International Journal of
Molecular Sciences

Special Issue Reprint

Neurodegenerative Disease

From Molecular Basis to Therapy, 2nd Edition

Edited by
Claudia Ricci

mdpi.com/journal/ijms

MDPI

Neurodegenerative Disease: From Molecular Basis to Therapy, 2nd Edition

Neurodegenerative Disease: From Molecular Basis to Therapy, 2nd Edition

Guest Editor

Claudia Ricci

MDPI

Basel • Beijing • Wuhan • Barcelona • Belgrade • Novi Sad • Cluj • Manchester

Guest Editor
Claudia Ricci
Medical, Surgical and
Neurological Sciences
University of Siena
Siena
Italy

Editorial Office
MDPI AG
Grosspeteranlage 5
4052 Basel, Switzerland

This is a reprint of the Special Issue, published open access by the journal *International Journal of Molecular Sciences* (ISSN 1422-0067), freely accessible at: www.mdpi.com/journal/ijms/special_issues/SNB17VCR4V.

For citation purposes, cite each article independently as indicated on the article page online and using the guide below:

Lastname, A.A.; Lastname, B.B. Article Title. *Journal Name* **Year**, *Volume Number*, Page Range.

ISBN 978-3-7258-3508-9 (Hbk)
ISBN 978-3-7258-3507-2 (PDF)
https://doi.org/10.3390/books978-3-7258-3507-2

Contents

About the Editor

Claudia Ricci

Claudia Ricci is a Research Scientist at the Neurogenetics Laboratory of the Department of Medical, Surgical, and Neurological Sciences at the University of Siena. After completing a PhD in Biotechnology, she extended her interest to the genetics of cerebral vascular malformations and motor neuron diseases, particularly amyotrophic lateral sclerosis (ALS), and she increased her expertise in the up-to-date techniques of genetic screening and biomarker research. She collaborates with the Italian Consortium for the study of genetics in ALS (ITALSGEN) and the Italy–USA Network and participates in wide studies on the genetic basis of ALS, leading to the identification of several genes related to this disease, including C9orf72, TARDBP, and FUS. Her publication list includes approximately 70 papers in peer-reviewed journals (ORCID 0000-0002-2431-0308). Since 2021, she has been a member of the Scientific Committee of the master's degree programmes "Regulatory Medical Writer" and "Science Popularization" at the University of Siena.

International Journal of
Molecular Sciences

MDPI

Editorial

Neurodegenerative Disease: From Molecular Basis to Therapy, 2nd Edition

Claudia Ricci

Department of Medical, Surgical and Neurological Sciences, University of Siena, 53100 Siena, Italy; claudia.ricci@unisi.it

Neurodegenerative diseases, characterised by the progressive degeneration of neurons, are a heterogeneous group of largely age-related disorders that affect millions of people worldwide. Age is the single most important risk factor for the development of all neurodegenerative diseases, but genetic and environmental factors can also enhance the risk. The prevalence of these diseases is increasing with increasing life expectancy, resulting in a growing socio-economic burden associated with neurodegenerative diseases. Current treatments are mostly symptomatic, without addressing the underlying cause of the disease, and have little or no effect on disease progression. Despite their different manifestations, some mechanisms, such as the presence of misfolded protein aggregates and abnormal protein accumulation, are common to several neurodegenerative diseases. On the other hand, in several cases, it is becoming clear that the same disease can be caused by different factors in different people, making a precision medicine approach necessary. Understanding these mechanisms is fundamental to the development of future effective therapies. While significant progress has been made in recent years in elucidating critical mechanisms underlying the pathogenesis of neurodegenerative diseases, this progress is only beginning to be effectively translated into clinical practice.

The aim of this Special Issue is to provide an up-to-date overview of progress in neurodegenerative disease research, from understanding the molecular basis to developing new therapies. Although the challenge remains daunting, there is some evidence to suggest that we are on the right track to identifying effective therapies, also in the context of a precision medicine approach.

A large proportion of the papers in this Special Issue focus on therapeutic approaches to Alzheimer's disease (AD), both as a review of previously published studies and as future perspectives. In their review, Kiss and colleagues [1] provide an up-to-date overview of the experimental evidence documenting the neuroprotective activities of artemisinins, highlighting the potential of these drugs for the treatment of Alzheimer's disease in humans and suggesting their consideration for carefully designed clinical trials. Artemisinin and its derivatives are plant-based drugs successfully used to treat malaria caused by Plasmodium parasites [2]. The authors describe the relatively large number of well-conducted studies, indicating the beneficial effects of these drugs in the preclinical setting of Alzheimer's disease, showing improved pathological features and pointing to multiple disease causes that can be modulated to enhance cognitive function. At the same time, they underline that the lack of concerted validation of the doses and specific efficacy of each artemisinin compound, and comparisons of their relative efficacy in different animal models makes direct translation into clinical trials difficult. The authors point out that questions about dosing regimens, long-term safety and potential interactions with existing drugs, as well as toxicities that may be associated with treatment in Alzheimer's patients can only be adequately answered by well-conducted clinical trials.

check for updates

Received: 14 February 2025
Accepted: 21 February 2025
Published: 24 February 2025

Citation: Ricci, C. Neurodegenerative Disease: From Molecular Basis to Therapy, 2nd Edition. *Int. J. Mol. Sci.* **2025**, *26*, 1929. https://doi.org/10.3390/ijms26051929

Rakovskaya and colleagues [3] focused on one of the key pathogenic events associated with Alzheimer's disease, the dysregulation of neuronal calcium (Ca^{2+}). Pharmacological agents capable of stabilising neuronal Ca^{2+} signalling have been identified as potential disease-modifying agents in Alzheimer's disease. The authors evaluated the effects of a set of novel positive allosteric regulators (PAMs) of the sarco/endoplasmic reticulum Ca^{2+} ATPase (SERCA) pump agents on the HEK293T cell line and 5XFAD transgenic mice modelling Alzheimer's disease. Several SERCA PAM compounds showed neuroprotective properties, confirming their potential role as a therapeutic target for the treatment of AD, with the compound NDC-9009 showing the best results, offering promising prospects for the development of disease-modifying agents for Alzheimer's disease.

5XFAD transgenic mice were also used as an AD model in the study performed by Park and colleagues [4]. They investigated the potential of adoptive regulatory T-cell (Treg) therapy for the treatment of Alzheimer's disease. The authors developed a Treg preparation protocol to facilitate the clinical application of this therapy and evaluated the therapeutic effects in 5XFAD mice. In addition to improving cognitive function, Aβ-specific Tregs reduced Aβ and pTAU accumulation in the hippocampus of 5XFAD mice and inhibited microglial neuroinflammation. These effects were observed at very low doses. The results of this study suggest that Aβ-specific Tregs can attenuate AD pathology in 5XFAD mice, opening new perspectives for targeted immunotherapy of AD.

Kim and colleagues [5] propose a novel approach to characterise novel mediators in Alzheimer's disease pathology. Their study highlights the importance of understanding the impact of exosomes on neural networks to improve our understanding of intracerebral neuronal communication and its impact on neurological disorders such as AD. The exosomes, derived from the nasal lavage fluid of 5XFAD mice, were studied using a high-density multielectrode array (HD-MEA) system, a novel technology that allows simultaneous recordings from thousands of neurons in primary cortical neuron cultures and organotypic hippocampal slices. The results showed increased neuronal firing rates and disoriented connectivity, reflecting the effects of pathological amyloid-beta oligomer treatment. Abnormal rhythmicity and increased current source density were also seen in local field potentials in exosome-treated hippocampal brain slices. This groundbreaking research is only a first exploration, but it shows the potential of exosomes to modulate neural networks and highlights the importance of understanding this modulation during the progression of Alzheimer's disease.

The availability of appropriate animal models is a key issue in the development of new treatments for Alzheimer's disease. In their perspective article [6], Volloch and Rits-Volloch provide an exhaustive review of the animal models currently used in AD research and point out their limitations. First, they are unable to develop the full spectrum of Alzheimer's pathology. Secondly, they are very responsive to drugs that are completely ineffective in the treatment of symptomatic Alzheimer's disease. This leads the authors to conclude that both the transgenic animal models and the drugs closely reflect the theory that guided their design, and that both fail because of the inadequacy of the underlying theory. They introduce a new, all-encompassing theory of conventional AD—the ACH2.0. The theory is also well described in the second paper of Volloch and Rits-Volloch present in this Special Issue [7]. In brief, it proposes that AD is a two-stage disease. Both stages are driven by intraneuronal (rather than extracellular) Aβ (iAβ), albeit from two distinct origins. The first asymptomatic stage is the accumulation of iAβ derived from the Aβ protein precursor (AβPP) over decades until a critical threshold is reached. This triggers the activation of the self-sustaining AβPP-independent iAβ production pathway and the onset of the second, symptomatic stage of AD. Importantly, AβPP-independent Aβ production is maintained intraneuronally. It drives AD pathology and perpetuates pathway function. In light of this

theory, the authors conclude that current animal models are inadequate because they do not take into account the intraneuronal AβPP-independent iAβ production pathway and that this mechanism must be incorporated into any successful AD model that faithfully mimics the disease. The authors also propose principles for the design of novel transgenic animal models of the disease and describe the molecular details of their construction [6]. At the same time, the ACH2.0 could also guide a next-generation therapeutic strategy for the treatment and prevention of both AD, as described in the second paper [7]. It should lead to the depletion of iAβ via its transient, short-lived, targeted degradation. The authors also propose two plausible ACH2.0-based drugs, activators of the physiologically occurring intra-iAβ-cleaving capabilities of BACE1 and/or BACE2, as potential novel treatments.

The study by Butler and colleagues [8] investigated the dysregulation of (AD)-associated protein expression in polycystic ovary syndrome (PCOS). The authors measured the plasma levels of amyloid-associated proteins (Amyloid-precursor protein (APP), alpha-synuclein (SNCA), amyloid P-component (APCS), Pappalysin (PAPPA), Microtubule-associated protein tau (MAPT), apolipoprotein E (apoE), apoE2, apoE3, apoE4, Serum amyloid A (SAA), Noggin (NOG) and apoA1 in weight and aged-matched non-obese PCOS and control women. The dementia-related proteins fibronectin (FN), FN1.3 and FN1.4; Von Willebrand factor (VWF); and extracellular matrix protein 1 (ECM1) were also measured. Only APCS differed between groups, being elevated in non-obese PCOS women compared to non-obese controls. This differed markedly from the elevated APP, APCS, ApoE, FN, FN1.3, FN1.4 and VWF previously reported in obese women with PCOS [9]. Non-obese PCOS subjects had a lower AD-associated protein pattern risk profile than obese PCOS women and were more similar to non-obese controls. This suggests that maintaining optimal body weight may be fundamental to reducing the long-term risk of AD in women with PCOS.

Parkinson's disease (PD) is another major focus of this Special Issue. Again, particular attention is paid to understanding the molecular mechanisms responsible for the disease and identifying future therapeutic targets. In their review, Battis and colleagues [10] describe the bidirectional interaction of α-synuclein with lipids and how its alterations may be related to the pathogenesis of Parkinson's disease. The authors provide an accurate description of lipids and lipid metabolism in the central nervous system, describe their alteration in PD, and focus on the interactions between lipids and α-synuclein in physiological and pathological conditions. Finally, they propose several therapeutic approaches based on strategies to modulate the lipid-α-synuclein interaction.

It is known that the accumulation of misfolded and aggregated α-synuclein can induce ER stress and unfolded protein response (UPR), leading to apoptotic cell death in Parkinson's disease (PD) patients. A key role in the regulation of the UPR is played by glucose-regulated protein 78 (GRP78), the major ER chaperone [11]. In rat models of α-synuclein pathology, its overexpression can modulate the UPR, block apoptosis and promote survival of nigral dopamine neurons. Pazi and colleagues [12] investigated the therapeutic potential of intranasal exogenous GRP78 to prevent or slow PD-like neurodegeneration in a rat model. The intranasally administered GRP78 was rapidly internalised by neurons and microglia in the substantia nigra pars compacta and other affected regions of the brain and prevented the development of the neurodegenerative process in the nigrostriatal system. GRP78 treatment significantly reversed the abnormal accumulation of phosphorylated pS129-α-synuclein and activation of the pro-apoptotic pathway of the UPR. In addition, exogenous GRP78 inhibited both microglial activation and pro-inflammatory cytokine production. In light of these findings, the authors suggest that exogenous GRP78 may have neuroprotective and anti-inflammatory effects and may be an effective therapeutic agent for PD and other synucleinopathies.

Salemi and colleagues [13] carried out a transcriptome analysis of post mortem mRNA extracted from the substantia nigra of both PD patients and healthy controls. Using an RNA sequencing approach, they identified 33 mRNAs that were significantly up-regulated and 59 mRNAs that were down-regulated in PD compared to controls. An examination of statistically significant pathways using KEGG and GO enrichment analyses revealed the involvement of several signalling pathways including cardiac muscle contraction, GABAergic synapse, autophagy, and Fc gamma receptor-mediated phagocytosis. These results show that genes that are conventionally associated with electrical conduction mechanisms in cardiac muscle may also play a role in the brain, suggesting new pathophysiological mechanisms that underlie Parkinson's disease. This knowledge could improve our understanding of Parkinson's disease and contribute to the development of future targeted therapies.

Other papers in this Special Issue focus on the understanding of the general mechanisms underlying neurodegeneration, using animal models of specific conditions. Druga and colleagues [14] address the neurodegeneration associated with epilepsy using LiCl/pilocarpine to induce status epilepticus (SE) in rat pups. This is a widely accepted model of temporal lobe epilepsy that causes spontaneous recurrent seizures, cognitive and behavioural deficits, and extensive brain damage. The authors analysed the location of degenerating neurons in the dorsal (insular) claustrum (DCL and VCL) and the dorsal, intermediate and ventral endopiriform nucleus (DEn, IEn and VEn) after induction of SE at different postnatal days. This study showed that status epilepticus induced in the early stages of life causes neurodegeneration in the claustral complex. Age at SE induction and time intervals after SE were highly related to the extent and distribution of degenerating neurons. The severity of the damage increased with age at the time of SE and reached a peak at 24 h after SE. In the DCL, degenerating neurons predominated in the zone close to the medial and dorsal margins. Little degeneration was observed in the VCl, suggesting a protective role against SE-induced damage.

Neuroinflammation and immune activation are widely accepted as significant contributing factors to the pathophysiology of neurodegenerative disease. Aries and colleagues [15] used low-level chronic peripheral LPS to induce neutrophil activation in the periphery and brain as a model to understand the role of inflammation in brain diseases. Subclinical levels of LPS were injected intraperitoneally into mice to study its effect on neutrophil numbers and activation. Since neutrophil activation in the periphery was higher in LPS-injected mice than in saline-injected mice after 4 weeks, but not after 8 weeks of injections, the time for brain examination was set at 4 weeks. Within this window, chronic LPS injections increased neutrophil activation in the periphery and brain of mice. These results indicate that subclinical levels of peripheral LPS induce neutrophil activation in the periphery and brain and define the experimental parameters. This model could be used for understanding how neutrophils may be mediators of the periphery–brain axis of inflammation in neurodegenerative or neuroinflammatory diseases.

Neurodegeneration may also involve progressive and relentless tissue loss in areas connected to an initial infarct-damaged zone, as in the case of stroke-related secondary neurodegeneration. Focusing on stroke, Hamblin and colleagues [16] examined the effects of MMP-3 genetic knockout (MMP-3 KO) on infarct volume and gene expression in the brains of mice subjected to middle cerebral artery occlusion followed by reperfusion. An RNA-seq analysis revealed a significant downregulation of gene expression signatures for neuroinflammation, endothelial and epithelial–mesenchymal transition, integrin cell surface signalling and apoptosis in the stroke brains of MMP-3 KO mice compared to MMP-3 wild-type controls, with a greater extent in females. Based on these results, the authors suggest that MMP-3 is a promising therapeutic target for improving stroke outcome because it affects multiple cellular pathways after stroke.

Given the evidence that increasing histamine levels has beneficial effects on memory [17] and that dihydroergotamine (DHE), an FDA-approved drug for the treatment of migraine, inhibits histamine N-methyltransferase (HNMT), the enzyme responsible for inactivating histamine in the brain [18], Hernández-Rodríguez and colleagues [19] evaluated the effect of DHE on histamine levels in the hippocampus and its effects on memory using a scopolamine-induced amnesia mouse model. Their results showed that DHE improves memory in the scopolamine-induced amnesia model by increasing histamine levels in the hippocampus through its activity as an HNMT inhibitor. As increasing histamine levels in the brain has been proposed as a promising approach to treating neurological disorders that cause memory impairment, these results may open up new therapeutic perspectives.

In their review, Ruqa and colleagues focus on the terminal nerve, a highly conserved and versatile nerve that is located just above the olfactory bulbs in humans and in several other species of vertebrates [20]. The authors summarise the main findings on the terminal nerve in order to clarify its anatomy and the various functions attributed to it, and to better interpret its possible involvement in pathological processes. They point out that the terminal nerve has been well studied in various animal species, but only a few studies have been carried out in humans. Therefore, its function remains unknown. The authors review studies suggesting a role in olfaction due to its proximity to the olfactory nerve. Others suggest a role in reproduction and sexual behaviour. It is thought to be involved in the unconscious perception of specific odours that influence the autonomic and reproductive hormone systems via the hypothalamic–pituitary–gonadal axis. Finally, a section of the review is devoted to the potential role of the terminal nerve in diseases such as Kallmann syndrome (a genetic form of hypogonadotropic hypogonadism) and COVID-19.

Last but not least, the review by Cantara and colleagues [21] offers real hope for the advancement of therapeutic interventions in neurodegenerative disorders, addressing motor neuron diseases, namely spinal muscular atrophy (SMA), amyotrophic lateral sclerosis (ALS) and spinal bulbar muscular atrophy (SBMA). The authors reviewed the use of antisense oligonucleotides (ASOs), short oligodeoxynucleotides designed to bind to specific regions of target mRNA, as therapeutic agents in these diseases. This approach has led to major successes, such as the ASO known as nusinersen, the first effective treatment for SMA that can improve symptoms and slow disease progression. Another success is tofersen, an ASO designed to treat ALS patients with *SOD1* gene mutations. Both ASOs have received FDA and EMA approval and represent a milestone in the treatment of two diseases previously thought to be incurable. On the other hand, ASO treatment in ALS patients carrying the *C9orf72* gene mutation has failed to improve disease progression. The authors highlight the successes, failures, strengths and limitations of current ASO research and suggest approaches that could lead to more effective treatments.

In summary, this Special Issue addresses the problem of treating neurodegenerative diseases from a variety of perspectives, from basic research into the molecular mechanisms responsible for a disease to reviews of the most advanced therapies available. This topic can provide exciting insights into new therapeutic approaches for various neurodegenerative disorders, expanding our knowledge of the biological basis and clinical research, as well as new challenges and future perspectives in neurodegeneration.

Conflicts of Interest: The author declares no conflicts of interest.

References

1. Kiss, E.; Kins, S.; Gorgas, K.; Venczel Szakács, K.H.; Kirsch, J.; Kuhse, J. Another Use for a Proven Drug: Experimental Evidence for the Potential of Artemisinin and Its Derivatives to Treat Alzheimer's Disease. *Int. J. Mol. Sci.* **2024**, *25*, 4165. [CrossRef] [PubMed]
2. Krishna, S.; Bustamante, L.; Haynes, R.K.; Staines, H.M. Artemisinins: Their Growing Importance in Medicine. *Trends Pharmacol. Sci.* **2008**, *29*, 520–527. [CrossRef]
3. Rakovskaya, A.; Erofeev, A.; Vinokurov, E.; Pchitskaya, E.; Dahl, R.; Bezprozvanny, I. Positive Allosteric Modulators of SERCA Pump Restore Dendritic Spines and Rescue Long-Term Potentiation Defects in Alzheimer's Disease Mouse Model. *Int. J. Mol. Sci.* **2023**, *24*, 13973. [CrossRef] [PubMed]
4. Park, S.-Y.; Yang, J.; Yang, H.; Cho, I.; Kim, J.Y.; Bae, H. Therapeutic Effects of Aβ-Specific Regulatory T Cells in Alzheimer's Disease: A Study in 5XFAD Mice. *Int. J. Mol. Sci.* **2024**, *25*, 783. [CrossRef]
5. Kim, S.; Jeon, J.; Ganbat, D.; Kim, T.; Shin, K.; Hong, S.; Hong, J. Alteration of Neural Network and Hippocampal Slice Activation through Exosomes Derived from 5XFAD Nasal Lavage Fluid. *Int. J. Mol. Sci.* **2023**, *24*, 14064. [CrossRef] [PubMed]
6. Volloch, V.; Rits-Volloch, S. On the Inadequacy of the Current Transgenic Animal Models of Alzheimer's Disease: The Path Forward. *Int. J. Mol. Sci.* **2024**, *25*, 2981. [CrossRef] [PubMed]
7. Volloch, V.; Rits-Volloch, S. Next Generation Therapeutic Strategy for Treatment and Prevention of Alzheimer's Disease and Aging-Associated Cognitive Decline: Transient, Once-in-a-Lifetime-Only Depletion of Intraneuronal Aβ (iAβ) by Its Targeted Degradation via Augmentation of Intra-iAβ-Cleaving Activities of BACE1 and/or BACE2. *Int. J. Mol. Sci.* **2023**, *24*, 17586. [CrossRef]
8. Butler, A.E.; Moin, A.S.M.; Sathyapalan, T.; Atkin, S.L. A Cross-Sectional Study of Protein Changes Associated with Dementia in Non-Obese Weight Matched Women with and without Polycystic Ovary Syndrome. *Int. J. Mol. Sci.* **2024**, *25*, 2409. [CrossRef] [PubMed]
9. Butler, A.E.; Moin, A.S.M.; Sathyapalan, T.; Atkin, S.L. A Cross-Sectional Study of Alzheimer-Related Proteins in Women with Polycystic Ovary Syndrome. *Int. J. Mol. Sci.* **2024**, *25*, 1158. [CrossRef] [PubMed]
10. Battis, K.; Xiang, W.; Winkler, J. The Bidirectional Interplay of α-Synuclein with Lipids in the Central Nervous System and Its Implications for the Pathogenesis of Parkinson's Disease. *Int. J. Mol. Sci.* **2023**, *24*, 13270. [CrossRef] [PubMed]
11. Gorbatyuk, M.S.; Shabashvili, A.; Chen, W.; Meyers, C.; Sullivan, L.F.; Salganik, M.; Lin, J.H.; Lewin, A.S.; Muzyczka, N.; Gorbatyuk, O.S. Glucose Regulated Protein 78 Diminishes α-Synuclein Neurotoxicity in a Rat Model of Parkinson Disease. *Mol. Ther.* **2012**, *20*, 1327–1337. [CrossRef] [PubMed]
12. Pazi, M.B.; Belan, D.V.; Komarova, E.Y.; Ekimova, I.V. Intranasal Administration of GRP78 Protein (HSPA5) Confers Neuroprotection in a Lactacystin-Induced Rat Model of Parkinson's Disease. *Int. J. Mol. Sci.* **2024**, *25*, 3951. [CrossRef]
13. Salemi, M.; Ravo, M.; Lanza, G.; Schillaci, F.A.; Ventola, G.M.; Marchese, G.; Salluzzo, M.G.; Cappelletti, G.; Ferri, R. Gene Expression Profiling of Post Mortem Midbrain of Parkinson's Disease Patients and Healthy Controls. *Int. J. Mol. Sci.* **2024**, *25*, 707. [CrossRef] [PubMed]
14. Druga, R.; Mares, P.; Salaj, M.; Kubova, H. Degenerative Changes in the Claustrum and Endopiriform Nucleus after Early-Life Status Epilepticus in Rats. *Int. J. Mol. Sci.* **2024**, *25*, 1296. [CrossRef]
15. Aries, M.; Cook, M.; Hensley-McBain, T. A Pilot Study to Investigate Peripheral Low-Level Chronic LPS Injection as a Model of Neutrophil Activation in the Periphery and Brain in Mice. *Int. J. Mol. Sci.* **2024**, *25*, 5357. [CrossRef] [PubMed]
16. Hamblin, M.H.; Boese, A.C.; Murad, R.; Lee, J.-P. MMP-3 Knockout Induces Global Transcriptional Changes and Reduces Cerebral Infarction in Both Male and Female Models of Ischemic Stroke. *Int. J. Mol. Sci.* **2024**, *25*, 7383. [CrossRef] [PubMed]
17. Kamei, C.; Chen, Z.; Nakamura, S.; Sugimoto, Y. Effects of Intracerebroventricular Injection of Histamine on Memory Deficits Induced by Hippocampal Lesions in Rats. *Methods Find. Exp. Clin. Pharmacol.* **1997**, *19*, 253–259. [PubMed]
18. Jiménez, E.M.; Żołek, T.; Hernández Perez, P.G.; Miranda Ruvalcaba, R.; Nicolás-Vázquez, M.I.; Hernández-Rodríguez, M. Drug Repurposing to Inhibit Histamine N-Methyl Transferase. *Molecules* **2023**, *28*, 576. [CrossRef] [PubMed]
19. Hernández-Rodríguez, M.; Mera Jiménez, E.; Nicolás-Vázquez, M.I.; Miranda-Ruvalcaba, R. Dihydroergotamine Increases Histamine Brain Levels and Improves Memory in a Scopolamine-Induced Amnesia Model. *Int. J. Mol. Sci.* **2024**, *25*, 3710. [CrossRef]
20. Ruqa, W.A.; Pennacchia, F.; Rusi, E.; Zoccali, F.; Bruno, G.; Talarico, G.; Barbato, C.; Minni, A. Smelling TNT: Trends of the Terminal Nerve. *Int. J. Mol. Sci.* **2024**, *25*, 3920. [CrossRef] [PubMed]
21. Cantara, S.; Simoncelli, G.; Ricci, C. Antisense Oligonucleotides (ASOs) in Motor Neuron Diseases: A Road to Cure in Light and Shade. *Int. J. Mol. Sci.* **2024**, *25*, 4809. [CrossRef]

International Journal of
Molecular Sciences

MDPI

Review

Another Use for a Proven Drug: Experimental Evidence for the Potential of Artemisinin and Its Derivatives to Treat Alzheimer's Disease

Eva Kiss [1,2,*], Stefan Kins [3], Karin Gorgas [1], Kinga Hajnal Venczel Szakács [2], Joachim Kirsch [1] and Jochen Kuhse [1,*]

[1] Institute of Anatomy and Cell Biology, University of Heidelberg, 69120 Heidelberg, Germany; gorgas@ana.uni-heidelberg.de (K.G.); joachim.kirsch@urz.uni-heidelberg.de (J.K.)
[2] Department of Cellular and Molecular Biology, George Emil Palade University of Medicine, Pharmacy, Science and Technology of Târgu Mures, 540142 Târgu Mures, Romania; kingahajnalszakacs@gmail.com
[3] Department of Human Biology and Human Genetics, University of Kaiserslautern, 69120 Kaiserslautern, Germany; s.kins@biologie.uni-kl.de
* Correspondence: kiss@ana.uni-heidelberg.de (E.K.); jochen.kuhse@urz.uni-heidelberg.de (J.K.)

Abstract: Plant-derived multitarget compounds may represent a promising therapeutic strategy for multifactorial diseases, such as Alzheimer's disease (AD). Artemisinin and its derivatives were indicated to beneficially modulate various aspects of AD pathology in different AD animal models through the regulation of a wide range of different cellular processes, such as energy homeostasis, apoptosis, proliferation and inflammatory pathways. In this review, we aimed to provide an up-to-date overview of the experimental evidence documenting the neuroprotective activities of artemisinins to underscore the potential of these already-approved drugs for treating AD also in humans and propose their consideration for carefully designed clinical trials. In particular, the benefits to the main pathological hallmarks and events in the pathological cascade throughout AD development in different animal models of AD are summarized. Moreover, dose- and context-dependent effects of artemisinins are noted.

Keywords: Alzheimer's disease; artemisinins; multitargeting neurotherapeutics

Citation: Kiss, E.; Kins, S.; Gorgas, K.; Venczel Szakács, K.H.; Kirsch, J.; Kuhse, J. Another Use for a Proven Drug: Experimental Evidence for the Potential of Artemisinin and Its Derivatives to Treat Alzheimer's Disease. *Int. J. Mol. Sci.* **2024**, *25*, 4165. https://doi.org/10.3390/ijms25084165

Academic Editor: Claudia Ricci

Received: 5 February 2024
Revised: 28 March 2024
Accepted: 29 March 2024
Published: 9 April 2024

1. Introduction

Alzheimer's disease (AD) is the most common form of dementia characterized by progressive cognitive decline, pathological hallmarks of extracellular amyloid plaques formed by amyloid β peptides (Aβ), and intracellular deposits of hyperphosphorylated tau protein as neurofibrillary tangles in the brain [1]. However, a much better pathological correlate of cognitive dysfunction observed in AD is synaptic loss [2–4].

Sporadic forms of AD (i.e., late-onset) mostly start after age 65, whereas symptoms of the inherited forms of the disease usually develop before age 50. These "early-onset" forms compose less than 5% of all AD cases and are associated with mutations in genes involved in the amyloid-processing pathway, such as presenilin 1 (PSEN1) and 2 (PSEN2) and amyloid precursor protein (APP) [5]. The impaired APP cleavage caused by the mutations results in the increased production of amyloid beta $(Aβ)_{1–42}$ peptides and failure in the Aβ clearance, thus providing an explanation for the Aβ accumulation in the brain of early-onset AD patients [1]. The identification of these gene mutations initiated the proposal of the "amyloid cascade hypothesis" in the early 1990s. It suggests that the generation and aggregation of Aβ are the initiator and, further, central factors in the cascade of cellular and molecular events that, ultimately, lead to AD [6,7]. Further supporting this theory, both genetic (e.g., ApoE4, TREM2, RIN3, CLU and PTK2B) and nongenetic (e.g., diabetes and obesity) risk factors for late-onset AD have also been identified to influence Aβ generation and/or Aβ clearance [8].

Aβ is released from APP through the amyloidogenic pathway after sequential cleavage by β-secretase (BACE1) and γ-secretase during the course of its trafficking to the cell membrane. In addition to Aβ, other molecules such as sAPPβ (a soluble ectodomain of APP), CTFβ (C-terminal fragment β or C99) and AICD (APP intracellular domain) are also formed in the amyloidogenic pathway. Along the nonamyloidogenic pathway, membrane-anchored APP is cleaved by α-secretase within the Aβ sequence, thus preventing Aβ production [1,9]. Under physiological conditions, the nonamyloidogenic pathway predominates, and augmentation of the amyloidogenic pathway results in increased Aβ generation and AD pathogenesis. Under pathological conditions, there is also a change in the $A\beta_{1–42}/A\beta_{1–40}$ ratio in favor of an increased level of $A\beta_{1–42}$, exhibiting decreased solubility and increased tendencies for fibril assembly and plaque formation [1,9]. After secretion, these Aβ peptides spontaneously aggregate and deposit into oligomers, fibrils, and plaques, which then progressively induce a series of events, including synaptic failure, aberrant proteostasis, such as tau phosphorylation and fibrillary tangle formation, cytoskeletal abnormalities, impaired energy homeostasis, DNA and RNA damage, increased inflammation and neuronal death [1]. All of these processes can also represent a link to the alteration of different forms of synaptic plasticity, changes that apparently develop long before the onset of clinical symptoms of AD [10]. Evidence supports that complex compensation mechanisms may work in the brain to maintain an almost normal cognitive performance for decades, with AD symptoms only starting when pathological cellular reactions are initiated [11]. Accordingly, the initial effects of "proteopathic" stress exerted by Aβ on various cells in the brain are physiological, involving primarily the lysosomal/endolysosomal system and, in particular, autophagy, to maintain homeostasis in the proteostatic network and various synaptic plasticity mechanisms. Even inflammatory reactions contribute initially to sustain homeostasis [11]. It is when these compensatory cellular homeostatic mechanisms fail that the clinical phase of the disease is initiated, and then it is no longer the accumulation of Aβ but other downstream events, such as neuroinflammation and tau accumulation, that are the main drivers of the neurodegeneration, eventually, in a synergistic manner.

In addition to Aβ, other proteolytic fragments of APP may also participate in the pathogenesis of AD via differential mechanisms. Specifically, carboxy-terminal fragments (CTFs) of APP were found to exhibit even higher levels of neurotoxicity than Aβ [12]. CTFs were reported to translocate into the nucleus, where binding with Fe65 and CP2 affected the transcription of genes, including GSK-3 (glycogen synthase kinase-3), resulting in increased tau phosphorylation and the formation of neurofibrillary tangles [13]. More recently, overproduction of CTFs was indicated to cause alterations in mitochondrial structure and function, as well as failure of basal mitophagy, in vivo [14].

Another interesting aspect of AD pathogenesis is the demonstration that APP and APP cleavage products have important physiological roles, raising the question of whether their loss contributes to AD development [15,16]. The extracellular proteolytic protein of APP (sAPPα) [17,18], as well as Aβ, exert neuroprotective effects and have neurotrophic roles in synaptogenesis and neurogenesis [19,20]. For example, Aβ monomers can induce pathways mediated by the CREB (cAMP-response element-binding protein)-induced transcription of BDNF (brain-derived neurotrophic factor), known to be involved in adult hippocampal neurogenesis [21]. Further, it has been suggested that a hormetic mechanism for Aβ may operate, thus exerting opposing effects at low and high concentrations. Low concentrations of Aβ strengthen both synaptic plasticity and memory, whereas high concentrations result in the well-known impairment of cognition [19]. Neurotoxic Aβ aggregates are connected with damage to the blood–brain barrier (BBB), since low levels of Aβ peptides may function as a seal that maintains the BBB's integrity [22]. Moreover, CTFs seem to be essential for endosomal and lysosomal functions and have a regulatory role in autophagy and mitochondrial function [14], whereas full lengths APP as a cell surface protein fulfill important functions for synaptic homeostasis and participate in signal transduction [17,23].

Thus, considering the complexity of AD and the failure or only very limited clinical effects of most single-target therapies [24,25], it seems essential that future therapeutic approaches target several pathogenic factors of the disease and, so far as possible, in a stage-dependent manner [8,26]. This includes exploring the potentials of natural products with neuroprotective effects that have a multitarget capacity and mild adverse events. Recent research has explored the potential benefits of specific floral extracts and by-products in the context of AD. For instance, some studies have evaluated the roles of flowers, such as rose x hybrida petals [27] and tubalghia volacea petals [28]. Certain by-products, including olive leaves, have also shown promise in combating AD [29]. Moreover, the potential therapeutic effects of honey in the context of AD have been explored (e.g., [30,31]). Additionally, over the several last years, an increasing number of studies in animal models have indicated the capability of different plant extracts used in traditional Chinese medicine to treat AD [32–36]. Moreover, an oral compound extracted from brown seaweed was approved in China, in 2019, to treat patients with mild to moderate forms of the disease [37]. Artemisinins represent another promising member of these plant-derived groups of drugs, holding the additional privilege of already being approved for the treatment of malaria with a known clinical safety and efficacy.

2. Artemisinins: Chemical Structure, Pharmacokinetic Behaviors and Antimalaria Activities

Artemisinin and its derivatives (collectively termed as artemisinins) are sesquiterpene lactones derived from the plant sweet wormwood (Artemisia annua), which has been applied in traditional Chinese medicine to treat "fever". Currently, artemisinins are first-line drugs in the treatment of malaria caused by Plasmodium parasites [38]. For the isolation and discovery of artemisinin, the active compound of the plant, as an antimalarial drug, the Chinese scientist Tu Youyou received the Nobel Prize in Physiology or Medicine in 2015.

Since it was first isolated, in 1972, several artemisinin analogs with improved solubi-lity and pharmacokinetic profiles have been developed [39]. These include dihydroartemisinin (DHA), artemether, arteether, and, especially, artesunate, which is a hemisuccinate ester of DHA. Artesunate because of its substantial water solubility and high oral bioavailability is considered superior to artemisinin and other derivatives that are lipid-soluble [40]. In a relatively recent study based on computer simulations and pharmacokine-tics, the oral bioavailability of artemisinin was found to be 12.2 $\pm$ 0.832% [41], since the oral bioavailability of artesunate, which shows high variability, can reach 60% [42,43]. DHA, which is the common active metabolite of artemisinin derivatives, into which they are converted in the body upon administration, but it is also available as an independent drug, has an even higher bioavailability of >80% after oral administration [44]. However, all artemisinins have very short in vivo half-lives, ranging from 2 to 5 h for artemisinin, <1 h for artesunate and DHA and 2 to 4 h for artemether [43,44]. Therefore, they are commonly coadministered antimalarial agents with longer half-lives. These combinations also help to slow the development of parasite resistance [45,46]. The fast elimination of artemisinins also explains, at least partially, their favorable safety profiles. Furthermore, because of their ability to easily cross the BBB, artemi-sinins are highly effective in the treatment of the cerebral form of the disease [42].

All forms of the drug encompass a tetracyclic core bearing an endoperoxide bridge (C-O-O-C), which is essential for the antimalarial activity of these lactons. For this, artemisinins are thought to be activated through an interaction with intraparasitic heme in erythrocytes—a byproduct of hemoglobin endocytosis and catabolism within the malaria parasite—resulting in heme iron (II) oxide-mediated cleavage of the endoperoxide bridge. The subsequently generated carbon-centered free radicals then alkylate and damage susceptible cellular proteins, lipids and other molecules, as well as generate reactive oxygen species (ROS), resulting in the death of the parasite [47]. Additionally, there is evidence suggesting that DHA can kill malaria parasites, inducing proteostatic stress by compromis-

ing parasite proteasome function, at which time the accumulation of unfolded/da-maged and polyubiquitinated proteins will activate the ER stress responses [48].

Presently, extensive in vitro and in vivo preclinical data support the therapeutic efficacy of artemisinins in a variety of human disease conditions beyond malaria, such as cancer, diabetes, atherosclerosis, viral infections, autoimmune diseases and, not least, in neurodegenerative diseases [49]. These effects seem to be mediated by artemisinins-induced changes in several signaling pathways, that interfere with multiple hallmarks of the respective diseases and probably rely on multitarget and promiscuous interactions of artemisinins with cellular proteins [50]. However, the exact molecules and substances that directly interact with artemisinins have yet to be determined.

3. Alzheimer's Disease Mouse Models Used for Testing Artemisinins

Wild-type mice do not develop Aβ plaques during the course of normal aging, thus the most commonly used animal models for AD are transgenic mice that rely on the neural overexpression of human genes carrying mutations associated with familial AD (FAD). It was observed that the expression of multiple FAD-associated mutations at one time results in transgenic mice with a more severe pathology that develops at a younger age [51]. Thus, a vast majority of transgenic mice express mutated human APP in combination with PSEN1, resulting in increased Aβ production, Aβ aggregation and formation of amyloid plaques with or without human MAPT (microtubule-associated protein tau), which results in the formation of neurofibrillary tangles [52]. It is important to emphasize that none of the available animal models replicate all features of human AD; they only recapitulate one or more features of AD pathology, commonly in a nonphysiological manner, which represents their major limitation. In addition, the exact phenotype, including the type and time course of the AD pathology, strongly depends on the FAD mutation, promoter used, expression levels of transgene in the brain and, not least, the background mouse strain, thus making absolute comparisons among models difficult [51]. Nevertheless, the results generated using experimental models have contributed substantially to the elucidation of the molecular pathogenesis of AD and development of diagnostic biomarkers and therapeutic strategies, although in the latter with a very high rate of failure when tested in clinical settings. This has led some scientists to question the validity of the available mouse models for developing therapeutic strategies in humans [51,53]. The contrary is supported by the monoclonal antibodies targeting of different forms of Aβ recently approved by the US Food and Drug Administration (FDA) for the treatment of AD. Prior to clinical trials, these antibodies were tested in several preclinical studies decreasing pathogenic Aβ levels and preventing Aβ deposition in the brain of transgenic mice [54,55]. Furthermore, the use of more than one model to evaluate potential drugs should enhance the chances of a successful translation from preclinical studies to patient therapy. Here, we summarize the main characteristics of AD mouse models used by the different research groups to test the effects of artemisinins on various aspects of the disease.

$APP_{swe}PS1_{L166P}$—APP/PS1 mice are double transgenic mice coexpressing the KM670/671NL "Swedish"-mutated amyloid precursor protein (APP) and the L166P-mutation carrying human presenilin 1 (PS1) under the control of a neuron-specific Thy1 promoter element. The $A\beta_{40}$ and $A\beta_{42}$ concentrations increase with advancing age in the brain of APP/PS1 mice. Amyloid plaque deposition starts at approximately 6 weeks of age in the neocortex and 3–4 months of age in the hippocampus in parallel to plaque-associated neuroinflammation (microgliosis and astrogliosis), similar to that in human AD. Cognitive impairment, including deficits in the Morris Water maze, was reported at seven months of age. The major limitations of APP/PS1 mice are a lack of widespread neuronal loss and neurofibrillary tangles (NFTs), yet they show increased tau hyperphosphorylation [56,57].

APPswe/PSEN1dE9—APP/PS1 mice represent the most widely used AD model and were bred by crossing transgenic APP animals expressing the Swedish mutation with those expressing PSEN1dE9 (PSEN1 gene without exon 9). In comparison to the $APP_{swe}PS1_{L166P}$ model, these mice start developing Aβ deposits later, by six months of age, showing

abundant plaques in the hippocampus and cortex by 9 months, with further increases up to 12 months of age [58,59]. In parallel, astrocytosis develops, indicated by extensive GFAP staining throughout the cortex by 15 months [60]. Modest neuronal loss was observed adjacent to plaques between 8 and 10 months of age [61] but tangles were not detected in this model.

The 5xFAD mouse model carries five FAD mutations, specifically the Swedish ($APP_{K670N/M671L}$), London (APP_{V717I}) and Florida (APP_{I716V}) APP mutations and the $PS1_{M146L}$ and $PS1_{L286V}$ mutations, driven by the Thy-1 promoter [62]. In these mice, a very early intraneuronal Aβ accumulation (6 weeks) is followed by plaque formation at 2 months, when astrogliosis and microgliosis also begin to develop. Soluble $A\beta_{42}$ is already detectable at 1.5 months. The $A\beta_{42}/A\beta_{40}$ ratios are very high in young mice, averaging ∼25, but they decrease to ∼5 as a result of the increase in $A\beta_{40}$ levels with age. The mice exhibit synaptic degeneration and neuronal loss, altered spatial working memory, and develop progressive cognitive deficits as early as 4–5 months of age. However, abnormal tau hyperphosphorylation was not noticed in the 5XFAD mice, and they also failed to develop NFTs. The early onset and aggressive amyloidosis render this moue model for the study of, specifically, AD-like amyloidosis and the effects of plaques on the brain and testing potential therapies on it [62].

The 3xTg mouse model is considered the most complete transgenic mouse model of AD pathology available that combines the tau (MAPT) mutation P301L with the APP Swedish mutation and PSEN1 mutation M146V. The APP and MAPT expressions are driven by the Thy-1.2 promoter, while PSEN1 expression is driven by the endogenous PSEN1 promoter [63]. These mice develop a progressive neuropathology, including intracellular (3–4 months of age) and extracellular Aβ deposits (6 months of age) and phosphorylated tau aggregates (10–12 months of age), which start in the hippocampus and then expanding to the neocortex, thus closely mimicking the development pattern of the pathology in the brain of humans with AD [64]. Gliosis may occur earlier than 7 months [65]. Mice also show minor, localized neuronal cell loss, synaptic impairment and cognitive deficits from 4 months, when plaques and tangles are not yet apparent [51]. Interestingly, recent reports indicate that, since the original report, in 2003 [63], the development of pathology has been substantially delayed (~18 months of age), and a sex difference manifested for both plaques and tangles, only emerging in female mice [66]. The model is considered suitable for assessing relationships between amyloid and tau pathologies, as well as cognition and testing of potential therapies [67].

Intracerebral injections of Aβ oligomers: injection or infusion of soluble Aβ peptide into the brain is considered an alternative to transgenic animals to mimic AD pathology in physiologically normal, nontransgenic mice or rats and to study the effects of increased soluble amyloid species in the brain without the presence of plaque. The results appear to depend on the site of injection and the nature of the peptide used [68]. The injection of $A\beta_{1–42}$ into the rat\mouse hippocampus was able to induce memory deficits and increase the level of oxidative stress and inflammatory response and even apoptosis of cholinergic neurons, indicating that these phenomena are general consequences of $A\beta_{1–42}$ administration in the brain. Additionally, phosphorylated tau proteins and some neurofibrillary tangles were also observed in the hippocampus of these rodents [68]. The model is considered a valid tool to evaluate the potential for compounds to directly target Aβ or its downstream mechanism early in AD.

4. Effects of Artemisinins on Hallmarks of AD Pathogenesis

The reported effects of artemisinins on hallmarks of AD, observed using in vitro and in vivo preclinical models, are summarized in Figure 1.

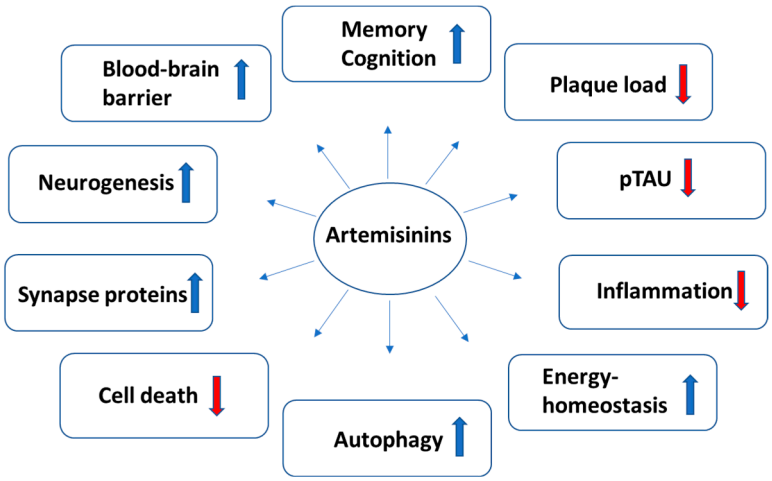

Figure 1. Reported effects of artemisinins on the hallmarks of Alzheimer's disease. The arrows indicate changes induced by artemisinins in the specified pathogenetic factors and hallmarks of AD in preclinical studies; ↑ (increase) and ↓ (decrease) compared to AD condition.

4.1. Aβ Pathology—Plaque Formation

According to the amyloid hypothesis, the accumulation of pathological forms of Aβ represents the primary pathological process in AD pathogenesis, which is driven by an imbalance between Aβ production and Aβ clearance, resulting in the formation of amyloid plaques [1]. Aβ aggregation may disrupt cell-to-cell communication, and it was shown to induce neuroinflammation and, finally, neuronal cell death. Moreover, increasing evidence indicates that soluble Aβ oligomers and the intermediate products of APP cleavage by β-secretase (CTFs) could also trigger tau alterations and contribute to neurotoxicity and neurodegeneration [1,69], leading to cognitive decline. Correspondingly, extensive experimental data propose that the inhibition of Aβ generation and plaque formation should reduce Aβ pathology and attenuate tauopathy [8]. The new, recently FDA-approved antibody drugs (aducanumab, lecanemab and donanemab) for use in AD therapy targeting the formation of Aβ plaques have shown an ability to slow down cognitive decline in patients with early symptoms, strengthening the hypothesis of a causal role of Aβ in the pathogenesis of AD [70,71]. However, the magnitude of the clinical effect elicited by these drugs (an approximately 30% slower rate of decline) is rather modest, suggesting the contribution of additional pathological mechanisms to the disease.

In this context, it is important to note that several independent studies have reported a reduction in Aβ production and plaque load in the cortex and hippocampus of various AD mouse models upon treatment with different artemisinins. Already one decade ago, Shi et al. demonstrated that artemisinin treatment in 5-month-old APPswe/PS1dE9 transgenic mice at a dose of 40 mg/kg/day for 30 days decreased the neuritic plaque burden by approximately 48% and 61% in the cortex and hippocampus, respectively. Moreover, these authors have shown that artemisinin reduced APP processing through inhibition of the β-secretase activity, evidenced by decreased BACE1 levels in transgenic mice brains [72]. Very similar results were obtained when 6-month-old male APPswe/PSEN1dE9 mice were treated with DHA at a dose of 20 mg/kg/day. In this study, the oral administration of DHA for 3 months reduced thioflavin S-stained Aβ deposits and the quantities of amyloid plaques in the cortex and hippocampus sections of the treated group in parallel with markedly reduced $A\beta_{42}$ levels in both the cortex and hippocampus homogenates. Compared with the control group, the levels of APP and BACE1 protein were also down-regulated after DHA treatment, indicating reduced Aβ production [73]. In another study, 3-month-old male APPswePSEN1dE9/Nju mice were fed with relative high concentrations of DHA, specifically 50 mg/kg or 300 mg/kg, until they reached 9 months of age. Thioflavin T-staining of brain tissue sections revealed that both low and high doses of DHA significantly reduced Aβ plaque aggregations in the CA3, CA1 and DG subregions of the

hippocampus and in the cortex of AD mice, importantly, without toxicity or side effects on mice livers and kidneys [74]. Interestingly, in this study glycine silver staining was used to detect NFTs, evidencing their significant reduction in the brains of DHA-treated mice. Further, using the same mouse model, Qin et al. reported that the semisynthetic derivative of artemisinin, artesunate, also alleviated AD phenotypes in these APP/PS1 mice, reducing Aβ deposition in brain sections, as well as the levels of soluble and insoluble $A\beta_{1–42}$ in brain tissue, both by 40–50% [75]. In all of these studies, the treatment of APPswe/PSEN1dE9 mice corresponded mostly to the initial stage of Aβ deposition in this mouse model, supporting a preventive potential of artemisinins treatment in AD.

In line with this, very recently, artesunate was administered (32 mg/kg/day, i.p.) to 3-month-old 5xFAD mice that were also deficient in phosphatidylinositol-binding clathrin assembly protein PICALM (*Picalm*$^{+/-}$; *5XFAD* mice), a protein involved in the regulation of endocytosis and internalization of cell receptors, as well as intracellular protein trafficking [68]. After two months of treatment with artesunate, these mice exhibited relatively early-stage Aβ pathologies, two-fold increases in brain capillary PICALM levels and, in parallel, reduced $A\beta_{42}$ and $A\beta_{40}$ levels, Aβ load, and thioflavin S-positive amyloid deposition in the cortex and hippocampus of 34–51%. However, in this study, no differences in APP processing, as shown by comparable levels in the brain for APP, APP-CTF, BACE1 or Aβ degrading enzymes (neprilysin and insulin-degrading enzyme) were found [76].

In our own study, 12-month-old male $APP_{swe}/PS1_{L166P}$ mice, characterized with early onset amyloid plaque development, were evaluated after 3 months of oral administration of artemisinin or artesunate. The administration started at a relatively advanced stage of amyloidosis, and both drugs, at a dose of 10 mg/kg/day, reduced the plaque load in the cortex and hippocampus by ~40–50%, and a weaker effect or none at all was observed at a higher dose of 100 mg/kg/day [77]. In addition, artesunate treatment resulted in a significant decrease in APP cleavage products, specifically CTF levels and soluble Aβ concentrations in the hippocampus homogenates of 12-month-old APP/PS1 mice, altogether supporting that artemisinins, especially artesunate, can not only prevent but eventually reverse the progression of amyloid deposition in the brain of APP/PS1 mice. In conclusion, these different studies demonstrate convincingly that artemisinins treatment is an efficient method to reduce the level of amyloid plaques in AD models, although no complete elimination of amyloid plaques could be achieved in neither study. Furthermore, dose- and drug-dependent effects have to be considered.

4.2. Tau Pathology

Aβ pathology is thought to promote the development of tau pathology by favoring the conversion of tau from a normal to a toxic state that can even enhance Aβ toxicity via a feedback loop [78]. The reduction in cerebrospinal fluid and plasma p-tau by the recently approved anti-amyloid monoclonal antibodies in clinical trials support a downstream effect of amyloid-reducing agents on AD tau pathology as well [71]. Several studies using the 3xTg mouse model that exhibits both amyloid plaques and NFTs have shown that in addition to Aβ, artemisinins also beneficially modulate tau homeostasis.

Under normal physiological conditions, tau protein is a microtubule-associated protein highly expressed in the axons of neurons and involved in promoting the assembly and stabilization of microtubules. In AD, tau protein has been found in a hyperphospho-rylated state at certain serine/threonine residues forming aggregates of insoluble paired helical filaments and NFTs, which then lead to impairment of axonal transport compromising both neuronal and synaptic functions [79]. Interestingly, tau can also be secreted into the synaptic cleft in an activity-dependent manner, subsequently being internalized by a postsynaptic neuron or glia cells, spreading to other brain regions [80]. It was found that mostly phosphorylated soluble tau oligomers accumulate in both pre- and postsynaptic terminals, suggesting that mainly these tau forms spread trans-synaptically. These and other findings support a specific role for soluble pathological forms of tau in the neuropathology of AD [81].

Li et al. reported, in 2019, that artemether administered at doses of 5 mg/kg or 20 mg/kg, reduced both the Aβ deposition and phosphorylation of tau (Ser 416) by 20–40% in the brain cortex of 10-month-old 3xTg AD mice after treatment for four weeks [82]. In another study, the beneficial effects of artemether against $A\beta_{25–35}$-induced cognitive impairments in a rat model were correlated with the downregulation of the endogenous expressions of Aβ, BACE1, mTOR and tau proteins in N2a cells [83]. Artemisinin was also tested in 3xTg mice. Treatment for 1 month at doses of 1, 5 or 10 mg/kg/day for one month resulted in a significant reduction in with Aβ antibodies and Congo red staining detected Aβ levels and plaque load in the cortex and hippocampus of 12-month-old 3xTg mice. Additionally, significant reductions in the phosphorylated tau (Ser396 and Thr212) levels but not in total tau levels were recorded in the brains of artemisinin-treated mice when compared to control 3xTg mice [84]. These results were confirmed by a recently published study using Artemisia annua extracts in different concentration rather than isolated artemisinins [85]. In this study, the oral administration of the extract (6.7 mg/mL vs. 20 mg/mL) to 9-month-old female 3xTg AD mice for 3 months reduced both Aβ accumulation and tau hyper-phosphorylation (Thr181) to within a comparable range in the cortex and hippocampus. Interestingly, similar to our own observations, some clear dose dependent effects of the extract were evidenced. The effect of extract on Aβ deposition and APP and $A\beta_{1–42}$ levels in brain homogenates was higher in animals treated with lower concentrations of the extract since mice receiving the dosage of 20 mg/mL exhibited a more prominent reduction in tau-phosphorylation compared to animals treated with 6.7 mg/mL. The plant extract did not affect the expression of total tau, altogether indicating an eventual direct effect of the artemisinin extract on tau pathology [85].

In conclusion, several independent studies convincingly demonstrate that artemisinins treatment is an efficient method to reduce the level of Aβ and amyloid plaques, as well as tau hyperphosphorylation, in different AD mouse models, mimicking different stages of the disease, although the range of these reductions did not exceed 40–50% in either study.

4.3. Inflammation

Inflammation is another central feature of AD pathology, defined mainly by activation of CNS-residing glial cells and release of inflammatory factors. Inflammatory biomarkers are elevated in AD patients [86], and glial cells, such as microglia and astrocytes, that surround senile plaques and affected neurons are usually observed in the brain of AD patients [87]. Data from genome-wide association studies (GWASs) on sporadic AD cases showing associations between AD and genes involved in innate immunity (e.g., TREM2, CD33) suggest that inflammation is probably not only a consequence of the accumulation of Aβ and p-tau in the AD brain but may also modulate disease progression [87,88]. Both microglia and astrocytes can adopt neuroprotective and neurotoxic phenotypes, which seem primarily related to the stage of the disease. Microglia are the primary immune cells of the CNS and thought to protect against the incidence of AD due to the clearance of Aβ aggregates. Indeed, the ability of microglia to prevent plaque development by removing pathogenic Aβ is part of a first-line defense in addition to the inhibition of tau hyperphosphorylation and the production and release of neurotrophic factors. On the other hand, the Aβ-mediated activation of these cells can cause the release of pro-inflammatory cytokines, such as tumor necrosis factor (TNF)-α, interleukin (IL)-1β, and IL-6, and induce the generation of neurotoxic factors, such as nitric oxide and ROS, resulting in neuronal damage [89]. Aβ- or microglia-activated astrocytes also have neuroprotective functions in AD, ensuring the functional integrity of neurons and synapses with the release of neurotrophic factors and by blunting plaque formation by Aβ clearance and maintenance of BBB integrity. However, they may also favor neuroinflammation through the delivery of inflammatory cytokines and chemokines [87]. Pro-inflammatory cytokines can then upregulate β- and γ-secretases, generating a self-sustaining cycle in which cytokines and Aβ load reciprocally increase. Cytokines, especially IL-6, stimulating CDK5 activation promote the hyperphosphorylation of tau, indicating that long-lasting neuroinflammation

can also exacerbate Aβ and tau pathologies in AD [90,91]. Thus, modulation of neuroglial activation may represent another effective intervention to control the pathophysiology of neurodegenerative diseases [92].

Aβ-activated glial cells' production of different pro-inflammatory cytokines involves NF-κB activation that also favors the stimulation of NLRP3 inflammasome signaling cascades, resulting in the activation of caspase-1 and the secretion of IL-1β and IL-18 [93,94]. Thus, molecules that influence NF-kB activity can indirectly alter NALP3 priming. The involvement of this mechanism in the pathogenesis of AD is supported by the finding that the inhibition of NLAP3 in in vivo AD models can rescue cognitive deficits.

A large number of studies provide evidence for the anti-inflammatory activities of artemisinins in AD mouse brain. In 2013, Shi et al. had already reported that artemisinin treatment in 5-month-old APPswe/PS1dE9 transgenic mice at a dose of 40 mg/kg/day for 30 days reduced the nuclear translocation of NF-κB p65 and increased I-κBα expression, which led to the inhibition of NF-κB activity and a decrease in the production of downstream cytokines (IL-6 and TNF-α) of 37.16% and 34.46% in transgenic mice brains [72]. Additionally, in the artemisinin-treated mice, the level of NALP3 significantly decreased by 37%, and the level of the downstream molecule caspase-1 p20 subunit and the production of IL-1β decreased by 50% and 29.73%, respectively. Thus, artemisinin was shown to inhibit NF-κB activity and NALP3 activation in APPswe/PS1dE9 double-transgenic mice in a relative early stage of AD pathogenesis, preventing tissue damage. More recently, in the same mouse model artesunate administration from 2 to 6 month of age at either a 5 or 10 mg/kg/day dose effectively reduced the expressions of TNF-α, IL-6, and IL-1β and also reversed the alterations in the mitochondrial dynamics and mitophagy in mouse brain tissues [75]. Correspondingly, in the same study, artesunate suppressed Aβ-induced activation of BV-2 microglial cells and N2a neuronal cells reducing the secretion of TNF-α, IL-6, and IL-1β (protein and mRNA levels) to 100 and 200 nM but not 50 nM concentrations. In a very similar fashion, Artemisia annua extract was recently shown to attenuate neuroinflammation in the brain of 12-month-old female 3xTg mice after 3 months of treatment. GFAP and Iba-1 (a microglia marker) expressions, as well as levels of IL-6, TNF-α, and IL-1β, were significantly reduced in the hippocampus and cortex of the mice treated with either 6.7 mg/mL or 20 mg/mL, in parallel exhibiting lower Aβ accumulation, tau hyperphosphorylation, and milder cognitive deficits [85]. These results are supported by findings in nontransgenic mouse AD models. In a study by Qiang et al., male KM mice, pretreated for 2 weeks by intragastric administration of artemisinin B (20, 40 or 80 mg/kg), were injected via the lateral ventricle with $A\beta_{25–35}$ and treated for an additional week post-surgery, resulting in increased levels of anti-inflammatory IL-10 and reduced amounts of pro-inflammatory TNF-α in the cortex and hippocampus, as well suppressing Iba1-positive cell activation in the hippocampal CA1 region [95]. In a more recent study, six-week-old C57 mice, pretreated for one month with intraperitoneal administration of artemisinin at 5 mg/kg/day, were injected with $A\beta_{1–42}$ into the hippocampus. The analysis of the hippocampi at day 7 postsurgery revealed that artemisinin treatment significantly reduced the number of GFAP- and Iba1-positive cells, as well as the release of the inflammatory factors TNF-α, IL-1β and IL-6. Moreover, the protein levels of NF-κB, p65 and Toll-like receptor 4 (TLR4) also decreased, supporting earlier findings that the anti-inflammatory effect of artemisinins may be achieved by suppressing the NF-κB signaling pathway [96]. Further support for the anti-inflammatory effect of artemisinins in AD models was provided by a current publication showing that artesunate (32 mg/kg/day, i.p.) also suppressed the neuroinflammatory response in the hippocampus and cortex of *Picalm*$^{+/-}$; *5XFAD* mice, as indicated by the detection of significantly lower numbers of Iba1-positive microglia (by 28–25%) and GFAP-positive astrocytes (by 23–36%) [76].

In conclusion, several studies convincingly support a strong anti-inflammatory function of different artemisinin derivatives in AD models, which is in agreement with many other works that describe the anti-inflammatory potential of artemisinins in another context [33].

4.4. Oxidative Stress and Mitochondrial Dysfunction

The overproduction of ROS in combination with insufficient antioxidant defense leads to cellular oxidative stress. Markers of oxidative stress, including high levels of oxidatively modified nucleic acids, lipids, and proteins, were found in postmortem brain tissue and biological fluids from patients with preclinical or early stages of AD and ApoE4 (apolipoprotein E epsilon-4) carriers, as well as in animal AD models. Moreover, in AD, the levels of antioxidant enzymes were also altered [97]. Among the multiple factors that can contribute to ROS production in AD brains, such as neuroinflammation and abnormal metal homeostasis (Fe, Cu and Zn), mitochondria are the major source of ROS generation [98]. It is thought that Aβ oligomers trigger a significant influx of Ca^{2+} into the mitochondria, causing membrane depolarization, enhanced ROS production, metabolic dysfunction, and eventually cytochrome C release, initiating apoptosis [99]. The evidence of altered energy and oxygen metabolisms and mitochondrial dysfunction early in AD pathogenesis, before any sign of Aβ or tau pathology, led to the mitochondrial cascade hypothesis proposing that the aggregations of Aβ and tau in AD might be a compensatory response to underlying oxidative stress [100]. Either way, once initiated, a "vicious cycle" may be created in which dysfunction of mitochondria contributes to disease progression directly affecting synaptic activity and neurotransmission, leading to cognitive deficits [101]. Nevertheless, supplementation with antioxidants that target total ROS in the orga-nism (e.g., vitamins E and C and α-lipoic acid) has shown a small modifying effect on AD development in clinical trials. This may rely, at least partially, on the dual role of ROS, implying that in addition to their implication in neurodegeneration, some oxidant species, such as superoxide and hydrogen peroxide ($O_2{}^{2-}$ and H_2O_2) function as signaling molecules of essential redox-dependent signaling pathways [101]. Thus, antioxidants that directly target mitochondria seem to represent a more efficient approach to attenuating local ROS production, and some of these compounds have already led to promising results in clinical trials [102].

A number of different studies indicate that artemisinins alleviate oxidative stress and mitochondrial damage in in vivo and in vitro models of AD. Li et al. reported, in 2019, that artemether attenuated oxidative stress in the brain cortex of 10-month-old 3xTg-AD mice. After artemether treatment at a dose of 20 mg/kg but not at 5 mg/kg, the levels of the lipid peroxidation product MDA (malondialdehyde) and antioxidant enzyme SOD (superoxide dismutase) reversed by approximately 25% in brain extracts of 3xTg-AD mice in comparison to untreated AD mice [82]. Similar findings were reported in a rat model of streptozotocin-induced AD and diabetes after the administration of 50mg/kg artemisinin for 4 weeks [103]. Furthermore, it was demonstrated that artemether stimulated AMPK/GSK3β(Ser9)/Nrf2 signaling, resulting in an increased level of the antioxidant protein heme oxygenase-1 (HO-1), both in vivo and in vitro, in $A\beta_{1–42}$-treated PC12 cell cultures, correlating with a reduction in neuronal cell death [82]. Notably, transcription factor nuclear factor erythroid-2-related factor 2 (Nrf2) is generally activated in cells as an additional mechanism to protect against oxidative stress activating expressions of cytoprotective genes [104]. Additionally, it was shown that pretreatment with 10–100 μM of artemether in PC12 cells diminished also the $A\beta_{1–42}$ induced decline in mitochondrial membrane potential. Similar findings, of reduced ROS levels and restored mitochondrial membrane potential attenuating apoptosis after exposure to $A\beta_{1–42}$ were reported for artemisinin in SH-SY5Y human neuroblastoma cells [73] and for both artemisinin (0.25–1 μM) and artesunate (100 and 200 nM) in BV2 microglial cells [75,96]. Remarkably, artesunate was shown, not only to recover the depolarization of mitochondrial membranes suppressing $A\beta$ induced oxidative stress but also to regulate mitochondrial dynamics in BV-2 and N2a neuronal cells [75].

Coordinated cycles of fission and fusion are essential for maintaining mitochondrial morphology and functions and requires the adequate expression of genes coding proteins such as dynamic-related protein-1 (Drp-1), mitochondrial fission-1 (Fis-1), fusion proteins (Mfn1, Mfn2 and Opa1), that are disturbed by both Aβ and CTFs already in early-stage AD, resulting in mitochondrial fragmentation [105,106]. To maintain mitochondrial homeostasis,

damaged mitochondria regularly undergo mitophagy, involving the engulfment of altered mitochondria by the autophagic vacuoles and their fusion with lysosomes, followed by subsequent degradation and recycling. In both, AD patients and animal models, an age-dependent accumulation of defective mitochondria and impaired mitophagy were coupled with increase in oxidative stress and dysfunctional neurons, whereas mitophagy stimulation improves memory impairments [107,108]. Qin et al. recently demonstrated that artesunate antagonized the effects of Aβ on mitochondria dynamics proteins (Drp-1, Fis-1, Mfn-1 and Opa-1) and reversed the suppression of autophagy and mito-phagy related proteins induced by Aβ in BV-2 and N2a cells as well as in APPswe/PS1dE9 double transgenic mice [75]. Thus, several studies on different models strongly suggest that the artemisinins' neuroprotective effects in AD are mediated in part by their antioxidant activities including reduction in pro-oxidant molecules and increasing production of endogenous antioxidants as well as regulating mitochondrial dynamics and mitophagy. However, the beneficial effects of artemisinins treatment on mitochondrial structure and function seem to be strongly concentration- and context-dependent, since higher concentrations of artesunate (20 μM to 40 μM) were found to inhibit mitochondrial respiration in cancer cells, resulting in oxidative stress and cell damage [109].

4.5. Autophagy

Autophagy is the process by which not only damaged cellular organelles but also protein aggregates and cellular debris are degraded via lysosomes, thus representing an important cellular defense mechanism for maintaining cellular homeostasis. The autophagic process comprises several steps, including sequestration, fusion and degradation, and its dysregulation has been observed in AD patients' brains and animal models [110,111]. The increased numbers of autophagosomes and autolysosomes observed in the brains of patients with AD are probably caused, on the one hand, by the activation of autophagy and, on the other hand, the reduction in degradation by autolysosomes. Specifically, hyperactivation of mTORC1 (mammalian target of rapamycin complex 1) signaling was demonstrated in AD, which may prevent autophagy initiation and autophagosome formation. Consequently, the enhancement of autophagy to remove Aβ, CTFβ and p-tau proteins, preventing cell death, may be a promising therapeutic strategy, especially in the early stages of AD [111,112]. In this context, a study by Zhao et al. has convincingly demonstrated that DHA, the active metabolite of artemisinins corrected autophagy dysfunction in the initial stage of Aβ pathology in APPswe/PSEN1dE9 mice and in cell models of AD (N2a-APP and SH-SY5Y-APP) by acting on multiple targets within the autophagic process [99]. Transmission electron microscopy and measurements of autophagy stage-specific proteins have evidenced that DHA treatment not only activates autophagy via the upregulation of ATG5, ATG12, ATG16L and LC3 II/I and decrease in ubiquitin-binding p62 protein levels, but it also promoted the fusion of autophagosomes and lysosomes (increases in Beclin1, ATG14, Rab7 and RILP levels) and, thus, elevated the number of lysosomes and their degradation function. Moreover, their findings indicated that DHA can activate autophagy by suppressing the mTOR/ ULK1 (unc-51-like kinase) junction within the autophagy-regulating signaling network [113].

4.6. Cell Death

Neuronal loss is one of the main features of AD, but it is difficult to detect in real time because of the limited accessibility of dying cells by immunohistochemical methods [114]. Loss of neurons in AD begins in the preclinical stage of the disease and progresses during MCI and dementia, correlating well with the degree of cognitive deficits. Multiple sources of evidence indicate that different forms of cell death can occur in AD, including apoptosis, necroptosis, pyroptosis, autophagic cell death, ferroptosis and necrosis in different stages of the disease [114]. However, it is not yet clear which pathway is dominant in the different stages of the disease and/or whether there is a combinatorial effect among coactivated death pathways [115].

The features of apoptosis, a type of regulated cell death, include cytoplasmic shrinkage, blebbing of the plasma membrane, nuclear condensation and fragmentation, and the formation of apoptotic bodies can be observed in neurons incubated with Aβ peptide and AD brain tissue [114]. Apoptosis can be triggered by two distinct pathways: the intrinsic (also called the mitochondrial or Bcl-2-regulated) pathway and the extrinsic (also called the death receptor) pathway, with the latter precipitated by the binding of extracellular death ligands, such as TNF-α, FasL, and TRAIL (tumor necrosis factor (TNF)-related apoptosis-inducing ligand), to transmembrane death receptors. In the intrinsic pathway, mitochondrial membrane depolarization, as a result of cellular injury, such as DNA damage, metabolic stress, and ROS, leads to the release of cytochrome C from the mitochondria, resulting in the activation of effector caspases and apoptotic death. Proteolytic enzymes, known as caspases, are involved in both pathways. Moreover, the family of B-cell lymphoma-2 (Bcl-2) proteins, including pro-apoptotic and anti-apoptotic members, were identified as essential integrators of signals that trigger cell survival or apoptosis [116]. TUNEL staining, the in situ labeling technique for apoptotic cell detection, and the levels of caspase 3, the main executive caspase functioning in multiple apoptotic signaling pathways, have been reported as elevated in cortical and hippocampal neurons from AD patients. In addition, the expressions of several pro- and anti-apoptotic members of the Bcl-2 family, such as Bcl-2, Bcl-xl, Bax, and Bak, are altered in AD brain extracts, including humans and mouse models [114].

The effects of artemisinins on apoptotic cell death were studied in different models of AD, and the results indicated clearly anti-apoptotic properties of artemisinins. Li et al. reported, in 2019, a reduced number of TUNEL-positive apoptotic neurons in the brain cortex of 10-month-old 3xTg-AD mice following treatment with 5 mg/kg or 20 mg/kg of artemether and in different $A\beta_{1–42}$-exposed neuronal cell cultures (PC12, SH-SY5Y, mice primary cortical neurons) pretreated with artemether (10–100 μM), concomitant with decreased caspase 3 activity. Moreover, the expression of the anti-apoptotic protein Bcl-2 increased, whereas the pro-apoptotic protein Bax decreased in brain homogenates of treated 3xTg AD mice. These authors linked the inhibition of brain cortical apoptosis and attenuation of cognitive deficits in the 3xTg mice model to AMPK/GSK3β(Ser9)/Nrf2 activation and consecutively increased antioxidant effects of artemether [82]. In addition, Zhao et al. observed, in parallel with attenuated histopathological changes, a reduction in the number of apoptotic cortical neurons in 12-month-old 3xTg-AD mice after one month of treatment with artemisinin (1, 5 or 10 mg/kg). Cytochrome C, caspase 9 and caspase 3 activities decreased, as the ratio of Bcl-2/Bax increased in response to the artemisinin treatment, both in the 3xTg mice and the $A\beta_{1–42}$-induced SH-SY5Y cells (12.5 μM). The rise in the expression levels of p-ERK1/2 and p-CREB detected both in vivo and in vitro suggested that artemisinin reduced brain neuronal apoptosis through the ERK/p-CREB/Bcl-2 axis [117]. These results are in concordance with a much earlier in vitro study describing the protective effect of 25 μM artemisinin against $A\beta_{25–35}$-induced cell death in neuronal PC12 cells through activation of the ERK1/2 pathway [118]. Moreover, it was shown that artemisinin (5 mg/kg/day) reduced apoptotic cell death in the cerebral cortex of C57 mice after intrahippocampal injection with $A\beta_{1–42}$. Additionally, these authors found that artemisinin-pretreated microglia medium reduced PC12 cell apoptosis and increased PC12 cell viability, demonstrating that artemisinin protects against neuronal cell apoptosis by improving the inflammatory environment [96]. Accordingly, in cocultures of Aβ-pretreated microglial BV-2 and neuronal N2a cells, when BV2 cells were pretreated with both Aβ and artesunate they failed to induce apoptosis of N2a cells [75]. Consistently, DHA (20 mg/kg/day), the active metabolite of all artemisinin compounds, rescued neuronal loss in the hippocampal CA1 area of 9-month-old APPswe/PSEN1dE9 mice and downregulated the protein expression levels of full-length caspase 3, cleaved caspase 3 and Bax while also increasing the level of the anti-apoptotic Bcl-2 protein. Concurrently, DHA corrected the abnormal levels of brain-derived neurotrophic factor (BDNF) [117]. More recently, an artemisia extract was reported to rescue neuronal cell apoptosis in 9-month-old

3xTg AD mice accompanied by changes in the expressions of different apoptosis regulators. In addition to the emodulation of Bax, Bcl-2 and cleaved caspase 3 levels, artemisinin extract treatment activated YAP/TEAD2/Survivin signaling, promoting a significant increase in anti-apoptotic Survivin protein levels, while significantly reducing the level of pro-apoptotic promyelocytic leukemia protein [85]. YAP (Yes-associated protein) is a transcriptional cofactor that regulates cell death and survival by binding to different transcription factors such as p73 and TEAD (TEA-domain family member) and seems to be a key player in the molecular network of AD [119]. Since a YAP-mediated increase in the TEAD activity has been implicated in cell proliferation, differentiation, and survival, reduced TEAD activity is thought to primarily promote necrotic cell death [120]. Interestingly, recent findings on MCI vs. AD patients and early- vs. late-stage 5xFAD mice strongly support that intracellular Aβ-triggered Hippo/YAP pathway-dependent necrosis occurs from the very early presymptomatic to late stages in both human and mouse AD pathologies. Moreover, residual Aβ after neuronal necrosis seems to be the seed for the formation of extracellular beta-amyloid plaques. Thus, early-stage interventions for molecules involved in the regulation of Hippo pathway-dependent apoptosis and necrosis could suppress progression of late-stage AD pathological changes, possibly including the limitation of extracellular Aβ aggregation [120].

Traditionally, necrosis is considered an unregulated form of cell death characterized by cell and organelle swelling, loss of membrane integrity and release of intracellular contents into the extracellular environment, usually triggering an inflammatory response. A main ultrastructural feature of intracellular Aβ-induced YAP-deprivation-mediated Hippo pathway-dependent necrosis is endoplasmic reticulum (ER) ballooning [121]. In a recent study, Zhao et al. reported that TEM analysis of neurons in brain sections of DHA-treated APPswe/PSEN1dE9 mice showed significantly reduced swelling of the ER [118]. Other forms of cell death acting in different stages of AD pathogenesis might also represents targets of artemisinins. Necroptosis, the regulated form of necrosis, exhibits the morphological features of necrosis but is associated with the activation of the RIP kinase cascade and the formation of the necrosome, and it can be induced by the stimulation of TNFR1, TLRs and certain other receptors [122]. Necroptosis has been primarily implicated in neuronal loss in the later stages of AD when they are exposed to amyloid plaques and tau tangles, possibly involving TNF-α inflammatory pathway signaling [123,124]. Pyro-ptosis is another form of necrotic programmed cell death involving the activation of caspase-1 by inflammasomes and the release of various inflammatory cytokines such as IL-1β and IL-18. The occurrence of pyroptosis (accompanied by inflammasome activation and elevated levels of IL-1β and IL-18) has been documented for many neurodegenerative diseases, including AD [125]. Ferroptosis refers to a form of iron-dependent necrotic programmed cell death that involves the accumulation of ROS and lipid peroxidation products and the depletion of reduced glutathione, caused by an imbalance in cellular redox homeostasis [126]. The specific role of ferroptosis in an AD setting is difficult to establish because of the overall presence of lipid peroxidation, altered iron homoeostasis and reduced glutathione in neurodegeneration; however, ferroptosis inhibitors manifested protection in animal models of AD and in clinical trials [127].

Altogether, a handful of different in vivo and in vitro data convincingly demonstrate that artemisinins protect directly against Aβ-dependent apoptotic neuronal cell death by regulating the expression of pro- and anti-apoptotic proteins and the activity of molecules involved in multiple intersecting pathways related to cell survival and cell death. In addition, the improved mitochondrial function and energy metabolism and diminished oxidative stress, as well as reduced neuroinflammation, by artemisinins, as outlined above, can presumably protect indirectly against apoptosis, necrosis and different forms of programmed necrotic cell death. Autophagy activation and autophagy flux correction can also play important roles in maintaining cell viability in the AD brain via artemisinins.

It is notable that in another context the cellular response to exposure to artemisinin and its derivatives include oxidative stress, DNA damage and repair, and induction of

various modes of cell death [128]. Interestingly, artesunate was used as a ferroptosis inducer to selectively promote ROS- and lysosomal-iron-dependent cell death in KRAS-transformed PDAC cells, a cancer of the exocrine pancreas, while it exerted no effect on nonneoplastic human pancreatic ductal epithelial cells, further underscoring the multifaceted intervention potential of artemisinins [129].

4.7. Synapse Pathology

Both the direct effects of Aβ and tau on synaptic integrity and the indirect effects, through processes such as inflammation and mitochondrial dyshomeostasis, are likely to drive synaptic dysfunction and loss in AD [130,131]. Synapse dysfunction is thought to start long before the loss of memory and accelerate as the disease progress. There are widespread changes in synapse number, size, shape and structure of synaptic protein expression in AD brains, all suggestive of synaptic dysfunction that, predictably, will lead to changes in network oscillations [132,133]. There is evidence of a disrupted balance between excitatory and inhibitory neuronal activities (E/I imbalance) early before the onset of clinical symptoms, both in AD patients and animal models, and is seen as a main driver of AD pathogenesis promoting cognitive deficits [134,135]. It is well established that changes in excitatory synaptic transmission contribute to the E/I imbalance and AD progression due to aberrant activation of glutamate receptors, resulting in glutamatergic and cholinergic neuronal hyperexcitability and degeneration. Meanwhile, there is significant evidence suggesting that disruption to the inhibitory GABAergic synaptic transmission is also important and occurs early in the disease process [10,135–138]. Preclinical and clinical studies support that modulation of the GABAergic system may improve E/I imbalance and AD pathology, proposing it as a target for AD therapy [139].

In this context, it is interesting to note that several studies reported a significant impact of artemisinins on different components of the GABAergic system. In pancreatic islet cells, artemisinins were reported to increase GABAergic signaling resulting in elevated insulin secretion [140]. In contrast, studies using cultured spinal cord and hippocampal neurons described a decrease in glycinergic signaling and reductions in gephyrin and $GABA_AR$ coclustering [141]. These effects were found to be dependent on gephyrin, the main scaffold protein of inhibitory synapses, identified as a direct target of artemisinins. In particular, it was demonstrated that artemisinins bind competitively to the GlyRβ and $GABA_A$ receptor-anchoring pockets of gephyrin. Moreover, in an additional study, it was shown that artemisinins bind to and inhibit the enzyme pyridoxal kinase, synthesizing pyridoxal 5-phosphate, an essential cofactor of glutamic acid decarboxylase (GAD) involved in the synthesis of GABA, with the therapy, thus, resulting in reduced inhibitory neurotransmission in vitro [142]. In comparison to these nonamyloidogenic in vitro experiments, in our own in vivo studies, artemisinin and artesunate, at two different doses (10 mg/kg and 100 mg/kg), rescued the expression levels of key proteins of inhibitory synapses, such as gephyrin and $GABA_AR$-γ2, to approximately WT levels in the hippocampus of 12-month-old APP/PS1 ($APP_{Sw}PSEN1_{L166P}$), whereas in untreated APP/PS1 mice a robust reduction in synaptic protein levels and the number of synapses were detected [77,136]. Moreover, artemisinin, at a lower dose (10 mg/kg), was found to increase gephyrin protein levels, as well as the phosphorylation of gephyrin at serine 270 already in a preplaque stage of the disease (3 months old), suggesting a more direct effect of artemisinin on gephyrin expression than a downstream effect of an ameliorated Aβ-dependent pathology [143]. Since CDK5-dependent phosphorylation at Ser270 may result in higher gephyrin and $GABA_AR$-γ2 receptor densities at postsynaptic membrane specializations, this finding also indicates a supporting function of low-dose artemisinin treatment on inhibitory synapse structure. In a more resent study, we reported the modulation of the glycinergic inhibitory system after artesunate treatment in APP/PS1 mice. Analy-zing the glycine receptor (GlyR) α1, α2 and α3 subunit distribution in hAPPswe-expressing cultured hippocampal neurons and brain slices of 12-month-old APP/PS1 mice, we demonstrated that artesunate (10 mg/kg) can rescue the, probably, Aβ-induced loss of extrasynaptic GlyR α3 clusters

both in vitro and in vivo, which are thought to play a role in tonic inhibition, an important mechanism in controlling neuronal excitability [144]. Altogether, these few studies indicate that artemisinins can maintain or restore inhibitory synapse protein expression levels in animal models of AD, very likely involving a direct influence on gene expression rather than indirect effects through modulation of other pathogenic mechanisms involved in AD, such as amyloid pathology or reduced cell death. Moreover, fewer data are available concerning the effects of artemisinins on excitatory synapses. Zhou et al. reported that Artemisia annua extract (6.7 mg/mL and 20 mg/mL) elevated the expression levels of synaptophysin, a protein found in presynaptic terminals, and PSD95, a key postsynaptic protein of excitatory synapses, above wild-type levels in the brains of 9-month-old 3xTg AD mice [85]. In our own studies, a significant increase in the PSD95 mRNA level was measured in APP/PS1 mice brains upon treatment with 100 mg/kg artesunate compared to the control APP/PS1 mice [77]. The maintenance of synapses after other artemisinins was also reported; in 9-month-old APPswe/PSEN1dE9 mice, DHA (20 mg/kg/day) upregulated the level of synaptophysin in brain homogenates and promoted neurite outgrowth [117], and in mice injected with $A\beta_{25–35}$ into the lateral ventricle, artemisinin B inhibited synaptophysin loss in the neurons of the hippocampal CA1 region [95].

Taken together, a limited number of studies have so far demonstrated that the reduced expression levels of proteins from both excitatory and inhibitory synapses in different AD models are restored upon treatment with artemisinin compounds. In support of this, in a streptozotocin-induced AD–diabetes rat model [145] and in a mouse model overexpressing human tau (hTau) in the hippocampus, improved synaptic plasticity indicated by increased long-term potentiation (LTP) was reported after artemisinin and DHA treatment, respectively, with improved learning and memory tests. Interestingly, the latter study suggested, as an underlying mechanism for this finding, a DHA-induced modulation of the crosstalk between O-GlcNAcylation and the phosphorylation of tau [146].

4.8. Neurogenesis

Adult neurogenesis, comprising the proliferation of progenitor cells derived from neural stem cells upon asymmetric division and their subsequent migration, differentiation into neurons or glia cells and maturation, contributes to the homeostasis of the central nervous system. Cell morphology, expression of transcription factors and a set of marker proteins allow for distinguishing the different stages occurring during the transition from stem cell to mature neuron [147]. The evidence supports a deregulated adult neurogenesis in Alzheimer's disease associated with learning and memory deficits. It seems to be an early event in Alzheimer's disease pathogenesis, mediated by intracellular Aβ oligomers [148]. A progressive decline in neurogenesis in AD brains was detected and correlated with disease progression [149], since interventions that promote neurogenesis have been found to alleviate disease symptoms [150,151]. Therefore, it is important to point out a recent study that reported improved neurogenesis in 12-month-old 3xTg AD mice after 3 months of treatment with an extract of Artemisia annua (6.7 mg/mL and 20 mg/mL) containing artemisinin acid, arteether and deoxyartemisinin, correlating with ameliorated cognitive deficits. Specifically, the proliferation and survival of neuronal progenitor cells were promoted. as indicated by significantly increased numbers of $Sox2^+$ and $Brdu^+$ cells in the hippocampus and cortex of the treated mice [85].

4.9. Blood–Brain Barrier

The blood–brain barrier (BBB) is composed of endothelial cells sealed by tight junctions, pericytes and astrocytes, and it is crucial for Aβ homeostasis including clearance dynamics. Structural and functional alterations in the BBB, specifically its endothelial cells, are part of the early pathology of AD brains [152]. The BBB controls the entry of Aβ from plasma into the brain via the receptor for advanced glycation end products (RAGE), whereas the low-density lipoprotein receptor-related protein (LRP1) promotes the removal of brain-derived Aβ. The expressions of both receptors were found to be altered in AD [152,153].

Interestingly, despite suppressed NF-κB-mediated inflammatory signaling and decreased neuritic plaque burden, Shi et al. could not detect significant changes in peripheral blood $A\beta_{42}$ concentration and expression levels of LRP1 and RAGE in brains with relative early pathology in 6-month-old APPswe/PS1dE9 mice after a 30-day treatment with artemisinin (40 mg/kg/day) [72]. In contrast, very recently, Kisler et al. reported that early artesunate (32 mg/kg/day) treatment for 2 months increased blood serum $A\beta_{42}$ and $A\beta_{40}$ levels by approximately two-fold, suggesting the accelerated clearance of Aβ from brain-to-blood in 5-month-old 5XFAD mice that correlated with a reduced Aβ pathology and improved behavioral performance in cognition tests [76]. In this study, it was demonstrated that artesunate specifically increased endothelial PICALM (phosphatidylinositol-binding clathrin assembly protein) levels, a protein that interacts with LRP1 and is involved in internalization of cell surface receptors, as well as in intracellular trafficking of different proteins [154]. It is noteworthy that a 60% reduction in PICALM endothelial levels was measured in human AD brains, correlating inversely with the Aβ load, Braak stage, and clinical dementia, leading to the proposal of a change in the endothelial PICALM level as a significant susceptibility factor for late-onset AD [154].

4.10. Memory and Cognition

Qiang et al. reported, in 2018, that artemisinin B parallelly reduced neuroinflammation and significantly improved learning and memory abilities of dementia mice in the Morris water maze (MWM) test, including navigation and space exploration experiments, as well as the step-through test, which analyzes the characteristics of mice that prefer dark places and avoid light [95]. In the same study, the open field test, broadly used to evaluate spontaneous activity and exploratory behavior in mice, showed that the drug had no obvious excitatory or inhibitory effects on the mental state and activity of mice. Shortly thereafter, Li et al. reported results of Morris water maze tests in 10-month-old 3xTg AD mice after artemether therapy. Since untreated 3xTg-AD mice showed significant impairment in learning tasks compared to the wild-type mice, with longer times needed to find the hidden platform, artemether treatment, both at 5 and 20 mg/kg/day doses, significantly shortened the swimming distance of 3xTg-AD mice and decreased the escape latency in comparison to untreated 3xTg AD mice [82]. Thus, artemether treatment rescued spatial learning and reference memory deficits in the 3xTg AD mouse model. These findings were later corroborated by several other studies in different mouse and rat AD models and for various artemisinin compounds. Our literature research identified altogether twelve publications reporting beneficial effects of artemisinins on memory and cognition in AD models that are summarized in Table 1. Most of these studies tested learning and memory abilities using the MWM test, the classic behavioral experiment studying primarily long-term memory, which is affected more in later stages of the disease [155]. In one very recent study, the behavioral performances of 5-month-old 5xFAD mice was evaluated using novel object location, recognition, nesting, and burrowing tests that were improved by artesunate and was correlated with increased expression of a key protein involved in regulating the trans-endothelial transport and clearance of Aβ (PICALM) in brain capillaries [66]. Altogether, these studies provide evidence that the positive modulation of various pathogenic components of AD by artemisinins in rodent models is translated into improvements in memory and cognitive deficits.

Table 1. Summary of the studies and their main findings from testing different artemisinins in in vivo and in vitro AD models. Doses, route and period of administration, as well as the start of therapy applied in animal models or concentrations used in cell culture experiments, are included. The minimal doses or concentrations to achieve a significant improvement are also shown. Changes induced by the therapy in the given hallmarks of AD are indicated by ↓ (decrease) or ↑ (increase). The arrows in the first row illustrate the changes that occur under AD conditions in comparison to healthy conditions. Key molecular pathways or protein expression alterations are indicated by (+) (increase) or (−) decrease. i.p.—Intra-peritoneally; i.g.—intragastric; p.o.—per oral.

Aβ	pTau	Inflammation	ROS	Autophagy	Cell Death	Synapse Proteins	Neurogenesis	BBB	Memory Cognition	Substance	Dose/Day, Route and Duration of Administration/ Concentration	Lowest Efficient Dose/ Concentration	Molecular Mechanisms	System/Start of Therapy	References
↑	↑	↑	↑	↓	↑	↓	↓	↓	↓	-	-	-	-	-	-
↓		↓								Artemisinin	40 mg/kg, i.p., 30 days	40 mg/kg	NF-κB, IL-6, TNF-α NALP3 BACE1	(−) (−) (−)	APPswe/PS1dE9 mice, 4-month-old	Shi et al., (2013) [72]
			↓		↓					Artemisinin	3.1–100 μM	1.5 μM	ERK1/2 pathway Caspase-3 and -7	(+) (−)	PC12 cells + $A\beta_{25-35}$	Zeng et al., (2017) [118]
		↓				↑			↑	Artemisinin B	20-, 40-, and 80 mg/kg, i.g., 1–2 weeks 1–8 μM	20 mg/kg 1 μM	TLR4, MyD88, NF-κB IL-1β, IL-6, TNF-α	(−) (−)	KM mice- intra-ventricular $A\beta_{25-35}$ start:immediately after surgery BV2 cells	Qiang et al., (2018) [95]
↓	↓		↓		↓				↑	Artemether	5- and 20 mg/kg, i.p., 4 weeks, 3–100 μM	5 mg/kg 10 μM	AMPK/GSK3β/Nrf2 Bcl-2 Bax	(+) (+) (−)	3xTg mice, 8-month-old PC12 and SH-SY5Y, primary cortical neurons	Li et al., (2019) [82]
↓	↓	↓	↓		↓				↑	Artemisinin	1-, 5- and 10 mg/kg, i.p., 30 days 3.125–100 μM	1 mg/kg, 6.25 μM	ERK/CREB pathway Cytochrome C Caspase-3 and -9 Bcl-2/Bax	(+) (−) (−) (+)	3xTg mice, 11-month-old SH-SY5Y cells	Zhao et al., (2020) [84]
↓				↑					↑	Dihydro-artemisinin	20 mg/kg, p.o., 90 days	20 mg/kg	BACE1 mTOR/ ULK1	(−) (+)	APPswe/PSEN1dE9, 6-month-old N2a-APP and SH-SY5Y-APP cells	Zhao et al., (2020) [73]
					↓	↑				Dihydro artemisinin	20 mg/kg. p.o., 90 days	20 mg/kg	Caspase-3, Bax. Bcl-2	(−) (+)	APPswe/PSEN1dE9, 6-month-old	Zhao et al., (2020) [117]
↓						↑				Artemisinin, Artesunate	10- and 100 mg/kg, p.o., 3 months 0.05, 0.125, 0.25 μM	10 mg/kg 0.05 μM	CTFs	(−)	$APP_{swe}/PS1_{L166P}$, 9-month-old Hippocampal neurons	Kiss et al., (2021) [77]
						↑				Artemisinin	10- and 100 mg/kg, p.o., 6 weeks	10 mg/kg	Gephyrin phosphorylation	(+)	$APP_{swe}/PS1_{L166P}$, 6-week-old	Kiss et al., (2021) [143]
↓		↓	↓							Artemisinin	50 mg/kg, i.p., 4 weeks	50 mg/kg	ROS, TNF-α Blood glucose	(−) (−)	Streptozotocin-induced AD and diabetes in rats	Poorgholam et al., (2021) [103]
↓	↓								↑	Artemether	n.n.	n.n.	BACE1, mTOR	(−)	$A\beta_{25-35}$-treated rats N2a cells	Li et al., (2021) [83]
↓		↓	↓	↑	↓				↑	Artesunate	5- and 10 mg/kg, p.p., 6 months 0.01, 0.05, 0.1, 0.2, 0.5, 1.0 μM	5 mg/kg 0.1 μM	TNFα, IL-6, IL-1β PINK1. Parkin	(−) (+) (+)	APPswe/PS1, 2-month-old BV-2-, N2a cells	Qin et al., (2022) [75]

Table 1. *Cont.*

Aβ	pTau	Inflammation	ROS	Autophagy	Cell Death	Synapse Proteins	Neurogenesis	BBB	Memory Cognition	Substance	Dose/Day, Route and Duration of Administration/ Concentration	Lowest Efficient Dose/ Concentration	Molecular Mechanisms		System/Start of Therapy	References
		↓	↓		↓				↑	Artemisinin	5 mg/kg, i.p., 4 weeks 0.25, 0.5, 1.0 μM	5 mg/kg 0.25 μM	TLR4/NF-κB TNF-α, IL-1β, IL-6	(−) (−)	C57 mice injected with $A\beta_{1-42}$ into the hippocampus, start:4 weeks pre BV2 Cells	Zhao et al., (2022) [96]
↓	↓								↑	Dihydro-artemisinin	50- and 300 mg/kg, p.o., 4/6 months	50 mg/kg	-		APPswePSEN1dE9/Nju, 3-month-old	Xiao et al., (2022) [74]
↓		↓						↑	↑	Artesunate	32 mg/kg, i.p., 2 months, 3 μM	EC_{50}: 2.1 μM	Brain capillary PICALM	(+)	5XFAD mice, 3-month-old HEK293t luciferase reporter line	Kisler et al., (2023) [76]
						↑				Artesunate	10- and 100 mg/kg, p.o., 1.5/3 months	10 mg/kg	-		APP_{swe} /$PS1_{L166P}$, 1.5-/ 9-month- old	Kuhse et al., (2023) [144]
						↑			↑	Artemisinin	50 mg/kg, i.p., 4 weeks,	50 mg/kg;	Blood glucose	(−)	Streptozotocin-induced AD and diabetes in rats, 4-month-old	Poorgholam et al., (2023) [145]
↓	↓	↓	↓		↓	↑	↑		↑	Artemisia annua extract	6.7- and 20 mg/mL, p.o., 3 months 1–10,000 μg/mL	6.7 mg/mL 30 μg/mL	IL-6, TNF-α, IL1β Hippo/YAP signaling Bax Bcl-2	(−) (+) (−) (+)	3xTg mice, 9-month-old SH-SY5Y, primary neurons PC12 cells	Zhou et al., (2023) [85]

5. Artemisinins Toxicity

Artemisinin compounds have been in clinical use for more than two decades, and several clinical studies support their high safety and efficacy during the treatment of malaria. The most commonly reported adverse reactions in malaria patients are gastrointestinal nature, including nausea, vomiting, diarrhea, and transient transaminase elevation [156,157]. However, animal and in vitro studies have shown that high doses of artemisinins can be neurotoxic [158,159]. One explanation might be that since human subjects were administered doses of 2–8 mg/kg body weight per day for 3–5 days, most studied animals have been exposed to much higher doses for longer periods of time. The dose causing neurotoxicity or death in 50% of adult mice (Swiss albino) was approximately 300 mg/kg/day for oral artemether and artesunate in comparison to 50 mg/kg/day of intramuscular artemether, both administered for 28 days [158]. In this context, it should be emphasized that APPswePSEN1dE9/Nju mice after oral DHA treatment for 6 months at relatively high doses of 50 and even 300 mg/kg/day exhibited improved behavior in the MWM and open field tests compared to untreated AD mice. Furthermore, in this study, no toxic effects of the DHA treatment were detected on the liver, as evidenced by the unchanged aspartate transferase and alanine aminotransferase levels and on the kidneys, and blood lipid levels were evenly suppressed [74]. In comparison, artesunate at 40 mg/kg administered as a single dose or at 13.4 mg/kg/day given for 3 days at 24 h intervals (i.v.) was found to exert toxic effects on spermatozoa at the morphological and molecular levels in Swiss albino mice, probably involving oxidative mechanisms [160]. Moreover, another study demonstrated that the treatment of zebrafish with artesunate at high doses resulted in acute cardiotoxicity, whereas a low-dose treatment exerted cardioprotective effects [161]. Altogether a biphasic dose-dependent response generated by artemisinins seems to emerge, characterized by beneficial effects at low doses and inhibitory or toxic effects on cellular processes at high doses. However, even this hormetic behavior is strongly context dependent.

Thus, one can conclude, that the bioactivities of artemisinins depend on multiple factors, including dosage, time, drug delivery routes, target cell or tissue types and, probably, from compound chemical characteristics and even species differences [162]. Further, preclinical and clinical studies on pharmacokinetics, long term effect/toxicity and drug–drug interactions are required to understand the reasons for the discrepancies in artemisinin-compounds effects and eventually find the optimal dose in humans with AD that can be administered for long term without toxic effects.

6. Conclusions and Future Directions

A relatively large number of well-conducted studies indicate the beneficial effects of artemisinins in preclinical settings of AD, evidencing improvements in pathological hallmarks and pointing to multiple pathogenetic targets within disease development, whose modulation, ultimately, resulted in improved cognitive functions. Different doses of artemisinin and its derivative were tested and found to be effective in the same or different models of AD, which altogether strengthens their therapeutic potential as multitarget drug candidates for a complex disease such as AD. At the same time, the lack of concerted validations of doses and specific efficacies for any artemisinin compound, as well as comparisons of their relative potencies in different animal models, make a direct translation into clinical trials difficult. However, the very context-dependent activity of artemisinins strongly suggests that questions concerning dosing regimens, safety over long-term use, and possible interactions with existing medications, as well as toxicities that could eventually occur linked to treatment in AD patients can be answered appropriately only by well conducted clinical trials.

Author Contributions: E.K. and J.K. (Jochen Kuhse) conceptualized, designed and wrote the primary draft of the manuscript. S.K., K.G., K.H.V.S. and J.K. (Joachim Kirsch) edited and revised the final version manuscript. All authors have read and agreed to the published version of the manuscript.

Funding: This work was supported by a grant from the Romanian Ministry of Research and Innovation (CNCS-UEFISCDI) (PN-III-P4-PCE-2021-1089).

Conflicts of Interest: The authors declare no conflict of interest.

References

1. Selkoe, D.J.; Hardy, J. The amyloid hypothesis of Alzheimer's disease at 25 years. *EMBO Mol. Med.* **2016**, *8*, 595–608. [CrossRef] [PubMed]
2. Terry, R.D.; Masliah, E.; Salmon, D.P.; Butters, N.; DeTeresa, R.; Hill, R.; Hansen, L.A.; Katzman, R. Physical basis of cognitive alterations in Alzheimer's disease: Synapse loss is the major correlate of cognitive impairment. *Ann. Neurol.* **1991**, *30*, 572–580. [CrossRef] [PubMed]
3. DeKosky, S.T.; Scheff, S.W.; Styren, S.D. Structural correlates of cognition in dementia: Quantification and assessment of synapse change. *Neurodegeneration* **1996**, *5*, 417–421. [CrossRef] [PubMed]
4. Mecca, A.P.; O'Dell, R.S.; Sharp, E.S.; Banks, E.R.; Bartlett, H.H.; Zhao, W.; Lipior, S.; Diepenbrock, N.G.; Chen, M.K.; Naganawa, M.; et al. Synaptic density and cognitive performance in Alzheimer's disease: A PET imaging study with [^{11}C]UCB-J. *Alzheimers Dement.* **2022**, *18*, 2527–2536. [CrossRef] [PubMed]
5. Bekris, L.M.; Yu, C.E.; Bird, T.D.; Tsuang, D.W. Genetics of Alzheimer disease. *J. Geriatr. Psychiatry Neurol.* **2010**, *23*, 213–227. [CrossRef] [PubMed]
6. Hardy, J. The discovery of Alzheimer-causing mutations in the APP gene and the formulation of the "amyloid cascade hypothesis". *FEBS J.* **2017**, *284*, 1040–1044. [CrossRef] [PubMed]
7. Kepp, K.P.; Robakis, N.K.; Høilund-Carlsen, P.F.; Sensi, S.L.; Vissel, B. The amyloid cascade hypothesis: An updated critical review. *Brain* **2023**, *146*, 3969–3990. [CrossRef]
8. Zhang, Y.; Chen, H.; Li, R.; Sterling, K.; Song, W. Amyloid β-based therapy for Alzheimer's disease: Challenges, successes and future. *Sig. Transduct. Target. Ther.* **2023**, *8*, 248. [CrossRef]
9. Knopman, D.S.; Amieva, H.; Petersen, R.C.; Chételat, G.; Holtzman, D.M.; Hyman, B.T.; Nixon, R.A.; Jones, D.T. Alzheimer disease. *Nat. Rev. Dis. Primers* **2021**, *7*, 33. [CrossRef]
10. Zott, B.; Busche, M.A.; Sperling, R.A.; Konnerth, A. What Happens with the Circuit in Alzheimer's Disease in Mice and Humans? *Annu. Rev. Neurosci.* **2018**, *41*, 277–297. [CrossRef]
11. De Strooper, B.; Karran, E. The Cellular Phase of Alzheimer's Disease. *Cell* **2016**, *164*, 603–615. [CrossRef] [PubMed]
12. Chang, K.A.; Suh, Y.H. Pathophysiological roles of amyloidogenic carboxy-terminal fragments of the beta-amyloid precursor protein in Alzheimer's disease. *J. Pharmacol. Sci.* **2005**, *97*, 461–471. [CrossRef]
13. Xu, Y.; Kim, H.S.; Joo, Y.; Choi, Y.; Chang, K.A.; Park, C.H.; Shin, K.Y.; Kim, S.; Cheon, Y.H.; Baik, T.K.; et al. Intracellular domains of amyloid precursor-like protein 2 interact with CP2 transcription factor in the nucleus and induce glycogen synthase kinase-3beta expression. *Cell Death Differ.* **2007**, *14*, 79–91. [CrossRef] [PubMed]
14. Vaillant-Beuchot, L.; Mary, A.; Pardossi-Piquard, R.; Bourgeois, A.; Lauritzen, I.; Eysert, F.; Kinoshita, P.F.; Cazareth, J.; Badot, C.; Fragaki, K.; et al. Accumulation of amyloid precursor protein C-terminal fragments triggers mitochondrial structure, function, and mitophagy defects in Alzheimer's disease models and human brains. *Acta Neuropathol.* **2021**, *141*, 39–65. [CrossRef] [PubMed]
15. van der Kant, R.; Goldstein, L.S. Cellular functions of the amyloid precursor protein from development to dementia. *Dev. Cell* **2015**, *32*, 502–515. [CrossRef] [PubMed]
16. Müller, U.C.; Deller, T.; Korte, M. Not just amyloid: Physiological functions of the amyloid precursor protein family. *Nat. Rev. Neurosci* **2017**, *18*, 281–298. [CrossRef] [PubMed]
17. Goodman, Y.; Mattson, M.P. Secreted forms of beta-amyloid precursor protein protect hippocampal neurons against amyloid beta-peptide-induced oxidative injury. *Exp. Neurol.* **1994**, *128*, 1–12. [CrossRef] [PubMed]
18. Richter, M.C.; Ludewig, S.; Winschel, A.; Abel, T.; Bold, C.; Salzburger, L.R.; Klein, S.; Han, K.; Weyer, S.W.; Fritz, A.K.; et al. Distinct in vivo roles of secreted APP ectodomain variants APPsα and APPsβ in regulation of spine density, synaptic plasticity, and cognition. *EMBO J.* **2018**, *37*, e98335. [CrossRef] [PubMed]
19. Puzzo, D.; Privitera, L.; Palmeri, A. Hormetic effect of amyloid-β peptide in synaptic plasticity and memory. *Neurobiol. Aging* **2012**, *33*, 1484.e15–1484.e24. [CrossRef]
20. Coronel, R.; Palmer, C.; Bernabeu-Zornoza, A.; Monteagudo, M.; Rosca, A.; Zambrano, A.; Liste, I. Physiological effects of amyloid precursor protein and its derivatives on neural stem cell biology and signaling pathways involved. *Neural Regen. Res.* **2019**, *14*, 1661–1671.
21. Zimbone, S.; Monaco, I.; Gianì, F.; Pandini, G.; Copani, A.G.; Giuffrida, M.L.; Rizzarelli, E. Amyloid Beta monomers regulate cyclic adenosine monophosphate response element binding protein functions by activating type-1 insulin-like growth factor receptors in neuronal cells. *Aging Cell* **2018**, *17*, e12684. [CrossRef] [PubMed]
22. Atwood, C.S.; Bishop, G.M.; Perry, G.; Smith, M.A. Amyloid-beta: A vascular sealant that protects against hemorrhage? *J. Neurosci. Res.* **2002**, *70*, 356. [CrossRef]
23. Chen, J.; Chen, J.S.; Li, S.; Zhang, F.; Deng, J.; Zeng, L.H.; Tan, J. Amyloid Precursor Protein: A Regulatory Hub in Alzheimer's Disease. *Aging Dis.* **2023**, *15*, 201–225. [CrossRef]
24. Sevigny, J.; Chiao, P.; Bussière, T.; Weinreb, P.H.; Williams, L.; Maier, M.; Dunstan, R.; Salloway, S.; Chen, T.; Ling, Y.; et al. The antibody aducanumab reduces Aβ plaques in Alzheimer's disease. *Nature* **2016**, *537*, 50–56. [CrossRef] [PubMed]

25. Wright, A.C.; Lin, G.A.; Whittington, M.D.; Agboola, F.; Herron-Smith, S.; Rind, D.; Pearson, S.D. The effectiveness and value of lecanemab for early Alzheimer disease: A summary from the Institute for Clinical and Economic Review's California Technology Assessment Forum. *J. Manag. Care Spec. Pharm.* **2023**, *29*, 1078–1083. [CrossRef] [PubMed]
26. Uddin, M.S.; Kabir, M.T.; Rahman, M.S.; Behl, T.; Jeandet, P.; Ashraf, G.M.; Najda, A.; Bin-Jumah, M.N.; El-Seedi, H.R.; Abdel-Daim, M.M. Revisiting the Amyloid Cascade Hypothesis: From Anti-Aβ Therapeutics to Auspicious New Ways for Alzheimer's. Disease. *Int. J. Mol. Sci.* **2020**, *21*, 5858. [CrossRef] [PubMed]
27. Rivas-García, L.; Quiles, J.L.; Roma-Rodrigues, C.; Raposo, L.R.; Navarro-Hortal, M.D.; Romero-Márquez, J.M.; Esteban-Muñoz, A.; Varela-López, A.; García, L.C.; Cianciosi, D.; et al. Rosa x hybrida extracts with dual actions: Antiproliferative effects against tumour cells and inhibitor of Alzheimer disease. *Food Chem. Toxicol.* **2021**, *149*, 112018. [CrossRef]
28. Rivas-García, L.; Romero-Márquez, J.M.; Navarro-Hortal, M.D.; Esteban-Muñoz, A.; Giampieri, F.; Sumalla-Cano, S.; Battino, M.; Quiles, J.L.; Llopis, J.; Sánchez-González, C. Unravelling potential biomedical applications of the edible flower Tulbaghia violacea. *Food Chem.* **2022**, *381*, 132096. [CrossRef]
29. Romero-Márquez, J.M.; Forbes-Hernández, T.Y.; Navarro-Hortal, M.D.; Quirantes-Piné, R.; Grosso, G.; Giampieri, F.; Lipari, V.; Sánchez-González, C.; Battino, M.; Quiles, J.L. Molecular Mechanisms of the Protective Effects of Olive Leaf Polyphenols against Alzheimer's Disease. *Int. J. Mol. Sci.* **2023**, *24*, 4353. [CrossRef]
30. Navarro-Hortal, M.D.; Romero-Márquez, J.M.; Muñoz-Ollero, P.; Jiménez-Trigo, V.; Esteban-Muñoz, A.; Tutusaus, K.; Giampieri, F.; Battino, M.; Sánchez-González, C.; Rivas-García, L.; et al. Amyloid β-but not Tau-induced neurotoxicity is suppressed by Manuka honey via HSP-16.2 and SKN-1/Nrf2 pathways in an in vivo model of Alzheimer's disease. *Food Funct.* **2022**, *13*, 11185–11199. [CrossRef]
31. Romero-Márquez, J.M.; Navarro-Hortal, M.D.; Orantes, F.J.; Esteban-Muñoz, A.; Pérez-Oleaga, C.M.; Battino, M.; Sánchez-González, C.; Rivas-García, L.; Giampieri, F.; Quiles, J.L.; et al. In Vivo Anti-Alzheimer and Antioxidant Properties of Avocado (*Persea americana* Mill.) Honey from Southern Spain. *Antioxidants* **2023**, *12*, 404. [CrossRef] [PubMed]
32. Uddin, M.S.; Hasana, S.; Ahmad, J.; Hossain, M.F.; Rahman, M.M.; Behl, T.; Rauf, A.; Ahmad, A.; Hafeez, A.; Perveen, A.; et al. Anti-Neuroinflammatory Potential of Polyphenols by Inhibiting NF-κB to Halt Alzheimer's Disease. *Curr. Pharm. Des.* **2021**, *27*, 402–414. [CrossRef] [PubMed]
33. Ho, W.E.; Peh, H.Y.; Chan, T.K.; Wong, W.S. Artemisinins: Pharmacological actions beyond anti-malarial. *Pharmacol. Ther.* **2014**, *142*, 126–139. [CrossRef] [PubMed]
34. Seo, E.J.; Fischer, N.; Efferth, T. Phytochemicals as inhibitors of NF-κB for treatment of Alzheimer's disease. *Pharmacol. Res.* **2018**, *129*, 262–273. [CrossRef] [PubMed]
35. Li, Q.; Rubin, L.; Silva, M.; Li, S.; Yang, C.; Lazarovici, P.; Zheng, W. Current Progress on Neuroprotection Induced by Artemisia, Ginseng, Astragalus, and Ginkgo Traditional Chinese Medicines for the Therapy of Alzheimer's Disease. *Oxid. Med. Cell Longev.* **2022**, *14*, 3777021. [CrossRef] [PubMed]
36. Dai, R.; Sun, Y.; Su, R.; Gao, H. Anti-Alzheimer's disease potential of traditional chinese medicinal herbs as inhibitors of BACE1 and AChE enzymes. *Biomed Pharmacother.* **2022**, *154*, 113576. [CrossRef]
37. Syed, Y.Y. Sodium Oligomannate: First Approval. *Drugs* **2020**, *80*, 441–444. [CrossRef] [PubMed]
38. Krishna, S.; Bustamante, L.; Haynes, R.K.; Staines, H.M. Artemisinins: Their growing importance in medicine. *Trends Pharmacol. Sci.* **2008**, *29*, 520–527. [CrossRef] [PubMed]
39. Shi, C.; Li, H.; Yang, Y.; Hou, L. Anti-inflammatory and immunoregulatory functions of artemisinin and its derivatives. *Mediat. Inflamm.* **2015**, *2015*, 435713. [CrossRef] [PubMed]
40. Navaratnam, V.; Mansor, S.M.; Sit, N.W.; Grace, J.; Li, Q.; Olliaro, P. Pharmacokinetics of artemisinin-type compounds. *Clin. Pharmacokinet.* **2000**, *39*, 255–270. [CrossRef]
41. Fu, C.; Shi, H.; Chen, H.; Zhang, K.; Wang, M.; Qiu, F. Oral Bioavailability Comparison of Artemisinin, Deoxyartemisinin, and 10-Deoxoartemisinin Based on Computer Simulations and Pharmacokinetics in Rats. *ACS Omega* **2020**, *6*, 889–899. [CrossRef]
42. de Vries, P.J.; Dien, T.K. Clinical pharmacology and therapeutic potential of artemisinin and its derivatives in the treatment of malaria. *Drugs* **1996**, *52*, 818–836. [CrossRef] [PubMed]
43. Morris, C.A.; Duparc, S.; Borghini-Fuhrer, I.; Jung, D.; Shin, C.S.; Fleckenstein, L. Review of the clinical pharmacokinetics of artesunate and its active metabolite dihydroartemisinin following intravenous, intramuscular, oral or rectal administration. *Malar. J.* **2011**, *10*, 263. [CrossRef]
44. Gautam, A.; Ahmed, T.; Batra, V.; Paliwal, J. Pharmacokinetics and pharmacodyamics of endoperoxide antimalarials. *Curr. Drug Metab.* **2009**, *10*, 289–306. [CrossRef] [PubMed]
45. Aweeka, F.T.; German, P.I. Clinical Pharmacology of Artemisinin-Based Combination Therapies. *Clin. Pharmacokinet.* **2008**, *47*, 91–102. [CrossRef]
46. Lu, F.; He, X.-L.; Richard, C.; Cao, J. A brief history of artemisinin: Modes of action and mechanisms of resistance. *Chin. J. Nat. Med.* **2019**, *17*, 331–336. [CrossRef]
47. Ribbiso, K.A.; Heller, L.E.; Taye, A.; Julian, E.; Willems, A.V.; Roepe, P.D. Artemisinin-Based Drugs Target the Plasmodium falciparum Heme Detoxification Pathway. *Antimicrob. Agents Chemother.* **2021**, *65*, e02137-20. [CrossRef]
48. Bridgford, J.L.; Xie, S.C.; Cobbold, S.A.; Pasaje, C.F.A.; Herrmann, S.; Yang, T.; Gillett, D.L.; Dick, L.R.; Ralph, S.A.; Dogovski, C.; et al. Artemisinin kills malaria parasites by damaging proteins and inhibiting the proteasome. *Nat. Commun.* **2018**, *9*, 3801. [CrossRef] [PubMed]

49. Posadino, A.M.; Giordo, R.; Pintus, G.; Mohammed, S.A.; Orhan, I.E.; Fokou, P.V.T.; Sharopov, F.; Adetunji, C.O.; Gulsunoglu-Konuskan, Z.; Ydyrys, A.; et al. Medicinal and mechanistic overview of artemisinin in the treatment of human diseases. *Biomed. Pharmacother.* **2023**, *163*, 114866. [CrossRef]
50. Yuan, D.S.; Chen, Y.P.; Tan, L.L.; Huang, S.Q.; Li, C.Q.; Wang, Q.; Zeng, Q.P. Artemisinin: A Panacea Eligible for Unrestrictive Use? *Front. Pharmacol.* **2017**, *8*, 737. [CrossRef]
51. Drummond, E.; Wisniewski, T. Alzheimer's disease: Experimental models and reality. *Acta Neuropathol.* **2017**, *133*, 155–175. [CrossRef] [PubMed]
52. Sasaguri, H.; Nilsson, P.; Hashimoto, S.; Nagata, K.; Saito, T.; De Strooper, B.; Hardy, J.; Vassar, R.; Winblad, B.; Saido, T.C. APP mouse models for Alzheimer's disease preclinical studies. *EMBO J.* **2017**, *36*, 2473–2487. [CrossRef] [PubMed]
53. Egan, K.J.; Vesterinen, H.M.; Beglopoulos, V.; Sena, E.S.; Macleod, M.R. From a mouse: Systematic analysis reveals limitations of experiments testing interventions in Alzheimer's disease mouse models. *Evid.-Based Preclin. Med.* **2016**, *3*, e00015. [CrossRef] [PubMed]
54. Tucker, S.; Möller, C.; Tegerstedt, K.; Lord, A.; Laudon, H.; Sjödahl, J.; Söderberg, L.; Spens, E.; Sahlin, C.; Waara, E.R.; et al. The murine version of BAN2401 (mAb158) selectively reduces amyloid-β protofibrils in brain and cerebrospinal fluid of tg-ArcSwe mice. *J. Alzheimer's Dis.* **2015**, *43*, 575–588. [CrossRef] [PubMed]
55. Söllvander, S.; Nikitidou, E.; Gallasch, L.; Zyśk, M.; Söderberg, L.; Sehlin, D.; Lannfelt, L.; Erlandsson, A. The Aβ protofibril selective antibody mAb158 prevents accumulation of Aβ in astrocytes and rescues neurons from Aβ-induced cell death. *J. Neuroinflamm.* **2018**, *15*, 98. [CrossRef] [PubMed]
56. Ye, L.; Rasmussen, J.; Kaeser, S.A.; Marzesco, A.M.; Obermüller, U.; Mahler, J.; Schelle, J.; Odenthal, J.; Krüger, C.; Fritschi, S.K.; et al. Aβ seeding potency peaks in the early stages of cerebral β-amyloidosis. *EMBO Rep.* **2017**, *18*, 1536–1544. [CrossRef] [PubMed]
57. Radde, R.; Bolmont, T.; Kaeser, S.A.; Coomaraswamy, J.; Lindau, D.; Stoltze, L.; Calhoun, M.E.; Jäggi, F.; Wolburg, H.; Gengler, S.; et al. Abeta42-driven cerebral amyloidosis in transgenic mice reveals early and robust pathology. *EMBO Rep.* **2006**, *7*, 940–946. [CrossRef] [PubMed]
58. Jankowsky, J.L.; Slunt, H.H.; Gonzales, V.; Jenkins, N.A.; Copeland, N.G.; Borchelt, D.R. APP processing and amyloid deposition in mice haplo-insufficient for presenilin 1. *Neurobiol. Aging* **2004**, *25*, 885–892. [CrossRef]
59. Garcia-Alloza, M.; Robbins, E.M.; Zhang-Nunes, S.X.; Purcell, S.M.; Betensky, R.A.; Raju, S.; Prada, C.; Greenberg, S.M.; Bacskai, B.J.; Frosch, M.P. Characterization of amyloid deposition in the APPswe/PS1dE9 mouse model of Alzheimer disease. *Neurobiol. Dis.* **2006**, *24*, 516–524. [CrossRef]
60. Kamphuis, W.; Mamber, C.; Moeton, M.; Kooijman, L.; Sluijs, J.A.; Jansen, A.H.; Verveer, M.; de Groot, L.R.; Smith, V.D.; Rangarajan, S.; et al. GFAP isoforms in adult mouse brain with a focus on neurogenic astrocytes and reactive astrogliosis in mouse models of Alzheimer disease. *PLoS ONE* **2012**, *7*, e42823. [CrossRef]
61. Jackson, R.J.; Rudinskiy, N.; Herrmann, A.G.; Croft, S.; Kim, J.M.; Petrova, V.; Ramos-Rodriguez, J.J.; Pitstick, R.; Wegmann, S.; Garcia-Alloza, M.; et al. Human tau increases amyloid β plaque size but not amyloid β-mediated synapse loss in a novel mouse model of Alzheimer's disease. *Eur. J. Neurosci.* **2016**, *44*, 3056–3066. [CrossRef] [PubMed]
62. Oakley, H.; Cole, S.L.; Logan, S.; Maus, E.; Shao, P.; Craft, J.; Guillozet-Bongaarts, A.; Ohno, M.; Disterhoft, J.; Van, E.L.; et al. Intraneuronal beta-amyloid aggregates, neurodegeneration, and neuron loss in transgenic mice with five familial Alzheimer's disease mutations: Potential factors in amyloid plaque formation. *J. Neurosci.* **2006**, *26*, 10129–10140. [CrossRef] [PubMed]
63. Oddo, S.; Caccamo, A.; Shepherd, J.D.; Murphy, M.P.; Golde, T.E.; Kayed, R.; Metherate, R.; Mattson, M.P.; Akbari, Y.; LaFerla, F.M. Triple-transgenic model of Alzheimer's disease with plaques and tangles: Intracellular Abeta and synaptic dysfunction. *Neuron* **2003**, *39*, 409–421. [CrossRef]
64. Oddo, S.; Caccamo, A.; Kitazawa, M.; Tseng, B.P.; LaFerla, F.M. Amyloid deposition precedes tangle formation in a triple transgenic model of Alzheimer's disease. *Neurobiol. Aging* **2003**, *24*, 1063–1070. [CrossRef] [PubMed]
65. Caruso, D.; Barron, A.M.; Brown, M.A.; Abbiati, F.; Carrero, P.; Pike, C.J.; Garcia-Segura, L.M.; Melcangi, R.C. Age-related changes in neuroactive steroid levels in 3xTg-AD mice. *Neurobiol. Aging* **2013**, *34*, 1080–1089. [CrossRef] [PubMed]
66. Javonillo, D.I.; Tran, K.M.; Phan, J.; Hingco, E.; Kramár, E.A.; da Cunha, C.; Forner, S.; Kawauchi, S.; Milinkeviciute, G.; Gomez-Arboledas, A.; et al. Systematic Phenotyping and Characterization of the 3xTg-AD Mouse Model of Alzheimer's Disease. *Front. Neurosc.* **2022**, *15*, 785276. [CrossRef]
67. Kitazawa, M.; Medeiros, R.; Laferla, F.M. Transgenic mouse models of Alzheimer disease: Developing a better model as a tool for therapeutic interventions. *Curr. Pharm. Des.* **2012**, *18*, 1131–1147. [CrossRef] [PubMed]
68. Chambon, C.; Wegener, N.; Gravius, A.; Danysz, W. Behavioural and cellular effects of exogenous amyloid-β peptides in rodents. *Behav Brain Res.* **2011**, *225*, 623–641. [CrossRef]
69. Lauritzen, I.; Pardossi-Piquard, R.; Bauer, C.; Brigham, E.; Abraham, J.D.; Ranaldi, S.; Fraser, P.; St-George-Hyslop, P.; Le Thuc, O.; Espin, V.; et al. The β-secretase-derived C-terminal fragment of βAPP, C99, but not Aβ, is a key contributor to early intraneuronal lesions in triple-transgenic mouse hippocampus. *J. Neurosci.* **2012**, *32*, 16243–16255. [CrossRef]
70. Sims, J.R.; Zimmer, J.A.; Evans, C.D.; Lu, M.; Ardayfio, P.; Sparks, J.; Wessels, A.M.; Shcherbinin, S.; Wang, H.; Monkul Nery, E.S.; et al. Donanemab in Early Symptomatic Alzheimer Disease: The TRAILBLAZER-ALZ 2 Randomized Clinical Trial. *JAMA* **2023**, *330*, 512–527. [CrossRef]

71. Cummings, J.; Osse, A.M.L.; Cammann, D.; Powell, J.; Chen, J. Anti-Amyloid Monoclonal Antibodies for the Treatment of Alzheimer's Disease. *BioDrugs* **2024**, *38*, 5–22. [CrossRef] [PubMed]
72. Shi, J.Q.; Zhang, C.C.; Sun, X.L.; Cheng, X.X.; Wang, J.B.; Zhang, Y.D.; Xu, J.; Zou, H.Q. Antimalarial drug artemisinin extenuates amyloidogenesis and neuroinflammation in APPswe/PS1dE9 transgenic mice via inhibition of nuclear factor-κB and NLRP3 inflammasome activation. *CNS Neurosci. Ther.* **2013**, *19*, 262–268. [CrossRef] [PubMed]
73. Zhao, Y.; Long, Z.; Ding, Y.; Jiang, T.; Liu, J.; Li, Y.; Liu, Y.; Peng, X.; Wang, K.; Feng, M.; et al. Dihydroartemisinin Ameliorates Learning and Memory in Alzheimer's Disease Through Promoting Autophagosome-Lysosome Fusion and Autolysosomal Degradation for Aβ Clearance. *Front. Aging Neurosci.* **2020**, *12*, 47. [CrossRef] [PubMed]
74. Xiao, M.; Xiang, W.; Chen, Y.; Peng, N.; Du, X.; Lu, S.; Zuo, Y.; Li, B.; Hu, Y.; Li, X. DHA Ameliorates Cognitive Ability, Reduces Amyloid Deposition, and Nerve Fiber Production in Alzheimer's Disease. *Front. Nutr.* **2022**, *9*, 852433. [CrossRef] [PubMed]
75. Qin, Y.R.; Ma, C.Q.; Jiang, J.H.; Wang, D.P.; Zhang, Q.Q.; Liu, M.R.; Zhao, H.R.; Fang, Q.; Liu, Y. Artesunate restores mitochondrial fusion-fission dynamics and alleviates neuronal injury in Alzheimer's disease models. *J. Neurochem.* **2022**, *162*, 290–304. [CrossRef] [PubMed]
76. Kisler, K.; Sagare, A.P.; Lazic, D.; Bazzi, S.; Lawson, E.; Hsu, C.J.; Wang, Y.; Ramanathan, A.; Nelson, A.R.; Zhao, Z.; et al. Anti-malaria drug artesunate prevents development of amyloid-β pathology in mice by upregulating PICALM at the blood-brain barrier. *Mol. Neurodegener.* **2023**, *18*, 7. [CrossRef] [PubMed]
77. Kiss, E.; Kins, S.; Zöller, Y.; Schilling, S.; Gorgas, K.; Groß, D.; Schlicksupp, A.; Rosner, R.; Kirsch, J.; Kuhse, J. Artesunate restores the levels of inhibitory synapse proteins and reduces amyloid-β and C-terminal fragments (CTFs) of the amyloid precursor protein in an AD-mouse model. *Mol. Cell. Neurosci.* **2021**, *113*, 103624. [CrossRef] [PubMed]
78. Bloom, G.S. Amyloid-β and tau: The trigger and bullet in Alzheimer disease pathogenesis. *JAMA Neurol.* **2014**, *71*, 505–508. [CrossRef] [PubMed]
79. Kolarova, M.; García-Sierra, F.; Bartos, A.; Ricny, J.; Ripova, D. Structure and pathology of tau protein in Alzheimer disease. *Int. J. Alzheimers Dis.* **2012**, *2012*, 731526. [CrossRef]
80. Pooler, A.M.; Polydoro, M.; Wegmann, S.; Nicholls, S.B.; Spires-Jones, T.L.; Hyman, B.T. Propagation of tau pathology in Alzheimer's disease: Identification of novel therapeutic targets. *Alzheimer's Res. Ther.* **2013**, *5*, 49. [CrossRef]
81. Naseri, N.N.; Wang, H.; Guo, J.; Sharma, M.; Luo, W. The complexity of tau in Alzheimer's disease. *Neurosci. Lett.* **2019**, *705*, 183–194. [CrossRef] [PubMed]
82. Li, S.; Zhao, X.; Lazarovici, P.; Zheng, W. Artemether Activation of AMPK/GSK3β(ser9)/Nrf2 Signaling Confers Neuroprotection towards β-Amyloid-Induced Neurotoxicity in 3xTg Alzheimer's Mouse Model. *Oxidative Med. Cell. Longev.* **2019**, *2019*, 1862437. [CrossRef] [PubMed]
83. Li, H.J.; Wang, T.Z.; Hou, C.; Liu, H.Y.; Zhang, Y.; Xue, Z.Z.; Cai, Q.C.; Chen, D.M.; Gao, C.W.; Yang, J.L.; et al. Artemether Attenuates Aβ25-35-Induced Cognitive Impairments by Downregulating Aβ, BACE1, mTOR and Tau Proteins. *Clin. Lab.* **2021**, *67*. [CrossRef] [PubMed]
84. Zhao, X.; Li, S.; Gaur, U.; Zheng, W. Artemisinin Improved Neuronal Functions in Alzheimer's Disease Animal Model 3xtg Mice and Neuronal Cells via Stimulating the ERK/CREB Signaling Pathway. *Aging Dis.* **2020**, *11*, 801–819. [CrossRef] [PubMed]
85. Zhou, W.; Lei, B.; Yang, C.; Silva, M.; Xing, X.; Yu, H.; Lu, J.; Zheng, W. Artemisia annua Extract Improves the Cognitive Deficits and Reverses the Pathological Changes of Alzheimer's Disease via Regulating YAP Signaling. *Int. J. Mol. Sci.* **2023**, *24*, 5259. [CrossRef] [PubMed]
86. Morgan, A.R.; Touchard, S.; Leckey, C.; O'Hagan, C.; Nevado-Holgado, A.J.; NIMAConsortium Barkhof, F.; Bertram, L.; Blin, O.; Bos, I.; Dobricic, V.; et al. Annex: NIMA–Wellcome Trust Consortium for Neuroimmunology of Mood Disorders and Alzheimer's Disease. Inflammatory biomarkers in Alzheimer's disease plasma. *Alzheimer's Dement. J. Alzheimer's Assoc.* **2019**, *15*, 776–787. [CrossRef] [PubMed]
87. Heneka, M.T.; Carson, M.J.; El Khoury, J.; Landreth, G.E.; Brosseron, F.; Feinstein, D.L.; Jacobs, A.H.; Wyss-Coray, T.; Vitorica, J.; Ransohoff, R.M.; et al. Neuroinflammation in Alzheimer's disease. *Lancet Neurol.* **2015**, *14*, 388–405. [CrossRef] [PubMed]
88. Kinney, J.W.; Bemiller, S.M.; Murtishaw, A.S.; Leisgang, A.M.; Salazar, A.M.; Lamb, B.T. Inflammation as a central mechanism in Alzheimer's disease. *Alzheimers Dement.* **2018**, *4*, 575–590. [CrossRef] [PubMed]
89. Singh, A.; Kukreti, R.; Saso, L.; Kukreti, S. Oxidative Stress: A Key Modulator in Neurodegenerative Diseases. *Molecules* **2019**, *24*, 1583. [CrossRef]
90. Carret-Rebillat, A.S.; Pace, C.; Gourmaud, S.; Ravasi, L.; Montagne-Stora, S.; Longueville, S.; Tible, M.; Sudol, E.; Chang, R.C.; Paquet, C.; et al. Neuroinflammation and Aβ accumulation linked to systemic inflammation are decreased by genetic PKR down-regulation. *Sci. Rep.* **2015**, *5*, 8489. [CrossRef]
91. Di Benedetto, G.; Burgaletto, C.; Bellanca, C.M.; Munafò, A.; Bernardini, R.; Cantarella, G. Role of Microglia and Astrocytes in Alzheimer's Disease: From Neuroinflammation to Ca^2Homeostasis Dysregulation. *Cells* **2022**, *11*, 2728. [CrossRef]
92. Rauf, A.; Badoni, H.; Abu-Izneid, T.; Olatunde, A.; Rahman, M.M.; Painuli, S.; Semwal, P.; Wilairatana, P.; Mubarak, M.S. Neuroinflammatory Markers: Key Indicators in the Pathology of Neurodegenerative Diseases. *Molecules* **2022**, *27*, 3194. [CrossRef] [PubMed]
93. Kelley, N.; Jeltema, D.; Duan, Y.; He, Y. The NLRP3 inflammasome: An overview of mechanisms of activation and regulation. *Int. J. Mol. Sci.* **2019**, *20*, 3328. [CrossRef]

94. Jha, D.; Bakker, E.N.T.P.; Kumar, R. Mechanistic and therapeutic role of NLRP3 inflammasome in the pathogenesis of Alzheimer's disease. *J. Neurochem.* **2023**. *Online ahead of print*. [CrossRef] [PubMed]
95. Qiang, W.; Cai, W.; Yang, Q.; Yang, L.; Dai, Y.; Zhao, Z.; Yin, J.; Li, Y.; Li, Q.; Wang, Y.; et al. Artemisinin B Improves Learning and Memory Impairment in AD Dementia Mice by Suppressing Neuroinflammation. *Neuroscience* **2018**, *395*, 1–12. [CrossRef] [PubMed]
96. Zhao, X.; Huang, X.; Yang, C.; Jiang, Y.; Zhou, W.; Zheng, W. Artemisinin Attenuates Amyloid-Induced Brain Inflammation and Memory Impairments by Modulating TLR4/NF-κB Signaling. *Int. J. Mol. Sci.* **2022**, *23*, 6354. [CrossRef] [PubMed]
97. Buccellato, F.R.; D'Anca, M.; Fenoglio, C.; Scarpini, E.; Galimberti, D. Role of Oxidative Damage in Alzheimer's Disease and Neurodegeneration: From Pathogenic Mechanisms to Biomarker Discovery. *Antioxidants* **2021**, *10*, 1353. [CrossRef] [PubMed]
98. Wang, W.; Zhao, F.; Ma, X.; Perry, G.; Zhu, X. Mitochondria dysfunction in the pathogenesis of Alzheimer's disease: Recent advances. *Mol. Neurodegener.* **2020**, *15*, 30. [CrossRef] [PubMed]
99. Nikolaeva, N.S.; Yandulova, E.Y.; Aleksandrova, Y.R.; Starikov, A.S.; Neganova, M.E. The Role of a Pathological Interaction between β-amyloid and Mitochondria in the Occurrence and Development of Alzheimer's Disease. *Acta Naturae* **2022**, *14*, 19–34. [CrossRef]
100. Swerdlow, R.H. Mitochondria and mitochondrial cascades in Alzheimer's disease. *J. Alzheimer's Dis.* **2018**, *62*, 1403–1416. [CrossRef]
101. Tönnies, E.; Trushina, E. Oxidative Stress, Synaptic Dysfunction, and Alzheimer's Disease. *J. Alzheimer's Dis.* **2017**, *57*, 1105–1121. [CrossRef] [PubMed]
102. Fields, M.; Marcuzzi, A.; Gonelli, A.; Celeghini, C.; Maximova, N.; Rimondi, E. Mitochondria-Targeted Antioxidants, an Innovative Class of Antioxidant Compounds for Neurodegenerative Diseases: Perspectives and Limitations. *Int. J. Mol. Sci.* **2023**, *24*, 3739. [CrossRef] [PubMed]
103. Poorgholam, P.; Yaghmaei, P.; Noureddini, M.; Hajebrahimi, Z. Effects of artemisinin and TSP-1-human endometrial-derived stem cells on a streptozocin-induced model of Alzheimer's disease and diabetes in Wistar rats. *Acta Neurobiol. Exp.* **2021**, *81*, 141–150.
104. Loboda, A.; Damulewicz, M.; Pyza, E.; Jozkowicz, A.; Dulak, J. Role of Nrf2/HO-1 system in development, oxidative stress response and diseases: An evolutionarily conserved mechanism. *Cell. Mol. Life Sci.* **2016**, *73*, 3221–3247. [CrossRef] [PubMed]
105. Sirk, D.; Zhu, Z.; Wadia, J.S.; Shulyakova, N.; Phan, N.; Fong, J.; Mills, L.R. Chronic exposure to sub-lethal beta-amyloid (Abeta) inhibits the import of nuclear-encoded proteins to mitochondria in differentiated PC12 cells. *J. Neurochem.* **2007**, *103*, 1989–2003. [CrossRef]
106. Bhatia, S.; Rawal, R.; Sharma, P.; Singh, T.; Singh, M.; Singh, V. Mitochondrial Dysfunction in Alzheimer's Disease: Opportunities for Drug Development. *Curr. Neuropharmacol.* **2022**, *20*, 675–692. [CrossRef] [PubMed]
107. Kerr, J.S.; Adriaanse, B.A.; Greig, N.H.; Mattson, M.P.; Cader, M.Z.; Bohr, V.A.; Fang, E.F. Mitophagy and Alzheimer's Disease: Cellular and Molecular Mechanisms. *Trends Neurosci.* **2017**, *40*, 151–166. [CrossRef] [PubMed]
108. Fang, E.F.; Hou, Y.; Palikaras, K.; Adriaanse, B.A.; Kerr, J.S.; Yang, B.; Lautrup, S.; Hasan-Olive, M.M.; Caponio, D.; Dan, X.; et al. Mitophagy inhibits amyloid-β and tau pathology and reverses cognitive deficits in models of Alzheimer's disease. *Nat. Neurosci.* **2019**, *22*, 401–412. [CrossRef]
109. Xiao, Q.; Yang, L.; Hu, H.; Ke, Y. Artesunate targets oral tongue squamous cell carcinoma via mitochondrial dysfunction-dependent oxidative damage and Akt/AMPK/mTOR inhibition. *J. Bioenerg. Biomembr.* **2020**, *52*, 113–121. [CrossRef]
110. Sanchez-Varo, R.; Trujillo-Estrada, L.; Sanchez-Mejias, E.; Torres, M.; Baglietto-Vargas, D.; Moreno-Gonzalez, I.; De Castro, V.; Jimenez, S.; Ruano, D.; Vizuete, M.; et al. Abnormal accumulation of autophagic vesicles correlates with axonal and synaptic pathology in young Alzheimer's mice hippocampus. *Acta Neuropathol.* **2012**, *123*, 53–70. [CrossRef]
111. Uddin, M.S.; Stachowiak, A.; Mamun, A.A.; Tzvetkov, N.T.; Takeda, S.; Atanasov, A.G.; Bergantin, L.B.; Abdel-Daim, M.M.; Stankiewicz, A.M. Autophagy and Alzheimer's Disease: From Molecular Mechanisms to Therapeutic Implications. *Front. Aging Neurosci.* **2018**, *10*, 4. [CrossRef] [PubMed]
112. Liu, J.; Li, L. Targeting Autophagy for the Treatment of Alzheimer's Disease: Challenges and Opportunities. *Front. Mol. Neurosci.* **2019**, *12*, 203. [CrossRef] [PubMed]
113. Holczer, M.; Hajdú, B.; Lőrincz, T.; Szarka, A.; Bánhegyi, G.; Kapuy, O. Fine-tuning of AMPK-ULK1-mTORC1 regulatory triangle is crucial for autophagy oscillation. *Sci. Rep.* **2020**, *10*, 17803. [CrossRef] [PubMed]
114. Goel, P.; Chakrabarti, S.; Goel, K.; Bhutani, K.; Chopra, T.; Bali, S. Neuronal cell death mechanisms in Alzheimer's disease: An insight. *Front. Mol. Neurosci.* **2022**, *15*, 937133. [CrossRef] [PubMed]
115. Brokaw, D.L.; Piras, I.S.; Mastroeni, D.; Weisenberger, D.J.; Nolz, J.; Delvaux, E.; Serrano, G.E.; Beach, T.G.; Huentelman, M.J.; Coleman, P.D. Cell death and survival pathways in Alzheimer's disease: An integrative hypothesis testing approach utilizing -omic data sets. *Neurobiol. Aging* **2020**, *95*, 15–25. [CrossRef] [PubMed]
116. Warren, C.F.A.; Wong-Brown, M.W.; Bowden, N.A. BCL-2 family isoforms in apoptosis and cancer. *Cell Death Dis.* **2019**, *10*, 177. [CrossRef] [PubMed]
117. Zhao, Y.; Long, Z.; Liu, Y.; Luo, M.; Qiu, Y.; Idris, N.F.B.; Song, A.; Wang, K.; He, G. Dihydroartemisinin Ameliorates Decreased Neuroplasticity-Associated Proteins and Excessive Neuronal Apoptosis in APP/PS1 Mice. *Curr. Alzheimer Res.* **2020**, *17*, 916–925. [CrossRef] [PubMed]
118. Zeng, Z.; Xu, J.; Zheng, W. Artemisinin protects PC12 cells against β-amyloid-induced apoptosis through activation of the ERK1/2 signaling pathway. *Redox Biol.* **2017**, *12*, 625–633. [CrossRef] [PubMed]

119. Xu, M.; Zhang, D.F.; Luo, R.; Wu, Y.; Zhou, H.; Kong, L.L.; Bi, R.; Yao, Y.G. A systematic integrated analysis of brain expression profiles reveals YAP1 and other prioritized hub genes as important upstream regulators in Alzheimer's disease. *Alzheimers Dement.* **2018**, *14*, 215–229. [CrossRef]
120. Tanaka, H.; Homma, H.; Fujita, K.; Kondo, K.; Yamada, S.; Jin, X.; Waragai, M.; Ohtomo, G.; Iwata, A.; Tagawa, K.; et al. YAP-dependent necrosis occurs in early stages of Alzheimer's disease and regulates mouse model pathology. *Nat. Commun.* **2020**, *11*, 507. [CrossRef]
121. Sachet, M.; Liang, Y.Y.; Oehler, R. The immune response to secondary necrotic cells. *Apoptosis* **2017**, *22*, 1189–1204. [CrossRef] [PubMed]
122. Linkermann, A.; Green, D.R. Necroptosis. *N. Engl. J. Med.* **2014**, *370*, 455–465. [CrossRef] [PubMed]
123. Caccamo, A.; Branca, C.; Piras, I.S.; Ferreira, E.; Huentelman, M.J.; Liang, W.S.; Readhead, B.; Dudley, J.T.; Spangenberg, E.E.; Green, K.N.; et al. Necroptosis activation in Alzheimer's disease. *Nat. Neurosci.* **2017**, *20*, 1236–1246. [CrossRef] [PubMed]
124. Balusu, S.; Horré, K.; Thrupp, N.; Craessaerts, K.; Snellinx, A.; Serneels, L.; T'syen, D.; Chrysidou, I.; Arranz, A.M.; Sierksma, A.; et al. MEG3 activates necroptosis in human neuron xenografts modeling Alzheimer's disease. *Science* **2023**, *381*, 1176–1182. [CrossRef] [PubMed]
125. Liao, Y.; Wang, X.; Huang, L.; Qian, H.; Liu, W. Mechanism of pyroptosis in neurodegenerative diseases and its therapeutic potential by traditional Chinese medicine. *Front. Pharmacol.* **2023**, *14*, 1122104. [CrossRef] [PubMed]
126. Gao, M.; Monian, P.; Pan, Q.; Zhang, W.; Xiang, J.; Jiang, X. Ferroptosis is an autophagic cell death process. *Cell Res.* **2016**, *26*, 1021–1032. [CrossRef] [PubMed]
127. Chen, K.; Jiang, X.; Wu, M.; Cao, X.; Bao, W.; Zhu, L.Q. Ferroptosis, a Potential Therapeutic Target in Alzheimer's Disease. *Front. Cell Dev. Biol.* **2021**, *9*, 704298. [CrossRef] [PubMed]
128. Khanal, P. Antimalarial and anticancer properties of artesunate and other artemisinins: Current development. *Monatsh. Chem.* **2021**, *152*, 387–400. [CrossRef] [PubMed]
129. Eling, N.; Reuter, L.; Hazin, J.; Hamacher-Brady, A.; Brady, N.R. Identification of artesunate as a specific activator of ferroptosis in pancreatic cancer cells. *Oncoscience* **2015**, *2*, 517–532. [CrossRef]
130. Rajmohan, R.; Reddy, P.H. Amyloid-Beta and Phosphorylated Tau Accumulations Cause Abnormalities at Synapses of Alzheimer's disease Neurons. *J. Alzheimers Dis.* **2017**, *57*, 975–999. [CrossRef]
131. Griffiths, J. Grant SGN Synapse pathology in Alzheimer's disease. *Semin. Cell Dev. Biol.* **2023**, *139*, 13–23. [CrossRef] [PubMed]
132. Hollnagel, J.O.; Elzoheiry, S.; Gorgas, K.; Kins, S.; Beretta, C.A.; Kirsch, J.; Kuhse, J.; Kann, O.; Kiss, E. Early alterations in hippocampal perisomatic GABAergic synapses and network oscillations in a mouse model of Alzheimer's disease amyloidosis. *PLoS ONE* **2019**, *14*, e0209228. [CrossRef] [PubMed]
133. Meftah, S.; Gan, J. Alzheimer's disease as a synaptopathy: Evidence for dysfunction of synapses during disease progression. *Front. Synaptic Neurosci.* **2023**, *15*, 1129036. [CrossRef] [PubMed]
134. Palop, J.J.; Chin, J.; Roberson, E.D.; Wang, J.; Thwin, M.T.; Bien-Ly, N.; Yoo, J.; Ho, K.O.; Yu, G.Q.; Kreitzer, A.; et al. Aberrant excitatory neuronal activity and compensatory remodeling of inhibitory hippocampal circuits in mouse models of Alzheimer's disease. *Neuron* **2007**, *55*, 697–711. [CrossRef] [PubMed]
135. Palop, J.J.; Mucke, L. Network abnormalities and interneuron dysfunction in Alzheimer disease. *Nat. Rev. Neurosci.* **2016**, *17*, 777–792. [CrossRef]
136. Kiss, E.; Gorgas, K.; Schlicksupp, A.; Groß, D.; Kins, S.; Kirsch, J.; Kuhse, J. Biphasic Alteration of the Inhibitory Synapse Scaffold Protein Gephyrin in Early and Late Stages of an Alzheimer Disease Model. *Am. J. Pathol.* **2016**, *186*, 2279–2291. [CrossRef] [PubMed]
137. Ambrad Giovannetti, E.; Fuhrmann, M. Unsupervised excitation: GABAergic dysfunctions in Alzheimer's disease. *Brain Res.* **2019**, *1707*, 216–226. [CrossRef]
138. Mori, H.; Yoshino, Y.; Iga, J.I.; Ochi, S.; Funahashi, Y.; Yamazaki, K.; Kumon, H.; Ozaki, Y.; Ueno, S.I. Aberrant Expression of GABA-Related Genes in the Hippocampus of 3xTg-AD Model Mice from the Early to End Stages of Alzheimer's Disease. *J. Alzheimer's Dis.* **2023**, *94*, 177–188. [CrossRef] [PubMed]
139. Calvo-Flores Guzmán, B.; Vinnakota, C.; Govindpani, K.; Waldvogel, H.J.; Faull, R.L.M.; Kwakowsky, A. The GABAergic system as a therapeutic target for Alzheimer's disease. *J. Neurochem.* **2018**, *146*, 649–669. [CrossRef]
140. Li, J.; Casteels, T.; Frogne, T.; Ingvorsen, C.; Honoré, C.; Courtney, M.; Huber, K.V.; Schmitner, N.; Kimmel, R.A.; Romanov, R.A.; et al. Artemisinins Target GABAA Receptor Signaling and Impair α Cell Identity. *Cell* **2017**, *168*, 86–100.e15. [CrossRef]
141. Kasaragod, V.B.; Hausrat, T.J.; Schaefer, N.; Kuhn, M.; Christensen, N.R.; Tessmer, I.; Maric, H.M.; Madsen, K.L.; Sotriffer, C.; Villmann, C.; et al. Elucidating the Molecular Basis for Inhibitory Neurotransmission Regulation by Artemisinins. *Neuron* **2019**, *101*, 673–689.e11. [CrossRef] [PubMed]
142. Kasaragod, V.B.; Pacios-Michelena, A.; Schaefer, N.; Zheng, F.; Bader, N.; Alzheimer, C.; Villmann, C.; Schindelin, H. Pyridoxal kinase inhibition by artemisinins down-regulates inhibitory neurotransmission. *Proc. Natl. Acad. Sci. USA* **2020**, *117*, 33235–33245. [CrossRef] [PubMed]
143. Kiss, E.; Kins, S.; Gorgas, K.; Orlik, M.; Fischer, C.; Endres, K.; Schlicksupp, A.; Kirsch, J.; Kuhse, J. Artemisinin-treatment in pre-symptomatic APP-PS1 mice increases gephyrin phosphorylation at Ser270: A modification regulating postsynaptic GABAAR density. *Biol. Chem.* **2021**, *403*, 73–87. [CrossRef] [PubMed]

144. Kuhse, J.; Groeneweg, F.; Kins, S.; Gorgas, K.; Nawrotzki, R.; Kirsch, J.; Kiss, E. Loss of Extrasynaptic Inhibitory Glycine Receptors in the Hippocampus of an AD Mouse Model Is Restored by Treatment with Artesunate. *Int. J. Mol. Sci.* **2023**, *24*, 4623. [CrossRef] [PubMed]
145. Poorgholam, P.; Yaghmaei, P.; Noureddini, M.; Hajebrahimi, Z. Artemisin and human endometrial-derived stem cells improve cognitive function and synaptic plasticity in a rat model of Alzheimer disease and diabetes. *Metab. Brain Dis.* **2023**, *38*, 1925–1936. [CrossRef] [PubMed]
146. Xia, L.; Pang, Y.; Li, J.; Wu, B.; Du, Y.; Chen, Y.; Luo, M.; Wang, Y.; Dong, Z. Dihydroartemisinin Induces O-GlcNAcylation and Improves Cognitive Function in a Mouse Model of Tauopathy. *J. Alzheimer's Dis.* **2021**, *84*, 239–248. [CrossRef] [PubMed]
147. Kempermann, G.; Song, H.; Gage, F.H. Neurogenesis in the Adult Hippocampus. *Cold Spring Harb. Perspect. Biol.* **2015**, *7*, a018812. [CrossRef]
148. Scopa, C.; Marrocco, F.; Latina, V.; Ruggeri, F.; Corvaglia, V.; La Regina, F.; Ammassari-Teule, M.; Middei, S.; Amadoro, G.; Meli, G.; et al. Impaired adult neurogenesis is an early event in Alzheimer's disease neurodegeneration, mediated by intracellular Aβ oligomers. *Cell Death Differ.* **2020**, *27*, 934–948. [CrossRef] [PubMed]
149. Moreno-Jiménez, E.P.; Flor-García, M.; Terreros-Roncal, J.; Rábano, A.; Cafini, F.; Pallas-Bazarra, N.; Ávila, J.; Llorens-Martín, M. Adult hippocampal neurogenesis is abundant in neurologically healthy subjects and drops sharply in patients with Alzheimer's disease. *Nat. Med.* **2019**, *2*, 554–560. [CrossRef]
150. Toda, T.; Parylak, S.L.; Linker, S.B.; Gage, F.H. The role of adult hippocampal neurogenesis in brain health and disease. *Mol. Psychiatry* **2019**, *24*, 67–87. [CrossRef]
151. Sasaki, K.; Geribaldi-Doldán, N.; Wu, Q.; Davies, J.; Szele, F.G.; Isoda, H. Microalgae *Aurantiochytrium* Sp. Increases Neurogenesis and Improves Spatial Learning and Memory in Senescence-Accelerated Mouse-Prone 8 Mice. *Front. Cell Dev. Biol.* **2021**, *8*, 600575. [CrossRef]
152. Petrushanko, I.Y.; Mitkevich, V.A.; Makarov, A.A. Effect of β-amyloid on blood-brain barrier properties and function. *Biophys. Rev.* **2023**, *15*, 183–197. [CrossRef]
153. Sweeney, M.D.; Sagare, A.P.; Zlokovic, B.V. Blood-brain barrier breakdown in Alzheimer disease and other neurodegenerative disorders. *Nat. Rev. Neurol.* **2018**, *14*, 133–150. [CrossRef]
154. Ando, K.; Nagaraj, S.; Küçükali, F.; de Fisenne, M.A.; Kosa, A.C.; Doeraene, E.; Lopez Gutierrez, L.; Brion, J.P.; Leroy, K. PICALM and Alzheimer's Disease: An Update and Perspectives. *Cells* **2022**, *11*, 3994. [CrossRef] [PubMed]
155. Puzzo, D.; Lee, L.; Palmeri, A.; Calabrese, G.; Arancio, O. Behavioral assays with mouse models of Alzheimer's disease: Practical considerations and guidelines. *Biochem. Pharmacol.* **2014**, *88*, 450–467. [CrossRef]
156. Mssusa, A.K.; Fimbo, A.M.; Nkayamba, A.F.; Irunde, H.F.; Sillo, H.B.; Shewiyo, D.H.; Hill, G.; Minzi, O.M. Safety Profile of Artemether-Lumefantrine: A Cohort Event Monitoring Study in Public Health Facilities in Tanzania. *Clin. Drug Investig.* **2016**, *36*, 401–411. [CrossRef] [PubMed]
157. Roussel, C.; Caumes, E.; Thellier, M.; Ndour, P.A.; Buffet, P.A.; Jauréguiberry, S. Artesunate to treat severe malaria in travellers: Review of efficacy and safety and practical implications. *J. Travel Med.* **2017**, *24*, taw093. [CrossRef]
158. Nontprasert, A.; Pukrittayakamee, S.; Nosten-Bertrand, M.; Vanijanonta, S.; White, N.J. Studies of the neurotoxicity of oral artemisinin derivatives in mice. *Am. J. Trop. Med. Hyg.* **2000**, *62*, 409–412. [CrossRef] [PubMed]
159. Wesche, D.L.; DeCoster, M.A.; Tortella, F.C.; Brewer, T.G. Neurotoxicity of artemisinin analogs in vitro. *Antimicrob. Agents Chemother.* **1994**, *38*, 1813–1819. [CrossRef]
160. Singh, S.; Giri, A.; Giri, S. The antimalarial agent artesunate causes sperm DNA damage and hepatic antioxidant defense in mice. *Mutat. Res. Genet. Toxicol. Environ. Mutagen.* **2015**, *777*, 1–6. [CrossRef]
161. Zheng, C.; Shan, L.; Tong, P.; Efferth, T. Cardiotoxicity and Cardioprotection by Artesunate in Larval Zebrafish. *Dose-Response* **2020**, *18*, 1559. [CrossRef] [PubMed]
162. Gordi, T.; Lepist, E.I. Artemisinin derivatives: Toxic for laboratory animals, safe for humans? *Toxicol. Lett.* **2004**, *147*, 99–107. [CrossRef] [PubMed]

International Journal of
Molecular Sciences

MDPI

Article

Positive Allosteric Modulators of SERCA Pump Restore Dendritic Spines and Rescue Long-Term Potentiation Defects in Alzheimer's Disease Mouse Model

Anastasiya Rakovskaya [1,†], Alexander Erofeev [1,†], Egor Vinokurov [1], Ekaterina Pchitskaya [1], Russell Dahl [2] and Ilya Bezprozvanny [1,3,*]

[1] Laboratory of Molecular Neurodegeneration, Peter the Great St. Petersburg Polytechnical University, St. Petersburg 195251, Russia; rakovskaya_av@spbstu.ru (A.R.); alexandr.erofeew@spbstu.ru (A.E.); vinokurov.ek@edu.spbstu.ru (E.V.); pchitskaya_ei@spbstu.ru (E.P.)
[2] Neurodon Corporation, 9800 Connecticut Drive, Crown Point, IN 46307, USA; rdahl@neurodon.net
[3] Department of Physiology, UT Southwestern Medical Center at Dallas, Dallas, TX 75390, USA
* Correspondence: ilya.bezprozvanny@utsouthwestern.edu
† These authors contributed equally to this work.

Abstract: Alzheimer's disease (AD) is a neurodegenerative disorder that affects memory formation and storage processes. Dysregulated neuronal calcium (Ca^{2+}) has been identified as one of the key pathogenic events in AD, and it has been suggested that pharmacological agents that stabilize Ca^{2+} neuronal signaling can act as disease-modifying agents in AD. In previous studies, we demonstrated that positive allosteric regulators (PAMs) of the sarco/endoplasmic reticulum Ca^{2+} ATPase (SERCA) pump might act as such Ca^{2+}-stabilizing agents and exhibit neuroprotective properties. In the present study, we evaluated effects of a set of novel SERCA PAM agents on the rate of Ca^{2+} extraction from the cytoplasm of the HEK293T cell line, on morphometric parameters of dendritic spines of primary hippocampal neurons in normal conditions and in conditions of amyloid toxicity, and on long-term potentiation in slices derived from 5xFAD transgenic mice modeling AD. Several SERCA PAM compounds demonstrated neuroprotective properties, and the compound NDC-9009 showed the best results. The findings in this study support the hypothesis that the SERCA pump is a potential therapeutic target for AD treatment and that NDC-9009 is a promising lead molecule to be used in the development of disease-modifying agents for AD.

Keywords: SERCA; positive allosteric modulators; calcium; Alzheimer's disease; beta-amyloid; dendritic spines; calcium imaging; long-term potentiation

Citation: Rakovskaya, A.; Erofeev, A.; Vinokurov, E.; Pchitskaya, E.; Dahl, R.; Bezprozvanny, I. Positive Allosteric Modulators of SERCA Pump Restore Dendritic Spines and Rescue Long-Term Potentiation Defects in Alzheimer's Disease Mouse Model. *Int. J. Mol. Sci.* **2023**, *24*, 13973. https://doi.org/10.3390/ijms241813973

Academic Editor: Claudia Ricci

Received: 21 August 2023
Revised: 7 September 2023
Accepted: 8 September 2023
Published: 12 September 2023

1. Introduction

Alzheimer's disease (AD) is a neurodegenerative disorder that affects memory formation and storage processes. Several hypotheses about the causes of AD have been proposed, but the so-called "amyloid cascade hypothesis" is a dominant model of AD pathogenesis. It states that increased production of the amyloidogenic Aβ42 peptide (or an increase in the Aβ42:Aβ40 ratio) is driving AD, causing a decreased number of synapses and neuronal death [1]. Therefore, great efforts have been made to develop agents that can reduce Aβ production or eliminate Aβ from the brain. Recently, the FDA approved Aduhelm and Leqembi (monoclonal antibodies against Aβ developed by Biogen and Eisai) for AD. However, these approvals were based primarily on amyloid clearance endpoints, and clinical benefits of these antibodies appear to be very limited despite potential serious side effects reported for both [2–5]. Therefore, a substantial unmet need exists for the development of safer therapies for Alzheimer's disease (AD) that can potentially offer clinical benefits to patients. It is noteworthy that the immune system interacts with synapses as well as immune cells and mediators participating in synapse elimination during development and

contributing to synaptic plasticity during adulthood [6,7]. Therefore, in the context of drug development, it is imperative to consider their impact on the immune system.

An alternative approach to developing AD treatments is based on the "calcium hypothesis" of AD [8,9]. This hypothesis proposes that dysregulation in cellular calcium homeostasis is the main driving force of neurodegeneration in AD [8,9]. The pharmacological normalization of calcium signaling in neurons is a promising approach for the development of therapeutic agents, and its potential efficacy and applicability is demonstrated through the example of memantine [10]—a noncompetitive NMDA glutamate receptor antagonist. Memantine is also a dopamine agonist and increases dopaminergic transmission. In cognitive terms, memantine primarily increases attention and episodic memory. Memantine offers no benefit in mild AD, but it improves symptoms in patients with moderate to severe AD and exhibits a favorable safety and tolerability profile [11]. One potentially interesting and relatively unexplored Ca^{2+}-related target is the sarco/endoplasmic reticulum calcium ATPase (SERCA) Ca^{2+} pump. Compounds from a new class of substances—positive allosteric modulators (PAM)—do not affect the basal activity of SERCA but are capable of enhancing the extraction of Ca^{2+} from the cytoplasm into the endoplasmic reticulum, with significant increases in calcium concentration. Such an effect will avoid undesirable effects on normal calcium-sensitive processes, thereby minimizing possible side effects while preventing toxic increases in cytoplasmic calcium concentrations. In our recent study, it was demonstrated that a novel SERCA PAM agent (compound NDC-1173) improved the performance in behavioral studies and offered a robust benefit in reducing ER stress in the APP/PS1 transgenic AD mouse model [12]. Encouraging results have also been obtained for this class of compounds in earlier studies with preclinical models of AD [13].

In this research, we aimed to study the activity of a new class of SERCA PAMs in vitro and their potential protective and therapeutic effects on in vitro and in vivo AD models. We describe the identification and evaluation of several novel positive allosteric modulators of the SERCA pump: NDC-9009, NDC-9033, NDC-9136, and NDC-9342. We demonstrate that these SERCA PAMs facilitate Ca^{2+} clearance from the cytoplasm during its pathological increase, protect hippocampal dendritic spines from amyloid toxicity-induced degenerative changes in vitro, and efficiently recover synaptic plasticity in brain slices from 6-month-old 5xFAD mice, an aggressive Aβ model of AD.

2. Results

2.1. Identification and Functional Analysis of Novel SERCA PAMs

Our previous work utilizing a high-throughput fluorescence resonance energy transfer (FRET) assay consisting of labeled SERCA and phospholamban enabled the identification of an aminoquinoline class of compounds that perturb SERCA conformation [14]. This finding is significant because of SERCA's reputation as an intractable target and also because the only previously reported small-molecule SERCA activators were based on istaroxime, a steroid-based molecule with polypharmacology (specifically Na^+,K^+-ATPase inhibition), a narrow therapeutic index, and reported toxicity [15,16]. Identified compounds acted as either inhibitors or activators of SERCA, and a standard ATPase assay was employed to identify only activators. Medicinal chemistry optimization of this series identified the four SERCA PAMs: NDC-9009, NDC-9033, NDC-9136, and NDC-9342. The structures of these compounds and their basic biochemical properties are summarized in Table 1.

2.2. SERCA PAMs Enhance the Rate of Calcium Extraction from the Cytosol in HEK293T Cell Line

To analyze the effect of SERCA PAMs on the rate of calcium extraction from the cytosol, HEK293T cells were transfected with the protein calcium-sensor GCaMP using polyethyleneamine. Cells were placed in ADMEM with 2 mM of Ca^{2+}, and then one of four different PAMs (NDC-9009, NDC-9033, NDC-9136, or NDC-9342) was added at a final concentration of 0.1 μM along with the ionomycin (Io) ionophore at a final concentration of 1 μM (Figure 1A). Analysis of the results showed that NDC-9009, NDC-9136, and NDC-

9342 inhibited the increase in calcium levels caused by the addition of ionomycin: the peak value of the GCaMP signal for the control group was 7.2 ± 0.6; with the addition of NDC-9009, it was 4.78 ± 0.3 (***: $p < 0.001$); for NDC-9136, it was 4.9 ± 0.5 (**: $p < 0.01$); and for NDC-9342, it was 5.9 ± 0.4 (*: $p < 0.05$,) (Figure 1B) (Table 2). The rate of increase in cytosolic calcium was estimated by calculating the tangent of the slope (tanα). PAMs caused a tanα decrease: for NDC-9009, to 0.021 ± 0.002 (***: $p < 0.001$); for NDC-9136, to 0.016 ± 0.002 (***: $p < 0.001$); and for NDC-9342, to 0.026 ± 0.003 (***: $p < 0.001$) (Figure 1C) (Table 2).

Table 1. Biochemical properties of SERCA PAMs.

Compound	MW	Structure	% SERCA Activation @ 2 μM	Solubility (μM) in PBS @ pH 7.4
NDC-9009	305	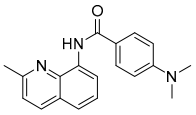	17.1 ± 1.0	0.23
NDC-9033	320	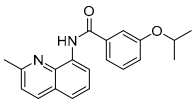	16.5 ± 2.5	0.05
NDC-9136	320	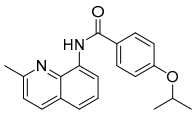	13.9 ± 2.1	0.10
NDC-9342	426	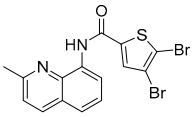	28.4 ± 1.2	0.03

Table 2. Results of evaluation of the neuroprotective effect of SERCA PAMs. Data are expressed as the mean ± SEM. Statistical significance was determined by using a Conover–Iman test in the analysis of the spines' head area and Dunn's test for the calcium signal and curve slope (* $p < 0.05$, ** $p < 0.001$, *** $p < 0.001$ compared to control).

Criterion	Control	NDC-9009	NDC-9033	NDC-9136	NDC-9342
Spines' head area in normal conditions, μm^2	0.583 ± 0.025	0.588 ± 0.026	0.511 ± 0.026 *	0.598 ± 0.029	0.430 ± 0.019 ***
Spines' head area in conditions of amyloid toxicity, μm^2	0.481 ± 0.019	0.576 ± 0.041 *	0.530 ± 0.020	0.560 ± 0.028 *	0.563 ± 0.031 *
Calcium signal (dF/F0)	7.2 ± 0.6	4.78 ± 0.3 ***	7.97 ± 0.7	4.9 ± 0.5 **	5.9 ± 0.4 *
Curve slope (tanα)	0.061 ± 0.006	0.021 ± 0.002 ***	0.048 ± 0.006	0.016 ± 0.002 ***	0.026 ± 0.003 ***

It was confirmed that NDC-9009, NDC-9136, and NDC-9342 reduced the calcium concentration with its pathological increase. The rate of calcium extraction during SERCA activation was also evaluated, and the best results were also demonstrated by these three compounds. Next, it was necessary to evaluate the neuroprotective potential of SERCA PAMs in primary hippocampal neurons in conditions of amyloid toxicity, modeling Alzheimer's disease.

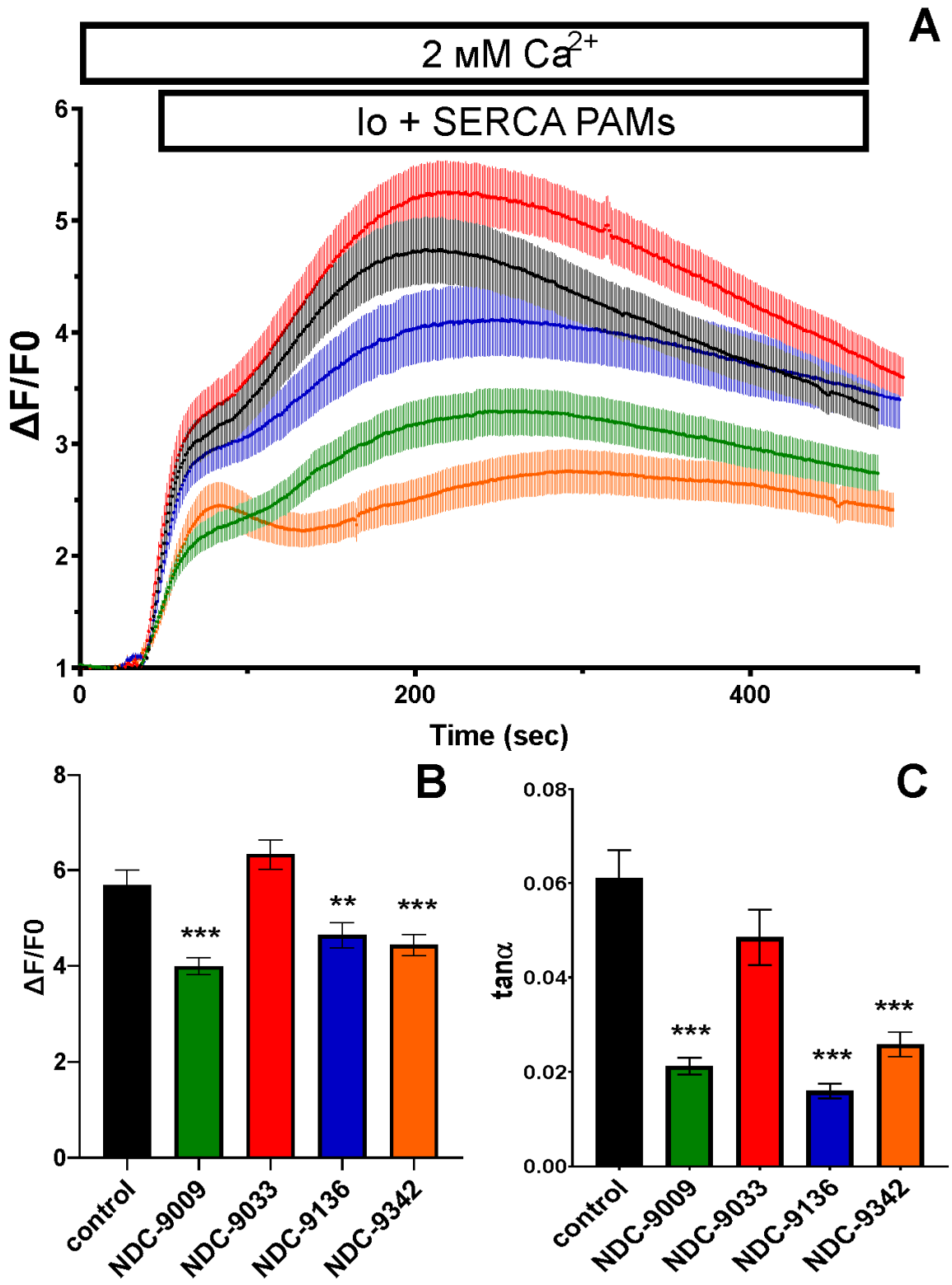

Figure 1. SERCA PAMs increased the rate of calcium extraction from the cytoplasm of the HEK293T cell line. (**A**) Calcium signal dF/F0 after addition of 1 µM of ionomycin (Io) in the control group and with the addition of PAMs. (**B**) Peak value of dF/F0 and (**C**) curve slope (tanα) for the control group and with the addition of PAMs. Data are presented as the mean ± SEM ($n \geq 15$ cells from 3 batches of cultures); Dunn's test was used for multiple comparison (**: $p < 0.01$,***: $p < 0.001$ compared to control).

2.3. Effects of SERCA PAMs on the Morphology of Dendritic Spines of Primary Hippocampal Neurons in Normal Conditions and in Conditions of Amyloid Toxicity

To assess the neuroprotective potential of positive allosteric modulators (PAMs), primary hippocampal neurons were visualized via calcium phosphate transfection with the GFP plasmid on day 7 of in vitro culture (DIV). Seventy-two hours before fixation, cells were treated with Aβ42 (final concentration of 0.1 μM) oligomers to model amyloid synaptotoxicity conditions in vitro. The cells were incubated with 0.1 μM of one of the four PAMs (NDC-9009, NDC-9033, NDC-9136, or NDC-9342) or an equal volume of DMSO for 24 h. At DIV 16-17, cultures were fixed, and an analysis of the dendritic spine morphology was performed by using confocal microscopy (2048 × 2048 pixels with a resolution of 0.032 μm/pixel). Image processing was performed using the SpineJ plugin in ImageJ software. The micrographs in Figure 2C illustrate changes in the morphology of the dendritic spines of the hippocampal neurons after addition of PAM in normal conditions and in conditions of amyloid toxicity, simulating AD in vitro. A decrease in the area of the head of the dendritic spines was demonstrated for NDC-9033 (0.511 ± 0.026 μm^2) (*: $p < 0.05$) and NDC-9342 (0.430 ± 0.019 μm^2) (***: $p < 0.001$) (Figure 2A), while increases were shown in the neck length for the other two PAMs: NDC-9009 (0.696 ± 0.044 μm) (***: $p < 0.001$) and NDC-9136 (0.654 ± 0.049 μm) (*: $p < 0.05$) (Figure 2B). However, the ratio of neck length to spine length increased only when exposed to NDC-9009 ($36 \pm 1\%$) (***: $p < 0.001$) (Figure 2E), and no differences in density were observed compared to the control (Figure 2D). The spines' head area decreased to 0.481 ± 00.019 μm^2 (*: $p < 0.05$) in conditions of amyloid toxicity, consistent with the data obtained and characteristic of the in vitro AD model (Figure 2F). NDC-9009, NDC-9136, and NDC-9342 demonstrated a neuroprotective effect in the condition of amyloid toxicity by increasing the head area of the dendritic spines to 0.576 ± 0.041 μm^2 (#: $p < 0.05$), 0.560 ± 0.028 μm^2 (#: $p < 0.05$), and 0.563 ± 0.031 μm^2 (#: $p < 0.05$) (Figure 2F) (Table 2), respectively. The length of the neck of the dendritic spines increased in conditions of amyloid toxicity from 0.488 ± 0.029 μm to 0.757 ± 0.057 μm (***: $p < 0.001$); however, the addition of PAM did not show statistical differences in this criterion (Figure 2G). There were no statistical differences between the groups in the density of dendritic spines per 10 μm (Figure 2H). The ratio of neck length to spine length increased from $30 \pm 1\%$ to $39 \pm 2\%$ (***: $p < 0.001$) in conditions of amyloid toxicity, but the addition of PAM reduced this parameter: NDC-9033—up to $34 \pm 2\%$ (#: $p < 0.05$); NDC-9342—up to $35 \pm 2\%$ (#: $p < 0.05$) (Figure 2I) (Table 2).

Based on the results of the experiments summarized in Table S1, it can be concluded that the NDC-9009 compound demonstrated the best neuroprotective effect and the highest efficiency, and thus it was chosen for further experiments to evaluate its neuroprotective potential in vivo.

2.4. Effects of NDC-9009 on Long-Term Potentiation in an AD Mouse Model

Hippocampal synaptic plasticity occurs in multiple phases involving short-term and long-term changes in the synapse [17]. Changes within 0–2 min after high-frequency stimulation (HFS) are thought to reflect post-tetanic potentiation associated with alterations in presynaptic neurotransmitter release properties [18]. Changes in the last 10 min after HFS stimulation are considered long-term potentiation [19]. We conducted experiments to assess post-tetanic potentiation (PTP) and long-term potentiation (LTP) in control and experimental groups of wild-type (WT) and Alzheimer's mice (5xFAD) characterized by the production and aggregation of beta-amyloid protein (Figure 3; representative images of amyloid plaques in the brains of 6-month-old 5xFAD and WT mice are presented in Figure S1). Both the wild-type and AD experimental groups were administered intraperitoneal injections of NDC-9009 at a 10 mg/kg dose (DMSO + NDC9009:TWEEN 80:water) for one month starting at 5 months of age. The control group received a vehicle solution (DMSO:TWEEN 80:water).

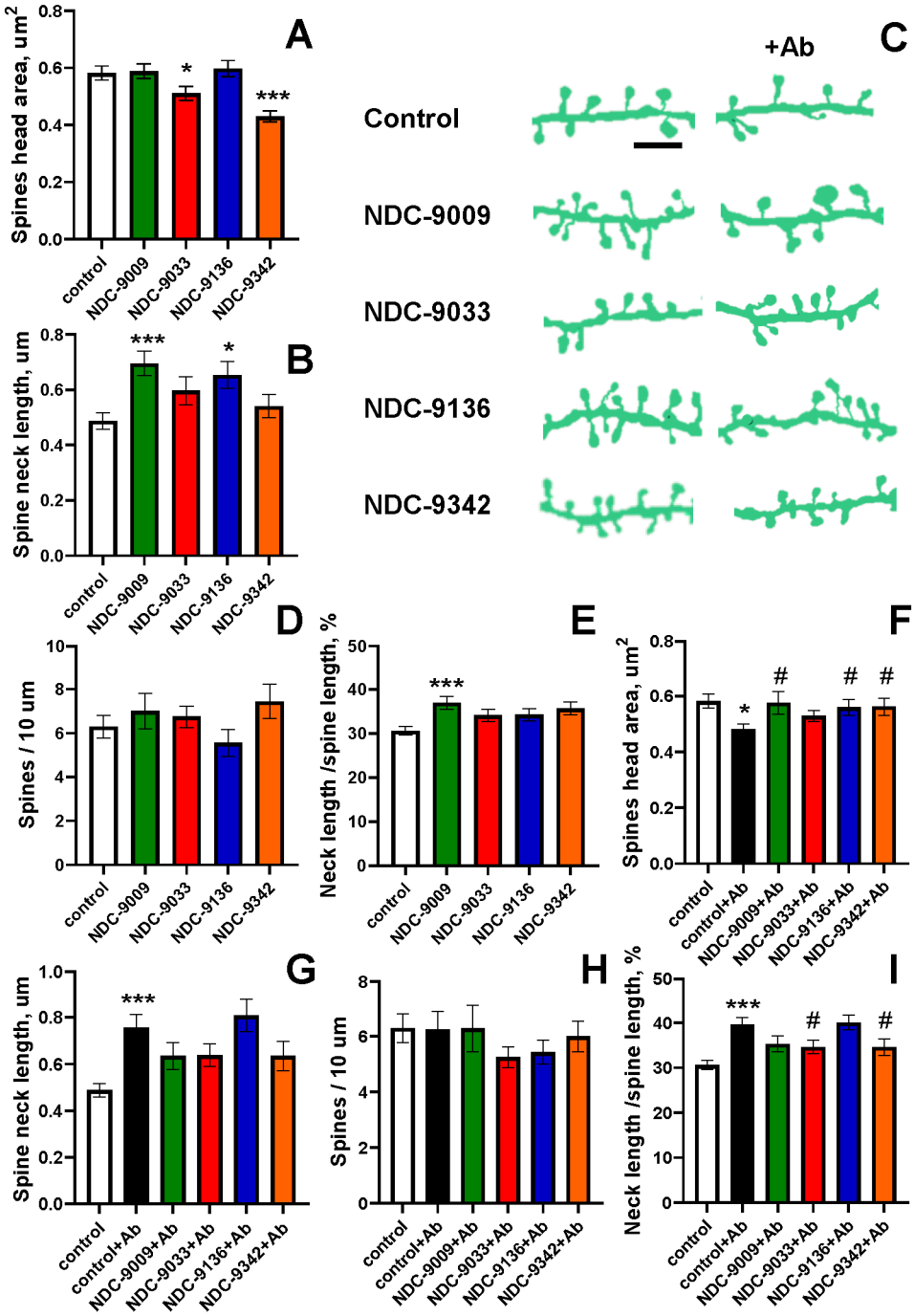

Figure 2. Positive allosteric modulators of calcium ATPase SERCA have a neuroprotective effect on hippocampal neurons in conditions of low amyloid toxicity. (**A**,**B**,**F**,**G**) The spines' head area and spine length neck for each group of cells shown in panel C in the normal conditions (**A**,**B**) and in conditions of amyloid toxicity (Ab) (**F**,**G**) are presented as the mean ± SEM ($n \geq 10$ neurons from 1 batch of cultures). (**C**) Binarized images of dendrites of wild-type (WT) hippocampal neurons transfected with GFP plasmid at DIV 7; one of four PAMs were added 24 h before fixation, and the culture was fixed at DIV 16-17. Scale bar corresponds to 5 µm. (**D**,**E**,**H**,**I**) Number of spines per 10 µm dendrite length and the ratio of the length of the neck to the length of the dendrite for each group of cells shown in panel C in normal conditions (**D**,**E**) and in conditions of amyloid toxicity (Ab) (**H**,**I**) are presented as the mean ± SEM (neurons ≥ 10, spines ≥ 70 from 1 batch of cultures). Statistical analysis was performed using a Conover–Iman test (*: $p < 0.05$, ***: $p < 0.001$ compared to control; #: $p < 0.05$ compared to control + Ab).

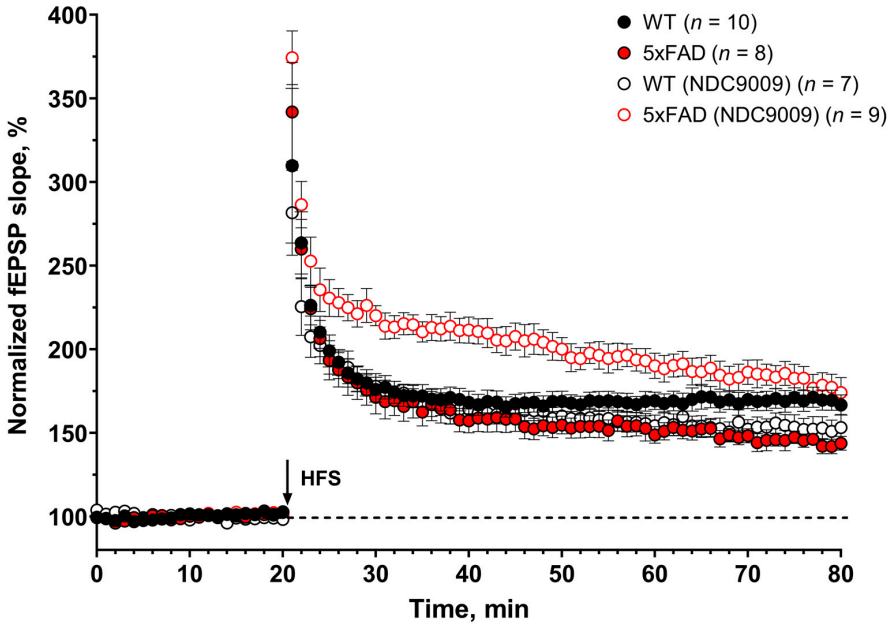

Figure 3. Positive allosteric modulators of SERCA pump (NDC-9009) restores LTP impairment in 6-month-old 5xFAD mice. The figure shows summary plots of the normalized fEPSP slope (%) in the recording time. The fEPSPs were induced by HFS (black arrow). After HFS, the fEPSP slope increased over time in all groups. The increments in the slope of the fEPSP were slower in 5xAFD mice than the wild-type (WT) mice in the control group and changed in the experimental group with NDC-9009. Data are presented as the mean ± SEM.

Analysis of the PTP (2 min after high-frequency stimulation) revealed no difference in the fEPSP slope between the WT and 5xFAD control groups at 6 months old, with values of 299 ± 22 and 306 ± 24, respectively (Figure 4A). However, NDC-9009 administration significantly increased the PTP fEPSP slope of the 5xFAD mice in comparison to WT, with values of 340 ± 13 and 258 ± 20, respectively.

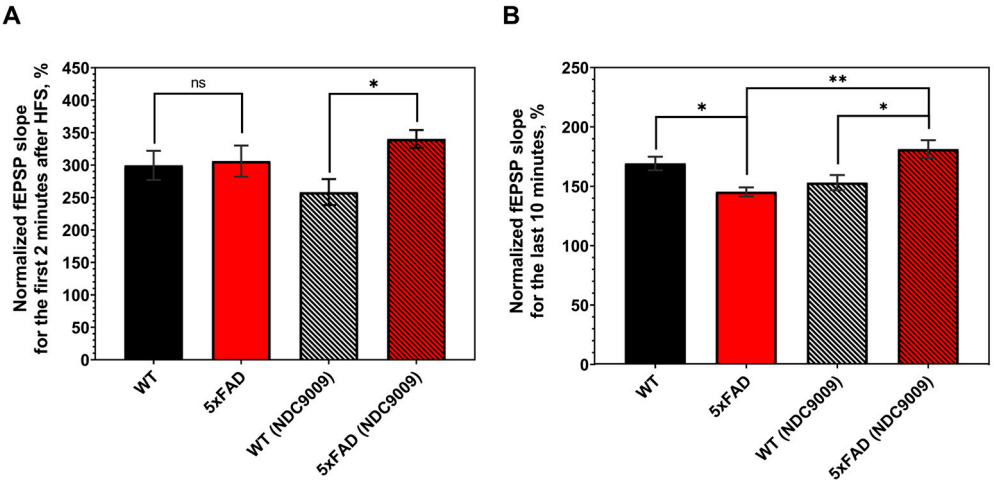

Figure 4. Positive allosteric modulators of SERCA pump (NDC-9009) restores LTP impairment in 6-month-old 5xFAD mice. (**A**) Normalized fEPSP slope (%) for post-tetanic potentiation (2 min after high-frequency stimulation). (**B**) Normalized fEPSP slope (%) for long-term potentiation (last 10 min after high-frequency stimulation). Groups: WT: n = 10; 5xFAD: n = 8; WT (NDC-9009): n = 7; 5xFAD (NDC-9009): n = 9. Statistical analysis was performed using a Kruskal–Wallis test with a post hoc Dunn's test for PTP analysis and one-way ANOVA with a post hoc Tukey's test for LTP analysis (*: $p < 0.05$, **: $p < 0.01$). Data are presented as the mean ± SEM.

We next examined the LTP expression (last 10 min after high-frequency stimulation) in 6-month-old mice (Figure 4B). After HFS, the fEPSP slope increased over time in all groups. The increments in the slope of the fEPSP were slower in 5xAFD mice than in the wild-type mice in the control group and changed in the experimental group with NDC-9009. Normalized to baseline, the percentage of slope (LTP, last 10 min after HFS) values was lower in 5xFAD mice (145 $\pm$ 3) than in WT mice (169 $\pm$ 5) in the control group.

At the same time, significant differences (*: $p < 0.05$) were observed in the magnitude of long-term potentiation between the wild-type mice (153 $\pm$ 6) and 5xFAD mice (181 $\pm$ 7) in the experimental group. Furthermore, a significant difference (**: $p < 0.01$) in long-term potentiation was observed in both the control and experimental groups of 5xFAD mice. Specifically, the LTP value within the experimental group of 5xFAD mice exceeded that observed in the corresponding control group. In the case of the wild-type mice, no statistically differences in the long-term potentiation (LTP) value were discerned between the experimental and control groups of mice.

Based on our findings, it can be inferred that the positive allosteric modulator of calcium ATPase SERCA NDC-9009 exhibits a neuroprotective effect. The intraperitoneal administration of NDC-9009 led to an increase in the magnitude of long-term potentiation in 6-month-old 5xFAD mice compared to the control group of mice.

3. Discussion

Alzheimer's disease (AD) is a neurodegenerative disorder that affects memory formation and storage processes. Several hypotheses about the causes of AD have been proposed, but the so-called "amyloid cascade hypothesis" is a dominant model of AD pathogenesis. It states that increased production of amyloidogenic Aβ42 peptide is driving AD, causing a decreased number of synapses and neuronal death [1]. As an alternative viewpoint, the "calcium hypothesis" of AD has also been suggested [20]. This hypothesis assumes that dysregulation in cellular calcium homeostasis mechanisms is the main driving force of neurodegeneration in AD [8,9].

In addition to the adverse effect of amyloid β-protein, Ca^{2+} dysregulation in AD is caused by mutated presenilins [21]. Different cellular models expressing AD mutant presenilin demonstrate an overloading of the endoplasmic reticulum (ER) with Ca^{2+} and an excessive Ca^{2+} release through the $InsP_3R$ [22–25], altering parts of the neuronal calcium signaling machinery such as the store-operated Ca^{2+} influx [26] and induction of excessive ryanodine receptor (RyR) calcium release [25]. Most of the AD-causing mutations block the pore formed by presenilin, leading to ER calcium overload [22,23], which subsequently results in excessive calcium release through the RyR [25]. A reduction in the RyR calcium release was proposed as a therapeutic strategy for AD treatment. However, experiments with its inhibitor (dantrolene) have yielded contradictory results, possibly due to its lack of selectivity [27,28]. Recent findings suggest that the neuronal-store-operated calcium entry (SOCE) pathway plays a role in AD pathogenesis. The SOCE pathway is activated following depletion of ER Ca^{2+} levels and is reduced in AD. The most obvious reason for SOCE alteration is the reduced expression level of the ER Ca^{2+} sensor STIM2/STIM1 [29–31]. Pharmacological restoration of the SOCE pathway is one potential method for drug development in AD [29].

The primary focus of this article centers on the SERCA Ca^{2+} pump. SERCA's well-established role is to preserve low cytosolic Ca^{2+} levels by pumping free Ca^{2+} ions into the ER lumen by utilizing ATP hydrolysis. It has been suggested that presenilins can directly interact with SERCA and physiologically regulate its activity and confer resistance to endoplasmic reticulum stress [32]. SERCA ensures proper Ca^{2+} handling in cells and may act as a therapeutic target for the disease associated with dysregulation of calcium ions [33]; therefore, development of its selective activators is under scientific investigation. Recently, a small transmembrane SERCA-binding protein known as the Dwarf Open Reading Frame (DWORF) was discovered as a direct activator of SERCA. This fundamental discovery about the physiological regulation of SERCA holds promise for the development of a new generation of its activators [34]. Also, a study conducted on a pyridone derivative

was found to activate the SERCA2a isoform [35]. Furthermore, it was observed that the pyridone derivative stimulated the Ca^{2+}-dependent ATPase activity of cardiac sarcoplasmic reticulum (SR) vesicles. This indicates that the derivative enhances the ability of SR to transport calcium ions, which is an essential process for proper cardiac function. This results in improved cardiac function at both the cellular and organ level. Therefore, this pyridone derivative is suggested as a promising candidate for therapeutic applications in heart failure [35]. Another study demonstrated that CDN1163, when activating the SERCA2b isoform in the liver, can reduce endoplasmic reticulum (ER) stress and improve mitochondrial efficiency. Additionally, metabolic parameters were improved, suggesting that CDN1163 or other SERCA activators have the potential to be pharmacological agents for treating diabetes and metabolic dysfunction [14,36]. Additionally, small-molecule activation of SERCA2 by the quinoline derivative CDN1163 [37] was supposed to be a potential pharmacotherapeutic target in Alzheimer's and Parkinson's diseases [38]. CDN1163 has been demonstrated to be effective in the APP/PS1 double transgenic mouse model of Alzheimer's disease [13].

Previous studies confirmed that SERCA PAM CDN1163 can exert beneficial effects in APP/PS1 mice [13]. Our recent paper also concluded that another SERCA PAM—compound NDC-1173—could enhance memory in both object and spatial memory tasks in an AD mouse [12]. In the present study, we report the activity of another SERCA PAM molecule—compound NDC-9009. When compared to other molecules (NDC-9033, NDC-9136, and NDC-9342), this compound demonstrated the most consistent effects on Ca^{2+} dynamics (Figure 1) and in the spine rescue assay (Figure 2) in hippocampal neuronal cultures (Table 2). We demonstrated the in vitro calcium ATPase activity using SERCA PAMs on the HEK293T cell line. Additionally, we evaluated the neuroprotective potential of SERCA PAMs in conditions of amyloid toxicity, which is believed to be the primary driver of AD pathology. NDC-9009 also exhibited effectiveness in the LTP rescue assay using hippocampal slices from 5xFAD mice (Figures 3 and 4). It is worth noting that we investigated alterations in long-term potentiation in 6-month-old 5xFAD male mice. We used exclusively male mice in our research and examined a single concentration of the compound. To gain a more comprehensive understanding of the compound under investigation, further experiments involving a range of concentrations and both male and female mice are warranted. Based on these findings, we concluded that NDC-9009 is the most promising SERCA PAM from this compound series for the development of potential AD therapeutic agents.

However, several limitations of this study should be noted. First, future studies are needed to analyze another system (heart or pancreas) after using SERCA PAMs in vivo to rule out potential side effects. Second, we focused our study on the 5xFAD mice model, which is a very aggressive model of AD and has its critics [39]. Testing NDC-9009 or other SERCA PAMs in "second generation" AD models such as APPKI mice [40] may provide further insights into their mechanism of action.

4. Materials and Methods

4.1. Synthesis of SERCA PAMs

NDC-9009. Into a stirred solution of 4-(dimethylamino) benzoic acid (2.50 g, 15.134 mmol) and DMF (50.00 µL) in DCM (30.0 mL), oxalyl chloride (9 mL, 2 M in DCM) was added dropwise at 0 °C under nitrogen. The resulting mixture was stirred for 1 h at room temperature and then concentrated under reduced pressure. The crude product was used in the next step directly without further purification. The residue was dissolved in DCM (30.0 mL) and added dropwise into a stirred solution of 2-methylquinolin-8-amine (1.30 g, 8.217 mmol) and TEA (3.33 g, 32.868 mmol) in DCM (30.0 mL) at 0 °C. The resulting mixture was stirred for 2 h at room temperature under a nitrogen atmosphere. LCMS showed that the SM was consumed and the product was formed. The mixture was washed with water, extracted with DCM, and dried over anhydrous Na_2SO_4. After filtration, the filtrate was concentrated under reduced pressure. The residue was purified via silica gel column chromatography eluting with EtOAc/DCM (0–5%) to afford the crude product. The residue was dissolved in DCM

(50 mL) and washed with 1N of HCl (50 mL). The aqueous layer was adjusted to pH 8 with $NaHCO_3$ and extracted with DCM (50 mL). The organic layers were dried over anhydrous Na_2SO_4 and concentrated under reduced pressure. The residue was recrystallized from PE: EtOAc = 10:1 (50 mL) to afford 1.46 g (58% yield) of the title compound as a light yellow solid. LC-MS: (ESI, m/z): $[M + H]^+ = 306$. ^{1}H NMR (400 MHz, DMSO-d_6) δ 10.58 (s, 1H), 8.71–8.67 (m, 1H), 8.31 (d, J = 8.4 Hz, 1H), 7.88 (d, J = 9.2 Hz, 2H), 7.63–7.50 (m, 3H), 6.86 (d, J = 8.8 Hz, 2H), 3.03 (s, 6H), 2.78 (s, 3H).

NDC-9033. Into a stirred solution of 3-isopropoxybenzoic acid (1.80 g, 9.989 mmol) and DMF (50.00 µL, 0.684 mmol) in DCM (30.0 mL), oxalyl chloride (6 mL, 2 M in DCM) was added dropwise at 0 °C under nitrogen. The resulting mixture was stirred for 1 h at room temperature and then concentrated under reduced pressure. The crude product was used in the next step directly without further purification. The residue was dissolved in DCM (30.0 mL) and added dropwise into a stirred solution of 2-methylquinolin-8-amine (1.74 g, 10.998 mmol) and TEA (2.02 g, 19.978 mmol) in DCM (30.0 mL) at 0 °C. The resulting mixture was stirred for 2 h at room temperature under a nitrogen atmosphere. LCMS showed that the SM was consumed and the product was formed. The mixture was washed with water and dried over anhydrous Na_2SO_4. After filtration, the filtrate was concentrated under reduced pressure. The residue was purified via silica gel column chromatography eluting with EtOAc/DCM (0–5%) to afford the crude product. The crude product was further purified in a pre-packed C18 column (solvent gradient: 0–50% ACN in water (10 mmol/L NH_4HCO_3)) to afford 1.92 g (59% yield) of the title compound as a white solid. LC-MS: (ESI, m/z): $[M + H]^+ = 321$. ^{1}H NMR (400 MHz, DMSO-d_6) δ 10.68 (s, 1H), 8.70–8.67 (m, 1H), 8.33 (d, J = 8.4 Hz, 1H), 7.70–7.66 (m, 1H), 7.59–7.52 (m, 5H), 7.23–7.19 (m, 1H), 4.78–4.72 (m, 1H), 2.75 (s, 3H), 1.34 (d, J = 6.0 Hz, 6H).

NDC-9136. Into a stirred solution of 4-isopropoxybenzoic acid (1.80 g, 9.989 mmol) and DMF (50.0 µL) in DCM (30.0 mL), oxalyl chloride (6.0 mL, 2 M in DCM) was added dropwise at 0 °C under nitrogen. The resulting mixture was stirred for 1 h at room temperature and then concentrated under reduced pressure. The crude product was used in the next step directly without further purification. The residue was dissolved in DCM (30.0 mL) and added dropwise into a stirred solution of 2-methylquinolin-8-amine (1.70 g, 10.746 mmol) and TEA (2.17 g, 21.445 mmol) in DCM (30.0 mL) at 0 °C. The resulting mixture was stirred for 2 h at room temperature under a nitrogen atmosphere. LCMS showed that the SM was consumed and the product was formed. The resulting mixture was washed with water and dried over anhydrous Na_2SO_4. After filtration, the filtrate was concentrated under reduced pressure. The residue was purified via silica gel column chromatography eluting with EtOAc/DCM (0–5%) to afford the crude product. The crude product was dissolved in DCM (50 mL) and washed with 1N HCl (50 mL) and 10% $NaHCO_3$ (50 mL). The organic layers were dried over anhydrous Na_2SO_4. After filtration, the filtrate was concentrated under reduced pressure to afford 1.8 g (52% yield) of the title compound as a white solid. LC-MS: (ESI, m/z): $[M + H]^+ = 321$. ^{1}H NMR (400 MHz, DMSO-d_6) δ 10.63 (s, 1H), 8.71–8.67 (m, 1H), 8.33 (d, J = 8.4 Hz, 1H), 8.01–7.95 (m, 2H), 7.68–7.63 (m, 1H), 7.59–7.52 (m, 2H), 7.13 (d, J = 9.2 Hz, 2H), 4.82–4.72 (m, 1H), 2.78 (s, 3H), 1.32 (d, J = 6.0 Hz, 6H).

NDC-9342. To a stirred solution of 4,5-dibromothiophene-2-carboxylic acid (7.00 g, 24.5 mmol) in DCM (70 mL), DMF was added (47.2 mg, 0.646 mmol), and the mixture was allowed to cool down to 0 °C. Then, oxalic dichloride (6.30 g, 49.6 mmol) was added dropwise at 0 °C under a nitrogen atmosphere. The resulting mixture was stirred for 2 h at room temperature under a nitrogen atmosphere. The resulting mixture was concentrated under reduced pressure. The crude product was used in the next step directly without further purification. The residue was dissolved in DCM (30 mL) and added dropwise into a stirred solution of 2-methylquinolin-8-amine (4.40 g, 27.8 mmol) and TEA (7.10 g, 70.2 mmol) in DCM (40 mL) at 0 °C. The resulting mixture was stirred for 2 h at room temperature under a nitrogen atmosphere. The desired product could be detected via LC-MS. The mixture was washed with 100 mL of water, and the aqueous phase was extracted with DCM (80 mL). The combined organic layers were concentrated under reduced

pressure. The residue was purified via silica gel column chromatography and eluted with PE/EA = 63/37 to afford 9.00 g of the product. Then, 30 mL of EA was added carefully into 4,5-dibromo-N-(2-methylquinolin-8-yl)thiophene-2-carboxamide (purity >95%) to form a light yellow slurry. The resulting slurry was stirred for 36 h at room temperature. After filtration, the solid was collected and dried overnight at 40 °C to afford 4,5-dibromo-N-(2-methylquinolin-8-yl)thiophene-2-carboxamide (6.55 g, 62%) as an off-white solid. LC/MS (ESI, m/z): $[M + H]^+$ = 426.6. ^{1}H NMR (300 MHz, $CDCl_3$) δ 10.61 (s, 1H), 8.72 (dd, J = 6.2, 2.8 Hz, 1H), 8.10 (d, J = 8.4 Hz, 1H), 7.56–7.47 (m, 3H), 7.38–7.36 (m, 1H), 2.78 (s, 3H).

4.2. Biochemical Analysis of SERCA PAMs

SERCA Activity Assay. ATPase assays in HEK 293 lysates were carried out using the ATPase Assay Kit (Colorimetric; Cat. No. ab234055; Abcam, Cambridge, UK) as per the manufacturer's instructions. Briefly, HEK 293 cells and either DMSO as a control or 2 μM of the test compound were incubated in the provided assay buffer containing ATPase substrate and developed at 25 °C for 20 min, and the A_{650} was measured using an Accuris SmartReader 96 Microplate Reader (Benchmark Scientific Inc., Sayreville, NJ, USA).

4.3. Animals

Albino inbred mice (FVB/NJ) were obtained from the Jackson Laboratory (Jackson Laboratory, Bar Harbor, ME, USA, strain #001800) and used as a source of brain tissue for experiments with primary hippocampal cultures. The 5xFAD mice (Jackson Laboratory, Bar Harbor, ME, USA, strain #034840-JAX) in a B6SJLF1 background were obtained from the Jackson Laboratory and used as a source of brain slices for LTP induction experiments. These mice were established and maintained in a vivarium with 4 to 5 mice per cage and a 12-hour light/dark cycle in the animal facility. Food and water were available ad libitum. All procedures adhered to the principles of the European Convention and the Declaration of Helsinki regarding the humane treatment of animals and were approved by the Bioethics Committee of Peter the Great St. Petersburg Polytechnic University in St. Petersburg, Russia (Ethical Permit No. 2-n-b from 25 January 2021).

4.4. Primary Hippocampal Cultures, Calcium Phosphate Transfection, and Immunohistochemistry

Primary hippocampal neuronal cultures of dissociated hippocampal cells were prepared from newborn FVB mice and maintained in culture as described previously [31]. Briefly, the hippocampus from postnatal day 0–1 was incubated with papain solution for 30 min at 37 °C (Worthington Biochemical Corp., Lakewood, NJ, USA, #3176) then dissociated with a solution of deoxyribonuclease I (5 mg/mL; Macherey Nagel GMBH, Germany, #R1542S). The neurons were placed in a 24-well plate on 12 mm glass cover glasses pre-coated with 1% poly-D-lysine (Sigma-Aldrich, St Louis, MO, USA, #p-7886). Cells were grown in 1 mL Neurobasal-A (Thermo Fisher Scientific, Waltham, MA, USA, #10888022) supplemented with 2% B27 (Thermo Fisher Scientific, Waltham, MA, USA, #17504044), 1% heat-inactivated fetal bovine serum (FBS, Thermo Fisher Scientific, Waltham, MA, USA, #10500064), and 0.5 mM L-glutamine (Thermo Fisher Scientific, Waltham, MA, USA, #25030024), and were maintained at 37 °C in a 5% CO_2 incubator in a 24-well glass plate. Transfection was performed according to [41] with a calcium transfection kit purchased from Clontech (Takara Bio, Kusatsu, Japan, #631312) with GFP plasmid. Preparation of the oligomeric beta-amyloid was described in [31]. Cells were incubated with Aβ for 72 h. The cells were incubated with 0.1 μM of one of the four PAMs (NDC-9009, NDC-9033, NDC-9136, or NDC-9342) or an equal volume of DMSO for 24 h before fixation.

4.5. HEK293T Cultures and Transfection with Polyethyleneamine

HEK293T line cells with 50–70% of confluency were co-transfected with the GCaMP5.3 plasmid using a polyethylenimine reagent (Polysciences Inc., Warrington, PA, USA, #23966) in serum-free Opti-MEM medium (Thermo Fisher Scientific, Waltham, MA, USA, #11058-021). After 3 h of incubation in a CO_2 incubator, the Opti-MEM was replaced with full

DMEM (Thermo Fisher Scientific, Waltham, MA, USA, #41965-039; 10% FBS; 1% Pen Strep, Thermo Fisher Scientific, Waltham, MA, USA, #15140-122). HEK293T cells were grown to a confluence of 40% to 50% on round coverslips (12 mm diameter) in one well of a 24-well culture plate.

4.6. Intraperitoneal Administration

In order to evaluate the neuroprotective efficacy of a positive allosteric modulator on long-term potentiation (LTP), NDC9009 was administered intraperitoneally (10 mg/kg; DMSO + NDC9009:TWEEN80:water at a 10:10:80 ratio) with daily injections for 4 weeks (5 days every week) starting at 5 months [13]. Control mice were administered the vehicle, which consisted of DMSO:TWEEN80:water at a 10:10:80 ratio. The daily injections occurred for 4 weeks on weekdays only starting when the mice were 5 months of age.

4.7. Long-Term Potentiation Recording

For the long-term potentiation experiments, male wild-type mice and the 5xFAD mouse line were utilized. At 6 months of age, acute living hippocampal slices from injected mice were prepared, and field excitatory postsynaptic potentials (fEPSPs) were recorded to evaluate the magnitude of long-term potentiation. For this purpose, mice were anesthetized with isoflurane (1.5–2%) and perfused transcardially with ice-cold modified artificial cerebrospinal fluid containing (in mM) 25 D-glucose, 5 HEPES, 124 NaCl, 2.5 KCl, 3 Na-pyruvate, 1.25 $NaH_2PO_4 \cdot 2H_2O$, 24 $NaHCO_3$, 0.5 $CaCl_2 \cdot 2H_2O$, and 10 $MgSO_4 \cdot 7H_2O$ (pH 7.3–7.4). Brains were rapidly removed into ice-cold modified artificial cerebrospinal fluid. The 400 µm thick slices were cut on a vibratome (Leica Microsystems, Wetzlar, Germany) and immediately transferred to an incubation chamber. The slices were incubated to recover at 32 °C for 30 min and transferred to an incubation chamber artificial cerebrospinal fluid containing (in mM) 25 D-glucose, 5 HEPES, 124 NaCl, 2.5 KCl, 1.25 $NaH_2PO_4 \cdot 2H_2O$, 24 $NaHCO_3$, 2.6 $CaCl_2 \cdot 2H_2O$, and 1.3 $MgSO_4 \cdot 7H_2O$ (pH 7.3–7.4) for 60 min at room temperature. During the slice preparation and recording, artificial cerebrospinal fluid was continuously mixed with the gas, including 95% O_2 and 5% CO_2. Following incubation at room temperature, the hippocampus slice was transferred to the recording chamber and allowed to equilibrate for an additional 20 min prior to the recording of fEPSPs.

The stimulating bipolar electrode was prepared by double-twisting two platinum-iridium wires with a diameter of 50 microns (A-M Systems Inc., Carlsborg, WA, USA). The CA1 region located at the boundary between the CA1 and CA2 regions of the hippocampus was chosen as the stimulation site; the recording site was determined by the occurrence of an fEPSP response in the CA1 area. The fEPSPs were evoked by a Model 2100 isolated pulse stimulator (A-M Systems Inc., Carlsborg, WA, USA); the stimulation current (from 10 µA in steps of 5–10 µA) was adjusted accordingly until the occurrence of a population spike. The evoked fEPSPs were amplified with a MultiClamp 700B (Molecular Devices, San Jose, CA, USA) and digitized with a Digidata 1440A (Molecular Devices, San Jose, CA, USA) at a 20 kHz sampling rate. Baseline responses were stabilized (fEPSP slope deviation of less than 10%) and then recorded for 20 min at 0.05 Hz of stimulation. Long-term potentiation was then induced by high-frequency stimulation (HFS), which consisted of two bursts with an interval of 20 s; each burst had a duration of 1s and a stimulation frequency of 100 Hz. After HFS, the stimulus was repeatedly delivered once every 20 s for 60 min to observe any changes in the LTP magnitude. The LTP magnitude was defined as the ratio between the average fEPSP slope after HFS during the last 10 min and the average slope of the baseline fEPSPs. Post-tetanic potentiation (PTP) was defined as the ratio between the average fEPSP slope after HFS during the first 2 min and the average slope of the baseline fEPSPs. Traces were obtained and analyzed using the pClamp 10.7 software program (Molecular Devices, San Jose, CA, USA).

4.8. Analysis of Dendritic Spine Morphology in Primary Hippocampal Cultures

For assessment of the dendritic spine morphology, a Z-stack of the optical section was captured with a confocal microscope (Leica TCS SP8). For dendritic analysis, 2048 × 2048-pixel images with a 0.032 µm/pixel resolution were captured with Z interval of 0.2 µm using a 10× objective lens (NA = 0.85, UPlanSApo; Olympus, Tokyo, Japan). The images were pre-processed with ImageJ's built-in "Median" filter to remove noise. Quantitative analysis of the dendritic spines, including measurements of the dendritic spine head area, neck length, and neck length/dendritic spine length ratio, was performed using SpineJ v1.0 software [42].

4.9. Calcium Imaging

Cells of the HEK293T line were transfected with a GCaMP5.3 expression plasmid using polyethyleneamine, as described earlier. Live fluorescent images were collected every 0.5 s using an Olympus IX73 fluorescent microscope with a 10× objective (UPlanFL N, Olympus, Tokyo, Japan) and a ZYLA 4.2 sCMOS camera (Andor Technology Ltd, Belfast, UK). Cells were incubated in 2 M Ca^{2+} ADMEM solution (110 mM NaCl, 5.3 mM KCl, 25 mM D-glucose, and 10 mM HEPES; pH = 7.4) for 10 min. After recording basal fluorescent signals in the 2 M Ca^{2+} ADMEM solution for 30 s, release of ER Ca^{2+} was induced via puff application of 0.2 µL of ionomycin and 1 µL of one of the four PAMs (NDC-9009, NDC-9033, NDC-9136, or NDC-9342). Analysis of the data was performed using ImageJ software. The ROI used in the image analysis was chosen to correspond to spines, and the signal was normalized to the baseline.

4.10. Statistical Analyses

Statistical data analysis was performed using R studio software and GraphPad Prism software. To determine the distribution, the Shapiro–Wilk test or Lillifors test was calculated. If the distribution was not normal, the Kruskal–Wallis test was used. For multiple pairwise comparisons, Dunn's nonparametric test or the Conover–Iman test were used. The one-way ANOVA test was employed to analyze the data assuming a normal distribution. Subsequently, the Tukey test was applied to facilitate multiple pairwise comparisons. Statistical tests are indicated in the figure legends. The data are presented as the mean ± S.E.M.

Supplementary Materials: The following supporting information can be downloaded at: https://www.mdpi.com/article/10.3390/ijms241813973/s1, Figure S1: Representative images of amyloid plaques (indicated by white triangles) in the brains of 6-month-old 5xFAD and WT mice in the hippocampal CA1 region and the cortical S1 region.

Author Contributions: Conceptualization, I.B. and E.P.; methodology, A.R., A.E. and R.D.; formal analysis, A.R. and A.E; investigation, A.R., A.E., E.V. and R.D.; resources, R.D. and I.B.; data curation, A.R., A.E., E.V. and R.D.; writing—original draft preparation, A.R. and A.E.; writing—review and editing, E.P., R.D. and I.B.; visualization, A.R. and A.E.; supervision, E.P. and I.B.; project administration, E.P.; funding acquisition, R.D. and I.B. All authors have read and agreed to the published version of the manuscript.

Funding: This research was funded by the Russian Science Foundation under grant 22-15-00049 (I.B.), by the National Institutes of Health under grants R01AG071310 (I.B.) and R42AG062001 (R.D.), and by the Neurodon Corporation (R.D.).

Institutional Review Board Statement: The study was conducted in accordance with the Declaration of Helsinki and approved by the Bioethics Committee of Peter the Great St. Petersburg Polytechnic University in St. Petersburg, Russia (Ethical Permit No. 2-n-b from 25 January 2021).

Informed Consent Statement: Not applicable.

Data Availability Statement: Not applicable.

Acknowledgments: The authors thank members of the Molecular Neurodegeneration Laboratory for their help, Asya Bolshakova for lab management and reagent supply, and Olga Vlasova for organizational support. I.B. holds the Carl J. and Hortense M. Thomsen Chair in Alzheimer's Disease Research.

Conflicts of Interest: R.D. is an inventor of the US patents 11,730,729 and 10,772,881 ("Quinolines that modulate SERCA and their use for treating disease") and US patent application 17/401,642, which describe all of the compounds disclosed herein and are assigned to the Neurodon Corporation. Part of the cost of this research was paid for by Neurodon. R.D. is an employee of Neurodon. I.B. is a member of Neurodon SAB. R.D. and I.B. hold Neurodon stock or stock options.

References

1. Selkoe, D.J.; Hardy, J. The amyloid hypothesis of Alzheimer's disease at 25 years. *EMBO Mol. Med.* **2016**, *8*, 595–608. [CrossRef] [PubMed]
2. Wojtunik-Kulesza, K.; Rudkowska, M.; Orzel-Sajdlowska, A. Aducanumab-Hope or Disappointment for Alzheimer's Disease. *Int. J. Mol. Sci.* **2023**, *24*, 4367. [CrossRef] [PubMed]
3. Tampi, R.R.; Forester, B.P.; Agronin, M. Aducanumab: Evidence from clinical trial data and controversies. *Drugs Context* **2021**, *10*, 2021–2027. [CrossRef]
4. Kepp, K.P.; Sensi, S.L.; Johnsen, K.B.; Barrio, J.R.; Hoilund-Carlsen, P.F.; Neve, R.L.; Alavi, A.; Herrup, K.; Perry, G.; Robakis, N.K.; et al. The Anti-Amyloid Monoclonal Antibody Lecanemab: 16 Cautionary Notes. *J. Alzheimers Dis.* **2023**, *94*, 497–507. [CrossRef] [PubMed]
5. Hoilund-Carlsen, P.F.; Revheim, M.E.; Costa, T.; Alavi, A.; Kepp, K.P.; Sensi, S.L.; Perry, G.; Robakis, N.K.; Barrio, J.R.; Vissel, B. Passive Alzheimer's immunotherapy: A promising or uncertain option? *Ageing Res. Rev.* **2023**, *90*, 101996. [CrossRef] [PubMed]
6. Desai, B.N.; Leitinger, N. Purinergic and calcium signaling in macrophage function and plasticity. *Front. Immunol.* **2014**, *5*, 580. [CrossRef]
7. Sebastiao, A.M.; Ribeiro, J.A. Neuromodulation and metamodulation by adenosine: Impact and subtleties upon synaptic plasticity regulation. *Brain Res.* **2015**, *1621*, 102–113. [CrossRef]
8. Bezprozvanny, I.; Mattson, M.P. Neuronal calcium mishandling and the pathogenesis of Alzheimer's disease. *Trends Neurosci.* **2008**, *31*, 454–463. [CrossRef] [PubMed]
9. Alzheimer's Association Calcium Hypothesis Workgroup; Khachaturian, Z.S. Calcium hypothesis of Alzheimer's disease and brain aging: A framework for integrating new evidence into a comprehensive theory of pathogenesis. *Alzheimer's Dement.* **2017**, *13*, 178–182.e17.
10. Lipton, S.A. Paradigm shift in neuroprotection by NMDA receptor blockade: Memantine and beyond. *Nat. Rev. Drug Discov.* **2006**, *5*, 160–170. [CrossRef]
11. McShane, R.; Westby, M.J.; Roberts, E.; Minakaran, N.; Schneider, L.; Farrimond, L.E.; Maayan, N.; Ware, J.; Debarros, J. Memantine for dementia. *Cochrane Database Syst. Rev.* **2019**, *3*, CD003154. [CrossRef]
12. Dahl, R.; Moore, A.C.; Knight, C.; Mauger, C.; Zhang, H.; Schiltz, G.E.; Koss, W.A.; Bezprozvanny, I. Positive Allosteric Modulator of SERCA Pump NDC-1173 Exerts Beneficial Effects in Mouse Model of Alzheimer's Disease. *Int. J. Mol. Sci.* **2023**, *24*, 11057. [CrossRef]
13. Krajnak, K.; Dahl, R. A new target for Alzheimer's disease: A small molecule SERCA activator is neuroprotective in vitro and improves memory and cognition in APP/PS1 mice. *Bioorganic Med. Chem. Lett.* **2018**, *28*, 1591–1594. [CrossRef]
14. Cornea, R.L.; Gruber, S.J.; Lockamy, E.L.; Muretta, J.M.; Jin, D.; Chen, J.; Dahl, R.; Bartfai, T.; Zsebo, K.M.; Gillispie, G.D.; et al. High-throughput FRET assay yields allosteric SERCA activators. *J. Biomol. Screen.* **2013**, *18*, 97–107. [CrossRef]
15. Khan, H.; Metra, M.; Blair, J.E.; Vogel, M.; Harinstein, M.E.; Filippatos, G.S.; Sabbah, H.N.; Porchet, H.; Valentini, G.; Gheorghiade, M. Istaroxime, a first in class new chemical entity exhibiting SERCA-2 activation and Na-K-ATPase inhibition: A new promising treatment for acute heart failure syndromes? *Heart Fail. Rev.* **2009**, *14*, 277–287. [CrossRef] [PubMed]
16. Gobbini, M.; Armaroli, S.; Banfi, L.; Benicchio, A.; Carzana, G.; Fedrizzi, G.; Ferrari, P.; Giacalone, G.; Giubileo, M.; Marazzi, G.; et al. Novel analogues of istaroxime, a potent inhibitor of Na^+,K^+-ATPase: Synthesis and structure-activity relationship. *J. Med. Chem.* **2008**, *51*, 4601–4608. [CrossRef]
17. Chakroborty, S.; Kim, J.; Schneider, C.; West, A.R.; Stutzmann, G.E. Nitric oxide signaling is recruited as a compensatory mechanism for sustaining synaptic plasticity in Alzheimer's disease mice. *J. Neurosci.* **2015**, *35*, 6893–6902. [CrossRef] [PubMed]
18. Fioravante, D.; Regehr, W.G. Short-term forms of presynaptic plasticity. *Curr. Opin. Neurobiol.* **2011**, *21*, 269–274. [CrossRef]
19. Frey, U.; Huang, Y.Y.; Kandel, E.R. Effects of cAMP simulate a late stage of LTP in hippocampal CA1 neurons. *Science* **1993**, *260*, 1661–1664. [CrossRef]
20. Khachaturian, Z.S. Calcium, membranes, aging, and alzheimers-disease-introduction and overview. *Ann. N. Y. Acad. Sci.* **1989**, *568*, 1–4. [CrossRef] [PubMed]
21. Chami, M.; Checler, F. Alterations of the endoplasmic reticulum (ER) calcium signaling molecular components in Alzheimer's disease. *Cells* **2020**, *9*, 2577. [CrossRef] [PubMed]
22. Tu, H.; Nelson, O.; Bezprozvanny, A.; Wang, Z.; Lee, S.-F.; Hao, Y.-H.; Serneels, L.; De Strooper, B.; Yu, G.; Bezprozvanny, I. Presenilins form ER Ca^{2+} leak channels, a function disrupted by familial Alzheimer's disease-linked mutations. *Cell* **2006**, *126*, 981–993. [CrossRef]
23. Nelson, O.; Tu, H.; Lei, T.; Bentahir, M.; De Strooper, B.; Bezprozvanny, I. Familial Alzheimer disease–linked mutations specifically disrupt Ca^{2+} leak function of presenilin 1. *J. Clin. Investig.* **2007**, *117*, 1230–1239. [CrossRef]

24. Cheung, K.-H.; Mei, L.; Mak, D.-O.D.; Hayashi, I.; Iwatsubo, T.; Kang, D.E.; Foskett, J.K. Gain-of-function enhancement of IP3 receptor modal gating by familial Alzheimer's disease–linked presenilin mutants in human cells and mouse neurons. *Sci. Signal.* **2010**, *3*, ra22. [CrossRef]
25. Stutzmann, G.E.; Smith, I.; Caccamo, A.; Oddo, S.; LaFerla, F.M.; Parker, I. Enhanced ryanodine receptor recruitment contributes to Ca2+ disruptions in young, adult, and aged Alzheimer's disease mice. *J. Neurosci.* **2006**, *26*, 5180–5189. [CrossRef]
26. Yoo, A.S.; Cheng, I.; Chung, S.; Grenfell, T.Z.; Lee, H.; Pack-Chung, E.; Handler, M.; Shen, J.; Xia, W.; Tesco, G. Presenilin-mediated modulation of capacitative calcium entry. *Neuron* **2000**, *27*, 561–572. [CrossRef] [PubMed]
27. Krause, T.; Gerbershagen, M.; Fiege, M.; Weisshorn, R.; Wappler, F. Dantrolene–a review of its pharmacology, therapeutic use and new developments. *Anaesthesia* **2004**, *59*, 364–373. [CrossRef]
28. Liu, J.; Supnet, C.; Sun, S.; Zhang, H.; Good, L.; Popugaeva, E.; Bezprozvanny, I. The role of ryanodine receptor type 3 in a mouse model of Alzheimer disease. *Channels* **2014**, *8*, 230–242. [CrossRef] [PubMed]
29. Zhang, H.; Sun, S.; Wu, L.; Pchitskaya, E.; Zakharova, O.; Tacer, K.F.; Bezprozvanny, I. Store-operated calcium channel complex in postsynaptic spines: A new therapeutic target for Alzheimer's disease treatment. *J. Neurosci.* **2016**, *36*, 11837–11850. [CrossRef]
30. Zhang, H.; Wu, L.; Pchitskaya, E.; Zakharova, O.; Saito, T.; Saido, T.; Bezprozvanny, I. Neuronal store-operated calcium entry and mushroom spine loss in amyloid precursor protein knock-in mouse model of Alzheimer's disease. *J. Neurosci.* **2015**, *35*, 13275–13286. [CrossRef]
31. Popugaeva, E.; Pchitskaya, E.; Speshilova, A.; Alexandrov, S.; Zhang, H.; Vlasova, O.; Bezprozvanny, I. STIM2 protects hippocampal mushroom spines from amyloid synaptotoxicity. *Mol. Neurodegener.* **2015**, *10*, 37. [CrossRef]
32. Jin, H.; Sanjo, N.; Uchihara, T.; Watabe, K.; George-Hyslop, P.S.; Fraser, P.E.; Mizusawa, H. Presenilin-1 holoprotein is an interacting partner of sarco endoplasmic reticulum calcium-ATPase and confers resistance to endoplasmic reticulum stress. *J. Alzheimer's Dis.* **2010**, *20*, 261–273. [CrossRef]
33. Rahate, K.; Bhatt, L.K.; Prabhavalkar, K.S. SERCA stimulation: A potential approach in therapeutics. *Chem. Biol. Drug Des.* **2020**, *95*, 5–15. [CrossRef]
34. Fisher, M.L.E.; Bovo, E.; Aguayo-Ortiz, R.; Cho, E.E.; Pribadi, M.P.; Dalton, M.P.; Rathod, N.; Lemieux, M.J.; Espinoza-Fonseca, L.M.; Robia, S.L. Dwarf open reading frame (DWORF) is a direct activator of the sarcoplasmic reticulum calcium pump SERCA. *Elife* **2021**, *10*, e65545. [CrossRef]
35. Kaneko, M.; Yamamoto, H.; Sakai, H.; Kamada, Y.; Tanaka, T.; Fujiwara, S.; Yamamoto, S.; Takahagi, H.; Igawa, H.; Kasai, S. A pyridone derivative activates SERCA2a by attenuating the inhibitory effect of phospholamban. *Eur. J. Pharmacol.* **2017**, *814*, 1–8. [CrossRef]
36. Gruber, S.J.; Cornea, R.L.; Peterson, K.C.; Gillispie, G.D.; Robia, S.L.; Thomas, D.D. Discovery of enzyme modulators via high-throughput time-resolved FRET in living cells. *Biophys. J.* **2014**, *106*, 427a–428a. [CrossRef]
37. Sordi, G.; Goti, A.; Young, H.S.; Palchetti, I.; Tadini-Buoninsegni, F. Stimulation of Ca2+-ATPase Transport Activity by a Small-Molecule Drug. *ChemMedChem* **2021**, *16*, 3293–3299. [CrossRef]
38. Britzolaki, A.; Cronin, C.C.; Flaherty, P.R.; Rufo, R.L.; Pitychoutis, P.M. Chronic but not acute pharmacological activation of SERCA induces behavioral and neurochemical effects in male and female mice. *Behav. Brain Res.* **2021**, *399*, 112984. [CrossRef]
39. Sasaguri, H.; Hashimoto, S.; Watamura, N.; Sato, K.; Takamura, R.; Nagata, K.; Tsubuki, S.; Ohshima, T.; Yoshiki, A.; Sato, K.; et al. Recent Advances in the Modeling of Alzheimer's Disease. *Front. Neurosci.* **2022**, *16*, 807473. [CrossRef]
40. Saito, T.; Matsuba, Y.; Mihira, N.; Takano, J.; Nilsson, P.; Itohara, S.; Iwata, N.; Saido, T.C. Single App knock-in mouse models of Alzheimer's disease. *Nat. Neurosci.* **2014**, *17*, 661–663. [CrossRef]
41. Sun, S.; Zhang, H.; Liu, J.; Popugaeva, E.; Xu, N.-J.; Feske, S.; White, C.L.; Bezprozvanny, I. Reduced synaptic STIM2 expression and impaired store-operated calcium entry cause destabilization of mature spines in mutant presenilin mice. *Neuron* **2014**, *82*, 79–93. [CrossRef] [PubMed]
42. Levet, F.; Tønnesen, J.; Nägerl, U.V.; Sibarita, J.-B. SpineJ: A software tool for quantitative analysis of nanoscale spine morphology. *Methods* **2020**, *174*, 49–55. [CrossRef]

International Journal of
Molecular Sciences

MDPI

Article

Therapeutic Effects of Aβ-Specific Regulatory T Cells in Alzheimer's Disease: A Study in 5xFAD Mice

Seon-Young Park [1], Juwon Yang [2], Hyejin Yang [1], Inhee Cho [2], Jae Yoon Kim [3] and Hyunsu Bae [1,2,*]

[1] Department of Science in Korean Medicine, College of Korean Medicine, Graduate School, Kyung Hee University, 26 Kyungheedae-ro, Dongdaemun-gu, Seoul 02447, Republic of Korea; psys12@naver.com (S.-Y.P.); emilly86@naver.com (H.Y.)
[2] Department of Korean Medicine, College of Korean Medicine, Graduate School, Kyung Hee University, 26 Kyungheedae-ro, Dongdaemun-gu, Seoul 02447, Republic of Korea; jwyang@khu.ac.kr (J.Y.); okoriental@naver.com (I.C.)
[3] Institute of Life Science & Biotechnology, VT Bio. Co., Ltd., 16 Samseong-ro 76-gil, Gangnam-gu, Seoul 06185, Republic of Korea; jykim@vtbio.co.kr
* Correspondence: hbae@khu.ac.kr

Abstract: The aging global population is placing an increasing burden on healthcare systems, and the social impact of Alzheimer's disease (AD) is on the rise. However, the availability of safe and effective treatments for AD remains limited. Adoptive Treg therapy has been explored for treating neurodegenerative diseases, including AD. To facilitate the clinical application of Treg therapy, we developed a Treg preparation protocol and highlighted the therapeutic effects of Tregs in 5xFAD mice. $CD4^+CD25^+$ Tregs, isolated after Aβ stimulation and expanded using a G-rex plate with a gas-permeable membrane, were adoptively transferred into 5xFAD mice. Behavioral analysis was conducted using Y-maze and passive avoidance tests. Additionally, we measured levels of Aβ, phosphorylated tau (pTAU), and nitric oxide synthase 2 (NOS2) in the hippocampus. Real-time RT-PCR was employed to assess the mRNA levels of pro- and anti-inflammatory markers. Our findings indicate that Aβ-specific Tregs not only improved cognitive function but also reduced Aβ and pTAU accumulation in the hippocampus of 5xFAD mice. They also inhibited microglial neuroinflammation. These effects were observed at doses as low as 1.5×10^3 cells/head. Collectively, our results demonstrate that Aβ-specific Tregs can mitigate AD pathology in 5xFAD mice.

Keywords: Alzheimer's disease; regulatory T cells; Amyloid-β

Citation: Park, S.-Y.; Yang, J.; Yang, H.; Cho, I.; Kim, J.Y.; Bae, H. Therapeutic Effects of Aβ-Specific Regulatory T Cells in Alzheimer's Disease: A Study in 5xFAD Mice. *Int. J. Mol. Sci.* **2024**, *25*, 783. https://doi.org/10.3390/ijms25020783

Academic Editor: Claudia Ricci

Received: 15 December 2023
Revised: 5 January 2024
Accepted: 5 January 2024
Published: 8 January 2024

1. Introduction

Presently, over 55 million individuals worldwide are affected by dementia, with nearly 10 million new cases emerging annually. Alzheimer's disease (AD) stands as the predominant form, constituting 60–70% of all dementia cases [1].

The neuropathological characteristics of AD encompass chronic neuroinflammation linked to the extracellular deposition of amyloid-β (Aβ), intraneural neurofibrillary tangles, astrocytosis, and microgliosis [2,3]. In central nervous system (CNS) disorders, including AD, neuroinflammation plays a role in the progression of pathology by influencing blood-brain barrier (BBB) integrity [4,5]. Amyloid-β and phosphorylated tau, distinctive AD proteins, form extracellular neuritis plaques and intracellular neurofibrillary tangles, representing focal points in AD research [6].

Regulatory T cells (Tregs) are indispensable for suppressing moderate immune responses and maintaining immune homeostasis. Several mechanisms of Treg-mediated suppression include the secretion of immunosuppressive cytokines by the Treg, cell-contact-dependent suppression, and functional modification or killing of antigen-presenting cells [7]. Their significance extends to neuroinflammation in the CNS [8]. Notably, impaired

Treg function has been identified in patients with multiple sclerosis (MS), and Treg accumulation has been linked to recovery in experimental autoimmune encephalomyelitis (EAE) models [9,10]. Similarly, a reduction in the number of Tregs has been reported in patients with mild AD [11].

Treg-based therapies have emerged as promising strategies, broadly categorized into two approaches. One involves the administration of immunomodulatory interventions designed to foster the expansion and enhance the function of Tregs in vivo. The alternative approach entails the adoptive transfer of Tregs that have been expanded in vitro. Tregs themselves can be further classified into antigen-specific and expanded polyclonal Tregs [12]. Polyclonal Treg-based cell therapy has successfully transitioned into clinical practice, with trials demonstrating the safety and efficacy of this Treg therapeutic approach. Moreover, in animal models, antigen-specific Tregs have shown functional superiority compared to polyclonal Tregs [13].

In our previous study, we manufactured antigen-specific Tregs and demonstrated their effectiveness in treating CNS disorders in a mouse model. We observed that the adoption of Aβ-specific Tregs attenuates the progression of AD [14], and administration of alpha-synuclein-specific Tregs ameliorates PD progression [15].

5xFAD and 3xTg represent the most commonly employed mouse models in AD research. 5xFAD mice bear mutations in the APP and presenilin (PS) genes, exhibiting amyloid deposition as early as 2 months. They swiftly manifest key AD pathology features, including neuronal loss and memory impairment, in contrast to 3xTg mice. Cognitive impairment resulting from these alterations can be evaluated through behavioral assessments, such as maze tests [16–18]. In our previous study, we manufactured antigen-specific Tregs and demonstrated their effectiveness in treating CNS disorders.

In a previous investigation, we used the 3xTg AD mouse model to explore the neuroprotective effect of improving the cognitive function of Tregs in AD [19]. Based on the results, we employed young 5xFAD mice and successfully replicated the therapeutic effects of Tregs.

In the present study, we employed a young AD mouse model to examine the impact of Aβ-specific Tregs and refined the Treg expansion protocol using Gas-permeable Rapid Expansion (G-Rex). Our objective was to enhance the reproducibility of experiments involving human Tregs and propel them toward becoming a viable treatment option for AD.

2. Results

2.1. Ex Vivo Expansion of Aβ-Specific Treg

For the development of a reproducible method for expanding Aβ-specific Treg for clinical applications, $CD4^+CD25^+$ Tregs were initially isolated and subsequently expanded using G-rex plates in vitro. We obtained splenocytes from wild-type (WT) mice and depleted CD8 cells to obtain CD8-cells. For antigen presentation, CD8-cells were incubated with Aβ and bee venom phospholipase A2 for a duration of 4 days and $CD4^+CD25^+$ Treg was isolated and expanded for 2 weeks (details provided in 'Section 4') (Figure 1A).

The purity of the isolated cells was assessed by flow cytometry. CD8-cells were stained with FITC-CD8 after CD8 depletion and, as a result, it was confirmed that most CD8+ cells were depleted. After Treg isolation, the isolated Tregs were stained with PE-Cy5-CD4 and APC-cy7-CD25, and the purity of Tregs was confirmed to be over 97%. Tregs cultured in G-rex were confirmed to be expanded by staining with PE-Cy5-CD4 and APC-cy7-CD25 (Figure 1B).

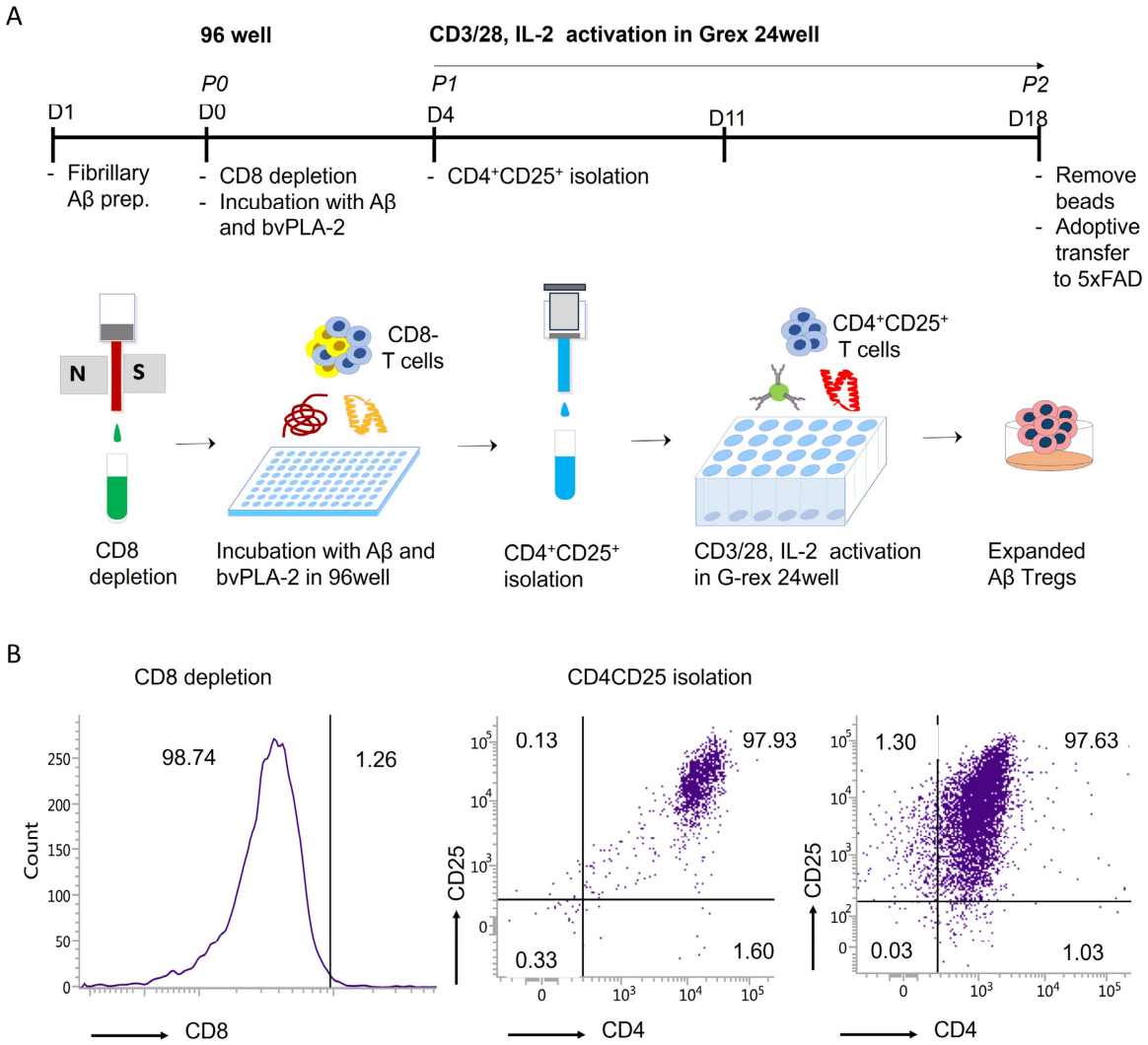

Figure 1. Ex vivo expansion of Aβ-specific Treg. (**A**) Schematic representation of the ex vivo expansion of Aβ-specific Treg. (**B**) The purity of isolated Aβ-specific Treg was analyzed by flow cytometry. Aβ-specific Tregs were stained with FITC-CD8 after CD8 depletion and PE-Cy5-CD4 and APC-cy7-CD25 after Treg isolation and expansion.

2.2. Treg Transfer Ameliorates Cognitive Dysfunction in 5xFAD Mice

To evaluate the therapeutic effects of ex vivo-expanded Tregs in AD, groups of 5xFAD mice were administered 1.5×10^3, 10^4, and 10^5 ex vivo-expanded Tregs. Behavioral tests were conducted after eight weeks (Figure 2A). Y-maze alternation tests were employed to assess cognitive function (Figure 2B). Mice were allowed to explore all three arms of the Y-maze freely, and spontaneous alternation was calculated. The ex vivo-expanded Tregs improved alternation scores, which were reduced in 5xFAD mice. In the passive avoidance experiment, mice were trained to escape the conditioning chamber with the foot shock. The test result showed that the escape latency of passive avoidance in the ex vivo-expanded Tregs injected group was significantly increased compared to the 5xFAD mice (Figure 2C). Notably, these effects on cognitive function were dose-dependent.

2.3. Treg Transfer Reduces Accumulation of aβ and Phosphorylated-Tau in 5xFAD Mice

The accumulation of Aβ stands as a prominent pathological hallmark in AD [20]. We extracted the brains of mice that completed behavioral testing for 8 weeks after infusion of Tregs expanded at various doses and quantified Aβ levels in the hippocampal CA1 region using immunofluorescence (Figure 3A). Aβ fluorescence intensity increased in the 5xFAD

mice compared to WT (Figure 3B) but significantly decreased in the group transferred ex vivo-expanded Tregs ($p < 0.001$).

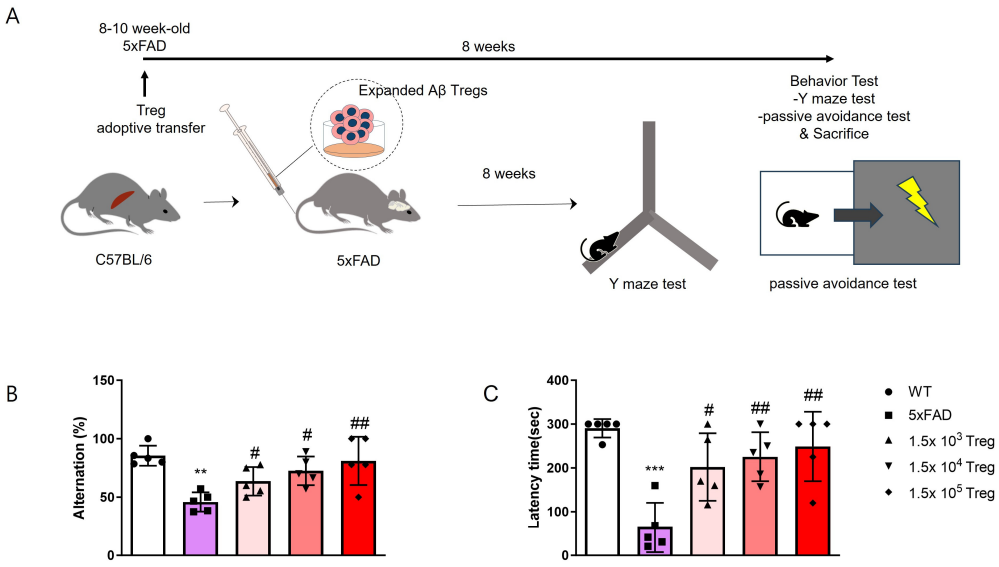

Figure 2. Treg transfer ameliorates cognitive dysfunction in 5xFAD mice. (**A**) Schematic representation of Treg adoptive transfer to 5xFAD mice and behavior test. (**B**) The alternation of Y maze test. (**C**) The latency time in the passive avoidance test (** $p < 0.01$, *** $p < 0.001$ vs. the WT group and # $p < 0.05$, ## $p < 0.01$, vs. the 5xFAD group, one-way ANOVA, Newman-Keuls multiple comparison test ($n = 5$). Data are presented as the mean ± SEM).

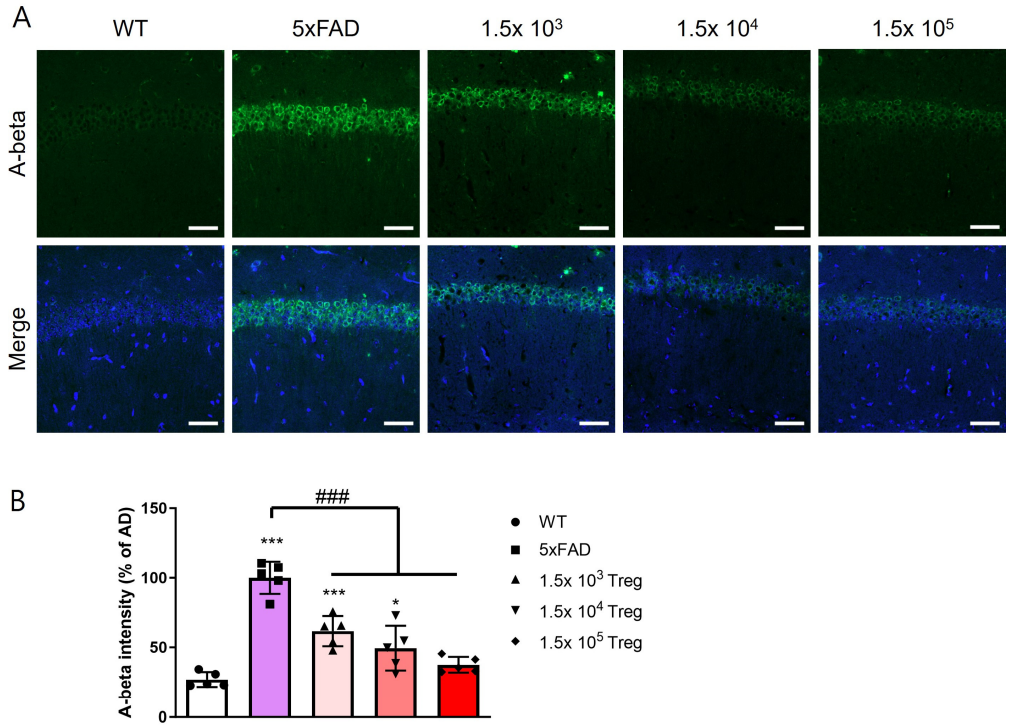

Figure 3. Treg transfer reduces the accumulation of Aβ in 5xFAD mice. (**A**) The expression levels of Aβ in the CA1 of the hippocampus were assessed with immunostaining. (**B**) Aβ intensity in the CA1 of the hippocampus (* $p < 0.05$, *** $p < 0.001$ vs. the WT group and ### $p < 0.001$ vs. the 5xFAD group, one-way ANOVA, Newman–Keuls multiple comparison test ($n = 5$). Data are shown as the mean ± SEM).

Additionally, we assessed the levels of phosphorylated tau (p-tau), another hallmark of AD (Figure 4A). In 5xFAD mice, p-tau deposition was elevated compared to that in WT group, yet this elevation was mitigated by the transfer of ex vivo-expanded Tregs (Figure 4B). The fluorescence intensity of p-tau in groups of 1.5×10^4 and 10^5 ex vivo-expanded Tregs transfered with 5xFAD mice is similar to WT. These findings imply that ex vivo-expanded Tregs play a role in ameliorating AD pathology.

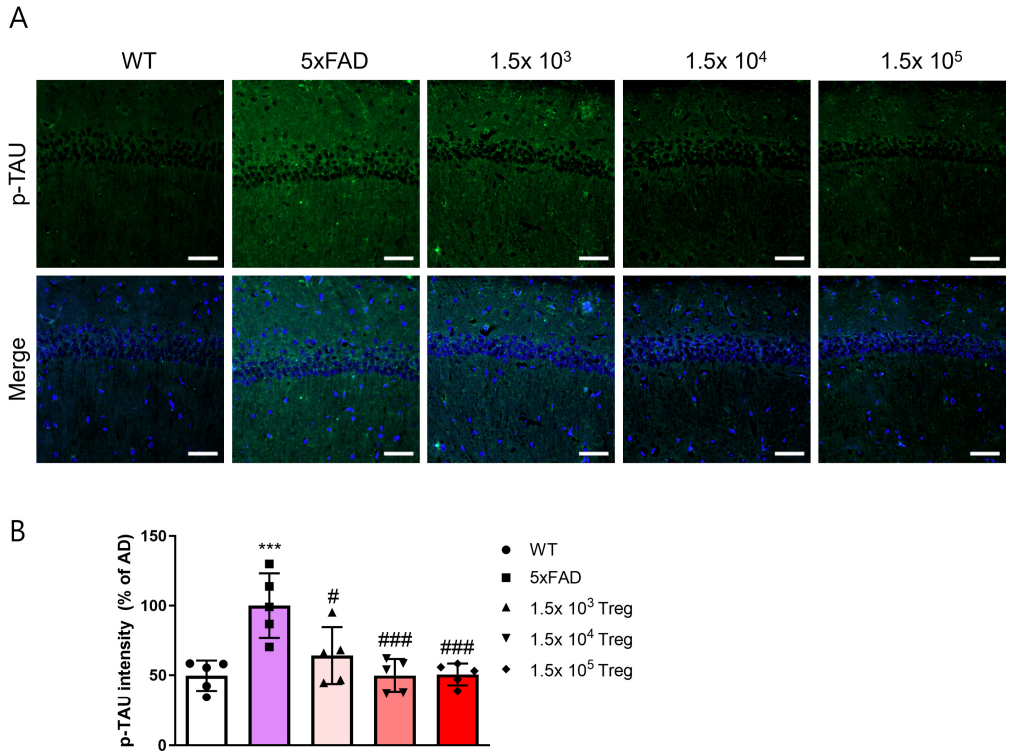

Figure 4. Treg transfer reduces the accumulation of p-TAU in 5xFAD mice. (**A**) The expression levels of p-TAU in the CA1 of the hippocampus were assessed with immunostaining. (**B**) p-TAU intensity in the CA1 of the hippocampus (*** $p < 0.001$ vs. the WT group and # $p < 0.05$, ### $p < 0.001$ vs. the 5xFAD group, one-way ANOVA, Newman–Keuls multiple comparison test ($n = 5$). Data are shown as the mean ± SEM).

2.4. Treg Transfer Modulates Neuroinflammation of 5xFAD Mice

This study investigates the impact of ex vivo-expanded Tregs on neuroinflammation. We quantified the levels of NOS2 in the hippocampus using immunofluorescence (Figure 5A). In 5xFAD mice, NOS2 deposition was elevated compared to that in WT group, yet the transfer of ex vivo-expanded Tregs mitigated this elevation. Additionally, we assessed the mRNA expression of pro-inflammatory markers (NOS2, TNF-α, IL-1β, and IL-6) and anti-inflammatory markers (Arg1 and Mrc1) by RT-qPCR (Figure 5B). The transfer of ex vivo-expanded Tregs effectively suppresses the pro-inflammatory response while bolstering the anti-inflammatory response. These findings substantiate the hypothesis that ex vivo -expanded Tregs play a role in alleviating neuroinflammation in mice models of AD.

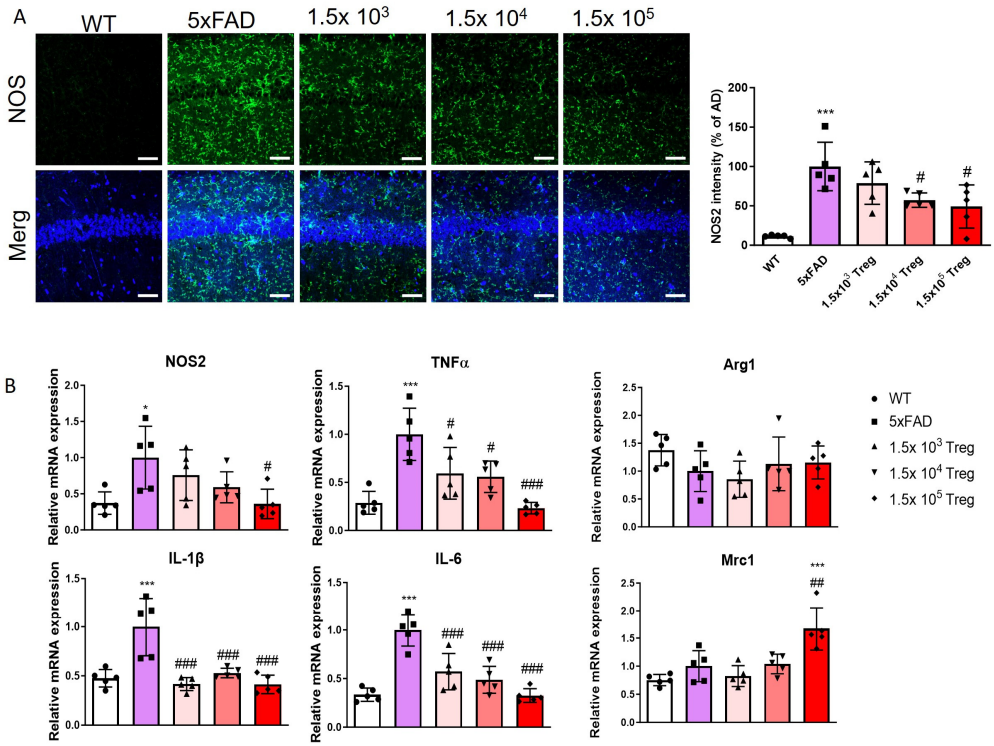

Figure 5. Treg transfer modulates neuroinflammation in 5xFAD mice. (**A**) The expression levels and intensity of NOS2 in the CA1 of the hippocampus assessed with immunostaining. (**B**) The mRNA expression of NOS2, TNF-α, IL-1β, Arg1, and Mrc1 (* $p < 0.05$, *** $p < 0.001$ vs. the WT group and # $p < 0.05$, ## $p < 0.01$, ### $p < 0.001$ vs. the 5xFAD group, one-way ANOVA, Newman–Keuls multiple [21] comparison test ($n = 5$). Data are shown as the mean ± SEM).

3. Discussion

The etiology of AD has been attributed to various pathological processes, with the Aβ toxicity and amyloid cascade hypotheses emerging prominently. These hypotheses propose that the accumulation of Aβ peptide and synaptic alterations in the brain plays a central role in AD pathology [21,22]. Studies have demonstrated that the extracellular deposition of Aβ peptide leads to the formation of senile plaques, while intracellular neurofibrillary tangles, composed of hyperphosphorylated tau protein, also develop [20,23]. Despite extensive research, drug trials targeting these pathological mechanisms have shown limited success.

Aducanumab is a monoclonal antibody designed to target amyloid beta and was approved for medical use by the U.S. Food and Drug Administration (FDA) in June 2021. Although it is the first treatment approved for Alzheimer's disease, it is controversial due to safety issues such as low clinical efficacy and side effects such as intracerebral microhemorrhage and edema [24]. Lecanemab is also a monoclonal antibody drug targeting amyloid beta and was approved by the FDA in July 2023. This is the second drug approved to reduce amyloid markers and significantly slow cognitive decline in early-stage Alzheimer's disease. However, as safety concerns have been raised about risks such as cerebral hemorrhage, long-term clinical trials are needed to confirm the efficacy and safety of lecanemab in early Alzheimer's disease [25,26]. Overall, there is a growing need for effective AD treatments without side effects.

The efficacy of Treg immunotherapy has been demonstrated in various disease models, including graft-versus-host disease, colitis, type 1 diabetes, and multiple sclerosis [27–30]. Specifically, the expansion of antigen-specific Tregs is a potential strategy currently under exploration in preclinical trials [31]. Advancing the clinical application of Treg therapy is crucial to enhance its efficiency and establish reproducibility in patients. This Treg expansion protocol using G-rex can be used for reproducibility of human Tregs isolated from peripheral blood mononuclear cells (hPBMC). Notably, in this study, it is significant

that even a low dose of 1.5×10^3 Aβ-specific Tregs demonstrated neuroprotective effects in 5xFAD mice.

Our research consistently focuses on Treg cell therapy for the treatment of AD. In 2016, we highlighted the potential of Treg therapy in AD [19] and further developed a Treg treatment strategy using Aβ antigen presentation. Our findings demonstrate that the administration of Aβ antigen-specific Tregs modulates the inflammatory state in AD [14]. In this study, we attempted antigen presentation and expansion using G-rex plates after Treg isolation, complementing the Aβ-specific Treg production method in the previous study. This research reinforces the effectiveness of Aβ-specific Treg therapy for AD, contributing valuable insights to future clinical research.

Animal models play a pivotal role in AD research. Various transgenic mouse models, such as 3xTg and 5xFAD, have been employed to investigate AD-related pathologies [32]. Recognizing the distinctions between the 5xFAD and 3xTg AD mouse models is imperative, as they capture different facets of Alzheimer's disease pathology. In our previous study on Treg therapy for AD, we utilized 3xTg mice that express human APP695, PS1, and Tau. In these mice, amyloid deposition and memory deficits manifested at 6 and 4.5 months, respectively. Pathological changes, especially amyloid deposition, occurred at a slower pace compared to 5xFAD mice. Consequently, the 3xTg model is well-suited for investigating the later stages of AD and the interplay between amyloid and tau pathologies [33]. In contrast, 5xFAD mice rapidly develop severe amyloid pathology, with extensive Aβ accumulation primarily in the brain, commencing as early as two months of age. This model proves particularly valuable for studying the early stages of amyloid deposition and its impact on neuronal function [18]. Our study aimed to exploit these distinctions to better understand the potential of Treg therapy across different stages and aspects of AD.

Some reports on the clinical application of cell therapy suggest a correlation between the cell dose and the occurrence and severity of cytokine-release storms. In the case of CAR-T cells, the usual administration range is from 1×10^5 to 1×10^{10} CAR-T cells/kg for patients undergoing cancer treatment [34]. In Treg therapy studies of neurodegenerative diseases such as AD, ALS, and PD, typically more than 5×10^5 Tregs are transferred to mice [19,35,36]. However, in our study, we transferred only 1.5×10^3, 10^4, and 10^5 Tregs to 5xFAD mice and observed significant neuroprotective effects even at lower doses (Figures 3 and 4). Although these effects were dose-dependent, the observation that as few as 10^3 Tregs could have therapeutic effects is promising for future clinical applications in humans.

In addition to our findings, it is crucial to highlight the methodological advancements presented in this study that significantly improved current methods for producing efficiently ex vivo-expanded Tregs. Our protocol, which employs G-rex plates for the expansion of antigen-specific Tregs, represents a substantial advancement over traditional methods. This approach not only enhances the expansion efficiency of Tregs but also ensures greater consistency and reproducibility, crucial for clinical applications. The ability to efficiently generate many antigen-specific Tregs ex vivo is a key step towards realizing the full therapeutic potential of Treg therapy in clinical settings. Moreover, the effectiveness of this method in generating Aβ-specific Tregs, as demonstrated in our study, opens new avenues for targeted immunotherapy in AD and potentially other neurodegenerative diseases. This advancement underscores our commitment to improving Treg-based therapies and sets a new benchmark for future research in this field.

4. Materials and Methods

4.1. Animals

Female 5xFAD mice, carrying transgenes encoding APP (Swedish, Florida, and London) and PS1 (M146L and L286V), along with control mice, were sourced from the Korea Research Institute of Bioscience and Biotechnology (KRIBB). C57BL/6 mice for Treg isolation were obtained from the Jackson Laboratory (Bar Harbor, ME, USA). All animals were housed in a controlled environment with a 12-h light/dark cycle and had ad libitum access

to food and water. The animal experiments strictly adhered to the guidelines for animal care and the guiding principles for experiments involving animals. The University of Kyung Hee Animal Care and Use Committee approved all experimental procedures under the protocol number KHUASP(SE)-21-255. Furthermore, all animal studies underwent thorough review and were conducted in accordance with the ARRIVE guidelines [37].

4.2. Regulatory T Cells Manufacturing and Adoptive Transfer

Aβ-specific Treg cells were induced by culturing CD8+ T cell-depleted splenocytes with fibrillized Aβ and bee venom phospholipase A2. The Amyloid-β (Aβ; Genscript, Piscataway, NJ, USA, catalog number (*Cat No*): RP10017) fibrillization process involved diluting 5 mM Aβ1-42 with 10 mM HCl to reach a final concentration of 100 μM. The resulting mixture was incubated at 37 °C overnight [38].

Spleens obtained from C57BL/6J mice underwent mechanical disruption using a 40 μm strainer. Following red blood cell (RBC) lysis, CD8+ cells were removed through the application of CD8a (Ly-2) MicroBeads (Miltenyi Biotec, Auburn, CA, USA, *Cat No*: 130-117-044).

For antigen presentation, CD8-cells were plated in 96-well U-bottom plates with 0.5 μM fibrillized Aβ and 0.4 μg/mL bee venom phospholipase A2 (bvPLA2; Sigma Aldrich, St. Louis, MO, USA *Cat No*: P9279) for a duration of 4 days.

Following antigen presentation, $CD4^+CD25^+$ regulatory T cells (Tregs) were isolated using a $CD4^+CD25^+$ Regulatory T Cell Isolation Kit (Miltenyi Biotec, *Cat No*: 130-091-041) and expanded for an additional 2 weeks. Purified Tregs were seeded into a G-Rex 24-well plate (Wilson Wolf Manufacturing, St. Paul, MN, USA, *Cat No*: 80192M) with CD 3/28 MACSiBead™ Particles of Treg Expansion Kit (Miltenyi Biotec, *Cat No*: 130-093-627) and 2000 U/mL rmIL-2 (R&D Systems, Minneapolis, MN, USA, *Cat No*: 402-ML-020/CF).

After Treg expansion, Ex vivo-expanded Tregs were washed with media to remove IL-2, and MACSiBead™ Particles were separated by MACSiMAG™ Separator (Miltenyi Biotec, *Cat No*: 130-092-168). 1×10^3, 1×10^4 and 1×10^5 Tregs were adoptively transferred to 5xFAD mice via intravenous.

The purity of isolated Treg was confirmed using flow cytometry after each isolation and expansion.

4.3. Flow Cytometry

To assess the purity of isolated cells, FITC-CD8 (Invitrogen, Carlsbad, CA, USA, *Cat No*: 11-0081-82) staining was performed after CD8 depletion. Following Treg isolation and expansion, PE-Cy5-CD4 (Invitrogen, *Cat No*: 15-0041-82) and APC-cy7-CD25 (BD Pharmingen, Franklin Lakes, NJ, USA, *Cat No*: 557658) staining was conducted in the dark at 4°C for 30 min. Subsequently, the samples were washed with BD FACS Stain buffer (BD Bioscience, San Jose, CA, USA, *Cat No*: 554656) and subjected to flow cytometry analysis. Data acquisition was carried out using a BD FACSlyric™ flow cytometer (BD bioscience, reference number (REF): 659 180), and analysis was performed using BD FACSuite software (BD bioscience, v1,2,1,5657).

4.4. Behaviour Test

Eight weeks after the transfer of Tregs, we conducted the Y-maze test to evaluate spatial memory in mice. The test, lasting 5 min, took place in a Y-shaped maze with three black opaque plastic arms positioned 120° apart. After entering the maze's center, mice were permitted to explore the three arms. We calculated the percentage of alternations by tracking the number of arm entries and triads, defining an entry as when all four limbs were within the arm. This test serves as a metric for quantifying cognitive deficits in mice and assessing the impact of novel treatments on cognition [39].

For the assessment of aversive memory, which stimulates amygdale and hippocampus, we employed the passive avoidance test (PAT), utilizing an apparatus measuring 20 × 20 × 30 cm, comprising a lit chamber and a dark chamber separated by a door. On training days, mice were positioned in the lit chamber facing away from the door. Upon entry into the dark chamber, the door closed, and a foot shock (0.35 mA, 2 s) was administered. Thirty seconds after the shock, the mice were euthanized. This trial was conducted over two days. On the test day, mice were placed in a light chamber, and the latency to enter the dark chamber was recorded within a 5-min window [40].

4.5. Immunofluorescence Analysis

For immunofluorescence, mice were anesthetized with isoflurane (Ifran Solution; Hana Pharm Co., Seoul, Republic of Korea, *Cat No*: 3003) and transcardially perfused with PBS. Brains were harvested and divided into two equal parts. One half of the brain was postfixed in 4% paraformaldehyde at 4 °C overnight, then transferred to a 30% sucrose solution and subsequently frozen-sectioned into 30 µm thick coronal sections using a cryomicrotome (HM525 NX; Thermo Fisher Scientific, Inc., Waltham, MA, USA, *Cat No*: 95-664-0EC). The brain sections underwent a series of treatments, beginning with a 5-min incubation in 50% formic acid at room temperature (RT), followed by heating in 10 mM sodium citrate buffer (pH 6.0) at 60 °C after washing with PBS. Blocking was performed by incubating the sections with 5% bovine serum albumin in TBSTr for 30 min. Subsequently, the sections were incubated with primary antibodies, including mouse monoclonal 4G8 antibody (1:500; BioLegend, San Diego, CA, USA, *Cat No*: 800701), phospho-Tau (1:1000; Invitrogen, REF: MN1020), and NOS2 (1:500; Santa Cruz Biotechnology, Santa Cruz, CA, USA, *Cat No*: sc-7271), for 3 days at 4 °C. Following primary antibody incubation, the brain sections were washed with Tris-buffered saline containing 0.5% Triton X-100 (TBSTr) and incubated for 2 h at RT with Alexa 488-conjugated IgG secondary antibodies (Invitrogen, *Cat No*: A32723. Slides were mounted with DAPI mounting medium (Vector Laboratories, Burlingame, CA, USA, *Cat No*: VEC-H-1200) and examined under an LSM 800 confocal laser scanning microscope (Carl Zeiss, Oberkochen, Germany). Staining intensity was quantified by measuring the integral density of the region of interest from monochromatic images using ImageJ software (National Institutes of Health, USA, v1.52a). The percentage staining intensity was calculated relative to 5xFAD and multiplied by 100 for normalization purposes.

4.6. RNA Extraction and RT-PCR Assays

Total RNA was extracted from hippocampal brain tissue using the easy-BLUE RNA extraction kit (iNtRON Biotechnology, Republic of Korea, *Cat No*: 17061). Subsequently, cDNA synthesis was carried out with Cyclescript reverse transcriptase (Bioneer, Republic of Korea, *Cat No*: E-3131). Real-time RT-PCR samples were prepared using the SensiFAST SYBR no-Rox kit (Bioline, Republic of Korea, *Cat No*: BIO-98005), and the amplification was conducted on the CFX Connect System (Bio-Rad, Hercules, CA, USA, *Cat No*: 1855201).

The cycling conditions comprised an initial denaturation cycle at 95 °C for 30 s, followed by 49 cycles of denaturation at 95 °C for 10 s, annealing at 55 °C for 30 s, and a final melting curve stage at 95 °C for 10 s, 50 °C for 5 s, with a gradual increase until reaching 95 °C. The quantification of target mRNAs was normalized to the expression levels of mouse β-actin, a designated housekeeping gene serving as an endogenous control. All fold changes are expressed relative to the WT. The primer sequences are provided in Table 1.

4.7. Statistical Analysis

The statistical analyses were conducted utilizing GraphPad Prism 5.01 software (GraphPad Software Inc., San Diego, CA, USA). A one-way analysis of variance (ANOVA) was employed, followed by Tukey's multiple comparison test. All experiments were conducted in a blinded manner and independently repeated under identical conditions. Statistical significance was considered at $p < 0.05$.

Table 1. Primer sequences for RT-PCR.

Gene Name	Forward Primer Sequence (5′–3′)	Reverse Primer Sequence (5′–3′)
β-actin	GTG CTA TGT TGC TCT AGA CTT CG	ATG CCA CAG GAT TCC ATA CC
NOS2	AGG ACA TCC TGC GGC AGC	GCT TTA ACC CCT CCT GTA
TNF-α	GGC AGG TTC TGT CCC TTT CAC	TTC TGT GCT CAT GGT GTC TTT TCT
IL-1β	AAG CCT CGT GCT GTC GGA CC	TGA GGC CCA AGG CCA CAG G
IL-6	TTC CAT CCA GTT GCC TTC TTG	GGG AGT GGT ATC CTC TGT GAA GTC
Arg1	CTC CAA GCC AAA GTC CTT AGA G	AGG AGC TGT CAT TAG GGA CAT C
Mrc1	TTC GGT GGA CTG TGG ACG AGC	ATA AGC CAC CTG CCA CTC CGG

Author Contributions: Author Contributions: Conceptualization, H.B.; methodology, S.-Y.P., H.Y. and J.Y.K.; formal analysis, J.Y. and I.C.; writing—original draft preparation, S.-Y.P. and J.Y.; writing—review and editing, J.Y. and H.B.; supervision: H.B.; funding acquisition, H.B. All authors have read and agreed to the published version of the manuscript.

Funding: This work was supported by the National Research Foundation of Korea (NRF) grant funded by the Korea government (MSIT) (RS-2023-00208347) and the Korea Health Technology R&D Project through the Kore Health Industry Development Institute (KHIDI), funded by the Ministry of Health & Welfare and Ministry of science and ICT, Republic of Korea (HU20C0026).

Institutional Review Board Statement: The animal study protocol was approved by the Institutional Animal Care and Use Committee of Kyung Hee University (KHUASP(SE)-22-148 and 20-240).

Informed Consent Statement: Not applicable.

Data Availability Statement: All data generated or analyzed during this study are included in this published article.

Conflicts of Interest: The authors declare that the research was conducted in the absence of any commercial or financial relationships that could be construed as a potential conflict of interest.

References

1. World Health Organization. *Global Action Plan on the Public Health Response to Dementia 2017–2025*; World Health Organization: Geneva, Switzerland, 2017.
2. Schenk, D.; Barbour, R.; Dunn, W.; Gordon, G.; Grajeda, H.; Guido, T.; Hu, K.; Huang, J.; Johnson-Wood, K.; Khan, K.; et al. Immunization with amyloid-beta attenuates Alzheimer-disease-like pathology in the PDAPP mouse. *Nature* **1999**, *400*, 173–177. [CrossRef]
3. Janus, C.; Pearson, J.; McLaurin, J.; Mathews, P.M.; Jiang, Y.; Schmidt, S.D.; Chishti, M.A.; Horne, P.; Heslin, D.; French, J.; et al. Aβ peptide immunization reduces behavioural impairment and plaques in a model of Alzheimer's disease. *Nature* **2000**, *408*, 979–982. [CrossRef]
4. Sardi, F.; Fassina, L.; Venturini, L.; Inguscio, M.; Guerriero, F.; Rolfo, E.; Ricevuti, G. Alzheimer's disease, autoimmunity and inflammation. The good, the bad and the ugly. *Autoimmun. Rev.* **2011**, *11*, 149–153. [CrossRef]
5. Stolp, H.B.; Dziegielewska, K.M. Review: Role of developmental inflammation and blood-brain barrier dysfunction in neurodevelopmental and neurodegenerative diseases. *Neuropathol. Appl. Neurobiol.* **2009**, *35*, 132–146. [CrossRef]
6. Zhang, H.; Wei, W.; Zhao, M.; Ma, L.; Jiang, X.; Pei, H.; Cao, Y.; Li, H. Interaction between Aβ and Tau in the Pathogenesis of Alzheimer's Disease. *Int. J. Biol. Sci.* **2021**, *17*, 2181–2192. [CrossRef]
7. Sakaguchi, S.; Yamaguchi, T.; Nomura, T.; Ono, M. Regulatory T cells and immune tolerance. *Cell* **2008**, *133*, 775–787. [CrossRef]
8. Kleinewietfeld, M.; Hafler, D.A. Regulatory T cells in autoimmune neuroinflammation. *Immunol. Rev.* **2014**, *259*, 231–244. [CrossRef]
9. Venken, K.; Hellings, N.; Broekmans, T.; Hensen, K.; Rummens, J.L.; Stinissen, P. Natural naive $CD4^+CD25^+CD127^{low}$ regulatory T cell (Treg) development and function are disturbed in multiple sclerosis patients: Recovery of memory Treg homeostasis during disease progression. *J. Immunol.* **2008**, *180*, 6411–6420. [CrossRef]
10. McGeachy, M.J.; Stephens, L.A.; Anderton, S.M. Natural recovery and protection from autoimmune encephalomyelitis: Contribution of $CD_4{}^+CD_{25}{}^+$ regulatory cells within the central nervous system. *J. Immunol.* **2005**, *175*, 3025–3032. [CrossRef]
11. Larbi, A.; Pawelec, G.; Witkowski, J.M.; Schipper, H.M.; Derhovanessian, E.; Goldeck, D.; Fulop, T. Dramatic shifts in circulating CD4 but not CD8 T cell subsets in mild Alzheimer's disease. *J. Alzheimers Dis.* **2009**, *17*, 91–103. [CrossRef]

12. Selck, C.; Dominguez-Villar, M. Antigen-Specific Regulatory T Cell Therapy in Autoimmune Diseases and Transplantation. *Front. Immunol.* **2021**, *12*, 661875. [CrossRef] [PubMed]
13. Mohseni, Y.R.; Tung, S.L.; Dudreuilh, C.; Lechler, R.I.; Fruhwirth, G.O.; Lombardi, G. The Future of Regulatory T Cell Therapy: Promises and Challenges of Implementing CAR Technology. *Front. Immunol.* **2020**, *11*, 1608. [CrossRef] [PubMed]
14. Yang, H.; Park, S.Y.; Baek, H.; Lee, C.; Chung, G.; Liu, X.; Lee, J.H.; Kim, B.; Kwon, M.; Choi, H.; et al. Adoptive therapy with amyloid-beta specific regulatory T cells alleviates Alzheimer's disease. *Theranostics* **2022**, *12*, 7668–7680. [CrossRef] [PubMed]
15. Park, S.-Y.; Yang, H.; Kim, S.; Yang, J.; Go, H.; Bae, H. Alpha-Synuclein-Specific Regulatory T Cells Ameliorate Parkinson’s Disease Progression in Mice. *Int. J. Mol. Sci.* **2023**, *24*, 15237.
16. Javonillo, D.I.; Tran, K.M.; Phan, J.; Hingco, E.; Kramár, E.A.; da Cunha, C.; Forner, S.; Kawauchi, S.; Milinkeviciute, G.; Gomez-Arboledas, A.; et al. Systematic Phenotyping and Characterization of the 3xTg-AD Mouse Model of Alzheimer's Disease. *Front. Neurosci.* **2021**, *15*, 785276. [CrossRef] [PubMed]
17. Lee, J.E.; Han, P.L. An update of animal models of Alzheimer disease with a reevaluation of plaque depositions. *Exp. Neurobiol.* **2013**, *22*, 84–95. [CrossRef] [PubMed]
18. Oakley, H.; Cole, S.L.; Logan, S.; Maus, E.; Shao, P.; Craft, J.; Guillozet-Bongaarts, A.; Ohno, M.; Disterhoft, J.; Van Eldik, L.; et al. Intraneuronal beta-amyloid aggregates, neurodegeneration, and neuron loss in transgenic mice with five familial Alzheimer's disease mutations: Potential factors in amyloid plaque formation. *J. Neurosci.* **2006**, *26*, 10129–10140. [CrossRef]
19. Baek, H.; Ye, M.; Kang, G.H.; Lee, C.; Lee, G.; Choi, D.B.; Jung, J.; Kim, H.; Lee, S.; Kim, J.S.; et al. Neuroprotective effects of $CD4^+CD25^+Foxp3^+$ regulatory T cells in a 3xTg-AD Alzheimer's disease model. *Oncotarget* **2016**, *7*, 69347–69357. [CrossRef]
20. Querfurth, H.W.; LaFerla, F.M. Alzheimer's disease. *N. Engl. J. Med.* **2010**, *362*, 329–344. [CrossRef]
21. Selkoe, D.J. Alzheimer's disease: Genes, proteins, and therapy. *Physiol. Rev.* **2001**, *81*, 741–766. [CrossRef]
22. Honjo, K.; Black, S.E.; Verhoeff, N.P. Alzheimer's disease, cerebrovascular disease, and the beta-amyloid cascade. *Can. J. Neurol. Sci.* **2012**, *39*, 712–728. [CrossRef] [PubMed]
23. Montine, T.J.; Phelps, C.H.; Beach, T.G.; Bigio, E.H.; Cairns, N.J.; Dickson, D.W.; Duyckaerts, C.; Frosch, M.P.; Masliah, E.; Mirra, S.S.; et al. National Institute on Aging-Alzheimer's Association guidelines for the neuropathologic assessment of Alzheimer's disease: A practical approach. *Acta Neuropathol.* **2012**, *123*, 1–11. [CrossRef] [PubMed]
24. Whitehouse, P.; Gandy, S.; Saini, V.; George, D.R.; Larson, E.B.; Alexander, G.C.; Avorn, J.; Brownlee, S.; Camp, C.; Chertkow, H.; et al. Making the Case for Accelerated Withdrawal of Aducanumab. *J. Alzheimers Dis.* **2022**, *87*, 1003–1007. [CrossRef] [PubMed]
25. van Dyck, C.H.; Swanson, C.J.; Aisen, P.; Bateman, R.J.; Chen, C.; Gee, M.; Kanekiyo, M.; Li, D.; Reyderman, L.; Cohen, S.; et al. Lecanemab in Early Alzheimer's Disease. *N. Engl. J. Med.* **2023**, *388*, 9–21. [CrossRef] [PubMed]
26. Reish, N.J.; Jamshidi, P.; Stamm, B.; Flanagan, M.E.; Sugg, E.; Tang, M.; Donohue, K.L.; McCord, M.; Krumpelman, C.; Mesulam, M.M.; et al. Multiple Cerebral Hemorrhages in a Patient Receiving Lecanemab and Treated with t-PA for Stroke. *N. Engl. J. Med.* **2023**, *388*, 478–479. [CrossRef] [PubMed]
27. Edinger, M.; Hoffmann, P.; Ermann, J.; Drago, K.; Fathman, C.G.; Strober, S.; Negrin, R.S. $CD4^+CD25^+$ regulatory T cells preserve graft-versus-tumor activity while inhibiting graft-versus-host disease after bone marrow transplantation. *Nat. Med.* **2003**, *9*, 1144–1150. [CrossRef] [PubMed]
28. Mottet, C.; Uhlig, H.H.; Powrie, F. Cutting edge: Cure of colitis by $CD4^+CD25^+$ regulatory T cells. *J. Immunol.* **2003**, *170*, 3939–3943. [CrossRef] [PubMed]
29. Tang, Q.; Henriksen, K.J.; Bi, M.; Finger, E.B.; Szot, G.; Ye, J.; Masteller, E.L.; McDevitt, H.; Bonyhadi, M.; Bluestone, J.A. In vitro-expanded antigen-specific regulatory T cells suppress autoimmune diabetes. *J. Exp. Med.* **2004**, *199*, 1455–1465. [CrossRef]
30. Kohm, A.P.; Carpentier, P.A.; Anger, H.A.; Miller, S.D. Cutting edge: $CD4^+CD25^+$ regulatory T cells suppress antigen-specific autoreactive immune responses and central nervous system inflammation during active experimental autoimmune encephalomyelitis. *J. Immunol.* **2002**, *169*, 4712–4716. [CrossRef]
31. Raffin, C.; Vo, L.T.; Bluestone, J.A. T(reg) cell-based therapies: Challenges and perspectives. *Nat. Rev. Immunol.* **2020**, *20*, 158–172. [CrossRef]
32. Elder, G.A.; Gama Sosa, M.A.; De Gasperi, R. Transgenic mouse models of Alzheimer's disease. *Mt. Sinai J. Med.* **2010**, *77*, 69–81. [CrossRef] [PubMed]
33. Oddo, S.; Caccamo, A.; Shepherd, J.D.; Murphy, M.P.; Golde, T.E.; Kayed, R.; Metherate, R.; Mattson, M.P.; Akbari, Y.; LaFerla, F.M. Triple-transgenic model of Alzheimer's disease with plaques and tangles: Intracellular Abeta and synaptic dysfunction. *Neuron* **2003**, *39*, 409–421. [CrossRef] [PubMed]
34. Zhao, L.; Cao, Y.J. Engineered T Cell Therapy for Cancer in the Clinic. *Front. Immunol.* **2019**, *10*, 2250. [CrossRef]
35. Beers, D.R.; Henkel, J.S.; Zhao, W.; Wang, J.; Huang, A.; Wen, S.; Liao, B.; Appel, S.H. Endogenous regulatory T lymphocytes ameliorate amyotrophic lateral sclerosis in mice and correlate with disease progression in patients with amyotrophic lateral sclerosis. *Brain A J. Neurol.* **2011**, *134 Pt 5*, 1293–1314. [CrossRef] [PubMed]
36. Reynolds, A.D.; Banerjee, R.; Liu, J.; Gendelman, H.E.; Mosley, R.L. Neuroprotective activities of $CD4^+CD25^+$ regulatory T cells in an animal model of Parkinson's disease. *J. Leukoc. Biol.* **2007**, *82*, 1083–1094. [CrossRef] [PubMed]
37. Kilkenny, C.; Browne, W.; Cuthill, I.C.; Emerson, M.; Altman, D.G. Animal research: Reporting in vivo experiments: The ARRIVE guidelines. *Br. J. Pharmacol.* **2010**, *160*, 1577–1579. [CrossRef]
38. Baek, H.; Park, S.Y.; Ku, S.J.; Ryu, K.; Kim, Y.; Bae, H.; Lee, Y.S. Bee Venom Phospholipase A2 Induces Regulatory T Cell Populations by Suppressing Apoptotic Signaling Pathway. *Toxins* **2020**, *12*, 198. [CrossRef] [PubMed]

39. Li, F.; Emmerton, K.K.; Jonas, M.; Zhang, X.; Miyamoto, J.B.; Setter, J.R.; Nicholas, N.D.; Okeley, N.M.; Lyon, R.P.; Benjamin, D.R.; et al. Intracellular Released Payload Influences Potency and Bystander-Killing Effects of Antibody-Drug Conjugates in Preclinical Models. *Cancer Res.* **2016**, *76*, 2710–2719. [CrossRef]
40. Eagle, A.L.; Wang, H.; Robison, A.J. Sensitive Assessment of Hippocampal Learning Using Temporally Dissociated Passive Avoidance Task. *Bio Protoc.* **2016**, *6*, e1821. [CrossRef]

International Journal of
Molecular Sciences

MDPI

Article

Alteration of Neural Network and Hippocampal Slice Activation through Exosomes Derived from 5XFAD Nasal Lavage Fluid

Sangseong Kim [1,*], Jaekyong Jeon [2], Dulguun Ganbat [2], Taewoon Kim [3], Kyusoon Shin [3], Sungho Hong [4] and Jongwook Hong [3,5,6,*]

[1] Department of Biomedical Science and Engineering, Gwangju Institute of Science and Technology, Gwangju 61005, Republic of Korea
[2] Department of Pharmacy, Hanyang University, Ansan 15588, Republic of Korea; abcde27230@gmail.com (J.J.); dulguun38584@gmail.com (D.G.)
[3] Department of Bionanotechnology, Graduate School, Hanyang University, Seoul 04763, Republic of Korea; xodns4922@hanyang.ac.kr (T.K.); 23btlsd32@gmail.com (K.S.)
[4] Computational Neuroscience Unit, Okinawa Institute of Science and Technology, Okinawa 904-0495, Japan; shhong@oist.jp
[5] Department of Medical and Digital Engineering, Graduate School, Hanyang University, Seoul 04763, Republic of Korea
[6] Department of Bionanoengineering, Hanyang University, Ansan 15588, Republic of Korea
* Correspondence: talpiot21@gist.ac.kr (S.K.); jwh@hanyang.ac.kr (J.H.)

Abstract: Exosomes, key mediators of intercellular transmission of pathogenic proteins, such as amyloid-beta and tau, significantly influence the progression and exacerbation of Alzheimer's disease (AD) pathology. Present in a variety of biological fluids, including cerebrospinal fluid, blood, saliva, and nasal lavage fluid (NLF), exosomes underscore their potential as integral mediators of AD pathology. By serving as vehicles for disease-specific molecules, exosomes could unveil valuable insights into disease identification and progression. This study emphasizes the imperative to investigate the impacts of exosomes on neural networks to enhance our comprehension of intracerebral neuronal communication and its implications for neurological disorders like AD. After harvesting exosomes derived from NLF of 5XFAD mice, we utilized a high-density multielectrode array (HD-MEA) system, the novel technology enabling concurrent recordings from thousands of neurons in primary cortical neuron cultures and organotypic hippocampal slices. The ensuing results revealed a surge in neuronal firing rates and disoriented neural connectivity, reflecting the effects provoked by pathological amyloid-beta oligomer treatment. The local field potentials in the exosome-treated hippocampal brain slices also exhibited aberrant rhythmicity, along with an elevated level of current source density. While this research is an initial exploration, it highlights the potential of exosomes in modulating neural networks under AD conditions and endorses the HD-MEA as an efficacious tool for exosome studies.

Keywords: exosome; nasal lavage fluid; 5XFAD; high-density multielectrode array; hippocampal slice; neural network

Citation: Kim, S.; Jeon, J.; Ganbat, D.; Kim, T.; Shin, K.; Hong, S.; Hong, J. Alteration of Neural Network and Hippocampal Slice Activation through Exosomes Derived from 5XFAD Nasal Lavage Fluid. *Int. J. Mol. Sci.* **2023**, *24*, 14064. https://doi.org/10.3390/ijms241814064

Academic Editor: Claudia Ricci

Received: 9 August 2023
Revised: 31 August 2023
Accepted: 5 September 2023
Published: 14 September 2023

1. Introduction

Exosomes have gained considerable attention in neurobiology, offering intricate insights into the multifaceted interactions that govern neural networks [1,2]. These tiny extracellular vesicles are secreted by various neural cell types—neurons, astrocytes, and microglia—all of which have unique roles to play in the functioning of the nervous system. When neurons release exosomes filled with neurotransmitters and synaptic proteins, these vesicles travel to synapses facilitating the synaptic plasticity crucial for learning, memory, and cognitive functions [3]. Astrocytes also secrete exosomes with a slightly different

molecular repertoire. These vesicles often contain growth factors, nutrients, and anti-inflammatory agents. Astrocyte-derived exosomes thus assist in maintaining the structural integrity and functional stability of neural networks [4]. They play roles in repairing damaged neurons, fortifying synaptic connections, and reconfiguring existing neural pathways, thus contributing to the adaptability and resilience of networks. In parallel, microglia, often referred to as the immune cells of the nervous system, produce exosomes loaded with cytokines. Depending on the nature of these cytokines, microglial exosomes can have pro-inflammatory or anti-inflammatory effects, impacting neuroinflammation, neuronal survival, and synaptic integrity [5].

While the beneficial aspects of exosomes are fascinating, their potential role in disease pathology, particularly in Alzheimer's disease (AD), is equally compelling [6,7]. Exosomes isolated from biological fluids like cerebrospinal fluid (CSF), blood, and saliva have been found to carry disease-specific molecules, such as amyloid-beta (Aβ) and tau proteins. These molecules have been implicated in the spread of AD, potentially serving as markers and mediators of disease progression. According to the clinical and experimental evidence, a connection between CSF and olfactory systems is observed, suggesting a new avenue for the role of exosomes in nasal discharge as diagnostic biomarkers [8,9]. The olfactory system, especially the olfactory epithelium, has been shown to display unique features in AD pathology, such as unusual secretase expression and heightened susceptibility to neuroinflammation [10,11]. Given that olfactory dysfunction often precedes cognitive impairment in AD and overlaps anatomically with early AD-affected regions, the potential for applying nasal lavage fluid (NLF) as a non-invasive diagnostic tool is promising. NLF, generated by mucous membranes in the olfactory mucosa, serves to protect these sensory tissues while also potentially capturing the neuropathology unfolding in the surrounding system [12]. Therefore, exosomes obtained from this fluid could offer a snapshot of the ongoing state of neurodegeneration. Due to the easy collectability, it provides an efficient means for early disease detection and monitoring, complementing the information gathered from other conventional biological fluids, such as CSF and blood. Even though the biomarkers in human NLF have been discovered [13], the volume of collectible NLF from mice is significantly constrained, often amounting to less than a milliliter. This limited quantity renders component-based analyses, such as RNA sequencing, technically unfeasible. As a preliminary investigation of this nature, the current study thus concentrates on exploring the overarching functional impact of NLF from AD animal models on live neurons and brain slices.

A comprehensive investigation into the exosomal effects on neural networks has, however, been a daunting task due to inadequate methods. Conventional techniques of detecting neural activity, such as calcium imaging or patch clamping, offer limited data due to the slow responsiveness of calcium dye and the restricted number of neurons that can be recorded [2]. Utilizing a multielectrode array (MEA) system has overcome these limitations by enabling the simultaneous recording of multiple neuronal signals. Some studies have provided critical insights into neural circuit development, signal transduction, gene regulation, and neural synchronization influenced by exosomes derived from various sources [1,14,15]. However, despite their contributions, MEA experiments face inherent constraints, such as a relatively sparse density of electrodes and a considerable gap between electrodes. In this study, we employed a high-density MEA (HD-MEA) featuring 4096 electrodes (64×64) to capture the neural network characteristics influenced by exosomes derived from NLF of 5XFAD AD model animals. The superior spatiotemporal resolution of HD-MEA permitted detailed observations of neural ensembles and circuitry [16]. Further analyses, like functional connectivity maps and current source density (CSD) characterization, coupled with conventional neural activity analysis depicted an integrated picture of neural information processing initiated by exosome treatment.

Though the number of repetitions of the experiment and brain slices analyzed were limited in this preliminary attempt, our findings underscore the potential implications of exosomes in modulating neural networks under neurodegenerative conditions. Thus, the results validate the potential of HD-MEA as an effective neurochip for exosome studies,

particularly in understanding their effect on neural networks. By investigating the role of exosomes in AD, we can enhance our understanding of disease mechanisms, potentially leading to the development of diagnostic tools, and explore innovative therapeutic strategies for this formidable neurodegenerative disorder.

2. Results

2.1. Characterization of Exosomes Isolated from the NLF of 5XFAD Mice Using the Flow Amplification Separation Technology (FAST)

To examine the role of NLF-derived exosomes from 5XFAD animals, FAST was used to collect intact exosomes from limited amounts of nasal fluid with high yield and purity [17–19] (Figure 1A). Under consistent temperature control, we determined the size distribution of particles isolated from NLF using nanoparticle tracking analysis (Figure 1B). The overall distribution pattern of 5XFAD mice showed higher peaks in particle concentration than control mice. The concentration of 35–205 nm particles isolated from the nasal fluid of 5XFAD mice was approximately 8.5×10^8 particles/mL, which was approximately 3.0-fold higher than that of the control (Figure 1C). According to transmission electron microscopy images, the majority of the collected exosomes were 30–150 nm in diameter (Figure 1D). Considering the same volume loaded onto the grid, the exosome density was higher in 5XFAD mice than that in control mice, as confirmed by a 3.2-fold increase in CD63 exosome marker expression levels (Figure 1E,F). Overall, the secretion of NLF-derived exosomes was enhanced in the AD animal model, similar to other body fluids [12,20]. After the concentration normalization, the neural network in the HD-MEA was measured for both neuronal cultures and organotypic hippocampal slice cultures (OHSCs) with the harvested intact exosomes (Figure S1).

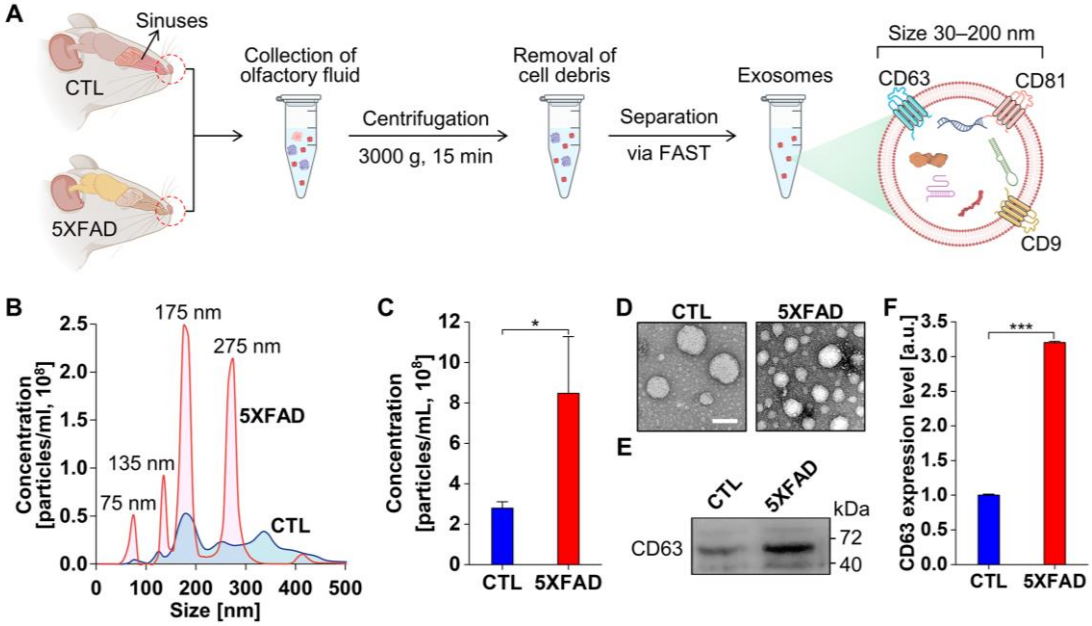

Figure 1. The workflow of exosome preparation from NLF and its quantification following functional tests in HD MEA. (**A**) Flow amplification separation technology (FAST) method to collect intact exosomes from NLF of 5XFAD and control (CTL) animals. Tetraspanins expression in the vesicle membrane, such as CD63, CD81, and CD9, as markers of exosomes. (**B**) Size distribution of particles isolated from NLF through nanoparticle tracking analysis. NLF exosomes from 5XFAD are in red with those from CTL in blue. (**C**) Particle concentration in the range of 35~205 nm. (**D**) Transmission electron microscope (TEM) images in the grids of the same volume loading with NLF-derived exosomes from 5XFAD and CTL. Scale bar = 100 nm. (**E**) Western blot of the exosome surface marker CD63. (**F**) The protein expression level of exosome surface marker CD63. The values are means ± SEMs from three independent experiments. *** $p < 0.005$, * $p < 0.05$; unpaired, two-tailed *t*-test with Welch's correction.

2.2. Altered Neuronal Excitability and Network Connectivity in Primary Cortical Neuron Cultures Stimulated with Aβ42 Oligomers and 5XFAD NLF-Derived Exosomes

During the developmental stages of AD symptoms, neuronal excitability has been frequently documented in vitro with pathologic Aβ42 oligomer treatment, as well as in functional magnetic resonance imaging (fMRI) imaging in patients with mild cognitive impairment (MCI). Using HD-MEA, we recorded primary cortical neurons for two weeks to measure the neuronal excitability induced by Aβ42 oligomers (neuronal culture image on CMOS chip in Figure S2B(a)). Additionally, 5XFAD NLF-derived exosomes were examined under the same conditions to compare their neuroexcitability. The basic topological properties of neural cultures were assessed on days in vitro (DIV) 7, 10, and 13 based on the number of spikes (NOS), interspike interval (ISI), and mean firing rate (MFR) for each group. During the culture aging process, NOS and MFR levels tended to increase in all groups (Figure 2A,C,D). Among them, the Aβ42 treatment group displayed the strongest activity. The control group exhibited a slightly higher NOS level and a lower MFR than the 5XFAD group. The ISI, indicative of the time interval between two consecutive spikes, tended to decrease with age, implying increased readiness in response to an input (Figure 2E). The average burst duration in the active electrodes decreased monotonically in the control, which was the reversal pattern in the other groups with the aging of cultures (Figure 2B,F). The mean NOS per burst remained consistent across different groups and DIVs, suggesting stable network mechanisms underlying individual burst events (Figure 2G). However, the burst frequency was increased in Aβ42 and 5XFAD NLF groups in older cultures, indicating a more recurrent generation of neuronal activation under these detrimental conditions (Figure 2H). Considering burst patterns in neuronal networks, the network burst duration in the interquartile range showed a steady increase in all groups (Figure 2I).

2.3. Differentiating Features of Neuronal Networks in 5XFAD NLF-Treated Neurons

To investigate network properties, it is necessary to apply reliable network parameters to describe their essential characteristics [21]. Among several parameters, we selected clustering coefficients (CCs), node degrees (NDs), and path lengths (PLs), given their credibility and relevance. First, the CC is primarily a measure of the tendency of neurons in a network to form clusters. Network clustering gradually increased in all groups (Figure 3B), albeit with sparser connections in the connectivity map, particularly from DIV 10 to 13 (Figures 3A and S5). The PLs and NDs are presented as average values and distribution histograms for each node (Figure 3C–F). The PL measures the number of steps involved in transmitting signals from one node to another. In the control culture, the PL values steadily decreased (Figure 3C; control, 5.25, 4.23, and 1.00 each for the median values from DIV 7 to 13), suggesting that neuronal communication became more efficient gradually. Given the increasing CCs, this phenomenon can be attributed to the maintenance of longer distances and local shortcut connections [22]. In contrast, PLs in the Aβ42 and 5XFAD NLF groups retained high means and wide deviations, as reflected in the box plots (Figure 3C; Aβ42, 4.14, 3.12, and 3.32; 5XFAD, 4.51, 3.75, and 4.84 for the median values from DIV 7 to 13). Likewise, the PL distribution of the Aβ42 and 5XFAD NLF groups at DIV13 displayed fatter tails compared to the control group, implying inefficient network organization (Figures 3E and S3A; control, 1.30; Aβ42, 3.70; 5XFAD, 5.65 for the PL values at the upper 70% cumulative node counts).

These data suggest that networks of the Aβ42 and 5XFAD groups added or maintained more local clustering connections over time, which increased CCs with insufficient long-distance shortcuts, resulting in degraded network efficiency when compared with that of the control. ND, representing the number of connections per node, provided further insights into gradual network changes compared with the control group. In the control group, the ND gradually declined, suggesting a network-wide pruning of connections. However, the Aβ42 group exhibited a substantial increase in the number of connections from DIV 7 to 10, followed by a slight decrease at DIV 13 (Figure 3A,D), and the 5XFAD group showed a similar tendency to a lesser degree. The ND distribution histogram

reflects quantitative changes across the DIVs (Figures 3F and S3B). In summary, the control group network evolved by losing connections while achieving higher CCs and lower PLs, developing a more efficient, 'small world'-like structure [22]. However, in both the Aβ42 and 5XFAD NLF groups, the networks added (from DIV 7 to DIV 10) and lost connections (from DIV 10 to 13), although the latter did not demonstrate a considerable improvement in efficiency, possibly due to a disrupted balance between local connections and long-distance shortcuts. This result demonstrates that 5XFAD NLF could induce pathological changes similar to Aβ42 in network activity patterns.

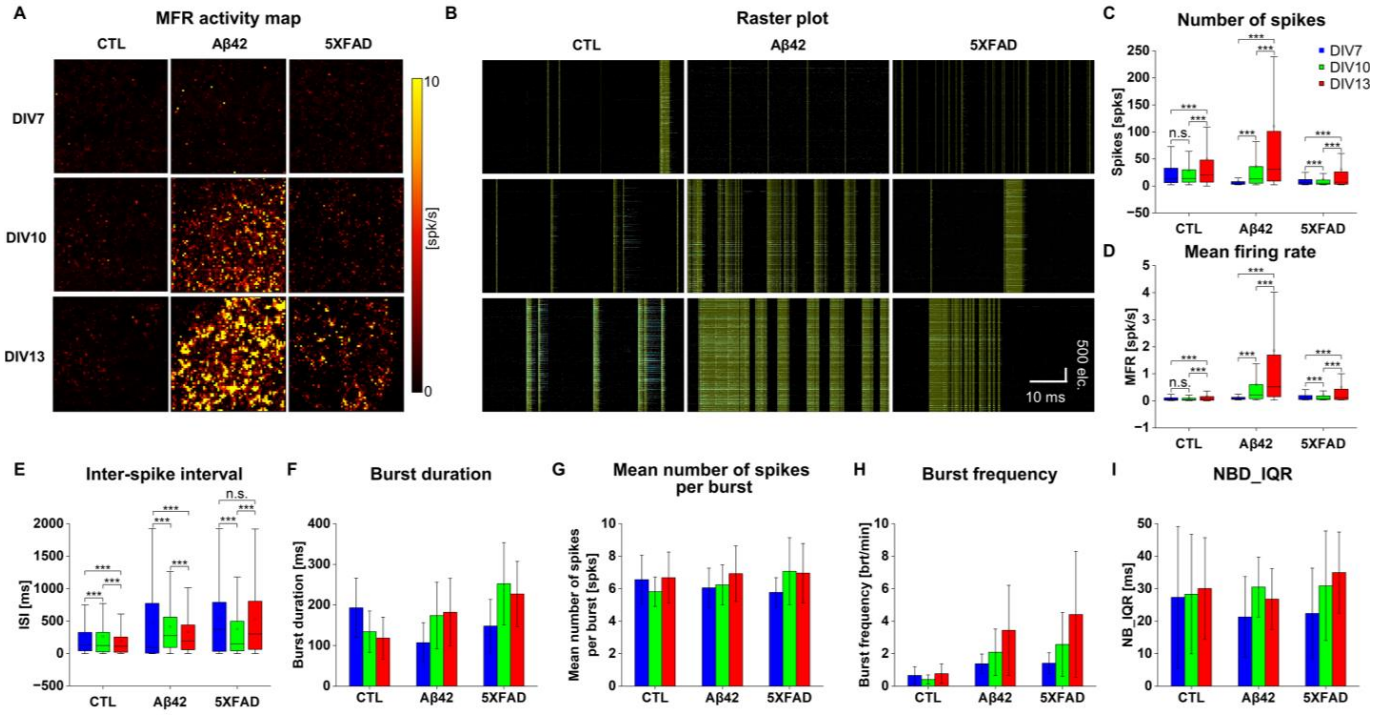

Figure 2. Topological properties of neuronal cultures on HD MEA recording with culture development. (**A**) MFR activity map in spontaneous neuronal activation during 60 s recordings represented from the 64 × 64 grid electrode arena (2.67 × 2.67 mm^2). Control, Aβ42, and 5XFAD NLF treatment groups on DIV 7, 10, and 13. The intensity scale ranges from 0 to 10 spikes per second. (**B**) Raster plot of neuronal spiking from 4096 electrodes (y-axis) for 60 s recording (x-axis). Mustard color represents spike network bursts and blue represents spike bursts. (**C**) Box plot of the number of total spikes for 60 s recordings in the individual culture chips. Blue for DIV 7, green for DIV 10, and red for DIV 13. (**D**) Box plot of mean firing rate (MFR) in spikes per second. (**E**) Box plot of interspike interval (ISI) in milliseconds. (**F**) Average burst duration with error bars in milliseconds. (**G**) Average of the mean number of spikes per burst in the raster plot with error bars. (**H**) Average of burst frequency in bursts per minute with error bars. (**I**) Average of network burst in interquartile range in milliseconds. In all the box plots above, the lower quartile as the borderline of the box nearest to zero expresses the 25th percentile, whereas the upper quartile as the borderline of the box farthest from zero indicates the 75th percentile. Error bars show SEMs. *** $p < 0.005$; unpaired, two-tailed *t*-test with Welch's correction; n.s. not significant.

2.4. The Effects of Aβ42 Oligomers and 5XFAD NLF-Derived Exosomes on the LFP Property and Oscillation in OHSCs

In contrast to the formation of intrinsic circuitry in the brain, neuronal culture is limited in its artificial construction. To determine the network properties of neurons in a more natural environment, we tested OHSCs incubated with Aβ42 oligomers and 5XFAD NLF-derived exosomes using HD-MEA (Nissl staining image of the cortical slice in Figure S2A). Under 4AP stimulation, LFP signals in slices were recorded after incubation for 12 days with each treatment. Due to the deleterious influence of the degenerative factors,

it was inevitable to rescue only single active OHSCs for each group from several slices in preparation. Figure 4A presents typical LFP traces for the dentate gyrus (DG) and cornu ammonis (CA) 1 and 2 overlaid on the MEA recording. As in neuronal cultures, internal connections within slices were represented in OHSCs that overlapped on top of the MFR responses (light-blue lines, Figures 4A and S2B(b–d)). After low-pass filtering (<200 Hz), certain oscillations were evident in the DG, CA1, and CA3 of each OHSC (Figure 4A). Based on the LFP analysis, Aβ42 (509.71 μV for the median) exhibited the highest average amplitude, followed by the 5XFAD NLF (370.36 μV) and control (278.82 μV), although the 5XFAD NLF still exhibited the widest deviation range (Figure 4B; control, 279; Aβ42, 25; 5XFAD, 186 for the number of active sites in the recording arena).

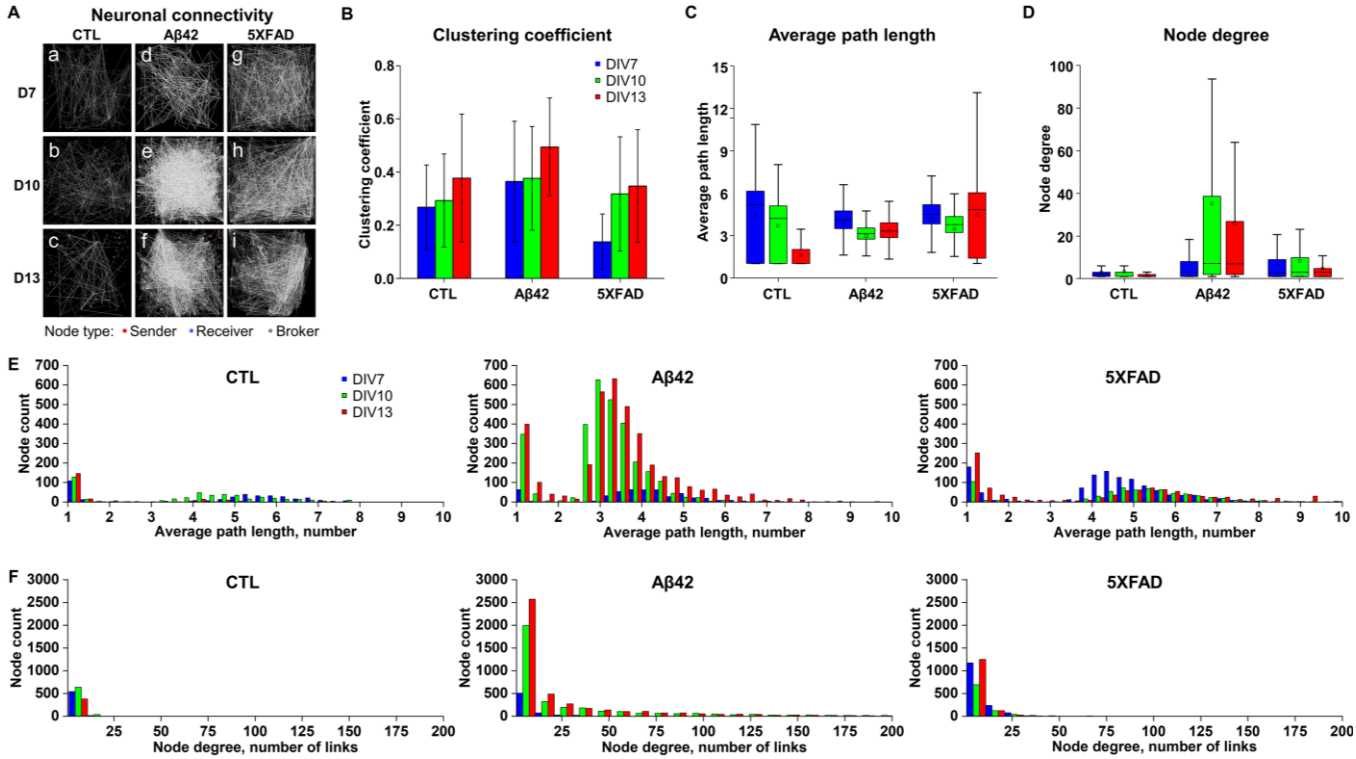

Figure 3. Characteristics of neuronal connectivity in networks. (**A**) Neuronal connectivity map in spontaneous neuronal activation during 60 s recordings represented from the 64 × 64 grid electrode arena (2.67 × 2.67 mm^2). Control (CTL; a–c), Aβ42 (d–f), and 5XFAD (g–i) NLF treatment groups on DIV 7, 10, and 13. The red dot represents a node of the sender, blue the receiver, and gray the broker. The white lines describe the connections between nodes. (**B**) Average clustering coefficients from neuronal connections for 60 s recordings in the individual culture chips. Blue for DIV 7, green for DIV 10, and red for DIV 13. (**C**) Box plot of average path length in a number of links. (**D**) Box plot of node degrees. (**E**) Distribution histogram of node counts to average path length in number. (**F**) Distribution histogram of node counts to node degree in a number of links.

Furthermore, the 5XFAD NLF maintained both the highest average value and a wide deviation in the LFP rate (Figure 4C; control, 60.05 ± 0.01 fp/min; Aβ42, 86.66 ± 7.23 fp/min; 5XFAD, 188.50 ± 73.37 fp/min) and duration (Figure 4D; control, 37.34 ± 1.74 ms; Aβ42, 15.71 ± 0.44 ms; 5XFAD, 61.77 ± 5.99 ms). Despite differences in the LFP characteristics, the energy levels in all slices were unaltered, suggesting that the activity dynamics were consistent across test samples (Figure 4E; control, 0.20 ± 0.01 μV·ms; Aβ42, 0.22 ± 0.02 μV·ms; 5XFAD, 0.18 ± 0.01 μV·ms).

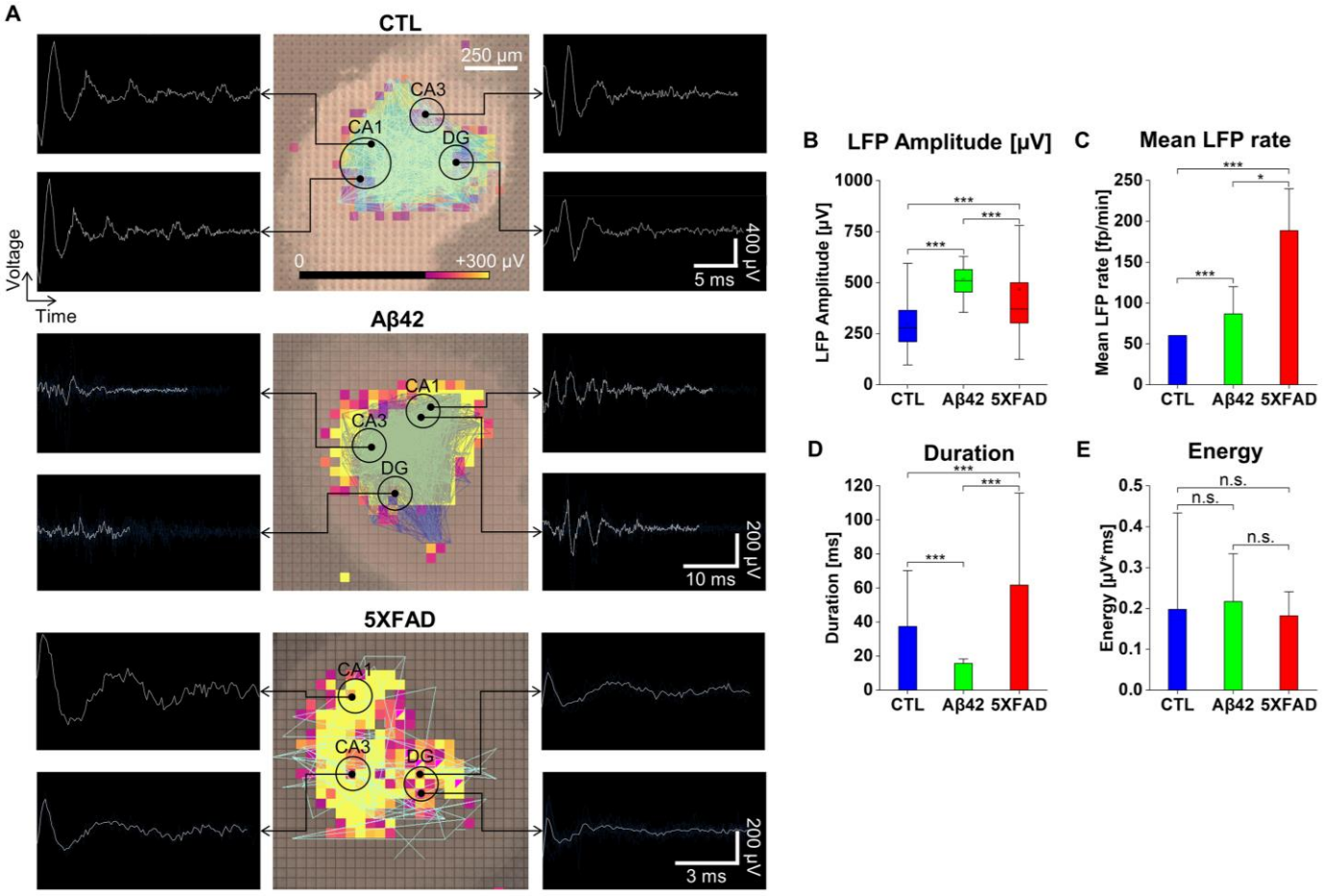

Figure 4. MEA record of LFP responses in organotypic hippocampal slices (OHCSs). (**A**) Overlay of LFP activities over the OHCSs with distinctive waveforms in DG, CA1, and -2 regions represented from the 64 × 64 grid electrode arena (2.67 × 2.67 mm^2). Control, Aβ42, and 5XFAD NLF treatment groups after incubation of 12 days. The intensity of LFP activity in the color scale from 0 to 300 μV. The white waveforms inside the black columns represent LFP signals from the specific locations denoted by arrows. The sky-blue lines overlaid on the slice images represent connections within the slices. LFP waveforms after the low-pass filter (<200 Hz). (**B**) Box plot of LFP amplitude in micro voltage. (**C**) Average of mean LFP rate in number of LFPs per minute with error bars. (**D**) The average duration of LFPs in milliseconds with error bars. (**E**) Average of mean LFP energy in charge unit of measurement for the area under a voltage–time curve. Error bars show SEMs. *** $p < 0.005$, * $p < 0.05$; unpaired, two-tailed *t*-test with Welch's correction; n.s. not significant.

2.5. Current Source Density (CSD) Analysis to Localize LFP Distribution in OHSCs

Although LFP analysis can deliver characteristic neural activity in brain slices, the vulnerability of the far-field effect to volume conduction is an intrinsic limitation of LFP analysis in terms of signal transmission in recording slices. To overcome this limitation, a second spatial derivative of LFP, the CSD, can be applied to estimate LFP distribution and propagation with high accuracy [23,24]. Comparing mean CSDs across groups, the 5XFAD NLF group exhibited the highest level, implying significantly larger electrical current sources than sinks on the recording slices (Figure 5A; control, 5.26; Aβ42, 5.76; 5XFAD, 7.52 for the median values). Although the mean value of the Aβ42 group was lower than that of the 5XFAD NLF group, the deviation was wider, suggesting that the data for individual slices were complex and spread between the control and 5XFAD NLF samples. The transformation of LFP data into CSD was generated in a time-series representation, illustrating the dynamic interplay of sinks and sources of neural activity. (Movies S1–S3). Representative photographic images were captured during the spread of activity (Figure 5B,C). Parsing

of CSD signals separated the sink and source waveforms, where the level and frequency of ridges and furrows of the wave spread were observed (Figure S4A–C). 5XFAD NLF showed the most volatile dynamics, followed by that of the Aβ42-treated OHSCs.

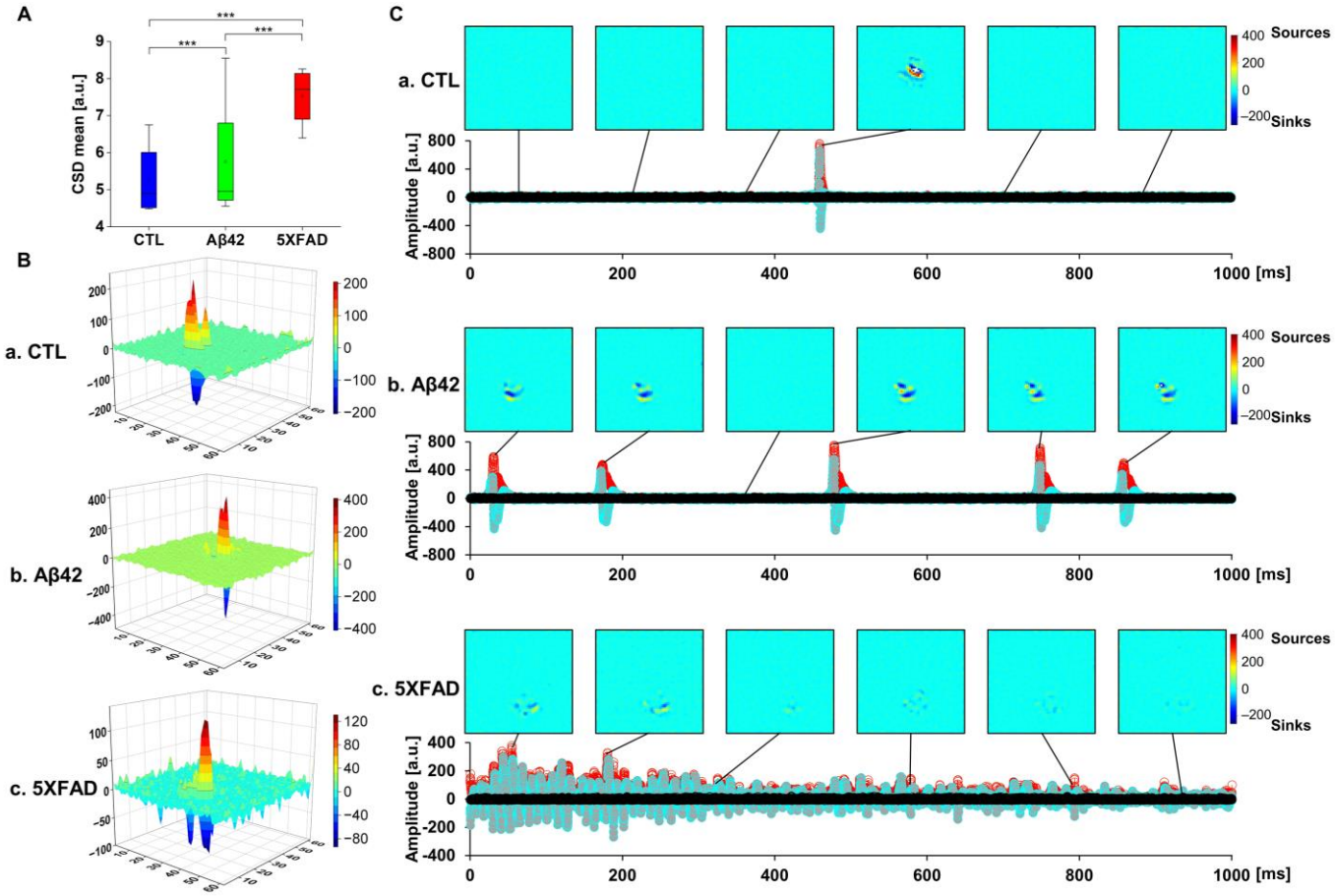

Figure 5. CSD propagation in organotypic hippocampal slices (OHCSs). (**A**) Box plot of CSD means in arbitrary units (a.u.). (**B**) Snapshot of CSD amplitude changes in 3D graph captured from Movies S1–S3 of respective CSD propagations. Blue for sinks and red for sources in the scale bar. (**C**) Distribution of CSD incidences over time in amplitude. The upper images were captured from Movies S1–S3 of the respective CSD propagations. Blue for sinks and red for sources in the scale bar. *** $p < 0.005$; unpaired, two-tailed *t*-test with Welch's correction.

3. Discussion

Exosome research, especially in relation to Alzheimer's disease (AD), has surged in recent years due to their critical role in cellular mediation. Pathological propagation akin to prion diseases has been found in Aβ42, a factor implicated in AD [25]. Despite this knowledge, the exact transfer mechanism of Aβ42 between cells remains elusive. Exosomes carrying Amyloid precursor protein (APP) and Aβ42 have been implicated in the AD pathogenesis, potentially aiding the dissemination of pathological agents [26–28]. In this study, we collected nasal lavage fluid (NLF), as it enables non-invasive and convenient procurement of large volumes of nasal washes in clinical settings. Given the strong correlation between olfactory dysfunction and dementia symptoms, we postulated that NLF-derived exosomes may contain AD-related pathological molecules [29–32]. We employed microfluidic sorting technology to obtain intact exosomes from clean nasal washes in mice [17,33]. However, due to the minimal amounts of exosomes present in the collected nasal washes, the characterization of internal contents faced technical hurdles. Moreover, proteomic or RNA sequencing analysis requires the collection of substantial volumes of nasal wash, thereby posing challenges when testing novel samples for the first time.

Neuronal hyperactivity is a distinctive early-stage AD feature implicated in epileptic seizures in both humans and animal AD models [34–36]. Our electrophysiological results concerning the treatment of neuronal cell cultures with soluble Aβ42 oligomers align with previous findings about neuronal hyperexcitability [37–40]. Surprisingly, treatment with 5XFAD NLF exosomes also amplified neuronal activity, consistent with a prior report on hippocampal hyperactivity using 5XFAD brain slices [41,42]. Based on accumulated evidence, this can be attributed to the attenuation of inhibitory postsynaptic currents and metabolic dysfunction between neurons and astrocytes in 5XFAD hippocampal neurons. Herein, the connectivity between neuronal networks could be systematically determined owing to the exceptional integrity of the HD-MEA recordings from 4096 electrodes in real time. The gradual increase in clustering coefficient values in aging cultures indicates that network stability can also be developed gradually in neurodegenerative conditions, such as Aβ42 oligomer and 5XFAD NLF exosome treatment. According to the quantitative dimensions of the network, this pathological environment stimulates cluster formation within neuronal cultures relevant to neuronal hyperexcitability. Apart from the superficial observation of the network, the qualitative analysis calculated from the PLs between nodes revealed that disintegration of network efficiency occurs during a long incubation period with 5XFAD NLF exosomes at a rate similar to that with Aβ42 treatment. A longitudinal study of soluble Aβ42 oligomers and 5XFAD NLF exosomes in OHSCs was also conducted to determine their neuromodulatory effects in mouse hippocampal slices. We noted increased LFP responses in Aβ42 oligomers and 5XFAD NLF exosomes in OHSCs, which mirrored the increase in neuronal activity observed in the dissociated cultures. The Aβ42 oligomer-treated neuronal cultures exhibited the strongest topological activation characteristics and connectivity. However, the LFP property was higher in 5XFAD NLF exosomes than in those treated with Aβ42 oligomers, which was also reflected in the CSD analysis. In this case, the intrinsic structure of the hippocampal slices possibly consists of neurons and glial cells interspersed within a specific circuit. Altered current conduction in hippocampal slices may result from the interaction of substances in NLF exosomes with diverse cells in the circuitry.

Utilizing HD-MEA recordings, we demonstrated the functional effect of NLF-derived exosomes from AD model animals. Despite being a preliminary trial to explore the influence of exosomes on the neural network of the AD brain, this study presents a novel possibility of NLF-derived exosomes inducing neuronal circuitry reorganization that would be a crucial sign in the disease progression. Applying the innovative technology used in this study, more conclusive results could be derived to characterize the neural network effect of exosomes derived from other types of neurodegenerative animal models, provided a sufficient amount of exosomes and a valid number of brain slices are available.

4. Materials and Methods

4.1. Animals

B6SJL-Tg (APPSwFlLon, PSEN1×M146L×L286V) (5XFAD) mice were purchased from The Jackson Laboratory (MMRRC Stock No.: 34840-JAX) (Bar Harbor, ME, USA), and experimental procedures were performed according to protocols approved by the Institutional Animal Care and Use Committee (IACUC) of KPCLab (approval number: P171011) (Matthews Urbana, IL, USA) and ©MEDIFRON DBT Inc. (approval number: Medifron 2017-1) (Seoul, Republic of Korea). C57BL/6 mice were obtained from OrientBio Inc. (Gyeonggi, Republic of Korea), and compliance with relevant ethical regulations and animal procedures was reviewed and approved by Seoul National University Hospital IACUC (approval number: 16-0043-c1a0). For the experiments, three animals from each group were used to obtain OHSCs. Two slices were selected based on the LFP activities for control, Aβ42, and 5XFAD in Figure 4.

4.2. Nasal Lavage Fluid Extraction

The procedure of NLF extraction was followed by the previous method [33]. After anesthesia, the left ventricle of the mice was cannulated, and blood was cleared by perfusion with cold PBS. Using scissor dissection, the upper airway, including the palatopharyngeal region, was separated, and the mouse head was separated at the larynx level of the upper airway. Two consecutive volumes of 350 µL of PBS were instilled through the pharyngeal opening into the choana. NLF fluids were centrifuged, and supernatants were stored at −80 °C until assayed. To negate the impact of the varying concentrations and scrutinize the effects of 5XFAD and CTL exosomes at equivalent concentrations, a normalization procedure for each exosome sample was implemented. Specifically, the isolated 5XFAD sample was amalgamated with a buffer to equilibrate the concentration of exosomes originating from CTL.

4.3. Nanoparticle Tracking Analysis

NTA was performed using an LM10 (NanoSight, Salisbury, UK) instrument. Exosomes separated from minuscule amounts of nasal lavage fluid were diluted with filtered phosphate-buffered saline (PBS) to examine 20 particles per frame and gently injected into the laser chamber. Each exosome sample was subjected to a red laser (642 nm) three times for 1 min; the detection threshold was set to 5 to allow the detection of nanosized particles. The data were analyzed using NTA software (ver. 3.1; NanoSight). All experiments were conducted at room temperature.

4.4. Exosome Purification

Nasal-derived exosome isolation was performed as described previously [17–19], with minor modifications. In brief, nasal lavage fluid harvested from the mouse model was filtered through a 0.2 µm syringe filter (Sartorius, Goettingen, Germany) to remove aggregates. The nasal fluid, including extracellular vesicles, was carefully collected and kept on ice before performing exosome separation using FAST. To isolate exosomes, the purification buffer was filtered through a 0.2 µm syringe filter. The flow ratio of sample:buffer: magnification was set at 5:95:75. Exosome-sized particles were separated from the other particles, and all samples were maintained at 4 °C during exosome purification.

4.5. Western Blotting

CD63 expression was quantitatively analyzed using Western blotting. Purified exosomes were mixed with 5% sodium dodecyl sulfate (SDS) sample buffer (Tech & Innovation, Gangwon, Republic of Korea), and sliced tissues were lysed and homogenized in radioimmunoprecipitation assay buffer (Tech & Innovation, Republic of Korea) containing protease inhibitors. The protein concentrations of the separated solutions were measured using the Bradford assay (Bio-Rad, Hercules, CA, USA). The samples were heated for 10 min at 97 °C. Next, 15 µg of protein from each sample was subjected to SDS-polyacrylamide gel electrophoresis (PAGE) (12%) and transferred to polyvinylidene difluoride (PVDF) membranes (Bio-Rad) for 90 min. Each membrane was blocked with 5% skim milk (BD Life Sciences, Franklin Lakes, NJ, USA) in TBST buffer (25 mM Tris, 190 mM NaCl, and 0.05% Tween 20, pH 7.5) for 1 h at room temperature, followed by incubation with primary antibodies (anti-CD63, 1:300; Novus Biologicals, Centennial, CO, USA) at 4 °C overnight. After five 20 min washes with TBST, each membrane was washed three times in Tween-20 and incubated with goat anti-mouse IgG for 2 h. Bands were visualized using an enhanced chemiluminescence system; the intensity of the blots was quantified with Image J 1.44 software (https://imagej.nih.gov/ij/plugins/index.html) [43].

4.6. Transmission Electron Microscopy

Separated exosomes were diluted and fixed with 2% glutaraldehyde overnight at 4 °C. The mixture of exosomes and fixation solution was then diluted 10-fold with PBS for electron microscopic observation. Briefly, 5 µL of each sample was plated onto a glow-

discharged carbon-coated grid (Harrick Plasma, Ithaca, NY, USA), which was immediately negatively stained using 1% uranyl acetate. The exosome samples on the grids were observed under a Tecnai 10 transmission electron microscope (FEI, Hillsboro, OR, USA) operated at 100 kV. Images were acquired with a 2K × 2K UltraScan CCD camera (Gatan, Pleasanton, CA, USA).

4.7. Aβ42 Oligomer Preparation

The peptide corresponding to human Aβ42 (Anaspec, Fremont, CA, USA, AS-64129-1, 1 mg) was dissolved in 100 µL of DMSO by vortexing for 30 min at room temperature, and then the solution was added to 900 µL of PBS for incubation at 4 °C for 24 h.

4.8. Primary Neuron Culture

Dissection medium Neurobasal Media (NBM) consisted of 45 mL Neurobasal Medium A, 1 mL B27 (50 X), 0.5 mM Glutamine sol, 25 µM Glutamate, 5 mL Horse serum, and 500 µL penicillin/streptomycin. And the culture medium consisted of 50 mL Neurobasal Medium A, 1 mL B27, 0.5 mM Glutamine sol, 500 µL penicillin/streptomycin, and 50 µL HEPES. The Biochip chamber (3Brain, Arena, Houston, TX, USA) was cleaned, filled with 70% ethanol for 20–30 min, rinsed with autoclaved DDW 3–4 times, and, dried in the clean bench overnight with NBM. On the day after, 30–90 µL filtered PDLO which dissolved in borate buffer on the active surface of the Biochip was added and placed overnight in the incubator. The Biochip was washed with autoclaved DDW 3 times before cell seeding. Primary cortical and hippocampal neuron cultures were prepared from postnatal 0-day mouse pups. The pups were decapitated with sterilized scissors and the whole brain was removed. The removed brain was chilled in a cold neurobasal medium with papain 0.003 g/mL solution at 4 °C in a 35 mm diameter dish. Surrounding meninges and excess white matter were pulled out under the microscope (Inverted microscope, Nikon, Tokyo, Japan) in the same solution and transferred to the second dish at 4 °C. The cortex and hippocampus parts were isolated from other parts of the brain, washed with NBM and papain solution, and minced into small pieces. The minced tissues were transferred into a 15 mL tube and incubated for 30 min in the 37 °C water bath. After, the tube was inverted gently every 5 min to be mixed. The tissues were washed with HBSS twice, after being settled down, and the cortex and hippocampi tissues were transferred into prewarmed NBM and triturated 20–30 times using a fire-polished Pasteur pipette. The number of cells was counted and 30–90 µL drops of the cells were plated in the Biochip, which contains ~1000–1500 cells/µL (incubated at 37 °C in 5% CO_2). From day 2 of the culture, the whole medium was replaced with a fresh feeding medium every 3 days. A quantity of 10 µM of Aβ42 oligomers was treated at DIV 7, 10, and 13. 5XFAD NLF exosomes were incubated from DIV 7 until DIV 13.

4.9. Organotypic Hippocampal Slice Culture

The dissection medium consisted of 40 mL Hibernate A, 0.5 mM L-Glutamine, and 10 mL Horse serum. Growth medium 1 consisted of 40 mL Neurobasal A, 20% Horse serum, and 400 µL penicillin/streptomycin solution. Growth medium 2 consisted of 40 mL Neurobasal A, 2% B27, and supplement, 400 µL penicillin/streptomycin solution. The organotypic hippocampal slice culture was prepared from postnatal 7-day mouse pups. Decapitation was performed under cervical dislocation, and the entire brain was removed with forceps and chilled in Hibernate A medium for 10 s at 4 °C. After that, the excess white matter and meninges surrounding the brain were removed under the microscope (inverted microscope; Nikon, Japan) carefully and the hippocampus was dissected with a spatula. The dissected hippocampus was placed on the tissue chopper instrument (Stoelting tissue slicer) which has filter-paper coverage and sliced transversally to 300 µm. The freshly cut sections were collected into the cold dissection medium and separated from each other with a spatula. From the best slices, up to 4 slices were transferred onto the cold culture membrane (Millicell membrane, 0.4 µm), which was then placed into the prewarmed 6-well

plate with growth medium 1. From day 2, the medium was changed with growth medium 2, and the whole medium was replaced every 3 days. Quantities of 10 μM of Aβ42 oligomers and 5XFAD NLF exosomes were treated at DIV 7 until DIV 13.

4.10. Neuronal Spike and LFP Recording with the High-Density Multielectrode Array (HD-MEA)

High-density multielectrode array (HD MEA) recording with 4096 electrodes in a CMOS Biochip (BiocamX, 3Brain GmbH, Pfäffikon, Switzerland) was conducted at a sampling rate of 9 KHz. The active electrode, which is 21 μm × 21 μm in size and 42 μm in pitch, is implanted in the array with a 64 × 64 grid (2.67 × 2.67 mm^2) centered in a working area (6 × 6 mm^2). The brain slice was positioned at the center of the Biochip under the square-shape platinum net anchor to prevent it from displacement by the perfusion flux. To overlay the real image of the slice at the site of recording, a stereomicroscope with transmitted illumination was settled over the slice with 20× magnification (Nikon, SMZ745T, Japan). The neuronal activities in cortex slices were recorded for approximately 35 min with and without additional chemicals. To generate spontaneous epileptic-like discharges, the slices were perfused with Kv1 channel blocker 4-Aminopyridine (4AP) 250 μM (Sigma-Aldrich, Saint Louis, MO, USA). The spontaneous response was recorded for the first 5 min following the oxygenated 4AP for up to 15 min. All recordings were conducted by Brainwave 5 software (3Brain GmbH, Switzerland; https://www.3brain.com/products/software/brainwave5).

4.11. HD MEA Data Analysis

Raw data were filtered with an IIR low-pass filter (cutoff at 200 Hz, order 5) before LFP detection. To identify LFP events, a standard hard double-threshold algorithm was used (upper threshold, 40 μV; lower threshold, −40 μV). When the signal overcame one of the two thresholds, an LFP was detected. To determine the duration of the LFP, the energy of the signal was calculated on a sliding window of 50 ms moving forward and backward around the peak until the energy was 1.5 times higher than the energy calculated on the noise. A refractory period (i.e., the minimum distance between two consecutive LFPs on an electrode) of 50 ms was set by the operator. An electrode was considered active if the LFP rate was at least 0.05 event/s. After detection, statistics on the LFP features were extracted by averaging the parameter on each electrode along the recording. The distribution of the feature was calculated by grouping electrodes belonging to the same anatomical area. To identify the different areas concerning the electrode's position, an image of the recorded slice was superimposed on the map of the electrode grid, allowing manual selection of electrodes for each area of interest. LFP events generally involved most of the area of interest, so to get rid of spurious false-positive detected events, an automated cleaning procedure was used before feature extraction. Detected LFPs were considered valid only if they occurred simultaneously on at least 40% of the total electrodes of an area within a time window of 300 ms. All the parameters from spike detection and LFP recording were calculated with brainwave 5 software (3Brain GmbH, Switzerland; https://www.3brain.com/products/software/brainwave5) [44].

4.12. Current Source Density (CSD) Analysis

In the two-dimensional CSD analysis, we first preprocessed the data in two steps: first, at each time point, we identified the saturated electrodes by simple thresholding and inpainted missing signals by linear interpolation with the data from surrounding regions. We monitored how much space the saturated electrodes occupied and checked whether this procedure caused any noticeable artifacts. Then, we smoothed the data spatially by a

Gaussian kernel with σ = dpitch. From this, the current source was estimated by applying the modified two-dimensional Laplacian:

$$\begin{aligned} CSD(x,y,t) &= -\nabla^2\phi(x,y,t) \\ &\approx -\tfrac{2}{3}\cdot[\phi(x\pm\Delta x,y,t)+\phi(x,y\pm\Delta y,t)-4\phi(x,y,t)] \\ &\quad -\tfrac{1}{6}\cdot[\phi(x\pm\Delta x,y\pm\Delta y,t)+\phi(x\pm\Delta x,y\mp\Delta y,t)-4\phi(x,y,t)]. \end{aligned}$$

From this, we isolated the CSD within the region of interest (ROI) and time window of interest (TOI), computed in the following way: We first estimated the dynamic amplitudes of LFP signals, $A(x,y,t)$, by applying Hilbert transformation (MATLAB function *hilbert*) and computing their absolute values. Then, for each (x, y), we computed the amplitude variability, $\xi(x,y) = \mathrm{STD}[A(x,y,t)]_t$, and the ROI was selected by a criterion, $\xi(x,y) > \mathrm{Median}[\xi(x,y)] + 2.326\ \mathrm{STD}[\xi(x,y)]$. For each (x, y) in the ROI, a TOI was selected by $A(x,y,t) > \mu_{\mathrm{noise}} + 2.326\ \sqrt{2}\ \sigma_{\mathrm{noise}}$, where $\mu_{\mathrm{noise}} = \left\langle \bar{A}(x,y) \right\rangle_{(x,y)\notin ROI}$, $\sigma_{\mathrm{noise}} = \mathrm{STD}\left[\bar{A}(x,y)\right]_{(x,y)\notin ROI}$, and $\bar{A}(x,y)$ is the temporal average of $A(x,y,t)$. Then, the average rectified CSD (rCSD) was computed by averaging the absolute value of the CSD, $|\mathrm{CSD}(x,y,t)|$, within the ROI and TOI.

All CSD analysis was performed by custom scripts in MATLAB 2018a (Mathworks Inc., Natick, MA, USA), which will be made available upon request.

5. Conclusions

Applying HD-MEA, our study illuminates the impacts of 5XFAD NLF-derived exosomes on neural networks, expanding our comprehension of intracerebral communication and its implications for AD. Analogous to the effects of amyloid-beta oligomer treatment, the exosomes result in the biphasic neural activation reminiscent of MCI patients' neurophysiology. These findings underscore the implication of exosomes in AD, additionally introducing a novel possibility of HD-MEA as an efficacious method for the study of neural networks.

Supplementary Materials: The following supporting information can be downloaded at: https://www.mdpi.com/article/10.3390/ijms241814064/s1.

Author Contributions: Conceptualization, S.K., J.J., D.G., T.K., K.S., S.H. and J.H. methodology, J.J. and D.G.; software, J.J., D.G., T.K., K.S. and S.H.; validation, J.J., D.G., T.K., K.S. and S.H.; formal analysis, S.K., J.J., D.G., T.K., K.S. and S.H.; investigation, S.K. and J.H.; resources, S.K. and J.H.; data curation, J.J., D.G., T.K., K.S. and S.H.; writing, S.K. and J.H.—original draft preparation, S.K.; writing—review and editing, S.K. and J.H.; visualization, S.K., J.J., D.G., T.K., K.S. and S.H.; supervision, S.K. and J.H.; project administration, S.K., and J.H.; funding acquisition, S.K. and J.H. All authors have read and agreed to the published version of the manuscript.

Funding: This research was supported by a grant from the Korea Health Technology R&D Project through the Korea Health Industry Development Institute (KHIDI), funded by the Ministry of Health and Welfare, Republic of Korea (grant number: HI17C1711). In addition, it was supported by the Bio & Medical Technology Development Program of the National Research Foundation (NRF), funded by the Ministry of Science and ICT (2018M3A9H1023323), and also by the National Research Foundation of Korea (NRF) grant, funded by the Korea government (MSIT) (2022R1A2C1093134). S.H. was supported by the Okinawa Institute of Science and Technology Graduate University.

Institutional Review Board Statement: The animal study protocol was approved by Hanyang University IACUC (protocol code 2019-0192A with date of approval 3 December 2019).

Data Availability Statement: All the data can be shared through the database of MDPI.

Acknowledgments: We thank Hyun Suk of Kangwon National University for his help in the preparation of TEM images and GENUV Inc. for providing the 5XFAD animals. We also appreciate Yunjong Lee for providing the Nissl staining image.

Conflicts of Interest: The authors declare no conflict of interest.

References

1. Sharma, P.; Mesci, P.; Carromeu, C.; McClatchy, D.R.; Schiapparelli, L.; Yates, J.R., 3rd; Muotri, A.R.; Cline, H.T. Exosomes regulate neurogenesis and circuit assembly. *Proc. Natl. Acad. Sci. USA* **2019**, *116*, 16086–16094. [CrossRef]
2. Spelat, R.; Jihua, N.; Sanchez Trivino, C.A.; Pifferi, S.; Pozzi, D.; Manzati, M.; Mortal, S.; Schiavo, I.; Spada, F.; Zanchetta, M.E.; et al. The dual action of glioma-derived exosomes on neuronal activity: Synchronization and disruption of synchrony. *Cell Death Dis.* **2022**, *13*, 705. [CrossRef]
3. Xia, X.; Wang, Y.; Qin, Y.; Zhao, S.; Zheng, J.C. Exosome: A novel neurotransmission modulator or non-canonical neurotransmitter? *Ageing Res. Rev.* **2022**, *74*, 101558. [CrossRef]
4. Gharbi, T.; Zhang, Z.; Yang, G.Y. The Function of Astrocyte Mediated Extracellular Vesicles in Central Nervous System Diseases. *Front. Cell Dev. Biol.* **2020**, *8*, 568889. [CrossRef]
5. Zhao, S.; Sheng, S.; Wang, Y.; Ding, L.; Xu, X.; Xia, X.; Zheng, J.C. Astrocyte-derived extracellular vesicles: A double-edged sword in central nervous system disorders. *Neurosci. Biobehav. Rev.* **2021**, *125*, 148–159. [CrossRef]
6. Rajendran, L.; Honsho, M.; Zahn, T.R.; Keller, P.; Geiger, K.D.; Verkade, P.; Simons, K. Alzheimer's disease beta-amyloid peptides are released in association with exosomes. *Proc. Natl. Acad. Sci. USA* **2006**, *103*, 11172–11177. [CrossRef]
7. Saeedi, S.; Israel, S.; Nagy, C.; Turecki, G. The emerging role of exosomes in mental disorders. *Transl. Psychiatry* **2019**, *9*, 122. [CrossRef]
8. Spera, I.; Cousin, N.; Ries, M.; Kedracka, A.; Castillo, A.; Aleandri, S.; Vladymyrov, M.; Mapunda, J.A.; Engelhardt, B.; Luciani, P.; et al. Open pathways for cerebrospinal fluid outflow at the cribriform plate along the olfactory nerves. *Ebiomedicine* **2023**, *91*, 104558. [CrossRef]
9. Mehta, N.H.; Sherbansky, J.; Kamer, A.R.; Carare, R.O.; Butler, T.; Rusinek, H.; Chiang, G.C.; Li, Y.; Strauss, S.; Saint-Louis, L.A.; et al. The Brain-Nose Interface: A Potential Cerebrospinal Fluid Clearance Site in Humans. *Front. Physiol.* **2021**, *12*, 769948. [CrossRef]
10. Ubeda-Banon, I.; Saiz-Sanchez, D.; Flores-Cuadrado, A.; Rioja-Corroto, E.; Gonzalez-Rodriguez, M.; Villar-Conde, S.; Astillero-Lopez, V.; Cabello-de la Rosa, J.P.; Gallardo-Alcaniz, M.J.; Vaamonde-Gamo, J.; et al. The human olfactory system in two proteinopathies: Alzheimer's and Parkinson's diseases. *Transl. Neurodegener.* **2020**, *9*, 22. [CrossRef]
11. Son, G.; Jahanshahi, A.; Yoo, S.J.; Boonstra, J.T.; Hopkins, D.A.; Steinbusch, H.W.M.; Moon, C. Olfactory neuropathology in Alzheimer's disease: A sign of ongoing neurodegeneration. *BMB Rep.* **2021**, *54*, 295–304. [CrossRef]
12. Jung, D.H.; Son, G.; Kwon, O.H.; Chang, K.A.; Moon, C. Non-Invasive Nasal Discharge Fluid and Other Body Fluid Biomarkers in Alzheimer's Disease. *Pharmaceutics* **2022**, *14*, 1532. [CrossRef]
13. Lasser, C.; O'Neil, S.E.; Ekerljung, L.; Ekstrom, K.; Sjostrand, M.; Lotvall, J. RNA-containing exosomes in human nasal secretions. *Am. J. Rhinol. Allergy* **2011**, *25*, 89–93. [CrossRef]
14. Bras, I.C.; Khani, M.H.; Riedel, D.; Parfentev, I.; Gerhardt, E.; van Riesen, C.; Urlaub, H.; Gollisch, T.; Outeiro, T.F. Ectosomes and exosomes modulate neuronal spontaneous activity. *J. Proteom.* **2022**, *269*, 104721. [CrossRef]
15. Frohlich, D.; Kuo, W.P.; Fruhbeis, C.; Sun, J.J.; Zehendner, C.M.; Luhmann, H.J.; Pinto, S.; Toedling, J.; Trotter, J.; Kramer-Albers, E.M. Multifaceted effects of oligodendroglial exosomes on neurons: Impact on neuronal firing rate, signal transduction and gene regulation. *Philos. Trans. R. Soc. B Biol. Sci.* **2014**, *369*, 20130510. [CrossRef]
16. Ganbat, D.; Jeon, J.K.; Lee, Y.; Kim, S.S. Exploring the Pathological Effect of Abeta42 Oligomers on Neural Networks in Primary Cortical Neuron Culture. *Int. J. Mol. Sci.* **2023**, *24*, 6641. [CrossRef]
17. Shin, S.; Han, D.; Park, M.C.; Mun, J.Y.; Choi, J.; Chun, H.; Kim, S.; Hong, J.W. Separation of extracellular nanovesicles and apoptotic bodies from cancer cell culture broth using tunable microfluidic systems. *Sci. Rep.* **2017**, *7*, 9907. [CrossRef]
18. Shin, K.; Lee, E.; Hong, J.W. Nanoparticles Are Separated in a Different Pattern from Microparticles with Focused Flow Control. *Langmuir* **2020**, *36*, 7210–7216. [CrossRef]
19. Karima, G.; Shin, K.; Jeong, J.; Choi, D.; Hwang, K.-G.; Hong, J.W. Stem Cell Oriented Exosomes Regulate Cell Proliferation in Hepatoma Carcinoma. *Biotechnol. Bioprocess Eng.* **2023**, *28*, 263–273. [CrossRef]
20. Yoo, S.J.; Son, G.; Bae, J.; Kim, S.Y.; Yoo, Y.K.; Park, D.; Baek, S.Y.; Chang, K.A.; Suh, Y.H.; Lee, Y.B.; et al. Longitudinal profiling of oligomeric Abeta in human nasal discharge reflecting cognitive decline in probable Alzheimer's disease. *Sci. Rep.* **2020**, *10*, 11234. [CrossRef]
21. Mossink, B.; Verboven, A.H.A.; van Hugte, E.J.H.; Klein Gunnewiek, T.M.; Parodi, G.; Linda, K.; Schoenmaker, C.; Kleefstra, T.; Kozicz, T.; van Bokhoven, H.; et al. Human neuronal networks on micro-electrode arrays are a highly robust tool to study disease-specific genotype-phenotype correlations in vitro. *Stem Cell Rep.* **2021**, *16*, 2182–2196. [CrossRef] [PubMed]
22. Watts, D.J.; Strogatz, S.H. Collective dynamics of 'small-world' networks. *Nature* **1998**, *393*, 440–442. [CrossRef] [PubMed]
23. Nicholson, C. Theoretical analysis of field potentials in anisotropic ensembles of neuronal elements. *IEEE Trans. Biomed. Eng.* **1973**, *20*, 278–288. [CrossRef] [PubMed]
24. Nicholson, C.; Freeman, J.A. Theory of current source-density analysis and determination of conductivity tensor for anuran cerebellum. *J. Neurophysiol.* **1975**, *38*, 356–368. [CrossRef] [PubMed]
25. Shankar, G.M.; Li, S.; Mehta, T.H.; Garcia-Munoz, A.; Shepardson, N.E.; Smith, I.; Brett, F.M.; Farrell, M.A.; Rowan, M.J.; Lemere, C.A.; et al. Amyloid-beta protein dimers isolated directly from Alzheimer's brains impair synaptic plasticity and memory. *Nat. Med.* **2008**, *14*, 837–842. [CrossRef]

26. Sharples, R.A.; Vella, L.J.; Nisbet, R.M.; Naylor, R.; Perez, K.; Barnham, K.J.; Masters, C.L.; Hill, A.F. Inhibition of gamma-secretase causes increased secretion of amyloid precursor protein C-terminal fragments in association with exosomes. *FASEB J.* **2008**, *22*, 1469–1478. [CrossRef]
27. Howitt, J.; Hill, A.F. Exosomes in the Pathology of Neurodegenerative Diseases. *J. Biol. Chem.* **2016**, *291*, 26589–26597. [CrossRef]
28. Yuyama, K.; Sun, H.; Mitsutake, S.; Igarashi, Y. Sphingolipid-modulated exosome secretion promotes clearance of amyloid-beta by microglia. *J. Biol. Chem.* **2012**, *287*, 10977–10989. [CrossRef]
29. Bathini, P.; Brai, E.; Auber, L.A. Olfactory dysfunction in the pathophysiological continuum of dementia. *Ageing Res. Rev.* **2019**, *55*, 100956. [CrossRef]
30. Doty, R.L. Olfactory dysfunction in neurodegenerative diseases: Is there a common pathological substrate? *Lancet Neurol.* **2017**, *16*, 478–488. [CrossRef]
31. Attems, J.; Jellinger, K.A. Olfactory tau pathology in Alzheimer disease and mild cognitive impairment. *Clin. Neuropathol.* **2006**, *25*, 265–271. [PubMed]
32. Marin, C.; Vilas, D.; Langdon, C.; Alobid, I.; Lopez-Chacon, M.; Haehner, A.; Hummel, T.; Mullol, J. Olfactory Dysfunction in Neurodegenerative Diseases. *Curr. Allergy Asthma Rep.* **2018**, *18*, 42. [CrossRef]
33. Cho, S.H.; Oh, S.Y.; Zhu, Z.; Lee, J.; Lane, A.P. Spontaneous eosinophilic nasal inflammation in a genetically-mutant mouse: Comparative study with an allergic inflammation model. *PLoS ONE* **2012**, *7*, e35114. [CrossRef] [PubMed]
34. Verret, L.; Mann, E.O.; Hang, G.B.; Barth, A.M.; Cobos, I.; Ho, K.; Devidze, N.; Masliah, E.; Kreitzer, A.C.; Mody, I.; et al. Inhibitory interneuron deficit links altered network activity and cognitive dysfunction in Alzheimer model. *Cell* **2012**, *149*, 708–721. [CrossRef] [PubMed]
35. Vossel, K.A.; Beagle, A.J.; Rabinovici, G.D.; Shu, H.; Lee, S.E.; Naasan, G.; Hegde, M.; Cornes, S.B.; Henry, M.L.; Nelson, A.B.; et al. Seizures and epileptiform activity in the early stages of Alzheimer disease. *JAMA Neurol.* **2013**, *70*, 1158–1166. [CrossRef]
36. Palop, J.J.; Chin, J.; Roberson, E.D.; Wang, J.; Thwin, M.T.; Bien-Ly, N.; Yoo, J.; Ho, K.O.; Yu, G.Q.; Kreitzer, A.; et al. Aberrant excitatory neuronal activity and compensatory remodeling of inhibitory hippocampal circuits in mouse models of Alzheimer's disease. *Neuron* **2007**, *55*, 697–711. [CrossRef]
37. Busche, M.A.; Chen, X.; Henning, H.A.; Reichwald, J.; Staufenbiel, M.; Sakmann, B.; Konnerth, A. Critical role of soluble amyloid-beta for early hippocampal hyperactivity in a mouse model of Alzheimer's disease. *Proc. Natl. Acad. Sci. USA* **2012**, *109*, 8740–8745. [CrossRef]
38. Busche, M.A.; Eichhoff, G.; Adelsberger, H.; Abramowski, D.; Wiederhold, K.H.; Haass, C.; Staufenbiel, M.; Konnerth, A.; Garaschuk, O. Clusters of hyperactive neurons near amyloid plaques in a mouse model of Alzheimer's disease. *Science* **2008**, *321*, 1686–1689. [CrossRef]
39. Muller, L.; Kirschstein, T.; Kohling, R.; Kuhla, A.; Teipel, S. Neuronal Hyperexcitability in APPSWE/PS1dE9 Mouse Models of Alzheimer's Disease. *J. Alzheimer's Dis.* **2021**, *81*, 855–869. [CrossRef]
40. Zott, B.; Simon, M.M.; Hong, W.; Unger, F.; Chen-Engerer, H.J.; Frosch, M.P.; Sakmann, B.; Walsh, D.M.; Konnerth, A. A vicious cycle of beta amyloid-dependent neuronal hyperactivation. *Science* **2019**, *365*, 559–565. [CrossRef]
41. Li, Y.; Zhu, K.; Li, N.; Wang, X.; Xiao, X.; Li, L.; Li, L.; He, Y.; Zhang, J.; Wo, J.; et al. Reversible GABAergic dysfunction involved in hippocampal hyperactivity predicts early-stage Alzheimer disease in a mouse model. *Alzheimer's Res. Ther.* **2021**, *13*, 114. [CrossRef] [PubMed]
42. Andersen, J.V.; Skotte, N.H.; Christensen, S.K.; Polli, F.S.; Shabani, M.; Markussen, K.H.; Haukedal, H.; Westi, E.W.; Diaz-delCastillo, M.; Sun, R.C.; et al. Hippocampal disruptions of synaptic and astrocyte metabolism are primary events of early amyloid pathology in the 5xFAD mouse model of Alzheimer's disease. *Cell Death Dis.* **2021**, *12*, 954. [CrossRef] [PubMed]
43. Schneider, C.A.; Rasband, W.S.; Eliceiri, K.W. NIH Image to ImageJ: 25 years of image analysis. *Nat. Methods* **2012**, *9*, 671–675. [CrossRef]
44. Hilgen, G.; Sorbaro, M.; Pirmoradian, S.; Muthmann, J.O.; Kepiro, I.E.; Ullo, S.; Ramirez, C.J.; Puente Encinas, A.; Maccione, A.; Berdondini, L.; et al. Unsupervised Spike Sorting for Large-Scale, High-Density Multielectrode Arrays. *Cell Rep.* **2017**, *18*, 2521–2532. [CrossRef] [PubMed]

International Journal of
Molecular Sciences

MDPI

Perspective

On the Inadequacy of the Current Transgenic Animal Models of Alzheimer's Disease: The Path Forward

Vladimir Volloch [1,*] and Sophia Rits-Volloch [2,3,*]

[1] Department of Developmental Biology, Harvard School of Dental Medicine, Boston, MA 02115, USA
[2] Division of Molecular Medicine, Children's Hospital, Boston, MA 02115, USA
[3] Department of Biological Chemistry and Molecular Pharmacology, Harvard Medical School, Boston, MA 02115, USA
* Correspondence: vladimir.volloch@gmail.com (V.V.); rits@crystal.harvard.edu (S.R.-V.)

Abstract: For at least two reasons, the current transgenic animal models of Alzheimer's disease (AD) appear to be patently inadequate. They may be useful in many respects, the AD models; however, they are not. First, they are incapable of developing the full spectrum of the AD pathology. Second, they respond spectacularly well to drugs that are completely ineffective in the treatment of symptomatic AD. These observations indicate that both the transgenic animal models and the drugs faithfully reflect the theory that guided the design and development of both, the amyloid cascade hypothesis (ACH), and that both are inadequate because their underlying theory is. This conclusion necessitated the formulation of a new, all-encompassing theory of conventional AD—the ACH2.0. The two principal attributes of the ACH2.0 are the following. One, in conventional AD, the agent that causes the disease and drives its pathology is the intraneuronal amyloid-β (*i*Aβ) produced in two distinctly different pathways. Two, following the commencement of AD, the bulk of Aβ is generated independently of Aβ protein precursor (AβPP) and is retained inside the neuron as *i*Aβ. Within the framework of the ACH2.0, AβPP-derived *i*Aβ accumulates physiologically in a lifelong process. It cannot reach levels required to support the progression of AD; it does, however, cause the disease. Indeed, conventional AD occurs if and when the levels of AβPP-derived *i*Aβ cross the critical threshold, elicit the neuronal integrated stress response (ISR), and trigger the activation of the AβPP-independent *i*Aβ generation pathway; the disease commences only when this pathway is operational. The *i*Aβ produced in this pathway reaches levels sufficient to drive the AD pathology; it also propagates its own production and thus sustains the activity of the pathway and perpetuates its operation. The present study analyzes the reason underlying the evident inadequacy of the current transgenic animal models of AD. It concludes that they model, in fact, not Alzheimer's disease but rather the effects of the neuronal ISR sustained by AβPP-derived *i*Aβ, that this is due to the lack of the operational AβPP-independent *i*Aβ production pathway, and that this mechanism must be incorporated into any successful AD model faithfully emulating the disease. The study dissects the plausible molecular mechanisms of the AβPP-independent *i*Aβ production and the pathways leading to their activation, and introduces the concept of conventional versus unconventional Alzheimer's disease. It also proposes the path forward, posits the principles of design of productive transgenic animal models of the disease, and describes the molecular details of their construction.

Keywords: Alzheimer's disease (AD); conventional AD; unconventional AD; amyloid cascade hypothesis (ACH); ACH-based models of AD; ACH-based AD drugs; ACH2.0; ACH2.0-based models of AD; intraneuronal Aβ (*i*Aβ); Aβ protein precursor (AβPP); AβPP-independent *i*Aβ production pathway

Citation: Volloch, V.; Rits-Volloch, S. On the Inadequacy of the Current Transgenic Animal Models of Alzheimer's Disease: The Path Forward. *Int. J. Mol. Sci.* **2024**, *25*, 2981. https://doi.org/10.3390/ijms25052981

Academic Editor: Claudia Ricci

Received: 13 February 2024
Revised: 27 February 2024
Accepted: 28 February 2024
Published: 4 March 2024

1. Theory of a Disease and the Theory-Guided Disease Models Are Inextricably Entangled: The Current Transgenic Animal AD Models Are Inadequate Because the Underlying Theory Is

The ultimate objective of this study is to introduce a new class of transgenic AD models. The design of this class of models is informed by the novel, recently proposed theory of conventional AD—the amyloid cascade hypothesis 2.0 (ACH2.0) [1–6]. The major

aspects and attributes of the ACH2.0 are described below. The present section elaborates the reasons that necessitated the formulation of this new theory, which in turn defines the principles of design of the adequate model systems.

1.1. The Theory of AD Defines the Construction of the Model Systems and Determines the Design of Potential Drugs: These Three Aspects Are Inextricable

Any model system of a disease is based upon and reflects the theory of that disease. The criteria of its success are simple: the pathology exhibited by it must epitomize the phenomenology of the actual disease. Accordingly, the failure of a model to faithfully reproduce the disease is indicative of the inadequacy of the underlying theory. By the same reasoning, the efficiency of drugs in the model system is only the first test. Drugs are expected to be efficient in the model system since both are based on the same theory. The real test of a drug comes with its implementation in the actual disease. If, despite its effectiveness in the model system, it were inefficient in the disease, this also would be indicative of the inadequacy of the underlying theory. Below, we examine the properties of the transgenic animal AD models and of the AD drugs designed and developed within the framework of the amyloid cascade hypothesis (ACH) theory of the disease.

1.2. The Amyloid Cascade Hypothesis: AD Is Caused and Driven by Extracellular Aβ Produced Solely in the AβPP Proteolytic/Secretory Pathway

The ACH was proposed over thirty years ago, in 1992 [7]. Its authors, Hardy and Higgins, defined it as follows: "Our hypothesis is that deposition of amyloid-β protein, the main component of the plaques, is the causative agent of Alzheimer's pathology and that the neurofibrillary tangles, cell loss, vascular damage, and dementia follow as the direct result of this deposition" [7]. When the ACH was proposed, the occurrence and composition of Aβ plaques had been known for a considerable time. The immediate principal basis for its formulation was the discovery of a mutation that affected the generation of Aβ in the AβPP proteolytic pathway [8]; this mutation segregated with and apparently caused AD [8]. The ACH theory of AD appeared, at the time of its formulation, to be consistent with the accumulated data; it served as the basis for the design of transgenic animal models of AD and the development of the candidate AD drugs.

1.3. The Current ACH-Based Transgenic AD Models Could Be Useful but Are Not Adequate

The ACH-guided approach to the design of the transgenic mouse models of AD was simple: express as much as possible of human Aβ, preferentially in the mouse neurons or CNS, and this will cause its overexpression and excessive secretion and extracellular deposition, and the disease will follow. This approach was, in fact, carried out. Numerous copies of DNA encoding human AβPP, under the control of a powerful CNS-specific promoter, were introduced into the mouse genome. As a result, Aβ was indeed overproduced and over-secreted. This caused the excessive deposition of extracellular Aβ plaques, but symptomatic manifestation of the disease was rather limited. Whereas certain neurodegeneration and cognitive impairments were observed, the formation of the neurofibrillary tau tangles, the major hallmark of AD, was not seen. In an attempt to address this issue, additional mutations known to cause the early onset of AD (familial AD, FAD) were introduced into the transgenes; those included not only AβPP/Aβ mutations but also mutations in the presenilins (PSEN) involved in the processing of AβPP. The effect, however, was only quantitative, such as earlier manifestation of neurodegeneration and of limited cognitive impairments; no NFT formation was observed in any animal model. Clearly, AD appears to entail more than the increased production/secretion of Aβ in the AβPP proteolytic pathway, even in combination with the FAD mutations. Yet, for reasons discussed below, Aβ is apparently both the cause and the driver of the disease. Moreover, as described in the following section, some cognitive defects observed in the current transgenic animal models of AD, such as impaired memory formation and learning are not necessarily AD-specific.

1.4. Elicitation of the Integrated Stress Response (ISR) in Neurons, Triggered by Aβ or Otherwise, Results in the Impairment of Synaptic Plasticity, Long-Term Memory Formation, and Learning

The integrated stress response (ISR) is an evolutionary conserved signaling pathway, which is activated in response to different environmental and pathological conditions [9–18]. Those include nutrient deprivation, variable stresses, such as oxidative stress, inflammation, viral infection, protein aggregation and misfolding, and protein homeostasis defects. The numerous and various stressors capable of the eliciting the ISR converge on a single event, namely, the phosphorylation of the eukaryotic initiation factor 2 alpha (eIF2α) at a specific position (serine residue 51), hence the "integrated" in the "integrated stress response". The elicitation of the ISR has far-reaching consequences: It reprograms and transforms both the transcriptional and translational landscapes of the affected cell. The former includes the activation of several transcription factors, and the latter results in a drastic reduction in total cellular protein synthesis via suppression of its 5′ cap-assisted initiation and the activation of cap-independent translation of a small subset of mRNA species.

The consequences of the ISR-initiated cellular reprogramming are numerous and some, relevant to the present subject, are discussed in the following sections below. One of these consequences is the impairment of synaptic plasticity, long-term memory formation and learning, all processes requiring de novo protein synthesis (suppressed by the ISR), in the affected organisms. The ISR and the consequent impairments are universally associated with AD and transgenic AD models, as well as with a variety of cognitive disorders, including Parkinson's disease, Huntington disease, amyotrophic lateral sclerosis (ALS), traumatic brain injury, Down syndrome, prion disease, and Charcot–Marie–Tooth disease [19–35]. A mutation in the eIF2α phosphatase causing its increased phosphorylation and consequently the ISR is associated with a severe cognitive impairment [36]. The accumulated evidence that the observed cognitive impairments are consequences of the ISR is exceptionally strong: the genetic or pharmacological inhibition of the ISR prevents them, and systemic suppression of the ISR with the small-molecule inhibitor ISRIB alleviates them in model systems including the current transgenic AD models [37–45]. As discussed below, in AD patients and in the current transgenic models of AD, the elicitation of the ISR in neurons and its cognitive repercussions is mediated by Aβ. Importantly, however, the elicitation of the ISR in neurons and the resulting cognitive impairment could be triggered by stressors other than Aβ, as seen, for example, in cases of traumatic brain injury.

1.5. ACH-Based AD Drugs Should Work in the ACH-Based AD Models and so They Did, Spectacularly

The ACH theory of AD suggested the design of drugs for the treatment of the condition, referred to henceforward as ACH-based drugs. The central presumption of the ACH is that sufficiently high levels of extracellular Aβ cause AD. Therefore, the rationale for the construction of ACH-based drugs is straightforward: reduce levels of extracellular Aβ and you will abrogate the disease. Since both models and drugs are based on the same theory, they could be expected to be compatible, and indeed they were. Numerous agents capable of such reduction have been generated over the time. The most effective of them fall into two categories. The first consists of various antibodies that sequester Aβ in different forms, both soluble and insoluble. The second category of ACH-based drugs includes agents that suppress the production of Aβ in the AβPP proteolytic/secretory pathway. The less Aβ is generated, the less is secreted, and in conjunction with the physiologically occurring extracellular Aβ clearance, its levels would be reduced. Many of the candidate ACH-based AD drugs were spectacularly effective in the current transgenic AD models [46–48]. They not only stopped the symptomatic progression of the disease, but in some cases also reversed it. These results engendered the hope that a successful therapy for the disease could be at hand.

1.6. ACH-Based Drugs Failed Utterly in the Treatment of Symptomatic AD

However, all ACH-based drugs failed in human clinical trials of symptomatic AD [49,50] as spectacularly as they succeeded on the transgenic models (the effects of two apparent exceptions, lecanemab and donanemab, are consistent with the above statement and are

discussed below and elsewhere [3–6]). Importantly, these drugs failed not because they could not do in human AD patients what they did in animal models. To the contrary, in both situations (AD models and AD patients), ACH-based drugs fulfilled their mechanistic mission very effectively, reducing substantially, up to 80%, levels of extracellular Aβ in AD patients [49,50]. The fact that the drugs were utterly ineffective in human AD patients reinforces the conclusion formulated above, namely, that the current transgenic models do not recapitulate AD and that the disease occurs significantly differently from its portrayal in the ACH theory. Taken cumulatively, the above reasoning suggests that neither current transgenic models of AD nor ACH-based AD drugs are adequate because their foundation, the ACH theory of the disease, is not.

1.7. Extracellular Aβ Can Be Ruled Out as the Causative Agent of AD

The results of clinical trials of ACH-based drugs, i.e., their complete inefficiency in treatment of symptomatic AD, indicate that extracellular Aβ is not the causative agent of AD. Indeed, the removal of the bulk of extracellular Aβ resulting in no therapeutic benefit can hardly be interpreted in any other way. This conclusion is strongly supported by the observation that there is, in fact, no good correlation between the levels of extracellular Aβ and the occurrence of the disease. Indeed, in a substantial fraction of the general population, up to 40%, extracellular Aβ accumulates, physiologically and in an aging-dependent manner, to the levels equal to or exceeding those seen in AD without causing any cognitive or neurodegenerative issues [51–57]. Moreover, the reverse is also correct, as follows from the observation of AD cases lacking the excessive accumulation of extracellular Aβ [58]. Taken cumulatively, these observations indicate emphatically that extracellular Aβ can be ruled out as the causative and driving agent of AD.

2. Amyloid Cascade Hypothesis 2.0

2.1. Intraneuronal Aβ Causes and Drives AD

In over thirty years since the discovery of the first Aβ-associated AD (FAD)-causing mutation [8], many more AD-causing mutations (and one that protects from the disease [59,60]) were detected. They occur either within Aβ or within AβPP in the vicinity of its Aβ segment, or within the presenilins. The common feature of these mutations is that they all, without exception, affect either the production or the structure of Aβ. With a single exception, they all cause the early onset of AD. The only exception is the Icelandic mutation. It changes a single amino acid residue in Aβ and this change is sufficient to confer to the carriers of this mutation protection from AD [59,60]. These observations leave very little doubt regarding the centrality and the causative role of Aβ in the disease. Since, as discussed above, extracellular Aβ can be ruled out as the causative agent of AD, this role falls to another pool of Aβ, the physiologically occurring intraneuronal Aβ—*i*Aβ. This inference is, in fact, supported by numerous studies indicating that intraneuronal *i*Aβ, rather than its extracellular counterpart, correlates with and is the major component of AD [61–73].

2.2. The Principal Attributes of the ACH2.0 Theory of AD

The rationale for and the strongest indication of the principal attributes of this novel theory of AD can be derived from the results of clinical trials of ACH-based drugs in general and from those of verubecestat in particular. Indeed, in AD patients, a substantial reduction in the levels of extracellular Aβ had no efficacy whatsoever. It follows that extracellular Aβ is neither the cause nor the driver of AD. Since, as discussed above, AD appears nevertheless to both cause and drive the disease, it has to be the intracellular pool of Aβ—*i*Aβ. Since the suppression of the production of Aβ in the AβPP proteolytic pathway (by verubecestat or other BACE1 inhibitors) had no effect on progression of the disease [49,50] either, it follows that in AD, Aβ is produced independently of AβPP and is retained intraneuronally. These two features, namely, the causative role of *i*Aβ in AD and its production and intracellular retention in the AβPP-independent pathway, are the major attributes of the ACH2.0 [1–6]. The conventional disease is triggered when the AβPP-

derived *i*Aβ reaches ISR-activating levels, and it commences when the AβPP-independent *i*Aβ production pathway becomes operational [1–6]. The dynamics of accumulation of AβPP-derived *i*Aβ is, therefore, the deciding factor determining the occurrence of AD [4,6]. This is consistent with data showing that virtually all known FAD mutations accelerate the accumulation of AβPP-derived *i*Aβ and thus cause the early onset of the disease, and that the protective Icelandic mutation suppresses the accumulation of AβPP-derived *i*Aβ and thus delays or prevents the disease [4].

2.3. Origins of AβPP-Derived Intraneuronal Aβ: Two Physiologically Occurring Pathways

Conventionally, Aβ is derived from AβPP via two proteolytic cleavages. The first, by beta-secretase (beta-site AβPP-cleaving enzyme, BACE) occurs between residues 671 and 672 of AβPP and generates the C-terminal fragment (CTF) containing Aβ at its N-portion and consisting of 99 residues (designated C99). C99 is further cleaved, at variable positions, by gamma-secretase, thus generating Aβ with variable C-terminus and, accordingly, of variable length (typically 40 or 42 residues). Both cleavages occur on cellular membranes. The latter typically takes place on the plasma membrane and the resulting Aβ is secreted. Ostensibly, this scenario does not leave space for intraneuronal Aβ. The question is where it comes from. In fact, the intraneuronal Aβ is of two origins. First, the gamma cleavage of C99 does not occur exclusively on the plasma membrane. It also takes place within numerous cellular organelles. Those include lysosomes, endosomes, endoplastic reticulum, Golgi, trans-Golgi network, and mitochondria [74–82]. Importantly, Aβ resulting from C99 processing at these locations is not secreted outside the cell but is retained within it. The retention of Aβ produced on the intracellular membranes occurs physiologically and constitutes one origin of *i*Aβ. The second origin of intraneuronal Aβ is the importation—in fact, the repatriation—of secreted Aβ. The cellular uptake of extracellular Aβ also occurs physiologically [83–88], requires prior oligomerization of Aβ as a prerequisite [87,88], and is facilitated by a variety of cellular receptors [89–97].

2.4. Upon Reaching the Critical Threshold, iAβ Triggers the Activation of eIF2α Kinases, PKR and HRI, and the Elicitation of the ISR

When AβPP-derived *i*Aβ accumulates to a sufficient level ("the critical threshold"), it triggers the activation of two eIF2alpha kinases, namely, PKR and HRI. The link between Aβ and the PKR activity has been established in numerous studies [98–100] that showed not only the activated kinase but also the phosphorylated eIF2α in cells and model systems overexpressing Aβ. Importantly, the activated PKR was detected in neurons of Alzheimer's patients [33,101]. It appears that *i*Aβ can activate PKR in two ways. One is via TNFα [26]. Another Aβ-mediated PKR activation pathway involves PKR ACTivator (PACT); its employment in AD is suggested by the observation of the co-localization of PACT and activated PKR in the neurons of AD patients [102].

The *i*Aβ-mediated activation of HRI in neuronal cells, on the other hand, is a consequence of the mitochondrial dysfunction. The connection between intracellular Aβ and mitochondrial dysfunction has been a subject of numerous investigation and is well established [103–120]. Mitochondrial distress has multiple ramifications for cellular physiology. One of the most important is the triggering of the integrated stress response. For the ISR to be elicited, a signal has to be conveyed from mitochondria to the cytosol. This involves two mitochondrial proteins. Fist, the mitochondrial distress activates the mitochondrial protease OMA1. OMA1, in turn, cleaves another mitochondrial protein, DELE1. One of the resulting fragments of DELE1 is exported to the cytosol. There, it binds to and activates the eIF2α kinase HRI [121,122], and the elicitation of the ISR follows. To summarize, the accumulation of AβPP-derived *i*Aβ to sufficient levels triggers, via two distinct pathways, the activation of two different eIF2α kinases, namely, PKR and HRI. As a result, eIF2α is phosphorylated at the serine residue 51 and the integrated stress response is elicited.

2.5. ISR-Reprogrammed Translation in Neuronal Cells Provides "Missing" Components of and Activates the AβPP-Independent iAβ Production Pathway: AD Commences

As discussed above, in conventional AD, the accumulation of *i*Aβ to the critical level triggers activation of the AβPP-independent *i*Aβ production pathway. The entire output of this pathway is retained within the cell; it drives the AD pathology, and the disease commences only when the pathway is activated [1–6]. What, apparently, leads to the activation of the AβPP-independent *i*Aβ generation pathway is the ISR. Under the ISR conditions, both transcription and translation are radically reprogrammed. The total protein production is severely suppressed but, concurrently, the translation of a small subset of cellular proteins is activated. Presumably [1–6], this subset includes the component(s), which are "missing" under regular conditions and are required for the activation and operation of the AβPP-independent *i*Aβ production pathway. When this/these component(s) become available, the pathway is activated and AD commences. It should be mentioned that whereas the end product of the AβPP-independent pathway is intraneuronally retained Aβ, *i*Aβ, its primary translation product is the C100 fragment of AβPP, i.e., the N-terminal methionine-containing C99; the etiology of C100 as well as its processing are described below.

2.6. Unconventional AD: The Disease Could Be Triggered via iAβ-Independent Elicitation of the ISR

In conventional AD, the elicitation of the ISR in neuronal cells and consequent activation of the AβPP-independent *i*Aβ production are mediated by AβPP-derived *i*Aβ. However, as long as the elicitation of the ISR is sufficient for the activation of the AβPP-independent *i*Aβ production pathway, this does not necessarily have to be the case. Potentially, the ISR can be elicited in neuronal cells by a variety of stressors capable of activating one or more of the four members of the family of eIF2α kinases. As soon as the ISR is elicited in neurons, the AβPP-independent *i*Aβ generation pathway would be activated and AD would commence. As described in the following subsection, the latter is, or eventually becomes, self-sustaining and its continuous operation is, therefore, independent from the initial ISR-eliciting stressor. AD driven by such a process would be unconventional. Both conventional and unconventional AD are identical in that they are driven by the same AβPP-independent *i*Aβ production pathway. They differ, however, in the cause that triggers the elicitation of the ISR in neuronal cells and consequently of the AβPP-independent *i*Aβ production pathway. In conventional disease, it is AβPP-derived *i*Aβ accumulated to sufficient levels; whereas in unconventional AD, it is any other stressor operating sufficiently long (or repeatedly) to allow *i*Aβ produced in the AβPP-independent pathway to accumulate over the critical threshold and for the pathway to become self-sustaining. Thus, unconventional AD may have multiple causes. These include, potentially, traumatic brain injury, chronic encephalopathy, chronic inflammation, and viral and bacterial infections.

2.7. iAβ Generated in the AβPP-Independent Pathway Drives the AD Pathology and Sustains and Perpetuates Its Own Production: The Engine That Drives AD

To recap the above discussion, the ACH2.0 envisions conventional AD as the process, which occurs in two stages. In the first stage, AβPP-derived *i*Aβ accumulates physiologically via two distinct mechanisms. One is the cellular uptake of secreted Aβ. Another is the intraneuronal retention of a fraction of Aβ produced by the processing of its immediate precursor, C99, on intracellular membranes within various cellular organelles. If and when the AβPP-derived *i*Aβ levels in neuronal cells reach and cross the critical threshold, the integrated stress response is elicited. The immediate cause of ISR elicitation is the phosphorylation of the eIF2α at the serine residue 51. This occurs, potentially, in two ways. One is the *i*Aβ-mediated activation of the PKR kinase via TNFα and/or the PKR activator PACT. Another way is through the *i*Aβ-triggered mitochondrial dysfunction and the associated activation of the mitochondrial protease OMA1. The activated OMA1 cleaves another mitochondrial protein, DELE1. One of the DELE1 fragments produced by the OMA1 cleavage is exported to the cytosol, where it binds to and activates the HRI kinase. When activated, either PKR or HRI, or both, phosphorylate eIF2α and the elicitation of the ISR ensues.

Under ISR conditions, cellular transcription and translation are reprogrammed and the global cellular protein synthesis is drastically suppressed. Concurrently, the translation of a small subset of cellular proteins, presumably in the cap-independent manner, is activated. Among those are the "missing" components required for the activity of the AβPP-independent *i*Aβ production pathway; when these components are made available, the pathway becomes operational. The entire *i*Aβ production output of the AβPP-independent pathway is retained within neuronal cells and its levels rapidly increase. This results in two major consequences. First, the elevated levels of *i*Aβ drive the AD pathology (AβPP-derived *i*Aβ cannot attain these levels), culminating in the formation of neurofibrillary tangles [123–126] and, ultimately, in the neuronal loss. Second, the resulting high levels of *i*Aβ sustain, via the continuous propagation of the ISR, its own production in the AβPP-independent pathway and consequently perpetuate its operation. Thus, in conventional AD, the ISR-eliciting stressor operating at the first stage of the disease (pre-ISR elicitation) is the same as the one operating at the second AD stage (post-ISR elicitation). In both cases, it is *i*Aβ, but of distinctly different origins. In the first AD stage, it is derived from AβPP via its proteolysis, whereas at the second stage it is produced independently of AβPP. When the AβPP-independent *i*Aβ production pathway is operational, it renders the influx of AβPP-derived *i*Aβ marginal and becomes fully independent from it. The repeated cycles of *i*Aβ-induced propagation of its own generation in the AβPP-independent pathway constitute the engine that powers AD—the AD Engine. The initiation and continuous operation of the AD Engine are depicted schematically in Figure 1.

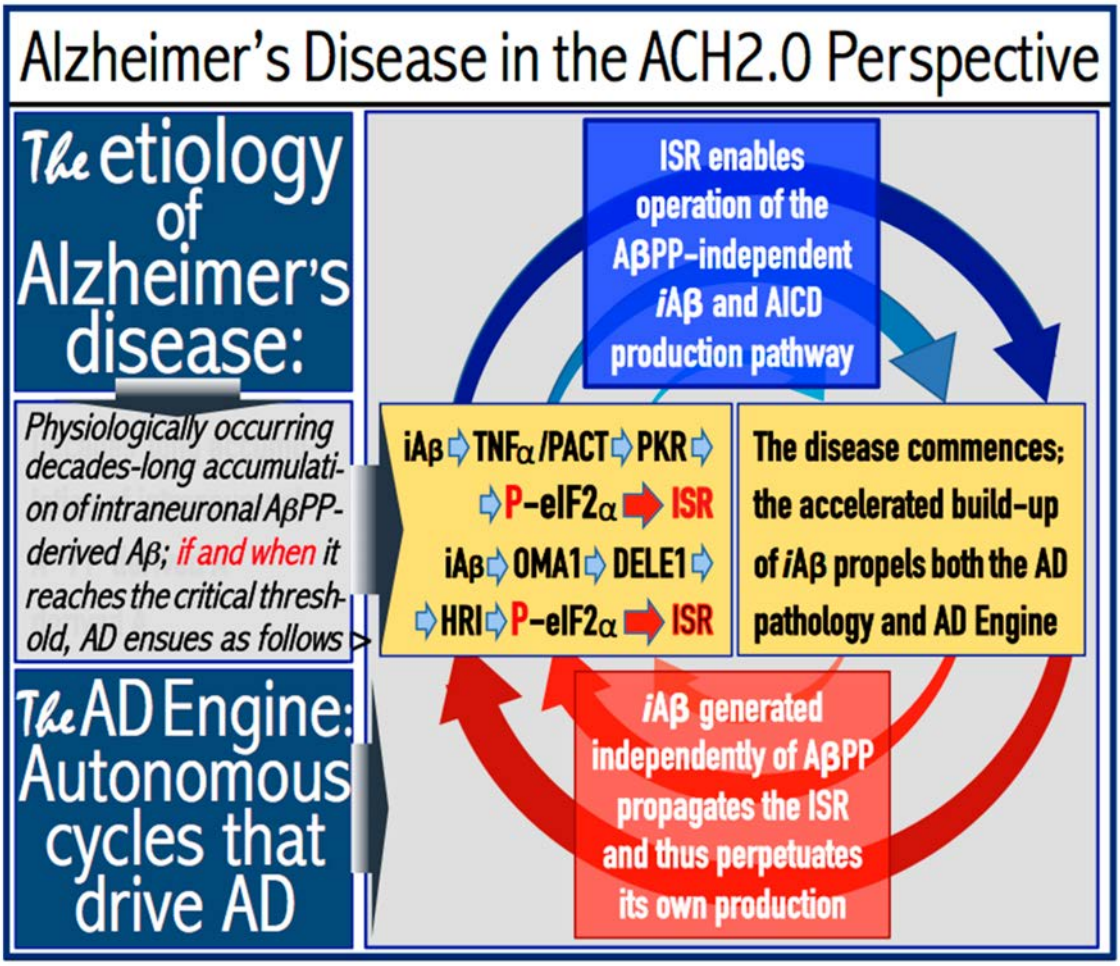

Figure 1. Conventional Alzheimer's disease is caused by AβPP-derived *i*Aβ, accumulated physiologically over the ISR-triggering threshold, and is driven by *i*Aβ produced in the self-sustaining AβPP-independent

pathway: the Engine that drives AD. *i*Aβ: intraneuronal Aβ. *eIF2α:* eukaryotic translation initiation factor 2alpha. *PKR*, *HRI:* kinases that phosphorylate eIF2α. *TNFα*: tumor necrosis factor/alpha (activates PKR); *PACT*: PKR activator. *OMA1:* mitochondrial protease activated by mitochondrial distress and cleaving DELE1; *DELE1:* mitochondrial protein mediating (after the cleavage by OMA1) the activation of HRI. *ISR:* integrated stress response, which is elicited by the phosphorylation of eIF2α and presumably activates the AβPP-independent *i*Aβ generation pathway. *AICD:* AβPP intracellular domain. *Gray box* (*left*): Physiologically occurring accumulation of *i*Aβ. If and when its levels reach the critical threshold, they trigger the activation of the PKR and/or HRI kinases. *Mustard-yellow box* (*left*)*:* Phosphorylation of eIF2α and the elicitation of the ISR; cellular protein synthesis is reprogrammed, resulting in the production of factor(s) required for the activation of the AβPP-independent *i*Aβ production pathway. *Blue box*: The AβPP-independent *i*Aβ generation pathway is initiated; its end products, *i*Aβ and AICD, are retained intraneuronally. *Mustard-yellow box* (*right*): Levels of *i*Aβ, driven by the AβPP-independent *i*Aβ production pathway, rapidly increase. *Red box:* High levels of *i*Aβ drive the AD pathology, sustain the activity of PKR and HRI, maintain the ISR conditions, and propagate the activity of the AβPP-independent pathway of its own production, thus perpetuating the operation of the AD Engine (arched blue and red arrows).

3. Dynamics of *i*Aβ Accumulation and Its Role in AD in the ACH2.0 Perspective

3.1. iAβ Dynamics in Health and Disease

In the ACH2.0, the dynamics of *i*Aβ accumulation in healthy individuals that do not develop AD in their lifetimes is single-phased. In these individuals, *i*Aβ is produced solely in the AβPP proteolytic pathway and accumulates, via its cellular uptake from the secreted extracellular pool and through the retention of a fraction generated by the processing of AβPP on the intracellular membranes, throughout the lifetime. As shown in panel A of Figure 2, its levels do not reach and never cross the threshold (T1 threshold), which triggers the activation of eIF2α kinases, the elicitation of the integrated stress response and the initiation of operation of the AβPP-independent *i*Aβ production pathway. Consequently, no AD occurs within the life span of an individual. It should be mentioned that if the T1 threshold is sufficiently high, the elevated, yet sub-T1, levels of *i*Aβ can cause aging-associated cognitive decline (AACD), a scenario that is outside the scope of the present study and that has been addressed elsewhere [4,6].

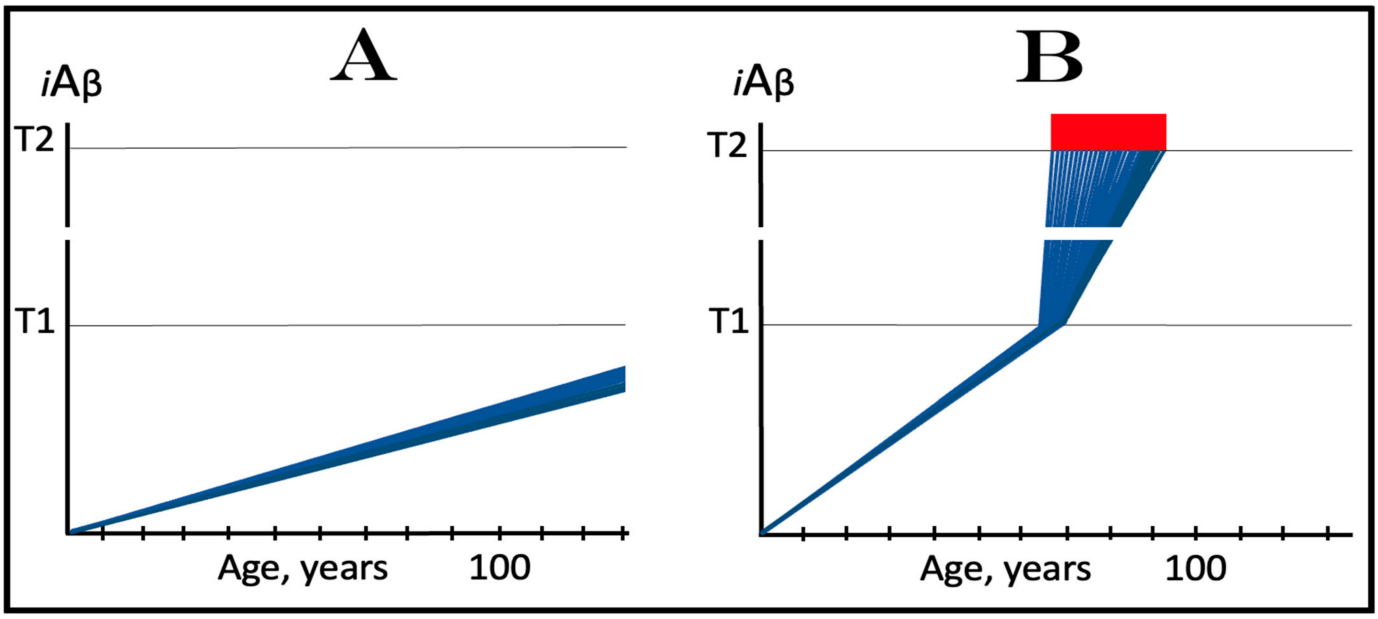

Figure 2. Dynamics of *i*Aβ accumulation in health and disease. *i*Aβ: intraneuronal Aβ. ***T1*** *threshold*: concentration of *i*Aβ that triggers activation of the eIF2α kinases, the elicitation of the ISR and the

initiation of the AβPP-independent *i*Aβ generation pathway. ***T2*** *threshold*: concentration of *i*Aβ, generated mainly in the AβPP-independent pathway, which triggers neuronal apoptosis or necroptosis. *Blue lines*: levels of *i*Aβ in individual neuronal cells. *Red box*: apoptotic zone, the range of *i*Aβ levels that cause the commitment to cell death. (**A**) The levels of AβPP-derived *i*Aβ neither reach nor cross the T1 threshold within the lifetime of an individual; no disease occurs. (**B**) The levels of *i*Aβ cross the T1 threshold within a narrow temporal window; the ISR is elicited, and the AβPP-independent *i*Aβ generation pathway is initiated. AD commences only with the activation of the latter, and *i*Aβ produced independently of AβPP drives the AD pathology and simultaneously propels the operation of the AβPP-independent *i*Aβ production pathway.

The dynamics of the *i*Aβ accumulation in AD-affected individuals, on the other hand, are two-phased. In the first phase, *i*Aβ is derived solely from AβPP. At this stage, the only difference from healthy individuals is that the rate of accumulation of AβPP-derived *i*Aβ is faster and/or the extent of the T1 threshold is lower, and it reaches and crosses the T1 threshold within the lifetime of an individual. In the second phase, the overwhelming bulk of *i*Aβ is generated independently of AβPP. Its levels rapidly increase, and when they reach and cross the T2 threshold, neurons commit apoptosis and/or necroptosis [127]. The two phases of the dynamics of *i*Aβ accumulation correspond to two stages of AD. The first AD stage is asymptomatic and culminates with the crossing of the T1 threshold [1–6]. The disease commences and its symptoms manifest at the second AD stage. At this stage, any interference with the production and/or accumulation of AβPP-derived *i*Aβ would have no effect whatsoever on the progression of AD because the disease is driven by *i*Aβ produced in the AβPP-independent pathway [1–6]. The dynamics of *i*Aβ accumulation in AD are presented diagrammatically in panel B of Figure 2.

3.2. Conditionality of the First AD Stage

Referring to the accumulation of AβPP-derived *i*Aβ prior to the crossing of the T1 threshold as "the first AD stage" creates a paradox. Indeed, there is obviously no AD at this stage. By definition, the disease commences and its symptoms manifest only with the activation of the AβPP-independent *i*Aβ production pathway at the second stage of AD. And if the T1 threshold were not crossed within the life span of an individual, a scenario currently predominating in the majority of general human population and illustrated in panel A of Figure 2, there would be no AD and, obviously, no first stage of it. Therefore, "the first stage of AD" is a conditional terminological construct. "The first AD stage" becomes such only post-factum, i.e., only if and when the T1 threshold is crossed, the AβPP-independent *i*Aβ production pathway activated, and the disease commences. Otherwise, the sub-T1 accumulation of AβPP-derived *i*Aβ is simply a normal physiological occurrence.

3.3. AD-Causing or -Preventing Mutations Act via the Augmentation or the Abatement of the Rate of Accumulation of AβPP-Derived iAβ

From the description of the dynamics of AβPP-derived *i*Aβ accumulation, it follows that it is the decisive factor, which determines the timing of the occurrence of the disease. The higher the rate of the AβPP-derived *i*Aβ accumulation is (and the lower the extent of the T1 threshold), the sooner the crossing of the T1 threshold occurs, AβPP-independent *i*Aβ production pathway become operational, and the disease commences. The slower the rate of AβPP-derived *i*Aβ accumulation (and the higher the extent of the T1 threshold), the later the T1 threshold is crossed and AD commences, and if the T1 is not reached within the life span of an individual, no AD occurs. These notions are supported by the observed effects of the mutations that either cause AD or protect from it. Not only the AD-causing mutations but also virtually all known factors that predispose to AD accelerate the kinetics of the AβPP-derived *i*Aβ accumulation. For instance, the internalization of extracellular Aβ requires ApoE. The latter can occur in several distinct isoforms. Of those, ApoE4 was shown to be more efficient in facilitating the cellular uptake of secreted Aβ than the rest of ApoE isoforms [66]. By increasing the influx of AβPP-derived *i*Aβ, it elevates

the rate of its accumulation; it is also the major factor that predisposes its carriers to AD. In another example, certain PSEN mutations result in the shift of the gamma-cleavage to the position 42 of Aβ [85] and thus in the increased secretion of the Aβ42 isoform. Aβ42, in turn, is taken up by the cell twice as efficiently as the other Aβ isoforms [84]. Consequently, these mutations accelerate the rate of AβPP-derived *i*Aβ accumulation; they also cause the early onset of AD. Mutations resulting in the increased processing of AβPP on the intracellular membranes and, consequently, in the increased intraneuronal retention of AβPP-derived iAβ also increase the rate of its accumulation; they also cause the early onset of AD. This type of mutation is represented by the Swedish mutation [128] and some PSEN mutations [129]. The Flemish Aβ mutation lowers the efficiency of the physiologically occurring intra-*i*Aβ cleavages [130] and consequently increases the rate of accumulation of AβPP-derived *i*Aβ; it also causes the early onset of AD. The Icelandic Aβ mutation, on the other hand, elevates the efficiency of the physiologically occurring intra-*i*Aβ cleavage [59,60] and thus reduces the rate of the accumulation of AβPP-derived *i*Aβ; it also protects from AD (i.e., either delays or prevents it).

3.4. Potential Role of AICD in AD

The processing of C99 (or of C100, as described below), results in two products. Aβ is only one of those. Regardless of whether Aβ generated by the gamma-cleavage is secreted or retained within the neuron, the other product is always retained intraneuronally [131]. Therefore, it is designated the AβPP intracellular domain (AICD). In numerous studies, AICD was shown to be far from inert. Thus, it is known to interact with multiple cellular signaling pathways and to affect numerous regulatory proteins [132–142]. It was shown to participate in the regulation of gene expression and to affect both cytoskeletal dynamics and apoptosis [143,144]. It affects the *i*Aβ clearance by influencing the production of neprilysin [145], influences the phosphorylation of tau protein, and consequently the formation of NFTs [132,143]. It was also shown to impact the neuronal activity and oscillations in hippocampus, and to cause deterioration in spatial memory encoding [146]. AICD is generated both during the production of Aβ by AβPP proteolysis and during the operation of the AβPP-independent *i*Aβ production pathway. Therefore, there is substantially more AICD in AD patients than in healthy individuals. Due to its multiple activities, it is conceivable that it contributes significantly to AD pathology. The extent of its contribution, however, remains to be elucidated.

3.5. Inevitability of AD within Sufficiently Long Human Life Span

The majority of the general human population does not develop AD within their lifetime. What renders these individuals resistant to the disease is simply the slow kinetics of the accumulation of AβPP-derived *i*Aβ. No T1 threshold is crossed and consequently no AβPP-independent *i*Aβ production pathway is activated and no AD occurs within their life spans. The "life span" is the key term in the preceding statement; given the constant rate of accumulation of AβPP-derived *i*Aβ, it is the limited human life span that prevents the occurrence of AD. If, however, the life span is considered variable, with no limitation on its duration, the situation changes drastically: Everyone would eventually and inevitably develop AD provided her/his life span is sufficiently long. Indeed, since the accumulation of AβPP-derived *i*Aβ is, apparently, a lifelong process, it is only a question of time when its levels would cross the T1 threshold, but the crossing would certainly occur and AD develop. As the average life span steadily increases, so does the fraction of the general population that develops AD, and one can safely predict that this trend would continue, with the affected fraction nearing 100% unless a preventive treatment is developed and is implemented routinely [1–6].

4. AβPP-Independent Production of Intraneuronally Retained Aβ Is Inoperative in the Current Transgenic Animal Models of AD: *i*Aβ Dynamics in the ACH2.0 Perspective

4.1. In the Current Transgenic AD Models, Levels of AβPP-Derived iAβ Cross the T1 Threshold and Elicit the ISR

In the ACH2.0 perspective, the observed limited symptoms of AD in the current transgenic models of the disease are caused mainly by the ISR triggered by intraneuronal AβPP-derived *i*Aβ accumulated over the critical threshold. As in humans, the latter has two origins. One is the cellular uptake of secreted Aβ, and another the intraneuronal retention of a fraction of AβPP-derived Aβ following the gamma-cleavage on the intracellular membranes. Both processes occur physiologically and both are enhanced by the acute overproduction of AβPP from multiple transgenes. As discussed below, at sufficient cellular concentrations, *i*Aβ is a stressor capable of eliciting the ISR. If and when the levels of AβPP-derived *i*Aβ cross the T1 threshold, they would trigger the activation of the PKR and/or HRI kinases, phosphorylation of eIF2α, and elicitation of the integrated stress response. There are strong indications that the above sequence of events indeed takes place and that the ISR is elicited in transgenic AD models. As described in the preceding sections, the ISR was shown to cause cognitive impairments such as defects in the neuronal plasticity, long-term memory formation, and learning, processes that require de novo protein synthesis, which is suppressed under ISR conditions. That the observed cognitive deficits in transgenic AD models are caused by the ISR was convincingly demonstrated in studies utilizing the small-molecule ISR inhibitor ISRIB as well as genetic prevention and pharmacological suppression of the ISR. Indeed, in these studies, inhibition of the ISR or the prevention of its elicitation resulted in the marked alleviation or in the preclusion of cognitive impairments in the current transgenic AD models [37–45].

4.2. Inactivity of the AβPP-Independent iAβ Production Pathway in Transgenic AD Models Defines the Single-Phased Dynamics of Its Accumulation

In conventional AD, the AβPP-derived *i*Aβ-mediated elicitation of the integrated stress response leads to the activation of the AβPP-independent *i*Aβ production pathway. Since the entire *i*Aβ output of this pathway is retained within neuronal cells, its levels rapidly increase. High levels of *i*Aβ, produced overwhelmingly in the AβPP-independent pathway, appear to be essential for both the commencement of the disease and the progression of the AD pathology [1–6]. In the current transgenic animal models of AD, as reasoned above, AβPP-derived *i*Aβ accumulates over the T1 threshold and the integrated stress response is elicited, but the AD pathology does not progress, judging by its major hallmark, the formation of neurofibrillary tangles, or rather by the lack thereof; indeed, there are no indications that the disease commences in the first place. It follows that in the current transgenic AD models, the elicitation of the ISR is not accompanied by the enhanced production and accumulation of *i*Aβ, i.e., that in transgenic AD models the elicitation of the ISR is not followed by the activation of the AβPP-independent *i*Aβ production, which remains inoperative. Under these circumstances, the AβPP proteolytic pathway would remain the only source of *i*Aβ and its accumulation would continue at the same rate as prior to the crossing the T1 threshold. Such dynamics of the *i*Aβ accumulation in the current transgenic AD models are illustrated diagrammatically in Figure 3. The figure shows two conditions. In normal (non-transgenic) mice, AβPP-derived *i*Aβ accumulates slowly, and neither crosses the T1 threshold nor causes the elicitation of the ISR and accompanying cognitive impairment within the lifetime of an animal. In contrast, in transgenic animals, the rate of the accumulation of AβPP-derived *i*Aβ is increased due to its massive overproduction from multiple transgenes, and, consequently, the T1 threshold is crossed; the ISR is elicited, and cognitive impairment manifests. However, with the AβPP-independent *i*Aβ production pathway inoperative, *i*Aβ does not reach, within the limits of the life span of an animal, levels essential to support the progression (and, apparently, even the commencement) of AD pathology and formation of NFTs. Since we define AD as a disease that initiates with the activation of the AβPP-independent *i*Aβ production pathway (see

above), it neither commences nor occurs in the current transgenic animal AD models. These models are useful in many respects; they, however, are not AD models.

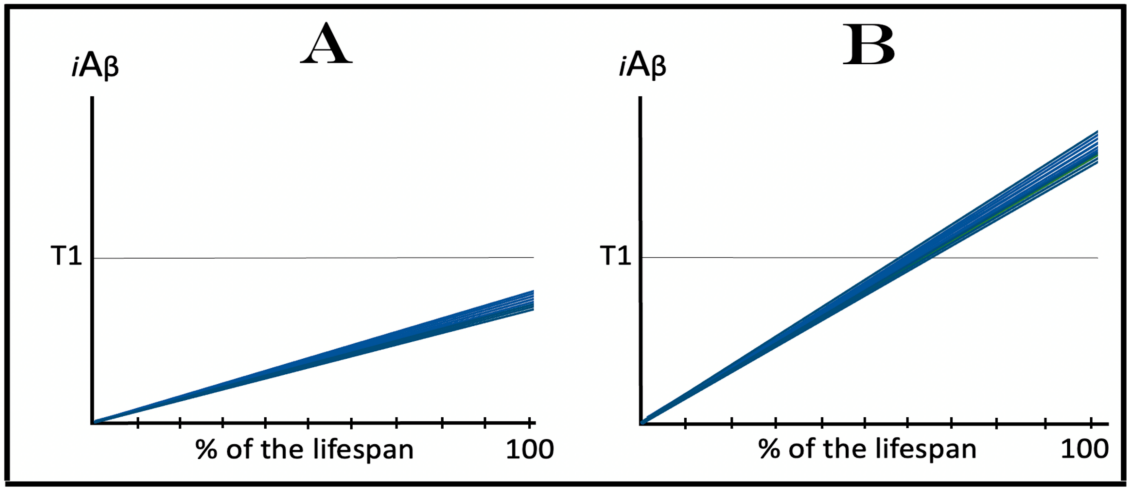

Figure 3. *i*Aβ dynamics in normal mice and in the current transgenic models of AD: the ACH2.0 perspective. *i*Aβ: intraneuronal Aβ. ***T1*** *threshold*: concentration of *i*Aβ that triggers activation of the eIF2α kinases, phosphorylation of eIF2α, and the elicitation of the ISR. *Blue lines*: levels of *i*Aβ in individual neuronal cells. (**A**) In normal mice, the levels of AβPP-derived *i*Aβ neither reach nor cross the T1 threshold within the lifetime of an animal. (**B**) Aβ is produced from multiple transgenes, and the rate of the accumulation of AβPP-derived *i*Aβ markedly increases. The levels of AβPP-derived *i*Aβ cross the T1 threshold, and the ISR is elicited. The resulting transcriptional and translational reprogramming and severe suppression of the total protein production cause impairment in cognitive functions requiring de novo protein synthesis. The AβPP-independent *i*Aβ generation pathway is not activated; no AD occurs. *i*Aβ is produced throughout the lifetime solely in the AβPP proteolytic pathway, and its rate of accumulation does not change.

5. Why ACH-Based AD Drugs Are Effective in Current Transgenic AD Models, but Not in Symptomatic AD Patients

5.1. Effect of ACH-Based Drugs in Current Transgenic AD Models

The dynamics of the accumulation of AβPP-derived *i*Aβ in the current transgenic animal models of AD, described in the preceding section, explain why ACH-based AD drugs are so effective in these models. ACH-based drugs were designed to reduce levels of extracellular Aβ. They can be divided into two categories. One consists of drugs that either degrade extracellular Aβ or sequester it, as in the cases of numerous monoclonal antibodies. Another category includes drugs that suppress the production and consequently secretion of Aβ in the AβPP proteolytic pathway. These drugs are exemplified by various BACE1 inhibitors, such as verubecestat. In the ACH2.0 perspective, these drugs should also be effective (see limitations below), because by reducing the pool of extracellular Aβ, they also reduce the rate of its uptake into the cell. Moreover, the second category of ACH-based drugs reduce not only its importation but also its intraneuronal retention (less produced, less retained). When implemented, such drugs would reduce the rate of AβPP-derived *i*Aβ accumulation and could even reverse it due to the physiologically ongoing *i*Aβ clearance; this would obviously be therapeutically beneficent. The expected, and apparently observed, effect of ACH-based drugs in current transgenic animal AD models is illustrated in Figure 4. The drug is administered when the T1 threshold has already been crossed, the ISR elicited, and cognitive impairment manifested. For the duration of drug administration, the rate of *i*Aβ accumulation is reversed. When its levels are reduced below the T1 threshold, the ISR is no longer in effect, the normal protein synthesis is restored and the cognitive impairment is relieved. The key to the drugs' efficiency in transgenic animal models is the inactivity of the AβPP-independent *i*Aβ production pathway, which is insensitive to these drugs.

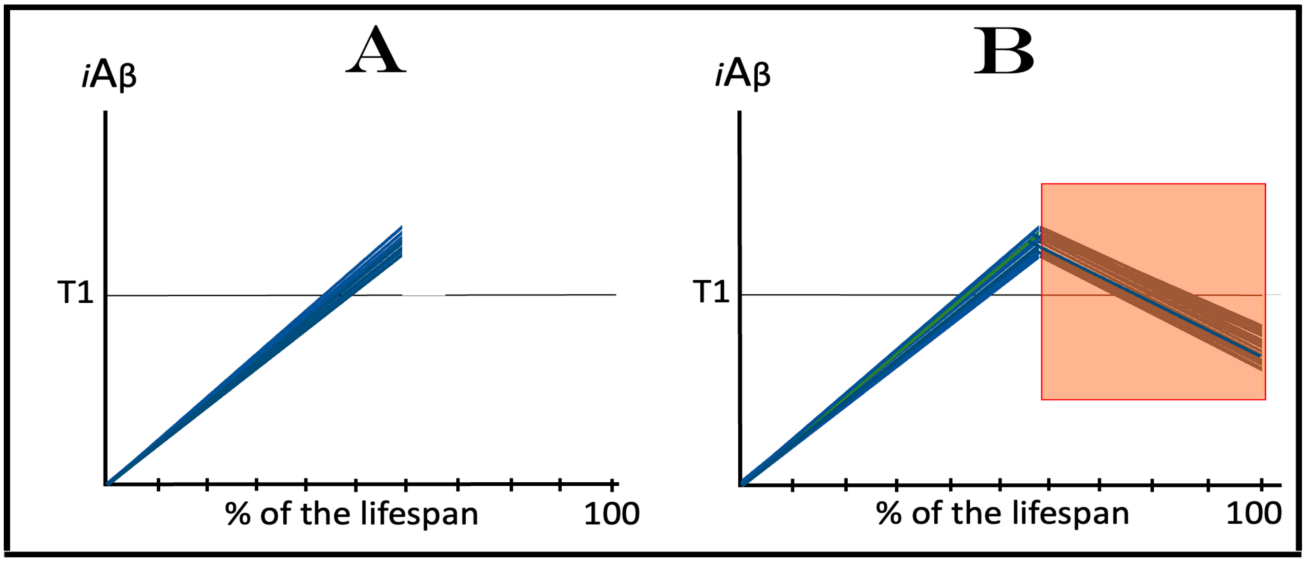

Figure 4. Effect of ACH-based drugs in the current transgenic animal AD models. *i*Aβ: intraneuronal Aβ. ***T1*** *threshold*: concentration of *i*Aβ that triggers activation of the eIF2α kinases, phosphorylation of eIF2α, and the elicitation of the ISR. *Blue lines*: levels of *i*Aβ in individual neuronal cells. *Orange Box:* duration of the administration of the ACH-based drug. (**A**) The initial state of the levels of *i*Aβ in the individual neurons at the commencement of drug's administration. The levels of AβPP-derived *i*Aβ have crossed the T1 threshold. The ISR has been elicited, and the ISR-caused cognitive impairments (due to the suppression of cellular protein synthesis) have manifested. (**B**) Evolution of the initial state in the presence of the ACH-based drug (for the definition of ACH-based drugs and their mechanism of action, see the main text). The drug reduces the influx of *i*Aβ and consequently lowers its rate of accumulation. In the best-case scenario (shown in the Figure), due to the physiologically ongoing *i*Aβ clearance, its rate of accumulation is reversed. When the levels of *i*Aβ are reduced below the T1 threshold, the ISR is no longer in effect; the normal protein synthesis is restored and the cognitive impairment is relieved for the duration of the drug's administration.

5.2. Effect of ACH-Based Drugs in Symptomatic AD

In the framework of the ACH2.0, the outcome of the implementation of ACH-based drugs in symptomatic AD patients is expected to be, and evidently was, drastically different. The key to this difference is the operational AβPP-independent *i*Aβ production pathway. As shown in Figure 5, at the time of drug administration, levels of AβPP-derived *i*Aβ have crossed the T1 threshold and the AβPP-independent *i*Aβ production pathway has been activated in all affected neurons [1–6]. At this stage, *i*Aβ is overwhelmingly produced in the AβPP-independent pathway. Whereas the activation of this pathway is triggered by AβPP-derived *i*Aβ, its operation is completely independent of the latter. Indeed, the AβPP-independent *i*Aβ production pathway is self-sustaining because its *i*Aβ product propagates its own generation (this is the reason why it is referred to as the AD Engine) and also drives the AD pathology. On the other hand, with the AβPP-independent *i*Aβ production pathway operative, the contribution of the AβPP proteolytic pathway to the cellular *i*Aβ pool becomes marginal and inconsequential for the progression of the disease. ACH-based drugs can, and apparently do, interfere with the accumulation of AβPP-derived *i*Aβ, but they cannot affect the production or accumulation of *i*Aβ in the AβPP-independent pathway. Therefore, the implementation of ACH-based drugs would be futile in symptomatic AD, as was indeed observed in clinical trials.

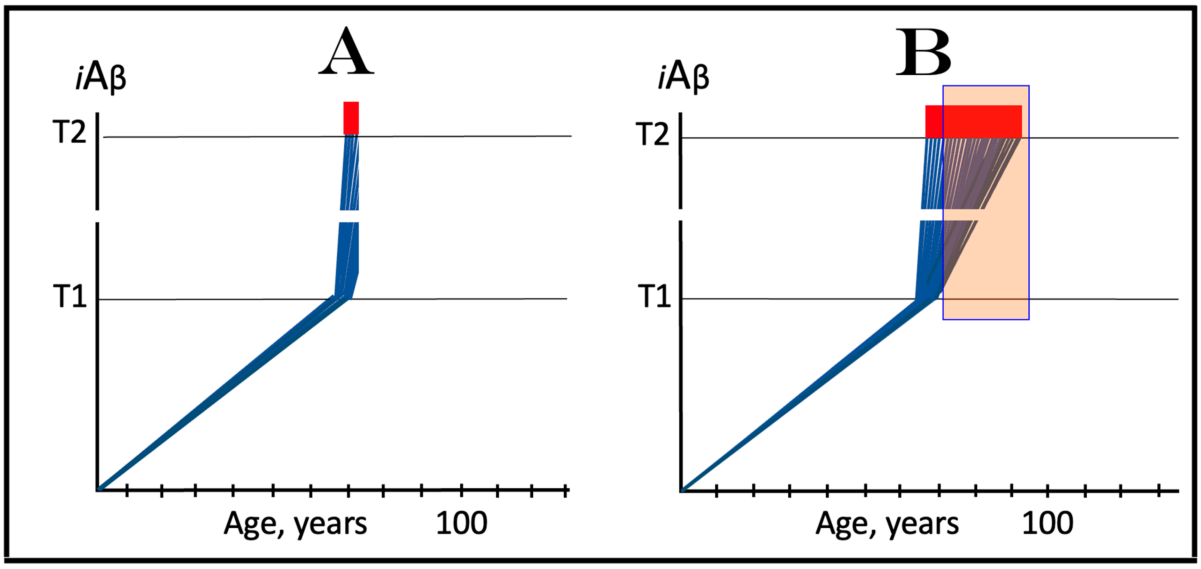

Figure 5. Effect of ACH-based drugs in symptomatic Alzheimer's disease. *i*Aβ: intraneuronal Aβ. ***T1*** *threshold*: concentration of *i*Aβ that triggers activation of the eIF2α kinases, the elicitation of the ISR and the initiation of the AβPP-independent *i*Aβ generation pathway. ***T2*** *threshold*: concentration of *i*Aβ, generated mainly in the AβPP-independent pathway, which triggers neuronal apoptosis or necroptosis. *Blue lines*: levels of *i*Aβ in individual neuronal cells. *Red Box*: apoptotic zone, the range of *i*Aβ levels that cause the commitment to cell death. *Orange Box:* duration of the administration of the ACH-based drug. (**A**) The initial state of the levels of *i*Aβ in the individual neurons at the commencement of drug administration. The levels of AβPP-derived *i*Aβ have crossed the T1 threshold. The ISR has been elicited, and the AβPP-independent *i*Aβ production pathway was activated in all affected neurons. A fraction of the affected neurons have crossed the T2 threshold, committed apoptosis, and AD symptoms have manifested. (**B**) Evolution of the initial state in the presence of the ACH-based drug. The drug reduces the influx and lowers the rate of accumulation of AβPP-derived *i*Aβ. At this stage, however, *i*Aβ is overwhelmingly produced in the AβPP-independent pathway. The contribution of the AβPP-derived *i*Aβ into the cellular *i*Aβ pool is marginal, and its suppression is inconsequential and has no impact whatsoever on the progression of AD. *i*Aβ continues to accumulate, its levels cross the T2 threshold, and when a sufficient fraction of the neurons commit apoptosis, the disease enters the end stage.

5.3. ACH-Based Drugs Would Be Effective in Prevention of AD for the Same Reason They Are Effective in Transgenic AD Models

On the other hand, in the ACH2.0 perspective, ACH-based drugs could potentially be effective in prevention of AD, if administered prior to the commencement of the disease, for exactly the same reason they are effective in transgenic AD models: the inactivity of the AβPP-independent *i*Aβ production pathway at this stage. Preventive implementation of ACH-based drugs infers that they are administered prior to the crossing of the T1 threshold. At this stage, *i*Aβ is derived solely from AβPP via its proteolysis. Therefore, interference with its accumulation either through the reduction of the rate of its importation from the extracellular pool or via the suppression of its intraneuronal retention by the inhibition of its production would delay or prevent the crossing of the T1 threshold and the commencement and indeed the occurrence of AD. This expected preventive effect of ACH-based drugs is shown in Figure 6. In panel A, the rate of the accumulation of AβPP-derived *i*Aβ is reduced but its levels continue to increase, albeit more slowly. Eventually, they would reach and cross the T1 threshold. The ISR would be elicited, the AβPP-independent *i*Aβ production pathway would be activated, and AD would commence, but all this would occur with a considerable delay in comparison to an untreated individual. In panel B, the influx of AβPP-derived *i*Aβ is reduced sufficiently to reverse the rate of its accumulation.

Consequently, no T1 would be crossed, no AβPP-independent *i*Aβ production pathway would be activated, and no AD would occur for the duration of the treatment.

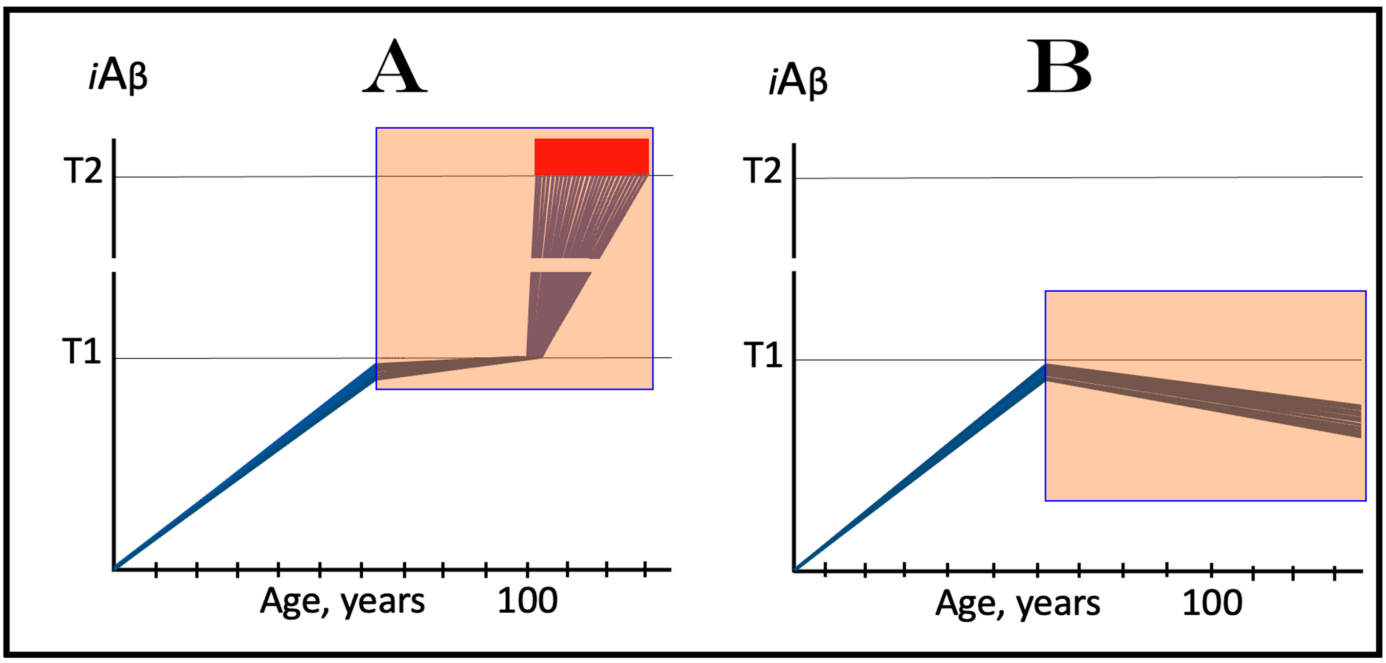

Figure 6. Effect of ACH-based drugs in prevention of AD. *i*Aβ: intraneuronal Aβ. ***T1*** *threshold*: concentration of *i*Aβ that triggers activation of the eIF2α kinases, the elicitation of the ISR and the initiation of the AβPP-independent *i*Aβ generation pathway. ***T2*** *threshold*: concentration of *i*Aβ, generated mainly in the AβPP-independent pathway, which triggers neuronal apoptosis or necroptosis. *Blue lines*: levels of *i*Aβ in individual neuronal cells. *Red box*: apoptotic zone, the range of *i*Aβ levels that cause the commitment to cell death. *Orange boxes:* duration of the administration of the ACH-based drug. The drug is administered prior to the crossing of the T1 threshold. At this stage, the AβPP-independent *i*Aβ production pathway is inoperative and *i*Aβ is derived solely from AβPP via its proteolysis. Therefore, the interference with its accumulation would delay or prevent the crossing of the T1 threshold and the commencement and indeed the occurrence of AD. (**A**) The rate of the accumulation of AβPP-derived *i*Aβ is reduced, but its levels continue to increase. Eventually, they would reach and cross the T1 threshold. The ISR would be elicited, the AβPP-independent *i*Aβ production pathway would be activated, and AD would commence, but all this would occur with a considerable delay in comparison to an untreated individual. (**B**) The influx of AβPP-derived *i*Aβ is reduced sufficiently to reverse the rate of its accumulation. Consequently, no T1 would be crossed, no AβPP-independent *i*Aβ production pathway would be activated, and no AD would occur for the duration of the treatment.

5.4. ACH-Based Drugs Can Be Only Marginally Effective in Early Symptomatic AD: Effects of Lecanemab and Donanemab, the Proverbial Exceptions That Prove the Rule

The preventive potential of ACH-based drugs in AD explains both the nature of their observed effect at the very early stages of the disease, as was seen in the recent clinical trials of lecanemab and donanemab, and why this effect was only marginal. In contrast to the preceding clinical trials of potential AD drugs, which utilized participants at relatively advanced stages of AD, in the clinical trials in question [147–151], only subjects at the very early stages of the disease were employed. As described above and elsewhere [1–6], in AD patients, the levels of AβPP-derived *i*Aβ in individual affected neurons cross the T1 threshold, and thus initiate the disease, within a narrow temporal window. Consequently, when AD symptoms manifest, the bulk if not the entire population of the affected neurons have crossed the T1 threshold and activated the AβPP-independent *i*Aβ production pathway. As reasoned above, the implementation of ACH-based drugs at this point would be

futile. As shown in Figure 7, in the clinical trials of lecanemab and donanemab, however, at the time of the drug administration, due to the early stages of the disease, a fraction of the affected neurons in individual subjects have not yet crossed the T1 threshold and therefore were responsive to the drug. The beneficial effect of the drags in these clinical trials was thus preventive, not curative. It was marginal because the fraction of sub-T1 neurons was marginal. It should be emphasized that there is nothing special about lecanemab and donanemab. What made the difference (in comparison with the preceding trials) was the early timing of their administration. Any typical ACH-based drug, administered at the same early stage of AD, would have similar effect. Thus, whereas the preventive implementation of ACH-based AD drugs could be feasible, this is, apparently, not the case in symptomatic AD patients.

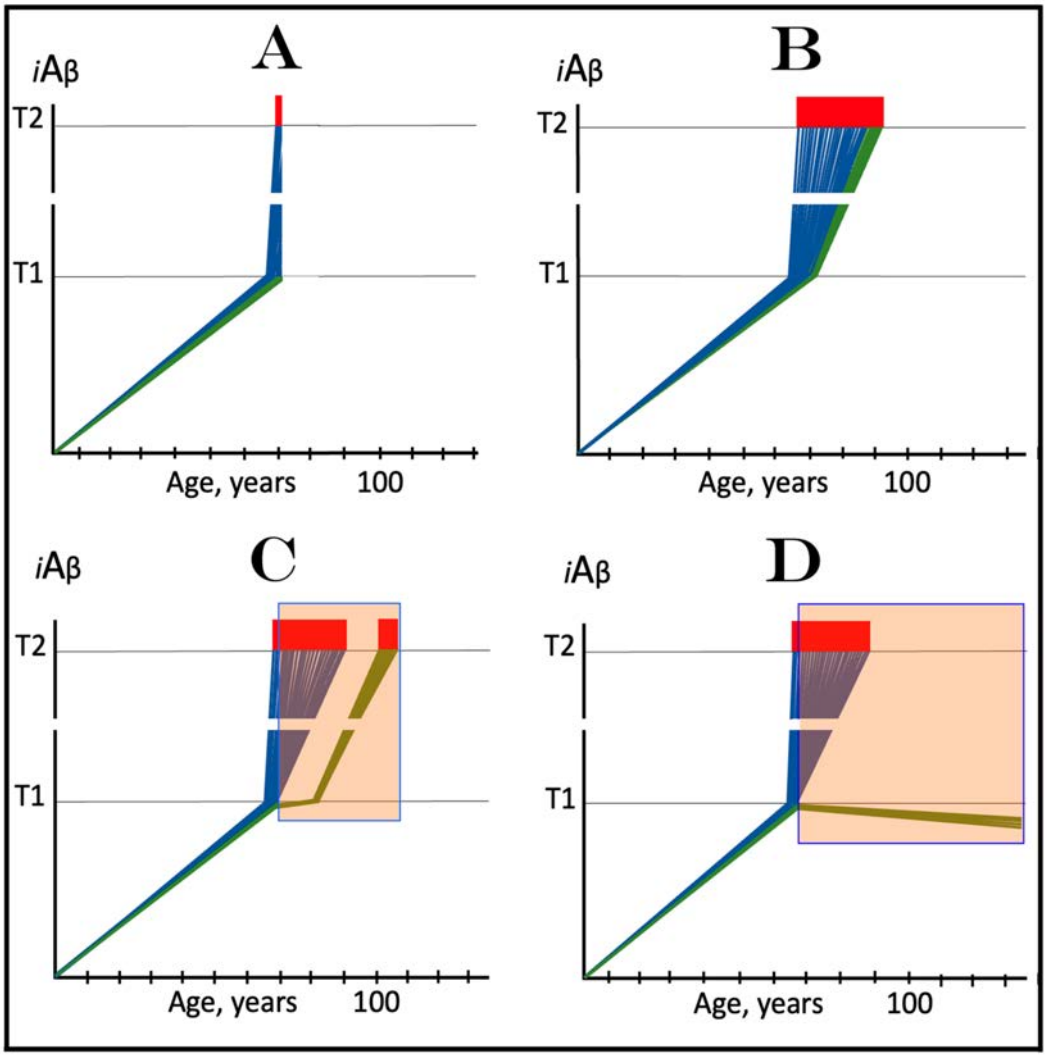

Figure 7. Effect of ACH-based drugs in early symptomatic AD: lecanemab and donanemab. *i*Aβ: intraneuronal Aβ. ***T1*** *threshold*: concentration of *i*Aβ that triggers activation of the eIF2α kinases, the elicitation of the ISR and the initiation of the AβPP-independent *i*Aβ generation pathway. ***T2*** *threshold*: concentration of *i*Aβ, generated mainly in the AβPP-independent pathway, which triggers neuronal apoptosis or necroptosis. *Blue lines*: levels of *i*Aβ in individual neuronal cells. Green lines: neurons with levels of AβPP-derived *i*Aβ below the T1 threshold at the commencement of the treatment. *Red box*: apoptotic zone, the range of *i*Aβ levels that cause the commitment to cell death. *Orange boxes:* duration of the administration of the ACH-based drug. (**A**) The initial state of *i*Aβ levels in individual neurons

at the commencement of the drug's administration. The levels of AβPP-derived *i*Aβ have crossed the T1 threshold and the AβPP-independent *i*Aβ production pathway has been activated in the bulk of the neurons, but a small neuronal fraction remains sub-T1. (**B**) Evolution of the initial state in the absence of a treatment. The initial sub-T1 neuronal fraction crosses the T1 threshold and activates the AβPP-independent *i*Aβ production pathway. The disease progresses until it reaches the end stage. (**C**,**D**) Evolution of the initial state in the presence of the drug. In both panels, the drug affects only the sub-T1 neuronal fraction and has no effect in neurons with the operational AβPP-independent *i*Aβ generation pathway. (**C**) In the initial sub-T1 neuronal fraction, the drug reduces the influx of AβPP-derived *i*Aβ and lowers the rate of its accumulation, but its levels are increasing and eventually reach the T1 threshold. The AβPP-independent *i*Aβ production pathway would be activated, the cells would become unresponsive to the drug, and their fate would be the same as of the rest of the neuronal population, albeit with a certain delay. (**D**) The influx of AβPP-derived *i*Aβ is reduced sufficiently to reverse its accumulation, and its levels are decreasing. In this neuronal fraction, the T1 threshold would not be reached for the duration of the drug's administration. In either case, the overall effect would be only marginal because the drug would affect only a marginal neuronal sub-population.

6. AβPP-Independent Production of *i*Aβ Is the Cornerstone of Any Adequate Model of AD

The AβPP-independent *i*Aβ production pathway appears to constitute the essence, the active core of AD. Indeed, the accumulation of *i*Aβ produced in the AβPP proteolytic pathway alone appears insufficient to reach the levels required to initiate and drive the disease. The efficiency of the AβPP-independent *i*Aβ generation pathway greatly exceeds that of its production in the AβPP proteolytic pathway. The reasons for this are multiple. Whereas only a minute fraction of Aβ produced by AβPP proteolysis ends up as *i*Aβ, the entire output the AβPP-independent *i*Aβ production pathway is, presumably, retained intraneuronally. The primary translation product of the AβPP-independent pathway of *i*Aβ generation (100 amino acid residues long) constitutes only 13% of the full-size AβPP (771 residues long) and requires only one, rather than two, proteolytic cleavage; accordingly, its production is an order of magnitude more efficient. Moreover, as discussed in detail below, it appears plausible that the AβPP-independent *i*Aβ generation pathway is powered by the asymmetric amplification of AβPP mRNA. In this scenario, every conventionally transcribed AβPP mRNA serves repeatedly as a template for transcription of multiple mRNAs encoding C100 [4], and the rate of its production in such a case would be orders of magnitude greater than that of C99 production by AβPP proteolysis. In relation to the AβPP-independent *i*Aβ production pathway, AβPP-derived *i*Aβ plays an auxiliary role: just as the starter motor ignites the car engine (and remains redundant for the duration of the engine's operation), so too does AβPP-derived *i*Aβ, when accumulated over the T1 threshold, ignite the autonomous, self-sustaining AD Engine and is rendered marginal, if not redundant, afterwards. The bottom line of this reasoning is that the operation of the AβPP-independent *i*Aβ production pathway is necessary and probably sufficient for AD; the disease cannot occur without it. This pathway, therefore, is the cornerstone of and has to be incorporated in any adequate model of the disease.

7. Human Neuronal Cell-Based Models of AD

The present section describes the design, construction, and utilization of the human neuronal cell-based AD models capable of displaying the full spectrum of cellular AD pathology. These models are sufficient to address numerous aspects of the disease and to support the development and testing of novel AD drugs. Importantly, they also constitute the essential intermediate step in the development of adequate transgenic animal models of AD.

7.1. Rationale

Conceivably, for more than one reason, the best and apparently the only currently available adequate model of AD is one based on human neuronal cells. AD appears to be a

human-specific condition. It is possible that it occurs in other species, but so far it has been observed exclusively in humans (all claims to the contrary have been made on the basis of the appearance of Aβ plaques, a criterion that has little relevance to AD in the ACH2.0 perspective [1–6]). Closely related primate species possibly do not live long enough to develop the disease, but even in long-lived mammals such as elephants, no AD has been detected. Since the ACH2.0 defines AD as a disease driven by the production of *i*Aβ in the AβPP-independent pathway, it can be assumed that this attribute is possibly unique (or at least relatively unique) to humans and is inoperative (or operative rarely) in non-human mammalian species. Thus, choosing human neuronal cells as the basis for the development of AD model confers two advantages. One, these cells originate from the species known to be affected by the disease. Another, related, advantage is that it can be presumed that they are capable of operating molecular pathways underlying the disease; more specifically that they are capable, when properly induced, to generate *i*Aβ in the AβPP-independent pathway. Given this capability, the design of the human neuronal cell-based model of AD is obvious: activate the AβPP-independent *i*Aβ production pathway and ascertain that it is self-sustaining, i.e., that the AD Engine is operative, and the cellular AD pathology would follow; the activity of the AβPP-independent *i*Aβ generation pathway can be assessed as described in Section 12 below. At this point, the cellular AD pathology would become, short of therapeutic intervention, irreversible and the appearance of neurofibrillary tau tangles could serve as the benchmark for the occurrence and the progression of the disease at the cellular level.

7.2. Exogenous iAβ-Mediated Elicitation of the ISR

According to the ACH2.0, the activation of the AβPP-independent *i*Aβ production pathway is preceded by the elicitation of the ISR: the latter causes the former. One way to elicit the ISR is via the accumulation of exogenous *i*Aβ. Such an approach would emulate the physiological development of conventional AD. Presumably, once the levels of *i*Aβ reach the T1 threshold, the PKR and/or HRI kinases would be activated, eIF2α would be phosphorylated, the ISR would be elicited and the operation of the AβPP-independent pathway of production of endogenous *i*Aβ would be initiated. Exogenous AβPP can be produced transiently or stably, from multiple AβPP-encoding transgenes. To prevent the diffusion of secreted Aβ (and consequent reduction of its importation), cells can be maintained in a semi-solid medium such as Matrigel. Utilization of the proper AβPP mutants would accelerate the accumulation of AβPP-derived *i*Aβ. Thus, mutants producing predominantly Aβ42 would elevate the rate of its cellular uptake and also lower the extent of the T1 threshold [4]. Utilization of the Swedish AβPP mutant, in another example, would result, as discussed above, in the increased rate of intraneuronal retention of Aβ produced on the intracellular membranes.

In another approach, *i*Aβ can be produced exogenously from vectors or from transgenes expressing only Aβ42. In this approach, its entire output would remain within the cell (it lacks the transmembrane domain, which is present within C99 at the junction of its Aβ and AICD segments and is requisite for secretion) and would rapidly accumulate. When its levels cross the T1 threshold, the ISR would be elicited and the AβPP-independent endogenous production of *i*Aβ would be activated. Since at the time of the activation of the AβPP-independent *i*Aβ production pathway, the basal *i*Aβ level would be above the T1 threshold, operation of the pathway would be self-sustainable as soon as it is active.

7.3. iAβ-Independent Elicitation of the ISR

In the framework of the ACH2.0, elicitation of the ISR in human neuronal cells by means other than AβPP-derived *i*Aβ would be sufficient to activate the endogenous AβPP-independent *i*Aβ production pathway and to trigger the progression of the AD pathology. This is, in all likelihood, the way in which traumatic brain injury, chronic encephalopathy, chronic inflammation, and viral and bacterial infections contribute to the development of AD. To trigger the elicitation of the ISR in human neuronal cells, it is sufficient to activate

any of the four eIF2α kinases: PKR, PERK, GCN2, and HRI. There are numerous stressors capable of activating these kinases. For example, HRI could be conveniently activated via mitochondrial disorder as was described for various cell types, including neuronal cells [121,122]. In this approach, however, when the ISR is elicited and the endogenous AβPP-independent *i*Aβ production pathway is activated, the basal level of *i*Aβ would be below the T1 threshold. Consequently, at the time of its activation, the AβPP-independent *i*Aβ production pathway wouldn't be self-sustainable, and if the initial ISR-eliciting stressor is removed and the ISR is not in effect anymore, operation of the pathway would cease. It follows that in this approach the initial stressor should be present, to maintain the ISR, long enough to allow *i*Aβ produced in the AβPP-independent pathway to accumulate over the T1 threshold. At this level, *i*Aβ becomes the stressor, which maintains the ISR (via activation of the PKR and/or HRI kinases) and perpetuates the operation of the AβPP-independent pathway of its own production; the continuous presence or the removal of the initial ISR-eliciting stressor would be, at this point, irrelevant and inconsequential for operation of the pathway.

7.4. Proof of Concept: "Alzheimer's in the Dish"

As was discussed above, the appearance of neurofibrillary tau tangles can serve as the benchmark for the progression of the cellular AD pathology in human neuronal cell-based AD models. But are cultured human neuronal cells capable of displaying the full spectrum of cellular AD pathology, including the NFTs? The answer to this question is affirmative. The formation of NFTs was indeed observed in human neuronal cells overexpressing exogenous Aβ and cultured in Matrigel [152] (a model popularly known as "Alzheimer's in the dish"). The authors of that study interpreted (in the ACH terms) the results as the affirmation of the AD-causing effect of extracellular Aβ. The interpretation of these results in the ACH2.0 framework, however, indicated that in this study, the endogenous self-sustaining AβPP-independent *i*Aβ production pathway was activated and that this pathway propelled the cellular AD pathology, including the formation of the NFTs. In the study in question, a polycistronic lentiviral construct was employed to overexpress human AβPP carrying two FAD mutations, namely, London (V717I) and Swedish (K670N/M671L), as well as PSEN1 with the E9 FAD mutation. The construct was transfected into human neural progenitor cells, which were cultured and differentiated in Matrigel. In the resulting neuronal cells, the Swedish mutation promoted, as discussed above, the processing of C99 on intracellular membranes and the retention of *i*Aβ. The London mutation shifted the AβPP processing toward production of the Aβ42 isoform, as did the PSEN1 E9 mutation. Since, as discussed above, the rate of importation of extracellular Aβ42 (which did not diffuse due to the cultivation of cells in Matrigel) is twice that of other Aβ isoforms, and because of the increased retention of AβPP-derived *i*Aβ produced on intracellular membranes, the rate of accumulation of exogenous *i*Aβ significantly accelerated; eventually it crossed the T1 threshold and triggered the activation of the endogenous AβPP-independent *i*Aβ production pathway. With this pathway operative, the cellular AD pathology progressed and reached the benchmark of the NFTs formation.

The study under discussion [152] serves as proof of concept for the suitability of human neuronal cells as the basis for the models of AD. As described above and elsewhere [1,4], the design of human neuronal cell-based models of AD can be significantly streamlined, but the model utilized in [152] can also be legitimately employed in further studies.

7.5. Human Neuronal Cell-Based AD Model as a Tool for Validation of the Occurrence of AβPP-Independent iAβ Production and for Elucidation of the Molecular Nature of the Underlying Mechanism

Above, we reasoned that to generate the adequate transgenic animal model of AD, the operative inducible AβPP-independent *i*Aβ production pathway has to be introduced. The problem is that we do not know the identity of this pathway and need an adequate AD model in order to test for it. Human neuronal cell-based AD models solve this problem. With such a model, we do not have to know the nature of the mechanism, which produces

*i*Aβ independently of AβPP, in order to employ the model. It is sufficient to know that it is incorporated into the model. And because the model is based on human neuronal cells, we are certain that it is, intrinsically. The availability of such an AD model provides a tool for validation of operation of the AβPP-independent *i*Aβ generation pathway and for elucidation of its molecular nature. In Section 12 below, we describe how the operation of this pathway can be verified. We also define four distinct mechanisms capable of generating *i*Aβ independently of AβPP and describe how they can be tested for and identified with the help of human neuronal cell-based AD models (Section 13 below).

7.6. Human Neuronal Cell-Based AD Model as a Tool for Testing Novel AD Drugs

Human neuronal cell-based models of AD can also be employed to evaluate potential therapeutic effects of the novel AD strategies, such as, for example, the depletion of *i*Aβ by its targeted degradation via the activation of BACE1 and/or BACE2. The rationale for this strategy, described in detail in [4,6], is, briefly, the following. The AβPP-derived *i*Aβ production pathway, which drives the AD pathology, is self-sustainable. It is propagated by *i*Aβ at the levels above the T1 threshold. If *i*Aβ were depleted to the levels below the T1 threshold, operation of the pathway would cease and the progression of the AD pathology would be arrested. This can be achieved by the transient activation of BACE1 and/or BACE2. Both possess intra-*i*Aβ cleaving activities (distinctly different; secondary in BACE1 and primary in BACE2) that are capable of depleting *i*Aβ if sufficiently enhanced (reviewer in [4,6]; in fact, this is what takes place in carriers of the protective Icelandic Aβ mutation). The disease would not recur until the levels of *i*Aβ (now produced solely in the AβPP proteolytic pathway) would be restored to the T1 (i.e., the ISR-activating) threshold, possibly a decades-long process. To evaluate their therapeutic potential, BACE1 and/or BACE2 can be exogenously overexpressed in human neuronal cell-based AD model. Assaying for the effects of BACE1/2 overexpression would include monitoring *i*Aβ levels, expected to be reduced, measuring the activity of the AβPP-independent *i*Aβ generation pathway (expected to cease if the strategy is successful), as described in Section 12 below, and testing for the occurrence of NFTs.

Human neuronal cell-based AD models can also be employed to evaluate the feasibility of the ISR inhibitors as potential AD drugs. Indeed, in the ACH2.0 paradigm, if the ISR is prevented or suppressed, the AβPP-independent *i*Aβ production pathway cannot operate, and consequently AD cannot occur (or progress). The means to inhibit the integrated stress response are currently available: the small-molecule ISR inhibitor ISRIB. Depending on the timing of its administration and on the duration of treatment, it could be anticipated that the implementation of ISRIB would either prevent both the activation of the AβPP-independent *i*Aβ production pathway and the formation of neurofibrillary tangles (if dispensed prior to the elicitation of the ISR) or stop operation of the former (if applied following the elicitation of the ISR; approaches to assess the activity of this pathway are discussed below). If successful, the results of such assessment would establish the ISR inhibitors as potential AD drugs. It should be mentioned that the utilization of the ISR inhibitors as AD drugs would require the long-term duration of treatment, which could be problematic in view of the pivotal physiological role of the ISR.

8. Potential Mechanisms Enacting AβPP-Independent *i*Aβ Production in AD: The Singularity of the AUG Encoding Met671 of Human AβPP

8.1. Pivotal Role of the AUG Encoding Met671 of AβPP in the AβPP-Independent Generation of iAβ

All conceivable mechanisms potentially underlying operation of the AβPP-independent *i*Aβ production pathway have one common feature: in all, translation initiates from the AUG conventionally encoding methionine 671 of human AβPP [4]. This pivotal role of the AUG codon in question stems from its singular position within the human AβPP gene, and, consequently, within AβPP mRNA. In 1987, three research groups cloned and sequenced human AβPP cDNA [153–155]. Shortly afterwards, two researchers, Breimer and Danny, have noticed that in the human AβPP nucleotide sequence, the portion encoding C99

is preceded immediately, contiguously, and in-frame by an AUG codon [156]. Just this observation would be a sufficient ground for the far-reaching speculations, but there was more to it. The AUG codon under discussion is positioned within the optimal translation initiation nucleotide context (known as the Kozak motif). Moreover, as if this were not enough, this particular AUG codon is singular in that of twenty methionine-encoding AUG codons in human AβPP mRNA, it is the only one embedded within the optimal translation initiation nucleotide context. Strikingly, not even the translation-initiating AUG encoding Met1 of human AβPP is situated within the optimal translation initiation nucleotide context. Such extraordinary localization of the AUG encoding Met671 of human AβPP has sweeping implications: (a) translation can potentially initiate from this position, and (b) the initiation of translation from the AUG under discussion would result in C99 (C100) and, subsequently, Aβ produced independently of AβPP.

8.2. Internal Initiation of Translation from the AUG Encoding Met671 of Human AβPP Cannot Be Ruled Out

Following their observation, Breimer and Danny reasoned that the unique and propitious localization of the AUG encoding Met671 of human AβPP may be not random but rather reflects the underlying physiological function [156]. They suggested that, in Alzheimer's disease, translation of the intact AβPP mRNA initiates internally from the AUG encoding Met671 of AβPP and results in C99 generated independently of AβPP [156]. This proposition attracted significant interest and was eventually addressed experimentally by two research groups. The rationale for both attempts was that if translation indeed initiates internally from the AUG in question, manipulation of AβPP coding nucleotide sequence upstream from it would not interfere with the process. Accordingly, multiple frame-shifting mutations were introduced upstream from the AUG of interest in one study [157]. In another study, translational stop codon was inserted upstream of it [158]. Both studies reasoned that if translation initiates internally, the introduced mutations would not affect it. However, in both studies, the mutations completely stopped the production of C99 and Aβ, and, consequently, the internal initiation of translation was ruled out. This conclusion may be correct, but for the wrong reasons. The process posited by Breimer and Danny in [156] was proposed to occur in AD-affected human neurons in a disease-inducible manner. Both studies described above [157,158], however, were carried out in non-neuronal cells and definitely not under AD conditions. Breimer and Danny's proposition [156], therefore, remains potentially valid and should be reevaluated in an adequate human neuronal cell-based model system.

8.3. Internal Initiation of Transcription Can Produce 5′-Truncated AβPP mRNA where the AUG Encoding Met671 Is the First Translation Initiation Codon

The unconventional internal initiation of translation within the intact human AβPP mRNA is, however, not the only way to utilize the AUG encoding Met 671 for the AβPP-independent production of Aβ. The identical result can be achieved in a conventional manner by generating suitably 5′-truncated AβPP mRNA where the AUG in question becomes the first, 5′-most, in-frame translation initiation codon. One way to generate such 5′-truncated AβPP mRNA is via the internal initiation of transcription within the AβPP gene. Such initiation of transcription should, obviously, occur upstream of the AUG under discussion and it would lead to the production of mRNA encoding C99 (or rather C100, see below) and, subsequently to the generation of C99 independently of AβPP. This process would require the production of a specialized transcription factor or co-factor expressed in the AD-affected neurons, presumably as a result of the ISR-mediated transcriptional/translational reprogramming.

8.4. Site-Specific Cleavage of AβPP mRNA Can Also Generate Suitably 5′-Truncated AβPP mRNA

Another way to generate a suitably 5′-truncated AβPP mRNA where the AUG normally encoding Met671 is the first translation initiation codon is to cleave the intact AβPP

mRNA in a site-specific manner. The requirements for the position of the site of such cleavage are the same as for that of the site of the internal initiation of transcription discussed above: it should be positioned upstream of the AUG in question, with no other functional in-frame translation initiation codons in-between. The primary translation product of so truncated mRNA would be C100 (see below) produced independently of AβPP. The truncated mRNA would be cap-less; it would be, nevertheless, a functional translation template under the conditions of the ISR (sustained, as discussed above, by *i*Aβ produced independently of AβPP), which enable cap-independent translation. Such site-specific cleavage of the intact AβPP mRNA would depend on the de novo production of a specialized nuclease, expressed, presumably, within the framework of ISR-mediated transcriptional/translational reprogramming.

8.5. Unconventional Generation of 5′-Truncated Chimeric AβPP mRNA Encoding the C100 Fragment of AβPP

Apparently, the most plausible mechanism underlying the operation of the AβPP-independent *i*Aβ production pathway is unconventional. It is the generation of 5′-truncated chimeric AβPP mRNA encoding the C100 fragment where the first in-frame translation initiation codon is the AUG normally encoding Met671 of AβPP; it is "chimeric" because its 5′ untranslated region (5′UTR) includes a 3′-terminal segment of the antisense AβPP RNA. The plausibility of this mechanism is strongly supported empirically, and it provides a mechanistic explanation as to why the AβPP-independent *i*Aβ production and, consequently, AD occur in humans but not in mice and in the current transgenic animal AD models; it also instructs how to overcome this limitation and construct an adequate animal AD model. Due to its potential importance, this mechanism and its application to AβPP-independent *i*Aβ production in AD are further discussed in the following three sections below.

9. RNA-Dependent Amplification of Mammalian mRNA: General Principles

Mammalian RNA-dependent mRNA amplification, described in detail elsewhere [159–168], occurs physiologically in situations requiring the large-scale production of specific proteins, for example, in some types of terminal differentiation [159–161] or during deposition of extracellular matrix proteins [162]. This process may potentially occur in two stages. The first stage is a "chimeric" pathway, named so because it yields a chimeric mRNA where a portion of or the entire 5′UTR consists of the 3′-terminal segment of the antisense RNA strand. In this pathway, every conventionally transcribed mRNA serves repeatedly as a template; this process is thus linear. Subject to certain requirements, it can, upon completion, expand into the second stage that operates in a PCR-like manner where every newly transcribed amplified RNA molecule serves as a transcription template; this process is exponential. The second mRNA amplification stage, although very interesting, has no relevance to the present discussion subject, and only the chimeric mRNA amplification pathway is described below. The latter is of special interest because it is capable of generating 5′-truncated human AβPP mRNA encoding only the C100 fragment.

The chimeric pathway of RNA-dependent amplification of mammalian mRNA is depicted schematically in the upper and middle panels of Figure 8. The amplification process begins with the generation of the antisense strand of a conventionally gene-transcribed mRNA molecule by the RNA-dependent RNA polymerase, RdRp. It initiates within the 3′-terminal poly(A) region of mRNA and results in a double-stranded RNA containing strands in both, sense and antisense, orientation. The double-stranded RNA structure is resolved by helicase activity, which commences at the 3′-terminal poly(A) and proceeds in the 5′ direction. When separated, conventionally produced mRNA can be repeatedly reutilized in the amplification process.

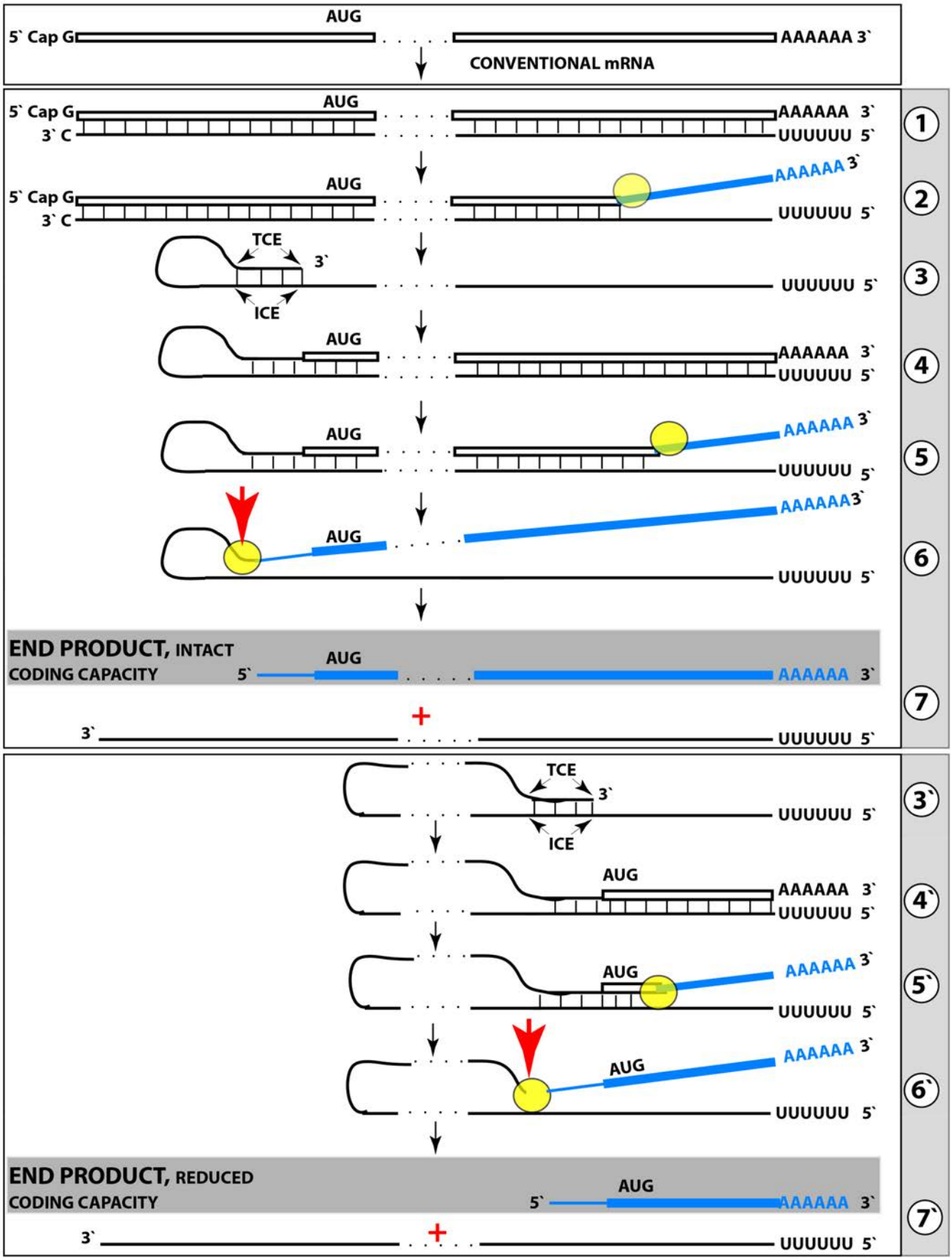

Figure 8. RNA-dependent amplification of mammalian mRNA amplification: principal stages. *Boxed*

line: sense RNA. *Single line*: antisense RNA. "*AUG*": codon for translation-initiating methionine. "*TCE*": 3′-terminal complementary element of the antisense RNA; "*ICE*": internal complementary element of the antisense RNA. *Yellow circle*: helicase complex; it also includes nucleotide-modifying activity. *Blue lines* (both single and boxed): RNA strands following their separation by the helicase/nucleotide-modifying complex. *Red arrows*: position of the cleavage of the chimeric RNA intermediate. (**Top panel**) Conventional, genome-transcribed mRNA, the "progenitor" in the mRNA amplification pathway. (**Middle panel**) Principal stages of the chimeric pathway of mammalian RNA-dependent mRNA amplification. Stage **1**: The antisense RNA is transcribed from the conventional mRNA progenitor by RdRp. Stage **2**: Sense and antisense strands are separated. The helicase complex mounts 3′-terminal poly(A) of the sense RNA and moves along it, modifying on average every fifth nucleotide along the way. Stage **3**: TCE–ICE-assisted folding of the antisense RNA into a self-priming configuration; Stage **4**: Extension of the self-primed antisense RNA. Its 3′ terminus is extended into the sense RNA, resulting in a hairpin-like structure. Stage **5**: Strand separation. The helicase complex mounts the 3′-terminal poly(A) of the sense strand and moves along it, separating it from the antisense strand. Simultaneously introduced nucleotide modifications presumably prevent the strands from re-annealing. Stage **6**: Upon reaching the single-stranded portion of the hairpin structure, the helicase complex cleaves the chimeric RNA intermediate; Stage **7**: 3′-truncated antisense RNA and chimeric mRNA end products of the chimeric mRNA amplification pathway. Note that in the above sequence, the ICE is positioned within a segment of the antisense RNA corresponding to the 5′UTR of the mRNA progenitor; in this scenario, the chimeric RNA end product contains the intact coding region of the conventional mRNA molecule. (**Bottom panel**) The ICE is positioned within a segment of the antisense RNA corresponding to the coding region of the mRNA progenitor. In this scenario, the amplified chimeric RNA end product contains a 5′-truncated coding region of the conventional mRNA progenitor. The translational outcome is defined by the position of the first translation initiation codon. If the first functional translation initiation codon is in-frame, translation would result in the C-terminal fragment of the conventionally encoded polypeptide. Stages **3′** through **7′** correspond to stages **3** through **7**.

The newly synthesized antisense RNA, when separated from its mRNA template, undergoes folding and assumes a self-priming configuration. This requires the presence within the antisense RNA strand of two not only complementary (or sufficiently complementary) but also topologically compatible segments. One of this segments has to be strictly 3′-terminal [169] (referred to as the terminal complementary element, TCE) whereas another segment can be situated any place within the antisense RNA strand (referred to as the internal complementary element, ICE). The TCE–ICE may contain internal mismatches; the only requirement for them is to be capable of forming a stable double-stranded structure without 3′-terminal overhang. Upon formation of a self-priming structure, the 3′ terminus of the antisense strand is extended into RNA in the sense orientation; the position of the initiation of extension of the antisense into sense RNA constitutes the "chimeric junction", i.e., the point of the conversion of RNA orientation. When the extension is completed, it produces a hairpin-like structure. The double-stranded portion of this structure is separated by a helicase complex invoked above. Upon reaching the single-stranded segment of the hairpin-like structure, the helicase cleaves the RNA molecule. The cleavage occurs either at the 3′ end of the hairpin loop or at one of the TCE–ICE mismatches.

One of the two resulting end products of the chimeric mRNA amplification pathway is the 3′-truncated antisense RNA. It misses either the entire TCE (if the cleavage occurs at the 3′ end of the hairpin loop) or a portion of it (if the cleavage occurs at the TCE–ICE mismatch). In the chimeric mRNA amplification pathway, the 3′-truncated antisense RNA end product is capable of limited re-use if the cleavage occurs at the TCE–ICE mismatch and leaves a substantial portion of the TCE intact (see below). However, if the amplification process is expanded and continues into the second stage, its fate is interesting and exciting: it gets polyadenylated at the 3′ end in conjunction with the cleavage, and serves as the initial template in the PCR stage of amplification {it has poly(A) at the 3′ end and poly(U) transcribed from the 3′-terminal poly(A) of mRNA at its 5′ end; its transcript, generated by RdRp, would likewise possess 3′-terminal poly(A) and 5′-terminal poly(U)} [160,161].

Another, functional (i.e., protein-encoding), end product of the chimeric amplification pathway is chimeric mRNA. It consists of the 5′-truncated mRNA and a covalently attached segment of the antisense RNA, actually its cleaved-off TCE (if the cleavage took place at the 5′ end of the TCE) or a portion thereof (the latter if the cleavage occurred at the TCE–ICE mismatch). The anticipated uncapped nature of the amplified chimeric mRNA end product is consistent and functionally compatible with the preferential cap-independent type of translation under the ISR conditions. In the reported cases of mammalian RNA-dependent mRNA amplification, those of globin and laminin mRNAs [159–162], the folding of the antisense RNA occurs within its segment corresponding to a portion of the 5′UTR of mRNA. This is the scenario depicted in the middle panel of Figure 8. In such cases, the resulting chimeric mRNA retains the complete coding capacity of the conventional mRNA progenitor, and upon translation yields the polypeptide identical to the translational product of the conventional mRNA. This, however, is not always the case.

10. Asymmetric RNA-Dependent Mammalian mRNA Amplification: Amplified mRNA Encodes Only CTF of the Conventionally Produced Polypeptide

The 3′-terminal TCE is, as reflected in its designation, always 3′-terminal. This is a strict requirement crucial for its potential to prime transcription of RNA. In contrast, the ICE can be any place within the antisense RNA. If the ICE occurs within a portion of the antisense RNA corresponding to the 5′UTR of conventional mRNA, the amplified mRNA would retain the complete coding capacity of the mRNA progenitor, but this is only one of many possibilities (for detailed discussion of the subject, see [164]). For example, the amplified chimeric RNA may encode a CTF of the original protein or even a polypeptide non-contiguously encoded in the genome [164]. What scenario will play out depends on two factors. One is the position of the ICE within the antisense RNA. It defines the site of the initiation of transcription and the extent of the 5′ truncation of the amplified mRNA. Another factor is the position of the first functional translation initiation codon within the amplified chimeric RNA.

The present section considers a scenario that results in the production of CTF of a conventional protein. This scenario is of special interest due to its relevance to the potential of generating C99 (a CTF) independently of AβPP. In this scenario, diagrammatically illustrated in the bottom panel of Figure 8, the ICE is positioned within a segment of the antisense RNA corresponding to the coding region of conventionally produced mRNA. Consequently, self-primed extension of the 3′ terminus of the antisense RNA would generate only the 3′-terminal segment of conventional mRNA containing only a 3′ portion of its coding region. Subsequent strand separation and cleavage would produce a chimeric mRNA truncated within its coding region. The translational outcome of this scenario would be defined by the position of the first functional translation initiation codon (AUG or any other initiation-competent codon). If it occurs within the remaining portion of the coding region and if it were in-frame, translation initiated at this position would generate a CTF of conventionally produced polypeptide. Thus, this type of RNA-dependent mRNA amplification would be asymmetric: the amplified RNA would contain only the 3′-terminal portion of the coding region of mRNA progenitor and would yield, upon translation, only a CTF of the conventional polypeptide.

11. Human AβPP mRNA Is RdRp-Compatible Template Eligible for Asymmetric Amplification Yielding 5′-Truncated, C99-Encoding mRNA

The asymmetric pathway of chimeric mRNA amplification appears to be, in principle, capable of generating C99 (C100) independently of AβPP, provided that in the resulting 5′-truncated chimeric mRNA the first functional translation initiation codon were the AUG encoding Met671 of AβPP. There are, however, many barriers on the way. One is the distances (in nucleotides) involved in this process. The AUG encoding Met671 is situated over 2000 nucleotides downstream from the 5′ terminus of human AβPP mRNA. Provided that suitable TCE and ICE do occur in the antisense RNA, the location of the ICE would have to be 3′ from but in the vicinity of the complement of the AUG in question and thus

separated from the TCE also by about 2000 nucleotides. Given the highly complex nature of RNA folding, especially over long distances, the question is whether the TCE and ICE (if they are present within the antisense AβPP RNA to begin with) would be topologically compatible, i.e., would they find each other in the folded antisense RNA configuration? In other words, the question is whether human AβPP mRNA is the eligible template for RNA-dependent mRNA amplification. Its eligibility can be assessed in the following general approach, applicable to any mammalian mRNA species; actually, any RNA species containing 3′-terminal poly(A).

11.1. Evaluation of the Eligibility of an mRNA Species for the Chimeric mRNA Amplification Process: General Approach

To assess the eligibility of any mRNA species for RNA-dependent mRNA amplification, the mRNA of interest is first transcribed by reverse transcriptase (RT) starting at the 3′-terminal poly(A) segment. This produces its antisense strand, cDNA. The mRNA component is then removed by RNase H, usually present in preparations of RT (unless eliminated genetically). At this point, we have the antisense strand, separated from its mRNA template, in the presence of an enzyme (RT) capable to extend it if it forms a suitable self-primed structure, a situation equivalent to that depicted in the initial stages of Figure 8. If the resulting cDNA is the complete transcript of mRNA, if it contains the TCE and ICE, if the TCE and ICE (provided they are present in the cDNA) are topologically compatible, the cDNA would fold into a self-priming configuration. RT would then extend the 3′ end of cDNA into the sense strand. The nucleotide-sequencing analysis would determine whether the extension occurred, thus defining whether or not the topologically compatible TCE and ICE are present in the antisense transcript. If affirmative, this would establish the eligibility of the mRNA species of interest for RNA-dependent mRNA amplification, and the junction between the antisense and sense portions of the resulting product would determine the site of the initiation of self-primed extension, define the 5′ end of the ICE and enable the identification of both complementary elements.

11.2. Human AβPP mRNA Is the Eligible Template for Asymmetric Amplification Resulting in mRNA Encoding C100

The evaluation described above was, in fact, carried out, albeit inadvertently, for human AβPP mRNA. As was mentioned above, in 1987, three research groups cloned and sequenced human AβPP cDNA. Shortly after these studies were published, one group reported cloning and sequencing of much larger human AβPP cDNA that was substantially extended at its 3′ terminus [170]. This study speculated that the 3′-extended AβPP cDNA was templated by the corresponding 5′-extended AβPP mRNA, and that this 5′-extended mRNA, in turn, originated by the initiation of transcription at a site upstream from the transcription start site (TSS) defined by previously sequenced AβPP cDNAs [153–155]. At the time [170] was published, the genomic sequence upstream from human AβPP was not yet known. Soon afterwards, however, it was determined [171], and it became apparent that the reported 3′ extension of human AβPP cDNA did not correspond to and therefore could not have originated from a genomic transcript. As a result, the group that detected the 3′-extended human AβPP cDNA declared their finding an artifact and published a correction to this effect [170] (correction).

However, the careful analysis of the 3′-extended human AβPP cDNA in question showed that the extension is actually a segment of a human AβPP sense strand [172–174]. This result leaves little doubt regarding the origin of the extended segment. It is clear that it was produced during the preparation of cDNA by its self-primed extension, which occurred just as described in the preceding subsection. The analysis of the antisense–sense junction showed that the extension initiated about 2000 nucleotides from the 3′ end of the cDNA. It also defined the 5′ end of the ICE and thus allowed the identification of the TCE and ICE sequences [172–174]. These results thus established that human AβPP mRNA is eligible for RNA-dependent mRNA amplification. Moreover, the results affirmed that amplification of human AβPP would occur asymmetrically. The next key question is where translation of

the amplified chimeric RNA would initiate. As became clear from the sequence analysis, the first translation initiation codon within the extended sense-orientation portion of cDNA is actually the ATG encoding Met671 of human AβPP [172–174].

The projected folding into self-priming configuration and the extension of human antisense AβPP RNA into the sense strand encoding the C100 fragment of AβPP is presented in Figure 9 (panels "a," "b," and "c" correspond to stages 3′, 4′, and 6′ in Figure 8). As shown, human antisense AβPP RNA possesses the TCE and ICE, which are separated by over 2000 nucleotides. They are, nevertheless, topologically compatible, i.e., mutually accessible in the folded RNA structure. If and when RdRp is available, the TCE, acting as a primer, is extended into the sense AβPP RNA. Upon completion of the extension process, complementary strands are separated by the helicase complex and the cleavage takes place either at one of the TCE–ICE mismatches or at the 5′ terminus of the TCE (only the latter is shown in the Figure). The process is asymmetric. It generates chimeric mRNA whose antisense portion consists either of the TCE or of the portion thereof (if cleavage occurs at one of the TCE–ICE mismatches). Its sense portion consists of the 5′-truncated coding region and the 3′UTR. In terms of the translation outcome, its most important attribute is the presence of the in-frame translation initiation codon. It is located 58 nucleotides from the chimeric junction and it is the AUG encoding Met 671 of AβPP. Upon translation of this RNA, C99 (C100) and, subsequently, Aβ would be produced independently of AβPP.

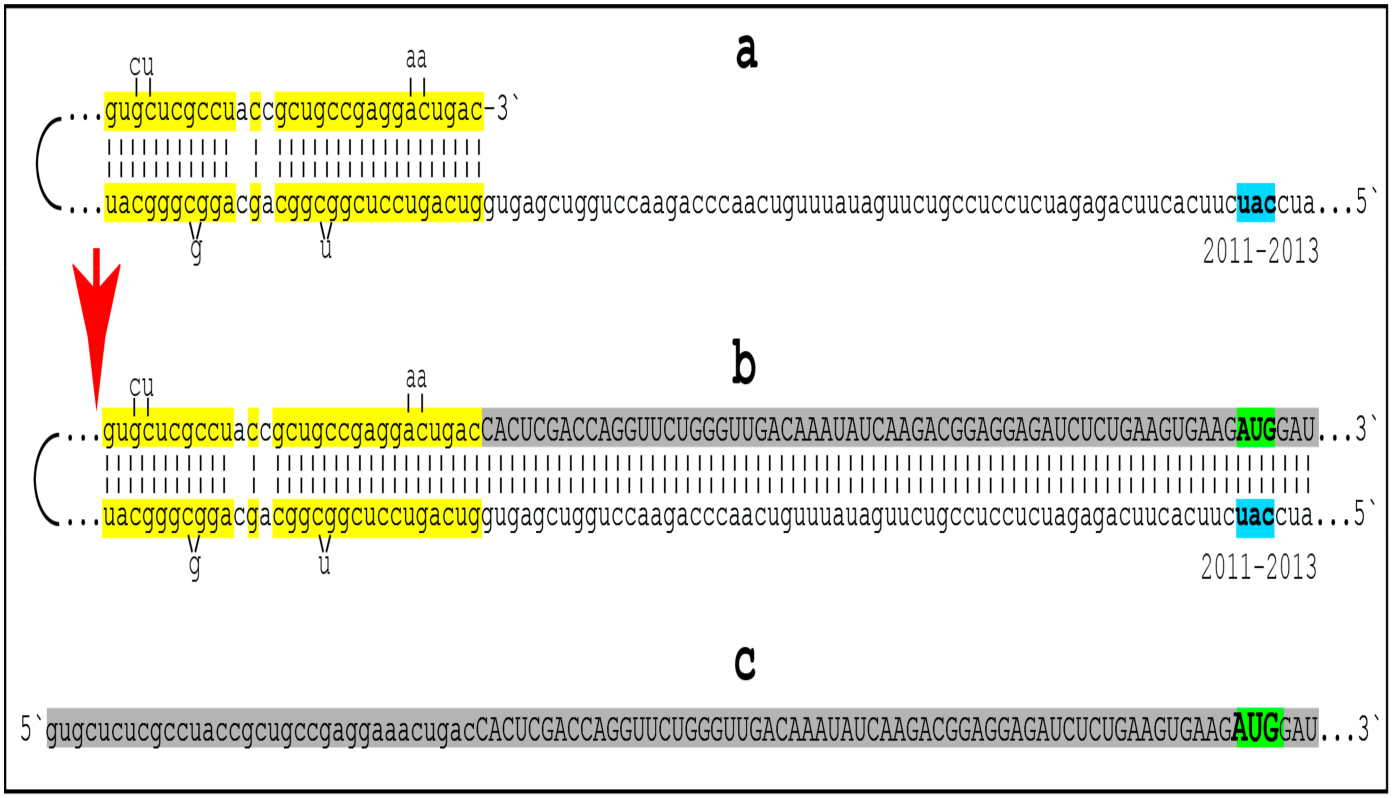

Figure 9. Human AβPP mRNA is the eligible template for asymmetric amplification resulting in mRNA encoding C100. *Lowercase letters*: nucleotide sequence of the antisense RNA. *Uppercase letters*: nucleotide sequence of the sense RNA. Highlighted *in yellow*: the TCE (top) and the ICE (bottom) elements of the human antisense AβPP RNA. *"2011–2013"*: nucleotide positions (counted from the 3′ terminus of the antisense AβPP RNA) of the "uac" (highlighted *in blue*), the complement of the "AUG" (highlighted *in green*) encoding Met671 in the human AβPP mRNA. Panels (**a**–**c**) correspond to stages 3′, 4′, and 6′ of Figure 8. (**a**) TCE–ICE-assisted folding of the human AβPP antisense RNA into the self-priming conformation. (**b**) Extension of the self-primed AβPP antisense RNA into the sense RNA

(highlighted *in gray*). *Red arrow*: cleavage of chimeric RNA intermediate following separation of sense and antisense RNA. Note that the cleavage is shown at the 3′ end of the single-stranded loop portion of the hairpin structure; it may also take place at one of the mismatches within the TCE–ICE. (**c**) Chimeric RNA end product of RNA-dependent amplification of human AβPP mRNA (highlighted *in gray*). It contains the antisense portion extended into the 5′-truncated coding region of human AβPP mRNA (note that the antisense–sense junction can shift if the cleavage occurs at one of the TCE–ICE mismatches; this aspect is addressed in Section 14 below). In the chimeric RMA end product, the first translation initiation codon is the in-frame AUG (highlighted *in green*) that encodes Met671 of human AβPP; when translated, the chimeric mRNA end product would produce C100 independently of AβPP.

12. Testing for the Occurrence of the AβPP-Independent Production of *i*Aβ in the Human Neuronal Cell-Based AD Model

The production of C99 and, consequently, of Aβ independently of AβPP is the quintessential and cardinal requirement within the framework of the ACH2.0. Obtaining a proof for this phenomenon would firmly establish the new AD paradigm. Auspiciously, making this determination appears feasible. When Breimer and Danny [156] suggested that the AUG encoding Met671 of AβPP could be used in the initiation of translation, obtaining such proof seemed unattainable. Indeed, according to the state of art at that time, it was assumed that, following the initiation of translation at the AUG in question, the initiating methionine would be removed co-translationally, as commonly happens, by the N-terminal methionine aminopeptidases 1/2 (MAP1/2). The resulting primary product, therefore, would be C99 that could be cleaved by gamma-secretase to generate Aβ. Thus, in the Breimer and Danny's narrative [156], the products of translation initiated at the AUG in question (independently of AβPP) would be identical in every way to and indistinguishable from the corresponding products of the AβPP proteolysis. However, the ensuing investigations into the processing of the N-terminus of the newly synthesized polypeptides have proven this presumption incorrect.

12.1. Initiation of Translation at the AUG Encoding Met671 of AβPP Results Not in C99 but in the C100 Fragment: The Initiating Methionine Is Not Removed Co-Translationally

Translation of the overwhelming majority of cellular proteins is initiated with methionine. The initiating methionine is usually removed co-translationally by the MAP1 or MAP2, and the resulting primary translation product starts at the N-end with a residue that follows the translation-initiating Met. This, however, is not always the case [175–180]. For the translation-initiating methionine to be cleaved co-translationally, it, and the residue that follows it, should be accommodated within the active site of MAP1/MAP2. This is, strictly speaking, a topological requirement and it cannot always be satisfied. With the size of the initiating methionine constant, the dimensions of the pair are defined by the size of its second residue. The size of an amino acid residue is determined by the radius of gyration of its side chain (RG). The RG is zero in glycine (no side chain), 0.77 Angstrom in alanine, 1.08 in serine, 1.22 in cysteine, 1.24 in threonine, 1.25 in proline, and 1.25 in valine. When the translation-initiating methionine is followed by any of these seven residues, the pair fits within the MAP1/MAP2 active site and the cleavage occurs co-translationally. When the translation-initiating methionine is followed by any other residue (all of them larger than valine), the pair cannot be accommodated within the MAP1/MAP2 active site, co-translational cleavage does not occur, and the primary translation product retains the initiating methionine [175–180].

Met671 of human AβPP is followed by the aspartate (RG 1.43 Angstrom). The Met/Asp combination does not fit within the MAP1/MAP2 active site. Therefore, if translation initiates with the methionine normally in position 671 of AβPP (regardless of the mechanism underlying such translation initiation), the initiating Met is not removed co-translationally and the primary translation product is the C100 (Met-C99) fragment of AβPP. This is not a unique situation; in cases like this, when the initiating Met is re-

tained in the primary translation product, it is usually removed by one of the numerous aminopeptidases with a broad specificity [180]. Thus, C100 is eventually converted into C99. If C100 were cleaved by gamma-secretase prior to the removal of its N-terminal methionine, this would result in Met-Aβ. In such a case, Met-Aβ would be eventually converted into Aβ by the same mechanism that converts C100 into C99. Importantly, the removal of the N-terminal translation-initiating methionine by an aminopeptidase other than MAP1/MAP2 unvaryingly occurs post-translationally.

12.2. Validation of the AβPP-Independent Production of C100 and Met-Aβ

Since the removal of the N-terminal methionine from C100 and Met-Aβ would always occur post-translationally, their pools should be present in the AD-affected human neuronal cells. The sizes of these pools would reflect the rate of the removal of the translation-initiating methionine, and, in the case of Met-Aβ, the relative rates of the aminopeptidase versus gamma-secretase cleavages, but these pools should exist in live AD-affected neurons. The occurrence of such pools would report on and validate the operation of the AβPP-independent *i*Aβ production pathway regardless of the nature of an underlying mechanism. The human neuronal cell-based AD model is suitable for testing the validity of the production of Aβ independently of AβPP. It should be commented at this point that the C100 and Met-Aβ pools would not be present in postmortem samples. This is because in dying cells, synthetic processes cease well in advance of proteolytic cleavages. Accordingly, in the absence of the influx of C100 and Met-Aβ, the remaining initiating methionine-containing molecules would be rapidly and completely converted into C99 and Aβ. An alternative, albeit more complicated, approach to validate the occurrence of the AβPP-independent production of C100 initiating at the AUG normally encoding Met671 of AβPP is described in the following section.

13. Elucidation of Molecular Nature of the AβPP-Independent *i*Aβ Production Mechanism in Human Neuronal Cell-Based AD Model

The occurrence of the initiation of translation from the AUG encoding Met671 of AβPP can also be assessed utilizing the same procedures as those employed previously [157,158] but in the appropriate model system, a human neuronal cell-based AD model. More specifically, a frame-shifting mutation or a translational stop-codon mutation can be edited in the endogenous AβPP gene upstream from the AUG encoding Met671. If the initiation of translation from the AUG in question does not occur, no Aβ would be produced endogenously in this model system. If it does, neither mutation would interfere with it. The criterion for the occurrence of the endogenous Aβ generation would be the presence of C100 and, possibly, Met-Aβ (more precisely, the presence of the N-terminal methionine in these molecules).

In another approach, in addition to the mutations upstream from the potentially translation-initiating AUG in the endogenous AβPP gene, one of the FAD mutation can be introduced within the Aβ-coding segment of the endogenous AβPP gene or, alternatively, within the Aβ-coding segment of a transgene. In either case, Aβ produced endogenously would be distinguishable from exogenously expressed Aβ, and the presence of the former would validate the occurrence of the endogenous initiation of translation at the AUG encoding Met671 of AβPP independently of the appearance and detection of the N-terminal Met in C100 or Met-Aβ. This approach can complement or substitute the detection of C100 or Met-Aβ as the validation test and could be useful if C100/Met-Aβ pools are too small for their unambiguous detection. The modification of the endogenous AβPP gene in this approach should be minimal in order not to interfere with the folding of the antisense AβPP RNA (e.g., the translational stop codon could be introduced with the replacement of a single nucleotide).

The relevant studies discussed above [157,158] attempted similar approaches for determination of the occurrence of the internal initiation of translation within the intact AβPP mRNA. However, the experiments described in [157,158] and in the present section above

address only the possible initiation of translation from the AUG encoding Met671 of human AβPP. They cannot distinguish between the mechanisms underlying this phenomenon. If and when the occurrence of the AβPP-independent *i*Aβ production in the human neuronal cell-based AD model is verified as discussed above, the subject of the nature of the mechanism underlying the operation of this pathway can be considered. Thus, the assignment of the origin of such phenomenon to the internal initiation of translation within the intact human AβPP mRNA would require evaluation of the operational occurrence of the IRES, which can be addressed using standard analytical approaches [181–186].

Whether the internal initiation of endogenous transcription within human AβPP gene or the site-specific cleavage of the intact human endogenously produced AβPP mRNA do take place, both occurring upstream of the AUG encoding Met671 of AβPP, could be suggested by the observation of the appropriately 5′-truncated AβPP mRNA where the first translation initiation codon is the AUG in question. If such RNA were observed, the presence of the cap structure at its 5′ terminus would indicate the occurrence of the internal initiation of transcription. If the 5′-terminal cap structure were not present, this would be consistent with the site-specific cleavage of the intact AβPP mRNA (for the approaches to detect the operation of the chimeric RNA-dependent human AβPP mRNA amplification pathway, see Section 14 below).

The procedures to evaluate the remaining and, arguably, the most plausible option, namely, that the human AβPP-independent production of IAβ is enabled by the asymmetric RNA-dependent amplification of human AβPP mRNA in the chimeric pathway, are analyzed in detail in the following section.

14. Validation of the Occurrence of Asymmetric AβPP mRNA Amplification: Search for the Chimeric RNA Intermediate

14.1. Why the Chimeric RNA Intermediate (Rather than Chimeric mRNA End Product)?

To assess the possibility that the AβPP-independent *i*Aβ production pathway is powered by the asymmetric RNA-dependent amplification of human AβPP mRNA in the chimeric pathway, it is sufficient to test for the presence of the chimeric mRNA end product. As shown in stage 7′ of Figure 9, the end product of human AβPP mRNA amplification would contain severely 5′-truncated coding region and, at its 5′-terminus, as a part of the 5′UTR, a 3′-terminal segment of the AβPP antisense RNA, more precisely its TCE element or a part thereof (if the cleavage occurs at one of the TCE–ICE mismatches). Due to the nature of the amplification process, where every conventionally genome-transcribed AβPP mRNA can be repeatedly utilized as a template (a situation analogous to a massive gene amplification), the chimeric mRNA end product should be highly ubiquitous and thus easy to detect. This, however, is not the case. This is because when the extension of the self-primed antisense RNA is completed, the helicase complex mounts the newly synthesized 3′ poly(A) and proceeds along this strand, separating it from its template (sages 5, 5′ and 6, 6′ in Figure 9). While separating this RNA strand, the helicase activity also modifies on average its every fifth nucleotide [160,161]. Ostensibly, the function of these modifications is to prevent the re-annealing of just-separated strands: the nature of these modifications is such that they interfere with nucleic acid hybridization [160,161]. Consequently, they also interfere with cDNA synthesis and cDNA-based sequencing. Therefore, the chimeric mRNA end product, although ubiquitous, cannot be used as a reporter of the RNA-dependent mRNA amplification process [160].

Therefore, the role of a reporter falls to its immediate precursor, the chimeric intermediate of the mRNA amplification. The region of interest that defines the chimeric nature of the molecule, its "identifier," is the region around and including the junction of sense and antisense segments, the "chimeric junction." The chimeric junction is created concurrently with the commencement of the extension of the self-primed antisense RNA. At this point, it is not modified. It remains unmodified for the duration of the extension (stages 4, 4′ in Figure 9) and for the time period it takes the helicase complex to traverse the distance between the 3′-terminal poly(A) and the vicinity of the chimeric junction (stages 5, 5′ in

Figure 9). This means that there is a defined duration, roughly between the commencement of the extension of the self-primed antisense RNA and the cleavage generating the chimeric RNA end product, when the chimeric junction region is not yet modified and is therefore detectable by the conventional means. If detected, the occurrence of the chimeric junction sequences would report on the occurrence of the RNA-dependent amplification of human AβPP mRNA. Such an approach was indeed validated in the detection of chimeric junctions generated during RNA-dependent amplification of globin and laminin mRNAs [160–162].

14.2. Potential Human AβPP mRNA Amplification-Generated Chimeric Junctions

As discussed above, each conventionally genome-transcribed mRNA molecule can be repeatedly utilized in cycles of amplification. Each cycle produces one antisense RNA molecule, which in turn might produce several distinctly different chimeric RNA intermediates. If the TCE and ICE elements are present within this molecule and are fully complementary, each antisense RNA transcript would produce only one chimeric RNA intermediate (the full-size antisense RNA extended into sense RNA) and, correspondingly, only one chimeric mRNA end product: the helicase complex would advance to the 5′ end of the TCE and cleave it off, as shown in stages 6, 6′ in Figure 9. In such a case, only one chimeric RNA intermediate molecule would be generated, with chimeric junction occurring at the 3′ end of the TCE element. If, however, the TCE–ICE combinations contain mismatches (and in all described cases of RNA-dependent mRNA amplification they do), the outcome would be different. In such a case, the helicase would cleave at the first (3′-most) mismatch, liberating the chimeric RNA end product with only a 3′-terminal portion of the TCE at its 5′ end. If the self-primed antisense RNA structure remains stable (despite its shortened TCE), it would be capable of another extension. In the resulting chimeric RNA intermediate, however, the chimeric junction would be shifted because the TCE is shorter (missing it cleaved-off 3′-terminal portion). This phenomenon is referred to as the "chimeric junction shift" and was, in fact, observed empirically [160,161]. If more than one mismatch is present in a particular TCE–ICE pair, more than one chimeric junction shift may occur and more than one chimeric RNA intermediate (and, subsequently, more than one chimeric RNA end product) would be generated from one antisense RNA molecule.

14.3. Differentiating between Mechanistic Possibilities

The putative end product of the RNA-dependent human AβPP mRNA amplification is a cap-less RNA molecule, which cannot be translated under the regular conditions. It would be, however, preferentially translated under the ISR conditions. This circumstance opens up an alternative mechanistic explanation of the AβPP-independent *i*Aβ production in the AD-affected neurons. Indeed, it can be speculated that the RNA-dependent amplification of human AβPP mRNA does occur constitutively in healthy AD-unaffected neurons but the resulting chimeric mRNA product remains untranslated, "silent." In such a case, the elicitation of the ISR, rather than activating the RNA-dependent mRNA amplification, enables translation of the otherwise "silent" uncapped C100-encoding chimeric mRNA. The assay described above would allow distinguishing between the two possibilities. If chimeric intermediates of AβPP mRNA amplification were found in human neuronal cell-based model system only when the ISR is elicited, this would indicate the inducible nature of the amplification process. If, on the other hand, the intermediates were detected also prior to the ISR elicitation, this would suggest the constitutive operation of the AβPP mRNA amplification mechanism in the human neuronal cells.

14.4. Putative Nucleotide Sequences of Human AβPP mRNA Amplification-Generated Chimeric Junctions to Search for in Human Neuronal Cell-Based AD Model

In cases of RNA-dependent human AβPP mRNA amplification, there is potential for the generation of three or four different chimeric RNA intermediates, and, accordingly, for the detection of three or four distinct chimeric junctions. One arises by the initial extension of the self-primed human antisense AβPP RNA whereas others are generated via

the chimeric junction shift in subsequent extension events. The mechanics of this process as well as the sequences of the putative chimeric RNA intermediates are presented in Figure 10. The detection of any of the chimeric junctions would constitute a proof of the occurrence of the chimeric RNA-dependent amplification of human AβPP mRNA.

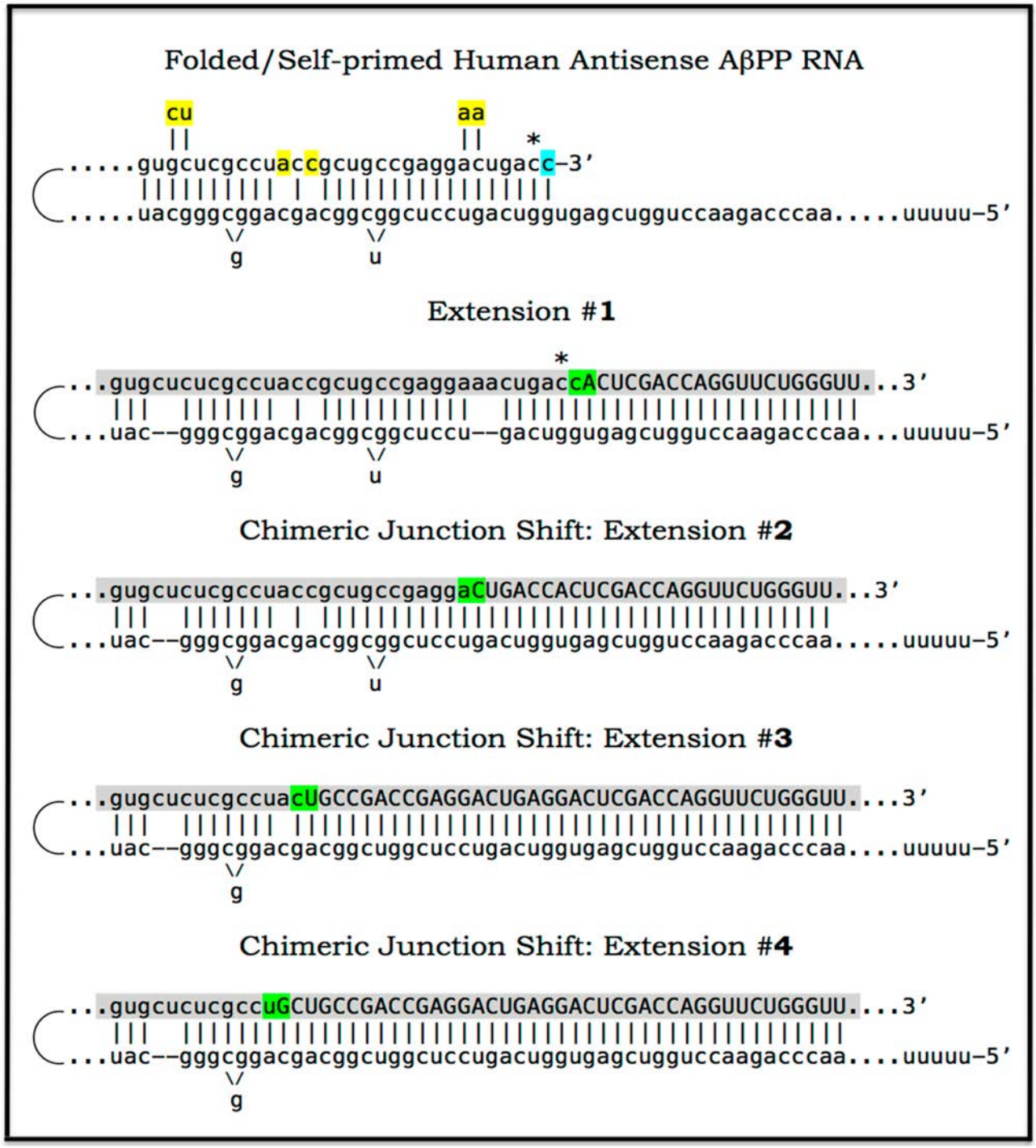

Figure 10. Chimeric junction shifts can generate multiple distinct chimeric RNA intermediates: the nucleotide sequences to look for. *Lowercase letters*: nucleotide sequence of the antisense RNA. *Uppercase letters*: nucleotide sequence of the sense RNA. Highlighted *in yellow*: mismatches within the TCE–ICE complex. Highlighted *in green*: chimeric junctions, the sites of the initiation of the extension of the self-primed antisense RNA into the sense RNA strand. *Asterisk*: the nucleotide position on the antisense RNA corresponding to the TSS of human AβPP mRNA (position (−)149 upstream from the

"A" of the translation-initiating AUG codon). Highlighted *in blue*: "C" transcribed from the 5′-terminal cap "G" of AβPP mRNA (not encoded in the genome; addressed in Section 20 below). Highlighted *in gray*: regions containing chimeric junctions, the "identifier" nucleotide sequences to look for. "Extension #1" of the self-primed AβPP antisense RNA produces chimeric RNA intermediate containing the full-size TCE. If, at the strand separation stage, the cleavage occurs at the first (3′-most) mismatch and the self-priming antisense RNA structure (now with a shorter TCE) remains stable, it would be capable of another extension. In the resulting chimeric RNA intermediate, however, the chimeric junction would be shifted because the TCE is shorter (missing its cleaved-off 3′-terminal portion). If more than one mismatch is present, more than one chimeric junction shift may occur ("Extension #2," etc.) and more than one chimeric RNA intermediate (and, subsequently, more than one chimeric RNA end product) would be generated from one antisense RNA molecule. In cases of RNA-dependent human AβPP mRNA amplification, there is potential for the generation of three or four different chimeric RNA intermediates, and, accordingly, for the detection of three or four distinct chimeric junctions. The nucleotide sequences to search for are highlighted in gray.

As was mentioned above, in the Authors' opinion and for the reasons discussed above, the asymmetric RNA-dependent amplification of human AβPP mRNA in AD-affected neuronal cells appears to be the most plausible mechanism powering the AβPP-independent *i*Aβ production pathway. For the purposes of the further discussion, it is presumed that this is the case. Even if this were not the case, the following discussion would illuminate the general principles of construction of an adequate transgenic animal model of AD, which are applicable to other potential mechanisms underlying the production of *i*Aβ in the AβPP-independent manner.

15. Generation of an Adequate Transgenic Animal Model of AD, Part I: Elicitation of the ISR in Neuronal Cells

15.1. Utilization of the Current Transgenic Animal AD Models

In light of the above discussion, the generation of an adequate transgenic animal model of AD consists of two parts. The first part is the elicitation of the integrated stress response in the neuronal cells. A practical approach to this is, apparently, the utilization of the current transgenic animal AD models. In these models, exogenously produced *i*Aβ accumulates via its importation from the extracellular pool and through its intraneuronal retention following the gamma cleavage of C99 on the intracellular membranes. Moreover, as discussed above, it is apparent that in these models, the levels of exogenous *i*Aβ have crossed the T1 threshold and triggered the elicitation of the ISR. This is because under ISR conditions, the de novo protein synthesis is reprogrammed and severely suppressed. Since neuronal plasticity, long-term memory and learning capacity all depend on de novo protein synthesis, they are all impaired under the ISR. As discussed above, inhibition of the ISR by the small-molecule inhibitor ISRIB abrogates this impairment, and the prevention of the elicitation of the ISR by genetic and pharmacological means precludes this impairment in the current transgenic AD models [37–45]. It follows that the first requirement for the successful generation of an adequate transgenic model of AD is already fulfilled in the current models.

15.2. Elicitation of the ISR in Neuronal Cells via Exogenous Overexpression of Intraneuronally Retained iAβ42

The current transgenic animal models of AD are ineffective in the accumulation of *i*Aβ. Although in these models AβPP is massively overproduced, only a small fraction of the resulting Aβ ends up inside the neuron as *i*Aβ. Indeed, only a small fraction of secreted Aβ is imported back inside the cell and only a small fraction of AβPP is processed (including the gamma-cleavage) on the intracellular membranes thus yielding *i*Aβ. The rate of accumulation of AβPP-derived *i*Aβ can potentially be greatly increased if the bulk or the entire production output of exogenous Aβ is retained intraneuronally. This can be achieved by employing transgenes encoding only Aβ. In these models, the AUG normally encoding Met671 of AβPP would be utilized as the translation initiation codon.

Since it is situated within the optimal initiation context, translation would be efficient. As discussed above, the primary translation product would be not Aβ, but Met-Aβ. The translation-initiating methionine, however, would be removed post-translationally by one of the cellular aminopeptidases with broad specificity; this will generate Aβ. Since it is lacking the transmembrane domain, this Aβ would be retained intraneuronally as *i*Aβ. Expressing exogenously *i*Aβ42 would be more efficient in the elicitation of the ISR than utilizing other isoforms of Aβ. This is because, due to its propensity to aggregate, *i*Aβ42 is more cytotoxic than other Aβ isoforms and would lower the T1 threshold for the activation of eIF2α kinases and the consequent elicitation of the ISR (discussed in detail in [4]).

15.3. iAβ-Independent Elicitation of the ISR in Neuronal Cells

In conventional AD, the elicitation of the integrated stress response is triggered by the accumulation of AβPP-derived *i*Aβ over the T1 threshold. However, within the framework of the ACH2.0, elicitation of the ISR in neuronal cells by any means, including stressors other than *i*Aβ, should be sufficient to provide the "missing" components of the mechanism enabling the AβPP-independent *i*Aβ production pathway and to activate its operation. Such *i*Aβ-independent elicitation of the ISR apparently underlie the cases of unconventional AD, such as those that are caused by traumatic brain injury, chronic encephalopathy, chronic inflammation, and viral and bacterial infection. The choice of a stressor in this approach would be largely defined by which one of the four eIF2α kinases is targeted for the activation. For example, for the activation of the HRI kinase, mitochondrial dysfunction could be triggered, whereas viral infection could be employed for the activation of the PKR kinase; the activation of one or more of the eIF2α kinases would be followed by the elicitation of the ISR. When the AβPP-independent *i*Aβ production pathway is activated in an AD model, it must be self-sustainable in order to drive the AD pathology. Whereas the AβPP-independent *i*Aβ production pathway triggered by the accumulation of AβPP-derived *i*Aβ over the T1 threshold is always self-sustainable (discussed above), this is not necessarily the case when the activation of this pathway is triggered by a stressor other than *i*Aβ; this issue is addressed in the following section.

16. Generation of an Adequate Transgenic Model of AD, Part II: Securing Self-Sustainable AβPP-Independent Production of *i*Aβ

The second part of the construction of an adequate transgenic animal model of AD is securing self-sustainable AβPP-independent production of *i*Aβ. The operation of this pathway seems to be essential for the occurrence of the disease [1–6]. Without it, the levels of *i*Aβ required to drive the AD pathology apparently cannot be achieved. In conventional AD, when the AβPP-independent *i*Aβ generation pathway is activated, it is immediately self-sustainable. This is because the initial stressor eliciting the ISR, in this case *i*Aβ, is already over the T1 threshold, and its production independently of AβPP assures that it stays so and, in addition to driving the AD pathology, propagates is own production. This would also be the case in transgenic animal models of the disease where the elicitation of the ISR is achieved through the accumulation of exogenous *i*Aβ over the T1 threshold.

If the ISR is elicited in neuronal cells by a stressor other than *i*Aβ, and, in turn, initiates the generation of *i*Aβ independently of AβPP, the activated AβPP-independent *i*Aβ production pathway would not be immediately self-sustainable. Indeed, if the initial ISR-eliciting stressor is withdrawn, operation of the AβPP-independent *i*Aβ production pathway would cease. For it to become self-sustainable, the ISR should be in effect for a sufficient duration to allow *i*Aβ produced independently of AβPP to accumulate over the T1 threshold. Repeated elicitations of the ISR for shorter durations would also achieve this by increasing the baseline levels of *i*Aβ (produced independently of AβPP) stepwise until they reach and cross the T1 threshold. However it is done in a perspective transgenic AD model where the ISR is initially elicited independently of *i*Aβ, for the model to be adequate, it must be ascertained that the ISR-activated AβPP-independent *i*Aβ production pathway attains self-sustainability. In unconventional cases of AD, both approaches mentioned above are,

apparently, utilized: in chronic encephalopathy it is the repeated trauma (i.e., the repeated elicitation of the ISR and a stepwise increase in the levels of *i*Aβ produced independently of AβPP), whereas in chronic inflammation and prolonged viral and bacterial infections, it is a sufficient duration of the ISR elicitation, which ensures the accumulation of *i*Aβ (produced in the AβPP-independent pathway) to levels exceeding the T1 threshold.

The above considerations are relevant and applicable only if the integrated stress response *does* activate the AβPP-independent generation of *i*Aβ. This, however, *does not* happen in the current transgenic animal models of AD. Why this is so and how to overcome this deficiency is addressed in the following sections.

17. Mice Possess and Utilize Physiologically the RNA-Dependent mRNA Amplification Pathway

One way to explain why the AβPP-independent *i*Aβ production pathway is inoperative in mice is to assume that this species does not possess the machinery required to enable the pathway's activity. In more precise terms, the assumption would be that mice lack the functional RNA-dependent mRNA amplification-competent RdRp. Such an assumption, however, would be incorrect. RNA-dependent mRNA amplification-competent RdRp was shown to be present and vigorously operating in mice physiologically. Two such instances have been described in detail. One is RNA-dependent amplification of alpha and beta globin mRNAs in differentiating erythroid cells [159–161]. The power of this process in terms of the production of mRNA is considerable: at the height of the erythroid differentiation the amount of globin mRNA produced in the RNA-dependent amplification pathway is about 1500 fold greater than the amount of globin mRNA generated conventionally during the same period in the same cells [160,161]. Another example is RNA-dependent amplification of mRNA species encoding alpha1, beta1, and gamma1 laminin in cells producing and secreting extraordinary amounts of this extracellular matrix component [162].

As in both examples above, the RNA-dependent mRNA amplification pathway appears to operate in circumstances requiring rapid production of immense quantities of particular polypeptides; thus, in erythroid differentiation cells are literally filled with hemoglobin (resulting in reticulocytes and, eventually, erythrocytes) within 48–72 h. Arguably, the extracellular matrix proteins are produced in even greater quantities within comparable time periods. In both examples and, probably, in general, RNA-dependent mRNA amplification is, apparently, activated under the ISR conditions, which, presumably, supply, via transcriptional/translational reprogramming, the component(s) of the RdRp complex that are "missing" under regular conditions. In cases of erythroid differentiation, it appears that the ISR is elicited via the activation of the heme-regulated HRI kinase, which, in turn, is triggered by the deficiency of free heme; the deficiency arises due to the increased conventional production of globin and the resulting sequestration of heme within the hemoglobin tetramer structure. As in Alzheimer's disease (discussed above), the activation of the RNA-dependent globin mRNA amplification and, eventually, greatly elevated production of globin polypeptides, creates the Engine that maintains the ISR and thus drives the amplification process: this occurs because as more globin is produced, more heme is sequestered, and its deficiency, and consequently the activity of HRI, are sustained. In the case of laminins, the increased conventional production of the ECM proteins apparently saturates the endoplasmic reticulum and causes the ER stress, thus activating PERK, another eIF2α kinase, and triggering the elicitation of the ISR and consequently of RNA-dependent mRNA amplification. The dramatically increased production of laminins (and other ECM proteins) sustains the ER stress, maintains the ISR conditions, and propagates the operation of the RNA-dependent mRNA amplification pathway [162].

In addition to the competent RdRp, the operation of the RNA-dependent mRNA amplification pathway requires the occurrence of an amplification-eligible RdRp mRNA template. In the examples presented above, both alpha and beta globin mRNA, as well as all three laminin mRNA species, are eligible RdRp templates [160–162]. The requirements

for such eligibility, described in the preceding sections, are strict. Some requirements are inviolable, such as, for example, the lack of the 3′-terminal overhang within the TCE–ICE complex. But "loosening" of more minor requirements also significantly affects the efficiency of the amplification process. For example, even single-nucleotide changes within the 5′UTR of human beta globin mRNA, that do not affect the efficiency of its translation but reduce the extent of its TCE–ICE complementarity, interfere with its amplification and cause beta thalassemia [164]. It follows that since mice possess functional RNA-dependent mRNA amplification machinery, and since the ISR is elicited and RdRp complex is, presumably, assembled in the neurons of the current transgenic animal models of AD, the highly plausible deficiency preventing the operation of the AβPP-independent *i*Aβ production pathway is, as discussed in the following section, the lack of the RdRp-compatible, RNA-dependent amplification-eligible AβPP mRNA.

18. Mouse AβPP mRNA Is Ineligible for RNA-Dependent Amplification and So Are AβPP mRNAs Produced in the Current Models of AD from Human AβPP Transgenes

18.1. Mouse AβPP mRNA Is Not a Competent RdRp Template and Therefore Is Ineligible for RNA-Dependent Amplification

In humans, the AβPP-independent *i*Aβ production pathway could, apparently, be powered by the RNA-dependent amplification of AβPP mRNA. Activating this pathway is then synonymous with assembling the competent RdRp complex. In these terms, and according to the discussion in the preceding sections, the transcriptional/translational reprogramming by the integrated stress response provides missing component(s), potentially co-factors, of the RdRp complex. With the competent RdRp complex assembled, for the mRNA amplification process to occur, the only needed companion is an RdRp-compatible RNA template, i.e., an mRNA, which is eligible for the RdRp-mediated amplification by virtue of satisfying two requirements: 1. The occurrence of the TCE and ICE elements within the antisense RNA strand and 2. The topological compatibility of the TCE and ICE elements, i.e., their mutual accessibility in the folded antisense RNA configuration. As discussed above, human AβPP mRNA constitutes just such an RdRp-compatible, RNA-dependent amplification-eligible template.

Mouse AβPP mRNA, on the other hand, *is not* a legitimate RdRp template. For this mRNA species, the second requirement formulated above, that of an appropriate antisense RNA folding requirement, may or may not be satisfied. That this requirement is satisfied in human AβPP mRNA does not signify that it is also satisfied in its mouse counterpart; although the two encode nearly identical polypeptides, over one-third of nucleotides in these two RNA species are different, and the folding patterns of their antisense RNA counterparts could be highly diverse. This consideration, however, is irrelevant in the context of the present discussion. This is because in mouse AβPP mRNA, the first requirement, namely, the occurrence of the TCE and ICE elements within the antisense RNA strand, is clearly not satisfied. Upon the analysis of the nucleotide sequence of the mouse antisense AβPP RNA, it become apparent that its 3′-terminal segment does not have, within the entire AβPP antisense RNA, a sufficiently complementary companion that could allow the formation of a stable double-stranded structure with no 3′ overhang [173,174]. Indeed, as shown in Figure 11, in terms of complementarity, the relationship between the 3′-terminal segment of the mouse antisense AβPP RNA and its internal segment corresponding to the TCE and ICE elements within human antisense AβPP RNA is not much stronger than random, and a substantial overhang at the 3′ terminus of the mouse RNA prohibits its utilization as a transcription primer.

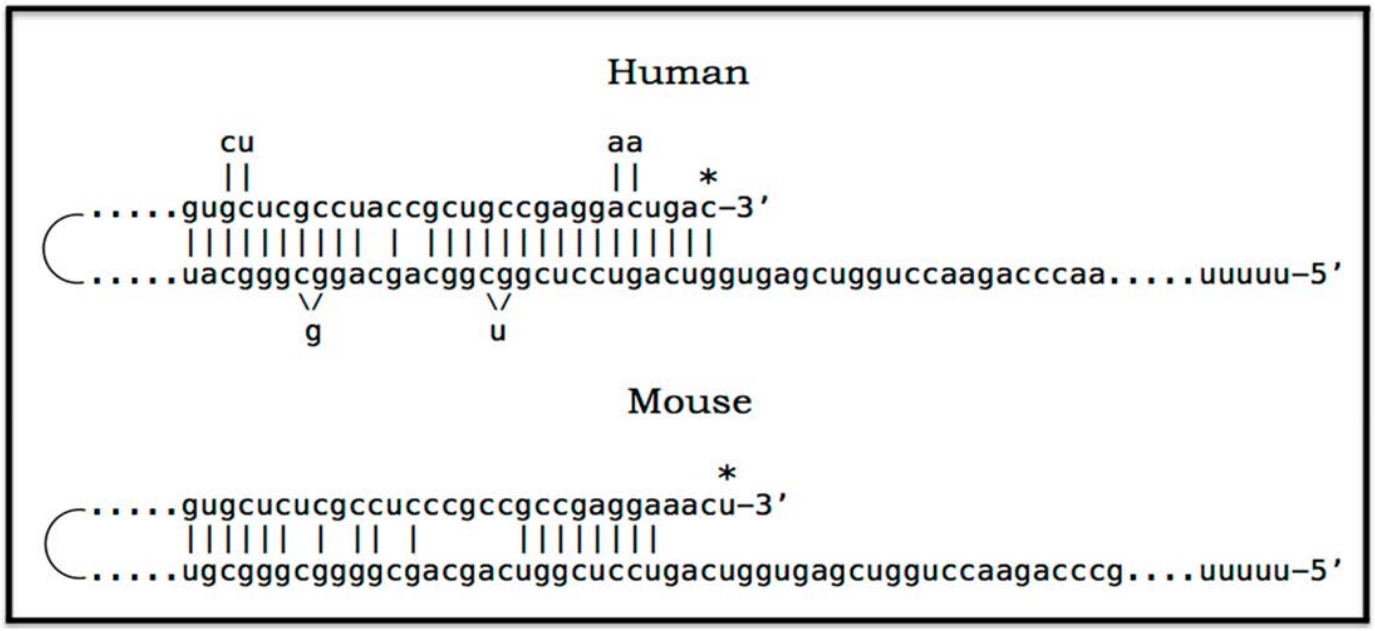

Figure 11. Mouse AβPP mRNA is ineligible for the amplification process: comparison of the relationships of the TCE and ICE elements within human antisense AβPP RNA and of analogous segments within mouse antisense AβPP RNA. *"Human"*: human antisense AβPP RNA folded into self-priming configuration. "Mouse": the relationship between the analogous segments of the mouse antisense AβPP RNA. *Asterisk*: the nucleotide position on the antisense RNA corresponding to the TSS of human or mouse AβPP mRNA (in both cases, position (−)149 upstream from the "A" of the translation-initiating AUG codon). Note that the relationship between the 3′-terminal segment of the mouse antisense AβPP RNA and its internal segment corresponding to the TCE and ICE elements within human antisense AβPP RNA is not much stronger than random, and a substantial overhang at the 3′ terminus of the mouse RNA prohibits its utilization as a transcription primer.

18.2. mRNA Products of Human AβPP Transgenes in the Current Animal AD Models Are Also Ineligible for the RNA-Dependent Amplification Process

If, upon the elicitation of the ISR in the current transgenic animal AD models (and, as discussed above, the ISR is elicited in these models via the accumulation of AβPP-derived *i*Aβ), the RNA-dependent mRNA amplification-competent RdRp complex is assembled (and, as discussed above, it is highly plausible that it is), it could be argued that since human AβPP mRNA is the eligible RdRp template, and because it is human AβPP mRNA, which is expressed from the transgenes in the current animal AD models, its amplification should occur. This, however, is not the case. The amplification depends on the highly delicate and precise TCE-ICE interaction, which occurs within the antisense complement of the *intact* human AβPP mRNA. But human AβPP mRNA expressed in the current transgenic animal AD models *is not intact*, i.e., not identical to endogenous human AβPP mRNA. The 5′-terminal portion of these transgenes, the very segment harboring the TCE element in the "intact" mRNA, is heavily modified during their construction. Consequently, the 5′UTR of the resulting mRNA is substantially changed and so is the 3′-terminal segment of the corresponding antisense AβPP RNA. Since this is the segment containing the TCE element, this element is profoundly altered and loses both its ability to interact with the ICE and its functionality as the transcription primer.

19. If Attempted, the "Legitimization" of Endogenous Mouse AβPP mRNA Transcripts via Facilitation of the TCE–ICE Interaction Would Likely Be Futile Due to the Thermodynamics of RNA Folding

Mouse Aβ differs in amino acid content from its human counterpart, and, in the past, attempts have been made to generate mouse models of AD by "humanizing" its Aβ. These

attempts were unfruitful. In light of the ACH2.0 and of the considerations presented above, a different type of "humanization" of mouse AβPP gene could appear justified. Thus, it could be argued that if the endogenous mouse AβPP gene is modified so that its transcripts contain sufficiently complementary TCE and ICE elements lacking the 3′ overhang, the elicitation of the ISR via overexpression of exogenous Aβ or by other means (discussed above) would activate RNA-dependent amplification of the endogenous AβPP mRNA and consequently the AβPP-independent *i*Aβ production pathway, and that this, in turn, would trigger the commencement and progression of AD. This, however, is implausible because the second requirement for the functionality of the TCE–ICE elements (the first being a sufficient complementarity and the lack of the 3′-terminal overhang), namely, their mutual accessibility in the folded antisense RNA configuration, is unlikely to be satisfied.

Indeed, the change of only a few (possibly a single) nucleotides in key positions can radically alter the thermodynamics of the RNA folding process. In mouse AβPP mRNA, over a third of nucleotides differ from those in the corresponding positions in human AβPP mRNA (although their amino acid contents remain highly analogous); the same applies to their antisense RNA counterparts. It can be anticipated with a great degree of certainty that the folding conformation of mouse antisense AβPP RNA is substantially different from that of its human counterpart. Consequently, there is a significant probability that the TCE and ICE elements, "legitimized" by arranging their sufficient complementarity, would nevertheless be mutually inaccessible in the folded configuration of mouse antisense AβPP RNA.

20. Design of the Transgene Encoding Human AβPP mRNA Eligible for RNA-Dependent Amplification

20.1. Transcription of Human AβPP mRNA Can Be Initiated at the Multiple Locations; Only One of Them Is Compatible with the Amplification Process

The AβPP gene belongs to the category of the TATA-less genes, i.e., genes lacking the "TATA box" as their control element. When present, the TATA box defines the precise position of the initiation of transcription, the "transcription start site," TSS. In its absence, transcription usually initiates at multiple sites, albeit within narrow margins, i.e., within relatively small gene segment. This is indeed the case with the human AβPP gene. Within this gene, there are five known TSS sites [171]. They are situated at the following positions (distances in nucleotides counts are given from the "A" of the translation-initiating AUG codon): (−)150, (−)149, (−)146, (−)144, and (−)143 (corresponding positions on the antisense RNA are marked by asterisks in Figure 12). What is important for the present considerations is the requirement that there is no 3′-terminal overhang within the TCE–ICE complex in the folded antisense RNA. When analyzing the compliance with this requirement for AβPP antisense RNA generated from human AβPP transcripts initiated at each of the five TSS positions, one additional prerequisite should be taken into consideration: the additional 3′-terminal "C" transcribed by RdRp from the 5′-terminal cap "G", not encoded in the genome, must be accommodated in the double-stranded TCE–ICE structure. This is because it was shown that RdRp is capable of transcribing the cap "G" of an mRNA template; this phenomenon was observed in all cases of RNA-dependent mRNA amplification analyzed to date, and thus appears to be the general case [160–162]. With the inclusion of the 3′-terminal genome-unencoded "C" transcribed by RdRp from the cap "G" of mRNA, the potential TCE–ICE complexes ("potential" because not all would be functional) within the corresponding antisense RNAs would appear as presented in Figure 12.

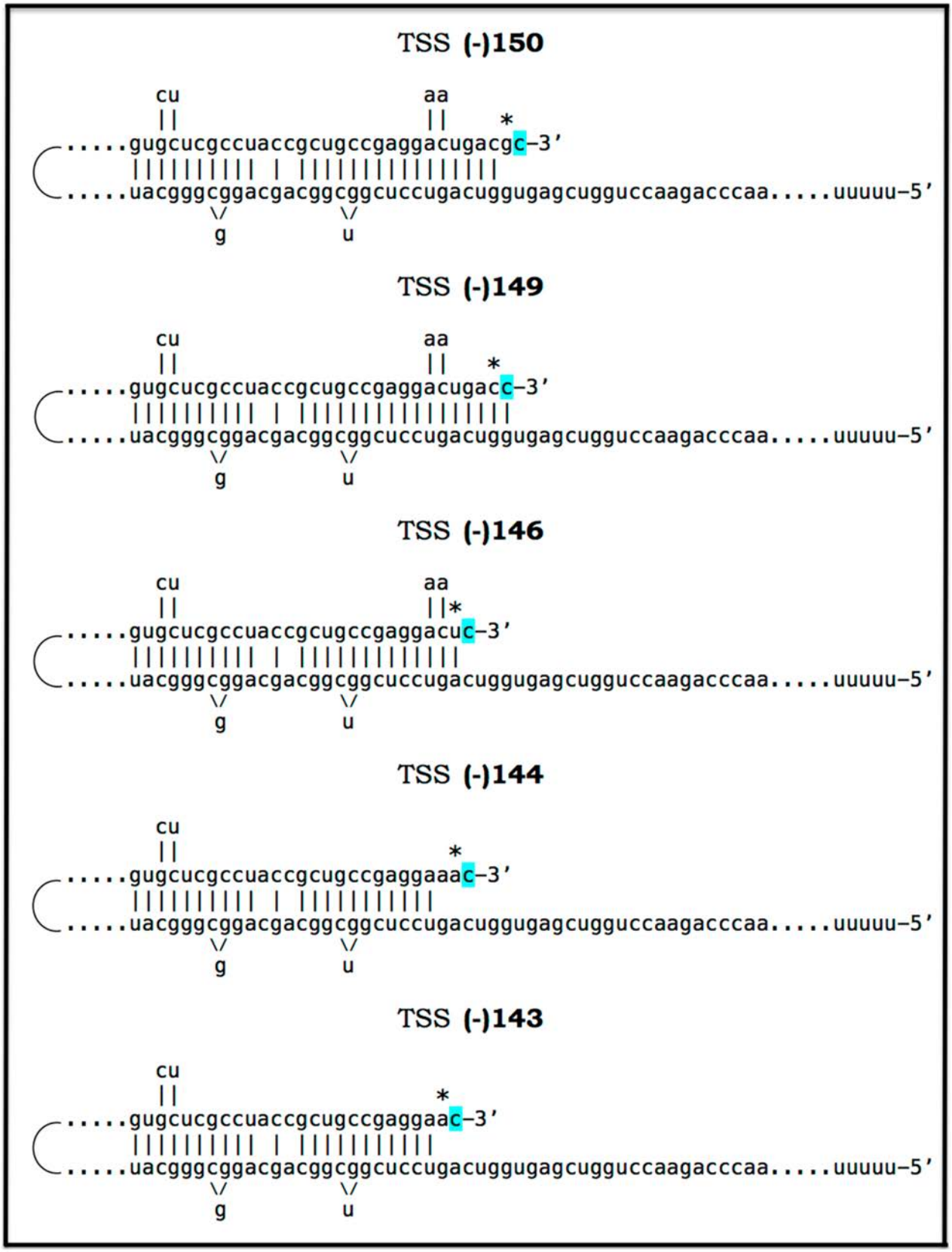

Figure 12. Folding of the antisense RNA originated from human AβPP mRNA initiated at the multiple TSS positions. *TSS*: transcription start site. (−)*150*, (−)*149*, (−)*146*, (−)*144*, (−)*143*: positions of the known TSSs of human AβPP mRNA. *Asterisk*: the nucleotide position on the antisense RNA

corresponding to the TSS of human AβPP mRNA. Highlighted *in blue*: "C" transcribed from the 5′-terminal cap "G" of AβPP mRNA (not encoded in the genome). Shown in the figure are the interactions of the 3′-terminal segment of each antisense RNA type with its complementary counterpart within the molecule. Note that only one type of the antisense AβPP RNA species, namely, that generated from AβPP mRNA initiated at the TSS (−)149, would contain fully functional TCE and ICE elements capable of forming a self-priming structure. In the other four antisense AβPP RNA types, the 3′-terminal overhangs would preclude self-priming or at least substantially reduce its efficiency.

As shown in Figure 12, the analysis of the interaction of the 3′-terminal segment of the antisense RNA produced by RdRp from human AβPP mRNA initiated at the various TSS positions with its potential ICE counterpart indicates that only one type of the antisense AβPP RNA species, namely, that generated from AβPP mRNA initiated at the TSS (−)149, would contain fully functional TCE and ICE elements capable of forming a self-priming structure. In other four antisense AβPP RNA types, the 3′-terminal overhangs would preclude self-priming or at least substantially reduce its efficiency.

20.2. The Key to Success: Precisely Defined Initiation of Transcription from Human AβPP Transgenes Would Produce RdRp-Compatible AβPP mRNA Eligible for the RNA-Dependent Amplification Process

It follows from the preceding subsection that the key to success in generating a transgenic animal model capable of operating the AβPP-independent *i*Aβ production pathway and consequently of supporting the commencement and progression of AD is to utilize transgenes expressing human AβPP mRNA initiated at the TSS in position (−)149. One of the approaches to ensure the initiation of transcription from this particular position is to place human AβPP transgenes under the control of the appropriately positioned TATA box. In such experimental system, the elicitation of the ISR, either via the accumulation of exogenous *i*Aβ over the T1 threshold or by other means discussed above, would be followed by the transcriptional/translational reprogramming and the production of the "missing" component(s) required for the functional, amplification-competent RdRp complex. With the latter assembled, the presence of the RdRp-compatible, RNA-dependent amplification-eligible AβPP mRNA template would enable the operation of the amplification process and consequently of the AβPP-independent *i*Aβ production pathway. This in turn would empower the commencement and progression of AD.

21. "One-Stage" Construction of an Adequate AD Model: Analogues of the Current Transgenic Animal AD Models Expressing Amplification-Eligible Human AβPP mRNA Would Efficiently Emulate the Disease

The preceding sections addressed the principles of the "two-stage" construction of a transgenic animal model of AD. In such an approach, the origins or the nature of the agents eliciting the integrated stress response and those produced via the RNA-dependent amplification of human AβPP mRNA and driving the disease are different. In these models, the first stage, elicitation of the ISR, is enacted either by *i*Aβ produced from amplification-ineligible AβPP mRNA expressed by the exogenous transgenes (the current transgenic AD models are, in fact, the "first-stage" models), by *i*Aβ42 expressed from C100-encoding transgenes, or by various stressors other than *i*Aβ. The essence of the second stage is the RNA-dependent amplification of exogenous RdRp-compatible human AβPP mRNA and the resulting generation of *i*Aβ in quantities sufficient to drive the AD pathology (and to perpetuate its own production). Such models are "two-stage" because even if we utilize the current AD models as the "first-stage," express *i*Aβ42, or elicit the ISR independently of *i*Aβ to enable the "second-stage," we still have to introduce transgenes expressing human AβPP mRNA eligible for the amplification process. Would it not be simpler to do only the latter?

Indeed, the construction of a single-stage model can, with one exception, reproduce that of the current transgenic animal models of AD. The exception is that the transgenes should be designed and constructed in such a way as to express human RdRp-compatible

and consequently RNA-amplification eligible AβPP mRNA. As discussed in the preceding sections, we know that the quantities of exogenous *i*Aβ expressed from human transgenes and derived conventionally in the AβPP proteolytic pathway would be sufficient to cause the activation of the eIF2α kinases and to trigger the elicitation of the ISR in neuronal cells. This would enable the assembly of the amplification-competent RdRp complex, and, provided exogenous AβPP mRNA is amplification-eligible, its RNA-dependent amplification would follow. This process would enable the operation of the AβPP-independent *i*Aβ production pathway, which in turn would empower the commencement and progression of AD.

Paradoxically, the single-stage model described above could be "too" efficient. In AD, RNA-dependent amplification of AβPP mRNA is based on the conventional expression of a single gene. In a human neuronal cell-based AD model, endogenous amplification of AβPP mRNA, transcribed from a single gene, presumably causes formation of NFTs in just a few days. In the proposed one-stage transgenic animal model of AD, the amplification of human AβPP mRNA would be based on the conventional exogenous expression of dozens, possibly around hundred, transgenes. This would increase the rate of *i*Aβ accumulation by an additional two orders of magnitude. As a result, the duration of the AD pathology could be significantly condensed, and the pathology itself possibly altered; this could make it difficult to be used in some applications, such as the testing of potential AD drugs. In such a case, the two-stage approach should be employed in the construction of a model: the number of transgenes expressing RdRp-compatible amplification-eligible human AβPP mRNA should be minimized, and the ISR should be elicited via the expression of amplification-ineligible AβPP or Aβ mRNA or through utilization of stressors other than *i*Aβ.

Alternatively, a current transgenic animal model of AD can be manipulated with a similar effect. Human AβPP transgenes in such a model could potentially be edited with the double aim of (a) restoring the 5′ termini of transgenes to their origin and (b) ascertaining that their transcription would initiate at the TSS (−)149. Accomplishing this would lead to the production of RdRp-compatible RNA-dependent amplification-eligible human AβPP mRNA transcripts. If only a fraction of the AβPP transgenes in a current transgenic AD model were successfully edited along the above lines, it could be sufficient to generate an adequate animal model of the disease.

22. Conclusions

The present study examines the suitability of the current transgenic models of Alzheimer's disease. It concludes that these models are inadequate, and, moreover, that their inadequacy reflects that of the theory of AD that guided their design—the ACH. Furthermore, the insufficiencies of the ACH and of ACH-based AD models also encompass the inefficiency of ACH-based AD drugs, emphasizing the inextricable connection between the three. These shortcomings have necessitated the formulation of a new theory of AD that is consistent with the accumulated empirical data, fully explains the phenomenology of the disease, and can serve as a basis for the design and construction of adequate AD models and effective AD drugs.

The recently introduced novel interpretation of AD, referred to as ACH2.0 since it retains the centrality and the causative role of Aβ in the disease, appears to constitute just such a theory. It posits that AD is driven by *i*Aβ produced independently of AβPP and retained intraneuronally. The AβPP-independent *i*Aβ production pathway in neuronal cells is activated as a consequence of the integrated stress response. The ISR initiates transcriptional/translational reprogramming, and some of the newly synthesized proteins provide the necessary component(s) of the AβPP-independent *i*Aβ generation pathway, which are missing under normal conditions, and thus enable its operation. The ISR in neuronal cells is elicited via the phosphorylation of eIF2α at its serine residue 51. This is enacted by one (or more) of the four eIF2α kinases PERK (PKR-like ER kinase), PKR (protein kinase double-stranded RNA-dependent), GCN2 (general control non-derepressible-2),

and HRI (heme-regulated inhibitor). In conventional AD, AβPP-derived *i*Aβ, accumulated over the critical threshold, triggers the neuronal activation of the PKR and/or HRI kinases, whereas in unconventional AD, one or more of the eIF2α kinases are activated in neurons by stressors other than *i*Aβ. The levels of *i*Aβ produced in the AβPP proteolytic pathway alone are insufficient to cause and support the progression of AD; the disease commences only following the activation of the AβPP-independent pathway of *i*Aβ generation. Within the framework of the disease, *i*Aβ produced independently of AβPP performs two principal functions: it drives the AD pathology and sustains the ISR condition, thus propagating its own production and perpetuating the operation of the AβPP-independent *i*Aβ production pathway, a cyclical process referred to as the AD Engine.

Apparently, the principal problem with the current transgenic animal models of AD is that, for the reasons elaborated in the preceding sections, they lack the operational AβPP-independent *i*Aβ production pathway. They model, in fact, not Alzheimer's disease but rather the effects of the neuronal ISR sustained by AβPP-derived *i*Aβ. This explains why they are incapable of developing the full spectrum of AD pathology, and why ACH-based drugs were spectacularly successful in current transgenic AD models, but completely inefficient in treating the disease. The present study concludes that any adequate transgenic animal model of AD must incorporate the operational AβPP-independent pathway of *i*Aβ generation. It also discusses cellular mechanisms potentially enabling the operation of the AβPP-independent *i*Aβ generation pathway, posits the principles of design of adequate, physiologically suitable ACH2.0-guided models of AD, and describes the molecular details of their construction.

Author Contributions: Conceptualization, V.V. and S.R.-V.; writing, V.V.; editing, V.V. and S.R.-V. All authors have read and agreed to the published version of the manuscript.

Funding: This research was funded by National Institutes of Health, grant numbers: NIH R21 GM056179; NIH RO1 AR036819.

Acknowledgments: Authors are grateful to Bjorn R. Olsen (Harvard Medical School) for his support, Hailong Gao (Children's Hospital, Boston) for the assistance with figure preparation, and Michael J. Foley and his associates for logistical support.

Conflicts of Interest: The authors declare no conflicts of interest.

References

1. Volloch, V.; Rits-Volloch, S. The Amyloid Cascade Hypothesis 2.0: On the possibility of once-in-a-lifetime-only treatment for prevention of Alzheimer's disease and for its potential cure at symptomatic stages. *J. Alzheimer Dis. Rep.* **2022**, *6*, 369–399. [CrossRef]
2. Volloch, V.; Rits-Volloch, S. The Amyloid Cascade Hypothesis 2.0: Generalization of the Concept. *J. Alzheimer Dis. Rep.* **2023**, *7*, 21–35. [CrossRef]
3. Volloch, V.; Rits-Volloch, S. Effect of Lecanemab and Donanemab in Early Alzheimer's Disease: Mechanistic Interpretation in the Amyloid Cascade Hypothesis 2.0 Perspective. *J. Alzheimer Dis.* **2023**, *93*, 1277–1284. [CrossRef]
4. Volloch, V.; Rits-Volloch, S. The Amyloid Cascade Hypothesis 2.0 for Alzheimer's Disease and Aging-Associated Cognitive Decline: From Molecular Basis to Effective Therapy. *Int. J. Mol. Sci.* **2023**, *24*, 12246. [CrossRef]
5. Volloch, V.; Rits-Volloch, S. Principles of Design of Clinical Trials for Prevention and Treatment of Alzheimer's Disease and Aging-Associated Cognitive Decline in the ACH2.0 Perspective: Potential Outcomes, Challenges and Solutions. *J. Alzheimer Dis. Rep.* **2023**, *7*, 921–955. [CrossRef] [PubMed]
6. Volloch, V.; Rits-Volloch, S. Next Generation Therapeutic Strategy for Treatment and Prevention of Alzheimer's Disease and Aging-Associated Cognitive Decline: Transient, Once-in-a-Lifetime-Only Depletion of Intraneuronal Aβ (iAβ) by Its Targeted Degradation via Augmentation of Intra-iAβ-Cleaving Activities of BACE1 and/or BACE2. *Int. J. Mol. Sci.* **2023**, *24*, 17586.
7. Hardy, J.A.; Higgins, G.A. Alzheimer's disease: The amyloid cascade hypothesis. *Science* **1992**, *256*, 184–185. [CrossRef] [PubMed]
8. Goate, A.; Chartier-Harlin, M.C.; Mullan, M.; Brown, J.; Crawford, F.; Fidani, L.; Giuffra, L.; Haynes, A.; Irving, N.; James, L.; et al. Segregation of a missense mutation in the amyloid precursor protein gene with familial Alzheimer's disease. *Nature* **1991**, *349*, 704–706. [CrossRef] [PubMed]
9. Pakos-Zebrucka, K.; Koryga, I.; Mnich, K.; Ljujic, M.; Samali, A.; Gorman, A.M. The integrated stress response. *EMBO Rep.* **2016**, *17*, 1374–1395. [CrossRef] [PubMed]

10. Ron, D. Translational control in the endoplasmic reticulum stress response. *J. Clin. Investig.* **2002**, *110*, 1383–1388. [CrossRef] [PubMed]
11. Harding, H.P.; Zhang, Y.; Zeng, H.; Novoa, I.; Lu, P.D.; Calfon, M.; Sadri, N.; Yun, C.; Popko, B.; Paules, R.S.; et al. An Integrated Stress Response Regulates Amino Acid Metabolism and Resistance to Oxidative Stress. *Mol. Cell* **2003**, *11*, 619–633. [CrossRef] [PubMed]
12. Brostrom, C.O.; Prostko, C.R.; Kaufman, R.J.; Brostrom, M.A. Inhibition of translational initiation by activators of the glucose-regulated stress protein and heat shock protein stress response systems. Role of the interferon-inducible double-stranded RNA-activated eukaryotic initiation factor 2alpha kinase. *J. Biol. Chem.* **1996**, *271*, 24995–25002. [CrossRef] [PubMed]
13. Dever, T.E.; Feng, L.; Wek, R.C.; Hinnebusch, A.G. Phosphorylation of initiation factor 2 alpha by protein kinase GCN2 mediates gene-specific translational control of GCN4 in yeast. *Cell* **1992**, *68*, 585–596. [CrossRef] [PubMed]
14. Wek, R.C.; Jiang, H.Y.; Anthony, T.G. Coping with stress: eIF2 kinases and translational control. *Biochem. Soc. Trans.* **2006**, *34*, 7–11. [CrossRef]
15. Rzymski, T.; Milani, M.; Pike, L.; Buffa, F.; Mellor, H.R.; Winchester, L.; Pires, I.; Hammond, E.; Ragoussis, I.; Harris, A.L. Regulation of autophagy by ATF4 in response to severe hypoxia. *Oncogene* **2010**, *29*, 4424–4435. [CrossRef]
16. Ye, J.; Kumanova, M.; Hart, L.S.; Sloane, K.; Zhang, H.; De Panis, D.N.; Bobrovnikova-Marjon, E.; Diehl, J.A.; Ron, D.; Koumenis, C. The GCN2-ATF4 pathway is critical for tumour cell survival and proliferation in response to nutrient deprivation. *EMBO J.* **2010**, *29*, 2082–2096. [CrossRef]
17. Garcia, M.A.; Meurs, E.F.; Esteban, M. The dsRNA protein kinase PKR: Virus and cell control. *Biochimie* **2007**, *89*, 799–811. [CrossRef]
18. Harding, H.P.; Zhang, Y.; Ron, D. Protein translation and folding are coupled by an endoplasmic-reticulum-resident kinase. *Nature* **1999**, *397*, 271–274. [CrossRef]
19. Costa-Mattioli, M.; Walter, P. The integrated stress response: From mechanism to disease. *Science* **2020**, *368*, eaat5314. [CrossRef] [PubMed]
20. Romero-Ramírez, L.; Nieto-Sampedro, M.; Barreda-Manso, M.A. Integrated Stress Response as a Therapeutic Target for CNS Injuries. *BioMed Res. Int.* **2017**, *2017*, 6953156. [CrossRef] [PubMed]
21. Costa-Mattioli, M.; Gobert, D.; Stern, E.; Gamache, K.; Colina, R.; Cuello, C.; Sossin, W.; Kaufman, R.; Pelletier, J.; Rosenblum, K.; et al. eIF2α Phosphorylation Bidirectionally Regulates the Switch from Short- to Long-Term Synaptic Plasticity and Memory. *Cell* **2007**, *129*, 195–206. [CrossRef]
22. Rosi, S.; Frias, E.S. The Integrated Stress Response: A Central Memory Switch in Down Syndrome. *Cell Metab.* **2020**, *31*, 15–17. [CrossRef]
23. Kim, H.-J.; Raphael, A.R.; LaDow, E.S.; McGurk, L.; Weber, R.A.; Trojanowski, J.Q.; Lee, V.M.-Y.; Finkbeiner, S.; Gitler, A.D.; Bonini, N.M. Therapeutic modulation of eIF2α phosphorylation rescues TDP-43 toxicity in amyotrophic lateral sclerosis disease models. *Nat. Genet.* **2014**, *46*, 152–160. [CrossRef]
24. Abisambra, J.F.; Jinwal, U.K.; Blair, L.J.; O'Leary, J.C., 3rd; Li, Q.; Brady, S.; Wang, L.; Guidi, C.E.; Zhang, B.; Nordhues, B.A.; et al. Tau accumulation activates the unfolded protein response by impairing endoplasmic reticulum-associated degradation. *J. Neurosci.* **2013**, *33*, 9498–9507. [CrossRef]
25. Moreno, J.A.; Radford, H.; Peretti, D.; Steinert, J.R.; Verity, N.; Martin, M.G.; Halliday, M.; Morgan, J.; Dinsdale, D.; Ortori, C.A.; et al. Sustained translational repression by eIF2alpha-P mediates prion neurodegeneration. *Nature* **2012**, *485*, 507–511. [CrossRef]
26. Lourenco, M.V.; Clarke, J.R.; Frozza, R.L.; Bomfim, T.R.; Forny-Germano, L.; Batista, A.F.; Sathler, L.B.; Brito-Moreira, J.; Amaral, O.B.; Silva, C.A.; et al. TNFalpha mediates PKR-dependent memory impairment and brain IRS-1 inhibition induced by Alzheimer's beta-amyloid oligomers in mice and monkeys. *Cell Metab.* **2013**, *18*, 831–843. [CrossRef]
27. Baleriola, J.; Walker, C.A.; Jean, Y.Y.; Crary, J.F.; Troy, C.M.; Nagy, P.L.; Hengst, U. Axonally Synthesized ATF4 Transmits a Neurodegenerative Signal across Brain Regions. *Cell* **2014**, *158*, 1159–1172. [CrossRef] [PubMed]
28. Halliday, M.J.; Radford, H.; Sekine, Y.; Moreno, J.J.; Verity, N.; Le Quesne, J.P.C.; Ortori, C.A.; Barrett, D.A.; Fromont, C.; Fischer, P.M.; et al. Partial restoration of protein synthesis rates by the small molecule ISRIB prevents neurodegeneration without pancreatic toxicity. *Cell Death Dis.* **2015**, *6*, e1672. [CrossRef] [PubMed]
29. Cheng, W.; Wang, S.; Mestre, A.A.; Fu, C.; Makarem, A.; Xian, F.; Hayes, L.R.; Lopez-Gonzalez, R.; Drenner, K.; Jiang, J.; et al. C9ORF72 GGGGCC repeat-associated non-AUG translation is upregulated by stress through eIF2α phosphorylation. *Nat. Commun.* **2018**, *9*, 51. [CrossRef] [PubMed]
30. Martínez, G.; Khatiwada, S.; Costa-Mattioli, M.; Hetz, C. ER Proteostasis Control of Neuronal Physiology and Synaptic Function. *Trends Neurosci.* **2018**, *41*, 610–624. [CrossRef] [PubMed]
31. Wong, Y.L.; Le Bon, L.; Basso, A.M.; Kohlhaas, K.L.; Nikkel, A.L.; Robb, H.M.; Donnelly-Roberts, D.L.; Prakash, J.; Swensen, A.M.; Rubinstein, N.D.; et al. eIF2B activator prevents neurological defects caused by a chronic integrated stress response. *eLife* **2019**, *8*, e42940. [CrossRef]
32. Zhu, P.J.; Khatiwada, S.; Cui, Y.; Reineke, L.C.; Dooling, S.W.; Kim, J.J.; Li, W.; Walter, P.; Costa-Mattioli, M. Activation of the ISR mediates the behavioral and neurophysiological abnormalities in Down syndrome. *Science* **2019**, *366*, 843–849. [CrossRef] [PubMed]
33. Chang, R.C.; Wong, A.K.; Ng, H.K.; Hugon, J. Phosphorylation of eukaryotic initiation factor-2alpha (eIF2alpha) is associated with neuronal degeneration in Alzheimer's disease. *Neuroreport* **2002**, *13*, 2429–2432. [CrossRef] [PubMed]

34. Page, G.; Bilan, A.R.; Ingrand, S.; Lafay-Chebassier, C.; Pain, S.; Pochat, M.P.; Bouras, C.; Bayer, T.; Hugon, J. Activated double-stranded RNA-dependent protein kinase and neuronal death in models of Alzheimer's disease. *Neuroscience* **2006**, *139*, 1343–1354. [CrossRef]
35. Segev, Y.; Barrera, I.; Ounallah-Saad, H.; Wibrand, K.; Sporild, I.; Livne, A.; Rosenberg, T.; David, O.; Mints, M.; Bramham, C.R.; et al. PKR Inhibition Rescues Memory Deficit and ATF4 Overexpression in ApoE epsilon4 Human Replacement Mice. *J. Neurosci.* **2015**, *35*, 12986–12993. [CrossRef]
36. Kernohan, K.D.; Liwak-Muir, U.; Geraghty, M.T.; Qin, W.; Venkateswaran, S.; Davila, J.; Holcik, M.; Majewski, J.; Richer, J.; Boycott, K.M.; et al. Homozygous mutation in the eukaryotic translation initiation factor 2alpha phosphatase gene, PPP1R15B, is associated with severe microcephaly, short stature and intellectual disability. *Hum. Mol. Genet.* **2015**, *24*, 6293–6300. [CrossRef]
37. Hu, Z.; Yu, P.; Zhang, Y.; Yang, Y.; Zhu, M.; Qin, S.; Xu, J.-T.; Duan, D.; Wu, Y.; Wang, D.; et al. Inhibition of the ISR abrogates mGluR5-dependent long-term depression and spatial memory deficits in a rat model of Alzheimer's disease. *Transl. Psychiatry* **2022**, *12*, 96. [CrossRef]
38. Oliveira, M.M.; Lourenco, M.V.; Longo, F.; Kasica, N.P.; Yang, W.; Ureta, G.; Ferreira, D.D.P.; Mendonça, P.H.J.; Bernales, S.; Ma, T.; et al. Correction of eIF2-dependent defects in brain protein synthesis, synaptic plasticity, and memory in mouse models of Alzheimer's disease. *Sci. Signal.* **2021**, *14*, eabc5429. [CrossRef]
39. Ma, T.; A Trinh, M.; Wexler, A.J.; Bourbon, C.; Gatti, E.; Pierre, P.; Cavener, D.R.; Klann, E. Suppression of eIF2α kinases alleviates Alzheimer's disease–related plasticity and memory deficits. *Nat. Neurosci.* **2013**, *16*, 1299–1305. [CrossRef] [PubMed]
40. Chou, A.; Krukowski, K.; Jopson, T.; Zhu, P.J.; Costa-Mattioli, M.; Walter, P.; Rosi, S. Inhibition of the integrated stress response reverses cognitive deficits after traumatic brain injury. *Proc. Natl. Acad. Sci. USA* **2017**, *114*, E6420–E6426. [CrossRef]
41. Zhu, P.J.; Huang, W.; Kalikulov, D.; Yoo, J.W.; Placzek, A.N.; Stoica, L.; Zhou, H.; Bell, J.C.; Friedlander, M.J.; Krnjević, K.; et al. Suppression of PKR Promotes Network Excitability and Enhanced Cognition by Interferon-γ-Mediated Disinhibition. *Cell* **2011**, *147*, 1384–1396. [CrossRef] [PubMed]
42. Stern, E.; Chinnakkaruppan, A.; David, O.; Sonenberg, N.; Rosenblum, K. Blocking the eIF2α Kinase (PKR) Enhances Positive and Negative Forms of Cortex-Dependent Taste Memory. *J. Neurosci.* **2013**, *33*, 2517–2525. [CrossRef] [PubMed]
43. Ounallah-Saad, H.; Sharma, V.; Edry, E.; Rosenblum, K. Genetic or Pharmacological Reduction of PERK Enhances Cortical-Dependent Taste Learning. *J. Neurosci.* **2014**, *34*, 14624–14632. [CrossRef] [PubMed]
44. Batista, G.; Johnson, J.L.; Dominguez, E.; Costa-Mattioli, M.; Pena, J.L.; Albert Einstein College of Medicine, United States; Baylor College of Medicine, United States. Translational control of auditory imprinting and structural plasticity by eIF2α. *eLife* **2016**, *5*, e17197. [CrossRef]
45. Sidrauski, C.; Acosta-Alvear, D.; Khoutorsky, A.; Vedantham, P.; Hearn, B.R.; Li, H.; Gamache, K.; Gallagher, C.M.; Ang, K.K.-H.; Wilson, C.; et al. Pharmacological brake-release of mRNA translation enhances cognitive memory. *eLife* **2013**, *2*, e00498. [CrossRef]
46. Keskin, A.D.; Kekuš, M.; Adelsberger, H.; Neumann, U.; Shimshek, D.R.; Song, B.; Zott, B.; Peng, T.; Förstl, H.; Staufenbiel, M.; et al. BACE inhibition-dependent repair of Alzheimer's pathophysiology. *Proc. Natl. Acad. Sci. USA* **2017**, *114*, 8631–8636. [CrossRef]
47. Hu, X.; Das, B.; Hou, H.; He, W.; Yan, R. BACE1 deletion in the adult mouse reverses preformed amyloid deposition and improves cognitive functions. *J. Exp. Med.* **2018**, *10*, 1084. [CrossRef]
48. Kennedy, M.E.; Stamford, A.W.; Chen, X.; Cox, K.; Cumming, J.N.; Dockendorf, M.F.; Egan, M.; Ereshefsky, L.; Hodgson, R.A.; Hyde, L.A.; et al. The BACE1 inhibitor verubecestat (MK-8931) reduces CNS β-amyloid in animal models and in Alzheimer's disease patients. *Sci. Transl. Med.* **2016**, *8*, 363ra150. [CrossRef] [PubMed]
49. Egan, M.F.; Kost, J.; Tariot, P.N.; Aisen, P.S.; Cummings, J.L.; Vellas, B.; Sur, C.; Mukai, Y.; Voss, T.; Furtek, C.; et al. Randomized trials of verubecestat for mild-to-moderate Alzheimer's disease. *N. Engl. J. Med.* **2018**, *378*, 1691–1703. [CrossRef] [PubMed]
50. Egan, M.F.; Kost, J.; Voss, T.; Mukai, Y.; Aisen, P.S.; Cummings, J.L.; Tariot, P.N.; Vellas, B.; van Dyck, C.H.; Boada, M.; et al. Randomized trial of verubecestat for prodromal Alzheimer's disease. *N. Engl. J. Med.* **2019**, *380*, 1408–1420. [CrossRef]
51. Katzman, R.; Terry, R.; DeTeresa, R.; Brown, T.; Davies, P.; Fuld, P.; Renbing, X.; Peck, A. Clinical, pathological, and neurochemical changes in dementia: A subgroup with preserved mental status and numerous neocortical plaques. *Ann. Neurol.* **1988**, *23*, 138–144. [CrossRef]
52. Delaere, P.; Duyckaerts, C.; Masters, C.; Beyreuther, K.; Piette, F.; Hauw, J. Large amounts of neocortical beta A4 deposits without neuritic plaques nor tangles in a psychometrically assessed, non-demented person. *Neurosci. Lett.* **1990**, *116*, 87–93. [CrossRef]
53. Dickson, D.; Crystal, H.; Mattiace, L.; Masur, D.; Blau, A.; Davies, P.; Yen, S.; Aronson, M. Identification of normal and pathological aging in prospectively studied nondemented elderly humans. *Neurobiol. Aging* **1992**, *13*, 178–189. [CrossRef] [PubMed]
54. Aizenstein, H.; Nebes, R.; Saxton, J.; Price, J.; Mathis, C.; Tsopelas, N.; Ziolko, S.; James, J.; Snitz, B.; Houck, P.; et al. Frequent amyloid deposition without significant cognitive impairment among the elderly. *Arch. Neurol.* **2008**, *65*, 1509–1517. [CrossRef] [PubMed]
55. Klunk, W.; Mathis, C.; Price, J.; DeKosky, S.; Lopresti, B.; Tsopelas, N.; Saxton, J.; Nebes, R. Amyloid imaging with PET in Alzheimer's disease, mild cognitive impairment, and clinically unimpaired subjects. In *PET in the Evaluation of Alzheimer's Disease and Related Disorders*; Silverman, D., Ed.; Springer: New York, NY, USA, 2009; pp. 119–147.
56. Villemagne, V.; Pike, K.; Chételat, G.; Ellis, K.; Mulligan, R.; Bourgeat, P.; Ackermann, U.; Jones, G.; Szoeke, C.; Salvado, O.; et al. Longitudinal assessment of Abeta and cognition in aging and Alzheimer disease. *Ann. Neurol.* **2011**, *69*, 181–192. [CrossRef] [PubMed]

57. Seto, M.; Weiner, R.L.; Dumitrescu, L.; Hohman, T.J. Protective genes and pathways in Alzheimer's disease: Moving towards precision interventions. *Mol. Neurodegen.* **2021**, *16*, 29. [CrossRef] [PubMed]
58. Makin, S. The amyloid hypothesis on trial. *Nature* **2018**, *559*, S4–S7. Available online: https://media.nature.com/original/magazine-assets/d41586-018-05719-4/d41586-018-05719-4.pdf (accessed on 1 January 2024). [CrossRef] [PubMed]
59. Jonsson, T.; Atwal, J.K.; Steinberg, S.; Snaedal, J.; Jonsson, P.V.; Bjornsson, S.; Stefansson, H.; Sulem, P.; Gudbjartsson, D.; Maloney, J.; et al. A mutation in APP protects against Alzheimer's disease and age-related cognitive decline. *Nature* **2012**, *488*, 96–99. [CrossRef]
60. Harper, A.R.; Nayee, S.; Topol, E.J. Protective alleles and modifier variants in human health and disease. *Nat. Rev. Genet.* **2015**, *16*, 689–701. [CrossRef] [PubMed]
61. Casas, C.; Sergeant, N.; Itier, J.M.; Blanchard, V.; Wirths, O.; Van Der Kolk, N.; Vingtdeux, V.; Van De Steeg, E.; Ret, G.; Canton, T.; et al. Massive CA1/2 neuronal loss with intraneuronal and N-terminal truncated Abeta42 accumulation in a novel Alzheimer transgenic model. *Am. J. Pathol.* **2004**, *165*, 1289–1300. [CrossRef]
62. Bayer, T.A.; Wirths, O. Review on the APP/PS1KI mouse model: Intraneuronal Abeta accumulation triggers axonopathy, neuron loss and working memory impairment. *Genes Brain Behav.* **2008**, *7* (Suppl. S1), 6–11. [CrossRef]
63. Bayer, T.A.; Breyhan, H.; Duan, K.; Rettig, J.; Wirths, O. Intraneuronal beta-amyloid is a major risk factor--novel evidence from the APP/PS1KI mouse model. *Neurodegener. Dis.* **2008**, *5*, 140–142. [CrossRef]
64. Wirths, O.; Breyhan, H.; Cynis, H.; Schilling, S.; Demuth, H.U.; Bayer, T.A. Intraneuronal pyroglutamate-Abeta 3-42 triggers neurodegeneration and lethal neurological deficits in a transgenic mouse model. *Acta Neuropathol.* **2009**, *118*, 487–496. [CrossRef]
65. Christensen, D.Z.; Bayer, T.A.; Wirths, O. Intracellular Aß triggers neuron loss in the cholinergic system of the APP/PS1KI mouse model of Alzheimer's disease. *Neurobiol. Aging* **2010**, *31*, 1153–1163. [CrossRef]
66. Christensen, D.Z.; Schneider-Axmann, T.; Lucassen, P.J.; Bayer, T.A.; Wirths, O. Accumulation of intraneuronal Abeta correlates with ApoE4 genotype. *Acta Neuropathol.* **2010**, *119*, 555–566. [CrossRef]
67. Bayer, T.A.; Wirths, O. Intracellular accumulation of amyloid-Beta—A predictor for synaptic dysfunction and neuron loss in Alzheimer's disease. *Front. Aging Neurosci.* **2010**, *2*, 1359. [CrossRef]
68. Bayer, T.A.; Wirths, O. Intraneuronal Aβ as a trigger for neuron loss: Can this be translated into human pathology? *Biochem. Soc. Trans.* **2011**, *39*, 857–861. [CrossRef] [PubMed]
69. Wirths, O.; Bayer, T.A. Intraneuronal Aβ accumulation and neurodegeneration: Lessons from transgenic models. *Life Sci.* **2012**, *91*, 1148–1152. [CrossRef] [PubMed]
70. Kumar, S.; Wirths, O.; Theil, S.; Gerth, J.; Bayer, T.A.; Walter, J. Early intraneuronal accumulation and increased aggregation of phosphorylated Abeta in a mouse model of Alzheimer's disease. *Acta Neuropathol.* **2013**, *125*, 699–709. [CrossRef] [PubMed]
71. Ripoli, C.; Cocco, S.; Li Puma, D.D.; Piacentini, R.; Mastrodonato, A.; Scala, F.; Puzzo, D.; D'Ascenzo, M.; Grassi, C. Intracellular accumulation of amyloid-β (Aβ) protein plays a major role in Aβ-induced alterations of glutamatergic synaptic transmission and plasticity. *J. Neurosci.* **2014**, *34*, 12893–12903. [CrossRef] [PubMed]
72. Scala, F.; Fusco, S.; Ripoli, C.; Piacentini, R.; Li Puma, D.D.; Spinelli, M.; Laezza, F.; Grassi, C.; D'Ascenzo, M. Intraneuronal Aβ accumulation induces hippocampal neuron hyperexcitability through A-type K(+) current inhibition mediated by activation of caspases and GSK-3. *Neurobiol. Aging* **2015**, *36*, 886–900. [CrossRef]
73. Christensen, D.Z.; Kraus, S.L.; Flohr, A.; Cotel, M.C.; Wirths, O.; Bayer, T.A. Transient intraneuronal Abeta rather than extracellular plaque pathology correlates with neuron loss in the frontal cortex of APP/PS1KI mice. *Acta Neuropathol.* **2008**, *116*, 647–655. [CrossRef]
74. Kinoshita, A.; Fukumoto, H.; Shah, T.; Whelan, C.M.; Irizarry, M.C.; Hyman, B.T. Demonstration by FRET of BACE interaction with the amyloid precursor protein at the cell surface and in early endosomes. *J. Cell Sci.* **2003**, *116*, 3339–3346. [CrossRef] [PubMed]
75. Xu, H.; Greengard, P.; Gandy, S. Regulated formation of Golgi secretory vesicles containing Alzheimer β-amyloid precursor protein. *J. Biol. Chem.* **1995**, *270*, 23243–23245. [CrossRef] [PubMed]
76. Mizuguchi, M.; Ikeda, K.; Kim, S. Differential distribution of cellular forms of β-amyloid precursor protein in murine glial cell cultures. *Brain Res.* **1992**, *584*, 219–225. [CrossRef] [PubMed]
77. Cook, D.G.; Forman, M.S.; Sung, J.C.; Leight, S.; Kolson, D.L.; Iwatsubo, T.; Lee, V.M.Y.; Doms, R.W. Alzheimer's Aβ42 is generated in the endoplasmic reticulum/intermediate compartment of NT2N cells. *Nature Med.* **1997**, *3*, 1021–1023. [CrossRef] [PubMed]
78. Hartmann, T.; Bieger, S.C.; Brühl, B.; Tienari, P.J.; Ida, N.; Allsop, D.; Roberts, G.W.; Masters, C.L.; Dotti, C.G.; Unsicker, K.; et al. Distinct sites of intracellular production for Alzheimer's disease Aβ40/42 amyloid peptides. *Nature Med.* **1997**, *3*, 1016–1020. [CrossRef]
79. Wild-Bode, C.; Yamazaki, T.; Capell, A.; Leimer, U.; Steiner, H.; Ihara, Y.; Haass, C. Intracellular generation and accumulation of amyloid beta-peptide terminating at amino acid 42. *J. Biol. Chem.* **1997**, *272*, 16085–16088. [CrossRef]
80. Lee, S.J.; Liyanage, U.; Bickel, P.E.; Xia, W.; Lansbury, P.T., Jr.; Kosik, K.S. A detergent-insoluble membrane compartment contains Aβ in vivo. *Nature Med.* **1998**, *4*, 730–734. [CrossRef]
81. Skovronsky, D.; Doms, R.; Lee, V. Detection of a novel intraneuronal pool of insoluble amyloid β protein that accumulates with time in culture. *J. Cell Biol.* **1998**, *141*, 1031–1039. [CrossRef]

82. Manczak, M.; Anekonda, T.S.; Henson, E.; Park, B.S.; Quinn, J.; Reddy, P.H. Mitochondria are a direct site of Aβ accumulation in Alzheimer's disease neurons: Implications for free radical generation and oxidative damage in disease progression. *Hum. Mol. Genet.* **2006**, *15*, 1437–1449. [CrossRef] [PubMed]
83. Chafekar, S.; Baas, F.; Scheper, W. Oligomer-specific amyloid-beta toxicity in cell models is mediated by selective uptake. *Biochem. Biophys. Acta* **2008**, *9*, 523–531.
84. Wesen, E.; Jeffries, G.; Dzebo, M.; Esbjorner, M. Endocytic uptake of monomeric amyloid-β peptides is clathrin- and dynamin-independent and results in selective accumulation of Aβ(1–42) compared to Aβ(1–40). *Sci. Rep.* **2017**, *7*, 2021. [CrossRef] [PubMed]
85. Kumar-Singh, S.; Theuns, J.; Van Broeck, B.; Pirici, D.; Vennekens, K.L.; Corsmit, E.; Cruts, M.; Dermaut, B.; Wang, R.; Van Broeckhoven, C. Mean age-of-onset of familial Alzheimer disease caused by presenilin mutations correlates with both increased Aβ42 and decreased Aβ40. *Hum. Mutat.* **2006**, *27*, 686–695. [CrossRef] [PubMed]
86. Hu, X.; Crick, S.L.; Bu, G.; Frieden, C.; Pappu, R.V.; Lee, J.M. Amyloid seeds formed by cellular uptake, concentration, and aggregation of the amyloid-beta peptide. *Proc. Natl. Acad. Sci. USA* **2009**, *106*, 20324–20329. [CrossRef] [PubMed]
87. Yajima, R.; Tokutake, T.; Koyama, A.; Kasuga, K.; Tezuka, T.; Nishizawa, M.; Ikeuchi, T. ApoE-isoform-dependent cellular uptake of amyloid-β is mediated by lipoprotein receptor LR11/SorLA. *Biochem. Biophys. Res. Comm.* **2015**, *456*, 482–488. [CrossRef]
88. Omtri, R.S.; Davidson, M.W.; Arumugam, B.; Poduslo, J.F.; Kandimalla, K.K. Differences in the Cellular Uptake and Intracellular Itineraries of Amyloid Beta Proteins 40 and 42: Ramifications for the Alzheimer's Drug Discovery. *Mol. Pharm.* **2012**, *9*, 1887–1897. [CrossRef]
89. Bu, G.; Cam, J.; Zerbinatti, C. LRP in amyloid-β production and metabolism. *Ann. N. Y. Acad. Sci.* **2006**, *1086*, 35–53. [CrossRef]
90. Wang, H.Y.; Lee, D.H.; D'Andrea, M.R.; Peterson, P.A.; Shank, R.P.; Reitz, A.B. β-Amyloid1–42 binds to α7 nicotinic acetylcholine receptor with high affinity. Implications for Alzheimer's disease pathology. *J. Biol. Chem.* **2000**, *275*, 5626–5632. [CrossRef]
91. Nagele, R.; D'Andrea, M.; Anderson, W.; Wang, H. Intracellular accumulation of Aβ42 in neurons is facilitated by the α 7 nicotinic acetylcholine receptor in Alzheimer's disease. *Neuroscience* **2002**, *110*, 199–211. [CrossRef]
92. Oddo, S.; Caccamo, A.; Green, K.N.; Liang, K.; Tran, L.; Chen, Y.; Leslie, F.M.; LaFerla, F.M. Chronic nicotine administration exacerbates tau pathology in a transgenic model of Alzheimer's disease. *Proc. Natl. Acad. Sci. USA* **2005**, *102*, 3046–3051. [CrossRef] [PubMed]
93. Yan, S.D.; Chen, X.I.; Fu, J.; Chen, M.; Zhu, H.; Roher, A.; Slattery, T.; Zhao, L.; Nagashima, M.; Morser, J.; et al. RAGE and amyloid-β peptide neurotoxicity in Alzheimer's disease. *Nature* **1996**, *382*, 685–691. [CrossRef] [PubMed]
94. Sasaki, N.; Toki, S.; Chowei, H.; Saito, T.; Nakano, N.; Hayashi, Y.; Takeuchi, M.; Makita, Z. Immunohistochemical distribution of the receptor for advanced glycation end products in neurons and astrocytes in Alzheimer's disease. *Brain Res.* **2001**, *888*, 256–262. [CrossRef] [PubMed]
95. Deane, R.; Du Yan, S.; Submamaryan, R.K.; LaRue, B.; Jovanovic, S.; Hogg, E.; Welch, D.; Manness, L.; Lin, C.; Yu, J.; et al. RAGE mediates amyloid-β peptide transport across the blood–brain barrier and accumulation in brain. *Nature Med.* **2003**, *9*, 907–913. [CrossRef] [PubMed]
96. Iribarren, P.; Zhou, Y.; Hu, J.; Le, Y.; Wang, J. Role of formyl peptide receptor-like 1 (FPRL1/FPR2) in mononuclear phagocyte responses in Alzheimer disease. *Immunol. Res.* **2005**, *31*, 165–176. [CrossRef] [PubMed]
97. Snyder, E.M.; Nong, Y.; Almeida, C.G.; Paul, S.; Moran, T.; Choi, E.Y.; Nairn, A.C.; Salter, M.W.; Lombroso, P.J.; Gouras, G.K.; et al. Regulation of NMDA receptor trafficking by amyloid-β. *Nature Neurosci.* **2005**, *8*, 1051–1058. [CrossRef]
98. Chang, R.C.; Suen, K.C.; Ma, C.H.; Elyaman, W.; Ng, H.K.; Hugon, J. Involvement of double-stranded RNA-dependent protein kinase and phosphorylation of eukaryotic initiation factor-2alpha in neuronal degeneration. *J. Neurochem.* **2002**, *83*, 1215–1225. [CrossRef]
99. Peel, A.L. PKR activation in neurodegenerative disease. *J. Neuropathol. Exp. Neurol.* **2004**, *63*, 97–105. [CrossRef]
100. Peel, A.L.; Bredesen, D.E. Activation of the cell stress kinase PKR in Alzheimer's disease and human amyloid precursor protein transgenic mice. *Neurobiol. Dis.* **2003**, *14*, 52–62. [CrossRef] [PubMed]
101. Onuki, R.; Bando, Y.; Suyama, E.; Katayama, T.; Kawasaki, H.; Baba, T.; Tohyama, M.; Taira, K. An RNA-dependent protein kinase is involved in tunicamycin-induced apoptosis and Alzheimer's disease. *EMBO J.* **2004**, *23*, 959–968. [CrossRef] [PubMed]
102. Paquet, C.; Mouton-Liger, F.; Meurs, E.F.; Mazot, P.; Bouras, C.; Pradier, L.; Gray, F.; Hugon, J. The PKR activator PACT is induced by Abeta: Involvement in Alzheimer's disease. *Brain Pathol.* **2012**, *22*, 219–229. [CrossRef] [PubMed]
103. Zhu, X.; Perry, G.; Moreira, P.I.; Aliev, G.; Cash, A.D.; Hirai, K.; Smith, M.A. Mitochondrial abnormalities and oxidative imbalance in Alzheimer disease. *J. Alzheimers Dis.* **2006**, *9*, 147–153. [CrossRef]
104. Blass, J.P. The mitochondrial spiral. An adequate cause of dementia in the Alzheimer's syndrome. *Ann. N. Y. Acad. Sci.* **2000**, *924*, 170–183. [CrossRef]
105. Manczak, M.; Park, B.S.; Jung, Y.; Reddy, P.H. Differential expression of oxidative phosphorylation genes in patients with Alzheimer's disease: Implications for early mitochondrial dysfunction and oxidative damage. *Neuromol. Med.* **2004**, *5*, 147–162. [CrossRef]
106. Qin, W.; Haroutunian, V.; Katsel, P.; Cardozo, C.P.; Ho, L.; Buxbaum, J.D.; Pasinetti, G.M. PGC-1alpha expression decreases in the Alzheimer disease brain as a function of dementia. *Arch. Neurol.* **2009**, *66*, 352–361. [CrossRef]
107. Du, H.; Guo, L.; Yan, S.; Sosunov, A.A.; McKhann, G.M.; Yan, S.S. Early deficits in synaptic mitochondria in an Alzheimer's disease mouse model. *Proc. Natl. Acad. Sci. USA* **2010**, *107*, 18670–18675. [CrossRef] [PubMed]

108. Lin, M.T.; Simon, D.K.; Ahn, C.H.; Kim, L.M.; Beal, M.F. High aggregate burden of somatic mtDNA point mutations in aging and Alzheimer's disease brain. *Hum. Mol. Genet.* **2002**, *11*, 133–145. [CrossRef]
109. Calkins, M.; Manczak, M.; Mao, P.; Shirendeb, U.; Reddy, P.H. Impaired mitochondrial biogenesis, defective axonal transport of mitochondria, abnormal mitochondrial dynamics and synaptic degeneration in a mouse model of Alzheimer's disease. *Hum. Mol. Genet.* **2011**, *20*, 4515–4529. [CrossRef]
110. Anandatheerthavarada, H.K.; Biswas, G.; Robin, M.A.; Avadhani, N.G. Mitochondrial targeting and a novel transmembrane arrest of Alzheimer's amyloid precursor protein impairs mitochondrial function in neuronal cells. *J. Cell Biol.* **2003**, *161*, 41–54. [CrossRef]
111. Caspersen, C.; Wang, N.; Yao, J.; Sosunov, A.; Chen, X.; Lustbader, J.W.; Xu, H.W.; Stern, D.; McKhann, G.; Du Yan, S. Mitochondrial Abeta: A potential focal point for neuronal metabolic dysfunction in Alzheimer's disease. *FASEB J.* **2005**, *19*, 2040–2041. [CrossRef]
112. Chen, J.X.; Yan, S.S. Role of mitochondrial amyloid-beta in Alzheimer's disease. *J. Alzheimers Dis.* **2010**, *20*, S569–S578. [CrossRef]
113. Hansson Petersen, C.A.; Alikhani, N.; Behbahani, H.; Wiehager, B.; Pavlov, P.F.; Alafuzoff, I.; Leinonen, V.; Ito, A.; Winblad, B.; Glaser, E.; et al. The amyloid beta-peptide is imported into mitochondria via the TOM import machinery and localized to mitochondrial cristae. *Proc. Natl. Acad. Sci. USA* **2008**, *105*, 13145–13150. [CrossRef]
114. de la Monte, S.M.; Luong, T.; Neely, T.R.; Robinson, D.; Wands, J.R. Mitochondrial DNA damage as a mechanism of cell loss in Alzheimer's disease. *Lab. Investig.* **2000**, *80*, 1323–1335. [CrossRef] [PubMed]
115. Brooks, W.M.; Lynch, P.J.; Ingle, C.C.; Hatton, A.; Emson, P.C.; Faull, R.L.; Starkey, M.P. Gene expression profiles of metabolic enzyme transcripts in Alzheimer's disease. *Brain Res.* **2007**, *1127*, 127–135. [CrossRef]
116. Wang, X.; Perry, G.; Smith, M.A.; Zhu, X. Amyloid-beta-derived diffusible ligands cause impaired axonal transport of mitochondria in neurons. *Neurodegener. Dis.* **2007**, *7*, 56–59. [CrossRef] [PubMed]
117. Wang, X.; Su, B.; Fujioka, H.; Zhu, X. Dynamin-like protein 1 reduction underlies mitochondrial morphology and distribution abnormalities in fibroblasts from sporadic Alzheimer's disease patients. *Am. J. Pathol.* **2008**, *173*, 470–482. [CrossRef]
118. Wang, X.; Su, B.; Lee, H.G.; Li, X.; Perry, G.; Smith, M.A.; Zhu, X. Impaired balance of mitochondrial fission and fusion in Alzheimer's disease. *J. Neurosci.* **2009**, *29*, 9090–9103. [CrossRef]
119. Wang, X.; Su, B.; Siedlak, S.L.; Moreira, P.I.; Fujioka, H.; Wang, Y.; Casadesus, G.; Zhu, X. Amyloid-beta overproduction causes abnormal mitochondrial dynamics via differential modulation of mitochondrial fission/fusion proteins. *Proc. Natl. Acad. Sci. USA* **2008**, *105*, 19318–19323. [CrossRef]
120. Brewer, G.; Herrera, R.; Philipp, S.; Sosna, J.; Reyes-Ruiz, J.; Glabe, C. Age-Related Intraneuronal Aggregation of Amyloid-β in Endosomes, Mitochondria, Autophagosomes, and Lysosomes. *J. Alzheimers Dis.* **2020**, *73*, 229–246. [CrossRef] [PubMed]
121. Guo, X.; Aviles, G.; Liu, Y.; Tian, R.; Unger, B.A.; Lin, Y.H.T.; Wiita, A.P.; Xu, K.; Correia, M.A.; Kampmann, M. Mitochondrial stress is relayed to the cytosol by an OMA1-DELE1-HRI pathway. *Nature* **2020**, *579*, 427–432. [CrossRef]
122. Fessler, E.; Eckl, E.-M.; Schmitt, S.; Mancilla, I.A.; Meyer-Bender, M.F.; Hanf, M.; Philippou-Massier, J.; Krebs, S.; Zischka, H.; Jae, L.T. A pathway coordinated by DELE1 relays mitochondrial stress to the cytosol. *Nature* **2020**, *579*, 433–437. [CrossRef]
123. Almeida, C.; Takahashi, R.; Gouras, G. β-amyloid accumulation impairs multivesicular body sorting by inhibiting the ubiquitin–proteasome system. *J. Neurosci.* **2006**, *26*, 4277–4288. [CrossRef]
124. Gregori, L.; Fuchs, C.; Figueiredo-Pereira, M.; Van Nostrand, W.; Goldgaber, D. Amyloid β-protein inhibits ubiquitin-dependent protein degradation in vitro. *J. Biol. Chem.* **1995**, *270*, 19702–19708. [CrossRef]
125. Oh, S.; Hong, H.S.; Hwang, E.; Sim, H.J.; Lee, W.; Shin, S.J.; Mook-Jung, I. Amyloid peptide attenuates the proteasome activity in neuronal cells. *Mech. Ageing Dev.* **2005**, *126*, 1292–1299. [CrossRef]
126. Tseng, B.; Green, K.; Chan, J.; Blurton-Jones, M.; LaFerla, F. Aβ inhibits the proteasome and enhances amyloid and tau accumulation. *Neurobiol. Aging* **2008**, *29*, 1607–1618. [CrossRef] [PubMed]
127. Balusu, S.; Horré, K.; Thrupp, N.; Craessaerts, K.; Snellinx, A.; Serneels, L.; T'syen, D.; Chrysidou, I.; Arranz, A.M.; Sierksma, A.; et al. MEG3 activates necroptosis in human neuron xenografts modeling Alzheimer's disease. *Science* **2023**, *381*, 1176–1182. [CrossRef] [PubMed]
128. Martin, B.; Schrader-Fischer, G.; Busciglio, J.; Duke, M.; Paganetti, P.; Yankner, B. Intracellular accumulation of beta-amyloid in cells expressing the Swedish mutant amyloid precursor protein. *J. Biol. Chem.* **1995**, *270*, 26727–26730. [CrossRef] [PubMed]
129. Sannerud, R.; Esselens, C.; Ejsmont, P.; Mattera, R.; Rochin, L.; Tharkeshwar, A.K.; De Baets, G.; De Wever, V.; Habets, R.; Baert, V.; et al. Restricted Location of PSEN2/gamma-secretase determines substrate specificity and generates an intracellular Abeta pool. *Cell* **2016**, *166*, 193–208. [CrossRef] [PubMed]
130. De Jonghe, C.; Zehr, C.; Yager, D.; Prada, C.-M.; Younkin, S.; Hendriks, L.; Van Broeckhoven, C.; Eckman, C.B. Flemish and Dutch Mutations in Amyloid β Precursor Protein Have Different Effects on Amyloid β Secretion. *Neurobiol. Dis.* **1998**, *5*, 281–286. [CrossRef]
131. Pardossi-Piquard, R.; Checler, F. The physiology of the β-amyloid precursor protein intracellular domain AICD. *J. Neurochem.* **2011**, *120*, 109–124. [CrossRef]
132. Szögi, T.; Schuster, I.; Borbély, E.; Gyebrovszki, A.; Bozsó, Z.; Gera, J.; Rajkó, R.; Sántha, M.; Penke, B.; Fülöp, L. Effects of the Pentapeptide P33 on Memory and Synaptic Plasticity in APP/PS1 Transgenic Mice: A Novel Mechanism Presenting the Protein Fe65 as a Target. *Int. J. Mol. Sci.* **2019**, *20*, 3050. [CrossRef]
133. Borg, J.-P.; Yang, Y.; De Taddeo-Borg, M.; Margolis, B.; Turner, R.S. The X11α protein slows cellular amyloid precursor protein processing and reduces Aβ40 and Aβ42 secretion. *J. Biol. Chem.* **1998**, *273*, 14761–14766. [CrossRef]

134. Dunning, C.J.R.; Black, H.L.; Andrews, K.L.; Davenport, E.C.; Conboy, M.; Chawla, S.; Dowle, A.A.; Ashford, D.; Thomas, J.R.; Evans, G.J.O. Multisite tyrosine phosphorylation of the N-terminus of Mint1/X11α by Src kinase regulates the trafficking of amyloid precursor protein. *J. Neurochem.* **2016**, *137*, 518–527. [CrossRef]
135. Miller, C.C.J.; McLoughlin, D.M.; Lau, K.-F.; Tennant, M.E.; Rogelj, B. The X11 proteins, Aβ production and Alzheimer's disease. *Trends Neurosci.* **2006**, *29*, 280–285. [CrossRef]
136. Tamayev, R.; Zhou, D.; D'Adamio, L. The interactome of the amyloid β precursor protein family members is shaped by phosphorylation of their intracellular domains. *Mol. Neurodegener.* **2009**, *4*, 28. [CrossRef] [PubMed]
137. Hoe, H.-S.; Tran, T.S.; Matsuoka, Y.; Howell, B.W.; Rebeck, G.W. DAB1 and Reelin Effects on Amyloid Precursor Protein and ApoE Receptor 2 Trafficking and Processing. *J. Biol. Chem.* **2006**, *281*, 35176–35185. [CrossRef] [PubMed]
138. Russo, C.; Dolcini, V.; Salis, S.; Venezia, V.; Zambrano, N.; Russo, T.; Schettini, G. Signal Transduction through Tyrosine-phosphorylated C-terminal Fragments of Amyloid Precursor Protein via an Enhanced Interaction with Shc/Grb2 Adaptor Proteins in Reactive Astrocytes of Alzheimer's Disease Brain. *J. Biol. Chem.* **2002**, *277*, 35282–35288. [CrossRef]
139. Tarr, P.E.; Roncarati, R.; Pelicci, G.; Pelicci, P.G.; D'Adamio, L. Tyrosine Phosphorylation of the β-Amyloid Precursor Protein Cytoplasmic Tail Promotes Interaction with Shc. *J. Biol. Chem.* **2002**, *277*, 16798–16804. [CrossRef]
140. Bukhari, H.; Glotzbach, A.; Kolbe, K.; Leonhardt, G.; Loosse, C.; Müller, T. Small things matter: Implications of APP intracellular domain AICD nuclear signaling in the progression and pathogenesis of Alzheimer's disease. *Prog. Neurobiol.* **2017**, *156*, 189–213. [CrossRef]
141. Chang, K.-A.; Kim, H.-S.; Ha, T.-Y.; Ha, J.-W.; Shin, K.Y.; Jeong, Y.H.; Lee, J.-P.; Park, C.-H.; Kim, S.; Baik, T.-K.; et al. Phosphorylation of Amyloid Precursor Protein (APP) at Thr668 Regulates the Nuclear Translocation of the APP Intracellular Domain and Induces Neurodegeneration. *Mol. Cell. Biol.* **2006**, *26*, 4327–4338. [CrossRef] [PubMed]
142. Ando, K.; Iijima, K.-I.; Elliott, J.I.; Kirino, Y.; Suzuki, T. Phosphorylation-dependent Regulation of the Interaction of Amyloid Precursor Protein with Fe65 Affects the Production of β-Amyloid. *J. Biol. Chem.* **2001**, *276*, 40353–40361. [CrossRef] [PubMed]
143. Müller, T.; Meyer, H.E.; Egensperger, R.; Marcus, K. The amyloid precursor protein intracellular domain (AICD) as modulator of gene expression, apoptosis, and cytoskeletal dynamics—Relevance for Alzheimer's disease. *Prog. Neurobiol.* **2008**, *85*, 393–406. [CrossRef] [PubMed]
144. Shu, R.; Wong, W.; Ma, Q.H.; Yang, Z.Z.; Zhu, H.; Liu, F.J.; Wang, P.; Ma, J.; Yan, S.; Polo, J.M.; et al. APP intracellular domain acts as a transcriptional regulator of miR-663 suppressing neuronal differentiation. *Cell Death Dis.* **2015**, *6*, e1651. [CrossRef] [PubMed]
145. Grimm, M.O.W.; Mett, J.; Stahlmann, C.P.; Grösgen, S.; Haupenthal, V.J.; Blümel, T.; Hundsdörfer, B.; Zimmer, V.C.; Mylonas, N.T.; Tanila, H.; et al. APP intracellular domain derived from amyloidogenic β-and γ-secretase cleavage regulates neprilysin expression. *Front. Aging Neurosci.* **2015**, *7*, 77. [CrossRef] [PubMed]
146. Pousinha, P.A.; Mouska, X.; Bianchi, D.; Temido-Ferreira, M.; Rajão-Saraiva, J.; Gomes, R.; Fernandez, S.P.; Salgueiro-Pereira, A.R.; Gandin, C.; Raymond, E.F.; et al. The Amyloid Precursor Protein C-Terminal Domain Alters CA1 Neuron Firing, Modifying Hippocampus Oscillations and Impairing Spatial Memory Encoding. *Cell Rep.* **2019**, *29*, 317–331.e5. [CrossRef]
147. van Dyck, C.H.; Swanson, C.J.; Aisen, P.; Bateman, R.J.; Chen, C.; Gee, M.; Kanekiyo, M.; Li, D.; Reyderman, L.; Cohen, S.; et al. Lecanemab in Early Alzheimer's Disease. *N. Engl. J. Med.* **2023**, *388*, 9–21. [CrossRef]
148. Mintun, M.A.; Lo, A.C.; Evans, C.D.; Wessels, A.M.; Ardayfio, P.A.; Andersen, S.W.; Shcherbinin, S.; Sparks, J.; Sims, J.R.; Brys, M.; et al. Donanemab in Early Alzheimer's Disease. *N. Engl. J. Med.* **2021**, *384*, 1691–1704. [CrossRef]
149. Lilly, E. Donanemab Significantly Slowed Cognitive and Functional Decline in Phase 3 Study of Early Alzheimer's Disease. 2023. Press Release. Available online: https://investor.lilly.com/news-releases/news-release-details/lillys-donanemab-significantly-slowed-cognitive-and-functional (accessed on 1 January 2024).
150. Sims, J.R.; Zimmer, J.A.; Evans, C.D.; Lu, M.; Ardayfio, P.; Sparks, J.; Wessels, A.M.; Shcherbinin, S.; Wang, H.; Nery, E.S.M.; et al. Donanemab in Early Symptomatic Alzheimer Disease. *JAMA* **2023**, *330*, 512–527. [CrossRef]
151. Abbott, A. The next generation of Alzheimer's treatments. *Nature* **2023**, *616*, 26–28. [CrossRef] [PubMed]
152. Choi, S.H.; Kim, Y.H.; Hebisch, M.; Sliwinski, C.; Lee, S.; D'Avanzo, C.; Chen, H.; Hooli, B.; Asselin, C.; Muffat, J.; et al. A three-dimensional human neural cell culture model of Alzheimer's disease. *Nature* **2014**, *515*, 274–278. [CrossRef] [PubMed]
153. Kang, J.; Lemaire, H.G.; Unterbeck, A.; Salbaum, J.M.; Masters, C.L.; Grzeschik, K.H.; Multhaup, G.; Beyreuther, K.; Müller-Hill, B. The precursor of Alzheimer's disease amyloid A4 protein resembles a cell-surface receptor. *Nature* **1987**, *325*, 733–736. [CrossRef] [PubMed]
154. Robakis, N.K.; Ramakrishna, N.; Wolfe, G.; Wisniewski, H.M. Molecular cloning and characterization of a cDNA encoding the cerebrovascular and the neuritic plaque amyloid peptides. *Proc. Natl. Acad. Sci. USA* **1987**, *84*, 4190–4194. [CrossRef] [PubMed]
155. Tanzi, R.E.; Gusella, J.F.; Watkins, P.C.; Bruns, G.A.; St George-Hyslop, P.; Van Keuren, M.L.; Patterson, D.; Pagan, S.; Kurnit, D.M.; Neve, R.L. Amyloid beta protein gene: cDNA, mRNA distribution, and genetic linkage near the Alzheimer locus. *Science* **1987**, *235*, 880–884. [CrossRef] [PubMed]
156. Breimer, L.; Denny, P. Alzheimer amyloid aspects. *Nature* **1987**, *326*, 749–750. [CrossRef] [PubMed]
157. Citron, M.; Haass, C.; Selkoe, D. Production of amyloid beta peptide by cultured cells: No evidence for internal initiation of translation at Met596. *Neurobiol. Aging* **1993**, *14*, 571–573. [CrossRef] [PubMed]
158. Macq, A.; Philippe, B.; Octave, N. The amyloid peptide of Alzheimer's disease is not produced by internal initiation of translation generating C-terminal amyloidogenic fragments of its precursor. *Neurosci. Lett.* **1994**, *182*, 227–230. [CrossRef]

159. Volloch, V.; Schweitzer, B.; Rits, S. Antisense Globin RNA in Murine Erythroid Tissues: Structure, Origin and Possible Function. *Proc. Natl. Acad. Sci. USA* **1996**, *93*, 2476–2481. [CrossRef]
160. Volloch, V. Protein-encoding RNA-to-RNA information transfer in mammalian cells: Principles of RNA-dependent mRNA amplification. *Ann. Integr. Mol. Med.* **2019**, *1*, 1002. [CrossRef]
161. Rits, S.; Olsen, B.; Volloch, V. Protein-encoding RNA to RNA information transfer in mammalian cells: RNA-dependent mRNA amplification. Identification of chimeric RNA intermediates and putative RNA end products. *Ann. Integr. Mol. Med.* **2019**, *1*, 23. [PubMed]
162. Volloch, V.; Rits, S.; Olsen, B. RNA-dependent amplification of mammalian mRNA encoding extracellullar matrix proteins: Identification of chimeric RNA intermediates for α1, β1, and γ1 chains of laminin. *Ann. Integr. Mol. Med.* **2019**, *1*, 48. [CrossRef] [PubMed]
163. Volloch, V.; Olsen, B.; Rits, S. Precursor-independent overproduction of beta-amyloid in AD: Mitochondrial dysfunction as possible initiator of asymmetric RNA-dependent APP mRNA amplification. An engine that drives Alzheimer's disease. *Ann. Integr. Mol. Med.* **2019**, *1*, 61. [CrossRef]
164. Volloch, V.; Olsen, B.; Rits, S. AD "Statin": Alzheimer's disorder is a "fast" disease preventable by therapeutic intervention initiated even late in life and reversible at the early stages. *Ann. Integr. Mol. Med.* **2020**, *2*, 75. [CrossRef] [PubMed]
165. Volloch, V.; Olsen, B.; Rits, S. Alzheimer's disease is driven by intraneuronally retained beta-amyloid produced in the AD-specific, APP-independent pathway: Current perspective and experimental models for tomorrow. *Ann. Integr. Mol. Med.* **2020**, *2*, 90. [CrossRef] [PubMed]
166. Volloch, V.; Olsen, B.; Rits, S. Alzheimer's disease prevention and treatment: Case for optimism. *Ann. Integr. Mol. Med.* **2020**, *2*, 115. [CrossRef] [PubMed]
167. Volloch, V.; Rits-Volloch, S. News from Mars: Two-Tier Paradox, Intracellular PCR, Chimeric Junction Shift, Dark Matter mRNA and Other Remarkable Features of Mammalian RNA-Dependent mRNA Amplification. Implications for Alzheimer's Disease, RNA-Based Vaccines and mRNA Therapeutics. *Ann. Integr. Mol. Med.* **2019**, *2*, 131–173. [CrossRef] [PubMed]
168. Volloch, V.; Rits-Volloch, S. Alzheimer's disease is driven by beta-amyloid generated in the amyloid precursor protein-independent pathway and retained intraneuronally: Research and therapeutic strategies in a new AD paradigm. *Ann. Integr. Mol. Med.* **2021**, *2*, 1010. [CrossRef]
169. Volloch, V.; Schwetizer, B.; Rits, S. Evolutionarily Conserved Elements in the 5′-untranslated Region of β Globin mRNA Mediate Site-specific Priming of a Unique Hairpin Structure during cDNA Synthesis. *Nucl. Acids Res.* **1994**, *22*, 5302–5309. [CrossRef] [PubMed]
170. Mita, S.; Sadlock, J.; Herbert, J.; Schon, E. A cDNA specifying the human amyloid beta precursor protein encodes a 95-kDa polypeptide. *Nucl. Acids Res.* **1988**, *16*, 9351, Correction in *Nucl. Acids Res.* **1988**, *16*, 11402. [CrossRef] [PubMed]
171. Salbaum, J.; Weidemann, A.; Lemaire, H.; Masters, C.; Beyreuther, K. The promoter of Alzheimer's disease amyloid A4 precursor gene. *EMBO J.* **1988**, *7*, 2807–2813. [CrossRef]
172. Volloch, V. A mechanism for β-amyloid overproduction in Alzheimer's disease: Precursor-independent generation of β-amyloid via antisense RNA-primed mRNA synthesis. *FEBS Lett.* **1996**, *390*, 124–128. [CrossRef]
173. Volloch, V. Mechanism for β-amyloid overproduction in sporadic Alzheimer's Disease: Possible antisense RNA-mediated generation of a 5′-truncated ßAPP mRNA encoding 12 kDa C-terminal fragment of βAPP, the immediate precursor of Aβ. In *Molecular Mechanisms of Dementia*; Wasco, W., Tanzi, R., Eds.; Humana Press: New York, NY, USA, 1997.
174. Volloch, V. Possible mechanism for resistance to Alzheimer's disease (AD) in mice suggests new approach to generate a mouse model for sporadic AD and may explain familial resistance to AD in man. *Exp. Neurobiol.* **1997**, *144*, 214–218. [CrossRef]
175. Frottin, F.; Martinez, A.; Peynot, P.; Mitra, S.; Holz, R.C.; Giglione, C.; Meinnel, T. The Proteomics of N-terminal Methionine Cleavage. *Mol. Cell. Proteom.* **2006**, *5*, 2336–2349. [CrossRef]
176. Xiao, Q.; Zhang, F.; Nacev, B.A.; Liu, J.O.; Pei, D. Protein N-Terminal Processing: Substrate Specificity of Escherichia coli and Human Methionine Aminopeptidases. *Biochemistry* **2010**, *49*, 5588–5599. [CrossRef]
177. Varshavsky, A. The N-end rule pathway and regulation by proteolysis. *Protein Sci.* **2011**, *20*, 1298–1345. [CrossRef]
178. Wingfield, P. N-Terminal Methionine Processing. *Curr. Protoc. Protein Sci.* **2017**, *88*, 6.14.1–6.14.3. [CrossRef]
179. Varland, S.; Osberg, C.; Arnesen, T. N-terminal modifications of cellular proteins: The enzymes involved, their substrate specificities and biological effects. *Proteomics* **2015**, *15*, 2385–2401. [CrossRef] [PubMed]
180. Polevoda, B.; Sherman, F. N-terminal Acetyltransferases and Sequence Requirements for N-terminal Acetylation of Eukaryotic Proteins. *J. Mol. Biol.* **2003**, *325*, 595–622. [CrossRef] [PubMed]
181. Hellen, C.U.; Sarnow, P. Internal ribosome entry sites in eukaryotic mRNA molecules. *Genes Dev.* **2001**, *15*, 1593–1612. [CrossRef] [PubMed]
182. Yang, T.-H.; Wang, C.-Y.; Tsai, H.-C.; Liu, C.-T. Human IRES Atlas: An integrative platform for studying IRES-driven translational regulation in humans. *Database* **2021**, *2021*, baab025. [CrossRef] [PubMed]
183. Kieft, J.S.; Costantino, D.A.; Filbin, M.E.; Hammond, J.; Pfingsten, J.S. Structural methods for studying IRES function. *Methods Enzymol.* **2007**, *430*, 333–371. [PubMed]
184. Wang, Q.S.; Au, H.H.; Jan, E. Methods for studying IRES-mediated translation of positive-strand RNA viruses. *Methods* **2013**, *59*, 167–179. [CrossRef] [PubMed]

185. Thompson, S.R. So you want to know if your message has an IRES? *WIREs RNA* **2012**, *3*, 697–705. [CrossRef] [PubMed]
186. Francisco-Velilla, R.; Fernandez-Chamorro, J.; Lozano, G.; Diaz-Toledano, R.; Martínez-Salas, E. RNA–protein interaction methods to study viral IRES elements. *Methods* **2015**, *91*, 3–12. [CrossRef] [PubMed]

International Journal of
Molecular Sciences

MDPI

Perspective

Next Generation Therapeutic Strategy for Treatment and Prevention of Alzheimer's Disease and Aging-Associated Cognitive Decline: Transient, Once-in-a-Lifetime-Only Depletion of Intraneuronal Aβ (*i*Aβ) by Its Targeted Degradation via Augmentation of Intra-*i*Aβ-Cleaving Activities of BACE1 and/or BACE2

Vladimir Volloch [1,*] and Sophia Rits-Volloch [2,3,*]

[1] Department of Developmental Biology, Harvard School of Dental Medicine, Boston, MA 02115, USA
[2] Division of Molecular Medicine, Children's Hospital, Boston, MA 02115, USA
[3] Department of Biological Chemistry and Molecular Pharmacology, Harvard Medical School, Boston, MA 02115, USA
* Correspondence: vladimir.volloch@gmail.com (V.V.); rits@crystal.harvard.edu (S.R.-V.)

Abstract: Although the long-standing Amyloid Cascade Hypothesis (ACH) has been largely discredited, its main attribute, the centrality of amyloid-beta (Aβ) in Alzheimer's disease (AD), remains the cornerstone of any potential interpretation of the disease: All known AD-causing mutations, without a single exception, affect, in one way or another, Aβ. The ACH2.0, a recently introduced theory of AD, preserves this attribute but otherwise differs fundamentally from the ACH. It posits that AD is a two-stage disorder where both stages are driven by *intraneuronal* (rather than extracellular) Aβ (*i*Aβ) albeit of two distinctly different origins. The first asymptomatic stage is the decades-long accumulation of Aβ protein precursor (AβPP)-derived *i*Aβ to the critical threshold. This triggers the activation of the self-sustaining AβPP-*independent* *i*Aβ production pathway and the commencement of the second, symptomatic AD stage. Importantly, Aβ produced independently of AβPP is retained intraneuronally. It drives the AD pathology and perpetuates the operation of the pathway; continuous cycles of the *i*Aβ-stimulated propagation of its own AβPP-independent production constitute an engine that drives AD, the AD Engine. It appears that the dynamics of AβPP-derived *i*Aβ accumulation is the determining factor that either drives Aging-Associated Cognitive Decline (AACD) and triggers AD or confers the resistance to both. Within the ACH2.0 framework, the ACH-based drugs, designed to lower levels of extracellular Aβ, could be applicable in the prevention of AD and treatment of AACD because they reduce the rate of accumulation of AβPP-derived *i*Aβ. The present study analyzes their utility and concludes that it is severely limited. Indeed, their short-term employment is ineffective, their long-term engagement is highly problematic, their implementation at the symptomatic stages of AD is futile, and their evaluation in conventional clinical trials for the prevention of AD is impractical at best, impossible at worst, and misleading in between. In contrast, the ACH2.0-guided Next Generation Therapeutic Strategy for the treatment and prevention of both AD and AACD, namely the depletion of *i*Aβ via its transient, short-duration, targeted degradation by the novel ACH2.0-based drugs, has none of the shortcomings of the ACH-based drugs. It is potentially highly effective, easily evaluable in clinical trials, and opens up the possibility of once-in-a-lifetime-only therapeutic intervention for prevention and treatment of both conditions. It also identifies two plausible ACH2.0-based drugs: activators of physiologically occurring intra-*i*Aβ-cleaving capabilities of BACE1 and/or BACE2.

Keywords: Alzheimer's disease (AD); Aging-Associated Cognitive Decline (AACD); Amyloid Cascade Hypothesis 2.0 (ACH2.0); intraneuronal Aβ (*i*Aβ); Aβ protein precursor (AβPP); AβPP-independent *i*Aβ production pathway; ACH2.0-based drugs; BACE1/BACE2 activators

Citation: Volloch, V.; Rits-Volloch, S. Next Generation Therapeutic Strategy for Treatment and Prevention of Alzheimer's Disease and Aging-Associated Cognitive Decline: Transient, Once-in-a-Lifetime-Only Depletion of Intraneuronal Aβ (*i*Aβ) by Its Targeted Degradation via Augmentation of Intra-*i*Aβ-Cleaving Activities of BACE1 and/or BACE2. *Int. J. Mol. Sci.* **2023**, *24*, 17586. https://doi.org/10.3390/ijms242417586

Academic Editor: Claudia Ricci

Received: 19 October 2023
Revised: 4 December 2023
Accepted: 5 December 2023
Published: 18 December 2023

1. Introduction: From the ACH to the ACH2.0

1.1. Amyloid Cascade Hypothesis: Extracellular Aβ Causes and Drives AD

The Amyloid Cascade Hypothesis 2.0 (ACH2.0) was formulated [1–5] to fill in an acute need for a new, all-encompassing theory of Alzheimer's disease following the discreditation of the initial Amyloid Cascade Hypothesis, ACH, that was introduced over three decades ago [6]. At that time, it was assumed that extracellular plaques containing amyloid-beta (Aβ) as their main component are specific for the disease. However, the immediate rationale for the introduction of the ACH was a discovery of the Aβ protein precursor (AβPP) mutation [7] affecting the production of Aβ and segregating with, and apparently causing the early onset of AD (familiar AD, FAD). The ACH postulated that increased levels of extracellular Aβ drive the disease and trigger a cascade of cellular events, including the formation of neurofibrillary tangles (NFTs, or tau-tangles), which culminates in neuronal loss. At the time of its introduction, the ACH appeared consistent with and provided a sufficient explanation for the accumulated body of empirical data; it was widely accepted and extracellular Aβ became the major target for numerous candidate AD drugs.

1.2. Inconsistencies of the ACH: Extracellular Aβ Can Be Ruled out as the Causative Agent of AD

A number of those drugs exhibited spectacular successes in stopping the progression of and even reversing the disease in various AD models [8–10]. They all, however, failed as spectacularly in human clinical symptomatic AD trials despite fulfilling their mechanistic mission, e.g., reducing substantially, up to 80%, levels of extracellular Aβ [11,12] (two apparent exceptions, clinical trials of lecanemab and donanemab, are discussed and interpreted in detail below). The complete inefficacy of the depletion of extracellular Aβ in numerous clinical trials for symptomatic AD indicated that the underlying theory, ACH, is incorrect. Moreover, as observational data accumulated, it became clear that there is no good correlation between levels of extracellular Aβ and the occurrence of AD. In a substantial fraction, about a third, of the general population, extracellular Aβ accumulates with aging to levels equal to or exceeding those seen in AD patients, yet without any cognitive impairment or the accompanying neurodegeneration [13–19]. The reverse is also true: cases of AD without an excessive extracellular Aβ deposition were detected [20]. Thus, the observations described above, taken cumulatively, decidedly rule out extracellular Aβ as the causative agent and driver of AD pathology.

1.3. Centrality and Causative Role of Aβ Are the Cornerstone of Any Theory of AD: Intraneuronal Aβ, iAβ

On the other hand, another category of accumulated data asserts undisputedly the centrality and causative role of Aβ in Alzheimer's disease. Indeed, since 1991, when the first FAD-causing mutation was discovered [7], numerous other mutations that cause the early onset of AD were detected. All of them, without a single exception, affect either the structure or the production of Aβ. Moreover, a mutation that replaces a single residue in Aβ, the Icelandic mutation, confers upon its carriers the protection from both AD and Aging-Associated Cognitive Decline, AACD [21,22]. Together, these observations make the case for the central and causative role of Aβ in AD (and AACD) powerfully persuasive (reviewed in [1,4]). Moreover, they suggest that these two features, the centrality and the causative role of Aβ in AD, constitute the essential cornerstone of any conceivable theory of AD. At first glance, it appears that this assertion contradicts the above statement that extracellular Aβ can be ruled out as the cause of the disease. The two, however, are not inconsistent because of the occurrence of another pool of amyloid-beta, namely intraneuronal Aβ, *i*Aβ.

1.4. Amyloid Cascade Hypothesis 2.0: The Essence

The ACH2.0 preserves this cornerstone, i.e., the centrality and the causative role of Aβ in AD [1] (hence "ACH" in the ACH2.0) and, in addition, posits that it is also the central and causative agent in AACD [2,4]. This is the only "overlap" between the two theories of

AD, but even it is rather superficial: in the ACH2.0, the Aβ in question is intraneuronal, whereas in the ACH, it is extracellular. All other features of the ACH2.0 are drastically different from those of the ACH. Thus, the ACH2.0 posits that AD is a two-stage disease (in contrast to its single-stage nature in the ACH). The first stage is asymptomatic. In it, *i*Aβ produced in the AβPP proteolytic pathway accumulates in a decades-long, even a life-long, process. If and when it reaches and crosses the critical threshold, it triggers the activation of the self-sustaining AβPP-independent *i*Aβ production pathway and the commencement of the second, devastating AD stage that includes the tau pathology and culminates in neuronal loss. The dynamics of AβPP-derived *i*Aβ accumulation appear to be the determining factor that either drives AACD and triggers AD or confers the resistance to both [4]. Thus, *all* known mutations that cause the early onset of AD augment the rate of accumulation of AβPP-derived *i*Aβ, resulting in the earlier, accelerated crossing of the second-AD-stage-activating threshold, activation of the AβPP-independent *i*Aβ production pathway, and commencement of the disease [4]. In sharp contrast, the protective Icelandic mutation reduces the rate of accumulation of AβPP-derived *i*Aβ, resulting in the delay or prevention of the threshold crossing, of the activation of the AβPP-independent *i*Aβ generation pathway, and, consequently, of the commencement of symptomatic AD [4]; it also delays or prevents the crossing of the AACD-triggering threshold and thus protects from this condition as well [2,4].

1.5. The AβPP-Independent Aβ Generation Pathway: The Active Core of AD

The AβPP-independent Aβ generation pathway is, therefore, the active core of AD. Its product is not secreted but is retained within the cell [1,4]; it both drives the AD pathology and propagates the operation of the AβPP-independent pathway that, in turn, produces more of it. The rationale for these two attributes of the ACH2.0, i.e., that in AD *i*Aβ is produced in the AβPP-independent pathway and that the bulk and, possibly, the entire production output is retained intraneuronally, is straightforward. In this theory of AD, *i*Aβ causes and drives the disease. Yet, the documented suppression of Aβ production by the AβPP proteolysis had no effect on the progression of AD [11,12]; hence, it is generated independently of AβPP in the disease. Likewise, a substantial depletion of the levels of extracellular Aβ had no efficacy whatsoever in clinical symptomatic AD trials; hence, Aβ generated in the AβPP-independent pathway is retained intraneuronally (reviewed in [1,4]).

2. The Engine That Drives AD

2.1. Life-Long Accumulation of AβPP-Derived iAβ at the First AD Stage: Mechanistic Aspects

Conventionally, Aβ is produced in the proteolytic/secretory pathway by two cleavages within the AβPP. The first, beta-cleavage, occurs between residues 671 and 672 and produces the C99, 99 amino acids long C-terminal fragment, which contains Aβ in its N-terminal portion. Subsequent gamma-cleavage occurs within an internal segment of C99 and generates Aβ of variable length, typically 40 (most common) or 42 residues long. The bulk of the gamma-cleavages of C99 take place on the plasma membranes, and the resulting Aβ is secreted. However, a small fraction of gamma-cleavages of C99 occurs physiologically on the intracellular membranes within various organelles, such as endoplasmic reticulum, endosomes, lysosomes, Golgi apparatus, trans-Golgi network (TGN), and mitochondria [23–31]. Aβ resulting from gamma-cleavages of C99 at these locations is not secreted but is retained intraneuronally and remains *i*Aβ. The physiologically occurring intraneuronal retention of a small fraction of AβPP-derived Aβ constitutes one of the two sources of *i*Aβ. The second source is the internalization of secreted Aβ [32–37]. In this case, extracellular Aβ is converted to *i*Aβ. It appears that the oligomerization of extracellular Aβ is a prerequisite for its importation inside the cell [35–37]. Aβ42, for example, is taken up by the cell twice as effectively as other Aβ species [33] because of its propensity to aggregate and form soluble oligomers. The importation of extracellular Aβ into the cell is facilitated by multiple cellular receptors [38–46]. As discussed below, when AβPP-derived

*i*Aβ reaches the critical threshold, it triggers the activation of the AβPP-independent *i*Aβ production pathway, ignites the AD Engine and commences the second AD stage.

2.2. AβPP-Derived iAβ Accumulation Triggers AD but Is a Normal Physiological Process: At the First AD Stage the Difference between Health and Disease Is Quantitative, Not Qualitative

Numerous studies have demonstrated that *i*Aβ is the major cause of Alzheimer's pathology [47–59]. It should be emphasized, however, that the mechanisms underlying the occurrence of AβPP-derived *i*Aβ, both the importation of extracellular Aβ inside the cell and the intraneuronal retention of Aβ derived from AβPP processed on the intracellular membranes, are normal physiological processes. They are capable of causing the disease, yet they occur in both healthy individuals who never develop AD and in future AD patients. Both accumulate AβPP-derived *i*Aβ but at different rates, and/or the extents of their second-AD-stage-activating thresholds are, apparently, also different. Thus, the difference between the two is not qualitative but quantitative, i.e., it is not how *i*Aβ accumulates but how fast it accumulates and how soon (if at all) it reaches the critical second-AD-stage-activating threshold, as illustrated further in the following sections below. Indeed, all known factors that facilitate the accumulation of *i*Aβ either predispose to or cause AD. For example, the cellular uptake of extracellular Aβ was shown to require ApoE [36], which occurs in several isoforms. One of those, ApoE4, was demonstrated to be much more effective in mediating the importation of extracellular Aβ than other ApoE isoforms [36,52]; it also constitutes the major risk factor for the disease. Some presenilins (PSEN) mutations cause increased production and secretion of Aβ42 [34], and thus facilitate, as discussed above, the cellular uptake of secreted Aβ. These mutations also cause the early onset of AD [34]. The Swedish AβPP mutation causes a marked increase in the fraction of AβPP processed on intracellular membranes [60] and, consequently, the augmented rate of its intraneuronal retention and so do certain PSEN mutations [61]. Both types of mutations also cause the early onset of AD [60,61]. On the other hand, the Icelandic Aβ mutation increases the rate of physiologically occurring cleavage within *i*Aβ and, consequently decreases the rate of its accumulation [21,22]; it also protects from the disease [21,22]. In an inverse example, the Flemish Aβ mutation decreases the rate of physiologically occurring cleavages within *i*Aβ [62] and thus increases the rate of its accumulation; it also causes the early onset of AD [62].

2.3. iAβ-Mediated Activation of the PKR and HRI Kinases Elicits the Integrated Stress Response (ISR) and Triggers Operation of the AβPP-Independent iAβ Production Pathway: Transition to the Second AD Stage

Ultimately, AβPP-derived *i*Aβ, accumulated to sufficient levels (the "critical threshold" referred to above), triggers activation of the operation of the AβPP-independent *i*Aβ production pathway and thus initiates the second AD stage. This, however, occurs indirectly, in several distinct steps. The first step is *i*Aβ-mediated activation of the PKR and HRI kinases. The connection between the occurrence and levels of *i*Aβ and the activity of PKR has been established in numerous studies in cell and animal models [63–65]. Physiologically importantly, activated PKR was detected in neuronal cells of AD patients [66,67]. Studies with animal models suggested the involvement of TNFα in the *i*Aβ-mediated activation of PKR [68]. Another possible mechanism involves the participation of the PKR Activator (PACT). The occurrence of the latter was indicated by the detection of co-localized PACT and activated PKR in the AD-affected human neuronal cells [69].

On the other hand, the *i*Aβ-mediated activation of the HRI kinase results from mitochondrial distress. The connection between AD and mitochondrial dysfunction is well established [70–87]; mitochondrial distress is, actually, one of the earliest pathological occurrences in the progression of AD. For mitochondrial distress to activate a cytoplasmic enzyme, a signal has to be transmitted across the mitochondrial membrane to the cytosol. This occurs via mitochondrial dysfunction-activated proteolytic cascade. First, the dysfunction activates the OMA1 mitochondrial protease, which cleaves another mitochondrial

protein, DELE1. One of the two resulting fragments of DELE1 is exported to the cytosol. There, it binds to and thus activates the HRI kinase [88,89].

Both PKR and HRI are members of the eIF2α family of kinases [90] (the other two members are PERK and GNS2). When activated, either PKR or HRI, or both, phosphorylate eIF2α at its serine-51 residue thus triggering the integrated stress response, ISR. The eIF2α phosphorylation is, in fact, the "integrating" factor of the ISR: all numerous and variable cellular events and stresses that activate the ISR do so by the phosphorylation of eIF2α at the serine 51 [90–99]. The main manifestation of the ISR is a substantial reduction in global cellular protein synthesis. This occurs via the inhibition of the cap-dependent initiation of translation. At the same time, the integrated stress response propagates cap-independent translation of certain mRNAs. Notably, those include mRNA species encoding numerous transcription factors. The ACH2.0 posits that either some of these transcription factors or products of the genes regulated by them are the "missing" component(s) required for the operation of the AβPP-independent *i*Aβ production pathway [1]. Once these components are available, the pathway is activated and the second AD stage commences [1,4].

2.4. AβPP-Independent iAβ Production (and Retention) Pathway: Potential Underlying Mechanisms

There are several, at least four, cellular mechanisms capable of generating Aβ independently of AβPP [1,4]. Regardless of their nature (discussed below), they all share one common feature: in every conceivable AβPP-independent Aβ production pathway, translation initiates from the AUG encoding methionine 671 (Met671) of AβPP and preceding immediately, contiguously, and in-frame the C99 (and Aβ)-encoding segment of human AβPP mRNA. The occurrence of an AUG codon in such a propitious position was recognized [100] soon after human AβPP cDNA had been cloned and sequenced [101–103]. Moreover, not only is its location auspicious, it is situated within an optimal translation initiation nucleotide context [100], and in this respect, is unique for human AβPP mRNA where of 20 in-frame AUG codons, the AUG in question is the only one located within an optimal translation initiation nucleotide context; even the AUG encoding Met1 (the translation-initiating methionine) of human AβPP is not in an optimal translation initiation complex [100]. This circumstance suggested a possibility that the AUG encoding Met671 of human AβPP is utilized physiologically to generate C99 and Aβ independently of AβPP and that this pathway is operating inducibly in AD and, in fact, is underlying the disease.

One proposed mechanism capable of generating C99 and Aβ independently of AβPP is the internal initiation of translation of the intact AβPP mRNA commencing with the Met671 [100]. Following this proposal, several studies were carried out to test it [104,105]. They excluded it on dubious premises, as discussed elsewhere [4]. This possibility remains, in fact, viable and should be tested in a suitable AD model (see [4] on the subject of a suitable AD model). Three more potential mechanisms of AβPP-independent generation of Aβ utilize 5′-truncated AβPP mRNAs as translational templates. In every case, the AUG encoding Met671 of AβPP is the first functional translation initiation codon; in each of these three mechanisms, translation initiates conventionally (rather than via an unconventional internal initiation). One such mechanism is the internal initiation of transcription of the AβPP gene, which produces a suitable 5′-truncated AβPP mRNA. Another mechanism is a site-specific cleavage of the intact AβPP mRNA, which produces a molecule where the AUG in question is the first translation initiation codon. The third and apparently the most plausible mechanism is the asymmetric RNA-dependent amplification of human AβPP mRNA, which produces 5′-truncated AβPP mRNA with the AUG in question in the conventional translation-initiating position [1,4]. Importantly, this mechanism is not specific to AβPP mRNA but is rather widely used physiologically with a variety of mRNA species. It is defined by the activity of the RNA-dependent mRNA amplification pathway and the eligibility of mRNA species. Human AβPP mRNA is eligible and its amplification requires only the activation of the pathway; this option was, in fact, tested and proven plausible in a model experiment (rev. in [4]). It should be noted that another, arguably less

probable, version of this option, yielding the same end result, is also possible, namely that the AβPP mRNA amplification pathway is constitutively operative in human neurons but the resulting C100-encoding mRNA is functionally, i.e., translationally, "silent" because it is cap-less, and its translation is enabled only under the ISR conditions.

Regardless of which of the mechanisms discussed above is employed in the AβPP-independent production of C99 and Aβ, the primary translation product in each case is not C99 but rather C100, i.e., Met-C99. This is because, when the translation-initiating methionine is followed by a residue larger than valine (in case of C100, the initialing Met is followed by aspartate, much larger than valine), it cannot, due to the geometry of the active site, be removed by the N-terminal aminopeptidases 1 and 2 (MAP1 and MAP2) that cleave-off the initiating methionine co-translationally [106–111]. When MAP1/MAP2 are inoperative, the translation-initiating methionine is eventually removed by other aminopeptidases [111] with broad specificity, but this happens, invariably, post-translationally. If C100 and, potentially, Met-Aβ were indeed produced in AD-affected neurons, the detection of either species would constitute proof of the occurrence of the process. Such proof cannot be obtained from postmortem samples because, in dying cells, C100 synthesis would cease long before the proteolysis does, and without its influx, N-terminal methionine would be completely removed from both Met-C99 and Met-Aβ. On the other hand, both C100 and Met-Aβ should be readily detectable in a suitable AD model, as described elsewhere [1,4]. The detection of Met-Aβ would be feasible because, in the ACH2.0 framework, it is retained intraneuronally [1,4]. This is presumably because Met-C99 and C99 produced independently from AβPP are processed only or mainly on the intracellular membranes. Not only this type of C99 processing was shown to occur, but also C99 gamma-cleavage on ER and TGN membranes was shown to be neuron-specific [26,27].

2.5. Collateral Effect: AβPP-Independent iAβ Production Pathway also Generates AβPP Intracellular Domain, AICD

Aβ is only one of the two molecules that are given rise to by the cleavage of C99. The other is AβPP Intracellular Domain, AICD. Roughly one AICD molecule is produced per molecule of Aβ generated by C99 (or C100) cleavage (in both AβPP-dependent and -independent pathways). It is generated by the epsilon cleavage of C99 (downstream from, preceding and apparently independent of the gamma-cleavage) [112], and it is not inert. AβPP intracellular domain was shown to interact with and affect a number of cellular signaling pathways and regulatory proteins [113–123]. It was implicated in the regulation of gene expression, in cytoskeletal dynamics, and in apoptosis [124,125]. It was demonstrated to influence the expression of neprilysin [126] and, consequently, the *i*Aβ clearance, and to impact the phosphorylation of tau protein, thus potentially contributing to the formation of neurofibrillary tangles [113,124]. It affects neuronal activity, impacts oscillations in the hippocampus, and causes deterioration of spatial memory encoding [127].

The production and accumulation of AICD produced by AβPP proteolysis occurs at the first AD stage alongside the accumulation of AβPP-derived *i*Aβ, and it is conceivable that both contribute to the transition to the second AD stage. The operation of the AβPP-independent *i*Aβ and AICD production pathway at the second AD stage markedly increases the levels of both. Therefore, there is significantly more AICD in Alzheimer's patients (i.e., at the second AD stage) than in healthy individuals (or at the first AD stage). It is highly plausible that augmented levels of AICD contribute to AD pathology; however, the full extent of this contribution remains to be elucidated. Importantly, any drug interfering with the operation of the AβPP-independent *i*Aβ and AICD-generating pathway (see below on the subject) would stop the production of not only *i*Aβ but also of AICD generated in an AβPP-independent manner.

2.6. The AD Engine: Continuous Cycles of the iAβ-Stimulated Propagation of Its Own AβPP-Independent Production

To summarize the above discourse, the ACH2.0 posits that AD is a two-stage disease. At the first, asymptomatic stage AβPP-derived *i*Aβ accumulates in a decades-long process.

This occurs via the retention of a fraction of Aβ resulting from the processing of AβPP on intracellular membranes and through the importation into the cell of a fraction of secreted Aβ. When AβPP-derived *i*Aβ reaches and crosses the critical threshold, it triggers the activation of the AβPP-independent *i*Aβ (and AICD) production pathway. More specifically, it mediates, via the engagement of TNFα and/or PACT, activation of the PKR kinase. Alternatively or additionally, it triggers mitochondrial distress, which, in turn, activates mitochondrial protease OMA1. OMA1 cleaves another mitochondrial protein, DELE1. One of the resulting two DELE1 fragments is exported into the cytosol where it finds, binds, and thus activates the HRI kinase. Both PKR and HRI are members of the eIF2α family of kinases. Upon activation, they phosphorylate eIF2α at the specific site thus eliciting the integrated stress response. The global cellular protein synthesis is drastically reduced via inhibition of cap-dependent initiation of translation but, concurrently, translation of a subset of mRNA species is increased in a cap-independent manner. This subset includes mRNA species encoding several transcription factors, and the ACH2.0 postulates that some of these transcription factors or products of genes up-regulated by them are the components required for the operation of the AβPP-independent *i*Aβ (and AICD) production pathway and absent in unstressed neuronal cells.

When the "missing" components are supplied, the AβPP-independent *i*Aβ generation pathway becomes operational. This marks the commencement of the second stage of AD. At this stage, the difference between health and disease is patently qualitative. The bulk or the entire Aβ output of this pathway is retained intraneuronally and *i*Aβ levels rapidly increase. This has two major consequences. First, elevated *i*Aβ levels drive AD pathology, including the generation of misfolded or unfolded *i*Aβ aggregates and the formation of neurofibrillary tangles. They can do the latter by, for example, suppressing the ubiquitin-proteosome system, consequently accelerating the accumulation of tau protein and expediting its phosphorylation [128–131] (reviewed in [4]). The second major consequence is the perpetualization of the operation of the AβPP-independent *i*Aβ production pathway for the remaining lifespan of the affected neurons. Indeed, the increasing levels of *i*Aβ produced independently of AβPP and retained intraneuronally sustain the activity of eIF2α kinases; this, in turn, maintains the integrated stress response. With all required components of the AβPP-independent *i*Aβ generation pathway continuously supplied, the pathway's operation is perpetuated. These continuous cycles of the *i*Aβ-stimulated propagation of its own AβPP-independent production constitute the engine driving AD, the AD Engine.

The activation and operation of the AD Engine are illustrated in Figure 1. The left box of Figure 1 depicts a decades-long accumulation of *i*Aβ produced in the AβPP proteolytic/secretory pathway and constituting the first AD stage. As shown in the middle (green) box, if and when AβPP-derived *i*Aβ levels reach and cross a critical threshold, it mediates the activation of PKR (via TNFα and/or PACT) and HRI (by triggering mitochondrial distress, which, in turn, activates the OMA1-DELE1-HRI signaling cascade). Activated kinases phosphorylate eIF2α, thus eliciting the integrated stress response. Among new proteins produced under the ISR conditions, there are component(s) required for the operation of the AβPP-independent *i*Aβ (and AICD) production pathway. When they are supplied, the pathway is activated (upper blue box). Aβ produced independently of AβPP is retained intraneuronally and its cellular levels rapidly increase (right pink box). Steadily increasing levels of *i*Aβ propagate the ISR and perpetuate its own production via the operation of the AβPP-independent *i*Aβ/AICD generation pathway (bottom red box). Arched blue and red arrows indicate the repeated feedback cycles and denote the operation of the AD Engine; it culminates in neuronal death. Please note that while the AD Engine is operational, it is self-sustaining (due to the influx of *i*Aβ produced independently of AβPP) and completely independent from the influx of *i*Aβ produced by the AβPP proteolysis, which at this point contributes only marginally to the cellular *i*Aβ pool.

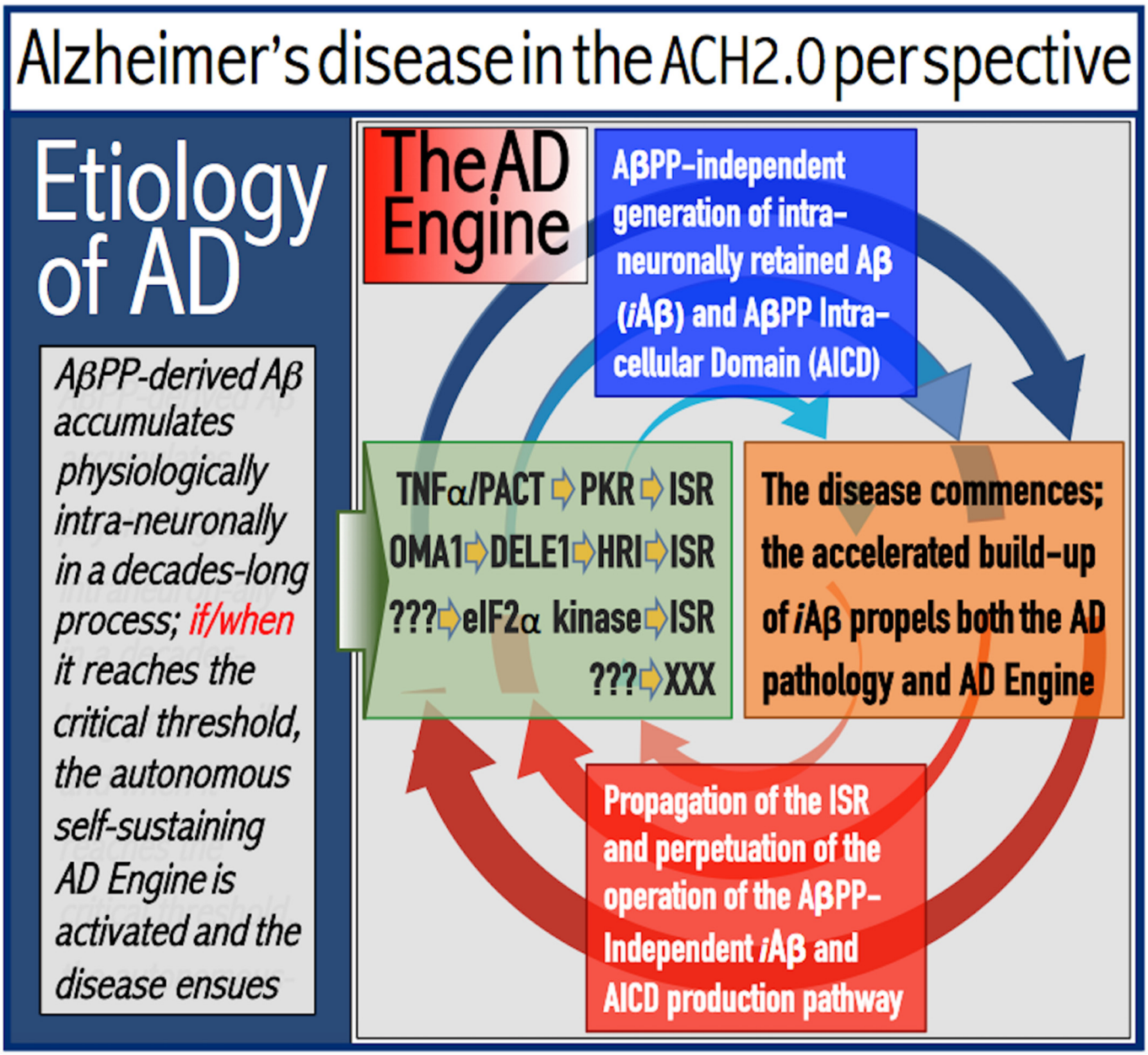

Figure 1. Etiology of AD in the ACH2.0 perspective: Continuous cycles of the *i*Aβ-stimulated propagation of its own AβPP-independent production constitute the engine that drives AD. *i*Aβ: Intraneuronal Aβ. *eIF2α*: Eukaryotic translation initiation factor 2 alpha. *PKR*, *HRI*: eIF2α kinases. *TNFα*—tumor necrosis factor alpha, *PACT*-PKR activator; both mediators of the activation of PKR. *OMA1*, *DELE1*: Mitochondrial proteins mediating the activation of HRI. *ISR*: Integrated stress response. *AICD*: AβPP intracellular domain. "*???*": Yet-unidentified mediator(s). Note that it can act independently of AβPP-derived *i*Aβ, as apparently occurs in the case of chronic neuronal inflammation. "*XXX*": Yet-unknown pathway activating AβPP-independent production of *i*Aβ. *Left (gray) box*: Decades-long accumulation of AβPP-derived *i*Aβ. *Middle (green) box*: Sufficient levels of *i*Aβ mediate the phosphorylation of eIF2α and the elicitation of the ISR; some proteins synthesized under the ISR conditions are the "missing" components required for the operation of the AβPP-independent *i*Aβ production pathway; alternatively, the ISR enables translation of constitutively expressed, otherwise "silent", Met-C99-encoding cap-less mRNA. *Top (blue) box*: The AβPP-independent *i*Aβ production pathway is activated; its end products, *i*Aβ and AICD are both retained intraneuronally. *Right (pink) box*: Following the activation of the AβPP-independent *i*Aβ

production pathway, steady-state levels of *i*Aβ rapidly increase. *Bottom (red) box*: The increased levels of *i*Aβ propagate the ISR and perpetuate the operation of the AβPP-independent pathway of its further production; they also drive the AD pathology. *Large Grey box*: The continuous cycles of the *i*Aβ-stimulated propagation of its own AβPP-independent generation constitute an engine that drives AD, the AD Engine; when ignited, it is autonomous, self-sustaining, and completely independent of AβPP-derived *i*Aβ.

Thus, AD is a disease that is due to and completely depends upon the operation of the AβPP-independent *i*Aβ production pathway, and, apparently, the elicitation of the ISR is sufficient to activate this pathway. In other words, the AD Engine could be ignited by means other than AβPP-derived *i*Aβ. In these terms, the observed role of the persistent neuronal inflammation in the predisposition to AD could be due to its contribution to the elicitation of the integrated stress response in neuronal cells and, consequently, to the facilitation of activation of the AβPP-independent *i*Aβ production pathway even if the levels of AβPP-derived *i*Aβ are below the critical ISR-triggering threshold (further discussed in Section 17.3).

3. Dynamics of AβPP-Derived *i*Aβ Accumulation in Health and Disease: Alzheimer's Disorder and Aging-Associated Cognitive Decline and the Conditionality of the "First Stage of AD"

3.1. Dynamics of AβPP-Derived iAβ Accumulation in Health and Disease: Alzheimer's Disease

The dynamics of *i*Aβ accumulation in health and disease are depicted in Figure 2. Panel A of Figure 2 shows the dynamics of AβPP-derived *i*Aβ accumulation in individuals who do not develop AD in their lifetime. The T1 threshold, which triggers the activation of the AβPP-independent *i*Aβ production pathway, is not reached, the pathway is not activated, and there is no disease. Panel B of Figure 2 illustrates the dynamics of *i*Aβ accumulation in individuals who develop sporadic AD. The levels of *i*Aβ produced in the AβPP proteolytic pathway reach and cross the T1 threshold within a relatively narrow temporal window [1,4]. This triggers the activation of eIF2α kinases, the elicitation of the integrated stress response, and the initiation of the AβPP-independent *i*Aβ generation pathway. The activation of the latter commences the second AD stage. Levels of *i*Aβ in individual neurons increase in a broad stochastic distribution [1,4], and when they reach and cross the T2 threshold, cells commit apoptosis. When a sufficient fraction of the affected neurons lose functionality or die, AD symptoms manifest. Importantly, by the time the symptoms manifest, the bulk of the affected neurons have already crossed the T1 threshold and activated the AβPP-independent *i*Aβ production pathway [1,4]. With the continuous loss of the affected neurons, the disease eventually reaches its end state.

3.2. Conditionality of the "First Stage of AD"

The scenario depicted in panel A of Figure 2 is the prevailing one: the majority of the population does not develop AD. This, however, is not because these individuals are resistant to AD but because of the kinetics of their AβPP-derived *iAβ* accumulation. They simply are running out of time, i.e., the lifetime, to accumulate enough *i*Aβ and to cross the T1 threshold. Moreover, in terms of the ACH2.0, given sufficiently long lifetime, *every* individual would eventually develop AD. As discussed above, the difference between health and disease at the first AD stage is purely quantitative, AβPP-derived *i*Aβ accumulates by the very same, normal, physiological mechanisms in both cases. In individuals who eventually develop AD, either the rate of this accumulation is faster or the extent of the T1 threshold is lower. Therefore, the first AD stage cannot be defined unconditionally as a "decades-long accumulation of AβPP-derived *i*Aβ". This is precisely what is depicted in panel A of Figure 2, yet there is no disease there and therefore no "first stage" of it. It follows that the "first stage of AD" can be such only conditionally and, moreover, only post-factum, if and when the T1 crossing occurs and the disease develops. Under any other circumstances, it is just a normal physiological occurrence. Furthermore, the "first AD stage" is mostly a term of convenience since there is no AD prior to the

T1 crossing. The disease commences only with the crossing of the T1 threshold and the activation of the AβPP-independent *i*Aβ production pathway, a phase referred to in the ACH2.0 as the "second stage of AD". Accordingly, in terms of ACH2.0, the terms "second stage of AD" and "AD" are synonymous and can be used interchangeably.

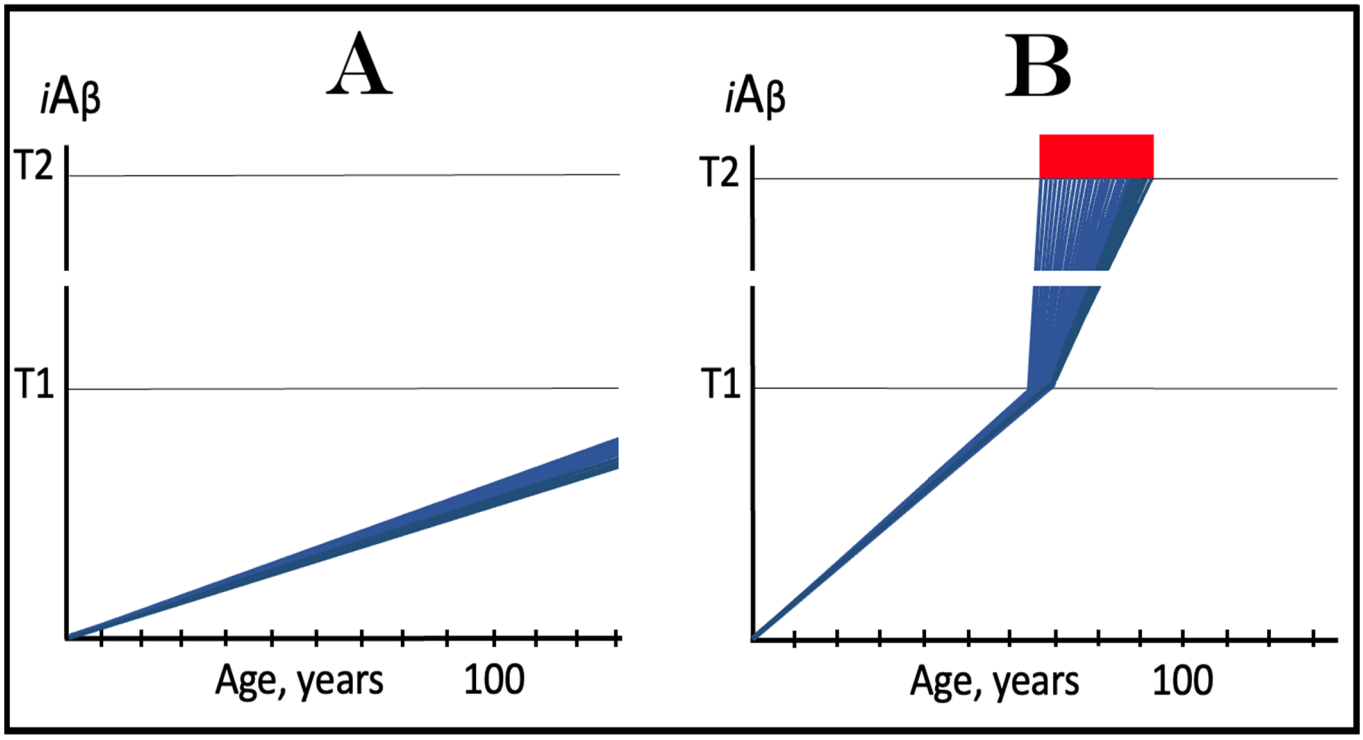

Figure 2. Dynamics of AβPP-derived *i*Aβ accumulation in health and in Alzheimer's disease. *i*Aβ: Intraneuronal Aβ. *Blue lines*: Levels of *i*Aβ in individual neurons. ***T1*** *threshold*: The concentration of AβPP-derived *i*Aβ that mediates elicitation of the ISR and triggers the activation of the AβPP-independent *i*Aβ production pathway. ***T2*** *threshold*: The level of *i*Aβ, produced mainly in the AβPP-independent pathway, which triggers neuronal apoptosis. *Red box*: Apoptotic Zone, the range of *i*Aβ concentrations that cause the commitment to apoptosis. Panel (**A**): The levels of *i*Aβ do not cross the T1 threshold within the lifespan of a person; consequently, no disease occurs. Panel (**B**): The levels of *i*Aβ reach and cross the T1 threshold within a narrow temporal window; the AβPP-independent *i*Aβ production pathway is activated and AD commences. Eventually, the *i*Aβ levels cross the **T2** threshold. When a sufficient fraction of neurons die or lose functionality, the disease enters the end stage.

3.3. Dynamics of AβPP-Derived iAβ Accumulation in Health and Disease: Aging-Associated Cognitive Decline

The above considerations make it clear that the lower extent of the T1 threshold would accelerate its crossing by AβPP-derived *i*Aβ and, consequently, would expedite the commencement of the second AD stage. And indeed, statistically, in individuals predisposed to AD, the extent of the T1 threshold appears to be relatively low, lower than in the general population [132,133]. Therefore, in these individuals, as AβPP-derived *i*Aβ accumulates, no significant *i*Aβ-related damage would occur until post-T1 crossing. It is easy to visualize that with the increase in the extent of the T1 threshold, a sub-T1 level of AβPP-derived *i*Aβ would be eventually reached that causes consequential neuronal damage [4]. The ACH2.0 defines it as the T^0 threshold: the sub-T1 level of AβPP-derived *i*Aβ, which triggers neuronal damage that manifests as Aging-Associated Cognitive Decline [2,4]. Within the framework of the ACH2.0, AACD is defined as an extended segment of the first AD stage, which occurs in individuals with a sufficiently high T1 threshold and is driven by AβPP-derived *i*Aβ. Moreover, the ACH2.0 establishes the T^0 and T1 thresholds as the

boundaries of the "AACD Zone": the condition commences with the crossing of the former and morphs into AD when the latter is traversed [4].

The dynamics of *i*Aβ accumulation in AACD versus that in health is presented diagrammatically in Figure 3. The extents of the T^0 and T1 thresholds are identical in both panels of Figure 3. In panel A, the rate of AβPP-derived *i*Aβ accumulation is such that it does not reach the T^0 threshold within the lifespan of an individual. Neither the T^0 crossing nor AACD occurs. In contrast, in panel B of Figure 3, the levels of AβPP-derived *i*Aβ cross the T^0 threshold and trigger AACD. If, subsequently, the T1 threshold were not crossed within the individual's lifetime, the AACD would persist for the remaining lifespan, increasing in its severity in parallel with the increase in the levels of AβPP-derived *i*Aβ. If, however, the T1 threshold would be crossed within the lifetime of an individual, AACD would morph into AD (see Section 12 below on the potential overlap of AACD and AD symptoms).

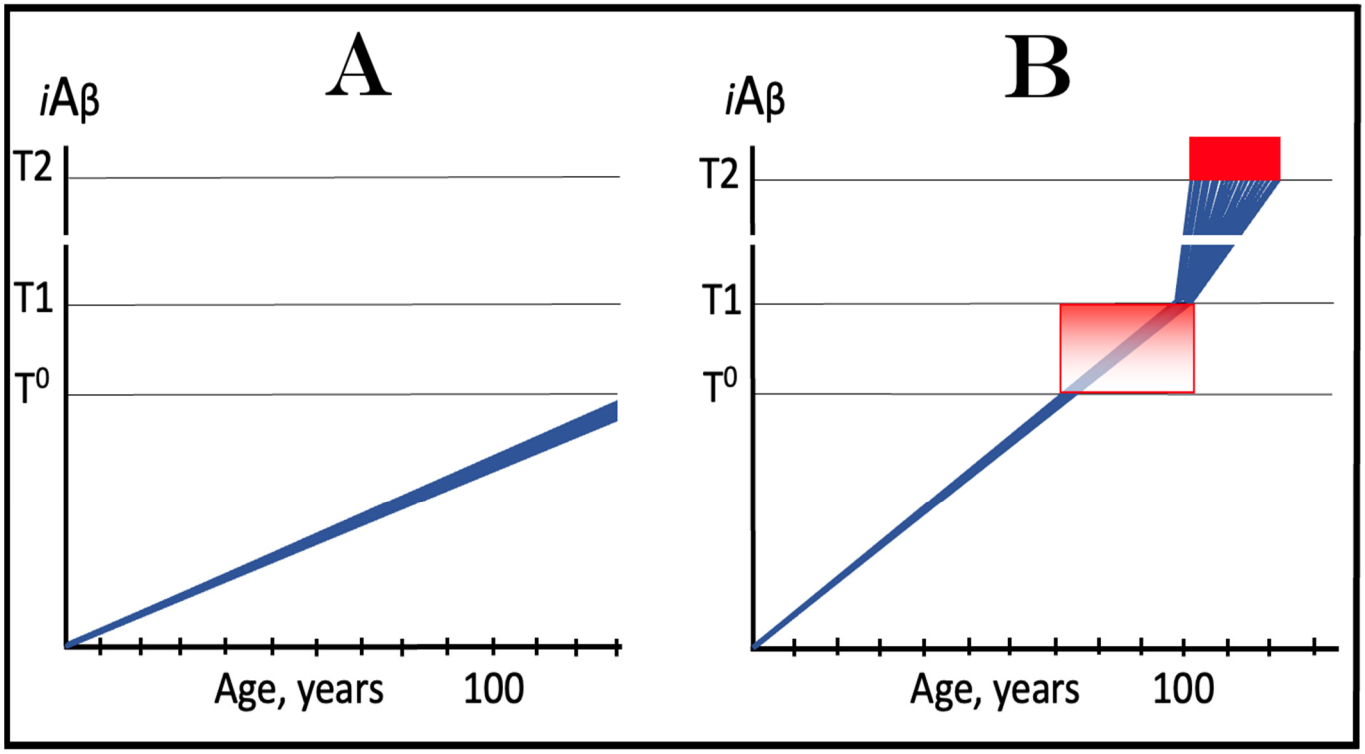

Figure 3. Dynamics of AβPP-derived *i*Aβ accumulation in health and in Aging-Associated Cognitive Decline. *i*Aβ: Intraneuronal Aβ. *Blue lines*: Levels of *i*Aβ in individual neurons. ***T*^{0}** *threshold*: The concentration of *i*Aβ that triggers the neurodegeneration manifesting as AACD. ***T1*** *threshold*: The concentration of AβPP-derived *i*Aβ that mediates elicitation of the ISR and triggers the activation of the AβPP-independent *i*Aβ production pathway. ***T2*** *threshold*: The level of *i*Aβ, produced mainly in the AβPP-independent pathway, which triggers neuronal apoptosis. *Pink gradient box*: AACD Zone, the range of concentration of AβPP-derived *i*Aβ between the T^0 and T1 boundaries. *Red box*: Apoptotic Zone, the range of *i*Aβ concentrations that cause the commitment to apoptosis. Panel (**A**): The levels of *i*Aβ do not cross the T^0 threshold within the lifespan of a person; consequently, no AACD occurs. Panel (**B**): The levels of *i*Aβ reach and cross the T^0 threshold; this triggers the commencement of AACD. If the T1 threshold is not crossed within the lifespan of an individual, the condition will persist for the remaining lifetime. If the T1 threshold was crossed (provided the lifespan is long enough), AACD would morph into AD. For detail, see the main text.

4. ACH-Based AD Drugs: A Definition

Below, the present study analyzes the limits of the utility of the type of AD drugs that have been developed to date and are being utilized currently. It concludes that this type

of drug is patently unsuitable for the treatment of AD despite its efficiency in fulfilling its mechanistic mission. The type of drug in question is comprised of ACH-based drugs, the drugs suggested by and designed on the basis of the ACH theory of AD. In the framework of the ACH, the disease is caused and driven by the extracellular Aβ. Accordingly, the rational way to treat the disease is to eliminate or reduce the cause, i.e., extracellular Aβ. Therefore, ACH-based AD drugs can be defined as agents that reduce the levels of extracellular Aβ. ACH-based AD drugs can be divided into two categories. One category comprises drugs that act outside the cell. It is exemplified by lecanemab, donanemab or other monoclonal antibodies that sequester Aβ. Any agent directly degrading or clearing or removing in any imaginable way extracellular Aβ would fall into this category. Another category of ACH-based drugs consists of agents that interfere with the intracellular production and secretion of Aβ. Since in terms of the ACH, Aβ is produced solely in the AβPP proteolytic/secretory pathway, this category includes drugs that interfere with the AβPP proteolysis. It is exemplified by verubecestat, a small-molecule drug that penetrates inside the neuron and inhibits the activity of BACE1 (Beta-Site Cleaving Enzyme). This category of drugs can be quite effective: they prevent the production and, consequently, secretion of AβPP-derived Aβ and enable effective physiological clearance of extracellular Aβ. In human clinical trials, for example, verubecestat reduced, in a dose-dependent manner, the levels of extracellular Aβ by up to 80% [11,12]. The ACH-based AD drugs fulfilled their mechanistic mission, i.e., significantly reduced the levels of extracellular Aβ, and were spectacularly successful in relieving and even reversing [8–10] symptoms of the disease in transgenic AD models but not in human clinical trials of symptomatic AD. The reasons for this are discussed below.

5. In the ACH2.0 Paradigm, Conceptually, ACH-Based Drugs Cannot Be Effective at Symptomatic Stages of AD

All tested ACH-based drugs were ineffective for symptomatic AD in human clinical trials (marginal effect of lecanemab and donanemab is discussed in Section 7 below). In light of their efficiency in animal models, their failure in human clinical trials was highly unexpected in the framework of the ACH, but this is precisely how it should be in the ACH2.0 paradigm: ACH-based drugs *cannot* be effective in symptomatic AD. The reason for this is the AβPP-independent *i*Aβ production pathway. Within the ACH2.0 framework, this process is, in fact, the cornerstone of the disease. In relation to it, AβPP-derived *i*Aβ carries out, in a way, the same function that the starter motor does in a car: when it accumulates over a critical threshold, it triggers the activation of *i*Aβ generation in an AβPP-independent manner, i.e., it ignites the AD Engine. Only then does AD commence. The production of *i*Aβ in the AβPP proteolytic pathway is simply not sufficient to drive AD pathology. On the other hand, following the activation of the AβPP-independent pathway, the production of *i*Aβ increases drastically for several reasons. First, the entire Aβ output of the pathway is retained within the neuron (in contrast to only a small fraction of the Aβ output of the AβPP proteolysis). Second, the primary translation product derived independently of AβPP (C100) comprises only 13% of 771 residues-long protein precursor of the proteolytic pathway; its production would be significantly more efficient. Third, if, as suggested elsewhere [1,4], the AβPP-independent *i*Aβ generation pathway employs the asymmetric amplification of AβPP mRNA [4], the rate of generation of *i*Aβ in this pathway would be orders of magnitude higher than the rate of production of Aβ in the AβPP proteolytic pathway. Importantly, similarly to the starter motor/engine relationship in a car, once activated, the operation of the AβPP-independent *i*Aβ production pathway is, as described above, self-sustaining and completely independent from the contribution of *i*Aβ produced by AβPP proteolysis (which becomes at this point marginal in comparison with that generated independently of AβPP). Thus, once ignited, the AβPP-independent *i*Aβ production pathway (the "AD Engine") renders the AβPP proteolytic pathway irrelevant to the progression of AD and makes any attempt at the therapeutic utilization of the ACH-based drugs futile.

6. In the ACH2.0 Paradigm, Conceptually, ACH-Based Drugs Can Be Effective in Prevention of AD

Whereas, as argued in the preceding section, the production of *i*Aβ in the AβPP proteolytic pathway is irrelevant to the progression of symptomatic AD, it is, in the ACH2.0 paradigm, instrumental in triggering the disease. For this to happen, the levels of AβPP-derived *i*Aβ should reach and cross the T1 threshold (see Figure 2 above); if the T1 threshold is not crossed within the lifetime of an individual, no AβPP-independent *i*Aβ production pathway is activated and no AD occurs. This presumption lucidly suggests an effective therapeutic strategy: suppress AβPP-derived *i*Aβ accumulation and preclude its levels from reaching the T1 threshold and you will prevent the disease. And in this, the ACH-based drugs could potentially be quite effective.

As discussed above, the influx of AβPP-derived *i*Aβ occurs in two ways. One is the importation into the cell of the secreted extracellular Aβ. This is clearly a function of the levels of soluble extracellular Aβ. Reduce the levels of soluble extracellular Aβ and the rate of its cellular uptake will be reduced. The ACH-based drugs, such as monoclonal Aβ antibodies, were designed to do just this (the first category of the ACH-based AD drugs; see Section 4 above). Another mechanism of the influx of AβPP-derived *i*Aβ is the intraneuronal retention of Aβ (*i*Aβ) resulting from a fraction of AβPP processed on intracellular rather than on plasma membranes. The way to reduce the influx of retained *i*Aβ is to suppress the AβPP proteolytic pathway: less Aβ will be produced and less will be retained. Drugs, such as verubecestat (the second category of the ACH-based AD drugs; see Section 4 above), carry this out effectively [10–12]. ACH-based drugs of this type, actually, perform a double duty by suppressing both venues of the influx of AβPP-derived *i*Aβ. By reducing the production of AβPP-derived Aβ, they reduce its retention, whereas by lowering its secretion (less produced, less secreted), they decrease its extracellular levels and reduce the rate of its cellular uptake. By reducing the influx of AβPP-derived *i*Aβ, the ACH-based drugs would suppress the rate of its accumulation and thus delay or prevent the crossing of the T1 threshold and, consequently, the occurrence of AD.

6.1. Long-Term Treatment with ACH-Based Drugs: Two Possible Modes of Action

Panels A and B of Figure 4 depict two potential modes of action of the ACH-based drugs initiated prior to the crossing of the T1 threshold and administered for a long duration. In one scenario (panel A), the influx of AβPP-derived *i*Aβ is reduced. Consequently, the rate of accumulation of AβPP-derived *i*Aβ is lowered, but its influx still outbalances the efflux and its levels continue to rise. The continuous increase in the levels of AβPP-derived *i*Aβ can result in one of two possible outcomes: (a) the T1 threshold is not crossed within the lifetime of an individual, and (b) provided the lifespan is long enough, the T1 threshold is crossed and AD develops but with a considerable delay (in comparison with the absence of the treatment).

In another scenario, illustrated in panel B of Figure 4, the drug-mediated decrease in the influx of AβPP-derived *i*Aβ is sufficient for its efflux (i.e., physiologically occurring degradation and clearance) to outbalance the influx and, consequently, its accumulation is reversed and its levels steadily decrease for the duration of the treatment. In this scenario, the T1 threshold would not be crossed within the lifetime of an individual (provided that the treatment lasts sufficiently long-term) and the disease would not occur.

6.2. Inefficiency of Short-Duration Treatment with ACH-Based AD Drugs

Panels A' and B' of Figure 4 consider the consequences of the preventive treatment with the ACH-based AD drugs administered for a short duration. Its efficiency would, obviously, depend on the degree of a decrease in the levels of AβPP-derived *i*Aβ during the treatment period. In panel A' of Figure 4, the levels of AβPP-derived *i*Aβ do not decrease, but rather increase (albeit at a slower rate), for the duration of the treatment. Consequently, following the cessation of the treatment, the accumulation of AβPP-derived *i*Aβ would resume with a rate equal to that exhibited prior to the treatment, the T1 threshold would

be crossed and AD would ensue. In this scenario, the commencement of AD would be delayed by less than the duration of the treatment (because at the end of the treatment, the levels of AβPP-derived *i*Aβ would be higher than at its beginning).

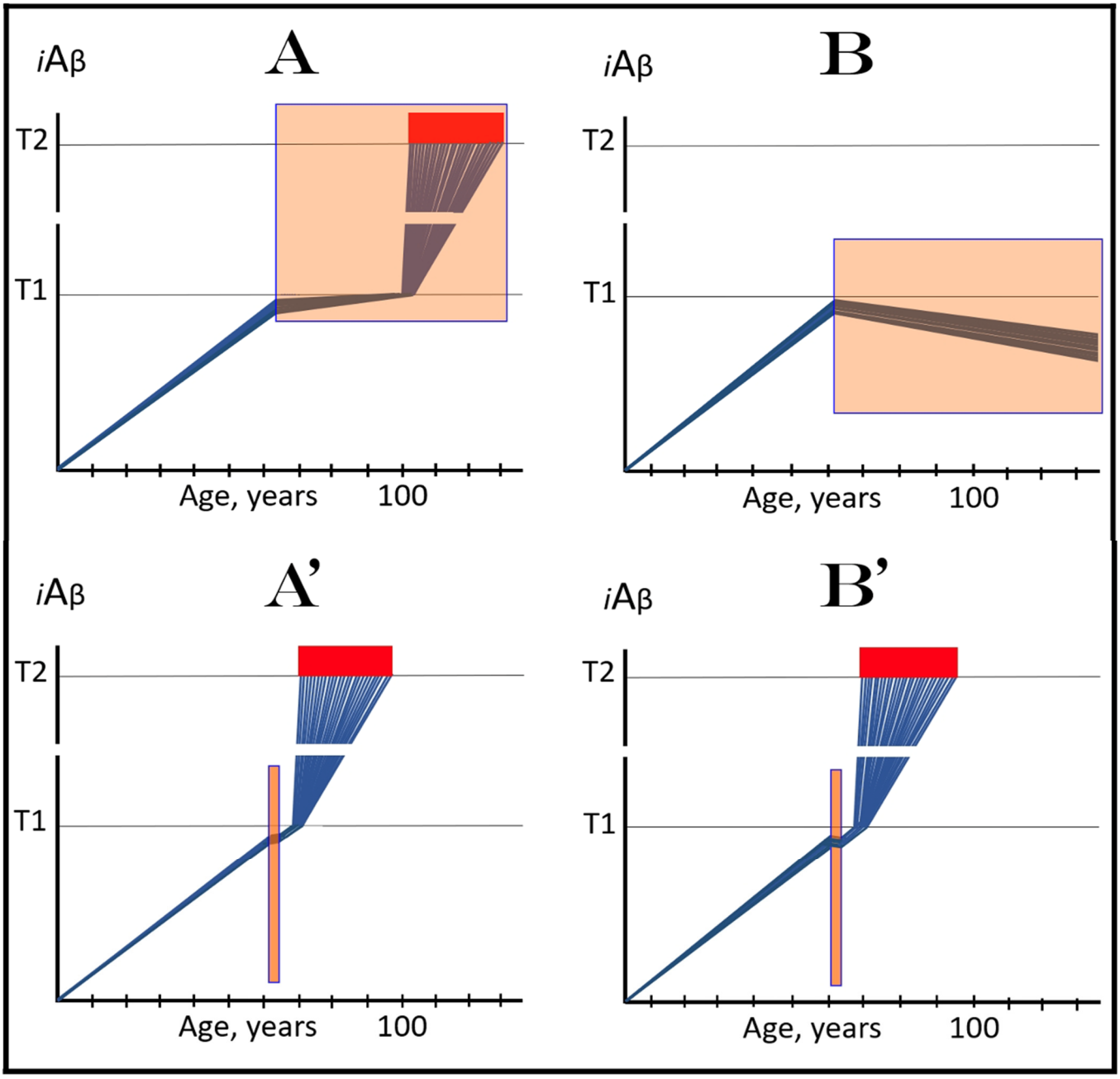

Figure 4. ACH-based drugs in prevention of AD. *i*Aβ: Intraneuronal Aβ. *Blue lines*: Levels of *i*Aβ in individual neurons. ***T1*** *threshold*: The concentration of AβPP-derived *i*Aβ that mediates elicitation of the ISR and triggers the activation of the AβPP-independent *i*Aβ production pathway. ***T2*** *threshold*: The level of *i*Aβ, produced mainly in the AβPP-independent pathway, which triggers neuronal apoptosis. *Red boxes*: Apoptotic Zone, the range of *i*Aβ concentrations that cause the commitment to apoptosis. *Orange boxes*: The duration of administration of the ACH-based drug. Panels (**A**,**B**): The administration of the ACH-based drug commences prior to the T1 crossing and continues for the remaining lifetime. Panel (**A**): The drug lowers the influx of AβPP-derived *i*Aβ and reduces the rate of its accumulation, but its levels are still increasing. Provided a sufficient lifespan, the levels of AβPP-derived *i*Aβ would eventually cross the T1 threshold and AD would

ensue. Panel (**B**): The reduction in the influx of AβPP-derived *i*Aβ is sufficient to reverse its accumulation; its levels are steadily decreasing. They would not reach the T1 threshold and no AD would occur for the duration of the treatment. Panels (**A′**,**B′**): Effects of the short-term, pre-T1 crossing, administration of the ACH-based drug. Panel (**A′**): Following the cessation of the treatment, the accumulation of AβPP-derived *i*Aβ would resume at a rate equal to that exhibited prior to the treatment, the T1 threshold would be crossed and AD would ensue. In this scenario, the commencement of AD would be delayed by less than the duration of the treatment. Panel (**B′**): Upon termination of the treatment, the accumulation of AβPP-derived *i*Aβ would resume at the pre-treatment rate, the T1 threshold would be crossed, the AβPP-independent *i*Aβ production pathway would be activated, and AD would commence. In this scenario, the delay in the occurrence of the disease would be only slightly longer than the duration of the treatment.

In panel B′ of Figure 4, the accumulation of AβPP-derived *i*Aβ is reversed and its levels decrease. The drug-mediated decrease in the levels of AβPP-derived *i*Aβ is, however, unlikely to be substantial. This is because of the "passive" nature of the decline: it depends on the naturally occurring clearance processes rather than on the direct action of a drug. The notion that the ACH-based drugs do not reduce or do not substantially reduce the levels of AβPP-derived *i*Aβ is consistent with the outcomes of clinical trials of lecanemab (see the following section below), where the pretreatment rate of cognitive decline resumed shortly after the cessation of the treatment. Upon termination of the short-term treatment, the accumulation of AβPP-derived *i*Aβ would resume at the pre-treatment rate, the T1 threshold would be crossed, the AβPP-independent *i*Aβ production pathway would be activated, and AD would commence. In this scenario, the delay in the occurrence of the disease (in comparison with the absence of the treatment) would be slightly longer than the duration of the treatment; more precisely, it would be equal to the duration of the treatment plus the time needed to restore AβPP-derived *i*Aβ to the pre-treatment levels at the pre-treatment rate.

7. Effect of Lecanemab and Donanemab in Early AD: A Dual Proof of Concepts for Inefficiency of ACH-Based Drugs in Symptomatic AD and for Their Applicability in Prevention of AD

7.1. Effect of Lecanemab and Donanemab in Early AD: Mechanistic Interpretation in the ACH2.0 Perspective

Two recently concluded clinical trials of the ACH-based drugs in early symptomatic AD, one of lecanemab and another of donanemab, resulted, for the first time, in a limited (very limited) success [134–137]. In both cases, the rate of cognitive decline decreased, albeit marginally, for the duration of the treatment. Both drugs are ACH-based drugs, i.e., they were designed within the ACH framework with the purpose of decreasing the levels of extracellular Aβ and thus diminishing its toxic effect. The marginal success of both drugs has been construed as evidence that the strategy worked and that the reduction in the extracellular Aβ levels indeed diminished its cytotoxicity. This, however, is inconsistent with the results of multiple preceding clinical trials where levels of extracellular Aβ were significantly reduced (to no lesser degree) by either monoclonal antibodies or by BACE inhibitors but without any efficacy whatsoever. This apparent controversy (within the ACH framework) is convincingly resolved in the ACH2.0 terms, which explain not only how the drugs worked but also why the effect was only marginal.

In both clinical trials, the drugs were administered to the patients exhibiting AD symptoms. In terms of the ACH2.0, these ACH-based drugs were not supposed to work, yet they did. Why? How? The key to understanding the "why" is the timing of the administration of the drugs. In both trials, the earliest measurable symptoms were utilized in the selection of the trials' subjects [134,137]. In terms of ACH2.0, when symptoms manifest, the bulk of the neurons of an affected individual have already crossed the T1 threshold. However, because the T1 crossing is temporally distributed (albeit narrowly) a fraction of neurons may remain sub-T1 in early symptomatic AD, and the earlier symptoms are utilized, the more substantial this fraction is. In the lecanemab and donanemab trials,

in every medicated trial subject, the drugs could not affect the over-T1 neurons but were effective in the sub-T1 neuronal fraction. As an unintended consequence of their design, both drugs, by reducing the levels of extracellular Aβ, lowered the rate of its cellular uptake, decreased the influx of *i*Aβ, and suppressed the rate of AβPP-derived *i*Aβ accumulation. This answers the "how" part: the reduction in the rate of AβPP-derived *i*Aβ accumulation delayed or prevented the crossing of the T1 threshold by and the commencement of AD pathology in the sub-T1 neuronal fraction. The effect of the drugs was marginal because they affected only a marginal fraction of neurons.

The above reasoning is illustrated in Figure 5. Panel A of Figure 5 depicts diagrammatically the neuronal distribution immediately prior to drugs' administration (referred to as the initial state). The bulk of neurons have crossed the T1 threshold and activated the AβPP-independent *i*Aβ production pathway, and some have reached the T2 threshold and committed apoptosis; a small fraction (depicted in green), however, remains sub-T1 at this point. Panel B illustrates the evolution of the initial state in an untreated patient. All affected neurons, including the green fraction, have crossed the T2 threshold; the disease reached its end stage. Panels C and D illustrate two potential outcomes in treated patients. The drugs have no impact on the over-T1 neuronal population; the effect is limited solely to the sub-T1 neuronal fraction. In panel C, the influx of AβPP-derived *i*Aβ is reduced, but it still accumulates, albeit at a slower rate. Eventually, it crosses the T1 threshold, activates the AβPP-independent *i*Aβ production pathway, reaches the T2 threshold, and cells commit apoptosis. This fraction was redeemed, but only temporarily. In panel D, on the other hand, the influx of AβPP-derived *i*Aβ was reduced sufficiently to reverse its accumulation. Its levels are declining and this fraction of neurons is redeemed for the duration of the treatment. It appears likely that in clinical trials either the scenario depicted in panel C played out or, if the levels of AβPP-derived *i*Aβ were actually reduced, the reduction was insignificant. This is because, upon the termination of the treatment, the pre-treatment rate of cognitive decline rapidly resumed [138].

7.2. Outcomes of Lecanemab and Donanemab Clinical Trials Constitute Dual Proof of Concepts: ACH-Based Drugs Are Inefficient in Symptomatic AD but Can Be Effective Preventively

It appears, therefore, that both lecanemab and donanemab worked, albeit in a very limited fashion, not because they are conceptually different from other, "failed" AD drugs but because of the early timing of their administration. In terms of the ACH2.0, it can be safely assumed that any drug lowering the extracellular Aβ levels (and, consequently, reducing its cellular uptake), including multiple Aβ-sequestering monoclonal antibodies, or inhibiting AβPP proteolysis, such as verubecestat, would have a similar effect if administered at the same early symptomatic AD stage, provided that their potential cellular toxicity would not obscure their therapeutic impact.

The outcomes of the clinical trials of lecanemab and donanemab are consistent with the notions explored in the preceding sections, namely that ACH-based drugs cannot be effective in symptomatic AD but could be efficient in the prevention of the disease. Moreover, these results, as interpreted from the ACH2.0 perspective, constitute a dual proof of concepts for these notions. In the preceding sections, when analyzing AD, we considered the "pre-symptomatic" and "symptomatic" phases of the disease. However, the analysis of the effect of lecanemab and donanemab makes it clear that such division is not entirely correct, and that in mechanistic terms, a division into pre-T1 crossing and post-T1 crossing should be always utilized when considering the effects of the ACH-based drugs. This aspect is addressed further in the following sections.

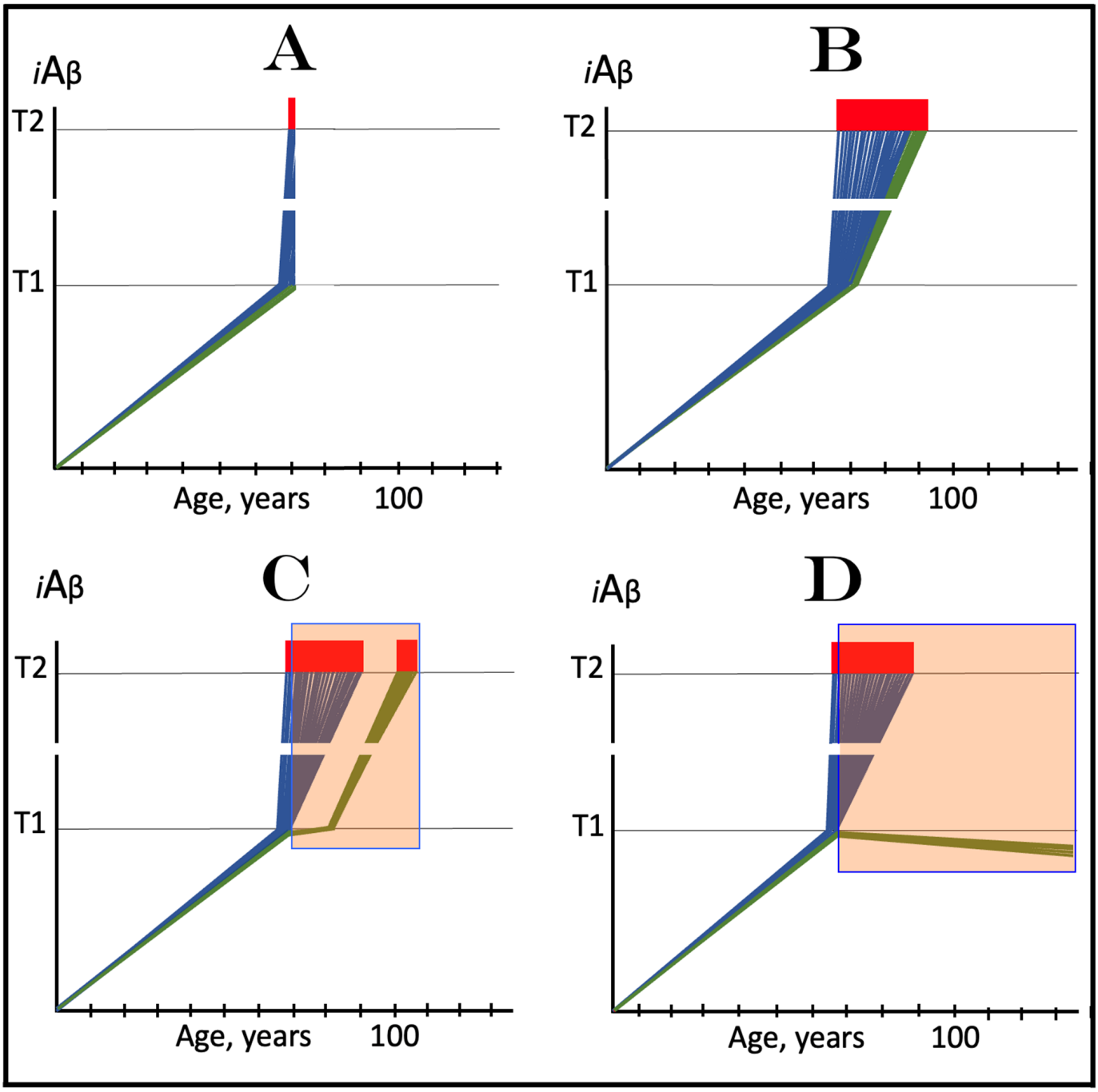

Figure 5. ACH-based drugs can be only marginally effective in early symptomatic AD: lecanemab and donanemab case study. *i*Aβ: Intraneuronal Aβ. *Blue and green lines*: Levels of *i*Aβ in individual neurons. *Green lines*: A neuronal fraction that was sub-T1 at the commencement of a drug administration. ***T1*** *threshold*: The concentration of AβPP-derived *i*Aβ that mediates elicitation of the ISR and triggers the activation of the AβPP-independent *i*Aβ production pathway. ***T2*** *threshold*: The level of *i*Aβ, produced mainly in the AβPP-independent pathway, which triggers neuronal apoptosis. *Red boxes*: Apoptotic Zone, the range of *i*Aβ concentrations that cause the commitment to apoptosis. *Orange boxes*: The duration of administration of lecanemab or donanemab. Panel (**A**): The initial state of *i*Aβ levels in individual neurons at the commencement of the treatment. Most neurons have crossed the T1 threshold but a small neuronal fraction is still sub-T1. Panel (**B**): Evolution of the initial state in the absence of a drug; AD progresses and reaches the end stage. Panels (**C**,**D**): Evolution of the initial state in the presence of lecanemab or

donanemab. Importantly, the drug has no effect in the over-T1 neurons. Panel (**C**): The drug lowers the influx of AβPP-derived *i*Aβ and reduces the rate of its accumulation, but its levels are still increasing and eventually crosses the T1 threshold in the initially sub-T1 neurons; these cells will reach and cross the T2 threshold and commit apoptosis. The effect of the drug would be not only marginal but also temporary. Panel (**D**): The reduction in the influx of AβPP-derived *i*Aβ is sufficient to reverse its accumulation; its levels are steadily decreasing. They would not reach the T1 threshold for the duration of the treatment; the overall effect, however, would be only marginal. For details, see the main text.

8. ACH-Based AD Drugs: Complications with the Long-Term Treatment for Prevention of AD

8.1. Long-Term Treatment with Current ACH-Based Drugs Is Inconceivable in Low-Risk Individuals

Above, in Section 6.2, we have established that the short-term preventive treatment with ACH-based drugs would have little or no effect beyond the duration of the treatment. To be effective, the treatment has to be for a long duration, potentially for the remaining lifetime of an individual, as shown in panels A and B of Figure 4 above. This, however, is entirely inconceivable for the currently available drugs. These drugs have to be delivered intravenously and frequently [134–138]. But this is a minor inconvenience considering their adverse effect: both lecanamab and donanemab caused life-threatening brain swelling and bleeding in treated individuals [134–138]. It can be firmly stated that in low-risk individuals, the possible harm from these drugs significantly outweighs their potential benefits. Conceivably, other types of drugs that reduce the influx of AβPP-derived *i*Aβ could be developed. For example, a small-molecule drug that suppresses the cellular uptake of extracellular Aβ would be no less, and possibly more, effective in the prevention of AD than lecanemab and donanemab. Inhibitors of AβPP proteolysis could be even more effective (because they would suppress both venues of the influx of AβPP-derived *i*Aβ, its retention and importation) provided their toxicity, such as was seen with verubecestat, is substantially reduced or eliminated. These proposed drugs are ACH-based. On the other hand, the present study suggests, as reflected in its title, a new, ACH2.0-based class of drugs that would be equally effective in both the prevention and treatment of AD and would render the ACH-based drugs obsolete (see below).

8.2. Long-Term ACH-Based Drugs Treatment for Prevention of Sporadic AD Would Be Inefficient in High-Risk Individuals

One may argue that whereas the employment of current ACH-based drugs for the prevention of AD is unacceptable in low-risk individuals, it is justified in high-risk persons. This may be correct in principle. The reality, however, is different. The reason is a profound distinction between the crossing of the T1 threshold and the manifestation of AD symptoms. The former signifies the commencement of the disease. It is closely followed by the activation of the AβPP-independent *i*Aβ production pathway. This pathway is self-sustainable and thus irreversible unless interfered with therapeutically, which is currently impossible. There is, however, a substantial gap between the times the levels of AβPP-derived *i*Aβ cross the T1 threshold and, consequently, the neurons "commit", via the activation of the AβPP-independent *i*Aβ production pathway, to the progression of the disease, and the times AD symptoms manifest. This is the period required for sufficient accumulation of *i*Aβ produced in the AβPP-independent pathway, and it could be measured potentially in years. By definition, a high-risk individual is one who is asymptomatic but presents indications for an imminent development of AD symptoms. It could be assumed, with high probability, that in such an individual, a substantial portion, if not the majority or even the entirety, of the affected neurons have already crossed the T1 threshold. These neurons would be completely unresponsive to the ACH-based drugs. The drugs would delay or prevent the T1 crossing by a still sub-T1 neuronal fraction but its overall therapeutic effect would be insignificant.

The above scenario is illustrated in Figure 6. Panel A depicts the initial state of the neuronal population of a high-risk individual. The levels of AβPP-derived *i*Aβ have crossed the T1 threshold and the AβPP-independent *i*Aβ production pathway has been activated in the majority of the affected neurons (referred to as "over-T1"), whereas a fraction of affected neurons remains sub-T1 by the time of the drug administration. Panel B of Figure 6 shows the evolution of the initial state in the absence of the treatment. The levels of AβPP-derived *i*Aβ reach and cross the T1 threshold in the initially sub-T1 neuronal fraction. The AβPP-independent *i*Aβ production pathway is activated in all affected neurons. The T2 threshold is crossed and apoptosis is triggered in all affected neurons; the disease reaches the end stage. Panel C of Figure 6 shows the evolution of the initial state of the neuronal population in a high-risk individual treated with an ACH-based drug (orange box). As discussed above, the over-T1 neurons are not affected by the drug. In these cells, *i*Aβ, produced independently of AβPP, accumulates and drives AD pathology. AD symptoms manifest, neurons reach and cross the T2 threshold, and commit apoptosis. The sub-T1 neurons, on the other hand, are protected by the drug (to simplify the discussion, the best case scenario is assumed: the drug reverses the accumulation of AβPP-derived *i*Aβ and its levels steadily decrease). This neuronal fraction is redeemed for the duration of the treatment but the overall therapeutic effect of the drug could be insignificant.

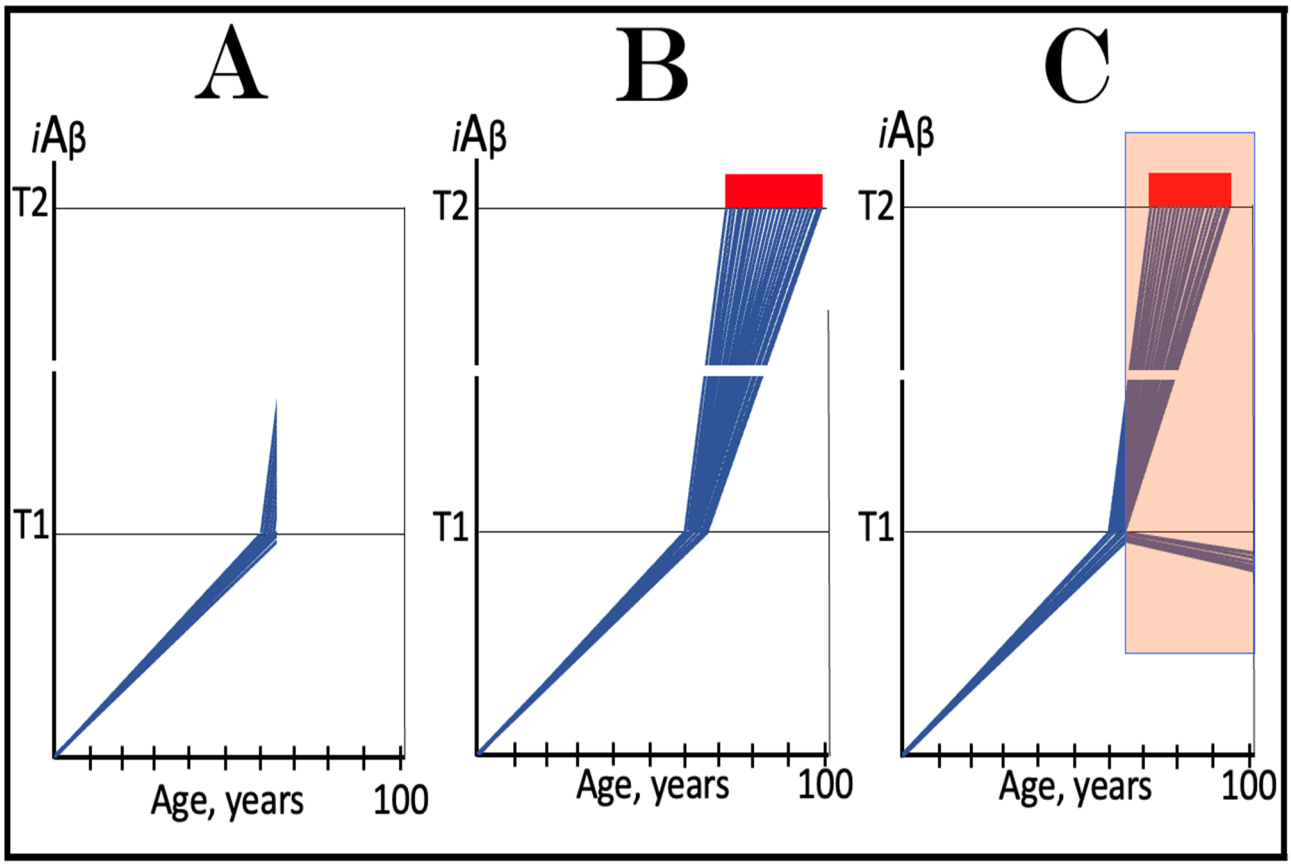

Figure 6. ACH-based drugs would be inefficient for prevention of AD in high-risk individuals. *i*Aβ: Intraneuronal Aβ. *Blue lines*: Levels of *i*Aβ in individual neurons. ***T1*** *threshold*: The concentration of AβPP-derived *i*Aβ that mediates elicitation of the ISR and triggers the activation of the AβPP-independent *i*Aβ production pathway. ***T2*** *threshold*: The level of *i*Aβ, produced mainly in the AβPP-independent pathway, which triggers neuronal apoptosis. *Red boxes*: Apoptotic Zone, the range of *i*Aβ concentrations that cause the commitment to apoptosis. *Orange box*: The duration of administration of an ACH-based drug. Panel (**A**): The initial state of the *i*Aβ levels in the neuronal population. The individual is asymptomatic, yet a significant fraction of the affected neurons have

crossed the T1 threshold and activated the AβPP-independent *i*Aβ production pathway; these neurons are insensitive to the ACH-based drugs. Panel (**B**): The evolution of the initial state in the absence of the treatment. The levels of *i*Aβ cross the T1 threshold in all affected neurons. Eventually, the T2 threshold is crossed, cells commit apoptosis, and the disease reaches the end stage. Panel (**C**): The evolution of the initial stage in the presence of the ACH-based drug. The over-T1 neurons are not affected by the drug. In these cells, *i*Aβ, produced independently of AβPP, accumulates and drives the AD pathology; neurons reach and cross the T2 threshold and commit apoptosis. The sub-T1 neurons, on the other hand, are protected by the drug (to simplify discussion, the best case scenario is assumed: the drug reverses the accumulation of AβPP-derived *i*Aβ and its levels steadily decrease). This neuronal fraction is redeemed for the duration of the treatment but the overall therapeutic effect of the drug could be insignificant.

9. In the ACH2.0 Paradigm, ACH-Based Drugs Should Be Effective in Treatment of AACD

In terms of ACH2.0, Aging-Associated Cognitive Decline is a segment of the first stage of AD in individuals with a sufficiently high extent of the T1 threshold [2,4]. AACD commences upon the crossing of the T^0 threshold and either continues for the remaining lifespan or morphs into AD if the T1 threshold is subsequently crossed (illustrated in Figure 3 above). Like Alzheimer's disease, it is driven by *i*Aβ but, in contrast to AD, it is solely AβPP-derived *i*Aβ at levels ranging from the T^0 to T1 thresholds ("AACD Zone" is defined above as sub-T1 levels of AβPP-derived *i*Aβ causing neuronal damage manifesting as AACD). It follows that the ACH-based drugs could potentially be effective in the treatment, even cure, of AACD. Indeed, if a drug is administered that lowers the rate of accumulation of AβPP-derived *i*Aβ, the rate of the progression of the condition will slow down accordingly for the duration of the treatment. Moreover, if an ACH-based drug were employed, which suppresses the influx of AβPP-derived *i*Aβ sufficiently to reverse its accumulation, its levels would be steadily declining for the duration of the treatment. Eventually, the levels of AβPP-derived *i*Aβ can cross, in a reverse direction, the T^0 threshold. If and when this occurs, the levels of AβPP-derived *i*Aβ would be below the T^0 threshold and the patient would be cured (technically; the degree of cure would depend on the ability of the affected neurons to restore their functionality and of cognitive functions to recover). The potential outcomes of these scenarios appear to be AACD stage-specific and are further discussed and illustrated in Section 11 below.

10. ACH-Based Drugs Were Spectacularly Successful in Transgenic AD Models for the Same Reason They Would Be in AACD: Mechanistic Interpretation in the ACH2.0 Perspective

In contrast to their complete inefficiency in symptomatic AD, the ACH-based drugs were spectacularly effective in transgenic AD models: they reduced, even reversed, various symptoms of the disease [8–10]. In terms of ACH2.0, the reason for this is the AβPP-independent *i*Aβ production pathway. In humans, it renders the Aβ production in the AβPP proteolytic pathway irrelevant to the progression of the disease and brands its targeting at symptomatic stages as futile (see above). *In mice, however, it is inoperative*. Indeed, Alzheimer's disease appears to be human-specific, or at least species-specific; it does not occur even in long-living mammals such as elephants. As discussed elsewhere [4], four physiologically occurring mechanisms could be responsible for the operation of the AβPP-independent *i*Aβ production pathway in humans. Of those, the most plausible is the asymmetric RNA-dependent amplification of AβPP mRNA [4]. While human AβPP mRNA is eligible for this process, its mouse counterpart is not, and human AβPP mRNA expressed in transgenic models is also rendered ineligible due to its altered (during transgene construction) 5′ terminus [4].

The absence of the AβPP-independent *i*Aβ generation pathway in transgenic AD models explains why they never develop the full spectrum of AD pathology, most notably neurofibrillary tau tangles. Moreover, it can be unequivocally stated that *the current transgenic AD models can never develop AD; they are not really "AD models"*. This is in accordance

with the definition of AD as a condition initiated and driven by the AβPP-independent *i*Aβ production pathway and with the presumed mechanistic inability to reach the adequate AD pathology-driving levels of *i*Aβ with the AβPP-independent pathway of its production inoperative. From this perspective, the transgenic AD models are, in fact, models of AACD, or of "enhanced" AACD. As in AACD, transgenic models accumulate AβPP-derived *i*Aβ via its intraneuronal retention and through cellular uptake of secreted Aβ. Because, in these models, Aβ is acutely overproduced from multiple AβPP transgenes (typically containing FAD and/or PSEN mutations), AβPP-derived *i*Aβ accumulates faster and to a higher extent, and could cause symptoms more severe than in typical AACD, hence "enhanced AACD". In addition, in these models, the levels of *i*Aβ are sufficient to elicit the ISR, which, in turn, causes the impairment of learning and long-term memory formation due to suppression of protein synthesis. Therefore, it can be stated that the ACH-based drugs were spectacularly effective in the treatment of symptoms in transgenic models precisely for the same reason they should be effective in AACD, namely due to their ability to reduce or reverse the rate of AβPP-derived *i*Aβ accumulation. The current transgenic "AD" models can be useful for multiple purposes, but their utility in the investigation of AD is acutely limited. The principles of design and construction of an adequate human-neuronal-cell-based AD model are described elsewhere [1,2,4]. Eventually, with a fuller understanding of the molecular mechanism underlying the AβPP-independent *i*Aβ generation pathway, transgenic animal models can be developed where this pathway is operative, and which faithfully epitomizes the disease. In the ACH2.0 paradigm, the operative AβPP-independent *i*Aβ production pathway is the fundamental requirement for any such model.

11. ACH-Based Drugs in Treatment of Different Stages of AACD

The present section addresses only the effects of the long-duration employment of ACH-based drugs in the treatment of AACD. This is because the short-term deployment of these drugs is inapplicable in AACD for the same reason they are unsuitable, as discussed in Section 6.2 above, for the prevention of AD, with the effect lasting not much longer, and possibly shorter, than the duration of the treatment.

In virtually any disease, the earliest possible intervention is the most beneficial. This is certainly the case with AACD. The essence of the treatment of AACD is either the reduction in the rate of accumulation of AβPP-derived *i*Aβ or the reversal of its accumulation and the decrease in its levels (the latter is, of course, preferable, but it depends on the efficiency of the drug in suppressing the influx of AβPP-derived *i*Aβ). The sooner after the diagnosis the treatment starts, the lower the AβPP-derived *i*Aβ baseline is, the less neurodegeneration occurs, and the more effective the treatment will be. Figure 7 depicts two possible modes of action of the ACH-based drugs administered at the early and progressively advancing stages of AACD.

In panels A and B of Figure 7, the levels of AβPP-derived *i*Aβ have just crossed the T^0 threshold in all affected neurons of AACD patients; the condition has commenced and is progressing. It has a long way to go: in a typical AACD case, the extent of the T1 threshold appears to be substantially higher than that of T^0, as suggested by the observation that AACD patients develop AD only infrequently. Panel A shows the effect of an ACH-based drug that reduces the rate of AβPP-derived *i*Aβ accumulation. The accumulation continues but the *i*Aβ levels increase significantly slower than pre-treatment. Consequently, since the severity of the disease is a function of the levels of AβPP-derived *i*Aβ within the AACD Zone [4], the condition is substantially milder than it would have been if untreated. Panel B of Figure 7 illustrates the effect of an ACH-based drug that reduces the influx of AβPP-derived *i*Aβ sufficiently to reverse its accumulation. Its levels steadily decrease and eventually cross, in reverse, the T^0 threshold. At this point, the patient is technically cured and remains disease-free for the duration of the treatment. Arguably, this is one of only a few scenarios where the utilization of the current ACH-based drugs could be justified, due to the certainty of the outcomes.

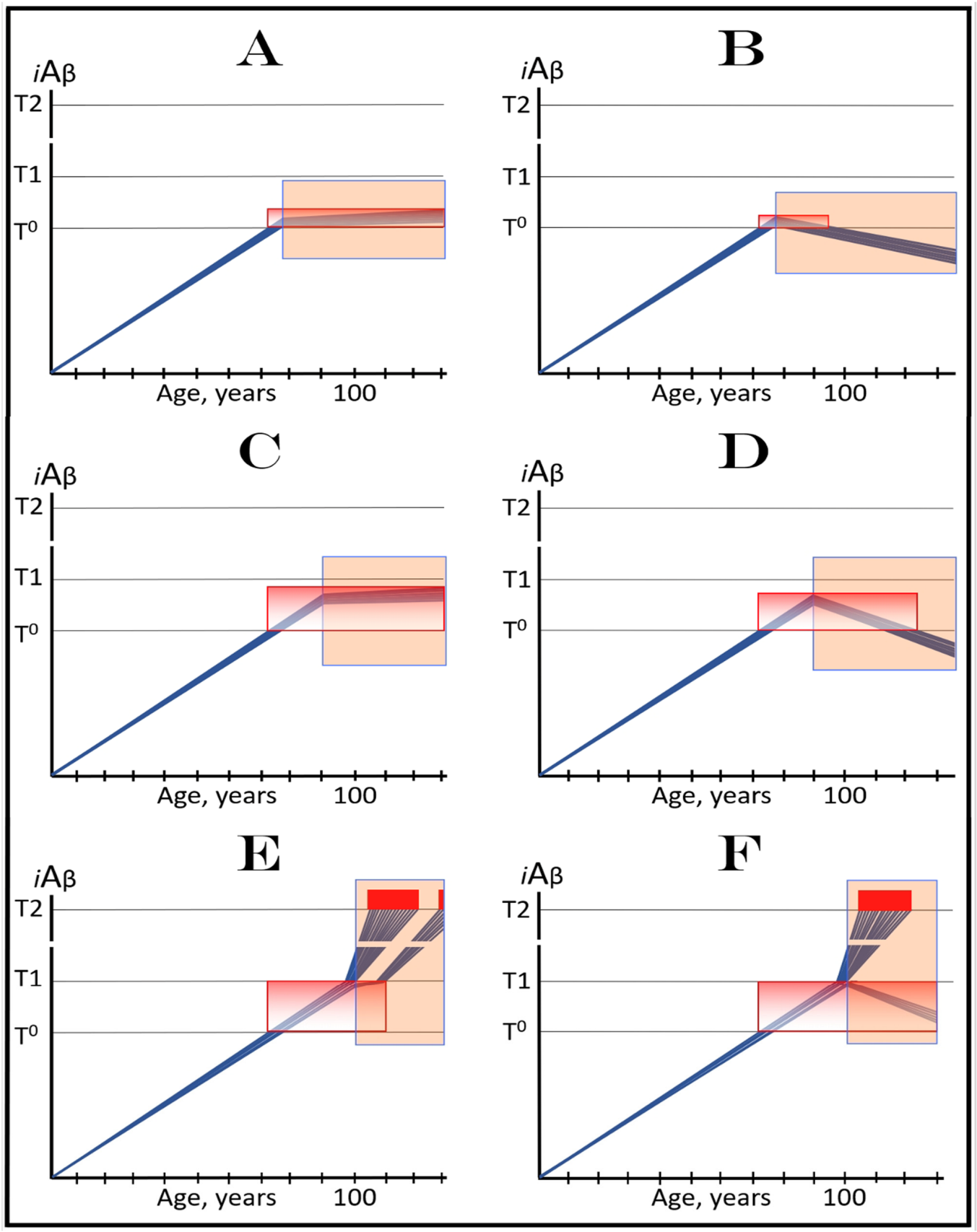

Figure 7. ACH-based drugs could be effective in the treatment of AACD but not at its late stages. *i*Aβ: Intraneuronal Aβ. *Blue lines*: Levels of *i*Aβ in individual neurons. ***T*^{0}** *threshold*: The concentration of *i*Aβ that triggers the neurodegeneration manifesting as AACD. ***T1*** *threshold*: The

concentration of AβPP-derived *i*Aβ that mediates elicitation of the ISR and triggers the activation of the AβPP-independent *i*Aβ production pathway. ***T2*** *threshold*: The level of *i*Aβ, produced mainly in the AβPP-independent pathway, which triggers neuronal apoptosis. *Pink gradient boxes*: AACD Zone, the range of concentration of AβPP-derived *i*Aβ between the T^0 and T1 boundaries. *Red boxes*: Apoptotic Zone, the range of *i*Aβ concentrations that cause the commitment to apoptosis. *Orange boxes*: The duration of administration of an ACH-based drug. Panels (**A**,**B**): ACH-based drugs in early AACD. Panel (**A**): The drug reduces the rate of AβPP-derived *i*Aβ accumulation and its levels increase significantly slower than pre-treatment. Since the severity of the disease is a function of the levels of AβPP-derived *i*Aβ within the AACD Zone, the condition is substantially milder than it would have been if untreated. Panel (**B**): The drug reverses the rate of the AβPP-derived *i*Aβ accumulation. Its levels steadily decrease and eventually cross, in reverse, the T^0 threshold. At this point the patient is technically cured and remains disease-free for the duration of the treatment. Panels (**C**,**D**): Effect of an ACH-based drug at mid-stage of AACD. Panel (**C**): The drug reduces the rate of AβPP-derived *i*Aβ accumulation. AACD progresses significantly slower and is milder than it would in the absence of a drug. Panel (**D**): The drug reverses the rate of accumulation of AβPP-derived *i*Aβ and causes steady decrease in its levels; the condition of a patient is likely to stabilize and even improve for the duration of the treatment. Panels (**E**,**F**): ACH-based drugs in late AACD. The patient is asymptomatic for AD but a substantial neuronal fraction has crossed the T1 threshold and was rendered insensitive to ACH-based drugs; these neurons eventually cross the T2 threshold and commit apoptosis. In panel (**E**), the drug reduces the rate of AβPP-derived *i*Aβ accumulation. The initially sub-T1 neurons cross the T1 and proceed toward the T2 threshold and eventual apoptosis but with a considerable delay. In panel (**F**), the rate of AβPP-derived *i*Aβ accumulation is reversed. The sub-T1 neurons are protected for the duration of the treatment but the overall effect in panels (**E**,**F**) is insignificant.

In panels C and D of Figure 7, the levels of AβPP-derived *i*Aβ in the affected neurons of AACD patients have traversed about half the distance between the T^0 and T1 thresholds. This is the initial state at the time of the administration of a drug. Panel C illustrates the effect of an ACH-based drug that reduces the rate of accumulation of AβPP-derived *i*Aβ. Its levels continue to increase as a function of time but much slower than prior to the commencement of the treatment. Likewise, AACD progresses significantly slower and is milder than it would in the absence of a drug. Moreover, in contrast to an untreated patient, the levels of AβPP-derived *i*Aβ would not cross, as shown, the T1 threshold within the lifetime of an individual (or would cross it much later) and AACD would not evolve into AD (or would with a significant delay). Panel D of Figure 7 depicts the effect of an ACH-based drug that reverses the rate of accumulation of AβPP-derived *i*Aβ and causes a steady decrease in its levels. As a result, the condition of a patient is likely to stabilize and even improve for the duration of the treatment.

Panels E and F of Figure 7 depict a scenario where a fraction of the affected neurons have reached and crossed the T1 threshold but an AACD patient is asymptomatic for AD. The evolution of this initial state in the presence of a drug is more complex than in the two preceding scenarios. Regardless of the effect of an ACH-based drug on the rate of accumulation of AβPP-derived *i*Aβ, it will have no therapeutic effect on the over-T1 neurons because in these cells, the AβPP-independent *i*Aβ production pathway has been already activated. The levels of *i*Aβ generated in this pathway will steadily increase and cross the T2 threshold; cells will commit apoptosis and this neuronal fraction will be lost. Any ACH-based drug would affect only the neurons that are still sub-T1. In panel E of Figure 7, an ACH-based drug suppresses the rate of accumulation of AβPP-derived *i*Aβ but its levels keep increasing. Eventually, they will reach and cross the T1 threshold in all initially sub-T1 neurons. The AβPP-independent *i*Aβ production pathway will be activated, and AACD will evolve into AD. In this scenario, therefore, a fraction of affected neurons would be redeemed by an ACH-based drug but only temporarily. In panel F of Figure 7, on the other hand, an ACH-based drug suppresses the influx of

AβPP-derived *i*Aβ sufficiently to reverse the rate of its accumulation and its levels are steadily decreasing. In this scenario, although the over-T1 neuronal fraction will be eventually lost, the sub-T1 neurons will be redeemed for the duration of the treatment. In either case (panels E and F), however, the overall effect of the ACH-based drug would be insignificant.

12. Symptoms of AACD-Related Cognitive Impairment Overlap with and Are Indistinguishable from Those of AD-Associated MCI: Ramifications for ACH-Based Drugs Therapy

The AACD Zone is, by definition, a range of *i*Aβ concentrations that trigger the neurodegeneration, which manifests as AACD [4]. The lower boundary of this range is the T^0 and the upper boundary is the T1 threshold. However, whereas the former is tangible, the latter is not. For the sake of argument, we can define AACD Zone as a range of *i*Aβ concentrations starting at the T^0 threshold and continuing upward to some arbitrary level. If the upper level happens to be the T1 threshold, the two definitions are identical. Alternatively, we can envision this scenario as the end of the lifespan coinciding with the moment when AβPP-derived *i*Aβ reaches (but does not cross) the T1 threshold, as shown in Figure 8, panel A. But what if the T1 threshold is lower than the chosen upper level, or if AβPP-derived *i*Aβ crosses the T1 threshold within the range defined above? This is an important question because the same symptoms could be attributable to different sources. One situation where this issue arises is depicted in panel B of Figure 8. As we reasoned earlier, upon the T1 crossing, the AβPP-independent *i*Aβ production pathway is activated, AD commences, and AACD morphs into AD. Since, by definition, the extent of the neurodegeneration and, accordingly, the symptoms reflect the *i*Aβ concentrations, the same symptoms would manifest within the same *i*Aβ range (gradient pink boxes; the extents of the T^0 threshold are identical in all panels of Figure 8). While in panel A, these symptoms can be clearly defined as AACD-related cognitive impairment, in panel B, they are composed of AACD-related impairment and AD-associated mild cognitive impairment (MCI). An even more drastic situation is presented in panel C of Figure 8. In this panel, the extent of the T^0 threshold is the same as in panels A and B, but it is higher than the T1 threshold. Technically, there is neither an AACD Zone nor an AACD Zone. Here, the range of *i*Aβ concentrations corresponding to that considered in panels A and B consists mostly of *i*Aβ generated independently of AβPP, but since the range (gradient pink box) is the same in panels A, B, and C, so are the symptoms. In panel C, however, the symptoms are attributable, in their entirety, to AD-associated MCI. The point of this discussion is to demonstrate that within a certain range, symptoms of AACD on MCI are overlapping and indistinguishable (they can be properly attributed only by measuring the activity of the AβPP-independent *i*Aβ production pathway; see below). In the above scenarios, the only tangible difference is that when the levels of *i*Aβ cross the T1 threshold, the integrated stress response is elicited. At this point, as discussed above, cellular protein synthesis is reprogrammed and largely inhibited. Eventually, this inhibition would affect learning and long-term memory formation, which require de novo protein synthesis; there is, however, a considerable gap between the elicitation of the ISR and the manifestation of these consequences. It could be argued that the difference in the attribution of similar symptoms to AACD or AD is purely a semantic exercise; however, it is not.

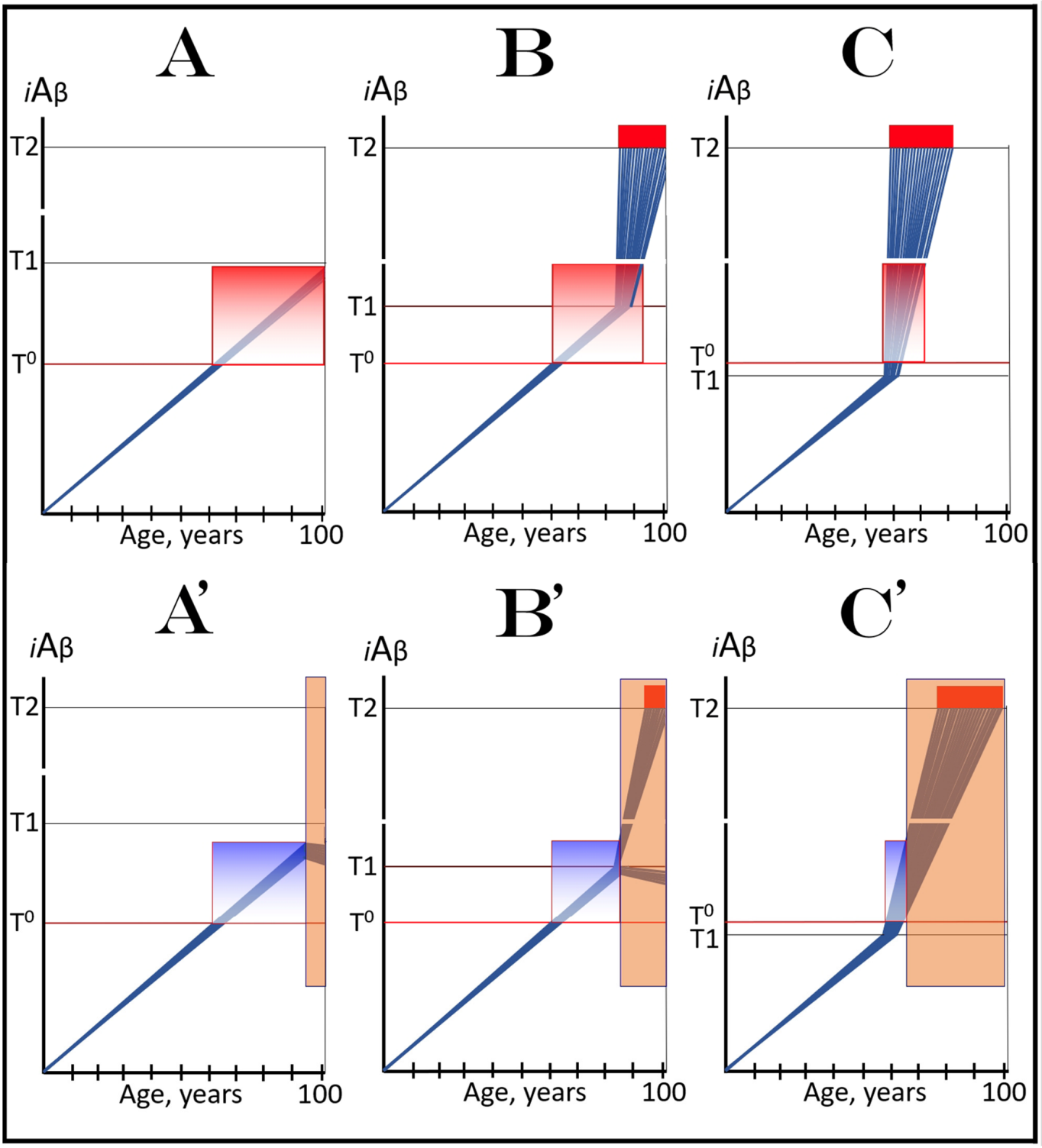

Figure 8. Symptoms of AACD overlap with and are indistinguishable from those of AD-Associated MCI: Ramifications for ACH-based drugs therapy. *i*Aβ: Intraneuronal Aβ. *Blue lines*: Levels of *i*Aβ in individual neurons. ***T*^{0}** *threshold:* The concentration of *i*Aβ that triggers the neurodegeneration manifesting as AACD. ***T1*** *threshold*: The concentration of AβPP-derived *i*Aβ that mediates elicitation of the ISR and triggers the activation of the AβPP-independent *i*Aβ production pathway. ***T2*** *threshold*: The level of *i*Aβ, produced mainly in the AβPP-independent pathway, which triggers neuronal apoptosis. *Pink gradient boxes*: AACD Zone or its equivalents in terms of the range of concentrations of AβPP-derived *i*Aβ. *Blue boxes*: The defined range of concentrations of AβPP-derived *i*Aβ within

AACD Zone or its equivalents. *Red boxes*: Apoptotic Zone, the range of *i*Aβ concentrations that cause the commitment to apoptosis. *Orange boxes*: The duration of administration of an ACH-based drug. Panel (**A**): The T1 threshold is not crossed. AACD commences with the crossing of the T^0 threshold and continues for the remaining lifespan; the *i*Aβ–caused cognitive impairment is entirely attributable to AACD. Panel (**B**): The T1 threshold is lowered. The same range of *i*Aβ consists of the pre-T1 crossing and post-T1 crossing portions. The symptoms caused by the former are AACD-associated whereas those caused by the latter constitute AD-associated mild cognitive impairment. Panel (**C**): The T1 threshold is further lowered. The same range of *i*Aβ concentrations is wholly post-T1 crossing, and the corresponding symptoms are attributable entirely to AD-associated MCI. Panel (**A'**): ACH-based drug is administered prior to the T1 crossing and protects the entire neuronal population for the duration of the treatment. Panel (**B'**): The drug is administered when a significant neuronal fraction has already crossed the T1 threshold. This fraction is eventually lost; only the sub-T1 neuronal fraction is protected for the duration of the treatment. Panel (**C'**): ACH-based drug is administered within the same *i*Aβ range, but after the entire neuronal population has crossed the T1 threshold; it has no protective effect whatsoever. For details, see the main text.

The designations of symptoms as AACD-related cognitive impairment of AD-associated MCI are of great functional importance because they implicate fundamentally different underlying mechanisms. AACD-related impairment is propagated by *i*Aβ produced by AβPP proteolysis, whereas AD-associated MCI is driven by *i*Aβ generated in the AβPP-independent pathway. Thus, the distinction between etiological origins of potentially overlapping symptoms is not semantic but a functional and practical issue, as illustrated in panels A' through C' of Figure 8. In panel A', the treatment with an ACH-based drug is implemented when the levels of AβPP-derived *i*Aβ are within the AACD Zone, i.e., below the T1 and above the T^0 thresholds (the *i*Aβ range between the T^0 threshold and the level of the treatment implementation is shown as blue boxes), and the symptoms are, unquestionably, AACD-related cognitive impairment. The ACH-based drug would be very effective in this situation (to simplify the discussion, the "best case scenario" is shown: the drug reverses the accumulation of AβPP-derived *i*Aβ and causes a steady decrease in its levels), levels of AβPP-derived *i*Aβ would steadily decrease for the duration of the treatment, and the condition of the patient would stabilize and potentially improve. In panel B' of Figure 8, the treatment is administered when the levels of *i*Aβ have reached the same extent as in panel A'. At this time, however, a fraction of the affected neurons have already crossed the T1 threshold and activated the AβPP-independent *i*Aβ production pathway. The drug is effective only in the still sub-T1 neurons; in this neuronal subpopulation, the accumulation of AβPP-derived *i*Aβ is reversed and cells are redeemed for the duration of the treatment. On the other hand, the drug has no effect on the over-T1 neuronal fraction; it reaches the T2 threshold and is eventually lost. In panel C' of Figure 8, the entire "blue" range is above the T1 threshold, and the patient's condition is unquestionably AD-associated MCI. Because the AβPP-independent *i*Aβ production pathway has been activated, the drug has no effect; *i*Aβ levels would progress to the T2 threshold and trigger apoptosis in the entire neuronal population. The bottom line is that in panels A' through C', the ACH-based drug was administered at the same symptomatic stage but with drastically different consequences. The reason for this is that the treatment was implemented at different conditions (i.e., AACD versus AD), indistinguishable to us due to the current inability to detect the T1 crossing in human patients (practically, the T1 crossing can be ascertained only via the detection of the operation of the AβPP-independent *i*Aβ production pathway, not feasible currently in human subjects). It follows that if a drug would be able to reduce the levels of not only AβPP-derived *i*Aβ but also of *i*Aβ generated independently of AβPP, it would be equally effective in all three situations (panels A' through C'). Just such a class of drugs, the ACH2.0-based drugs, is, in fact, described below.

13. Clinical Trials of ACH-Based Drugs in Prevention of AD with All Participants at Sub-T1 Levels of *i*Aβ: Apparently Straightforward but Impractical

Above, we have established that ACH-based drugs are limited in their utility. Indeed, their short-term employment is ineffective, their long-term engagement is highly problematic, and their implementation at the symptomatic stages of AD is futile. Severe limitations of ACH-based drugs apply not only to their utilization but extend also to the evaluation of their efficiency in clinical trials. The present and two following sections analyze the potential outcomes of clinical trials of ACH-based drugs in the prevention of AD. The decisive variable in such trials is the composition of a trial's cohorts. The present section considers an ideal scenario and concludes that it is impractical. The following section analyzes the outcomes of a trial with cohorts reflecting the general population of age close to or exceeding the statistical age of the late onset of AD and decides that they could be grossly misleading. Section 15 examines the outcomes of a trial with cohorts composed of high-risk individuals and establishes that they would be either impossible or uninformative.

Figure 9 illustrates the outcomes of an "ideal" clinical trial of an ACH-based drug in the prevention of AD, with every line representing an individual trial subject. Such a trial is "ideal" in that all its subjects are not just asymptomatic for AD but sub-T1, i.e., the levels of AβPP-derived *i*Aβ in all their neurons are below the T1 threshold. Panel A of Figure 9 shows the initial state of the levels of *i*Aβ in trial subjects immediately prior to the administration of a drug. Panel B depicts the evolution of the initial state in the placebo group. In this cohort, a fraction of trial participants would cross the T1 threshold and activate the AβPP-independent *i*Aβ generation pathway. The levels of *i*Aβ produced in this pathway would rapidly increase. Upon reaching the Ts threshold (Ts signifies the symptomatic threshold) and crossing into the Symptomatic Zone (pink box), they would trigger the manifestation of symptoms of AD.

Panels C and D of Figure 9 illustrate the evolution of the initial state in medicated trial subjects (orange boxes show the duration of the treatment). In panel C, the ACH-based drug decreases the influx of AβPP-derived *i*Aβ and thus suppresses the rate of its accumulation. The reduction in the rate of accumulation, however, is not sufficient to reverse it, and the levels of AβPP-derived *i*Aβ keep increasing. Following the T1 crossing, the AβPP-independent *i*Aβ production pathway, which is insensitive to the ACH-based drugs, would be activated and the progression of the disease would be identical to that in the placebo cohort; the manifestation of the symptoms of AD would eventually occur but with a significant delay. In some participants, this delay is sufficient to prevent the occurrence of AD within their lifetimes. In panel D of Figure 9, the reduction in the influx of AβPP-derived *i*Aβ is sufficient to reverse the rate of its accumulation. The levels of AβPP-derived *i*Aβ steadily decrease and would not cross the T1 threshold for the duration of the treatment. In this scenario, the drug would prevent the disease.

In such an "ideal" trial for the prevention of AD, the outcomes would be clear and easily interpretable. Such a trial, however, is impractical. The problem is the selection of trial subjects with levels of AβPP-derived *i*Aβ certainly below the T1 threshold. Sporadic AD symptoms start manifesting, statistically, at about the age of 65. The T1 threshold, however, is crossed long, probably years, before the manifestation of the symptoms [4]. Upon the T1 crossing, the AβPP-independent *i*Aβ generation pathway is activated, which renders ACH-based drugs completely inadequate: they would still suppress the influx of AβPP-derived *i*Aβ but now its contribution to the cellular *i*Aβ pool is only marginal and thus irrelevant to the progression of the disease. Since currently, as discussed above, we lack tools for detecting the T1 crossing in human subjects, the only means to ascertain that over-T1 individuals are not included in a trial is to limit the age of the trial subject to that well below the statistical age of the late onset of AD. This, however, translates into a long wait, possibly a decade or more, for AD cases to develop (at least in the placebo cohort), thus rendering this type of trial impractical. The following two sections address the consequences of the inclusion of asymptomatic over-T1 individuals in clinical trials.

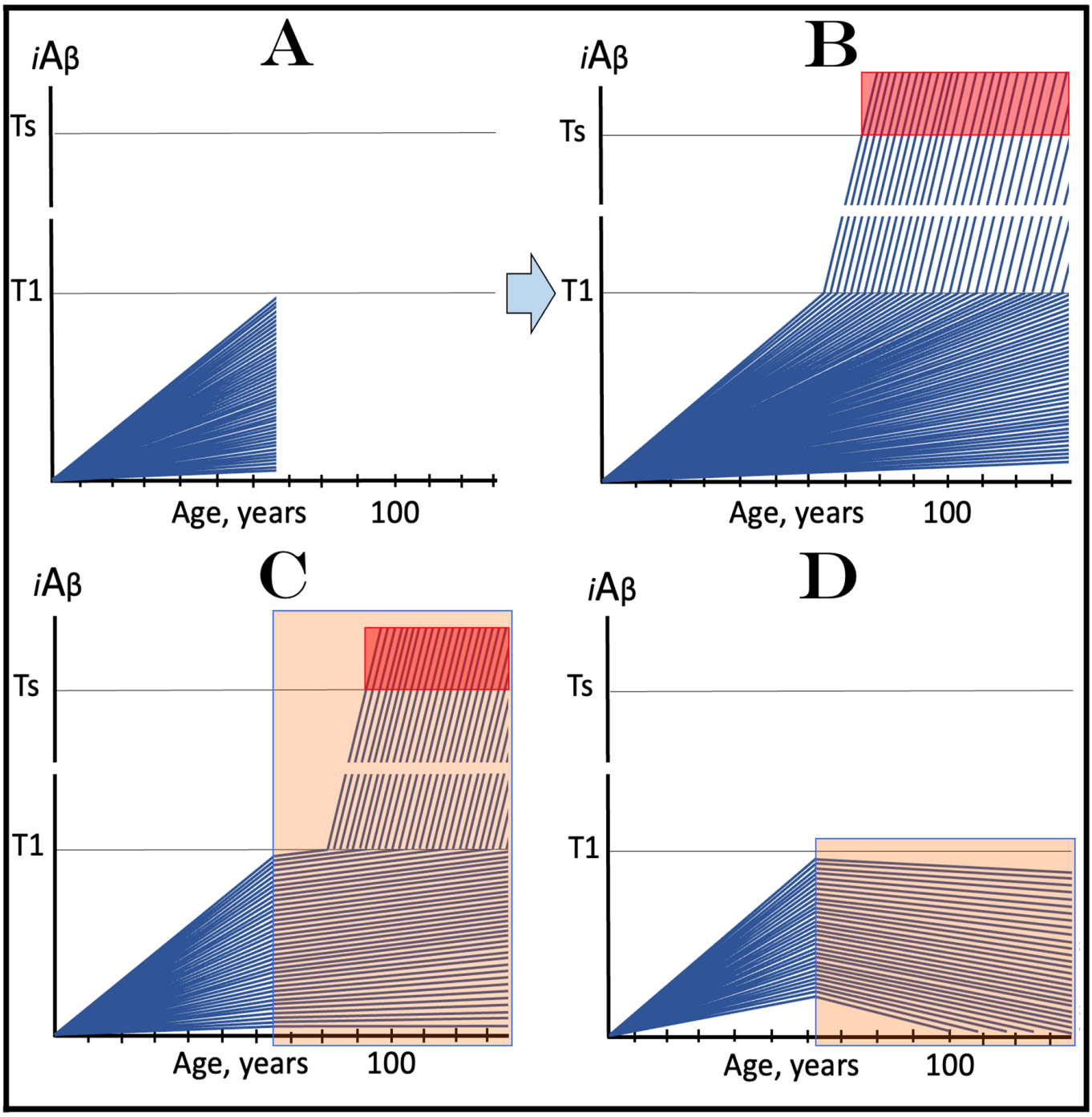

Figure 9. Clinical trials of ACH-based drugs in prevention of AD with all trial subjects at sub-T1 levels of *i*Aβ. *i*Aβ: Intraneuronal Aβ. *Blue lines*: The levels of *iA*β in individual trial subjects. ***T1*** *threshold*: The concentration of AβPP-derived *i*Aβ that mediates elicitation of the ISR and triggers the activation of the AβPP-independent *i*Aβ production pathway. ***Ts*** *threshold*: The levels of *i*Aβ that trigger the manifestation of AD symptoms. *Pink boxes*: Symptomatic Zone, the range of *i*Aβ concentrations above the Ts threshold. *Orange boxes:* The duration of administration of an ACH-based drug. Panel (**A**): The initial state of *i*Aβ levels in individual trial subjects at the commencement of the treatment. Panel (**B**): The evolution of the initial state in the untreated individuals (the placebo group). In the majority of subjects, the levels of *i*Aβ do not cross the T1 threshold within the lifespan of an individual. In those subjects where it does, the AβPP-independent pathway of *i*Aβ production

is triggered, the levels of *i*Aβ cross the Ts threshold and AD symptoms manifest. Panels (**C**,**D**): The evolution of the initial state in the medicated trial participants. Panel (**C**): The drug lowers the rate of accumulation of AβPP-derived *i*Aβ but its levels keep increasing. In a fraction of participants, they cross the T1 threshold and trigger the AD symptoms. The outcome is principally the same as in the placebo group, but is preceded by a lag period; in another fraction, the delay is sufficient to prevent the disease. Panel (**D**): The drug causes the reversal of the accumulation of AβPP-derived *i*Aβ. Its levels do not cross the **T1** threshold; no disease occurs in trial participants for the duration of the treatment.

14. Clinical Trials of ACH-Based Drugs in Prevention of AD with Participants Representing a Cross-Section of the General Population Aged 65 and Over: Results Could Be Grossly Misleading

14.1. The Overall Picture

The present section considers clinical trials of ACH-based drugs in the prevention of AD with participants representing a cross-section of the general population close to and over the statistical age of the late onset of AD (about 65 years). At this age, only a minor fraction of the population is going to develop AD (about 10% at 65 and increasing with age). All trial subjects are asymptomatic for AD. It is, however, inevitable that in some the levels of AβPP-derived *i*Aβ have already crossed the T1 threshold, and the AβPP-independent *i*Aβ production pathway has been already activated. Such an initial state is depicted in panel A of Figure 10. The evolution of this initial state in the placebo cohort, shown in panel B of Figure 10, is identical to that presented in Figure 9 above. In some participants, the levels of AβPP-derived *i*Aβ will not cross the T1 threshold within their lifetime. In those trial subjects whose levels of AβPP-derived *i*Aβ will cross the T1 threshold, the AβPP-independent *i*Aβ generation pathway would become operational, and its product will rapidly accumulate, cross the Ts threshold, and trigger the manifestation of the symptoms of AD.

The evolution of the initial state in the medicated (orange boxes) subjects (panels C and D of Figure 10) is complex. With the exception of cases where *i*Aβ levels were over T1 prior to the drug administration, it is the same as presented in the preceding section. In panel C, the ACH-based drug decreases the influx of AβPP-derived *i*Aβ and thus reduces the rate of its accumulation. The reduction, however, is not sufficient to reverse it, and the levels of AβPP-derived *i*Aβ continue to increase. Following the T1 crossing, the AβPP-independent *i*Aβ production pathway, which is insensitive to the ACH-based drugs, would be activated and the progression of the disease would be identical to that in the placebo cohort; the manifestation of the symptoms of AD would eventually occur but with a significant delay. In some participants, this delay is sufficient to prevent the occurrence of AD within their lifetimes. In panel D of Figure 10, the reduction in the influx of AβPP-derived *i*Aβ is sufficient to reverse the rate of its accumulation, and its levels steadily decrease. They would not cross the T1 threshold and AD would not occur for the duration of the treatment. In both scenarios, however, the drug would be ineffective in initially over-T1 trial subjects. In these cases, the progression of AD would continue uninterrupted, and the levels of *i*Aβ, produced mainly independently of AβPP, would cross the Ts threshold and trigger the manifestation of AD symptoms. Therefore, for a significant period of time, measured in years, the outcomes in the drug recipients would closely resemble the outcomes in the placebo cohort. Since in asymptomatic initially over-T1 medicated individuals, a fraction of neurons could be still sub-T1 and therefore would be protected by the drug for the duration of the treatment, AD symptoms may develop marginally slower than in the placebo group. But, even in such a case, the actual effect of an ACH-based drug would be obscured or distorted by the outcome of a trial. Eventually, the outcomes would diverge but the wait could be impractically long. In view of the importance of these considerations, they are analyzed further and in greater detail in the following sub-section below.

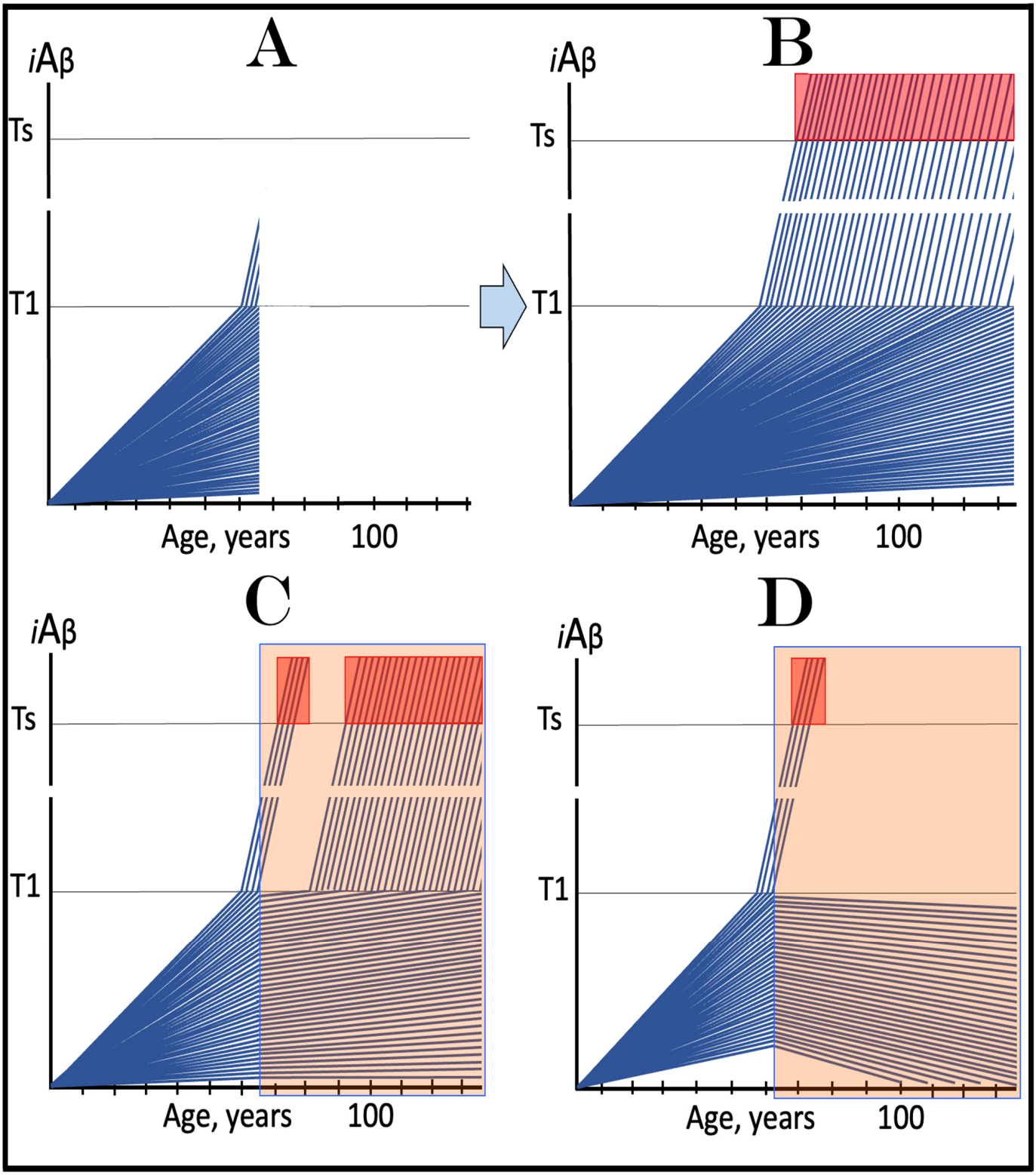

Figure 10. Clinical trials of ACH-based drugs in prevention of AD with a cross-section of the general population aged 65 and over. *i*Aβ: Intraneuronal Aβ. *Blue lines*: The levels of *i*Aβ in individual trial subjects. ***T1*** *threshold*: The concentration of AβPP-derived *i*Aβ that mediates elicitation of the ISR and triggers the activation of the AβPP-independent *i*Aβ production pathway. ***Ts*** *threshold*: The levels of *i*Aβ that trigger the manifestation of AD symptoms. *Pink boxes*: Symptomatic Zone,

the range of *i*Aβ concentrations above the Ts threshold. *Orange boxes:* The duration of administration of an ACH-based drug. Panel (**A**): The initial state of *i*Aβ levels in individual trial subjects at the commencement of the treatment. Importantly, in a fraction of the subjects, these levels have crossed the T1 threshold. Panel (**B**): The evolution of the initial state in the untreated individuals (the placebo cohort). It is principally identical to that shown in panel B of Figure 9, except it occurs faster. Panels (**C**,**D**): The evolution of the initial state in the medicated trial participants. Note that in both panels, the initial over-T1 fraction is not affected by the drug due to the operation of the AβPP-independent *i*Aβ production pathway. Panel (**C**): In the initial sub-T1 fraction, the rate of accumulation of AβPP-derived *i*Aβ is lowered but its levels keep increasing. After a delay (in comparison with the placebo group), they cross the **T1** threshold and eventually reach the Symptomatic Zone in a fraction of the subjects. In another fraction, the delay is sufficient to prevent the disease. Panel (**D**): In the initial sub-T1 fraction, the drug causes the reversal of the accumulation of AβPP-derived *i*Aβ. Its levels do not cross the **T1** threshold; no disease occurs in these trial participants for the duration of the treatment. However, in both panels (**C**,**D**), the initial over-T1 neuronal fraction progresses into the Symptomatic Zone, unaffected by the drug. Therefore, for a considerable duration, the trial outcomes in the treated cohort would be nearly identical to the outcomes in the placebo cohort thus obscuring the effect of the drug.

14.2. Detailed Analysis: Duration of Trials Could Be Prohibitively Excessive Prior to the Divergence of the Outcomes in Medicated and Placebo Groups

To better understand the nature of the overlap in the evolution of the medicated and placebo cohorts in a scenario considered above, this sub-section examines a limited time interval (the "time interval of concern"): from the commencement of the drug administration until all initially over-T1 subjects cross the Ts threshold and enter the Symptomatic Zone. This analysis is illustrated in Figure 11. Panel A of Figure 11 depicts the initial state. Its main attribute of concern is the inclusion of asymptomatic subjects whose levels of *i*Aβ are over T1 and where the AβPP-independent *i*Aβ production pathway has already been activated. Panel B depicts the evolution of the initial state in the placebo cohort within the time interval of concern (green box). In the initially over-T1 subjects, *i*Aβ levels steadily increase, subjects enter the Symptomatic Zone, and AD symptoms manifest. Within the same time interval of concern, the levels of AβPP-derived *i*Aβ cross the T1 threshold in multiple additional participants from the placebo cohort. In these trial participants, the AβPP-independent *i*Aβ generation pathway is activated and the second AD stage commences. Importantly, by the conclusion of the time interval of concern, the levels of *i*Aβ (produced mainly independently of AβPP) have not yet reached the Ts threshold in the initially sub-T1 trial subjects.

In panels C and D of Figure 11, the administration of an ACH-based drug prevents the crossings of the T1 threshold in the initially sub-T1 trial subjects for the time interval of concern. Within the same time period, however, the initially over-T1 individuals cross the Ts threshold and enter the Symptomatic Zone at nearly the same rate as in the placebo group. At the conclusion of the time interval of concern, there is, apparently, a marked distinction between the medicated and the placebo cohorts: In both, the initially over-T1 subjects entered the Symptomatic Zone and developed AD symptoms, but only in the latter did additional numerous subjects cross the T1 threshold. These additional subjects, however, did not reach the Ts threshold. They remain asymptomatic and thus "invisible" in the evaluation of the outcomes of the trial. Therefore, within the time interval of concern, the outcomes in the medicated and the placebo cohorts would be similar, possibly indistinguishable, despite the efficiency of a drug. This time interval could be of a substantial duration. Following it, when the "additional" placebo cases enter the Symptomatic Zone, the outcomes would diverge drastically. But were the trial terminated within the time interval of concern, it would be considered a failure.

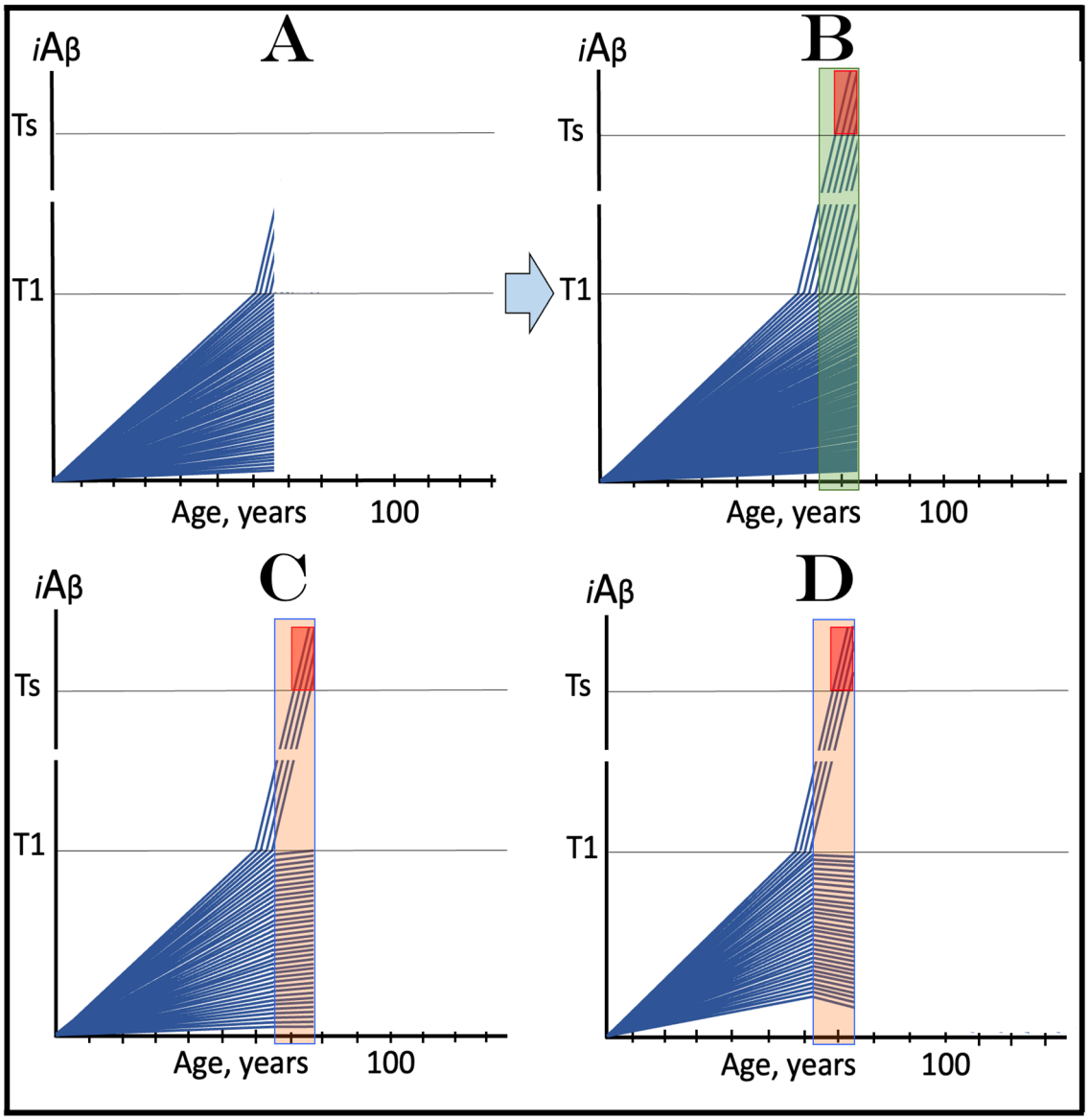

Figure 11. Clinical trials of ACH-based drugs in prevention of AD with a cross-section of the general population: a detailed analysis. *i*Aβ: Intraneuronal Aβ. *Blue lines*: The levels of *i*Aβ in individual trial subjects. ***T1*** *threshold*: The concentration of AβPP-derived *i*Aβ that mediates elicitation of the ISR and triggers the activation of the AβPP-independent *i*Aβ production pathway. ***Ts*** *threshold*: The levels of *i*Aβ that trigger the manifestation of AD symptoms. *Pink boxes*: Symptomatic Zone, the range of *i*Aβ concentrations above the Ts threshold. *Orange boxes:* The duration of administration of an ACH-based drug. *Green box:* The duration of the evolution of the initial over-T1 fraction of trial subjects ("time interval of concern"). Panel (**A**): The initial state of *i*Aβ levels in individual trial subjects at the commencement of the treatment. Importantly, in a fraction of the subjects these levels have crossed the T1 threshold. Panel (**B**): Evolution of the initial state in the placebo cohort for the duration of the time interval of concern. The initial over-T1 fraction crosses the Ts threshold and the AD symptoms manifest. During this time interval, additional participants cross the T1 threshold but none reaches the Ts threshold. Panels (**C**,**D**): The evolution of the initial state in the medicated cohort during the time interval of concern. In both panels the initial over-T1 fraction crosses into the Symptomatic Zone and AD symptoms manifest. No additional crossings of the T1 threshold occur during the period of interest. The outcomes in the medicated and placebo cohorts within the time interval of concern are differentiated only by the presence in the placebo group of additional participants who crossed the T1 threshold but remain asymptomatic and thus "invisible" in the analysis of the results.

15. Clinical Trials of ACH-Based Drugs in Prevention of AD with High-Risk Participants: Practically Impossible and Self-Defeating

The problem with the currently ongoing clinical trials of lecanemab and donanemab in the prevention of AD is that they employ, and apparently are limited to, high-risk participants [138]. Importantly, this problem is not specific to lecanemab and donanemab but is general for any ACH-based drug. The high-risk individuals are asymptomatic persons who, by a number of indicators, would develop AD symptoms shortly or imminently. They are also the individuals who, highly probably, have already crossed the T1 threshold. Whereas in a cross-section of the general population aged 65 or over, considered above, the initially over-T1 asymptomatic individuals represent only a few percentage points, in a high-risk cohort, they would constitute the majority of, if not the entire cohort. The consequences of the utilization of high-risk asymptomatic persons in clinical trials of ACH-based drugs in the prevention of AD are considered in Figure 12.

Three parts of Figure 12 (upper, middle, and bottom) depict three situations with different proportions of asymptomatic over-T1 subjects in a selected cohort (the initial state). In the upper part of Figure 12, the initial state is such that about half of the selected participants are already over T1 (panel A). In these subjects, the AβPP-independent *i*Aβ production pathway has been activated but the levels of *i*Aβ (produced at this stage mainly independently of AβPP) have not yet reached the Ts threshold. Panel B shows the evolution of the initial stage in the placebo group. The levels of AβPP-derived *i*Aβ cross the T1 threshold in all trial subjects. The AβPP-independent *i*Aβ generation pathway becomes operational, *i*Aβ levels increase and cross the Ts threshold, subjects enter the Symptomatic Zone and AD symptoms manifest (provided a sufficiently long lifespan). Panel C depicts the evolution of the initial state in the presence of an ACH-based drug (orange box). To simplify the discussion, only the best-case scenario is considered: a drug that is capable of reversing the accumulation of AβPP-derived *i*Aβ and causing a steady decline in its levels. In the sub-T1 trial subjects, the influx of AβPP-derived *i*Aβ is suppressed and its rate of accumulation is reversed. These subjects would not cross the T1 threshold for the duration of the treatment. However, the drug would be ineffective in the initially over-T1 trial participants. Those would progress toward the Ts threshold, enter the Symptomatic Zone, and AD symptoms would manifest at a rate similar to or indistinguishable from that in the placebo group. The outcomes in the medicated and the placebo group would eventually diverge but only after an impracticably long, well over a decade, period of overlap.

In the middle and the bottom parts of Figure 12, the proportion of asymptomatic but over-T1 trial subjects in the initial state increases. In the middle part of Figure 12, it is about three-quarters of the cohort (panel A'); in the bottom part of Figure 12, it is the entire cohort (panel A''). The evolution of the initial state in the placebo groups for the middle and the bottom parts of Figure 12, shown in panels B' and B'', respectively, is no different from that depicted in panel B. In the initially over-T1 subjects the disease progresses, and the sub-T1 participants cross the T1 threshold. Eventually, all subjects reach the Ts threshold, cross into the Symptomatic Zone, and AD symptoms manifest. The evolution of the initial state in the presence of the drug (orange boxes) for the middle and the bottom parts of Figure 12 is shown in panels C' and C'', respectively. In panel C', the drug is ineffective in three-quarters of the trial subjects who already have crossed the T1 threshold and activated the AβPP-independent *i*Aβ production pathway. Only the initially sub-T1 subjects are protected for the duration of the treatment. However, the overlap between the outcomes in the medicated and placebo cohorts is even greater than that shown in panel C. In panel C'', the entire cohort is largely unresponsive to the ACH-based drug. The evolution of the initial state is principally the same as in the placebo group, and it would not be conceptually possible to gain any information regarding the efficiency of the drug. It should be emphasized here that the composition of high-risk cohorts would differ from trial to trial but, on average, it would most resemble that depicted in the lower panel of Figure 12 (panel A''). The bottom line for this and the preceding sections is that the

selection of low-risk subjects for clinical trials of the ACH-based drugs in the prevention of AD is impractical, whereas the selection of high-risk trial participants is self-defeating.

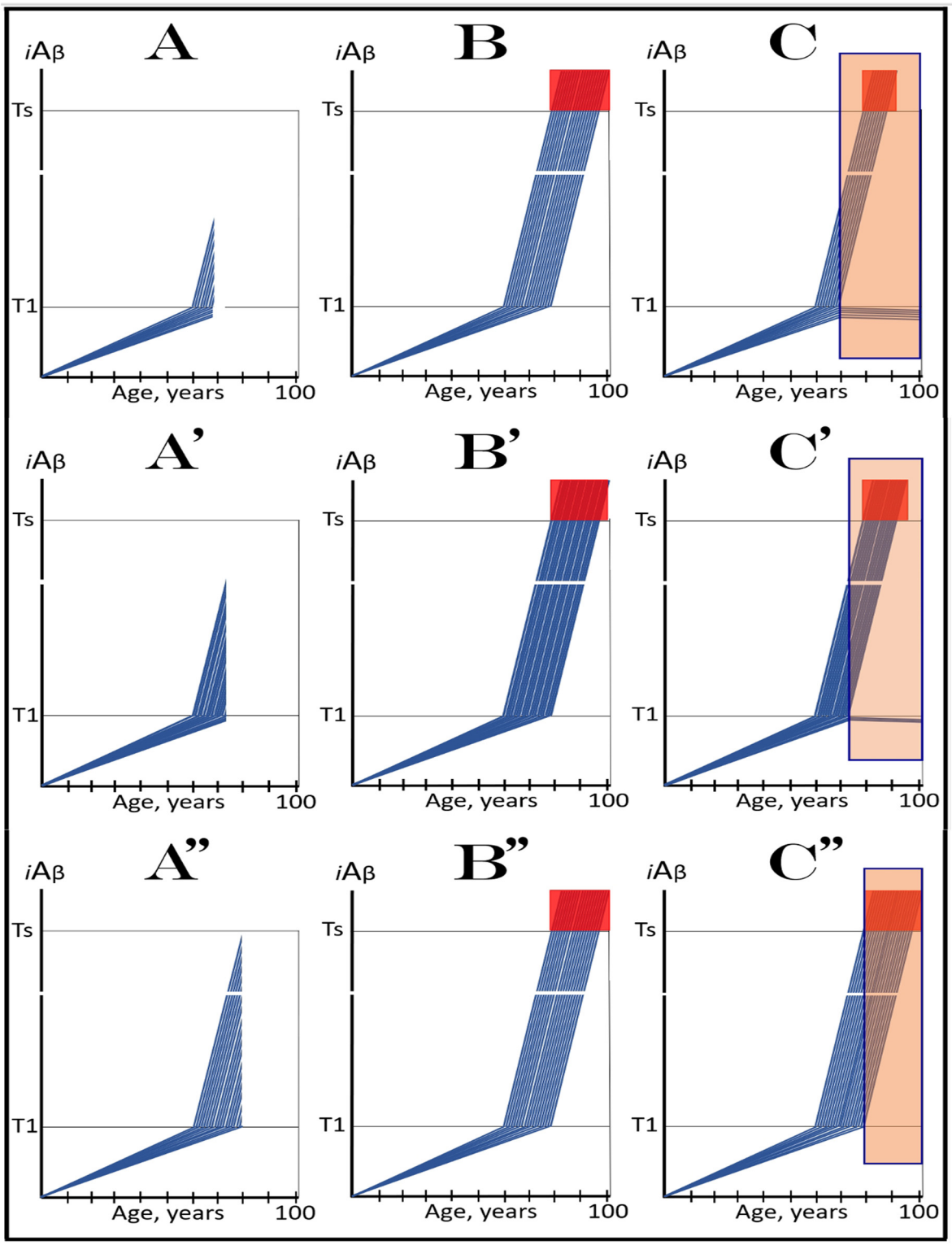

Figure 12. Clinical trials of ACH-based drugs in prevention of AD with high-risk cohorts. *i*Aβ: Intraneuronal Aβ. *Blue lines*: The levels of *i*Aβ in individual trial subjects. ***T1*** *threshold*: The concentration of AβPP-derived *i*Aβ that mediates elicitation of the ISR and triggers the activation of the AβPP-independent *i*Aβ production pathway. ***Ts*** *threshold*: The levels of *i*Aβ that trigger the manifestation of AD symptoms. *Pink boxes*: Symptomatic Zone, the range of *i*Aβ concentrations above the Ts threshold.

Orange boxes: The duration of administration of an ACH-based drug. Panel (**A**): All trial subjects are asymptomatic but about 50% have crossed the T1 threshold and activated the AβPP-independent *i*Aβ production pathway. Panel (**B**): The evolution of the initial stage in the placebo group. The levels of AβPP-derived *i*Aβ cross the T1 threshold and the AβPP-independent *i*Aβ generation pathway becomes operational in all trial subjects. *i*Aβ levels increase and cross the Ts threshold, subjects enter the Symptomatic Zone and AD symptoms manifest. Panel (**C**): The evolution of the initial state in the presence of an ACH-based drug (orange box). To simplify the discussion, only the best-case scenario is considered: a drug that is capable of reversing the accumulation of AβPP-derived *i*Aβ and causing a steady decline in its levels. In the sub-T1 trial subjects, the influx of AβPP-derived *i*Aβ is suppressed and its rate of accumulation is reversed. These subjects would not cross the T1 threshold for the duration of the treatment. However, the drug would be ineffective in the initially over-T1 trial participants. Those would progress toward the Ts threshold, enter the Symptomatic Zone, and AD symptoms would manifest at a rate similar to or indistinguishable from that in the placebo group. The outcomes in the medicated and the placebo group would eventually diverge but only after an impracticably long period of overlap. Panels (**A′–C′**,**A″–C″**) reiterate the same sequence as shown in panels A through C but with increasing proportions of asymptomatic over-T1 subjects: 75% in (**A′–C′**) and 100% in (**A″–C″**). In both cases, the evolutions of the initial states in the absence and the presence of the ACH-based drug are similar to those described above but the overlap between the outcomes in the medicated and placebo cohorts increases in the former and the two are practically indistinguishable in the latter, reflecting the notion that selection of high-risk subjects for AD-preventive trials of ACH-based drugs is self-defeating.

16. Clinical Trials of ACH-Based Drugs in Treatment of AACD

16.1. Clinical Trials of ACH-Based Drugs in Treatment of AACD with Subjects including Late-Stage Patients: Potential Complications

A clinical trial of a drug for the treatment of a condition is always easier to conduct than a trial for its prevention. This is because the selection of the trial subjects is greatly simplified. Potentially, the trial's cohort can be composed of patients at different stages of a disease; such inclusiveness may enrich the outcomes and conclusions of a trial. This, however, is not the case with clinical trials of ACH-based drugs in the treatment of AACD. The potential problem with such a trial arises if it includes late-stage patients. The consequences of such inclusion are illustrated in Figure 13.

If the criterion for selection of the trial subjects is solely the diagnosis of AACD, regardless of its stage, it is inevitable that the trial cohort would include late-stage AACD patients who are asymptomatic for AD but nevertheless have the *i*Aβ levels exceeding the T1 threshold (over-T1 trial subjects). The initial state of such a scenario is depicted in panel A of Figure 13. In all subjects, the levels of AβPP-derived *i*Aβ have crossed the T^0 threshold and all exhibit AACD symptoms (pink gradient box). A fraction of the late-stage patients has also crossed the T1 threshold and activated the AβPP-independent *i*Aβ generation pathway but remains asymptomatic for AD. The evolution of this initial state in the placebo group is shown in panel B. The levels of AβPP-derived *i*Aβ increase, cross the T1 threshold, and trigger the activation of AβPP-independent *i*Aβ production pathway in all initially sub-T1 patients (provided a sufficient lifespan). The levels of *i*Aβ, produced now mainly independently of AβPP, reach and cross the Ts threshold, and AD symptoms manifest.

Panels C and D of Figure 13 illustrate the evolution of the initial state in the presence of an ACH-based drug (orange boxes). The drug is effective only in patients who were still sub-T1 at the time of its administration and can yield two possible outcomes. In panel C, the drug reduces the influx of AβPP-derived *i*Aβ, the rate of its accumulation decreases but its levels are still increasing. In a fraction of the trial subjects, the decrease in the rate of AβPP-derived *i*Aβ accumulation is sufficient to prevent the T1 crossing (and AD) within the lifetime of a patient. In the rest of the initially sub-T1 subjects, the levels of AβPP-derived *i*Aβ would cross the T1 threshold, the AβPP-independent *i*Aβ production pathway would be activated, and AD would ensue but with a considerable delay in comparison with the

placebo group. In panel D of Figure 13, the reduction in the influx of AβPP-derived *i*Aβ is sufficient to reverse its accumulation. Its levels are steadily decreasing for the duration of the treatment. There will be no T1 crossing and no AD in these subjects. Moreover, their condition would improve and some of them will be even cured upon the reverse crossing of the T^0 threshold.

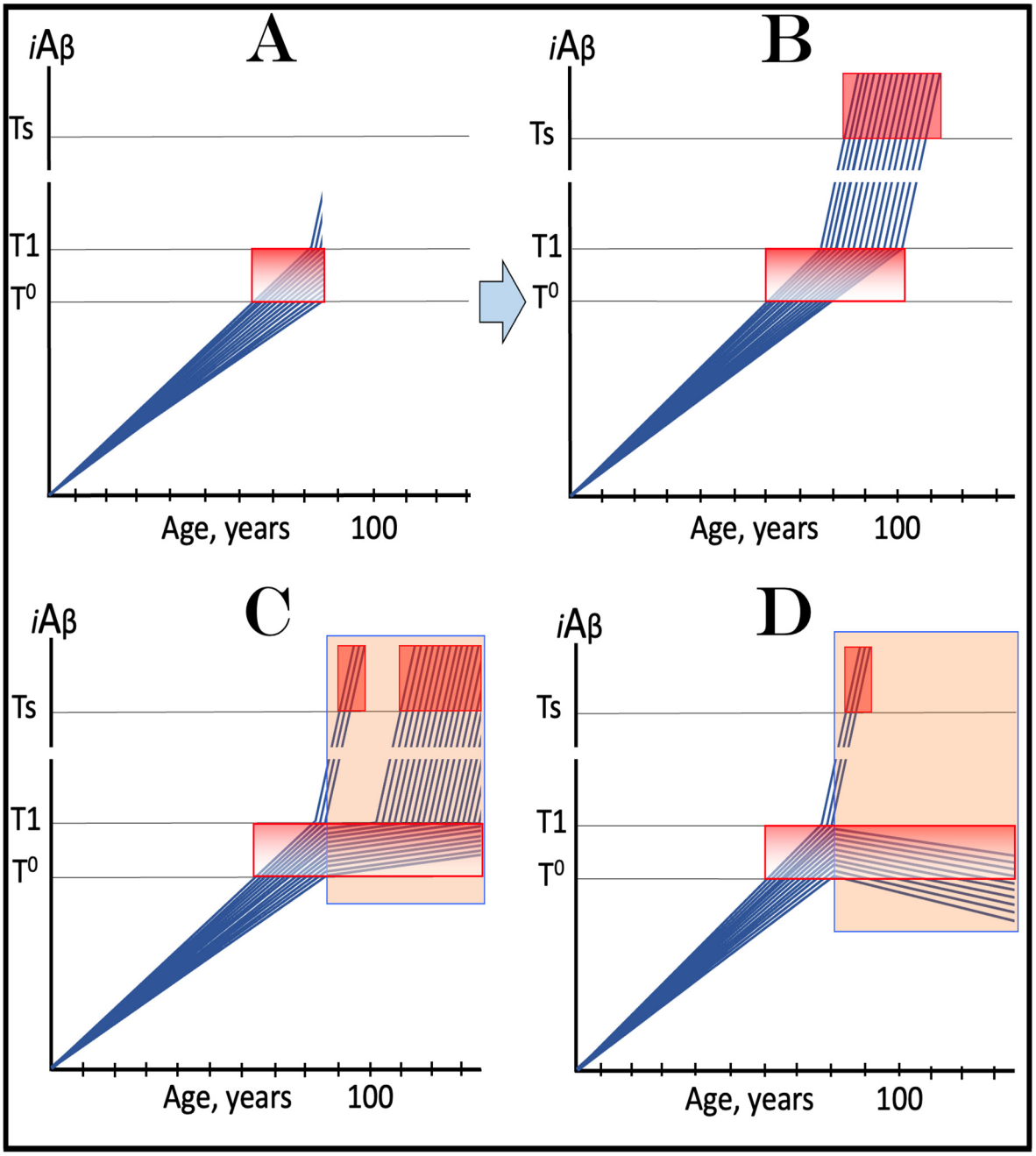

Figure 13. Clinical trials of ACH-based drugs in treatment of AACD with subjects including late-stage patients. *i*Aβ: Intraneuronal Aβ. *Blue lines*: The levels of *iA*β in individual trial subjects. ***T*^{0}** *threshold*: The concentration of *i*Aβ that triggers the neurodegeneration manifesting as AACD. ***T1*** *threshold*: The concentration of AβPP-derived *i*Aβ that mediates elicitation of the ISR and triggers the activation of the AβPP-independent *i*Aβ production pathway. ***Ts*** *threshold*: The levels of *i*Aβ that trigger the manifestation of AD symptoms. *Pink gradient boxes*: AACD Zone, the range of concentration of AβPP-derived *i*Aβ between the T^0 and T1 boundaries. *Pink boxes*: Symptomatic Zone, the range of *i*Aβ concentrations above the Ts threshold. *Orange boxes*: The duration of administration of

an ACH-based drug. Panel (**A**): The initial state. All subjects exhibit the AACD symptoms and are asymptomatic for AD. In the majority of trial participants, the levels of *i*Aβ are confined between the boundaries of the T^0 and T1 thresholds. In a fraction of trial subjects, the levels of *i*Aβ have crossed the T1 threshold and triggered the activation of the AβPP-independent *i*Aβ production pathway. Panel (**B**): The evolution of the initial state in the placebo group. The initial sub-T1 fraction of the trial subjects crossed the T1 threshold; the AβPP-independent *i*Aβ production pathway is now operative in all participants. *i*Aβ rapidly accumulates, crosses the Ts threshold, and the AD symptoms manifest. Panels (**C**,**D**): The evolution of the initial state in the medicated trial subjects. In both panels, the drug has no effect in the initial over-T1 fraction; in these subjects, AD progresses and, when the Ts threshold is crossed, its symptoms manifest. Panel (**C**): The drug lowers the rate of accumulation of AβPP-derived *i*Aβ. In a fraction of subjects, this is sufficient to prevent the T1 crossing and the occurrence of AD. In another fraction of the trial participants, the T1 threshold is crossed and AD ensues but with a considerable delay. Panel (**D**): The drug reverses the rate of AβPP-derived *i*Aβ accumulation. The T1 threshold would not be crossed and AD would not occur in the initial sub-T1 fraction. Moreover, if/when the T^0 threshold would be reverse-crossed, the patients would be technically cured. However, because of the presence of the initially over-T1 subjects, the outcomes in the medicated and placebo cohorts would overlap for a substantial duration before they diverge drastically.

However, the drug will be inefficient in the initially over-T1 subjects because of the operation of the AβPP-independent *i*Aβ production pathway, which is insensitive to the ACH-based drugs. In these subjects, the levels of *i*Aβ (produced mostly independently of AβPP) would increase and eventually cross the Ts threshold. Consequently, this fraction of trial participants would enter the Symptomatic Zone and exhibit AD symptoms at a rate similar to that in the placebo group. The problem with such clinical trial, therefore, is akin to that discussed above: the outcomes in the medicated and the placebo cohorts would be similar for a substantial duration, measured in years, before diverging, and would obscure and distort the actual effect of the drug.

16.2. Clinical Trials of ACH-Based Drugs in Treatment of Early AACD: The Only Unproblematic Clinical Trials of ACH-Based Drugs

It follows that the reliable approach to conducting clinical trials of ACH-based drugs in the treatment of AACD is to employ only trial subjects at the early AACD stages. Because, as discussed above, the extent of the T1 threshold appears to be substantially greater than that of the T^0 threshold, the inclusion of the over-T1 trial subjects is highly unlikely if only the early-stage AACD patients are selected. This approach and its possible outcomes are illustrated in Figure 14. Panel A depicts the initial state. All selected subjects have crossed the T^0 threshold and are exhibiting the early symptoms of AACD. Panel B of Figure 14 illustrates the evolution of the initial state in the placebo group. AβPP-derived *i*Aβ continues to accumulate and the condition progresses in all subjects in the placebo cohort. Eventually, provided a sufficiently long lifespan, the levels of AβPP-derived *i*Aβ would cross the T1 threshold and trigger the activation of the AβPP-independent *i*Aβ production pathway and the commencement of AD. The rate of accumulation of *i*Aβ (now produced mostly independently from AβPP) would increase. Its levels would reach and cross the Ts threshold in all participants in the placebo group and AD symptoms would manifest.

Panels C and D of Figure 14 depict diagrammatically the evolution of the initial state in the presence of an ACH-based drug. In panel C, the drug reduces the influx of AβPP-derived *i*Aβ and suppresses its rate of accumulation. Its levels, however, continue to increase albeit much slower than prior to the drug administration. The T1 threshold would not be crossed and a low-grade, rather mild, AACD would persist for the remaining portions of the lifespans of treated trial subjects or for the duration of the treatment. In panel D of Figure 14, the reduction in the influx of AβPP-derived *i*Aβ is sufficient to reverse its accumulation, and its levels are steadily decreasing. The condition of the medicated

subjects would be improving. Moreover, when the levels of AβPP-derived *i*Aβ would reverse-cross the T^0 threshold, the patients would be technically cured (subject to full restoration of neuronal functionality). It should be emphasized that this scenario, i.e., trials of treatment of early AACD, is the only type of clinical trial of the ACH-based drugs that is capable of generating clear and unequivocal results.

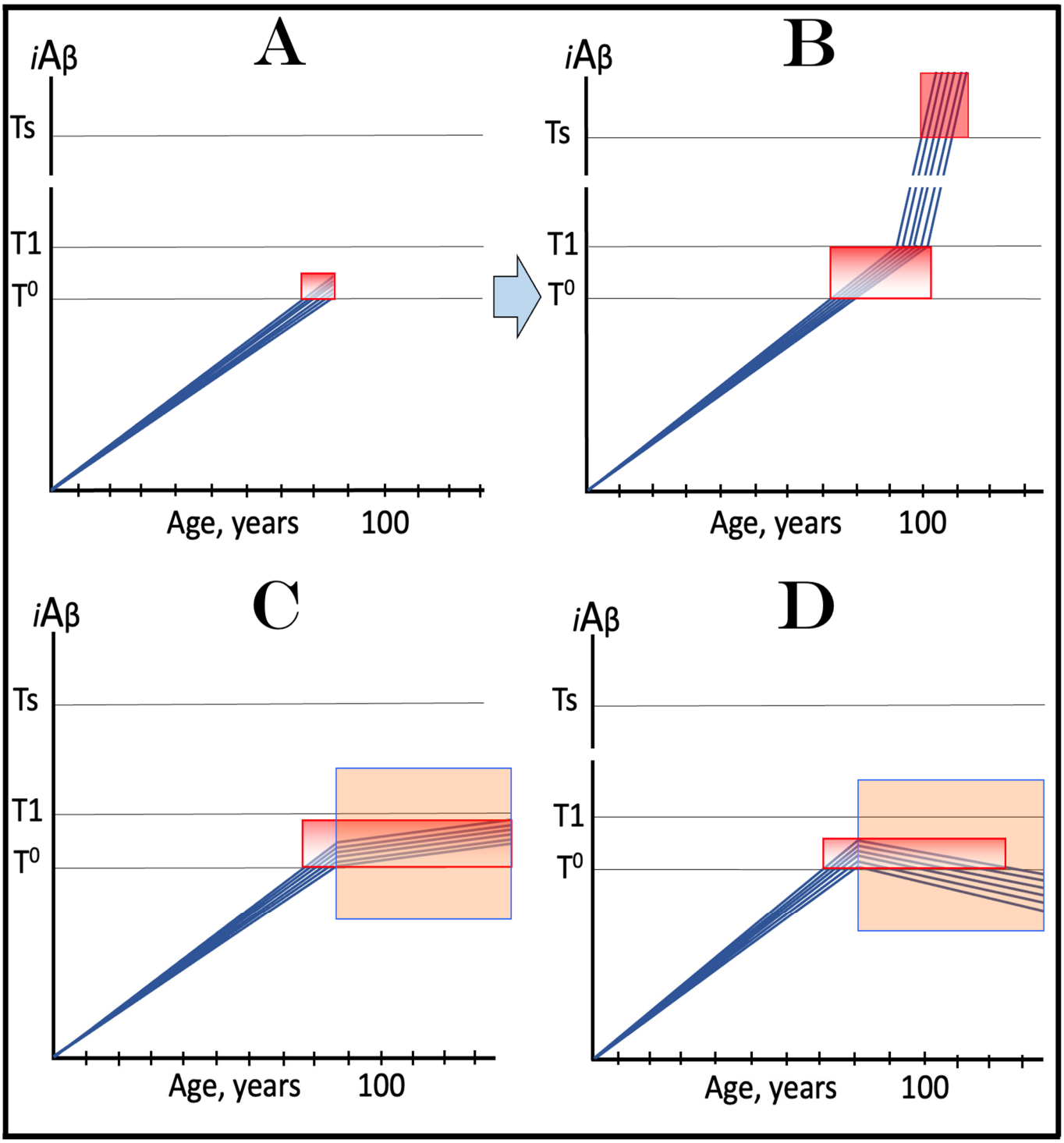

Figure 14. Clinical trials of ACH-based drugs in treatment of early AACD. *i*Aβ: Intraneuronal Aβ. *Blue lines*: The levels of *i*Aβ in individual trial subjects. ***T*^{0}** *threshold*: The concentration of *i*Aβ that triggers the neurodegeneration manifesting as AACD. ***T1*** *threshold*: The concentration of AβPP-derived

*i*Aβ that mediates elicitation of the ISR and triggers the activation of the AβPP-independent *i*Aβ production pathway. ***Ts*** *threshold*: The levels of *i*Aβ that trigger the manifestation of AD symptoms. *Pink gradient boxes*: AACD Zone, the range of concentration of AβPP-derived *i*Aβ between the T^0 and T1 boundaries. *Pink boxes*: Symptomatic Zone, the range of *i*Aβ concentrations above the Ts threshold. *Orange boxes*: The duration of administration of an ACH-based drug. Panel (**A**): The initial state. All trial participants exhibit only early AACD symptoms; the AβPP-derived *i*Aβ levels have just crossed the T^0 threshold. Panel (**B**): The evolution of the initial state in the untreated trial subjects (the placebo group). AβPP-derived *i*Aβ steadily accumulates. If and when its levels cross the T1 threshold (subject to the longevity of trial participants), AD ensues. Panels (**C**,**D**): The evolution of the initial state in participants treated with an ACH-based drug. Panel (**C**): The drug reduces the rate of accumulation of the AβPP-derived *i*Aβ and its levels do not reach the T1 threshold for the duration of the treatment. AACD progresses, but much slower than in the absence of the drug. Panel (**D**): The drug reverses the rate of AβPP-derived *i*Aβ accumulation and its levels are steadily decreasing. The condition of the patients is expected to improve and, when the *i*Aβ levels reverse-cross the T^0 threshold, they will be technically cured. In this trial there is no overlap between the outcomes in the medicated and the placebo cohorts; it is the only type of clinical trial of ACH-based drugs (due to the feasibility of selection of the trial subjects that are highly likely to be sub-T1) that is capable of generating clear and unequivocal results.

17. The ACH2.0-Guided Next Generation Therapeutic Strategy for AD and AACD: The Depletion of *i*Aβ via Its Targeted Degradation

17.1. Effective AD Therapy Requires Both the Reduction of the Levels of iAβ and Cessation of the Operation of the AβPP-Independent Pathway of Its Production

To briefly summarize the preceding sections, the ACH-based drugs could be highly problematic both in their utilization and in their evaluation. The focal point of all principal problems with ACH-based drugs is the occurrence of the operational AβPP-independent *i*Aβ generation pathway. Indeed, as discussed above, the ACH-based drugs are rendered completely ineffective as soon as the AβPP-independent *i*Aβ production pathway is activated. That the ACH-based drugs would be effective were it not for the operation of the AβPP-independent *i*Aβ generation pathway is exemplified by numerous studies with transgenic mice lacking the operational AβPP-independent *i*Aβ production pathway and overexpressing Aβ solely in the AβPP proteolytic pathway, where the suppression of its production or the removal of extracellular Aβ (both leading to the reduction in the levels of *i*Aβ) relieved or reversed the neurodegeneration [8–10]. These results are consistent with and strongly support the major tenet of the ACH2.0, namely that *i*Aβ, produced in AD mainly in the AβPP-independent pathway, triggers and drives the neurodegeneration and that its depletion would be therapeutically beneficial. Thus, the first component of the ACH2.0-guided Next Generation Therapeutic Strategy for AD and AACD is the reduction in the levels of total *i*Aβ, regardless of its origin. This, however, is not enough, because the continuous and very efficient production of *i*Aβ in the AβPP-independent pathway would be unceasingly replenishing its levels. Therefore, for the Next Generation Therapeutic Strategy to be effective, another component needs to be enacted: cessation of the operation of the AβPP-independent *i*Aβ generation pathway. Propitiously, as reasoned below, achieving the former accomplishes the latter.

17.2. A Sufficient Depletion of iAβ Would Cease the Activity of the AβPP-Independent iAβ Production Pathway

Indeed, the activation and operation of the AβPP-independent *i*Aβ production pathway requires sufficiently high, more specifically over-T1, levels of *i*Aβ. Those are initially supplied by the AβPP proteolysis. When the levels of AβPP-derived *i*Aβ cross the T1 threshold, the AβPP-independent *i*Aβ production pathway is activated and transformed into the AD Engine. This is because the increasing levels of *i*Aβ stimulate its own AβPP-independent production and thus perpetuate the operation of the Engine. As discussed elsewhere [1,4], of several ways to stop the operation of the

AβPP-independent *i*Aβ production pathway (regardless of the nature of its underlying mechanism), only one is viable and feasible: the depletion of *i*Aβ below the T1 threshold. With insufficient *i*Aβ levels, the operation of the AβPP-independent pathway of its production would cease. The production of *i*Aβ in the AβPP proteolytic pathway, on the other hand, would continue, and as soon as AβPP-derived *i*Aβ levels are restored to the T1 threshold, they would re-ignite the AD Engine. The accumulation of AβPP-derived *i*Aβ is, however, a very slow process: it takes decades to build up its levels to the T1 threshold in sporadic AD cases, and in the majority of the population, the T1 threshold is not reached (and AD does not occur) within the lifetime of an individual. Therefore, if the *i*Aβ levels were depleted sufficiently deep, close to its initial baseline, its accumulation would resume, solely in the AβPP proteolytic pathway, from a low starting point. This would provide additional decades of AD- and AACD-free lifetime. In fact, both conditions would be unlikely to occur (if the treatment were preventive) or recur (if the treatment were curative) within an individual's lifespan. Thus, the Next Generation Therapeutic Strategy can be enacted through the substantial depletion of *i*Aβ via its targeted degradation by the drugs specifically designed for this purpose, the ACH2.0-based drugs.

17.3. Inhibition of the ISR Is Not a Viable Option for AD

In a Fraction of AD Cases, the Effective Therapy May Require Anti-Inflammatory Treatment in Addition to the Depletion of iAβ

In terms of ACH2.0, the elicitation of the integrated stress response in neuronal cells results in the production of the component(s) that are necessary and sufficient for the activation of the AβPP-independent *i*Aβ production pathway and the commencement of AD. It follows that the elicitation of the ISR by means other than AβPP-derived *i*Aβ-mediated activation of eIF2α kinases could be sufficient to activate the AβPP-independent *i*Aβ generation pathway and trigger the disease. In such a scenario, the depletion of *i*Aβ below the T1 threshold alone in AD would not cease the operation of the AβPP-independent *i*Aβ production pathway; the cause of the ISR elicitation should be removed or reduced as well. This scenario is exemplified by the instances of AD in individuals who are predisposed to the disease due to persistent neuronal inflammation (resulting, for example, from a concussion or from multiple concussions). In this category, prior to the activation of the AβPP-independent *i*Aβ production pathway, the long-term anti-inflammatory therapy would protect from the onset of AD (by precluding the elicitation of the ISR and, consequently, of the AβPP-independent *i*Aβ production pathway), whereas after the commencement of AD, the implementation of the transient *i*Aβ depletion via its targeted degradation would be effective if it is paralleled by the long-term anti-inflammatory therapy.

In terms of the ACH2.0, potentially, the activation of the AβPP-independent *i*Aβ generation pathway can be precluded or its operation suppressed, and, accordingly, AD could be prevented or its progression stopped by the inhibition of the ISR, e.g., with the small molecule ISR inhibitor ISRIB. However, due to the ISR's pivotal role in cellular physiology, its long-term suppression (it would be effective in both prevention and treatment of AD only if implemented long-term) is highly likely to result in widespread adverse effects and is not a viable option.

18. ACH2.0-Based Drugs for Prevention and Treatment of AD and AACD: A Definition

In accordance with the preceding section, the ACH2.0-based drugs are the agents that enact or mediate the targeted degradation of *i*Aβ, thus causing its depletion. This class of drugs differs fundamentally from the ACH-based drugs. The latter lower or, hopefully, reverse the rate of accumulation of only AβPP-derived *i*Aβ and do it rather indirectly, "passively", by limiting its influx. As long as the influx occurs, the ACH-based drugs cannot cause the reduction in AβPP-derived *i*Aβ levels on their own; for this, they rely on the naturally occurring clearance processes. Thus, treatment with the

ACH-based drugs can potentially (if the rate of accumulation is reversed) result in a limited depletion of AβPP-derived *i*Aβ, but this depletion is "passive" and, even if it occurs, is apparently insignificant, as suggested by recent results with lecanemab and donanemab [134–138].

In contrast, ACH2.0-based drugs are capable of enacting the "active" depletion of total *i*Aβ, regardless of its origin. The agents can be potentially designed that penetrate inside the neuron, recognize *i*Aβ, and specifically cleave it. Another category of ACH2.0-based drugs includes the agents devised to activate or enhance the intrinsic neuronal activities capable of specific degradation of *i*Aβ. This approach is, in fact, feasible; two highly plausible prime candidates are discussed in Section 26 below. Such degradation is "active" because it is actively forced; in comparison, "passive" degradation is not forced but relies upon physiologically occurring processes. The direct, targeted degradation of *i*Aβ could be substantially more effective than its "passive" counterpart. It is conceivable, therefore, that the treatment with ACH2.0-based drugs could achieve its purpose, i.e., a substantial depletion of *i*Aβ, in a transient manner, within a duration measured in days, akin to that of an antibiotic treatment. As discussed in the following sections, such treatment can be implemented preventively, prior to the manifestation of AD or AACD symptoms; in similarity to their ACH counterparts, ACH2.0-based drugs can also treat symptomatic AACD. Ultimately and uniquely, as described below, ACH2.0-based drugs can deliver the "Holy Grail" of Alzheimer's research: the efficient treatment of AD at its symptomatic stages. When implemented prior to the T1 crossing, such treatment can be relatively short because, in the absence of the operational AβPP-independent *i*Aβ production pathway, the cellular pool of *i*Aβ would be relatively low. The duration of the treatment would be probably longer in symptomatic AD, where, due to the activity of the AβPP-independent *i*Aβ generation pathway, the levels of *i*Aβ would be significantly higher. In sharp contrast to the ACH-based drugs, their ACH2.0-based counterparts can be easily and unambiguously evaluated in clinical trials for both the prevention and treatment of AD and AACD (see below). Remarkably, as described in the following sections, the effective transient treatment with an ACH2.0-based drug opens up the possibility of its once-in-a-lifetime administration for the prevention of AD and AACD and for their efficient treatment at symptomatic stages.

19. Implementation of ACH2.0-Based Drugs in Prevention of AD by Depletion of *i*Aβ via Its Transient, Short-Duration, Targeted Degradation

19.1. Prevention of AD by Transient Depletion of iAβ via Its Targeted Degradation in Asymptomatic Low-Risk Individuals with the Entire Neuronal Population Sub-T1

Figure 15 considers the prevention of AD via transient depletion of *i*Aβ by its targeted degradation. In this Figure, it is assumed that not only is an individual asymptomatic for AD but also that the levels of *i*Aβ have not yet crossed the T1 threshold in the entire neuronal population. Moreover, the case under consideration is that of an individual who would, unless preventively treated, develop the disease. To simplify the discussion, it is also assumed that the depletion treatment resets the levels of *i*Aβ completely or nearly completely to the original baseline. Panel A of Figure 15 depicts the initial state of the levels of *i*Aβ in the neuronal population of an individual: they all are below the T1 threshold. Panel B shows the evolution of the initial state in the absence of the treatment. The levels of *i*Aβ in individual neurons would continue to increase and eventually would cross the T1 threshold. The AβPP-independent *i*Aβ generation pathway would be activated; its product would rapidly accumulate, reach and cross the T2 threshold, and trigger apoptosis. Panel C of Figure 15 illustrates the evolution of the initial state following the *i*Aβ depletion treatment with an ACH2.0-based drug. The treatment substantially reduces the levels of *i*Aβ and its accumulation resumes from a low baseline. If the depletion is deep enough and if the treatment were administered mid-life, as shown in the figure, the levels of AβPP-derived *i*Aβ would not reach the T1 threshold within the lifetime of the treated individual.

Thus, the single, once-in-a-lifetime-only transient *i*Aβ depletion by an ACH2.0-based drug is potentially capable of protecting from AD for life.

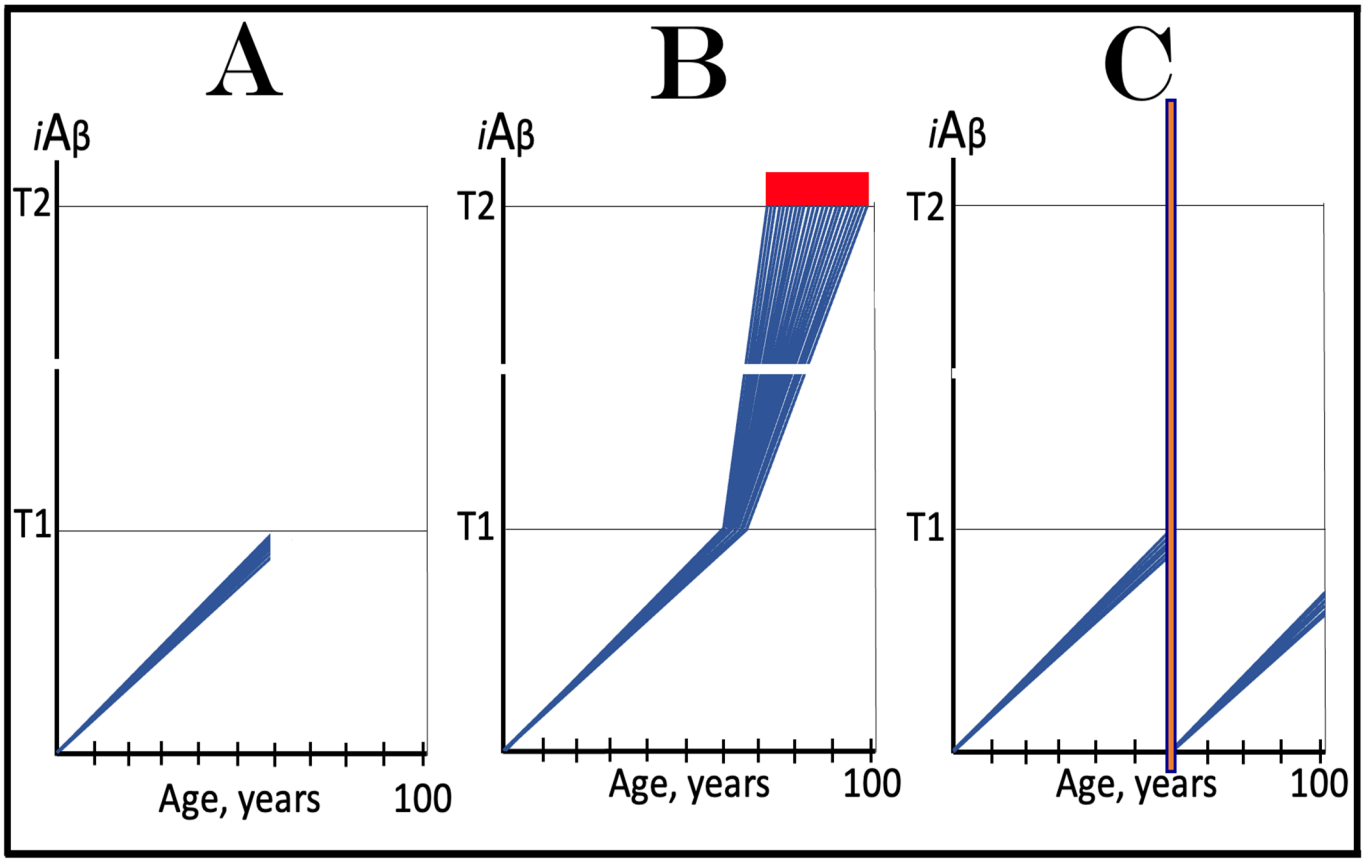

Figure 15. Prevention of AD by transient depletion of iAβ via its targeted degradation in asymptomatic low-risk individuals. *i*Aβ: Intraneuronal Aβ. *Blue lines*: Levels of *i*Aβ in individual neurons. ***T1*** *threshold*: The concentration of AβPP-derived *i*Aβ that mediates elicitation of the ISR and triggers the activation of the AβPP-independent *i*Aβ production pathway. ***T2*** *threshold*: The level of *i*Aβ, produced mainly in the AβPP-independent pathway, which triggers neuronal apoptosis. *Red box*: Apoptotic Zone, the range of *i*Aβ concentrations that cause the commitment to apoptosis. *Orange box*: The duration of the transient administration of an ACH2.0-based drug. Panel (**A**): The initial state of the levels of *i*Aβ in the neuronal population of an individual; they all are below the T1 threshold. Panel (**B**): The evolution of the initial state in the absence of the treatment. The levels of *i*Aβ in individual neurons would continue to increase and eventually would cross the T1 threshold. The AβPP-independent *i*Aβ generation pathway would be activated; its product would rapidly accumulate, reach and cross the T2 threshold, and trigger apoptosis. Panel (**C**): The evolution of the initial state following the *i*Aβ depletion treatment with an ACH2.0-based drug. The treatment substantially reduces the levels of *i*Aβ and its accumulation resumes from a low baseline. If the depletion is deep enough and if the treatment were administered mid-life, as shown in the figure, the levels of AβPP-derived *i*Aβ would not reach the T1 threshold within the lifetime of the treated individual. Thus, the single, once-in-a-lifetime-only transient *i*Aβ depletion by an ACH2.0-based drug is potentially capable of protecting from AD for life.

19.2. Prevention of AD by Transient Depletion of iAβ via Its Targeted Degradation in Asymptomatic High-Risk Individuals with Over-T1 Neuronal Subpopulation

Figure 16 considers a situation where the transient *i*Aβ depletion treatment is administered to an asymptomatic high-risk individual. Whereas no AD symptoms have yet manifested, a fraction of the neuronal population has already crossed the T1 threshold and activated the AβPP-independent *i*Aβ production pathway. This initial state of the

neuronal population is depicted in panel A of Figure 16. The evolution of this initial state in an untreated individual is shown in panel B of Figure 16. In addition to the initially over-T1 neuronal subpopulation, the remaining, initially sub-T1, affected neurons cross the T1 threshold in a relatively narrow temporal window [1,4]. The AβPP-independent *i*Aβ generation pathway is now active in all affected neurons. The levels of *i*Aβ rapidly increase, cross the T2 threshold, and trigger apoptosis. When a sufficient proportion of neurons lose their functionality or die, the disease enters the end stage. The evolution of the initial state following the transient *i*Aβ depletion treatment with an ACH2.0 drug is illustrated in panel C of Figure 16. *i*Aβ is depleted in all neurons, including the initial over-T1 neuronal fraction, and the operation of the AβPP-independent *i*Aβ production pathway in this neuronal subpopulation ceases. The de novo accumulation of *i*Aβ, produced at this point solely in the AβPP proteolytic pathway, resumes from the low baseline. Provided the depletion was sufficiently deep, the T1 threshold would not be reached and AD would not occur within the lifetime of the treated individual. Thus, the one-time-only transient administration of the ACH2.0-based drug can potentially provide lifelong protection from AD even in high-risk individuals. It should be emphasized that the ACH2.0-based drugs-mediated *i*Aβ depletion treatment would confer protection from symptomatic AD if administered any time prior to the manifestation of symptoms of the disease (rather than prior to the crossing of the T1 threshold, as is the case with the ACH-based drugs; compare with Figure 6 in Section 8.2 above).

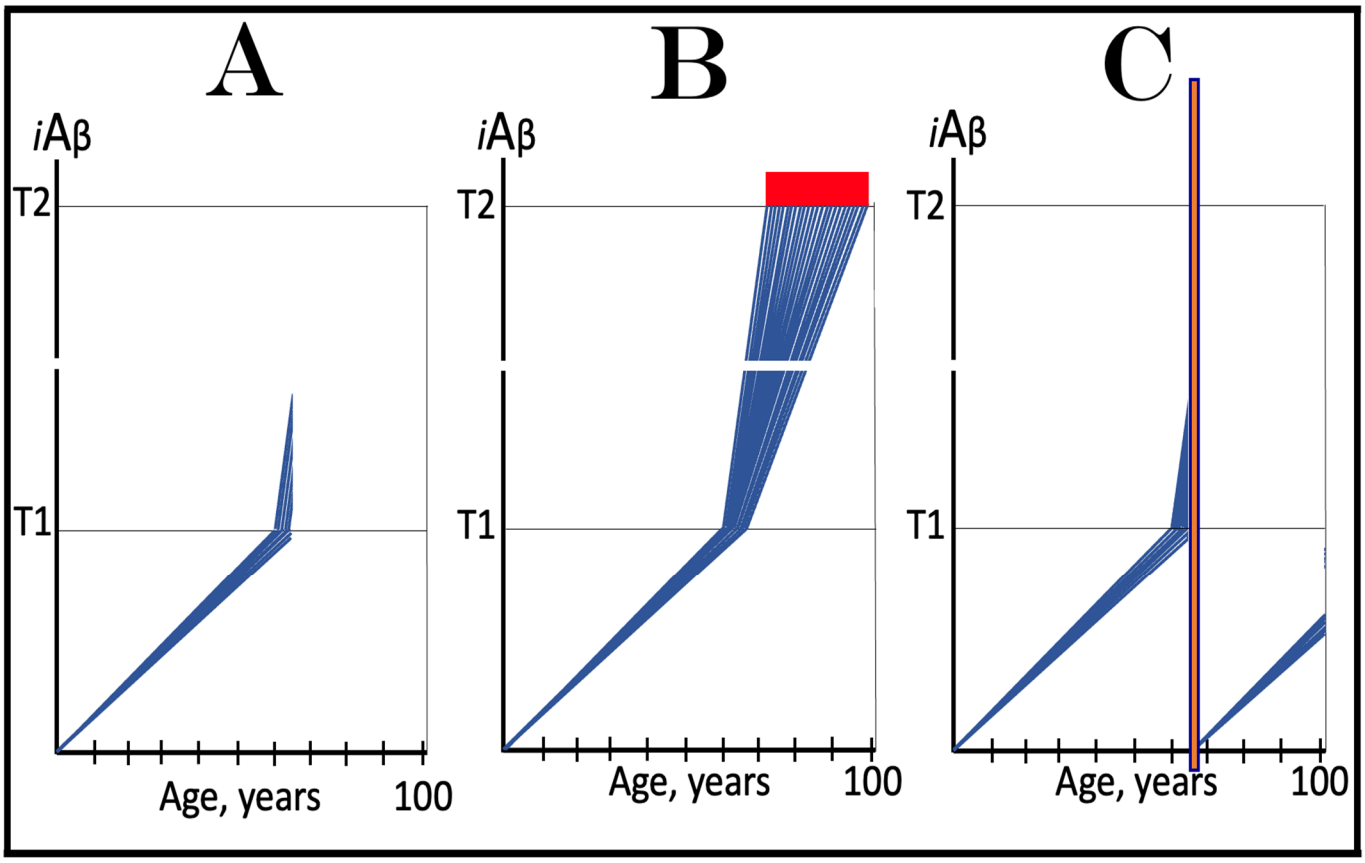

Figure 16. Prevention of AD by transient depletion of iAβ via its targeted degradation in asymptomatic high-risk individuals. *i*Aβ: Intraneuronal Aβ. *Blue lines*: Levels of *i*Aβ in individual neurons. ***T1*** *threshold*: The concentration of AβPP-derived *i*Aβ that mediates elicitation of the ISR and triggers the activation of the AβPP-independent *i*Aβ production pathway. ***T2*** *threshold*: The level of *i*Aβ, produced mainly in the AβPP-independent pathway, which triggers neuronal apoptosis. *Red box*: Apoptotic Zone, the range of *i*Aβ concentrations that cause the commitment to apoptosis. *Orange box*:

The duration of the transient administration of an ACH2.0-based drug. Panel (**A**): The initial state of the levels of *i*Aβ in the neuronal population of an individual. A significant fraction of the neuronal population has already crossed the T1 threshold and activated the AβPP-independent *i*Aβ production pathway. Panel (**B**): The evolution of the initial state in the absence of the treatment. The initially sub-T1 neurons cross the T1 threshold; the AβPP-independent *i*Aβ generation pathway is now active in all affected neurons. The levels of *i*Aβ rapidly increase, cross the T2 threshold and trigger apoptosis. When a sufficient proportion of neurons lose their functionality or die, the disease enters the end stage. Panel (**C**): The evolution of the initial state following the *i*Aβ depletion treatment with an ACH2.0-based drug. *i*Aβ is depleted in all neurons, including the initial over-T1 neuronal fraction, and the operation of the AβPP-independent *i*Aβ production pathway in this neuronal subpopulation ceases. The de novo accumulation of *i*Aβ, produced at this point solely in the AβPP proteolytic pathway, resumes from the low baseline. Provided the depletion was sufficiently deep, the T1 threshold would not be reached and AD would not occur within the lifetime of the treated individual. Thus, the one-time-only transient administration of the ACH2.0-based drug can potentially provide lifelong protection from AD even in high-risk individuals. Note that this result is in sharp contrast to the outcome of the long-term employment of the ACH-based drugs in a similar setting, shown in Figure 6 above.

20. Implementation of ACH2.0-Based Drugs in Prevention and Treatment of AACD

20.1. Transient iAβ Depletion Treatment in Prevention of AACD

In terms of ACH2.0, preventing AACD requires precluding the levels of AβPP-derived *i*Aβ from reaching the T^0 threshold. Panels A through C of Figure 17 depict the implementation of an ACH2.0-based drug in achieving this objective. Panel A shows the initial state of the levels of AβPP-derived *i*Aβ in the neuronal population of an individual. They have not yet reached the T^0 threshold, and no AACD symptoms have manifested. Panel B of Figure 17 shows the evolution of the initial state in the untreated individual. The AβPP-derived *i*Aβ levels reach the T^0 threshold and cross into the AACD Zone (defined above). AACD symptoms manifest and the condition progresses in parallel with the increase in the levels of AβPP-derived *i*Aβ. Provided the sufficient lifespan of the individual, the levels of AβPP-derived *i*Aβ would reach and cross the T1 threshold, trigger the activation of the AβPP-independent *i*Aβ production pathway, and AD would ensue. Panel C of Figure 17 illustrates the evolution of the initial state following the transient *i*Aβ depletion treatment with an ACH2.0-based drug. As a result of the treatment, the *i*Aβ levels are substantially reset, and the de novo accumulation of AβPP-derived *i*Aβ resumes from a low baseline. Provided the *i*Aβ depletion is sufficiently deep, its levels would not reach the T^0 threshold within the lifetime of the treated individual and no AACD (and, moreover, no AD) would occur. It should be noted that since the age of the onset of AACD is statistically greater than that of AD (discussed above), the potentially once-in-a-lifetime AD-preventive transient iAb depletion treatment would also protect from AACD.

20.2. Transient iAβ Depletion Treatment in Early AACD

The ACH2.0-based drugs are potentially also capable of treating and curing AACD. Indeed, in the ACH2.0 framework, this condition is driven by AβPP-derived *i*Aβ within a certain range of concentrations (T^0 to T1 thresholds; the AACD Zone). The successful treatment, therefore, requires the depletion of the *i*Aβ levels below the T^0 level. If, following the *i*Aβ depletion treatment, the affected neurons are capable of restoring their functionality, the treated AACD patient would be cured. Panels A′ through C′ of Figure 17 show the implementation of the transient *i*Aβ depletion therapy in the treatment of early AACD. Panel A′ depicts the initial state of the *i*Aβ levels in the neuronal population of the patient. They all have crossed the T^0 threshold and the early AACD symptoms have manifested; none have yet crossed the T1 threshold. Panel B′ of Figure 17 shows the evolution of the initial state in the untreated AACD patient. It is, essentially, the same as in panel B of the same figure: AβPP-derived *i*Aβ would

further accumulate and the condition would progress. If and when (depending on the longevity of the patient), its levels cross the T1 threshold, the AβPP-independent *i*Aβ production pathway would be activated, and the AD would commence. Panel C' of Figure 17 illustrates the effect of the transient *i*Aβ depletion treatment on the evolution of the initial state. The levels of *i*Aβ are substantially reduced; at this point, the patient is technically cured. The de novo accumulation of AβPP-derived *i*Aβ commences from a low baseline and, assuming it proceeds at the pre-treatment rate, the restoration of its levels would require decades. Consequently, neither the crossing of the T^0 threshold would occur nor would AACD recur within the lifetime of the treated patient.

20.3. Transient iAβ Depletion Treatment in Late AACD

In terms of ACH2.0, AACD is driven by AβPP-derived *i*Aβ. Therefore, as discussed above, AACD can be potentially treated with ACH-based drugs. These drugs, however, are ineffective in the late AACD cases that are asymptomatic for AD but where a fraction of, and, possibly, the entire neuronal population have already crossed the T1 threshold (see Section 11 above) and where *i*Aβ is produced mainly in the AβPP-independent pathway, which is insensitive to ACH-based drugs. On the other hand, such a scenario presents no difficulties for ACH2.0-based drugs. Indeed, as illustrated in panels A" through C" of Figure 17, the transient *i*Aβ depletion therapy would be as effective in the late AACD cases as it presumably is in the early instances of this condition. Panel A" of Figure 17 depicts the initial state of the *i*Aβ levels in the neuronal population of a late-stage AACD patient. In all neurons, the *i*Aβ levels have crossed the T^0 threshold and progressed deep into the AACD Zone. The patient is asymptomatic for AD but in a subpopulation of his neurons, the levels of *i*Aβ have already crossed the T1 threshold, and the AβPP-independent *i*Aβ production pathway is operational. Panel B" of Figure 17 shows the evolution of the initial state in the untreated patient. The initially over-T1 neuronal subpopulation continues to accumulate *i*Aβ, produced mainly in the AβPP-independent pathway. The initially sub-T1 neuronal fraction crosses the T1 threshold, the AβPP-independent *i*Aβ generation pathway becomes operational in all affected neurons, and the AD progresses toward the end stage. Panel C" of Figure 17 illustrates the evolution of the initial state following the transient administration of an ACH2.0-based drug. *i*Aβ is substantially depleted, and its levels are reduced to nearly the initial baseline in *all* neurons, both sub-T1 and over-T1. At this stage, the patient is cured, subject to the restoration of full functionality in the affected neurons. In the initially over-T1 neuronal subpopulation, the operation of the AβPP-independent *i*Aβ production pathway ceases. The de novo accumulation of *i*Aβ, produced now solely in the AβPP proteolytic pathway, resumes from the low baseline. The levels of AβPP-derived *i*Aβ would not reach the T^0 threshold and neither AACD would recur nor would AD occur within the lifetime of the treated patient. In this situation, the remarkable efficiency of the ACH2.0-based drug is due to its ability to switch off the operation of the AβPP-independent *i*Aβ production pathway by interrupting the self-sustaining cycle and depriving the pathway of its stimulant. This ability of the ACH2.0-based drugs is at the core of its potential effect in symptomatic AD, discussed in the following section.

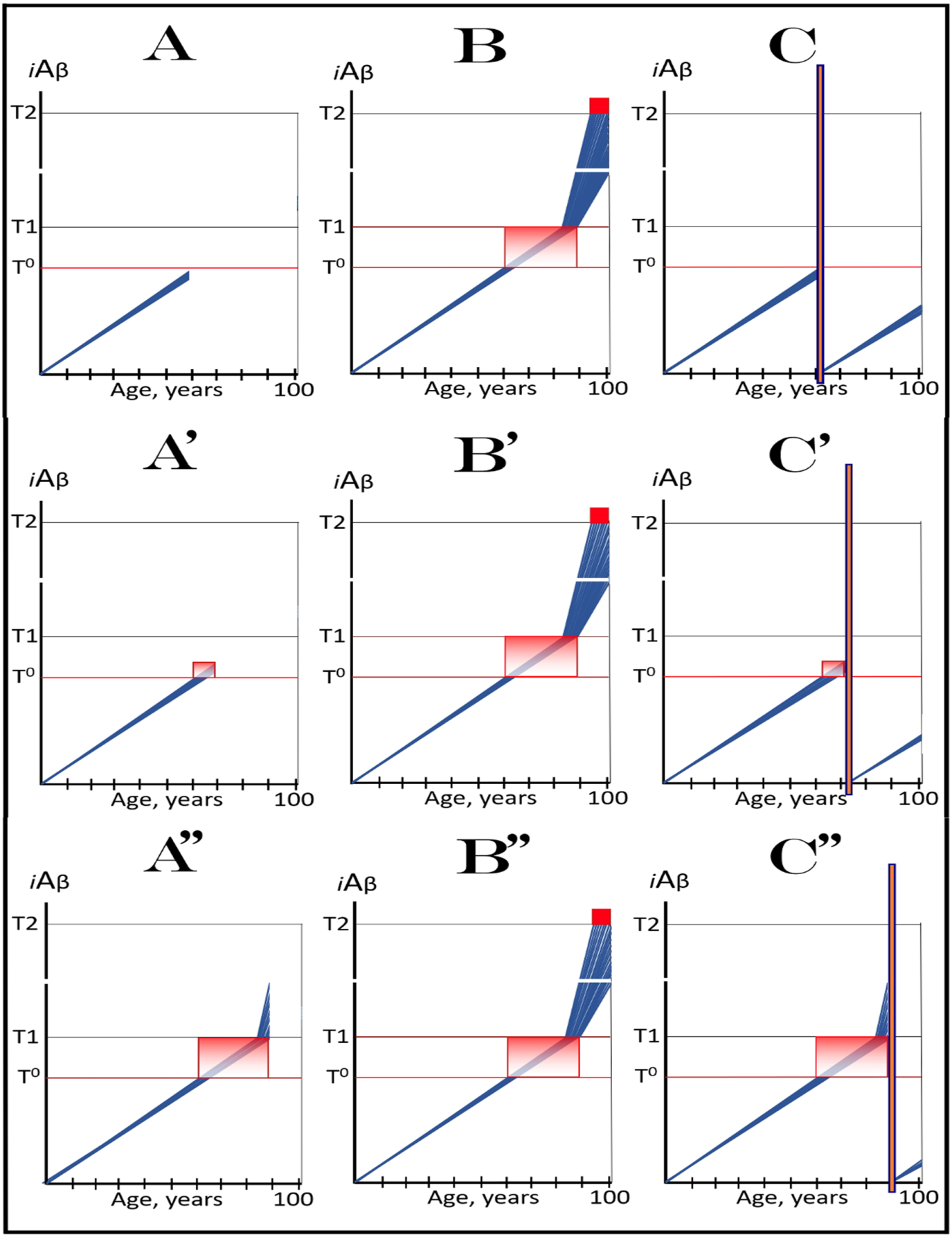

Figure 17. ACH2.0-based drugs in prevention and treatment of AACD. *i*Aβ: Intraneuronal Aβ. *Blue lines*: Levels of *i*Aβ in individual neurons. T^0 *threshold*: The concentration of *i*Aβ that triggers

the neurodegeneration manifesting as AACD. ***T1*** *threshold*: The concentration of AβPP-derived *i*Aβ that mediates elicitation of the ISR and triggers the activation of the AβPP-independent *i*Aβ production pathway. ***T2*** *threshold*: The level of *i*Aβ, produced mainly in the AβPP-independent pathway, which triggers neuronal apoptosis. *Pink gradient boxes*: AACD Zone, the range of concentration of AβPP-derived *i*Aβ between the T^0 and T1 boundaries. *Red boxes*: Apoptotic Zone, the range of *i*Aβ concentrations that cause the commitment to apoptosis. *Orange boxes*: The duration of the transient administration of an ACH2.0-based drug. Panels (**A**–**C**): Transient *i*Aβ depletion treatment in prevention of AACD. Panel (**A**): The initial state of the levels of AβPP-derived *i*Aβ in the neuronal population of an individual; they have not yet reached the T^0 threshold, and no AACD symptoms have yet manifested. Panel (**B**): The evolution of the initial state in the untreated individual. The AβPP-derived *i*Aβ levels reach the T^0 threshold and cross into the AACD Zone. AACD symptoms manifest and the condition progresses in parallel with the increase in the levels of AβPP-derived *i*Aβ. Provided a sufficient lifespan, the levels of AβPP-derived *i*Aβ would cross the T1 threshold, trigger the activation of the AβPP-independent *i*Aβ production pathway, and AD would ensue. Panel (**C**): The evolution of the initial state following the transient *i*Aβ depletion treatment with an ACH2.0-based drug. The *i*Aβ levels are substantially reset, and the de novo accumulation of AβPP-derived *i*Aβ resumes from a low baseline. Provided the *i*Aβ depletion is sufficiently deep, its levels would not reach the T^0 threshold within the lifetime of the treated individual and no AACD (and, moreover, no AD) would occur. Panels (**A′**–**C′**): Transient *i*Aβ depletion treatment in early AACD. Panel (**A′**): The initial state of the *i*Aβ levels in the neuronal population of the patient; they all have crossed the T^0 threshold and the early AACD symptoms have manifested; none has yet crossed the T1 threshold. Panel (**B′**): The evolution of the initial state in the untreated AACD patient; essentially, the same as in panel (**B**) above. Panel (**C′**): The effect of the transient *i*Aβ depletion treatment on the evolution of the initial state. The levels of *i*Aβ are substantially reduced; at this point, the patient is technically cured. The de novo accumulation of AβPP-derived *i*Aβ commences from a low baseline and the restoration of its levels would require decades. Neither the crossing of the T^0 threshold would occur, nor AACD would recur within the lifetime of the treated patient. Panels (**A″**–**C″**): Transient *i*Aβ depletion treatment in late AACD. Panel (**A″**): the initial state of the *i*Aβ levels in the neuronal population of a late-stage AACD patient. In all neurons, the *i*Aβ levels have crossed the T^0 threshold and progressed deep into the AACD Zone. The patient is asymptomatic for AD but in a subpopulation of his neurons, the levels of *i*Aβ have already crossed the T1 threshold, and the AβPP-independent *i*Aβ production pathway is operational. Panel (**B″**): The evolution of the initial state in the untreated patient. The initially sub-T1 neuronal fraction crosses the T1 threshold, the AβPP-independent *i*Aβ generation pathway becomes operational in all affected neurons, and the AD progresses toward the end stage. Panel (**C″**): The evolution of the initial state following the transient administration of an ACH2.0-based drug. *i*Aβ is substantially depleted, and its levels are reduced to nearly the initial baseline in *all* neurons, both sub-T1 and over-T1; the operation of the AβPP-independent *i*Aβ production pathway ceases. At this stage, the patient is cured, subject to the restoration of full functionality in the affected neurons. The de novo accumulation of *i*Aβ, produced now solely in the AβPP proteolytic pathway, resumes from the low baseline. The levels of AβPP-derived *i*Aβ would not reach the T^0 threshold and neither AACD would recur nor AD would occur within the lifetime of the treated patient.

21. The Proverbial "Holy Grail" of the Alzheimer's Research Attained: ACH2.0-Based Drugs Are Capable of Treatment of AD at Its Symptomatic Stages

Arguably, the prevention of AD is of the greatest strategic importance in addressing the disorder. Practically and emotionally, however, the ability to treat and possibly cure the disease at its devastating symptomatic stages has always been and remains the "Holy Grail" of Alzheimer's research. No drug developed to date has even approached this goal. As discussed above, in terms of the ACH2.0, the implementation of the ACH-based drugs, although potentially useful in the prevention of AD, conceptually would be, and was, in fact, shown in multiple clinical trials to be futile at the symptomatic stages of Alzheimer's

disease. This is because, following the crossing of the T1 threshold and the commencement of AD, its pathology is driven by *i*Aβ generated mainly in the AβPP-independent pathway, which is completely insensitive to the ACH-based drugs. The key to the efficient treatment of AD at its symptomatic stages is, therefore, the reduction in the levels of *i*Aβ (i.e., the removal of the driver of the disease) and the cessation of its supply, i.e., the termination of the operation of the AβPP-independent *i*Aβ production pathway. The ACH2.0-based drugs fulfill both objectives: by achieving the former, they accomplish the latter. Indeed, conceptually, the ACH2.0-based drugs are the agents capable of the efficiently targeted degradation of *i*Aβ (see Section 26 below on the highly plausible prime candidates for this role). On the other hand, the operation of the AβPP-independent *i*Aβ production pathway requires, depends upon, and is propagated and perpetuated by sufficient levels of *i*Aβ; this is the essence of the AD Engine defined above. When the *i*Aβ levels are reduced to those below the T1 threshold, the operation of the AβPP-independent *i*Aβ generation pathway ceases and the AD Engine stops. Following its transient depletion, the accumulation of *i*Aβ resumes de novo but, at this point, its only source is the AβPP proteolysis. If the ACH2.0-based drug-mediated *i*Aβ depletion is "deep" enough, the single, once-in-a-lifetime transient treatment could be sufficient to preclude the AβPP-derived *i*Aβ levels from reaching the T1 threshold within the lifetime of the treated AD patient. In the absence of its driver, the progression of the disease would stop; the condition of the patient would at least stabilize and possibly improve, subject to the stage of intervention, the proportion of the remaining viable neurons, and their capacity for functional restoration.

The above scenario is illustrated in Figure 18. The transient *i*Aβ depletion treatment is administered at the different stages of AD. It is assumed that the treatment completely, or nearly completely, depletes the levels of *i*Aβ and that the rate of AβPP-derived *i*Aβ accumulation is the same both pre- and post-treatment. In panel A of Figure 18, the transient *i*Aβ depletion treatment is administered at the early symptomatic stage. A fraction of the patient's neurons have crossed both the T1 and T2 thresholds, initiated apoptosis, and triggered the manifestation of AD symptoms. This neuronal fraction is unredeemable. A substantial neuronal subpopulation, the majority at this early symptomatic stage, did not yet reach the T2 threshold. In these neurons, cellular damage is either insubstantial or reversible. The *i*Aβ depletion therapy resets the levels of *i*Aβ to a low baseline. The operation of the AβPP-independent *i*Aβ production pathway ceases. The accumulation of *i*Aβ resumes de novo from the initial or the nearly initial baseline, and is supported solely by its production in the AβPP proteolytic pathway. Its levels would not reach the T1 threshold and the disease would not re-ignite within the lifetime of the treated patient. The progression of the disease would be certainly stopped. The condition of the patient and their cognitive functions are expected to improve. Provided the still-viable neurons are capable of recovering their functionality and reconnecting, the patient would be at least partially cured.

Panels B through D of Figure 18 illustrate the effects of the administration of the transient *i*Aβ depletion treatment at various symptomatic stages of AD. Conceptually, the effect at the advanced stages of AD is the same as at its early stage, depicted in panel A. The difference is the proportion of remaining viable neurons at the time of the treatment administration. As the disease advances, progressively more affected neurons cross the T2 threshold and commit apoptosis; they are either dead or unresponsive to the treatment. This leaves a progressively smaller number of still-viable, treatment-responsive neurons. In these cells, following the reduction in the *i*Aβ levels, the operation of the AβPP-independent *i*Aβ generation pathway would stop. The accumulation of *i*Aβ would recommence de novo from the low baseline and only in the AβPP proteolytic pathway. Its levels would not reach the T1 threshold and the disease would not resume within the remaining lifespan of the treated patient. The treatment would certainly stop or decelerate the progression of the disease and the conditions of the treated patients are expected to improve but the restoration of the cognitive functions would be progressively less likely at more advanced stages of AD.

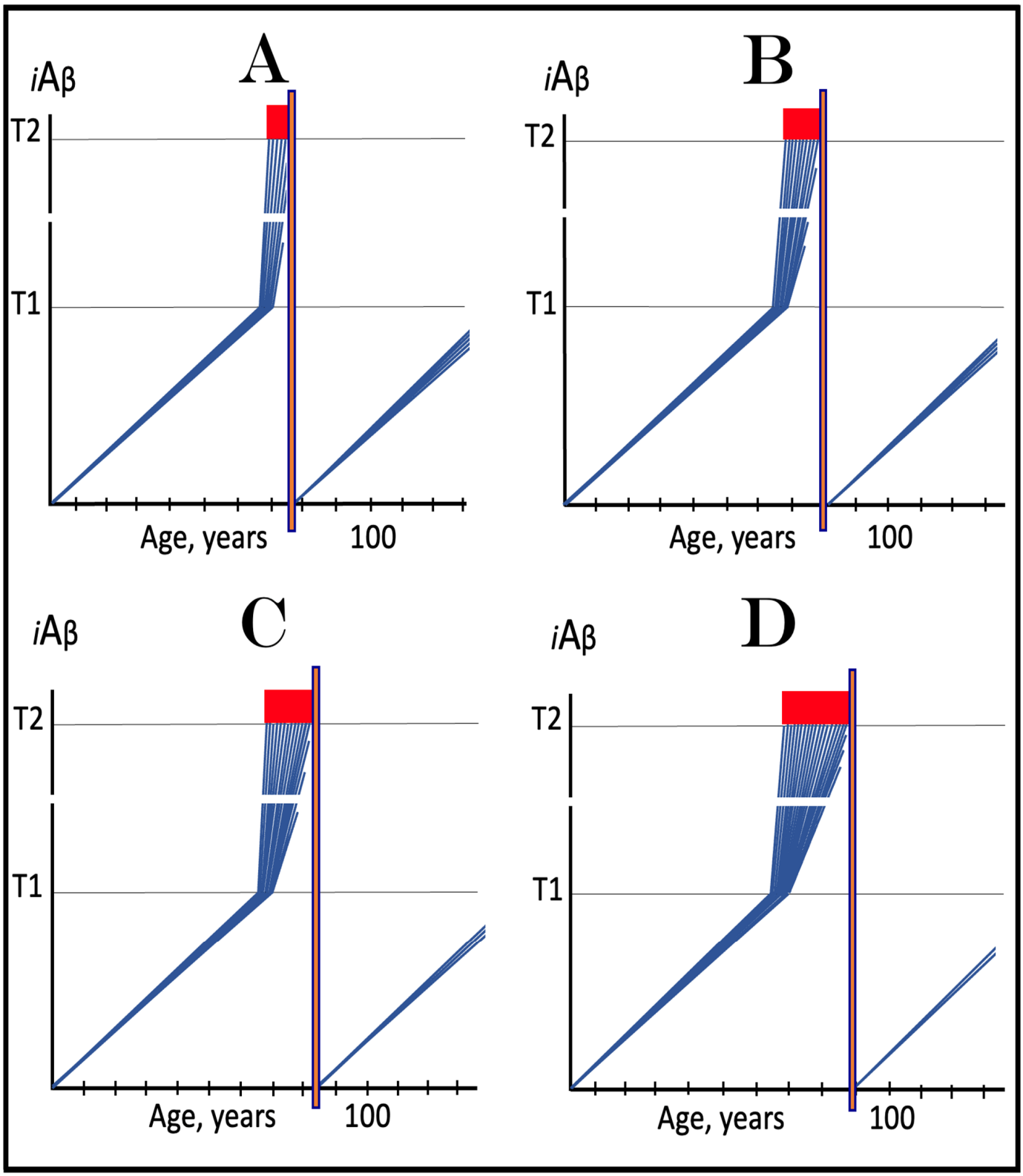

Figure 18. ACH2.0-based drugs are capable of treatment of AD at its symptomatic stages. *i*Aβ: Intraneuronal Aβ. *Blue lines*: Levels of *i*Aβ in individual neurons. ***T1*** *threshold*: The concentration of AβPP-derived *i*Aβ that mediates elicitation of the ISR and triggers the activation of the AβPP-independent *i*Aβ production pathway. ***T2*** *threshold*: The level of *i*Aβ, produced mainly in the AβPP-

independent pathway, which triggers neuronal apoptosis. *Red boxes*: Apoptotic Zone, the range of *i*Aβ concentrations that cause the commitment to apoptosis. *Orange boxes*: The duration of the transient administration of an ACH2.0-based drug. Panel (**A**): The transient administration of the ACH2.0-based drug is implemented at the early stage of AD. At this time the majority of the affected neurons have not yet reached the T2 threshold and are still viable and capable of recovering and reconnecting. The treatment resets the levels of *i*Aβ to nearly their initial baseline. The operation of the AβPP-independent *i*Aβ production pathway ceases, and the *i*Aβ accumulation commences de novo from the low baseline and solely in the AβPP proteolytic pathway. Provided the post-treatment rate of accumulation of AβPP-derived *i*Aβ is similar to that occurring pre-treatment, the T1 threshold would not be reached and the disease would not recur within the remaining lifespan of the treated patient. Panels (**B**–**D**): The transient administration of the ACH2.0-based drug is executed at more and more advanced stages of the disease. The outcomes are principally identical to the one described above except that with the advancement of the disease, the progressively increasing proportions of the affected neurons cross the T2 threshold and commit apoptosis; this leaves fewer and fewer viable neurons capable of recovering their functionality. In this case, the progression of AD would stop but the recovery of cognitive functions would depend of the proportion of the redeemed neurons.

It should be emphasized that at the symptomatic stages of AD, the duration of the *i*Aβ depletion treatment depends on both the reduction in the levels of *i*Aβ to a sufficiently low baseline and the cessation of the operation of the AβPP-independent *i*Aβ production pathway. This is because, in these circumstances, the former does not directly and immediately trigger the latter. The *i*Aβ-driven AD pathology involves the generation of various stressors, such as substantial levels of unfolded and/or misfolded proteins. As a result, if the ISR alone is sufficient to maintain the activity of the AβPP-independent *i*Aβ generation pathway, then even after the depletion of *i*Aβ below the T1 threshold, these stressors may sustain the operation of the pathway until their levels are sufficiently reduced through the action of cellular chaperones. Consequently, if the *i*Aβ depletion therapy is terminated while the AβPP-independent *i*Aβ production pathway is still operational, *i*Aβ could rapidly accumulate to over-T1 levels and re-ignite the AD Engine.

22. Clinical Trials of ACH2.0-Based Drugs in Prevention of AD: Unambiguous Evaluation Even with High-Risk Over-T1 Participants

The present and the two following sections analyze the evaluation of the efficiency of the ACH2.0-based drugs in clinical trials. These sections consider three situations where the assessment of the ACH-based drugs was shown problematic or impossible. They conclude that the evaluation of the efficacy of the ACH2.0-based drugs in the same circumstances would yield unequivocal conclusions. The present section examines clinical trials of ACH2.0-based drugs for the prevention of AD in high-risk individuals (compared with Section 15 above, which concluded that clinical trials of the ACH-based drugs in the same setting are practically impossible and/or self-defeating). Figure 19 presents three different situations identical to those considered in Figure 12 (Section 15 above) but with drastically distinct outcomes. In all three parts of Figure 19, all selected subjects are asymptomatic for AD but are at high risk for developing the disease. As discussed above, it is inevitable that a substantial proportion of trial participants or even the entire cohort are over T1, i.e., the levels of AβPP-derived *i*Aβ in their neurons have crossed the T1 threshold. Panel A in the upper part of Figure 19 depicts the initial state where about 50% of the trial participants are over T1. In these individuals, the AβPP-independent *i*Aβ production pathway is operational; its product (*i*Aβ generated independently of AβPP) is rapidly accumulating but has not yet reached the Ts threshold ("symptomatic threshold"), and the subjects remain asymptomatic. Panel B in the upper part of Figure 19 shows the evolution of the initial state in the untreated (placebo) cohort. The levels of AβPP-derived *i*Aβ in initially sub-T1 trial subjects cross the T1 threshold and trigger the activation of the AβPP-independent *i*Aβ production pathway. At this

point, all subjects are over T1. The levels of *i*Aβ, produced mainly independently of AβPP, rapidly increase and eventually cross the Ts threshold. All subjects enter the Symptomatic Zone (pink box) and the AD symptoms manifest. Panel C in the upper part of Figure 19 illustrates the evolution of the initial state following the transient *i*Aβ depletion therapy (orange box). As a result of the treatment, the levels of *i*Aβ are substantially reduced in *all* subjects, and the operation of the AβPP-independent *i*Aβ generation pathway in over-T1 subjects ceases. The de novo accumulation of *i*Aβ, now produced solely in the AβPP proteolytic pathway, resumes from the low baselines in all treated participants. Its levels would not reach the T1 threshold within the lifetime of the treated subjects; the disease would be prevented in all subjects, there would be no overlap of any sort with the outcomes in the placebo cohort, and the outcomes of the trial would be unambiguously clear and lucidly interpretable.

In the middle part of Figure 19, panel A' depicts the initial state where about 75% of the trial subjects are over T1 and produce *i*Aβ in the AβPP-independent pathway. The levels of *i*Aβ, however, have not yet reached the Ts threshold and these subjects remain asymptomatic for AD. The evolution of this initial state, shown in panel B' of Figure 19, is similar to that depicted in panel B of the same Figure: the levels of *i*Aβ, produced mainly independently of AβPP, increase, reach the Ts threshold, cross into the Symptomatic Zone, and the AD symptoms manifest in all subjects. Panel C' in the middle part of Figure 19 illustrates the evolution of the initial state following the implementation of the transient *i*Aβ depletion therapy. The levels of *i*Aβ substantially decreased in all trial participants. The AβPP-independent *i*Aβ production pathway is rendered inoperative, and Aβ, and consequently *i*Aβ, are produced only by the AβPP proteolysis. The accumulation of AβPP-derived *i*Aβ resumes de novo and its levels would not reach the T1 threshold within the remaining lifespans of treated trial participants. The disease is fully prevented in the medicated cohort, there is no overlap with the outcomes in the placebo group, and the conclusions of the trial are unequivocal.

Panel A" in the bottom part of Figure 19 shows the initial state where the levels of AβPP-derived *i*Aβ have crossed the T1 threshold and the AβPP-independent *i*Aβ production pathway has been activated in all trial subjects; they all are over T1, but remain asymptomatic. As a practical aspect, it should be emphasized that this is the most likely situation if only high-risk subjects are selected. Panel B" in the bottom part of Figure 19 depicts the evolution of this initial state. Conceptually, it is identical to those depicted in panels B and B', only faster. The levels of *i*Aβ reach the Ts threshold, cross into the Symptomatic Zone, and the symptoms of AD manifest. In panel C" of Figure 19, the participants are subjected to transient *i*Aβ depletion therapy (orange box). This results in the levels of *i*Aβ being reduced to the initial or nearly initial baseline. The activity of the AβPP-independent *i*Aβ production pathway stops. The accumulation of *i*Aβ is resumed de novo and only in the AβPP proteolytic pathway. Its levels would not reach the T1 threshold within the lifetime of the treated subjects; the disease is prevented in all treated trial participants. This outcome is drastically distinct from results with the ACH-based drugs in the same situation, where all treated participants develop AD and the outcomes in the medicated and placebo cohorts are indistinguishable. With ACH2.0-based drugs, in sharp contrast, the outcomes of the trial are unambiguous.

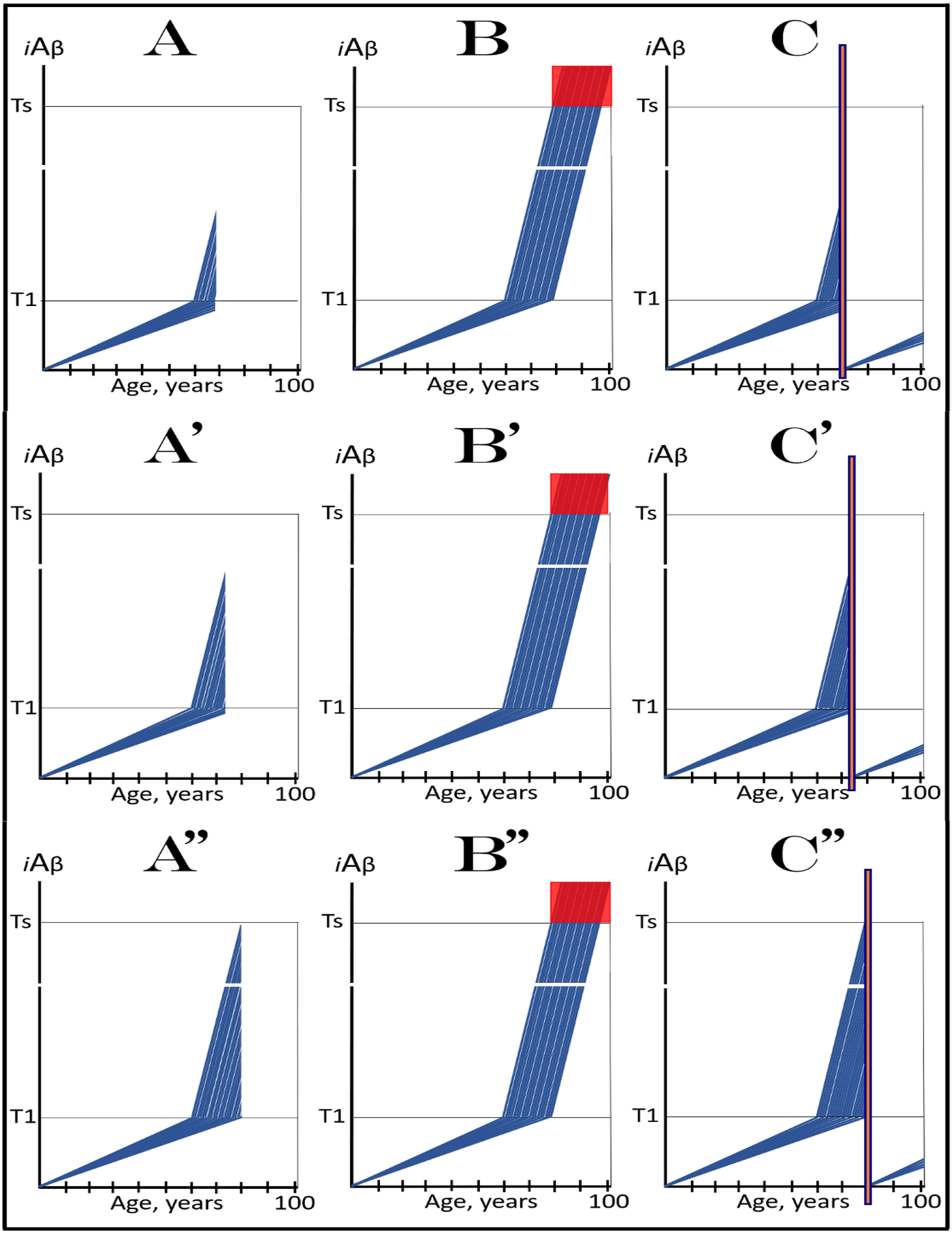

Figure 19. Clinical trials of ACH2.0-based drugs in prevention of AD with high-risk cohorts. *i*Aβ: Intraneuronal Aβ. *Blue lines*: The levels of *i*Aβ in individual trial subjects. ***T1*** *threshold*: The concentration

of AβPP-derived *i*Aβ that mediates elicitation of the ISR and triggers the activation of the AβPP-independent *i*Aβ production pathway. ***Ts*** *threshold*: The levels of *i*Aβ that trigger the manifestation of AD symptoms. *Pink boxes*: Symptomatic Zone, the range of *i*Aβ concentrations above the Ts threshold. *Orange boxes*: The duration of administration of an ACH-based drug. Panel (**A**): All trial subjects are asymptomatic but about 50% have crossed the T1 threshold and activated the AβPP-independent *i*Aβ production pathway. Panel (**B**): The evolution of the initial stage in the placebo group. The levels of AβPP-derived *i*Aβ cross the T1 threshold and the AβPP-independent *i*Aβ generation pathway becomes operational in all trial subjects. *i*Aβ levels increase and cross the Ts threshold, subjects enter the Symptomatic Zone and AD symptoms manifest. Panel (**C**): The evolution of the initial state following the transient administration of an ACH2.0-based drug (orange box). The transient *i*Aβ depletion via its targeted degradation resets the levels of *i*Aβ to nearly its initial baseline in all trial subjects, both over-T1 and sub-T1. The operation of the AβPP-independent *i*Aβ production pathway ceases and the accumulation of *i*Aβ resumes de novo supported now only by its production in the AβPP proteolytic pathway. The levels of AβPP-derived *i*Aβ would not reach the T1 threshold and AD would not occur (for initially sub-T1 patients) or recur (for initially over-T1 patients) within the remaining lifetimes of the treated individuals. Panels (**A′**–**C′**,**A″**–**C″**) reiterate the same sequence as shown in panels A through C but with increasing proportions of asymptomatic over-T1 subjects: 75% in (**A′**–**C′**) and 100% in (**A″**–**C″**). In both cases, the evolutions of the initial states in the treated and the placebo cohorts are identical to those described above. In all three scenarios, the outcomes in the treated cohorts are unequivocally distinct from those in the placebo groups and are unambiguously interpretable.

23. Clinical Trials of ACH2.0-Based Drugs in Treatment of AACD: No Complications Even with Late-Stage Participants

Above, a setting for the AD-preventive clinical trials was examined that is self-defeating for the ACH-based drugs but informatively straightforward for the ACH2.0-based drugs. Another conceptually similar example is the evaluation of a drug's efficiency in the treatment of AACD in a setting that includes late-stage AACD patients. The analysis presented in Section 16 above concluded that such an assessment would be unfeasible for ACH-based drugs. The present section examines the performance of the ACH2.0-based drugs in an identical setting and establishes that it would result in unequivocal conclusions. The situation under discussion is illustrated in Figure 20. Panel A of Figure 20 depicts the initial state of clinical trials for the treatment of AACD. The only criteria for participation in this trial are the presentation of the AACD symptoms. In all selected participants the levels of AβPP-derived *i*Aβ have crossed the T^0 threshold and entered the AACD Zone (pink gradient box); all participants are asymptomatic for AD. In a fraction of participating late-stage AACD patients, however, AβPP-derived *i*Aβ has crossed the T1 threshold and triggered the activation of the AβPP-independent *i*Aβ production pathway, yet these participants remain asymptomatic for AD. The evolution of this initial state in the untreated trial subjects is not shown here since it is presented in panel B of Figure 13 above. Briefly, AACD would progress, the levels of AβPP-derived *i*Aβ would eventually cross the T1 threshold in all initially sub-T1 subjects, and, provided sufficiently long lifespans, AD would ensue. The evolution of the initial state following the transient *i*Aβ depletion therapy (orange box) is shown in panel B of Figure 20. As a result of the treatment, the levels of *i*Aβ are substantially reduced in all patients, including the initially over-T1 fraction. In this fraction, the operation of the AβPP-independent *i*Aβ production pathway ceases. All treated trial subjects are technically cured. The de novo accumulation of *i*Aβ resumes solely in the AβPP proteolytic pathway. Its levels would not reach the T^0 threshold and AACD would not recur within the lifetime of the treated trial subjects. The outcomes in the medicated cohort would not overlap in any way with those in the placebo group and thus would be unambiguously interpretable.

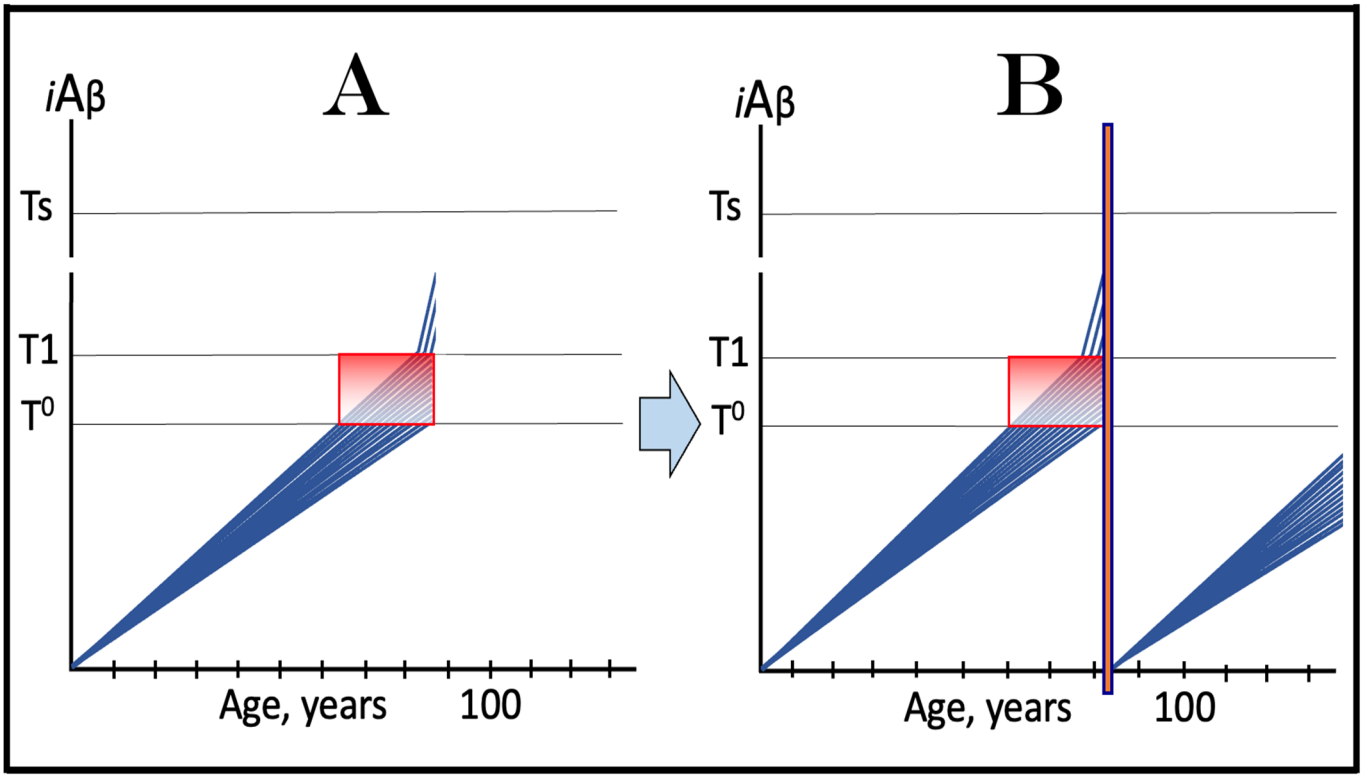

Figure 20. Clinical trials of ACH2.0-based drugs in treatment of AACD are feasible even with late-stage patients. *i*Aβ: Intraneuronal Aβ. *Blue lines*: The levels of *i*Aβ in individual trial subjects. ***T*^{0}** *threshold*: The concentration of *i*Aβ that triggers the neurodegeneration manifesting as AACD. ***T1*** *threshold*: The concentration of AβPP-derived *i*Aβ that mediates elicitation of the ISR and triggers the activation of the AβPP-independent *i*Aβ production pathway. ***Ts*** *threshold*: The levels of *i*Aβ that trigger the manifestation of AD symptoms. *Pink gradient boxes*: AACD Zone, the range of concentration of AβPP-derived *i*Aβ between the T^{0} and T1 boundaries. *Orange box*: The duration of administration of an ACH-based drug. Panel (**A**): The initial state. All subjects exhibit the AACD symptoms and are asymptomatic for AD. In the majority of trial participants, the levels of *i*Aβ are confined between the boundaries of the T^{0} and T1 thresholds. In a fraction of trial subjects the levels of *i*Aβ have crossed the T1 threshold and triggered the activation of the AβPP-independent *i*Aβ production pathway. The evolution of this initial state in the placebo cohort is depicted in panel B of Figure 13 and is not shown here (briefly, all subjects cross the T1 threshold and AD ensues). Panel (**B**): The evolution of the initial state following the *i*Aβ depletion via transient administration of the ACH2.0-based drug (orange box). The transient *i*Aβ depletion via its targeted degradation resets the levels of *i*Aβ to nearly its initial baseline in all trial subjects, both over-T1 and sub-T1. The operation of the AβPP-independent *i*Aβ production pathway ceases. At this point, the treated trial participants are cured. The accumulation of *i*Aβ resumes de novo supported now only by its production in the AβPP proteolytic pathway. The levels of AβPP-derived *i*Aβ would not reach the T^{0} threshold and AACD would not recur within the remaining lifetimes of the treated individuals. The outcome in the treated cohort is distinctly different from that in the placebo group and can be unambiguously interpreted.

24. Clinical Trials of ACH2.0-Based Drugs in Treatment of Symptomatic AD: Lucidly Interpretable Outcomes at All Stages of the Disease

The final example of AD clinical trials, impossible with the ACH-based drugs but straightforward and informative with the ACH2.0-based drugs, is their evaluation in the treatment of symptomatic AD. Such trials are impossible with the ACH-based drugs because these drugs would have at best only marginal effect in very early AD (when a fraction of the neurons may not yet have crossed the T1 threshold), as exemplified by the clinical

trials of lecanemab and donanemab, and would yield no beneficial effect whatsoever in the advanced stages of the disease when the AβPP-independent *i*Aβ production pathway has been activated in all affected neurons. In contrast, as discussed in Section 19 above, ACH2.0-based drugs would be effective in stopping the progression of the disease regardless of its stage. The design and the outcomes of the clinical trial examining the effect of ACH2.0-based drugs in symptomatic AD are considered in Figure 21. Panel A of Figure 21 depicts the initial state of the trial. All trial participants are symptomatic for AD; this is the only criterion for their inclusion. The levels of *i*Aβ, produced mainly in the AβPP-independent pathway, have crossed the Ts threshold and entered the Symptomatic Zone (pink box) in all trial subjects. The cohort covers the entire spectrum of AD pathology: in different subjects, the symptoms vary from very early and mild to very advanced and severe.

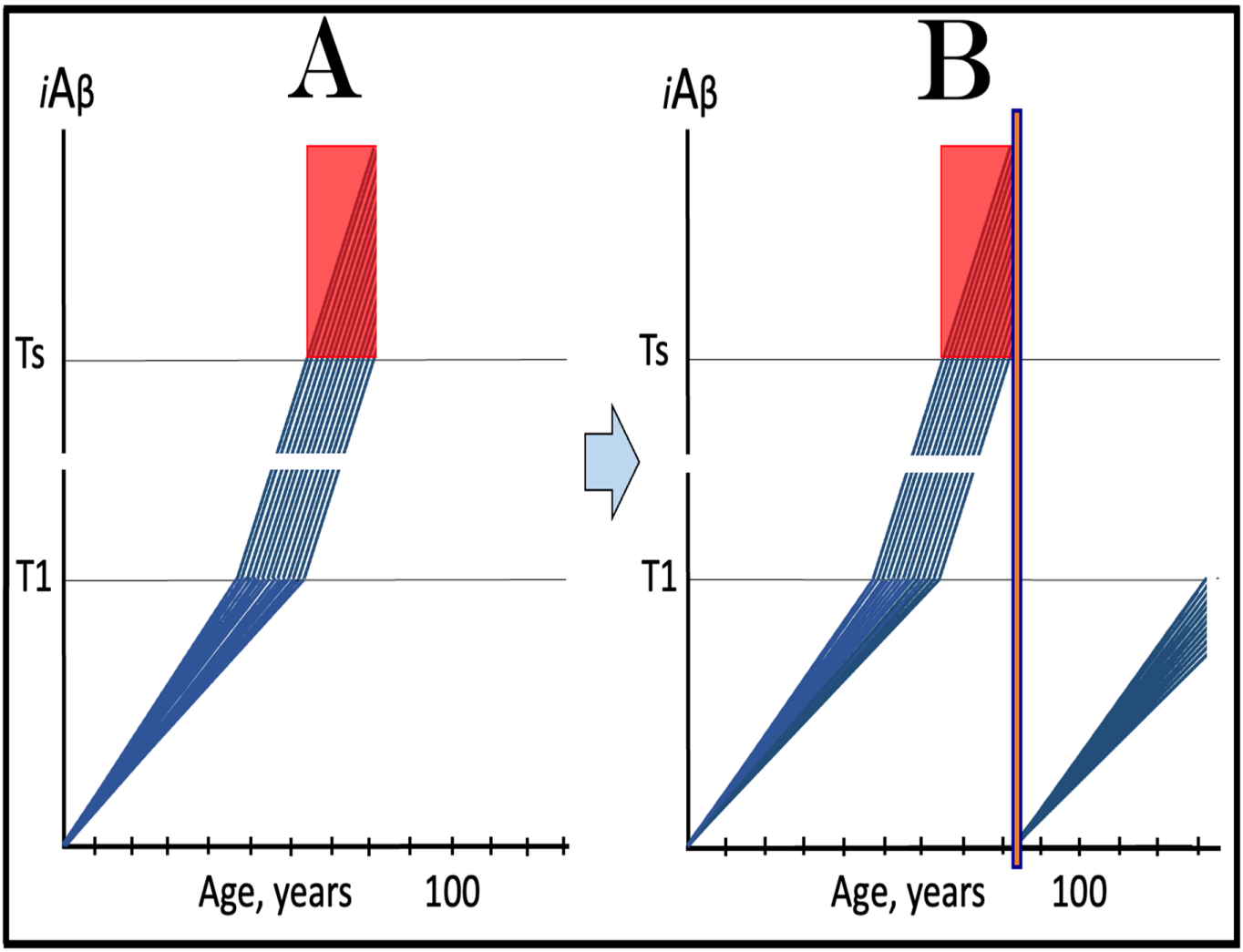

Figure 21. Clinical trials of ACH2.0-based drugs in treatment of symptomatic AD. *i*Aβ: Intraneuronal Aβ. *Blue lines*: The levels of *i*Aβ in individual trial subjects. ***T1** threshold*: The concentration of AβPP-derived *i*Aβ that mediates elicitation of the ISR and triggers the activation of the AβPP-independent *i*Aβ production pathway. ***Ts** threshold*: The levels of *i*Aβ that trigger the manifestation of AD symptoms. *Pink boxes*: Symptomatic Zone, the range of *i*Aβ concentrations above the Ts threshold. *Orange box*: The duration of the transient administration of an ACH2.0-based drug. Panel (**A**): The initial state of *i*Aβ levels in individual trial subjects at the commencement of the treatment. All trial participants are symptomatic for AD; this is the only criterion for their inclusion. The levels of *i*Aβ,

produced mainly in the AβPP-independent pathway, have crossed the Ts threshold and entered the Symptomatic Zone (pink box) in all trial subjects. The cohort covers the entire spectrum of AD pathology: in different subjects, the symptoms vary from very early and mild to very advanced and severe. The evolution of this initial state in the placebo group is obvious: in all subjects, the disease progresses toward the end stage. Panel (**B**): Evolution of the initial state following the *i*Aβ depletion treatment. The levels of *i*Aβ are reset and substantially reduced in all trial subjects. The operation of the AβPP-independent pathway of *i*Aβ production ceases and it is now generated solely in the AβPP proteolytic pathway. Due to the insufficient levels of its principal driver, the progression of AD is arrested. The accumulation of the *i*Aβ initiates de novo, supported only by the AβPP proteolysis. The AβPP-derived *i*Aβ levels would not reach the T1 threshold and the disease would not resume within the lifetimes of the treated patients, the outcome that is unequivocally distinguishable from that occurring in the placebo cohort.

The evolution of the initial state in untreated trial subjects is obvious: the symptoms develop further, and the disease progresses and reaches the end stage in all untreated participants. The evolution of the initial state following the *i*Aβ depletion treatment is shown in panel B of Figure 21. The levels of *i*Aβ are reset and substantially reduced in all trial subjects. The operation of the AβPP-independent pathway of *i*Aβ production ceases and it is now generated solely in the AβPP proteolytic pathway. Due to the insufficient levels of its principal driver, the progression of AD is arrested. The accumulation of the *i*Aβ initiates de novo, supported only by the AβPP proteolysis. The AβPP-derived *i*Aβ levels would not reach the T1 threshold and the disease would not resume within the lifetimes of the treated patients. The prognostic outcomes would differ individually depending on the initial symptomatic stage of a patient. At the early stages, the majority of the neuronal population of an individual trial participant remains viable at the time of the treatment and is redeemed. It could be expected that the affected yet still-viable neurons would recover their functionality and reconnect; the cognitive functions would improve and the patient could be cured, at least partially. At more advanced stages of the disease, fewer neurons remain viable and thus redeemable by the treatment. The progression of the disease would cease or decelerate at every stage, however advanced, but the cognitive recovery would be increasingly less certain.

25. The Uniform Mechanistic Effect of the ACH2.0-Based Drugs Elicits Distinctly Stage-Specific Outcomes

The preceding sections establish that, if effective in the depletion of *i*Aβ via its targeted degradation, the ACH2.0-based drugs are therapeutically multi-potential. They are capable of the prevention of AACD and AD, they are efficient in curing AACD, and they are effective in the treatment of AD at its symptomatic stages. Such versatility of the ACH2.0-based drugs may create an impression of their mechanistic variability, i.e., that their mechanism of action is different in different circumstances. This impression, however, would be erroneous. The ACH-based drugs act in one way only: they actively deplete or mediate the direct "active" (as defined above) depletion of *i*Aβ. What differs distinctly and is the disease stage-specific, are the effects (rather than mechanisms of action) of the ACH2.0-based drugs and, accordingly, the outcomes of their deployment in different settings. In every case, the transient utilization of the ACH2.0 drugs would deplete *i*Aβ, force the reduction in its levels to the nearly initial baseline, and necessitate its de novo decades-long accumulation. When the levels of AβPP-derived *i*Aβ have not yet reached the T1 or T^0 thresholds, this would preclude the T1 and/or T^0 crossing, and thus prevent AACD and/or AD. At symptomatic stages of AACD and AD, the action of the ACH2.0-based drugs would be precisely the same, namely the reduction in the levels of *i*Aβ and the enforcement of its de novo accumulation from a low baseline. In these settings, however, the outcomes would be not the prevention but the treatment and, potentially, the cure of AACD or AD. Despite the dissimilarity of the outcomes, the underlying mechanism is the same: when a condition

is treated, the driver of this condition is eliminated; when a condition is prevented, its potential driver is not allowed to come into play.

26. Activators of Physiologically Occurring Intra-*i*Aβ-Cleaving Capabilities of BACE1 and/or BACE2: Highly Plausible ACH2.0-Based Drugs for Prevention and Treatment of AD and AACD

The ACH2.0-based drugs were defined above as the agents that enact or mediate the targeted degradation of *i*Aβ, thus causing its "active", forced depletion. This definition would include, for example, a small molecule capable of crossing into the brain, penetrating the neurons, and catalyzing the targeted, i.e., specific, degradation of *i*Aβ. This, however, is easier said than done. On the other hand, the enzymatic activities capable of performing precisely this, the targeted degradation of *i*Aβ by its intra-molecular cleavage, are encoded in humans and expressed in the neuronal cells and could potentially be manipulated therapeutically. There are at least two such activities and, incidentally, they are either the major or the ancillary components of the two familiar players in the Alzheimer's play script: BACE1 and BACE2. Moreover, one of these activities confers protection from both AD and AACD when it is enhanced, whereas another activity operates in a physiologically protective capacity and its weakening causes the early onset of AD. In fact, these two activities are best known for their pivotal role in the functional outcomes of the two prominent Aβ mutations: "Icelandic" and "Flemish".

The Icelandic mutation, which substitutes an "A" in position 2 of Aβ with a "T", confers upon its carriers protection from both AD and AACD [21,22]. It does so by enhancing the efficiency of the BACE1-mediated cleavage at the alternative site within *i*Aβ. The primary cleavage site of BACE1 is known as the β-site. The alternative cleavage site, located ten residues downstream within *i*Aβ, is designated the β'-site. Cleavage at the β'-site of *i*Aβ degrades the molecule and thus depletes its levels. The augmentation of the β'-site cleavage is not limited to the carriers of the Icelandic mutation. It can be accomplished, apparently, by any increase in the activity of BACE1, for example, via its exogenous overexpression [139–142]. Indeed, the exogenous overexpression of human BACE1 in mouse models greatly elevated the rate of cleavage at the β'-site, increased the ratio of the N-truncated to the full-size Aβ, and significantly decreased the deposition of Aβ in mouse brain [140,141]. The β'-site is not the only alternative BACE1 cleavage site within the *i*Aβ molecule. As was shown in multiple investigations, BACE1 or BACE1-associated activity is also capable of cleaving between residues 34 and 35 of human iAβ [143–146]. Moreover, the exogenous overexpression of human BACE1 was demonstrated to substantially increase the rate of the *i*Aβ cleavage at residues 34/35 thus producing an intermediate in the iAβ clearance process [145].

As for the Flemish mutation, which causes the early onset of AD (FAD), the occurrence of this phenomenon is indicative of the protective physiological function of the BACE1 analog, BACE2. In contrast to BACE1 operation, where the major cleavage activity occurs at the β-site (thus generating Aβ), the main cleavage activity of BACE2 is at the two positions within *i*Aβ, at its residues 19 and 20, both phenylalanines [147]. Apparently, the physiological function of BACE2 is a protective one: to control and, if necessary, to limit the production and the levels of *i*Aβ [148]. Indeed, the inhibition of BACE2 in model systems resulted in a substantial elevation in the production of Aβ [62,148]. Moreover, the recent results obtained with the human pluripotent stem cell-derived brain organoids indicated that BACE2 could protect neuronal cells from Aβ-mediated apoptosis, whereas the deficiency of BACE2 activity may represent a common pathological mechanism not only for AD but also for Hirschsprung disease [149]. The notion that BACE2 is a physiologically occurring protective agent is strongly supported by the effect of Flemish mutation. This mutation occurs at the residue 21 of Aβ, contiguously downstream from the BACE2 cleavage sites. It substantially reduces the main cleavage activity of BACE2 and, consequently, leads to the elevation of the levels of *i*Aβ [62]. This, in turn, results in the early onset of AD.

It appears, therefore, highly plausible that a sufficient increase, potentially mediated by small-molecule activators, of the main activity of BACE2 or of the ancillary *i*Aβ-cleaving activities of BACE1 would be capable of the "active", forced depletion of *i*Aβ either in the preventive or in the curative settings discussed in the preceding sections above. The transient activation of either BACE2 alone or of only the intra-*i*Aβ-cleaving activities of BACE1 could be sufficient to achieve a substantial, therapeutically meaningful depletion of *i*Aβ and the reduction in its levels. On the other hand, the concerted activation of the intra-*i*Aβ-cleaving capabilities of both, BACE1 and BACE2 would greatly synergize the process because these activities target different sites within *i*Aβ and, in addition, operate in different sub-cellular locations [150]. If, however, only one activity could be feasibly manipulated at a time, BACE2 appears the natural choice because the enhancement of its activity would constitute the augmentation of its physiological protective function. On the other hand, since the intra-*i*Aβ cleavage is the main activity of BACE2, it could be, evolutionary, already optimized physiologically and its efficiency may be hard to improve upon. In contrast, the intra-*i*Aβ-cleaving capabilities of BACE1 are its secondary, minor activities and, as such, could possibly be more amenable to optimization and enhancement, as exemplified by the effect of the Icelandic mutation.

It should be strongly emphasized that the activation of the intra-*i*Aβ-cleaving activities of BACE1 and/or BACE2 is the first choice in terms of therapeutic strategy for prevention and treatment of AD and AACD only because it is both feasible and plausible. Importantly, however, *any* suitable agent capable of a substantial depletion of *i*Aβ via its direct or mediated targeted degradation would constitute a potential ACH2.0-based drug.

27. Conclusions

The present study introduces the Amyloid Cascade Hypothesis 2.0, ACH2.0, a novel theory of Alzheimer's disease and of Aging-Associated Cognitive Decline, and describes the class of potentially highly effective drugs suggested by this theory; this class is designated as the ACH2.0-based drugs. The study offers a comparative evaluation of the therapeutic potentials of the ACH2.0-based drugs versus those of the drugs whose design was informed by the Amyloid Cascade Hypothesis, referred to here as the ACH-based drugs. This analysis concludes that the utility of the ACH-based drugs is severely limited. Their short-term employment is ineffective, their long-term engagement is highly problematic, their implementation at the symptomatic stages of AD is futile, and their assessment in conventional clinical trials for prevention of AD is at best impractical, at worst impossible, and could be deceitful in between. In sharp contrast, the ACH2.0-based drugs have none of those shortcomings and are capable of delivering the proverbial "Holy Grail" of Alzheimer's research: the ability to treat and potentially cure the disease at its symptomatic stages. The ACH2.0-based drugs would also be effective in the prevention of AD and AACD and in the treatment of the latter. Remarkably, the *modus operandi* of the ACH2.0-based drugs opens up the possibility of once-in-a-lifetime only, transient, short-duration therapy for the treatment and prevention of both AD and AACD.

The ACH2.0-based drugs act by substantially reducing the levels of *i*Aβ and necessitating its de novo accumulation from a low baseline. This may not be sufficient in cases where the ISR in neuronal cells is elicited by means other than AβPP-derived *i*Aβ-mediated activation of eIF2α kinases, such as in individuals predisposed to AD due to the persistent neuronal inflammation (resulting, for example, from repeated concussions). In these individuals, as discussed above, either the T1 threshold is lowered due to the increased basal level of cellular (neuronal) stress or the ISR is elicited and, subsequently, the AβPP-independent *i*Aβ production pathway is activated as the consequence of the inflammatory processes-associated stressors in neuronal cells even if the levels of AβPP-derived *i*Aβ do not reach the T1 threshold. In the latter cases, the anti-inflammatory treatment would act preventively prior to the onset of AD (i.e., prior to the activation of the AβPP-independent *i*Aβ production pathway), whereas, following its commencement,

the transient implementation of the ACH2.0-based drugs should be combined with the long-term anti-inflammatory therapy.

In the framework of the ACH2.0, potentially, as discussed in [4], AD could be prevented, or its progression could be ceased via long-term inhibition of the ISR, for example with the small molecule ISR inhibitor ISRIB; this would preclude or stop the operation of the AβPP-independent *i*Aβ generation pathway and, consequently, of the AD Engine. This, apparently, is not a viable option, since, due to the central role of the integrated stress response in cellular physiology, its long-term suppression is highly likely to result in significant adverse effects.

In addition, the present study offers a solution for the conundrum of the spectacular efficiency of the ACH-based drugs in animal models versus their complete inefficacy in human clinical trials for symptomatic AD. Lastly, it posits that the prime candidates for the efficient ACH2.0-based drugs are the activators of the intra-*i*Aβ-cleaving capabilities of BACE1 and BACE2.

Author Contributions: Conceptualization, writing, V.V.; conceptualization, editing S.R.-V. All authors have read and agreed to the published version of the manuscript.

Funding: NIH R21 GM056179; NIH RO1 AR036819.

Informed Consent Statement: Neither human nor animal subjects were involved in the present study.

Acknowledgments: The authors are grateful to Bjorn R. Olsen (Harvard Medical School) for his support, to Hailong Gao (Children's Hospital, Boston) for assistance with the figure preparation, and to Michael J. Foley and his associates for logistical support.

Conflicts of Interest: The authors declare no conflict of interest.

References

1. Volloch, V.; Rits-Volloch, S. The Amyloid Cascade Hypothesis 2.0: On the possibility of once-in-a-lifetime-only treatment for prevention of Alzheimer's disease and for its potential cure at symptomatic stages. *J. Alz Dis. Rep.* **2022**, *6*, 369–399. [CrossRef]
2. Volloch, V.; Rits-Volloch, S. The Amyloid Cascade Hypothesis 2.0: Generalization of the Concept. *J. Alz Dis. Rep.* **2023**, *7*, 21–35. [CrossRef]
3. Volloch, V.; Rits-Volloch, S. Effect of Lecanemab and Donanemab in Early Alzheimer's Disease: Mechanistic Interpretation in the Amyloid Cascade Hypothesis 2.0 Perspective. *J. Alz Dis.* **2023**, *93*, 1277–1284. [CrossRef]
4. Volloch, V.; Rits-Volloch, S. The Amyloid Cascade Hypothesis 2.0 for Alzheimer's Disease and Aging-Associated Cognitive Decline: From Molecular Basis to Effective Therapy. *Int. J. Mol. Sci.* **2023**, *24*, 12246. [CrossRef]
5. Volloch, V.; Rits-Volloch, S. Principles of Design of Clinical Trials for Prevention and Treatment of Alzheimer's Disease and Aging-Associated Cognitive Decline in the ACH2.0 Perspective: Potential Outcomes, Challenges and Solutions. *J. Alz Dis. Rep.* **2023**, *7*, 921–955. [CrossRef]
6. Hardy, J.A.; Higgins, G.A. Alzheimer's disease: The amyloid cascade hypothesis. *Science* **1992**, *256*, 184–185. [CrossRef]
7. Goate, A.; Chartier-Harlin, M.C.; Mullan, M.; Brown, J.; Crawford, F.; Fidani, L.; Giuffra, L.; Haynes, A.; Irving, N.; James, L.; et al. Segregation of a missense mutation in the amyloid precursor protein gene with familial Alzheimer's disease. *Nature* **1991**, *349*, 704–706. [CrossRef]
8. Keskin, A.D.; Kekuš, M.; Adelsberger, H.; Neumann, U.; Shimshek, D.R.; Song, B.; Zott, B.; Peng, T.; Förstl, H.; Staufenbiel, M.; et al. BACE inhibition-dependent repair of Alzheimer's pathophysiology. *Proc. Natl. Acad. Sci. USA* **2017**, *114*, 8631–8636. [CrossRef]
9. Hu, X.; Das, B.; Hou, H.; He, W.; Yan, R. BACE1 deletion in the adult mouse reverses preformed amyloid deposition and improves cognitive functions. *J. Exp. Med.* **2018**, *10*, 1084. [CrossRef]
10. Kennedy, M.E.; Stamford, A.W.; Chen, X.; Cox, K.; Cumming, J.N.; Dockendorf, M.F.; Egan, M.; Ereshefsky, L.; Hodgson, R.A.; Hyde, L.A.; et al. The BACE1 inhibitor verubecestat (MK-8931) reduces CNS β-amyloid in animal models and in Alzheimer's disease patients. *Sci. Transl. Med.* **2016**, *8*, 363ra150. [CrossRef]
11. Egan, M.F.; Kost, J.; Tariot, P.N.; Aisen, P.S.; Cummings, J.L.; Vellas, B.; Sur, C.; Mukai, Y.; Voss, T.; Furtek, C.; et al. Randomized trials of verubecestat for mild-to-moderate Alzheimer's disease. *N. Engl. J. Med.* **2018**, *378*, 1691–1703. [CrossRef]
12. Egan, M.F.; Kost, J.; Voss, T.; Mukai, Y.; Aisen, P.S.; Cummings, J.L.; Tariot, P.N.; Vellas, B.; van Dyck, C.H.; Boada, M.; et al. Randomized trial of verubecestat for prodromal Alzheimer's disease. *N. Engl. J. Med.* **2019**, *380*, 1408–1420. [CrossRef]
13. Katzman, R.; Terry, R.; DeTeresa, R.; Brown, T.; Davies, P.; Fuld, P.; Rebing, X.; Peck, A. Clinical, pathological, and neurochemical changes in dementia: A subgroup with preserved mental status and numerous neocortical plaques. *Ann. Neurol.* **1988**, *23*, 138–144. [CrossRef]

14. Delaere, P.; Duyckaerts, C.; Masters, C.; Beyreuther, K.; Piette, F.; Hauw, J. Large amounts of neocortical beta A4 deposits without neuritic plaques nor tangles in a psychometrically assessed, non-demented person. *Neurosci. Lett.* **1990**, *116*, 87–93. [CrossRef]
15. Dickson, D.; Crystal, H.; Mattiace, L.; Masur, D.; Blau, A.; Davies, P.; Yen, S.; Aronson, M. Identification of normal and pathological aging in prospectively studied nondemented elderly humans. *Neurobiol. Aging* **1992**, *13*, 178–189. [CrossRef]
16. Aizenstein, H.; Nebes, R.; Saxton, J.; Price, J.; Mathis, C.; Tsopelas, N.; Ziolko, S.; James, J.; Snitz, B.; Houck, P.; et al. Frequent amyloid deposition without significant cognitive impairment among the elderly. *Arch. Neurol.* **2008**, *65*, 1509–1517. [CrossRef]
17. Klunk, W.; Mathis, C.; Price, J.; DeKosky, S.; Lopresti, B.; Tsopelas, N.; Saxton, J.; Nebes, R. Amyloid imaging with PET in Alzheimer's disease, mild cognitive impairment, and clinically unimpaired subjects. In *PET in the Evaluation of Alzheimer's Disease and Related Disorders*; Silverman, D., Ed.; Springer: New York, NY, USA, 2009; pp. 119–147.
18. Villemagne, V.; Pike, K.; Chételat, G.; Ellis, K.; Mulligan, R.; Bourgeat, P.; Ackermann, U.; Jones, G.; Szoeke, C.; Salvado, O.; et al. Longitudinal assessment of Abeta and cognition in aging and Alzheimer disease. *Ann. Neurol.* **2011**, *69*, 181–192. [CrossRef]
19. Seto, M.; Weiner, R.L.; Dumitrescu, L.; Hohman, T.J. Protective genes and pathways in Alzheimer's disease: Moving towards precision interventions. *Mol. Neurodegen* **2021**, *16*, 29. [CrossRef]
20. Makin, S. The amyloid hypothesis on trial. *Nature* **2018**, *559*, S4–S7. Available online: https://media.nature.com/original/magazine-assets/d41586-018-05719-4/d41586-018-05719-4.pdf (accessed on 1 March 2021). [CrossRef]
21. Jonsson, T.; Atwal, J.K.; Steinberg, S.; Snaedal, J.; Jonsson, P.V.; Bjornsson, S.; Stefansson, H.; Sulem, P.; Gudbjartsson, D.; Maloney, J.; et al. A mutation in APP protects against Alzheimer's disease and age-related cognitive decline. *Nature* **2012**, *488*, 96–99. [CrossRef] [PubMed]
22. Harper, A.R.; Nayee, S.; Topol, E.J. Protective alleles and modifier variants in human health and disease. *Nat. Rev. Genet.* **2015**, *16*, 689–701. [CrossRef]
23. Kinoshita, A.; Fukumoto, H.; Shah, T.; Whelan, C.M.; Irizarry, M.C.; Hyman, B.T. Demonstration by FRET of BACE interaction with the amyloid precursor protein at the cell surface and in early endosomes. *J. Cell Sci.* **2003**, *116*, 3339–3346. [CrossRef]
24. Xu, H.; Greengard, P.; Gandy, S. Regulated formation of Golgi secretory vesicles containing Alzheimer β-amyloid precursor protein. *J. Biol. Chem.* **1995**, *270*, 23243–23245. [CrossRef] [PubMed]
25. Mizuguchi, M.; Ikeda, K.; Kim, S. Differential distribution of cellular forms of β-amyloid precursor protein in murine glial cell cultures. *Brain Res.* **1992**, *584*, 219–225. [CrossRef] [PubMed]
26. Cook, D.G.; Forman, M.S.; Sung, J.C.; Leight, S.; Kolson, D.L.; Iwatsubo, T.; Lee, V.M.; Doms, R.W. Alzheimer's Aβ-42 is generated in the endoplasmic reticulum/intermediate compartment of NT2N cells. *Nature Med.* **1997**, *3*, 1021–1023. [CrossRef] [PubMed]
27. Hartmann, T.; Bieger, S.C.; Brühl, B.; Tienari, P.J.; Ida, N.; Allsop, D.; Roberts, G.W.; Masters, C.L.; Dotti, C.G.; Unsicker, K.; et al. Distinct sites of intracellular production for Alzheimer's disease Aβ-40/42 amyloid peptides. *Nature Med.* **1997**, *3*, 1016–1020. [CrossRef] [PubMed]
28. Wild-Bode, C.; Yamazaki, T.; Capell, A.; Leimer, U.; Steiner, H.; Ihara, Y.; Haass, C. Intracellular generation and accumulation of amyloid beta-peptide terminating at amino acid 42. *J. Biol. Chem.* **1997**, *272*, 16085–16088. [CrossRef] [PubMed]
29. Lee, S.J.; Liyanage, U.; Bickel, P.E.; Xia, W.; Lansbury, P.T., Jr.; Kosik, K.S. A detergent-insoluble membrane compartment contains Aβ in vivo. *Nature Med.* **1998**, *4*, 730–734. [CrossRef]
30. Skovronsky, D.; Doms, R.; Lee, V. Detection of a novel intraneuronal pool of insoluble amyloid β protein that accumulates with time in culture. *J. Cell Biol.* **1998**, *141*, 1031–1039. [CrossRef]
31. Manczak, M.; Anekonda, T.S.; Henson, E.; Park, B.S.; Quinn, J.; Reddy, P.H. Mitochondria are a direct site of Aβ accumulation in Alzheimer's disease neurons: Implications for free radical generation and oxidative damage in disease progression. *Hum. Mol. Genet* **2006**, *15*, 1437–1449. [CrossRef]
32. Chafekar, S.; Baas, F.; Scheper, W. Oligomer-specific amyloid-beta toxicity in cell models is mediated by selective uptake. *Biochem. Biophys. Acta* **2008**, *9*, 523–531.
33. Wesen, E.; Jeffries, G.; Dzebo, M.; Esbjorner, M. Endocytic uptake of monomeric amyloid-β peptides is clathrin- and dynamin-independent and results in selective accumulation of Aβ(1–42) compared to Aβ(1–40). *Sci. Rep.* **2017**, *7*, 2021. [CrossRef] [PubMed]
34. Kumar-Singh, S.; Theuns, J.; Van Broeck, B.; Pirici, D.; Vennekens, K.; Corsmit, E.; Cruts, M.; Dermaut, B.; Wang, R.; Van Broeckhoven, C. Mean age-of-onset of familial Alzheimer disease caused by presenilin mutations correlates with both increased Abeta42 and decreased Abeta40. *Hum. Mutat.* **2006**, *27*, 686–695. [CrossRef] [PubMed]
35. Hu, X.; Crick, S.L.; Bu, G.; Frieden, C.; Pappu, R.V.; Lee, J.M. Amyloid seeds formed by cellular uptake, concentration, and aggregation of the amyloid-beta peptide. *Proc. Natl. Acad. Sci. USA* **2009**, *106*, 20324–20329. [CrossRef]
36. Yajima, R.; Tokutake, T.; Koyama, A.; Kasuga, K.; Tezuka, T.; Nishizawa, M.; Ikeuchi, T. ApoE-isoform-dependent cellular uptake of amyloid-β is mediated by lipoprotein receptor LR11/SorLA. *Biochem. Biophys. Res. Comm.* **2015**, *456*, 482–488. [CrossRef] [PubMed]
37. Omtri, R.S.; Davidson, M.W.; Arumugam, B.; Poduslo, J.F.; Kandimalla, K.K. Differences in the cellular uptake and intracellular itineraries of amyloid beta proteins 40 and 42: Ramifications for the Alzheimer's drug discovery. *Mol. Pharm.* **2012**, *9*, 1887. [CrossRef]
38. Bu, G.; Cam, J.; Zerbinatti, C. LRP in amyloid-β production and metabolism. *Ann. N. Y. Acad. Sci.* **2006**, *1086*, 35–53. [CrossRef] [PubMed]

39. Wang, H.Y.; Lee, D.H.; D'Andrea, M.R.; Peterson, P.A.; Shank, R.P.; Reitz, A.B. β-Amyloid1–42 binds to α7 nicotinic acetylcholine receptor with high affinity. Implications for Alzheimer's disease pathology. *J. Biol. Chem.* **2000**, *275*, 5626–5632. [CrossRef]
40. Nagele, R.; D'Andrea, M.; Anderson, W.; Wang, H. Intracellular accumulation of Aβ42 in neurons is facilitated by the α7 nicotinic acetylcholine receptor in Alzheimer's disease. *Neuroscience* **2002**, *110*, 199–211. [CrossRef]
41. Oddo, S.; Caccamo, A.; Green, K.N.; Liang, K.; Tran, L.; Chen, Y.; Leslie, F.M.; LaFerla, F.M. Chronic nicotine administration exacerbates tau pathology in a transgenic model of Alzheimer's disease. *Proc. Natl. Acad. Sci. USA* **2005**, *102*, 3046–3051. [CrossRef]
42. Yan, S.D.; Chen, X.; Fu, J.; Chen, M.; Zhu, H.; Roher, A.; Slattery, T.; Zhao, L.; Nagashima, M.; Morser, J.; et al. RAGE and amyloid-β peptide neurotoxicity in Alzheimer's disease. *Nature* **1996**, *382*, 685–691. [CrossRef] [PubMed]
43. Sasaki, N.; Toki, S.; Chowei, H.; Saito, T.; Nakano, N.; Hayashi, Y.; Takeuchi, M.; Makita, Z. Immunohistochemical distribution of the receptor for advanced glycation end products in neurons and astrocytes in Alzheimer's disease. *Brain Res.* **2001**, *888*, 256–262. [CrossRef] [PubMed]
44. Deane, R.; Du Yan, S.; Submamaryan, R.K.; LaRue, B.; Jovanovic, S.; Hogg, E.; Welch, D.; Manness, L.; Lin, C.; Yu, J.; et al. RAGE mediates amyloid-β peptide transport across the blood–brain barrier and accumulation in brain. *Nat. Med.* **2003**, *9*, 907–913. [CrossRef] [PubMed]
45. Iribarren, P.; Zhou, Y.; Hu, J.; Le, Y.; Wang, J. Role of formyl peptide receptor-like 1 (FPRL1/FPR2) in mononuclear phagocyte responses in Alzheimer disease. *Immunol. Res.* **2005**, *31*, 165–176. [CrossRef] [PubMed]
46. Snyder, E.M.; Nong, Y.; Almeida, C.G.; Paul, S.; Moran, T.; Choi, E.Y.; Nairn, A.C.; Salter, M.W.; Lombroso, P.J.; Gouras, G.K.; et al. Regulation of NMDA receptor trafficking by amyloid-β. *Nat. Neurosci.* **2005**, *8*, 1051–1058. [CrossRef] [PubMed]
47. Casas, C.; Sergeant, N.; Itier, J.M.; Blanchard, V.; Wirths, O.; van der Kolk, N.; Vingtdeux, V.; van de Steeg, E.; Ret, G.; Canton, T.; et al. Massive CA1/2 neuronal loss with intraneuronal and N-terminal truncated Abeta42 accumulation in a novel Alzheimer transgenic model. *Am. J. Pathol.* **2004**, *165*, 1289–1300. [CrossRef]
48. Bayer, T.A.; Wirths, O. Review on the APP/PS1KI mouse model: Intraneuronal Abeta accumulation triggers axonopathy, neuron loss and working memory impairment. *Genes Brain Behav.* **2008**, *1*, 6–11. [CrossRef]
49. Bayer, T.A.; Breyhan, H.; Duan, K.; Rettig, J.; Wirths, O. Intraneuronal beta-amyloid is a major risk factor--novel evidence from the APP/PS1KI mouse model. *Neurodegener. Dis.* **2008**, *5*, 140–142. [CrossRef]
50. Wirths, O.; Breyhan, H.; Cynis, H.; Schilling, S.; Demuth, H.U.; Bayer, T.A. Intraneuronal pyroglutamate-Abeta 3-42 triggers neurodegeneration and lethal neurological deficits in a transgenic mouse model. *Acta Neuropathol.* **2009**, *118*, 487–496. [CrossRef]
51. Christensen, D.Z.; Bayer, T.A.; Wirths, O. Intracellular Aβ triggers neuron loss in the cholinergic system of the APP/PS1KI mouse model of Alzheimer's disease. *Neurobiol. Aging* **2010**, *31*, 1153–1163. [CrossRef]
52. Christensen, D.Z.; Schneider-Axmann, T.; Lucassen, P.J.; Bayer, T.A.; Wirths, O. Accumulation of intraneuronal Abeta correlates with ApoE4 genotype. *Acta Neuropathol.* **2010**, *119*, 555–566. [CrossRef] [PubMed]
53. Bayer, T.A.; Wirths, O. Intracellular accumulation of amyloid-Beta—A predictor for synaptic dysfunction and neuron loss in Alzheimer's disease. *Front. Aging Neurosci.* **2010**, *2*, 8. [CrossRef] [PubMed]
54. Bayer, T.A.; Wirths, O. Intraneuronal Aβ as a trigger for neuron loss: Can this be translated into human pathology? *Biochem. Soc. Trans.* **2011**, *39*, 857–861. [CrossRef] [PubMed]
55. Wirths, O.; Bayer, T.A. Intraneuronal Aβ accumulation and neurodegeneration: Lessons from transgenic models. *Life Sci.* **2012**, *91*, 1148–1152. [CrossRef] [PubMed]
56. Kumar, S.; Wirths, O.; Theil, S.; Gerth, J.; Bayer, T.A.; Walter, J. Early intraneuronal accumulation and increased aggregation of phosphorylated Abeta in a mouse model of Alzheimer's disease. *Acta Neuropathol.* **2013**, *125*, 699–709. [CrossRef] [PubMed]
57. Ripoli, C.; Cocco, S.; Li Puma, D.D.; Piacentini, R.; Mastrodonato, A.; Scala, F.; Puzzo, D.; D'Ascenzo, M.; Grassi, C. Intracellular accumulation of amyloid-β (Aβ) protein plays a major role in Aβ-induced alterations of glutamatergic synaptic transmission and plasticity. *J. Neurosci.* **2014**, *34*, 12893–12903. [CrossRef]
58. Scala, F.; Fusco, S.; Ripoli, C.; Piacentini, R.; Li Puma, D.D.; Spinelli, M.; Laezza, F.; Grassi, C.; D'Ascenzo, M. Intraneuronal Aβ accumulation induces hippocampal neuron hyperexcitability through A-type K^+ current inhibition mediated by activation of caspases and GSK-3. *Neurobiol. Aging* **2015**, *36*, 886–900. [CrossRef]
59. Christensen, D.Z.; Kraus, S.L.; Flohr, A.; Cotel, M.C.; Wirths, O.; Bayer, T.A. Transient intraneuronal Abeta rather than extracellular plaque pathology correlates with neuron loss in the frontal cortex of APP/PS1KI mice. *Acta Neuropathol.* **2008**, *116*, 647–655. [CrossRef]
60. Martin, B.; Schrader-Fischer, G.; Busciglio, J.; Duke, M.; Paganetti, P.; Yankner, B. Intracellular accumulation of beta-amyloid in cells expressing the Swedish mutant amyloid precursor protein. *J. Biol. Chem.* **1995**, *270*, 26727–26730. [CrossRef]
61. Sannerud, R.; Esselens, C.; Ejsmont, P.; Mattera, R.; Rochin, L.; Tharkeshwar, A.K.; De Baets, G.; De Wever, V.; Habets, R.; Baert, V.; et al. Restricted Location of PSEN2/gamma-secretase determines substrate specificity and generates an intracellular Abeta pool. *Cell* **2016**, *166*, 193–208. [CrossRef]
62. De Jonghe, C.; Zehr, C.; Yager, D.; Prada, C.M.; Younkin, S.; Hendriks, L.; Van Broeckhoven, C.; Eckman, C.B. Flemish and Dutch mutations in amyloid beta precursor protein have different effects on amyloid beta secretion. *Neurobiol. Dis.* **1998**, *5*, 281–286. [CrossRef] [PubMed]

63. Chang, R.C.; Suen, K.C.; Ma, C.H.; Elyaman, W.; Ng, H.K.; Hugon, J. Involvement of double-stranded RNA-dependent protein kinase and phosphorylation of eukaryotic initiation factor-2alpha in neuronal degeneration. *J. Neurochem.* **2002**, *83*, 1215–1225. [CrossRef] [PubMed]
64. Peel, A.L. PKR activation in neurodegenerative disease. *J. Neuropathol. Exp. Neurol.* **2004**, *63*, 97–105. [CrossRef] [PubMed]
65. Peel, A.L.; Bredesen, D.E. Activation of the cell stress kinase PKR in Alzheimer's disease and human amyloid precursor protein transgenic mice. *Neurobiol. Dis.* **2003**, *14*, 52–62. [CrossRef]
66. Chang, R.C.; Wong, A.K.; Ng, H.K.; Hugon, J. Phosphorylation of eukaryotic initiation factor-2alpha (eIF2alpha) is associated with neuronal degeneration in Alzheimer's disease. *Neuroreport* **2002**, *13*, 2429–2432. [CrossRef]
67. Onuki, R.; Bando, Y.; Suyama, E.; Katayama, T.; Kawasaki, H.; Baba, T.; Tohyama, M.; Taira, K. An RNA-dependent protein kinase is involved in tunicamycin-induced apoptosis and Alzheimer's disease. *EMBO J.* **2004**, *23*, 959–968. [CrossRef] [PubMed]
68. Lourenco, M.V.; Clarke, J.R.; Frozza, R.L.; Bomfim, T.R.; Forny-Germano, L.; Batista, A.F.; Sathler, L.B.; Brito-Moreira, J.; Amaral, O.B.; Silva, C.A.; et al. TNF-alpha mediates PKR-dependent memory impairment and brain IRS-1 inhibition induced by Alzheimer's beta-amyloid oligomers in mice and monkeys. *Cell Metab.* **2013**, *18*, 831–843. [CrossRef]
69. Paquet, C.; Mouton-Liger, F.; Meurs, E.F.; Mazot, P.; Bouras, C.; Pradier, L.; Gray, F.; Hugon, J. The PKR activator PACT is induced by Abeta: Involvement in Alzheimer's disease. *Brain Pathol.* **2012**, *22*, 219–229. [CrossRef]
70. Zhu, X.; Perry, G.; Moreira, P.I.; Aliev, G.; Cash, A.D.; Hirai, K.; Smith, M.A. Mitochondrial abnormalities and oxidative imbalance in Alzheimer disease. *J. Alzheimers Dis.* **2006**, *9*, 147–153. [CrossRef]
71. Blass, J.P. The mitochondrial spiral. An adequate cause of dementia in the Alzheimer's syndrome. *Ann. N. Y. Acad. Sci.* **2000**, *924*, 170–183. [CrossRef]
72. Manczak, M.; Park, B.S.; Jung, Y.; Reddy, P.H. Differential expression of oxidative phosphorylation genes in patients with Alzheimer's disease: Implications for early mitochondrial dysfunction and oxidative damage. *Neuromolecular Med.* **2004**, *5*, 147–162. [CrossRef]
73. Qin, W.; Haroutunian, V.; Katsel, P.; Cardozo, C.P.; Ho, L.; Buxbaum, J.D.; Pasinetti, G.M. PGC-1alpha expression decreases in the Alzheimer disease brain as a function of dementia. *Arch. Neurol.* **2009**, *66*, 352–361. [CrossRef]
74. Du, H.; Guo, L.; Yan, S.; Sosunov, A.A.; McKhann, G.M.; Yan, S.S. Early deficits in synaptic mitochondria in an Alzheimer's disease mouse model. *Proc. Natl. Acad. Sci. USA* **2010**, *107*, 18670–18675. [CrossRef]
75. Lin, M.T.; Simon, D.K.; Ahn, C.H.; Kim, L.M.; Beal, M.F. High aggregate burden of somatic mtDNA point mutations in aging and Alzheimer's disease brain. *Hum. Mol. Genet.* **2002**, *11*, 133–145. [CrossRef] [PubMed]
76. Calkins, M.; Manczak, M.; Mao, P.; Shirendeb, U.; Reddy, P.H. Impaired mitochondrial biogenesis, defective axonal transport of mitochondria, abnormal mitochondrial dynamics and synaptic degeneration in a mouse model of Alzheimer's disease. *Hum. Mol. Genet.* **2011**, *20*, 4515–4529. [CrossRef] [PubMed]
77. Anandatheerthavarada, H.K.; Biswas, G.; Robin, M.A.; Avadhani, N.G. Mitochondrial targeting and a novel transmembrane arrest of Alzheimer's amyloid precursor protein impairs mitochondrial function in neuronal cells. *J. Cell Biol.* **2003**, *161*, 41–54. [CrossRef] [PubMed]
78. Caspersen, C.; Wang, N.; Yao, J.; Sosunov, A.; Chen, X.; Lustbader, J.W.; Xu, H.W.; Stern, D.; McKhann, G.; Yan, S.D. Mitochondrial Abeta: A potential focal point for neuronal metabolic dysfunction in Alzheimer's disease. *FASEB J.* **2005**, *19*, 2040–2041. [CrossRef] [PubMed]
79. Chen, J.X.; Yan, S.S. Role of mitochondrial amyloid-beta in Alzheimer's disease. *J. Alzheimers Dis.* **2010**, *20*, S569–S578. [CrossRef] [PubMed]
80. Hansson Petersen, C.A.; Alikhani, N.; Behbahani, H.; Wiehager, B.; Pavlov, P.F.; Alafuzoff, I.; Leinonen, V.; Ito, A.; Winblad, B.; Glaser, E.; et al. The amyloid beta-peptide is imported into mitochondria via the TOM import machinery and localized to mitochondrial cristae. *Proc. Natl. Acad. Sci. USA* **2008**, *105*, 13145–13150. [CrossRef] [PubMed]
81. de la Monte, S.M.; Luong, T.; Neely, T.R.; Robinson, D.; Wands, J.R. Mitochondrial DNA damage as a mechanism of cell loss in Alzheimer's disease. *Lab. Investig.* **2000**, *80*, 1323–1335. [CrossRef]
82. Brooks, W.M.; Lynch, P.J.; Ingle, C.C.; Hatton, A.; Emson, P.C.; Faull, R.L.; Starkey, M.P. Gene expression profiles of metabolic enzyme transcripts in Alzheimer's disease. *Brain Res.* **2007**, *1127*, 127–135. [CrossRef] [PubMed]
83. Wang, X.; Perry, G.; Smith, M.A.; Zhu, X. Amyloid-beta-derived diffusible ligands cause impaired axonal transport of mitochondria in neurons. *Neurodegener. Dis.* **2007**, *7*, 56–59. [CrossRef] [PubMed]
84. Wang, X.; Su, B.; Fujioka, H.; Zhu, X. Dynamin-like protein 1 reduction underlies mitochondrial morphology and distribution abnormalities in fibroblasts from sporadic Alzheimer's disease patients. *Am. J. Pathol.* **2008**, *173*, 470–482. [CrossRef]
85. Wang, X.; Su, B.; Lee, H.G.; Li, X.; Perry, G.; Smith, M.A.; Zhu, X. Impaired balance of mitochondrial fission and fusion in Alzheimer's disease. *J. Neurosci.* **2009**, *29*, 9090–9103. [CrossRef]
86. Wang, X.; Su, B.; Siedlak, S.L.; Moreira, P.I.; Fujioka, H.; Wang, Y.; Casadesus, G.; Zhu, X. Amyloid-beta overproduction causes abnormal mitochondrial dynamics via differential modulation of mitochondrial fission/fusion proteins. *Proc. Natl. Acad. Sci. USA* **2008**, *105*, 19318–19323. [CrossRef]
87. Brewer, G.; Herrera, R.; Philipp, S.; Sosna, J.; Reyes-Ruiz, J.; Glabe, C. Age-Related Intraneuronal Aggregation of Amyloid-β in Endosomes, Mitochondria, Autophagosomes, and Lysosomes. *J. Alzheimers Dis.* **2020**, *73*, 229–246. [CrossRef]
88. Guo, X.; Aviles, G.; Liu, Y.; Tian, R.; Unger, B.A.; Lin, Y.T.; Wiita, A.P.; Xu, K.; Correia, M.A.; Kampmann, M. Mitochondrial stress is relayed to the cytosol by an OMA1-DELE1-HRI pathway. *Nature* **2020**, *579*, 427–432. [CrossRef]

89. Fessler, E.; Eckl, E.M.; Schmitt, S.; Mancilla, I.A.; Meyer-Bender, M.F.; Hanf, M.; Philippou-Massier, J.; Krebs, S.; Zischka, H.; Jae, L.T. A pathway coordinated by DELE1 relays mitochondrial stress to the cytosol. *Nature* **2020**, *579*, 433–437. [CrossRef]
90. Pakos-Zebrucka, K.; Koryga, I.; Mnich, K.; Ljujic, M.; Samali, A.; Gorman, A.M. The integrated stress response. *EMBO Rep.* **2016**, *17*, 1374–1395. [CrossRef]
91. Ron, D. Translational control in the endoplasmic reticulum stress response. *J. Clin. Investig.* **2002**, *110*, 1383–1388. [CrossRef]
92. Harding, H.P.; Zhang, Y.; Zeng, H.; Novoa, I.; Lu, P.D.; Calfon, M.; Sadri, N.; Yun, C.; Popko, B.; Paules, R.; et al. An integrated stress response regulates amino acid metabolism and resistance to oxidative stress. *Mol. Cell* **2003**, *11*, 619–633. [CrossRef]
93. Brostrom, C.O.; Prostko, C.R.; Kaufman, R.J.; Brostrom, M.A. Inhibition of translational initiation by activators of the glucose-regulated stress protein and heat shock protein stress response systems. Role of the interferon-inducible double-stranded RNA-activated eukaryotic initiation factor 2alpha kinase. *J. Biol. Chem.* **1996**, *271*, 24995–25002. [CrossRef] [PubMed]
94. Dever, T.E.; Feng, L.; Wek, R.C.; Hinnebusch, A.G. Phosphorylation of initiation factor 2 alpha by protein kinase GCN2 mediates gene-specific translational control of GCN4 in yeast. *Cell* **1992**, *68*, 585–596. [CrossRef] [PubMed]
95. Wek, R.C.; Jiang, H.Y.; Anthony, T.G. Coping with stress: eIF2 kinases and translational control. *Biochem. Soc. Trans.* **2006**, *34*, 7–11. [CrossRef] [PubMed]
96. Rzymski, T.; Milani, M.; Pike, L.; Buffa, F.; Mellor, H.R.; Winchester, L.; Pires, I.; Hammond, E.; Ragoussis, I.; Harris, A.L. Regulation of autophagy by ATF4 in response to severe hypoxia. *Oncogene* **2010**, *29*, 4424–4435. [CrossRef] [PubMed]
97. Ye, J.; Kumanova, M.; Hart, L.S.; Sloane, K.; Zhang, H.; De Panis, D.N.; Bobrovnikova-Marjon, E.; Diehl, J.A.; Ron, D.; Koumenis, C. The GCN2-ATF4 pathway is critical for tumour cell survival and proliferation in response to nutrient deprivation. *EMBO J.* **2010**, *29*, 2082–2096. [CrossRef] [PubMed]
98. Garcia, M.A.; Meurs, E.F.; Esteban, M. The dsRNA protein kinase PKR: Virus and cell control. *Biochimie* **2007**, *89*, 799–811. [CrossRef] [PubMed]
99. Harding, H.P.; Zhang, Y.; Ron, D. Protein translation and folding are coupled by an endoplasmic-reticulum-resident kinase. *Nature* **1999**, *397*, 271–274. [CrossRef]
100. Breimer, L.; Denny, P. Alzheimer amyloid aspects. *Nature* **1987**, *326*, 749–750. [CrossRef]
101. Kang, J.; Lemaire, H.G.; Unterbeck, A.; Salbaum, J.M.; Masters, C.L.; Grzeschik, K.H.; Multhaup, G.; Beyreuther, K.; Müller-Hill, B. The precursor of Alzheimer's disease amyloid A4 protein resembles a cell-surface receptor. *Nature* **1987**, *325*, 733–736. [CrossRef]
102. Robakis, N.K.; Ramakrishna, N.; Wolfe, G.; Wisniewski, H.M. Molecular cloning and characterization of a cDNA encoding the cerebrovascular and the neuritic plaque amyloid peptides. *Proc. Natl. Acad. Sci. USA* **1987**, *84*, 4190–4194. [CrossRef] [PubMed]
103. Tanzi, R.E.; Gusella, J.F.; Watkins, P.C.; Bruns, G.A.; St George-Hyslop, P.; Van Keuren, M.L.; Patterson, D.; Pagan, S.; Kurnit, D.M.; Neve, R.L. Amyloid beta protein gene: cDNA, mRNA distribution, and genetic linkage near the Alzheimer locus. *Science* **1987**, *235*, 880–884. [CrossRef] [PubMed]
104. Citron, M.; Haass, C.; Selkoe, D. Production of amyloid beta peptide by cultured cells: No evidence for internal initiation of translation at Met596. *Neurobiol. Aging* **1993**, *14*, 571–573. [CrossRef]
105. Macq, A.; Philippe, B.; Octave, N. The amyloid peptide of Alzheimer's disease is not produced by internal initiation of translation generating C-terminal amyloidogenic fragments of its precursor. *Neurosci. Lett.* **1994**, *182*, 227–230. [CrossRef] [PubMed]
106. Frottin, F.; Martinez, A.; Peinot, P.; Mitra, S.; Holz, R.; Giglione, C.; Meinnel, T. The proteomics of N-terminal methionine cleavage. *Mol. Cell Proteom. MCP* **2006**, *5*, 2336–2349. [CrossRef]
107. Xiao, Q.; Zhang, F.; Nacev, B.; Liu, J.; Pei, D. Protein N-Terminal Processing: Substrate Specificity of Escherichia coli and Human Methionine Aminopeptidases. *Biochemistry* **2010**, *49*, 5588–5599. [CrossRef] [PubMed]
108. Varshavsky, A. The N-end rule pathway and regulation by proteolysis. *Protein Sci.* **2011**, *20*, 1298–1345. [CrossRef] [PubMed]
109. Wingfield, P. N-Terminal Methionine Processing. *Curr. Protoc. Protein Sci.* **2017**, *88*, 6.14.1–6.14.3. [CrossRef]
110. Varland, S.; Osberg, C.; Arnesen, T. N-terminal modifications of cellular proteins: The enzymes involved, their substrate specificities and biological effects. *Proteomics* **2015**, *15*, 2385–2401. [CrossRef]
111. Polevoda, B.; Sherman, F. N-terminal acetyltransferases and sequence requirements for N-terminal acetylation of eukaryotic proteins. *J. Mol. Biol.* **2003**, *325*, 595–622. [CrossRef]
112. Pardossi-Piquard, R.; Checler, F. The physiology of the β-amyloid precursor protein intracellular domain AICD. *J. Neurochem.* **2012**, *120* (Suppl. S1), 109–124. [CrossRef]
113. Szögi, T.; Schuster, I.; Borbély, E.; Gyebrovszki, A.; Bozsó, Z.; Gera, J.; Rajkó, R.; Sántha, M.; Penke, B.; Fülöp, L. Effects of the Pentapeptide P33 on Memory and Synaptic Plasticity in APP/PS1 Transgenic Mice: A Novel Mechanism Presenting the Protein Fe65 as a Target. *Int. J. Mol. Sci.* **2019**, *20*, 3050. [CrossRef] [PubMed]
114. Borg, J.-P.; Yang, Y.; De Taddeo-Borg, M.; Margolis, B.; Turner, R.S. The X11α protein slows cellular amyloid precursor protein processing and reduces Aβ40 and Aβ42 secretion. *J. Biol. Chem.* **1998**, *273*, 14761–14766. [CrossRef] [PubMed]
115. Dunning, C.J.R.; Black, H.L.; Andrews, K.L.; Davenport, E.C.; Conboy, M.; Chawla, S.; Dowle, A.A.; Ashford, D.; Thomas, J.R.; Evans, G.J.O. Multisite tyrosine phosphorylation of the N-terminus of Mint1/X11α by Src kinase regulates the trafficking of amyloid precursor protein. *J. Neurochem.* **2016**, *137*, 518–527. [CrossRef] [PubMed]
116. Miller, C.C.J.; McLoughlin, D.M.; Lau, K.-F.; Tennant, M.E.; Rogelj, B. The X11 proteins, Aβ production and Alzheimer's disease. *Trends Neurosci.* **2006**, *29*, 280–285. [CrossRef] [PubMed]
117. Tamayev, R.; Zhou, D.; D'Adamio, L. The interactome of the amyloid β precursor protein family members is shaped by phosphorylation of their intracellular domains. *Mol. Neurodegener.* **2009**, *4*, 28. [CrossRef]

118. Hoe, H.-S.; Tran, T.S.; Matsuoka, Y.; Howell, B.W.; Rebeck, G.W. DAB1 and Reelin Effects on Amyloid Precursor Protein and ApoE Receptor 2 Trafficking and Processing. *J. Biol. Chem.* **2006**, *281*, 35176–35185. [CrossRef]
119. Russo, C.; Dolcini, V.; Salis, S.; Venezia, V.; Zambrano, N.; Russo, T.; Schettini, G. Signal Transduction through Tyrosine-phosphorylated C-terminal Fragments of Amyloid Precursor Protein via an Enhanced Interaction with Shc/Grb2 Adaptor Proteins in Reactive Astrocytes of Alzheimer's Disease Brain. *J. Biol. Chem.* **2002**, *277*, 35282–35288. [CrossRef]
120. Tarr, P.E.; Roncarati, R.; Pelicci, G.; Pelicci, P.G.; D'Adamio, L. Tyrosine phosphorylation of the β-amyloid precursor protein cytoplasmic tail promotes interaction with Shc. *J. Biol. Chem.* **2002**, *277*, 16798–16804. [CrossRef]
121. Bukhari, H.; Glotzbach, A.; Kolbe, K.; Leonhardt, G.; Loosse, C.; Mueller, T. Small things matter: Implications of APP intracellular domain AICD nuclear signaling in the progression and pathogenesis of Alzheimer's disease. *Prog. Neurobiol.* **2017**, *156*, 189–213. [CrossRef]
122. Chang, K.-A.; Kim, H.-S.; Ha, T.-Y.; Ha, J.-W.; Shin, K.Y.; Jeong, Y.H.; Lee, J.-P.; Park, C.-H.; Kim, S.; Baik, T.-K.; et al. Phosphorylation of amyloid precursor protein (APP) at Thr668 regulates the nuclear translocation of the APP intracellular domain and induces neurodegeneration. *Mol. Cell. Biol.* **2006**, *26*, 4327–4338. [CrossRef] [PubMed]
123. Ando, K.; Iijima, K.-I.; Elliott, J.I.; Kirino, Y.; Suzuki, T. Phosphorylation-dependent regulation of the interaction of amyloid precursor protein with Fe65 affects the production of β-amyloid. *J. Biol. Chem.* **2001**, *276*, 40353–40361. [CrossRef] [PubMed]
124. Müller, T.; Meyer, H.E.; Egensperger, R.; Marcus, K. The amyloid precursor protein intracellular domain (AICD) as modulator of gene expression, apoptosis, and cytoskeletal dynamics-relevance for Alzheimer's disease. *Prog. Neurobiol.* **2008**, *85*, 393–406. [CrossRef]
125. Shu, R.; Wong, W.; Ma, Q.H.; Yang, Z.Z.; Zhu, H.; Liu, F.J.; Wang, P.; Ma, J.; Yan, S.; Polo, J.M.; et al. APP intracellular domain acts as a transcriptional regulator of miR-663 suppressing neuronal differentiation. *Cell Death Dis.* **2015**, *6*, e1651. [CrossRef]
126. Grimm, M.O.; Mett, J.; Stahlmann, C.P.; Grösgen, S.; Haupenthal, V.J.; Blümel, T.; Hundsdörfer, B.; Zimmer, V.C.; Mylonas, N.T.; Tanila, H.; et al. APP intracellular domain derived from amyloidogenic β- and γ-secretase cleavage regulates neprilysin expression. *Front. Aging Neurosci.* **2015**, *7*, 77. [CrossRef]
127. Pousinha, P.A.; Mouska, X.; Bianchi, D.; Temido-Ferreira, M.; Rajão-Saraiva, J.; Gomes, R.; Fernandez, S.P.; Salgueiro-Pereira, A.R.; Gandin, C.; Raymond, E.F.; et al. The Amyloid Precursor Protein C-Terminal Domain Alters CA1 Neuron Firing, Modifying Hippocampus Oscillations and Impairing Spatial Memory Encoding. *Cell Rep.* **2019**, *29*, 317–331.e5. [CrossRef]
128. Almeida, C.; Takahashi, R.; Gouras, G. β-amyloid accumulation impairs multivesicular body sorting by inhibiting the ubiquitin–proteasome system. *J. Neurosci.* **2006**, *26*, 4277–4288. [CrossRef]
129. Gregori, L.; Fuchs, C.; Figueiredo-Pereira, M.; Van Nostrand, W.; Goldgaber, D. Amyloid β-protein inhibits ubiquitin-dependent protein degradation in vitro. *J. Biol. Chem.* **1995**, *270*, 19702–19708. [CrossRef]
130. Oh, S.; Hong, H.S.; Hwang, E.; Sim, H.J.; Lee, W.; Shin, S.J.; Mook-Jung, I. Amyloid peptide attenuates the proteasome activity in neuronal cells. *Mech. Ageing Dev.* **2005**, *126*, 1292–1299. [CrossRef]
131. Tseng, B.; Green, K.; Chan, J.; Blurton-Jones, M.; LaFerla, F. Aβ inhibits the proteasome and enhances amyloid and tau accumulation. *Neurobiol. Aging* **2008**, *29*, 1607–1618. [CrossRef]
132. Tucker-Drob, E.M. Cognitive Aging and Dementia: A Life Span Perspective. *Annu. Rev. Dev. Psychol.* **2019**, *1*, 177–196. [CrossRef] [PubMed]
133. Matthews, F.E.; Arthur, A.; Barnes, L.E.; Bond, J.; Jagger, C.; Robinson, L.; Brayne, C. Medical Research Council Cognitive Function and Ageing Collaboration. A two-decade comparison of prevalence of dementia in individuals aged 65 years and older from three geographical areas of England: Results of the Cognitive Function and Ageing Study I and II. *Lancet.* **2013**, *382*, 1405–1412. [PubMed]
134. van Dyck, C.H.; Swanson, C.J.; Aisen, P.; Bateman, R.J.; Chen, C.; Gee, M.; Kanekiyo, M.; Li, D.; Reyderman, L.; Cohen, S.; et al. Lecanemab in Early Alzheimer's Disease. *N. Engl. J. Med.* **2023**, *388*, 9–21. [CrossRef] [PubMed]
135. Mintun, M.; Lo, A.; Duggan-Evans, C.; Wessels, A.; Ardayfio, P.; Andersen, S.; Shcherbinin, S.; Sparks, J.; Sims, J.; Brys, M.; et al. Donanemab in Early Alzheimer's Disease. *N. Engl. J. Med.* **2021**, *384*, 1691–1704. [CrossRef] [PubMed]
136. Lilly, E. Donanemab Significantly Slowed Cognitive and Functional Decline in Phase 3 Study of Early Alzheimer's Disease. Press-rlease. 2023. Available online: https://investor.lilly.com/news-releases/news-release-details/lillys-donanemab-significantly-slowed-cognitive-and-functional (accessed on 1 October 2023).
137. Sims, J.; Zimmer, J.; Evans, C.; Lu, M.; Ardayfio, P.; Sparks, J.; Wessels, A.; Sncherbinin, S.; Wang, H.; Nery, E.; et al. Donanemab in Early Symptomatic Alzheimer Disease: The TRAILBLAZER-ALZ 2 Randomized Clinical Trial. *JAMA* **2023**, *330*, 512–527. [CrossRef]
138. Abbott, A. The next generation of Alzheimer's treatments. *Nature* **2023**, *616*, 26–28. [CrossRef]
139. Huse, J.; Liu, K.; Pijak, D.; Carlin, D.; Lee VDoms, R. Beta-secretase processing in the trans-Golgi network preferentially generates truncated amyloid species that accumulate in Alzheimer's disease brain. *J. Biol. Chem.* **2002**, *277*, 16278–16284. [CrossRef]
140. Liu, K.; Doms, R.; Lee, M. Glu11 site cleavage and N-terminally truncated A beta production upon BACE overexpression. *Biochemistry* **2002**, *41*, 3128–3136. [CrossRef]
141. Lee, E.B.; Zhang, B.; Liu, K.; Greenbaum, E.A.; Doms, R.W.; Trojanowski, J.Q.; Lee, V.M. BACE overexpression alters the subcellular processing of APP and inhibits Aβ deposition in vivo. *J. Cell Biol.* **2005**, *168*, 291–302. [CrossRef]

142. Kimura, A.; Hata, S.; Suzuki, T. Alternative selection of beta-site APP-cleaving enzyme 1 (BACE1) cleavage sites in amyloid beta-protein precursor (APP) harboring protective and pathogenic mutations within the Abeta sequence. *J. Biol. Chem.* **2016**, *291*, 24041–24053. [CrossRef]
143. Fluhrer, R.; Multhaup, G.; Schlicksupp, A.; Okochi, M.; Takeda, M.; Lammich, S.; Willem, M.; Westmeyer, G.; Bode, W.; Walter, J.; et al. Identification of a beta-secretase activity, which truncates amyloid beta-peptide after its presenilin-dependent generation. *J. Biol. Chem.* **2003**, *278*, 5531–5538. [CrossRef] [PubMed]
144. Shi, X.P.; Tugusheva, K.; Bruce, J.E.; Lucka, A.; Wu, G.X.; Chen-Dodson, E.; Price, E.; Li, Y.; Xu, M.; Huang, Q.; et al. Beta-secretase cleavage at amino acid residue 34 in the amyloid beta peptide is dependent upon gamma-secretase activity. *J. Biol. Chem.* **2003**, *278*, 21286–21294. [CrossRef] [PubMed]
145. Liebsch, F.; Kulic, L.; Teunissen, C.; Shobo, A.; Ulku, I.; Engelschalt, V.; Hancock, M.A.; van der Flier, W.M.; Kunach, P.; Rosa-Neto, P.; et al. Abeta34 is a BACE1-derived degradation intermediate associated with amyloid clearance and Alzheimer's disease progression. *Nat. Commun.* **2019**, *10*, 2240. [CrossRef] [PubMed]
146. Garcia-Gonzales, L.; Pilat, D.; Rivera, S. Emerging Alternative Proteinases in APP Metabolism and Alzheimer's Disease Pathogenesis. *Front. Aging Neurosci.* **2019**, *11*, 244. [CrossRef]
147. Farzan, M.; Schnitzler, C.E.; Vasilieva, N.; Leung, D.; Choe, H. BACE2, a β-secretase homolog, cleaves at the β site and within the amyloid-β region of the amyloid-β precursor protein. *Proc. Natl. Acad. Sci. USA* **2000**, *97*, 9712–9717. [CrossRef]
148. Yan, R.; Munzner, J.; Shuck, M.; Bienkowski, M. BACE2 functions as an alternative alpha secretase in cells. *J. Biol. Chem.* **2001**, *276*, 34019–34027. [CrossRef]
149. Luo, J.; Zou, H.; Guo, Y.; Huang, K.; Ngan, E.S.; Li, P. BACE2 variant identified from HSCR patient causes AD-like phenotypes in hPSC-derived brain organoids. *Cell Death Discov.* **2022**, *8*, 47. [CrossRef]
150. Basi, G.; Frigon, N.; Barbour, R.; Doan, T.; Gordon, G.; McConlogue, L.; Sinha, S.; Zeller, M. Antagonistic effects of beta-site amyloid precursor protein-cleaving enzymes 1 and 2 on beta-amyloid peptide production in cells. *J. Biol. Chem.* **2003**, *278*, 31512–31520. [CrossRef]

International Journal of
Molecular Sciences

MDPI

Article

A Cross-Sectional Study of Protein Changes Associated with Dementia in Non-Obese Weight Matched Women with and without Polycystic Ovary Syndrome

Alexandra E. Butler [1,*], Abu Saleh Md Moin [1], Thozhukat Sathyapalan [2] and Stephen L. Atkin [1]

[1] Research Department, Royal College of Surgeons of Ireland, Busaiteen P.O. Box 15503, Bahrain; amoin@rcsi.com (A.S.M.M.); satkin@rcsi.com (S.L.A.)
[2] Academic Endocrinology, Diabetes and Metabolism, Hull York Medical School, Hull HU6 7RU, UK; thozhukat.sathyapalan@hyms.ac.uk
* Correspondence: aeb91011@gmail.com or abutler@rcsi.com; Tel.: +973-66760313

Abstract: Dysregulated Alzheimer's disease (AD)-associated protein expression is reported in polycystic ovary syndrome (PCOS), paralleling the expression reported in type 2 diabetes (T2D). We hypothesized, however, that these proteins would not differ between women with non-obese and non-insulin resistant PCOS compared to matched control subjects. We measured plasma amyloid-related proteins levels (Amyloid-precursor protein (APP), alpha-synuclein (SNCA), amyloid P-component (APCS), Pappalysin (PAPPA), Microtubule-associated protein tau (MAPT), apolipoprotein E (apoE), apoE2, apoE3, apoE4, Serum amyloid A (SAA), Noggin (NOG) and apoA1) in weight and aged-matched non-obese PCOS (n = 24) and control (n = 24) women. Dementia-related proteins fibronectin (FN), FN1.3, FN1.4, Von Willebrand factor (VWF) and extracellular matrix protein 1 (ECM1) were also measured. Protein levels were determined by Slow Off-rate Modified Aptamer (SOMA)-scan plasma protein measurement. Only APCS differed between groups, being elevated in non-obese PCOS women (p = 0.03) relative to the non-obese control women. This differed markedly from the elevated APP, APCS, ApoE, FN, FN1.3, FN1.4 and VWF reported in obese women with PCOS. Non-obese, non-insulin resistant PCOS subjects have a lower AD-associated protein pattern risk profile versus obese insulin resistant PCOS women, and are not dissimilar to non-obese controls, indicating that lifestyle management to maintain optimal body weight could be beneficial to reduce the long-term AD-risk in women with PCOS.

Keywords: polycystic ovary syndrome; PCOS; amyloid-associated proteins; Alzheimer's disease

Citation: Butler, A.E.; Moin, A.S.M.; Sathyapalan, T.; Atkin, S.L. A Cross-Sectional Study of Protein Changes Associated with Dementia in Non-Obese Weight Matched Women with and without Polycystic Ovary Syndrome. *Int. J. Mol. Sci.* **2024**, *25*, 2409. https://doi.org/10.3390/ijms25042409

Academic Editor: Claudia Ricci

Received: 24 January 2024
Revised: 14 February 2024
Accepted: 16 February 2024
Published: 18 February 2024

1. Introduction

There is an increased prevalence of metabolic features including T2D, hypertension, fatty liver disease and cardiovascular disease [1] in women with polycystic ovary disease (PCOS) that is thought to be related to the degree of insulin resistance and inflammation driven by obesity [1,2], characteristics typically found in the condition. Women with PCOS are reported to suffer more from mood disorders, such as anxiety and depression, and sleep disturbances compared to women without PCOS, indicative of a neurological component to the PCOS disease spectrum [3].

Dementia is predicted to increase markedly as the population ages, potentially rising to 115.4 million by 2050 [4], of which Alzheimer's disease (AD) accounts for 80% of all cases [5]. Obesity is associated with AD [6], and increased insulin resistance (IR) is also associated with AD independently [7], as insulin is able to freely cross the blood brain barrier [7], and it has been suggested that the underlying molecular mechanisms of IR and AD are due to insulin receptor substrate 1 (IRS-1) and insulin-like growth factor 1 (IGF-1) receptor dysregulation [8]. It has been suggested that the link between obesity, depression and AD is enhanced neuroinflammation [9]. Obesity and increased IR are both characteristic

features found in T2D and the increased risk for T2D patients developing AD has been well established [10–12]. It has been reported that a pattern of AD-related risk proteins, particularly amyloid precursor proteins (APP), amyloid P component (APCS) and alpha synuclein (SNCA) are found in T2D [13] and recently a similar pattern of these proteins was reported in PCOS [14]. Perhaps this similarity is not surprising as both obesity and increased IR are commonly found in PCOS and it is reported that 10% may develop diabetes [15]. In addition, mood disorders that include both anxiety and depression, and sleep disturbances are more commonly found in women with PCOS compared to those women that do not have PCOS [3]; thus, the combination noted above of obesity and depression with AD [9] may also reflect an enhanced risk of AD in PCOS. Indeed, there is increasing evidence to suggest that there may be a link between Alzheimer's disease and PCOS [16]. The underlying mechanism has been suggested to be multifactorial with contributions from insulin resistance, obesity and hormonal imbalance from both the pituitary and the ovaries associated with the PCOS condition, all of which can affect cognitive function and increase inflammation [17]. Functional magnetic resonance (MRI) studies have suggested that there are cerebral changes in areas associated with cognition that relate to insulin resistance [18] and to luteinizing hormone (LH) level changes [19], whilst others have suggested that changes in PCOS-related cognitive function are exacerbated by hormonal changes involving increased testosterone [20] and insulin levels [21].

In a proteomic study used to analyze proteins in a comparison between AD, frontotemporal dementia (FTD) and controls, it was reported that five proteins, fibronectin (FN), fibronectin fragment 3 (FN1.3), fibronectin fragment 4 (FN1.4), Von Willebrand factor (VWF) and extracellular matrix protein 1 (ECM1) were discriminatory being increased in AD in comparison to both FTD and controls [22], and which may prove to be important biomarkers for AD in the future. Other proteins central to the biology of amyloid Beta (Aβ), a characteristic pathological feature of AD, include APP, SNCA, APCS, Pappalysin (PAPPA), Microtubule-associated protein tau (MAPT) and apolipoprotein E (apoE) and its alleles (apoE2, E3 and E4) and thus their levels were determined here.

An elevation of APP and APCS, which are associated with AD, and decreased SNCA were found in patients with T2D [13], and this was reflected in a similar pattern of protein expression in obese and insulin resistant subjects with PCOS [14]. Given that obesity and IR are so closely associated with PCOS they are not easily accounted for statistically; therefore, only a study in PCOS of non-obese women without insulin resistance could answer the question of whether the inherent pathophysiology of PCOS infers a greater risk for AD. Thus, we hypothesized that the pattern of AD-related protein changes found in obese women with PCOS [14] would not have been different to matched controls if weight and insulin resistance had been accounted for in the study design; therefore, we analyzed AD-related protein levels in non-obese, non-insulin resistant women with PCOS compared to a matched non-PCOS control population.

2. Results

Baseline data for the 24 PCOS subjects and 24 controls are shown in Table 1. The two cohorts were weight and age-matched, and did not have insulin resistance, but subjects with PCOS did have hyperandrogenemia, with increased C-reactive protein (CRP, an inflammatory marker) and anti-Müllerian hormone (AMH).

Table 1. Demographics, baseline, hormonal and metabolic parameters of the polycystic ovary syndrome (PCOS) subjects and controls (mean ± SD).

	Control (*n* = 24)	**PCOS (*n* = 24)**	***p*-Value**
Age (years)	32.5 ± 4.1	31 ± 6.4	0.14
BMI (kg/m^2)	24.8 ± 1.1	25.9 ± 1.8	0.56
Fasting glucose (nmol/L)	4.9 ± 0.4	4.7 ± 0.8	0.06

Table 1. *Cont.*

	Control (n = 24)	PCOS (n = 24)	p-Value
HbA1C (mmol/mol)	30.9 ± 6.5	31.8 ± 3.0	0.9
HOMA-IR	1.8 ± 1.0	1.9 ± 1.6	0.97
SHBG (nmol/L)	104.2 ± 80.3	71.7 ± 62.2	0.01
Free androgen index (FAI)	1.3 ± 0.5	4.2 ± 2.9	0.0001
CRP (mg L^{-1})	2.34 ± 2.34	2.77 ± 2.57	0.43
AMH (ng/mL)	24.3 ± 13.1	57.2 ± 14.2	0.0001

BMI—Body Mass Index; HbA1c—glycated hemoglobin; HOMA-IR—Homeostasis model of assessment—insulin resistance; CRP—C reactive protein; SHBG—sex hormone binding globulin; AMH—Anti-Müllerian hormone.

The results of the Somascan analysis of Alzheimer's disease-related proteins are shown in Table 2 for the PCOS and control women.

Table 2. Levels of Alzheimer's-related proteins in non-obese women with polycystic ovary syndrome (n = 24; PCOS) versus controls (n = 24). Data presented are Mean ± 1 Standard Deviation of Relative Fluorescent Units (RFU).

	Control Mean (SD)	PCOS Mean (SD)	p-Value
APP	31,246 (19,569)	28,300 (22,332)	0.60
SNCA	9673 (3322)	10,012 (3343)	0.70
APCS	35,663 (11,717)	41,518 (11,879)	0.03
PAPPA	10,201 (5799)	10,065 (4505)	0.92
MAPT	129 (48)	130 (36)	0.89
apoE	25,296 (11,517)	26,588 (13,321)	0.69
apoE2	214,964 (67,686)	221,851 (56,020)	0.68
apoE3	148,321 (59,451)	157,453 (59,480)	0.56
apoE4	170,531 (57,851)	173,799 (63,642)	0.84
SAA	1211 (1150)	1585 (2774)	0.51
NOG	3081 (1063)	3203 (2582)	0.82
apoA1	12,344 (2248)	12,392 (2448)	0.94
vWF	11,481 (14,223)	10,746 (9306)	0.82
FN	18,553 (16,585)	19,991 (12,729)	0.71
FN1.3	4360 (7520)	3368 (2021)	0.50
FN1.4	63,653 (33,196)	69,376 (26,468)	0.47
ECM1	18,037 (6143)	19,345 (5284)	0.39

Amyloid-precursor protein (APP), alpha-synuclein (SNCA), amyloid P-component (APCS), Pappalysin (PAPPA), Microtubule-associated protein tau (MAPT), apolipoprotein E (apoE), apoE2, apoE3, apoE4, Serum amyloid A (SAA), Noggin and apoA1; von Willebrand factor (vWF); Fibronectin (FN); Fibronectin fragment 3 (FN1.3); Fibronectin fragment 4 (FN1.4); Extracellular matrix protein 1 (ECM1).

2.1. Levels of Alzheimer's-Related Proteins in PCOS

Only APCS differed between groups, being elevated in non-obese PCOS women (p = 0.03) relative to the non-obese control women (Table 1). The levels of other Alzheimer's-related proteins, namely APP, SNCA, PAPPA, MAPT, apoE, apoE2, apoE3, apoE4, SAA, NOG and apoA1 were comparable between PCOS subjects and controls (Table 2). The dementia-related proteins FN, FN1.3, FN1.4, VWF and ECM1 did not differ between the non-obese non-insulin resistant PCOS and controls.

2.2. Correlation Analyses

For the APCS protein that differed between non-obese non-insulin resistant PCOS subjects and control women, correlations with age, BMI, insulin resistance (HOMA-IR), testosterone, C-reactive protein (CRP) and circulating levels of selected inflammatory proteins and protective heat shock proteins (HSPs) (interleukin 6 (IL6), tumor necrosis

factor alpha (TNFa), heat shock protein 90 (HSP90AA1, HSP90) and heat shock protein family D protein 1 (HSPD1, HSP60) were determined.

BMI correlated positively with APCS (r = 0.52, $p = 0.003$) and apoE ($r = 0.44$, $p = 0.02$) in PCOS women; Homeostasis model of assessment–insulin resistance (HOMA-IR) correlated positively with apoE ($r = 0.37$, $p = 0.04$) in PCOS women. Testosterone correlated negatively with APCS ($r = -0.45$, $p = 0.02$) in PCOS women (Figure 1).

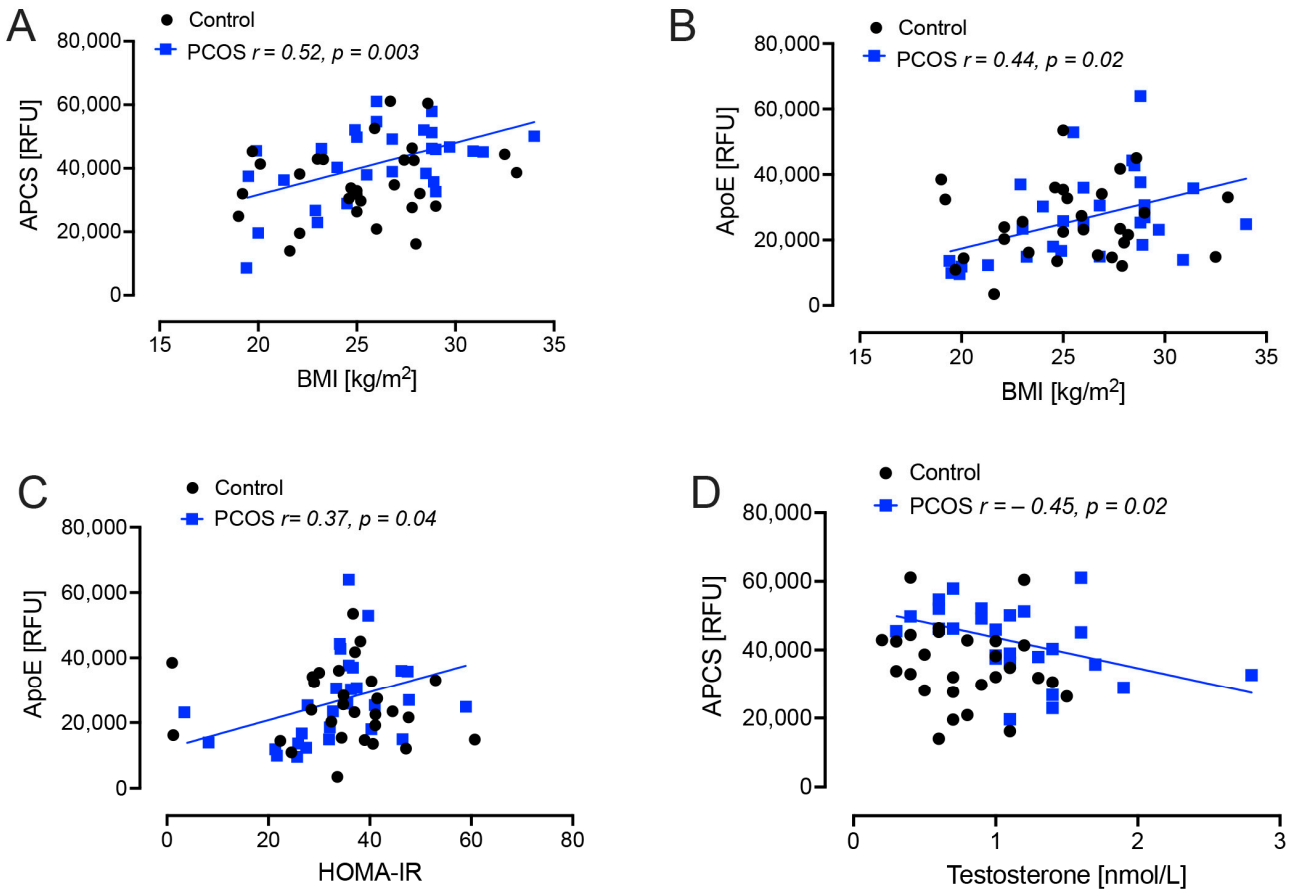

Figure 1. Demographic and biochemical correlations with plasma amyloid-related proteins levels in polycystic ovary syndrome (PCOS) and control subjects; amyloid P-component (APCS) and apolipoprotein E (apoE) with body mass index (BMI), insulin resistance (HOMA-IR) and testosterone in weight and aged-matched non-obese PCOS ($n = 24$) and control ($n = 24$) women. (**A**), positive correlation of APCS with BMI ($p = 0.003$); (**B**), positive correlation of ApoE with BMI ($p = 0.02$); (**C**), positive correlation of ApoE with HOMA-IR ($p = 0.04$); (**D**), negative correlation of APCS with testosterone ($p = 0.02$).

Interleukin 6 (IL6) correlated positively with APP ($r = 0.37$, $p = 0.04$) and negatively with apoE ($r = -0.38$, $p = 0.04$) in PCOS women. Heat shock protein 90 (HSP90AA1, HSP90) correlated positively with APP in both control and PCOS women ($r = 0.35$, $p = 0.04$ and $r = 0.60$, $p = 0.0006$, respectively), and correlated positively with SNCA ($r = 0.44$, $p = 0.01$) in PCOS women. Heat shock protein family D protein 1 (HSPD1, HSP60) correlated positively with APP ($r = 0.60$, $p = 0.0006$) and SNCA ($r = 0.51$, $p = 0.004$) in PCOS women (Figure 2).

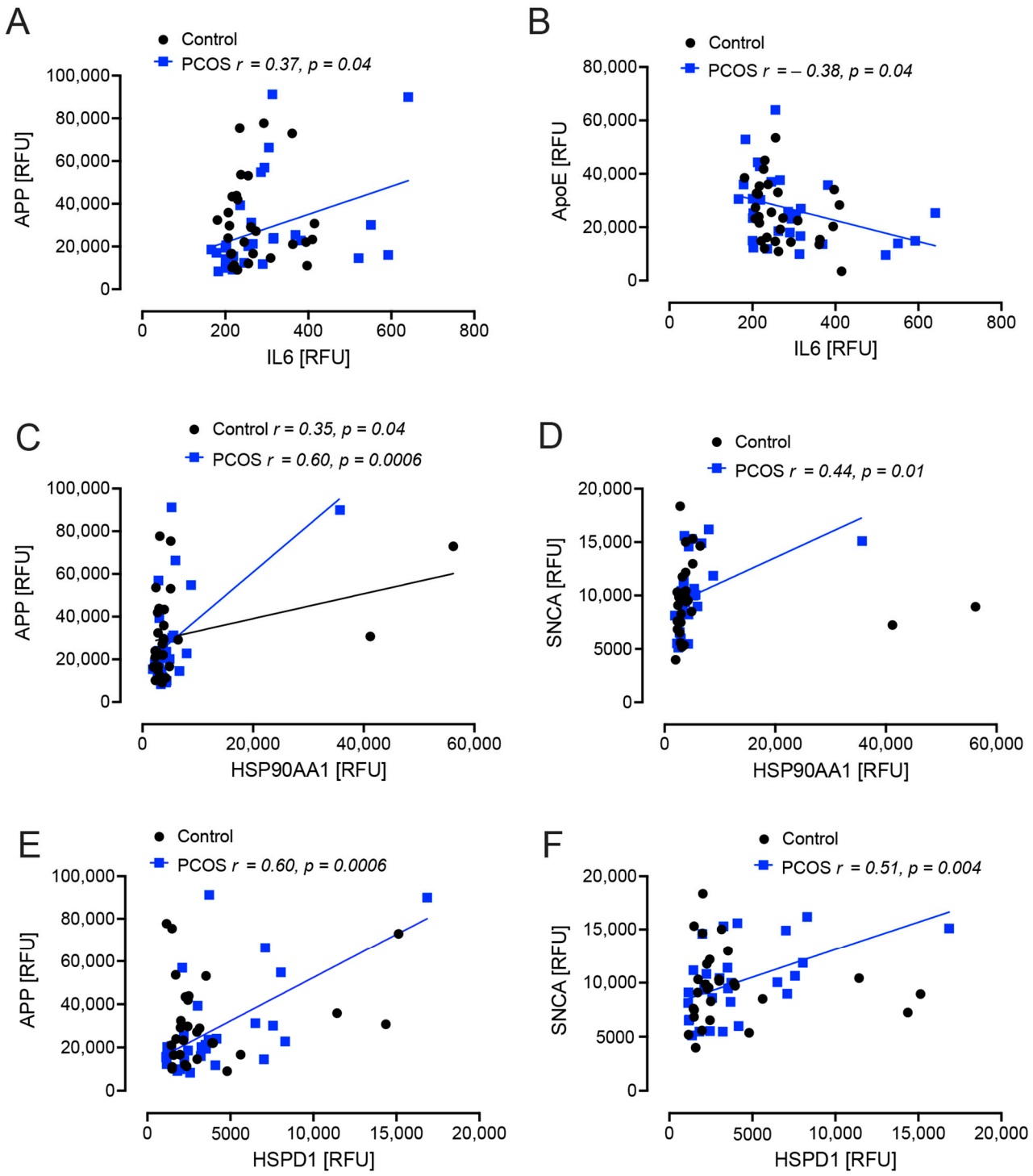

Figure 2. Correlations of Alzheimer's-related proteins with interleukin 6 (IL6) and heat shock proteins in polycystic ovary syndrome (PCOS) and control subjects. APP correlated positively with IL6 in PCOS (p = 0.04) (**A**); ApoE correlated negatively with IL6 in PCOS (p = 0.04) (**B**); in both PCOS (p = 0.0006) and control women (p = 0.04) APP corelated positively with heat shock protein 90 (HSP90AA1) (**C**); SNCA correlated positively with HSP90AA1 (p = 0.01) (**D**), APP correlated positively with heat shock protein 60 (HSPD1: p = 0.0006) (**E**); SNCA correlated positively with HSPD1 (p = 0.004) (**F**). Controls: black open circles; PCOS: blue squares.

3. Discussion

Here, we show that the only change in plasma Alzheimer's-related proteins in subjects with PCOS who were non-obese and not insulin resistant was an increase in APCS ($p = 0.03$) relative to weight matched control women. Of note, an increase in APCS was also found in obese women with PCOS [14]. Amyloid P component (APCS) is found in plaques and the neurofibrillary tangles characteristic of Alzheimer's disease [23], and its role may be involved in the decreased proteolysis of Aβ deposits, leading to further plaque formation [24] therefore, increased serum levels may be detrimental. APCS was shown to accurately discriminate between AD compared to normal brain samples [25]. Overall, the results in this study are in contrast to what has been reported in a cohort of obese women with PCOS from a PCOS biobank [14] where the circulatory AD-related protein pattern reflected what was seen in T2D subjects with elevated APP and lower SNCA [26–28]. In this study, the plasma levels of APP, SNCA and apoE were not different between the non-obese PCOS and control women; however, in the prior study reporting AD-related protein changes in PCOS, all the PCOS subjects had the metabolic phenotype A according to the Rotterdam criteria. PCOS phenotype A, that expresses all three of the diagnostic criteria, is reported to be at higher risk of adverse metabolic and cardiovascular outcomes compared to the other phenotypes, and phenotype D is the least severe [29]. In this study, all of the PCOS subjects had anovulatory infertility but half were phenotype B (irregular menses with hyperandrogenism) and half were phenotype C (irregular menses and polycystic ovaries on transvaginal scanning); there were too few subjects, and less than the power analysis would allow, to do a subgroup analysis. Therefore, the expression of AD-related proteins needs to be clarified for the individual PCOS phenotypes to determine if there is a potential increased risk only for the PCOS subjects with the type A phenotype.

It has been suggested that PCOS may have an increased risk of AD, with documented changes in cognition [16,18–21], and it is well recognized that patients with T2D have evidence of an increased risk for developing AD [10–12]; however, what this study shows is that, if the obesity and insulin resistance in these patients is addressed, that any AD-risk could possibly be normalized to that of matched controls. What is unknown is whether, once obesity and insulin resistance are established in PCOS, any intervention(s) to reverse these also positively impacts on the AD-risk proteins; however, this is inferred from the results that showed BMI correlated positively with APCS and apoE in PCOS women and that HOMA-IR correlated positively with apoE in PCOS women suggesting that, should weight and insulin resistance increase with an increased BMI, that these parameters would also increase. It has been suggested that underlying insulin resistance associated with PCOS is responsible for the alterations in cognitive function and, additionally, increases in inflammation [17]. Obesity is commonly a sequela of both PCOS and T2D, and obesity is also associated with an increased risk of AD [30]. This then leads to a complex milieu, with insulin resistance promoting increasing obesity due to compensatory hyperinsulinemia [31]; conversely, obesity, through mechanisms of chronic inflammation, adipokine activation, mitochondrial dysfunction [17], promotes insulin resistance. Thus, a vicious cycle may result. The inflammation that results from the insulin resistance/obesity may then be reflected in the development of cognitive impairment and the progression to AD [32,33]. In this study, those parameters associated with inflammation such as IL6 and the heat shock response proteins correlated with APP, SNCA and ApoE in the PCOS subjects but not the normal controls, suggesting that those with PCOS could be predisposed to enhanced changes of these proteins with the onset of inflammation induced by obesity and insulin resistance.

What role testosterone may have in the development of AD is debated but has been reported in men that a lower testosterone level was associated with AD [34]. Whether testosterone has a role in the development of AD in women is unclear, and in this study APCS negatively correlated with testosterone; however, this was the converse found in obese PCOS where APCS positively correlated; however, in both studies, testosterone levels

did not correlate in the normal controls. Future studies to determine if testosterone in women has a positive or negative effect on AD risk need to be undertaken.

Intervention through recommended lifestyle management with 5–10% weight loss and undertaking regular physical exercise [35] does impact positively on obesity and insulin resistance [36], but is often difficult to sustain [37]; further, it is unknown whether AD-related risk factors are improved. Bariatric surgery has been shown to have a marked effect in PCOS, with reduction in BMI, insulin resistance, androgen levels and a return of regular menses, but no reports on AD-related risk factors are available [38]; however, the current evidence would suggest that early and sustained lifestyle changes may have a long term beneficial effect on cognition and AD-related risk and, at the very least, would not be harmful. Prospective studies on the effect of weight gain and weight loss and their effects on AD-related proteins in those women with PCOS would be highly informative.

A strength of this study is that it was performed on a homogeneous white Caucasian population though this would therefore need to be repeated to consider ethnic differences. The primary limitation of this study is that BMI was the only anthropometric analysis used and a more precise analysis of body composition, such as dual energy X-ray absorptiometry (DXA), resistance analysis, abdominal circumference or waist-to-hip ratio, would add value. In addition, the comparison between the protein levels between obese and the nonobese PCOS are limited, and the studies should be run using the same proteomic platforms; however, rigorous control samples included in every run would serve to mitigate this. Subsequent validation of the protein changes described with additional quantitative methods would also add value to the findings. Adjusting for BMI and insulin resistance is very difficult as both are so highly correlated with PCOS that regression adjustment for either or both would remove the PCOS effects; therefore, to determine if a decrease in AD-related risk factors is dependent on obesity and insulin resistance, this study provides the only design that would answer the question, with the caveat that it would have biased the PCOS phenotype recruited given that they all had to be non-obese.

4. Materials and Methods

Study Design

In a cross-sectional analysis, plasma levels of Alzheimer's-related proteins were measured in women with PCOS (n = 24) and control (n = 24) women recruited from the Hull IVF clinic [39]. Control women were age and BMI matched to the PCOS patients. All procedures performed in studies involving human participants were in accordance with the ethical standards of the Yorkshire and The Humber NRES ethical committee, UK, that provided approval for the study, and with the 1964 Helsinki declaration and its later amendments or comparable ethical standards. For the diagnosis of PCOS, the Rotterdam consensus criteria were used: (1) clinical (Ferriman-Gallwey score of >8) and biochemical hyperandrogenemia (a free androgen index (FAI) of >4) (2) oligomenorrhea or amenorrhea and (3) polycystic ovaries seen on transvaginal ultrasound [40]. Study participants had no other condition or illness and were required to be medication-free for nine months preceding study enrollment, including the exclusion of over-the-counter medication. Testing was undertaken to ensure that no patient had any of the following endocrine conditions: non-classical 21-hydroxylase deficiency, hyperprolactinemia, Cushing's disease or an androgen-secreting tumor as per the recommendations [41]. Of note, both women with PCOS and control women had maintained a stable weight for at least 3 months prior to enrollment in the study. Demographic data for both control and PCOS women is shown in Table 1.

Patients presented after fasting overnight; height, weight and waist circumference and body mass index (BMI) were performed according to WHO guidelines [42]. BMI was defined as weight in kilograms and height in centimeters, with the formula kg/m^2. Blood was withdrawn fasting and prepared by centrifugation at $3500\times\ g$ for 15 min, aliquoted and stored at $-80\ ^{\circ}C$. Analysis for sex hormone binding globulin (SHBG), insulin (DPC Immulite 200 analyser, Euro/DPC, Llanberis, UK), and plasma glucose (to calculate homeostasis model assessment-insulin resistance (HOMA-IR)) (Synchron LX20

analyser, Beckman-Coulter, High Wycombe, UK) was undertaken. Free androgen index (FAI) was derived from total testosterone divided by SHBG $\times 100$. Insulin resistance (IR) was determined by HOMA-IR (insulin $\times$ glucose)/22.5). Serum testosterone was quantified using isotope-dilution liquid chromatography tandem mass spectrometry (LC-MS/MS) [39].

Plasma Alzheimer's-related proteins were measured by the Slow Off-rate Modified Aptamer (SOMA)-scan platform (Somalogic, Boulder, CO, USA) [43]. Calibration was based on standards as previously described [44].

The protein quantification was performed using a Slow Off-rate Modified Aptamer (SOMAmer)–based protein array, as previously described [45,46]. Briefly, EDTA plasma samples were measured as follows (1) Analyte and primer beads binding-SOMAmers (fully synthetic fluorophore-labeled SOMAmer coupled to a biotin moiety through a photocleavable linker) were equilibrated; (2) Analyte/SOMAmers complex immobilization on streptavidin-substituted support. (3) Long-wave ultraviolet light cleavage to release analyte-SOMAmer complexes into the solution; (4) Analyte-SOMAmer complexes were immobilized on streptavidin support through analyte-borne biotinylation. (5) Elution of analyte-SOMAmer complexes with the released SOMAmers acting as surrogates for analyte quantification; (6) Quantification by hybridization to SOMAmer-complementary oligonucleotides. Normalization of raw intensities, hybridization, median signal and calibration signal were standardized for each [43,44].

Version 3.1 of the SOMAscan Assay was used, targeting the following proteins: Amyloid-precursor protein (APP), alpha-synuclein (SNCA), amyloid P-component (APCS), Pappalysin (PAPPA), Microtubule-associated protein tau (MAPT), apolipoprotein E (apoE), apoE2, apoE3, apoE4, Serum amyloid A (SAA), Noggin (NOG) and apoA1. In addition, proteins related to dementia were measured: fibronectin (FN), FN1.3, FN1.4, Von Willebrands factor (VWF) and extracellular matrix protein 1 (ECM1). Supplemental analysis of inflammatory proteins and protective heat shock proteins (HSPs) were determined that included Interleukin-6 (IL6), tumor necrosis factor-alpha (TNFa), HSP90AA1 (HSP90) and HSPD1 (HSP60).

5. Statistics

Power was based on APCS protein changes reported to be different in obese PCOS [14] (nQuery version 9, Statsol, Boston, MA, USA). APCS: for an alpha of 0.05 with an effect size of 0.9 then a total of 40 subjects (20 per arm) would be needed for 80% power if these proteins were to be significantly different in PCOS. Visual inspection of the data was undertaken followed by Student's *t*-tests for normally distributed data and Mann-Whitney tests for non-normally distributed data as determined by the Kolmogorov-Smirnov Test. All analyses were performed using Graphpad Prism version 9.4.1 (San Diego, CA, USA).

6. Conclusions

PCOS patients who are non-obese and not insulin resistant show a lower AD-associated protein pattern risk profile that was no different to non-obese controls, indicating that lifestyle and interventional management to maintain optimal body weight may also be beneficial for the reduction of long-term risk for AD in PCOS.

Author Contributions: A.S.M.M. and A.E.B. analyzed the data and wrote the manuscript. T.S. supervised clinical studies and edited the manuscript. S.L.A. contributed to study design, data interpretation and the writing of the manuscript. A.E.B. is the guarantor of this work. All authors have read and agreed to the published version of the manuscript.

Funding: No funding was received to perform this study.

Institutional Review Board Statement: The study was conducted in accordance with the Declaration of Helsinki, and approved by The Humber NRES ethical committee, UK (approval number 0203043, 31 January 2014).

Informed Consent Statement: Informed consent was obtained from all subjects involved in the study.

Data Availability Statement: All the data for this study will be made available upon reasonable request to the corresponding author.

Conflicts of Interest: No authors have any conflict of interest or competing interests to declare.

References

1. Sathyapalan, T.; Atkin, S.L. Recent advances in cardiovascular aspects of polycystic ovary syndrome. *Eur. J. Endocrinol./Eur. Fed. Endocr. Soc.* **2012**, *166*, 575–583. [CrossRef]
2. Armanini, D.; Boscaro, M.; Bordin, L.; Sabbadin, C. Controversies in the Pathogenesis, Diagnosis and Treatment of PCOS: Focus on Insulin Resistance, Inflammation, and Hyperandrogenism. *Int. J. Mol. Sci.* **2022**, *23*, 4110. [CrossRef]
3. Brutocao, C.; Zaiem, F.; Alsawas, M.; Morrow, A.S.; Murad, M.H.; Javed, A. Psychiatric disorders in women with polycystic ovary syndrome: A systematic review and meta-analysis. *Endocrine* **2018**, *62*, 318–325. [CrossRef]
4. Prince, M.; Bryce, R.; Albanese, E.; Wimo, A.; Ribeiro, W.; Ferri, C.P. The global prevalence of dementia: A systematic review and metaanalysis. *Alzheimer's Dement.* **2013**, *9*, 63–75.e62. [CrossRef]
5. Alzheimer's Association. 2014 Alzheimer's disease facts and figures. *Alzheimer's Dement.* **2014**, *10*, e47–e92.
6. Picone, P.; Di Carlo, M.; Nuzzo, D. Obesity and Alzheimer's disease: Molecular bases. *Eur. J. Neurosci.* **2020**, *52*, 3944–3950. [CrossRef]
7. Sedzikowska, A.; Szablewski, L. Insulin and Insulin Resistance in Alzheimer's Disease. *Int. J. Mol. Sci.* **2021**, *22*, 9987. [CrossRef] [PubMed]
8. Talbot, K.; Wang, H.-Y.; Kazi, H.; Han, L.-Y.; Bakshi, K.P.; Stucky, A.; Fuino, R.L.; Kawaguchi, K.R.; Samoyedny, A.J.; Wilson, R.S.; et al. Demonstrated brain insulin resistance in Alzheimer's disease patients is associated with IGF-1 resistance, IRS-1 dysregulation, and cognitive decline. *J. Clin. Investig.* **2012**, *122*, 1316–1338. [CrossRef] [PubMed]
9. Ly, M.; Yu, G.Z.; Mian, A.; Cramer, A.; Meysami, S.; Merrill, D.A.; Samara, A.; Eisenstein, S.A.; Hershey, T.; Babulal, G.M.; et al. Neuroinflammation: A Modifiable Pathway Linking Obesity, Alzheimer's disease, and Depression. *Am. J. Geriatr. Psychiatry* **2023**, *31*, 853–866. [CrossRef] [PubMed]
10. Ott, A.; Stolk, R.P.; van Harskamp, F.; Pols, H.A.; Hofman, A.; Breteler, M.M. Diabetes mellitus and the risk of dementia: The Rotterdam Study. *Neurology* **1999**, *53*, 1937–1942. [CrossRef] [PubMed]
11. Sims-Robinson, C.; Kim, B.; Rosko, A.; Feldman, E.L. How does diabetes accelerate Alzheimer disease pathology? *Nat. Rev. Neurol.* **2010**, *6*, 551–559. [CrossRef]
12. Zilkens, R.R.; Davis, W.A.; Spilsbury, K.; Semmens, J.B.; Bruce, D.G. Earlier age of dementia onset and shorter survival times in dementia patients with diabetes. *Am. J. Epidemiol.* **2013**, *177*, 1246–1254. [CrossRef]
13. Moin, A.S.M.; Al-Qaissi, A.; Sathyapalan, T.; Atkin, S.L.; Butler, A.E. Hypoglycaemia in type 2 diabetes exacerbates amyloid-related proteins associated with dementia. *Diabetes Obes. Metab.* **2021**, *23*, 338–349. [CrossRef] [PubMed]
14. Butler, A.E.; Moin AS, M.; Sathyapalan, T.; Atkin, S.L. A Cross-Sectional Study of Alzheimer-Related Proteins in Women with Polycystic Ovary Syndrome. *Int. J. Mol. Sci.* **2024**, *25*, 1158. [CrossRef] [PubMed]
15. Kakoly, N.S.; Khomami, M.B.; Joham, A.E.; Cooray, S.D.; Misso, M.L.; Norman, R.J.; Harrison, C.L.; Ranasinha, S.; Teede, H.J.; Moran, L.J. Ethnicity, obesity and the prevalence of impaired glucose tolerance and type 2 diabetes in PCOS: A systematic review and meta-regression. *Hum. Reprod. Update* **2018**, *24*, 455–467. [CrossRef] [PubMed]
16. Sarahian, N.; Sarvazad, H.; Sajadi, E.; Rahnejat, N.; Eskandari Roozbahani, N. Investigation of common risk factors between polycystic ovary syndrome and Alzheimer's disease: A narrative review. *Reprod. Health* **2021**, *18*, 156. [CrossRef] [PubMed]
17. Barber, T.M.; Kyrou, I.; Randeva, H.S.; Weickert, M.O. Mechanisms of Insulin Resistance at the Crossroad of Obesity with Associated Metabolic Abnormalities and Cognitive Dysfunction. *Int. J. Mol. Sci.* **2021**, *22*, 546. [CrossRef] [PubMed]
18. Li, G.; Hu, J.; Zhang, S.; Fan, W.; Wen, L.; Wang, G.; Zhang, D. Changes in Resting-State Cerebral Activity in Women With Polycystic Ovary Syndrome: A Functional MR Imaging Study. *Front. Endocrinol.* **2020**, *11*, 603279. [CrossRef] [PubMed]
19. Lai, W.; Li, X.; Zhu, H.; Zhu, X.; Tan, H.; Feng, P.; Chen, L.; Luo, C. Plasma luteinizing hormone level affects the brain activity of patients with polycystic ovary syndrome. *Psychoneuroendocrinology* **2020**, *112*, 104535. [CrossRef]
20. Schattmann, L.; Sherwin, B.B. Testosterone levels and cognitive functioning in women with polycystic ovary syndrome and in healthy young women. *Horm. Behav.* **2007**, *51*, 587–596. [CrossRef]
21. Macut, D.; Bjekić-Macut, J.; Rahelić, D.; Doknić, M. Insulin and the polycystic ovary syndrome. *Diabetes Res. Clin. Pract.* **2017**, *130*, 163–170. [CrossRef]
22. Teunissen, C.; Del Campo, M.; Peeters, C.; Meeter, L.; Seelaar, H.; Koel-Simmelink, M.; Ramakers, I.; Middelkoop, H.; De Deyn, P.; Claessen, J. Blood-based protein biomarkers in definite frontotemporal dementia: A case-control study. 2022, *preprint*.
23. Nishiyama, E.; Iwamoto, N.; Kimura, M.; Arai, H. Serum amyloid P component level in Alzheimer's disease. *Dementia* **1996**, *7*, 256–259. [CrossRef]
24. Verwey, N.A.; Schuitemaker, A.; van der Flier, W.M.; Mulder, S.D.; Mulder, C.; Hack, C.E.; Scheltens, P.; Blankenstein, M.A.; Veerhuis, R. Serum amyloid p component as a biomarker in mild cognitive impairment and Alzheimer's disease. *Dement. Geriatr. Cogn. Disord.* **2008**, *26*, 522–527. [CrossRef]

25. Roberts, J.A.; Varma, V.R.; Candia, J.; Tanaka, T.; Ferrucci, L.; Bennett, D.A.; Thambisetty, M. Unbiased proteomics and multivariable regularized regression techniques identify SMOC1, NOG, APCS, and NTN1 in an Alzheimer's disease brain proteomic signature. *NPJ Aging* **2023**, *9*, 18. [CrossRef] [PubMed]
26. Baldacci, F.; Daniele, S.; Piccarducci, R.; Giampietri, L.; Pietrobono, D.; Giorgi, F.S.; Nicoletti, V.; Frosini, D.; Libertini, P.; Lo Gerfo, A.; et al. Potential Diagnostic Value of Red Blood Cells alpha-Synuclein Heteroaggregates in Alzheimer's Disease. *Mol. Neurobiol.* **2019**, *56*, 6451–6459. [CrossRef] [PubMed]
27. Yun, S.M.; Cho, S.J.; Jo, C.; Park, M.H.; Han, C.; Koh, Y.H. Elevation of plasma soluble amyloid precursor protein beta in Alzheimer's disease. *Arch. Gerontol. Geriatr.* **2020**, *87*, 103995. [CrossRef] [PubMed]
28. Bush, A.I.; Beyreuther, K.; Masters, C.L. Beta A4 amyloid protein and its precursor in Alzheimer's disease. *Pharmacol. Ther.* **1992**, *56*, 97–117. [CrossRef] [PubMed]
29. Sachdeva, G.; Gainder, S.; Suri, V.; Sachdeva, N.; Chopra, S. Comparison of the Different PCOS Phenotypes Based on Clinical Metabolic, and Hormonal Profile, and their Response to Clomiphene. *Indian J. Endocrinol. Metab.* **2019**, *23*, 326–331. [CrossRef] [PubMed]
30. Rahmani, F.; Wang, Q.; McKay, N.S.; Keefe, S.; Hantler, N.; Hornbeck, R.; Wang, Y.; Hassenstab, J.; Schindler, S.; Xiong, C.; et al. Sex-Specific Patterns of Body Mass Index Relationship with White Matter Connectivity. *J. Alzheimers Dis.* **2022**, *86*, 1831–1848. [CrossRef] [PubMed]
31. Pennings, N.; Jaber, J.; Ahiawodzi, P. Ten-year weight gain is associated with elevated fasting insulin levels and precedes glucose elevation. *Diabetes/Metab. Res. Rev.* **2018**, *34*, e2986. [CrossRef]
32. Akiyama, H.; Barger, S.; Barnum, S.; Bradt, B.; Bauer, J.; Cole, G.M.; Cooper, N.R.; Eikelenboom, P.; Emmerling, M.; Fiebich, B.L.; et al. Inflammation and Alzheimer's disease. *Neurobiol. Aging* **2000**, *21*, 383–421. [CrossRef] [PubMed]
33. Lee, S.; Tong, M.; Hang, S.; Deochand, C.; de la Monte, S. CSF and Brain Indices of Insulin Resistance, Oxidative Stress and Neuro-Inflammation in Early versus Late Alzheimer's Disease. *J. Alzheimers Dis. Park.* **2013**, *3*, 128. [CrossRef]
34. Marriott, R.J.; Murray, K.; Flicker, L.; Hankey, G.J.; Matsumoto, A.M.; Dwivedi, G.; Antonio, L.; Almeida, O.P.; Bhasin, S.; Dobs, A.S.; et al. Lower serum testosterone concentrations are associated with a higher incidence of dementia in men: The UK Biobank prospective cohort study. *Alzheimer's Dement.* **2022**, *18*, 1907–1918. [CrossRef] [PubMed]
35. Norman, R.J.; Teede, H.J. A new evidence-based guideline for assessment and management of polycystic ovary syndrome. *Med. J. Aust.* **2018**, *209*, 299–300. [CrossRef] [PubMed]
36. Kim, C.H.; Lee, S.H. Effectiveness of Lifestyle Modification in Polycystic Ovary Syndrome Patients with Obesity: A Systematic Review and Meta-Analysis. *Life* **2022**, *12*, 308. [CrossRef]
37. Ee, C.; Pirotta, S.; Mousa, A.; Moran, L.; Lim, S. Providing lifestyle advice to women with PCOS: An overview of practical issues affecting success. *BMC Endocr. Disord.* **2021**, *21*, 234. [CrossRef] [PubMed]
38. Hu, L.; Ma, L.; Xia, X.; Ying, T.; Zhou, M.; Zou, S.; Yu, H.; Yin, J. Efficacy of Bariatric Surgery in the Treatment of Women With Obesity and Polycystic Ovary Syndrome. *J. Clin. Endocrinol. Metab.* **2022**, *107*, e3217–e3229. [CrossRef]
39. Cunningham, T.K.; Allgar, V.; Dargham, S.R.; Kilpatrick, E.; Sathyapalan, T.; Maguiness, S.; Mokhtar Rudin, H.R.; Abdul Ghani, N.M.; Latiff, A.; Atkin, S.L. Association of Vitamin D Metabolites With Embryo Development and Fertilization in Women With and Without PCOS Undergoing Subfertility Treatment. *Front. Endocrinol.* **2019**, *10*, 13. [CrossRef]
40. Revised 2003 consensus on diagnostic criteria and long-term health risks related to polycystic ovary syndrome (PCOS). *Hum. Reprod.* **2004**, *19*, 41–47. [CrossRef]
41. Legro, R.S.; Arslanian, S.A.; Ehrmann, D.A.; Hoeger, K.M.; Murad, M.H.; Pasquali, R.; Welt, C.K. Diagnosis and Treatment of Polycystic Ovary Syndrome: An Endocrine Society Clinical Practice Guideline. *J. Clin. Endocrinol. Metab.* **2013**, *98*, 4565–4592. [CrossRef]
42. World Health Organization. *Waist Circumference and Waist–Hip Ratio. Report of a WHO Expert Consultation, Geneva*; World Health Organization: Geneva, Switzerland, 2008.
43. Kahal, H.; Halama, A.; Aburima, A.; Bhagwat, A.M.; Butler, A.E.; Graumann, J.; Suhre, K.; Sathyapalan, T.; Atkin, S.L. Effect of induced hypoglycemia on inflammation and oxidative stress in type 2 diabetes and control subjects. *Sci. Rep.* **2020**, *10*, 4750. [CrossRef] [PubMed]
44. Kraemer, S.; Vaught, J.D.; Bock, C.; Gold, L.; Katilius, E.; Keeney, T.R.; Kim, N.; Saccomano, N.A.; Wilcox, S.K.; Zichi, D.; et al. From SOMAmer-based biomarker discovery to diagnostic and clinical applications: A SOMAmer-based, streamlined multiplex proteomic assay. *PLoS ONE* **2011**, *6*, e26332. [CrossRef] [PubMed]
45. Gold, L.; Ayers, D.; Bertino, J.; Bock, C.; Bock, A.; Brody, E.N.; Carter, J.; Dalby, A.B.; Eaton, B.E.; Fitzwater, T.; et al. Aptamer-based multiplexed proteomic technology for biomarker discovery. *PLoS ONE* **2010**, *5*, e15004. [CrossRef] [PubMed]
46. Suhre, K.; Arnold, M.; Bhagwat, A.M.; Cotton, R.J.; Engelke, R.; Raffler, J.; Sarwath, H.; Thareja, G.; Wahl, A.; DeLisle, R.K.; et al. Connecting genetic risk to disease end points through the human blood plasma proteome. *Nat. Commun.* **2017**, *8*, 14357. [CrossRef]

International Journal of
Molecular Sciences

MDPI

Review

The Bidirectional Interplay of α-Synuclein with Lipids in the Central Nervous System and Its Implications for the Pathogenesis of Parkinson's Disease

Kristina Battis, Wei Xiang and Jürgen Winkler *

Department of Molecular Neurology, University Hospital Erlangen, Friedrich-Alexander-University Erlangen-Nürnberg, 91054 Erlangen, Germany; kristina.battis@uk-erlangen.de (K.B.); wei.xiang@uk-erlangen.de (W.X.)
* Correspondence: juergen.winkler@uk-erlangen.de

Abstract: The alteration and aggregation of alpha-synuclein (α-syn) play a crucial role in neurodegenerative diseases collectively termed as synucleinopathies, including Parkinson's disease (PD). The bidirectional interaction of α-syn with lipids and biomembranes impacts not only α-syn aggregation but also lipid homeostasis. Indeed, lipid composition and metabolism are severely perturbed in PD. One explanation for lipid-associated alterations may involve structural changes in α-syn, caused, for example, by missense mutations in the lipid-binding region of α-syn as well as post-translational modifications such as phosphorylation, acetylation, nitration, ubiquitination, truncation, glycosylation, and glycation. Notably, different strategies targeting the α-syn-lipid interaction have been identified and are able to reduce α-syn pathology. These approaches include the modulation of post-translational modifications aiming to reduce the aggregation of α-syn and modify its binding properties to lipid membranes. Furthermore, targeting enzymes involved in various steps of lipid metabolism and exploring the neuroprotective potential of lipids themselves have emerged as novel therapeutic approaches. Taken together, this review focuses on the bidirectional crosstalk of α-syn and lipids and how alterations of this interaction affect PD and thereby open a window for therapeutic interventions.

Keywords: α-synuclein; lipids; Parkinson's disease; post-translational modification

Citation: Battis, K.; Xiang, W.; Winkler, J. The Bidirectional Interplay of α-Synuclein with Lipids in the Central Nervous System and Its Implications for the Pathogenesis of Parkinson's Disease. *Int. J. Mol. Sci.* **2023**, *24*, 13270. https://doi.org/10.3390/ijms241713270

Academic Editor: Claudia Ricci

Received: 31 July 2023
Revised: 23 August 2023
Accepted: 24 August 2023
Published: 26 August 2023

1. Introduction

Alpha-synuclein (α-syn) is a small 14-kDa protein first discovered by Maroteaux and colleagues in 1988 [1]. In the central nervous system (CNS), α-syn is expressed abundantly in neurons [2], while it is also present in the peripheral nervous system (PNS), gut, muscle, liver, heart, lungs, kidney, and blood cells [3,4]. Since α-syn is enriched in presynaptic terminals and associated with synaptic vesicles, a large number of studies indicates the important role of α-syn in neurotransmission and synaptic plasticity [5–7]. In addition, α-syn plays a role in transcriptional regulation of dopamine synthesis [8]. Diverse physiological forms of α-syn have been reported: the protein may exist as unstructured monomer [9,10], α-helical monomer or multimer [11,12] that interacts with biological membranes [13]. Pathological alterations in the α-syn structure are predominantly linked to its abnormal aggregation from monomers to oligomeric or fibrillar species [11,14] showing varying degrees of assembly, solubility, and pathogenicity [15]. Neurotoxic effects of aggregated α-syn are multifaceted. For example, addition of α-syn oligomers to primary neurons in culture induces reactive oxygen species, increases cytosolic calcium, disrupts membranes, and thus leads to cell death [15,16]. Furthermore, exposure of neurons to fibrillar forms of α-syn induces prion-like propagation of α-syn aggregation, resulting in the formation of inclusions that are morphologically and biochemically similar to those detected in diseased brains [17,18]. Diseases associated with α-syn aggregation are collectively

termed synucleinopathies, consisting of Parkinson's disease (PD), multiple system atrophy (MSA), and Lewy body disease [19].

PD is the most prevalent neurodegenerative movement disorder and is clinically characterized by motor deficits such as bradykinesia, rigidity, and resting tremor [20,21]. The neuropathological hallmarks of PD are the formation of Lewy bodies or Lewy neurites containing aggregated α-syn accompanied with a substantial loss of dopaminergic neurons in the substantia nigra [22,23]. The involvement of α-syn in dopaminergic neuronal cell death was suggested after the identification of the first missense mutations (A30P, E46K, and A53T) in the α-syn encoding gene, *SNCA*, linked to monogenic PD phenotypes [22,24,25]. The primary structure of α-syn is composed of three well-described domains that determine its biological functions: the N-terminal amphipathic region [26,27], responsible for lipid binding [27]; the central hydrophobic non-amyloid-β component (NAC) region [28], important for aggregation of the protein [29,30] as well as axonal transport [31]; and the acidic C-terminal domain [32], decisive for protein interactions [33] and oligomerization of the protein [34] (Figure 1). Interestingly, all missense mutations linked so far to familial forms of PD (e.g., A30P, E46K, H50Q, G51D, A53E, and A53T) reside in the lipid-interacting N-terminal domain of α-syn [22,24,25,35] (Figure 1). Thus, these mutations may represent a functional "hot spot" resulting in a detrimental impact on the lipid-binding properties of α-syn and its physiological function. Moreover, α-syn conformation and aggregation propensity may be consequently changed after exposure to distinct lipid classes [36].

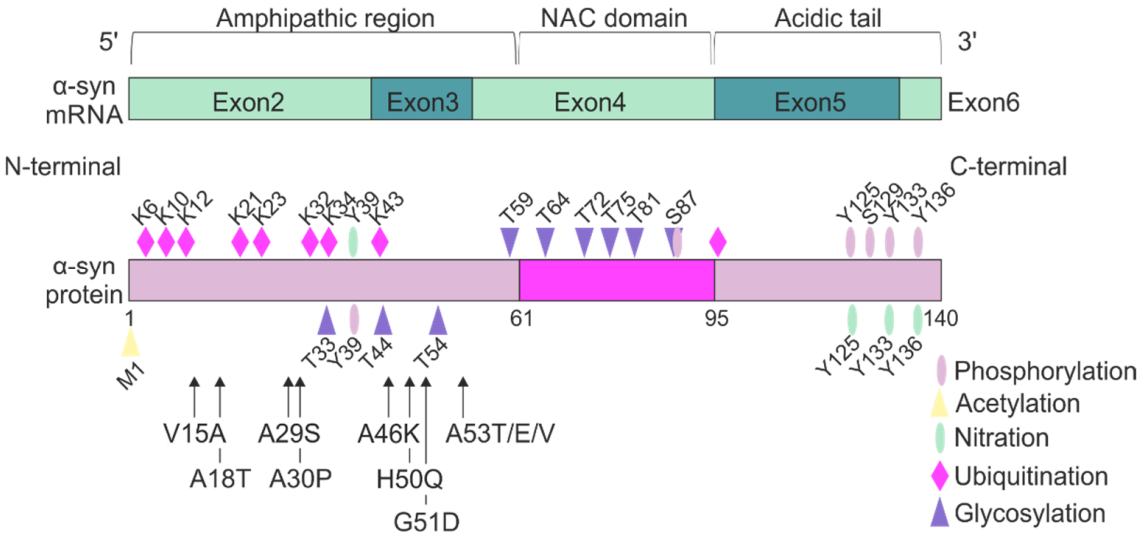

Figure 1. Structure of alpha-synuclein (α-syn). α-syn is encoded by the *SNCA* gene. This gene is transcribed into mRNA consisting of five exons. Following translation, the protein consists of distinct domains: the amphipathic region at the N-terminus, the non-amyloid-β component (NAC) domain, and the C-terminal acidic tail. Moreover, α-syn undergoes a variety of post-translational modifications (PTMs), including phosphorylation, acetylation, nitration, ubiquitination, truncation, glycosylation, and glycation. Monogenic PD-associated point mutations are indicated with arrows and are exclusively present in the N-terminal amphipathic region.

Lipids play an essential role in the CNS. Besides ensuring compartmentalization of cells and organelles through the formation of lipid-rich membranes, lipids act as bioactive signaling molecules [37]. Furthermore, they participate in mitochondrial metabolism [37]. In the CNS, lipids are predominantly metabolized in neurons and astrocytes [37]. However, lipids are one of the main components of myelin sheaths generated by oligodendrocytes and thus present a major player in lipid metabolism as well [38]. Furthermore, there is a physiological interaction of α-syn with different lipid classes, especially biomembranes, [27,39,40] and lipids are dysregulated in PD [41]. Since current therapeutic approaches for PD predominantly restore dopaminergic tone to control motor symptoms, though without

altering disease progression, interfering with the interaction between α-syn and lipids offers potential avenues for therapeutic strategies in PD [42].

Thus, this review focuses on two key aspects related to the reciprocal interplay between α-syn and lipids: (1) changes in lipid composition or metabolism that may impact the biochemical dynamic of α-syn aggregation and (2) alterations in the α-syn structure due to mutations or post-translational modifications (PTMs) that could influence its interaction with lipids. The final goal of this review is to elucidate this bidirectional crosstalk and how this may drive the pathological events in PD, thus offering novel targets for therapeutic interventions.

2. Lipids and Lipid Metabolism

The four major classes of biomolecules in a mammalian cell are carbohydrates, proteins, nucleic acids, and lipids [43]. The latter are an essential component of the brain. Indeed, the brain has the second highest lipid content after adipose tissue in the human body, accounting 50% of the brain's dry weight [44]. In contrast to adipose tissue, where fatty acids (FAs) are predominantly stored as triglycerides (TAG) for energy storage, the brain primarily utilizes lipids as structural components for membranes [44]. Regular biomembranes typically have a lipid:protein ratio of about 50%:50%. However, in the case of myelination in oligodendrocytes, lipids play a particularly crucial role, as myelin is characterized by an exceptionally high proportion of lipids, with a lipid:protein ratio of 70–85%:15–30% [45]. In general, lipids fulfill a broad range of roles throughout the body such as energy supply, membrane components, and precursors of vitamins and hormones. Moreover, they contribute to blood coagulation and to immune responses [46]. Lipids are taken up by nutrition or are synthesized de novo. Multiple different neural cells are able to produce its own lipids. In this review, we focus on the four major types of lipids: sterols, (including cholesterol), FAs, sphingolipids, and glycerophospholipids (Figure 2). Other lipid classes such as saccharolipids, polyketides, and prenol lipids have been reviewed elsewhere [47].

2.1. Lipid Metabolism in the Brain

All lipids except sterols, such as cholesterol, are generated from FAs [48]. While FAs pass across the blood–brain barrier [49], the entry of cholesterol into the brain is largely restricted [50]. Thus, there is a crucial need for cholesterol synthesis within the CNS [51]. In general, cholesterol can be synthesized de novo by all cells in the brain [52]. However, the neural cell type primarily responsible for cholesterol synthesis shifts from development to adulthood (Figure 3). During embryogenesis, neurons are the primary producers of cholesterol. However, during postnatal myelination, the production site shifts to oligodendrocytes, and later in adulthood, it primarily transitions to astrocytes [51,52]. Astrocytes are considered the major neural cells taking over lipid production in the brain not only of cholesterol, but also of diacylglycerol (DAG) and triacylglycerol (TAG) [53]. Thus, in the adult brain, neurons and oligodendrocytes mainly take up lipids derived from astrocytes to support synaptic function [54] and myelination [53,55]. A simplified overview of lipid metabolism in the brain is depicted in Figure 3.

2.1.1. Cholesterol

The de novo cholesterol synthesis pathway is based on the acetyl-CoA pool that is converted to cholesterol in a multistep mechanism primarily in the endoplasmatic reticulum (ER) (Figure 2). The transport of cholesterol from astrocytes to neurons and oligodendrocytes is facilitated by apolipoprotein E (ApoE), also produced by astrocytes themselves [56]. Bound to ApoE, cholesterol is exported by ATP-binding cassette (ABCA1) transporters [57]. The cholesterol-ApoE complex is consequently endocytosed by low-density lipoprotein receptors (LDLR) expressed by neurons [58,59] and oligodendrocytes [60] (Figure 3). Within oligodendrocytes, cholesterol associates with the proteolipid protein (PLP) and is integrated into the myelin sheath during myelination [61,62].

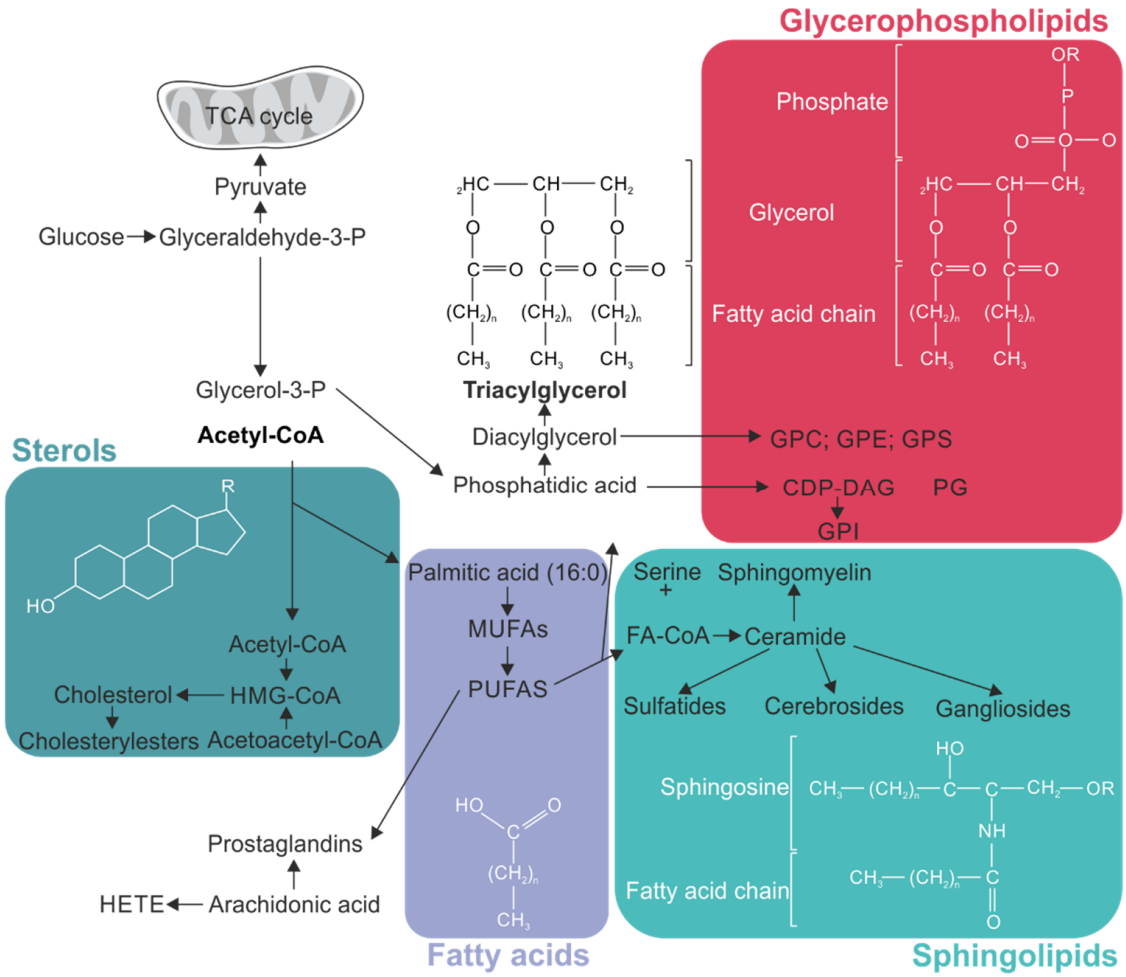

Figure 2. Overview of different lipid classes and their synthesis pathways. The major classes of lipids (sterols, fatty acids (FAs), sphingolipids, and glycerophospholipids) important for this review are depicted with their chemical structure and the key steps of their synthesis pathway. Eicosanoids, such as arachidonic acid, are classified as a type of FAs. CDP = cytidine diphosphate; CoA = Coenzyme A; GPC = glycerophosphocholine; GPE = glycerophosphoethanolamine; GPS = glycerophosphoserine; HETE = hydroxyeicosatetraenoic acids; HMG = β-hydroxy-β-methylglutaryl; MUFAs = monounsaturated fatty acids; P = phosphate; PUFAs = polyunsaturated fatty acids; TCA = tricarboxylic acid.

2.1.2. Fatty Acids

FAs are essential for various components of cell membranes and myelin, as well as for providing energy. Although FAs are able to cross the blood–brain barrier and pass through cellular membranes, neurons, oligodendrocytes, and astrocytes are able to synthesize the majority of required saturated and monounsaturated fatty acids (MUFAs) by themselves (reviewed by [63]). However, the brain and other organs severely lack the ability to produce polyunsaturated fatty acids (PUFAs) [64]. Thus, PUFAs need to be taken up by the diet [65]. FA synthesis takes place in the cytoplasm and the ER [66]. Besides serving as basis for the synthesis of complex lipids, FAs are stored as energy-rich TAGs in lipid droplets. Astrocytes are the most prominent cell type responsible for producing lipid droplets in the adult brain. However, neurons and oligodendrocytes also generate lipid droplets (as reviewed in [67]). Lipid droplets serve two important purposes: first, they help sequester free cytosolic FAs which, in the absence of lipid droplets, can be toxic to cellular structures like mitochondria by disrupting their membranes (reviewed by [68]); second, lipid droplets facilitate the transport of FAs into mitochondria, providing an essential energy supply during starvation and enabling β-oxidation [69,70]. In the brain, β-oxidation, the process

of degrading FAs, is primarily observed in astrocytes, and it is also present in neurons and oligodendrocytes [71].

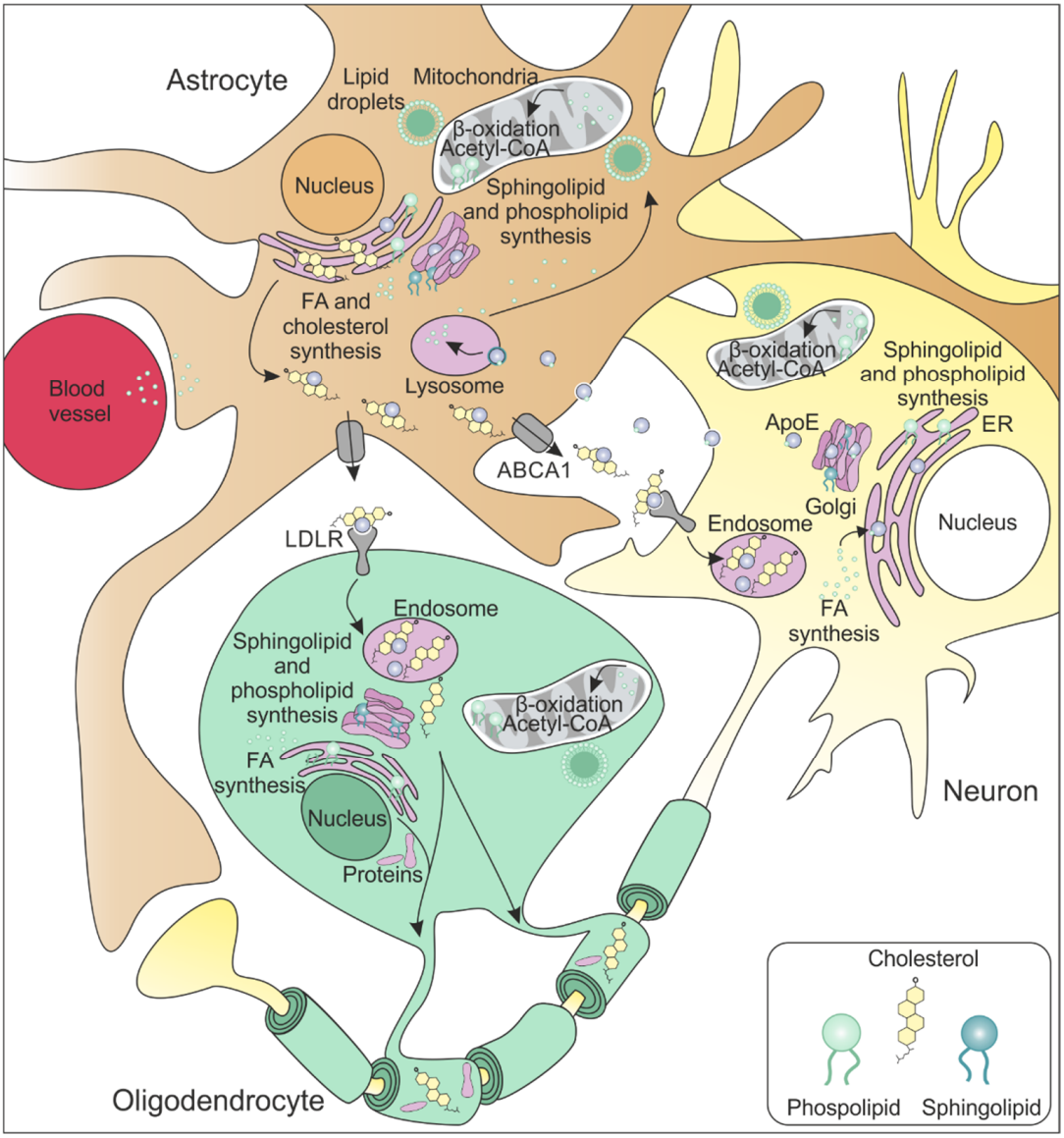

Figure 3. Lipid metabolism in the adult brain. All lipids are produced based on two main components: cholesterol and FAs. Cholesterol is synthesized primarily at the ER of astrocytes and is further transported to neurons and oligodendrocytes via ApoE and ABCA1 transporters. FAs, however, are produced by neurons, astrocytes, and oligodendrocytes. Additionally, FAs also bind to ApoE for their transport. FAs are used as a fuel source in β-oxidation predominantly by astrocytes, but also by neurons and oligodendrocytes. Alternatively, all neural cell types contain lipid droplets for storage. Finally, all cells are able to produce phospholipids and sphingolipids within the ER. ABCA1 = ATP-binding cassette transporter A1; ApoE = apolipoprotein E; ER = endoplasmatic reticulum; LDLR = low-density lipoprotein receptor.

2.1.3. Sphingolipids

Sphingolipids, including glycolipids such as gangliosides, cerebrosides, and sulfatides, require FAs for their production, particularly ceramide, which is subsequently incorporated into various complex sphingolipids, predominantly in the Golgi (reviewed by [72]).

2.1.4. Phospholipids

Phospholipids, the main component of biological membranes, are produced by all the major neural cells in the brain using FAs as biochemical building blocks. The synthesis of all classes of phospholipids takes place in the ER and is initiated by two common precursors: phosphatidic acid (PA) and DAG (reviewed by [73]).

3. α-syn and Lipids

α-syn was originally discovered in the nucleus and the presynaptic terminals [1], where it is involved in neurotransmission and synaptic plasticity [74]. Immediately after the discovery of α-syn within Lewy bodies [75], the lipid-binding properties of α-syn were described in numerous studies where α-syn was found to associate with synaptic membranes [76]. It displays a preference for binding to negatively charged head groups of anionic lipids. This interaction is mediated by the amphipathic N-terminal region of α-syn, which is rich in lysine residues [77]. Additionally, α-syn exhibits a specific affinity to the phospholipids phosphatidylethanolamine (PE), PA, phosphatidylinositol (PI), and ganglioside due to their acidic head groups, rather than to phosphatidylserine (PS) or phosphatidylglycerol (PG) [78–81]. Moreover, α-syn contains a cholesterol-binding site (residues 67–78) [82] as well as one for glycosphingolipids (residues 34–45) [83]. It also interacts with membranes, including myelin, with a preferential interaction with membranes containing unsaturated FAs [84]. Further, α-syn preferably binds to lipid raft domains of membranes [85]. Intracellularly, α-syn also associates with mitochondrial membranes [86], although the physiological role of this interaction is still unclear.

After α-syn is bound to a membrane, it forms an α-helical structure. Membrane binding of monomeric α-syn is mediated by two steps: (1) anchoring to the membrane with the N-terminal residues 3–25, and (2) a coil-to-helix transition of residues 26–97 that are responsible for the lipid binding and act as membrane sensors [87–89]. Physiologically, binding of α-syn to membranes and the consecutive formation of an α-helical structure are important for soluble N-ethylmaleimide-sensitive-factor attachment receptor (SNARE)-complex assembly [14,90].

The interaction of α-syn monomers with membranes was investigated extensively; however, binding of α-syn multimers to membranes remains elusive. While monomer binding to the membrane leads to the formation of an α-helical structure, multimers do not change their secondary structure upon membrane binding [16,91]. Moreover, different α-syn multimers species with distinct structures and membrane interaction properties exist [16,92]. Nevertheless, similar to monomeric α-syn, multimers prefer binding to lipids having acidic, negatively charged head groups [78,93] and lipid raft domains of membranes [78].

There are different mechanisms underlying the interaction of α-syn and lipids in PD, which will be further elaborated in this review: (1) multiple alterations in lipid classes and metabolism have been observed in PD patients and PD models affecting the aggregation propensity of α-syn; (2) missense mutations of α-syn identified so far in familial monogenic PD are localized at the *N*-terminus, where lipid binding takes place, and indeed change its lipid-binding properties; and (3) PTMs of α-syn change its binding properties toward different forms of lipids.

3.1. Alterations of Lipids and Their Metabolism in PD

PD is frequently characterized as a proteinopathy; however, emerging evidence suggests that it might be described as a lipidopathy, or most likely as a combination of both (reviewed by Fanning and colleagues [94]). An analysis of three genome-wide association studies (GWAS) revealed four main biological processes relevant for PD—oxidative stress response, endosomal-lysosomal functioning, ER stress response, and immune response activation [95]. Interestingly, lipids and lipoproteins are key to all four processes [95]. Furthermore, α-syn is involved in several lipid metabolic pathways, including FA [96–98], TAG [99], and cholesterol metabolism [100]. Indeed, alterations in lipid metabolism have

been found throughout different metabolic pathways, including FA [101,102], cholesterol [103,104], sphingolipid [105,106], and glycerophospholipid metabolism [102].

3.1.1. FA Metabolism

Recently, it was demonstrated that α-syn overexpression in yeast-, rodent-, and induced pluripotent stem cell (iPSC)-derived neurons increased the formation of MUFAs, specifically oleic acid, which subsequently enhanced α-syn toxicity by altering the equilibrium of the membrane bound to soluble α-syn [107]. Coincidentally, neuronal and plasma levels of PUFAS are increased in PD patients [108,109]. Along this line, α-syn oligomerization is regulated by PUFA levels [110]. Especially docosahexaenoic acid (DHA) and α-linolenic acid (ALA) are able to bind α-syn and elevate its aggregation at low ratios, while reducing the aggregation at high ratios.

3.1.2. Cholesterol Metabolism

Several oxysterols are increased in PD brains [111], and, importantly, cholesterol accumulates in lysosomes of glucocerebrosidase (*GBA*)-PD patients [112]. *GBA* mutations are associated with monogenic PD. Moreover, an increased brain cholesterol level was detected in methyl-4-phenyl-1,2,3,6-tetrahydropyridine (MPTP) mice, which is a neurotoxin-induced PD model, exacerbating dopaminergic loss in the striatum and substantia nigra. Furthermore, a high-cholesterol diet alleviated motor functions in the animals [113]. Similarly, high cholesterol levels in SH-SY5Y-differentiated neurons led to decreased dopaminergic neuronal survival [114]. Thus, selectively targeting cholesterol synthesis in the CNS might be a promising therapeutic approach.

3.1.3. Sphingolipid Metabolism

Notably, several enzymes involved in sphingolipid metabolism are associated with PD. Emerging evidence implies that distinct variants within the genes for *GBA* [115] and serine palmitoyltransferase (*SPTLC1*) [116] are important risk factors for developing PD. Moreover, sphingolipids can associate with cholesterol to form lipid rafts involved in signal transduction and membrane trafficking [117], while sphingolipid metabolites such as ceramides and sphingosine-1-phosphate play important roles in cell proliferation, differentiation and apoptosis [118,119]. Thus, pharmaceutical intervention in the sphingolipid metabolic pathway might be useful for intervening in pathological processes in PD.

3.1.4. Glycerophospholipid Metabolism

Farmer and colleagues observed that 17 glycerophosphocholine and lysophosphatidylcholine species were significantly reduced in the substantia nigra of 6-hydroxydopamine (6-OHDA)-lesioned PD mice using high-performance liquid chromatography coupled with mass spectrometry [120]. Specifically, the lysophosphatidylcholine species (16:0/0:0) and (18:1/0:0) were increased in this mouse model, which were also found to be increased in human fibroblasts deficient in *PARKIN*, being a risk factor for monogenic PD [121]. Both lysophosphatidylcholine species contribute to inflammatory signaling in the pathogenesis of PD [122]. Moreover, the *PARKIN*-mutant fibroblasts exhibit higher levels of glycerophosphoserine, glycerophosphoinositol, and gangliosides GM2 and GM3 [121]. Elevated levels of glycerophosphoinositol and glycerophosphoserine may cause defects in mitochondrial turnover [121]. Additionally, PE was found to be reduced in the substantia nigra and midbrain of PD patients [123,124]. In yeast cells, PE deficiency has been linked to the disturbance of α-syn homeostasis, highlighting a potential functional role in the pathology of PD [125]. To produce glycerophospholipids, DAGs are needed. Moreover, DAG is able to act as second messenger in nuclear lipid signaling. Using liquid chromatography–mass spectrometry, Wood and colleagues identified increased levels of DAGs, with both monounsaturated and polyunsaturated hydrocarbon chains, in the frontal cortex of PD patients correlating with the severity of neuropathology [126]. Moreover, they observed a significant decrease in the levels of PA 16:0 in PD patients [126].

3.2. Effects of Missense Mutations on the Binding Capacity of α-syn to Lipids

While membrane binding of α-syn may be important for its physiological function, abnormal alterations of α-syn such as overexpression, aggregation, or mutation may have pathological effects upon membrane binding. For example, association of abnormal α-syn with mitochondrial membranes has detrimental effects [127,128]. In dopaminergic and primary neurons overexpressing α-syn, mitochondrial impairment associated with an increase in oxidative stress and reduced cell viability was observed [128,129]. Typically, α-syn binds to membranes with its first 25 amino acid residues at the N-terminus when the lipid-to-protein ratio is high. However, a reduction in the lipid-to-protein ratio causes α-syn to interact with the membrane by binding with the first 97 amino acid residues [130]. Thus, the N-terminal domain of the α-syn gene, where missense mutations identified so far in familial PD have been found, is of special interest.

Missense mutations within the N-terminal region of the *SNCA* gene have detrimental effects on the binding capacity of α-syn to lipids. Here, we present a summary of the impact of point mutations in the *SNCA* gene (V15A, A18T, A29S, A30P, E46K, H50Q, G51D, A53E, A53T, A53V) associated with monogenic PD, focusing on their effects on α-syn aggregation and, in particular, their interaction with lipids (Table 1). The effect of the mutations on the aggregation of α-syn is reviewed more comprehensively elsewhere [131].

Table 1. Summary of PD-related point mutations of α-syn and their effects on its binding capacity to membranes.

Mutation	Effects on Lipid Membranes	Ref.
V15A	• decreased affinity to phospholipids accompanied by an increased aggregation and seeding activity	[132]
A18T	• less toxic than wildtype α-syn • altered triglycerides reduce α-syn toxicity	[133]
A29S	• less toxic than wildtype α-syn • altered triglycerides decrease α-syn toxicity • enhanced acetylation or SUMOylation are protective against α-syn toxicity	[133]
A30P	• reduced binding to membranes • formation of metal ion-induced pathologic oligomers was increased • fibril formation is slower in A30P mutants compared to wildtype • interaction of α-syn with lipid rafts is hindered	[85,134–136]
E46K	• increased lipid interactions and disrupted membrane selectivity • increased N-to-C interactions and coil compactness in the structure of lipid-unbound α-syn • conformation of α-syn is altered upon interaction with a curved lipid bilayer	[137,138]
H50Q	• enhances α-syn aggregation and toxicity without affecting the binding capacity to lipid membranes	[139]
G51D	• decreased binding to lipid membrane • fibril formation was accelerated	[136]
A53E	• α-syn exhibits a low lipid binding capacity compared to wildtype	[140]

Table 1. *Cont.*

Mutation	Effects on Lipid Membranes	Ref.
A53T	• does not change the binding capacity of α-syn to membranes • formation of metal ion-induced pathologic oligomers and fibril formation are increased • α-syn monomers cause membrane thinning and facilitate the interaction with artificial lipid rafts • iron-mediated oligomers do not impair the membrane, but facilitate the interaction with artificial lipid rafts • no effect on the interaction of α-syn with lipid rafts	[85,136,141,142]
A53V	• low binding affinity to membranes compared to wildtype • less toxic than wildtype α-syn • altered triglycerides reduce α-syn toxicity • enhanced acetylation or SUMOylation are protective against α-syn toxicity	[133,140]

A recently discovered V15A mutation led to alterations in the binding capacity of α-syn to lipids in vitro [132]. V15A-mutated α-syn showed a decreased affinity to phospholipids accompanied by an increased aggregation property and seeding activity compared to wildtype α-syn [132].

A18T and A29S are less toxic than wildtype α-syn in yeast [133]. Moreover, yeast strains with altered triglycerides reduce α-syn toxicity in both variants [133].

A reduced binding to membrane lipids was observed in the A30P variant in vitro [134] and in vivo [135]. Fibril formation was slower compared to wildtype α-syn in the A30P variant [136]. Interestingly, lipid raft association is required for the synaptic localization of α-syn, and the interaction of α-syn with lipid rafts is hindered by the A30P mutation [85].

It is additionally noteworthy that alterations at the N-terminal glutamate residues appear to exert a significant influence on the interaction between α-syn and lipids. Several studies have demonstrated that three glutamate-to-lysine mutations, namely, the pathogenic mutation E46K and two additional artificial mutations, E35K and E61K, in different combinations ("1K": E46K; "2K": E35K, E46K; and "3K": E35K, E46K, E61K) enhance lipid interactions and disrupt membrane selectivity [137,138]. In these studies, the lipid-binding and lipid-remodeling abilities of "3K" were characterized. Nuber and colleagues first observed that E46K mutants increase N-to-C interactions and coil compactness in the structure of the lipid-unbound protein. Moreover, the conformation of α-syn was also affected upon interaction with a curved lipid bilayer in the E46K-like mutants. Interestingly, glutamate-to-lysine mutations mildly increased the affinity for curved membranes and caused a progressive loss of curvature selectivity [137].

The H50Q mutation enhances α-syn aggregation and toxicity without affecting the binding capacity to membranes in vitro [139,143].

In the G51D variant, a reduced binding to membrane lipids was detected in vitro [134] and in vivo [135]. Furthermore, the formation of metal ion-induced pathologic oligomers was increased, and fibril formation was accelerated in this variant [136].

While fibril formation was increased in the A53T variant [136], the binding capacity of α-syn to membranes was not changed [141]. Perissinotto and colleagues analyzed the interaction of A53T α-syn specifically with artificial lipid bilayers mimicking lipid rafts [142]. They demonstrated that distinct monomeric and multimeric α-syn species interact differently with the artificial lipid rafts. The α-syn monomers caused membrane thinning, while iron-mediated oligomers did not impair the membrane. In both aggregation states, the A53T variant facilitated the interaction with membrane lipids [142].

Furthermore, recent studies have shed light on a potential impact of α-syn mutation on retromer-mediated endosomal trafficking. The proposition arises from the identification of mutations in the retromer gene VPS35, known to cause late-onset PD [144]. Retromer is a multi-subunit protein complex coating the cytosolic site of early endosomes, and it plays a pivotal role in endosomal trafficking and sorting [145]. Notably, a recent yeast model study provided mechanistic insights by revealing that the A53T α-syn mutation specifically reduces retromer-mediated trafficking of the conserved membrane-bound proprotein convertase Kex 2 [146]. This disruption might be caused by alterations in the binding ability of the A53T α-syn to the anionic phospholipid phosphatidylinositol 3′-phosphate (PI3P) in the endosomal membrane [146].

Surface plasmon resonance spectroscopy suggests that the A53V and A53E variants exhibit a low binding affinity to membranes compared to wildtype [140]. This low membrane binding capacity may be due to the nonpolar nature of valine which does not interact with the negatively charged membrane surface [140].

3.3. Binding Capacity of Posttranslational Modified α-syn to Lipids

Numerous studies have demonstrated that the interaction between α-syn and membranes is modified by PTMs. Despite its small size, α-syn undergoes a variety of PTMs including phosphorylation, acetylation, nitration, ubiquitination, truncation, glycosylation, and glycation (reviewed by [147]) (Figure 1). PTMs regulate the physiological function of α-syn but may also be linked to the pathogenic potential of the protein. Specifically, PTMs significantly influence the structure and aggregation propensity of α-syn as well as its interactions with lipids. The effects of PTMs on protein aggregation and toxicity have been extensively reviewed elsewhere [148–151]. Here, we in particular address the impact of PTMs on α-syn-lipid interactions. An overview of the detailed effects of PTMs on α-syn-lipid interactions is depicted in Table 2.

Table 2. Summary of PD-related point mutations of α-syn and their effects on its binding to membranes.

PTM	Position	Effects on Membranes	Ref.
Phosphorylation	Y39	• diminished lipid binding of α-syn and increased axonal pathology in transgenic PD mice	[152]
	S87	• conformational change in membrane-bound α-syn • decreased affinity to lipid vesicles • reduced aggregation of α-syn	[153]
	S129	• reduced binding of α-syn monomers and Fe^{3+}-induced oligomers to lipid vesicles • fewer α-helical structures, decreased binding, and disruption of lipid vesicles • no difference in membrane binding to synaptosomes • in the A30P variant, α-syn membrane binding was increased, leading to disruption of membranes • in the A53T variant, binding to membranes was reduced	[154–156]

Table 2. *Cont.*

PTM	Position	Effects on Membranes	Ref.
Acetylation	M1	• increased affinity of α-syn to membrane binding without structural alterations	[157]
Nitration	Y39	• less α-helical structure formation upon lipid vesicle binding • disrupted binding affinity of α-syn to membranes	[158]
	Y125	• less α-helical structure formation upon lipid vesicle binding • disrupted binding affinity of α-syn to membranes	
	Y133, Y136	• disrupted binding affinity of α-syn to lipid vesicles	
Ubiquitination	K6, K23, K43, K96	• no alterations in secondary structure of α-syn upon lipid binding	[159,160]
Truncation	1–100	• less potential inducing curvature upon membrane binding compared to full-length protein	[161]
	1–103	• produces mature fibrils in the presence of phospholipid vesicles	[162]
	1–115	• upon lipid binding, 1–115 truncated α-syn shows higher α-helical levels compared to full-length α-syn facilitating lipid binding	[163]
	1–119	• aggregates faster than full-length α-syn in the presence of phospholipid vesicles	[162]
	1–120	• reduced α-syn fibrillation and increased lipid binding predisposition upon methylphenidate treatment	[164]
	1–121	• similar aggregation to full-length α-syn in the presence of phospholipid vesicles • decreased ability to distort phospholipid membranes • higher toxicity compared to full-length α-syn	[165]

Table 2. *Cont.*

PTM	Position	Effects on Membranes	Ref.
Glycosylation	T72	• reduction in fibril formation, aggregation, and toxicity of monomeric α-syn in vitro, while binding affinity to lipid vesicles was unaltered	[166]
	T75	• reduction in fibril formation, aggregation, and toxicity of monomeric α-syn in vitro, while binding affinity to lipid vesicles was unaltered	
	T81	• reduction in fibril formation, aggregation, and toxicity of monomeric α-syn in vitro, while binding affinity to lipid vesicles was unaltered	
	S87	• reduction in fibril formation, aggregation, and toxicity of monomeric α-syn in vitro, while binding affinity to lipid vesicles was unaltered	
	T72, T75, and T81	• inhibited the α-helical structure of α-syn upon membrane binding	
Glycation	Lysine	• reduced binding affinity towards sodium dodecyl sulfate (SDS) micelles without affecting the α-helical structure of α-syn • disruption of lipid vesicles upon α-syn binding	[167]

3.3.1. Phosphorylation

Phosphorylation is mediated by kinases [168] and reversed by phosphatases, respectively [169]. Phosphorylation is an esterification reaction involving the attachment of a phosphoryl group to the hydroxyl group of the side-chains of specific amino acids such as serine, tyrosine, and threonine [170]. α-syn is most commonly phosphorylated on serine [153,171] and tyrosine residues [172–175]. In particular, phosphorylated α-syn at S87 [153] and S129 [171] is enriched in Lewy bodies [176]. S129 is even enriched by 90% [176]. The current literature presents divergent findings concerning the adverse and beneficial effects of phosphorylation on the interaction of α-syn with lipids. Phosphorylation on S87 and S129 was shown to alter the conformation of membrane-bound α-syn by destabilizing the α-helical conformation, leading to a decreased affinity to lipid vesicles [153–155]. However, conflicting results from Samuel and colleagues demonstrated no difference in membrane binding to synaptosomes upon phosphorylation at S129 [156].

3.3.2. Acetylation

Acetylation of α-syn is mediated by irreversible addition of an acetyl group to the amine group of the N-terminus (methionine) by histone acetyl transferase, resulting in a decreased positive charge [177]. It has been estimated that over 80% of α-syn molecules are acetylated [171]. Interestingly, acetylated α-syn is found to be enriched in Lewy bodies and affected brain regions from PD patients [171,178]. N-terminal acetylation induced α-helical structures of monomeric, soluble α-syn and thereby decreased its aggregation rates [179]. Due to the decreased positive charge upon acetylation, binding to negatively charged phospholipid head groups is influenced in a way that the affinity of α-syn for membrane binding is enhanced [157], while its structural properties were not altered [157]. In addition, N-terminal acetylated α-syn localizes to highly curved, ordered membranes

with a preference for lipid rafts under cell-free conditions [180]. The effect of site-specific acetylation as well as its neurotoxic potential need to be further investigated.

3.3.3. Nitration

Nitration is an irreversible aversive PTM that occurs on tyrosine residues, in particular in the presence of oxidative stress [181]. This PTM has been associated with several neurodegenerative diseases, including PD [181,182]. Nitrated α-syn was not only enriched in Lewy bodies [181,183], but also led to increased oligomerization of α-syn [184] as well as cytotoxicity in cells [185] and in the substantia nigra of rats [186]. Furthermore, α-syn nitration induced a reduced formation of α-helical structures and a decreased binding affinity of α-syn to negatively charged lipid vesicles [158]. Specifically, after nitration at Y39 or Y125, α-helix formation upon α-syn binding to lipid vesicles was diminished, and fibrils showed a distinct morphology compared to wildtype α-syn [158]. Moreover, nitration of Y125, Y133, and Y136 interfered with the binding affinity of α-syn to lipid vesicles [158].

3.3.4. Ubiquitination

Ubiquitination is a reversible PTM important for intracellular protein homeostasis. This type of PTM involves the attachment of ubiquitin, a small regulatory protein consisting of 76 amino acids, to lysine residues of a target protein through an isopeptide bond. This process is essential for targeted degradation and is mediated by three enzymes: the ubiquitin-activating enzyme E1, the ubiquitin-conjugating enzyme E2, and the ubiquitin ligase E3 [187]. α-syn contains nine lysine residues potentially being ubiquitinated (K6, K10, K12, K21, K23, K32, K34, K43, and K96). Ubiquitinated α-syn is present in Lewy bodies [188] and promotes fibril formation to a different degree depending on the position of ubiquitination in α-syn [189]. In detail, ubiquitination at K10 and K23 displayed similar fibril levels with altered kinetics of formation compared to wildtype α-syn, while K6, K12, and K21 slightly reduced fibril formation, and K32, K34, K43, and K96 reduced fibril formation more severely [189]. Moreover, it was demonstrated that ubiquitination at K6, K23, K43, and K96 had no effect on the α-helical secondary structure of α-syn after binding to lipid vesicles [159,160]. Alterations of the lipid-binding properties of α-syn upon ubiquitination are still largely unknown. It was suggested that ubiquitination of lysine residues within the N-terminal KTKEGV repeat motifs may prevent membrane binding of α-syn [190].

3.3.5. Truncation

Truncation of proteins occurs due to a dysfunctional protein homeostasis machinery leading to incomplete metabolization of α-syn by a number of enzymes, such as plasmin [191], neurosin [192], cathepsin D [193], caspase 1 [194], calpain 1 [195], and other proteinases [196]. α-syn is irreversibly truncated at the N- or C-terminus and present in over 15% of α-syn in Lewy bodies [197]. An overview of the possible truncations of α-syn is reviewed by Sorrentino and colleagues [198]. Notably, N-terminally truncated α-syn variants, 5–140, 39–140, 65–140, 66–140, 68–140, and 71–140, and C-terminally truncated α-syn variants, 1–101. 1–103, 1–115, 1–122, 1–124, 1–135, and 1–139 have been detected in different brain regions of PD patients so far [171,197,199]. Since the N-terminal domain of α-syn determines its lipid-binding capacity, truncation within this site may reduce physiological membrane binding. In general, truncation of α-syn is able to induce aggregation and toxicity in vitro [200] and in vivo [201] by increasing the spread of α-syn through synaptically coupled neuroanatomical tracts [202]. The impact of C-terminal truncations of α-syn on the aggregation of the protein was investigated in more detail, since oligomerization and aggregation of α-syn is mediated mainly by the C-terminus [162]. In any case, C-terminal truncation of α-syn reduces its solubility and affects its membrane-binding properties as well leading to site-specific neurotoxic effects [161–165].

3.3.6. Glycosylation

Glycosylation is a type of reversible enzyme-dependent PTM, in which N-acetylglucosamine (GlcNAc), an amide derivative of glucose, is transferred from uridine diphosphate-GlcNAc (UDP-GlcNAc) to the hydroxyl group of threonine or serine residues of a protein [203]. The addition of GlcNAc is catalyzed by O-GlcNAc-transferase, while its removal is mediated by O-GlcNAcase [203]. So far, nine residues of α-syn (T33, T44, T54, T59, T64, T72, T75, T81, and S87) have been reported as potential sites of glycosylation [204–206]. In general, glycosylation of α-syn at various position reduces aggregation and toxicity of α-syn [207,208], though it does not affect binding of α-syn to phospholipid membranes [166]. Interestingly, triple glycosylation at T72, T75, and T81 inhibited theα-helical structure of α-syn upon membrane binding [166]. Notably, glycosylation has an impact on other PTMs. In particular, glycosylation of α-yn was shown to prevent its phosphorylation at S129, whereas it promotes phosphorylation at S87 [207]. No aversive effects have been reported so far for glycosylation of α-syn.

3.3.7. Glycation

Glycation of α-syn is based upon a non-enzymatic reaction of its lysine residues with reactive carbonyl species as a side product of glycolysis, known as glycation [209]. One of the most prevalent end products of glycation is Nε-(carboxyethyl)lysine (CEL) [210]. It was demonstrated that glycation potentiates α-syn-associated neurodegeneration in PD [211]. Recently, it was observed that CEL formation on α-syn reduces its binding affinity towards sodium dodecyl sulfate (SDS) micelles used as a membrane mimic without affecting the α-helical structure of α-syn [167]. In PD, glycation of α-syn is implicated in protein aggregation and Lewy body formation, while site-specific effects are still poorly understood.

4. Therapeutic Potential

Due to the importance of the interaction of α-syn with lipids, strategies are emerging to modulate this interaction. Several therapeutic approaches have already been investigated and are currently being tested in multiple clinical trials (Table 3). A schematic of the bidirectional interaction of α-syn and lipids and the possible therapeutic interventions is depicted in Figure 4.

Table 3. Summary of current therapeutic approaches investigated experimentally or in clinical trials. https://www.clinicaltrials.gov, accessed on 3 August 2023.

Compound	Target	Effect	Clinical Trial	Clinical Trial PD	Ref.
Lovastatin	HMG-CoA reductase	reduces α-syn accumulation and its phosphorylation in vitro in HEK293 cells, SH-SY5Y cells, and in primary human neurons and in vivo in different transgenic mouse models that neuronally overexpress human α-syn	rheumatoid arthritis, cancer, etc.	Phase II	[212–214]
Simvastatin	HMG-CoA reductase	prevents MPTP-induced striatal dopamine depletion and protein tyrosine nitration in mice, and protects dopaminergic neurons in the substantia nigra, attenuates the expression of proinflammatory molecules, and improves motor deficits in the MPTP model of PD	hyper-lipidemia, diabetes, MS, etc.	Phase II	[212,215,216]

Table 3. *Cont.*

Compound	Target	Effect	Clinical Trial	Clinical Trial PD	Ref.
Myriocin	de novo ceramide synthesis	reduced oxidative stress and inflammation and increased vesicular trafficking in SH-SY5Y cells treated with α-syn fibrils	no	no	[217]
Ellagic acid	α-syn	polyphenolic compound that has an inhibitory effect toward oligomerization and fibrillation of α-syn in vitro, reduces α-syn aggregation, and increases cell survival	prostate cancer phase III	no	[218]
Squalamine	competitive of α-syn	specifically inhibits the initiation of aggregation of α-syn and alleviates its toxicity in neuronal cells and in a *Caenorhabditis elegans* model of PD	macular degeneration phase II and III	no	[219]
Nilotinib	α-syn kinase c-Abl	enhanced clearance of α-syn, reduced neurotoxicity, and improved motor behavior in a mouse model of PD	AD phase 3, leukemia, etc.	no	[220]
MC1568	class IIa histone deacetylases	increased neurite density and cell survival and protected against the neurotoxin-treated SY5Y cells	cancer	no	[221]
VX-765	caspase-1	reduces neurodegeneration, motor symptoms, and neuroinflammation in a mouse model of MSA	no	no	[222]
Arachidonic acid	α-syn	essential FA that induces the formation of ordered, α-helical structured α-syn multimers being resistant to fibrillation	autism, fibrosis, diabetes, etc.	no	[223]
Niacin/Nicotin-amide	Poly (ADP-ribose) polymerase	precursor of NADH and cofactor of mitochondrial enzymes that protects from MPTP-induced neurotoxicity in mice and prevents mitochondrial dysfunction in a cellular model and improves motor behavior in a *Drosophila* model of PD	hyperlipidemia, myopathy, etc.	interventional study	[224–226]
Deferiprone	ferric ions	iron chelator that reduces iron depositions in the substantia nigra accompanied by alleviated motor deficits in a clinical trial in early PD	HIV, ALS, heart disease, etc.	failed	[227]

4.1. Enzymes Involved in Lipid Metabolism

One potential approach is targeting activities of proteins involved in lipid metabolism, including enzymes and lipid transporters. For example, Vincent and colleagues were able to ameliorate α-syn-induced cytotoxicity by inhibiting the highly conserved enzyme stearoyl-CoA desaturase in iPSC-derived neuronal models [228]. This enzyme catalyzes the rate-limiting step in the formation of MUFAs; thus, inhibition of this enzyme reduces the levels of unsaturated membrane lipids [229]. Moreover, inhibition of stearoyl-CoA desaturase was able to reduce the formation of α-syn inclusions in the "3K" variant of the E46K mutation [230]. This result was confirmed by Nuber and colleagues in cultured human neurons, in "3K" neural cultures, and "3K" α-syn mice [42].

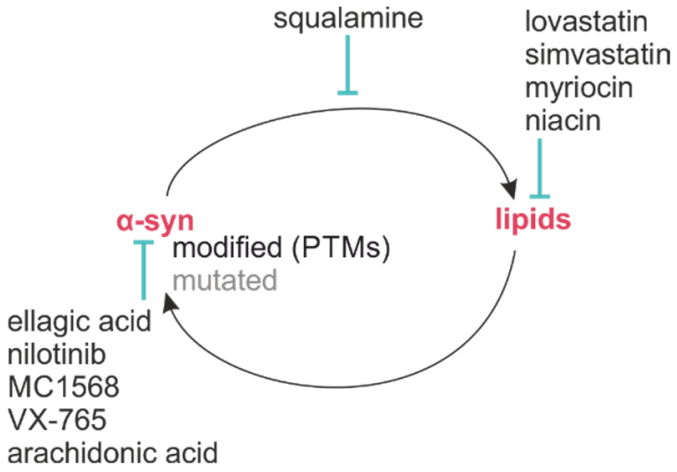

Figure 4. Bidirectional interaction of α-syn and lipids. Modifications of α-syn via mutation or PTMs can alter lipid-binding properties, while changes in lipid composition or metabolism alter pathological properties of α-syn. Moreover, different therapeutics may be used to modulate α-syn and lipids within the CNS, or the interaction between both.

Along this line, inhibition of the key enzymes within the cholesterol biosynthesis pathway induced accumulation of 8, 9-unsaturated sterols driving oligodendrocyte formation and remyelination [231]. For example, Lovastatin reduces cholesterol levels by inhibiting HMG-CoA reductase, which catalyzes the rate-limiting step in the cholesterol synthesis pathway [232]. Thereby, Lovastatin reduces α-syn accumulation and its phosphorylation in vitro in HEK293 cells, SH-SY5Y cells, and in primary human neurons [212,213] and in vivo in different transgenic mouse models that neuronally overexpress human α-syn [214]. Similarly, Simvastatin or other statins can be used as therapeutic approaches [212].

Furthermore, the inhibition of the de novo ceramide synthesis by myriocin, an inhibitor of serine palmitoyltransferase, reduced oxidative stress and inflammation and increased vesicular trafficking in SH-SY5Y cells treated with α-syn fibrils [217].

In summary, these observations suggest that inhibition of important enzymes participating in lipid metabolism may be able to prevent α-syn-mediated toxicity. Based on this evidence, development of inhibitors specifically targeting these enzymes is emerging as potential therapeutic strategy for PD and other synucleinopathies.

4.2. Membrane Binding of α-syn

Another possibility is to modulate binding of altered α-syn to membranes, for example, by using competitive compounds. It has been described that polyphenolic compounds compete effectively with α-syn for membrane binding and are thus considered a strong potential therapeutic candidate for PD and other synucleinopathies [219]. One polyphenolic compound that has an inhibitory effect toward α-syn oligomerization and fibrillation in vitro is ellagic acid [218]. Hence, α-syn aggregation was reduced, and cell survival increased [218]. Another molecule is squalamine [219], an antimicrobial aminosterol originally discovered in 1993 in the dogfish shark, *Squalus acanthias* [233]. Indeed, squalamine carries a net positive charge and shows a high binding affinity for anionic phospholipids [234]. By competing with α-syn for binding to the membranes, squalamine specifically inhibits the initiation of the aggregation process of α-syn [219]. Thus, it alleviates the toxicity of α-syn oligomers in neuronal cells and in a *Caenorhabditis elegans* model of PD [219].

4.3. PTMs

Since PTMs modify the interaction of α-syn with lipids, interfering with PTM pathways is considered as a novel therapeutic target for PD. Modulation of phosphorylation of α-syn is achieved by pharmacological modulation of kinases and phosphatases [235–238].

For example, using nilotinib, a Food and Drug Administration (FDA)-approved cancer treatment, to inhibit the kinase c-Abl leads to reduced phosphorylation, enhanced clearance of α-syn, reduced neurotoxicity, and improved motor behavior in a mouse model of PD [220].

Another possibility is to enhance the phosphatase activity of phosphoprotein phosphatase 2A (PP2A) by increasing methylation of the enzyme to decrease α-syn phosphorylation at S129, leading to decreased α-syn aggregation and toxicity in mice [239].

To target ubiquitination, antibodies inhibiting the ubiquitin E3 ligase were developed, which decreased the expression and aggregation of α-syn and improved cell viability in vitro [240].

Pharmacological inhibition of class IIa histone deacetylases (HDACs), which are important enzymes for the modulation of α-syn by acetylation, using MC1568 increased neurite density and cell survival and protected against the neurotoxin-treated SY5Y cells [221]. However, effects on the binding capacity of α-syn to lipids are not yet known.

Truncations of α-syn may be reduced by immunotherapy or pharmacological inhibition of caspases [222,241]. So far, therapeutic approaches concentrate on C-terminal truncations. One example is VX-765 that inhibits caspase-1, which cleaves α-syn at D121, thereby improving motor symptoms, neurodegeneration, and neuroinflammation in a transgenic mouse model of MSA [222].

Since glycosylation of α-syn reduces α-syn aggregation, pharmacological inhibition of O-GlcNAcase increases the glycosylation levels of α-syn, resulting in a lower aggregation of α-syn [242]. Moreover, glycosylation inhibits calpain-mediated C-terminal α-syn truncations, thus reducing aggregation of α-syn as well. Similarly, glycosylation competes with phosphorylation in targeting hydroxyl groups on serine and threonine residues, thereby protecting α-syn from increased aggregation caused by phosphorylation [207]. Along this line, accumulation of S129 α-syn was reduced in the substantia nigra in an adeno-associated virus-generated A53T mouse model of PD by pharmacological inhibition of O-GlcNAcase [243].

4.4. Neuroprotective Lipids

Given the neuroprotective effects of some lipids, their direct administration is emerging as a promising therapeutic strategy to alleviate α-syn-mediated cytotoxicity. One example is arachidonic acid, an essential FA that induces the formation of ordered, α-helical structured α-syn multimers being resistant to fibrillation [223]. Another target are PUFAs, especially omega-3, an important component of membranes (reviewed by [244]). Among other positive effects on PD, omega-3 PUFAs inhibit neuroinflammation, maintain α-syn degradation, and improve membrane fluidity (reviewed by [244]), thus emerging as a therapeutic strategy. Another potential nutrient is niacin/nicotinamide, a precursor of NADH and cofactor of mitochondrial enzymes [245,246]. Nicotinamide has already been linked to neuroprotection in PD and has shown to protect against MPTP induced neurotoxicity in mice [224,225]. Furthermore, nicotinamide prevented mitochondrial dysfunction in a cellular model and improved motor behavior in a *Drosophila* model of PD [226].

4.5. Environmental Factors

Since a variety of environmental factors affect lipid homeostasis, targeting these factors is a promising approach. Dietary nutrients are the main substrates of the gut microbiota and can have an impact on the composition and metabolic activity of these microbiota (reviewed by [247]). These processes lead to the production of intermediate metabolites affecting host energy homeostasis, glucose, and lipid metabolism [248]. For example, nutrition rich in antioxidants might be neuroprotective in PD [249]. Since increased lipid droplet formation in dopaminergic neurons has been correlated with iron accumulation, pharmacological administration of iron chelators such as deferiprone arises as a therapeutic strategy. Deferiprone reduces iron depositions in the substantia nigra accompanied by

alleviated motor deficits in an initial clinical trial in early PD [227]. However, it could not be confirmed lately.

Overall, lipids and their metabolism in the CNS contribute profoundly to the identification of novel therapeutic interventions for PD.

5. Conclusions

α-syn has been associated with PD and other synucleinopathies for over two decades. However, this discovery has not yet led to the development of effective and causative therapeutic approaches. Thus, this review focuses on an important aspect of α-syn, namely its interaction with lipids in the CNS. On the one hand, alterations of lipids and different metabolic pathways influence the function and the dysfunction of this protein. On the other hand, the interference of α-syn with lipids is changed in PD due to different factors, such as point mutations within the lipid-binding region (Table 1) or PTMs (Table 2). Focusing on PTMs, researchers have identified compounds that modulate PTMs, which reduce the aggregation of α-syn and modify its binding properties to membranes. Moreover, targeting enzymes involved in various stages of lipid metabolism and exploring the neuroprotective potential of certain lipids have emerged as promising therapeutic avenues. Efforts toward a more detailed characterization of α-syn interventions in lipid metabolism and function will lead to a more in-depth assessment of the protein's implications for therapeutic purposes. In conclusion, investigation of the bidirectional interaction of α-syn with lipids is advancing our comprehension of the pathology in PD and other synucleinopathies, suggesting that these disorders are not solely a consequence of protein pathology but also influenced by lipid-related processes. Thus, PD is not simply a synucleinopathy but rather a meta-disease composed of several different aspects.

Author Contributions: Conceptualization, K.B., W.X. and J.W.; writing, K.B.; review and editing, W.X. and J.W. All authors have read and agreed to the published version of the manuscript.

Funding: Funding was received from the Deutsche Forschungsgemeinschaft (DFG, German Research Foundation) 270949263/GRK2162 and the Bavarian Research Association "Interaction of Human Brain Cells" (ForInter) funded by the Bavarian State Ministry of Science and the Arts.

Institutional Review Board Statement: Not applicable.

Informed Consent Statement: Not applicable.

Data Availability Statement: Not applicable.

Acknowledgments: All figures were created with CorelDraw X6.

Conflicts of Interest: The authors declare no conflict of interest.

References

1. Maroteaux, L.; Campanelli, J.T.; Scheller, R.H. Synuclein: A neuron-specific protein localized to the nucleus and presynaptic nerve terminal. *J. Neurosci.* **1988**, *8*, 2804–2815. [CrossRef]
2. Iwai, A.; Masliah, E.; Yoshimoto, M.; Ge, N.; Flanagan, L.; De Silva, H.R.; Kittel, A.; Saitoh, T. The precursor protein of non-Aβ component of Alzheimer's disease amyloid is a presynaptic protein of the central nervous system. *Neuron* **1995**, *14*, 467–475. [CrossRef]
3. Gardai, S.J.; Mao, W.; Schüle, B.; Babcock, M.; Schoebel, S.; Lorenzana, C.; Alexander, J.; Kim, S.; Glick, H.; Hilton, K. Elevated alpha-synuclein impairs innate immune cell function and provides a potential peripheral biomarker for Parkinson's disease. *PLoS ONE* **2013**, *8*, e71634. [CrossRef]
4. Badawy, S.M.M.; Okada, T.; Kajimoto, T.; Hirase, M.; Matovelo, S.A.; Nakamura, S.; Yoshida, D.; Ijuin, T.; Nakamura, S.-I. Extracellular α-synuclein drives sphingosine 1-phosphate receptor subtype 1 out of lipid rafts, leading to impaired inhibitory G-protein signaling. *J. Biol. Chem.* **2018**, *293*, 8208–8216. [CrossRef]
5. Bellani, S.; Sousa, V.L.; Ronzitti, G.; Valtorta, F.; Meldolesi, J.; Chieregatti, E. The regulation of synaptic function by α-synuclein. *Commun. Integr. Biol.* **2010**, *3*, 106–109. [CrossRef] [PubMed]
6. Di Rosa, G.; Puzzo, D.; Sant Angelo, A.; Trinchese, F.; Arancio, O. Alpha-synuclein: Between synaptic function and dysfunction. *Histol. Histopathol.* **2003**, *18*, 1257–1266.
7. Cheng, F.; Vivacqua, G.; Yu, S. The role of alpha-synuclein in neurotransmission and synaptic plasticity. *J. Chem. Neuroanat.* **2011**, *42*, 242–248. [CrossRef]

8. Baptista, M.J.; O'Farrell, C.; Daya, S.; Ahmad, R.; Miller, D.W.; Hardy, J.; Farrer, M.J.; Cookson, M.R. Co-ordinate transcriptional regulation of dopamine synthesis genes by α-synuclein in human neuroblastoma cell lines. *J. Neurochem.* **2003**, *85*, 957–968. [CrossRef]
9. Fauvet, B.; Mbefo, M.K.; Fares, M.-B.; Desobry, C.; Michael, S.; Ardah, M.T.; Tsika, E.; Coune, P.; Prudent, M.; Lion, N. α-Synuclein in central nervous system and from erythrocytes, mammalian cells, and Escherichia coli exists predominantly as disordered monomer. *J. Biol. Chem.* **2012**, *287*, 15345–15364. [CrossRef]
10. Weinreb, P.H.; Zhen, W.; Poon, A.W.; Conway, K.A.; Lansbury, P.T. NACP, a protein implicated in Alzheimer's disease and learning, is natively unfolded. *Biochemistry* **1996**, *35*, 13709–13715. [CrossRef]
11. Dettmer, U.; Newman, A.J.; Soldner, F.; Luth, E.S.; Kim, N.C.; von Saucken, V.E.; Sanderson, J.B.; Jaenisch, R.; Bartels, T.; Selkoe, D. Parkinson-causing alpha-synuclein missense mutations shift native tetramers to monomers as a mechanism for disease initiation. *Nat. Commun.* **2015**, *6*, 7314. [CrossRef]
12. Bartels, T.; Choi, J.G.; Selkoe, D.J. α-Synuclein occurs physiologically as a helically folded tetramer that resists aggregation. *Nature* **2011**, *477*, 107–110. [CrossRef]
13. Wang, W.; Perovic, I.; Chittuluru, J.; Kaganovich, A.; Nguyen, L.T.; Liao, J.; Auclair, J.R.; Johnson, D.; Landeru, A.; Simorellis, A.K. A soluble α-synuclein construct forms a dynamic tetramer. *Proc. Natl. Acad. Sci. USA* **2011**, *108*, 17797–17802. [CrossRef]
14. Burre, J.; Sharma, M.; Sudhof, T.C. alpha-Synuclein assembles into higher-order multimers upon membrane binding to promote SNARE complex formation. *Proc. Natl. Acad. Sci. USA* **2014**, *111*, E4274–E4283. [CrossRef] [PubMed]
15. Chen, S.W.; Drakulic, S.; Deas, E.; Ouberai, M.; Aprile, F.A.; Arranz, R.; Ness, S.; Roodveldt, C.; Guilliams, T.; De-Genst, E.J.; et al. Structural characterization of toxic oligomers that are kinetically trapped during alpha-synuclein fibril formation. *Proc. Natl. Acad. Sci. USA* **2015**, *112*, E1994–E2003. [CrossRef]
16. Fusco, G.; Chen, S.W.; Williamson, P.T.; Cascella, R.; Perni, M.; Jarvis, J.A.; Cecchi, C.; Vendruscolo, M.; Chiti, F.; Cremades, N. Structural basis of membrane disruption and cellular toxicity by α-synuclein oligomers. *Science* **2017**, *358*, 1440–1443. [CrossRef]
17. Volpicelli-Daley, L.A.; Luk, K.C.; Patel, T.P.; Tanik, S.A.; Riddle, D.M.; Stieber, A.; Meaney, D.F.; Trojanowski, J.Q.; Lee, V.M. Exogenous alpha-synuclein fibrils induce Lewy body pathology leading to synaptic dysfunction and neuron death. *Neuron* **2011**, *72*, 57–71. [CrossRef]
18. Osterberg, V.R.; Spinelli, K.J.; Weston, L.J.; Luk, K.C.; Woltjer, R.L.; Unni, V.K. Progressive aggregation of alpha-synuclein and selective degeneration of lewy inclusion-bearing neurons in a mouse model of parkinsonism. *Cell. Rep.* **2015**, *10*, 1252–1260. [CrossRef]
19. Coon, E.A.; Singer, W. Synucleinopathies. *Continuum* **2020**, *26*, 72–92. [CrossRef]
20. Parkinson, J. An essay on the shaking palsy. *Arch. Neurol.* **1969**, *20*, 441–445. [CrossRef]
21. National Collaborating Centre for Chronic Conditions. *Parkinson's Disease: National Clinical Guideline for Diagnosis and Management in Primary and Secondary Care*; Royal College of Physicians of London: London, UK, 2006.
22. Polymeropoulos, M.H.; Lavedan, C.; Leroy, E.; Ide, S.E.; Dehejia, A.; Dutra, A.; Pike, B.; Root, H.; Rubenstein, J.; Boyer, R. Mutation in the α-synuclein gene identified in families with Parkinson's disease. *Science* **1997**, *276*, 2045–2047. [CrossRef] [PubMed]
23. Damier, P.; Hirsch, E.; Agid, Y.; Graybiel, A. The substantia nigra of the human brain: II. Patterns of loss of dopamine-containing neurons in Parkinson's disease. *Brain* **1999**, *122*, 1437–1448. [CrossRef]
24. Krüger, R.; Kuhn, W.; Müller, T.; Woitalla, D.; Graeber, M.; Kösel, S.; Przuntek, H.; Epplen, J.T.; Schols, L.; Riess, O. AlaSOPro mutation in the gene encoding α-synuclein in Parkinson's disease. *Nat. Genet* **1998**, *18*, 106–108. [CrossRef]
25. Zarranz, J.J.; Alegre, J.; Gómez-Esteban, J.C.; Lezcano, E.; Ros, R.; Ampuero, I.; Vidal, L.; Hoenicka, J.; Rodriguez, O.; Atarés, B. The new mutation, E46K, of α-synuclein causes parkinson and Lewy body dementia. *Ann. Neurol. Off. J. Am. Neurol. Assoc. Child Neurol. Soc.* **2004**, *55*, 164–173. [CrossRef]
26. George, J.M.; Jin, H.; Woods, W.S.; Clayton, D.F. Characterization of a novel protein regulated during the critical period for song learning in the zebra finch. *Neuron* **1995**, *15*, 361–372. [CrossRef]
27. Davidson, W.S.; Jonas, A.; Clayton, D.F.; George, J.M. Stabilization of a-Synuclein Secondary Structure upon Binding to Synthetic Membranes. *J. Biol. Chem.* **1998**, *273*, 9443–9449. [CrossRef] [PubMed]
28. Rodriguez, J.A.; Ivanova, M.I.; Sawaya, M.R.; Cascio, D.; Reyes, F.E.; Shi, D.; Sangwan, S.; Guenther, E.L.; Johnson, L.M.; Zhang, M. Structure of the toxic core of α-synuclein from invisible crystals. *Nature* **2015**, *525*, 486–490. [CrossRef]
29. Salveson, P.J.; Spencer, R.K.; Nowick, J.S. X-ray crystallographic structure of oligomers formed by a toxic β-hairpin derived from α-synuclein: Trimers and higher-order oligomers. *J. Am. Chem. Soc.* **2016**, *138*, 4458–4467. [CrossRef]
30. Giasson, B.I.; Murray, I.V.; Trojanowski, J.Q.; Lee, V.M.-Y. A hydrophobic stretch of 12 amino acid residues in the middle of α-synuclein is essential for filament assembly. *J. Biol. Chem.* **2001**, *276*, 2380–2386. [CrossRef]
31. Anderson, E.N.; Hirpa, D.; Zheng, K.H.; Banerjee, R.; Gunawardena, S. The non-amyloidal component region of α-synuclein is important for α-synuclein transport within axons. *Front. Cell. Neurosci.* **2020**, *13*, 540. [CrossRef]
32. Park, S.M.; Jung, H.Y.; Chung, K.C.; Rhim, H.; Park, J.H.; Kim, J. Stress-Induced Aggregation Profiles of GST− α-Synuclein Fusion Proteins: Role of the C-Terminal Acidic Tail of α-Synuclein in Protein Thermosolubility and Stability. *Biochemistry* **2002**, *41*, 4137–4146. [CrossRef]
33. Kim, T.D.; Paik, S.R.; Yang, C.-H. Structural and functional implications of C-terminal regions of α-synuclein. *Biochemistry* **2002**, *41*, 13782–13790. [CrossRef]

34. Farzadfard, A.; Pedersen, J.N.; Meisl, G.; Somavarapu, A.K.; Alam, P.; Goksøyr, L.; Nielsen, M.A.; Sander, A.F.; Knowles, T.P.; Pedersen, J.S. The C-terminal tail of α-synuclein protects against aggregate replication but is critical for oligomerization. *Commun. Biol.* **2022**, *5*, 123. [CrossRef]
35. Flagmeier, P.; Meisl, G.; Vendruscolo, M.; Knowles, T.P.; Dobson, C.M.; Buell, A.K.; Galvagnion, C. Mutations associated with familial Parkinson's disease alter the initiation and amplification steps of α-synuclein aggregation. *Proc. Natl. Acad. Sci. USA* **2016**, *113*, 10328–10333. [CrossRef]
36. Zunke, F.; Moise, A.C.; Belur, N.R.; Gelyana, E.; Stojkovska, I.; Dzaferbegovic, H.; Toker, N.J.; Jeon, S.; Fredriksen, K.; Mazzulli, J.R. Reversible Conformational Conversion of alpha-Synuclein into Toxic Assemblies by Glucosylceramide. *Neuron* **2018**, *97*, 92–107. [CrossRef]
37. Tracey, T.; Kirk, S.; Steyn, F.; Ngo, S. The role of lipids in the central nervous system and their pathological implications in amyotrophic lateral sclerosis. *Semin. Cell Dev. Biol.* **2021**, *112*, 69–81. [CrossRef]
38. Vandenheuvel, F.A. Study of biological structure at the molecular level with stereomodel projections I. The lipids in the myelin sheath of nerve. *J. Am. Oil Chem. Soc.* **1963**, *40*, 455–471. [CrossRef]
39. Eliezer, D.; Kutluay, E.; Bussell, R., Jr.; Browne, G. Conformational properties of α-synuclein in its free and lipid-associated states. *J. Mol. Biol.* **2001**, *307*, 1061–1073.
40. Bussell Jr, R.; Eliezer, D. A structural and functional role for 11-mer repeats in α-synuclein and other exchangeable lipid binding proteins. *J. Mol. Biol.* **2003**, *329*, 763–778. [CrossRef]
41. Willingham, S.; Outeiro, T.F.; DeVit, M.J.; Lindquist, S.L.; Muchowski, P.J. Yeast genes that enhance the toxicity of a mutant huntingtin fragment or α-synuclein. *Science* **2003**, *302*, 1769–1772. [CrossRef]
42. Nuber, S.; Nam, A.Y.; Rajsombath, M.M.; Cirka, H.; Hronowski, X.; Wang, J.; Hodgetts, K.; Kalinichenko, L.S.; Müller, C.P.; Lambrecht, V. A Stearoyl–Coenzyme A Desaturase Inhibitor Prevents Multiple Parkinson Disease Phenotypes in α-Synuclein Mice. *Ann. Neurol.* **2021**, *89*, 74–90. [CrossRef]
43. Pranav, K.; Usha, M. *Life Sciences Fundamental and Practice Part-1*; Pathfinder Publishers: Sydney, Australia, 2014.
44. Morell, P.; Toews, A.D. Biochemistry of lipids. *Handb. Clin. Neurol.* **1996**, *22*, 33–49.
45. Williams, K.A.; Deber, C.M. The structure and function of central nervous system myelin. *Crit. Rev. Clin. Lab. Sci.* **1993**, *30*, 29–64. [CrossRef]
46. Masoro, E.J. Lipids and Lipid Metabolism. *Ann. Rev. Physioi.* **1977**, *39*, 301–321. [CrossRef]
47. Fahy, E.; Cotter, D.; Sud, M.; Subramaniam, S. Lipid classification, structures and tools. *Biochim. Biophys. Acta (BBA)-Mol. Cell Biol. Lipids* **2011**, *1811*, 637–647. [CrossRef] [PubMed]
48. Rustan, A.C.; Drevon, C.A. Fatty acids: Structures and properties. *e LS* **2001**, 1–7. [CrossRef]
49. Spector, R. Fatty acid transport through the blood-brain barrier. *J. Neurochem.* **1988**, *50*, 639–643. [CrossRef]
50. Abbott, N.J.; Patabendige, A.A.; Dolman, D.E.; Yusof, S.R.; Begley, D.J. Structure and function of the blood-brain barrier. *Neurobiol. Dis.* **2010**, *37*, 13–25. [CrossRef]
51. Jurevics, H.; Morell, P. Cholesterol for synthesis of myelin is made locally, not imported into brain. *J. Neurochem.* **1995**, *64*, 895–901. [CrossRef]
52. Saher, G.; Stumpf, S.K. Cholesterol in myelin biogenesis and hypomyelinating disorders. *Biochim. Biophys. Acta* **2015**, *1851*, 1083–1094. [CrossRef] [PubMed]
53. Hofmann, K.; Rodriguez-Rodriguez, R.; Gaebler, A.; Casals, N.; Scheller, A.; Kuerschner, L. Astrocytes and oligodendrocytes in grey and white matter regions of the brain metabolize fatty acids. *Sci. Rep.* **2017**, *7*, 10779.
54. van Deijk, A.L.F.; Camargo, N.; Timmerman, J.; Heistek, T.; Brouwers, J.F.; Mogavero, F.; Mansvelder, H.D.; Smit, A.B.; Verheijen, M.H. Astrocyte lipid metabolism is critical for synapse development and function in vivo. *Glia* **2017**, *65*, 670–682.
55. Camargo, N.; Goudriaan, A.; van Deijk, A.-L.F.; Otte, W.M.; Brouwers, J.F.; Lodder, H.; Gutmann, D.H.; Nave, K.-A.; Dijkhuizen, R.M.; Mansvelder, H.D. Oligodendroglial myelination requires astrocyte-derived lipids. *PLoS Biol.* **2017**, *15*, e1002605.
56. Chen, J.; Zhang, X.; Kusumo, H.; Costa, L.G.; Guizzetti, M. Cholesterol efflux is differentially regulated in neurons and astrocytes: Implications for brain cholesterol homeostasis. *Biochim. Biophys. Acta* **2013**, *1831*, 263–275. [CrossRef]
57. Hirsch-Reinshagen, V.; Zhou, S.; Burgess, B.L.; Bernier, L.; McIsaac, S.A.; Chan, J.Y.; Tansley, G.H.; Cohn, J.S.; Hayden, M.R.; Wellington, C.L. Deficiency of ABCA1 impairs apolipoprotein E metabolism in brain. *J. Biol. Chem.* **2004**, *279*, 41197–41207.
58. Swanson, L.W.; Simmons, D.M.; Hofmann, S.L.; Goldstein, J.L.; Brown, M.S. Localization of mRNA for low density lipoprotein receptor and a cholesterol synthetic enzyme in rabbit nervous system by in situ hybridization. *Proc. Natl. Acad. Sci. USA* **1988**, *85*, 9821–9825.
59. Pitas, R.; Boyles, J.; Lee, S.; Hui, D.; Weisgraber, K. Lipoproteins and their receptors in the central nervous system. Characterization of the lipoproteins in cerebrospinal fluid and identification of apolipoprotein B, E (LDL) receptors in the brain. *J. Biol. Chem.* **1987**, *262*, 14352–14360.
60. Zhao, S.; Hu, X.; Park, J.; Zhu, Y.; Zhu, Q.; Li, H.; Luo, C.; Han, R.; Cooper, N.; Qiu, M. Selective expression of LDLR and VLDLR in myelinating oligodendrocytes. *Dev. Dyn. Off. Publ. Am. Assoc. Anat.* **2007**, *236*, 2708–2712.
61. Simons, M.; Krämer, E.-M.; Thiele, C.; Stoffel, W.; Trotter, J. Assembly of Myelin by Association of Proteolipid Protein with Cholesterol- and Galactosylceramid-rich Membrane Domains. *J. Cell Biol.* **2000**, *151*, 143–153.

62. Werner, H.B.; Krämer-Albers, E.M.; Strenzke, N.; Saher, G.; Tenzer, S.; Ohno-Iwashita, Y.; De Monasterio-Schrader, P.; Möbius, W.; Moser, T.; Griffiths, I.R. A critical role for the cholesterol-associated proteolipids PLP and M6B in myelination of the central nervous system. *Glia* **2013**, *61*, 567–586.
63. Garcia Corrales, A.V.; Haidar, M.; Bogie, J.F.J.; Hendriks, J.J.A. Fatty Acid Synthesis in Glial Cells of the CNS. *Int. J. Mol. Sci.* **2021**, *22*, 8159. [CrossRef]
64. Moore, S.A. Polyunsaturated fatty acid synthesis and release by brain-derived cells in vitro. *J. Mol. Neurosci.* **2001**, *16*, 195–200.
65. Bazan, N. Supply of n-3 polyunsaturated fatty acids and their significance in the central nervous system. *Nutr. Brain* **1990**, *8*, 1–24.
66. Chandel, N.S. Lipid metabolism. *Cold Spring Harb. Perspect. Biol.* **2021**, *13*, a040576.
67. Ralhan, I.; Chang, C.-L.; Lippincott-Schwartz, J.; Ioannou, M.S. Lipid droplets in the nervous system. *J. Cell Biol.* **2021**, *220*, e202102136.
68. Unger, R.H.; Clark, G.O.; Scherer, P.E.; Orci, L. Lipid homeostasis, lipotoxicity and the metabolic syndrome. *Biochim. Biophys. Acta (BBA)-Mol. Cell Biol. Lipids* **2010**, *1801*, 209–214.
69. Rambold, A.S.; Cohen, S.; Lippincott-Schwartz, J. Fatty acid trafficking in starved cells: Regulation by lipid droplet lipolysis, autophagy, and mitochondrial fusion dynamics. *Dev. Cell* **2015**, *32*, 678–692. [CrossRef]
70. Cabodevilla, A.; Sánchez-Caballero, L.; Picatoste, F.; Gubern, A.; Claro, E. Cell survival during complete nutrient deprivation depends on lipid droplet-fueled β-oxidation of fatty acids (577.3). *FASEB J.* **2014**, *28*, 577-3.
71. Edmond, J.; Robbins, R.; Bergstrom, J.; Cole, R.; De Vellis, J. Capacity for substrate utilization in oxidative metabolism by neurons, astrocytes, and oligodendrocytes from developing brain in primary culture. *J. Neurosci. Res.* **1987**, *18*, 551–561.
72. Hannun, Y.A.; Obeid, L.M. Sphingolipids and their metabolism in physiology and disease. *Nat. Rev. Mol. Cell Biol.* **2018**, *19*, 175–191. [CrossRef]
73. Tracey, T.J.; Steyn, F.J.; Wolvetang, E.J.; Ngo, S.T. Neuronal Lipid Metabolism: Multiple Pathways Driving Functional Outcomes in Health and Disease. *Front. Mol. Neurosci.* **2018**, *11*, 10. [CrossRef] [PubMed]
74. Burré, J. The synaptic function of α-synuclein. *J. Park. Dis.* **2015**, *5*, 699–713. [CrossRef] [PubMed]
75. Spillantini, M.G.; Schmidt, M.L.; Lee, V.M.-Y.; Trojanowski, J.Q.; Jakes, R.; Goedert, M. α-Synuclein in Lewy bodies. *Nature* **1997**, *388*, 839–840. [CrossRef] [PubMed]
76. Jensen, P.H.; Nielsen, M.S.; Jakes, R.; Dotti, C.G.; Goedert, M. Binding of α-synuclein to brain vesicles is abolished by familial Parkinson's disease mutation. *J. Biol. Chem.* **1998**, *273*, 26292–26294. [CrossRef]
77. Segrest, J.P.; Jackson, R.L.; Morrisett, J.D.; Gotto Jr, A.M. A molecular theory of lipid—Protein interactions in the plasma lipoproteins. *FEBS Lett.* **1974**, *38*, 247–253. [CrossRef]
78. van Rooijen, B.D.; Claessens, M.M.; Subramaniam, V. Lipid bilayer disruption by oligomeric α-synuclein depends on bilayer charge and accessibility of the hydrophobic core. *Biochim. Biophys. Acta (BBA)-Biomembr.* **2009**, *1788*, 1271–1278. [CrossRef]
79. Jo, E.; McLaurin, J.; Yip, C.M.; George-Hyslop, P.S.; Fraser, P.E. α-Synuclein membrane interactions and lipid specificity. *J. Biol. Chem.* **2000**, *275*, 34328–34334. [CrossRef]
80. Rhoades, E.; Ramlall, T.F.; Webb, W.W.; Eliezer, D. Quantification of α-synuclein binding to lipid vesicles using fluorescence correlation spectroscopy. *Biophys. J.* **2006**, *90*, 4692–4700. [CrossRef]
81. Narayanan, V.; Guo, Y.; Scarlata, S. Fluorescence studies suggest a role for α-synuclein in the phosphatidylinositol lipid signaling pathway. *Biochemistry* **2005**, *44*, 462–470. [CrossRef]
82. Fantini, J.; Carlus, D.; Yahi, N. The fusogenic tilted peptide (67-78) of alpha-synuclein is a cholesterol binding domain. *Biochim. Biophys. Acta* **2011**, *1808*, 2343–2351. [CrossRef]
83. Fantini, J.; Yahi, N. Molecular basis for the glycosphingolipid-binding specificity of alpha-synuclein: Key role of tyrosine 39 in membrane insertion. *J. Mol. Biol.* **2011**, *408*, 654–669. [CrossRef]
84. Wang, G.F.; Li, C.; Pielak, G.J. 19F NMR studies of alpha-synuclein-membrane interactions. *Protein Sci.* **2010**, *19*, 1686–1691. [CrossRef] [PubMed]
85. Fortin, D.L.; Troyer, M.D.; Nakamura, K.; Kubo, S.; Anthony, M.D.; Edwards, R.H. Lipid rafts mediate the synaptic localization of alpha-synuclein. *J. Neurosci.* **2004**, *24*, 6715–6723. [CrossRef] [PubMed]
86. Li, W.-W.; Yang, R.; Guo, J.-C.; Ren, H.-M.; Zha, X.-L.; Cheng, J.-S.; Cai, D.-F. Localization of α-synuclein to mitochondria within midbrain of mice. *Neuroreport* **2007**, *18*, 1543–1546. [CrossRef] [PubMed]
87. Bodner, C.R.; Maltsev, A.S.; Dobson, C.M.; Bax, A. Differential phospholipid binding of α-synuclein variants implicated in Parkinson's disease revealed by solution NMR spectroscopy. *Biochemistry* **2010**, *49*, 862–871. [CrossRef]
88. Fusco, G.; De Simone, A.; Gopinath, T.; Vostrikov, V.; Vendruscolo, M.; Dobson, C.M.; Veglia, G. Direct observation of the three regions in α-synuclein that determine its membrane-bound behaviour. *Nat. Commun.* **2014**, *5*, 3827. [CrossRef]
89. Bartels, T.; Ahlstrom, L.S.; Leftin, A.; Kamp, F.; Haass, C.; Brown, M.F.; Beyer, K. The N-terminus of the intrinsically disordered protein α-synuclein triggers membrane binding and helix folding. *Biophys. J.* **2010**, *99*, 2116–2124. [CrossRef]
90. Burré, J.; Sharma, M.; Tsetsenis, T.; Buchman, V.; Etherton, M.R.; Südhof, T.C. α-Synuclein promotes SNARE-complex assembly in vivo and in vitro. *Science* **2010**, *329*, 1663–1667. [CrossRef] [PubMed]
91. Fusco, G.; Pape, T.; Stephens, A.D.; Mahou, P.; Costa, A.R.; Kaminski, C.F.; Kaminski Schierle, G.S.; Vendruscolo, M.; Veglia, G.; Dobson, C.M. Structural basis of synaptic vesicle assembly promoted by α-synuclein. *Nat. Commun.* **2016**, *7*, 12563. [CrossRef] [PubMed]

92. Cremades, N.; Cohen, S.I.; Deas, E.; Abramov, A.Y.; Chen, A.Y.; Orte, A.; Sandal, M.; Clarke, R.W.; Dunne, P.; Aprile, F.A. Direct observation of the interconversion of normal and toxic forms of α-synuclein. *Cell* **2012**, *149*, 1048–1059. [CrossRef]
93. Grey, M.; Linse, S.; Nilsson, H.; Brundin, P.; Sparr, E. Membrane interaction of α-synuclein in different aggregation states. *J. Park. Dis.* **2011**, *1*, 359–371. [CrossRef]
94. Fanning, S.; Selkoe, D.; Dettmer, U. Parkinson's disease: Proteinopathy or lipidopathy? *NPJ Park. Dis.* **2020**, *6*, 3. [CrossRef]
95. Klemann, C.; Martens, G.J.M.; Sharma, M.; Martens, M.B.; Isacson, O.; Gasser, T.; Visser, J.E.; Poelmans, G. Integrated molecular landscape of Parkinson's disease. *NPJ Park. Dis.* **2017**, *3*, 14. [CrossRef]
96. Golovko, M.Y.; Faergeman, N.J.; Cole, N.B.; Castagnet, P.I.; Nussbaum, R.L.; Murphy, E.J. α-synuclein gene deletion decreases brain palmitate uptake and alters the palmitate metabolism in the absence of α-synuclein palmitate binding. *Biochemistry* **2005**, *44*, 8251–8259. [CrossRef] [PubMed]
97. Golovko, M.Y.; Rosenberger, T.A.; Faergeman, N.J.; Feddersen, S.; Cole, N.B.; Pribill, I.; Berger, J.; Nussbaum, R.L.; Murphy, E.J. Acyl-CoA synthetase activity links wild-type but not mutant α-synuclein to brain arachidonate metabolism. *Biochemistry* **2006**, *45*, 6956–6966. [CrossRef]
98. Golovko, M.Y.; Rosenberger, T.A.; Feddersen, S.; Færgeman, N.J.; Murphy, E.J. α-Synuclein gene ablation increases docosahexaenoic acid incorporation and turnover in brain phospholipids. *J. Neurochem.* **2007**, *101*, 201–211. [CrossRef]
99. Campos, S.S.; Alza, N.P.; Salvador, G.A. Lipid metabolism alterations in the neuronal response to A53T α-synuclein and Fe-induced injury. *Arch. Biochem. Biophys.* **2018**, *655*, 43–54. [CrossRef] [PubMed]
100. Barceló-Coblijn, G.; Golovko, M.Y.; Weinhofer, I.; Berger, J.; Murphy, E.J. Brain neutral lipids mass is increased in α-synuclein gene-ablated mice. *J. Neurochem.* **2007**, *101*, 132–141. [CrossRef]
101. Ruipérez, V.; Darios, F.; Davletov, B. Alpha-synuclein, lipids and Parkinson's disease. *Prog. Lipid Res.* **2010**, *49*, 420–428. [CrossRef] [PubMed]
102. Xicoy, H.; Wieringa, B.; Martens, G.J. The role of lipids in Parkinson's disease. *Cells* **2019**, *8*, 27. [CrossRef]
103. Jin, U.; Park, S.J.; Park, S.M. Cholesterol metabolism in the brain and its association with Parkinson's disease. *Exp. Neurobiol.* **2019**, *28*, 554. [CrossRef]
104. Huang, X.; Sterling, N.W.; Du, G.; Sun, D.; Stetter, C.; Kong, L.; Zhu, Y.; Neighbors, J.; Lewis, M.M.; Chen, H. Brain cholesterol metabolism and Parkinson's disease. *Mov. Disord.* **2019**, *34*, 386–395. [CrossRef] [PubMed]
105. Indellicato, R.; Trinchera, M. The link between Gaucher disease and Parkinson's disease sheds light on old and novel disorders of sphingolipid metabolism. *Int. J. Mol. Sci.* **2019**, *20*, 3304. [CrossRef] [PubMed]
106. Quinville, B.M.; Deschenes, N.M.; Ryckman, A.E.; Walia, J.S. A comprehensive review: Sphingolipid metabolism and implications of disruption in sphingolipid homeostasis. *Int. J. Mol. Sci.* **2021**, *22*, 5793. [CrossRef] [PubMed]
107. Fanning, S.; Haque, A.; Imberdis, T.; Baru, V.; Barrasa, M.I.; Nuber, S.; Termine, D.; Ramalingam, N.; Ho, G.P.H.; Noble, T.; et al. Lipidomic Analysis of alpha-Synuclein Neurotoxicity Identifies Stearoyl CoA Desaturase as a Target for Parkinson Treatment. *Mol. Cell* **2019**, *73*, 1001–1014. [CrossRef]
108. Yoo, D.; Lim, Y.; Son, Y.; Rho, H.; Shin, C.; Ahn, T.-B. Dietary intake and plasma levels of polyunsaturated fatty acids in early-stage Parkinson's disease. *Sci. Rep.* **2021**, *11*, 12489. [CrossRef]
109. Assayag, K.; Yakunin, E.; Loeb, V.; Selkoe, D.J.; Sharon, R. Polyunsaturated fatty acids induce α-synuclein-related pathogenic changes in neuronal cells. *Am. J. Pathol.* **2007**, *171*, 2000–2011. [CrossRef]
110. Sharon, R.; Bar-Joseph, I.; Mirick, G.E.; Serhan, C.N.; Selkoe, D.J. Altered fatty acid composition of dopaminergic neurons expressing α-synuclein and human brains with α-synucleinopathies. *J. Biol. Chem.* **2003**, *278*, 49874–49881. [CrossRef]
111. Cheng, D.; Jenner, A.M.; Shui, G.; Cheong, W.F.; Mitchell, T.W.; Nealon, J.R.; Kim, W.S.; McCann, H.; Wenk, M.R.; Halliday, G.M. Lipid pathway alterations in Parkinson's disease primary visual cortex. *PLoS ONE* **2011**, *6*, e17299. [CrossRef]
112. García-Sanz, P.; Orgaz, L.; Fuentes, J.M.; Vicario, C.; Moratalla, R. Cholesterol and multilamellar bodies: Lysosomal dysfunction in GBA-Parkinson disease. *Autophagy* **2018**, *14*, 717–718. [CrossRef]
113. Paul, R.; Choudhury, A.; Kumar, S.; Giri, A.; Sandhir, R.; Borah, A. Cholesterol contributes to dopamine-neuronal loss in MPTP mouse model of Parkinson's disease: Involvement of mitochondrial dysfunctions and oxidative stress. *PLoS ONE* **2017**, *12*, e0171285. [CrossRef]
114. Raju, A.; Jaisankar, P.; Borah, A.; Mohanakumar, K.P. 1-methyl-4-phenylpyridinium-induced death of differentiated SH-SY5Y neurons is potentiated by cholesterol. *Ann. Neurosci.* **2017**, *24*, 243–251. [CrossRef]
115. Mullin, S.; Hughes, D.; Mehta, A.; Schapira, A. Neurological effects of glucocerebrosidase gene mutations. *Eur. J. Neurol.* **2019**, *26*, 388-e329. [CrossRef] [PubMed]
116. McCampbell, A.; Truong, D.; Broom, D.C.; Allchorne, A.; Gable, K.; Cutler, R.G.; Mattson, M.P.; Woolf, C.J.; Frosch, M.P.; Harmon, J.M. Mutant SPTLC1 dominantly inhibits serine palmitoyltransferase activity in vivo and confers an age-dependent neuropathy. *Hum. Mol. Genet* **2005**, *14*, 3507–3521. [CrossRef]
117. Simons, K.; Ikonen, E. Functional rafts in cell membranes. *Nature* **1997**, *387*, 569–572. [CrossRef] [PubMed]
118. Hannun, Y.A.; Obeid, L.M. Principles of bioactive lipid signalling: Lessons from sphingolipids. *Nat. Rev. Mol. Cell Biol.* **2008**, *9*, 139–150. [CrossRef]
119. Futerman, A.H.; Riezman, H. The ins and outs of sphingolipid synthesis. *Trends Cell Biol.* **2005**, *15*, 312–318. [CrossRef]
120. Farmer, K.; Smith, C.A.; Hayley, S.; Smith, J. Major alterations of phosphatidylcholine and lysophosphotidylcholine lipids in the substantia nigra using an early stage model of Parkinson's disease. *Int. J. Mol. Sci.* **2015**, *16*, 18865–18877. [CrossRef]

121. Lobasso, S.; Tanzarella, P.; Vergara, D.; Maffia, M.; Cocco, T.; Corcelli, A. Lipid profiling of parkin-mutant human skin fibroblasts. *J. Cell. Physiol.* **2017**, *232*, 3540–3551. [CrossRef] [PubMed]
122. Cunningham, T.J.; Yao, L.; Lucena, A. Product inhibition of secreted phospholipase A2 may explain lysophosphatidylcholines' unexpected therapeutic properties. *J. Inflamm.* **2008**, *5*, 17. [CrossRef]
123. Riekkinen, P.; Rinne, U.K.; Pelliniemi, T.-T.; Sonninen, V. Interaction between dopamine and phospholipids: Studies of the substantia nigra in parkinson disease patients. *Arch. Neurol.* **1975**, *32*, 25–27. [CrossRef] [PubMed]
124. Hattingen, E.; Magerkurth, J.; Pilatus, U.; Mozer, A.; Seifried, C.; Steinmetz, H.; Zanella, F.; Hilker, R. Phosphorus and proton magnetic resonance spectroscopy demonstrates mitochondrial dysfunction in early and advanced Parkinson's disease. *Brain* **2009**, *132*, 3285–3297. [CrossRef]
125. Wang, S.; Zhang, S.; Liou, L.-C.; Ren, Q.; Zhang, Z.; Caldwell, G.A.; Caldwell, K.A.; Witt, S.N. Phosphatidylethanolamine deficiency disrupts α-synuclein homeostasis in yeast and worm models of Parkinson disease. *Proc. Natl. Acad. Sci. USA* **2014**, *111*, E3976–E3985. [CrossRef] [PubMed]
126. Wood, P.L.; Tippireddy, S.; Feriante, J.; Woltjer, R.L. Augmented frontal cortex diacylglycerol levels in Parkinson's disease and Lewy Body Disease. *PLoS ONE* **2018**, *13*, e0191815. [CrossRef]
127. Nakamura, K.; Nemani, V.M.; Wallender, E.K.; Kaehlcke, K.; Ott, M.; Edwards, R.H. Optical reporters for the conformation of α-synuclein reveal a specific interaction with mitochondria. *J. Neurosci.* **2008**, *28*, 12305–12317. [CrossRef] [PubMed]
128. Parihar, M.; Parihar, A.; Fujita, M.; Hashimoto, M.; Ghafourifar, P. Mitochondrial association of alpha-synuclein causes oxidative stress. *Cell. Mol. Life Sci.* **2008**, *65*, 1272–1284. [CrossRef] [PubMed]
129. Banerjee, K.; Sinha, M.; Pham, C.L.L.; Jana, S.; Chanda, D.; Cappai, R.; Chakrabarti, S. α-Synuclein induced membrane depolarization and loss of phosphorylation capacity of isolated rat brain mitochondria: Implications in Parkinson's disease. *FEBS Lett.* **2010**, *584*, 1571–1576. [CrossRef] [PubMed]
130. Bodner, C.R.; Dobson, C.M.; Bax, A. Multiple tight phospholipid-binding modes of α-synuclein revealed by solution NMR spectroscopy. *J. Mol. Biol.* **2009**, *390*, 775–790. [CrossRef]
131. Pancoe, S.X.; Wang, Y.J.; Shimogawa, M.; Perez, R.M.; Giannakoulias, S.; Petersson, E.J. Effects of Mutations and Post-Translational Modifications on α-Synuclein In Vitro Aggregation. *J. Mol. Biol.* **2022**, *434*, 167859. [CrossRef] [PubMed]
132. Daida, K.; Shimonaka, S.; Shiba-Fukushima, K.; Ogata, J.; Yoshino, H.; Okuzumi, A.; Hatano, T.; Motoi, Y.; Hirunagi, T.; Katsuno, M. α-Synuclein V15A Variant in Familial Parkinson's Disease Exhibits a Weaker Lipid-Binding Property. *Mov. Disord.* **2022**, *37*, 2075–2085. [CrossRef]
133. Grassel, A.; Borland, C.; Bertolotti, F.; Osselborn, R.; Nassuna, T.; Zabat, B.; DebBurman, S. Insight into Parkinson's Disease From a Yeast Model: How Three Alpha-Synuclein Mutants (A18T, A29S, & A53V) Generate Toxicity. *FASEB J.* **2022**, *36*. [CrossRef]
134. Kim, Y.S.; Laurine, E.; Woods, W.; Lee, S.-J. A novel mechanism of interaction between α-synuclein and biological membranes. *J. Mol. Biol.* **2006**, *360*, 386–397. [CrossRef]
135. Kuwahara, T.; Tonegawa, R.; Ito, G.; Mitani, S.; Iwatsubo, T. Phosphorylation of α-synuclein protein at Ser-129 reduces neuronal dysfunction by lowering its membrane binding property in Caenorhabditis elegans. *J. Biol. Chem.* **2012**, *287*, 7098–7109. [CrossRef]
136. Ruf, V.C.; Nubling, G.S.; Willikens, S.; Shi, S.; Schmidt, F.; Levin, J.; Botzel, K.; Kamp, F.; Giese, A. Different Effects of alpha-Synuclein Mutants on Lipid Binding and Aggregation Detected by Single Molecule Fluorescence Spectroscopy and ThT Fluorescence-Based Measurements. *ACS Chem. Neurosci.* **2019**, *10*, 1649–1659. [CrossRef] [PubMed]
137. Rovere, M.; Powers, A.E.; Jiang, H.; Pitino, J.C.; Fonseca-Ornelas, L.; Patel, D.S.; Achille, A.; Langen, R.; Varkey, J.; Bartels, T. E46K-like alpha-synuclein mutants increase lipid interactions and disrupt membrane selectivity. *J. Biol. Chem.* **2019**, *294*, 9799–9812. [CrossRef] [PubMed]
138. Fredenburg, R.A.; Rospigliosi, C.; Meray, R.K.; Kessler, J.C.; Lashuel, H.A.; Eliezer, D.; Lansbury, P.T. The impact of the E46K mutation on the properties of α-synuclein in its monomeric and oligomeric states. *Biochemistry* **2007**, *46*, 7107–7118. [CrossRef] [PubMed]
139. Khalaf, O.; Fauvet, B.; Oueslati, A.; Dikiy, I.; Mahul-Mellier, A.L.; Ruggeri, F.S.; Mbefo, M.K.; Vercruysse, F.; Dietler, G.; Lee, S.J.; et al. The H50Q mutation enhances alpha-synuclein aggregation, secretion, and toxicity. *J. Biol. Chem.* **2014**, *289*, 21856–21876. [CrossRef]
140. Mohite, G.M.; Kumar, R.; Panigrahi, R.; Navalkar, A.; Singh, N.; Datta, D.; Mehra, S.; Ray, S.; Gadhe, L.G.; Das, S. Comparison of kinetics, toxicity, oligomer formation, and membrane binding capacity of α-synuclein familial mutations at the A53 site, including the newly discovered A53V mutation. *Biochemistry* **2018**, *57*, 5183–5187. [CrossRef]
141. Ghosh, D.; Sahay, S.; Ranjan, P.; Salot, S.; Mohite, G.M.; Singh, P.K.; Dwivedi, S.; Carvalho, E.; Banerjee, R.; Kumar, A. The newly discovered Parkinson's disease associated Finnish mutation (A53E) attenuates α-synuclein aggregation and membrane binding. *Biochemistry* **2014**, *53*, 6419–6421. [CrossRef]
142. Perissinotto, F.; Stani, C.; De Cecco, E.; Vaccari, L.; Rondelli, V.; Posocco, P.; Parisse, P.; Scaini, D.; Legname, G.; Casalis, L. Iron-mediated interaction of alpha synuclein with lipid raft model membranes. *Nanoscale* **2020**, *12*, 7631–7640. [CrossRef]
143. Xiang, W.; Menges, S.; Schlachetzki, J.; Meixner, H.; Hoffmann, A.-C.; Schlötzer-Schrehardt, U.; Becker, C.-M.; Winkler, J.; Klucken, J. Posttranslational modification and mutation of histidine 50 trigger alpha synuclein aggregation and toxicity. *Mol. Neurodegener.* **2015**, *10*, 8. [CrossRef]
144. Vilariño-Güell, C.; Wider, C.; Ross, O.A.; Dachsel, J.C.; Kachergus, J.M.; Lincoln, S.J.; Soto-Ortolaza, A.I.; Cobb, S.A.; Wilhoite, G.J.; Bacon, J.A. VPS35 mutations in Parkinson disease. *Am. J. Hum. Genet* **2011**, *89*, 162–167. [CrossRef]

145. Patel, D.; Witt, S.N. Sorting Out the Role of α-Synuclein in Retromer-Mediated Endosomal Protein Sorting. *J. Exp. Neurosci.* **2018**, *12*, 1179069518796215. [CrossRef]
146. Rajasekaran, S.; Peterson, P.P.; Liu, Z.; Robinson, L.C.; Witt, S.N. α-synuclein inhibits Snx3-retromer retrograde trafficking of the conserved membrane-bound proprotein convertase Kex2 in the secretory pathway of Saccharomyces cerevisiae. *Hum. Mol. Genet* **2022**, *31*, 705–717. [CrossRef]
147. He, S.; Wang, F.; Yung, K.K.L.; Zhang, S.; Qu, S. Effects of α-Synuclein-associated post-translational modifications in Parkinson's disease. *ACS Chem. Neurosci.* **2021**, *12*, 1061–1071. [CrossRef] [PubMed]
148. Schaffert, L.-N.; Carter, W.G. Do post-translational modifications influence protein aggregation in neurodegenerative diseases: A systematic review. *Brain Sci.* **2020**, *10*, 232. [CrossRef] [PubMed]
149. Delenclos, M.; Burgess, J.D.; Lamprokostopoulou, A.; Outeiro, T.F.; Vekrellis, K.; McLean, P.J. Cellular models of alpha-synuclein toxicity and aggregation. *J. Neurochem.* **2019**, *150*, 566–576. [CrossRef]
150. Gadhavi, J.; Patel, M.; Bhatia, D.; Gupta, S. Neurotoxic or neuroprotective: Post-translational modifications of α-synuclein at the cross-roads of functions. *Biochimie* **2022**, *192*, 38–50. [CrossRef]
151. Oueslati, A.; Fournier, M.; Lashuel, H.A. Role of post-translational modifications in modulating the structure, function and toxicity of α-synuclein: Implications for Parkinson's disease pathogenesis and therapies. *Prog. Brain Res.* **2010**, *183*, 115–145. [PubMed]
152. Mahul-Mellier, A.-L.; Fauvet, B.; Gysbers, A.; Dikiy, I.; Oueslati, A.; Georgeon, S.; Lamontanara, A.J.; Bisquertt, A.; Eliezer, D.; Masliah, E. c-Abl phosphorylates α-synuclein and regulates its degradation: Implication for α-synuclein clearance and contribution to the pathogenesis of Parkinson's disease. *Hum. Mol. Genet* **2014**, *23*, 2858–2879. [CrossRef]
153. Paleologou, K.E.; Oueslati, A.; Shakked, G.; Rospigliosi, C.C.; Kim, H.-Y.; Lamberto, G.R.; Fernandez, C.O.; Schmid, A.; Chegini, F.; Gai, W.P. Phosphorylation at S87 is enhanced in synucleinopathies, inhibits α-synuclein oligomerization, and influences synuclein-membrane interactions. *J. Neurosci.* **2010**, *30*, 3184–3198. [CrossRef]
154. Nubling, G.S.; Levin, J.; Bader, B.; Lorenzl, S.; Hillmer, A.; Hogen, T.; Kamp, F.; Giese, A. Modelling Ser129 phosphorylation inhibits membrane binding of pore-forming alpha-synuclein oligomers. *PLoS ONE* **2014**, *9*, e98906. [CrossRef] [PubMed]
155. Ma, M.-R.; Hu, Z.-W.; Zhao, Y.-F.; Chen, Y.-X.; Li, Y.-M. Phosphorylation induces distinct alpha-synuclein strain formation. *Sci. Rep.* **2016**, *6*, 37130. [CrossRef]
156. Samuel, F.; Flavin, W.P.; Iqbal, S.; Pacelli, C.; Renganathan, S.D.S.; Trudeau, L.-E.; Campbell, E.M.; Fraser, P.E.; Tandon, A. Effects of serine 129 phosphorylation on α-synuclein aggregation, membrane association, and internalization. *J. Biol. Chem.* **2016**, *291*, 4374–4385. [CrossRef] [PubMed]
157. Runfola, M.; De Simone, A.; Vendruscolo, M.; Dobson, C.M.; Fusco, G. The N-terminal acetylation of α-synuclein changes the affinity for lipid membranes but not the structural properties of the bound state. *Sci. Rep.* **2020**, *10*, 204. [CrossRef]
158. Sevcsik, E.; Trexler, A.J.; Dunn, J.M.; Rhoades, E. Allostery in a disordered protein: Oxidative modifications to α-synuclein act distally to regulate membrane binding. *J. Am. Chem. Soc.* **2011**, *133*, 7152–7158. [CrossRef]
159. Lewis, Y.E.; Abeywardana, T.; Lin, Y.H.; Galesic, A.; Pratt, M.R. Synthesis of a Bis-thio-acetone (BTA) Analogue of the Lysine Isopeptide Bond and its Application to Investigate the Effects of Ubiquitination and SUMOylation on α-Synuclein Aggregation and Toxicity. *ACS Chem. Biol.* **2016**, *11*, 931–942. [CrossRef] [PubMed]
160. Hejjaoui, M.; Haj-Yahya, M.; Kumar, K.A.; Brik, A.; Lashuel, H.A. Towards Elucidation of the Role of Ubiquitination in the Pathogenesis of Parkinson's Disease with Semisynthetic Ubiquitinated α-Synuclein. *Angew. Chem. Int. Ed.* **2011**, *50*, 405–409. [CrossRef] [PubMed]
161. Caparotta, M.; Bustos, D.M.; Masone, D. Order–disorder skewness in alpha-synuclein: A key mechanism to recognize membrane curvature. *Phys. Chem. Chem. Phys.* **2020**, *22*, 5255–5263. [CrossRef]
162. van der Wateren, I.M.; Knowles, T.P.; Buell, A.K.; Dobson, C.M.; Galvagnion, C. C-terminal truncation of α-synuclein promotes amyloid fibril amplification at physiological pH. *Chem. Sci.* **2018**, *9*, 5506–5516. [CrossRef]
163. Flynn, J.D.; Gimmen, M.Y.; Dean, D.N.; Lacy, S.M.; Lee, J.C. Terminal Alkynes as Raman Probes of α-Synuclein in Solution and in Cells. *ChemBioChem* **2020**, *21*, 1582–1586. [CrossRef] [PubMed]
164. Faustini, G.; Longhena, F.; Bruno, A.; Bono, F.; Grigoletto, J.; La Via, L.; Barbon, A.; Casiraghi, A.; Straniero, V.; Valoti, E. Alpha-synuclein/synapsin III pathological interplay boosts the motor response to methylphenidate. *Neurobiol. Dis.* **2020**, *138*, 104789. [CrossRef] [PubMed]
165. Ma, L.; Yang, C.; Zhang, X.; Li, Y.; Wang, S.; Zheng, L.; Huang, K. C-terminal truncation exacerbates the aggregation and cytotoxicity of α-Synuclein: A vicious cycle in Parkinson's disease. *Biochim. Biophys. Acta (BBA)-Mol. Basis Dis.* **2018**, *1864*, 3714–3725. [CrossRef]
166. Levine, P.M.; Galesic, A.; Balana, A.T.; Mahul-Mellier, A.-L.; Navarro, M.X.; De Leon, C.A.; Lashuel, H.A.; Pratt, M.R. α-Synuclein O-GlcNAcylation alters aggregation and toxicity, revealing certain residues as potential inhibitors of Parkinson's disease. *Proc. Natl. Acad. Sci. USA* **2019**, *116*, 1511–1519. [CrossRef] [PubMed]
167. Uceda, A.B.; Frau, J.; Vilanova, B.; Adrover, M. Glycation of alpha-synuclein hampers its binding to synaptic-like vesicles and its driving effect on their fusion. *Cell Mol. Life Sci.* **2022**, *79*, 342. [CrossRef]
168. Manning, G.; Whyte, D.B.; Martinez, R.; Hunter, T.; Sudarsanam, S. The protein kinase complement of the human genome. *Science* **2002**, *298*, 1912–1934. [CrossRef]
169. Cohen, P. The structure and regulation of protein phosphatases. *Annu. Rev. Biochem.* **1989**, *58*, 453–508. [CrossRef]

170. Cohen, P. The origins of protein phosphorylation. *Nat. Cell Biol.* **2002**, *4*, E127–E130. [CrossRef]
171. Anderson, J.P.; Walker, D.E.; Goldstein, J.M.; De Laat, R.; Banducci, K.; Caccavello, R.J.; Barbour, R.; Huang, J.; Kling, K.; Lee, M. Phosphorylation of Ser-129 is the dominant pathological modification of α-synuclein in familial and sporadic Lewy body disease. *J. Biol. Chem.* **2006**, *281*, 29739–29752. [CrossRef]
172. Kosten, J.; Binolfi, A.; Stuiver, M.; Verzini, S.; Theillet, F.-X.; Bekei, B.; van Rossum, M.; Selenko, P. Efficient modification of alpha-synuclein serine 129 by protein kinase CK1 requires phosphorylation of tyrosine 125 as a priming event. *ACS Chem. Neurosci.* **2014**, *5*, 1203–1208. [CrossRef] [PubMed]
173. Zheng, W.; Zhang, Z.; Ye, Y.; Wu, Q.; Liu, M.; Li, C. Phosphorylation dependent α-synuclein degradation monitored by in-cell NMR. *Chem. Commun.* **2019**, *55*, 11215–11218. [CrossRef] [PubMed]
174. Schreurs, S.; Gerard, M.; Derua, R.; Waelkens, E.; Taymans, J.-M.; Baekelandt, V.; Engelborghs, Y. In vitro phosphorylation does not influence the aggregation kinetics of WT α-synuclein in contrast to its phosphorylation mutants. *Int. J. Mol. Sci.* **2014**, *15*, 1040–1067. [CrossRef] [PubMed]
175. Brahmachari, S.; Ge, P.; Lee, S.H.; Kim, D.; Karuppagounder, S.S.; Kumar, M.; Mao, X.; Shin, J.H.; Lee, Y.; Pletnikova, O. Activation of tyrosine kinase c-Abl contributes to α-synuclein–induced neurodegeneration. *J. Clin. Investig.* **2016**, *126*, 2970–2988. [CrossRef]
176. McFarland, N.R.; Fan, Z.; Xu, K.; Schwarzschild, M.A.; Feany, M.B.; Hyman, B.T.; McLean, P.J. α-Synuclein S129 phosphorylation mutants do not alter nigrostriatal toxicity in a rat model of parkinson disease. *J. Neuropathol. Exp. Neurol.* **2009**, *68*, 515–524. [CrossRef]
177. Dikiy, I.; Eliezer, D. N-terminal acetylation stabilizes N-terminal helicity in lipid- and micelle-bound alpha-synuclein and increases its affinity for physiological membranes. *J. Biol. Chem.* **2014**, *289*, 3652–3665. [CrossRef] [PubMed]
178. Bhattacharjee, P.; Öhrfelt, A.; Lashley, T.; Blennow, K.; Brinkmalm, A.; Zetterberg, H. Mass spectrometric analysis of Lewy body-enriched α-synuclein in Parkinson's disease. *J. Proteome Res.* **2019**, *18*, 2109–2120. [CrossRef]
179. Kang, L.; Moriarty, G.M.; Woods, L.A.; Ashcroft, A.E.; Radford, S.E.; Baum, J. N-Terminal acetylation of α-synuclein induces increased transient helical propensity and decreased aggregation rates in the intrinsically disordered monomer. *Protein Sci.* **2012**, *21*, 911–917. [CrossRef] [PubMed]
180. O'Leary, E.I.; Jiang, Z.; Strub, M.-P.; Lee, J.C. Effects of phosphatidylcholine membrane fluidity on the conformation and aggregation of N-terminally acetylated α-synuclein. *J. Biol. Chem.* **2018**, *293*, 11195–11205. [CrossRef]
181. Good, P.F.; Hsu, A.; Werner, P.; Perl, D.P.; Olanow, C.W. Protein nitration in Parkinson's disease. *J. Neuropathol. Exp. Neurol.* **1998**, *57*, 338–342. [CrossRef] [PubMed]
182. Paxinou, E.; Chen, Q.; Weisse, M.; Giasson, B.I.; Norris, E.H.; Rueter, S.M.; Trojanowski, J.Q.; Lee, V.M.-Y.; Ischiropoulos, H. Induction of α-synuclein aggregation by intracellular nitrative insult. *J. Neurosci.* **2001**, *21*, 8053–8061. [CrossRef] [PubMed]
183. Giasson, B.I.; Duda, J.E.; Murray, I.V.; Chen, Q.; Souza, J.M.; Hurtig, H.I.; Ischiropoulos, H.; Trojanowski, J.Q.; Lee, V.M. Oxidative damage linked to neurodegeneration by selective α-synuclein nitration in synucleinopathy lesions. *Science* **2000**, *290*, 985–989. [CrossRef]
184. Xiang, W.; Schlachetzki, J.C.; Helling, S.; Bussmann, J.C.; Berlinghof, M.; Schäffer, T.E.; Marcus, K.; Winkler, J.; Klucken, J.; Becker, C.-M. Oxidative stress-induced posttranslational modifications of alpha-synuclein: Specific modification of alpha-synuclein by 4-hydroxy-2-nonenal increases dopaminergic toxicity. *Mol. Cell. Neurosci.* **2013**, *54*, 71–83. [CrossRef]
185. Liu, Y.; Qiang, M.; Wei, Y.; He, R. A novel molecular mechanism for nitrated α-synuclein-induced cell death. *J. Mol. Cell. Biol.* **2011**, *3*, 239–249. [CrossRef] [PubMed]
186. Yu, Z.; Xu, X.; Xiang, Z.; Zhou, J.; Zhang, Z.; Hu, C.; He, C. Nitrated α-synuclein induces the loss of dopaminergic neurons in the substantia nigra of rats. *PLoS ONE* **2010**, *5*, e9956. [CrossRef]
187. Rape, M.; Komander, D. The ubiquitin code. *Annu. Rev. Biochem.* **2012**, *81*, 203–229.
188. Kuzuhara, S.; Mori, H.; Izumiyama, N.; Yoshimura, M.; Ihara, Y. Lewy bodies are ubiquitinated. *Acta Neuropathol.* **1988**, *75*, 345–353. [CrossRef] [PubMed]
189. Meier, F.; Abeywardana, T.; Dhall, A.; Marotta, N.P.; Varkey, J.; Langen, R.; Chatterjee, C.; Pratt, M.R. Semisynthetic, site-specific ubiquitin modification of α-synuclein reveals differential effects on aggregation. *J. Am. Chem. Soc.* **2012**, *134*, 5468–5471. [CrossRef]
190. Iyer, A.; Claessens, M.M. Disruptive membrane interactions of alpha-synuclein aggregates. *Biochim. Biophys. Acta (BBA)-Proteins Proteom.* **2019**, *1867*, 468–482. [CrossRef] [PubMed]
191. Kim, K.S.; Choi, Y.R.; Park, J.-Y.; Lee, J.-H.; Kim, D.K.; Lee, S.-J.; Paik, S.R.; Jou, I.; Park, S.M. Proteolytic cleavage of extracellular α-synuclein by plasmin: Implications for Parkinson disease. *J. Biol. Chem.* **2012**, *287*, 24862–24872. [CrossRef] [PubMed]
192. Iwata, A.; Maruyama, M.; Akagi, T.; Hashikawa, T.; Kanazawa, I.; Tsuji, S.; Nukina, N. Alpha-synuclein degradation by serine protease neurosin: Implication for pathogenesis of synucleinopathies. *Hum. Mol. Genet* **2003**, *12*, 2625–2635. [CrossRef]
193. Sevlever, D.; Jiang, P.; Yen, S.-H.C. Cathepsin D is the main lysosomal enzyme involved in the degradation of α-synuclein and generation of its carboxy-terminally truncated species. *Biochemistry* **2008**, *47*, 9678–9687. [CrossRef] [PubMed]
194. Wang, W.; Nguyen, L.T.; Burlak, C.; Chegini, F.; Guo, F.; Chataway, T.; Ju, S.; Fisher, O.S.; Miller, D.W.; Datta, D. Caspase-1 causes truncation and aggregation of the Parkinson's disease-associated protein α-synuclein. *Proc. Natl. Acad. Sci. USA* **2016**, *113*, 9587–9592. [CrossRef]
195. Diepenbroek, M.; Casadei, N.; Esmer, H.; Saido, T.C.; Takano, J.; Kahle, P.J.; Nixon, R.A.; Rao, M.V.; Melki, R.; Pieri, L. Overexpression of the calpain-specific inhibitor calpastatin reduces human alpha-Synuclein processing, aggregation and synaptic impairment in [A30P] αSyn transgenic mice. *Hum. Mol. Genet* **2014**, *23*, 3975–3989. [CrossRef] [PubMed]

196. Terada, M.; Suzuki, G.; Nonaka, T.; Kametani, F.; Tamaoka, A.; Hasegawa, M. The effect of truncation on prion-like properties of α-synuclein. *J. Biol. Chem.* **2018**, *293*, 13910–13920. [CrossRef] [PubMed]
197. Kellie, J.F.; Higgs, R.E.; Ryder, J.W.; Major, A.; Beach, T.G.; Adler, C.H.; Merchant, K.; Knierman, M.D. Quantitative measurement of intact alpha-synuclein proteoforms from post-mortem control and Parkinson's disease brain tissue by intact protein mass spectrometry. *Sci. Rep.* **2014**, *4*, 5797. [CrossRef] [PubMed]
198. Sorrentino, Z.A.; Giasson, B.I. The emerging role of α-synuclein truncation in aggregation and disease. *J. Biol. Chem.* **2020**, *295*, 10224–10244. [CrossRef] [PubMed]
199. Öhrfelt, A.; Zetterberg, H.; Andersson, K.; Persson, R.; Secic, D.; Brinkmalm, G.; Wallin, A.; Mulugeta, E.; Francis, P.T.; Vanmechelen, E. Identification of novel α-synuclein isoforms in human brain tissue by using an online nanoLC-ESI-FTICR-MS method. *Neurochem. Res.* **2011**, *36*, 2029–2042. [CrossRef]
200. Murray, I.V.; Giasson, B.I.; Quinn, S.M.; Koppaka, V.; Axelsen, P.H.; Ischiropoulos, H.; Trojanowski, J.Q.; Lee, V.M.-Y. Role of α-synuclein carboxy-terminus on fibril formation in vitro. *Biochemistry* **2003**, *42*, 8530–8540. [CrossRef] [PubMed]
201. Michell, A.W.; Tofaris, G.; Gossage, H.; Tyers, P.; Spillantini, M.; Barker, R. The effect of truncated human α-synuclein (1–120) on dopaminergic cells in a transgenic mouse model of Parkinson's disease. *Cell Transplant.* **2007**, *16*, 461–474. [CrossRef] [PubMed]
202. Sorrentino, Z.A.; Vijayaraghavan, N.; Gorion, K.-M.; Riffe, C.J.; Strang, K.H.; Caldwell, J.; Giasson, B.I. Physiological C-terminal truncation of α-synuclein potentiates the prion-like formation of pathological inclusions. *J. Biol. Chem.* **2018**, *293*, 18914–18932. [CrossRef]
203. Torres, C.-R.; Hart, G.W. Topography and polypeptide distribution of terminal N-acetylglucosamine residues on the surfaces of intact lymphocytes. Evidence for O-linked GlcNAc. *J. Biol. Chem.* **1984**, *259*, 3308–3317. [CrossRef]
204. Wang, Z.; Park, K.; Comer, F.; Hsieh-Wilson, L.C.; Saudek, C.D.; Hart, G.W. Site-specific GlcNAcylation of human erythrocyte proteins: Potential biomarker (s) for diabetes. *Diabetes* **2009**, *58*, 309–317. [CrossRef] [PubMed]
205. Alfaro, J.F.; Gong, C.-X.; Monroe, M.E.; Aldrich, J.T.; Clauss, T.R.; Purvine, S.O.; Wang, Z.; Camp, D.G.; Shabanowitz, J.; Stanley, P. Tandem mass spectrometry identifies many mouse brain O-GlcNAcylated proteins including EGF domain-specific O-GlcNAc transferase targets. *Proc. Natl. Acad. Sci. USA* **2012**, *109*, 7280–7285. [CrossRef]
206. Wang, S.; Yang, F.; Petyuk, V.A.; Shukla, A.K.; Monroe, M.E.; Gritsenko, M.A.; Rodland, K.D.; Smith, R.D.; Qian, W.J.; Gong, C.X. Quantitative proteomics identifies altered O-GlcNAcylation of structural, synaptic and memory-associated proteins in Alzheimer's disease. *J. Pathol.* **2017**, *243*, 78–88. [CrossRef] [PubMed]
207. Marotta, N.P.; Lin, Y.H.; Lewis, Y.E.; Ambroso, M.R.; Zaro, B.W.; Roth, M.T.; Arnold, D.B.; Langen, R.; Pratt, M.R. O-GlcNAc modification blocks the aggregation and toxicity of the protein α-synuclein associated with Parkinson's disease. *Nat. Chem.* **2015**, *7*, 913–920. [CrossRef]
208. Ryan, P.; Xu, M.; Davey, A.K.; Danon, J.J.; Mellick, G.D.; Kassiou, M.; Rudrawar, S. O-GlcNAc modification protects against protein misfolding and aggregation in neurodegenerative disease. *ACS Chem. Neurosci.* **2019**, *10*, 2209–2221. [CrossRef] [PubMed]
209. Salahuddin, P.; Rabbani, G.; Khan, R. The role of advanced glycation end products in various types of neurodegenerative disease: A therapeutic approach. *Cell. Mol. Biol. Lett.* **2014**, *19*, 407–437. [CrossRef]
210. Choi, Y.-G.; Lim, S. Nε-(carboxymethyl) lysine linkage to α-synuclein and involvement of advanced glycation end products in α-synuclein deposits in an MPTP-intoxicated mouse model. *Biochimie* **2010**, *92*, 1379–1386. [CrossRef]
211. Vicente Miranda, H.; Szegő, É.M.; Oliveira, L.M.; Breda, C.; Darendelioglu, E.; de Oliveira, R.M.; Ferreira, D.G.; Gomes, M.A.; Rott, R.; Oliveira, M. Glycation potentiates α-synuclein-associated neurodegeneration in synucleinopathies. *Brain* **2017**, *140*, 1399–1419. [CrossRef]
212. Bar-On, P.; Crews, L.; Koob, A.O.; Mizuno, H.; Adame, A.; Spencer, B.; Masliah, E. Statins reduce neuronal α-synuclein aggregation in in vitro models of Parkinson's disease. *J. Neurochem.* **2008**, *105*, 1656–1667. [CrossRef]
213. Dai, L.; Wang, J.; He, M.; Xiong, M.; Tian, Y.; Liu, C.; Zhang, Z. Lovastatin Alleviates α-Synuclein Aggregation and Phosphorylation in Cellular Models of Synucleinopathy. *Front. Mol. Neurosci.* **2021**, *14*, 682320. [CrossRef] [PubMed]
214. Koob, A.O.; Ubhi, K.; Paulsson, J.F.; Kelly, J.; Rockenstein, E.; Mante, M.; Adame, A.; Masliah, E. Lovastatin ameliorates α-synuclein accumulation and oxidation in transgenic mouse models of α-synucleinopathies. *Exp. Neurol.* **2010**, *221*, 267–274. [CrossRef]
215. Selley, M.L. Simvastatin prevents 1-methyl-4-phenyl-1, 2, 3, 6-tetrahydropyridine-induced striatal dopamine depletion and protein tyrosine nitration in mice. *Brain Res.* **2005**, *1037*, 1–6. [CrossRef] [PubMed]
216. Ghosh, A.; Roy, A.; Matras, J.; Brahmachari, S.; Gendelman, H.E.; Pahan, K. Simvastatin inhibits the activation of p21ras and prevents the loss of dopaminergic neurons in a mouse model of Parkinson's disease. *J. Neurosci.* **2009**, *29*, 13543–13556. [CrossRef] [PubMed]
217. Mingione, A.; Pivari, F.; Plotegher, N.; Dei Cas, M.; Zulueta, A.; Bocci, T.; Trinchera, M.; Albi, E.; Maglione, V.; Caretti, A. Inhibition of Ceramide Synthesis Reduces α-Synuclein Proteinopathy in a Cellular Model of Parkinson's Disease. *Int. J. Mol. Sci.* **2021**, *22*, 6469. [CrossRef]
218. Kumar, S.; Kumar, R.; Kumari, M.; Kumari, R.; Saha, S.; Bhavesh, N.S.; Maiti, T.K. Ellagic Acid Inhibits alpha-Synuclein Aggregation at Multiple Stages and Reduces Its Cytotoxicity. *ACS Chem. Neurosci.* **2021**, *12*, 1919–1930. [CrossRef]
219. Perni, M.; Galvagnion, C.; Maltsev, A.; Meisl, G.; Müller, M.B.; Challa, P.K.; Kirkegaard, J.B.; Flagmeier, P.; Cohen, S.I.; Cascella, R. A natural product inhibits the initiation of α-synuclein aggregation and suppresses its toxicity. *Proc. Natl. Acad. Sci. USA* **2017**, *114*, E1009–E1017. [CrossRef] [PubMed]

220. Hebron, M.L.; Lonskaya, I.; Moussa, C.E.-H. Nilotinib reverses loss of dopamine neurons and improves motor behavior via autophagic degradation of α-synuclein in Parkinson's disease models. *Hum. Mol. Genet* **2013**, *22*, 3315–3328. [CrossRef]
221. Collins, L.M.; Adriaanse, L.J.; Theratile, S.D.; Hegarty, S.V.; Sullivan, A.M.; O'Keeffe, G.W. Class-IIa histone deacetylase inhibition promotes the growth of neural processes and protects them against neurotoxic insult. *Mol. Neurobiol.* **2015**, *51*, 1432–1442. [CrossRef]
222. Bassil, F.; Fernagut, P.-O.; Bezard, E.; Pruvost, A.; Leste-Lasserre, T.; Hoang, Q.Q.; Ringe, D.; Petsko, G.A.; Meissner, W.G. Reducing C-terminal truncation mitigates synucleinopathy and neurodegeneration in a transgenic model of multiple system atrophy. *Proc. Natl. Acad. Sci. USA* **2016**, *113*, 9593–9598. [CrossRef] [PubMed]
223. Iljina, M.; Tosatto, L.; Choi, M.L.; Sang, J.C.; Ye, Y.; Hughes, C.D.; Bryant, C.E.; Gandhi, S.; Klenerman, D. Arachidonic acid mediates the formation of abundant alpha-helical multimers of alpha-synuclein. *Sci. Rep.* **2016**, *6*, 33928. [CrossRef] [PubMed]
224. Beal, M.F. Bioenergetic approaches for neuroprotection in Parkinson's disease. *Ann. Neurol. Off. J. Am. Neurol. Assoc. Child. Neurol. Soc.* **2003**, *53*, S39–S48. [CrossRef] [PubMed]
225. Anderson, D.W.; Bradbury, K.A.; Schneider, J.S. Neuroprotection in Parkinson models varies with toxin administration protocol. *Eur. J. Neurosci.* **2006**, *24*, 3174–3182. [CrossRef]
226. Jia, H.; Li, X.; Gao, H.; Feng, Z.; Li, X.; Zhao, L.; Jia, X.; Zhang, H.; Liu, J. High doses of nicotinamide prevent oxidative mitochondrial dysfunction in a cellular model and improve motor deficit in a Drosophila model of Parkinson's disease. *J. Neurosci. Res.* **2008**, *86*, 2083–2090. [CrossRef]
227. Devos, D.; Moreau, C.; Devedjian, J.C.; Kluza, J.; Petrault, M.; Laloux, C.; Jonneaux, A.; Ryckewaert, G.; Garçon, G.; Rouaix, N. Targeting chelatable iron as a therapeutic modality in Parkinson's disease. *Antioxid. Redox Signal.* **2014**, *21*, 195–210. [CrossRef]
228. Vincent, B.M.; Tardiff, D.F.; Piotrowski, J.S.; Aron, R.; Lucas, M.C.; Chung, C.Y.; Bacherman, H.; Chen, Y.; Pires, M.; Subramaniam, R. Inhibiting stearoyl-CoA desaturase ameliorates α-synuclein cytotoxicity. *Cell Rep.* **2018**, *25*, 2742–2754. E2731. [CrossRef] [PubMed]
229. Liu, X.; Strable, M.S.; Ntambi, J.M. Stearoyl CoA desaturase 1: Role in cellular inflammation and stress. *Adv. Nutr.* **2011**, *2*, 15–22. [CrossRef]
230. Imberdis, T.; Negri, J.; Ramalingam, N.; Terry-Kantor, E.; Ho, G.P.; Fanning, S.; Stirtz, G.; Kim, T.-E.; Levy, O.A.; Young-Pearse, T.L. Cell models of lipid-rich α-synuclein aggregation validate known modifiers of α-synuclein biology and identify stearoyl-CoA desaturase. *Proc. Natl. Acad. Sci. USA* **2019**, *116*, 20760–20769. [CrossRef]
231. Hubler, Z.; Allimuthu, D.; Bederman, I.; Elitt, M.S.; Madhavan, M.; Allan, K.C.; Shick, H.E.; Garrison, E.; Karl, M.T.; Factor, D.C. Accumulation of 8, 9-unsaturated sterols drives oligodendrocyte formation and remyelination. *Nature* **2018**, *560*, 372–376. [CrossRef]
232. Alberts, A.; Chen, J.; Kuron, G.; Hunt, V.; Huff, J.; Hoffman, C.; Rothrock, J.; Lopez, M.; Joshua, H.; Harris, E. Mevinolin: A highly potent competitive inhibitor of hydroxymethylglutaryl-coenzyme A reductase and a cholesterol-lowering agent. *Proc. Natl. Acad. Sci. USA* **1980**, *77*, 3957–3961. [CrossRef]
233. Moore, K.S.; Wehrli, S.; Roder, H.; Rogers, M.; Forrest Jr, J.N.; McCrimmon, D.; Zasloff, M. Squalamine: An aminosterol antibiotic from the shark. *Proc. Natl. Acad. Sci. USA* **1993**, *90*, 1354–1358. [CrossRef]
234. Selinsky, B.S.; Smith, R.; Frangiosi, A.; Vonbaur, B.; Pedersen, L. Squalamine is not a proton ionophore. *Biochim. Biophys. Acta (BBA)-Biomembr.* **2000**, *1464*, 135–141. [CrossRef]
235. Guttuso Jr, T.; Andrzejewski, K.L.; Lichter, D.G.; Andersen, J.K. Targeting kinases in Parkinson's disease: A mechanism shared by LRRK2, neurotrophins, exenatide, urate, nilotinib and lithium. *J. Neurol. Sci.* **2019**, *402*, 121–130. [CrossRef]
236. Braithwaite, S.P.; Voronkov, M.; Stock, J.B.; Mouradian, M.M. Targeting phosphatases as the next generation of disease modifying therapeutics for Parkinson's disease. *Neurochem. Int.* **2012**, *61*, 899–906. [CrossRef] [PubMed]
237. Braithwaite, S.P.; Stock, J.B.; Mouradian, M.M. α-Synuclein phosphorylation as a therapeutic target in Parkinson's disease. *Rev. Neurosci.* **2012**, *23*, 191–198. [CrossRef]
238. Bell, R.; Vendruscolo, M. Modulation of the Interactions Between alpha-Synuclein and Lipid Membranes by Post-translational Modifications. *Front. Neurol.* **2021**, *12*, 661117. [CrossRef]
239. Lee, K.-W.; Chen, W.; Junn, E.; Im, J.-Y.; Grosso, H.; Sonsalla, P.K.; Feng, X.; Ray, N.; Fernandez, J.R.; Chao, Y. Enhanced phosphatase activity attenuates α-synucleinopathy in a mouse model. *J. Neurosci.* **2011**, *31*, 6963–6971. [CrossRef] [PubMed]
240. Cai, Z.; Xu, J.; Xue, S.; Liu, Y.; Zhang, Y.; Zhang, X.; Wang, X.; Wu, F.; Li, X. The E3 ubiquitin ligase seven in absentia homolog 1 may be a potential new therapeutic target for Parkinson's disease. *Neural Regen. Res.* **2015**, *10*, 1286. [CrossRef] [PubMed]
241. Games, D.; Valera, E.; Spencer, B.; Rockenstein, E.; Mante, M.; Adame, A.; Patrick, C.; Ubhi, K.; Nuber, S.; Sacayon, P. Reducing C-terminal-truncated alpha-synuclein by immunotherapy attenuates neurodegeneration and propagation in Parkinson's disease-like models. *J. Neurosci.* **2014**, *34*, 9441–9454. [CrossRef]
242. Tavassoly, O.; Yue, J.; Vocadlo, D.J. Pharmacological inhibition and knockdown of O-GlcNAcase reduces cellular internalization of α-synuclein preformed fibrils. *FEBS J.* **2021**, *288*, 452–470. [CrossRef]
243. Lee, B.E.; Kim, H.Y.; Kim, H.-J.; Jeong, H.; Kim, B.-G.; Lee, H.-E.; Lee, J.; Kim, H.B.; Lee, S.E.; Yang, Y.R. O-GlcNAcylation regulates dopamine neuron function, survival and degeneration in Parkinson disease. *Brain* **2020**, *143*, 3699–3716. [CrossRef]
244. Li, P.; Song, C. Potential treatment of Parkinson's disease with omega-3 polyunsaturated fatty acids. *Nutr. Neurosci.* **2022**, *25*, 180–191. [CrossRef] [PubMed]
245. Kirsch, M.; De Groot, H. NAD (P) H, a directly operating antioxidant? *FASEB J.* **2001**, *15*, 1569–1574. [CrossRef] [PubMed]

246. Higdon, J. *An Evidence-Based Approach to Vitamins and Minerals Health Benefits and Intake Recommendations*; Thieme Medical Publishers, Inc.: New York, NY, USA, 2003.
247. Schoeler, M.; Caesar, R. Dietary lipids, gut microbiota and lipid metabolism. *Rev. Endocr. Metab. Disord.* **2019**, *20*, 461–472. [CrossRef] [PubMed]
248. Mao, X.-Y.; Yin, X.-X.; Guan, Q.-W.; Xia, Q.-X.; Yang, N.; Zhou, H.-H.; Liu, Z.-Q.; Jin, W.-L. Dietary nutrition for neurological disease therapy: Current status and future directions. *Pharmacol. Ther.* **2021**, *226*, 107861. [CrossRef]
249. Zhao, B. Natural antioxidants protect neurons in Alzheimer's disease and Parkinson's disease. *Neurochem. Res.* **2009**, *34*, 630–638. [CrossRef]

International Journal of
Molecular Sciences

MDPI

Article

Intranasal Administration of GRP78 Protein (HSPA5) Confers Neuroprotection in a Lactacystin-Induced Rat Model of Parkinson's Disease

Maria B. Pazi [1,*], Daria V. Belan [1], Elena Y. Komarova [2] and Irina V. Ekimova [1,*]

[1] Sechenov Institute of Evolutionary Physiology and Biochemistry, Russian Academy of Sciences, 44 Thorez pr., St. Petersburg 194223, Russia; daf205@yandex.ru
[2] Institute of Cytology, Russian Academy of Sciences, 4 Tikhoretsky pr., St. Petersburg 194064, Russia; elpouta@yahoo.com
* Correspondence: pazimariia@gmail.com (M.B.P.); irina-ekimova@mail.ru (I.V.E.); Tel.: +7-812-552-7901 (I.V.E.)

Abstract: The accumulation of misfolded and aggregated α-synuclein can trigger endoplasmic reticulum (ER) stress and the unfolded protein response (UPR), leading to apoptotic cell death in patients with Parkinson's disease (PD). As the major ER chaperone, glucose-regulated protein 78 (GRP78/BiP/HSPA5) plays a key role in UPR regulation. GRP78 overexpression can modulate the UPR, block apoptosis, and promote the survival of nigral dopamine neurons in a rat model of α-synuclein pathology. Here, we explore the therapeutic potential of intranasal exogenous GRP78 for preventing or slowing PD-like neurodegeneration in a lactacystin-induced rat model. We show that intranasally-administered GRP78 rapidly enters the substantia nigra pars compacta (SNpc) and other afflicted brain regions. It is then internalized by neurons and microglia, preventing the development of the neurodegenerative process in the nigrostriatal system. Lactacystin-induced disturbances, such as the abnormal accumulation of phosphorylated pS129-α-synuclein and activation of the pro-apoptotic GRP78/PERK/eIF2α/CHOP/caspase-3,9 signaling pathway of the UPR, are substantially reversed upon GRP78 administration. Moreover, exogenous GRP78 inhibits both microglia activation and the production of proinflammatory cytokines, tumor necrosis factor-α (TNF-α) and interleukin-6 (IL-6), via the nuclear factor kappa-light-chain-enhancer of activated B cells (NF-κB) signaling pathway in model animals. The neuroprotective and anti-inflammatory potential of exogenous GRP78 may inform the development of effective therapeutic agents for PD and other synucleinopathies.

Keywords: Parkinson's disease; lactacystin; GRP78; ER stress; neuroprotection; substantia nigra; microglia

Citation: Pazi, M.B.; Belan, D.V.; Komarova, E.Y.; Ekimova, I.V. Intranasal Administration of GRP78 Protein (HSPA5) Confers Neuroprotection in a Lactacystin-Induced Rat Model of Parkinson's Disease. *Int. J. Mol. Sci.* **2024**, *25*, 3951. https://doi.org/10.3390/ijms25073951

Academic Editor: Claudia Ricci

Received: 31 January 2024
Revised: 23 March 2024
Accepted: 31 March 2024
Published: 2 April 2024

1. Introduction

Parkinson's disease (PD) is an age-related chronic neurodegenerative disorder ranking second in frequency after Alzheimer's disease [1]. About 16 million people worldwide suffer from PD, and it is estimated that the number of PD patients will rise by 1.5–2-fold within the next 20–30 years due to the increase in centenarians [2]. The etiology of PD is largely unknown, with more than 90% of PD cases being sporadic [3]. Older age in combination with genetic profile and/or exposure to environmental pollution (herbicides, pesticides, infectious agents, etc.) are considered causative factors of sporadic PD onset and progression [4,5]. PD diagnosis relies on clinically significant symptoms, such as resting tremors, bradykinesia, muscular rigidity, and loss of balance. These symptoms are indicative of motor dysfunctions, which are associated with the degeneration of 50–60% of dopaminergic (DA) neurons in the substantia nigra pars compacta (SNpc), resulting in a reduction of dopamine in the striatum [6,7]. Such a delayed diagnosis of PD, when most specific neurons are already lost, explains the low effectiveness of existing PD therapies, primarily aimed at relieving symptoms. However, neuronal death also occurs in

extranigral brain regions responsible for non-motor symptoms that may manifest in the pre-symptomatic (preclinical) PD stage, 20–30 years prior to the first motor symptoms [8]. A wide range of non-motor symptoms in PD includes sleep disorders, olfactory disturbances, enteral dysfunction, etc. [6]. Therefore, progress in treating PD is linked to the advancement of early diagnosis technologies and pathogenetically significant therapy, aiming to prevent or attenuate neurodegeneration in its early stage [9].

A pathological hallmark of PD is the overexpression and/or abnormal accumulation and misfolding of α-synuclein (α-syn) followed by the formation of Lewy bodies and Lewy neurites [10,11]. The Lewy bodies consist of up to 90% of α-syn phosphorylated at serine-129 (Ser129), and this post-translational modification appears to be associated with the formation and/or toxicity of aggregated proteins [12,13]. The intraneuronal accumulation of aberrant α-syn forms (misfolded and phosphorylated at Ser129) results from the dysfunction of both the ubiquitin–proteasome system (UPS) and the autophagy–lysosomal pathway [14–16]. The weakening of conformational control mechanisms ensured by heat shock proteins also contributes to protein aggregation [17–19]. The discovery of UPS functional insufficiency in familial and sporadic PD has promoted the development of novel in vivo PD models based on proteasome inhibitors, such as lactacystin (LC) [20,21]. LC is a metabolite of ubiquitous soil and water bacteria, e.g., Streptomyces lactacystinaeus. Given the lipophilic properties of LC and its ability to enter the human body with food, water, or dust and accumulate over time, exposure to this proteasome inhibitor can underlie some cases of PD [22]. When injected directly into the SNpc in rats, LC replicates the key neuropathological features of PD in the nigrostriatal and extranigral systems stage by stage, with the effects varying in a dose-dependent manner [21]. This sets LC apart from other neurotoxins used to model PD, making it one of the most promising substances for testing therapeutic strategies that can slow down neurodegeneration at various stages of PD development. In this study, we established an LC-induced model of early PD. This stage is particularly crucial for effective treatment since the majority of DA neurons are still preserved.

A growing body of evidence from animal models of PD and postmortem studies in PD patients suggests that the accumulation of α-syn oligomers can trigger neuronal death via the apoptosis pathway coupled with microglial activation, which contributes to the pathogenesis of progressive PD [10,23–27]. In addition to the cytosol of neurons, α-syn pathologically aggregates and accumulates in the endoplasmic reticulum (ER) lumen. This, in turn, induces ER stress, initiating an adaptive response through the activation of the unfolded protein response (UPR) [26,28–32]. The UPR includes three signaling pathways initiated by the PKR-like ER kinase (PERK), inositol-requiring transmembrane kinase/endoribonuclease 1α (IRE1α), or the activating transcription factor 6 (ATF6) [33]. A member of the 70 kDa heat-shock protein (HSP) chaperone family, the ER-associated 78 kDa glucose-regulated protein, also known as the immunoglobulin heavy chain-binding protein (GRP78/BiP), is a key regulator of the UPR signaling pathways. Under normal conditions, GRP78 binds IRE1α, PERK, and ATF6, maintaining their inactive state. When misfolded proteins accumulate within the ER, GRP78 binds them to prevent further misfolding and, thus, dissociates from the three ER stress receptors mediating the UPR. Biologically, the UPR aims to restore the ER function and protect cells against the toxic build-up of un-/misfolded proteins.

However, if ER stress is prolonged or exceeds the adaptive capacity of the cell, it can lead to the activation of apoptosis signaling and cell death. The PERK protein plays a crucial role in the regulation of ER-stress-induced apoptosis due to its involvement in many branching pathways [31,34]. Another important player is the C/EBP homologous protein (CHOP), a transcription factor and a downstream regulator of the PERK pathway. pPERK and its phosphorylated downstream target eukaryotic initiation factor 2α (eIF2a), both markers of UPR activation, are detected in neuromelanin-containing DA SNpc neurons in PD cases but not in age-matched controls [28]. The induction of the UPR has been documented in various in vitro and in vivo models of PD [26,30,35]. Overall, these findings

indicate the involvement of the ER-stress PERK/CHOP pathway in neurodegeneration in PD. Therefore, modulating ER stress and inhibiting the PERK/CHOP-dependent pro-apoptotic UPR pathway could be a prospective therapeutic approach.

GRP78 chaperone is a specific modulator of ER stress, ensuring conformational control of nascent membrane-bound or secretory proteins. Unlike the cytosolic HSP members, GRP78 contains a signal sequence that targets it in the ER. In vivo and in vitro studies have shown that within cells containing α-syn aggregates, α-syn binds to the ER-stress sensor GRP78 [26,30]. This indicates that α-syn is a molecular target for GRP78. Chaperone GRP78 is a multifunctional protein that assists in a wide range of folding and refolding processes, the proteasomal endoplasmic-reticulum-associated protein degradation (ERAD) of misfolded proteins, maintaining calcium homeostasis, and regulating the UPR signaling [32,36]. Moreover, extracellular and exogenous GRP78 proteins demonstrate long-term anti-inflammatory and immunomodulatory properties in inflammatory diseases [37]. The literature data indicate that the mobilization of the GRP78-based chaperone mechanism serves as the first "line of defense" against the fatal consequences of α-syn toxicity and prolonged ER stress. The overexpression of GRP78 can reduce the death of DA neurons in the SNpc and loss of striatal dopamine by halting ER stress and apoptosis in an α-syn model of PD in rats [30,38].

These findings suggest that GRP78 can be a potential therapeutic target for the treatment of PD. Notably, GRP78 protein levels decrease in the SNpc with aging and in sporadic PD patients, which reflects the weakening of the protein conformational control and increased vulnerability of DA neurons to ER stress [38,39]. GRP78 is required for the survival of nigral neurons, and its lower level is suggested to be a predisposing factor for the onset and progression of PD and synucleinopathies in humans [38]. One of the ways to increase GRP78 in brain neurons is the intranasal delivery of the recombinant GRP78 protein. The intranasal method of GRP78 administration is informed by the in vitro data on the ability of exogenous GRP78 to penetrate living cells, translocate to the ER, and directly affect proteostasis and cell physiology [40]. Our preliminary experiments have shown that intranasal GRP78 administration helps mitigate the process of neurodegeneration in the nigrostrial system, suggesting the bioavailability of exogenous GRP78 [41]. This study aimed to develop a new neuroprotective approach to PD therapy through the intranasal administration of recombinant GRP78. We hypothesized that elevating GRP78 levels in the SNpc would prevent the abnormal accumulation and formation of pathological α-syn, modulate the UPR, block apoptosis, and inhibit microglial activation. Consequently, this would promote the survival of nigral neurons in the proteasome inhibitor-induced rat model of PD.

2. Results

2.1. GRP78 Treatment Prevents Neuronal Loss in the Substantia Nigra Pars Compacta in a Lactacystin-Induced Rat Model of Parkinson's Disease

To assess the therapeutic potential of exogenous GRP78, we used an LC-induced model of PD in rats, reproducing key pathological signs of PD [20,21]. At a dose of 0.4 μg, LC was injected into each side of the SNpc twice, with a 7-day interval (n = 8, group LC). Recombinant human GRP78 was administered intranasally (n = 8) at a dose of 1.6 μg/8 μL to each nostril 4 h and 28 h after each LC microinjection, as well as 7 days after the last microinjection (group LC+GRP78, see Figure 1 for details). Control rats (n = 8) were treated similarly but received an equivalent volume of the vehicle instead of LC and GRP78 (group vehicle). GRP78 was also introduced to naïve animals (n = 3, group GRP78). Twenty-one days after the first LC or vehicle microinjection, behavior tests were performed and then the animals were sacrificed for further immunohistochemical and biochemical analyses. In preliminary experiments [41], using motor behavior tests (sunflower seed test, Suok test, inverted horizontal grid test), we showed that double injections of 0.4 μg LC in the SNpc lead to no motor dysfunction. To assess the number of surviving DA neurons and their

axons, brain sections were stained with antibodies against tyrosine hydroxylase (TH), the marker of DA neurons.

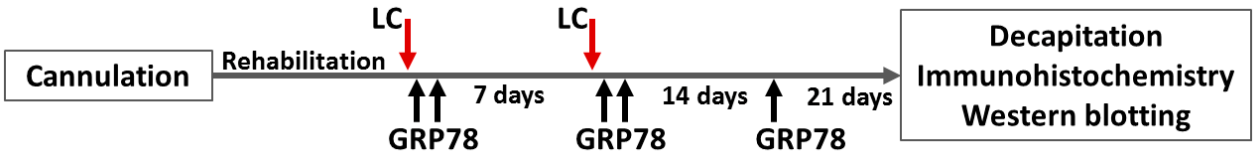

Figure 1. Experimental design. The timing and sequence of LC and GRP78 injections and procedures are shown. Red arrows, LC—microinjections of the proteasome inhibitor lactacystin into the SNpc (0.4 μg/1 μL). Black arrows, GRP78—treatment with recombinant human heat shock protein GRP78 (1.6 μg/8 μL) or the corresponding vehicle, sterile PBS, administered intranasally 4 h and 28 h following each microinjection of LC or vehicle and 7 days after the last injection.

The morphological analysis of nigrostriatal sections revealed the loss of 27% of DA neurons in the SNpc and 19.4% of their axons in the dorsal striatum after LC administration compared to the vehicle (Figure S1). This suggests the development of neurodegeneration imitating the pre-symptomatic (preclinical) stage of PD, as motor dysfunction symptoms do not manifest until at least 50–60% of the DA neurons in the SNpc are lost [9]. Treatment with GRP78 significantly prevented the loss of DA neurons in the SNpc (Figure S1a,c) and their axons in the dorsal striatum (Figure S1b,d). On the other hand, GRP78 did not affect the number of TH-positive neurons in the SNpc in rats untreated with LC, indicating that GRP78 administration is not responsible for neurodegeneration. Thus, our data demonstrate that exogenous GRP78 mitigates the neurodegenerative process in the nigrostriatal system in the LC-induced rat model of PD, and chaperone therapy has a neuroprotective effect.

2.2. Exogenous GRP78 Can Penetrate Brain Structures and Be Internalized by Neurons and Microgliocytes in a Lactacystin Rat Model of Parkinson's Disease

The neuroprotective potential of exogenous GRP78 shown in the LC model of PD suggests its bioavailability to the brain upon intranasal administration. To experimentally prove that exogenous GRP78 can penetrate the brain and be internalized by cells when administered intranasally, we analyzed the localization of the fluorescently labeled protein in brain structures pathogenetically significant for PD. GRP78, labeled by Alexa-555, was administered intranasally to rats after the microinjection of LC and after the injection of the LC vehicle (phosphate buffer saline, PBS) into the SNpc. Using antibodies against TH, we found that labeled GRP78 (red signal, Figure 2d–j) penetrates the brain and localizes in the cytosol, but not in the nuclei of DA neurons of the SNpc 3 h after its intranasal administration, both after LC injections (Figure 2a,d,g,i) or after LC vehicle injection (Figure S2). The merged signal (yellow) illustrates the co-localization of labeled GRP78 and TH in cell bodies in the SNpc (Figure 2g,j). A red fluorescent signal was absent following the intranasal administration of unlabeled GRP78 to a rat receiving the LC microinjection into the SNpc (Figure S3).

Next, we stained SNpc brain sections with antibodies against GRP78 and evaluated the optical density of GRP78 in SNpc neurons in animals treated with Alexa-labeled GRP78 and control animals receiving its solvent (PBS). The analysis showed a clear trend towards increased protein levels GRP78 in neurons of the SNpc; the content of GRP78 increased 1.4 times ($p = 0.06$) 3 h after its administration compared with the control (Figure S4). This further confirms that GRP78 penetrates the brain and starts to accumulate in neurons 3 h after its intranasal administration.

Since proteins can undergo proteolysis in the brain, we stained the SNpc sections of rats that received Alexa-555-labeled GRP78 with antibodies against GRP78. We showed that GRP78, recognized by specific antibodies (green signal, Figure 2b), co-localized (the merged signal, yellow) with exogenous labeled GRP78 (Figure 2h,k). Importantly, exogenous

GRP78 also migrated to other brain regions affected by PD in humans [8,42], such as the ventral tegmental area and locus coeruleus. There, GRP78 was able to cross the plasma membranes of neurons and localize in their cytosol, as illustrated in Figure S5. Thus, we can conclude that the loss of fewer DA neurons in the SNpc is linked to an increase in the content of the exogenous GRP78 protein after its intranasal administration and its neuroprotective properties in the LC-induced PD model.

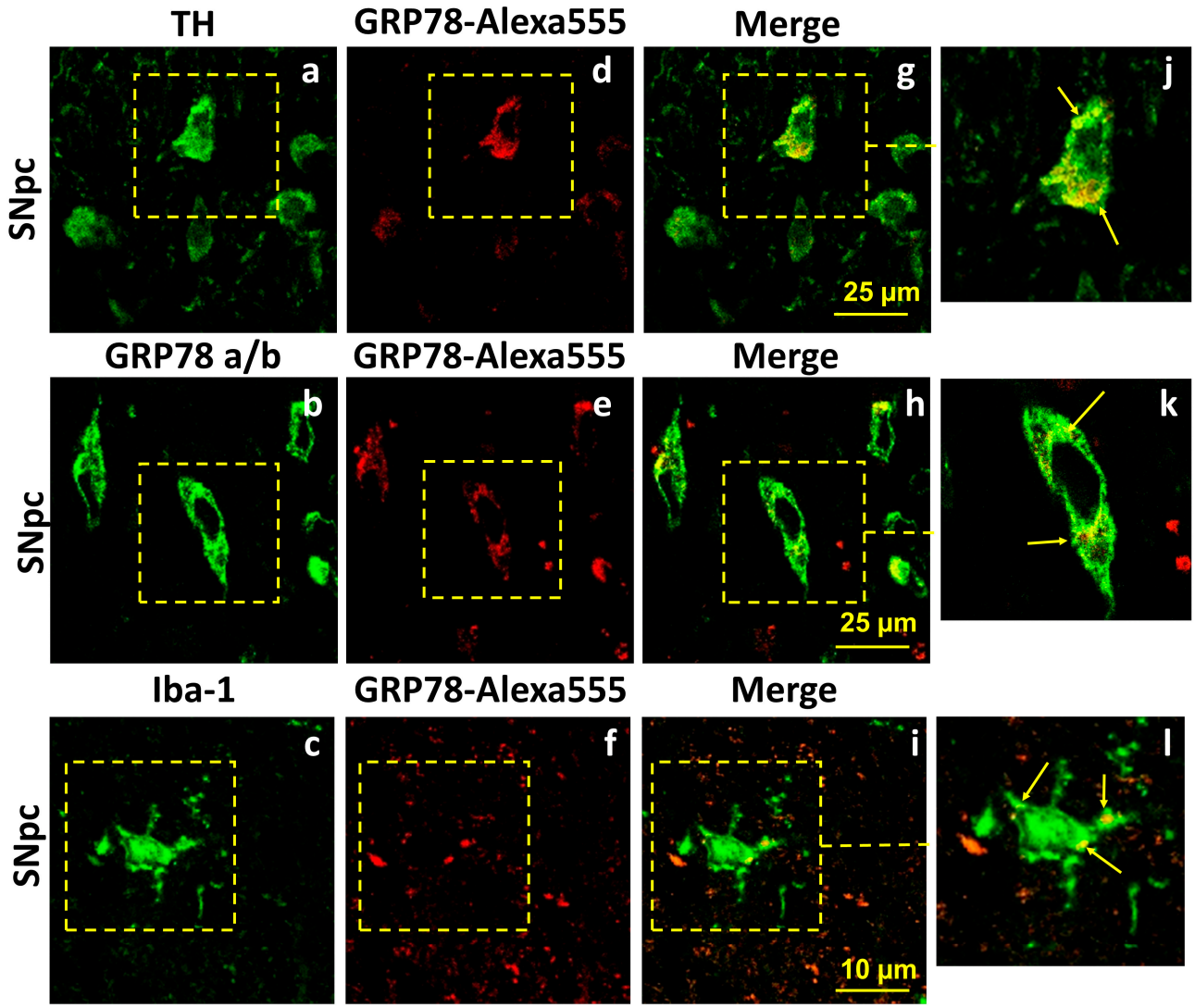

Figure 2. Labeled GRP78 penetrates the brain and is localized in DA neurons and microglial cells of the substantia nigra pars compacta (SNpc) 3 h after its intranasal administration in a rat model of Parkinson's disease. GRP78 protein labeled by Alexa-555 was administered intranasally to rats (n = 4) after a microinjection of lactacystin as described in the Materials and Methods. Brain sections were stained with (**a**) specific anti-TH antibodies (green signal), (**b**) anti-Grp78 antibodies specific to human protein (green signal), and (**c**) anti-Iba-1 antibodies (green signal). (**d**–**f**) Localization of labeled GRP78 is seen as a red signal. (**g**–**i**) Panels show co-localization of labeled GRP78 and anti-TH, anti-Grp78, or anti-Iba-1 signals. (**j**–**l**) Panels show magnified representative images of the co-localization within neurons and microglia cells marked by yellow box. Arrows indicate co-localization of labeled GRP78 with corresponding proteins. Images were obtained using confocal microscopy. Scale bars are 25 µm for neurons in the SNpc and 10 µm for microglia.

As shown previously, exogenous GRP78 is rapidly internalized by monocytes in the peripheral blood, directly impacting various phenotypical and metabolic functions of

myeloid cells [37,43]. We assumed that microglial brain cells could internalize exogenous GRP78, mediating its immunomodulatory effect. To test our assumption, we used antibodies against the microglial surface marker Iba-1 (ionized calcium-binding adaptor molecule) (Figure 2c). As seen in Figure 2f, GRP78 (red signal) was efficiently internalized by the microgliocytes of the SNpc (Figure 2i,l).

Thus, the protective effect of exogenous GRP78 on DA neurons of the SNpc appears to be associated with its ability to penetrate neurons and microglia and directly influence proteostasis and cell physiology during the development of PD-like pathology.

2.3. Exogenous GRP78 Prevents Abnormal Accumulation of Phosphorylated pS129-α-syn in Nigral Tissue in the Lactacystin Model of Parkinson's Disease

In order to find out whether the protective effect of exogenous GRP78 on DA-ergic neurons is associated with a decrease in the signs of α-syn pathology, we analyzed the total content of the water-soluble α-syn protein and its phosphorylated form pS129 using a Western blot analysis with antibodies against α-syn and pS129-α-syn. We tested nigral tissue samples of rats, treated or untreated with GRP78, 21 days after the first LC microinjection (see the experimental scheme for details, Figure 1).

Our results showed that the total concentration of water-soluble monomeric α-syn and its pS129 form in the SNpc of rats in the LC-induced PD model is 1.3 and 1.4 times higher, respectively, compared to the vehicle control (Figure 3a,b,d). As Figure 3c,d illustrate, the pS129/total soluble α-syn ratio increased with LC treatment. Therefore, pS129-α-syn predominates in the water-soluble monomeric α-syn fraction. At the same time point, the neurodegeneration of DA neurons in the SNpc and their axons in the dorsal striatum was observed after LC microinjections (Figure S1), which may be a consequence of the pS129-α-syn toxicity.

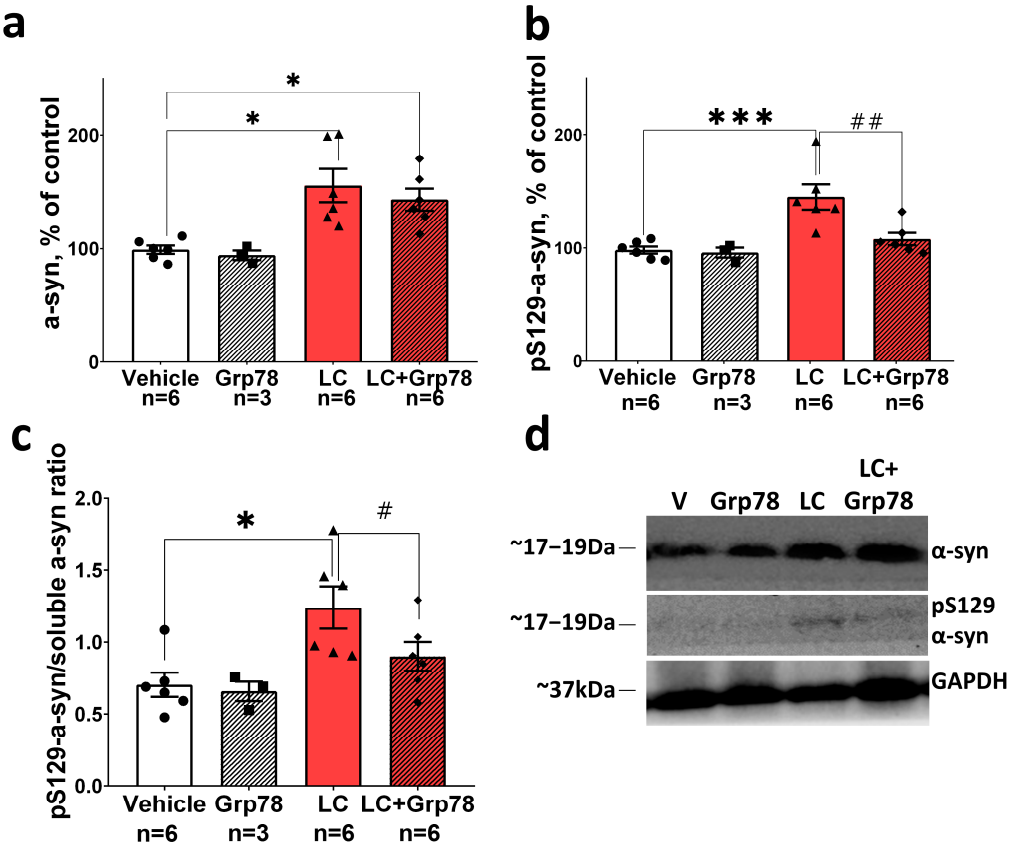

Figure 3. Exogenous GRP78 prevents abnormal accumulation of α-syn phosphorylated at S129 (pS129) in nigral tissue in rat model of Parkinson's disease. Nigral content of (**a**) soluble form of α-syn, (**b**) α-syn phosphorylated at S129 (pS129), (**c**) phosphorylated to soluble α-syn ratio. Western

blot analysis of nigral tissue was conducted with the antibodies against soluble and S129-phosphorylated forms of α-syn. Anti-GAPDH antibody staining was used as the loading control. (**d**) Representative Western blots are shown in panel. The results are presented as percentages of the control (100%) in (**a**–**c**) panels. Bar charts indicate mean values with standard errors. The dots, squares, triangles and rhombus show individual values per rat. Two-way ANOVA test followed by Tukey's post hoc analysis were performed to determine the effects of GRP78 therapy. Asterisks indicate significant differences between groups according to Tukey's post hoc tests: * $p < 0.05$, *** $p < 0.001$, vs. the vehicle group; # $p < 0.05$, ## $p < 0.01$, vs. the LC group. Interaction factor for soluble α-syn F (1, 15) = 7.329 $p = 0.0162$; Grp78 factor F (1, 15) = 14.34 $p = 0.0018$; LC (lactacystin) factor F (1, 15) = 13.63 $p = 0.0022$; Interaction factor for pS129-α-syn F (1, 17) = 4.982 $p = 0.0394$; Grp78 factor F (1, 17) = 6.399 $p = 0.0216$; LC factor F (1, 17) = 14.16 $p = 0.0016$.

Treatment with GRP78 prevented the LC-induced accumulation of pS129 α-syn (Figure 3b–d), while levels of total water-soluble α-syn remained elevated (Figure 3a,d). This effect coincided with a better survival of TH-positive neurons in the nigrostriatal system (Figure S1). GRP78 did not change the amount of water-soluble α-syn protein and pS129 α-syn in LC-untreated control rats. Thus, our data demonstrate that the treatment of LC-animals with exogenous GRP78 can reduce the content of potentially cytotoxic pS129 α-syn form.

2.4. Exogenous GRP78 Counteracts the Activation of the GRP78/eIF2α/CHOP/Caspase-3,9 Pro-Apoptotic UPR Signaling Pathway in the Lactacystin Model of Parkinson's Disease

To determine whether exogenous GRP78 counteracts the activation of the PERK/CHOP pro-apoptotic pathway of the UPR, we measured the GRP78 level and phosphorylation of eIF2α as ER stress indicators in nigral tissue using Western blot analyses. Furthermore, we assessed the levels of a pro-apoptotic transcription factor CHOP and well-known effectors of neuronal apoptosis—cleaved forms of caspase-3 and caspase-9—which play a crucial role in cell degeneration through the canonical mitochondrial apoptosis pathway.

Using specific antibodies against GRP78 and against total and phosphorylated (Ser51) forms of eIF2α, we found that the GRP78 protein level increased by 66 ± 13.2% ($p \leq 0.001$) in the SNpc on day 21 after the first LC injection compared to the vehicle control (Figure 4a,d). eIF2a phosphorylation (Ser51) also increased in the LC-treated animals, which suggests that there is ER stress in the SNpc (Figure 4b,d). Next, we investigated whether the upregulation of pSer51-eIF2 coincided with elevated levels of pro-apoptotic factors in the SNpc, such as CHOP and cleaved caspase-9 and caspase-3. We found that the CHOP protein was upregulated in LC-injected animals compared to the vehicle control (Figure 4c,d). We also observed a 23 ± 7% increase in cleaved caspase-9 protein levels ($p \leq 0.05$) and a 24 ± 4.8% increase in cleaved caspase-3 levels ($p \leq 0.01$) after LC administration (Figure 4e–g), indicating the activation of the pro-apoptotic PERK-CHOP branch of the UPR and the development of neuronal apoptosis induced by ER stress.

In contrast, treatment with GRP78 downregulated ER stress mediators and the level of pro-apoptotic proteins in LC-injected animals. The Western blot assessment showed no increase in the levels of GPR78 or pSer51-eIF2a in the SNpc (Figure 4b,d). Moreover, GRP78 prevented the upregulation of the pro-apoptotic factor CHOP, as evidenced by a decrease in CHOP protein levels compared to control values (Figure 4c,d). We also found that the levels of cleaved caspase-9 and cleaved caspase-3 returned to normal in the SNpc after GRP78 administration (Figure 4e–g). There was no change in the GRP78 content in the group of GRP78-treated animals. This is due to the fact that the content of GRP78 was measured 7 days after the last administration of exogenous GRP78. Thus, we suggest that by this time point, the administered exogenous GRP78 protein degraded. Consequently, in our experiments in the LC+GRP78 group, the elevation of GRP78 content was not observed for two reasons: (i) exogenous GRP78 had degraded by this time; (ii) treatment with GRP78

prevented the development of ER stress; therefore, the expression of endogenous GRP78 did not occur.

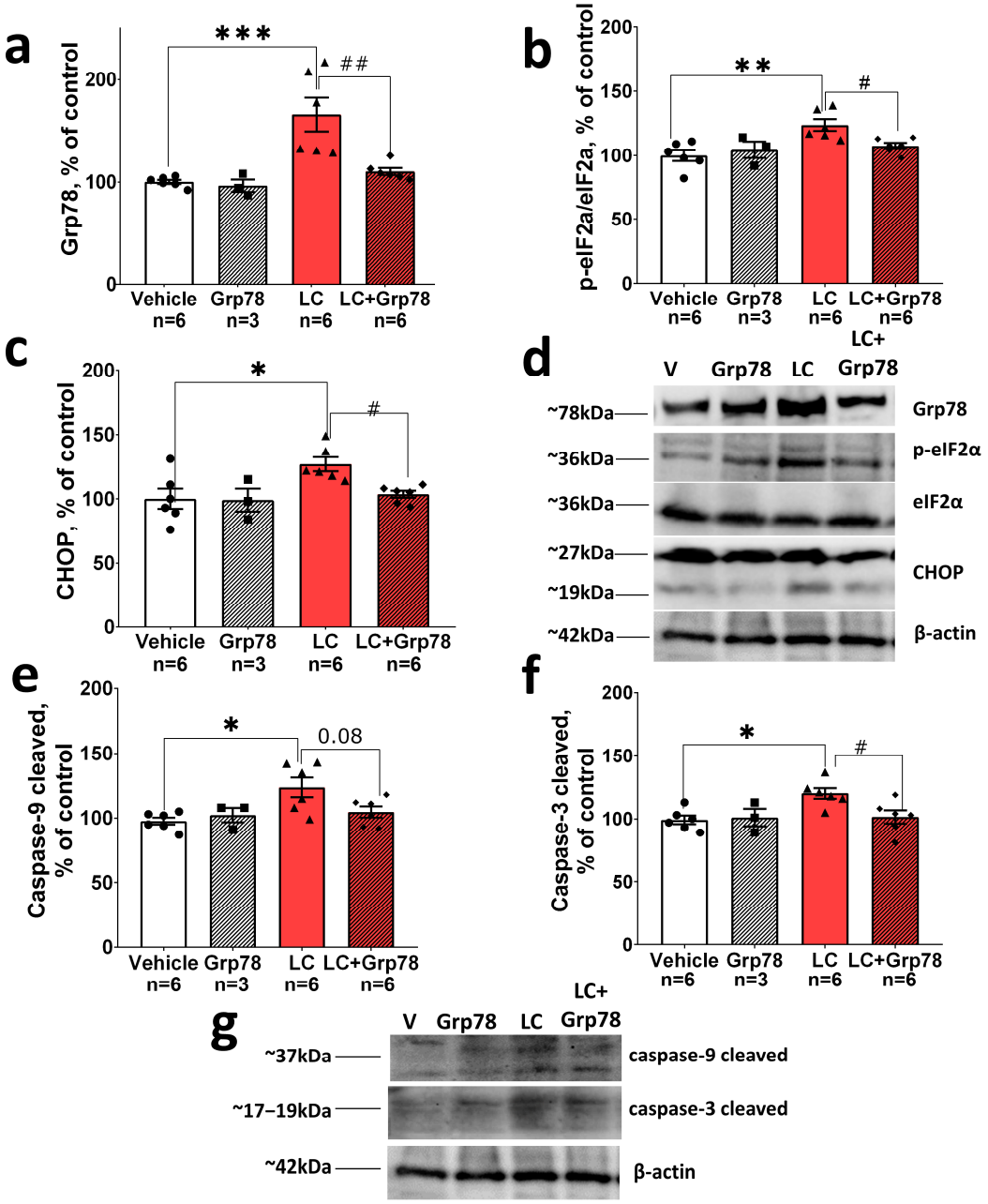

Figure 4. Exogenous GRP78 blocks the pro-apoptotic GRP78/eIF2α/CHOP/caspase-3,9 signaling pathway of the UPR in nigral tissue in a rat model of Parkinson's disease. Nigral content of (**a**) GRP78, (**b**) phosphorylated to total eIF2α, (**c**) CHOP. (**d**) Representative immunoblots. Nigral content of (**e**) cleaved caspase-9, (**f**) cleaved caspase-3. (**g**) Representative immunoblots. Western blot analysis of the nigral tissue was conducted with the antibodies against GRP78 (1:1000, rabbit, Abcam, Cambridge, UK), eIF2a (1:750, rabbit, Affinity Biosciences, Zhenjiang, China), pSer51-eIF2a (1:1000, rabbit, Abcam, Cambridge, UK), CHOP (1:1000, rabbit, Affinity Biosciences, Zhenjiang, China), cleaved caspase-9 (1:1000, rabbit, Affinity Biosciences, Zhenjiang, China), and cleaved caspase-3 (1:1000, rabbit, Affinity Biosciences, Zhenjiang, China). Staining with anti-β-Actin antibodies (1:1000, mouse, Santa Cruz Biotechnology, Dallas, TX, USA) was used as the loading control. The results are presented as percentages of the control (panels (**a**–**c**,**e**,**f**)). Bar charts indicate mean values with standard errors. The dots, squares,

triangles and rhombus indicate individual values per rat. Two-way ANOVA test followed by Tukey's post hoc analysis were performed to determine the effects of GRP78 therapy. Asterisks indicate significant differences between groups according to Tukey's post hoc tests: * $p < 0.05$; ** $p < 0.01$. *** $p < 0.001$, vs. the vehicle group; # $p < 0.05$, ## $p < 0.01$, vs. the LC group. Interaction factor for GRP78 F (1, 20) = 8.83 $p = 0.0076$; Grp78 treatment factor F (1, 20) = 7.413 $p = 0.0131$; LC (lactacystin) factor F (1, 20) = 15.89 $p = 0.0007$. Interaction factor for p-eIF2a/eIF2a ratio F (1, 19) = 5.68 $p = 0.0278$; Grp78 treatment factor F (1, 19) = 1.874 $p = 0.1869$; LC factor F (1, 19) = 7.819 $p = 0.0115$. Interaction factor for CHOP F (1, 16) = 3.126 $p = 0.0961$; Grp78 treatment factor F (1, 16) = 3.672 $p = 0.0734$; LC factor F (1, 16) = 47.898 $p = 0.0418$. Interaction factor for cleaved caspase-9 F (1, 17) = 4.124 $p = 0.0582$; Grp78 treatment factor F (1, 17) = 1.513 $p = 0.2355$; LC factor F (1, 17) = 5.911 $p = 0.0264$. Interaction factor for cleaved caspase-3 F (1, 17) = 6.417 $p = 0.0214$; Grp78 treatment factor F (1, 17) = 5.646 $p = 0.0295$; LC factor F (1, 17) = 7.451 $p = 0.0143$.

At the same time, the Western blot analysis demonstrated no significant changes in GRP78, p-eIF2, CHOP, activated caspase-3, and caspase-9 in the SNpc in control (LC-untreated) rats. This indicates that GPR78 itself does not induce ER stress or apoptosis in healthy animals.

In summary, our results showed that the intranasal administration of GRP78 prevented the activation of the GRP78/eIF2/CHOP signaling pathway, caspase-9, and caspase-3. This inhibition effectively mitigated the ER stress response and reduced apoptosis in the SNpc in the LC model of the preclinical stage of PD in rats.

2.5. Exogenous GRP78 Inhibits Microglia Activation and the Production of Proinflammatory Cytokines TNF-α and IL-6 via the NF-κB Signaling Pathway in the Lactacystin Model of Parkinson's Disease

We then investigated whether exogenous GRP78 has anti-inflammatory properties. As an increased number of activated microgliocytes is a marker of neuroinflammation [44], we first assessed the status of microglia in the SNpc of LC-treated rats. For this purpose, we implemented immunohistochemistry using antibodies against the microglial marker Iba-1 to quantify the number of Iba-1-immunopositive cells. We showed that LC caused a 38% ($p = 0.002$) increase in Iba-1-positive cells in the SNpc on day 21 after the first injection compared to the vehicle control (Figure 5a,b). During the visual analysis under a light microscope, we observed LC-induced morphological changes, such as larger soma sizes and less ramified processes (Figure 5a, lower panel). This indicates an increase in the number of microglial cells adopting an activated phenotype.

Next, we investigated whether the activation of microglia is associated with the release of pro-inflammatory cytokines TNF-α and IL-6, which participate in the pathogenesis of PD [44]. The immunoblot analysis demonstrated that the levels of TNF-α and IL-6 in the SNpc increased by ~2 times in LC-injected rats compared to the control (Figure 6). Taken together, these data indicate the development of the inflammatory process in the SNpc coupled with the death of DA neurons in the LC-induced rat model of the preclinical stage of PD.

In contrast, treatment with GRP78 decreased reactive microgliosis, as indicated by a 20% ($p < 0.05$) decrease in Iba-1-positive cells (Figure 5), and inhibited the production of pro-inflammatory cytokines TNF-α and IL-6 (Figure 6) in the SNpc of model animals. The administration of GRP78 alone affected neither the number of Iba-1-positive cells nor TNF-α and IL-6 levels in the SNpc. The results show that GRP78 can provide neuronal protection against the excessive activation of microglia in the LC-induced rat model of PD.

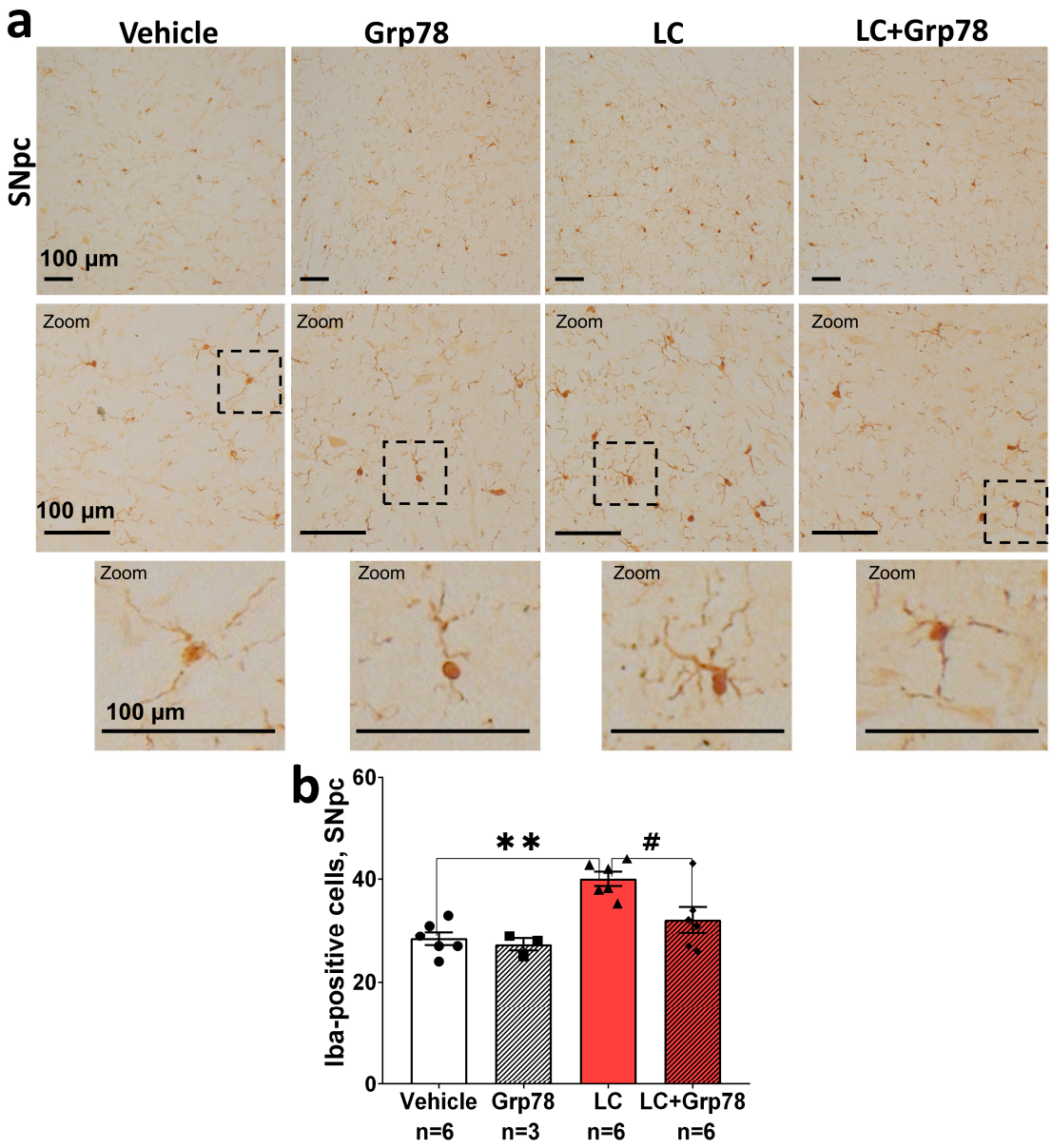

Figure 5. Exogenous GRP78 inhibits microglia activation in a lactacystin rat model of Parkinson's disease. (**a**) Brain sections (10 µm) of the substantia nigra pars compacta (SNpc, (**a**)) were prepared according to the brain atlas and stained with antibodies against Iba-1 (1:500; rabbit, Novus Biologicals, Centennial, CO, USA). The images were obtained using a Zeiss Axio Imager A1 microscope (Carl Zeiss, Oberkochen, Germany) with a built-in video camera and Axio-Vision 4.8 software. Original images are shown in the upper panel. Scale bars are 100 µm. The second panel show magnified images of microglia cells (zoom). The third panel show magnified images of microglia morphology of cells within dotted box area (zoom). (**b**) Quantitative analysis was performed using 10–12 sections from each animal at the same level of the studied zones, separated by approximately 70 µm. The number of cells accounted for a standard area of tissue captured by a light microscope camera using ×20 lens. The analysis was performed using the PhotoM freeware version 1.21 (http://www.t_lambda.chat.ru/ accessed on 11 December 2019). Bar charts indicate mean values with standard errors. The dots, squares, triangles and rhombus show individual values per rat. Two-way ANOVA test followed by Tukey's post hoc analysis were performed to determine the effects of GRP78 therapy. Asterisks indicate significant differences between groups according to Tukey's post hoc tests: ** $p < 0.01$ vs. the vehicle group; # $p < 0.05$ vs. the LC group. Interaction factor for microglia in SNpc F (2, 23) = 2.099; Grp78 factor F (2, 23) = 5.466 $p = 0.0284$; LC factor F (2, 23) = 17.04 $p = 0.0004$.

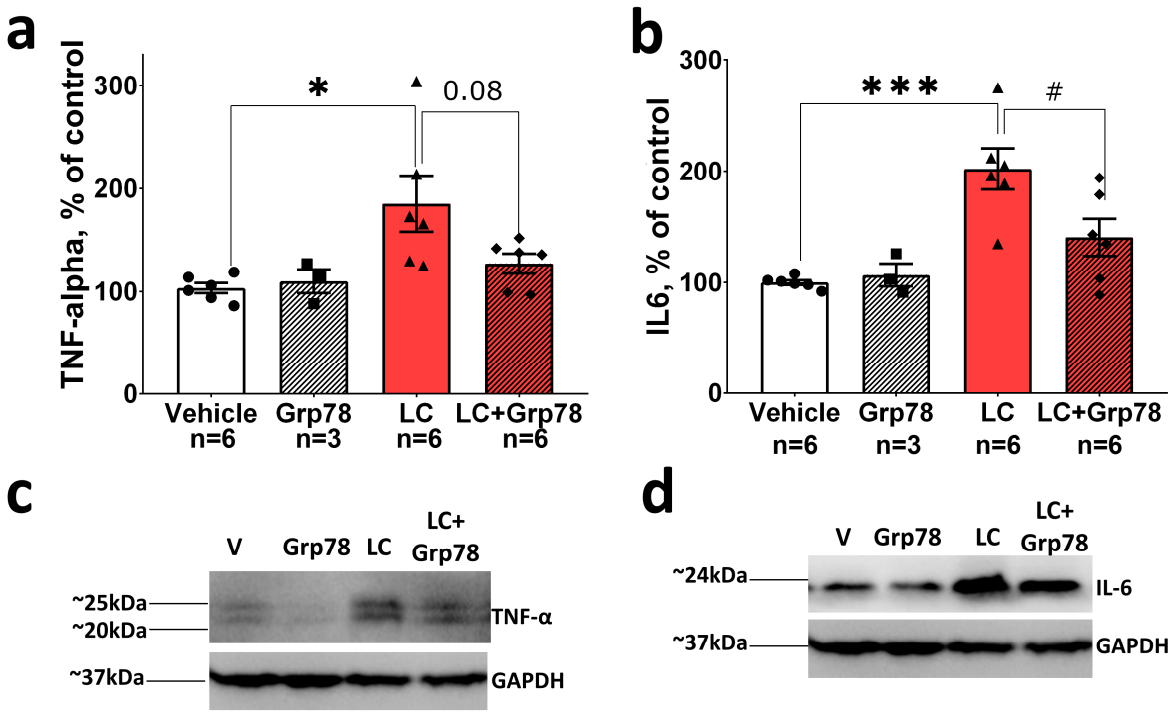

Figure 6. Exogenous GRP78 inhibits the production of pro-inflammatory cytokines TNF-α and IL-6 in a lactacystin rat model of Parkinson's disease. Content of (**a**) TNF-α and (**b**) IL-6 in SNpc tissue in the LC-induced model of PD. (**c**,**d**) Representative Western blots. Western blot analysis was conducted with the antibodies against TNF-α (1:1000, rabbit, Affinity Biosciences, Zhenjiang, China), IL-6 (1:1000, rabbit, Affinity Biosciences, Zhenjiang, China). Anti-GAPDH antibodies (1:1000, mouse, Affinity Biosciences, Zhenjiang, China) were used for loading control. Bar charts indicate mean values with standard errors. The dots, squares, triangles and rhombus show individual values per rat. Two-way ANOVA test followed by Tukey's post hoc analysis were performed to determine the effects of GRP78 therapy. Asterisks indicate significant differences between groups according to Tukey's post hoc tests: * $p < 0.05$, *** $p < 0.001$, vs. the vehicle group; # $p < 0.05$, vs. the LC group. Interaction factor for TNF-α F (1, 17) = 3.228 $p = 0.0902$; Grp78 treatment factor F (1, 17) = 2.034 $p = 0.1719$; LC (lactacystin) factor F (1, 17) = 7.614 $p = 0.0134$. Interaction factor for IL-6 F (1, 17) = 4.896 $p = 0.0409$; Grp78 treatment factor F (1, 17) = 3.164 $p = 0.0932$; F (1, 17) = 19.58 $p = 0.0004$.

To establish the mechanism enabling the GRP78-mediated inhibition of the microglia activation, we explored the activity of the NF-κB-dependent p65/RelA signaling pathway. This pathway facilitates the induction of proinflammatory cytokines [45] and NF-κB dysregulation has been found in patients with PD and in the substantia nigra of MPTP-treated mice [46]. Post-mortem studies showed an increase p65 nuclear translocation in melanized neurons of the substantia nigra that is supportive of NF-κB activation in PD. We assessed the expression patterns of p65 and phosphorylated-p65 (p-p65) after LC treatment with or without GRP78 using Western blot analysis. The level of p-p65 was found to increase in the LC group only, suggesting the activation of NF-κB during PD development. However, GPR78 inhibited the increase of p-p65 expression in the SNpc in the LC model (Figure 7), while no significant changes were found in LC-untreated rats. Hence, the decrease in p65 phosphorylation can be an essential factor in inhibiting activated microglia by exogenous GRP78.

Taken together, our data demonstrate that GRP78 can protect neurons from the excessive activation of microglia via NF-κB signaling pathways in the LC-induced rat model of PD.

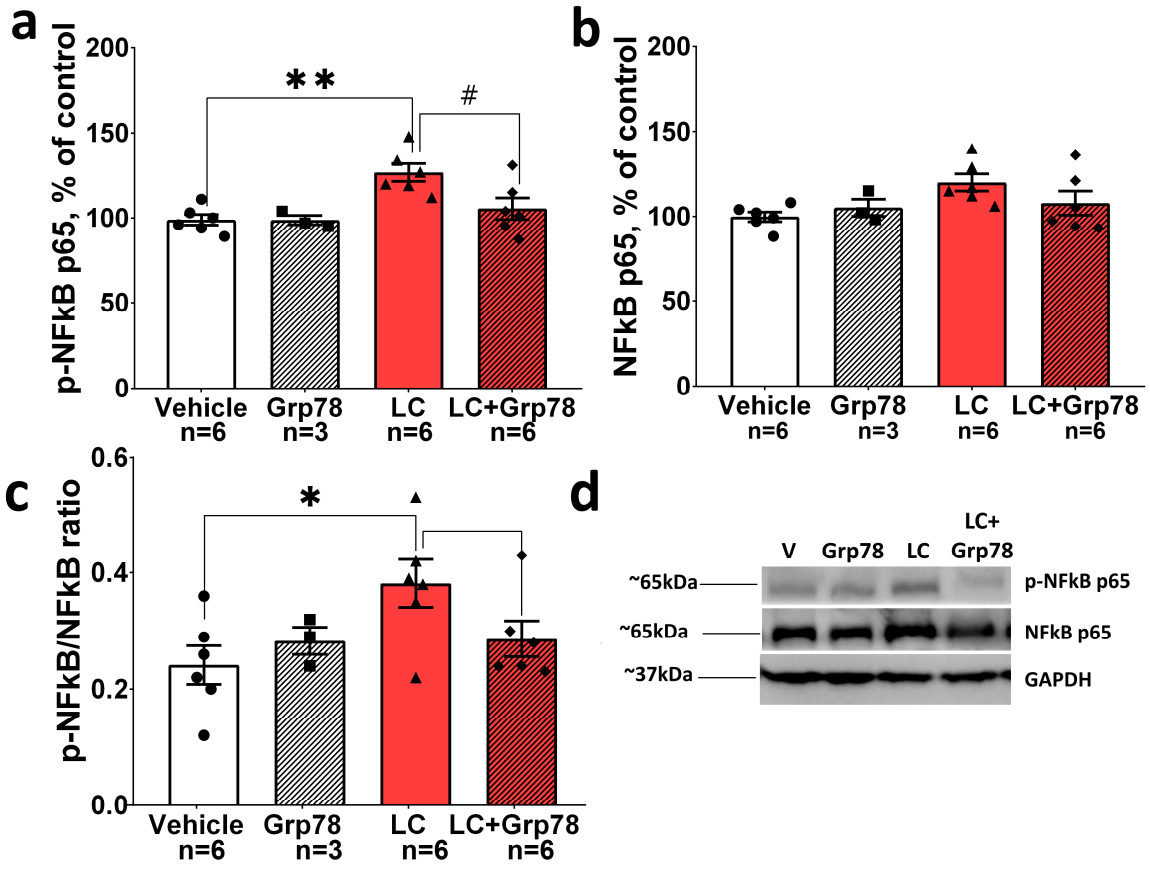

Figure 7. GRP78 can protect neurons from the excessive activation of microglia via NF-κB signaling pathways in the LC-induced rat model of PD. Content of (**a**) NF-κB p65, (**b**) phosphorylated NF-κB p65 (Ser536), and (**c**) phosphorylated to total NF-κB p65 ratio in SNpc in LC model of PD. (**d**) Representative immunoblots. Western blot analysis of the nigral tissue was conducted with the antibodies against NF-κB p65 (1:1000, mouse, Cell Signaling, Danvers, MA, USA), and phosphorylated NF-κB p65 (Ser536) (1:1000, rabbit, Cell Signaling, Danvers, MA, USA). Anti-GAPDH antibodies (1:1000, mouse, Affinity Biosciences, China) were used for loading control. Bar charts indicate mean values with standard errors. The dots, squares, triangles and rhombus show individual values per rat. Two-way ANOVA test followed by Tukey's post hoc analysis were performed to determine the effects of GRP78 therapy. Asterisks indicate significant differences between groups according to Tukey's post hoc tests: * $p < 0.05$, ** $p < 0.01$, vs. the vehicle group; # $p < 0.05$ vs. the LC group. Interaction factor for total NF-κB F (1, 17) = 2.337 $p = 0.1447$; Grp78 treatment factor F (1, 17) = 0.3563 $p = 0.5584$; LC factor F (1, 17) = 3.978 $p = 0.0624$. Interaction factor for phosphorylated NF-κB (Ser536) F (1, 17) = 3.776 $p = 0.0687$; Grp78 treatment factor F (1, 17) = 3.897 $p = 0.0648$; LC factor F (1, 17) = 10.29 $p = 0.0052$. Interaction factor for p-NF-κB (Ser536)/NF-κB ratio F (1, 17) = 5.358 $p = 0.0334$; Grp78 treatment factor F (1, 17) = 1.339 $p = 0.2631$; LC factor F (1, 17) = 2.477 $p = 0.1339$.

3. Discussion

With the population aging rapidly, the global prevalence of PD is rising, which significantly contributes to the increase in healthcare costs. Developing preventive PD therapy has proven challenging due to the limited bioavailability of neuroprotective drugs, partly because of the blood–brain barrier. One of the new approaches is the intranasal route of administration, delivering the drug from the nasal cavity directly to the brain via the olfactory and trigeminal nerves. It allows neurotherapeutic agents, including both small and large molecules, to bypass the blood–brain barrier [47,48]. Intranasal administration has shown therapeutic effects in animal and human studies of different pathologies [48].

In this study, we evaluated the neuroprotective potential of the intranasally administered recombinant human protein GRP78 in a rat PD model. The intranasal route was chosen considering that GRP78 protein can leave the ER, traverse the cell membrane, and enter the extracellular space [49], cerebrospinal fluid, and peripheral blood under normal and pathological conditions [37,50–52]. Moreover, when administered intravenously, exogenous GRP78 or its synthetic analog IRL201805 can be rapidly internalized by monocytes in the peripheral blood and directly impact various phenotypical and metabolic functions of myeloid cells [37]. It is noteworthy that the ability to enter the mammalian brain and neurons has been observed for another member of the same chaperone family, HSP70 (HSPA1). After intranasal administration, human recombinant HSP70 demonstrates therapeutic effects in animal models of PD and Alzheimer's disease [53,54]. This highlights the potential of using the intranasal delivery of chaperones to the brain for neuroprotection.

Neuroprotective interventions are most effective at the early (preclinical) stage of the pathological process. Therefore, we utilized a previously developed LC-induced model [21,55] that reproduces the main pathogenetic signs of the preclinical stage of PD in rats. These include the degeneration of 27% of DA neurons in the SNpc (a level that is characteristic of the preclinical PD stage [8] (Figure S1), development of α-syn pathology (Figure 3), and signs of chronic neuroinflammation (Figures 5 and 6)). At the molecular level, the model is characterized by the activation of the pro-apoptotic GRP78/PERK/eIF2/CHOP UPR pathway, caspases-9 and -3 (Figure 4), and the NF-κB-dependent p65 inflammatory signaling pathway (Figure 7). Yet, no motor dysfunction is detected.

At the first stage of our research, we demonstrated that intranasally administered GRP78 penetrates the mammalian brain and is internalized by DA neurons in the SNpc and other brain regions that can be affected by PD in humans (Figure S2). In addition, we have shown that exogenous GRP78 penetrates the brain under normal conditions (Figure S2) and accumulates in the neurons of the SNpc 3 h after administration (Figure S4), but 7 days after administration, GRP78 degrades, since its concentration in the SNpc tissue does not change in comparison to control animals (Figure S4). The internalization of GRP78 is assumed to occur through nonspecific or receptor-mediated endocytosis [37]. However, it is unclear what specific receptors and/or docking proteins facilitate endocytosis.

Next, we showed that GRP78 treatment mitigated the process of neurodegeneration in the rat model that mimics the preclinical stage of PD. It is evidenced by an increase in the number of TH-positive neurons in the SNpc and TH-positive axons in the dorsal striatum (Figure S1). Furthermore, intranasal treatment with GRP78 in control animals, without LC, was characterized by neither neurodegeneration in the nigrostriatal system nor behavioral deficit. This indicates the absence of cytotoxic properties of GRP78. Similar neuroprotective effects of elevating GRP78 via its overexpression in the SNpc have been shown in α-syn pathology models in rats [30,38], the 1-methyl-4-phenyl-1,2,3,6-tetrahydropyridine (MPTP) PD model in mice [56], and the rotenone PD model in rats [57]. Taken together, our data, along with the existing literature, indicate the therapeutic significance of elevating GRP78 levels in the brain during the development of PD-like pathology.

The abnormal accumulation of α-syn, and especially its phosphorylated and oligomeric forms, in the ER lumen and cytosol of the SNpc DA neurons is known to play a critical role in neuronal death in PD, although the underlying mechanism is poorly understood [10,58,59]. We first focused on investigating whether the neuroprotective effect of exogenous GRP78 is related to its ability to prevent α-syn pathology and the induction of the pro-apoptotic ER stress branch. We assessed levels of total and phosphorylated α-syn accumulated in the SNpc in the LC-induced PD model (Figure 3a,b) and demonstrated that pS129-α-syn predominated in the water-soluble monomeric α-syn fraction (Figure 3c). Hence, the enhanced S129-phosphorylation of α-syn may play a key role in the death of DA neurons in the SNpc. This assumption is supported by evidence showing that blocking S129-phosphorylation results in fewer α-syn aggregates and reduces neuronal cell death induced by the mitochondrial toxin rotenone [59]. In addition, the increased phosphorylation of α-syn can contribute to its transformation into oligomers or even aggregates, thereby affecting the

cytotoxicity of α-syn and promoting neuronal death [12,59–61]. It is assumed that extensive S129 phosphorylation during PD-like pathology is most likely caused by an increased influx of extracellular Ca^{2+} due to mitochondrial impairment [62] and the increased expression and activity of polo-like kinase 2 (PLK2, also known as serum-inducible kinase or SNK) [63,64].

Here, we showed that treatment with GRP78 reduced the content of the pS129 α-syn form (Figure 3b–d) in the LC model of PD. This effect coincided with an increase in the survival of DA neurons in the SNpc. We suggest that, at least in part, it was mediated by the direct interaction of GRP78 with both phosphorylated and non-phosphorylated forms of α-syn [26,29,30]. Such interaction could prevent excessive S129-phosphorylation and inhibit the multistep aggregation pathway of α-syn, reducing related toxicity.

The accumulation of aberrant α-syn forms is a central element for the induction of the UPR that can trigger apoptotic cell death in PD [31]. Since the exogenous GRP78 protein prevented the development of α-syn pathology in our preclinical PD model in rats, we then tested the hypothesis that this effect can lead to the inhibition of the ER stress response and a reduction of apoptosis in the SNpc. Indeed, the accumulation of monomeric α-syn in the SNpc correlated with the activation of the pro-apoptotic PERK-dependent pathway of the UPR in LC-treated rats (Figure 4a–d). This was evidenced by an increase in the level of the sensor protein and UPR activator GRP78, as well as the activation of eIf2α and upregulation of the ATF4-dependent pro-apoptotic factor CHOP (Figure 4a–d). At the same time, CHOP upregulation resulted in the activation of caspase-9 and caspase-3 (Figure 4e–g), promoting cell degeneration through the canonical mitochondrial apoptosis pathway. Overall, our data indicate that the prolonged hyperactivation of the PERK/CHOP pathway of the UPR promotes ER stress-dependent apoptosis in the SNpc in the animal model of preclinical PD. These findings correlate with studies on postmortem tissues from PD patients [28,33] and animal models of PD [35,65–67] that demonstrate the activation of the pro-apoptotic PERK/CHOP pathway in nigral tissue. Treatment with GRP78 downregulated ER stress mediators of the PERK-dependent pathway of the UPR (Figure 4a–d) and prevented the activation of pro-apoptotic caspases-9 and -3 (Figure 4e–g), which contributed to the survival of DA neurons in the SNpc in LC-injected animals. These results support the data on the neuroprotective effect of GRP78 overexpression, which is associated with the downregulation of the pro-apoptotic factor CHOP and a reduction in apoptosis in the SNpc in the rat model of α-syn pathology [30].

Neuroinflammation manifests in microglia activation and lymphocyte infiltration. It can be provoked by the release of misfolded α-syn from damaged and dead neurons, leading to the development and progression of PD [23]. Activated microglia is a chronic source of pro-inflammatory cytokines, reactive oxygen species (ROS), and nitric oxide (NO), all of which can induce neuronal death [68]. Large numbers of activated microglia and elevated levels of TNF-alpha receptor R1 in the SNpc, along with activated caspase-1 and caspase-3, have been observed in PD [69–71]. Furthermore, in vivo imaging has confirmed that widespread microglial activation is associated with the pathological process in idiopathic PD [45]. In our LC-induced model of the preclinical PD, the number of Iba-1 positive cells of amoeboid-like phenotype (Figure 5) was correlated with an increase in pro-inflammatory cytokines TNF-α and IL-6 (Figure 6) in the SNpc. This indicates the development of reactive microgliosis and neuroinflammation, potentially contributing to the death of DA neurons. We showed that intranasally delivered GRP78 was efficiently internalized by the microgliocytes of the SNpc (Figure 2c,f,i,l) and directly affected cell physiology. Its protective action manifested in a decreased number of Iba1-positive cells and lower levels of TNF-α and IL-6; these data indicate reduced microglial activation and neuroinflammation in the SNpc. However, it is not yet clear whether the anti-inflammatory effect of GRP78 is associated with the phenotypic shift of pro-inflammatory M1 microglia to anti-inflammatory M2 microglia, which may promote neuroprotection. Notably, following the systemic administration of GRP78 or its analog IRL201805 in an animal model of rheumatoid arthritis, these proteins are rapidly internalized by monocytes, which even-

tually leads to an increased secretion of IL-10 and the suppression of TNF-α and IL-1β release [37]. These anti-inflammatory properties of exogenous GRP78 help regulate and resolve chronic inflammation.

Toll-like receptors (TLRs) can serve as essential immune receptors in PD, triggering neuroinflammation [72,73]. TLRs can recognize a wide variety of damage-associated molecular patterns, including misfolded α-syn, released by damaged and dead neurons. Upon the recognition of these molecules, TLRs trigger a signaling cascade that activates NF-κB factors. NF-κB factors play a crucial role in the regulation of inflammation and apoptosis, and are involved in the pathogenesis of PD [46]. To find out whether the anti-inflammatory effect of exogenous GRP78 depends on its ability to modulate the NF-κB signaling pathway, we assessed expression patterns of p65 and phosphorylated-p65. The NF-κB-dependent p65 signaling pathway was shown to be activated in the SNpc in the LC-induced model of preclinical PD. This may be a signal regulating the molecular activation of microglia at an early stage of the disease. However, treatment with GRP78 inhibited the nigral activation of NF-κB (Figure 6). Taken together, the results demonstrate that exogenous GRP78 exerts potent anti-inflammatory effects. It can protect neurons against the excessive activation of microglia by targeting NF-κB signaling pathways during the development of LC-induced PD-like pathology.

Overall, our data support the therapeutic relevance of delivering GRP78 intranasally to the brain to prevent and/or slow down PD-like neurodegeneration. We determined that the neuroprotective potential of exogenous GRP78 is linked to its ability to (i) prevent the manifestation of α-syn pathology, (ii) block ER stress-dependent apoptosis, and (iii) mitigate the excessive activation of microglia by targeting NF-κB signaling pathways in the LC-induced rat model of preclinical PD.

4. Materials and Methods

4.1. Animals

The study was carried out in 6-month-old male Wistar rats, weighing 280–310 g. The animals were housed in individual cages under standard environmental conditions (12:12 h light–dark cycle; ambient temperature 23 ± 2 °C; food and water available ad libitum). The experiments were conducted under the requirements of the EU Directive 2010/63/EU on the treatment of laboratory animals and those of the Sechenov Institute of Evolutionary Physiology and Biochemistry of the Russian Academy of Sciences (Protocol No # 1-17/2022, 27 January 2022). The rats were placed in groups randomly.

4.2. Implantation of Guiding Cannulas

Before implantation surgery, animals were anesthetized with intramuscular injection of Zoletil-100 (50 mg/kg; tiletamine hydrochloride and zolazepam; Virbac, Carros, France) and then placed into a stereotaxic device (Narishige, Tokyo, Japan). Two stainless-steel guide cannulas (internal diameter 0.3 mm) were implanted into the SNpc for bilateral drug injections. The coordinates were as follows: 5.0 mm caudal to the bregma, 2.0 mm lateral to the midline, and 7.5 mm deep from the skull surface [74]. The guide cannulas were secured with Akrodent dental cement (Stoma, Kharkiv, Ukraine). Then, animals were returned to their home cages, and experiments began no earlier than 7 days post-surgery.

4.3. Modeling Parkinson's Disease in Wistar Rats

Cannulated animals were used to model PD and evaluate the protective potential of intranasally administered GRP78. To create the PD model, we used a specific, irreversible proteasome inhibitor lactacystin (LC; Enzo Life Sciences, Farmingdale, NY, USA). Phosphate-buffered saline (PBS) was filtered through a sterilized syringe filter (30 mm, PVDF, 0.22 μm; JET BIOFIL®, Seoul, Republic of Korea). LC was diluted in sterile PBS to the final concentration of 0.4 μg/μL and injected immediately after dilution through cannulas to rats (n = 6–8, group LC). Two sequential bilateral microinjections of LC into the SNpc were performed at a dose of 0.4 μg/1 μL with a weekly interval. For microinjections,

we used a needle with an external diameter of 0.2 mm attached to a 1 μL Hamilton syringe (Hamilton, Reno, NV, USA) via a short length of polyethylene tubing. LC was injected at a flow rate of 0.1 μL/ min. Control rats were treated similarly but received an equivalent volume of vehicle (PBS) instead of LC.

4.4. GRP78 Treatment

Recombinant human heat shock protein GRP78 (Sigma, Livonia, MI, USA) was diluted in sterile PBS (pH 7.4) and administered intranasally (to each nostril) to rats (n = 6–8, group LC+GRP78) at a dose of 1.6 μg/8 μL, 4 h and 28 h after each microinjection of LC. Additional administration of GRP78 was performed 7 days after the last LC microinjection. The control group of animals (n = 6–8) received an equivalent volume of the vehicle (PBS) instead of LC and GRP78. GRP78 was also administered to intact animals, untreated with LC (n = 3, group GRP78) (see experimental design in Figure 1). Intranasal injections were performed using a 10 μL micropipette (JET BIOFIL®, Seoul, Republic of Korea) at a flow rate of 3 μL/min. Animals were given one-minute intervals to regain normal respiratory function. All the effects were evaluated 21 days later.

4.5. GRP78 Labeling and Confocal Microscopy

GRP78 protein was conjugated with a fluorescent Alexa-555 dye (Invitrogen, Waltham, MA, USA) according to the manufacturer's protocol. Briefly, 50 μL of 10 mg/mL Alexa-555 solution in dimethyl sulfoxide was slowly added to 5 mg of GRP78 in 500 μL of 0.1 M sodium bicarbonate, pH 8.3, and vortexed for 2 min. The mixture was incubated for 1 h at 4 °C with continuous stirring. The reaction was stopped by adding 50 μL of freshly prepared 1.5 M hydroxylamine, pH 8.5. The conjugate was separated from non-reacted labels through triple dialysis in PBS at 4 °C.

GRP78 protein labeled with Alexa-555 was administered intranasally to rats (n = 4) at a dose of 1.6 μg/8 μL, 4 h after a microinjection of LC or after PBS injection (n = 4) into SNpc. Animals after LC-injection into SNpc treated with unlabled-GRP78 (n = 4) were used as controls. Three hours later, the rats were anesthetized with Zoletil-100 (50 mg/kg, i.m.) and rapidly transcardially perfused with 0.1 M PBS (pH = 7.4) and 4% paraformaldehyde in 0.1 M PBS. After that, the animals were decapitated, and their brains were isolated and placed in the same fixative overnight at 4 °C. Following 48 h incubation in 30% sucrose/PBS at 4 °C for cryoprotection, the brains were frozen in cold isopentane (−42 °C) and stored at −80 °C for further use. Serial frontal brain sections were prepared using a Leica CM-1520 cryostat ("Leica Biosystems", Nussloch, Germany). Sections (10 and 20 μm) of the SNpc, the ventral tegmental area (VTA), and the locus coeruleus were prepared according to the brain atlas [74]. Eight to twelve alternate series of sections were mounted on SuperFrost Plus Adhesion Microscope Slides ("Gerhard Menzel GmbH", Braunschweig, Germany) and stored at −22 °C.

For confocal microscopy, brain sections were dried at 23 °C overnight, repeatedly washed in PBS or PBS with 0.1% Tween-20 (PBST), and pre-incubated in 4% blocking solution (2% bovine serum albumin and 2% normal goat serum diluted in PBST) for 1 h at 23 °C. Next, the sections were incubated with primary antibodies against tyrosine hydroxylase (TH; 1:900; rabbit, ab117112, Abcam, Cambridge, UK), GRP78 (1:300; rabbit, ab21685, Abcam, Cambridge, UK), or Iba (1:500; rabbit, Novus Biologicals, Centennial, CO, USA) for 24 h. After washing with PBS, the sections were incubated for 2 h at room temperature with secondary anti-rabbit IgG antibodies labeled with DyLight-488 (1:350; 35552, Thermo Scientific, Waltham, MA, USA). Following several PBS washes, the slides were coverslipped with Mowiol (Sigma, Burlington, MA, USA). Unlabeled sections were used to measure autofluorescence. Images were obtained on a DMI6000 confocal microscope with a Leica TCS SP5 laser scanning confocal setup (Leica Microsystems, Wetzlar, Germany) using a ×63 oil immersion objective. The resulting images were analyzed using the Leica LAS AF version 4.0 software package. To avoid cross-interference between

fluorochromes, images for Alexa-555 and DyLight-488 were acquired using the sequential image recording method.

4.6. Immunohistochemical Studies

21 days after the first LC microinjection, rats were anesthetized with Zoletil-100 and decapitated. One half of each brain was used for immunohistochemical assays. The second half was used for further biochemical analysis. For immunohistochemical assays, brains were isolated and placed in the 4% paraformaldehyde in 0.1 M PBS overnight at 4 °C. Following 48 h incubation in 30% sucrose/PBS at 4 °C, the brains were frozen in cold isopentane (−42 °C) and stored at −80 °C for further use. Serial frontal brain sections were prepared using a Leica CM-1520 cryostat ("Leica Biosystems", Nussloch, Germany). Sections (10 μm) of the SNpc were prepared according to the brain atlas [74]. Ten to twelve alternate series of sections were mounted on SuperFrost Plus Adhesion Microscope Slides ("Gerhard Menzel GmbH", Braunschweig, Germany) and stored at −22 °C.

For bright-field microscopic analysis, brain sections were dried at 23 °C overnight. Next, sections were repeatedly washed in PBS and were preincubated first with 3% H_2O_2–10% methanol for 20 min, and then with 4% blocking solution for 1 h at room temperature. Sections were incubated for 48 h at room temperature with primary antibodies against microglia marker Iba-1 (1:500; rabbit, Novus Biologicals, Centennial, CO, USA) or anti-GRP78 antibodies (1:400, rabbit, Affinity Biosciences, Zhenjiang, China). Following incubation with biotinylated secondary antibodies, sections were incubated with streptavidin–peroxidase (1:250; Vector Labs., Newark, CA, USA). Reactions were visualized using 3,3-diaminobenzidine (Sigma-Aldrich, St. Louis, MO, USA) as a chromogen. To ensure specificity of the immunohistochemical staining, staining reactions lacking primary antibodies were performed.

Images of the stained sections of SNpc were obtained using a Zeiss Axio Imager A1 microscope (Carl Zeiss, Jena, Germany) with a built-in camera and Axio-Vision 4.8 software. Quantitative analysis was performed using 10–12 sections from each animal at the same level of the studied zones, separated by approximately 70 μm. The number of cells accounted for a standard area of tissue captured by a light microscope camera using ×20 lens—697 × 523 μm for Iba staining, and ×10 lens—1389 × 1040 μm for GRP78 staining. The number of Iba-positive cell bodies was counted manually and expressed as the average number of positive stained microglia cells per SNpc section. The optical density reflecting the content of an GRP78-immunopositive substance was calculated as the difference between intensely colored neurons containing an immunoreactive substance and the intensity of background coloring (not containing an immunoreactive substance) on the same section. The results were presented in relative units of optical density.

The analysis was performed using the PhotoM freeware version 1.21 (http://www.t_lambda.chat.ru/ accessed on 11 December 2019).

4.7. Immunoblotting

The SNpc was dissected from the brain according to the brain atlas [74]. All samples were weighed, frozen at −80 °C, and stored until the analysis. SNpc tissue was then homogenized in lysis buffer containing 20 mM Tris–HCl (pH 7.5), 150 mM NaCl, 0.5% Triton X-100, and 2 mM EDTA supplemented with a protease inhibitor cocktail (Sigma Aldrich, St. Louis, MO, USA) and a phosphatase inhibitor cocktail (Roche, Basel, Switzerland). Next, homogenized tissue was incubated on ice for 1 h until the lysis of the samples was complete. Following centrifugation (13,500× g for 10 min), the supernatant was used for protein quantification and further assays. Protein concentration was measured by the Lowry assay with BSA as a standard. For Western blotting, the protein supernatant was mixed 2:1 with loading buffer (0.0625 M Tris–HCl (pH 6.8), 10% glycerol, 2% SDS, 0.1 mM EDTA, 0.006% bromophenol blue, 10% β-mercaptoethanol) and heated at 95 °C for 7 min. Equal volume aliquots containing 30 μg of total protein were loaded onto 11% polyacrylamide gel and separated by electrophoresis with the Precisions Plus Protein Dual

Xtra Standards marker (BioRad, Hercules, CA, USA). Protein bands were then transferred onto PVDF membranes (pore size 0.2 μm; BioRad, Hercules, CA, USA) by wet transfer with a TransBlot device (BioRad, Hercules, CA, USA).

To prevent nonspecific antibody binding, membranes were incubated in a blocking solution (PBS added with 0.1% Tween-20 and 3% BSA or PBS added with 0.1% Tween-20 and 5% Nonfat dairy milk, NFDM) for 1 h. The membranes were then incubated at 4 °C overnight in PBST solution containing 0.05% NaN_3 and 3% BSA or 5% NFDM and one of the following primary antibodies: monoclonal antibodies against GRP78 (1:1000, rabbit, ab21685, Abcam, Cambridge, UK), phospho-NFkB p65 (Ser536) (1:750, rabbit, mAb#3033, Cell Signaling, Danvers, MA, USA), NFkB p65 (1:750, rabbit, mAb#8242, Cell Signaling, Danvers, MA, USA), or polyclonal antibodies against phospho-eIF2α (Ser51) (1:750, rabbit, AF3087, Affinity Biosciences, Zhenjiang, China), eIF2α (1:1000, rabbit, ab5369 Abcam, Cambridge, UK), CHOP (1:1000, rabbit, DF6025 Affinity Biosciences, Zhenjiang, China), caspase-9 cleaved (Asp353) (1:1000, rabbit, AF6348, Affinity Biosciences, Zhenjiang, China), caspase-3 cleaved (Asp175) (1:1000, rabbit, AF7022 Affinity Biosciences, Zhenjiang, China), phospho-α-syn (Ser129) (1:1500, rabbit, AF3285, Affinity Biosciences, Zhenjiang, China), α-syn (1:1200, rabbit, AF6285, Affinity Biosciences, Zhenjiang, China), Interleukine-6 (1:1000, rabbit, MAA079Ra21, Affinity Biosciences, Zhenjiang, China), or TNF-α (1:1000, rabbit, Affinity Biosciences, Zhenjiang, China). The polyclonal antibodies against GAPDH (1:1000, rabbit, AF7021 Affinity Biosciences, Zhenjiang, China) and β-Actin (1:1000, mouse, sc-69879, Santa Cruz Biotechnology Inc, Dallas, TX, USA) were used to visualize loading controls. Then, membranes were washed with PBST three times for 10 min each and incubated at room temperature for 1 h with a PBS solution of secondary antibodies conjugated with horseradish peroxidase (1:10,000, HRP-Goat Anti-Rabbit IgG, 111-035-144, or HRP-Donkey Anti-Mouse IgG, 715-036-150, both Jackson ImmunoResearch Europe Ltd., Ely, UK). After three washes with PBST, bands were visualized using a chemiluminescence protocol with the Novex ECL HRP Chemiluminescent Substrate Reagent Kit (Invitrogen, Carlsbad, CA, USA) and a ChemiDoc MP imager (Bio-Rad, Hercules, CA, USA).

Protein levels were normalized to the GAPDH or β-Actin signal. The relative amounts of phospho-eIF2α (Ser51) or phospho-NFkB p65 (Ser536) were determined by adjusting for total eIF2α or NFkB p65 protein or for GAPDH. Densitometric analysis was performed in the open-source ImageJ 1.8 software (National Institutes of Health, New York, NY, USA). The ratios of the optical densities of specific protein bands to the total protein were compared to the mean of the control group.

4.8. Statistics

All data were analyzed using GraphPad Prism 8 (GraphPad Software, San Diego, CA, USA). The distribution normality was checked using the Kolmogorov–Smirnov test. Multiple comparisons between the groups of rats were run using the two-way ANOVA test followed by Tukey's post hoc tests. Intergroup differences were considered statistically significant at $p \leq 0.05$. All data were represented as the mean ± standard error of the mean (SEM) and as individual values.

5. Conclusions

In an LC-induced rodent model, we achieved the first successful treatment of PD-like pathology using an intranasal delivery of the recombinant human protein GRP78 to the brain. We report that intranasally administered GRP78 rapidly enters affected brain regions and prevents the development of neurodegeneration in the nigrostriatal system during the preclinical stage of PD in rats. LC-induced disturbances, including ER stress-dependent apoptosis and the abnormal accumulation of monomeric phosphorylated pS129-α-syn, are alleviated with GRP78 administration. Moreover, exogenous GRP78 exhibits anti-inflammatory properties and can protect neurons against the excessive activation of microglia, as well as the increased production of pro-inflammatory cytokines, TNF-α and IL-6, by targeting NF-κB signaling pathways. Although further investigation into

molecular mechanisms is still necessary, we anticipate that this therapeutic approach, based on intranasal exogenous GRP78, may contribute to the development of effective therapeutic agents for PD and other synucleinopathies in the future.

Supplementary Materials: The following supporting information can be downloaded at: https://www.mdpi.com/article/10.3390/ijms25073951/s1.

Author Contributions: Conceptualization, I.V.E.; methodology, M.B.P., D.V.B., E.Y.K. and I.V.E.; formal analysis, M.B.P. and I.V.E.; investigation, M.B.P., E.Y.K. and D.V.B.; resources M.B.P., D.V.B. and I.V.E.; data curation, I.V.E., D.V.B. and M.B.P.; writing—original draft preparation, M.B.P. and I.V.E.; writing—review and editing, M.B.P., D.V.B. and I.V.E.; supervision, I.V.E.; project administration, I.V.E.; funding acquisition, I.V.E. All authors have read and agreed to the published version of the manuscript.

Funding: The work was supported by the IEPhB Research Program 075-00264-24-00.

Institutional Review Board Statement: The study was conducted under the requirements of the EU Directive 2010/63/EU and those of the Sechenov Institute of Evolutionary Physiology and Biochemistry of the Russian Academy of Sciences (St. Petersburg, Russia) (protocol no 1-17/ 2022, 27 January 2022).

Informed Consent Statement: Not applicable.

Data Availability Statement: The data presented in this study are available on request from the corresponding author M.B.P. and I.V.E.

Acknowledgments: Biochemical and immunohistochemical studies were performed using the facilities of the Research Resource Centre for physiological, biochemical, and molecular–biological research of the Sechenov Institute of Evolutionary Physiology and Biochemistry of the Russian Academy of Sciences.

Conflicts of Interest: The authors declare no conflicts of interest.

Abbreviations

ATF6	activating transcription factor 6
α-syn	α-synuclein
CHOP	C/EBP homologous protein
DA	dopaminergic
eIF2α	eukaryotic initiation factor 2α
ERAD	ER-associated degradation
ER	endoplasmic reticulum
GAPDH	glyceraldehyde 3-phosphate dehydrogenase
GRP78/BiP	glucose-regulated protein 78/immunoglobulin heavy chain binding protein
HSP	heat-shock protein
IRE1α	inositol-requiring transmembrane kinase/endoribonuclease 1α
IL-6	Interleukin-6
Iba1	Ionized calcium-binding adaptor molecule 1
LC	lactacystin
MPTP	1-methyl-4-phenyl-1,2,3,6-tetrahydropyridine
NF-κB	nuclear factor kappa-light-chain-enhancer of activated B cells
PD	Parkinson's disease

References

1. Tysnes, O.-B.; Storstein, A. Epidemiology of Parkinson's Disease. *J. Neural Transm.* **2017**, *124*, 901–905. [CrossRef]
2. Dorsey, E.R.; Constantinescu, R.; Thompson, J.P.; Biglan, K.M.; Holloway, R.G.; Kieburtz, K.; Marshall, F.J.; Ravina, B.M.; Schifitto, G.; Siderowf, A.; et al. Projected Number of People with Parkinson Disease in the Most Populous Nations, 2005 through 2030. *Neurology* **2007**, *68*, 384–386. [CrossRef] [PubMed]
3. Thomas, B.; Beal, M.F. Parkinson's Disease. *Hum. Mol. Genet.* **2007**, *16*, R183–R194. [CrossRef] [PubMed]
4. Tanner, C.M. Is the Cause of Parkinson's Disease Environmental or Hereditary? Evidence from Twin Studies. *Adv. Neurol.* **2003**, *91*, 133–142. [PubMed]

5. Karpenko, M.N.; Muruzheva, Z.M.; Pestereva, N.S.; Ekimova, I.V. An Infection Hypothesis of Parkinson's Disease. *Neurosci. Behav. Physiol.* **2019**, *49*, 555–561. [CrossRef]
6. Hustad, E.; Aasly, J.O. Clinical and Imaging Markers of Prodromal Parkinson's Disease. *Front. Neurol.* **2020**, *11*, 395. [CrossRef] [PubMed]
7. Riederer, P.; Wuketich, S. Time Course of Nigrostriatal Degeneration in Parkinson's Disease. A Detailed Study of Influential Factors in Human Brain Amine Analysis. *J. Neural Transm.* **1976**, *38*, 277–301. [CrossRef]
8. Braak, H.; Del Tredici, K.; Rüb, U.; de Vos, R.A.I.; Jansen Steur, E.N.H.; Braak, E. Staging of Brain Pathology Related to Sporadic Parkinson's Disease. *Neurobiol. Aging* **2003**, *24*, 197–211. [CrossRef]
9. Ugrumov, M. Development of Early Diagnosis of Parkinson's Disease: Illusion or Reality? *CNS Neurosci. Ther.* **2020**, *26*, 997–1009. [CrossRef]
10. Ganguly, U.; Chakrabarti, S.S.; Kaur, U.; Mukherjee, A.; Chakrabarti, S. Alpha-Synuclein, Proteotoxicity and Parkinson's Disease: Search for Neuroprotective Therapy. *Curr. Neuropharmacol.* **2018**, *16*, 1086–1097. [CrossRef]
11. Roberts, H.; Brown, D. Seeking a Mechanism for the Toxicity of Oligomeric α-Synuclein. *Biomolecules* **2015**, *5*, 282–305. [CrossRef] [PubMed]
12. Sato, H.; Kato, T.; Arawaka, S. The Role of Ser129 Phosphorylation of α-Synuclein in Neurodegeneration of Parkinson's Disease: A Review of in Vivo Models. *Rev. Neurosci.* **2013**, *24*, 115–123. [CrossRef]
13. Creed, R.B.; Memon, A.A.; Komaragiri, S.P.; Barodia, S.K.; Goldberg, M.S. Analysis of hemisphere-dependent effects of unilateral intrastriatal injection of α-synuclein pre-formed fibrils on mitochondrial protein levels, dynamics, and function. *Acta Neuropathol. Commun.* **2022**, *10*, 78. [CrossRef] [PubMed]
14. Chu, Y.; Dodiya, H.; Aebischer, P.; Olanow, C.W.; Kordower, J.H. Alterations in Lysosomal and Proteasomal Markers in Parkinson's Disease: Relationship to Alpha-Synuclein Inclusions. *Neurobiol. Dis.* **2009**, *35*, 385–398. [CrossRef]
15. Dehay, B.; Bové, J.; Rodríguez-Muela, N.; Perier, C.; Recasens, A.; Boya, P.; Vila, M. Pathogenic Lysosomal Depletion in Parkinson's Disease. *J. Neurosci.* **2010**, *30*, 12535–12544. [CrossRef]
16. McNaught, K.S.P.; Jackson, T.; JnoBaptiste, R.; Kapustin, A.; Olanow, C.W. Proteasomal Dysfunction in Sporadic Parkinson's Disease. *Neurology* **2006**, *66*, S37–S49. [CrossRef]
17. Moreno, J.A.; Tiffany-Castiglioni, E. The Chaperone Grp78 in Protein Folding Disorders of the Nervous System. *Neurochem. Res.* **2015**, *40*, 329–335. [CrossRef]
18. Kim, Y.E.; Hipp, M.S.; Bracher, A.; Hayer-Hartl, M.; Hartl, F.U. Molecular Chaperone Functions in Protein Folding and Proteostasis. *Annu. Rev. Biochem.* **2013**, *82*, 323–355. [CrossRef]
19. Labbadia, J.; Morimoto, R.I. The Biology of Proteostasis in Aging and Disease. *Annu. Rev. Biochem.* **2015**, *84*, 435–464. [CrossRef] [PubMed]
20. Bentea, E.; Verbruggen, L.; Massie, A. The Proteasome Inhibition Model of Parkinson's Disease. *J. Park. Dis.* **2017**, *7*, 31–63. [CrossRef]
21. Ekimova, I.V.; Belan, D.V.; Lapshina, K.V.; Pastukhov, Y.F. The Use of the Proteasome Inhibitor Lactacystin for Modeling Parkinson's Disease: Early Neurophysiological Biomarkers and Candidates for Intranigral and Extranigral Neuroprotection. In *Handbook of Animal Models in Neurological Disorders*; Martin, C.R., Patel, V.B., Preedy, V.R., Eds.; Elsevier: Amsterdam, The Netherlands; Academic Press: Cambridge, MA, USA, 2023; Chapter 41; pp. 507–523. ISBN 9780323898331. [CrossRef]
22. McNaught, K.S.P.; Perl, D.P.; Brownell, A.; Olanow, C.W. Systemic Exposure to Proteasome Inhibitors Causes a Progressive Model of Parkinson's Disease. *Ann. Neurol.* **2004**, *56*, 149–162. [CrossRef] [PubMed]
23. Béraud, D.; Maguire-Zeiss, K.A. Misfolded α-Synuclein and Toll-like Receptors: Therapeutic Targets for Parkinson's Disease. *Park. Relat. Disord.* **2012**, *18* (Suppl. S1), S17–S20. [CrossRef] [PubMed]
24. Yi, S.; Wang, L.; Wang, H.; Ho, M.S.; Zhang, S. Pathogenesis of α-Synuclein in Parkinson's Disease: From a Neuron-Glia Crosstalk Perspective. *Int. J. Mol. Sci.* **2022**, *23*, 14753. [CrossRef] [PubMed]
25. Hartmann, A.; Hunot, S.; Michel, P.P.; Muriel, M.-P.; Vyas, S.; Faucheux, B.A.; Mouatt-Prigent, A.; Turmel, H.; Srinivasan, A.; Ruberg, M.; et al. Caspase-3: A Vulnerability Factor and Final Effector in Apoptotic Death of Dopaminergic Neurons in Parkinson's Disease. *Proc. Natl. Acad. Sci. USA* **2000**, *97*, 2875–2880. [CrossRef] [PubMed]
26. Bellucci, A.; Navarria, L.; Zaltieri, M.; Falarti, E.; Bodei, S.; Sigala, S.; Battistin, L.; Spillantini, M.; Missale, C.; Spano, P. Induction of the Unfolded Protein Response by α-Synuclein in Experimental Models of Parkinson's Disease. *J. Neurochem.* **2011**, *116*, 588–605. [CrossRef] [PubMed]
27. Tatton, N.A.; Kish, S.J. In Situ Detection of Apoptotic Nuclei in the Substantia Nigra Compacta of 1-Methyl-4-Phenyl-1,2,3,6-Tetrahydropyridine-Treated Mice Using Terminal Deoxynucleotidyl Transferase Labelling and Acridine Orange Staining. *Neuroscience* **1997**, *77*, 1037–1048. [CrossRef] [PubMed]
28. Hoozemans, J.J.M.; van Haastert, E.S.; Eikelenboom, P.; de Vos, R.A.I.; Rozemuller, J.M.; Scheper, W. Activation of the Unfolded Protein Response in Parkinson's Disease. *Biochem. Biophys. Res. Commun.* **2007**, *354*, 707–711. [CrossRef] [PubMed]
29. Colla, E.; Coune, P.; Liu, Y.; Pletnikova, O.; Troncoso, J.C.; Iwatsubo, T.; Schneider, B.L.; Lee, M.K. Endoplasmic Reticulum Stress Is Important for the Manifestations of α-Synucleinopathy In Vivo. *J. Neurosci.* **2012**, *32*, 3306–3320. [CrossRef] [PubMed]
30. Gorbatyuk, M.S.; Shabashvili, A.; Chen, W.; Meyers, C.; Sullivan, L.F.; Salganik, M.; Lin, J.H.; Lewin, A.S.; Muzyczka, N.; Gorbatyuk, O.S. Glucose Regulated Protein 78 Diminishes α-Synuclein Neurotoxicity in a Rat Model of Parkinson Disease. *Mol. Ther.* **2012**, *20*, 1327–1337. [CrossRef]

31. Smedley, G.D.; Walker, K.E.; Yuan, S.H. The Role of PERK in Understanding Development of Neurodegenerative Diseases. *Int. J. Mol. Sci.* **2021**, *22*, 8146. [CrossRef]
32. Kim, S.; Kim, D.K.; Jeong, S.; Lee, J. The Common Cellular Events in the Neurodegenerative Diseases and the Associated Role of Endoplasmic Reticulum Stress. *Int. J. Mol. Sci.* **2022**, *23*, 5894. [CrossRef] [PubMed]
33. da Costa, C.A.; El Manaa, W.; Duplan, E.; Checler, F. The Endoplasmic Reticulum Stress/Unfolded Protein Response and Their Contributions to Parkinson's Disease Physiopathology. *Cells* **2020**, *9*, 2495. [CrossRef] [PubMed]
34. Galehdar, Z.; Swan, P.; Fuerth, B.; Callaghan, S.M.; Park, D.S.; Cregan, S.P. Neuronal Apoptosis Induced by Endoplasmic Reticulum Stress Is Regulated by ATF4-CHOP-Mediated Induction of the Bcl-2 Homology 3-Only Member PUMA. *J. Neurosci.* **2010**, *30*, 16938–16948. [CrossRef] [PubMed]
35. Deng, C.; Tao, R.; Yu, S.-Z.; Jin, H. Inhibition of 6-Hydroxydopamine-Induced Endoplasmic Reticulum Stress by Sulforaphane through the Activation of Nrf2 Nuclear Translocation. *Mol. Med. Rep.* **2012**, *6*, 215–219. [CrossRef]
36. Brown, M.K.; Naidoo, N. The Endoplasmic Reticulum Stress Response in Aging and Age-Related Diseases. *Front. Physiol.* **2012**, *3*, 263. [CrossRef] [PubMed]
37. Eggleton, P.; De Alba, J.; Weinreich, M.; Calias, P.; Foulkes, R.; Corrigall, V.M. The Therapeutic Mavericks: Potent Immunomodulating Chaperones Capable of Treating Human Diseases. *J. Cell Mol. Med.* **2023**, *27*, 322–339. [CrossRef] [PubMed]
38. Salganik, M.; Sergeyev, V.G.; Shinde, V.; Meyers, C.A.; Gorbatyuk, M.S.; Lin, J.H.; Zolotukhin, S.; Gorbatyuk, O.S. The Loss of Glucose-Regulated Protein 78 (GRP78) during Normal Aging or from SiRNA Knockdown Augments Human Alpha-Synuclein (α-Syn) Toxicity to Rat Nigral Neurons. *Neurobiol. Aging* **2015**, *36*, 2213–2223. [CrossRef] [PubMed]
39. Esteves, A.R.; Cardoso, S.M. Differential Protein Expression in Diverse Brain Areas of Parkinson's and Alzheimer's Disease Patients. *Sci. Rep.* **2020**, *10*, 13149. [CrossRef]
40. Kakimura, J.; Kitamura, Y.; Taniguchi, T.; Shimohama, S.; Gebicke-Haerter, P.J. BiP/GRP78-Induced Production of Cytokines and Uptake of Amyloid-β(1-42) Peptide in Microglia. *Biochem. Biophys. Res. Commun.* **2001**, *281*, 6–10. [CrossRef]
41. Ekimova, I.V.; Pazi, M.B.; Plaksina, D.V. Assessment of the Neuroprotective Potential of Glucose-Regulated Heat Shock Protein in a Model of Parkinson's Disease in Rats. *Neurosci. Behav. Physiol.* **2020**, *50*, 119–125. [CrossRef]
42. Prakash, K.M.; Nadkarni, N.V.; Lye, W.-K.; Yong, M.-H.; Tan, E.-K. The Impact of Non-Motor Symptoms on the Quality of Life of Parkinson's Disease Patients: A Longitudinal Study. *Eur. J. Neurol.* **2016**, *23*, 854–860. [CrossRef]
43. Panayi, G.S.; Corrigall, V.M. Immunoglobulin Heavy-Chain-Binding Protein (BiP): A Stress Protein That Has the Potential to Be a Novel Therapy for Rheumatoid Arthritis. *Biochem. Soc. Trans.* **2014**, *42*, 1752–1755. [CrossRef]
44. DiSabato, D.J.; Quan, N.; Godbout, J.P. Neuroinflammation: The Devil Is in the Details. *J. Neurochem.* **2016**, *139* (Suppl. S2), 136–153. [CrossRef] [PubMed]
45. Liu, T.; Zhang, L.; Joo, D.; Sun, S.-C. NF-κB Signaling in Inflammation. *Signal Transduct. Target. Ther.* **2017**, *2*, 17023. [CrossRef] [PubMed]
46. Bellucci, A.; Bubacco, L.; Longhena, F.; Parrella, E.; Faustini, G.; Porrini, V.; Bono, F.; Missale, C.; Pizzi, M. Nuclear Factor-κB Dysregulation and α-Synuclein Pathology: Critical Interplay in the Pathogenesis of Parkinson's Disease. *Front. Aging Neurosci.* **2020**, *12*, 68. [CrossRef] [PubMed]
47. Pardeshi, C.V.; Belgamwar, V.S. Direct Nose to Brain Drug Delivery via Integrated Nerve Pathways Bypassing the Blood-Brain Barrier: An Excellent Platform for Brain Targeting. *Expert Opin. Drug Deliv.* **2013**, *10*, 957–972. [CrossRef]
48. Mittal, D.; Ali, A.; Md, S.; Baboota, S.; Sahni, J.K.; Ali, J. Insights into Direct Nose to Brain Delivery: Current Status and Future Perspective. *Drug Deliv.* **2014**, *21*, 75–86. [CrossRef]
49. Takemoto, H.; Yoshimori, T.; Yamamoto, A.; Miyata, Y.; Yahara, I.; Inoue, K.; Tashiro, Y. Heavy Chain Binding Protein (BiP/GRP78) and Endoplasmin Are Exported from the Endoplasmic Reticulum in Rat Exocrine Pancreatic Cells, Similar to Protein Disulfide-Isomerase. *Arch. Biochem. Biophys.* **1992**, *296*, 129–136. [CrossRef]
50. Baek, J.-H.; Mamula, D.; Tingstam, B.; Pereira, M.; He, Y.; Svenningsson, P. GRP78 Level Is Altered in the Brain, but Not in Plasma or Cerebrospinal Fluid in Parkinson's Disease Patients. *Front. Neurosci.* **2019**, *13*, 697. [CrossRef]
51. Casas, C. GRP78 at the Centre of the Stage in Cancer and Neuroprotection. *Front. Neurosci.* **2017**, *11*. [CrossRef]
52. Shields, A.M.; Thompson, S.J.; Panayi, G.S.; Corrigall, V.M. Pro-Resolution Immunological Networks: Binding Immunoglobulin Protein and Other Resolution-Associated Molecular Patterns. *Rheumatology* **2012**, *51*, 780–788. [CrossRef] [PubMed]
53. Pastukhov, Y.F.; Plaksina, D.V.; Lapshina, K.V.; Guzhova, I.V.; Ekimova, I.V. Exogenous Protein HSP70 Blocks Neurodegeneration in the Rat Model of the Clinical Stage of Parkinson's Disease. *Dokl. Biological. Sci.* **2014**, *457*, 225–227. [CrossRef] [PubMed]
54. Bobkova, N.V.; Garbuz, D.G.; Nesterova, I.; Medvinskaya, N.; Samokhin, A.; Alexandrova, I.; Yashin, V.; Karpov, V.; Kukharsky, M.S.; Ninkina, N.N.; et al. Therapeutic Effect of Exogenous Hsp70 in Mouse Models of Alzheimer's Disease. *J. Alzheimers Dis.* **2014**, *38*, 425–435. [CrossRef] [PubMed]
55. Ekimova, I.V.; Plaksina, D.V.; Pastukhov, Y.F.; Lapshina, K.V.; Lazarev, V.F.; Mikhaylova, E.R.; Polonik, S.G.; Pani, B.; Margulis, B.A.; Guzhova, I.V.; et al. New HSF1 Inducer as a Therapeutic Agent in a Rodent Model of Parkinson's Disease. *Exp. Neurol.* **2018**, *306*, 199–208. [CrossRef] [PubMed]
56. Takano, K.; Tabata, Y.; Kitao, Y.; Murakami, R.; Suzuki, H.; Yamada, M.; Iinuma, M.; Yoneda, Y.; Ogawa, S.; Hori, O. Methoxyflavones Protect Cells against Endoplasmic Reticulum Stress and Neurotoxin. *Am. J. Physiol. Cell Physiol.* **2007**, *292*, C353–C361. [CrossRef] [PubMed]

57. Xu, Q.; Yang, S.; Wu, F.; Lin, Y.; Zhong, J.; Tang, L.; Hu, X.; Cai, J. Congrong Shujing Granule-Induced GRP78 Expression Reduced Endoplasmic Reticulum Stress and Neuronal Apoptosis in the Midbrain in a Parkinson's Disease Rat Model. *Evid. Based Complement Altern. Med.* **2020**, *2020*, 4796236. [CrossRef] [PubMed]
58. Fields, C.R.; Bengoa-Vergniory, N.; Wade-Martins, R. Targeting Alpha-Synuclein as a Therapy for Parkinson's Disease. *Front. Mol. Neurosci.* **2019**, *12*, 299. [CrossRef] [PubMed]
59. Sugeno, N.; Takeda, A.; Hasegawa, T.; Kobayashi, M.; Kikuchi, A.; Mori, F.; Wakabayashi, K.; Itoyama, Y. Serine 129 Phosphorylation of α-Synuclein Induces Unfolded Protein Response-Mediated Cell Death. *J. Biol. Chem.* **2008**, *283*, 23179–23188. [CrossRef] [PubMed]
60. Fujiwara, H.; Hasegawa, M.; Dohmae, N.; Kawashima, A.; Masliah, E.; Goldberg, M.S.; Shen, J.; Takio, K.; Iwatsubo, T. α-Synuclein Is Phosphorylated in Synucleinopathy Lesions. *Nat. Cell Biol.* **2002**, *4*, 160–164. [CrossRef] [PubMed]
61. Barrett, P.J.; Timothy Greenamyre, J. Post-Translational Modification of α-Synuclein in Parkinson's Disease. *Brain Res.* **2015**, *1628*, 247–253. [CrossRef]
62. Arawaka, S.; Sato, H.; Sasaki, A.; Koyama, S.; Kato, T. Mechanisms Underlying Extensive Ser129-Phosphorylation in α-Synuclein Aggregates. *Acta Neuropathol. Commun.* **2017**, *5*, 48. [CrossRef] [PubMed]
63. Inglis, K.J.; Chereau, D.; Brigham, E.F. Polo-like kinase 2 (PLK2) phosphorylates alpha-synuclein at serine 129 in central nervous system. *J Biol Chem.* **2009**, *284*, 2598–2602. [CrossRef] [PubMed]
64. Bergeron, M.; Motter, R.; Tanaka, P. In vivo modulation of polo-like kinases supports a key role for PLK2 in Ser129 α-synuclein phosphorylation in mouse brain. *Neuroscience* **2014**, *256*, 72–82. [CrossRef] [PubMed]
65. Gorbatyuk, M.S.; Gorbatyuk, O.S. The Molecular Chaperone GRP78/BiP as a Therapeutic Target for Neurodegenerative Disorders: A Mini Review. *J. Genet. Syndr. Gene Ther.* **2013**, *4*, 128. [CrossRef]
66. Gully, J.C.; Sergeyev, V.G.; Bhootada, Y.; Mendez-Gomez, H.; Meyers, C.A.; Zolotukhin, S.; Gorbatyuk, M.S.; Gorbatyuk, O.S. Up-Regulation of Activating Transcription Factor 4 Induces Severe Loss of Dopamine Nigral Neurons in a Rat Model of Parkinson's Disease. *Neurosci. Lett.* **2016**, *627*, 36–41. [CrossRef] [PubMed]
67. Demmings, M.D.; Tennyson, E.C.; Petroff, G.N.; Tarnowski-Garner, H.E.; Cregan, S.P. Activating Transcription Factor-4 Promotes Neuronal Death Induced by Parkinson's Disease Neurotoxins and α-Synuclein Aggregates. *Cell Death Differ.* **2021**, *28*, 1627–1643. [CrossRef] [PubMed]
68. Subhramanyam, C.S.; Wang, C.; Hu, Q.; Dheen, S.T. Microglia-Mediated Neuroinflammation in Neurodegenerative Diseases. *Semin. Cell Dev. Biol.* **2019**, *94*, 112–120. [CrossRef] [PubMed]
69. Imamura, K.; Hishikawa, N.; Sawada, M.; Nagatsu, T.; Yoshida, M.; Hashizume, Y. Distribution of Major Histocompatibility Complex Class II-Positive Microglia and Cytokine Profile of Parkinson's Disease Brains. *Acta Neuropathol.* **2003**, *106*, 518–526. [CrossRef] [PubMed]
70. McGeer, P.L.; Itagaki, S.; Boyes, B.E.; McGeer, E.G. Reactive Microglia Are Positive for HLA-DR in the Substantia Nigra of Parkinson's and Alzheimer's Disease Brains. *Neurology* **1988**, *38*, 1285. [CrossRef] [PubMed]
71. Nagatsu, T.; Mogi, M.; Ichinose, H.; Togari, A. Changes in Cytokines and Neurotrophins in Parkinson's Disease. In *Advances in Research on Neurodegeneration*; Springer Vienna: Vienna, Austria, 2000; pp. 277–290. [CrossRef]
72. Mazzotta, G.M.; Ceccato, N.; Conte, C. Synucleinopathies Take Their Toll: Are TLRs a Way to Go? *Cells* **2023**, *12*, 1231. [CrossRef]
73. Heidari, A.; Yazdanpanah, N.; Rezaei, N. The Role of Toll-like Receptors and Neuroinflammation in Parkinson's Disease. *J. Neuroinflamm.* **2022**, *19*, 135. [CrossRef] [PubMed]
74. Paxinos, G.; Watson, C. *The Rat Brain in Stereotaxic Coordinates (EBook)*, 6th ed.; Elsevier: Amsterdam, The Netherland, 2007; ISBN 978012374121.

International Journal of
Molecular Sciences

MDPI

Article

Gene Expression Profiling of Post Mortem Midbrain of Parkinson's Disease Patients and Healthy Controls

Michele Salemi [1,*,†], Maria Ravo [2,3,†], Giuseppe Lanza [1,4], Francesca A. Schillaci [1], Giovanna Maria Ventola [2,3], Giovanna Marchese [2,3], Maria Grazia Salluzzo [1], Graziella Cappelletti [5] and Raffaele Ferri [1]

[1] Oasi Research Institute–IRCCS, 94018 Troin, Italy; glanza@oasi.en.it (G.L.); fran7.sch@gmail.com (F.A.S.); msalluzzo@oasi.en.it (M.G.S.); rferri@oasi.en.it (R.F.)
[2] Genomix4Life Srl, 94081 Baroniss, Italy; maria.ravo@genomix4life.com (M.R.); giovanna.ventola@genomix4life.com (G.M.V.); giovanna.marchese@genomix4life.com (G.M.)
[3] Genome Research Center for Health–CRGS, 94081 Baronissi, Italy
[4] Department of Surgery and Medical–Surgical Specialties, University of Catania, 95100 Catania, Italy
[5] Department of Biosciences, University of Milan, 20019 Milan, Italy; graziella.cappelletti@unimi.it
* Correspondence: msalemi@oasi.en.it
† These authors contributed equally to this work.

Abstract: Parkinson's disease (PD) stands as the most prevalent degenerative movement disorder, marked by the degeneration of dopaminergic neurons in the substantia nigra of the midbrain. In this study, we conducted a transcriptome analysis utilizing post mortem mRNA extracted from the substantia nigra of both PD patients and healthy control (CTRL) individuals. Specifically, we acquired eight samples from individuals with PD and six samples from CTRL individuals, with no discernible pathology detected in the latter group. RNA sequencing was conducted using the TapeStation 4200 system from Agilent Technologies. A total of 16,148 transcripts were identified, with 92 mRNAs displaying differential expression between the PD and control groups. Specifically, 33 mRNAs were significantly up-regulated, while 59 mRNAs were down-regulated in PD compared to the controls. The identification of statistically significant signaling pathways, with an adjusted *p*-value threshold of 0.05, unveiled noteworthy insights. Specifically, the enriched categories included cardiac muscle contraction (involving genes such as ATPase Na^+/K^+ transporting subunit beta 2 (*ATP1B2*), solute carrier family 8 member A1 (*SLC8A1*), and cytochrome c oxidase subunit II (*COX2*)), GABAergic synapse (involving GABA type A receptor-associated protein-like 1 (*GABARAPL1*), G protein subunit beta 5 (*GNB5*), and solute carrier family 38 member 2 (*SLC38A2*), autophagy (involving *GABARAPL1* and tumor protein p53-inducible nuclear protein 2 (*TP53INP2*)), and Fc gamma receptor (FcγR) mediated phagocytosis (involving amphiphysin (*AMPH*)). These findings uncover new pathophysiological dimensions underlying PD, implicating genes associated with heart muscle contraction. This knowledge enhances diagnostic accuracy and contributes to the advancement of targeted therapies.

Keywords: mRNAs; RNA sequencing; Parkinson's disease; transcriptome analysis; substantia nigra

Citation: Salemi, M.; Ravo, M.; Lanza, G.; Schillaci, F.A.; Ventola, G.M.; Marchese, G.; Salluzzo, M.G.; Cappelletti, G.; Ferri, R. Gene Expression Profiling of Post Mortem Midbrain of Parkinson's Disease Patients and Healthy Controls. *Int. J. Mol. Sci.* **2024**, *25*, 707. https://doi.org/10.3390/ijms25020707

Academic Editor: Claudia Ricci

Received: 13 November 2023
Revised: 28 December 2023
Accepted: 30 December 2023
Published: 5 January 2024

1. Introduction

PD stands out as the most prevalent movement disorder and neurodegenerative disease after Alzheimer's dementia, affecting approximately seven million people globally [1,2]. Clinically, PD is a heterogeneous condition primarily characterized by a resting tremor, bradykinesia, and rigidity, commonly regarded as the "core motor symptoms". However, PD is clinically diverse, presenting with various causes and clinical manifestations. While a resting tremor is often a prominent and traditionally associated sign of PD, its clinical variability can result in its absence in some cases.

Despite the multifaceted clinical presentation, current diagnosis remains primarily clinical, with laboratory tests, such as genetic testing, and instrumental exams, including structural and/or functional neuroimaging, reserved for patients with atypical presentations [3]. Diagnostic criteria define PD as the presence of bradykinesia combined with either a rest tremor, rigidity, or both [4]. However, the clinical spectrum encompasses additional motor symptoms and non-otor symptoms, some of which precede motor manifestations and are equally debilitating [5–8].

While non-specific symptoms, such as constipation, apathy, fatigue, or mild cognitive changes, are challenging to promptly link to PD onset or its preclinical/prodromal phase, others, like hyposmia, adult onset depression/anxiety, or REM sleep behavior disorder, are considered strong predictors of neurodegeneration. These symptoms play a crucial role in the early diagnosis of PD, even in the absence of common motor symptoms [9].

Among synucleinopathies, multiple system atrophy (MSA) and dementia with Lewy bodies (DLB) represent significant differential diagnoses. MSA is a sporadic neurodegenerative disease clinically characterized by parkinsonism or cerebellar ataxia, both combined with dysautonomia and a poor response to levodopa. Magnetic resonance imaging may reveal specific abnormalities, such as the "hot cross bun" sign and bilateral putaminal hyperintensity [10]. DLB is characterized by dementia preceding or developing alongside parkinsonism, with core features including fluctuating cognition, recurrent visual hallucinations, dysautonomia, and marked sensitivity to D2 receptor-blocking agents. Functional studies may show typical hypometabolism within the occipital cortex [11].

A comprehensive brain transcriptome study of subjects with MSA revealed the down-regulation of oligodendrocyte genes associated with a loss of myelination, particularly the *QKI* gene as a master regulator of this gene network. Additionally, they demonstrated the up-regulation of monomeric α-synuclein gene expression in neurons [12].

Despite considerable research efforts, encompassing both preclinical and clinical studies, PD remains incurable. The progressive loss of dopaminergic (DA) neurons in the substantia nigra pars compacta (SNpc), a crucial part of the midbrain regulating movement tone and velocity, persists without effective intervention, and the complete set of pathomechanisms behind this degeneration remains incompletely elucidated [1,13]. Pathophysiologically, PD exhibits a multifactorial origin, involving intricate interactions between various genetic and environmental factors, a phenomenon observed in other complex diseases, such as tumors [14]. While some factors exert their influence on the elderly population in general, others appear to be more specifically associated with this disorder [15]. It is noteworthy that post mortem studies consistently report that over 60% of DA neurons in the SNpc are already degenerated when overt clinical signs manifest. This indicates that PD is neuropathologically evident long before its clinical onset, suggesting a period during which the human brain can compensate for dopaminergic loss until reaching a "clinical threshold" for PD [16–18].

Histological studies reveal that PD is characterized by the abnormal deposition of the insoluble protein α-synuclein, forming aggregates known as Lewy bodies [19]. These protein aggregates progressively accumulate throughout the brainstem and various neocortical and limbic regions, reflecting the progressive degeneration of the entire central nervous system (CNS) [20]. More recently, a neuroinflammatory state has been observed in the brains of PD patients, particularly evident in the SNpc [21,22]. Both neuroinflammation and dysfunctional activation of the immune system within the CNS significantly contribute to PD pathology and pathophysiology [23]. The inflammasome, a crucial complex of immune-modulating receptors and sensors, plays a role in recruiting proteins associated with apoptotic mechanisms through caspase-1 activation [24,25]. Caspase-1, in turn, activates the proinflammatory cytokines interleukin (IL)-1β and IL-18, perpetuating the neuroinflammatory state in PD brains [25–29]. A recently proposed model suggests that alpha-synuclein activates the inflammasome in the SNpc, leading to IL-activated proinflammatory profiles, neuronal death, and clinical symptoms [30–32].

Genetically, several genes or gene variants, including leucine-rich repeat kinase 2 (*LRRK2*), synuclein alpha (*SNCA*), glucosylceramidase beta-1 (*GBA1*), Parkin RBR E3 ubiquitin protein ligase (*PARKIN*), and PTEN-induced kinase 1 (*PINK1*), have been implicated in causing PD [33–36]. Molecular profiling studies of post mortem SNpc samples, aimed at identifying differential molecular expression changes specific to PD compared to controls, have been conducted [37]. For instance, Simunovic et al. [38] used RNA microarrays to analyze SNpc gene expression in PD samples, identifying the dysregulation of known molecular regulatory pathways in PD, including dysfunction in mitochondrial and oxidative-stress-induced cellular responses [39,40]. In a recent comparative gene expression analysis on laser-dissected neurons from SNpc, Zaccaria et al. [41] revealed 52 dysregulated genes in PD samples compared to controls.

We recognize that synucleinopathies are neurodegenerative disorders associated with the misfolding and aggregation of Alpha-synuclein (*α-Syn*) [42]. Real-time tremor-induced conversion technology (RT-QuIC) is an in vitro amplification method initially developed for the analysis of the prion protein (PrP) [42]. Today, it is also employed for the biochemical assessment of different strains of *α-Syn* within synucleinopathies [42].

Although PD is encompassed within this family of pathologies (synucleinopathies), our study focused on transcriptome analysis by examining post mortem mRNA. This approach allows the targeted identification of gene expression, a critical condition for comprehending this well-known yet enigmatic pathology present in the global population. Transcriptomics enables the unveiling of microscopic changes, offering the potential to identify individuals at risk of developing the disease, even in the presence of non-motor symptoms, or to anticipate the evolution of the pathology.

The review by Rike and Stern [43] cites proteomic and transcriptomic studies involving post mortem brain samples from individuals with PD compared to controls. Some authors of these studies concentrated on the transcriptome in the substantia nigra [44,45]. The data obtained revealed that the dysregulated groups of genes/pathways/biological processes in individuals with PD, as opposed to controls, are more associated with extracellular matrix (ECM)-receptor interaction and cell adhesion molecules.

In our study, we conducted mRNA analysis and subsequent enrichment using the Kyoto Encyclopedia of Genes and Genomes (KEGG) and Gene Ontology (GO) to assess mRNAs extracted post mortem from the SN of subjects with PD and healthy controls. Utilizing samples obtained from Parkinson's UK Brain Bank (Imperial College London, London, UK), we specifically addressed a case history of PD at Braak LB Stage 6.

2. Results

In the examination of mRNA deregulation in the SNpc of PD patients, we conducted gene expression profiling on eight post mortem SNpc samples from PD patients and six from healthy CTRL subjects using next-generation sequencing (RNA-Seq). The aim was to identify specific and differential changes in molecular expression. Following the removal of low-quality reads and adapter sequences, the high-quality reads were aligned against the human genome reference (hg38). In detail, we identified a total of 16,148 transcripts (Supplementary Table S1, sheet A), with 92 mRNAs differentially expressed (DEGs) between the two groups (PD vs. CTRL). Among these, 33 mRNAs were significantly up-regulated (Table 1, Figure 1), while 59 mRNAs were significantly down-regulated in PD compared to CTRL (Table 2, Figure 1). The normalized count of mRNAs is available at ArrayExpress (E-MTAB-13295).

Table 1. mRNAs down-expressed in PD subjects compared to controls (padj ≤ 0.05 and $|FC| \geq 1.5$).

Gene ID	Fold Change	Gene ID	Fold Change
ETNPPL	−7.435	*AC093330.1*	−2.718
MTND4P12	−5.475	*MAP4*	−2.693
CP	−5.444	*SLC1A2*	−2.651
MLC1	−5.02	*TXNIP*	−2.625

Table 1. *Cont.*

Gene ID	Fold Change	Gene ID	Fold Change
PPDPF	−4.631	*AGT*	−2.61
PAQR6	−4.469	*RHOBTB3*	−2.604
ACBD7	−4.345	*CST3*	−2.562
MOBP	−4.315	*SPARCL1*	−2.55
AQP1	−4.069	*MTND2P28*	−2.544
TAGLN	−4.001	*HIPK2*	−2.427
MBP	−3.977	*ZEB2*	−2.425
PAIP2B	−3.892	*NDRG2*	−2.408
PPP1R1B	−3.766	*MTURN*	−2.382
MTATP6P1	−3.736	*DAAM2*	−2.381
MT-C02	−3.5	*NFIX*	−2.343
ELOVL7	−3.456	*FADS2*	−2.325
SCARA3	−3.419	*ATP1B2*	−2.268
MT-C03	−3.338	*HEPACAM*	−2.263
TP53INP2	−3.336	*SHTN1*	−2.203
FAM107A	−3.168	*FAR1*	−2.182
SEPTIN4	−3.158	*AHCYL1*	−2.157
ALAD	−3.122	*EPAS1*	−2.075
MT-CO1	−3.116	*PHLDB1*	−2.058
IRAG1	−3.089	*GFAP*	−2.043
PLAAT3	−3.056	*MAP4K4*	−2.041
MT-CYB	−3.045	*PADI2*	−1.938
CTNNA3	−2.949	*CNP*	−1.916
FAT3	−2.906	*PKP4*	−1.874
BCAS1	−2.857	*WNK1*	−1.714
TSC22D4	−2.767		

Table 2. mRNAs over-expressed in PD subjects compared to controls (padj ≤ 0.05 and $|FC| \geq 1.5$).

Gene ID	Fold Change	Gene ID	Fold Change
IL10RA	12.026	*FYB1*	4.204
AMPH	9.664	*ARHGDIB*	4.111
HS6ST3	8.405	*SLC38A2*	4.104
VSNL1	7.195	*GNB5*	3.998
COLGALT1	6.373	*NAA30*	3.930
PRDM11	6.234	*SLC8A1*	3.409
L1CAM	6.208	*DYNLL1*	2.680
GPR34	6.141	*HSPH1*	2.666
ZNF618	5.543	*SPP1*	2.660
RCSD1	5.419	*BSN*	2.518
CRCP	5.257	*GABARAPL1*	2.471
INA	4.831	*YWHAG*	2.443
PTPRT	4.812	*QDPR*	2.060
GUCY1B1	4.422	*DNAJC5*	2.042
SLC5A3	4.338	*NEAT1*	1.926
SRGN	4.250	*TNPO1*	1.890
SCN8A	4.236		

The heatmap (Figure 1A) illustrates statistically significant differences in mRNA expression profiles between PD and CTRL. The volcano plot (Figure 1B) depicts the distribution of differentially expressed transcripts by their fold change and *p*-values. The most-up-regulated genes are toward the right, the most-down-regulated are toward the left, and the most statistically significant genes are at the top.

We employed the pathfindR tool to analyze significant DEGs in PD based on the KEGG pathway database. Enrichment analysis was performed to explore functional variations between the two groups and investigate pathways potentially associated with PD.

Statistically significant signaling pathways included (hsa04260) cardiac muscle contraction, (hsa04727) GABAergic synapse, (hsa04140) autophagy, and (hsa04666) Fc gamma R-mediated phagocytosis (Figure 2A and Supplementary Table S1).

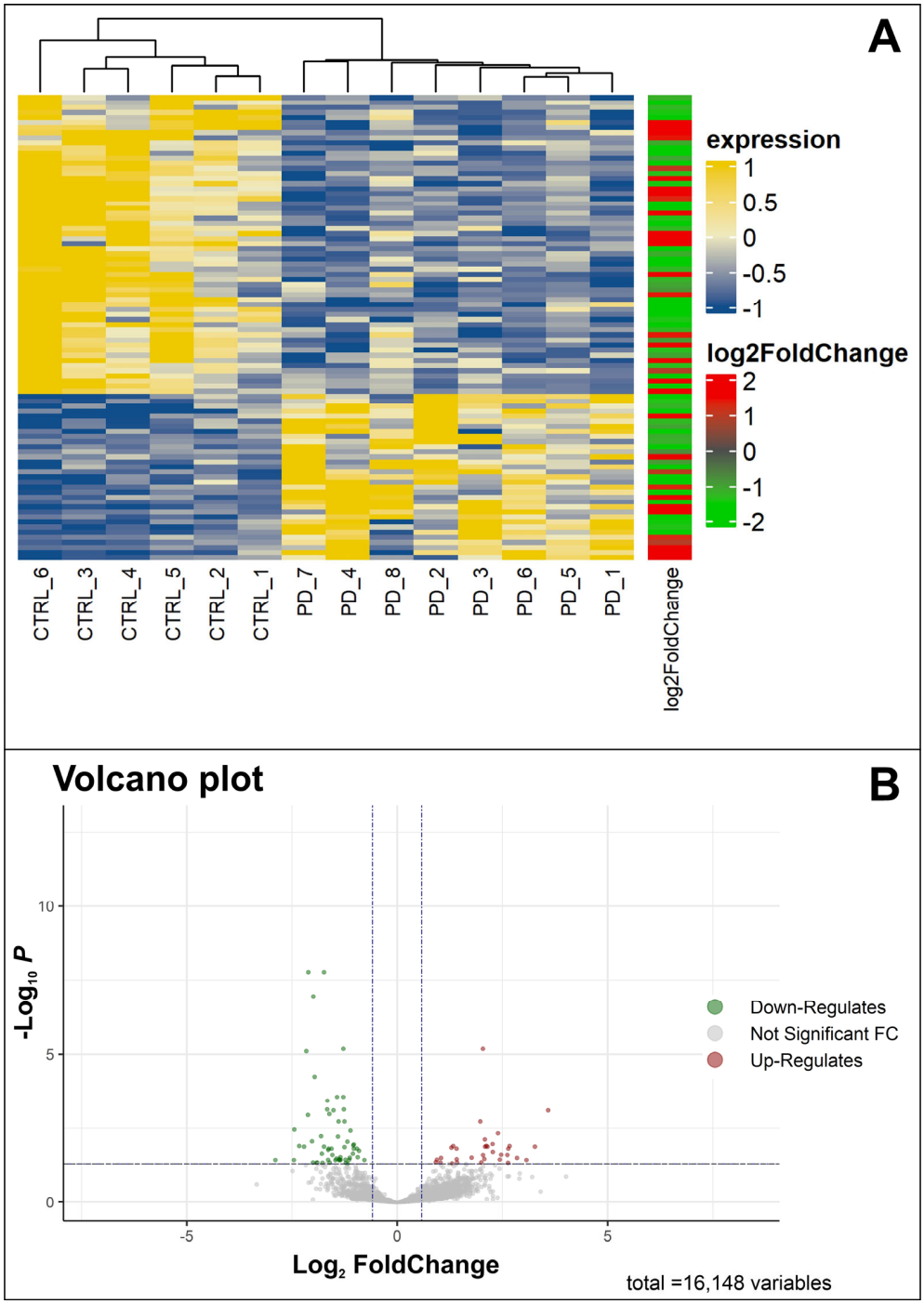

Figure 1. Visualization of differentially expressed genes (DEGs). (**A**) Heatmap of significant DEGs in patients with Parkinson's disease (PD) and healthy control (CTRL) individuals. In yellow, we see the genes with an up-normalized expression level, whereas in blue, we see the down genes. The log2 (foldChange) bar indicates, in red and in green, the up- and down-regulated genes, respectively. (**B**) Volcano plot of significant DEGs based on fold changes and *p*-values. The green color shows the down-regulated genes, whereas the red color shows the up-regulated genes.

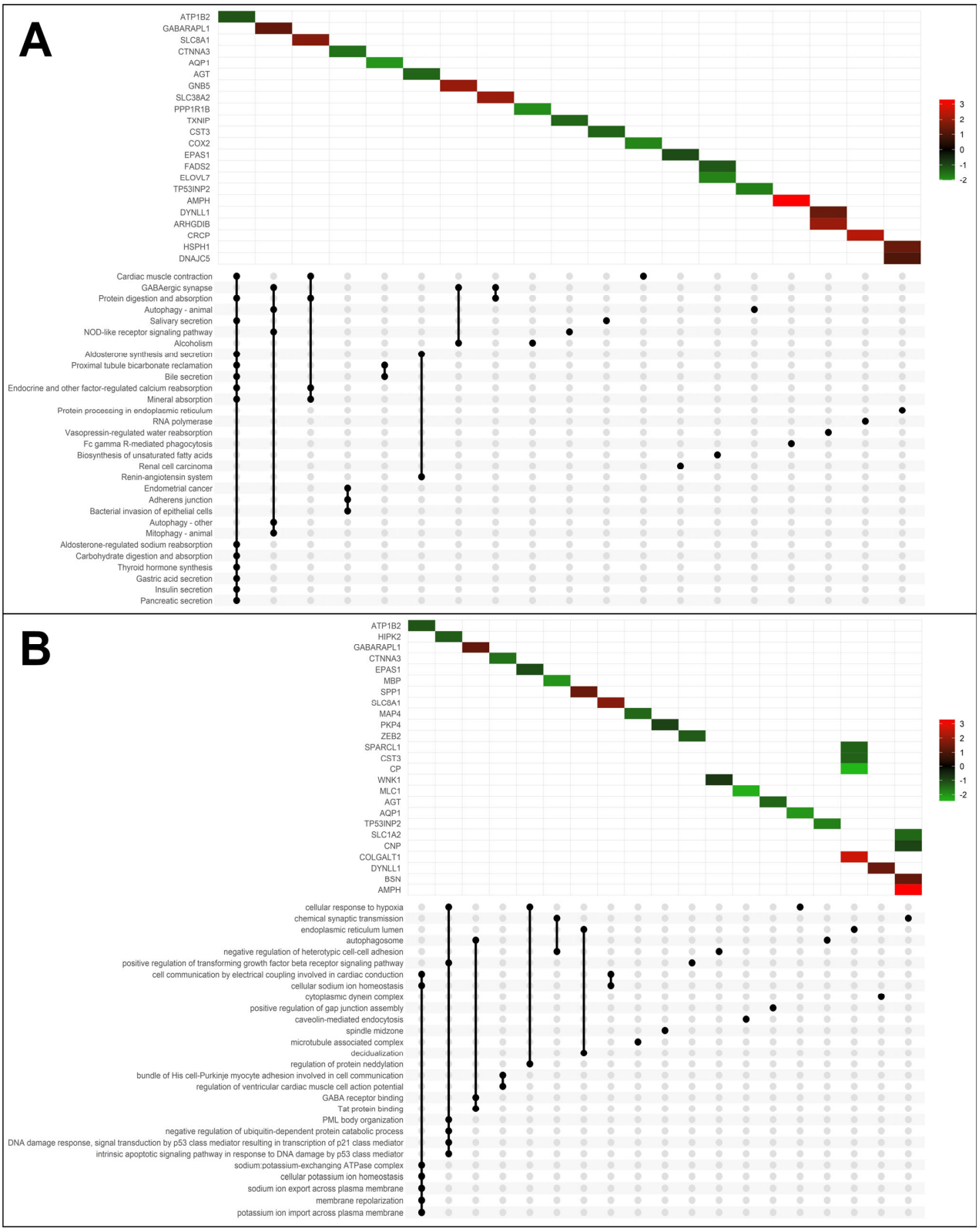

Figure 2. KEGG and GO enrichment analysis of differentially expressed genes. (**A**) UpSet Plot shows the intersections of significant genes and top 30 enriched KEGG pathway and (**B**) GO terms, with the Log2FoldChange scale.

For GO enrichment, we identified both down-regulated and up-regulated genes involved in various molecular functions or biological processes (Figure 2B and Supple-

mentary Table S2). Interestingly, among them, we found the enrichment of (GO:0007268) chemical synaptic transmission (*AMPH*, bassoon presynaptic cytomatrix protein (*BSN*), 2′,3′-cyclic nucleotide 3′ phosphodiesterase (*CNP*), myelin basic protein (MBP), solute carrier family 1 member 2 (*SLC1A2*), (GO:0071456) cellular response to hypoxia (aquaporin 1 (*AQP1*), endothelial PAS domain protein 1 (*EPAS1*), homeodomain-interacting protein kinase 2 (*HIPK2*), (GO:0000045) autophagosome assembly (*GABARAPL1, TP53INP2*), (GO:0050811) GABA type A receptor binding (*GABARAPL1*), and (GO:0086064) cell communication via electrical coupling involved in cardiac conduction (*SLC8A1, ATP1B2*).

To explore the Diseases and Biological Functions significantly enriched in DEGs and assess potential associations with PD susceptibility in the SNpc, we employed Ingenuity Pathway Analysis (IPA). The analysis revealed significant enrichment in Neurological Disease, with multiple annotations related to disorders of the basal ganglia, movement disorders, neuromuscular disease, dyskinesia, progressive motor neuropathy, familial neurological disorders, Parkinson's disease, progressive neurological disorders, abnormal morphology of the nervous system, and tauopathy (Figure 3 and Supplementary Table S3). The DEG IPA Network Analysis identified seven networks with nodes and interactions associated with the top Diseases or Function Annotations, such as Neurological Disease, Organismal Injury and Abnormalities, and Psychological Disorders (Figure 4 and Table 3).

Table 3. Molecule networks obtained via Ingenuity Pathway Analysis (IPA).

Molecules in Network	Score	Focus Molecules	Diseases and Functions
AHCYL1, Akt, Alp, *AQP1*, *ATP1B2*, *BCAS1*, *CP*, Creb, *CTNNA3*, cytochrome-c oxidase, *DNAJCS*, growth hormone, GTPase, *GUCY1B1*, Hdac, *HIPK2*, Hsp70, Hsp90, *HSPH1*, *IL1*, *L1CAM*, *MT-C01*, *MTC02*, *MT-C03*, *MT-CYB*, *NDRG2*, *NEAT1*, nuclear factor M1, *PHLDB1*, *PKP4*, *PLAAT3*, *ROCK*, secretase gamma, *SLCSA3*, *SLC8A1*	49	22	Neurological Disease, Organismal Injury and Abnormalities, Psychological Disorders
14-3-3, 20s proteasome, 26s Pro teasome, *ALAD*, *BSN*, calmodulin, calpain, *CG*, *CNP*, *COLGALT1*, collagen Alpha1, collagen type I (complex), collagen type IV, *EPAS1*, *ERK1/2*, *FAR1*, focal adhesion kinase, *GFAP*, *HEPACAM*, *INA*, insulin, *MAP4*, *MBP*, *MLC1*, *PDGFBB*, Pka, *PP2A*, *SEPTIN4*, *SLC1A2*, *SRGN*, *TAGLN*, Tgf beta, transglutaminase, *VSNL1*, *WNK1*	38	18	Cellular Function and Maintenance, Nervous System Development and Function, Tissue Development
AGT, *AMPH*, Ap1, *ARHGDIB*, calcineurin protein(s), CD3, collagen type I (family), cytokine, *ELOVL7*, *FYB1*, *GNBS*, Gsk3, IKK (complex), IL12 (complex), integrin, integrin alpha L beta 2, Jnk, *LDL*, *MAP4K4*, Mek, *MTURN*, NFAT (complex), Nfat (family), *NFIX*, NFkB (complex), Nrlh, P38 MAPK, *PAD12*, Pkc(s), *PPP1R1B*, Rac, *SPARCL1*, *SPP1*, TCR, voltage-gated calcium channel Act in, *AMPK*, Ck2, *CLEC9A*, *CST3*, *DYNLL1*	25	13	Cardiovascular Disease, Cell-To-Cell Signaling and Interaction, Organismal Injury and Abnormalities
Actin, *AMPK*, Ck2, *CLEC9A*, *CST3*, *DYNLL1*, *ERK*, F Actin, *FADS2*, FAM 107 A, *GABARAPL1*, *GPR34*, hemoglobin, histone h3, histone h4, IgG, *IL10RA*, IL12 (family), immunoglobulin, interferon alpha, Mapk, MHC class II (complex), Notch, P13K (complex), RNA polymerase 11, *SHTN1*, Siglech, SRC (family), trypsin, tubulin, *TXNIP*, ubiquitin, Vegf, *YWHAG*, *ZEB2*	20	11	Cell-To-Cell Signaling and Interaction, Infectious Diseases, Organismal Injury and Abnormalities
ACOD1, *CARD16*, *CASP8*, Cd24a, *COL2A1*, cytokine receptor, D-glucose, *DAAM2*, *FAT3*, *GBPS*, *HCAR2*, *HEPACAM2*, *IFNG*, ligp1, *IL10RB*, *IL17RE*, *IL18BP*, *IL2RA*, *IRAGl*, *LGALS1*, *LTC4S*, *MLKL*, *NAA30*, *NLRCS*, *PARVG*, *PLAAT3*, *PRDM11*, *QDPR*, *REL*, *RHOBTB3*, *SCARA3*, Tlr11, *TNFRSF10B*, *TP531NP2*, *ZBP1*	18	10	Gastrointestinal Disease, Inflammatory Response, Organismal Injury and Abnormalities
CFB, *CHADL*, *CNTLN*, *CSNK1A1*, *EP300*, *ETNPPL*, *FAM110D*, *FAM83G*, *FRMD4A*, *FRY*, *HDAC4*, *HDAC5*, *IKZF2*, *IL15RA*, importin alpha, *MECOM*, miR-129-Sp (and other miRNAs w/seed UUUUUGC), *MOBP*, *NRBP2*, *PAIP2B*, *PAQR6*, *PDCD1LG2*, *PPDPF*, *PRMT1*, *RCSD1*, *SCN8A*, *SMARCB1*, *SNX22*, *SNX24*, *SOX2*, *SOX9*, *TNP01*, *TSC22D4*, *ZDBF2*, *ZNF618*	18	10	Carbohydrate Metabolism, Cell Cycle, Cellular Assembly and Organization
ACBD7, betaestradiol, *CA2*, *CALCRL*, clathrin, *CRCP*, *DEFB116*, *DNPH1*, *DOCK3*, *ERBB*, *FMOS*, *HS6ST3*, *HTR4*, *INPP5F*, L-histidine, *L1CAM*, Ly6a (includes others), *MAL*, *NOS1*, *OGDHL*, *OGN*, Pplc, *PROTEASE*, *PTEN*, *PTPRT*, *PYGL*, *SEMA3A*, sGC, *SLC38A2*, *SLC02B1*, *SRC*, sulfotransferase, *SULT1C2*, *TBC1D24*, Wap	10	6	Cellular Development, Connective Tissue Development and Function, Skeletal and Muscular System Development and Function

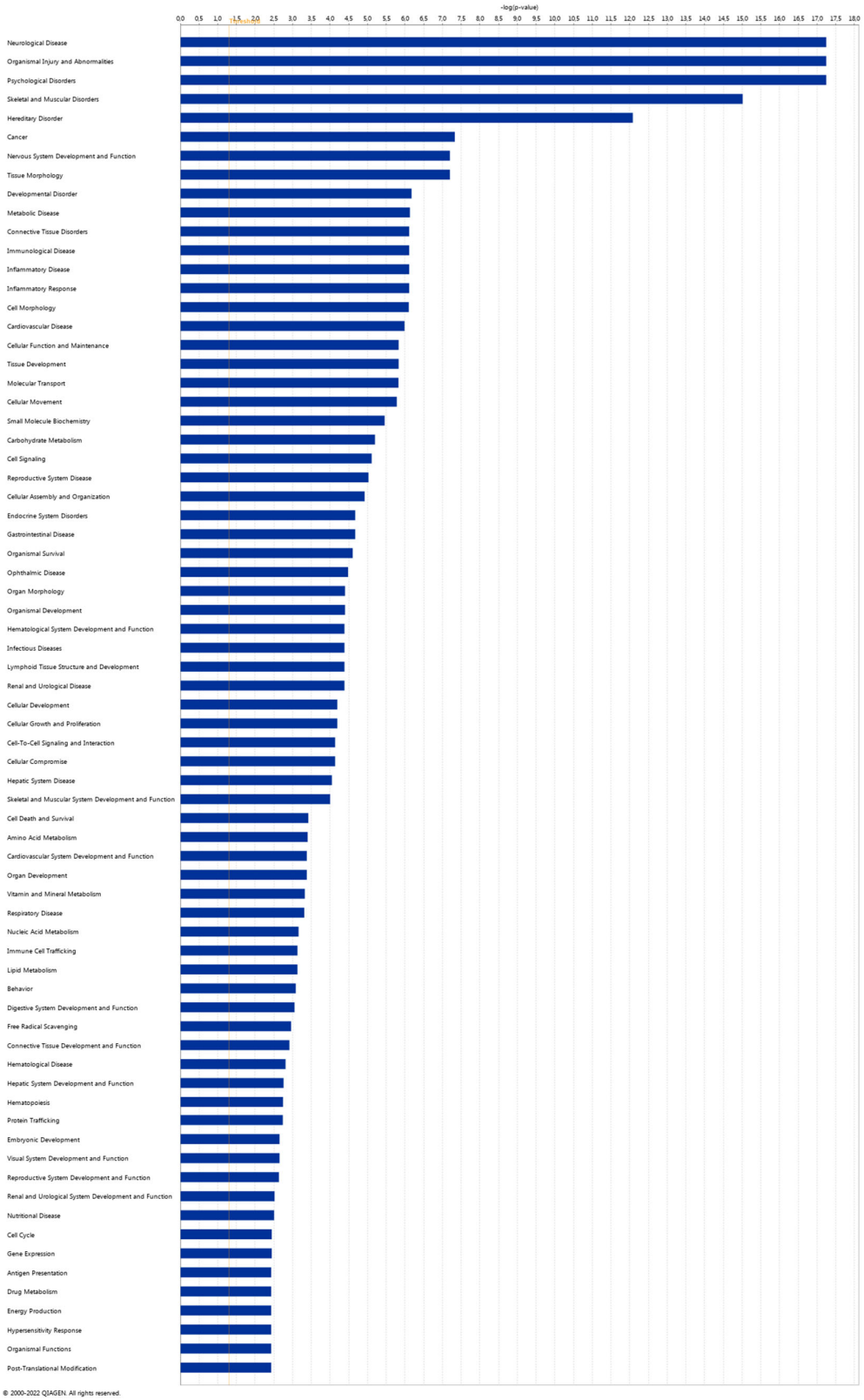

Figure 3. Ingenuity Pathway Analysis (IPA). Disease and Function analysis of differentially expressed genes in the IPA software (Prism version 9.4.1, 2022) with Log2 (*p*-value) scale.

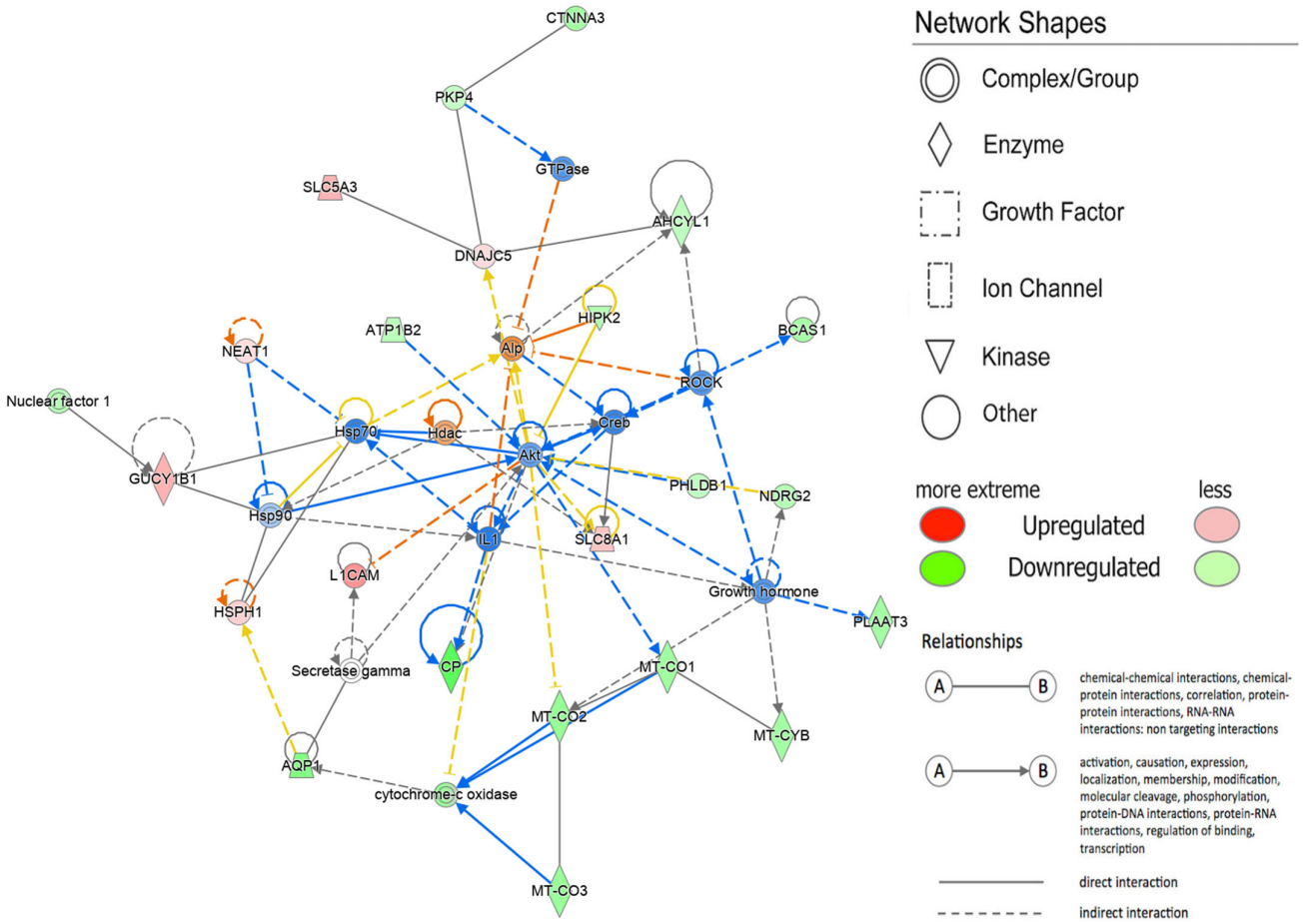

Figure 4. Network by Ingenuity Pathway Analysis (IPA). Neurological Disease, Organismal Injury and Abnormalities, Psychological Disorders. Red indicates the up-regulated transcripts, whereas green indicates the down-regulated transcripts. The color of the lines indicates the different relationship states. In particular, the orange lines show an activation, the blue lines show an inhibition, gray indicates non-predicted effects, and yellow indicates findings inconsistent with the state of the downstream molecule.

3. Discussion

While PD was initially described by James Parkinson in 1817, it remains a disease with several knowledge gaps, spanning the ethnic divide, gender differences, and the field of PD genetics [46]. Numerous studies in the field of omics sciences (genomics, transcriptomics, proteomics, metabolomics) have contributed to the identification of new genes, pathways, and proteins, providing insight into the extensive variability of PD in the context of current trends in personalized medicine [47].

Referring to the review by Rike and Stern [43], our study, at the pathway analysis level, reveals some overlaps with interaction mechanisms and cell adhesion molecules. Importantly, we have identified data that were not previously highlighted in the literature.

The results obtained indicate 33 significantly up-regulated mRNAs (padj ≤ 0.05 and $|FC| \geq 1.5$) and 59 significantly down-regulated mRNAs (padj ≤ 0.05 and $|FC| \leq -1.5$) in PD subjects compared with CTRLs.

Among these, the genes most involved in the highlighted pathways, functions, and networks include *ATP1B2*, *GABARAPL*, *SLC38A*, mitochondrially encoded cytochrome c oxidase I (*MT-CO1*), mitochondrially encoded cytochrome c oxidase II (*MT-CO2*), mitochondrially encoded cytochrome c oxidase III (*MT-CO3*), mitochondrially encoded cytochrome b (*MT-CYB*), and cytochrome oxidase.

ATP1B2, a plasma membrane pump with diverse functions, including homeostasis in cell differentiation and apoptosis, is particularly expressed in the brain [48]. In our study, the *ATP1B2* gene was under-expressed in PD brains compared to CTRLs (Table 1), confirming its peculiar expression in normal brains, as previously reported [49]. Following KEGG and GO enrichment analysis, *ATP1B2* correlated with most of the relevant pathways observed (Figure 2A,B). Notably, in KEGG analysis, one pathway is "contraction of cardiac muscles", while in GO analysis, *ATP1B2* correlates with the "cellular communication via electrical coupling involved in cardiac conduction" pathway (Figure 2A,B).

The cardiac sodium/calcium exchanger (*SLC8A1*), found to be overexpressed (Table 2) in our data, is a bidirectional calcium transporter contributing to the electrical activity of the heart. It is abundantly expressed in the heart and less so in the brain, retina, and skeletal muscle [50,51]. Enriched categories included different genes involved in cardiac muscle contraction, highlighting the known clinical and experimental evidence linking cardiac changes and PD. Although most dysautonomic symptoms in PD arise from alterations in the peripheral nerves of the autonomic nervous system [52], a direct role of myocardial cell pathology in PD patients cannot be excluded.

Recent evidence shows a close link between PD and cardiac cell dysfunction, with mitophagy likely playing a crucial role [53,54]. Proteins like those encoded by the *ATP1B2* gene, integral membrane proteins responsible for establishing and maintaining electrochemical gradients, may connect cardiac dysfunction with the PD patients studied here [55].

Notably, Bardutz et al. [56] recently suggested alterations in systolic function in PD patients, possibly related to dysfunctional cardiac muscle contraction. Oleksakova et al. [57] highlighted differences in baroreflex function and the baroreflex-mediated vasoconstriction response to orthostasis in PD patients. While data in the literature associate cardiac dysfunction with PD, our study directly underscores the dysregulation of genes related to cardiac contraction in the brain of PD patients. The specific role of these dysregulated genes in brain function remains unclear, but we cannot exclude their potential contribution to the neurodegeneration observed in PD.

Among the genes of interest, *GABARAPL1* was found to be overexpressed, as indicated via both KEGG and GO analyses, involving a distinct set of pathways (five and three, respectively): GABAergic synapse, autophagy—animal, the nucleotide-oligomerization-domain (NOD)-like receptor signaling pathway (a specialized group of intracellular proteins that plays a critical role in the regulation of the host innate immune response), autophagy—other, and mitophagy—animal (according to KEGG), as well as autophagosome, GABA type A receptor binding, and Tat protein binding (according to GO). The Tat protein serves as a nuclear transactive regulator of viral gene expression, either for human immunodeficiency virus (HIV) or the equivalent protein of another virus (https://www.uniprot.org/uniprotkb/P04610/entry; accessed on 10 December 2023). Nagel et al. [58] demonstrated that the Tat-heat shock protein 70 (Hsp70) complex effectively prevents neuronal cell death in both in vitro and in vivo models of PD.

Autophagy, a highly conserved cellular degradation process regulated by specific autophagy-related (Atg) factors, entails the formation of double-membrane autophagosomes that engulf cytoplasmic components for degradation. In mammals, this process is complex due to the presence of six Atg8 homologues, categorized into the GABA type A receptor-associated protein (*GABARAP*) and microtubule-associated protein 1 light-chain 3 (*MAP1LC3*) subfamilies [59]. *GABARAPL1/GEC1*, a member of the GABARAP subfamily, exhibits the highest mRNA expression among Atg8 homologues in the CNS. Notably, *GABARAPL1* brain expression is observable as early as embryonic day 11, increasing progressively to peak in adulthood. Significantly, *GABARAPL1* expression in the adult brain is particularly intense in neurons involved in motor and neuroendocrine functions, notably in the SNpc [60]. A dysregulation of Atg8 homologues has been observed in other synucleinopathies, such as Lewy-body dementia and multiple-system atrophy [61]. In PD, alterations in autophagic mechanisms are evident, as demonstrated by transcript levels of several autophagy genes in blood cells. A recent study found the overexpression of

autophagy-related genes, including *MAP1LC3B*, *GABARAP*, *GABARAPL1*, *GABARAPL2*, and sequestosome 1 (*P62/SQSTM1*), in PD patients, with potential implications for predicting markers and therapeutic responses [62].

Among the highlighted genes, *AMPH* stands out, as it was found to be overexpressed, as indicated via both the KEGG and GO analyses. This overexpression involves pathways such as phagocytosis mediated by Fc gamma R (according to KEGG) and chemical synaptic transmission (according to GO). The crystallizable fragment receptor (FcR) is a receptor with a specific binding capacity for the Fc region of the antibody tail and is responsible for inducing phagocytosis. When Fc gamma R on monocyte-macrophages or neutrophils combines with IgG through its Fc region, it triggers phagocytosis [63,64]. FcRs play a crucial role in normal responses to infection or tissue injury and are implicated in immune-related diseases and increasingly observed in neurodegenerative diseases [65]. The aberrant activation of FcRs in neural cells may contribute to the pathogenesis of major neurodegenerative conditions, including Alzheimer's disease, Parkinson's disease, ischemic stroke, and multiple sclerosis [65]. This observation aligns with the pathway expression found in our study sample.

Similarly, the *SLC38A2* gene was identified as overexpressed and associated with two relevant pathways according to KEGG: GABAergic synapse and protein digestion and absorption. This finding strengthens the connection between GABA overexpression, PD pathology, and neural degeneration. In a recent study using a rotenone-induced PD rat model [66], nardosinone, a biochemical compound enhancing NGF-mediated neurite outgrowth and synaptogenesis, demonstrated anti-PD efficacy. Transcriptome and proteome analyses suggested that the anti-PD target of nardosinone is the *SLC38A2* gene, potentially involving the GABAergic synaptic pathway. This underscores the *SLC38A2* gene as a potential target for PD treatment and emphasizes its modulatory effects as an anti-PD agent through the GABA system [66]. Diseases and Function analysis in the IPA software highlighted that DEGs correlated with Neurological Disease (Figures 3 and 4). Network IPA Analysis (Figure 4) revealed the down-regulation of many mitochondrial genes in the SN of PD subjects, including *MT-CO1*, *MT-CO2*, *MT-CO3*, *MT-CYB*, and cytochrome oxidase. This further supports mitochondrial dysfunction in PD, where mitochondria, involved in crucial functions, primarily energy generation, are essential for nearly all cellular activities. Alterations in mitochondrial functioning lead to insufficient energy production, particularly affecting the CNS [67]. Evidence indicates that mitochondrial respiratory-chain dysfunction plays a primary role in various neurodegenerative diseases, including PD [67,68]. Impaired elements of the respiratory chain, such as defects in complex I, have been associated with PD and frontal cortex dysfunction [69–72]. Damage to the electron transport chain increases oxidative stress and neuronal dysfunction, potentially contributing to the onset and progression of PD. Progressive mitochondrial damage results in the accumulation of non-functional mitochondria, further contributing to neuronal degeneration [73].

Looking at the down-regulated genes in the SN of PD patients, a group of genes involved in maintaining the structure and function of glial cells was noted. These genes include *MBP, CPN* (myelin protein cyclic nucleotide phosphodiesterase), *CTNNA3* (alpha-T-catenin), *AQP1*, and glial fibrillary acidic protein (*GFAP*). Among the up-regulated genes, *SLC8A1* is involved in linking trans-plasmalemmal gradients of sodium and calcium ions to the membrane potential of astrocytes. This outcome suggests the emerging important role of glial cells in neurodegeneration and PD pathogenesis [74–79].

4. Materials and Methods

4.1. Human Post Mortem Midbrain Samples

Human midbrain samples were generously provided by the Parkinson's UK Brain Bank (Imperial College London, London, UK). A total of 8 PD (6 males and 2 females; mean age 81.125 and SD of 5.693) and 6 CTRL (1 male and 5 females; mean age 78.166 and SD of 10.381) samples were acquired, and the specimens were histologically sectioned at the midbrain, encompassing the human SN in all slides. Each section had a thickness of 4 μm.

Supplementary Table S4 presents a concise summary of the clinical characteristics of PD subjects and controls, with the data sourced from the Parkinson's UK Brain Bank (Imperial College London, London, UK). It is noteworthy that all PD cases included in the study are classified at Braak LB Stage 6. The study adhered to the principles of the Declaration of Helsinki of 1964 and its subsequent amendments. The Ethics Committee of the Oasi Research Institute—IRCCS of Troina (Italy) granted approval for the protocol on 5 April 2022 (approval code: 2022/04/05/CE-IRCCS-OASI/52).

4.2. RNA Isolation from Human Midbrain Samples

RNA was extracted from 4 µm of Formalin-fixed paraffin-embedded (FFPE) slide-mounted sections using the RecoverAll Total Nucleic Acid Isolation Protocol (Thermo Fisher Scientific Inc., Waltham, MA, USA), following the manufacturer's instructions. Subsequently, the RNA was stored at -80 °C until further processing.

4.3. RNA Sequencing and Functional Analysis

RNA sequencing and subsequent data analysis were conducted by Genomix4Life Srl (Baronissi, Italy). The quality and quantity of RNA were assessed using a Qubit fluorometer (Thermo Fisher Scientific Inc.) and a TapeStation 4200 (Agilent Technologies, 5301 Stevens Creek Blvd), respectively.

Indexed libraries were prepared from 50 ng of purified RNA each, employing the Illumina Stranded Total RNA with Ribo-Zero Plus Kit (Illumina Inc., San Diego, CA, USA), following the manufacturer's guidelines. Library quantification was performed using the TapeStation 4200 (Agilent Technologies, Santa Clara, CA, USA) and Qubit. Subsequently, the indexed libraries were pooled in equimolar amounts, resulting in a final concentration of 2 nM. The Illumina NovaSeq 6000 System was utilized to sequence the pooled samples in a 2×75 paired-end format.

Trimming of short reads (<25 bp) and removal of adapter sequences were carried out with cutadapt (v.2.8) [80]. Using STAR [81] software (version 2.7.3a), the trimmed fastq files were mapped to the reference genome (GenCode (HG38-Release 37 (GRCh38.p13)). [https://www.gencodegenes.org/human/ accessed on 1 August 2023]) STAR [81] was used with standard parameters to create paired-end fastq files and wrote several output files, such as alignments (SAM/BAM). The next step of RNA-seq workflow, involved the gene quantification per sample, was performed using the featureCounts (version 2.0) tool. FeatureCounts is a highly efficient read summarization program that counts mapped reads (SAM/BAM files) for genomic features such as genes [https://bioweb.pasteur.fr/docs/modules/subread/1.4.6-p3/SubreadUsersGuide, accessed on 29 December 2023]. A Custom R script was employed for data normalization and differential expression analysis using the Bioconductor DESeq2 [82] package, based on negative binomial generalized linear models and on the estimates of dispersion and logarithmic fold changes incorporated in data-driven prior distributions. The threshold for considering genes as differentially expressed was set at Fold-Change ≥ 1.50 or ≤ -1.50 ($|FC| \geq 1.50$) with adjusted p-values ≤ 0.05 (padj). Volcano plots and heatmaps were generated using the En-hancedVolcano (10.18129/B9.bioc.EnhancedVolcano) and ComplexHeatmap [83] packages in R.

For functional analysis, KEGG pathway and GO database analyses were conducted using the R package pathfinder. Additionally, to gain a deeper understanding of the complex transcriptomics data, Ingenuity Pathway Analysis (IPA) (Prism version 9.4.1, 2022) [84] was performed, specifically for investigating diseases and function analysis.

The raw data (.fastq files) and the normalized count of identified mRNAs are available on ArrayExpress (E-MTAB-13295).

5. Conclusions

One of the study's limitations is undoubtably related to the number of cases examined, which stems from the necessity to select samples with a high yield of extracted mRNA.

A future objective includes expanding the sample size of PD subjects to enhance clinical heterogeneity and explore the pathological anatomy further. Another limitation is the absence of an expression study on non-coding RNAs (ncRNAs), which could be a focus of subsequent research.

The in-depth analysis conducted on the transcriptome of our samples revealed statistically significant findings pertaining to various signaling pathways, including cardiac muscle contraction, GABAergic synapse, autophagy, the Fc gamma R-mediated phagocytosis signaling pathway, the cellular response to chemical synaptic transmission, hypoxia, autophagosome assembly, GABA type A receptor binding, and cellular communication via electrical coupling involved in cardiac conduction. These results were obtained through KEGG and GO enrichment analyses. Notably, we highlight gene expression alterations affecting "cardiac muscle contraction" and "cellular communication via electrical coupling involved in cardiac conduction" in PD brain tissues compared to CTRLs. This leads us to speculate that genes conventionally associated with electrical conduction mechanisms in cardiac muscle might also play a role in the brain, with their function still unclear. We cannot exclude the involvement of differentially expressed genes, such as *SLC8A1* and *ATP1B2*, in various tissues within the context of PD.

Another significant finding is the altered expression of mitochondrial genes in the SN of subjects with PD. While this has been discussed in the literature, our study reaffirms it, emphasizing the central role of mitochondrial genes in PD. These discoveries may pave the way for improved diagnostic precision and the development of novel targeted therapies.

Supplementary Materials: The following supporting information can be downloaded at: https://www.mdpi.com/article/10.3390/ijms25020707/s1.

Author Contributions: Concept and design, M.S., G.C. and R.F.; next-generation sequencing analysis, M.R., G.M. and G.M.V.; acquisition of data or analysis, M.R., G.M., G.M.V. and M.S.; writing—original draft preparation, M.S., G.L., M.R., G.M., F.A.S., M.G.S., G.C. and R.F.; final approval, M.S., G.L., M.R. and R.F. All authors have read and agreed to the published version of the manuscript.

Funding: This research was funded by Italian Ministry of Health, grant number RC-2779777.

Institutional Review Board Statement: The study was conducted in accordance with the Declaration of Helsinki of 1964 and its later amendments, and the Ethics Committee of the Oasi Research Institute–IRCCS of Troina (Italy) approved the protocol on 5 April 2022 (approval code: 2022/04/05/CE-IRCCS-OASI/52).

Informed Consent Statement: The Centre for Blast Injury Studies fully complies with The Human Tissue Act 2004 (which replaced the Human Tissue Act 1961, the Anatomy Act 1984, and the Human Organ Transplants Act 1989), governed by the Human Tissue Authority, which outlines the use of human tissue for scientific purposes in the UK. Although the Human Tissue Act does not cover the use of tissues that are sourced outside the UK, the Centre also complies with its standards in its dealings with human tissue from overseas. Imperial College London also holds an institutional license from the Human Tissue Authority to collect, store, and use human tissue. As provided for in the Human Tissue Act, and depending on the nature of the research, organizations other than the Human Tissue Authority regulate the actual research on human tissue and, in the case of this study, this has been via the Ethics Committee of the Oasi Research Institute—IRCCS of Troina (Italy).

Data Availability Statement: https://www.bioinformatics.babraham.ac.uk/projects/fastqc/ accessed on 29 December 2023 (E-MTAB-13295).

Acknowledgments: We thank Parkinson's UK Brain Bank (Imperial College London, London, UK) for providing human midbrain samples.

Conflicts of Interest: The authors declare no conflict of interest.

References

1. Kalia, L.V.; Lang, A.E. Parkinson's Disease. *Lancet* **2015**, *386*, 896–912. [CrossRef]
2. Quik, M. Smoking, Nicotine and Parkinson's Disease. *Trends Neurosci.* **2004**, *27*, 561–568. [CrossRef] [PubMed]
3. Bloem, B.R.; Okun, M.S.; Klein, C. Parkinson's Disease. *Lancet* **2021**, *397*, 2284–2303. [CrossRef] [PubMed]

4. Postuma, R.B.; Berg, D.; Stern, M.; Poewe, W.; Olanow, C.W.; Oertel, W.; Obeso, J.; Marek, K.; Litvan, I.; Lang, A.E.; et al. MDS Clinical Diagnostic Criteria for Parkinson's Disease. *Mov. Disord.* **2015**, *30*, 1591–1601. [CrossRef] [PubMed]
5. Lang, A.E.; Obeso, J.A. Time to Move beyond Nigrostriatal Dopamine Deficiency in Parkinson's Disease. *Ann. Neurol.* **2004**, *55*, 761–765. [CrossRef] [PubMed]
6. Obeso, J.A.; Stamelou, M.; Goetz, C.G.; Poewe, W.; Lang, A.E.; Weintraub, D.; Burn, D.; Halliday, G.M.; Bezard, E.; Przedborski, S.; et al. Past, Present, and Future of Parkinson's Disease: A Special Essay on the 200th Anniversary of the Shaking Palsy. *Mov. Disord.* **2017**, *32*, 1264–1310. [CrossRef] [PubMed]
7. Figorilli, M.; Lanza, G.; Congiu, P.; Lecca, R.; Casaglia, E.; Mogavero, M.P.; Puligheddu, M.; Ferri, R. Neurophysiological Aspects of REM Sleep Behavior Disorder (RBD): A Narrative Review. *Brain Sci.* **2021**, *11*, 1588. [CrossRef] [PubMed]
8. Joza, S.; Hu, M.T.; Jung, K.-Y.; Kunz, D.; Stefani, A.; Dušek, P.; Terzaghi, M.; Arnaldi, D.; Videnovic, A.; Schiess, M.C.; et al. Progression of Clinical Markers in Prodromal Parkinson's Disease and Dementia with Lewy Bodies: A Multicentre Study. *Brain* **2023**, *146*, 3258–3272. [CrossRef]
9. Jankovic, J. Parkinson's Disease: Clinical Features and Diagnosis. *J. Neurol. Neurosurg. Psychiatry* **2008**, *79*, 368–376. [CrossRef]
10. Bhidayasiri, R.; Sringean, J.; Reich, S.G.; Colosimo, C. Red Flags Phenotyping: A Systematic Review on Clinical Features in Atypical Parkinsonian Disorders. *Park. Relat. Disord.* **2019**, *59*, 82–92. [CrossRef]
11. Caproni, S.; Colosimo, C. Diagnosis and Differential Diagnosis of Parkinson Disease. *Clin. Geriatr. Med.* **2020**, *36*, 13–24. [CrossRef] [PubMed]
12. Piras, I.S.; Bleul, C.; Schrauwen, I.; Talboom, J.; Llaci, L.; De Both, M.D.; Naymik, M.A.; Halliday, G.; Bettencourt, C.; Holton, J.L.; et al. Transcriptional Profiling of Multiple System Atrophy Cerebellar Tissue Highlights Differences between the Parkinsonian and Cerebellar Sub-Types of the Disease. *Acta Neuropathol. Commun.* **2020**, *8*, 76. [CrossRef] [PubMed]
13. Lang, A.E. A Critical Appraisal of the Premotor Symptoms of Parkinson's Disease: Potential Usefulness in Early Diagnosis and Design of Neuroprotective Trials. *Mov. Disord.* **2011**, *26*, 775–783. [CrossRef] [PubMed]
14. Salemi, M.; Mogavero, M.P.; Lanza, G.; Mongioì, L.M.; Calogero, A.E.; Ferri, R. Examples of Inverse Comorbidity between Cancer and Neurodegenerative Diseases: A Possible Role for Noncoding RNA. *Cells* **2022**, *11*, 1930. [CrossRef] [PubMed]
15. Fisicaro, F.; Lanza, G.; Cantone, M.; Ferri, R.; Pennisi, G.; Nicoletti, A.; Zappia, M.; Bella, R.; Pennisi, M. Clinical and Electrophysiological Hints to TMS in De Novo Patients with Parkinson's Disease and Progressive Supranuclear Palsy. *J. Pers. Med.* **2020**, *10*, 274. [CrossRef] [PubMed]
16. Cheng, H.-C.; Ulane, C.M.; Burke, R.E. Clinical Progression in Parkinson Disease and the Neurobiology of Axons. *Ann. Neurol.* **2010**, *67*, 715–725. [CrossRef] [PubMed]
17. Burke, R.E.; O'Malley, K. Axon Degeneration in Parkinson's Disease. *Exp. Neurol.* **2013**, *246*, 72–83. [CrossRef]
18. Dauer, W.; Przedborski, S. Parkinson's Disease: Mechanisms and Models. *Neuron* **2003**, *39*, 889–909. [CrossRef]
19. Braak, H.; Sandmann-Keil, D.; Gai, W.; Braak, E. Extensive Axonal Lewy Neurites in Parkinson's Disease: A Novel Pathological Feature Revealed by Alpha-Synuclein Immunocytochemistry. *Neurosci. Lett.* **1999**, *265*, 67–69. [CrossRef]
20. Braak, H.; Del Tredici, K.; Rüb, U.; de Vos, R.A.I.; Jansen Steur, E.N.H.; Braak, E. Staging of Brain Pathology Related to Sporadic Parkinson's Disease. *Neurobiol. Aging* **2003**, *24*, 197–211. [CrossRef]
21. Fearnley, J.M.; Lees, A.J. Ageing and Parkinson's Disease: Substantia Nigra Regional Selectivity. *Brain* **1991**, *114 Pt 5*, 2283–2301. [CrossRef]
22. Hirsch, E.C.; Breidert, T.; Rousselet, E.; Hunot, S.; Hartmann, A.; Michel, P.P. The Role of Glial Reaction and Inflammation in Parkinson's Disease. *Ann. N. Y. Acad. Sci.* **2003**, *991*, 214–228. [CrossRef]
23. Haque, M.E.; Akther, M.; Jakaria, M.; Kim, I.-S.; Azam, S.; Choi, D.-K. Targeting the Microglial NLRP3 Inflammasome and Its Role in Parkinson's Disease. *Mov. Disord.* **2020**, *35*, 20–33. [CrossRef]
24. De Rivero Vaccari, J.P.; Dietrich, W.D.; Keane, R.W. Therapeutics Targeting the Inflammasome after Central Nervous System Injury. *Transl. Res.* **2016**, *167*, 35–45. [CrossRef]
25. Martinon, F.; Burns, K.; Tschopp, J. The Inflammasome: A Molecular Platform Triggering Activation of Inflammatory Caspases and Processing of proIL-Beta. *Mol. Cell* **2002**, *10*, 417–426. [CrossRef]
26. Broz, P.; Dixit, V.M. Inflammasomes: Mechanism of Assembly, Regulation and Signalling. *Nat. Rev. Immunol.* **2016**, *16*, 407–420. [CrossRef]
27. Malik, A.; Kanneganti, T.-D. Inflammasome Activation and Assembly at a Glance. *J. Cell Sci.* **2017**, *130*, 3955–3963. [CrossRef]
28. Van Opdenbosch, N.; Lamkanfi, M. Caspases in Cell Death, Inflammation, and Disease. *Immunity* **2019**, *50*, 1352–1364. [CrossRef]
29. Franklin, B.S.; Bossaller, L.; De Nardo, D.; Ratter, J.M.; Stutz, A.; Engels, G.; Brenker, C.; Nordhoff, M.; Mirandola, S.R.; Al-Amoudi, A.; et al. The Adaptor ASC Has Extracellular and "prionoid" Activities That Propagate Inflammation. *Nat. Immunol.* **2014**, *15*, 727–737. [CrossRef]
30. Cabrera Ranaldi, E.D.L.R.M.; Nuytemans, K.; Martinez, A.; Luca, C.C.; Keane, R.W.; de Rivero Vaccari, J.P. Proof-of-Principle Study of Inflammasome Signaling Proteins as Diagnostic Biomarkers of the Inflammatory Response in Parkinson's Disease. *Pharmaceuticals* **2023**, *16*, 883. [CrossRef]
31. Codolo, G.; Plotegher, N.; Pozzobon, T.; Brucale, M.; Tessari, I.; Bubacco, L.; de Bernard, M. Triggering of Inflammasome by Aggregated α-Synuclein, an Inflammatory Response in Synucleinopathies. *PLoS ONE* **2013**, *8*, e55375. [CrossRef]
32. De Rivero Vaccari, J.P.; Dietrich, W.D.; Keane, R.W. Activation and Regulation of Cellular Inflammasomes: Gaps in Our Knowledge for Central Nervous System Injury. *J. Cereb. Blood. Flow Metab.* **2014**, *34*, 369–375. [CrossRef]

33. Funayama, M.; Nishioka, K.; Li, Y.; Hattori, N. Molecular Genetics of Parkinson's Disease: Contributions and Global Trends. *J. Hum. Genet.* **2023**, *68*, 125–130. [CrossRef]
34. Nalls, M.A.; Pankratz, N.; Lill, C.M.; Do, C.B.; Hernandez, D.G.; Saad, M.; DeStefano, A.L.; Kara, E.; Bras, J.; Sharma, M.; et al. Large-Scale Meta-Analysis of Genome-Wide Association Data Identifies Six New Risk Loci for Parkinson's Disease. *Nat. Genet.* **2014**, *46*, 989–993. [CrossRef]
35. Bandres-Ciga, S.; Diez-Fairen, M.; Kim, J.J.; Singleton, A.B. Genetics of Parkinson's Disease: An Introspection of Its Journey towards Precision Medicine. *Neurobiol. Dis.* **2020**, *137*, 104782. [CrossRef]
36. Dulski, J.; Uitti, R.J.; Ross, O.A.; Wszolek, Z.K. Genetic Architecture of Parkinson's Disease Subtypes—Review of the Literature. *Front. Aging Neurosci.* **2022**, *14*, 1023574. [CrossRef]
37. Redenšek, S.; Dolžan, V.; Kunej, T. From Genomics to Omics Landscapes of Parkinson's Disease: Revealing the Molecular Mechanisms. *OMICS* **2018**, *22*, 1–16. [CrossRef]
38. Simunovic, F.; Yi, M.; Wang, Y.; Macey, L.; Brown, L.T.; Krichevsky, A.M.; Andersen, S.L.; Stephens, R.M.; Benes, F.M.; Sonntag, K.C. Gene Expression Profiling of Substantia Nigra Dopamine Neurons: Further Insights into Parkinson's Disease Pathology. *Brain* **2009**, *132*, 1795–1809. [CrossRef]
39. Salemi, M.; Cosentino, F.; Lanza, G.; Cantone, M.; Salluzzo, M.G.; Giurato, G.; Borgione, E.; Marchese, G.; Santa Paola, S.; Lanuzza, B.; et al. MRNA Expression Profiling of Mitochondrial Subunits in Subjects with Parkinson's Disease. *Arch. Med. Sci.* **2023**, *19*, 678–686. [CrossRef]
40. Salemi, M.; Lanza, G.; Mogavero, M.P.; Cosentino, F.I.I.; Borgione, E.; Iorio, R.; Ventola, G.M.; Marchese, G.; Salluzzo, M.G.; Ravo, M.; et al. A Transcriptome Analysis of MRNAs and Long Non-Coding RNAs in Patients with Parkinson's Disease. *Int. J. Mol. Sci.* **2022**, *23*, 1535. [CrossRef] [PubMed]
41. Zaccaria, A.; Antinori, P.; Licker, V.; Kövari, E.; Lobrinus, J.A.; Burkhard, P.R. Multiomic Analyses of Dopaminergic Neurons Isolated from Human Substantia Nigra in Parkinson's Disease: A Descriptive and Exploratory Study. *Cell Mol. Neurobiol.* **2022**, *42*, 2805–2818. [CrossRef]
42. Okuzumi, A.; Hatano, T.; Fukuhara, T.; Ueno, S.; Nukina, N.; Imai, Y.; Hattori, N. α-Synuclein Seeding Assay Using RT-QuIC. *Methods Mol. Biol.* **2021**, *2322*, 3–16. [CrossRef]
43. Rike, W.A.; Stern, S. Proteins and Transcriptional Dysregulation of the Brain Extracellular Matrix in Parkinson's Disease: A Systematic Review. *Int. J. Mol. Sci.* **2023**, *24*, 7435. [CrossRef]
44. Liu, Y.; Zhou, Q.; Tang, M.; Fu, N.; Shao, W.; Zhang, S.; Yin, Y.; Zeng, R.; Wang, X.; Hu, G.; et al. Upregulation of alphaB-Crystallin Expression in the Substantia Nigra of Patients with Parkinson's Disease. *Neurobiol. Aging* **2015**, *36*, 1686–1691. [CrossRef]
45. Dumitriu, A.; Golji, J.; Labadorf, A.T.; Gao, B.; Beach, T.G.; Myers, R.H.; Longo, K.A.; Latourelle, J.C. Integrative Analyses of Proteomics and RNA Transcriptomics Implicate Mitochondrial Processes, Protein Folding Pathways and GWAS Loci in Parkinson Disease. *BMC Med. Genom.* **2016**, *9*, 5. [CrossRef]
46. González-Casacuberta, I.; Juárez-Flores, D.L.; Morén, C.; Garrabou, G. Bioenergetics and Autophagic Imbalance in Patients-Derived Cell Models of Parkinson Disease Supports Systemic Dysfunction in Neurodegeneration. *Front. Neurosci.* **2019**, *13*, 894. [CrossRef]
47. Gilbert, R.M.; Standaert, D.G. Bridging the Gaps: More Inclusive Research Needed to Fully Understand Parkinson's Disease. *Mov. Disord.* **2020**, *35*, 231–234. [CrossRef]
48. Li, Y.; Yang, J.; Li, S.; Zhang, J.; Zheng, J.; Hou, W.; Zhao, H.; Guo, Y.; Liu, X.; Dou, K.; et al. N-Myc Downstream-Regulated Gene 2, a Novel Estrogen-Targeted Gene, Is Involved in the Regulation of Na^+/K^+-ATPase. *J. Biol. Chem.* **2011**, *286*, 32289–32299. [CrossRef]
49. Mauri, N.; Kleiter, M.; Dietschi, E.; Leschnik, M.; Högler, S.; Wiedmer, M.; Dietrich, J.; Henke, D.; Steffen, F.; Schuller, S.; et al. A SINE Insertion in ATP1B2 in Belgian Shepherd Dogs Affected by Spongy Degeneration with Cerebellar Ataxia (SDCA2). *G3* **2017**, *7*, 2729–2737. [CrossRef] [PubMed]
50. Marchiano, S.; Nakamura, K.; Reinecke, H.; Neidig, L.; Lai, M.; Kadota, S.; Perbellini, F.; Yang, X.; Klaiman, J.M.; Blakely, L.P.; et al. Gene Editing to Prevent Ventricular Arrhythmias Associated with Cardiomyocyte Cell Therapy. *Cell Stem. Cell* **2023**, *30*, 396–414.e9. [CrossRef] [PubMed]
51. Khananshvili, D. The SLC8 Gene Family of Sodium-Calcium Exchangers (NCX)—Structure, Function, and Regulation in Health and Disease. *Mol. Asp. Med.* **2013**, *34*, 220–235. [CrossRef] [PubMed]
52. Cuenca-Bermejo, L.; Almela, P.; Navarro-Zaragoza, J.; Fernández Villalba, E.; González-Cuello, A.-M.; Laorden, M.-L.; Herrero, M.-T. Cardiac Changes in Parkinson's Disease: Lessons from Clinical and Experimental Evidence. *Int. J. Mol. Sci.* **2021**, *22*, 13488. [CrossRef] [PubMed]
53. Yu, W.; Wang, L.; Ren, W.-Y.; Xu, H.-X.; Wu, N.N.; Yu, D.-H.; Reiter, R.J.; Zha, W.-L.; Guo, Q.-D.; Ren, J. SGLT2 Inhibitor Empagliflozin Alleviates Cardiac Remodeling and Contractile Anomalies in a FUNDC1-Dependent Manner in Experimental Parkinson's Disease. *Acta Pharmacol. Sin.* **2023**. [CrossRef] [PubMed]
54. Ren, J.; Porter, J.E.; Wold, L.E.; Aberle, N.S.; Muralikrishnan, D.; Haselton, J.R. Depressed Contractile Function and Adrenergic Responsiveness of Cardiac Myocytes in an Experimental Model of Parkinson Disease, the MPTP-Treated Mouse. *Neurobiol. Aging* **2004**, *25*, 131–138. [CrossRef]

55. Piqueras-Flores, J.; López-García, A.; Moreno-Reig, Á.; González-Martínez, A.; Hernández-González, A.; Vaamonde-Gamo, J.; Jurado-Román, A. Structural and Functional Alterations of the Heart in Parkinson's Disease. *Neurol. Res.* **2018**, *40*, 53–61. [CrossRef]
56. Bardutz, H.; Singh, J.; Rehman, Z.; Bernat, P. Parkinson's Disease and the Cardiac Cycle: A Rapid Literature Review and Case Series. *Life* **2023**, *13*, 1003. [CrossRef]
57. Oleksakova, J.; Javorka, M.; Czippelova, B.; Mazgutova, N.; Grofik, M.; Babalova, L.; Skacik, P.; Kurca, E. Autonomic Control of Heart and Vessels in Patients with Very Early Stage of Parkinson Disease. *Physiol. Meas.* **2023**, *44*, 054002. [CrossRef]
58. Nagel, F.; Falkenburger, B.H.; Tönges, L.; Kowsky, S.; Pöppelmeyer, C.; Schulz, J.B.; Bähr, M.; Dietz, G.P.H. Tat-Hsp70 Protects Dopaminergic Neurons in Midbrain Cultures and in the Substantia Nigra in Models of Parkinson's Disease. *J. Neurochem.* **2008**, *105*, 853–864. [CrossRef]
59. Schaaf, M.B.E.; Keulers, T.G.; Vooijs, M.A.; Rouschop, K.M.A. LC3/GABARAP Family Proteins: Autophagy-(Un)Related Functions. *FASEB J.* **2016**, *30*, 3961–3978. [CrossRef]
60. Le Grand, J.N.; Bon, K.; Fraichard, A.; Zhang, J.; Jouvenot, M.; Risold, P.-Y.; Boyer-Guittaut, M.; Delage-Mourroux, R. Specific Distribution of the Autophagic Protein GABARAPL1/GEC1 in the Developing and Adult Mouse Brain and Identification of Neuronal Populations Expressing GABARAPL1/GEC1. *PLoS ONE* **2013**, *8*, e63133. [CrossRef]
61. Wakabayashi, K.; Tanji, K. Multiple system atrophy and autophagy. *Rinsho Shinkeigaku* **2014**, *54*, 966–968. [CrossRef] [PubMed]
62. El Haddad, S.; Serrano, A.; Moal, F.; Normand, T.; Robin, C.; Charpentier, S.; Valery, A.; Brulé-Morabito, F.; Auzou, P.; Mollet, L.; et al. Disturbed Expression of Autophagy Genes in Blood of Parkinson's Disease Patients. *Gene* **2020**, *738*, 144454. [CrossRef] [PubMed]
63. Fanger, N.A.; Wardwell, K.; Shen, L.; Tedder, T.F.; Guyre, P.M. Type I (CD64) and Type II (CD32) Fc Gamma Receptor-Mediated Phagocytosis by Human Blood Dendritic Cells. *J. Immunol.* **1996**, *157*, 541–548. [CrossRef] [PubMed]
64. Joshi, T.; Butchar, J.P.; Tridandapani, S. Fcγ Receptor Signaling in Phagocytes. *Int. J. Hematol.* **2006**, *84*, 210–216. [CrossRef] [PubMed]
65. Okun, E.; Mattson, M.P.; Arumugam, T.V. Involvement of Fc Receptors in Disorders of the Central Nervous System. *Neuromolecular Med.* **2010**, *12*, 164–178. [CrossRef] [PubMed]
66. Bian, L.-H.; Yao, Z.-W.; Wang, Z.-Y.; Wang, X.-M.; Li, Q.-Y.; Yang, X.; Li, J.-Y.; Wei, X.-J.; Wan, G.-H.; Wang, Y.-Q.; et al. Nardosinone Regulates the Slc38a2 Gene to Alleviate Parkinson's Symptoms in Rats through the GABAergic Synaptic and cAMP Pathways. *Biomed. Pharmacother.* **2022**, *153*, 113269. [CrossRef] [PubMed]
67. Lezi, E.; Swerdlow, R.H. Mitochondria in Neurodegeneration. *Adv. Exp. Med. Biol.* **2012**, *942*, 269–286. [CrossRef] [PubMed]
68. Power, J.H.T.; Barnes, O.L.; Chegini, F. Lewy Bodies and the Mechanisms of Neuronal Cell Death in Parkinson's Disease and Dementia with Lewy Bodies. *Brain Pathol.* **2017**, *27*, 3–12. [CrossRef]
69. Parker, W.D.; Boyson, S.J.; Parks, J.K. Abnormalities of the Electron Transport Chain in Idiopathic Parkinson's Disease. *Ann. Neurol.* **1989**, *26*, 719–723. [CrossRef]
70. Schapira, A.H.; Cooper, J.M.; Dexter, D.; Jenner, P.; Clark, J.B.; Marsden, C.D. Mitochondrial Complex I Deficiency in Parkinson's Disease. *Lancet* **1989**, *1*, 1269. [CrossRef]
71. Bindoff, L.A.; Birch-Machin, M.; Cartlidge, N.E.; Parker, W.D.; Turnbull, D.M. Mitochondrial Function in Parkinson's Disease. *Lancet* **1989**, *2*, 49. [CrossRef] [PubMed]
72. Parker, W.D.; Parks, J.K.; Swerdlow, R.H. Complex I Deficiency in Parkinson's Disease Frontal Cortex. *Brain Res.* **2008**, *1189*, 215–218. [CrossRef]
73. McCoy, M.K.; Cookson, M.R. Mitochondrial Quality Control and Dynamics in Parkinson's Disease. *Antioxid. Redox Signal.* **2012**, *16*, 869–882. [CrossRef] [PubMed]
74. Nave, K.-A.; Trapp, B.D. Axon-Glial Signaling and the Glial Support of Axon Function. *Annu. Rev. Neurosci.* **2008**, *31*, 535–561. [CrossRef] [PubMed]
75. Weng, A.; Rabin, E.E.; Flozak, A.S.; Chiarella, S.E.; Aillon, R.P.; Gottardi, C.J. Alpha-T-Catenin Is Expressed in Peripheral Nerves as a Constituent of Schwann Cell Adherens Junctions. *Biol. Open* **2022**, *11*, bio059634. [CrossRef] [PubMed]
76. Zhou, Z.; Zhan, J.; Cai, Q.; Xu, F.; Chai, R.; Lam, K.; Luan, Z.; Zhou, G.; Tsang, S.; Kipp, M.; et al. The Water Transport System in Astrocytes-Aquaporins. *Cells* **2022**, *11*, 2564. [CrossRef] [PubMed]
77. Phillips, C.L.; Faridounnia, M.; Armao, D.; Snider, N.T. Stability Dynamics of Neurofilament and GFAP Networks and Protein Fragments. *Curr. Opin. Cell Biol.* **2023**, *85*, 102266. [CrossRef]
78. Rose, C.R.; Ziemens, D.; Verkhratsky, A. On the Special Role of NCX in Astrocytes: Translating Na^+-Transients into Intracellular Ca^{2+} Signals. *Cell Calcium* **2020**, *86*, 102154. [CrossRef]
79. Valori, C.F.; Guidotti, G.; Brambilla, L.; Rossi, D. Astrocytes: Emerging Therapeutic Targets in Neurological Disorders. *Trends Mol. Med.* **2019**, *25*, 750–759. [CrossRef]
80. Kechin, A.; Boyarskikh, U.; Kel, A.; Filipenko, M. cutPrimers: A New Tool for Accurate Cutting of Primers from Reads of Targeted Next Generation Sequencing. *J. Comput. Biol.* **2017**, *24*, 1138–1143. [CrossRef]
81. Dobin, A.; Davis, C.A.; Schlesinger, F.; Drenkow, J.; Zaleski, C.; Jha, S.; Batut, P.; Chaisson, M.; Gingeras, T.R. STAR: Ultrafast Universal RNA-Seq Aligner. *Bioinformatics* **2013**, *29*, 15–21. [CrossRef] [PubMed]
82. Love, M.I.; Huber, W.; Anders, S. Moderated Estimation of Fold Change and Dispersion for RNA-Seq Data with DESeq2. *Genome Biol.* **2014**, *15*, 550. [CrossRef] [PubMed]

83. Gu, Z.; Eils, R.; Schlesner, M. Complex Heatmaps Reveal Patterns and Correlations in Multidimensional Genomic Data. *Bioinformatics* **2016**, *32*, 2847–2849. [CrossRef] [PubMed]
84. Krämer, A.; Green, J.; Pollard, J.; Tugendreich, S. Causal Analysis Approaches in Ingenuity Pathway Analysis. *Bioinformatics* **2014**, *30*, 523–530. [CrossRef]

International Journal of
Molecular Sciences

MDPI

Article

Degenerative Changes in the Claustrum and Endopiriform Nucleus after Early-Life Status Epilepticus in Rats

Rastislav Druga [1,2,3,*], Pavel Mares [2], Martin Salaj [1] and Hana Kubova [2,*]

[1] Institute of Anatomy, 2nd Medical Faculty, Charles University, 15006 Prague, Czech Republic; martin.salaj@lfmotol.cuni.cz
[2] Laboratory of Developmental Epileptology, Institute of Physiology, Czech Academy of Sciences, 14200 Prague, Czech Republic; maresp@biomed.cas.cz
[3] Institute of Anatomy, 1st Medical Faculty, Charles University, 12000 Prague, Czech Republic
* Correspondence: rastislav.druga@lf1.cuni.cz (R.D.); kubova@biomed.cas.cz (H.K.)

Abstract: The aim of the present study was to analyze the location of degenerating neurons in the dorsal (insular) claustrum (DCL, VCL) and the dorsal, intermediate and ventral endopiriform nucleus (DEn, IEn, VEn) in rat pups following lithium–pilocarpine status epilepticus (SE) induced at postnatal days [P]12, 15, 18, 21 and 25. The presence of Fluoro-Jade B-positive neurons was evaluated at 4, 12, 24, 48 h and 1 week later. A small number of degenerated neurons was observed in the CL, as well as in the DEn at P12 and P15. The number of degenerated neurons was increased in the CL as well as in the DEn at P18 and above and was highest at longer survival intervals. The CL at P15 and 18 contained a small or moderate number of degenerated neurons mainly close to the medial and dorsal margins also designated as DCl ("shell") while isolated degenerated neurons were distributed in the VCl ("core"). In P21 and 25, a larger number of degenerated neurons occurred in both subdivisions of the dorsal claustrum. The majority of degenerated neurons in the endopiriform nucleus were found in the intermediate and caudal third of the DEn. A small number of degenerated neurons was dispersed in the whole extent of the DEn with prevalence to its medial margin. Our results indicate that degenerated neurons in the claustrum CL and endopiriform nucleus are distributed mainly in subdivisions originating from the ventral pallium; their distribution correlates with chemoarchitectonics of both nuclei and with their intrinsic and extrinsic connections.

Keywords: status epilepticus; claustrum; endopiriform nucleus; claustroamygdaloid complex; neurodegeneration; ontogeny

Citation: Druga, R.; Mares, P.; Salaj, M.; Kubova, H. Degenerative Changes in the Claustrum and Endopiriform Nucleus after Early-Life Status Epilepticus in Rats. *Int. J. Mol. Sci.* **2024**, *25*, 1296. https://doi.org/10.3390/ijms25021296

Academic Editors: Ludmilla A. Morozova-Roche and Claudia Ricci

Received: 13 November 2023
Revised: 7 January 2024
Accepted: 17 January 2024
Published: 20 January 2024

1. Introduction

Status epilepticus (SE) is often used experimentally to trigger epileptogenesis and the development of complex structural and functional changes resembling human temporal lobe epilepsy [1]. Both limbic (amygdala, claustrum, endopiriform nucleus, piriform cortex, entorhinal cortex, hippocampal formation) but also extralimbic structures undergo substantial neuronal loss and structural reorganization after SE in adult as well as in young immature animals [2–9].

The claustrum is a subcortical telencephalic structure present in all mammals examined—from insectivora to primates and humans [10]. Two principal parts of this nucleus can be distinguished in all mammals, namely the dorsal (insular) claustrum, which underlies the insular cortex and the ventral claustrum (piriform claustrum, endopiriform nucleus), which adjoins the piriform cortex [11–15]. Expression patterns of the developmental regulatory genes indicate that the claustrum, the endopiriform nucleus and a part of the amygdala comprise an entity called the claustroamygdaloid complex [16,17] and that derivatives of the ventral and lateral pallium can be distinguished in the claustroamygdaloid complex. A major part of the dorsal claustrum (the dorsolateral claustrum, claustrum proper), the basolateral amygdala, posterolateral cortical amygdalar area and

dorsal part of the piriform cortex are considered derivatives of the lateral pallium, while the ventromedial claustrum (smaller, medial part of the dorsal claustrum adjoining the external capsule (see [17]), the endopiriform nucleus, several amygdalar nuclei and the ventral part of the piriform cortex are considered derivatives of the ventral pallium [16,17].

The claustrum nuclei (dorsal claustrum, endopiriform nucleus) contain mostly glutamatergic neurons and several subpopulations of GABAergic interneurons. Subpopulations of neurons within the CL and the ventral claustrum in rodents express GABA, calcium-binding proteins, neuropeptides and nitric oxide synthase (NOS) [12,15,18–23]. Calcium-binding proteins and neuropeptides in the CL and DEn are frequently colocalized [21,24]. Using single-cell RNA sequencing, it was demonstrated that claustrum contains two excitatory (glutamatergic) neuron subtypes, which differ in the expression of genes and form a core–shell organization [25].

In higher mammals, two principal parts of the claustrum (dorsal or insular and ventral or piriform claustrum) are distinguished [11,14], but in rodents, the traditional dorsal claustrum (CL) was recently parcelled into two subdivisions: the dorsal claustrum (DCl) and the ventral claustrum (VCl) [26]. These two parts differ in the expression of cadherins, calcium-binding proteins (parvalbumin, calretinin), the glutamate transporter GLUT2 and NOS. In contrast, the expression of cadherins might indicate three subdivisions [18,23,27]. Rat and guinea pig claustrum have been found to have complementary patterns of PV and CR immunoreactivity. The CL of the rat consists of two regions, the first being a CR negative zone in the core of the structure. This region is dorsally, medially and basally surrounded by CR-positive neuropil containing a small number of CR-positive neurons (shell). CR-negative zone corresponds to a strong PV-positive area containing a high density of PV-positive neurons and neuropil [4,12,23].

Similarly, the classical ventral (piriform) claustrum (the endopiriform nucleus) was further divided into the dorsal endopiriform nucleus (DEn), the intermediate endopiriform nucleus (IEn) and the ventral endopiriform nucleus (VEn) [26]. A recent analysis of the distribution of calcium-binding proteins and latexin in the CL and DEn of the short-tailed fruit bat proposes further subdivision of the shell subregion into four sectors [28].

Proteomic analyses indicate that the CL in the rat has a shorter anteroposterior extent and that the claustrum in rodents and primates is surrounded by layer VI of the insular cortex. Thus, the concept of the claustrum as an intracortically located structure (within layer VI), as originally introduced by Narkiewicz and Mamos [29], is supported and characterized by the expression of a specific protein [30].

Hodological analysis demonstrates that the CL has reciprocal connections with many neocortical regions, while the DEn has bidirectional connections with the piriform cortex and other limbic structures [13,15,31,32].

The functions of the CL were not yet sufficiently explained. Rich and bidirectional connections with many neocortical areas indicate that it may influence the responsiveness of these areas [33,34]. The claustrum might also integrate sensory information from many cortical areas and form a background for responses to complex stimuli [35].

Convergence of information from different levels of the olfactory system and from the amygdala occurs in the DEn. In addition, electrical and optical recordings indicate that olfactory and gustatory activity converges onto single neurons of the DEn [36–38].

The claustrum and piriform cortex play a role in temporal lobe epileptogenesis. The deep piriform region including the IEn, DEn and CL was identified as a region with an especially low threshold for the generation of epileptiform discharges. Microelectrode mapping indicates that the dorsal edge of the DEn is the site where these discharges are initiated [39]. In addition, the piriform cortex, IEn, DEn and CL are among the structures that exhibit severe pathologic changes in various epilepsy models in adult animals [2,3,8,9,40,41].

Our previous results demonstrated that the piriform cortex and the DEn and IEn are substantially damaged in young rats (P25) that survive lithium–pilocarpine SE, whereas the CL is relatively preserved [4]. More detailed data about the topography of degenerated

neurons and about the time- and age-dependent progression of neuronal degeneration in the ventral and dorsal claustrum (DEn and CL, respectively) are lacking.

In the present study, we stained neurons in these structures undergoing degeneration using FluoroJade-B (FJB) an efficient fluorochrome [42]. This dye was used to identify not only the distribution of neuronal damage but also the timing of damage in the dorsal (insular) claustrum (DCl, VCl) and the ventral (piriform) claustrum (DEn, IEN, VEn) of immature rats after lithium–pilocarpine induced SE. An additional aim was to relate the distribution of degenerating neurons to the recently introduced parcellation of the dorsal claustrum [16,18,23,26,27] (Figure 1).

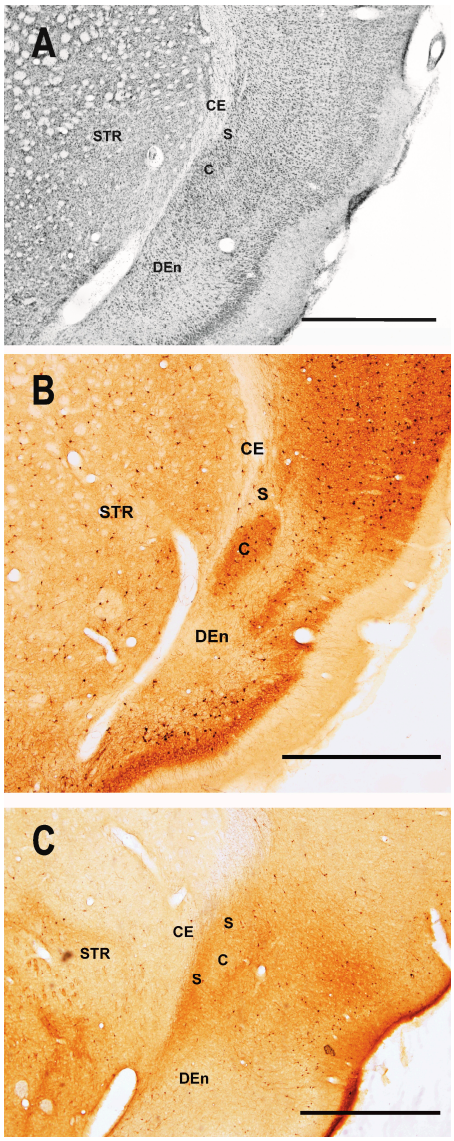

Figure 1. Low-power photomicrograph illustrating distribution of parvalbumin- and calretinin-positive neurons in the claustrum and dorsal endopiriform nucleus used for parcellation of the claustrum. (**A**) Shows cresyl-violet stained section indicating subdivisions of the claustrum. (**B**) Demonstrates the high density of parvalbumine (PVA)-immunopositive neurons in the ventral claustrum (i.e., in the "core"—C). In contrast, only sparse PVA-positive neurons were observed in the dorsal claustrum (i.e., in "shell"—S). The calretinin immunostaining is shown in (**C**). Abbreviations: CE—external capsule; C—dorsal claustrum, subdivision core; S—dorsal claustrum, subdivision shell; DEn—dorsal endopiriform nucleus, STR—striatum. Bar—500 µm.

2. Results

Status epilepticus was induced in all age groups used. Individual groups are signed according to the age of SE induction. Mortality increased with age at SE. No mortality was observed in the P12 group, whereas the highest mortality (35 and 32%, respectively) was observed in P21 and P25 rats.

2.1. Distribution of Degenerating Neurons and Severity of Damage

No FJB-positive neurons were observed in the control animals regardless of age and interval.

2.1.1. Severity of Damage and Distribution of Degenerating Neurons in the Dorsal (Insular) Claustrum (CL) in SE Animals

Both subdivisions of the CL differ significantly in the density of degenerating neurons. The majority of FJB-positive neurons were detected in the DCl (shell), whereas damage to the VCl (core) was rather negligible (Figures 2 and 3). In the DCl the majority of survival intervals exhibited the largest density of degenerating neurons in P21 and/or P25 animals.

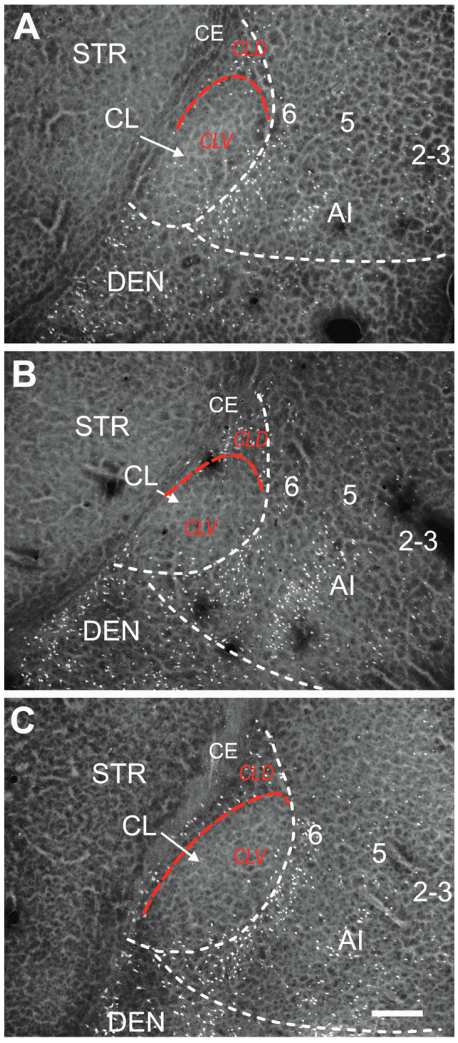

Figure 2. Distribution of FJB-positive neurons in the dorsal claustrum in the subdivisions shell (CLD) and core (CLV)(white dashed lines). Subdivisions are separated with dashed red lines. Panel (**A**) shows distribution and density of FJB-positive neurons in 18-day-old animal surviving 24 h after SE. Panel (**B**) illustrates neuronal damage in 21-day-old and Panel (**C**) in 25-day-old animals both in intervals 24 h after SE. Abbreviations: AI—agranular insular cortex, CE—external capsule, CLD—dorsal subdivision of the claustrum (shell), CLV—ventral subdivision of the claustrum (core), DEN—dorsal endopiriform nucleus, numbers indicate layers of the insular cortex. Bar—200 μm.

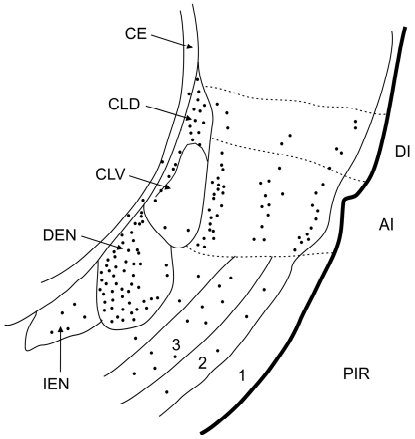

Figure 3. Schematic picture illustrating the parcellation of the claustrum and distribution of FJB-positive neurons (dots) in the claustral nuclei and adjoining cortical areas. Abbreviations: AI—agranular insular cortex, CE—external capsule, CLD—dorsal subdivision of the claustrum (shell), CLV—ventral subdivision of the claustrum (core), DEN—dorsal endopiriform nucleus, DI—disgranular insular cortex, IEN—intermediate endopiriform nucleus, PIR—piriform cortex, numbers indicate layers of the piriform cortex.

Two-way ANOVA revealed a significant effect of age at SE (F (4, 50) = 51.73; $p < 0.0001$) interval after SE (F (4, 50) = 35.25; $p < 0.0001$) and their interaction (F (16, 50) = 8.882; $p < 0.0001$) on the severity of damage in the CLD. The density of FJB-positive neurons (number of FJB-positive cells/mm^2) increased with age at SE and peaked at the 24 h interval. FJB-positive neurons were not observed in P12 in any interval after SE. In P15 rats, only sparse FJB-positive neurons (<10 per anatomic area) were found in intervals of 12–48 h. In P18 rats, the density of FJB-positive neurons was significantly lower 24 h after SE compared to P21 (Figure 4A, left panel). The mean number of FJB-positive cells per anatomic area (area of the CLD) in P21 and P25 was 48 and 55, respectively.

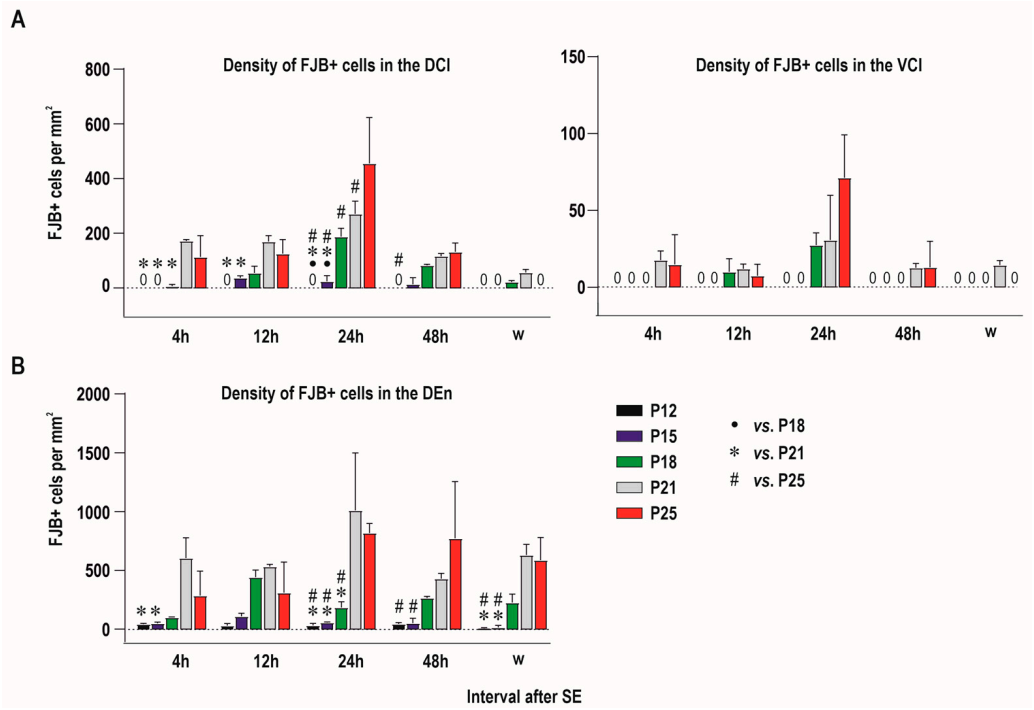

Figure 4. Graphs showing density (average number of FJB-positive neurons per mm^2—abscisae) in individual age (see inset on the bottom part of the graph) and interval groups (intervals after SE—ordinatae) in the claustrum in both DCl and VCl subdivisions (**A**) and in the dorsal endopiriform nucleus (DEN) (**B**). Results are presented as mean ± SD.

In the VCl, (core) density of FJB-positive neurons was negligible or negative with the exception of P18, P21 and P25 animals 24 h after SE. In this interval, 3 to 14 FJB-positive neurons per anatomic area were detected. In other age- and interval groups FJB-positive neurons occurred only sporadically and prevailed in marginal parts of the VCl (Figures 3 and 4A, right panel).

The area of neither the DCL nor VCL differed across individual age and interval groups (Figure 5A).

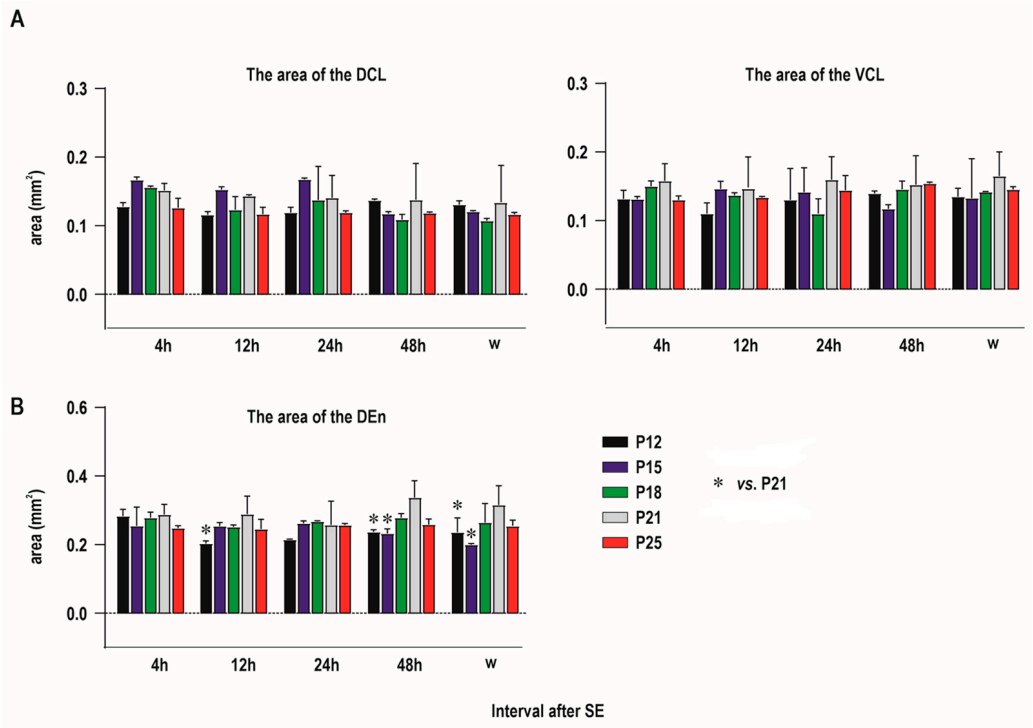

Figure 5. Graphs showing areas (in mm^2—abscisae) of both the claustrum (both DCl and VCl subdivisions, (**A**)) and DEN (**B**) in individual age (see inset on the bottom part of the graph) and interval groups (intervals after SE—ordinatae). Results are presented as mean ± SD.

2.1.2. Severity of Damage and Distribution of Degenerating Neurons in the Endopiriform Nucleus

FJB-positive neurons were detected in all age groups and at all intervals after SE. Two-way ANOVA revealed a significant effect of age at SE ($F(4, 50) = 43.26$; $p = 0.0283$), interval after SE ($F(4, 50) = 2.965$; $p < 0.0001$) and their interaction ($F(16, 50) = 2.776$; $p = 0.0030$) on the severity of damage expressed as a density of FJB-positive neurons (number of FJB-positive neurons per mm^2). In all intervals, the density of positive cells was lower in the three youngest age groups compared to P21 and P25 animals. The lowest density of FJB+ cells was found in P12 and P15 rats. In P18, the density of labeled cells was higher compared to younger age groups, but still significantly lower than in P21 and P25 animals 24 h after SE. FJB-positive neurons were equally distributed along the whole rostrocaudal length of the DEN in the caudal part of the DEN (Figures 4 and 6). In all intervals, FJB-positive neurons prevailed in the medial and basal parts of the DEN (Figures 3, 4 and 6).

Since P15 small number of degenerated neurons was dispersed in the IEN, while no FJB-positive neurons were detected in the VEN.

Two-way ANOVA revealed significant effects of age ($F(4, 50) = 9.743$; $p < 0.0001$), but not of interval after SE or age x and interval interaction on the DEN area. The DEN area tended to be higher in P21 animals in most of the intervals after SE, but post hoc analysis showed significant differences only between P21 animals and the two youngest groups of rats (Figure 5). The statistical differences have to be however interpreted with caution

because they were observed only in some intervals after SE and data were obtained from a relatively small number of animals.

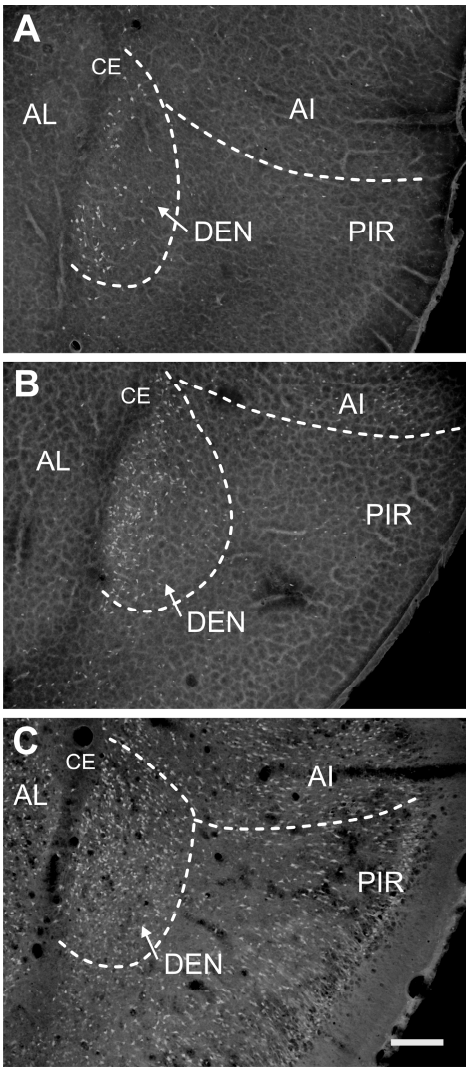

Figure 6. Distribution of FJB-positive neurons in the dorsal endopiriform nucleus (DEN) in 18-day-old (**A**), 21-day-old (**B**) and 25-day-old (**C**) rats 24 h after SE. All details as in Figure 2. Abbreviations: AI—agranular insular cortex, AL—lateral amygdalar nucleus, CE—external capsule, DEN—dorsal endopiriform nucleus, PIR—piriform cortex. White dash lines denote individual brain structures. Bar—200 μm.

2.2. Characteristics of Degenerated Neurons

FJB-positive small, rounded and less frequently bipolar neurons were characteristic in all subdivisions of the claustrum (DCl, VCl, DEN, IEn) at short survival intervals. In contrast, neurons of various sizes (15–33 μm) and with triangular (pyramidal) and multipolar perikarya and a variety of somatodendritic patterns represented approximately 80% of FJB-positive cells within the DCl, VCl and DEN at longer intervals, especially in P18 and older animals (Figure 7).

At shorter intervals up to 24 h after SE, FJB-positive neurons exhibited intense staining of the cell body and proximal dendrites. At longer survival intervals (48 h and 1 week), the DCl and DEN contained a mixture of intensely and less intensely stained neuronal bodies. Some of the less intensely stained (paler) neurons were shrunken with fragmented processes. Additionally, there were dispersed small stained particles formed probably by

disintegrated processes and axon terminals. These stained particles visible at a 1-week survival interval are responsible for a "dusty appearance" of the neuropil.

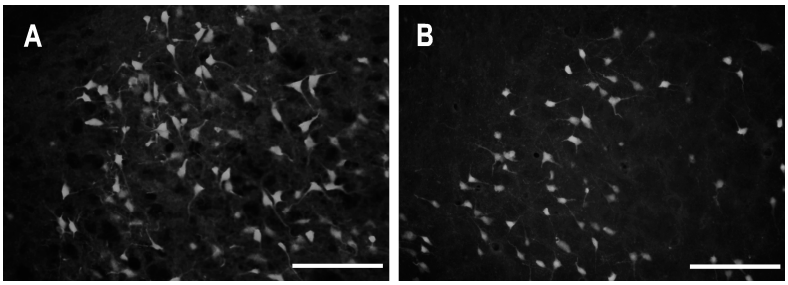

Figure 7. Somatodendritic morphology of FJB-positive neurons. (**A**) Morphology of degenerating neurons in the ventral claustrum, subdivision DEN in 25-day-old rats surviving 24 h after SE. (**B**) Morphology of degenerating neurons in the dorsal claustrum, subdivision DCl (shell) in the same animal. Bar 100 μm.

2.3. Distribution of Calretinin- and Parvalbumin-Positive Neurons

Immunostaining for calretinin (CR) and parvalbumin (PVA) demonstrates the complementary distribution of both calcium-binding proteins in the dorsal (insular) claustrum. The high density of PVA-positive neurons and neuropil was observed in the VCL (core subdivision). This subdivision is surrounded by the rim of CR-positive neurons in the DCL (shell subdivision). In this subdivision, which contained the majority of degenerating neurons, PVA-positive neurons were sparse (Figure 1). Our data are in line with previous studies.

Functioning at this age: The incidence and latency to the onset of continuous convulsions (i.e., SE) were registered. SE was interrupted after 1.5 h of continuous motor seizures by an intraperitoneal injection of paraldehyde (0.3 mL/kg in rat pups at P18 and younger, 0.6 mL/kg in animals at P21 and P25). After paraldehyde injection, the rats were subcutaneously injected with 0.9% NaCl (up to 3% of the body weight divided into 2–3 doses) to restore volume loss. For about 3–4 days after SE, animals 18 days old and older were fed a moist diet. The health status of animals was monitored daily until the end of the study.

Each age and interval group consisted of three animals. Control siblings (n = 2 per age and interval group) were treated with an equal volume of LiCl but the pilocarpine was replaced with saline. A corresponding dose of paraldehyde was administered 2 h after saline injection.

3. Discussion

LiCl/pilocarpine-induced status epilepticus (SE) leads to the development of spontaneous recurrent seizures, cognitive deficits and behavioral alterations and extensive brain damage. It is a widely accepted model of temporal lobe epilepsy. Temporal lobe epilepsy in humans is a complex disorder in which seizures start or involve one or both temporal lobe structures in the brain, specifically the hippocampal formation and amygdalar nuclei. In many patients, temporal lobe epilepsy is associated with a high prevalence of psychiatric comorbidities like cognitive impairment, depression and emotional disturbances. It has been hypothesized that both TLE and its psychiatric comorbidities share common neuropathological and neurobiological aspects. In animal models, several other structures functionally related to the hippocampus and amygdala like parahippocampal cortices, piriform cortex and claustral complex are also damaged. In addition to typical temporal lobe structures, distant nuclear complexes like thalamic nuclei and several neocortical areas hodologically related to hippocampal and amygdalar circuits are also damaged [1,5,43].

The present study provides evidence of region-specific neuronal damage in the claustrum. Neuronal degeneration in the CL is an age- as well as survival interval-dependent

process affecting all age categories. Degenerated neurons were detected in both subdivisions of the CL (DCL, VCL) but significantly prevailed in the DCl as well as in the endopiriform nucleus (DEn, IEn) at various intervals after lithium–pilocarpine induced SE. The number of degenerated neurons in the CL considerably increased in older animals (P21 and P25). A small number of degenerated neurons was detected in the CL (DCl) already in P12 and P15 pups. In older animals (P21 and P25) the number of positive neurons increased in the DCl but also in the VCl. In all groups of animals, FJB-positive neurons within the dorsal claustrum shared a similar topography; that is, in younger animals, they prevailed in the DCl (shell), and in older pups, a small number of degenerated neurons disseminated also to the VCl (core). The central part of the VCl was in younger animals (P15, P18) almost devoid of FJB-positive neurons. This part of the VCl contains many parvalbumin-immunoreactive neurons and a patch of strongly positive parvalbumin-immunoreactive fibers and terminals [19,23]. Very low immunostaining for calretinin is characteristic of the same area of the VCl, even though a small number of calretinin-immunoreactive neurons was detected in the periphery of this region (see Figures 2 and 3). This pale focal area (core) is devoid of calretinin-immunoreactive fibers and puncta and is surrounded medially and laterally by a rim of stronger calretinin-immunoreactive neuropil in the rat as well as in the mouse [12,23]. In addition to an almost complementary distribution pattern of parvalbumin and calretinin within the central area (core) of the CL corresponding to the VCl [26], this part of the CL is characterized by strong cadherin in older animals (P21, P25) (Cad8, rat), whereas there is little neuronal NOS and vesicular glutamate transporter VGLUT2 [16,27,44]. The differences in neuronal damage between shell and core subdivision of the CL in younger and older animals may be related to different structures and vulnerability of local neuronal circuits [45]. It should be taken into consideration that claustro-cortical projecting neurons within DCl (shell subdivision) and VCl (core subdivision) in mice differ in their gene expression and cortical targets. It has been shown that neurons projecting to the retrosplenial cortex are located in the core subdivision of the insular claustrum, while neurons projecting to the lateral entorhinal cortex were found in the shell subdivision [25]. In our experiments, the core subdivision of the claustrum was in younger animals almost preserved while the majority of degenerated neurons were found in the shell subdivision. Such distribution of degenerated neurons within the insular claustrum indicates that neurons projecting to the limbic structures are in younger pups more vulnerable to SE.

The differences in the distribution of degenerated neurons in the subdivisions of the CL (VCl, DCl) and in the DEn after SE may be associated with specific hodological, neurochemical and developmental features of both nuclei.

The neuronal damage in the DEn was heavier than that in the CL and differed significantly between age groups. A small number of FJB-positive neurons (with low densities) was characteristic for the P12 and P15 age groups. In older animals, the number of degenerated neurons increased and peaked at P21.

The DEn is reciprocally connected with the piriform cortex and several other cortical formations [31,37,46]. These projections are largely excitatory and might provide a substrate for regenerative feedback interactions. Epileptiform activities generated in the DEn can drive, via these massive projections, paroxysmal activity in the overlying piriform cortex and back to the DEn [31,37,39,46,47]. It is possible that hyperactivity and the synchronization of synaptic activity in these circuits lead to an increase in glutamate release with a subsequent cascade of neurotoxic events resulting in neuronal degeneration. The specific membrane properties of the DEn neurons may contribute to the susceptibility of this nucleus to epileptiform activity [48]. The other characteristics of the neuronal mechanism within the DEn that explain the susceptibility of the DEn to seizure induction and propagation and eventually to neuronal damage were recently revised [37].

The existence of long rostrally directed associative projections within the DEn which are supposed to be glutamatergic may also contribute to the synchronization of neuronal hyperactivity, glutamate neurotoxicity and consecutive neuronal degeneration in the whole anteroposterior extent of the DEn [46]. Such associative projections were never demon-

strated within the insular claustrum. The prevalence of neuronal degeneration in the caudal two thirds of the DEn might be explained by the additional influence of excitatory projections from several amygdalar nuclei (amygdalohippocampal area and other cortical amygdalar nuclei). These projections terminate in the intermediate and caudal part of the DEn [38].

The present study failed to demonstrate some specific features of neuronal degeneration in the dorsal part of the DEn that might be related to its specific role in the initiation of epileptiform activity [49]. A higher density of degenerated neurons, indicating a higher level of excitotoxicity, was evident in older animals (P18 and older) not only in the dorsal part of the DEn, but also in the medial and basal part of the nucleus. Neuronal degeneration within the DEn displays characteristics of a rather chronic process because the DEn in P18 and older animals contained a moderate number of FJB-positive neurons even 1 week after SE. In contrast to DEn, the IEn contained only a small number of degenerated neurons in all age groups and survival intervals. Negative findings were evident within the VEn.

It appears that the distribution pattern of degenerating neurons within the CL as well as in the DEn also has developmental relations. Degenerated neurons in the CL prevailed in the medial part of the VCl and in the DCl, which are probably derivatives of the ventral pallial histogenetic division. The lateral part of the VCl (called also dorsolateral claustrum, Cld) which is almost free of degenerated neurons is considered by Medina et al. [16] to be a derivative of the lateral pallial histogenetic division of the embryonic telencephalon. According to this developmental concept, the DEn which exhibited massive neuronal degeneration in the majority of survival intervals in our experiments is also considered a possible derivative of the ventral pallium. Thus, it appears that degenerated neurons within the CL (DCl, medial margin of the VCl) and the DEn are distributed predominantly in derivatives of the ventral pallium.

Comparison of the distribution of degenerated neurons in the dorsal and ventral claustrum with expression of Nurr1 (orphan nuclear receptor) and latexin indicated that Nurr+/Latexin- neurons prevailed in the parts of the claustral complex containing in our experiment FJB-positive neurons (DEn, DCl) [50–53].

The expression of a recently introduced marker of the CL, Gng2, indicates that in the rat hemisphere, the CL is discernible only at striatal levels and is surrounded medially and laterally by layer 6 insular cortex cells [30]. The Gng2-rich area probably corresponds to the lateral part of the subdivision of the CL designated by [26] as VCl. A small number of degenerating neurons were observed in this part of the CL in our experiments. In contrast, the medial part of the VCl and DCl contained degenerated neurons in an age- and survival interval-dependent manner.

The dynamics of neuronal degeneration in the DEn was similar to that in the CL (DCl) but the number of degenerated neurons in the DEn exceeded those in the CL. Larger neuronal damage of the DEn may be related to several hodological, cytochemical, structural and functional features. Among them, the pattern of local inhibitory interneurons may represent an important factor influencing the neuronal degeneration process. The core subdivision of the CL (VCl) contains many parvalbumin-immunoreactive neurons, a plexus of PV-ir fibers and a focus of parvalbumin-immunoreactive terminals, while PV-ir neurons are less frequent in the DEn [19]. In addition, the preservation of neurons within the core subdivision may be influenced by the synaptic organization of the neuronal circuits of this subdivision. The relationship among claustro-cortical neurons and PV-positive inhibitory neurons and feedforward inhibition of projecting neurons may represent substrate, which could contribute to the preservation of the core subdivision [45].

The DEn contains a large number of neuropeptide Y-positive neurons and the dorsalmost part of the DEn contains a large number of calretinin-positive boutons.

Summary and methodological considerations:

Our study demonstrated that there are rare degenerating neurons in both parts of the claustrum (DCl, DEn) if SE was elicited at the age of 12 days. Their number substantially increased if SE was induced in 18-day-old and older rats. In all age groups and survival

intervals, the dorsal endopiriform nucleus (DEn) exhibited a higher number of FJB-positive neurons than the dorsal claustrum (DCl, VCl) (Figures 5 and 6).

Taken together, our findings confirm the higher resistance of the immature brain to SE-induced damage. Several animal studies have already confirmed an increase in neurodegeneration with the age at SE. In rodents two weeks old or younger, damage to the hippocampus, amygdala complex or thalamus is small or even minuscule and the extent of neurodegeneration as well as the number of damaged structures increases with age at SE induction. In 3-week-old or older rats is comparable to those seen in adults [54–56].

The duration of SE together with the treatment chosen for termination of SE critically affects the severity and pattern of damage. Clinical studies have clearly shown that delayed treatment of SE is associated with an increased risk of morbidity and mortality as well as with a risk of treatment failure [57]. Clinical experience are supported by animal experiments showing a direct link between the duration of SE, its sequelae and the capability of treatment to stop seizure activity [58,59]. However, it also has to be emphasized that certain medications commonly used to terminate SE have been found to aggravate neuronal damage in immature rats [60]. In our experiments, a single dose of paraldehyde was administered after 1.5 h of ongoing motor seizure activity. In used doses, paraldehyde does not induce neurodegeneration in naïve P12 rats. Given treatment suppressed motor convulsions but it does not completely stop seizure activity in EEG [61]. In this respect, the SE model used for this study represents the model of long-lasting refractory status epilepticus associated with more serious consequences.

4. Materials and Methods

4.1. Animals

Male Wistar albino rats at P12, P15, P18, P21 and P25 postnatal days (P0 defined as the day of birth) were used. Animals (n = 125) were maintained with their dams on a 12/12 h light/dark cycle under controlled temperature (22 ± 1 °C) and humidity (50–60%), with free access to food and water until the end of the experiment. The experiments were approved by the Animal Care and Use Committee of the Institute of Physiology to be in agreement with the Animal Protection Law of the Czech Republic, which is fully compatible with European Commission Council directives 86/609/EEC.

4.2. Induction of Status Epilepticus

SE was induced by pilocarpine hydrochloride (#P6503, Sigma-Alrich® Brand, Merck KGaA, Darmstadt, Germany; 40 mg/kg i.p.) in 5 age groups of rats: 12- (P12), 15- (P15), 18- (P18), 21- (P21) and 25-days (P25) old (pretreated 24 h earlier with lithium chloride (#L9650, Sigma-Alrich® Brand, Merck KGaA, Darmstadt, Germany; 3 mEq/kg i.p.). Animals were observed for at least 2 h after pilocarpine administration. During experiments with 12- and 15-day-old pups, the temperature in Plexiglas cages used for observation was maintained at 32 ± 2 °C using an electric heating pad connected to a digital thermometer to compensate for immature thermoregulatory functioning at this age. The incidence and latency to the onset of continuous convulsions (i.e., SE) were registered. SE was interrupted after 1.5 h of continuous motor seizures by an intraperitoneal injection of paraldehyde (#P5520, Sigma-Alrich® Brand, Merck KGaA, Darmstadt, Germany; 0.3 mL/kg in rat pups at P18 and younger, 0.6 mL/kg in animals at P21 and P25). After paraldehyde injection, the rats were subcutaneously injected with 0.9% NaCl (up to 3% of the body weight divided into 2–3 doses) to restore volume loss. For about 3–4 days after SE, animals 18 days old and older were fed a moist diet. The health status of animals was monitored daily until the end of the study.

Each age and interval group consisted of three animals. Control siblings (n = 2 per age and interval group) were treated with an equal volume of LiCl but the pilocarpine was replaced with saline. A corresponding dose of paraldehyde was administered 2 h after saline injection.

4.3. Histology

Tissue preparation: Rats of all age groups were killed 4, 12, 24, 48 h and 1 week after SE. Rats were overdosed with 20% solution of urethane (#U2500, Sigma-Alrich® Brand, Merck KGaA, Darmstadt, Germany; 2.5 g/kg, i.p.) and perfused with phosphate-buffered saline (PBS, pH 7.4), followed by 4% paraformaldehyde (#P6148, Sigma-Alrich® Brand, Merck KGaA, Darmstadt, Germany; in 0.1 M phosphate buffer (pH 7.4, 4 °C). The brains were removed from the skull, post-fixed for 3 h and then cryoprotected in graded sucrose (10%, 20%, and 30% in PBS). The brains were frozen in dry ice and stored at −70 °C until cut. A series of 50 µm thick coronal sections were prepared for further processing.

FuoroJade B staining: To detect degenerating neurons, a 1-in-5 series of sections was mounted on gelatin-coated slides and processed for FJB histochemistry according to [41,42]. Sections were examined with an epifluorescence microscope using flourescein thiocyanate filter sets. To better delineate the cytoarchitectonic boundaries of the claustrum and adjoining cortical areas, parallel sections were stained with cresyl violet.

Immunohistochemistry: Adjacent sections were processed immunohistochemically with antibodies raised against parvalbumin (mouse monoclonal, dilution 1:10,000, #P3088, Sigma-Alrich® Brand, Merck KGaA, Darmstadt, Germany), or calretinin (mouse monoclonal, 1:8000, #MAB1568, Merck, NJ, USA) using the avidin–biotin method described previously in detail [12]. As a positive control, a thalamic section from an adult rat that experienced SE 24 h earlier was included into each set of immunostainings.

4.4. Parcellation of the Claustrum

For the description of the distribution of the degenerated (FJB-positive) neurons we used the parcellation of the rat claustrum according to Paxinos and Watson [26]. According to this parcellation, the dorsal (insular) claustrum (CL) was further subdivided into claustrum dorsale (DCl) and claustrum ventrale (VCl). Tracings of the CL, DEn and adjoining structures from adjacent series of Nissl stained sections and sections immunostained for parvalbumin and calretinin were used for identification of VCL and VCD borders (Figure 1).

4.5. Semiquantitative Analysis

Only neurons emitting intense yellow–green fluorescence that distinctly exceeded the background of the sections were included in a semi-quantitative analysis of damage severity. FJB-positive cells were counted in the dorsal endopiriform nucleus (DEn) and in the CLD and CLV subdivisions of the claustrum at 20-fold magnification directly from the sections using a microscopic grid. Counting of FJB+ cells in DEn was performed at three anteroposterior levels corresponding with Paxinos and Watson (2007) (23) AP +1.8 to AP −4.0. At each level, FJB^+ neurons were counted per the anatomic area in three to four sections. The size of each anatomic area was assessed using the Olympus BX51 microscope (Tokyo, Japan) and QuickPHOTOMicro 2.3 software (Promicra, Prague, Czech Republic). The cytoarchitectonic boundaries were verified using adjacent Nissl stained sections and the density of FJB+ cells (number of cells per mm^2) was calculated.

Degenerated neurons in the dorsal claustrum were counted in the CLD and CLV separately at the level AP 1.8–0.3 [26] at three consecutive sections.

4.6. Statistics

At the beginning of this study, simple randomization was used to assign each animal in individual age groups to a particular treatment and interval group. Data acquisition and analysis were conducted blinded to the treatment. Data were analyzed using GraphPad Prism 8 (GraphPad Software, Boston, MA, USA) software. Two-way ANOVA was used to identify the main effect of SE. Whenever a significant interaction was identified, the data were subjected to Tukey's post hoc test. p-value < 0.05 was required for significance.

5. Conclusions

Early-life status epilepticus leads to neurodegeneration in the claustral complex. The extent and distribution of degenerating, FJB-positive neurons is highly dependent on the age at SE induction and intervals after SE. The severity of damage increases with age at SE and peaks at 24 h after SE. In the dorsal (insular) claustrum degenerated neurons prevailed in the calretinin positive zone (DCl, i.e., subdivision shell). Low density or almost absence of FJB-positive neurons was observed in the VCl, (i.e., subdivision core) with a high density of parvalbumin-positive neurons suggesting its protective role against SE-induced damage.

Author Contributions: R.D., P.M. and H.K. conceived and designed the experiments. H.K. and R.D. were responsible for neuropathological analysis. H.K. performed animal experiments and statistical data evaluation. M.S. participated in the neuropathological analysis. All authors have read and agreed to the published version of the manuscript.

Funding: This study was supported by the grant of the Czech Science Foundation No. 23-05274S, by the project National Institute for Neurological Research (Programme EXCELES, ID Project No. LX22NPO5107), funded by the European Union–Next Generation EU the project and by support for long-term conceptual development of research organization RVO: 67985823.

Institutional Review Board Statement: All procedures involving animals and their care were conducted according to the ARRIVE guidelines (https://www.nc3rs.org.uk/arrive-guidelines) accessed on 09 December 2023 in compliance with national (Act No 246/1992 Coll.) and international laws and policies (EU Directive 2010/63/EU for animal experiments and the National Institutes of Health guide for the care and use of laboratory animals NIH Publications No. 8023, revised 1978). The experimental protocol was approved on 4 June 2018, by the Ethical Committee of the Czech Academy of Sciences (Approval No. 15/2018).

Informed Consent Statement: Not applicable.

Data Availability Statement: All data and original materials are available in the Laboratory of Developmental Epileptology, IPHYS.

Acknowledgments: The authors would like to thank Blanka Cejkova for her excellent technical assistance.

Conflicts of Interest: Authors declare no conflicts of interest.

References

1. Pitkanen, A.; Kharatishvili, I.; Karhunen, H.; Lukasiuk, K.; Immonen, R.; Nairismägi, J.; Gröhn, O.; Nissinen, J. Epileptogenesis in experimental models. *Epilepsia* **2007**, *48* (Suppl. 2), 13–20. [CrossRef] [PubMed]
2. Cavalheiro, E.A.; Silva, D.F.; Turski, W.A.; Calderazzo-Filho, L.S.; Bortolotto, Z.A.; Turski, L. The susceptibility of rats to pilocarpine-induced seizures is age-dependent. *Brain Res.* **1987**, *465*, 43–58. [CrossRef] [PubMed]
3. Covolan, L.; Mello, L.E. Temporal profile of neuronal injury following pilocarpine or kainic acid-induced status epilepticus. *Epilepsy Res.* **2000**, *39*, 133–152. [CrossRef]
4. Druga, R.; Kubová, H.; Suchomelová, L.; Haugvicová, R. Lithium/pilocarpine status epilepticus-induced neuropathology of piriform cortex and adjoining structures in rats is age-dependent. *Physiol. Res.* **2003**, *52*, 251–264. [CrossRef] [PubMed]
5. Druga, R.; Mares, P.; Otáhal, J.; Kubová, H. Degenerative neuronal changes in the rat thalamus induced by status epilepticus at different developmental stages. *Epilepsy Res.* **2005**, *63*, 43–65. [CrossRef] [PubMed]
6. Kubova, H.; Druga, R.; Haugvicová, R.; Suchomelová, L.; Pitkanen, A. Dynamic changes of status epilepticus-induced neuronal degeneration in the mediodorsal nucleus of the thalamus during postnatal development of the rat. *Epilepsia* **2002**, *43* (Suppl. 5), 54–60. [CrossRef]
7. Kubova, H.; Druga, R.; Lukasiuk, K.; Suchomelová, L.; Haugvicová, R.; Jirmanová, I.; Pitkänen, A. Status epilepticus causes necrotic damage in the mediodorsal nucleus of the thalamus in immature rats. *J. Neurosci.* **2001**, *21*, 3593–3599. [CrossRef]
8. Turski, W.A.; Cavalheiro, E.A.; Bortolotto, Z.A.; Mello, L.M.; Schwarz, M.; Turski, L. Seizures produced by pilocarpine in mice: A behavioral, electroencephalographic and morphological analysis. *Brain Res.* **1984**, *321*, 237–253. [CrossRef]
9. Turski, W.A.; Cavalheiro, E.A.; Schwarz, M.; Czuczwar, S.J.; Kleinrok, Z.; Turski, L. Limbic seizures produced by pilocarpine in rats: Behavioural, electroencephalographic and neuropathological study. *Behav. Brain Res.* **1983**, *9*, 315–335. [CrossRef]
10. Ashwell, K.W.; Hardman, C.; Paxinos, G. The claustrum is not missing from all monotreme brains. *Brain Behav. Evol.* **2004**, *64*, 223–241. [CrossRef]
11. Druga, R. The claustrum of the cat (Felis domestica). *Folia Morphol.* **1966**, *14*, 7–16.

12. Druga, R.; Salaj, M.; Barinka, F.; Edelstein, L.; Kubová, H. Calretinin immunoreactivity in the claustrum of the rat. *Front. Neuroanat.* **2014**, *8*, 160. [CrossRef] [PubMed]
13. Edelstein, L.R.; Denaro, F.J. The claustrum: A historical review of its anatomy, physiology, cytochemistry and functional significance. *Cell Mol. Biol.* **2004**, *50*, 675–702. [PubMed]
14. Narkiewicz, O. Degenerations in the Claustrum after Regional Neocortical Ablations in the Cat. *J. Comp. Neurol.* **1964**, *123*, 335–355. [CrossRef] [PubMed]
15. Druga, R. The structure and connections of the claustrum. In *The Claustrum. Structural, Functional and Clinical Neuroscience*; Edelstein, L.R., Smythies, J.R., Ramachandran, V.S., Eds.; Elsevier: San Diego, CA, USA, 2014; pp. 29–84.
16. Medina, L.; Legaz, I.; González, G.; De Castro, F.; Rubenstein, J.L.; Puelles, L. Expression of Dbx1, Neurogenin 2, Semaphorin 5A, Cadherin 8, and Emx1 distinguish ventral and lateral pallial histogenetic divisions in the developing mouse claustroamygdaloid complex. *J. Comp. Neurol.* **2004**, *474*, 504–523. [CrossRef] [PubMed]
17. Puelles, L.; Kuwana, E.; Puelles, E.; Bulfone, A.; Shimamura, K.; Keleher, J.; Smiga, S.; Rubenstein, J.L. Pallial and subpallial derivatives in the embryonic chick and mouse telencephalon, traced by the expression of the genes Dlx-2, Emx-1, Nkx-2.1, Pax-6, and Tbr-1. *J. Comp. Neurol.* **2000**, *424*, 409–438. [PubMed]
18. Davila, J.C.; Real, M.A.; Olmos, J.L.; Legaz, I.; Medina, L.; Guirado, S. Embryonic and postnatal development of GABA, calbindin, calretinin, and parvalbumin in the mouse claustral complex. *J. Comp. Neurol.* **2005**, *481*, 42–57. [CrossRef]
19. Druga, R.; Chen, S.; Bentivoglio, M. Parvalbumin and calbindin in the rat claustrum: An immunocytochemical study combined with retrograde tracing frontoparietal cortex. *J. Chem. Neuroanat.* **1993**, *6*, 399–406. [CrossRef]
20. Guirado, S.; Real, M.A.; Olmos, J.L.; Dávila, J.C. Distinct types of nitric oxide-producing neurons in the developing and adult mouse claustrum. *J. Comp. Neurol.* **2003**, *465*, 431–444. [CrossRef]
21. Kowianski, P.; Moryś, J.M.; Wójcik, S.; Dziewiatkowski, J.; Luczyńska, A.; Spodnik, E.; Timmermans, J.P.; Moryś, J. Neuropeptide-containing neurons in the endopiriform region of the rat: Morphology and colocalization with calcium-binding proteins and nitric oxide synthase. *Brain Res.* **2004**, *996*, 97–110. [CrossRef]
22. Kowianski, P.; Timmermans, J.P.; Morys, J. Differentiation in the immunocytochemical features of intrinsic and cortically projecting neurons in the rat claustrum—Combined immunocytochemical and axonal transport study. *Brain Res.* **2001**, *905*, 63–71. [CrossRef] [PubMed]
23. Real, M.A.; Davila, J.C.; Guirado, S. Expression of calcium-binding proteins in the mouse claustrum. *J. Chem. Neuroanat.* **2003**, *25*, 151–160. [CrossRef] [PubMed]
24. Kowianski, P.; Dziewiatkowski, J.; Moryś, J.M.; Majak, K.; Wójcik, S.; Edelstein, L.R.; Lietzau, G.; Moryś, J. Colocalization of neuropeptides with calcium-binding proteins in the claustral interneurons during postnatal development of the rat. *Brain Res. Bull.* **2009**, *80*, 100–106. [CrossRef]
25. Erwin, S.R.; Sullivan, K.E.; Kendrick, R.M.; Marriott, B.; Wang, L.; Clements, J.; Lemire, A.L.; Jackson, J.; Cembrowski, M.S. Spatially patterned excitatory neuron subtypes and projections of the claustrum. *Elife* **2021**, *10*, e68967. [CrossRef] [PubMed]
26. Paxinos, G.; Watson, C. *The Rat Brain in Stereotaxic Coordinates*, 6th ed.; Academic Press: San Diego, CA, USA, 2007.
27. Obst-Pernberg, K.; Medina, L.; Redies, C. Expression of R-cadherin and N-cadherin by cell groups and fiber tracts in the developing mouse forebrain: Relation to the formation of functional circuits. *Neuroscience* **2001**, *106*, 505–533. [CrossRef]
28. Morello, T.; Kollmar, R.; Ramzaoui, A.; Stewart, M.; Orman, R. Differential distribution of inhibitory neuron types in subregions of claustrum and dorsal endopiriform nucleus of the short-tailed fruit bat. *Brain Struct. Funct.* **2022**, *227*, 1615–1640. [CrossRef] [PubMed]
29. Narkiewicz, O.; Mamos, L. Relation of the insular claustrum to the neocortex in Insectivora. *J. Hirnforsch.* **1990**, *31*, 623–633.
30. Mathur, B.N.; Caprioli, R.M.; Deutch, A.Y. Proteomic analysis illuminates a novel structural definition of the claustrum and insula. *Cereb. Cortex* **2009**, *19*, 2372–2379. [CrossRef]
31. Majak, K.; Kowiánski, P.; Morýs, J.; Spodnik, J.; Karwacki, Z.; Wisniewski, H.M. The limbic zone of the rabbit and rat claustrum: A study of the claustrocingulate connections based on the retrograde axonal transport of fluorescent tracers. *Anat. Embryol.* **2000**, *201*, 15–25. [CrossRef]
32. Minciacchi, D.; Molinari, M.; Bentivoglio, M.; Macchi, G. The organization of the ipsi- and contralateral claustrocortical system in rat with notes on the bilateral claustrocortical projections in cat. *Neuroscience* **1985**, *16*, 557–576. [CrossRef]
33. Druga, R. Cortico-claustral connections. II. Connections from the parietal, temporal and occipital cortex to the claustrum. *Folia Morphol.* **1968**, *16*, 142–149.
34. Sherk, H.; LeVay, S. Contribution of the cortico-claustral loop to receptive field properties in area 17 of the cat. *J. Neurosci.* **1983**, *3*, 2121–2127. [CrossRef]
35. Crick, F.C.; Koch, C. What is the function of the claustrum? *Philos. Trans. R. Soc. Lond. B Biol. Sci.* **2005**, *360*, 1271–1279. [CrossRef] [PubMed]
36. Fu, W.; Sugai, T.; Yoshimura, H.; Onoda, N. Convergence of olfactory and gustatory connections onto the endopiriform nucleus in the rat. *Neuroscience* **2004**, *126*, 1033–1041. [CrossRef] [PubMed]
37. Majak, K.; Morys, J. Endopiriform nucleus connectivities: The implications for epileptogenesis and epilepsy. *Folia Morphol.* **2007**, *66*, 267–271.

38. Majak, K.; Pikkarainen, M.; Kemppainen, S.; Jolkkonen, E.; Pitkänen, A. Projections from the amygdaloid complex to the claustrum and the endopiriform nucleus: A Phaseolus vulgaris leucoagglutinin study in the rat. *J. Comp. Neurol.* **2002**, *451*, 236–249. [CrossRef]
39. Hoffman, W.H.; Haberly, L.B. Kindling-induced epileptiform potentials in piriform cortex slices originate in the underlying endopiriform nucleus. *J. Neurophysiol.* **1996**, *76*, 1430–1438. [CrossRef]
40. Ben-Ari, Y.; Tremblay, E.; Ottersen, O.P. Injections of kainic acid into the amygdaloid complex of the rat: An electrographic, clinical and histological study in relation to the pathology of epilepsy. *Neuroscience* **1980**, *5*, 515–528. [CrossRef]
41. Sperk, G.; Lassmann, H.; Baran, H.; Kish, S.J.; Seitelberger, F.; Hornykiewicz, O. Kainic acid induced seizures: Neurochemical and histopathological changes. *Neuroscience* **1983**, *10*, 1301–1315. [CrossRef]
42. Schmued, L.C.; Hopkins, K.J. Fluoro-Jade B: A high affinity fluorescent marker for the localization of neuronal degeneration. *Brain Res.* **2000**, *874*, 123–130. [CrossRef]
43. McDonald, A.J.; Mott, D.D. Functional neuroanatomy of amygdalohippocampal interconnections and their role in learning and memory. *J. Neurosci. Res.* **2017**, *95*, 797–820. [CrossRef] [PubMed]
44. Real, M.A.; Davila, J.C.; Guirado, S. Immunohistochemical localization of the vesicular glutamate transporter VGLUT2 in the developing and adult mouse claustrum. *J. Chem. Neuroanat.* **2006**, *31*, 169–177. [CrossRef] [PubMed]
45. Kim, J.; Matney, C.J.; Roth, R.H.; Brown, S.P. Synaptic Organization of the Neuronal Circuits of the Claustrum. *J. Neurosci.* **2016**, *36*, 773–784. [CrossRef] [PubMed]
46. Behan, M.; Haberly, L.B. Intrinsic and efferent connections of the endopiriform nucleus in rat. *J. Comp. Neurol.* **1999**, *408*, 532–548. [CrossRef]
47. Demir, R.; Haberly, L.B.; Jackson, M.B. Voltage imaging of epileptiform activity in slices from rat piriform cortex: Onset and propagation. *J. Neurophysiol.* **1998**, *80*, 2727–2742. [CrossRef] [PubMed]
48. Tseng, G.F.; Haberly, L.B. Deep neurons in piriform cortex. II. Membrane properties that underlie unusual synaptic responses. *J. Neurophysiol.* **1989**, *62*, 386–400. [CrossRef] [PubMed]
49. Demir, R.; Haberly, L.B.; Jackson, M.B. Epileptiform discharges with in-vivo-like features in slices of rat piriform cortex with longitudinal association fibers. *J. Neurophysiol.* **2001**, *86*, 2445–2460. [CrossRef]
50. Arimatsu, Y.; Matney, C.J.; Roth, R.H.; Brown, S.P. Organization and development of corticocortical associative neurons expressing the orphan nuclear receptor Nurr1. *J. Comp. Neurol.* **2003**, *466*, 180–196. [CrossRef]
51. Arimatsu, Y.; Kojima, M.; Ishida, M. Area- and lamina-specific organization of a neuronal subpopulation defined by expression of latexin in the rat cerebral cortex. *Neuroscience* **1999**, *88*, 93–105. [CrossRef]
52. Arimatsu, Y.; Nihonmatsu, I.; Hatanaka, Y. Localization of latexin-immunoreactive neurons in the adult cat cerebral cortex and claustrum/endopiriform formation. *Neuroscience* **2009**, *162*, 1398–1410. [CrossRef]
53. Arimatsu, Y.; Nihonmatsu, I.; Hirata, K.; Takiguchi-Hayashi, K. Cogeneration of neurons with a unique molecular phenotype in layers V and VI of widespread lateral neocortical areas in the rat. *J. Neurosci.* **1994**, *14*, 2020–2031. [CrossRef]
54. Kubova, H.; Mares, P. Are morphologic and functional consequences of status epilepticus in infant rats progressive? *Neuroscience* **2013**, *235*, 232–249. [CrossRef] [PubMed]
55. Sankar, R.; Shin, D.H.; Liu, H.; Mazarati, A.; Pereira de Vasconcelos, A.; Wasterlain, C.G. Patterns of status epilepticus-induced neuronal injury during development and long-term consequences. *J. Neurosci.* **1998**, *18*, 8382–8393. [CrossRef] [PubMed]
56. Scantlebury, M.H.; Heida, J.G.; Hasson, H.J.; Velísková, J.; Velísek, L.; Galanopoulou, A.S.; Moshé, S.L. Age-dependent consequences of status epilepticus: Animal models. *Epilepsia* **2007**, *48* (Suppl. 2), 75–82. [CrossRef] [PubMed]
57. Verrotti, A.; Mazzocchetti, C. Epilepsy: Timely treatment of refractory convulsive status epilepticus. *Nat. Rev. Neurol.* **2018**, *14*, 256–258. [CrossRef] [PubMed]
58. Klitgaard, H.; Matagne, A.; Vanneste-Goemaere, J.; Margineanu, D.G. Pilocarpine-induced epileptogenesis in the rat: Impact of initial duration of status epilepticus on electrophysiological and neuropathological alterations. *Epilepsy Res.* **2002**, *51*, 93–107. [CrossRef]
59. Mazarati, A.M.; Baldwin, R.A.; Sankar, R.; Wasterlain, C.G. Time-dependent decrease in the effectiveness of antiepileptic drugs during the course of self-sustaining status epilepticus. *Brain Res.* **1998**, *814*, 179–185. [CrossRef]
60. Torolira, D.; Suchomelova, L.; Wasterlain, C.G.; Niquet, J. Phenobarbital and midazolam increase neonatal seizure-associated neuronal injury. *Ann. Neurol.* **2017**, *82*, 115–120. [CrossRef]
61. Kubova, H.; Mares, P.; Suchomelová, L.; Brozek, G.; Druga, R.; Pitkänen, A. Status epilepticus in immature rats leads to behavioural and cognitive impairment and epileptogenesis. *Eur. J. Neurosci.* **2004**, *19*, 3255–3265. [CrossRef]

International Journal of
Molecular Sciences

MDPI

Article

A Pilot Study to Investigate Peripheral Low-Level Chronic LPS Injection as a Model of Neutrophil Activation in the Periphery and Brain in Mice

Michelle Aries [1], Makayla Cook [1] and Tiffany Hensley-McBain [1,2,*]

[1] McLaughlin Research Institute, Great Falls, MT 59405, USA; michelle.aries@mclaughlinresearch.org (M.A.)
[2] Department of Basic Sciences, Touro College of Osteopathic Medicine Montana, Great Falls, MT 59405, USA
* Correspondence: thmcbain@mclaughlinresearch.org

Abstract: Lipopolysaccharide-induced (LPS) inflammation is used as model to understand the role of inflammation in brain diseases. However, no studies have assessed the ability of peripheral low-level chronic LPS to induce neutrophil activation in the periphery and brain. Subclinical levels of LPS were injected intraperitoneally into mice to investigate its impacts on neutrophil frequency and activation. Neutrophil activation, as measured by CD11b expression, was higher in LPS-injected mice compared to saline-injected mice after 4 weeks but not 8 weeks of injections. Neutrophil frequency and activation increased in the periphery 4–12 h and 4–8 h after the fourth and final injection, respectively. Increased levels of G-CSF, TNFa, IL-6, and CXCL2 were observed in the plasma along with increased neutrophil elastase, a marker of neutrophil extracellular traps, peaking 4 h following the final injection. Neutrophil activation was increased in the brain of LPS-injected mice when compared to saline-injected mice 4–8 h after the final injection. These results indicate that subclinical levels of peripheral LPS induces neutrophil activation in the periphery and brain. This model of chronic low-level systemic inflammation could be used to understand how neutrophils may act as mediators of the periphery–brain axis of inflammation with age and/or in mouse models of neurodegenerative or neuroinflammatory disease.

Keywords: chronic inflammation; immune activation; neutrophil; extracellular traps; low-level LPS; IP injection; peripheral; brain; flow cytometry; microscopy; C57BL/6J; mice; timepoint optimization

Citation: Aries, M.; Cook, M.; Hensley-McBain, T. A Pilot Study to Investigate Peripheral Low-Level Chronic LPS Injection as a Model of Neutrophil Activation in the Periphery and Brain in Mice. *Int. J. Mol. Sci.* **2024**, *25*, 5357. https://doi.org/10.3390/ijms25105357

Academic Editors: Antonietta Bernardo and Claudia Ricci

Received: 5 March 2024
Revised: 20 April 2024
Accepted: 7 May 2024
Published: 14 May 2024

1. Introduction

Neuroinflammation and immune activation are widely accepted as significant contributing factors to the pathophysiology of Alzheimer's disease (AD), Parkinson's disease (PD), multiple sclerosis (MS), amyotrophic lateral sclerosis (ALS), Huntington's disease (HD), and other neurodegenerative diseases [1–3]. Moreover, neuroinflammation and immune activation are present before the onset of symptoms [4,5]. An increase in proinflammatory cytokines, such as tumor necrosis factor-alpha (TNFα) and interleukin-1b (IL-1b), and caustic molecules released during inflammation, such as nitric oxide (NO) and myeloperoxidase (MPO), have been associated with a worse prognosis across multiple neurodegenerative diseases [2,6]. Neuroinflammatory markers such as these, along with immune cells, including neutrophils and microglia, are potential therapeutic targets for multiple neurodegenerative diseases.

Neutrophils are of therapeutic interest because they are the most abundant circulating leukocyte in humans and have been shown in both human and mouse models to be associated with a worse prognosis in neurodegenerative diseases [7–9]. Genes involved in neutrophil activation and adhesion have been identified in areas with blood–brain barrier (BBB) disruption and associated with disease progression [10–13]. Furthermore, humanized AD mouse model studies have shown an increase in short-term spatial memory

and a decrease in capillary blood flow stalling when targeting neutrophil adhesion or accumulation [9,14,15].

Neutrophils are essential to fight invaders and clear debris [16]. Neutrophils mainly contain pathogens through phagocytosis, degranulation, and the formation of neutrophil extracellular traps (NETs). While neutrophils are important in fighting infection and repairing tissues, they can also cause damage to tissues through their release of antimicrobial peptides, enzymes meant to degrade the extracellular matrix, and reactive oxygen species [17–19]. Neutrophils are not commonly found in a healthy brain because of their exclusion by the BBB [16,20]. However, the BBB is disrupted in neurogenerative diseases such as AD [17,21] and PD [22]. Although neutrophils have been documented in the brain in several neuroinflammatory conditions and diseases, including stroke, multiple sclerosis, and AD, the role of peripheral inflammation in neutrophil infiltration and activation in the brain is unclear [14,17,21,23,24]. Administration of high levels of lipopolysaccharide (LPS) into the periphery as a model of sepsis results in neutrophil infiltration into the brain [25–27]. However, the level of inflammation that is induced in sepsis models is not representative of the chronic low-level inflammation that occurs with age and likely contributes to age-related neurological disease. Previous studies have also demonstrated that neutrophils adhere to the vasculature, infiltrate the brain parenchyma, and can return to the blood stream after interaction with microglia following acute systemic LPS exposure in mice and rats [28,29]. However, no studies have investigated chronic peripheral inflammation and subsequent neutrophil activation in the brain and periphery. With this pilot study, we demonstrate that low-level chronic LPS in the periphery induces neutrophil activation in the periphery of the brain. The LPS exposure model outlined in this pilot study can be further explored in future studies in mice of different genetic backgrounds to investigate the role of neutrophils in neuroinflammation and related brain disorders. This will be specifically useful to understand how peripheral mediators and genetic risk factors for disease may alter neutrophil responses to peripheral stimuli and if neutrophils are mechanistic drivers of the subsequent neuroinflammation and neurodegeneration.

2. Results

2.1. Comparing 4-Week vs. 8-Week Durations of Chronic LPS Exposure to Induce Peripheral Neutrophil Activation

No studies investigating chronic LPS-induced neuroinflammation and its potential cognitive consequences conducted to date have investigated the induction of neutrophil activation in the periphery or brain. As such, we sought to investigate the administration of 0.5 mg/kg of LPS once per week as a potential model of neutrophil activation in the brain. This LPS exposure represents the threshold of physiological changes in mice, and can be used to model low-level chronic inflammation, as may occur in persons with microbiome alterations or frequent GI or respiratory infections common in elderly individuals [30]. This dose has also been demonstrated to impact amyloid pathology and levels of inflammatory cytokines in AD mouse models [31,32]. It was therefore selected based on an interest to use this model in future studies to investigate neutrophilic contributions to AD.

We first sought to determine whether 4 or 8 weeks of chronic LPS injections was optimal to induce neutrophil activation in the periphery (Figure 1A). In this first iteration of the pilot study, male and female mice were injected IP with 0.5 mg/kg of LPS or saline once per week for 8 weeks, and blood was collected at baseline (pre-injection), 12 h after the 4th injection, and 12 h after the 8th injection (Figure 1A). Following injections, neutrophil activation was assessed via flow cytometry (Figure S1). CD11b expression in neutrophils was higher in LPS-injected mice compared to saline-injected mice after 4 weeks of injections ($p < 0.0001$) but not after 8 weeks of injections (Figure 1B). This could be due to increased tolerance, reflected as a slightly lower response in LPS-injected mice, or due to increased inflammation in a subset of saline-injected mice at 8 weeks (Figure 1B). Of note, neutrophil activation was non-significantly increased in the saline-injected group at both 4 weeks and 8 weeks, likely representing inflammation associated with injection and handling. Based

on these data, the next group of mice was injected for 4 weeks to investigate the timing of neutrophil activation in the brain following the final LPS injection (Figure 1C). Blood was drawn at baseline, and blood and brain tissue were collected 4 h, 8 h, or 12 h after the 4th and final injection (Figure 1C). As expected with this level of LPS, there were no significant changes in body weight in either the saline- or LPS-injected mice throughout the experiment (Figure 1D).

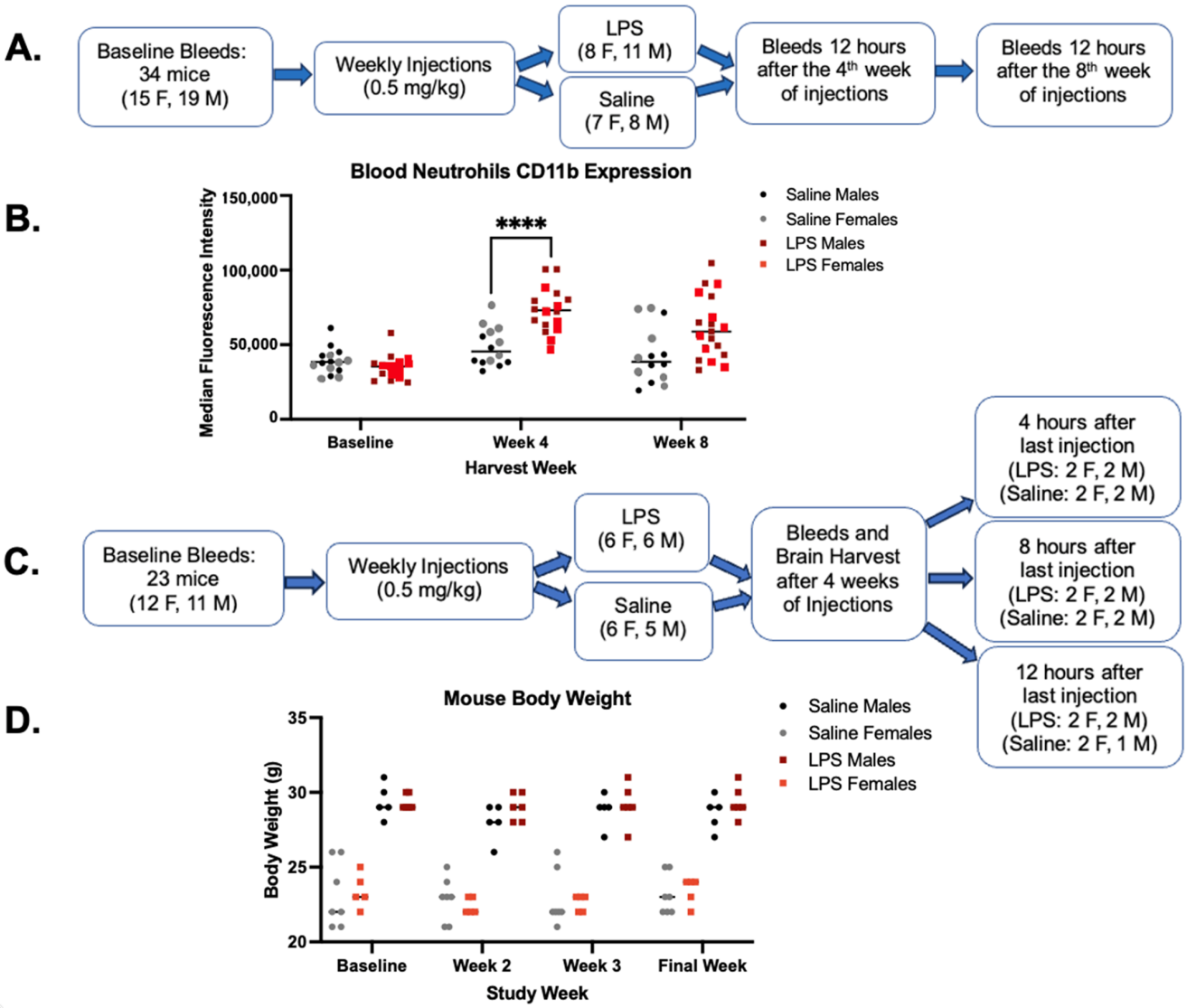

Figure 1. Study design iterations. (**A**) Schematic overview of the preliminary LPS pilot study design to compare 4 vs. 8 weeks of LPS or saline injections. (**B**) Median CD11b expression as measured by flow cytometry on peripheral neutrophils from the initial 8-week pilot described in (**A**) in LPS-injected mice and saline-injected mice demonstrating increased neutrophil activation. (**C**) Schematic overview of study design for the next iteration of the study. Blood and brain tissue were collected after 4 weeks of injections. Neutrophil frequency, activation, and soluble markers were measured 4 h, 8 h, and 12 h after the last injection. (**D**) Body weight throughout the duration of study is outlined in schematic C. Statistical significance was assessed between the LPS and saline groups across timepoints by repeated measures 2-way ANOVA followed by post hoc assessments within each timepoint using Tukey's multiple comparisons test. Multiplicity adjusted P values are represented as **** $p < 0.0001$.

2.2. Peripheral Neutrophil Activation following Low-Level Chronic LPS

Following 4 weeks of IP LPS injections, blood neutrophil frequency and activation were assessed via flow cytometry (Figure S1). No significant increases in blood neutrophil

frequency or activation were observed in the control mice receiving saline. Increases in neutrophil frequencies were observed 4 h after the final LPS injection and reached statistical significance 8 and 12 h following LPS injection, $p < 0.001$ (Figure 2A). Of note, the lack of a statistically significant increase compared to saline-injected mice at 4 h may be partially due to the slight increase in neutrophils in the saline-injected controls, potentially reflecting inflammation caused by handling and injection. Neutrophil CD11b expression increased 4 h after the final LPS injection ($p < 0.05$), peaking at 8 h following LPS injection ($p < 0.001$) (Figure 2A). Peripheral cytokines and chemokines with the ability to regulate neutrophil activation, maturation, and recruitment were measured in plasma via a multiplex bead array. Of the 12 total analytes measured, 5 showed a statistically significant change between the LPS and saline groups. G-CSF, TNFa, IL-6, and CXCL2 increased 4 h after LPS injection, with G-CSF remaining elevated 8 h post LPS administration ($p < 0.001$) (Figure 2B). The anti-inflammatory mediator IL-10 was also increased 4 h following the final LPS injection ($p < 0.01$), suggesting an early potential compensatory response following LPS injection [4,5]. Finally, neutrophil elastase (NE), a marker of neutrophil extracellular trap release [6], was measured via ELISA in plasma. NE was significantly increased 4 h following LPS injection ($p < 0.01$) and remained elevated but not significantly elevated 8 and 12 h following LPS injection (Figure 2C). Taken together, these data suggest that soluble mediators of neutrophil activation rapidly increase by 4 h after IP LPS injection, followed by an increase in neutrophil frequency and neutrophil activation in the blood that peaked 8 h after LPS administration. Soluble mediators of neutrophil responses and neutrophil activation begin to resolve 8–12 h following LPS. However, neutrophil frequency remains elevated 12 h post-LPS.

2.3. Brain Neutrophil Activation following Low-Level Chronic LPS

Brain neutrophil activation, as measured by CD11b expression, was significantly increased in mice receiving LPS 4 h ($p < 0.01$) and 8 h after injection ($p < 0.05$), which corresponds to what was observed for peripheral neutrophils (Figure 3A). We assessed total neutrophils in the brain via microscopy. Brain neutrophils were identified in sagittal sections via myeloperoxidase (MPO) staining using an antibody that has been validated to stain for neutrophils in mouse and human brain tissue (Figure 3B) [17]. A previous study has demonstrated that MPO-staining in mouse and human brain tissue is neutrophil-specific [17]. In addition, we validated the MPO staining of neutrophils by demonstrating that anti-MPO-positive cells have multilobed nuclei consistent with neutrophils and that MPO colocalizes with the neutrophil marker S100A8 (Figure S3). Neutrophils were counted and averaged across two entire sagittal sections and were variably elevated in the brain across timepoints (Figure 3C). Increased neutrophils in the brain were not statistically significant after accounting for statistical outliers in the 4 h and 8 h harvest groups. In addition, neutrophil frequencies were higher in the 8 h and 12 h groups of saline-injected mice compared to the 4 h groups. Neutrophil infiltration into specific brain regions was also variable, with influx into the cortex observed at 4 h and 12 h but not 8 h after the final LPS injection (Figure S2). Given the limited size and variability in neutrophil frequency, potential inferences about total neutrophils in the brain and in specific brain regions are limited with these data. However, different mice in the 4 h and 12 h LPS groups demonstrated over a 2-fold higher number of neutrophils in the brain, particularly in the cortex, suggesting that this may be an area of future study. Due to the potential for neutrophil-microglia crosstalk, we additionally assessed microglial frequencies in the brain in this model and found no statistically significant increase in microglia (Figure S4). Taken together these data indicate that neutrophils demonstrate increased activation in brain tissue within 4 h following peripheral low-level LPS injection.

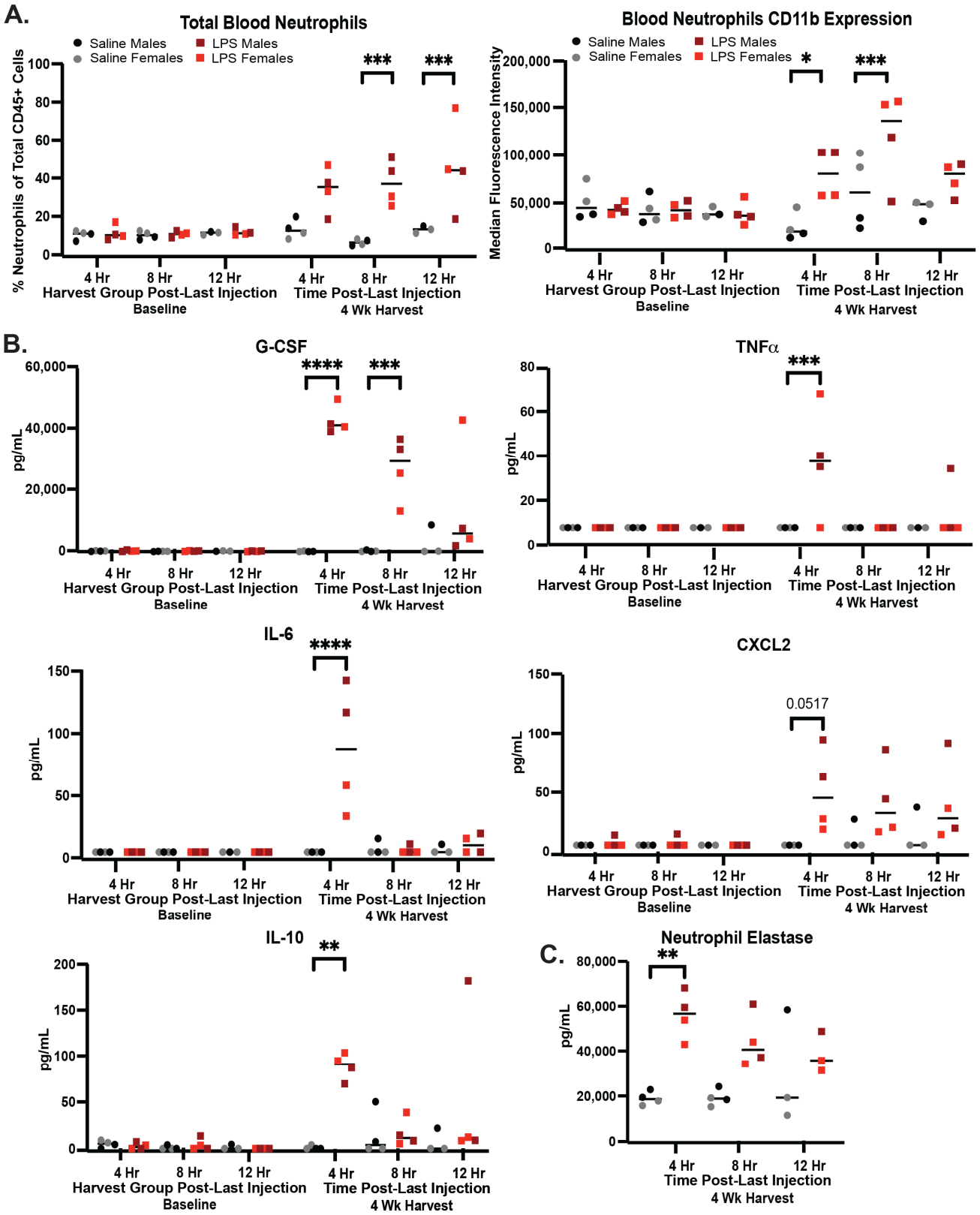

Figure 2. Increased peripheral neutrophil activation following 4 weeks of chronic low-level LPS injections. (**A**) Neutrophil frequency in peripheral blood and median CD11b expression on peripheral blood neutrophils as measured by flow cytometry in mice receiving LPS (red and dark red squares) or saline (grey and black circles). Neutrophils are defined as live, CD45+, CD11b+, Ly6G+ cells

(Figure S1). (**B**) Increased cytokines and chemokines in plasma as measured by multiplex bead array (LegendPlex) in mice receiving LPS (red and dark red squares) or saline (grey and black circles). (**C**) Increased neutrophil elastase in plasma as measured by ELISA in mice receiving LPS (red and dark red squares) or saline (grey and black circles). A and B were measured in submandibular blood, and C was measured in additional cardiac blood collected at time of euthanasia. Statistical significance was assessed between the LPS and saline groups across timepoints by 2-way ANOVA followed by post hoc assessments within each timepoint using Tukey's multiple comparisons test. Multiplicity adjusted p values are represented as * $p < 0.05$, ** $p < 0.01$, *** $p < 0.001$, **** $p < 0.0001$.

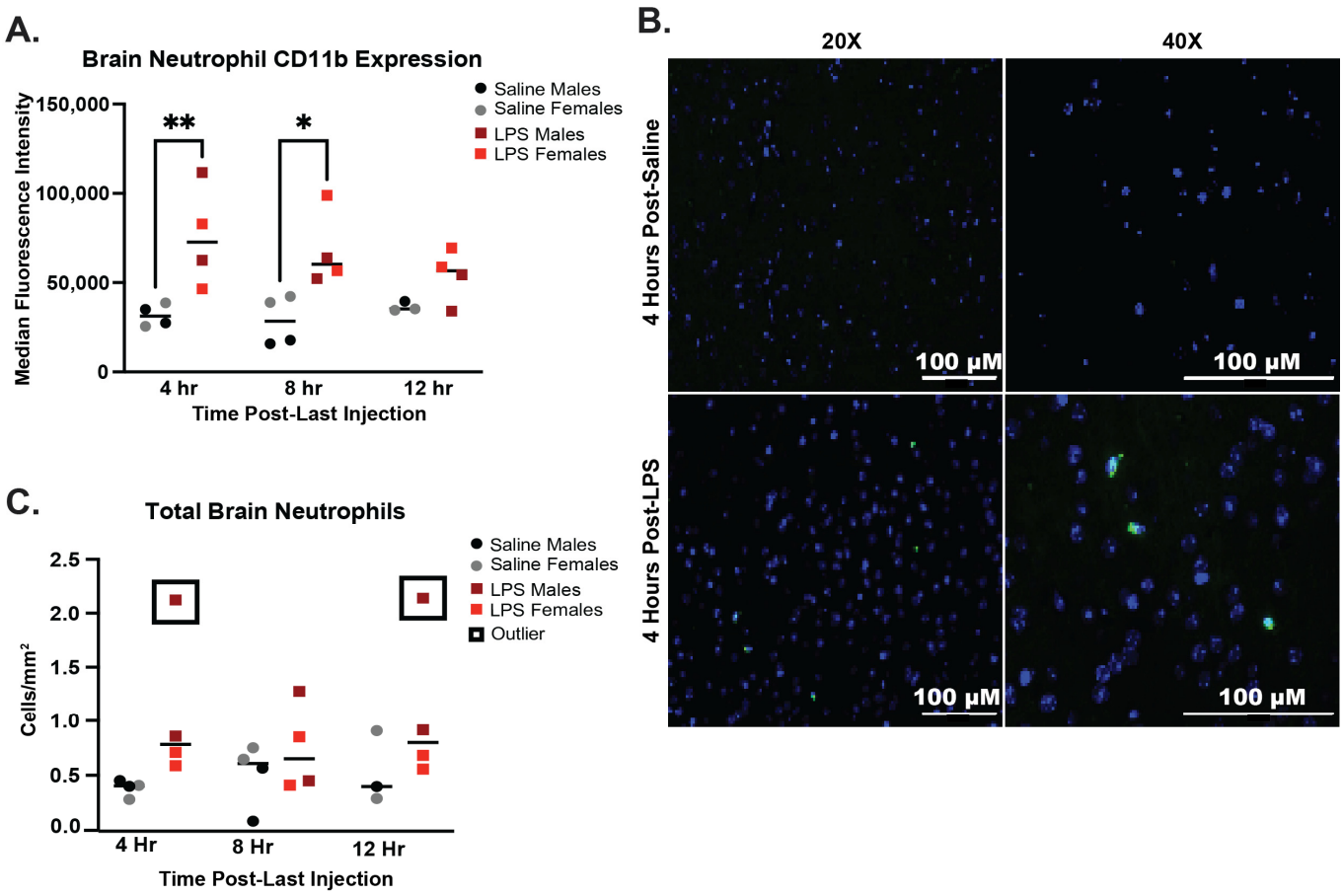

Figure 3. Infiltration of neutrophils into the brain and activation of brain neutrophils following 4 weeks of chronic low-level LPS injections. (**A**) Neutrophils in the brain were assessed by flow cytometry (Figure S1). Neutrophils were defined as CD45+CD11b+Ly6G+ cells, and activation was assessed via CD11b expression. (**B**) Example images of neutrophils stained with MPO-specific antibody (green) and DAPI (blue) in the visual area of the cortex of saline- and LPS-injected mice. (**C**) Neutrophils counted and averaged via microscopy in two sagittal brain sections and normalized by area in saline- and LPS-injected mice. Outliers were identified by ROUT method and indicated by a black box. Outliers were not included in statistical assessments. Statistical significance was assessed across timepoints by 2-way ANOVA followed by post hoc assessments within each timepoint using Tukey's multiple comparisons test. Multiplicity adjusted p values are represented as * $p < 0.05$, ** $p < 0.01$.

3. Discussion

LPS is a component of the outer membrane of Gram-negative bacteria that binds to toll-like receptor 4 (TLR-4) on immune cells. It is commonly used to induce inflammation in the periphery and brain. However, studies differ in their dose, frequency, and route of administration [3]. Most studies have investigated acute exposure to LPS, administering LPS intraperitoneally (IP) daily for 5–7 days at doses of 0.25–1 mg/kg. Chronic exposure

studies have demonstrated microglial and astrocyte activation and memory impairment with similar doses administered IP once or twice weekly for 4–6 weeks [33]. Despite LPS as a common model for peripheral immune activation and subsequent neuroinflammation, no studies have investigated the role of neutrophils in mediating the periphery–brain axis of inflammation induced by chronic low levels of LPS. Neutrophils in the periphery and vasculature could contribute to neuroinflammation and neurodegeneration in multiple ways, including their role in blood flow stalling and their direct release of proinflammatory cytokines and factors that disrupt the BBB [7,34]. In addition, peripheral inflammation could result in increased neutrophil adhesion molecules that result in their extravasation into the brain and release of granules and NET components that may directly damage tissue. Neutrophils in the brain could impact the surrounding tissue in multiple ways. Their release of ROS, NETs, and cytokines can activate microglia, and their release of extracellular histones can induce neuronal apoptosis [16,20,35]. The matrix metalloproteinases (MMPs) and proteases released by neutrophils during degranulation or the generation of NETs results in breakdown of the extracellular matrix and neuronal damage [16,20].

With this study, we sought to determine if low levels of peripheral LPS result in neutrophilic contributions to neuroinflammation. Models of various neurodegenerative diseases have demonstrated that chronic low-level LPS administered IP results in neuroinflammation, as evidenced by induced glial activation, cognitive dysfunction, cerebrovascular leakiness, and inflammatory cytokines in the brain [33]. Chronic peripheral LPS in these models also induced proteinopathy, with increased amyloid deposition in AD models and TDP-43 aggregation in ALS models [33]. The role of neutrophils in mediating neurodegeneration in response to low levels of chronic LPS in the periphery has never been examined. Here, we report that chronic IP LPS injections for 4 weeks induces increased neutrophils activation in the periphery and brain in mice. In our preliminary assessments, we found that neutrophil activation in the periphery was higher in LPS-injected mice compared with saline-injected mice after 4 weeks but not after 8 weeks of injections, therefore limiting our brain investigations to 4 weeks. Elevated neutrophil frequencies were observed through 12 h post-LPS in the periphery. Maintained elevated frequencies suggest that neutrophils released from the bone marrow are not yet undergoing homeostatic apoptosis by 12 h post-LPS [36]. Future studies should investigate the role of fewer and additional injections on neutrophils in the brain and the impact on the temporal nature of the response.

There are multiple mechanisms for how peripheral LPS may result in increased neutrophil activation in the brain. It has been demonstrated that LPS signaling through the TLR-4 receptor increases CD11b expression on neutrophils, and the binding of CD11b/CD18 (Mac 1) to ICAM-1 mediates adhesion and transmigration, which are necessary for extravasation into tissues [37]. We observed increased CD11b expression on peripheral and brain neutrophils following chronic low-level LPS. Therefore, it is possible that LPS increases neutrophil adhesion and extravasation into the brain through increased CD11b expression. Importantly, blood neutrophil CD11b expression is increased in persons with AD and correlates with disease severity, making it a relevant marker of neutrophil activation in models of neuroinflammation and neurodegeneration [38]. A previous study demonstrated that neutrophils enter the brain in 5xFAD mice, a mouse model for AD, through binding of LFA-1 to integrins, and LFA-1-dependent neutrophil recruitment has also been observed in a model of LPS-induced lung inflammation [9]. We did not measure LFA-1 (CD11a/CD18) on the surface of neutrophils in this study, nor did we measure receptor expression levels (e.g., ICAM-1). However, this model can be used to further understand how peripheral inflammation may result in neutrophil migration into the brain and decipher which adhesion molecules are involved. In addition, peripheral inflammation can contribute to BBB dysfunction, thus allowing for inflammatory cytokines and peripheral immune cells to more easily traffic into the brain and activate microglia that perpetuate neuroinflammation and continued BBB dysfunction [39]. Neutrophils have been found near areas of BBB dysfunction in AD mouse models, but whether the BBB is a cause or a consequence of neutrophil invasion remains to be determined [7].

Increased CD11b mediates phagocytosis and oxidative burst in neutrophils and is increased on peripheral neutrophils in AD [38,40], potentially due to increased TNFa [41–43]. In our study, TNFa increased 4 h following the final LPS injection but resolved by 8 h post-LPS, and CD11b expression was sustained through 8 h post-LPS in both the periphery and brain but resolved by 12 h post-LPS. This suggests that weekly LPS injections do not result in sustained elevations of TNFa and neutrophil activation at this very low dose. It will be interesting in future studies to determine how sustained exposure to subclinical inflammatory stimuli may alter these responses in comparison to intermittent stimuli, which we tested here. However, previous studies have demonstrated that exposure to this level of LPS early in life resulted in cognitive impairments 10 months later in mice [44,45], suggesting that damage caused by leukocytes that infiltrate temporarily may result in sustained impairment or may synergize later with age to contribute to degeneration. We did not investigate neurodegeneration or cognitive impairment in this pilot study. However, this will be an important area of future study. Finally, CD11b expression on neutrophils increases with age, so CD11b expression and neutrophil activation in mice receiving low-level chronic LPS should be further examined at different ages to determine how age impacts this model [46].

Overall, the data provided here are evidence that chronic, low-level LPS administered in the periphery increases neutrophil activation in the periphery and brain. While we did not study functionality of neutrophils in this study, the observed increase in NE is suggestive of increased NET release, which has been observed as a peripheral marker of neurodegeneration and neuroinflammation [35]. NET release in the brain is known to contribute to damage, so future studies should investigate NETs in the brain following low levels of peripheral LPS exposure. Of note, neutrophils may also have suppressive functions and contribute to the resolution of inflammation [7]. Studies have demonstrated that LPS may induce regulatory T cells that in turn result in the production of IL-10 by neutrophils, and this interaction is mediated by CD11b [47]. However, two observations suggest that this is not the main mechanism observed in our study: (1) IL-10 peaks at 4 h post-LPS, while neutrophils remain elevated through 8–12 h, suggesting that, at least at later timepoints, neutrophils are not producing high levels of IL-10. (2) Neutrophils that produce IL-10 were demonstrated to have decreased CD11b expression in a prior study [47], and neutrophils in this model upregulated CD11b expression following LPS injection. Future studies should perform functional assays to assess NET release, phagocytic ability, and ability to suppress T cell function to fully elucidate how neutrophils contribute to inflammation in this model. In addition, a detailed assessment of neutrophil dynamics as they relate to activation and frequency following LPS-injection will be of high importance. The relationship between CD11b expression and neutrophil frequency could be assessed by investigating neutrophil lifespan ex vivo and the expression of activation markers in conjunction with apoptosis markers, such as active Caspase-3, as we have previously investigated in human neutrophils [36].

This study has several limitations, some of which have already been discussed. First, this is a small pilot study, and although we included both male and female mice, we are underpowered to analyze them separately. Sex differences should be examined in the future to understand how this model may be applied to investigate sexual dimorphism in neuroinflammation. Given the sample size used herein, these results may not be generalizable, and future studies should further investigate the timing of neutrophil infiltration into the brain following this low-level chronic LPS model in additional mice, specifically in models with genetic modifications that will be useful to further probe the relationship between peripheral inflammation, neuroinflammation, and neurodegeneration. Second, we observed some activation of peripheral neutrophils and some higher neutrophil counts in the brain with some of the saline-injected groups. This makes the interpretations of sustained LPS-induced neutrophil infiltration into the brain beyond 4 h challenging. However, it depicts the continued need for control groups when performing injections and studying inflammation, as the injection itself, or simply handling the mice, may be mediators of inflammation [48]. While neutrophil responses in the brain to stress signals

have not been well characterized, studies have demonstrated that acute handling stress and social stress result in inflammation in the periphery that is dominated by neutrophils and neutrophil-specific transcriptional changes [49–51]. Finally, we are unable to speak to the longevity of neutrophil responses or how these responses compare to acute stimuli or stimuli given over a shorter duration (i.e., less than 4 weeks) based on this pilot. Future studies should investigate sustained neutrophil inflammation beyond 12 h following LPS injections and the potential for impacts weeks to months after injection. Future studies may also examine how this compares to acute responses to LPS and how chronic exposure changes the response with each subsequent injection. This model can also be used to assess interactions between neutrophils and other cell types in the periphery and brain and investigate molecular mechanisms of neutrophil activation models of neurodegeneration and neuroinflammation. This may be particularly important in the context of microglia, given that previous studies have shown that peripheral stimuli induce epigenetic reprogramming of microglia, suggestive of immune memory in the brain [52]. However, this study provides the foundation for an experimental model to induce neutrophil activation in the periphery and the brain with a subclinical peripheral stimulus, which can be used to understand the role of neutrophils in mediating the periphery–neuroinflammation axis in different mouse models of disease.

4. Materials and Methods

4.1. Animals

All mice in the study were generations F3 and F4 from the MRI C57BL/6J strain maintained in-house. The in-house lines are refreshed from The Jackson Laboratory periodically to reduce genetic drift. The mice were housed in individually ventilated and air-filtered cages in a super-barrier mouse room. All cages, bedding, water, and enrichment were autoclaved or UV-treated prior to contact with the mice. Mice always had free access to food and water. All mouse cages were only opened in a biological safety cabinet, and all personnel wore autoclaved lab coats and used sterile gloves. LPS and saline mice were co-housed to reduce cage-to-cage bias. No differences in the behavior of the LPS- vs. saline-injected mice were observable at any time point after injections or during the study. In the 8-week study (Figure 1A), 8 females and 11 males received LPS, and 7 females and 8 males received saline. In the subsequent 4-week study (Figure 1C), 6 females and 6 males received LPS, and 6 females and 5 males received saline.

4.2. LPS Injections

Mice were weighed weekly for 0.5 mg/kg by weight calculations. Vaccine-grade LPS from *Escherichia coli* 0111:B4 (InvivoGen, San Diego, CA, USA) or United States Pharmacopeia (USP) sterile-grade saline (z1376, Cytiva, Marlborough, MA, USA) were 0.22 uM sterile filtered prior to injections. Mice were injected IP with LPS or sterile saline once a week for 8 weeks for the preliminary study (Figure 1A) and once a week for 4 weeks for the next iteration (Figure 1C).

4.3. Blood and Brain Collection

Baseline blood was collected the day before the first injection. In the initial experiment, submandibular blood was collected 12 h after the 4-week and 8-week (final) LPS or saline injection. For the next iteration of the study, submandibular blood was collected at 4, 8, or 12 h after the 4-week (final) LPS or saline injection just prior to euthanasia and brain collection. Following the submandibular bleeds, deep anesthetization was carried out with avertin via IP injection. A cardiac puncture was then performed to obtain additional blood prior to whole body perfusion with 20 mL of PBS to flush the vasculature (until fluids ran clear). Success of the perfusion was determined based on coloration before proceeding as previously described [53]. Following perfusion, the brain was then removed and placed in R10 (10% fetal bovine serum in RPMI 1640 with L-glutamate and 25 mM HEPES) and kept on ice until tissue processing.

4.4. Brain Tissue Processing

One hemibrain was enzymatically digested with media (RPMI 1640 with L-glutamate and 25 mM HEPES) supplemented with Liberase (40 μg/ mL, Sigma-Aldrich, St. Louis, MO, USA) and DNAse (4 μg/mL, Sigma-Aldrich, St. Louis, MO, USA) for 45 min at 37 C with vigorous stirring and then ground through a 70 μm cell strainer, as previously described [54]. Isolated brain leukocytes were separated via a percoll gradient as previously described [55] for flow cytometry analysis. The second hemibrain was fixed in 10% buffered formalin for 24 h and then transferred to 70% ethanol until the paraffin-embedding procedure for microscopy staining.

4.5. Staining of Blood and Brain Tissue for Flow Cytometry

Plasma was removed from whole blood and frozen for cytokine analysis, and the volume removed was replaced with 1X phosphate buffered saline (PBS). Next, 25 μL of plasma-removed blood and was lysed for 10 min with 1× Red Blood Cell (RBC) Lysis Buffer (10× RBC, 420302, Biolegend, San Diego, CA, USA). All blood and brain samples were washed twice with 1× PBS and incubated for 5 min with a fixable viability stain (L34988, Invitrogen, San Diego, CA, USA). Samples were then incubated with a Fc block (TruStain FcX, 101320, Biolegend, San Diego, CA, USA) for 5 min. All samples were stained for 20 min with the following anti-mouse antibodies: Ly6G Brilliant Violet 421 (127628, Clone 1A8, Isotype Rat IgG2b, k, Biolegend, San Diego, CA, USA), CD45 APC (103112, Clone 30-F11, Isotype Rat IgG2b, k, Biolegend, San Diego, CA, USA), CD62L PE (104408, Clone MEL-14, Isotype Rat IgG2b, k, Biolegend, San Diego, CA, USA), and CD11b (101216, Clone M1/70, Isotype Rat IgG2b, k, Biolegend, San Diego, CA, USA). Samples were fixed with 1x fixation buffer for 20 min (420801, Biolegend, San Diego, CA, USA) and then washed twice with 1X PBS with 10% FBS wash (FACS wash). Fluorescence data were collected by flow cytometry on a Sony SH800S cell sorter. Compensation beads were stained with the fluorophore-conjugated antibodies used to stain the blood and brain samples, and compensation matrices were applied across all samples. Fluorescence minus one (FMO) tubes were run on each fluorophore-conjugated antibody used in the study to set positive gates. Unstained sample controls demonstrated consistent low background fluorescence across all channels. FlowJo (version 10.9.0, BD Biosciences, Franklin Lakes, NJ, USA) was used to analyze the data. Cells were gated based on surface marker expression and/or scatter properties (Figure S1) [56].

4.6. Soluble Analyte Analyses

Cytokine and chemokines involved in neutrophil mobilization and activation were measured using a custom multiplex bead array kit (LEGENDPlex, Biolegend, San Diego, CA, USA). Twelve cytokines were measured in duplicate, including CXCL1, CXCL2, G-CSF, IL-1b, IL-6, IL-4, TGFb, TNFa, GM-CSF, INFg, IL-17A, and IL-10. The assay was performed according to manufacturer's instructions, collected on an SH800 (Sony), and analyzed using the LEGENDPlex Cloud-Based Data Analysis Software version 2023-02-15 (Biolegend, San Diego, CA, USA and Qognit, San Carlos, CA, USA). Neutrophil elastase was measured via ELISA using a pre-validated kit following manufacturer's instructions (Abcam, Cambridge, UK) and read using a Mini ELISA Plate Reader (Biolegend, San Diego, CA, USA).

4.7. Immunohistochemistry

Formalin-fixed paraffin-embedded sections (5 μm thickness) were baked at 60 °C for 20 min, dewaxed in xylene for 1 h, and rehydrated through an alcohol series. Antigen retrieval with 1X Reveal Decloaker (Biocare Medical, Pacheco, CA, USA) was performed using the capillary gapping method with a steamer for 35 min. Once sections were cooled and washed, they were blocked in Background Sniper (Biocare Medical, Pacheco, CA, USA) for 10 min. Primary antibodies were diluted in Background Sniper as follows and added to sections overnight at 4 °C: Chicken anti-Mouse/Human/Rat GFAP (PA1-10004, Invitrogen, San Diego, CA, USA) and Rabbit anti-human/mouse Recombinant Anti-S100A8 (ab92331,

Abcam, Cambridge, UK) were diluted to 1µL/mL, and Goat anti-Human/Mouse MPO (AF3667, R&D, Minneapolis, MN, USA) was diluted to 0.5 µL/mL. Sections were washed in TBS with 0.1% Triton X (TBST) twice and incubated in species-specific secondary antibodies in the following dilutions for 2 h at room temperature: Donkey anti-Chicken Ax594 at a 2 µL/mL, Donkey anti-Rabbit Ax594 at 1 µL/mL, and Donkey anti-Goat IgG Ax488 at a 4 µL/mL. Slides were washed in TBST and distilled water, and then coverslips were mounted onto sections with Vectashield HardSet Antifade Mounting Medium with DAPI (Vector Laboratories, Newark, CA, USA) before imaging. Sections were imaged at 20× and 40× on an Olympus Fluoview FV1000, and neutrophils were counted on a Zeiss Axio Imager.M1 (20× and 40× objective).

4.8. Power Calculations and Statistical Analyses

This study was designed to have 0.81 power to detect a 20% difference in means with a standard deviation of 10% in neutrophils in the periphery between saline and LPS groups at each timepoint with an alpha level of 0.05 (n = 4 per timepoint). Statistical significance was assessed between the LPS and saline groups across timepoints by 2-way ANOVA followed by post hoc assessments within each timepoint using Tukey's multiple comparisons test.

Supplementary Materials: The following supporting information can be downloaded at: https://www.mdpi.com/article/10.3390/ijms25105357/s1.

Author Contributions: M.A. assisted with experimental procedures, conducted the study, conducted data analysis, drafted, and edited the article. M.C. conducted the study, conducted data analysis, and assisted with drafting and editing the article. T.H.-M. conceptualized, designed, and conducted the experiment, conducted data analysis, conceptualized, drafted, and edited the article. All authors have read and agreed to the published version of the manuscript.

Funding: This research was funded by the National Institute of General Medical Sciences of the National Institutes of Health under Award Number P20GM152335 and National Institutes of Health grant 1R56AG079224-01 awarded to T.H.-M. The content is solely the responsibility of the authors and does not necessarily represent the official views of the National Institutes of Health.

Institutional Review Board Statement: All animal studies were conducted at the McLaughlin Research Institute for Biomedical Sciences (MRI) between November 2022 and January 2023. MRI is an American Association of Laboratory Animal Science (AALAS)-certified institute. The studies reported herein were approved by the MRI Institutional Animal Care and Use Committee (IACUC) on 11 October 2021 under protocol number 2021-THM-050. All research protocols follow the NIH *Guide for the Care and Use of Laboratory Animals* [57], the *Public Health Service Policy on Humane Care and Use of Laboratory Animals* and the ARRIVE guidelines [58]. All procedures and experiments in this study were performed in accordance with all the above-named guidelines and regulations.

Informed Consent Statement: Not applicable.

Data Availability Statement: The datasets generated and analyzed during this study are available from the corresponding author upon reasonable request.

Acknowledgments: The authors would like to acknowledge colleagues and staff at the McLaughlin Research Institute for their support of these studies.

Conflicts of Interest: The authors declare that the research was conducted in the absence of competing interests.

References

1. Furman, D.; Campisi, J.; Verdin, E.; Carrera-Bastos, P.; Targ, S.; Franceschi, C.; Ferrucci, L.; Gilroy, D.W.; Fasano, A.; Miller, G.W.; et al. Chronic inflammation in the etiology of disease across the life span. *Nat. Med.* **2019**, *25*, 1822–1832. [CrossRef] [PubMed]
2. Rauf, A.; Badoni, H.; Abu-Izneid, T.; Olatunde, A.; Rahman, M.M.; Painuli, S.; Semwal, P.; Wilairatana, P.; Mubarak, M.S. Neuroinflammatory Markers: Key Indicators in the Pathology of Neurodegenerative Diseases. *Molecules* **2022**, *27*, 3194. [CrossRef] [PubMed]
3. Skrzypczak-Wiercioch, A.; Sałat, K. Lipopolysaccharide-Induced Model of Neuroinflammation: Mechanisms of Action, Research Application and Future Directions for Its Use. *Molecules* **2022**, *27*, 5481. [CrossRef]

4. Xie, J.; Van Hoecke, L.; Vandenbroucke, R.E. The Impact of Systemic Inflammation on Alzheimer's Disease Pathology. *Front. Immunol.* **2022**, *12*, 796867. [CrossRef] [PubMed]
5. Kinney, J.W.; Bemiller, S.M.; Murtishaw, A.S.; Leisgang, A.M.; Salazar, A.M.; Lamb, B.T. Inflammation as a central mechanism in Alzheimer's disease. *Alzheimer's Dement. Transl. Res. Clin. Interv.* **2018**, *4*, 575–590. [CrossRef] [PubMed]
6. Volkman, R.; Ben-Zur, T.; Kahana, A.; Garty, B.Z.; Offen, D. Myeloperoxidase Deficiency Inhibits Cognitive Decline in the 5XFAD Mouse Model of Alzheimer's Disease. *Front. Neurosci.* **2019**, *13*, 990. [CrossRef] [PubMed]
7. Aries, M.L.; Hensley-McBain, T. Neutrophils as a potential therapeutic target in Alzheimer's disease. *Front. Immunol.* **2023**, *14*, 1123149. [CrossRef] [PubMed]
8. Yan, Z.; Gibson, S.A.; Buckley, J.A.; Qin, H.; Benveniste, E.N. Role of the JAK/STAT signaling pathway in regulation of innate immunity in neuroinflammatory diseases. *Clin. Immunol.* **2018**, *189*, 4–13. [CrossRef] [PubMed]
9. Zenaro, E.; Pietronigro, E.; Bianca, V.D.; Piacentino, G.; Marongiu, L.; Budui, S.; Turano, E.; Rossi, B.; Angiari, S.; Dusi, S.; et al. Neutrophils promote Alzheimer's disease–like pathology and cognitive decline via LFA-1 integrin. *Nat. Med.* **2015**, *21*, 880–886. [CrossRef] [PubMed]
10. Song, L.; Yang, Y.T.; Guo, Q.; the ZIB Consortium; Zhao, X.-M. Cellular transcriptional alterations of peripheral blood in Alzheimer's disease. *BMC Med.* **2022**, *20*, 266. [CrossRef] [PubMed]
11. Duan, K.; Ma, Y.; Tan, J.; Miao, Y.; Zhang, Q. Identification of genetic molecular markers and immune infiltration characteristics of Alzheimer's disease through weighted gene co-expression network analysis. *Front. Neurol.* **2022**, *13*, 947781. [CrossRef] [PubMed]
12. Dong, Y.; Lagarde, J.; Xicota, L.; Corne, H.; Chantran, Y.; Chaigneau, T.; Crestani, B.; Bottlaender, M.; Potier, M.-C.; Aucouturier, P.; et al. Neutrophil hyperactivation correlates with Alzheimer's disease progression: Neutrophil Hyperactivation in Alzheimer's Disease. *Ann. Neurol.* **2018**, *83*, 387–405. [CrossRef] [PubMed]
13. Zhang, P.; Zhao, L.; Li, H.; Shen, J.; Li, H.; Xing, Y. Novel diagnostic biomarkers related to immune infiltration in Parkinson's disease by bioinformatics analysis. *Front. Neurosci.* **2023**, *17*, 1083928. [CrossRef] [PubMed]
14. Cruz Hernández, J.C.; Bracko, O.; Kersbergen, C.J.; Muse, V.; Haft-Javaherian, M.; Berg, M.; Park, L.; Vinarcsik, L.K.; Ivasyk, I.; Rivera, D.A.; et al. Neutrophil adhesion in brain capillaries reduces cortical blood flow and impairs memory function in Alzheimer's disease mouse models. *Nat. Neurosci.* **2019**, *22*, 413–420. [CrossRef] [PubMed]
15. Bracko, O.; Njiru, B.N.; Swallow, M.; Ali, M.; Haft-Javaherian, M.; Schaffer, C.B. Increasing cerebral blood flow improves cognition into late stages in Alzheimer's disease mice. *J. Cereb. Blood Flow. Metab.* **2020**, *40*, 1441–1452. [CrossRef]
16. Kanashiro, A.; Hiroki, C.H.; Da Fonseca, D.M.; Birbrair, A.; Ferreira, R.G.; Bassi, G.S.; Fonseca, M.D.; Kusuda, R.; Cebinelli, G.C.M.; Da Silva, K.P.; et al. The role of neutrophils in neuro-immune modulation. *Pharmacol. Res.* **2020**, *151*, 104580. [CrossRef] [PubMed]
17. Smyth, L.C.D.; Murray, H.C.; Hill, M.; van Leeuwen, E.; Highet, B.; Magon, N.J.; Osanlouy, M.; Mathiesen, S.N.; Mockett, B.; Singh-Bains, M.K.; et al. Neutrophil-vascular interactions drive myeloperoxidase accumulation in the brain in Alzheimer's disease. *Acta Neuropathol. Commun.* **2022**, *10*, 38. [CrossRef] [PubMed]
18. Rossi, B.; Constantin, G.; Zenaro, E. The emerging role of neutrophils in neurodegeneration. *Immunobiology* **2020**, *225*, 151865. [CrossRef]
19. de Oliveira, S.; Rosowski, E.E.; Huttenlocher, A. Neutrophil migration in infection and wound repair: Going forward in reverse. *Nat. Rev. Immunol.* **2016**, *16*, 378–391. [CrossRef] [PubMed]
20. Manda-Handzlik, A.; Demkow, U. The Brain Entangled: The Contribution of Neutrophil Extracellular Traps to the Diseases of the Central Nervous System. *Cells* **2019**, *8*, 1477. [CrossRef] [PubMed]
21. Zenaro, E.; Piacentino, G.; Constantin, G. The blood-brain barrier in Alzheimer's disease. *Neurobiol. Dis.* **2017**, *107*, 41–56. [CrossRef]
22. Wu, Y.-C.; Sonninen, T.-M.; Peltonen, S.; Koistinaho, J.; Lehtonen, Š. Blood-Brain Barrier and Neurodegenerative Diseases-Modeling with iPSC-Derived Brain Cells. *Int. J. Mol. Sci.* **2021**, *22*, 7710. [CrossRef]
23. Wangoo, A.; Shaw, R.J.; Diss, T.C.; Farrell, P.J.; du Bois, R.M.; Nicholson, A.G. Cryptogenic fibrosing alveolitis: Lack of association with Epstein-Barr virus infection. *Thorax* **1997**, *52*, 888–891. [CrossRef] [PubMed]
24. Denorme, F.; Portier, I.; Rustad, J.L.; Cody, M.J.; de Araujo, C.V.; Hoki, C.; Alexander, M.D.; Grandhi, R.; Dyer, M.R.; Neal, M.D.; et al. Neutrophil extracellular traps regulate ischemic stroke brain injury. *J. Clin. Investig.* **2022**, *132*, e154225. [CrossRef] [PubMed]
25. Byun, D.J.; Lee, J.; Yu, J.-W.; Hyun, Y.-M. NLRP3 Exacerbate NETosis-Associated Neuroinflammation in an LPS-Induced Inflamed Brain. *Immune Netw.* **2023**, *23*, e27. [CrossRef] [PubMed]
26. Thomson, C.A.; McColl, A.; Graham, G.J.; Cavanagh, J. Sustained exposure to systemic endotoxin triggers chemokine induction in the brain followed by a rapid influx of leukocytes. *J. Neuroinflamm.* **2020**, *17*, 94. [CrossRef] [PubMed]
27. He, H.; Geng, T.; Chen, P.; Wang, M.; Hu, J.; Kang, L.; Song, W.; Tang, H. NK cells promote neutrophil recruitment in the brain during sepsis-induced neuroinflammation. *Sci. Rep.* **2016**, *6*, 27711. [CrossRef]
28. Kim, Y.R.; Kim, Y.M.; Lee, J.; Park, J.; Lee, J.E.; Hyun, Y.-M. Neutrophils Return to Bloodstream through the Brain Blood Vessel after Crosstalk with Microglia During LPS-Induced Neuroinflammation. *Front. Cell Dev. Biol.* **2020**, *8*, 613733. [CrossRef] [PubMed]
29. Jeong, H.-K.; Jou, I.; Joe, E. Systemic LPS administration induces brain inflammation but not dopaminergic neuronal death in the substantia nigra. *Exp. Mol. Med.* **2010**, *42*, 823. [CrossRef] [PubMed]

30. Vaure, C.; Liu, Y. A Comparative Review of Toll-Like Receptor 4 Expression and Functionality in Different Animal Species. *Front. Immunol.* **2014**, *5*, 96623. [CrossRef] [PubMed]
31. Marottoli, F.M.; Katsumata, Y.; Koster, K.P.; Thomas, R.; Fardo, D.W.; Tai, L.M. Peripheral Inflammation, *Apolipoprotein E4*, and Amyloid-β Interact to Induce Cognitive and Cerebrovascular Dysfunction. *ASN Neuro* **2017**, *9*, 175909141771920. [CrossRef] [PubMed]
32. Thygesen, C.; Ilkjær, L.; Kempf, S.J.; Hemdrup, A.L.; von Linstow, C.U.; Babcock, A.A.; Darvesh, S.; Larsen, M.R.; Finsen, B. Diverse Protein Profiles in CNS Myeloid Cells and CNS Tissue from Lipopolysaccharide- and Vehicle-Injected APPSWE/PS1ΔE9 Transgenic Mice Implicate Cathepsin Z in Alzheimer's Disease. *Front. Cell. Neurosci.* **2018**, *12*, 397. [CrossRef] [PubMed]
33. Batista, C.R.A.; Gomes, G.F.; Candelario-Jalil, E.; Fiebich, B.L.; de Oliveira, A.C.P. Lipopolysaccharide-Induced Neuroinflammation as a Bridge to Understand Neurodegeneration. *IJMS* **2019**, *20*, 2293. [CrossRef]
34. Chakraborty, S.; Tabrizi, Z.; Bhatt, N.N.; Franciosa, S.A.; Bracko, O. A Brief Overview of Neutrophils in Neurological Diseases. *Biomolecules* **2023**, *13*, 743. [CrossRef] [PubMed]
35. Pietronigro, E.C.; Della Bianca, V.; Zenaro, E.; Constantin, G. NETosis in Alzheimer's Disease. *Front. Immunol.* **2017**, *8*, 228493. [CrossRef]
36. Hensley-McBain, T.; Wu, M.C.; Manuzak, J.A.; Cheu, R.K.; Gustin, A.; Driscoll, C.B.; Zevin, A.S.; Miller, C.J.; Coronado, E.; Smith, E.; et al. Increased mucosal neutrophil survival is associated with altered microbiota in HIV infection. *PLoS Pathog.* **2019**, *15*, e1007672. [CrossRef] [PubMed]
37. Zhou, X.; Gao, X.-P.; Fan, J.; Liu, Q.; Anwar, K.N.; Frey, R.S.; Malik, A.B. LPS activation of Toll-like receptor 4 signals CD11b/CD18 expression in neutrophils. *Am. J. Physiol.-Lung Cell. Mol. Physiol.* **2005**, *288*, L655–L662. [CrossRef] [PubMed]
38. Scali, C.; Prosperi, C.; Bracco, L.; Piccini, C.; Baronti, R.; Ginestroni, A.; Sorbi, S.; Pepeu, G.; Casamenti, F. Neutrophils CD11b and fibroblasts PGE(2) are elevated in Alzheimer's disease. *Neurobiol. Aging* **2002**, *23*, 523–530. [CrossRef] [PubMed]
39. Takata, F.; Nakagawa, S.; Matsumoto, J.; Dohgu, S. Blood-Brain Barrier Dysfunction Amplifies the Development of Neuroinflammation: Understanding of Cellular Events in Brain Microvascular Endothelial Cells for Prevention and Treatment of BBB Dysfunction. *Front. Cell. Neurosci.* **2021**, *15*, 661838. [CrossRef] [PubMed]
40. Coxon, A.; Rieu, P.; Barkalow, F.J.; Askari, S.; Sharpe, A.H. A Novel Role for the 2 Integrin CD11b/CD18 in Neutrophil Apoptosis: A Homeostatic Mechanism in Inflammation. *Immunity* **1996**, *5*, 653–666. [CrossRef] [PubMed]
41. Salamone, G.; Giordano, M.; Trevani, A.S.; Gamberale, R.; Vermeulen, M.; Schettinni, J.; Geffner, J.R. Promotion of Neutrophil Apoptosis by TNF-α. *J. Immunol.* **2001**, *166*, 3476–3483. [CrossRef] [PubMed]
42. Su, F.; Bai, F.; Zhang, Z. Inflammatory Cytokines and Alzheimer's Disease: A Review from the Perspective of Genetic Polymorphisms. *Neurosci. Bull.* **2016**, *32*, 469–480. [CrossRef] [PubMed]
43. Fillit, H.; Ding, W.; Buee, L.; Kalman, J.; Altstiel, L.; Lawlor, B.; Wolf-Klein, G. Elevated circulating tumor necrosis factor levels in Alzheimer's disease. *Neurosci. Lett.* **1991**, *129*, 318–320. [CrossRef] [PubMed]
44. Qin, L.; Wu, X.; Block, M.L.; Liu, Y.; Breese, G.R.; Hong, J.-S.; Knapp, D.J.; Crews, F.T. Systemic LPS causes chronic neuroinflammation and progressive neurodegeneration. *Glia* **2007**, *55*, 453–462. [CrossRef]
45. Bossù, P.; Cutuli, D.; Palladino, I.; Caporali, P.; Angelucci, F.; Laricchiuta, D.; Gelfo, F.; De Bartolo, P.; Caltagirone, C.; Petrosini, L. A single intraperitoneal injection of endotoxin in rats induces long-lasting modifications in behavior and brain protein levels of TNF-α and IL-18. *J. Neuroinflamm.* **2012**, *9*, 671. [CrossRef] [PubMed]
46. Van Avondt, K.; Strecker, J.-K.; Tulotta, C.; Minnerup, J.; Schulz, C.; Soehnlein, O. Neutrophils in aging and aging-related pathologies. *Immunol. Rev.* **2023**, *314*, 357–375. [CrossRef] [PubMed]
47. Lewkowicz, N.; Mycko, M.P.; Przygodzka, P.; Ćwiklińska, H.; Cichalewska, M.; Matysiak, M.; Selmaj, K.; Lewkowicz, P. Induction of human IL-10-producing neutrophils by LPS-stimulated Treg cells and IL-10. *Mucosal Immunol.* **2016**, *9*, 364–378. [CrossRef] [PubMed]
48. Meijer, M.K.; Spruijt, B.M.; Van Zutphen, L.F.M.; Baumans, V. Effect of restraint and injection methods on heart rate and body temperature in mice. *Lab. Anim.* **2006**, *40*, 382–391. [CrossRef]
49. Tang, L.; Cai, N.; Zhou, Y.; Liu, Y.; Hu, J.; Li, Y.; Yi, S.; Song, W.; Kang, L.; He, H. Acute stress induces an inflammation dominated by innate immunity represented by neutrophils in mice. *Front. Immunol.* **2022**, *13*, 1014296. [CrossRef]
50. Ishikawa, Y.; Kitaoka, S.; Kawano, Y.; Ishii, S.; Suzuki, T.; Wakahashi, K.; Kato, T.; Katayama, Y.; Furuyashiki, T. Repeated social defeat stress induces neutrophil mobilization in mice: Maintenance after cessation of stress and strain-dependent difference in response. *Br. J. Pharmacol.* **2021**, *178*, 827–844. [CrossRef] [PubMed]
51. Poller, W.C.; Downey, J.; Mooslechner, A.A.; Khan, N.; Li, L.; Chan, C.T.; McAlpine, C.S.; Xu, C.; Kahles, F.; He, S.; et al. Brain motor and fear circuits regulate leukocytes during acute stress. *Nature* **2022**, *607*, 578–584. [CrossRef]
52. Wendeln, A.-C.; Degenhardt, K.; Kaurani, L.; Gertig, M.; Ulas, T.; Jain, G.; Wagner, J.; Häsler, L.M.; Wild, K.; Skodras, A.; et al. Innate immune memory in the brain shapes neurological disease hallmarks. *Nature* **2018**, *556*, 332–338. [CrossRef]
53. Wu, J.; Cai, Y.; Wu, X.; Ying, Y.; Tai, Y.; He, M. Transcardiac Perfusion of the Mouse for Brain Tissue Dissection and Fixation. *Bio Protoc.* **2021**, *11*, e3988. [CrossRef] [PubMed]
54. Hensley-McBain, T.; Berard, A.R.; Manuzak, J.A.; Miller, C.J.; Zevin, A.S.; Polacino, P.; Gile, J.; Agricola, B.; Cameron, M.; Hu, S.-L.; et al. Intestinal damage precedes mucosal immune dysfunction in SIV infection. *Mucosal Immunol.* **2018**, *11*, 1429–1440. [CrossRef]

55. Guldner, I.H.; Golomb, S.M.; Wang, Q.; Wang, E.; Zhang, S. Isolation of mouse brain-infiltrating leukocytes for single cell profiling of epitopes and transcriptomes. *STAR Protoc.* **2021**, *2*, 100537. [CrossRef] [PubMed]
56. Srakočić, S.; Josić, P.; Trifunović, S.; Gajović, S.; Grčević, D.; Glasnović, A. Proposed practical protocol for flow cytometry analysis of microglia from the healthy adult mouse brain: Systematic review and isolation methods' evaluation. *Front. Cell. Neurosci.* **2022**, *16*, 1017976. [CrossRef] [PubMed]
57. National Research Council (US) Committee for the Update of the Guide for theCare and Use of Laboratory Animals. *Guide for the Care and Use of Laboratory Animals*, 8th ed.; National Academies Press (US): Washington, DC, USA, 2011; The National Academies Collection: Reports funded by National Institutes of Health. Available online: http://www.ncbi.nlm.nih.gov/books/NBK54050/ (accessed on 9 April 2024).
58. Percie du Sert, N.; Hurst, V.; Ahluwalia, A.; Alam, S.; Avey, M.T.; Baker, M.; Browne, W.J.; Clark, A.; Cuthill, I.C.; Dirnagl, U.; et al. The ARRIVE guidelines 2.0: Updated guidelines for reporting animal research. *PLoS Biol.* **2020**, *18*, e3000410. [CrossRef]

International Journal of
Molecular Sciences

MDPI

Article

MMP-3 Knockout Induces Global Transcriptional Changes and Reduces Cerebral Infarction in Both Male and Female Models of Ischemic Stroke

Milton H. Hamblin [1,2,*], Austin C. Boese [3], Rabi Murad [4] and Jean-Pyo Lee [1,5,*]

[1] Division of Biomedical Sciences, School of Medicine, University of California, Riverside, Riverside, CA 92521, USA
[2] Health Sciences Center, Tulane University, New Orleans, LA 70112, USA
[3] School of Medicine, Emory University, Atlanta, GA 30322, USA; austin.c.boese@emory.edu
[4] Bioinformatics, Sanford Burnham Prebys Medical Discovery Institute, La Jolla, CA 92037, USA; rmurad@sbpdiscovery.org
[5] Department of Physiology, Tulane University School of Medicine, New Orleans, LA 70112, USA
* Correspondence: milton.hamblin@ucr.edu (M.H.H.); jeanpyo.lee@ucr.edu (J.-P.L.)

Abstract: Ischemic stroke followed by reperfusion (IR) leads to extensive cerebrovascular injury characterized by neuroinflammation and brain cell death. Inhibition of matrix metalloproteinase-3 (MMP-3) emerges as a promising therapeutic approach to mitigate IR-induced stroke injury. We employed middle cerebral artery occlusion with subsequent reperfusion (MCAO/R) to model ischemic stroke in adult mice. Specifically, we investigated the impact of MMP-3 knockout (KO) on stroke pathophysiology using RNA sequencing (RNA-seq) of stroke brains harvested 48 h post-MCAO. MMP-3 KO significantly reduced brain infarct size following stroke. Notably, RNA-seq analysis showed that MMP-3 KO altered expression of 333 genes (252 downregulated) in male stroke brains and 3768 genes (889 downregulated) in female stroke brains. Functional pathway analysis revealed that inflammation, integrin cell surface signaling, endothelial- and epithelial-mesenchymal transition (EndMT/EMT), and apoptosis gene signatures were decreased in MMP-3 KO stroke brains. Intriguingly, MMP-3 KO downregulated gene signatures more profoundly in females than in males, as indicated by greater negative enrichment scores. Our study underscores MMP-3 inhibition as a promising therapeutic strategy, impacting multiple cellular pathways following stroke.

Keywords: inflammation; matrix metalloproteinase-3; RNA sequencing; ingenuity pathway analysis; gene set enrichment analysis; stroke; transcriptome

Citation: Hamblin, M.H.; Boese, A.C.; Murad, R.; Lee, J.-P. MMP-3 Knockout Induces Global Transcriptional Changes and Reduces Cerebral Infarction in Both Male and Female Models of Ischemic Stroke. *Int. J. Mol. Sci.* **2024**, *25*, 7383. https://doi.org/10.3390/ijms25137383

Academic Editor: Claudia Ricci

Received: 1 June 2024
Revised: 25 June 2024
Accepted: 25 June 2024
Published: 5 July 2024

1. Introduction

Stroke is a leading cause of death and disability in the United States [1]. Aging is a major risk factor for cerebrovascular diseases, and about 75% of strokes afflict individuals 65 years of age or older [2]. Approximately 87% of strokes are classified as ischemic [1] and occur due to thrombosis in cerebral arteries. Clinically, ischemia followed by reperfusion (IR) results in extensive cerebrovascular injury and neurological dysfunction [3,4]. Thrombolysis by tissue plasminogen activator (tPA) [5] and thrombectomy [6,7] are current primary treatments for acute ischemic stroke and have serious limitations. For instance, tPA, the only thrombolytic agent approved by the U.S. Food and Drug Administration, has a narrow therapeutic window of 4.5 hours (h) after stroke onset [8] and increases the chances of hemorrhagic transformation (HT) [9,10]. Thus, new drug targets for ischemic stroke are greatly needed.

Maintaining blood-brain barrier (BBB) integrity is critical for brain function and homeostasis [11–14]. Ischemic stroke compromises BBB integrity, which leads to further brain injury even after the initial ischemic insult [15,16]. Preclinical studies reveal that ischemia-reperfusion causes a biphasic BBB opening [17]; an initial but reversible opening

occurs several hours post-reperfusion [18], which is then followed by a later irreversible opening that exacerbates brain damage [19]. BBB injury results in part from inflammation and upregulation of matrix metalloproteinases (MMPs) [15,16,20–25]. Thus, ameliorating BBB damage is a promising therapeutic strategy for stroke. MMP-3 (stromelysin-1) is a 51-kDa protein [26] that degrades components of the extracellular matrix (ECM) and has important roles in tissue remodeling and wound healing [27]. As one of the major inducible MMPs, MMP-3 can also activate latent pro-MMP-9 [28–30]. MMP-3 is upregulated within several hours after stroke and this corresponds with the initial opening of the BBB [31]. MMP-3 deficient mice exhibit reduced tPA-induced HT after stroke [31], and MMP-3 exacerbates HT in hyperglycemic rats [32]. We previously reported significantly increased MMP-3 levels in the ipsilesional hemisphere of mouse brains at 48 h post-stroke [33]. We also found that human neural stem cell (hNSC) transplantation reduced MMP-3 levels in aged mouse stroke brains [33]. However, the molecular mechanisms through which MMP-3 contributes to subacute stroke IR injury remain poorly understood.

In this study, we assessed the effects of MMP-3 genetic knockout (MMP-3 KO) on infarct volume and gene expression in the brains of mice following middle cerebral artery occlusion with subsequent reperfusion (MCAO/R). Our RNA-seq analysis revealed significant downregulation of gene expression signatures for neuroinflammation, endothelial- and epithelial-mesenchymal transition (EndMT/EMT), and apoptosis in MMP-3 KO mouse stroke brains compared to MMP-3 wild-type (WT) controls. Stratification of gene expression by sex revealed depletion of similar gene signatures in both males and females, but to a greater extent in females. Our study is the first to utilize RNA-seq to identify altered gene signatures and pathways associated with improved subacute stroke phase outcome in MMP-3 KO mice.

2. Results

2.1. Genetic Knockout of MMP-3 Reduces Infarct Volume in Stroke Mouse Brains

We assessed the effects of MMP-3 genetic deletion on infarct volume in stroke brains. We measured ischemic lesion volume 48 h post-MCAO by staining brain sections with TTC. Compared to brains from MCAO/R WT mice, brains from MMP-3 KO mice had significantly smaller infarct sizes measured at 48 h post-stroke. The mean infarct volume of the ipsilesional hemisphere in male WT stroke brains was 52.02 $\pm$ 2.10% (**** $p < 0.0001$ vs. sham). In male MMP-3 KO stroke mice, the mean infarct volume was 18.27 $\pm$ 1.56% (**** $p < 0.0001$ vs. sham), which was significantly smaller than in the male WT MCAO/R group ($^{\#\#\#\#}$ $p < 0.0001$ vs. MCAO/R WT) (Figure 1A). The mean infarct volume of the ipsilesional hemisphere in female WT stroke brains was 38.99 $\pm$ 4.59% (**** $p < 0.0001$ vs. sham). In female MMP-3 KO stroke mice, the mean infarct volume was 11.55 $\pm$ 1.62% (**** $p < 0.0001$ vs. sham), which was significantly smaller than in the female WT MCAO/R group ($^{\#\#}$ $p < 0.01$ vs. MCAO/R WT) (Figure 1B). These results indicate that genetic deletion of MMP-3 attenuates brain tissue loss from ischemic stroke.

2.2. MMP-3 Deletion Induces Global Transcriptional Changes in the Brains of Male and Female Mice in the Subacute Stroke Phase

We performed RNA-seq of mouse brain tissue harvested at 48 h post-stroke to investigate the effect of MMP-3 KO on differential gene expression at a global level. Further analysis of differentially expressed genes (DEGs) between MMP-3 KO brains and WT brains was conducted to better understand the molecular mechanisms through which MMP-3 inhibition reduced tissue loss from ischemic stroke. We compared the transcriptomes of male MMP-3 KO mouse stroke brains to those of male WT stroke brains (MMP-3 KO MCAO vs. WT MCAO). Principal component analysis (PCA) showed clear separation between MMP-3 KO and WT stroke brain transcriptomes along PC1 which accounted for the greatest variability (30.25%) in the dataset (Figures 2A and A1). This suggested alterations in gene expression patterns due to MMP-3 deletion. We found 252 downregulated and 81 upregulated genes in MMP-3 KO stroke brains with a fold change >1.5 in either direction

(FDR < 0.05) (Figure 2B). The volcano plot (Figure 2B) indicates significant downregulation of genes already implicated in inflammation and apoptotic cell death following stroke such as *Ccr5*, *Casp8*, *Icam2*, *Mmp9*, *Pecam1*, and *Il6*. Further analysis of the TPM values for these genes from WT and MMP-3 KO male stroke brains confirmed our observation from the volcano plot (Figure A4B). These findings suggest that MMP-3 plays a pivotal role in mediating the expression of pathologically relevant genes in the subacute phase of ischemic stroke.

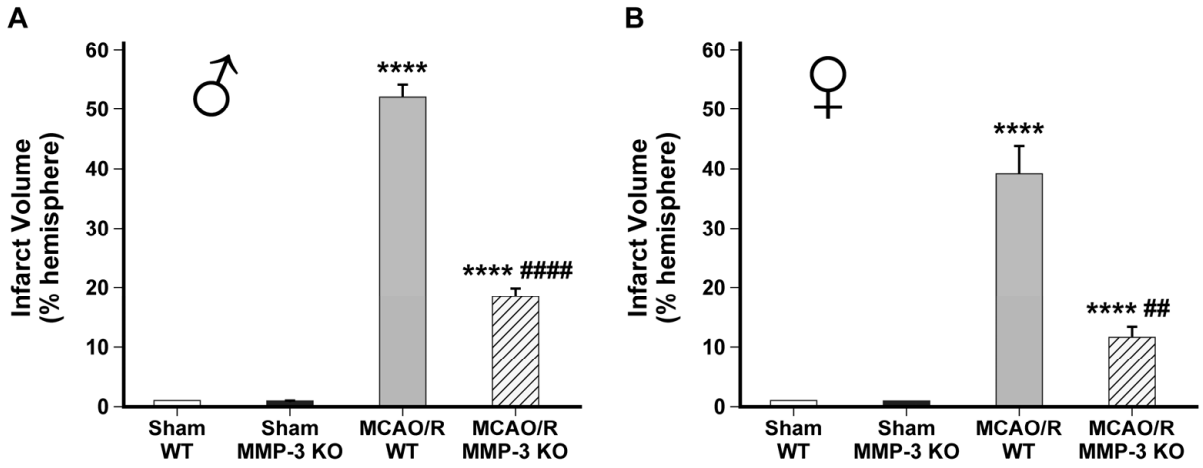

Figure 1. MMP-3 knockout reduces infarct volume in mice after ischemic stroke. (**A**) Infarct volume calculated by TTC staining of male mouse brains harvested 48 h post-MCAO (MMP-3 KO vs. WT). **** $p < 0.0001$ vs. sham; #### $p < 0.0001$ vs. MCAO/R WT. (n = 6, sham WT; n = 6, sham MMP-3 KO; n = 5, MCAO/R WT; n = 5, MCAO/R MMP-3 KO). (**B**) Infarct volume calculated by TTC staining of female mouse brains harvested 48 h post-MCAO (MMP-3 KO vs. WT). **** $p < 0.0001$ vs. sham; ## $p < 0.01$ vs. MCAO/R WT. (n = 6, sham WT; n = 6, sham MMP-3 KO; n = 5, MCAO/R WT; n = 5, MCAO/R MMP-3 KO). Data are presented as mean ± SEM. MCAO/R, middle cerebral artery occlusion with reperfusion.

We further analyzed DEGs to identify enriched or depleted biological pathways in MMP-3 KO mouse stroke brains. Our functional analysis revealed several enriched or depleted pathways in MMP-3 KO stroke brains. Gene Set Enrichment Analysis (GSEA) revealed negative enrichment scores (NES), indicating downregulation of gene sets for inflammation (78 genes, NES= −1.88), epithelial-mesenchymal transition (EMT) (98 genes, NES= −2.26), apoptosis (71 genes, NES= −1.63), and integrin cell surface interactions (40 genes, NES= −2.24) in brains of male MMP-3 KO MCAO mice (Figure 2C–F). This highlights the multifaceted role of MMP-3 in regulating several key biological processes after ischemic insult to the central nervous system (CNS). Notably, the negative enrichment scores across these pathways point to a potential protective or modulatory effect of MMP-3 knockout against ischemia-induced pathological changes. Key EMT-related genes that were downregulated upon MMP-3 KO in male stroke brains included *Fbn1*, *Fbln1*, *Tgfb1*, *Tgfbr3*, *Snai2*, and *Fgf2* (Figure 2C). Male MMP-3 KO stroke brains also exhibited downregulation of apoptosis-related genes such as *Casp9*, *Casp7*, *Bmf*, *Casp1*, *Bid*, *Casp6*, *Casp3*, *Casp2*, *Fas*, *Casp4*, and *Casp8* (Figure 2D). Genes related to inflammation such as *Ccl5*, *Cxcl5*, *Il1a*, *Tnfsf10*, *Nfkb1*, *Tnfrsf1b*, *Ccr7*, *Tnfrsf9*, *Ccl7*, *Il1b*, *Il6*, and *Ccl24* were also downregulated upon MMP-3 KO in male stroke brains (Figure 2E). Similarly, genes involved in integrin cell surface interactions including *Itga10*, *Itgb3*, *Vcam1*, *Itgb1*, *Itgae*, *Itgb7*, *Itga1*, *Itga5*, *Icam1*, *Itgb2*, *Pecam1*, and *Icam2* were depleted in male MMP-3 KO stroke brains (Figure 2F).

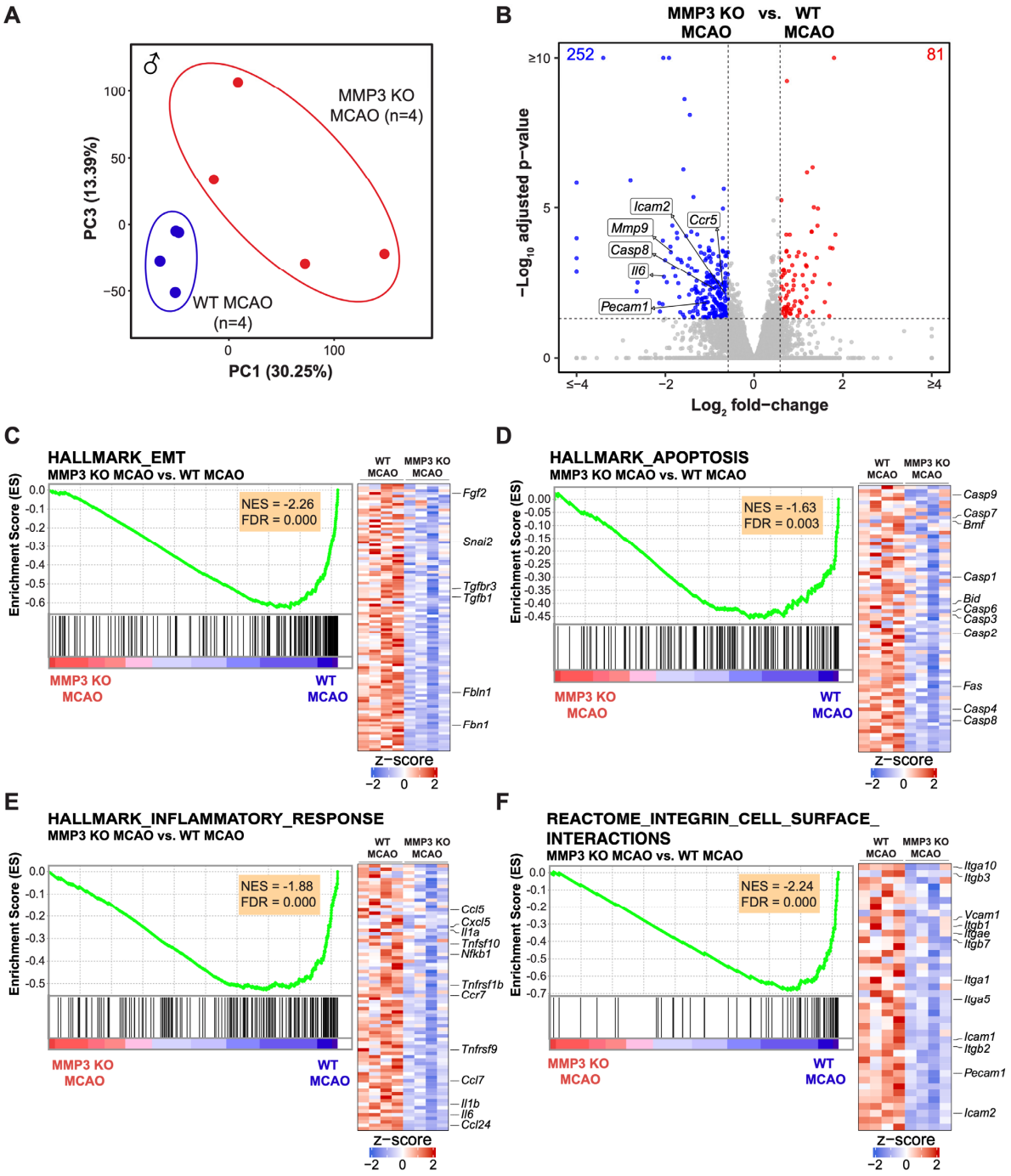

Figure 2. MMP-3 KO induces global transcriptional changes in the brains of male mice by 48 h post-stroke. (**A**) Principal component analysis (PCA) of transcriptomes from whole-brain tissue of male MMP-3 KO (n = 4, red) and male WT (n = 4, blue) mouse brains harvested at 48 h post-stroke. Each dot represents a biological replicate of an RNA-seq sample, and principal component 1 (PC1) splits the samples according to MMP-3 genetic status. (**B**) Volcano plot of differentially expressed genes (DEGs) Genes upregulated upon MMP-3 deletion in the subacute stroke phase are marked in red. Representative DEGs are labeled in black. (**C**–**F**) Enrichment plots and gene expression heatmaps for (**C**) Hallmark Epithelial-Mesenchymal Transition (EMT), (**D**) Hallmark Apoptosis, (**E**) Hallmark Inflammatory Response, and (**F**) Reactome Integrin Cell Surface Interactions gene sets. Row-wise z-scores were computed using transcripts per million (TPM). Core enriched genes of interest in each gene set are labeled in black. MCAO, middle cerebral artery occlusion with reperfusion.

We conducted Ingenuity Pathway Analysis (IPA) of DEGs to further interrogate cellular pathways affected by MMP-3 KO in male stroke brains. IPA of canonical pathways revealed downregulation of genes involved in leukocyte extravasation (7 genes, z = −1.414), acute phase response (8 genes, z = −2.236), and neuroinflammation (11 genes, z = −3.317). Meanwhile, MMP-3 KO brains showed enrichment of genes associated with inhibition of matrix metalloproteases (4 genes, z = 0.447) (Figure 3A,B). IPA of the Disease and Function category indicated downregulation of genes involved in leukocyte migration (64 genes, z = −5.066), blood cell adhesion (36 genes, z = −3.231), and the inflammatory response (54 genes, z = −4.305) upon MMP-3 KO in male brains at 48 h post-MCAO (Figure 3A,C). These results further confirm the importance of MMP-3 in regulating expression of pathologically relevant gene networks within the stroke-afflicted brain.

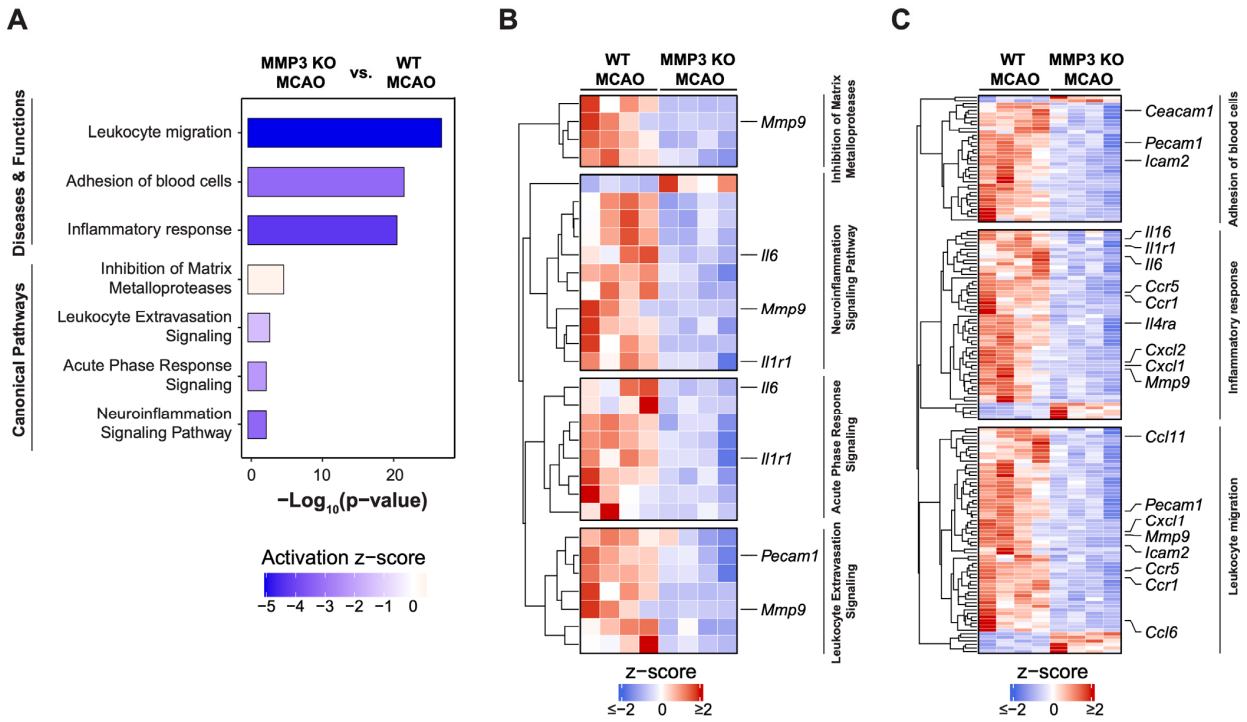

Figure 3. Pathway analysis of global transcriptional changes induced by MMP-3 deletion in male mouse brains 48 h post-stroke. (**A**) Ingenuity Pathway Analysis (IPA) of MMP-3 KO MCAO versus WT MCAO groups reveals pathways affected in male stroke brains. Activation z-scores comparing MMP-3 KO and WT groups are plotted for several signaling pathways and biological functions. Bar graphs show the negative logarithm of the calculated *p*-values for these pathways and functions. (**B**) Heatmap of Canonical Pathway gene expression signatures for leukocyte extravasation, acute phase response, neuroinflammation, and matrix metalloproteases in MMP-3 KO MCAO brains (MMP-3 KO MCAO vs. WT MCAO mice). (**C**) Heatmaps for gene signatures in the Disease and Function Annotation categories for leukocyte migration, blood cell adhesion, and inflammatory response in MMP-3 KO MCAO brains (MMP-3 KO MCAO vs. WT MCAO mice). (Row-wise z-scores were computed using transcripts per million (TPM). Heatmaps illustrate the expression levels (z-scores) of certain genes related to inflammation and cell migration, with color coding indicating the degree of expression from low (blue) to high (red). MCAO, middle cerebral artery occlusion with reperfusion.

We also compared the transcriptomes of female MMP-3 KO mouse stroke brains (n = 4) to those of female WT stroke brains (n = 4) (MMP-3 KO MCAO vs. WT MCAO). Like male brain samples, PCA was able to clearly separate the transcriptomes of female MMP-3 KO stroke brains from those of female WT stroke brains (Figure 4A). We found 889 downregulated and 2879 upregulated genes in female MMP-3 KO brains when compared to female WT brains at 48 h post-stroke with a fold change >1.5 into either direction (FDR < 0.05) (Figure 4B). Like their male counterparts, brains from MMP-3 KO female mice had downregulated expression of

pathologically relevant genes such as *Icam2*, *Tgfb1*, *Mmp9*, *Il6*, and *Pecam1* at 48 h post-MCAO (Figures 4B and A4B).

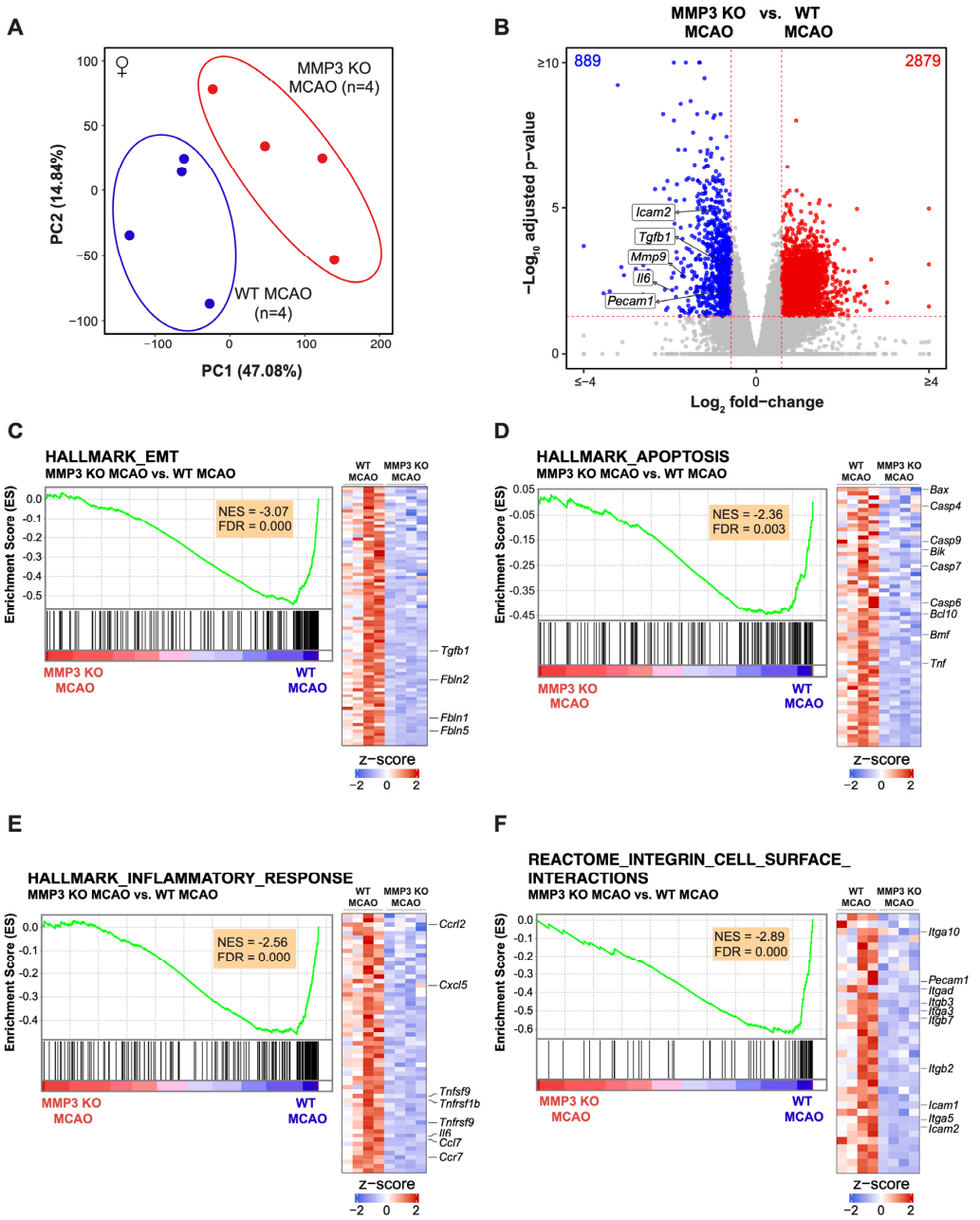

Figure 4. MMP-3 KO induces global transcriptional changes in the brains of female mice by 48 h post-stroke. (**A**) Principal component analysis (PCA) of transcriptomes from whole-brain tissue of female MMP-3 KO (n = 4, red) and female WT (n = 4, blue) mouse brains harvested at 48 h post-stroke. Each dot represents a biological replicate of an RNA-seq sample. Samples were split according to MMP-3 genetic status when plotted along PC1 which accounted for 47.08% of the variance between groups. (**B**) Volcano plot comparing the transcriptomes of MMP-3 KO MCAO versus WT MCAO groups. Statistically significant downregulated DEGs are marked in blue, while statistically significant upregulated DEGs are marked in red. Several representative downregulated genes in MMP-3 KO MCAO brains are labeled in black text. (**C-F**) Enrichment plots and gene expression heatmaps for (**C**) Hallmark Epithelial-Mesenchymal Transition (EMT), (**D**) Hallmark Apoptosis, (**E**) Hallmark Inflammatory Response, and (**F**) Reactome Integrin Cell Surface Interactions gene sets. Row-wise z-scores were computed using transcripts per million (TPM). Core enriched genes of interest in each gene set are labeled in black. MCAO, middle cerebral artery occlusion with reperfusion.

We performed further analysis of DEGs in female stroke brains to better assess the effects of MMP-3 KO during the subacute stroke phase (Figure 4). GSEA showed negative enrichment scores, indicating depletion, for sets of genes involved in EMT (81 genes, NES = −3.07), apoptosis (64 genes, NES = −2.36), inflammatory response (59 genes, NES = −2.56), and integrin cell surface interactions (36 genes, NES = −2.89) (Figure 4C–F). Key EMT-related genes that were downregulated in female MMP-3 KO stroke brains included *Fbln5*, *Fbln1*, *Fbln2*, and *Tgfb1* (Figure 4C). The apoptosis-related genes *Bax*, *Casp4*, *Casp9*, *Bik*, *Casp7*, *Casp6*, *Bcl10*, *Bmf*, and *Tnf* were all decreased in female MMP-3 KO brains when compared to female WT brains at 48 h post-MCAO (Figure 4D). Furthermore, genes related to the inflammatory response such as *Ccrl2*, *Cxcl5*, *Tnfsf9*, *Tnfrsf1b*, *Tnfrsf9*, *Il6*, *Ccl7*, and *Ccr7*, and genes involved in integrin cell surface interactions including *Itga10*, *Pecam1*, *Itgad*, *Itgb3*, *Itga3*, *Itgb7*, *Itgb2*, *Icam1*, *Itga5*, and *Icam2* were downregulated upon MMP-3 KO in female stroke brains (Figure 4E,F).

We performed IPA of transcriptome data from brains of female MMP-3 KO and female WT mice at 48 h post-stroke (Figure 5). Canonical pathway analysis revealed downregulation of macrophage classical activation signaling (32 genes, z = −3.212), acute phase response signaling (45 genes, z = −1.474), apoptosis signaling (17 genes, z = −0.6), and activation of matrix metalloproteases (7 genes, z = −1.667) (Figure 5A,B). Analysis of pathways in the Disease and Function category indicated downregulation of leukocyte migration (436 genes, z = −3.331), adhesion of blood cells (151 genes, z = −2.864), and the inflammatory response (323 genes, z = −4.186) in female MMP-3 KO brains (Figure 5A,C).

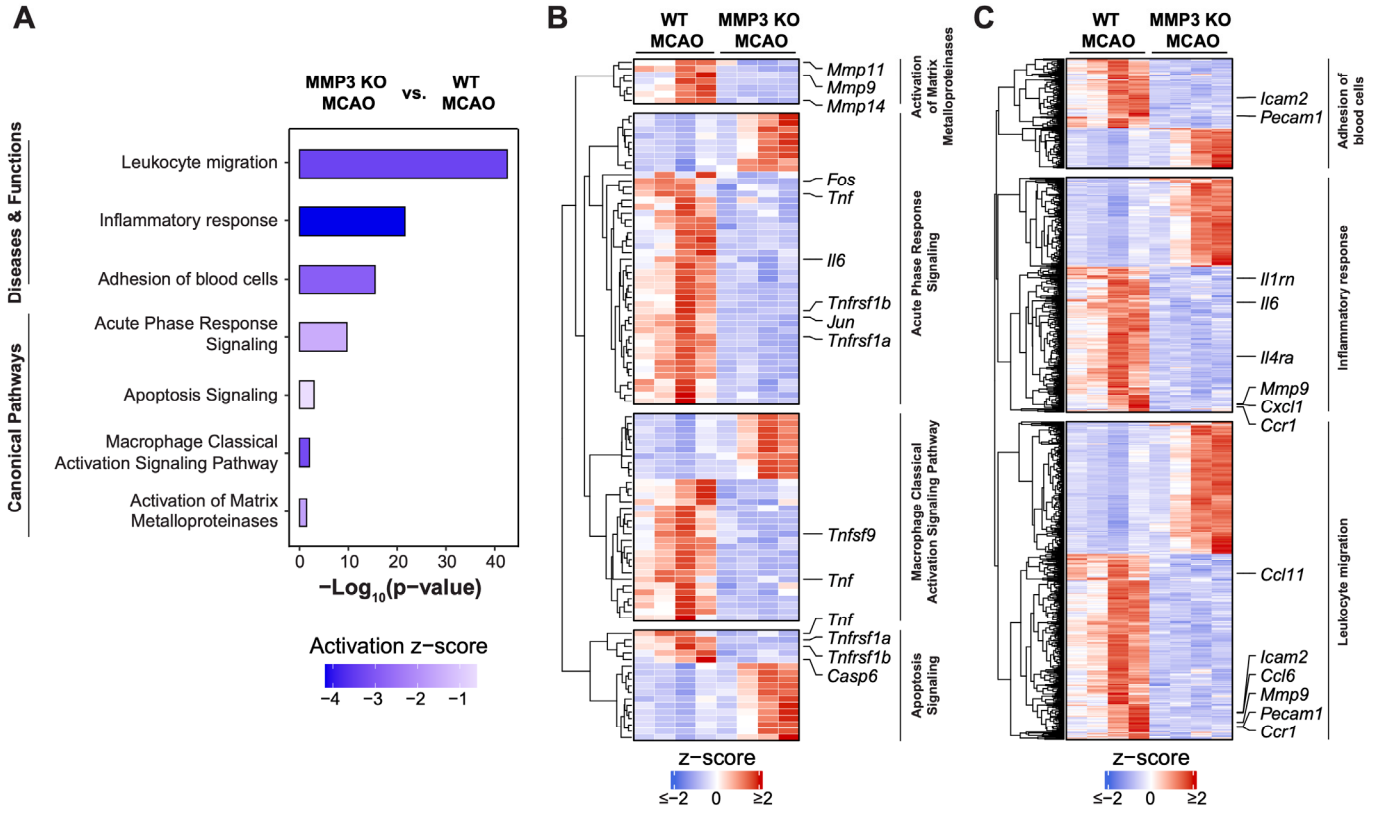

Figure 5. Pathway analysis of global transcriptional changes induced by MMP-3 deletion in female mouse brains at 48 h post-stroke. (**A**) Ingenuity Pathway Analysis (IPA) results of pathways affected by MMP-3 genetic deletion in female stroke brains. Activation z-scores comparing MMP-3 KO and WT groups are plotted for several signaling pathways and biological functions. Bar graphs show the negative logarithm of the calculated *p*-values for these pathways and functions. (**B**) Heatmap of Canonical Pathway gene expression signatures for apoptosis signaling, acute phase response signaling,

macrophage classical activation signaling, and activation of matrix metalloproteases in female MMP-3 KO stroke brains (MMP-3 KO MCAO vs. WT MCAO mice). (**C**) Heatmaps for gene signatures in the Disease and Function Annotation categories for leukocyte migration, adhesion of blood cells, and inflammatory response in female MMP-3 KO stroke brains (MMP-3 KO MCAO vs. WT MCAO mice). Row-wise z-scores were computed using transcripts per million (TPM). Heatmaps illustrate the expression levels (z-scores) of certain genes related to inflammation and cell migration, with color coding indicating the degree of expression from low (blue) to high (red). MCAO, middle cerebral artery occlusion with reperfusion.

Hierarchical clustering analysis was used to examine differences in expression of specific genes from the canonical pathways and disease and functions (activation z-score) results in females. Female MMP-3 KO stroke brains showed downregulation of the macrophage classical activation signaling genes *Tnf* and *Tnfsf9*, and decreased expression of the acute phage response genes *Tnfrsf1a*, *Jun*, *Tnfrsf1b*, *Il6*, *Tnf*, and *Fos*. Furthermore, female MMP-3 KO stroke brains showed decreased expression of apoptosis signaling genes *Casp6*, *Tnfrsf1b*, *Tnfrsf1a*, and *Tnf*, and downregulated expression of matrix metalloprotease genes *Mmp14*, *Mmp9*, and *Mmp11* (Figure 5B). Similar analysis of genes in the Disease and Function categories indicated that female MMP-3 KO stroke brains had decreased expression of leukocyte migration genes *Ccr1*, *Pecam1*, *Mmp9*, *Ccl6*, *Icam2*, and *Ccl11*. Female MMP-3 KO stroke brains also had decreased expression of blood cell adhesion genes *Pecam1* and *Icam2*, and decreased expression of inflammatory response genes *Ccr1*, *Cxcl1*, *Mmp9*, *Il4ra*, *Il6*, and *Il1rn* (Figure 5A–C).

We compared pathway enrichment results between male and female mouse brains to assess potential sex differences in the effects of MMP-3 inhibition on stroke infarct size (Figure 6). Both males (M) and females (F) showed significant negative normalized enrichment scores (NES) across several key biological processes, including integrin cell surface interactions, apoptosis, inflammatory response, and EMT. However, the data showed a greater magnitude of pathway depletion in female MMP-3 KO stroke brains than in male MMP-3 KO stroke brains for all gene sets (Figure 6).

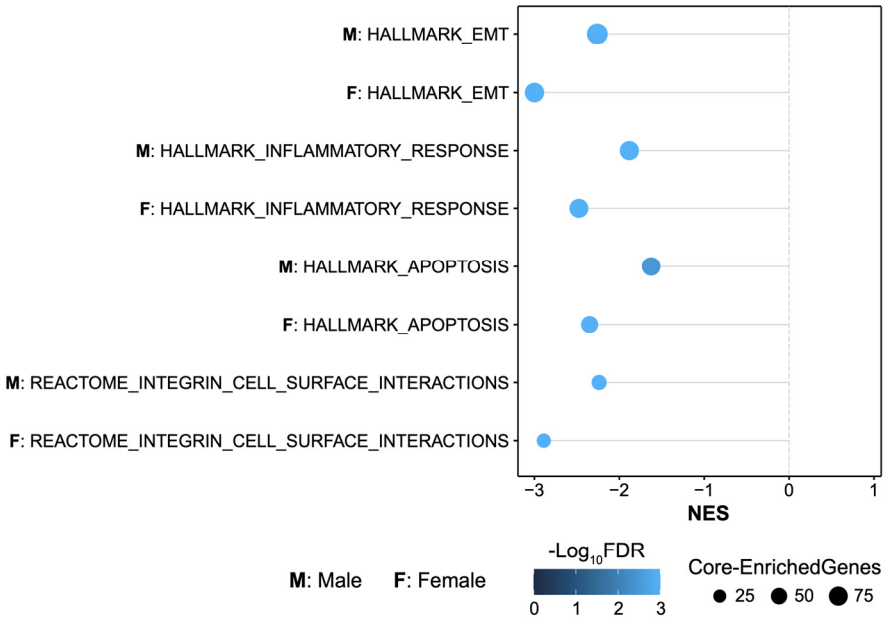

Figure 6. Pathway Enrichment results across key biological processes stratified by sex. Bubble plot of GSEA results in males (M) and females (F) (MMP-3 KO MCAO vs. WT MCAO) across several key biological processes: integrin cell surface interactions, apoptosis, inflammatory response, and epithelial-mesenchymal transition. Normalized enrichment score (NES) is plotted on the *x*-axis. Bubble colors correspond to FDR-q value. The size of the bubbles corresponds with the number of enriched genes in each gene set. MCAO, middle cerebral artery occlusion with reperfusion.

2.3. MMP-3 KO Decreases EMT Gene Expression in the Subacute Stroke Phase

To identify possible mechanisms underlying MMP-3 KO's effect on reducing stroke infarct volume, we performed additional clustering analysis of data from four samples each of MMP-3 KO and WT stroke brains. Clustering clearly distinguished the MMP-3 KO samples from WT samples (Figures 2C, 4C, A2 and A3).

MMP-3 is a secreted enzyme that degrades components of the extracellular matrix. Although it has important roles in development and tissue remodeling, MMP-3 induction can also be pathogenic. For instance, MMP-3 is upregulated in breast cancer [34], and MMP-3 can induce EMT and promote malignant transformation in cultured cells [35–37]. In vascular endothelial cells (ECs), proinflammatory factors can induce a very similar process termed endothelial-mesenchymal transition (EndMT) [38], which destabilizes blood vessels and contributes to cardiovascular disease [39,40]. In fact, ECs are reported to undergo EndMT following tMCAO [41]. Further analysis of DEGs from our RNA-seq data revealed that MMP-3 KO decreased expression of genes related to EMT in male mouse brains during the subacute stroke phase. Specifically, GSEA results showed downregulation of EMT-related genes in males (98 genes, NES = −2.26) (Figure 2C) and in females (81 genes, NES = −3.07) (Figure 4C). Key EMT-related genes that were downregulated in MMP-3 KO males included *Fbn1*, *Fbln1*, *Tgfb1*, *Tgfbr3*, *Snai2*, and *Fgf2*, while female MMP-3 KO stroke brains showed downregulation of *Fbln5*, *Fbln1*, *Fbln2*, and *Tgfb1*. Thus, although both male and female MMP-3 KO mice showed downregulation of EMT-related genes, there were still differences in the expression signatures between sexes. For instance, MMP-3 KO decreased *Snai1* expression to a greater extent in female stroke brains ($Log_2FC = -1.91$, FDR = 1.01e−8) than in male stroke brains ($Log_2FC = -0.99$, FDR = 0.058). In addition to *Snai1*, expression of the key EndMT/EMT-related genes *Tgfb1* and *Twist1* was decreased to a greater extent in females than in males. Nevertheless, our analyses clearly demonstrate that MMP-3 KO attenuated EndMT- and EMT-related gene expression in the brain during the subacute stroke phase, which correlated with reduced infarct volume.

2.4. MMP-3 KO Attenuates Inflammatory Mediator Gene Expression in the Brain during the Subacute Stroke Phase

Ischemic stroke elicits an inflammatory response that contributes to BBB breakdown and further brain tissue damage [42]. Thus, dampening neuroinflammation is an attractive therapeutic strategy for stroke. In both sexes, MMP-3 KO decreased inflammatory gene signatures in the brain during the subacute stroke phase. When compared to WT stroke brain controls, male MMP-3 KO stroke brains had decreased expression of 78 inflammation-related genes (NES= −1.88) (Figure 2E), while female MMP-3 KO stroke brains showed downregulation of 59 inflammation-related genes (NES= −2.56) (Figure 4E). Our IPA results revealed that female MMP-3 KO stroke brains had negative enrichment scores for inflammation-associated cellular pathways such as leukocyte migration (z = −3.331), inflammatory response (z = −4.186), macrophage classical activation signaling pathway (z = −3.212), and acute phase response signaling (z = −1.474) (Figure 5A,B). Key inflammation-associated genes downregulated upon MMP-3 KO in female stroke brains included *Tnfsf9*, *Il6*, *Tnfrsf9*, *Tnfrsf1b*, *Ccrl2*, *Cxcl5*, *Ccl7*, *Ccr7*, *Fos*, *Tnf*, *Jun*, *Tnfrsf1a*, *Icam2*, *Pecam1*, *Il1rn*, *Il4ra*, *Mmp9*, *Cxcl1*, *Ccr1*, and *Ccl11* (Figures 4E, 5A–C and A3C). IPA of males indicated that MMP-3 KO downregulated cellular pathways for leukocyte migration (z = −5.066), adhesion of blood cells (z = −3.231), inflammatory response (z = −4.305), leukocyte extravasation signaling (z = −1.414), acute phase response signaling (z = −2.236), and neuroinflammation signaling (z = −3.317) (Figure 3A,B). Key inflammation-associated genes downregulated upon MMP-3 KO in male stroke brains included *Ccr1*, *Cxcl1*, *Ccl11*, *Cxcl2*, *Ccl6*, *Il4ra*, *Irf1*, *Il15ra*, *Ccl5*, *Il10ra*, *Itgb3*, *Cxcl5*, *Il1a*, *Tlr*, *Tnfsf10*, *Nfkb1*, *Csf1*, *Adgre1*, *Tnfrsf1b*, *Ccr7*, *Mmp14*, *Mmp9*, *Nlrp3*, *Itga5*, *Tnfrsf9*, *Cd40*, *Il1r1*, *Ccl7*, *Sell*, *Icam1*, *Icam2*, *Lif*, *Il1b*, *Il6*, *Ccl24*, *Pecam1*, and *Ceacam1* (Figures 2E, 3A–C and A2C). Overall, female brains had more extensive downregulation of hallmark inflammation genes in the subacute stroke phase upon MMP-3 KO when compared to their MMP-3 KO male counterparts. In addition, IPA revealed subtle differences in modula-

tion of inflammation- and immune-related gene networks upon MMP-3 KO between males and females; both sexes had depletion of genes in the leukocyte migration, inflammatory response, and acute phase response signaling categories. However, male stroke brains with MMP-3 KO showed downregulation of genes in the neuroinflammation signaling pathway, while female MMP-3 KO stroke brains additionally showed downregulation of genes involved in the macrophage classical activation signaling pathway (Figures 2A–C and 4A–C). Nevertheless, MMP-3 deletion significantly downregulated several inflammatory pathways in both males and females during the subacute stroke phase.

2.5. MMP-3 KO Reduces Apoptotic Gene Expression in the Brain during the Subacute Stroke Phase

Apoptosis contributes to a significant proportion of neuronal death following acute brain ischemia [43]. Cerebral ischemia triggers two general pathways of apoptosis: the intrinsic pathway and the extrinsic pathway. The intrinsic pathway of apoptosis is triggered by various internal cellular stressors such as nutrient or oxygen depletion from ischemia and results in mitochondrial release of cytochrome c, formation of the apoptosome, and activation of executioner caspase-3 and caspase-7 by initiator caspase-9. On the other hand, the external pathway of apoptosis involves cell surface death receptor signaling that activates initiator caspase-8 to induce downstream executioner caspases [43]. Our GSEA results of male mouse brains revealed depletion of 71 genes related to both extrinsic and intrinsic apoptotic signaling pathways upon MMP-3 KO in the subacute stroke phase (NES = −1.63) (Figure 2D). Males with MMP-3 KO showed decreased gene expression of *Casp9*, *Casp7*, *Bmf*, *Casp1*, *Bid*, *Casp6*, *Casp3*, *Casp2*, *Fas*, *Casp4*, *Casp8*, *Aifm3*, *Irf1*, *Tnfrsf12a*, *Il1a*, *Tnfsf10*, *Ifngr1*, *Tgfbr3*, *Dap*, *Cd38*, *Il6*, and *Anxa1* (Figures 2D and A2B). In female MMP-3 KO mice, GSEA detected negative enrichment or downregulation of 64 genes related to apoptosis in the subacute stroke phase when compared to brains from WT controls (NES = −2.36) (Figure 4D). In addition to GSEA, IPA of RNA-seq data revealed downregulation of apoptosis signaling (z = −0.6) in the canonical pathway category for female MMP-3 KO mice in the subacute phase of stroke (Figure 5A). Representative apoptotic genes that were downregulated in female MMP-3 KO stroke brains included *Bax*, *Casp4*, *Casp9*, *Bik*, *Casp7*, *Casp6*, *Bcl10*, *Bmf*, *Tnf*, *Tnfrsf1a*, and *Tnfrsf1b* (Figures 4D, 5B and A3B). Overall, MMP-3 KO downregulated apoptotic gene expression to a greater extent in females than in males, but still had significant effects in both sexes.

2.6. MMP-3 KO Downregulates Expression of Genes Involved in Integrin Cell Surface Interactions

After stroke, the cerebral vasculature experiences altered integrin gene expression and degradation of the surrounding ECM [44]. Integrins are heterodimeric transmembrane proteins formed by the non-covalent binding of α and β subunits which can form 24 known combinations with varying roles [45]. The α subunit determines ligand binding specificity, while both the α and β subunits mediate intracellular signal transduction [46,47]. Upregulation of integrins following stroke is associated with angiogenesis, which plays an important role in tissue repair after stroke. However, this also contributes to BBB dysfunction and can contribute to IR injury in the subacute stroke phase [44]. We analyzed gene sets for integrin cell surface interactions in the mouse M2 REACTOME category to further explore biological mechanisms that might explain reduced infarct volume in MMP-3 KO mice. GSEA revealed that MMP-3 KO downregulated 40 genes related to integrin cell surface interactions in male mice (NES = −2.24) (Figures 2F and A2D). Key genes downregulated in male MMP-3 KO stroke brains included *Itga10*, *Itgb3*, *Vwf*, *Col9a2*, *Col13a1*, *Vcam1*, *Itgb1*, *Itgae*, *Itgb7*, *Col1a1*, *Col4a2*, *Col9a3*, *Col4a6*, *Col1a2*, *Itga1*, *Col8a1*, *Col6a5*, *Itga5*, *Col4a1*, *Col3a1*, *Icam1*, *Itgb2*, *Col2a1*, *Col7a1*, *Col5a2*, *Pecam1*, *Col6a3*, *Col18a1*, *Tnc*, *Icam2*, and *Col8a2* (Figures 2F and A2D). In female mice, MMP-3 genetic deletion decreased the expression of 36 genes related to integrin cell surface interactions at 48 h post-stroke (NES = −2.89) (Figures 4F and A3D). Key genes downregulated in female MMP-3 KO stroke brains included *Pecam1*, *Itgb2*, *Icam1*, *Itgb7*, *Icam2*, *Itga10*, *Itgb3*, *Itgad*, *Itga3*, and *Itga5* (Figures 4F and A3D). Females showed a

larger negative enrichment score than males, but MMP-3 KO nevertheless downregulated integrin signaling gene expression signatures in both sexes during the subacute stroke phase, which correlated with reduced infarct volume.

3. Discussion

The pathophysiology of ischemic stroke is complex, and damage to the CNS occurs through multiple mechanisms. Therefore, the Stroke Treatment Academic Industry Roundtable (STAIR) recommends targeting multiple pathways for future stroke therapies. Identifying druggable targets that regulate multiple pathophysiological cascades in the early stages of stroke is an attractive therapeutic strategy.

A large amount of brain damage following stroke is caused by reperfusion injury and BBB breakdown. The BBB plays crucial roles in maintaining brain homeostasis by providing a structural barrier that regulates molecular and cellular trafficking between the brain and circulatory system [48]. Thus, preserving BBB integrity is crucial for improving stroke outcome. Disruption of BBB tight junctions following ischemic stroke results from oxidative stress, EndMT, upregulation of proinflammatory factors, and induction of MMPs [15,49,50]. MMP-3 is a major inducible MMP and can activate latent pro-MMP-9 [28–30]. MMP-3 levels sharply increase within several hours after stroke; this coincides with the initial stages of BBB disruption [31]. Studies of human brains report upregulation of both MMP-3 and MMP-9 following stroke [51]. However, data from experiments using MMP-9 KO and MMP-3 KO mice suggest that MMP-3 contributes to delayed tPA-induced intracerebral hemorrhage more than MMP-9 does [31]. Moreover, pharmacological inhibition of MMP-3 improves stroke outcome and decreases hemorrhagic transformation in a diabetic female rat model of stroke [52]. However, the molecular mechanisms through which MMP-3 inhibition improves stroke outcome independent of downstream MMP-9 and MMP-2 activation remain largely unexplored. We hypothesized that inhibition of MMP-3 may improve stroke outcome through several other biochemical and cellular pathways in addition to activation of other latent MMPs.

We used a well-established transient MCAO/R model to study ischemic stroke [53]. In our study, genetic deletion of MMP-3 in mice reduced infarct volume following MCAO/R. We are the first to use RNA-sequencing analysis to identify global transcripts differentially expressed in MMP-3 KO mouse brains in the subacute stage of stroke. In male MMP-3 stroke brains, RNA-seq analysis identified 252 downregulated and 81 upregulated genes. In female stroke brains, MMP-3 deletion downregulated 889 genes and upregulated 2879 genes. Bioinformatic analysis of whole stroke brain RNA-seq data revealed depletion of gene signatures related to EMT, neuroinflammation, apoptosis, and integrin cell surface interactions upon MMP-3 deletion in both males and females. Here we present the first comprehensive analysis of gene networks in the brain altered by MMP-3 KO that correlate with reduced infarct volume following stroke.

Ischemic stroke triggers intrinsic and extrinsic apoptotic cell death pathways in brain cells, including neurons and endothelial cells (ECs) critical for BBB function. The intrinsic apoptotic pathway is triggered by energy failure from lack of oxygen and glucose, oxidative stress, and sodium and calcium imbalance from glutamate excitotoxicity [43]. During intrinsic apoptosis, cytochrome C is liberated from the mitochondria where it joins with Apaf-1 to activate initiator caspases and executioner caspase-3 and caspase-7 [43]. Stroke also activates apoptosis in injured brain cells through the extrinsic pathway, which occurs through signaling between tumor necrosis factor (TNF), Fas, and Trail cell surface death receptors. These external signals activate effector caspase-8 and caspase-10, which then converge on executioner caspases to propagate the apoptotic cascade [43]. Preclinical studies report that silencing of pro-apoptotic Bcl-2 family members improves neurological outcome in rodent models of stroke [54]. Interestingly, our RNA-seq analysis indicated downregulation of genes for both the intrinsic and extrinsic apoptosis pathways in the brains of male and female MMP-3 KO mice during the subacute stroke phase. Male and female MMP-3 KO brains both showed depletion of executioner *Casp7* as well as other

caspases such as *Casp9, Casp4,* and *Casp6.* Male MMP-3 KO brains showed downregulation of the cell membrane death receptor *Fas* and its downstream effector *Bid,* while female MMP-3 KO brains showed downregulation of the TNF signaling genes *Tnf*, *Tnfrsf1a*, and *Tnfrsf1b*. Compared to male brains, female brains had larger negative enrichment scores for the hallmark apoptosis gene set upon genetic ablation of MMP-3. In addition, IPA revealed a significant negative activation z-score for apoptosis signaling genes in female MMP-3 KO brains but not in males. Apoptosis occurs in multiple brain cell types after stroke. Downregulation of intrinsic apoptotic gene expression by MMP-3 KO may reduce infarct size after stroke by limiting IR injury and neuronal loss from intrinsic apoptosis induced by oxygen and glucose deprivation. On the other hand, downregulation of extrinsic apoptosis factor gene expression by MMP-3 KO may reduce stroke infarct volume by blocking apoptosis of neurons and cells of the BBB induced by death receptor signaling during the inflammatory response following the initial ischemic insult. We analyzed bulk RNA from whole brain tissue, so it remains unclear whether MMP-3 KO downregulated genes for apoptosis in neurons and ECs or in other cell types within the brain during the subacute stroke phase. Nevertheless, apoptosis results in a significant amount of tissue loss following stroke, and our results show that MMP-3 inhibition decreases apoptotic signatures and infarct size in the brain post-MCAO. MMP-3 inhibition may directly suppress apoptosis in neurons to reduce infarct volume, or MMP-3 inhibition may reduce infarct volume through downregulation of apoptosis in cell types that form the BBB. Nevertheless, our research suggests that MMP-3 is a pro-apoptotic factor in the stroke-afflicted brain.

Ischemia triggers the release of inflammatory factors from dying cells and stimulates an immune response that damages the BBB and leads to further tissue loss [55]. Damage-associated molecular patterns (DAMPs) and proinflammatory cytokines from injured tissue are released into the circulation and recruit peripheral immune cells such as macrophages, neutrophils, and T cells into the CNS through the compromised BBB [56,57]. DAMPs and cytokines bind to receptors on infiltrating immune cells and cause the upregulation and subsequent secretion of more inflammatory factors such as MMP-9, TNF-α, and interleukin (IL)-1β [56]. Research shows that activation of monocytes after stroke increases NF-κB signaling and TNF-α production, which correlates with worse stroke outcome [58]. Furthermore, incomplete clearance of DAMPs prolongs inflammation and exacerbates neuronal injury in mouse models of ischemic stroke [59]. Therefore, dampening the expression of proinflammatory factors within the brain may limit IR injury following ischemic stroke. GSEA of our transcriptomic data revealed that MMP-3 deletion significantly downregulated expression of genes in the hallmark inflammation gene set during the subacute stroke phase. Furthermore, male and female MMP-3 KO brains had negative activation z-scores for gene signatures indicative of acute phase response (APR) signaling, neuroinflammation, and the inflammatory response. The acute phase response is the early inflammatory response to infection or tissue injury such as stroke [60]. Clinical studies show that the magnitude of the acute phase response is strongly correlated with infarct size and long-term recovery in stroke patients; patients with higher serum APR protein levels often have poor neurological outcome [61]. Hierarchical clustering analysis of differentially expressed genes (DEGs) in MMP-3 KO mouse stroke brains revealed decreased expression of genes encoding TNF receptors and proinflammatory cytokines/chemokines and their receptors in both sexes. For example, MMP-3 KO downregulated brain expression of TNF receptor genes *Tnfrsf10b*, *Tnfrsf12a*, *Tnfrsf1b*, and *Tnfrsf1a*. Proinflammatory cytokines such as Il-6 are increased following stroke and correlate with poor stroke outcome [62]. Furthermore, chemokines secreted by activated microglia and astrocytes following stroke attract immune cells to the site of damage [49]. In addition to *Il6,* we also observed downregulation of *Il1a* and *Il1b* in male stroke brains, and downregulation of *Il1r1* in female stroke brains upon genetic ablation of MMP-3. Chemokines such as *Cxcl5* and *Ccr7* were also downregulated in both male and female stroke brains upon MMP-3 KO. We observed a sex-specific downregulation of other chemokines and *Nfkb1* upon MMP-3 deletion, but this was unsurprising considering well-established sex differences in the inflammatory response to stroke [63].

Nevertheless, our analysis suggests that MMP-3 inhibition may decrease stroke infarct volume by dampening the expression of inflammatory mediators that attract peripheral immune cells to the ischemic lesion and potentiate IR injury.

IR injury promotes inflammation and BBB disruption that enables invasion of peripheral immune cells into the brain [64]. Circulating lymphocytes contact inflamed vessels after stroke via P-selectin glycoprotein ligand-1, which interacts with E-selectin and P-selectin on ECs of the BBB [65]. Integrins on lymphocytes then bind to vascular cell adhesion molecule 1 (VCAM-1) and intercellular adhesion molecule 1 (ICAM-1) on ECs, which allows for leukocyte adhesion and migration along the BBB [66]. In addition, interactions between PECAM-1 and CD99 on leukocytes and ECs disrupt tight junctions and EC structure to promote diapedesis [67]. Preclinical studies indicate that trafficking of leukocytes into the brain after stroke worsens outcomes due to neuroinflammation-mediated neuronal cell death [68]. Integrin receptor α5β1 has been reported to promote leukocyte infiltration and BBB dysfunction; mice with conditional EC knockout of α5 integrin (α5 KO) show smaller infarct size and other markers of improved outcome in early stroke [69]. Integrin signaling also plays an important role in BBB homeostasis and becomes perturbed after ischemic stroke. For instance, upregulation of αvβ3 levels post-stroke induces the internalization of important tight junction proteins occludin and zonula occludens (ZO-1) in ECs and promotes the secretion of MMP-2 and MMP-9 [70–72]. Therefore, downregulation of integrins and adhesion molecules that compromise BBB integrity or facilitate the migration and invasion of peripheral immune cells into the CNS following stroke may limit IR injury. In both male and female stroke brains, we found that MMP-3 KO decreased the expression of *Itga10* and *Itgb3*, which encode the subunits that form integrin αvβ3. Thus, MMP-3 inhibition may reduce stroke infarct volume by decreasing the expression of genes that induce BBB dysfunction. In addition, our IPA results showed that MMP-3 KO reduced gene expression related to adhesion of blood cells, integrin signaling, leukocyte migration, and leukocyte extravasation at 48 h post-stroke. Clustering analysis of DEGs in male and female stroke brains revealed that MMP-3 KO decreased expression of genes that belong to the adhesion and leukocyte extravasation pathway such as *Esam*, *Icam1*, *Icam2*, *Mcam1*, and *Pecam1*. Thus, MMP-3 inhibition may reduce infarct volume after stroke by decreasing the expression of genes required for leukocyte adhesion and extravasation through the BBB, thereby limiting IR injury caused by prolonged cytotoxic inflammation. More research is needed to determine what specific cell types in the brain exhibit downregulation of integrins and adhesion molecules in response to MMP-3 inhibition.

In healthy brain blood vessels, specialized microvascular ECs of the BBB form tight junctions and regulate the passage of cells and substances into and out of the CNS. However, ischemic stroke induces endothelial dysfunction and BBB permeability. Epithelial- and endothelial-mesenchymal transition (EMT/EndMT) are pathological processes in which epithelial cells and ECs de-differentiate into mesenchymal cells and lose their specialized function in the vasculature. Although EndMT has important roles in embryogenesis and development, inappropriate activation of EndMT contributes to adult cardiovascular diseases, including stroke [73]. In general, EndMT is characterized by reduced expression of endothelial genes and increased expression of mesenchymal genes associated with transcription factors such as *Twist*, *Smad3*, *Zeb2*, *Snai1*, and *Snai2*. It has been reported that IR injury of the brain coincides with EndMT and vascular fibrosis through activation of the Let-7i/TGF-βR1 double-negative feedback loop [41]. Specifically, induction of TGF-βR1 and downregulation of Let-7i following ischemia modulates inflammatory pathways in ECs, while increasing Let-7i with a TGF-βR1 antagonist reduced infarct volume and BBB permeability and improved neurological outcome [41]. A previous study also shows that the circular RNA DLGAP4 improves stroke outcome by acting as a miR-143 sponge. This increased the expression of tight junction proteins and decreased the expression of mesenchymal genes in brain ECs [74]. Other studies implicate EndMT in BBB dysfunction in neurological diseases other than stroke. For instance, stimulation of human brain ECs with TGF-β1 and IL-1β promoted EndMT and increased markers of

multiple sclerosis in vitro. Immunohistochemistry results from the same study also showed EndMT-associated alterations in the brain vasculature of post-mortem multiple sclerosis patient brain tissue [40]. Targeting EndMT may hold therapeutic promise for stroke and other neurological disorders by preserving the structure and function of the BBB. Our RNA-seq analysis showed that genetic ablation of MMP-3 in our mouse model of stroke had a significant effect on EMT/EndMT gene expression in the brain during the subacute stroke phase when BBB dysfunction starts. Both male and female MMP-3 KO stroke brains showed decreased expression of genes involved in fibulin signaling (*Fbln1*, *Fbn1*, *Fbln2*, *Fbln5*), which are known to induce EMT during embryonic development [75]. Both sexes also exhibited downregulation of *Tgfb1*, which encodes the ligand for TGF-βR1. We also observed sex-specific alterations in other EndMT-associated genes; male MMP-3 KO stroke brains showed downregulation of *Tgfbr3* and the major EMT-associated transcription factor *Snai2*. Overall, our results suggest that MMP-3 inhibition may benefit stroke outcome by reducing expression of transforming growth factor and fibulin signaling factors within the brain to inhibit EndMT. This, in turn, would preserve BBB EC function and limit BBB breakdown and subsequent IR injury to reduce infarct size during the subacute stroke phase. However, since we employed bulk RNA-seq, it is unclear whether MMP-3 KO modulated expression of EndMT-related genes in BBB ECs or other cell types in the brain. Future studies would benefit from using targeted epigenetics assays such as single cell RNA-seq (scRNA-seq) or chromatin immunoprecipitation-seq (ChIP-seq) using brain ECs to see if MMP-3 inhibition does indeed modulate expression of these genes in the endothelium or in other brain cell types following stroke.

Although we observed similar trends in depleted pathways between male and female MMP-3 KO stroke brains, females overall showed a more profound downregulation of gene signatures as reflected in their more negative z-scores and enrichment scores. We observed slightly higher MMP-3 TPM values in female wild-type stroke brains compared to male wild-type stroke brains (Figure A4A). This suggests that females may have greater induction of MMP-3 expression in the brain following stroke than males do. It is possible that estrogen receptor and androgen receptor signaling drive differential expression of MMP-3 between females and males. Future studies should also investigate whether MMP-3 interacts directly or indirectly with estrogen receptors and androgen receptors in the nucleus to regulate gene expression in the brain; this may also account for some of our observed sex differences in response to MMP-3 KO following stroke. Although it is beyond of the scope of our study, future studies should consider age as a biological variable and potential confounder.

Our study had some limitations that can be addressed by future research. We demonstrated that MMP-3 KO reduces cerebral infarct size and is accompanied by global transcriptional changes. Although investigating the long-term neurological outcomes of MMP-3 KO is beyond the scope of this study, it would be beneficial for future research.

In this study, we analyzed bulk RNA harvested from whole brains to assess the effect of MMP-3 KO on stroke pathophysiology. Many cell types within the brain such as neurons, astrocytes, microglia, ECs, vascular smooth muscle cells, neutrophils, macrophages, and T cells, are affected by ischemic stroke in different ways. Gene expression is also context-dependent and determined by the input of many different signals. It is unlikely that MMP-3 regulates the genes identified in our study to the same degree across all cell types in the brain following stroke. Therefore, future studies would benefit from the use of scRNA-seq and other spatial transcriptomics techniques to better identify genes that MMP-3 regulates in specific cell types within the brain. In addition, epigenetic profiling technologies, such as ChIP-seq, should be employed in future research to determine if MMP-3 directly regulates gene expression by acting as a transcription factor or through other indirect mechanisms. The use of an additional genetically engineered mouse model that expresses a catalytically dead MMP-3 mutant may be able to delineate whether the protease activity of MMP-3 is required for its role in regulating gene expression.

In conclusion, genetic deletion of MMP-3 reduced brain infarct volume in our mouse model of ischemic stroke. MMP-3 KO altered gene expression signatures for neuroinflammation, apoptosis, EndMT, and integrin signaling during the subacute stroke phase, which coincides with BBB breakdown and IR injury. MMP-3′s canonical role is proteolytic cleavage of ECM proteins and other secreted extracellular substrates such as latent pro-MMP-9. However, some studies report that MMPs can localize within the nucleus of mammalian cells and exert transcription factor functions to regulate gene expression. For instance, MMP-3 is reported to be a trans regulator of the connective tissue growth factor gene (CCN2/CTGF) in chondrocytes [76]. More research is needed to determine whether MMP-3 directly regulates the expression of genes related to neuroinflammation, apoptosis, and EndMT in brain cells as a transcription factor or through another biochemical pathway such as signaling through extracellular substrate cleavage. Overall, our results highlight MMP-3 as an attractive therapeutic target to improve stroke outcome and our study warrants further investigation of MMP-3′s role in stroke pathophysiology.

4. Materials and Methods

4.1. Animals

MMP-3 KO mice and littermate controls (8–12 weeks) were obtained from Taconic Biosciences (Rensselaer, NY, USA). Mice were kept at 18–22 °C on a 12 h light-dark cycle. Mice were provided ad libitum access to water and food.

4.2. Animal Model of Stroke

The use of animals for this study was reviewed and approved by Tulane University (New Orleans, LA, USA) and University of California, Riverside (Riverside, CA, USA) Institutional Animal Care and Use Committees. Animals were managed and treated in compliance with the guidelines of Tulane University and UCR animal protocols, the American Veterinary Medical Association, and the National Institutes of Health Guide for the Care and Use of Laboratory Animals.

We used a well-established mouse model of transient focal cerebral ischemia [53]. Stroke surgery was performed as previously published [77–79]. Briefly, a 6-0 nylon monofilament (Doccol Corporation, Sharon, MA, USA) was used to induce middle cerebral artery occlusion (MCAO) for 1 h and then removed to enable reperfusion. As a control for the surgical procedure (sham control), mice underwent insertion and immediate removal of the filament. To confirm successful MCAO, we assessed regional cerebral blood flow (rCBF) with a transcranial laser Doppler (Perimed). A rCBF reduction of >80% indicated successful occlusion. Restoration of blood flow to >90% of baseline rCBF indicated successful post-MCAO/R recovery.

4.3. Quantification of Infarct Volume

Triphenyl tetrazolium chloride (TTC, Sigma, St. Louis, MO, USA) staining of mouse brain slices was utilized to evaluate ischemic lesions. To begin, 48 h after MCAO, 1-mm coronal brain sections were incubated in 2% TTC solution as previously published [77–79]. Image J software Version 1.54j (National Institutes of Health, Bethesda, MD, USA) was used to measure infarct area. To compensate for edema, cerebral infarct volume was calculated as a percent volume of the contralateral hemisphere: [volume of contralateral hemisphere—(volume of total ipsilesional hemisphere—volume of infarct area)]/volume of contralateral hemisphere.

4.4. RNA Sequencing (RNA-seq)

Poly(A) RNA was isolated using the NEBNext® Poly(A) mRNA Magnetic Isolation Module. RNA-sequencing libraries were constructed using the NEBNext® Ultra™ Directional RNA Library Prep Kit for Illumina® (NEB, Ipswich, MA, USA). Libraries were pooled and sequenced as single-end 75bp on an Illumina NextSeq 500 sequencer with a sequencing depth of 18–30 million reads.

4.4.1. RNA-seq Data Processing

Poly(A), Poly(T), and Illumina Truseq Adapter sequences were trimmed from raw sequencing reads with Cutadapt v2.3. Trimmed reads were aligned to mouse genome version 38 (mm10) using STAR aligner v2.7.0d_0221 [80] with parameters according to ENCODE long RNA-seq pipeline (https://github.com/ENCODE-DCC/long-rna-seq-pipeline, accessed on 10 June 2024). Estimated counts and transcripts per million (TPM) for each gene were quantified by RSEM v1.3.1 [81].

4.4.2. RNA-seq Quality Control and Quality Assurance (QC/QA)

RNA-seq alignment and quantification quality were assessed by FastQC v0.11.5 (https://www.bioinformatics.babraham.ac.uk/projects/fastqc/; RRID: SCR_014583, accessed on 10 June 2024) and MultiQC v1.8 [82]. Biological replicate concordance was assessed by principal component analysis (PCA) and pair-wise Pearson correlation analysis. Lowly expressed genes were filtered out by applying the following criterion: estimated counts (from RSEM) $\geq$ number of samples * 5.

4.4.3. Differential Gene Expression and Ingenuity Pathway Analysis (IPA)

Filtered estimated read counts from RSEM were compared with the R Bioconductor package DESeq2 v1.22.2 based on the generalized linear model and negative binomial distribution [83]. Significant differentially expressed genes (DEGs) were identified with the Wald test (BH adjusted p-value < 0.05) and had a fold-change >1.5 in either direction. IPA (Qiagen, Santa Clarita, CA, USA) of RNA-seq data was used to further assess cellular pathways affected by MMP-3 deletion in mouse stroke brains. Bioinformatics analysis was performed in the Sanford Burnham Prebys Medical Discovery Institute (SBP) Bioinformatics Core.

4.4.4. Gene Set Enrichment Analysis (GSEA)

Gene set enrichment analysis of MMP-3 KO and MMP-3 WT stroke brain transcriptomic data was performed using the desktop GSEA app version 4.3.2 [84] and TPM values from the RNA-seq samples. GSEA was run using the "Run GSEA" option with default parameters except "Permutation type = gene_set". The mouse-ortholog hallmark and M2 curated gene sets were used for testing.

4.5. Statistical Analysis

GraphPad Prism, version 6.0, SPSS Version 19.0 and R statistical software version 4.4.1 were used to perform analyses. Unless stated otherwise, one-way ANOVA with Fisher's LSD post-hoc test was used to assess differences between multiple groups. Results were considered statistically significant at $p < 0.05$. Data are presented as mean $\pm$ SEM.

Author Contributions: J.-P.L. conceived the study, designed the experiments, analyzed and interpreted data. M.H.H. designed and performed the experiments, analyzed and interpreted data. R.M. analyzed data and prepared figures; A.C.B. analyzed data; A.C.B., M.H.H. and J.-P.L. performed experiments, drafted, edited and revised the manuscript. All authors have read and agreed to the published version of the manuscript.

Funding: Dr. Jean-Pyo Lee is supported by the National Institute of Neurological Disorders and Stroke (Grant 7R01NS110370-06). Both Drs. Jean-Pyo Lee and Milton Hamblin are supported by startup funds from the Division of Biomedical Sciences, School of Medicine at the University of California, Riverside.

Institutional Review Board Statement: The animal study protocol was approved by the Institutional Review Board of Tulane University and the University of California, Riverside for studies involving animals.

Informed Consent Statement: Not applicable.

Data Availability Statement: The raw data supporting the conclusions of this article will be made available by the authors on request.

Conflicts of Interest: The authors declare no conflicts of interest. The funders had no role in the design of the study; in the collection, analyses, or interpretation of data; in the writing of the manuscript; or in the decision to publish the results.

Abbreviations

APR: acute phase response, BBB: blood-brain barrier, DEGs: differentially expressed genes, EC: endothelial cell, ECM: extracellular matrix, EndMT: endothelial-mesenchymal transition, EMT: epithelial-mesenchymal transition, GSEA: Gene Set Enrichment Analysis, HT: hemorrhagic transformation, IPA: Ingenuity Pathway Analysis, IR: ischemia followed by reperfusion, KO: knockout, MCAO/R: middle cerebral artery occlusion/reperfusion, MMP: matrix metalloprotease, NES: negative enrichment score, PCA: Principal Component Analysis.

Appendix A

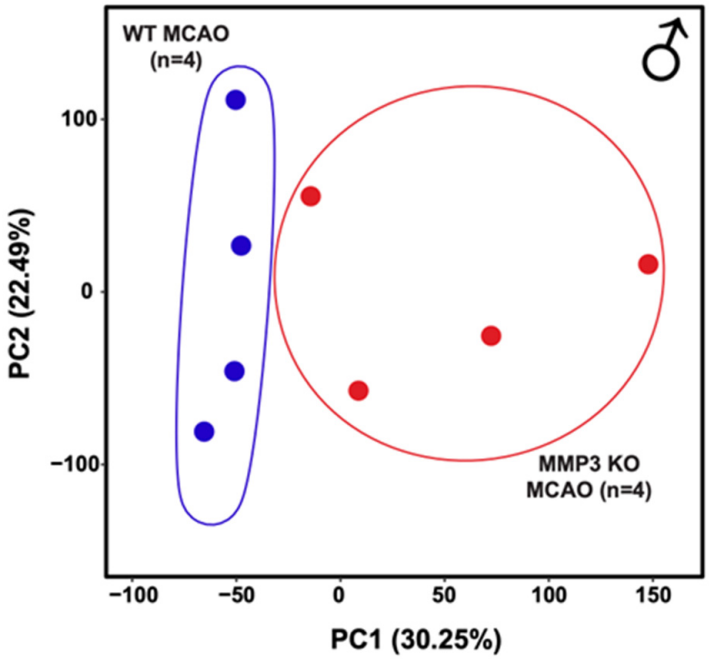

Figure A1. Principal component analysis (PCA) of transcriptomes from whole-brain tissue of male MMP-3 KO (n = 4, red) and male WT (n = 4, blue) mouse brains harvested at 48 h post-stroke. Each dot represents a biological replicate of an RNA-seq sample. Principal component 1 (PC1) splits the samples according to MMP-3 genetic status. MCAO, middle cerebral artery occlusion with reperfusion.

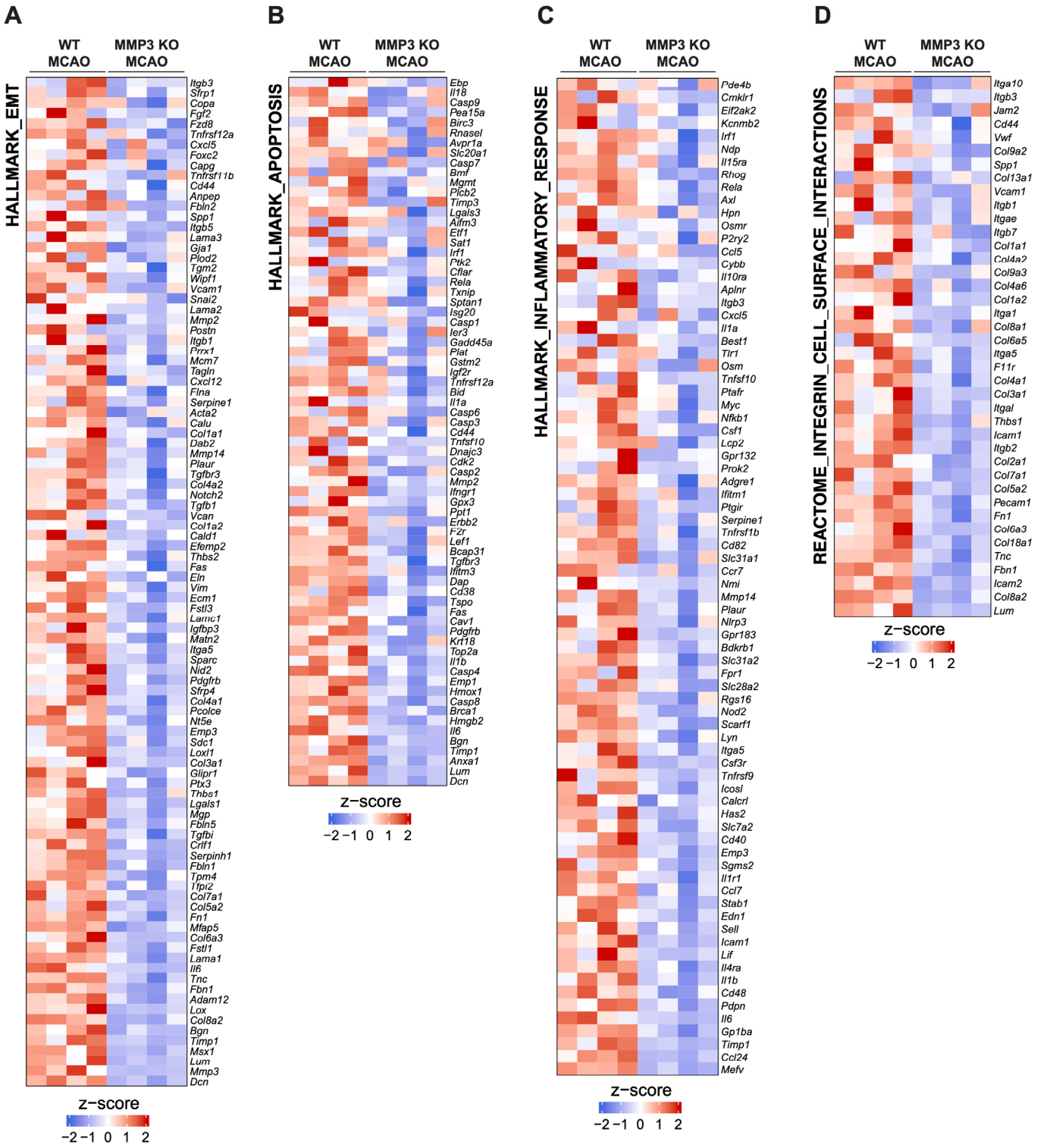

Figure A2. Heatmaps comparing gene expression profiles for (**A**) Hallmark Epithelial-Mesenchymal Transition (EMT), (**B**) Hallmark Apoptosis, (**C**) Hallmark Inflammatory Response, (**D**) Hallmark Integrin Cell Surface Interactions between male MMP-3 KO and male WT MCAO mice. Each panel (**A**–**D**) includes genes not explicitly highlighted in Figure 2. MCAO, middle cerebral artery occlusion with reperfusion. Red color indicates increased expression. Blue color indicates decreased expression.

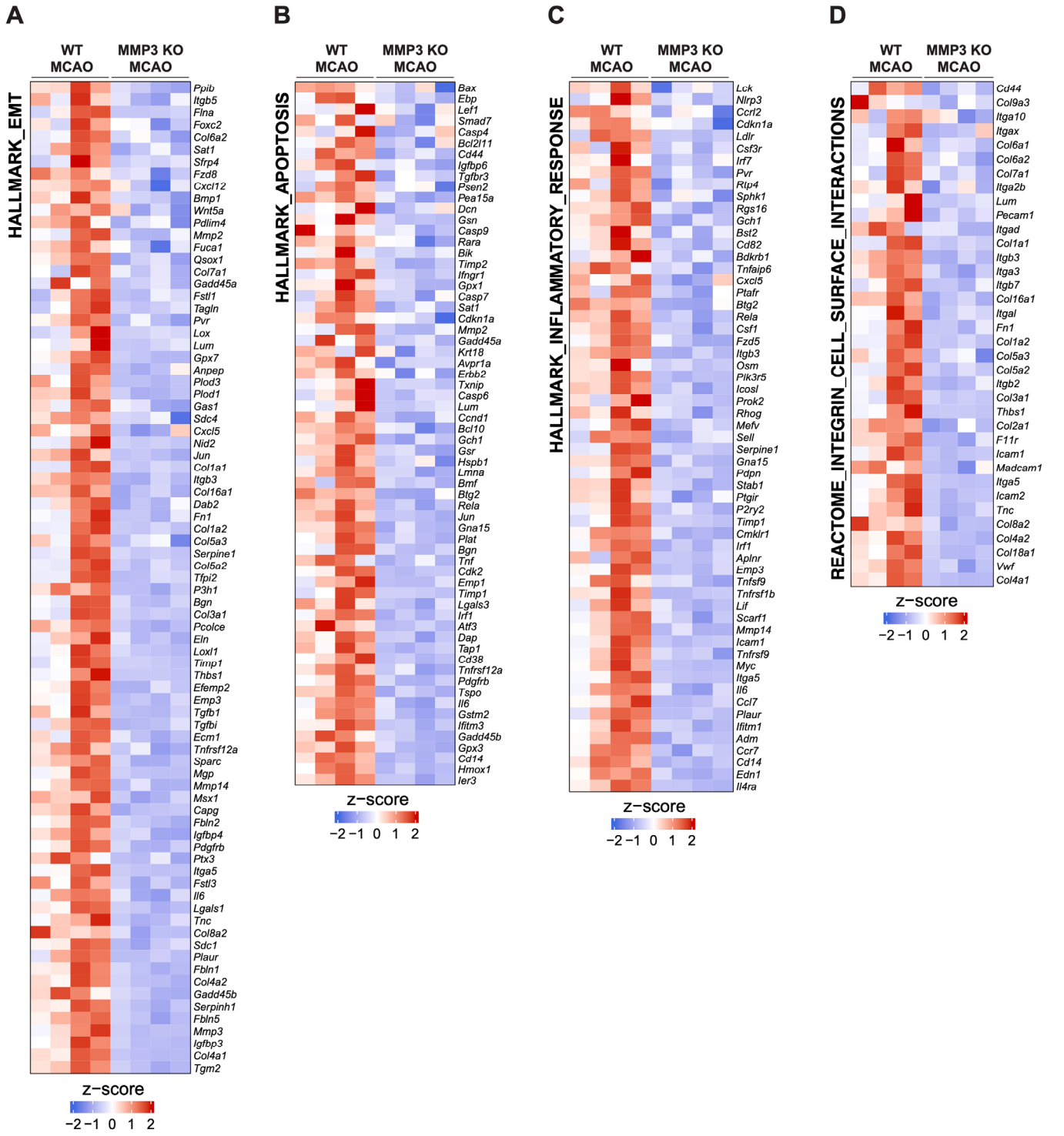

Figure A3. Heatmaps depicting gene expression profiles for the full set of genes in the (**A**) Hallmark Epithelial-Mesenchymal Transition (EMT), (**B**) Hallmark Apoptosis, (**C**) Hallmark Inflammatory Response, (**D**) Hallmark Integrin Cell Surface Interactions sets between female MMP-3 KO and female WT MCAO mice. Each panel (**A**–**D**) includes genes not explicitly highlighted in Figure 4. MCAO, middle cerebral artery occlusion with reperfusion. Red color indicates increased expression. Blue color indicates decreased expression.

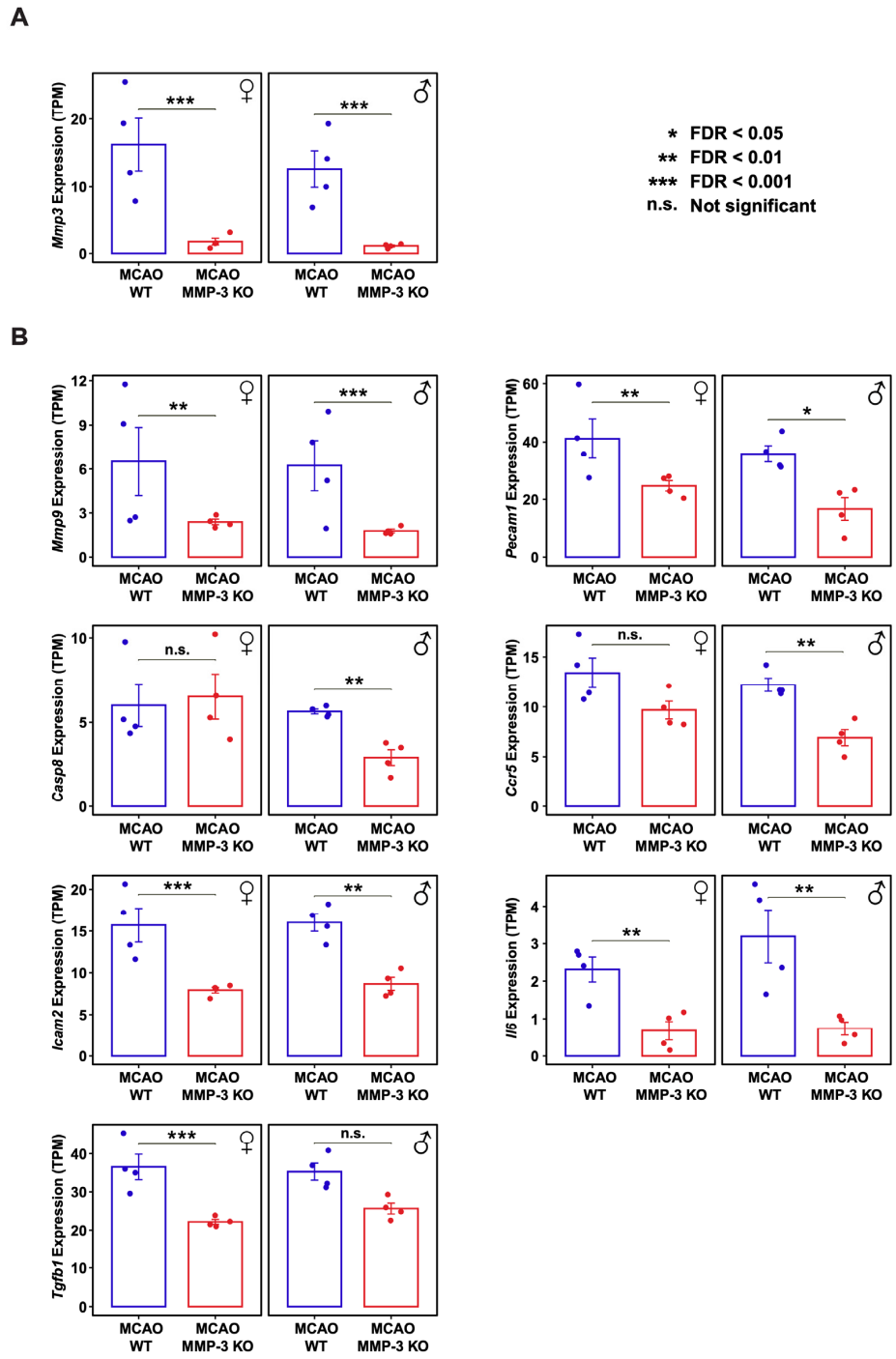

Figure A4. TPM levels of inflammatory mediators from stroke mouse brains harvested at 48 h post-stroke. (**A**) MMP-3 TPM values are higher in the WT MCAO group (blue) than in the MMP-3 KO MCAO group (red). There were no detectable levels of MMP-3 in sham control animals. Following stroke, the MMP-3 expression is significantly induced in WT MCAO group. As anticipated, MMP-3 expression is lower in the MMP-3 KO MCAO group at 48 h post-stroke as shown by RNA-seq analysis. *** FDR < 0.001. (n = 4, WT MCAO; n = 4, MMP-3 KO MCAO). (**B**) Expression of inflammatory mediators at 48 h post-stroke is lower in the MMP-3 KO MCAO group (red) than in the WT MCAO group (blue). * FDR < 0.05; ** FDR < 0.01; *** FDR < 0.001; n.s., not significant (n = 4, WT MCAO; n = 4, MMP-3 KO MCAO). Each dot represents a biological replicate of an RNA-seq sample. MCAO, middle cerebral artery occlusion with reperfusion; TPM, Transcripts Per Million.

References

1. Virani, S.S.; Alonso, A.; Benjamin, E.J.; Bittencourt, M.S.; Callaway, C.W.; Carson, A.P.; Chamberlain, A.M.; Chang, A.R.; Cheng, S.; Delling, F.N.; et al. Heart Disease and Stroke Statistics-2020 Update: A Report From the American Heart Association. *Circulation* **2020**, *141*, e139–e596. [CrossRef] [PubMed]
2. Feigin, V.L.; Forouzanfar, M.H.; Krishnamurthi, R.; Mensah, G.A.; Connor, M.; Bennett, D.A.; Moran, A.E.; Sacco, R.L.; Anderson, L.; Truelsen, T.; et al. Global and regional burden of stroke during 1990–2010: Findings from the Global Burden of Disease Study 2010. *Lancet* **2014**, *383*, 245–254. [CrossRef] [PubMed]
3. Moskowitz, M.A.; Lo, E.H.; Iadecola, C. The Science of Stroke: Mechanisms in Search of Treatments. *Neuron* **2010**, *67*, 181–198. [CrossRef] [PubMed]
4. Thom, T.; Haase, N.; Rosamond, W.; Howard, V.J.; Rumsfeld, J.; Manolio, T.; Zheng, Z.J.; Flegal, K.; O'Donnell, C.; Kittner, S.; et al. Heart disease and stroke statistics—2006 update: A report from the American Heart Association Statistics Committee and Stroke Statistics Subcommittee. *Circulation* **2006**, *113*, e85–e151. [PubMed]
5. Yamashita, T.; Deguchi, K.; Nagotani, S.; Abe, K. Vascular protection and restorative therapy in ischemic stroke. *Cell Transplant.* **2011**, *20*, 95–97. [CrossRef] [PubMed]
6. Sporns, P.B.; Minnerup, J.; Warneke, N.; Dziewas, R.; Hanning, U.; Berkemeyer, S.; Zoubi, T.; Heindel, W.; Schwindt, W.; Niederstadt, T. Impact of the Implementation of Thrombectomy with Stent Retrievers on the Frequency of Hemicraniectomy in Patients with Acute Ischemic Stroke. *Clin. Neuroradiol.* **2017**, *27*, 193–197. [CrossRef] [PubMed]
7. Wahlgren, N.; Moreira, T.; Michel, P.; Steiner, T.; Jansen, O.; Cognard, C.; Mattle, H.P.; van Zwam, W.; Holmin, S.; Tatlisumak, T.; et al. Mechanical thrombectomy in acute ischemic stroke: Consensus statement by ESO-Karolinska Stroke Update 2014/2015, supported by ESO, ESMINT, ESNR and EAN. *Int. J. Stroke* **2016**, *11*, 134–147. [CrossRef] [PubMed]
8. Roth, J.M. Recombinant tissue plasminogen activator for the treatment of acute ischemic stroke. *Bayl. Univ. Med. Cent. Proc.* **2011**, *24*, 257–259. [CrossRef]
9. Kilic, E.; Bahr, M.; Hermann, D.M. Effects of recombinant tissue plasminogen activator after intraluminal thread occlusion in mice: Role of hemodynamic alterations. *Stroke* **2001**, *32*, 2641–2647. [CrossRef]
10. Sumii, T.; Lo, E.H. Involvement of matrix metalloproteinase in thrombolysis-associated hemorrhagic transformation after embolic focal ischemia in rats. *Stroke* **2002**, *33*, 831–836. [CrossRef]
11. Begley, D.J.; Brightman, M.W. Structural and functional aspects of the blood-brain barrier. *Pept. Transp. Deliv. Into Cent. Nerv. Syst.* **2003**, *61*, 39–78.
12. Abbott, N.J. Astrocyte-endothelial interactions and blood-brain barrier permeability. *J. Anat.* **2002**, *200*, 629–638. [CrossRef] [PubMed]
13. Saunders, N.R.; Dreifuss, J.J.; Dziegielewska, K.M.; Johansson, P.A.; Habgood, M.D.; Mollgard, K.; Bauer, H.C. The rights and wrongs of blood-brain barrier permeability studies: A walk through 100 years of history. *Front. Neurosci.* **2014**, *8*, 404. [CrossRef] [PubMed]
14. Daneman, R.; Prat, A. The blood-brain barrier. *Cold Spring Harb. Perspect. Biol.* **2015**, *7*, a020412. [CrossRef] [PubMed]
15. Lochhead, J.J.; McCaffrey, G.; Quigley, C.E.; Finch, J.; DeMarco, K.M.; Nametz, N.; Davis, T.P. Oxidative stress increases blood-brain barrier permeability and induces alterations in occludin during hypoxia-reoxygenation. *J. Cereb. Blood Flow. Metab.* **2010**, *30*, 1625–1636. [CrossRef] [PubMed]
16. Yemisci, M.; Gursoy-Ozdemir, Y.; Vural, A.; Can, A.; Topalkara, K.; Dalkara, T. Pericyte contraction induced by oxidative-nitrative stress impairs capillary reflow despite successful opening of an occluded cerebral artery. *Nat. Med.* **2009**, *15*, 1031–1037. [CrossRef] [PubMed]
17. Kuroiwa, T.; Ting, P.; Martinez, H.; Klatzo, I. The biphasic opening of the blood-brain barrier to proteins following temporary middle cerebral artery occlusion. *Acta Neuropathol.* **1985**, *68*, 122–129. [CrossRef]
18. Shi, Y.; Zhang, L.; Pu, H.; Mao, L.; Hu, X.; Jiang, X.; Xu, N.; Stetler, R.A.; Zhang, F.; Liu, X.; et al. Rapid endothelial cytoskeletal reorganization enables early blood-brain barrier disruption and long-term ischaemic reperfusion brain injury. *Nat. Commun.* **2016**, *7*, 10523. [CrossRef] [PubMed]
19. Yang, Y.; Rosenberg, G.A. Blood-brain barrier breakdown in acute and chronic cerebrovascular disease. *Stroke* **2011**, *42*, 3323–3328. [CrossRef]
20. Defilippi, P.; Silengo, L.; Tarone, G. Alpha 6.beta 1 integrin (laminin receptor) is down-regulated by tumor necrosis factor alpha and interleukin-1 beta in human endothelial cells. *J. Biol. Chem.* **1992**, *267*, 18303–18307. [CrossRef]
21. Gasche, Y.; Fujimura, M.; Morita-Fujimura, Y.; Copin, J.C.; Kawase, M.; Massengale, J.; Chan, P.H. Early appearance of activated matrix metalloproteinase-9 after focal cerebral ischemia in mice: A possible role in blood-brain barrier dysfunction. *J. Cereb. Blood Flow. Metab.* **1999**, *19*, 1020–1028. [CrossRef] [PubMed]
22. Lu, B.; Rutledge, B.J.; Gu, L.; Fiorillo, J.; Lukacs, N.W.; Kunkel, S.L.; North, R.; Gerard, C.; Rollins, B.J. Abnormalities in monocyte recruitment and cytokine expression in monocyte chemoattractant protein 1-deficient mice. *J. Exp. Med.* **1998**, *187*, 601–608. [CrossRef] [PubMed]
23. Pettigrew, L.C.; Kindy, M.S.; Scheff, S.; Springer, J.E.; Kryscio, R.J.; Li, Y.; Grass, D.S. Focal cerebral ischemia in the TNFalpha-transgenic rat. *J. Neuroinflamm.* **2008**, *5*, 47. [CrossRef] [PubMed]
24. Rossi, B.; Angiari, S.; Zenaro, E.; Budui, S.L.; Constantin, G. Vascular inflammation in central nervous system diseases: Adhesion receptors controlling leukocyte-endothelial interactions. *J. Leukoc. Biol.* **2011**, *89*, 539–556. [CrossRef] [PubMed]

25. Wolpe, S.D.; Davatelis, G.; Sherry, B.; Beutler, B.; Hesse, D.G.; Nguyen, H.T.; Moldawer, L.L.; Nathan, C.F.; Lowry, S.F.; Cerami, A. Macrophages secrete a novel heparin-binding protein with inflammatory and neutrophil chemokinetic properties. *J. Exp. Med.* **1988**, *167*, 570–581. [CrossRef]
26. Chin, J.R.; Murphy, G.; Werb, Z. Stromelysin, a connective tissue-degrading metalloendopeptidase secreted by stimulated rabbit synovial fibroblasts in parallel with collagenase. Biosynthesis, isolation, characterization, and substrates. *J. Biol. Chem.* **1985**, *260*, 12367–12376. [CrossRef]
27. Klein, T.; Bischoff, R. Physiology and pathophysiology of matrix metalloproteases. *Amino Acids* **2011**, *41*, 271–290. [CrossRef] [PubMed]
28. Hahn-Dantona, E.; Ramos-DeSimone, N.; Sipley, J.; Nagase, H.; French, D.L.; Quigley, J.P. Activation of proMMP-9 by a plasmin/MMP-3 cascade in a tumor cell model. Regulation by tissue inhibitors of metalloproteinases. *Ann. N. Y. Acad. Sci.* **1999**, *878*, 372–387. [CrossRef]
29. Candelario-Jalil, E.; Yang, Y.; Rosenberg, G.A. Diverse roles of matrix metalloproteinases and tissue inhibitors of metalloproteinases in neuroinflammation and cerebral ischemia. *Neuroscience* **2009**, *158*, 983–994. [CrossRef]
30. Ramos-DeSimone, N.; Hahn-Dantona, E.; Sipley, J.; Nagase, H.; French, D.L.; Quigley, J.P. Activation of matrix metalloproteinase-9 (MMP-9) via a converging plasmin/stromelysin-1 cascade enhances tumor cell invasion. *J. Biol. Chem.* **1999**, *274*, 13066–13076. [CrossRef]
31. Suzuki, Y.; Nagai, N.; Umemura, K.; Collen, D.; Lijnen, H.R. Stromelysin-1 (MMP-3) is critical for intracranial bleeding after t-PA treatment of stroke in mice. *J. Thromb. Haemost.* **2007**, *5*, 1732–1739. [CrossRef] [PubMed]
32. Hafez, S.; Abdelsaid, M.; El-Shafey, S.; Johnson, M.H.; Fagan, S.C.; Ergul, A. Matrix Metalloprotease 3 Exacerbates Hemorrhagic Transformation and Worsens Functional Outcomes in Hyperglycemic Stroke. *Stroke* **2016**, *47*, 843–851. [CrossRef] [PubMed]
33. Hamblin, M.H.; Murad, R.; Yin, J.; Vallim, G.; Lee, J.P. Modulation of gene expression on a transcriptome-wide level following human neural stem cell transplantation in aged mouse stroke brains. *Exp. Neurol.* **2022**, *347*, 113913. [CrossRef] [PubMed]
34. Sternlicht, M.D.; Werb, Z. How matrix metalloproteinases regulate cell behavior. *Annu. Rev. Cell Dev. Biol.* **2001**, *17*, 463–516. [CrossRef] [PubMed]
35. Sternlicht, M.D.; Lochter, A.; Sympson, C.J.; Huey, B.; Rougier, J.P.; Gray, J.W.; Pinkel, D.; Bissell, M.J.; Werb, Z. The stromal proteinase MMP3/stromelysin-1 promotes mammary carcinogenesis. *Cell* **1999**, *98*, 137–146. [CrossRef] [PubMed]
36. Lochter, A.; Srebrow, A.; Sympson, C.J.; Terracio, N.; Werb, Z.; Bissell, M.J. Misregulation of stromelysin-1 expression in mouse mammary tumor cells accompanies acquisition of stromelysin-1-dependent invasive properties. *J. Biol. Chem.* **1997**, *272*, 5007–5015. [CrossRef] [PubMed]
37. Lochter, A.; Galosy, S.; Muschler, J.; Freedman, N.; Werb, Z.; Bissell, M.J. Matrix metalloproteinase stromelysin-1 triggers a cascade of molecular alterations that leads to stable epithelial-to-mesenchymal conversion and a premalignant phenotype in mammary epithelial cells. *J. Cell Biol.* **1997**, *139*, 1861–1872. [CrossRef] [PubMed]
38. Potenta, S.; Zeisberg, E.; Kalluri, R. The role of endothelial-to-mesenchymal transition in cancer progression. *Br. J. Cancer* **2008**, *99*, 1375–1379. [CrossRef] [PubMed]
39. Luo, Y.; Yang, H.; Wan, Y.; Yang, S.; Wu, J.; Chen, S.; Li, Y.; Jin, H.; He, Q.; Zhu, D.Y.; et al. Endothelial ETS1 inhibition exacerbate blood-brain barrier dysfunction in multiple sclerosis through inducing endothelial-to-mesenchymal transition. *Cell Death Dis.* **2022**, *13*, 462. [CrossRef]
40. Derada Troletti, C.; Fontijn, R.D.; Gowing, E.; Charabati, M.; van Het Hof, B.; Didouh, I.; van der Pol, S.M.A.; Geerts, D.; Prat, A.; van Horssen, J.; et al. Inflammation-induced endothelial to mesenchymal transition promotes brain endothelial cell dysfunction and occurs during multiple sclerosis pathophysiology. *Cell Death Dis.* **2019**, *10*, 45. [CrossRef]
41. Chen, D.; Li, L.; Wang, Y.; Xu, R.; Peng, S.; Zhou, L.; Deng, Z. Ischemia-reperfusion injury of brain induces endothelial-mesenchymal transition and vascular fibrosis via activating let-7i/TGF-βR1 double-negative feedback loop. *Faseb J* **2020**, *34*, 7178–7191. [CrossRef] [PubMed]
42. Jin, R.; Yang, G.; Li, G. Inflammatory mechanisms in ischemic stroke: Role of inflammatory cells. *J. Leukoc. Biol.* **2010**, *87*, 779–789. [CrossRef] [PubMed]
43. Radak, D.; Katsiki, N.; Resanovic, I.; Jovanovic, A.; Sudar-Milovanovic, E.; Zafirovic, S.; Mousad, S.A.; Isenovic, E.R. Apoptosis and Acute Brain Ischemia in Ischemic Stroke. *Curr. Vasc. Pharmacol.* **2017**, *15*, 115–122. [CrossRef] [PubMed]
44. Edwards, D.N.; Bix, G.J. Roles of blood-brain barrier integrins and extracellular matrix in stroke. *Am. J. Physiol. Cell Physiol.* **2019**, *316*, C252–C263. [CrossRef] [PubMed]
45. Takada, Y.; Ye, X.; Simon, S. The integrins. *Genome Biol.* **2007**, *8*, 215. [CrossRef] [PubMed]
46. Davis, M.J.; Wu, X.; Nurkiewicz, T.R.; Kawasaki, J.; Davis, G.E.; Hill, M.A.; Meininger, G.A. Integrins and mechanotransduction of the vascular myogenic response. *Am. J. Physiol. Heart Circ. Physiol.* **2001**, *280*, H1427-33. [CrossRef] [PubMed]
47. Wang, N.; Butler, J.P.; Ingber, D.E. Mechanotransduction across the cell surface and through the cytoskeleton. *Science* **1993**, *260*, 1124–1127. [CrossRef] [PubMed]
48. Obermeier, B.; Daneman, R.; Ransohoff, R.M. Development, maintenance and disruption of the blood-brain barrier. *Nat. Med.* **2013**, *19*, 1584–1596. [CrossRef] [PubMed]
49. Rochfort, K.D.; Cummins, P.M. The blood-brain barrier endothelium: A target for pro-inflammatory cytokines. *Biochem. Soc. Trans.* **2015**, *43*, 702–706. [CrossRef]

50. Pan, W.; Stone, K.P.; Hsuchou, H.; Manda, V.K.; Zhang, Y.; Kastin, A.J. Cytokine signaling modulates blood-brain barrier function. *Curr. Pharm. Des.* **2011**, *17*, 3729–3740. [CrossRef]
51. Cuadrado, E.; Rosell, A.; Penalba, A.; Slevin, M.; Alvarez-Sabin, J.; Ortega-Aznar, A.; Montaner, J. Vascular MMP-9/TIMP-2 and neuronal MMP-10 up-regulation in human brain after stroke: A combined laser microdissection and protein array study. *J. Proteome Res.* **2009**, *8*, 3191–3197. [CrossRef] [PubMed]
52. Abdul, Y.; Jamil, S.; Li, W.; Ergul, A. Cerebral microvascular matrix metalloproteinase-3 (MMP3) contributes to vascular injury after stroke in female diabetic rats. *Neurochem. Int.* **2023**, *162*, 105462. [CrossRef] [PubMed]
53. Engel, O.; Kolodziej, S.; Dirnagl, U.; Prinz, V. Modeling Stroke in Mice—Middle Cerebral Artery Occlusion with the Filament Model. *J. Vis. Exp.* **2011**, 2423.
54. Wei, N.; Xiao, L.; Xue, R.; Zhang, D.; Zhou, J.; Ren, H.; Guo, S.; Xu, J. MicroRNA-9 Mediates the Cell Apoptosis by Targeting Bcl2l11 in Ischemic Stroke. *Mol. Neurobiol.* **2016**, *53*, 6809–6817. [CrossRef] [PubMed]
55. Kono, H.; Rock, K.L. How dying cells alert the immune system to danger. *Nat. Rev. Immunol.* **2008**, *8*, 279–289. [CrossRef]
56. Qiu, Y.-M.; Zhang, C.-L.; Chen, A.-Q.; Wang, H.-L.; Zhou, Y.-F.; Li, Y.-N.; Hu, B. Immune Cells in the BBB Disruption After Acute Ischemic Stroke: Targets for Immune Therapy? *Front. Immunol.* **2021**, *12*, 678744. [CrossRef] [PubMed]
57. Gülke, E.; Gelderblom, M.; Magnus, T. Danger signals in stroke and their role on microglia activation after ischemia. *Ther. Adv. Neurol. Disord.* **2018**, *11*, 1756286418774254. [CrossRef] [PubMed]
58. Murray, K.N.; Buggey, H.F.; Denes, A.; Allan, S.M. Systemic immune activation shapes stroke outcome. *Mol. Cell Neurosci.* **2013**, *53*, 14–25. [CrossRef]
59. Shichita, T.; Ito, M.; Morita, R.; Komai, K.; Noguchi, Y.; Ooboshi, H.; Koshida, R.; Takahashi, S.; Kodama, T.; Yoshimura, A. MAFB prevents excess inflammation after ischemic stroke by accelerating clearance of damage signals through MSR1. *Nat. Med.* **2017**, *23*, 723–732. [CrossRef]
60. Baumann, H.; Gauldie, J. The acute phase response. *Immunol. Today* **1994**, *15*, 74–80. [CrossRef]
61. Dziedzic, T. Clinical significance of acute phase reaction in stroke patients. *Front. Biosci.* **2008**, *13*, 2922–2927. [CrossRef]
62. Shaafi, S.; Sharifipour, E.; Rahmanifar, R.; Hejazi, S.; Andalib, S.; Nikanfar, M.; Baradarn, B.; Mehdizadeh, R. Interleukin-6, a reliable prognostic factor for ischemic stroke. *Iran. J. Neurol.* **2014**, *13*, 70–76. [PubMed]
63. Tariq, M.B.; Lee, J.; McCullough, L.D. Sex differences in the inflammatory response to stroke. *Semin. Immunopathol.* **2023**, *45*, 295–313. [CrossRef]
64. Aktas, O.; Ullrich, O.; Infante-Duarte, C.; Nitsch, R.; Zipp, F. Neuronal damage in brain inflammation. *Arch. Neurol.* **2007**, *64*, 185–189. [CrossRef]
65. Rodrigues, S.F.; Granger, D.N. Blood cells and endothelial barrier function. *Tissue Barriers* **2015**, *3*, e978720. [CrossRef] [PubMed]
66. Shulman, Z.; Shinder, V.; Klein, E.; Grabovsky, V.; Yeger, O.; Geron, E.; Montresor, A.; Bolomini-Vittori, M.; Feigelson, S.W.; Kirchhausen, T.; et al. Lymphocyte crawling and transendothelial migration require chemokine triggering of high-affinity LFA-1 integrin. *Immunity* **2009**, *30*, 384–396. [CrossRef] [PubMed]
67. Schenkel, A.R.; Chew, T.W.; Muller, W.A. Platelet endothelial cell adhesion molecule deficiency or blockade significantly reduces leukocyte emigration in a majority of mouse strains. *J. Immunol.* **2004**, *173*, 6403–6408. [CrossRef] [PubMed]
68. Zera, K.A.; Buckwalter, M.S. The Local and Peripheral Immune Responses to Stroke: Implications for Therapeutic Development. *Neurotherapeutics* **2020**, *17*, 414–435. [CrossRef] [PubMed]
69. Roberts, J.; de Hoog, L.; Bix, G.J. Mice deficient in endothelial α5 integrin are profoundly resistant to experimental ischemic stroke. *J. Cereb. Blood Flow. Metab.* **2017**, *37*, 85–96. [CrossRef]
70. Okada, Y.; Copeland, B.R.; Hamann, G.F.; Koziol, J.A.; Cheresh, D.A.; del Zoppo, G.J. Integrin alphavbeta3 is expressed in selected microvessels after focal cerebral ischemia. *Am. J. Pathol.* **1996**, *149*, 37–44.
71. Alghisi, G.C.; Ponsonnet, L.; Rüegg, C. The Integrin Antagonist Cilengitide Activates αVβ3, Disrupts VE-Cadherin Localization at Cell Junctions and Enhances Permeability in Endothelial Cells. *PLoS ONE* **2009**, *4*, e4449. [CrossRef] [PubMed]
72. Bendeck, M.P.; Irvin, C.; Reidy, M.; Smith, L.; Mulholland, D.; Horton, M.; Giachelli, C.M. Smooth Muscle Cell Matrix Metalloproteinase Production Is Stimulated via αvβ3 Integrin. *Arterioscler. Thromb. Vasc. Biol.* **2000**, *20*, 1467–1472. [CrossRef] [PubMed]
73. Kovacic, J.C.; Dimmeler, S.; Harvey, R.P.; Finkel, T.; Aikawa, E.; Krenning, G.; Baker, A.H. Endothelial to Mesenchymal Transition in Cardiovascular Disease: JACC State-of-the-Art Review. *J. Am. Coll. Cardiol.* **2019**, *73*, 190–209. [CrossRef] [PubMed]
74. Bai, Y.; Zhang, Y.; Han, B.; Yang, L.; Chen, X.; Huang, R.; Wu, F.; Chao, J.; Liu, P.; Hu, G.; et al. Circular RNA DLGAP4 Ameliorates Ischemic Stroke Outcomes by Targeting miR-143 to Regulate Endothelial-Mesenchymal Transition Associated with Blood–Brain Barrier Integrity. *J. Neurosci.* **2018**, *38*, 32–50. [CrossRef] [PubMed]
75. Mahajan, D.; Kancharla, S.; Kolli, P.; Sharma, A.K.; Singh, S.; Kumar, S.; Mohanty, A.K.; Jena, M.K. Role of Fibulins in Embryonic Stage Development and Their Involvement in Various Diseases. *Biomolecules* **2021**, *11*, 685. [CrossRef] [PubMed]
76. Eguchi, T.; Kubota, S.; Kawata, K.; Mukudai, Y.; Uehara, J.; Ohgawara, T.; Ibaragi, S.; Sasaki, A.; Kuboki, T.; Takigawa, M. Novel transcription-factor-like function of human matrix metalloproteinase 3 regulating the CTGF/CCN2 gene. *Mol. Cell Biol.* **2008**, *28*, 2391–2413. [CrossRef] [PubMed]
77. Huang, L.; Wong, S.; Snyder, E.Y.; Hamblin, M.H.; Lee, J.P. Human neural stem cells rapidly ameliorate symptomatic inflammation in early-stage ischemic-reperfusion cerebral injury. *Stem Cell Res. Ther.* **2014**, *5*, 129. [CrossRef] [PubMed]

78. Eckert, A.; Huang, L.; Gonzalez, R.; Kim, H.S.; Hamblin, M.H.; Lee, J.P. Bystander Effect Fuels Human Induced Pluripotent Stem Cell-Derived Neural Stem Cells to Quickly Attenuate Early Stage Neurological Deficits After Stroke. *Stem Cells Transl. Med.* **2015**, *4*, 841–851. [CrossRef] [PubMed]
79. Boese, A.C.; Eckert, A.; Hamblin, M.H.; Lee, J.P. Human neural stem cells improve early stage stroke outcome in delayed tissue plasminogen activator-treated aged stroke brains. *Exp. Neurol.* **2020**, *329*, 113275. [CrossRef]
80. Dobin, A.; Davis, C.A.; Schlesinger, F.; Drenkow, J.; Zaleski, C.; Jha, S.; Batut, P.; Chaisson, M.; Gingeras, T.R. STAR: Ultrafast universal RNA-seq aligner. *Bioinformatics* **2013**, *29*, 15–21. [CrossRef]
81. Li, B.; Dewey, C.N. RSEM: Accurate transcript quantification from RNA-Seq data with or without a reference genome. *BMC Bioinform.* **2011**, *12*, 323. [CrossRef] [PubMed]
82. Ewels, P.; Magnusson, M.; Lundin, S.; Kaller, M. MultiQC: Summarize analysis results for multiple tools and samples in a single report. *Bioinformatics* **2016**, *32*, 3047–3048. [CrossRef] [PubMed]
83. Love, M.I.; Huber, W.; Anders, S. Moderated estimation of fold change and dispersion for RNA-seq data with DESeq2. *Genome Biol.* **2014**, *15*, 550. [CrossRef] [PubMed]
84. Subramanian, A.; Tamayo, P.; Mootha, V.K.; Mukherjee, S.; Ebert, B.L.; Gillette, M.A.; Paulovich, A.; Pomeroy, S.L.; Golub, T.R.; Lander, E.S.; et al. Gene set enrichment analysis: A knowledge-based approach for interpreting genome-wide expression profiles. *Proc. Natl. Acad. Sci. USA* **2005**, *102*, 15545–15550. [CrossRef] [PubMed]

International Journal of
Molecular Sciences

MDPI

Article

Dihydroergotamine Increases Histamine Brain Levels and Improves Memory in a Scopolamine-Induced Amnesia Model

Maricarmen Hernández-Rodríguez [1,*], Elvia Mera Jiménez [1,*], María Inés Nicolás-Vázquez [2] and Rene Miranda-Ruvalcaba [2]

[1] Laboratorio de Cultivo Celular, Neurofarmacología y Conducta, Escuela Superior de Medicina, Instituto Politécnico Nacional, Plan de San Luis y Díaz Mirón s/n, Ciudad de México 11340, Mexico
[2] Departamento de Ciencias Químicas, Facultad de Estudios Superiores Cuautitlán Campo 1, Universidad Nacional Autónoma de México, Avenida 1o de Mayo s/n, Colonia Santa María las Torres, Cuautitlán Izcalli 54740, Mexico; nicovain@yahoo.com.mx (M.I.N.-V.); mirruv@yahoo.com.mx (R.M.-R.)
* Correspondence: dra.hernandez.ipn@gmail.com or mhernandezrod@ipn.mx (M.H.-R.); elviamj@gmail.com or emeraj@ipn.mx (E.M.J.)

Abstract: The beneficial effects of increasing histamine levels on memory have acquired special interest due to their applicability to psychiatric conditions that cause memory impairments. In addition, by employing drug repurposing approaches, it was demonstrated that dihydroergotamine (DHE), an FDA drug approved to treat migraines, inhibits Histamine N Methyl Transferase (HNMT), the enzyme responsible for the inactivation of histamine in the brain. For this reason, in the present work, the effect of DHE on histamine levels in the hippocampus and its effects on memory was evaluated, employing the scopolamine-induced amnesia model, the Novel Object Recognition (NOR) paradigm, and the Morris Water Maze (MWM). Furthermore, the role of histamine 1 receptor (H1R) and histamine 2 receptor (H2R) antagonists in the improvement in memory produced by DHE in the scopolamine-induced amnesia model was evaluated. Results showed that the rats that received DHE (10 mg/kg, i.p.) showed increased histamine levels in the hippocampus after 1 h of administration but not after 5 h. In behavioral assays, it was shown that DHE (1 mg/kg, i.p.) administered 20 min before the training reversed the memory impairment produced by the administration of scopolamine (2 mg/kg, i.p.) immediately after the training in the NOR paradigm and MWM. Additionally, the effects in memory produced by DHE were blocked by pre-treatment with pyrilamine (20 mg/kg, i.p.) administered 30 min before the training in the NOR paradigm and MWM. These findings allow us to demonstrate that DHE improves memory in a scopolamine-induced amnesia model through increasing histamine levels at the hippocampus due to its activity as an HNMT inhibitor.

Keywords: histamine; dihydroergotamine; Morris water maze; novel object recognition

Citation: Hernández-Rodríguez, M.; Mera Jiménez, E.; Nicolás-Vázquez, M.I.; Miranda-Ruvalcaba, R. Dihydroergotamine Increases Histamine Brain Levels and Improves Memory in a Scopolamine-Induced Amnesia Model. *Int. J. Mol. Sci.* **2024**, *25*, 3710. https://doi.org/10.3390/ijms25073710

Academic Editors: Efthimios M. C. Skoulakis and Alberto Pérez-Mediavilla

Received: 15 February 2024
Revised: 18 March 2024
Accepted: 22 March 2024
Published: 26 March 2024

1. Introduction

Histamine is a biogenic amine that acts as a neurotransmitter to regulate several physiological functions in the brain, including wakefulness, feeding, energy intake, and memory, among others [1]. In the brain, histamine is produced by histaminergic neurons located in the tuberomamilar nucleus (TMN) by the enzyme histidine decarboxylase (HDC), which employs histidine as a substrate. Histamine exerts its effects by interacting with four types of histamine receptors: H1R, H2R, H3R, and H4R, which are protein G-coupled receptors [2]. H1R and H2R potentiate excitatory inputs while H3R downregulates histamine synthesis and release as well as the release of other neurotransmitters [3]. In contrast, although there is debate about the expression of H4R in the brain, it has been demonstrated that H4R regulates cytokine release by microglial cells [4].

The regulation of histamine levels in the synaptic cleft occurs predominantly through the action of the enzyme Histamine N Methyl Transferase (HNMT), located in astrocytes, which inactivates histamine to *t*-methylhistamine [5]. Thus, increased histamine levels in

the brain can be achieved by inhibiting HNMT, as was demonstrated by metoprine, an HNMT inhibitor [6].

Furthermore, the beneficial effects of increasing histamine levels in the brain were first described in 1986 by de Almeida and Izquierdo, showing that intra-cerebrovascular (i.c.v.) administration of 1 or 10 ng of histamine immediately after the training facilitated retention of step-down inhibitory avoidance tests in rats [7]. Interestingly, histamine infusion into the hippocampus of Wistar rats enhances retention in the inhibitory avoidance task in rats in a dose-dependent manner, and the effect was mimicked by hippocampal infusion with SKF-91844, which is an HNMT inhibitor [8]. In addition, the blockade of H1R and H2R receptors impaired memory retention in a novel object recognition (NOR) task when it was infused 30–120 min after training [9]. Furthermore, Prast H et al., 1996 showed that i.c.v. administration of histamine or histidine improved short-term recognition memory in rats. In contrast, depletion of neuronal histamine by alpha-fluoromethylhistidine (FMH) produces amnesia in rodents [10]. In addition, the effects of histamine on spatial memory have been demonstrated. Several reports have pointed out that both histamine and histidine ameliorate spatial memory deficits induced by aging, dorsal hippocampal lesions, and scopolamine, as determined by passive and active avoidance tasks and an eight-arm radial maze test for rats [11–13], thus highlighting the effects of the histaminergic system in memory processes.

Indeed, the effects of metoprine on cognitive performance have been demonstrated in a mouse model of scopolamine-induced amnesia [14]. In this sense, the study of effects on memory of HNMT inhibitors is of special interest.

Drug repurposing approaches employing computational and in vitro studies allowed us to demonstrate that dihydroergotamine (DHE, Figure 1), an FDA drug approved to treat migraines, inhibits HNMT [15]. For this reason, in the present work, the effect of DHE on histamine levels in the hippocampus and its effects on memory were evaluated, employing the scopolamine-induced amnesia model.

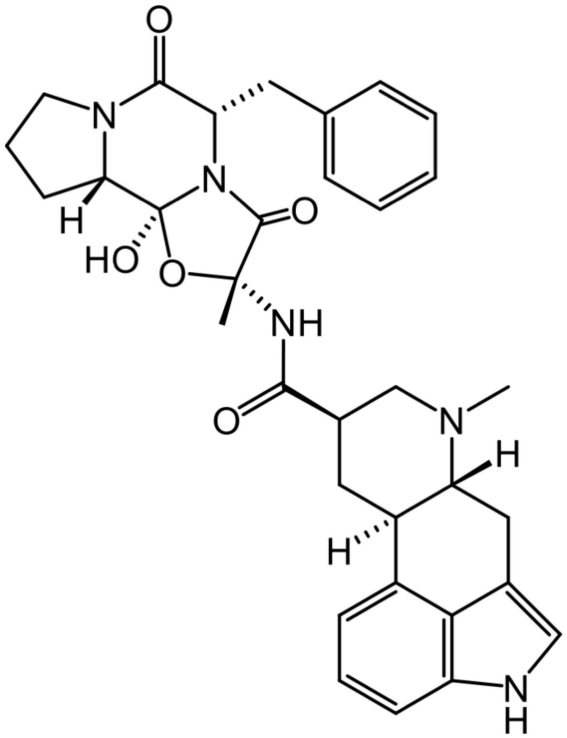

Figure 1. Chemical structure of dihydroergotamine (DHE).

2. Results

2.1. DHE Increases Histamine Levels in the Hippocampus

Histamine levels in the hippocampus of Wistar rats after 1 and 5 h of administration of saline solution (2 mL/kg), metoprine (10 mg/kg), or DHE (1 mg/kg), by i.p. routes were determined. As can be seen in Figure 2, the treatment groups displayed increased histamine levels after 1 h of administration in comparison with the control ($p < 0.5$). Interestingly, DHE induced an increase in histamine levels in the hippocampus similar to metoprine. However, histamine levels remain elevated only in the hippocampus of rats treated with metoprine after 5 h, as was previously reported [6], but not in the rats that received DHE.

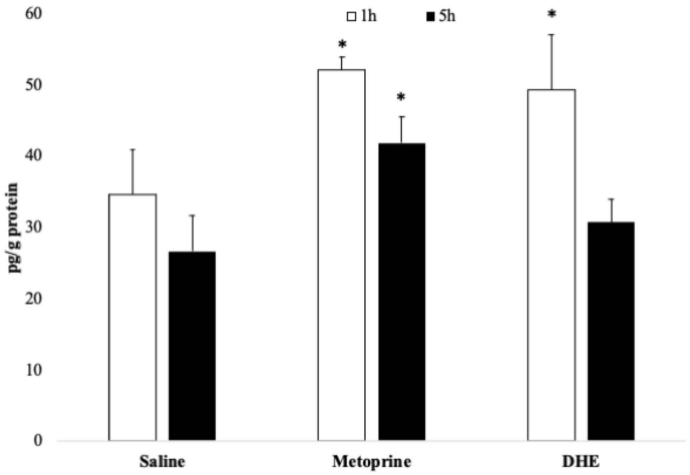

Figure 2. Histamine levels in the hippocampus of Wistar rats treated with metoprine and DHE. Rats were administered intraperitoneally with saline solution (2 mL/kg), metoprine (10 mg/kg), or DHE (1 mg/kg). After 1 and 5 h, rats were sacrificed and the brain histamine levels were determined employing a colorimetric competitive ELISA kit. The concentration of histamine in the samples was determined by comparing the O.D. at 450 nm with the standard curve. Data are expressed as Mean ± SEM, n = 3, and statistical analysis by one-way ANOVA (* $p < 0.05$ versus saline 1 h). For between-group comparisons, Tukey's test was used as a post-hoc test.

2.2. DHE Improves Memory Recognition in the Scopolamine-Induced Amnesia Model

As can be seen in Figure 3a, administration of 2 mg/kg (i.p.) scopolamine immediately after the training session significantly impaired remembering the exposition to a familiar object in the scopolamine group in comparison with the saline group. This fact is evidenced by a lower recognition index of the scopolamine group in comparison with the saline group (Figure 3b). Interestingly, in the piracetam group and DHE group, the effect produced by scopolamine was reversed, thus the rats spent more time exploring the novel object than exploring the familiar object ($p < 0.05$).

2.3. DHE Improves Spatial Learning and Memory in the Scopolamine-Induced Amnesia Model

Acquisition of the place task is represented by mean escape latencies on the four training trials. As shown in Figure 4, there is a decrease in the escape latency in all the groups on T2, T3, and T4, as compared to T1. However, the administration of scopolamine resulted in an increase in escape latency in the scopolamine group in comparison with the saline group ($p < 0.05$) during all the training days. Interestingly, treatment with piracetam 30 mg/kg i.p., a known nootropic drug, administered 20 min before the training session reverted the impairment produced by the administration of scopolamine, evidenced by similar escape latency times to the saline group (Figure 4). A similar effect was obtained with DHE (Figure 4).

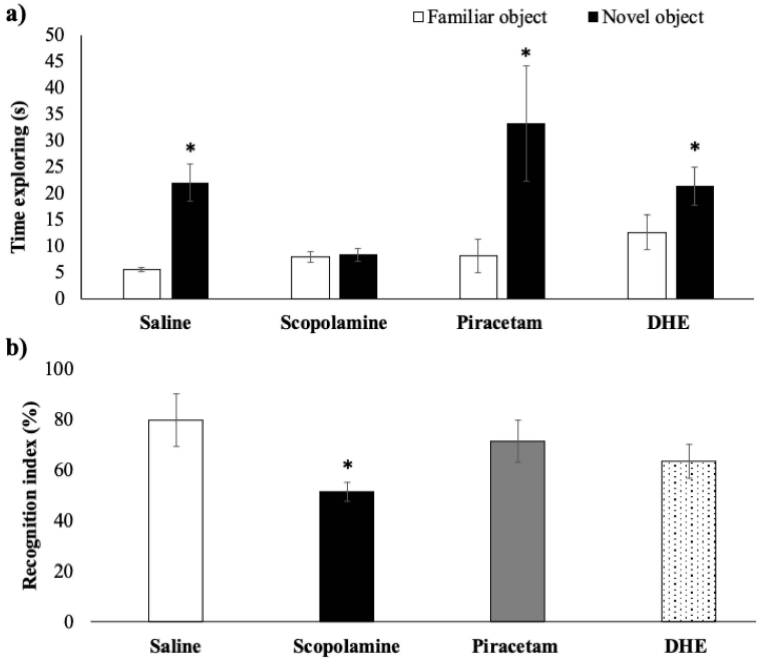

Figure 3. Effects of DHE in a scopolamine-induced amnesia model on recognition memory evaluated by the NOR paradigm. (**a**) In trials separated by 180 min, the rats from all groups, except for the scopolamine group, spent significantly more time exploring the novel object relative to the familiar object. Data are expressed as Mean ± SEM, n = 10. Statistical analysis was performed using paired Student *t*-test, * $p < 0.05$ were considered significant. (**b**) Graph plot for the recognition index. The recognition index is similar for all the groups except for the scopolamine group, which showed the lowest value. Data are expressed as Mean ± SEM, n = 10. Statistical analyses were performed by one-way ANOVA * $p < 0.05$. For between-group comparisons, Tukey's test was used as a post-hoc test.

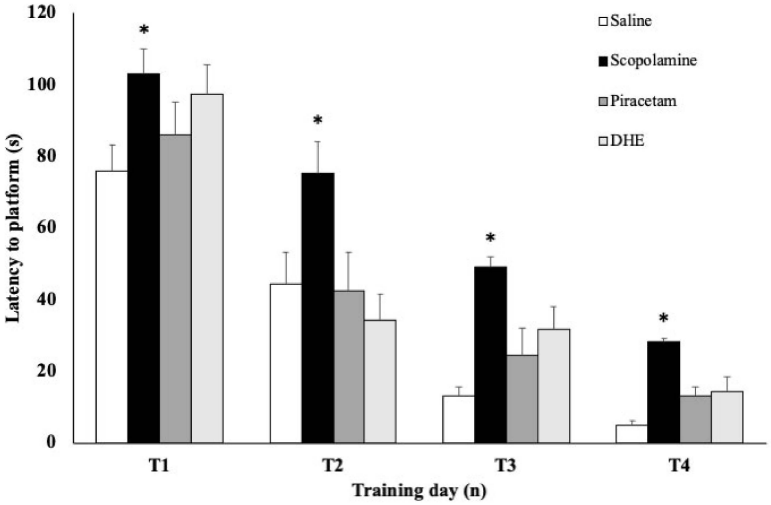

Figure 4. Effects of DHE in a scopolamine-induced amnesia model on escape latency during the training. This figure shows a significant increase in escape latency in the scopolamine group in comparison with the saline group. The impairment in learning was reversed by treatment with piracetam 30 mg/kg i.p. or DHE 1 mg/kg i.p. in the corresponding groups (the piracetam group and the DHE group). Values are presented as means ± SEM, n = 10. Statistical analyses were performed by one-way ANOVA * $p < 0.05$. For between-group comparisons, Tukey's test was used as a post-hoc test.

In addition, as can be seen in Figure 5, during the trial day, the saline group spent more time in the target quadrant than the opposite quadrant ($p < 0.05$). In contrast, the administration of scopolamine immediately after training affects memory, as is shown in the

scopolamine group, which does not show statistically significant differences in time spent in the target quadrant and the opposite quadrant (Figure 6). Interestingly, the piracetam group and the DHE group, which received treatment with piracetam 30 mg/kg i.p. or DHE 1 mg/kg i.p., respectively, reverted the impairment produced by the administration of scopolamine, evidenced by the rats spending more time in the target quadrant than the opposite quadrant ($p < 0.05$), similar to the saline group.

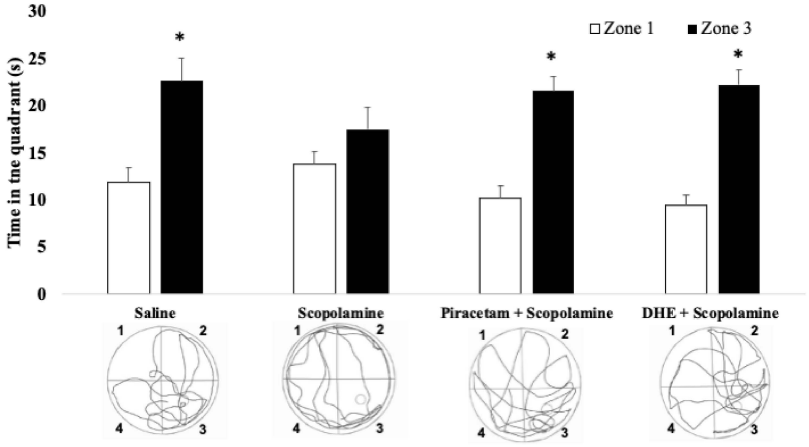

Figure 5. Effects of DHE in a scopolamine-induced amnesia model on path swim during the trial day. This figure shows a significantly lower time exploring quadrant 3, where the platform was located, versus the opposite quadrant 1, when the hidden platform was removed in the scopolamine group in comparison with the saline group. The impairment in remembering was reversed by treatment with piracetam 30 mg/kg i.p. or DHE 1 mg/kg i.p. in the corresponding groups (the piracetam group and the DHE group). Data are expressed as Mean ± SEM, n = 10. Statistical analysis was performed using paired Student *t*-tests, * $p < 0.05$ were considered significant A representative path swim diagram for each treatment group is shown.

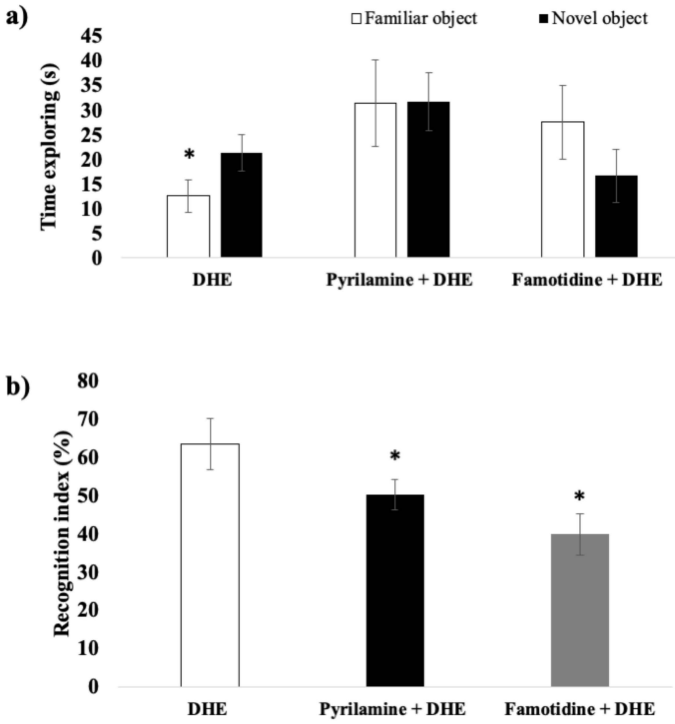

Figure 6. Effects of the blockade of H1R or H2R on the effects produced by DHE in a scopolamine-induced amnesia model evaluated by the NOR paradigm. (**a**) In trials separated by 180 min, the rats from all the groups, except for the scopolamine group, spent significantly more time exploring the

novel object relative to the familiar object. Data are expressed as Mean ± SEM, n = 10. Statistical analysis was performed using paired Student *t*-tests, * $p < 0.05$ were considered significant. (**b**) Graph plot for the recognition index. The recognition index is similar for all the groups except for the scopolamine group, which showed the lowest value. Data are expressed as Mean ± SEM, n = 10. Statistical analyses were performed by one-way ANOVA * $p < 0.05$. For between-group comparisons, Tukey's test was used as a post-hoc test.

2.4. H1R and H2R Antagonists Blockade the Improvement in Recognition Memory Produced by DHE in the Scopolamine-Induced Amnesia Model

To determine the contribution of increased histamine levels in the brain on the effects on memory produced by DHE, pre-treatment with pyrilamine (an H1R antagonist) or famotidine (an H2R antagonist) was evaluated. As can be seen in Figure 6a, pre-treatment with pyrilamine (20 mg/kg, i.p.) or famotidine (10 mg/kg, i.p.) caused a reversion of the improvement in the recognition memory of DHE in the scopolamine-induced amnesia model in the Pyrilamine + DHE group and the Famotidine + DHE group, respectively. This is evidenced by the rats exploring both the novel object and the familiar object for similar periods of time (Figure 6a), and lower discrimination indices for the Pyrilamine + DHE group and the Famotidine + DHE group than the DHE group ($p < 0.05$) (Figure 6b).

2.5. H1R Antagonist Blockades the Improvement in Spatial Learning and Memory Produced by DHE in the Scopolamine-Induced Amnesia Model

As can be seen in Figure 7, pre-treatment with pyrilamine (20 mg/kg, i.p.) in the pyrilamine + DHE group caused a reversion of the improvement of acquisition of the place task exhibited by DHE in the scopolamine-induced amnesia model ($p < 0.05$). In contrast, pre-treatment with famotidine in the famotidine + DHE group did not influence the anti-amnesic effect of DHE (Figure 7).

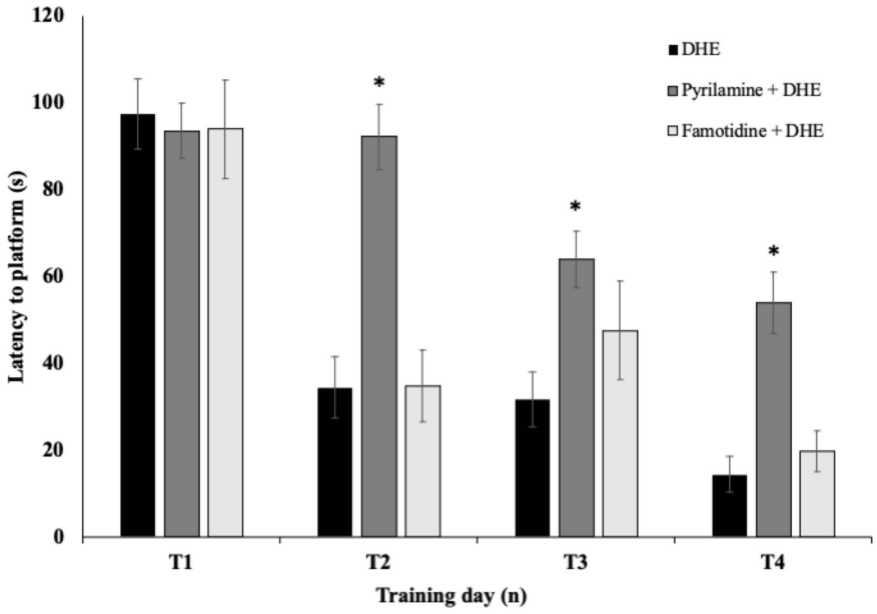

Figure 7. Effects of the blockade of H1R or H2R on the effects produced by DHE in a scopolamine-induced amnesia model in escape latency during the training. This figure shows a significant increase in escape latency in the Pyrilamine + DHE group, which received pre-treatment with pyrilamine 20 mg/kg i.p., in comparison with the DHE group. In contrast, pre-treatment with famotidine 10 mg/kg did not influence the anti-amnesic effect of DHE in the Famotidine + DHE group. Values are presented as means ± SEM, n = 10. Statistical analyses were performed by one-way ANOVA * $p < 0.05$. For between-group comparisons, Tukey's test was used as a post-hoc test.

However, as can be seen in Figure 8, during the trial day, it was shown that pyrilamine (20 mg/kg, i.p.) and famotidine (10 mg/kg i.p.) caused a reversion of improvement in the recognition memory of DHE in the scopolamine-induced amnesia model in the Pyrilamine + DHE group ($p < 0.05$). This is evidenced by the increase in the time spent in the opposite quadrant and the lowering of the time spent in the target quadrant, showing no statistically significant differences in the Pyrilamine + DHE group (Figure 8).

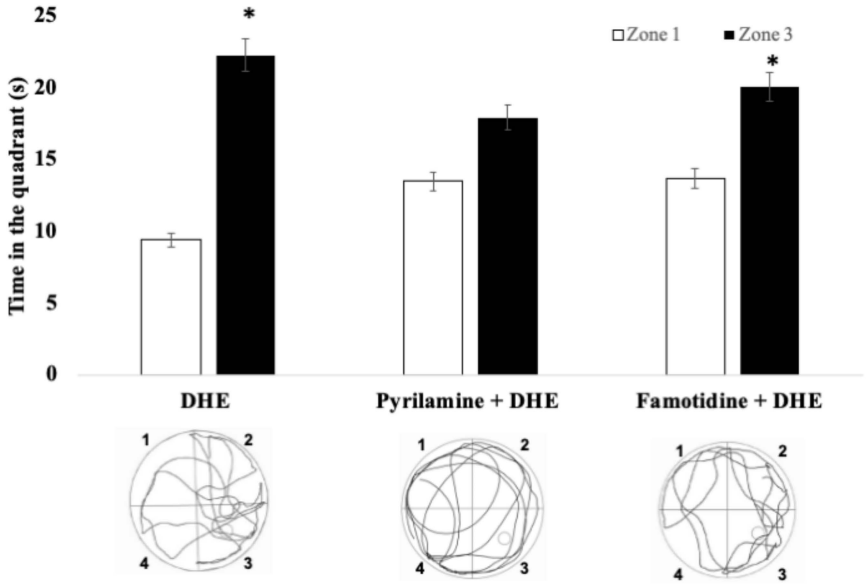

Figure 8. Effects of the blockade of H1R or H2R on the effects produced by DHE in a scopolamine-induced amnesia model in path swim during the trial day. Pre-treatment with pyrilamine (20 mg/kg, i.p.) or famotidine (10 mg/kg i.p.) caused a reversion of improvement in the recognition memory exhibited by DHE in the scopolamine-induced amnesia model in the Pyrilamine + DHE group and the Famotidine + DHE group, respectively. This is evidenced by the increase in the time spent in the opposite quadrant and the lowering of the time spent in the target quadrant. Data are expressed as Mean ± SEM, n = 10. Statistical analysis was performed using paired Student *t*-tests, * $p < 0.05$ were considered significant. A representative path swim diagram for each treatment group is shown.

3. Discussion

Over the last forty years, it has been demonstrated that histamine is a potent modulator of memory and learning [16,17]. Experiments performed by da Silva WC et al., 2006 showed that histamine infusion into the CA1 region of the dorsal hippocampus immediately after training enhances retention of inhibitory avoidance in rats [8]. In addition to the effect of exogenous histamine application, the requirements for endogenous histamine on memory consolidation have been reported [18].

For these reasons, increasing histamine levels in the brain has been proposed as a promising approach to treat neurological disorders that cause memory impairments, including Alzheimer's disease [19]. An increase in histamine levels in the brain can be achieved by inhibiting HNMT, the main enzyme that inactivates histamine in the central nervous system (CNS). Indeed, it has been demonstrated that HNMT inhibition by metoprine reverts amnesia produced by scopolamine a modified mouse passive avoidance test [14]. However, nowadays, there are few HNMT inhibitors, and most of them have a toxic adverse effect profile, including metoprine (cutaneous, gastrointestinal, and hematological toxicities) [20]. In addition, although they show HNMT inhibitory activity, some of these compounds, such as amodiaquine, do not increase brain histamine levels due to their poor blood–brain barrier (BBB) penetration [14,21]. Recently, it has been demonstrated that DHE, an FDA drug approved to treat migraines, inhibits HNMT [19]. Consequently, due to DHE being a drug employed for the treatment of neurological diseases, its safety and BBB penetration have already been corroborated. In the present study, it was demonstrated that DHE increases

histamine levels in the hippocampus 1 h after i.p. administration. However, the increase in histamine levels by DHE is not maintained after 5 h of administration. The transient increase in histamine levels could be related to the DHE peak plasmatic concentration [22]. Furthermore, although it has been demonstrated that the anti-migraine effect of DHE persists for days due to tissue binding, allowing the maintenance of DHE concentrations in the picogram range [23], the concentration could be insufficient to inhibit HNMT.

To evaluate the effects of increasing histamine levels in the hippocampus on memory, a scopolamine-induced amnesia model was employed. Scopolamine hydrobromide is a muscarinic receptor antagonist with amnestic properties that has been used for decades to induce impairment in murine performance in a variety of tasks requiring intact working and reference memory [24]. Although it has been demonstrated that chronic administration of scopolamine induces deleterious effects in the brain [25], we administered scopolamine immediately after the training due to its ability to reduce the cholinergic tone after its systemic administration by blocking muscarinic receptors in naïve animals [26]. This amnesia model allows the evaluation of several types of memory enhancers and is not only restricted to cholinergic-related compounds [27].

Treatments with the studied compounds were evaluated employing the NOR paradigm and the MWM assay, which are classical tasks widely used to assess memory parameters in rodents. Learning processes in both tasks involve the integrity of the hippocampus and associated regions [28].

The anti-amnesic effect of DHE on the NOR paradigm was evidenced by the restoration of novelty preference by spending more time on the novel object relative to the familiar object. Additionally, in the MWM assay, it was demonstrated that DHE treatment improved search errors during training trials produced by scopolamine, suggesting the amelioration of learning impairment. In addition, during the trial day, it was shown that DHE increased the time spent in the target quadrant, thus evincing the efficacy of DHE in improving memory impairment produced by scopolamine. Thus, the present study demonstrated that DHE exhibits an effect on memory similar to that previously demonstrated by metoprine [14].

In order to determine if the effects produced by DHE are related to the histaminergic system, pre-treatments with pyrilamine (H1R antagonist) or famotidine (H2R antagonist) were performed. H1R and H2R are found postsynaptically in all parts of the brain, including the cortex, hippocampus, striatum, and hypothalamus. The H1R is widely expressed in different areas of the brain, including the hippocampus where it is coupled to the Gi protein, mediating neuronal excitation through the stimulation of phospholipase C and thus the second messenger systems that lead to the release of IP_3 and Ca^{2+} from intracellular stores where they play an important role in neuronal functionality and thus in learning and memory formation [29]. H2R is coupled to Gs and stimulates adenylyl cyclase, thereby increasing intracellular cyclic adenosine monophosphate (cAMP), which in turn activates protein kinase A (PKA) and the transcription factor cAMP response element-binding protein (CREB). The cAMP-dependent CREB function in neurons has been associated with numerous intracellular processes, such as proliferation, differentiation, survival, long-term synaptic potentiation, neurogenesis, and neuronal plasticity [30]. However, beneficial effects on memory produced by DHE in MWM were reversed only by pyrilamine (an H1R antagonist). This could be due to differences in the contribution of H1R to the memory process in comparison with H2R. Previous studies in H1R-knockout (H1R-KO) mice revealed deficits in a variety of spatial learning and memory tasks [31]. Several reports suggest that H1R deficiency impairs learning and memory in response to novel objects, although the motivation to explore novel objects was unchanged [32,33]. Moreover, spatial learning and object recognition were impaired in H1R-deficient mice. Interestingly, like H1R-deficient mice, H2R-deficient mice also show impaired object recognition but improved auditory and contextual freezing [34]. These results indicate that H2R shares some, but not all, of its behavioral effects with H1R.

Another explanation of the lack of effect of famotidine on reversing the beneficial effects of DHE on spatial memory in the present study is associated with changes in other

neurotransmitter systems produced by DHE, which can contribute to their effect on memory. Piechal A. et al., 2021 demonstrated that administration of DHE to adult male Wistar Albino Glaxo rats produced changes in the concentration of monoaminergic neurotransmitters and their metabolites in the prefrontal cortex, striatum, cerebellum, medulla oblongata, and spinal cord [35]. Due to the above commentaries, it is necessary to continue with the exploration of DHE's effects on memory in additional behavioral assays.

4. Materials and Methods

4.1. Animals

Adult male Wistar rats weighing between 200–250 g were acquired from the animal facility of Instituto de Fisiología Celular from the Universidad Nacional Autónoma de México. The rats were kept and maintained in cages under standard conditions (12:12 h light/dark cycle, stress-free, water ad libitum, and standard diet). Prior to the experiment, the rats were allowed to acclimatize for a period of one week to reduce environmental stress. The animal procedures were conducted in accordance with the Mexican Official Standard NOM-062-ZOO-1999 [36].

4.2. Drugs

Drugs were purchased from Sigma–Aldrich (St. Louis, MO, USA). All drugs were dissolved in saline solution 0.9%. Drug concentrations were prepared in such a way that the necessary dose could be injected in a volume of 2 mL/kg by both subcutaneous intraperitoneal (i.p.) routes. Drugs were administered at the following doses: Metoprine 10 mg/kg i.p. [37], DHE 1 mg/kg i.p. [38], scopolamine 2 mg/kg i.p. [25], piracetam 30 mg/kg i.p. [14], pyrilamine 20 mg/kg i.p. [14], and famotidine 10 mg/kg i.p. [39].

4.3. Histamine Quantification in the Hippocampus

Wistar rats were intraperitoneally (i.p.) administered with the following treatments (n = 6); saline solution, metoprine (10 mg/kg), and DHE (1 mg/kg). After 1 h, three rats from each group were decapitated and the hippocampus from each group were isolated on ice. The same procedure was repeated for the remaining rats, 5 h after i.p. administration.

Hippocampal samples were rinsed with ice-cold PBS (0.01M, pH = 7.4) to remove excess hemolysis blood thoroughly. Tissue pieces were weighed, minced into small pieces, and homogenized, employing an ultrasonic cell disrupter (Tissuelyser) in PBS (4.5 mL PBS were employed for 1 g of tissue) on ice.

Histamine quantification in the hippocampus of Wistar rats was performed by employing a colorimetric Competitive ELISA kit (abcam, E.U.A., catalog number ab285333). The microtiter plate provided in this kit is pre-coated with histamine. During the reaction, histamine in the sample or standard competes with a fixed amount of histamine on the solid phase supporter for sites on the Biotinylated Detection Antibody specific to histamine. The concentration of histamine in the samples is then determined by comparing the O.D. at 450 nm with the standard curve.

4.4. Effects of DHE on the Scopolamine-Induced Amnesia Model

Scopolamine is a compound widely employed to produce memory deficits by disrupting cholinergic neurotransmission [40].

Thus, scopolamine can be employed to induce an amnesia model in rodents to screen anti-amnesic drugs [41–43].

Due to the comments, in the present study, the scopolamine-induced amnesia model was employed to evaluate the effects of dihydroergotamine on memory deficits, employing piracetam as a positive control due to its action as a nootropic [44].

For this propose, forty Wistar rats were randomized into 4 groups (n = 10) to undergo behavioral assays employing the NOR paradigm (days 1 and 2) and MWM (days 3 to 7). Pre-treatments and treatments were administered for each group as follows. Saline group: receive pre-treatment with isotonic saline solution 2 mL/kg i.p. (30 min before

behavioral training), treatment with saline solution 2 mL/kg i.p. (20 min before behavioral training), and saline solution 2 mL/kg i.p. immediately after the training. Scopolamine group: receive pre-treatment with isotonic saline solution 2 mL/kg i.p. (30 min before behavioral training), treatment with saline solution 2 mL/kg i.p. (20 min before behavioral training), and scopolamine 2 mg/kg i.p. immediately after the training. Piracetam group: receive pre-treatment with isotonic saline solution 2 mL/kg i.p. (30 min before behavioral training), treatment with piracetam 30 mg/kg i.p. (20 min before behavioral training), and scopolamine 2 mg/kg i.p. immediately after the training. DHE group: receive pre-treatment with isotonic saline solution 2 mL/kg i.p. (30 min before behavioral training), treatment with DHE 1 mg/kg i.p. (20 min before behavioral training), and scopolamine 2 mg/kg i.p. immediately after the training.

4.4.1. NOR Paradigm

The NOR is a memory test based on the natural propensity of rodents to explore novelty, which confers to the animals the ability to discriminate between novel and familiar entities. This paradigm is especially suited to test the effects of pharmacological interventions on learning and memory [45]. For this reason, the NOR paradigm was employed to evaluate recognition memory in the present study. For this purpose, the experimental apparatus consisted of an open field box ($40 \times 40 \times 40$ cm) made of a black acrylic material. The behavior test was conducted between 9:00 AM and 6:00 PM under dim-light illumination conditions (70 lux). The objects to be discriminated consist of a white circular cap of a culture medium bottle (familiar object) and a yellow rectangular Tupperware (new object). One day prior to the experiment, each rat was habituated to the open field box without any object for 10 min. On the experiment day, rats received pre-treatment and treatment as was previously described. After, each rat was placed in the open field for 5 min and allowed to freely explore the two identical objects (white circular cap of a culture medium bottle), receiving saline solution or scopolamine immediately according to the treatments described for each group. After 3 h of post-training sessions, one old object used during the training session was replaced by a novel object and the rat was left to explore the objects for 2 min. The time spent with each object was recorded and evaluated using ANY-maze software version 7.34 (Stoelting Co, Wood Dale, IL, USA). Both objects presented during the test session were different in texture, color, and size. The open field box was cleaned with 70% ethanol between runs to minimize scent trails. The recognition index was computed using the formula [TB/(TA + TB) * 100], where TA and TB are time spent exploring familiar object A and novel object B, respectively [46]. Exploration of an object was deemed when a rat sniffed or touched the object with its nose and/or forepaws.

4.4.2. MWM Assay

MWM is a widely used tool for assessing spatial learning and memory [47]. The water maze was a stainless steel circular pool, 150 cm in diameter and 60 cm high, filled with 20 ± 1 °C water to a depth of 30 cm. The maze was topographically divided into four equal quadrants with defined release points at each quadrant marked as N, E, S, and W. A hidden circular plexiglas platform (10 cm in diameter) was located in the center of the southeast quadrant and submerged 1.5 cm below the water level, thereby requiring the rats to find the platform based on their memory function. During the training (T1 to T4), the rats received pre-treatment and treatment as previously described. Then, the rats were trained to find the hidden platform during 120 seg. If the rat did not find the platform, it was placed by the experimenter on the platform and kept there for 30 s. Afterwards, the rat was removed from the platform to be gently dried and to immediately receive saline solution or scopolamine, according to the treatments described for each group. The latency and pathway to search the hidden platform were recorded and used to evaluate the ability of learning and memory. Latency to find the hidden platform during T1 to T4, and the time exploring the quadrant where the platform was located versus the opposite quadrant on trial day when the hidden platform was removed, were examined.

4.5. Effect of Blockading H1R and HR2 on the Effects on Memory Produced by DHE in the Scopolamine-Induced Amnesia Model

To determine the contribution of increased histamine levels in the brain on the effects on memory produced by DHE, pre-treatment with pyrilamine (an H1R antagonist) or famotidine (an H2R antagonist) was evaluated. For this purpose, twenty Wistar rats were randomized into 2 groups (n = 10) to undergo behavioral assays employing the NOR paradigm (days 1 and 2) and MWM (days 3 to 7). Pre-treatments and treatments were administered for each group as follows: DHE + Pyrilamine group: receive pre-treatment with pyrilamine 20 mg/kg i.p. (30 min before behavioral training), treatment with DHE 1 mg/kg i.p. (20 min before behavioral training), and scopolamine 2 mg/kg immediately after the training. DHE + Famotidine group: receive pre-treatment with famotidine 10 mg/kg i.p. (30 min before behavioral training), treatment with DHE 1 mg/kg i.p. (20 min before behavioral training), and scopolamine 2 mg/kg i.p. immediately after the training. Behavioral assays for NOR and MWM were performed as described previously in Sections 4.4.1 and 4.4.2.

4.6. Statistical Analysis

Data obtained from all studies were expressed as mean ± SEM. Statistical analysis was performed using paired Student *t*-tests or one-way analysis of variance (ANOVA), using Tukey's test as a post-hoc test. *p*-values of * $p < 0.05$ were considered statistically significant.

5. Conclusions

The present work demonstrated that dihydroergotamine improves memory in the scopolamine-induced amnesia model through increasing histamine levels in the hippocampus by its activity as an HNMT inhibitor.

Author Contributions: Conceptualization, writing—original draft preparation M.H.-R. and E.M.J.; literature search and writing—review and editing M.H.-R. and M.I.N.-V.; supervision, E.M.J., R.M.-R. and M.H.-R. All authors have read and agreed to the published version of the manuscript.

Funding: This research was funded by Consejo Nacional de Humanidades, Ciencias y Tecnologías (CONAHCYT) grant number 320862, PAPIIT-UNAM grant number IN212421, and Instituto Politécnico Nacional grant number 20227029, 20230708, 20241531, and 20241236.

Institutional Review Board Statement: Not applicable.

Informed Consent Statement: Not applicable.

Data Availability Statement: The data reported in this study are available upon request to dra.hernandez.ipn@gmail.com.

Acknowledgments: The authors acknowledge CONACyT for the financial support for this research through grant number 320862. Thanks to UNAM-PAPIIT-IN212421 and Instituto Politécnico Nacional grant numbers 20227029, 20230708, 20241531, and 20241236.

Conflicts of Interest: The authors declare no conflicts of interest.

References

1. Cheng, L.; Liu, J.; Chen, Z. The Histaminergic System in Neuropsychiatric Disorders. *Biomolecules* **2021**, *11*, 1345. [CrossRef] [PubMed]
2. Passani, M.B.; Blandina, P. Histamine receptors in the CNS as targets for therapeutic intervention. *Trends Pharmacol. Sci.* **2011**, *32*, 242–249. [CrossRef] [PubMed]
3. Brown, R.E.; Stevens, D.R.; Haas, H.L. The physiology of brain histamine. *Prog. Neurobiol.* **2001**, *63*, 637–672. [CrossRef] [PubMed]
4. Dong, H.; Zhang, W.; Zeng, X.; Hu, G.; Zhang, H.; He, S.; Zhang, S. Histamine induces upregulated expression of histamine receptors and increases release of inflammatory mediators from microglia. *Mol. Neurobiol.* **2014**, *49*, 1487–1500. [CrossRef]
5. Yoshikawa, T.; Nakamura, T.; Yanai, K. Analysis of brain histamine clearance using genetically engineered mice. *Nihon Yakurigaku Zasshi* **2018**, *152*, 16–20. [CrossRef] [PubMed]

6. Samotaeva, I.S.; Birioukova, L.M.; Midzyanovskaya, I.S.; Kuznetsova, G.D.; Bazyan, A.S.; Tuomisto, L. Metoprine induced behavioral modifications and brain regional histamine increase in WAG/Rij and Wistar rats. *Epilepsy Res.* **2012**, *101*, 148–156. [CrossRef]
7. de Almeida, M.A.; Izquierdo, I. Memory facilitation by histamine. *Arch. Int. Pharmacodyn. Ther.* **1986**, *283*, 193–198.
8. da Silva, W.C.; Bonini, J.S.; Bevilaqua, L.R.; Izquierdo, I.; Cammarota, M. Histamine enhances inhibitory avoidance memory consolidation through a H_2 receptor-dependent mechanism. *Neurobiol. Learn. Mem.* **2006**, *86*, 100–106. [CrossRef]
9. da Silveira, C.K.; Furini, C.R.G.; Benetti, F.; Monteiro, S.D.C.; Izquierdo, I. The role of histamine receptors in the consolidation of object recognition memory. *Neurobiol. Learn. Mem.* **2013**, *103*, 64–71. [CrossRef]
10. Prast, H.; Argyriou, A.; Philippu, A. Histaminergic neurons facilitate social memory in rats. *Brain Res.* **1996**, *734*, 316–318. [CrossRef]
11. Chen, Z. Effect of histamine H3-receptor antagonist clobenpropit on spatial memory of radial maze performance in rats. *Acta Pharmacol. Sin.* **2000**, *21*, 905–910. [PubMed]
12. Chen, Z.; Kamei, C. Facilitating effects of histamine on spatial memory deficit induced by scopolamine in rats. *Acta Pharmacol. Sin.* **2000**, *21*, 814–818. [PubMed]
13. Kamei, C.; Chen, Z.; Nakamura, S.; Sugimoto, Y. Effects of intracerebroventricular injection of histamine on memory deficits induced by hippocampal lesions in rats. *Methods Find. Exp. Clin. Pharmacol.* **1997**, *19*, 253–259. [PubMed]
14. Malmberg-Aiello, P.; Ipponi, A.; Bartolini, A.; Schunack, W. Antiamnesic Effect of Metoprine and of Selective Histamine H_1 Receptor Agonists in a Modified Mouse Passive Avoidance Test. *Neurosci. Lett.* **2000**, *288*, 1–4. [CrossRef] [PubMed]
15. Jiménez, E.M.; Zołek, T.; Hernández-Perez, P.G.; Miranda, R.; Nicolás-Vázquez, M.I.; Hernández-Rodríguez, M. Drug Repurposing to Inhibit Histamine N-Methyl Transferase. *Molecules* **2023**, *28*, 576. [CrossRef]
16. Nomura, H.; Shimizume, R.; Ikegaya, Y. Histamine: A Key Neuromodulator of Memory Consolidation and Retrieval. *Curr. Top. Behav. Neurosci.* **2022**, *59*, 329–353.
17. Nomura, H. Histamine signaling restores retrieval of forgotten memories. *Nihon Yakurigaku Zasshi* **2021**, *6*, 292–296. [CrossRef]
18. Nonaka, A.; Masuda, F.; Nomura, H.; Matsuki, N. Impairment of fear memory consolidation and expression by antihistamines. *Brain Res.* **2013**, *1493*, 19–26. [CrossRef] [PubMed]
19. Naddafi, F.; Mirshafiey, A. The neglected role of histamine in Alzheimer's disease. *Am. J. Alzheimer's Dis. Other Demen.* **2013**, *28*, 327–336. [CrossRef]
20. Yoshikawa, T.; Nakamura, T.; Yanai, K. Histamine *N*-Methyltransferase in the Brain. *Int. J. Mol. Sci.* **2019**, *20*, 737. [CrossRef]
21. Nowak, J.Z.; Zandarowska, E. Effect of amodiaquine on histamine level and histamine-methyltransferase activity in the rat brain. *Arch. Immunol. Ther. Exp.* **1980**, *28*, 927–930.
22. Saper, J.R.; Silberstein, S. Pharmacology of dihydroergotamine and evidence for efficacy and safety in migraine. *Headache* **2006**, *46* (Suppl. S4), S171–S181. [CrossRef] [PubMed]
23. Tfelt-Hansen, P. Clinical Pharmacology of Ergotamine. An Overview. In *Drug-Induced Headache*; Diener, H.C., Wilkinson, M., Eds.; Advances in Applied Neurological Sciences; Springer: Berlin/Heidelberg, Germany, 1988; Volume 5.
24. von Linstow Roloff, E.; Harbaran, D.; Micheau, J.; Platt, B.; Riedel, G. Dissociation of cholinergic function in spatial and procedural learning in rats. *Neuroscience* **2007**, *146*, 875–889. [CrossRef] [PubMed]
25. Hernández-Rodríguez, M.; Arciniega-Martínez, I.M.; García-Marín, I.D.; Correa-Basurto, J.; Rosales-Hernández, M.C. Chronic Administration of Scopolamine Increased GSK3βP9, Beta Secretase, Amyloid Beta, and Oxidative Stress in the Hippocampus of Wistar Rats. *Mol. Neurobiol.* **2020**, *57*, 3979–3988. [CrossRef] [PubMed]
26. Givens, B.; Olton, D.S. Local modulation of basal forebrain: Effects on working and reference memory. *J. Neurosci.* **1994**, *14*, 3578–3587. [CrossRef]
27. Chugh, Y.; Saha, N.; Sankaranarayanan, A.; Datta, H. Enhancement of memory retrieval and attenuation of scopolamine-induced amnesia following administration of 5-HT3 antagonist ICS 205-930. *Pharmacol. Toxicol.* **1991**, *69*, 105–106. [CrossRef] [PubMed]
28. Lissner, L.J.; Wartchow, K.M.; Toniazzo, A.P.; Gonçalves, C.A.; Rodrigues, L. Object recognition and Morris water maze to detect cognitive impairment from mild hippocampal damage in rats: A reflection based on the literature and experience. *Pharmacol. Biochem. Behav.* **2021**, *210*, 173273. [CrossRef] [PubMed]
29. Haas, H.L.; Sergeeva, O.A.; Selbach, O. Histamine in the nervous system. *Physiol. Rev.* **2008**, *88*, 1183–1241. [CrossRef]
30. Wang, H.; Xu, J.; Lazarovici, P.; Quirion, R.; Zheng, W. cAMP Response Element-Binding Protein (CREB): A Possible Signaling Molecule Link in the Pathophysiology of Schizophrenia. *Front. Mol. Neurosci.* **2018**, *11*, 255. [CrossRef]
31. Ambrée, O.; Buschert, J.; Zhang, W.; Arolt, V.; Dere, E.; Zlomuzica, A. Impaired spatial learning and reduced adult hippocampal neurogenesis in histamine H1-receptor knockout mice. *Eur. Neuropsychopharmacol.* **2014**, *24*, 1394–1404. [CrossRef]
32. Schneider, E.H.; Neumann, D.; Seifert, R. Modulation of behavior by the histaminergic system: Lessons from H_1R-and H_2R-deficient mice. *Neurosci. Biobehav. Rev.* **2014**, *42*, 252–266. [CrossRef] [PubMed]
33. Zlomuzica, A.; Ruocco, L.A.; Sadile, A.G.; Huston, J.P.; Dere, E. Histamine H1 receptor knockout mice exhibit impaired spatial memory in the eight-arm radial maze. *Br. J. Pharmacol.* **2009**, *157*, 86–91. [CrossRef]
34. Dai, H.; Kaneko, K.; Kato, H.; Fujii, S.; Jing, Y.; Xu, A.; Sakurai, E.; Kato, M.; Okamura, N.; Kuramasu, A.; et al. Selective cognitive dysfunction in mice lacking histamine H1 and H2 receptors. *Neurosci. Res.* **2007**, *57*, 306–313. [CrossRef]

35. Piechal, A.; Blecharz-Klin, K.; Joniec-Maciejak, I.; Pyrzanowska, J.; Krzysztoforska, K.; Mirowska-Guzel, D.; Widy-Tyszkiewicz, E. Dihydroergotamine affects spatial behavior and neurotransmission in the central nervous system of Wistar rats. *Ann. Agric. Environ. Med.* **2021**, *28*, 437–445. [CrossRef] [PubMed]
36. de Aluja, A.S. Laboratory animals and official Mexican norms (NOM-062-ZOO-1999). *Gac. Med. Mex.* **2002**, *138*, 295–298.
37. Lecklin, A.; Eriksson, L.; Leppäluoto, J.; Tarhanen, J.; Tuomisto, L. Metoprine-induced thirst and diuresis in Wistar rats. *Acta Physiol. Scand.* **1999**, *165*, 325–333. [CrossRef] [PubMed]
38. Rivera-Mancilla, E.; Avilés-Rosas, V.H.; Manrique-Maldonado, G.; Altamirano-Espinoza, A.H.; Villanueva-Castillo, B.; Maassen-VanDenBrink, A.; Villalón, C.M. The role of α1- and α2-adrenoceptor subtypes in the vasopressor responses induced by dihydroergotamine in ritanserin-pretreated pithed rats. *J. Headache Pain* **2017**, *18*, 104. [CrossRef]
39. Świąder, M.J.; Czuczwar, S.J. Interaction of famotidine, an H_2 histamine receptor antagonist, with conventional antiepileptic drugs in mice. *Pharmacol. Rep.* **2014**, *66*, 485–491. [CrossRef]
40. Levin, E.D.; Rose, J.E.; McGurk, S.R.; Butcher, L.L. Characterization of the cognitive effects of combined muscarinic and nicotinic blockade. *Behav. Neural Biol.* **1990**, *53*, 103–112. [CrossRef]
41. Katiyar, P.; Singh Rathore, A.; Banerjee, S.; Nathani, S.; Zahra, W.; Singh, S.P.; Sircar, D.; Roy, P. Wheatgrass extract imparts neuroprotective actions against scopolamine-induced amnesia in mice. *Food. Funct.* **2022**, *13*, 8474–8488. [CrossRef]
42. Mahnashi, M.H.; Ashraf, M.; Alhasaniah, A.H.; Ullah, H.; Zeb, A.; Ghufran, M.; Fahad, S.; Ayaz, M.; Daglia, M. Polyphenol-enriched *Desmodium elegans* DC. ameliorate scopolamine-induced amnesia in animal model of Alzheimer's disease: In Vitro, In Vivo and In Silico approaches. *Biomed. Pharmacother.* **2023**, *165*, 115144. [CrossRef] [PubMed]
43. Retinasamy, T.; Shaikh, M.F.; Kumari, Y.; Othman, I. Ethanolic Extract of Orthosiphon stamineus Improves Memory in Scopolamine-Induced Amnesia Model. *Front. Pharmacol.* **2019**, *10*, 1216. [CrossRef] [PubMed]
44. Piercey, M.F.; Vogelsang, G.D.; Franklin, S.R.; Tang, A.H. Reversal of scopolamine-induced amnesia and alterations in energy metabolism by the nootropic piracetam: Implications regarding identification of brain structures involved in consolidation of memory traces. *Brain Res.* **1987**, *424*, 1–9. [CrossRef] [PubMed]
45. Antunes, M.; Biala, G. The novel object recognition memory: Neurobiology, test procedure, and its modifications. *Cogn. Process.* **2012**, *13*, 93–110. [CrossRef] [PubMed]
46. Batool, Z.; Sadir, S.; Liaquat, L.; Tabassum, S.; Madiha, S.; Rafiq, S.; Tariq, S.; Batool, T.S.; Saleem, S.; Naqvi, F.; et al. Repeated administration of almonds increases brain acetylcholine levels and enhances memory function in healthy rats while attenuates memory deficits in animal model of amnesia. *Brain Res. Bull.* **2016**, *120*, 63–74. [CrossRef]
47. Othman, M.Z.; Hassan, Z.; Che Has, A.T. Morris water maze: A versatile and pertinent tool for assessing spatial learning and memory. *Exp. Anim.* **2022**, *71*, 264–280. [CrossRef]

International Journal of
Molecular Sciences

MDPI

Review

Smelling TNT: Trends of the Terminal Nerve

Wael Abu Ruqa [1,†], Fiorenza Pennacchia [1], Eqrem Rusi [2,†], Federica Zoccali [1], Giuseppe Bruno [2], Giuseppina Talarico [2], Christian Barbato [3,*] and Antonio Minni [1,4,*]

[1] Department of Sense Organs, Sapienza University of Rome, Policlinico Umberto I, 00161 Roma, Italy; aburuqa.1796600@studenti.uniroma1.it (W.A.R.); pennacchia.1748833@studenti.uniroma1.it (F.P.); federica.zoccali@uniroma1.it (F.Z.)
[2] Department of Human Neuroscience, Sapienza University of Rome, 00185 Rome, Italy; eqrem.rusi@uniroma1.it (E.R.); giuseppe.bruno@uniroma1.it (G.B.); giuseppina.talarico@uniroma1.it (G.T.)
[3] Institute of Biochemistry and Cell Biology (IBBC-CNR), Sapienza University Rome, Policlinico Umberto I, 00161 Roma, Italy
[4] Division of Otolaryngology-Head and Neck Surgery, ASL Rieti-Sapienza University, Ospedale San Camillo de Lellis, 02100 Rieti, Italy
* Correspondence: christian.barbato@cnr.it (C.B.); antonio.minni@uniroma1.it (A.M.)
† These authors contributed equally to this work.

Abstract: There is very little knowledge regarding the terminal nerve, from its implications in the involvement and pathogenesis of certain conditions, to its embryological origin. With this review, we try to summarize the most important evidence on the terminal nerve, aiming to clarify its anatomy and the various functions attributed to it, to better interpret its potential involvement in pathological processes. Recent studies have also suggested its potential role in the control of human reproductive functions and behaviors. It has been hypothesized that it plays a role in the unconscious perception of specific odors that influence autonomic and reproductive hormonal systems through the hypothalamic–pituitary–gonadal axis. We used the PubMed database and found different articles which were then selected independently by three authors. We found 166 articles, of which, after careful selection, only 21 were analyzed. The terminal nerve was always thought to be unimportant in our body. It was well studied in different types of animals, but few studies have been completed in humans. For this reason, its function remains unknown. Studies suggest a possible implication in olfaction due to the anatomical proximity with the olfactive nerve. Others suggest a more important role in reproduction and sexual behaviors. New emerging information suggests a possible role in Kallmann syndrome and COVID-19.

Keywords: terminal nerve; olfactory dysfunctions; Kallmann syndrome; GnRH; SARS-CoV-2

Citation: Ruqa, W.A.; Pennacchia, F.; Rusi, E.; Zoccali, F.; Bruno, G.; Talarico, G.; Barbato, C.; Minni, A. Smelling TNT: Trends of the Terminal Nerve. *Int. J. Mol. Sci.* **2024**, *25*, 3920. https://doi.org/10.3390/ijms25073920

Academic Editor: Claudia Ricci

Received: 14 March 2024
Revised: 29 March 2024
Accepted: 30 March 2024
Published: 31 March 2024

1. Introduction

The terminal nerve was first discovered in 1878 by Frisch in elasmobranchs, a subclass of Chondrichthyes, cartilaginous fish. Years later, it was also discovered in humans. More precisely, Johnston described it in human embryos in 1913 and in human adults the following year. Simultaneous with discoveries about its anatomical course and embryological studies, there had been a succession of names attributed to this nerve. Initially, it was named the following: nerve of Pinkus, tractus olfacto-commissuralis, new nerve, terminal nerve, nerve nulla (i.e., nothing, zero), and cranial nerve 13. Then, it was renamed "nervus terminalis" since it entered the region of the lamina terminalis, which is the currently accepted nomenclature [1]. The Latin name nervus terminalis, which has now been replaced by the names terminal nerve and terminalis nerve (TN), refers to a rudimentary structure found in human and higher mammals, which can be found in fetal stages. Still, there is a theoretical interest in its function [2,3].

It is a highly preserved and versatile nerve, located just above the olfactory bulbs in humans and different vertebrate species. In most instances, its fibers extend from the front

part of the brain to the olfactory and nasal epithelia. As the name suggests, this nerve penetrates the lamina terminalis of the forebrain, the slender layer of gray matter above the optic chiasm, forming the medial section of the anterior wall of the third ventricle [4] (Figure 1). In its initial segment, it runs within the nasal cavity, being one of the five systems that innervate the nasal cavity (the terminal system, the vomeronasal system, the olfactory system, the septal organ, and the trigeminal system). The fourth system originates from the original olfactory placode [4]. Within the nasal cavity, its fibers intermingle with those of the vomeronasal and olfactory nerves, respectively. However, the terminal nerve fibers travel medial to the nerve fibers of the 1st cranial nerve and into the anterosuperior portion of the nasal cavity. The fibers of the TN branch from the ganglion cells, towards the olfactory bulb and, intracranially, its fibers run independently. Studies conducted on embryos using high-resolution imaging have shown that medially the TN fibers are near the vomeronasal (VN) fibers and laterally, the olfactory fibers reach the olfactory bulb [4]. The terminalis nerve and the vomeronasal nerves penetrate through the cribriform plate, where the plexiform fibers of the terminalis nerve can be distinguished along the ganglion cell bodies that form the terminal ganglion. The plexus of the terminalis nerve is formed by numerous smaller strands that branch and anastomose with each other [2]. Ventrally on the surface of the brain and laterally to the olfactory bulbs, the terminalis nerve and the vomeronasal nerves resume their course along the fibers of cranial nerve I. The terminalis nerve plexus runs parallel to the olfactory tracts in the vicinity of the septal region, near the bifurcation of the anterior and middle cerebral arteries. Its fibers are non-myelinated and run alongside the dura mater, passing through the subarachnoid space and ultimately connecting to the pia mater in the gyri of the frontal lobes. It enters the brain through the lamina terminalis, implying penetration into the prosencephalon [1] (Figure 1). Roussel et al. have confirmed this in their work on the landmarks used during endonasal skull base surgery [5]. Many reports suggest that the terminal nerve projects various neuroanatomical structures, such as the medial pre-commissural septum, including the medial septal nucleus. It also sends fibers to the nasal mucosa and ventral rostral brain structures, mainly in olfactory and limbic areas (i.e., amygdala, hypothalamic nuclei) [6]. We have learned very little about this nerve since its discovery to the present, so it is not mentioned in most anatomy textbooks. Most studies on the TN have been conducted in animals, and a broader view of the TN in humans is important. In this brief review, we try to summarize what we know about this nerve, its anatomy, the hypotheses regarding its functions, and its possible pathological implications in human diseases.

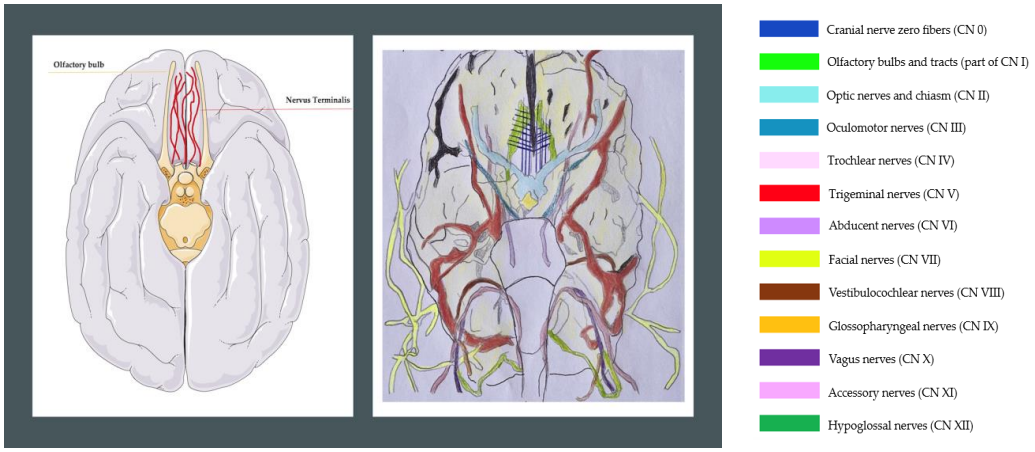

Figure 1. Representation of the ventral aspect of the human brain. The terminal nerve is reticulated in red (digital image on the left). On the right, the terminal nerve (TN) is reticulated in blue. The bilateral plexus of nerve fascicles of nervus terminalis covering the gyrus rectus of the human brain. This is an original drawing, showing the TN, during a surgery performed as part of the Specialization Program in Otolaryngology, La Sapienza University, Rome. "The accuracy of the handwriting cannot be assured since there is no verification".

2. Materials and Methods

For this research, the "PubMed" database was used. The terms used were as follows: (nervus terminalis OR Terminal Nerve OR cranial nerve 0 OR cranial nerve XIII). This search resulted in 166 possible articles. All non-English language articles and articles for which the full text was not available were excluded. We also had to exclude all the non-free studies that could not be accessed by Sapienza's institutional credentials. Of the remaining articles, three independent reviewers (F.P., W.A.R., and E.R.) checked them by titles and abstracts, selecting those relevant to the review topic. In this phase, most of the excluded articles were performed on animals without important correlations/implications for humans. We did not use a filter for human studies it our PubMed search because we did not want to risk excluding studies performed on animals with possible repercussions for humans. In the end, 145 studies were excluded, while the remaining 21 were analyzed and are discussed in this review. (Figure 2) (Table 1).

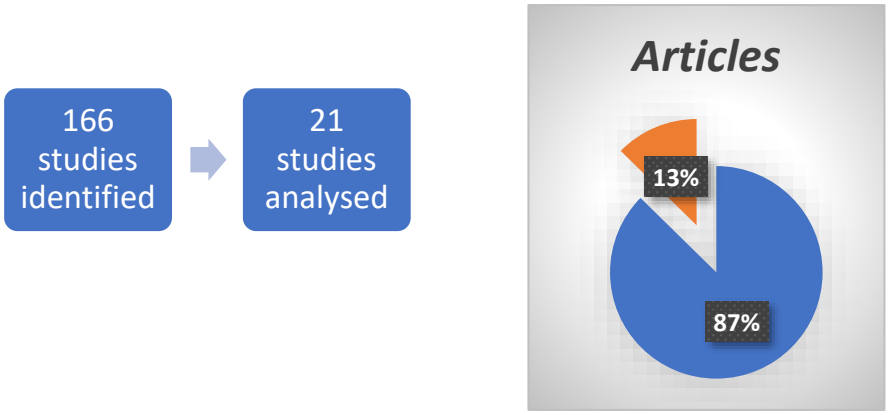

Figure 2. Left: From 166 studies 145 were excluded as non-relevant for our study; these include those in non-English languages and those with full text not available. Right: blue represents excluded articles; orange represents included and analyzed articles, as a percentage.

Table 1. This table summarizes the results extracted from the selected 21 articles. A summary of each is reported.

REFERENCE	ABSTRACT
[1]	The TN appears to have the same origin as the olfactory cells: the neural crest. Like other cranial nerves, its embryonic origins appear to lie in synergistic interactions during development between the neural and sensory crest placode.
[2]	Through the study of TN neurons in postnatal mice infected with a virus that traverses the olfactory pathways, an increase in gonadotropin-releasing hormone (GnRH) and choline acetyltransferase (CHAT) was identified.
[4]	The TN begins to develop at the edge of migrating neural crest cells with the olfactory and adenohypophyseal placodes.
[6]	The neural crest contributes to the subset of neurons that secrete GnRH. The TN neurons, indeed, appear to originate from the neural crest.
[7]	The TN seems to play a role in the olfactory function and in the reproductive function through the secretion of LHRH. Indeed, in women, the sense of smell is most acute during ovulation.
[8]	The TN shows a similar distribution of LHRH in both juvenile and adult animals. However, most of LHRH activity is greater in the adult brain.
[9]	Many studies on the fetal nervous system of animals have demonstrated the presence of cells that release gonadotropins, such as gonadotropin-releasing hormone (GnRH). The presence of gonadotropic cells present on the TN fibers was analyzed.
[10]	Through cadaveric dissections of animals and subsequent immunocytochemical procedures, TN GnRH fibers were found in the olfactory bulb region.

Table 1. *Cont.*

REFERENCE	ABSTRACT
[11]	In studies conducted on Atlantic stingrays, by stimulating the peripheral nervous trunk and analyzing the particles present in the cerebrospinal fluid, the levels of a compound like GnRH increase in the TN.
[12]	GnRH, the olfactory pathway is further distinguished by the existence of immunoreactive tyrosine hydroxylase. This cellular population has been observed within the nasal region and the human embryonic telencephalon, specifically among catecholaminergic neurons. These identical regions display positivity in GnRH investigations.
[13]	In relation to GnRH, both forms of this molecule are found in the brains of all significant vertebrate species. The research that confirmed the existence of these two forms of GnRH was carried out on adult and juvenile lungfish (Protopterus annectens) utilizing high-performance liquid chromatography and radioimmunoassay with specialized antisera. Given the identification of two forms of GnRH in animals, it could be hypothesized that forebrain and midbrain neurons might regulate species- and region-specific GnRH activity [13,14]
[14]	Analysis of GnRH highlighting the presence of mammalian, salmon, and chicken II GnRH and various pituitary hormones. From this analysis, both sGnRH and mGnRH appear.
[15]	Neuropeptide Y (NPY) plays a key role in the regulation of gonadotropin-releasing hormone (GnRH).The study shows associations and colocalizations of GnRHs in the ganglion cells of the terminal nerve, as well as in the hypothalamus.
[16]	Norepinephrine (NE) also exhibits activity on the TN activity level, and ganglion response to electrical stimuli is influenced by both NE and acetylcholine (ACh). ACh can have both excitatory and inhibitory effects on TN ganglion cells.
[17]	It was hypothesized that olfactory dysfunction in patients with COVID-19 may be correlated with the reduced average volume of the olfactory bulb and tract. The neurons of the terminal nerve express ACE2, and through the binding of the spike protein and this receptor, SARS-CoV-2 can infect these cells.
[18]	TN serves as a direct connection between the olfactory epithelium and the hypothalamus, bypassing the olfactory bulb. This indicates that the nervus terminalis can be a route for SARS-CoV-2 to reach the brain. This could explain why there is so much variability in the neuroinvasion of the brain, a characteristic that could not be explained by the classical route theory. The hypothesis that SARS-CoV-2 travels through the olfactory pathway has not been confirmed. This is because olfactory receptor neurons do not express ACE2 and TMPRSS2, which are the proteins which the virus penetrates. Therefore, they are not infected, or very rarely. For this reason, there are doubts about the ability of SARS-CoV-2 to use this pathway [18,19]. In the end, biopsies of the olfactory epithelium from COVID-19 patients showed that the virus infected non-neuronal cells. This has made it clear that anosmia is caused by the loss of cell function support and not the loss of neurons in the olfactory bulb [18]. This could justify the rapid appearance of viral particles in the hypothalamus, which do not localize in the parenchyma of the olfactory bulb but are instead found at the superficial margin of the olfactory bulb, where the neurons of the terminal nerve reside [18–20].
[19]	As reported in [18]
[20]	As reported in [18]
[21]	As reported in [18]

3. Results

3.1. Embryology

The specific embryological origin of the TN remains partly enigmatic. While some authors have reported that the nerve's origin is from the olfactory placode, where olfactory cells also originate, others indicate that it arises from the neural crest. The most widely accepted hypothesis is that, like other cranial nerves, its embryological origins lie in synergistic interactions during development between the neural crest and sensory placodes [1]. The terminalis nerve forms at the limit of migrating neural crest cells with the olfactory and adenohypophyseal placodes [4]. Furthermore, the neural crest may contribute to the subset of GnRH-secreting neurons [6].

3.2. Neurophysiology and Functional Aspects

Although there are different ideas about the functions of this nerve, in this paragraph we will delve into its potential functions (Figure 3). It is thought that the nerve does not play a role in the olfactive function but in the reproductive function. It secretes luteinizing hormone-releasing hormone (LHRH), which has been associated with reproductive behavior. It is speculated that the nerve's function in humans is to directly detect or more probably to modulate the activity of the olfactory epithelium, making pheromones more detectable. Pheromones are species-specific odors involved with sexual identification and arousal and therefore are important for mate selection. For example, the woman's sense of smell is most acute when she is ovulating. Odors are perceived differently throughout the menstrual cycle, making the same odors more pleasant and causing sexual arousal [7]. On the other hand, male odors have been shown to increase male sociosexual behavior. Also, a practical effect can be the phenomenon of women living together who tend to synchronize their menstrual cycles [7]. The TN may trigger hormonal responses, independently or together with other circuits, such as the kisspeptin neural network (mainly localized in the preoptic and infundibular regions of the hypothalamus) [7]. Also, the hormone GnRH/LHRH appears to serve as a coordinating system for the multitude of events occurring during reproduction, including changes in olfactory sensitivity to pheromones [4,7]. Luteinizing hormone-releasing hormone (LHRH) regulates the secretion of both the luteinizing hormone (LH) and follicle-stimulating hormone (FSH) from pituitary gonadotropic cells. The TN shows a similar distribution of LHRH in both juvenile and adult animals. However, most of the activity of LHRH is greater in the adult brain [8].

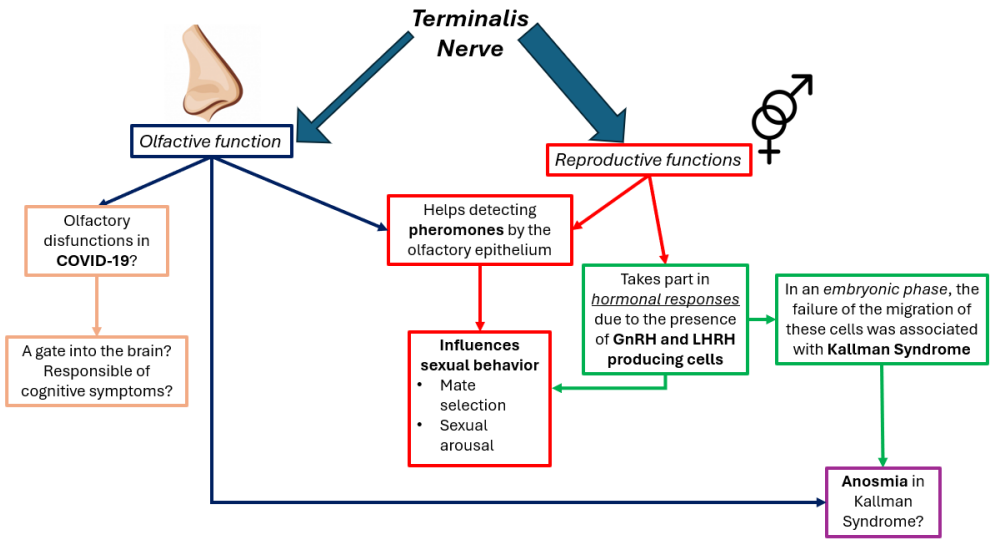

Figure 3. The figure illustrates the new proposed functions and pathological correlations of the terminalis nerve (TN). The first arrows have a different shape, demonstrating that most of the studies propose a more impactful role of TN in the reproductive function than in the olfactive one. Nevertheless, one does not exclude the other. Also, in this scheme associations between these two functions are present. Different colors were used: the left boxes (salmon color) show the hypothesis that COVID-19 is associated with the TN, while the red boxes show the role of this nerve in reproduction. The green boxes explain a possible etiology of Kallmann syndrome, in which a characteristic symptom is anosmia (violet box).

3.3. Neuronal Immunochemical Studies of the Nervus Terminalis

Many studies on the fetal nervous system of animals have shown the presence of gonadotropin-releasing cells. The presence of gonadotropic cells on nerve fibers was analyzed with GnRH immunoreactive molecular techniques. In the hypothalamus, groups of GnRH neurons are found as early as 20 weeks of gestation, as well as in the adult human

brain [9]. The hypothalamic population of GnRH neurons appears to continue rostrally in the TN in the adult and fetal human olfactory system. Standard immunocytochemical procedures seem to confirm the same origin from the olfactory placode. Through the cadaveric dissections of animals (South African clawed frogs, *X. laevis*) and subsequent immunocytochemical procedures, TN GnRH fibers were found in the olfactory bulb region. The fibers give rise to a dense plexus located ventrally to the bulb. Other fibers are also carried to more caudal levels of the telencephalon and diencephalon [10]. As another study shows, stimulating the peripheral trunk of the TN increases the levels of a GnRH-like compound in the cerebrospinal fluid of Atlantic stingrays [11]. This study was conducted in vivo on the species Dasyatis sabina by stimulating the peripheral nerve stem and analyzing the particles found in the cerebrospinal fluid [11]. In addition to GnRH, the olfactory pathway is also characterized by the presence of immunoreactive tyrosine hydroxylase. This cell population has been detected in the nasal region and the human embryonic telencephalon at the level of catecholaminergic neurons. These same areas are positive for GnRH research [12]. Considering GnRH, two forms of this molecule are present in the brains of all major vertebrate species. The study that demonstrated the presence of the two forms of GnRH was conducted on adult and juvenile lungfish (*Protopterus annectens*) using the high-performance liquid chromatography technique and radioimmunoassay with specific antisera [13]. As in the previous study, the analysis of GnRH led to the same conclusions, highlighting the presence of mammalian, salmon, and chicken II GnRH and various pituitary hormones, studied with double label immunocytochemistry [14]. Neuropeptide Y (NPY), instead, plays a key role in the regulation of gonadotropin-releasing hormone (GnRH), although its activity is not completely understood. A study of the forebrain of the teleost *Clarias batrachus* investigated one of the main roles of NPY in the regulation of GnRH. Dual immunocytochemistry shows associations and colocalizations of the two peptides in neurons of the olfactory system, and in the ganglion cells of the terminal nerve, as well as in the hypothalamus [15]. Finally, other molecules, such as Norepinephrine (NE), also have activity on TN. Norepinephrine (NE) has been shown to directly affect the TN activity level, and the ganglion response to electrical stimuli is influenced by both NE and acetylcholine (ACh), which demonstrated a variable effect on the total spectral power of TN activity. Given its activity, ACh can have both excitatory and inhibitory effects on TN ganglion cells [16].

3.4. Terminalis Nerve and Diseases

One of the pathognomonic symptoms of COVID-19 is olfactory dysfunction (Figure 3). The cause of this symptom is probably related to the reduced average volume of the olfactory bulb and tract in COVID-19 patients compared with the controls [17]. Theoretically, this can be explained by the neuroinvasive capacity of SARS-CoV-2. The hypothesis that SARS-CoV-2 travels via the olfactory route has not been confirmed. First, olfactory receptor neurons do not express the virus entry proteins ACE2 and TMPRSS2 and, therefore, are not infected, or extremely rarely infected, by SARS-CoV-2. This raises questions about the ability of SARS-CoV-2 to enter these neurons and travel along their axons into the brain. Moreover, the virus appears much more rapidly at downstream targets, which is inconsistent with axial transport and multiple transsynaptic transfers [18,19]. On the other hand, the nervus terminalis neurons express ACE2, and through the binding of the spike protein and this receptor, SARS-CoV-2 can infect these cells [17]. Furthermore, this cranial nerve serves as a direct connection between the olfactory epithelium and the hypothalamus, bypassing the olfactory bulb. Afterward, SARS-CoV-2 can penetrate the blood–brain barrier and can reach various neural circuits connected to the hypothalamus. This indicates that the nervus terminalis can be a route for the virus to reach the brain. This could explain why there is so much variability in the neuroinvasion of the brain, a characteristic that could not be explained by the classical route theory [18]. This hypothesis also justifies the rapid appearance of viral particles in the hypothalamus, which do not localize in the parenchyma of the olfactory bulb but are instead found at the superficial margin of the olfactory bulb,

where the neurons of the terminal nerve reside [18,20,21]. The major study in favor of this theory is the one conducted by Bilinska et al. They studied nervus terminalis neurons in postnatal mice, double-labeled with antibodies against ACE2, gonadotropin-releasing hormone (GnRH), and choline acetyltransferase (CHAT), proving the route for the virus from the nasal epithelium, possibly via the innervation of Bowman's glands, to brain targets, including the telencephalon and diencephalon [2]. In the end, biopsies of the olfactory epithelium from COVID-19 patients showed that the virus infected non-neuronal cells, defined as supporting cells of the olfactory epithelium. This implies that anosmia is caused by the loss of cell function support and not the loss of neurons in the olfactory bulb [18]. In the preceding section, we discussed the possible functions of the nervus terminalis, explaining its possible role in the reproductive system and how it modulates the olfactive system. The traumatic loss of the olfactory nerves is anecdotally associated with a reduction in libido [2]. Furthermore, it is thought that this nerve is implicated in Kallmann syndrome, a genetic form of hypogonadotropic hypogonadism. In more detail, in the embryonic phase, the failure of the migration of LHRH cells along the TN from the neural crest to the hypothalamus (through the olfactory placodes) results in the absence of LHRH cells, causing the diseases. Also, this syndrome is characterized by anosmia. The glycoprotein called "Anosmin-1", encoded by the KAL1 gene, is defective in human Kallmann syndrome [4]. The neuromodulatory role of the terminal nerve in reproductive behavior via GnRH establishes an important link with hypothalamic nuclei, specifically the preoptic (POA) and the infundibular (INF) nuclei, which form the "kisspeptin neuronal (KP) network" [6]. Over time, the KP circuit has been associated with various biological functions. Through the release of GnRH from the hypothalamus, it is linked to diverse endocrinological conditions such as sexual development and human reproductive functions. The KP network regulates the response of gonadotropins (FSH and LH), inducing the synthesis and release of hormones crucial for reproduction. There are suggestions that the TN may trigger hormonal responses independently of other pathways, such as the KP neural circuit. In addition to this, the kisspeptin system participates in various circuits within the limbic system that mediate anxiety, fear, other negative emotions, and olfaction [1]. The afferent neurons of the KP network are poorly studied. The TN has many projections like the nasal mucosa and the amygdala, but also the hypothalamus. Projections that reach one or both hypothalamic nuclei may represent a potential afferent component to the KP neurons regulating GnRH secretions. To date, this interesting hypothesis is only speculation [6].

4. Discussion

The TN is well-developed in vertebrates, but it exists only as a 'residue' in the adult human brain (Figure 3). This evolutionary divergence may reflect a different "olfactory ecosystem," driven by olfaction, climate change, and the potential evolution of the teleost fish forebrain [22]. Among the selected articles in this brief review, few deal with the human anatomy and physiology of the TN. However, some publications based on the study of the animal TN shows some interesting observations in humans, such as the migration from the olfactory placode to the central nervous system via the nasal septum. Also, studies conducted on embryos aim to demonstrate the presence of GnRH neurons in components of the adult and fetal human olfactory system [9]. According to this study, the migration of GnRH neurons in the fetal brain begins before the 10th week of gestation and these, once migrated, reach their maturity by the 20th week of gestation. To our knowledge, the projections, established during GnRH migration, continue to persist in the adult human olfactory system. The presence of GnRH neurons within the olfactory system in both the adult and fetal human brain, mirrors what has been found in other mammal species as well. Thus, GnRH neurons originate in the olfactory placode and migrate into the forebrain through the olfactory system. This also explains the hypogonadotropic hypogonadism that manifests as an olfactory deficiency in Kallmann syndrome [9]. Studies on Kallmann syndrome pathogenesis found that anosmin-1 (KAL1 gene) promotes axon outgrowth from the olfactory bulb and the branching into the olfactory cortex [23]. Furthermore, KAL1 is

necessary for the contact between different structures (olfactory bulb and olfactory and vomeronasal axons, with regions of the telencephalon). These axons form the tracks that permit GnRH1 neurons to migrate into the brain. The loss of KAL1/Anosmin-1 could lead not only to olfactory dysfunction, but also to hypogonadotropic hypogonadism, which is observed in Kallmann syndrome [23].

Further studies showed the role of the TN. The pioneer neurons composing the TN showed expression of Prokineticin 2/Prokineticin-Receptor-2 (Prokr2) genes, loss-of-function mutations of which are responsible for this syndrome [24]. These data underline that a correct genetic expression of the TN Pioneer neurons guarantees the correct development of the olfactory system. Studies carried out on mouse models showed abundant gene expression in the single-cell RNA of mutated Prokr2 genes in animals affected by Kallmann syndrome [24]. Studying the mechanisms that correlate smell and the GnRH-1 system may open a new frontier for clinical research because little is yet known about the impact that the gonadal axis has on smell and vice-versa. Another consideration that we need to make is the importance of pheromones in humans. The fact that GnRH levels are altered by pheromones indicates that pheromones are not only important in mate selection, maternal behavior, and sexual arousal, but can also have a role in different pathologies such as infertility or sexual arousal difficulties. The role of pheromones in these pathologies has remained unexplored until now [7]. In vertebrates, the sense of smell plays a very important role in various behaviors including mate choice, food selection, homing, and escape from predators. The olfactory system is in close relationship with the limbic system, which is a region of the brain that plays an important role in various functions such as memory, emotions, interactions with the endocrine system, and learning. The interaction between neuromodulatory hormones and odor signals is at the basis of the behaviors that allow an animal to adapt to an environment [25]. These odor signals are also important for marine species, allowing them to adapt to the environment, as in the teleost. The anterior brain, also known as the Rhinoencephalon, receives many inputs from olfactory sources, which can integrate it and generate behavioral responses to stimuli within social, emotional, or motivational contexts crucial for survival, including mating, aggression, and defense. Like other sensory systems, the size of the neural tissue within the central nervous system is proportional to the importance of the function performed. Animals that rely heavily on olfactory signals have a markedly different proportion of dedicated space. In humans, 50% of the genes coded for olfactory receptors are present [25–28]. Returning to the terminal nerve, the extensive projections of TN GnRH neurons in the forebrain, together with their endogenous rhythmic activities, suggest that they may act in the global modulation of circuits to adapt to changes in hormonal or environmental conditions in the animal [29]. Moreover, a demonstration is that the TN GnRH3 network and other forebrain regions participate in the neuromodulation of the olfactory system and thus play an important role in other mammals and fishes [30]. LHRH is an important component of the TN in other mammals as well, with localization mainly in nasal areas and developmental stages [8]. It is known that circulating estrogenic levels regulate the activity of GnRH neurons; a decrease in GnRH has been observed following oophorectomy and, on the other hand, an increase in GnRH has been observed following the administration of estrogens, and similar observations have also been made in humans [10]. Since two forms of GnRH have been identified in animals, it could therefore be hypothesized that the forebrain and midbrain neurons could modulate species- and region-specific GnRH activity [13,14]. Since late 2019 to early 2020, many researchers have focused on COVID-19 with a wide view. The hypothesis that TN could be "the gate" for SARS-CoV-2 entering the brain was very interesting. Recent studies suggested that, as was previously stated, SARS-CoV-2 was isolated along the superficial portion of the olfactory bulb, where the terminal nerve is located, and not in the parenchyma (where the cells of the olfactory nerve are located) [18,21]. This could suggest that the terminal nerve may be a communication pathway with the central nervous system that has not yet been studied, with important physio-pathological meanings. As consequence, the TN could be used as a model to study

viruses with a neuroinvasive capacity to fine-tune cognitive performance. The implication is that the nervus terminalis could also be an explanation for long COVID consequences, and post-COVID syndromes. Long COVID conditions could become an important public health issue in the future, considering that these post-COVID symptoms can last for years [31]. In this regard, neurological symptoms are very frequent and, in many cases, have an important impact on our patients' lives. The most common symptoms are anosmia and cognitive decline, perceived as memory loss and difficulty concentrating [32,33]. Researchers have proposed different mechanisms of how SARS-CoV-2 could enter the brain and cause neuronal damage to explain the neurological symptoms of long COVID. A new study published by Sauve et al. [34] associates cognitive decline with low testosterone levels, due to alterations in the HPG (hypothalamic-pituitary-gonadal) axis, specifically GnRH secretion (reduction or alterations of the pulsating release of the hormone). The authors found that the association between anosmia, cognitive decline, and hypogonadism is like swhat they observed in Trisomy 21 (Down syndrome), which is known as a neurodegeneration process similar to Alzheimer's disease [35]. The association between cognitive decline in Trisomy 21 and GnRH alterations was observed also in an animal model by Manfredi-Lozano and colleagues, where the replacement of GnRH improved cognition [36]. These observations plausibly suggest that the role of the TN might be larger than just as "a new route of entry into the CNS". TN impairment could be the reason not only for anosmia but also for the HPG and GnRH alterations that determine hormonal changes that can be responsible for the cognitive deficits observed in long COVID patients. The additive aspect of anosmia and the neuroinvasive capacity of SARS-CoV-2 was elucidated by De Melo et al. [37]. According to these authors, infected animals, i.e., golden hamsters, had different symptoms depending on which virus they encountered. Regardless of the viral variants, all forms are neuroinvasive. Thus, neuroinvasion and anosmia are independent phenomena of SARS-CoV-2 infection. (62.5% of animals infected with the main Wuhan strain presented anosmia while 12% were infected with Gamma and none (0%) of the animals infected with Delta and Omicron/BA.1 showed signs of anosmia). Also, another factor is the viral load with which the hamster is inoculated. The study shows that despite the presence of the virus in the olfactory bulbs, animals infected with a lower infective dose had a lower incidence of olfactory changes [37]. Infection of the olfactory bulb is common regardless of the variant, but olfactory dysfunction is not as common. An inflammatory response was observed in the olfactory bulb at the same time (regardless of variant), but even the inflammation of this region is not sufficient to explain why in some forms, odor perception remains the same in the golden hamster. One idea may concern the dysregulation of the olfactory mucosa, as recovery is related to the regeneration of the olfactory epithelium in hamsters [37]. Could the TN also influence the variability of the olfactory dysfunction? It is very important to note that the timing of the deciliation and odorant receptor gene downregulation is fundamental to untangling the route of COVID-19 infection [38].

5. Conclusions

Most of the scientific studies on the terminal nerve are conducted on vertebrates. In recent years, there has been an increased interest in identifying the anatomy and physiology of the TN in humans, as it is a highly conserved neural structure. Comparing studies conducted on animals, the terminal nerve is not a vestigial structure as was previously believed, but has a well-defined role, even in humans. The plexiform organization of the TN could have a significant role in the development of the GnRH system, in the modulation of smell, and the physiology of the reproductive system. The more knowledge we have about the terminal nerve, the more we will be able to understand human reproduction, the olfactory system, and their diseases. The need for new anatomical knowledge is important and that the exact location of the TN in humans can be very important to avoid complications in ENT surgeries [39]. In animals, lesions of the nerve were associated with GnRH deficiency [6]. ENT surgeons are essential to the advancement of this knowledge.

In conclusion, a better understanding of nerve anatomy and an easier way to identify this structure in vivo are needed.

Author Contributions: Conceptualization, A.M. and C.B.; methodology, W.A.R., F.P. and E.R.; writing—original draft preparation, W.A.R., F.P. and E.R.; writing—review and editing, W.A.R., F.P., E.R., F.Z. and C.B.; visualization, W.A.R. and F.Z.; resources, G.T. and G.B.; supervision, A.M. and C.B. All authors have read and agreed to the published version of the manuscript.

Funding: This research received no external funding.

Acknowledgments: We acknowledge the surgery staff of the Division of Otolaryngology-Head and Neck Surgery, Ospedale San Camillo de Lellis, Rieti.

Conflicts of Interest: The authors declare no conflict of interest.

References

1. López-Ojeda, W.; Hurley, R.A. Cranial Nerve Zero (CN 0): Multiple Names and Often Discounted yet Clinically Significant. *J. Neuropsychiatry* **2022**, *34*, A4–99. [CrossRef] [PubMed]
2. Vilensky, J.A. The neglected cranial nerve: Nervus terminalis (cranial nerve *N*). *Clin. Anat.* **2014**, *27*, 46–53. [CrossRef] [PubMed]
3. Jin, Z.W.; Cho, K.H.; Shibata, S.; Yamamoto, M.; Murakami, G.; Rodríguez-Vázquez, J.F. Nervus terminalis and nerves to the vomeronasal organ: A study using human fetal specimens. *Anat. Cell Biol.* **2019**, *52*, 278–285. [CrossRef] [PubMed]
4. Peña-Melián, Á.; la Rosa, J.P.C.-D.; Gallardo-Alcañiz, M.J.; Vaamonde-Gamo, J.; Relea-Calatayud, F.; González-López, L.; Villanueva-Anguita, P.; Flores-Cuadrado, A.; Saiz-Sánchez, D.; Martínez-Marcos, A. Cranial Pair 0: The Nervus Terminalis. *Anat. Rec.* **2019**, *302*, 394–404. [CrossRef] [PubMed]
5. Roussel, L.; Patron, V.; Maubert, E.; Escalard, C.; Goux, D.; Beaudouin, V.; Lechapt, E.; Moreau, S.; Hitier, M. New landmarks in endonasal surgery: From nasal bone to anterior cribriform plate including branches of anterior ethmoidal artery and nerve and terminal nerve. *Int. Forum Allergy Rhinol.* **2020**, *10*, 395–404. [CrossRef] [PubMed]
6. Sonne, J.; Reddy, V.; Lopez-Ojeda, W. Neuroanatomy, Cranial Nerve 0 (Terminal Nerve), StatPearls. 2023. Available online: https://www.ncbi.nlm.nih.gov/books/NBK459159/ (accessed on 26 February 2024).
7. Wirsig-Wiechmann, C.R. Function of gonadotropin-releasing hormone in olfaction. *Keio J. Med.* **2001**, *50*, 81–85. [CrossRef] [PubMed]
8. Valverde, F.; Heredia, M.; Santacana, M. Characterization of neuronal cell varieties migrating from the olfactory epithelium during prenatal development in the rat. Immunocytochemical study using antibodies against olfactory marker protein (OMP) and luteinizing hormone-releasing hormone (LH-RH). *Dev. Brain Res.* **1993**, *71*, 209–220. [CrossRef] [PubMed]
9. Kim, K.; Patel, L.; Tobet, S.; King, J.; Rubin, B.; Stopa, E. Gonadotropin-releasing hormone immunoreactivity in the adult and fetal human olfactory system. *Brain Res.* **1999**, *826*, 220–229. [CrossRef] [PubMed]
10. Wirsig-Wiechmann, C.R.; Lee, C.E. Estrogen Regulates Gonadotropin-Releasing Hormone in the Nervus Terminalis of *Xenopus laevis*. *Gen. Comp. Endocrinol.* **1999**, *115*, 301–308. [CrossRef]
11. Moeller, J.F.; Meredith, M. Increase in gonadotropin-releasing hormone (GnRH) levels in CSF after stimulation of the nervus terminalis in Atlantic stingray, Dasyatis sabina. *Brain Res.* **1998**, *806*, 104–107. [CrossRef]
12. Verney, C.; El Amraoui, A.; Zecevic, N. Comigration of tyrosine hydroxylase- and gonadotropin-releasing hormone-immunoreactive neurons in the nasal area of human embryos. *Dev. Brain Res.* **1996**, *97*, 251–259. [CrossRef] [PubMed]
13. King, J.A.; Millar, R.P.; Vallarino, M.; Pierantoni, R. Localization and characterization of gonadotropin-releasing hormones in the brain, gonads, and plasma of a dipnoi (lungfish, *Protopterus annectens*). *Regul. Pept.* **1995**, *57*, 163–174. [CrossRef]
14. Parhar, I.S.; Iwata, M. Gonadotropin releasing hormone (GnRH) neurons project to growth hormone and somatolactin cells in the steelhead trout. *Histochemistry* **1994**, *102*, 195–203. [CrossRef]
15. Gaikwad, A.; Biju, K.; Muthal, P.; Saha, S.; Subhedar, N. Role of neuropeptide Y in the regulation of gonadotropin releasing hormone system in the forebrain of *Clarias batrachus* (Linn.): Immunocytochemistry and high performance liquid chromatography-electrospray ionization-mass spectrometric analysis. *Neuroscience* **2005**, *133*, 267–279. [CrossRef]
16. White, J.; Meredith, M. Spectral analysis and modelling of ACh and NE effects on shark nervus terminalis activity. *Brain Res. Bull.* **1993**, *31*, 369–374. [CrossRef]
17. Bilinska, K.; von Bartheld, C.S.; Butowt, R. Expression of the ACE2 Virus Entry Protein in the Nervus Terminalis Reveals the Potential for an Alternative Route to Brain Infection in COVID-19. *Front. Cell. Neurosci.* **2021**, *15*, 674123. [CrossRef]
18. Butowt, R.; von Bartheld, C.S. The route of SARS-CoV-2 to brain infection: Have we been barking up the wrong tree? *Mol. Neurodegener.* **2022**, *17*, 20. [CrossRef] [PubMed]
19. Butowt, R.; Bilińska, K.; von Bartheld, C. Why Does the Omicron Variant Largely Spare Olfactory Function? Implications for the Pathogenesis of Anosmia in Coronavirus Disease 2019. *J. Infect. Dis.* **2022**, *226*, 1304–1308. [CrossRef]
20. Butowt, R.; Bilinska, K.; von Bartheld, C.S. Olfactory dysfunction in COVID-19: New insights into the underlying mechanisms. *Trends Neurosci.* **2023**, *46*, 75–90. [CrossRef] [PubMed]

21. von Bartheld, C.S.; Butowt, R. New evidence suggests SARS-CoV-2 neuroinvasion along the nervus terminalis rather than the olfactory pathway. *Acta Neuropathol.* **2024**, *147*, 1–3. [CrossRef]
22. Whitlock, K.E.; Palominos, M.F. The Olfactory Tract: Basis for Future Evolution in Response to Rapidly Changing Ecological Niches. *Front. Neuroanat.* **2022**, *16*, 831602. [CrossRef] [PubMed]
23. MacColl, G.; Bouloux, P.; Quinton, R. Kallmann Syndrome: Adhesion, Afferents, and Anosmia. *Neuron* **2002**, *34*, 675–678. [CrossRef] [PubMed]
24. Amato, E.; Taroc, E.Z.M.; Forni, P.E. Illuminating the Terminal Nerve: Uncovering the Link between GnRH-1 and Olfactory Development. *BioRxiv* **2023**. [CrossRef] [PubMed]
25. Palominos, M.F.; Calfún, C.; Nardocci, G.; Candia, D.; Torres-Paz, J.; Whitlock, K.E. The Olfactory Organ Is a Unique Site for Neutrophils in the Brain. *Front. Immunol.* **2022**, *13*, 881702. [CrossRef] [PubMed]
26. Morgane, P.J.; Galler, J.R.; Mokler, D.J. A review of systems and networks of the limbic forebrain/limbic midbrain. *Prog. Neurobiol.* **2005**, *75*, 143–160. [CrossRef] [PubMed]
27. Gerlach, G.; Wullimann, M.F. Neural pathways of olfactory kin imprinting and kin recognition in zebrafish. *Cell Tissue Res.* **2021**, *383*, 273–287. [CrossRef] [PubMed]
28. Mucignat-Caretta, C. Processing of intraspecific chemical signals in the rodent brain. *Cell Tissue Res.* **2021**, *383*, 525–533. [CrossRef]
29. Umatani, C.; Oka, Y. Multiple functions of non-hypophysiotropic gonadotropin releasing hormone neurons in vertebrates. *Zool. Lett.* **2019**, *5*, 1–10. [CrossRef] [PubMed]
30. Ueda, H. Physiological mechanisms of imprinting and homing migration in Pacific salmon *Oncorhynchus* spp. *J. Fish Biol.* **2012**, *81*, 543–558. [CrossRef] [PubMed]
31. The Lancet Respiratory Medicine Long COVID: Confronting a growing public health crisis. *Lancet Respir. Med.* **2023**, *11*, 663. [CrossRef]
32. Davis, H.E.; McCorkell, L.; Vogel, J.M.; Topol, E.J. Long COVID: Major findings, mechanisms and recommendations. *Nat. Rev. Microbiol.* **2023**, *21*, 133–146. [CrossRef] [PubMed]
33. Zhao, S.; Toniolo, S.; Hampshire, A.; Husain, M. Effects of COVID-19 on cognition and brain health. *Trends Cogn. Sci.* **2023**, *27*, 1053–1067. [CrossRef] [PubMed]
34. Sauve, F.; Nampoothiri, S.; Clarke, S.A.; Fernandois, D.; Coêlho, C.F.F.; Dewisme, J.; Mills, E.G.; Ternier, G.; Cotellessa, L.; Iglesias-Garcia, C.; et al. Long-COVID cognitive impairments and reproductive hormone deficits in men may stem from GnRH neuronal death. *EBioMedicine* **2023**, *96*, 104784. [CrossRef]
35. Dierssen, M. Down syndrome: The brain in trisomic mode. *Nat. Rev. Neurosci.* **2012**, *13*, 844–858. [CrossRef]
36. Manfredi-Lozano, M.; Leysen, V.; Adamo, M.; Paiva, I.; Rovera, R.; Pignat, J.-M.; Timzoura, F.E.; Candlish, M.; Eddarkaoui, S.; Malone, S.A.; et al. GnRH replacement rescues cognition in Down syndrome. *Science* **2022**, *377*, eabq4515. [CrossRef] [PubMed]
37. de Melo, G.D.; Perraud, V.; Alvarez, F.; Vieites-Prado, A.; Kim, S.; Kergoat, L.; Coleon, A.; Trüeb, B.S.; Tichit, M.; Piazza, A.; et al. Neuroinvasion and anosmia are independent phenomena upon infection with SARS-CoV-2 and its variants. *Nat. Commun.* **2023**, *14*, 4485. [CrossRef]
38. Butowt, R.; von Bartheld, C.S. Timing and cause of olfactory deciliation in COVID-19. *Physiol. Rev.* **2024**, *104*, 589–590. [CrossRef]
39. Perneczky, A. The Nervus terminalis. In *The Cranial Nerves*; Samii, M., Jannetta, P.J., Eds.; Springer: Berlin/Heidelberg, Germany, 1981. [CrossRef]

International Journal of
Molecular Sciences

MDPI

Review

Antisense Oligonucleotides (ASOs) in Motor Neuron Diseases: A Road to Cure in Light and Shade

Silvia Cantara [1], Giorgia Simoncelli [2] and Claudia Ricci [1,*]

[1] Department of Medical, Surgical and Neurological Sciences, University of Siena, 53100 Siena, Italy; cantara@unisi.it
[2] Unit of Neurology and Clinical Neurophysiology, Department of Neurological and Motor Sciences, Azienda Ospedaliero-Universitaria Senese, 53100 Siena, Italy; simoncelligiorgia1@gmail.com
* Correspondence: claudia.ricci@unisi.it

Abstract: Antisense oligonucleotides (ASOs) are short oligodeoxynucleotides designed to bind to specific regions of target mRNA. ASOs can modulate pre-mRNA splicing, increase levels of functional proteins, and decrease levels of toxic proteins. ASOs are being developed for the treatment of motor neuron diseases (MNDs), including spinal muscular atrophy (SMA), amyotrophic lateral sclerosis (ALS) and spinal and bulbar muscular atrophy (SBMA). The biggest success has been the ASO known as nusinersen, the first effective therapy for SMA, able to improve symptoms and slow disease progression. Another success is tofersen, an ASO designed to treat ALS patients with *SOD1* gene mutations. Both ASOs have been approved by the FDA and EMA. On the other hand, ASO treatment in ALS patients with the *C9orf72* gene mutation did not show any improvement in disease progression. The aim of this review is to provide an up-to-date overview of ASO research in MNDs, from preclinical studies to clinical trials and, where available, regulatory approval. We highlight the successes and failures, underline the strengths and limitations of the current ASO research, and suggest possible approaches that could lead to more effective treatments.

Keywords: antisense oligonucleotides (ASOs); motor neuron diseases; spinal muscular atrophy; amyotrophic lateral sclerosis; spinal and bulbar muscular atrophy; innovative therapy; nusinersen; tofersen; clinical trials

Citation: Cantara, S.; Simoncelli, G.; Ricci, C. Antisense Oligonucleotides (ASOs) in Motor Neuron Diseases: A Road to Cure in Light and Shade. *Int. J. Mol. Sci.* **2024**, *25*, 4809. https://doi.org/10.3390/ijms25094809

Academic Editor: Yohei Okada

Received: 28 February 2024
Revised: 23 April 2024
Accepted: 26 April 2024
Published: 28 April 2024

1. Introduction

In the landscape of modern medicine, the advent of molecular therapeutics has propelled the field towards unprecedented levels of precision and specificity. Among the groundbreaking innovations, antisense oligonucleotides (ASOs) have emerged as a class of therapeutic agents with transformative potential, offering a unique avenue for targeted genetic modulation [1–3]. These oligonucleotides, typically 15–25 bases in length, are designed to selectively modify protein synthesis by complementary binding to specific regions of target mRNA [1], steering away from the conventional paradigm of protein-focused therapeutics.

To fully understand the potential of ASOs, an exploration of their intricate composition is essential. Beyond their nucleotide sequence, ASOs undergo chemical modifications strategically incorporated into their backbone. Phosphorothioate linkages, 2′-O-methyl groups, and locked nucleic acids (LNAs) are among the key modifications. In phosphorothioate linkage, a sulphur atom replaces one of the non-bridging oxygen atoms in the phosphate group, enhancing stability and resistance to nuclease degradation [4]. The 2′-O-methyl groups refer to a chemical modification at the 2′ position of the ribose (or deoxyribose) sugar in nucleic acids in which a methyl group (-CH3) is added. This modification is preferred for RNA as it helps overcome some of the limitations associated with the natural susceptibility of RNA to degradation and affects the RNA's interaction with cellular machinery and proteins [5]. In LNAs, the ribose ring is chemically constrained by

a methylene bridge connecting the 2′-oxygen and the 4′-carbon of the ribose, creating a "locked" structure [5]. By incorporating LNAs into the ASO sequence, the resulting LNA-ASO exhibits increased stability, improved binding affinity, and enhanced resistance to nuclease degradation compared to traditional oligonucleotides. Additional modifications contributing to improved ASO pharmacokinetics include peptide nucleic acids (PNAs), replacing the sugar-phosphate backbone with a peptide-like structure [6]; GalNAc conjugation, facilitating liver targeting [7]; and hydrophobic modifications, enhancing cellular uptake and distribution [8]. These tailored molecular architectures ensure the longevity of ASOs in physiological environments and facilitate their efficient delivery to target cells, which are critical for therapeutic efficacy (Table 1).

Table 1. Main ASO modifications with advantages and disadvantages.

Name of Modification	Type of Modification	Advantages	Disadvantages
Single-stranded phosphorothioate	Replacement of one of the non-bridging oxygen atoms in the phosphate backbone with a sulphur atom	Improved nuclease resistance in plasma, tissues, and cells	Cytotoxicity when delivered at high concentrations due to non-specific binding with certain proteins
2′-O-Methoxyethyl (2′-MOE)-modification	Modifications at the 2′ position of the sugar moiety	Enhanced nuclease resistance, lower cell toxicity, and increased binding affinity	Impaired RNase H cleavage of the complementary RNA
2′-MOE gapmers	A central core of phosphorothioate-modified DNA is flanked by 2′-MOE-modified RNA bases	Induces RNase H cleavage, increases binding affinity to the target, mitigates non-specific cleavage	Immunogenic reaction still possible
2′-O-[2-(methylthio)ethyl] or 2′-O-MTE modification	Modifications at the 2′ position of the sugar moiety	Improved binding to human serum albumin, high binding affinity to target RNA	Limited resistance to exonuclease degradation
Phosphoryl guanidine backbone modification	Phosphoryl guanidine modification of the phosphate group at internucleotidic positions	Increased nuclease resistance, enhanced affinity and selectivity to target sites, enhances exon skipping	Reduced cellular uptake
Mixed-backbone oligonucleotides (MBOs)	Alternative phosphorothioate and phosphodiester linkages in the 2′-O-methylribonucleosides	Improved affinity to RNA, RNase H activation, better pharmacological and pharmacokinetic properties	The efficiency of gene silencing can vary depending on target mRNA secondary structure, accessibility, and cellular context. This variability may lead to unpredictable outcomes and require optimization for each specific target.
Locked nucleic aacids (LNA)	The ribose ring is chemically constrained by a methylene bridge connecting the 2′-oxygen and the 4′-carbon of the ribose, creating a "locked" structure	Increased binding affinity, enzymatic stability	Increased liver toxicity

The adaptability of ASOs stems from their ability to engage with target mRNA through precise Watson-Crick base pairing [9]. This interaction sets the stage for a multitude of mechanisms through which ASOs can exert their therapeutic effects. One paradigmatic mechanism involves the recruitment of cellular machinery, such as the endonuclease RNase H, triggering mRNA cleavage and subsequent degradation. This approach is particularly powerful when the therapeutic objective is to attenuate the expression of deleterious proteins associated with genetic disorders. However, the influence of ASOs extends beyond mere mRNA degradation (Figure 1). Steric hindrance, another aspect of their mechanism,

enables ASOs to interfere with the splicing process, dictating the inclusion or exclusion of specific exons [10] (Figure 2). This modulation of gene expression holds promise in conditions where aberrant splicing events underlie the pathophysiology, such as certain types of muscular dystrophy.

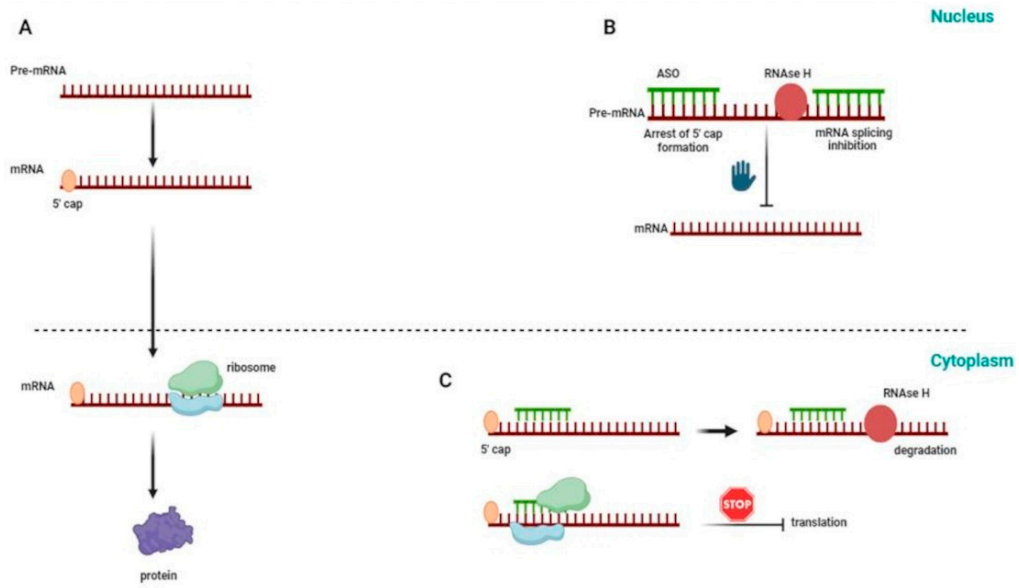

Figure 1. Mechanisms of ASO action in the regulation of gene expression: (**A**) Normal gene expression in the absence of ASO; (**B**) ASO can enter the nucleus and induce both 5′ cap formation and RNAse H-mediated mRNA splicing; (**C**) In the cytoplasm, ASO can either interfere with ribosome assembly or activate RNAse H-induced mRNA degradation due to ASO-mRNA heteroduplex formation.

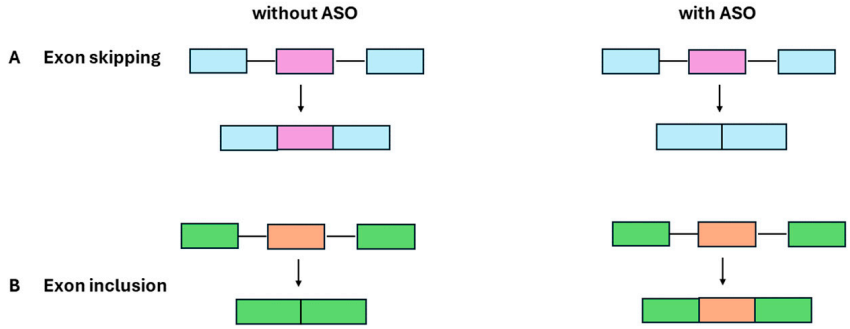

Figure 2. Mechanisms of ASO action in the regulation of RNA processing: (**A**) Exon skipping without or with ASO and (**B**) exon inclusion without or with ASO therapy.

In this paper we reviewed the use of ASOs as therapeutic agents in motor neuron diseases such as spinal muscular atrophy, amyotrophic lateral sclerosis, and spinal bulbar muscular atrophy, summarizing their mode of action and clinical trials.

2. Overcoming CNS Delivery Challenges: Strategies for Antisense Oligonucleotide Administration

The administration and delivery of ASOs in central nervous system (CNS) disorders are particularly challenging due to the presence of the blood–brain barrier (BBB), a highly selective semi-permeable layer of endothelial cells that acts as a filter. The chemical properties of ASOs, such as negative charge, high molecular weight, and hydrophilicity, prevent diffusion across the BBB and reduce the efficacy of systemic administration. To overcome these problems, intrathecal (IT) or intraventricular injection has been used to deliver ASOs directly into the CNS, bypassing the BBB. Following the injection of single-stranded phosphorothioate- and 2′-MOE-modified ASOs into the cerebrospinal fluid (CSF), rapid distribution throughout the spinal cord and to most regions of the brain is observed [11–16].

Approximately 20% of the injected dose remains in brain tissue with a peak 4–6 h after injection, while 80% or more is found in the systemic circulation [12,15] following normal CSF turnover pathways. In the case of 2′-MOE-modified oligonucleotides, the half-life in CNS tissues ranges from 3 weeks to 6 months, while the effects of single-stranded phosphorothioate ASOs on gene expression can last from 6 weeks to more than 6 months after a single injection, depending on the chemical design and method of administration [13,15,17]. The longest-lasting effects are achieved with 2′-MOE-modified oligonucleotides, where all internucleosidic linkages are phosphorothioate, combined with intracerebroventricular bolus injection as the method of delivery to the CNS. After intrathecal administration, the highest ASO concentrations are found near the injection site in the spinal cord, with lower concentrations in other regions of the spinal cord and cortical regions of the brain [12,15,18,19]. A similar distribution is found after intracerebral ventricular administration, but in this case, higher drug concentrations are found in the tissue surrounding the ventricle [20].

Given the invasiveness of this procedure, several approaches have been considered to deliver ASOs to the CNS. Intranasal administration, using the olfactory and trigeminal nerve pathways, can deliver drugs to the CNS [21–24]. In addition, the use of delivery particles has been shown to improve ASO transport into the CNS after systemic administration. Glucose-coated polymeric nanocarriers allow efficient brain accumulation of ASOs by non-invasive intravenous administration, presumably due to their multivalent binding to glucose transporter 1 expressed on the plasma membrane of brain capillary endothelial cells, with the highest brain accumulation shown when their size is less than 50 nm and the number and density of glucose are approximately 50 per 100 block copolymer strands on their surface [25]. Peptide-conjugated ASOs are another type of delivery particle that can bypass the blood–brain barrier. In a spinal muscular atrophy (SMA) disease model, these ASOs were present in the brain (cortex, brainstem, cerebellum), spinal cord, peripheral skeletal muscle, and liver after intravenous administration and were able to rescue the phenotype and dramatically extend the lifespan of severe SMA mice without significant side effects [26], making this approach very promising.

3. Motor Neuron Diseases

Motor neuron diseases (MNDs) are a group of sporadic and inherited neurodegenerative disorders that result in the total or predominant loss of motor neurons. Upper motor neurons are located in the primary motor cortex of the brain, and their axons connect to the brainstem (corticobulbar tract) and to the corticospinal tract of the spinal cord (corticospinal tract). Lower motor neurons are located in motor nuclei in the brainstem or in the anterior grey matter of the spinal cord. They are responsible for transmitting the signal from the upper motor neuron to the effector muscle, as their axons connect to the muscles of the limbs and bulbar region. Degeneration of motor neurons leads to loss of voluntary muscle function. Depending on which muscles are affected, patients with MNDs develop muscle weakness and atrophy, bulbar involvement, and respiratory failure.

MNDs generally include spinal muscular atrophy (SMA), amyotrophic lateral sclerosis (ALS), and spinal and bulbar muscular atrophy (SBMA).

4. Spinal Muscular Atrophy (SMA)

Spinal muscular atrophy (SMA) is an autosomal-recessive neuromuscular disease characterised by the progressive degeneration of alpha motor neurons in the anterior horn of the spinal cord, resulting in muscle atrophy and loss of muscle function [26]. Its incidence ranges from 1:6000 to 1:11,000 live births in the general population [27–29]. SMA is caused by deletions or point mutations in the *SMN1* gene, which encodes the survival motor neuron (SMN) protein. SMN plays a key role in the proper function and survival of motor neurons. Complete loss of the SMN protein is lethal at the embryonic stage [30]. Based on the age of onset and the severity of clinical symptoms, which is inversely related to the amount of SMN protein available at the motor neuron level, SMA is classified into different phenotypes (i.e., SMA type 0, type 1, type 2, type 3, and type 4) [31]. The severity of the

disease depends, at least in part, on the number of copies of a second gene, called *SMN2*, which is a centromeric copy of *SMN1* that arose from a duplication event during primate evolution [32]. The *SMN2* gene is almost identical to *SMN1*, but the transition of a C to a T in exon 7 inactivates a splicing enhancer and simultaneously introduces an exonic splicing silencer, resulting in abnormal mRNAs lacking exon 7 [33–37]. These transcripts lacking exon 7 produce very low levels of SMN protein because they are unstable and therefore degraded rapidly and cannot compensate for the loss of SMN protein caused by *SMN1* gene deletions/mutations. There is a variable number of copies of the *SMN1* and *SMN2* genes in the human population, including individuals with more than two copies of *SMN2*, with no known deleterious effect. Patients with type 1 SMA typically have two copies of the *SMN2* gene, patients with type 2 SMA have three copies of the *SMN2* gene, and patients with type 3 SMA have three to four copies of this gene. These observations support the idea that the number of copies of *SMN2* is a robust modifier of disease [38–41], suggesting that increasing the amount of SMN protein should have therapeutic effects in SMA.

Various ASOs have been designed to block intronic splicing silencers or induce splicing enhancers to prevent exon 7 skipping [42–44]. Nusinersen (trade name Spinraza) was the first SMA orphan drug approved by the Food and Drug Administration (FDA) and by the European Medicines Agency (EMA) for the treatment of SMA in children and adults. It is a 2′-MOE-modified ASO designed to increase SMN protein expression by modulating the splicing of the *SMN2* precursor messenger RNA (pre-mRNA) to restore a full-length mature messenger RNA (mRNA) from the *SMN2* pre-mRNA. Nusinersen targets a specific splicing silencer site (ISS-N1, intronic splice silencing) in intron 7 of *SMN2* and prevents the binding of specific splicing repressors, hnRNPA1 and hnRNPA2, to ISS-N1, allowing the integration of exon 7 into the final transcript and increasing the synthesis of a full-length functional SMN protein [45,46] (Figure 3).

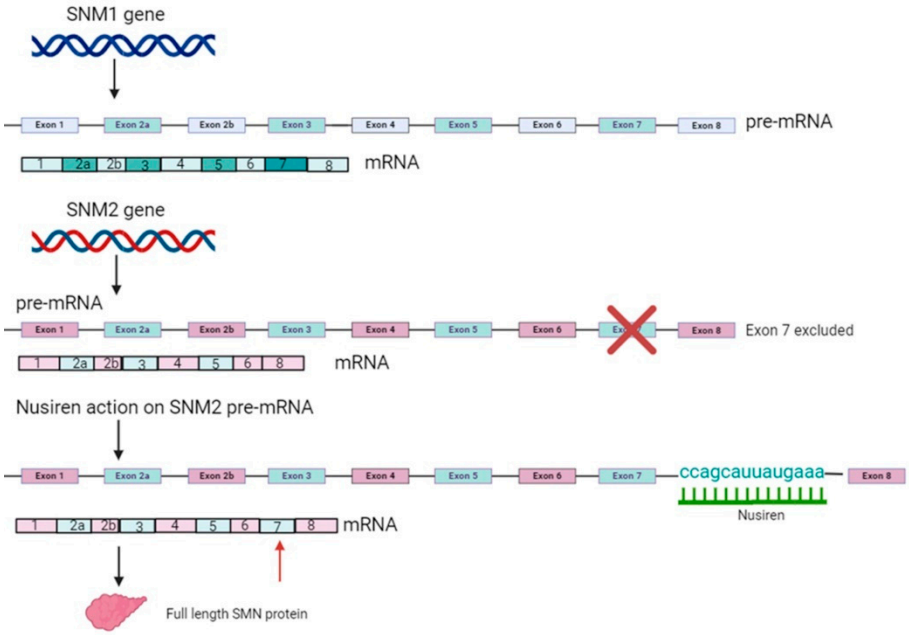

Figure 3. Nusinersen restoration of the SNM2 gene function: The *SNM1* gene leads to a full-length transcript resulting in a functional protein. The *SNM2* gene, on the contrary, results in a non-functional protein due to the skipping of exon 7. Nusinersen is able to restore a full-length protein by acting on pre-mRNA and avoiding the exclusion of exon 7.

As ASOs do not cross the blood–brain barrier, nusinersen must be administered intrathecally. A phase 1 clinical trial in which increasing doses of nusinersen were administered by lumbar puncture to children with type 2 and type 3 SMA showed that this ASO was well tolerated [47]. The phase 1 study was followed by two different open-label phase 2 studies, one in the same population as the phase 1 study and the second in infantile-onset

SMA infants. The first showed an increase in survival in nusinersen-treated patients compared with sham-treated patients [12,48]. In addition, nusinersen-treated infants showed an improvement in motor function scores that was never observed in the natural history of type 1 SMA patients [48]. Clinical trials in patients with type 2 SMA also showed improvement in motor function compared to a decline or no change in sham-treated patients [49]. These results led to the approval of nusinersen by the FDA in 2016 and by the EMA in 2017 for the treatment of all types of SMA, just five years to the day after the first patient was exposed to the drug [50]. Table 2 summarises the main steps of this pathway, while Table 3 reports nusinersen clinical trials.

Table 2. Summary of nusinersen preclinical studies.

Year	Results	Ref.
2006	Identification of the ISS-N1 sequence within *SMN2* intron 7 Synthesis of the first complementary ASO	[46]
2008	Synthesis of ASO 10–27 with high affinity to ISS-N1 First preclinical studies on an SMA mouse model	[45]
2010–2011	Improved SMN protein expression following administration of ASO 10–27 by intrathecal or intracerebroventricular injection in SMA mice Ameliorated disease phenotype No increase in lifespan of mice	[14]
2011	Amelioration of peripheral symptoms after subcutaneous injection of ASO 10–27 in SMA mice Improved lifespan by more than 25-fold	[51]
2011	Adequate distribution at the level of the spinal cord after intrathecal injection in non-human primates No significant side effects.	[14]

Table 3. Summary of Nusinersen clinical trials.

Phase	Type of Study	SMA Type	n° of Patients	Administration (Doses)	Clinical Outcomes	Ref.
I (NCT01494701) (NCT01780246)	Open-label	2/3	28	Intrathecal bolus injection (1, 3, 6, 9 mg)	Improved HFMSE scores in the 9 mg groups post-dose	[47]
II (NCT01839656)	Open-label	1	20	Intrathecal injection (6 mg and 12 mg equivalents)	Increased improvement in HINE-2 and CHOP-INTEND test assessments	[12]
III (ENDEAR NCT02193074)	Double-blind, randomised, and sham-controlled	1	121	Intrathecal injection (12 mg equivalents)	Higher percentage of motor-milestone response and higher percentage of CHOP-INTEND response compared to control group	[48]
III (CHERISH NCT02292537)	Double-blinded, multicentre and sham-controlled	later-onset SMA (2–12 years)	126	Intrathecal injection (12 mg)	Significant improvement in motor function compared to control group (increase from baseline to month 15 in the HFMSE score of at least 3 points)	[49]
II (NURTURE NCT02386553)	Open-label single-arm	1/2 presymptomatic	25	Intrathecal injection	Underway	[52,53]

HFMSE, Hammersmith Functional Motor Scale-Expanded; HINE-2, Hammersmith Infant Neurological Exam-Part 2; CHOP-INTEND, Children's Hospital of Philadelphia Infant Test of Neuromuscular Disorders.

A Phase 2 open-label, single-arm study (NURTURE—NCT02386553) is underway to evaluate the effects of nusinersen in infants with a genetic diagnosis of SMA (most likely to develop type 1 or type 2 SMA), where treatment is initiated before the onset of symptoms [52,53]. The main objective of the study is to determine whether nusinersen can prevent or delay the onset of the disease and/or result in a milder form of the disease (primary endpoint: time to death or respiratory intervention; secondary endpoints: attainment of motor milestones, change from baseline in growth parameters, proportion of participants developing clinically manifested SMA at 13 and 24 months of age). Since infants with a genetic diagnosis of SMA, with one functional copy of the *SMN1* gene and two or three copies of the *SMN2* gene, are expected to develop severe or fatal symptoms in the first years of life, an internal control group was considered unnecessary and ethically unjustifiable. The study is expected to be completed in early 2025.

In addition to nusinersen, a Phase 1 trial (NCT05575011) is currently underway for BIIB115, an ASO with an N-methylacetamide (NMA)-modified chemical backbone that improves efficacy and provides the opportunity to assess patient outcomes with long-interval dosing.

Nusinersen is a clear example of how it is feasible to implement collaborative strategies among different stakeholders (e.g., research centres, industry, and regulators) to build a robust pathway based on robust preclinical, translational, and clinical evidence to support the regulatory process [31]. In this way, it is possible to provide patients with effective therapies that can improve symptoms and slow disease progression, even in neurodegenerative diseases.

5. Amyotrophic Lateral Sclerosis (ALS)

ALS is a fatal neurodegenerative disease characterized by the progressive degeneration of motor neurons in the motor cortex, brainstem, and spinal cord, with consequent atrophy of voluntary muscles [54]. The incidence of ALS is approximately 1–2.6 cases per 100,000 person-years, and the average survival time from onset to death is 3–4 years [55]. There is no cure for ALS. The only approved drugs, riluzole and edaravone, provide only modest survival benefits and are often associated with multiple side effects [56,57]. Most cases of ALS occur sporadically, with no reported family history, whereas approximately 10% are familial (fALS), with autosomal dominant inheritance in most cases [58]. Pathogenic variants have been identified in more than 30 genes [59]. However, in approximately 70% of patients with familial ALS, the disease is associated with variants in four genes: chromosome 9 open reading frame 72 (*C9orf72*), superoxide dismutase 1 (*SOD1*), TAR DNA binding protein (*TARDBP*), and fused in sarcoma (*FUS*) [60].

Although a unique cellular pathway associated with mutations in these genes has not been identified, several studies have shown that the majority of the monogenic causes of ALS act through a toxic gain of function of the mutated gene [61]. In these cases, ASO therapies that directly modify the disease-causing genes and neutralise the toxic gene products hold great promise. At present, there are antisense therapies at various stages of development that directly target the transcripts of *SOD1*, *C9orf72*, and *FUS*.

5.1. SOD1 Gene

The first gene identified as a cause of ALS was *SOD1* [62], which accounts for about 20% of familial ALS cases and up to 2% of sporadic cases [63]. More than 200 different mutations in this gene have been associated with ALS (see https://alsod.ac.uk/, accessed on 25 April 2024). Although the exact pathogenic mechanism of *SOD1* mutations is not fully understood, several lines of evidence suggest that it is associated with a toxic gain of function that impairs neuronal function and survival [64]. Reducing the expression of toxic SOD1 proteins in rodent models of ALS has been shown to delay disease onset and increase survival [16,65–67].

Based on these observations, the first ASO therapy targeting *SOD1* mRNA via an RNase H1 mechanism of action was developed [16]. ASO 333611, a 2′-MOE gapmer,

produced a dose-dependent reduction in *SOD1* mRNA and protein in transgenic rats expressing human mutant $SOD1^{G93A}$ RNA, with a 40–60% reduction in the brainstem and spinal cord [16]. The reduction in SOD1 expression was well tolerated, delayed disease onset, and prolonged survival by 37% after disease onset in the transgenic rats. These encouraging preclinical data prompted a phase 1, double-blind, placebo-controlled clinical trial (NCT01041222) to evaluate the safety and tolerability of intrathecally delivered ASO 333611 in SOD1 ALS patients [68], making ASO 333611 the first experimental antisense drug to be administered intrathecally to patients for the treatment of a neurodegenerative disease. Given its novelty, a single course (12 h slow intrathecal infusion) of a low dose (0.15 to 3 mg) was used. No drug-related safety issues were observed in the study. Although no reduction of SOD1 protein levels in cerebrospinal fluid was observed, this study was a landmark for ASO therapy, demonstrating for the first time that intrathecal infusion of ASOs is safe in humans and effective in animals, and establishing a protocol to rapidly advance ASOs from initial selection into clinical trials.

Meanwhile, advances in ASO therapies for other neurological diseases, including SMA, identified more effective designs to improve the efficacy and tolerability of these drugs. As a result, the ASO approach to ALS was subsequently redesigned to incorporate more advanced technologies. The next-generation ASO, BIIB067 (IONIS-SOD1Rx, then called tofersen, trade name Qalsody), is a 2′-MOE mixed backbone ASO that was identified following an oligonucleotide screen in cell culture and $hSOD1^{G93A}$ transgenic mice and rats [19]. BIIB067, which targets a different region of the *SOD1* pre-mRNA and is designed for the treatment of ALS patients carrying mutations in the *SOD1* gene (Figure 3), was shown to be approximately six times more potent than ASO 333611 in cultured cells and three to four times more potent in inhibiting *SOD1* mRNA expression in transgenic rodents. In addition, administration of BIIB067 to transgenic $hSOD1^{G93A}$ rodents prior to disease onset significantly prolonged survival, slowed motor impairment, and reduced neuromuscular damage [19]. ASO therapy also reduced serum levels of phosphorylated neurofilament heavy chain (pNFH) [19], a cytoskeletal protein released in cerebrospinal fluid during axonal injury and correlated with disease severity [69]. When administered after disease onset, ASOs suppressed further increases in pNFH and restored neuromuscular activity close to baseline. Intrathecal injection of BIIB067 into non-human primates (NHPs) resulted in a dose-dependent reduction of *SOD1* mRNA and protein in CNS tissues and CSF.

Based on the strong functional recovery observed in rodent models and the favourable pharmacokinetics in NHPs, a randomised, double-blind, placebo-controlled Phase I/II study (VALOR; NCT02623699) was initiated to evaluate the tolerability and pharmacokinetics of intrathecal administration of tofersen in familial ALS patients carrying a mutation in the *SOD1* gene [70]. Single and multiple ascending doses were used. This and subsequent ASO trials used an intrathecal bolus rather than the intrathecal catheter and external pump employed in the first *SOD1* ASO trial. Tofersen was generally well tolerated and safe. The highest concentration of tofersen was more effective in reducing CSF SOD1 levels than lower doses. There was also a trend towards a slowing of the decline in ALSFRS-R measured in the highest dose group, particularly in the fast-progressing subgroup. Levels of plasma and CSF pNFH and neurofilament light chain (NfL) were also reduced in this group.

In light of these promising results, tofersen was advanced to a 28-week, randomised, double-blind, placebo-controlled Phase 3 trial (VALOR; NCT02623699) using the maximum dose from the previous study. Given the analysis from the tofersen Phase I/II trial, and to reduce the impact of the known heterogeneity of the patients, participants were divided into fast- and slow-progressing subgroups, with the effect on progression in the fast-progressing group as the primary outcome. This study showed that, after 28 weeks of treatment with tofersen, cerebrospinal fluid SOD1 and plasma neurofilament light chain levels were reduced, but clinical endpoints were not reached [71]. However, several secondary and exploratory endpoints supported favourable clinical and biomarker trends for tofersen

treatment. In particular, in the fast-progressing group, tofersen reduced CSF SOD1 and plasma NfL by 38% and 67%, respectively, and showed a benefit in respiratory (slow vital capacity) and muscle strength. Slow progressors exhibited similar but more limited reductions in SOD1 (26%) and NfL (48%) and very small reductions in ALSFRS-R, slow vital capacity, and muscle strength. Based on these results, the FDA approved tofersen in April 2023 for the treatment of patients with amyotrophic lateral sclerosis associated with a mutation in the *SOD1* gene, followed by the EMA's Committee for Human Medicines (CHMP) approval in February 2024. A long-term, open-label Phase 3 extension study (NCT03070119) is underway to follow participants who received tofersen and assess long-term safety, tolerability, and efficacy.

Figure 4 summarises the mechanism of action of tofersen.

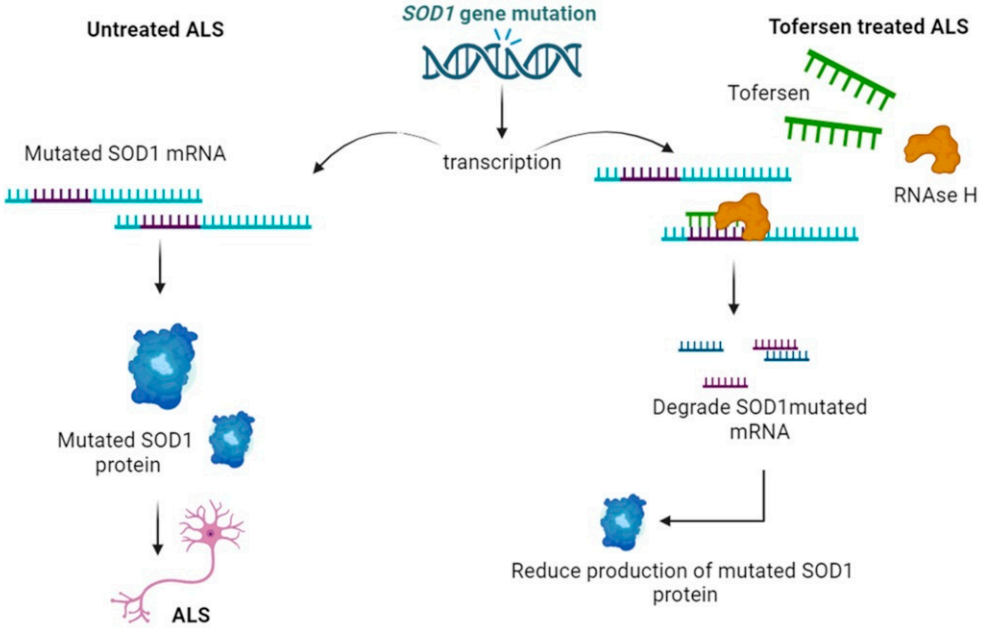

Figure 4. Tofersen mechanism of action in ALS: Mutated *SOD1* leads to mutated SOD1 protein which develops into ALS. Tofersen, through an RNAse H mechanism, degrades *SOD1* mutated mRNA, thus reducing the production of mutated SOD1 protein.

A recent study evaluating the effects of tofersen treatment in patients with *SOD1*-ALS in a "real-world setting" (a 12-month multicentre cohort study from the German Early Access Program) confirmed an effective therapeutic approach with a reduction in serum NfL levels, but also demonstrated a reduction in CSF pNFH. The therapy was safe, as no persistent symptoms were observed. Pleocytosis, increased protein levels, and intrathecal immunoglobulin synthesis were common CSF findings that need to be evaluated in future studies [72].

Based on the favourable safety and therapeutic outcomes for ALS patients, the SOD1-ASO is now being considered for the treatment of asymptomatic gene carriers in a new trial (ATLAS, NCT04856982). The hypothesis to be tested is that treating individuals with SOD1-ASO at the first evidence of biomarker changes, but before clinical evidence of motor neuron disease, may slow or prevent the onset of the disease. This randomised, placebo-controlled trial aims to recruit ~150 pre-symptomatic carriers without clinically manifest ALS (from May 2021 to August 2027). Participants will be monitored frequently for serum NfL levels. If a participant shows an increase in NfL, they will be randomised to receive either 100 mg tofersen or placebo every month for the following 2 years (1:1 to tofersen or placebo). The study endpoints will be the proportion of participants who develop clinically manifest ALS within 12 months and 24 months of randomisation and the time from randomisation to the development of clinically manifest ALS. An open-label extension period will allow participants who develop clinical ALS to receive tofersen in the

open-label arms of the study [73]. In Table 4, we summarised preclinical studies, and in Table 5, clinical studies of ASOs targeting *SOD1*.

Table 4. Summary of preclinical studies of ASOs targeting *SOD1*.

Year	Results	Ref.
2006	ASO 333611 produced a dose-dependent reduction of *SOD1* mRNA and protein in *SOD1*^{G93A} rats, delayed disease onset, and prolonged survival by 37% after the onset. The reduction in SOD1 expression was well tolerated.	[16]
2018	BIIB067 was more potent than ASO 333611 in inhibiting *SOD1* mRNA expression in cultured cells and in transgenic rodents. BIIB067 administration to transgenic *SOD1*^{G93A} rodents before disease onset significantly prolonged survival, slowed motor impairment, and reduced neuromuscular damage. ASO therapy reduced serum levels of pNFH.	[19]

pNFH: phosphorylated neurofilament heavy chain.

Table 5. Summary of clinical trial of ASOs targeting *SOD1*.

Phase	Type of Study	n° of Patients	Administration (Doses)	Clinical Outcome	Ref.
I (NCT01041222) ASO 333611	double-blind, placebo-controlled	22	A single course (12 h slow intrathecal infusion) of a low dose (0.15 to 3 mg)	No drug-related safety issues. No reduction of SOD1 protein levels in CSF	[68]
I/II (VALOR NCT02623699) BIIB067 (Tofersen)	Randomised, double-blind, placebo-controlled trial	50	Intrathecal injection (20, 40, 60, or 100 mg)	Tofersen was generally well tolerated and safe. The highest concentration was the most effective in reducing CSF SOD1 levels and slowed decline in ALSFRS-R	[70]
III (VALOR NCT02623699) BIIB067 (Tofersen)	Randomised, double-blind, placebo-controlled trial	108	Intrathecal injection (100 mg)	Reduction of CSF SOD1 and plasma neurofilament light chain levels after 28 weeks of treatment. Clinical endpoints were not reached. Several secondary and exploratory endpoints supported favourable clinical and biomarker trends, particularly in the fast-progressing group	[71]
III (NCT03070119) BIIB067 (Tofersen)	Long-term, open-label extension	138	Intrathecal injection (100 mg)	The aim is to assess long-term safety and tolerability of tofersen	[71]
III (ATLAS NCT04856982) BIIB067 (Tofersen)	Presymptomatic carrier	150 expected (2021–2027)	In case of an increse in NfL, the participant will be randomised to receive either 100 mg tofersen or placebo	The aim is to assess the effectiveness of tofersen in pre-symptomatic adult carriers of *SOD1* mutations with elevated neurofilament levels	[73]

CSF: cerebrospinal fluid.

5.2. C9orf72 Gene

The expanded GGGGCC hexanucleotide repeat in intron 1 of the *C9orf72* gene is the most common genetic cause of frontotemporal dementia (FTD) and ALS, accounting for ~40% of fALS cases and 5–7% of sALS cases [74]. The *C9orf72* gene contains between 2 and 30 repeats in healthy individuals. In ALS patients, however, the number of repeats can reach hundreds or thousands [75,76]. Transcription of this gene results in three main transcripts (V1, V2, V3). The repeat region is located in the first intron of transcripts V1 and

V3, whereas the V2 transcript contains the repeat in its promoter region. V1 encodes a short isoform of the C9orf72 protein, while V3 and V2 encode the same long isoform but contain different untranslated first exons (1a and 1b, respectively) [77].

The process by which *C9orf72* expansion leads to disease is not fully understood. Several mechanisms have been suggested: bidirectional transcription of the mutant *C9orf72* gene, with expression of sense and antisense RNA strands that can form RNA foci and fold the GGGGCC repeats into a G-quadruplex capable of sequestering important RNA-binding proteins and chromatin modifiers [78–80]; production of dipeptide repeat strings (DPRs) due to a non-canonical, repeat-associated, non-ATG-mediated (RAN) translation mechanism that alters cellular proteostasis [80–82]; haploinsufficiency of *C9orf72*, which limits its physiological functions (vesicle trafficking, autophagy, lysosomal processing, and immune response) [83,84]. It is likely that both gain- and loss-of-function mechanisms are responsible for the development of the disease [84,85]. Therefore, ASO therapies should mitigate the toxic gain of function resulting from the repeat expansions while maintaining the levels of the normal allele. This will reduce the toxicity of DPRs and repeat-containing RNA without suppressing physiological protein functions.

A unique opportunity for targeting C9orf72 arises from the multiple transcript variants produced. By targeting C9orf72 transcript variants 1 and 3, which carry the expansion, it is possible to reduce the expression of transcripts containing the expansion while preserving variant 2 and thus C9orf72 protein levels.

The studies performed in vitro and in animal models showed promising results. The use of ASOs was effective in reducing RNA foci in iPSC-derived neurons, and administration to transgenic mice ameliorated behavioural defects [85,86]. In addition, in a single patient carrying mutant *C9orf72*, CSF levels of polyGP dipeptide repeats, a stable biomarker of C9orf72-ALS [87], decreased following multiple intrathecal injections of ASOs. The procedure was well tolerated, demonstrating for the first time the possibility of using ASOs in the clinic for C9orf72 ALS [88].

The first clinical trial was conducted to assess the safety and tolerability of the ASO BIIB078, a phosphorothioate backbone ASO, which selectively targets *C9orf72* transcript variants 1 and 3 carrying the expansion, inducing RNAse H degradation, for the treatment of adult ALS patients with *C9orf72* expansion (NCT03626012). In this randomised, placebo-controlled Phase I clinical trial, 114 participants with C9orf72-ALS (excluding fast progressors) were recruited to receive ascending doses of BIIB078 or placebo by intrathecal infusion. BIIB078 was well tolerated but did not meet any of the endpoints (change in ALSFRS-R, slow vital capacity, and muscle strength) [89]. Moreover, patients receiving BIIB078 showed a trend toward greater clinical decline and increased levels of NfL in plasma, and further development of BIIB078 was discontinued.

A randomised, placebo-controlled Phase I/II clinical trial (NCT04931862) was also initiated to evaluate the safety, tolerability, and efficacy of the variant-selective, stereopure, phosphoryl guanidine backbone C9orf72-lowering ASO WVE-004 [90,91], in patients with ALS and/or FTD due to *C9orf72* expansion. This ASO targets a sequence near the exon 1b–intron junction, yielding more durable RNase H-mediated knockdown. Again, treatment with WVE-004 failed to show clinical benefit after 24 weeks, leading Wave to discontinue further development. Although a 48% reduction in CSF polyGP was observed, this was not associated with stabilisation or improvement in functional outcomes compared to placebo (https://www.globenewswire.com/news-release/2023/05/23/2674200/0/en/Wave-Life-Sciences-Announces-Topline-Results-from-Phase-1b-2a-FOCUS-C9-Study-of-WVE-004-for-C9orf72-associated-Amyotrophic-Lateral-Sclerosis-and-Frontotemporal-Dementia.html, accessed on 25 April 2024). Given that the *C9orf72* DNA containing the expansion is transcribed bidirectionally, producing both sense and antisense RNA strands that form RNA foci, and that all currently used ASOs bind and degrade only the sense strand, leaving DPRs and RNA foci produced by antisense *C9orf72* unaffected, it is hypothesised that the failure of these trials is due to their inability to neutralise antisense strands [89]. In this view, the results of these studies may provide valuable information that will lead to

a deeper understanding of this form of ALS, which is clearly much more complex than previously thought.

An Investigational New Drug Application (IND) approved by the FDA (IND141673) is currently underway to test the mixed backbone ASO afinersen in a single subject, a 60-year-old man with the *C9orf72* expansion [88]. Afinersen targets the intronic region flanking the GGGGCC repeat expansion. It suppresses the expression of V1 and V3 while allowing basal levels of V2. Prior to this application, toxicological studies in rodents, sheep, and monkeys supported the safety of afinersen [88]. Due to the chemical modification pattern used, no delivery vehicle was required, and the therapeutic was injected directly into the patient's spinal fluid to target the cells of interest. At the start of treatment, the patient had mild motor changes with elevated polyGP in the CSF. Eight escalating doses were administered intrathecally over 60 weeks, starting in August 2019. Afinersen was well distributed throughout the CSF, and compared to baseline, CSF polyGP levels decreased by 80%, indicating that this ASO is active and reduces C9orf72 expansion consequences. ALSFRS-R remained stable throughout treatment. At the time of this review, there are no registered clinical trials for afinersen.

Table 6 summarises preclinical studies, and Table 7 clinical studies of ASOs targeting *C9orf72*.

Table 6. Summary of preclinical studies of ASOs targeting *C9orf72*.

Year	Results	Ref.
2013	Studies in patient-derived fibroblasts [92], iPSC neurons [85], or motor neurons [93] demonstrate that C9orf72-targeting ASOs could potently reduce repeat-containing C9orf72 transcripts and clear intranuclear RNA foci	[85,92,93]
2016	Intracerebroventricular injection of intron-targeting ASOs ameliorates behavioural defects in transgenic mice carrying a bacterial artificial chromosome with the full human repeat-containing C9orf72	[86]

Table 7. Summary of clinical studies of ASOs targeting C9orf72.

Phase	Type of Study	n° of Patients	Administration (Doses)	Clinical Outcome	Ref.
I (NCT03626012) BIIB078	Randomised, placebo-controlled trial	114 (no fast progressors)	Intrathecal infusion of ascending doses (10 to 90 mg)	No drug-related adverse events No change in ALSFRS-R, slow vital capacity, and muscle strength trend toward a greater decline in patients receiving the highest dosage	[89]
I/II (NCT04931862) WVE-004	Randomised, double-blind, placebo-controlled trial	35	Intrathecal injection (single dose of 10, 30, or 60 mg OR multiple doses of 10 mg either every four or 12 weeks)	Single and multiple doses were generally well tolerated. Reduced poly(GP) levels in the CSF. No significant clinical benefits observed after six months on any efficacy measure	[90,91]
IND (IND141673 (Afinersen)	Investigational New Drug Application	1 (mild motor changes/ elevated polyGP in the CSF)	Intrathecal injection (Eight escalating doses from 0.5 mg/kg to 2.0 mg/kg)	Treatment safely tolerated. Good distribution throughout the CSF. CSF polydiGP levels reduced by approximately 80%. ALSFRS-R stable throughout treatment	[88]

5.3. FUS Gene

Mutations in the *FUS* gene are associated with a rare and aggressive form of ALS, often with juvenile onset [61]. FUS is an RNA-binding protein that plays a key role in RNA

metabolism, including regulation of splicing and translation of mRNA, and in DNA repair. To fulfil its role, FUS requires frequent nuclear/cytoplasmic translocation [94]. Mutations in the *FUS* gene are associated with cytoplasmic mislocalisation of the FUS protein, which forms cytoplasmic inclusions that are associated with neuronal degeneration [95]. Therefore, the pathogenetic mechanisms associated with *FUS* mutations appear to be due to loss of function in the nucleus and gain of toxic functions in the cytoplasm [96].

As *FUS* mutations are relatively rare, studies targeting them are limited. However, recent preclinical studies showed that the non-allele-specific FUS ASO ION363 (also called jacifusen), which targets intron 6 of the *FUS* gene, reduced the expression of both FUSP525L mutant and wild-type transcripts in the brain and spinal cord of a mouse model of FUS-ALS. ION363 also reduced levels of insoluble FUS protein and insoluble RNA-binding proteins found in FUS aggregates (Figure 5). In addition, ION363 prevented neurodegeneration of lumbar motoneurons and loss of neuromuscular junction innervation [97]. These results motivated the use of ION363 in a patient with the P525L mutation in FUS in a compassionate use IND application [97]. This application did not require toxicology studies in rodents or monkeys. The patient, a 26-year-old woman, received monthly ascending doses of 20 mg to a maximum of 120 mg intrathecally between June 2019 and March 2020. Treatment started six months after disease onset, when the disease was already at an advanced stage. The participant did not experience any serious adverse events. The patient died of ALS in May 2020. Neuropathological examination showed that ION363 reduced wild-type and mutant FUS protein with a decrease in FUS aggregates. There was little nuclear FUS staining in the spinal cord and motor cortex, and FUS-containing aggregates in motor neurons were reduced compared with the untreated ALS-FUSP525L control, in which FUS aggregates were abundant [97].

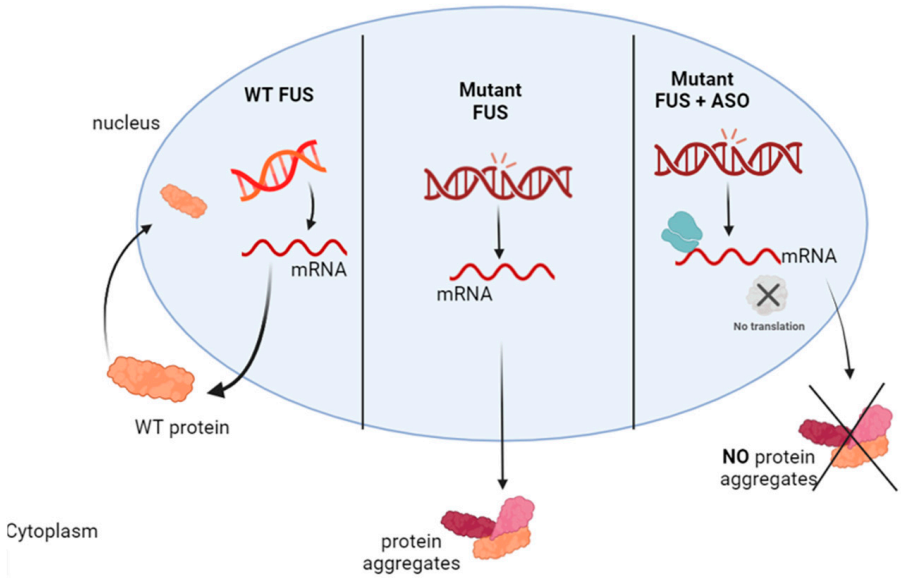

Figure 5. Mechanism of action of ASO in FUS-ALS: Mutated *FUS* leads to cytoplasmic mislocalisation of the FUS protein and formation of protein aggregates in the cytoplasm. ASO therapy, decreasing the expression of both FUS mutant and wild-type transcripts, reduces FUS-containing aggregates.

Based on these positive results, the clinical efficacy, safety, and pharmacology of ION363 (jacifusen) are being evaluated in Phase III clinical trials in ALS patients with *FUS* mutations (FUSION; NCT04768972). A total of 64 patients will be enrolled by March 2024 and will be randomised in a 2:1 ratio to receive jacifusen or placebo monthly or bimonthly for 29 weeks in part 1 of the study. Part 2 of the study will be a subsequent 72-week open-label extension period in which all patients will receive jacifusen. Participants will be transferred to the Part 2/open-label extension of the study if they show significant functional decline during Part 1. The primary outcome includes an assessment of the ALSFRS-R, the time to rescue, and the survival time without ventilator support. Secondary

outcomes will be the evaluation of muscle and lung function, survival, and changes in CSF FUS protein and neurofilaments. Results are expected in June 2025.

5.4. Other ALS-Related Genes

An interesting target for ALS therapy could be TDP-43, encoded by the *TARDBP* gene. It is a DNA/RNA-binding protein that plays a key role in RNA processing, regulating transcription, splicing, mRNA transport, mRNA stabilisation, and miRNA maturation [98]. Under normal conditions, TDP-43 is mainly located in the nucleus, but in many neurodegenerative diseases such as ALS, TDP-43 is sequestered in the cytoplasm, where it forms characteristic inclusions [99]. Nuclear depletion of TDP-43 leads to detrimental changes in the cell [98,100]. Given its fundamental role, an approach involving the total downregulation of TDP-43 levels must be ruled out [101–103]. An alternative approach is to attempt to correct the splicing defects of specific mRNAs that result from nuclear depletion of TDP-43. One interesting potential target is stathmin-2. Stathmin-2, encoded by the *STMN2* gene, is a microtubule-binding protein that is abundant in motor neurons and critical for axonal stability and regeneration. Its expression is reduced in both sporadic and familial ALS patients [104]. TDP-43 binds *STMN2* pre-mRNA and represses the inclusion of a cryptic exon in the mRNA. When TDP-43 is depleted, this cryptic exon is incorporated into the mRNA, resulting in a truncated, non-functional transcript. The subsequent decrease in the functional level of stathmin-2 appears to contribute to the pathogenesis of ALS [105]. An ASO that sterically blocks the cryptic splice site region of the stathmin-2 pre-mRNA, similar to the action of TDP-43, was able to restore normal splicing and functionality of stathmin-2 in human motor neurons and in a mouse model [106]. An ASO with a similar mechanism of action, called QRL-201, is being investigated in a randomised, double-blind, placebo-controlled Phase 1 study to assess its safety and tolerability in ALS (ANQUR, NCT05633459).

Another approach to developing ASO therapies is to consider modifier genes as potential targets. In this case, the target is not a causative gene, but a relatively common gene variant that confers an increasing risk of ALS. This strategy may be an important alternative for ALS patients without known mutations, mainly those with sporadic ALS. Ataxin-2 is a well-characterised example of such a modifier. It is an RNA-binding protein found in RNA-containing granules, encoded by the *ATXN2* gene. Ataxin-2 has a polyglutamine tract encoded by cytosine-adenine-guanine (CAG) repeats, which are less than 30 in healthy individuals. A number of CAG repeats of 34 or more is associated with the severe neurodegenerative disease spinocerebellar ataxia 2 (SCA2) [107], while intermediate CAG expansions (27–33 glutamines) are associated with an increased risk of ALS [108,109]. Treatment of a TDP-43 mouse model with an ASO that reduces ataxin-2 levels has been shown to have a beneficial effect on motor function and survival [108]. A placebo-controlled Phase 1/2 study was initiated in September 2020 to evaluate the safety and pharmacokinetics of the intrathecally administered BIIB105, an ASO designed to reduce ataxin-2 levels in ALS patients with or without intermediate CAG expansions (ALSpire; NCT04494256). The study is expected to end in July 2026.

6. Spinal Bulbar Muscular Atrophy (SBMA)

Spinal and bulbar muscular atrophy (SBMA), also known as Kennedy disease, is an X-linked recessive neuromuscular disease characterised primarily by the degeneration of lower motor neurons [110,111]. The disease typically affects only males, although females can be carriers and sometimes experience muscle cramps. The prevalence is 1–2 per 100,000 people [111,112]. Onset usually occurs at around 30–40 years of age, with a range of 18–64 years [113]. The disease is characterised by the progressive degeneration of muscle and lower motor neurons, resulting in muscle weakness, atrophy, and fasciculations. The progression is slow compared to other motor neuron diseases, with a decline in muscle strength of about 2% per year [114]. As the bulbar muscles become affected, people with SBMA develop difficulties with speech and swallowing [111].

SBMA is caused by a CAG repeat expansion in the androgen receptor (*AR*) gene on the X chromosome, with a corresponding increase in the length of a polyglutamine tract in the AR protein [115]. Notably, SBMA was the first of many neurological disorders caused by expanded polyglutamine tracts to be identified. In healthy individuals, the repeat is present with a range of 9–36 CAGs, whereas in SBMA patients it is expanded to 39–72 CAGs, with the repeat length correlating with age of onset and disease severity [115].

The AR is a ligand-dependent transcription factor that, through its N-terminal domain, interacts with coregulatory proteins to regulate the transcription of androgen-responsive target genes. Mutation of the *AR* gene causes both gain and loss of function of the receptor. However, the primary effect of the mutation is to alter the protein structure such that the receptor becomes toxic to motor neurons and muscle, causing a toxic gain of function of the protein. The loss-of-function effect results in partial androgen insensitivity with gynecomastia and reduced fertility, which does not appear to be directly related to the progressive weakness and loss of motor neurons [116]. The mechanisms underlying the neurodegenerative gain of function in SBMA are not fully understood [117]. Nuclear accumulation and aggregation of polyQ-ARs may contribute to motor neuron degeneration through a variety of molecular mechanisms involving disruption of multiple processes such as transcriptional regulation, protein homeostasis, intracellular trafficking, mitochondrial function, and cellular signalling [118].

Preclinical studies have shown that ASOs can mediate the degradation of mutant *AR* transcripts, reducing mRNA and protein levels in animal models. ASOs used in this case are gapmers that bind to AR mRNA and trigger RNase H cleavage and RNA degradation. A first study focused on two different 2′,4′-constrained ethyl (cEt) gapmers that caused a dose-dependent reduction of *AR* mRNA in HUVEC cells, named ASO1 and ASO2, and investigated whether they were able to ameliorate peripheral muscle pathology in transgenic SBMA mouse models [119]. ASO1 targets a region of the *AR* mRNA that is conserved between human and mouse transcripts, whereas ASO2 targets a human-specific region. ASO1 and ASO2 were administered subcutaneously to the AR113Q and humanised BAC fxAR121 SBMA mouse models, respectively. ASO treatment resulted in a significant knockdown of *AR* mRNA and an almost complete reduction of AR protein levels in the mouse quadriceps muscle, with an overall improvement in the disease phenotype. As the gapmers used in this study are unable to cross the blood–brain barrier, AR expression in the spinal cord was unaffected, demonstrating that skeletal muscle plays an important role in SBMA and can be considered as a target for ASO treatments.

A subsequent study used intracerebroventricular administration of ASOs in SBMA mice to evaluate the effect of knocking down AR transcripts in neurons rather than in muscle [120]. The AR-97Q mouse model, which expresses both murine and transgenic human AR protein, was treated with intracerebroventricular injection of either ASO-AR1 (targeting both human and murine *AR*) or ASO-2 (mouse-specific), both of which are 2′-MOE gapmers. Treatment resulted in a significant decrease in mutant AR mRNA and protein in the spinal cord and brain, while AR levels in peripheral muscle were unaffected. Mice treated with either ASO also showed a marked improvement in the clinical phenotype, which was confirmed by immunohistochemical analysis showing numerous markers of improvement, such as reduced neuronal degeneration and improved neuromuscular junction endplate maturation. Despite the negligible uptake of ASO into skeletal muscle, the muscles of ASO-AR1-treated mice showed restored fibre size and reduced atrophy compared to controls. The results of these preclinical studies are summarised in Table 8.

Taken together, these studies show that ASO treatment could be effective in SBMA and that AR knockdown in both peripheral tissues and the CNS is associated with an improved clinical phenotype of the disease. However, as both groups used gapmers that are unable to cross the blood–brain barrier, the treatments were mutually exclusive of either the CNS or peripheral muscles, depending on the route of administration. Given recent advances in the identification of nanocarriers and apoptotic bodies that can enhance oligonucleotide

blood–brain barrier penetration [25,121,122], the next generation of treatments for SBMA may consist of ASOs able to target both CNS and peripheral tissues with a single injection.

Table 8. Summary of preclinical studies of ASO targeting *AR*.

Year	Results	Ref.
2014	Subcutaneous administration of: ASO1 (targeting a region of the *AR* mRNA conserved between human and mouse transcripts) to the AR113Q mouse model, and ASO2 (which targets a human-specific region of the *AR* mRNA) to the humanised BAC fxAR121 SBMA mouse model. Significant knockdown of *AR* mRNA and an almost complete reduction of AR protein levels in the quadriceps muscle, with an overall improvement in the disease phenotype. AR expression in the spinal cord unaffected.	[119]
2015	Intracerebroventricular injection of either ASO-AR1 (targeting both human and murine AR) or ASO-2 (mouse-specific) in the AR-97Q mouse model, which expresses both murine and transgenic human AR protein. Significant decrease in mutant *AR* mRNA and protein in the spinal cord and brain. AR levels in peripheral muscle unaffected. Marked improvement in the clinical phenotype, confirmed by immunohistochemical analysis, with restored fibre size and reduced atrophy also in the muscles.	[120]

7. Discussion and Future Directions

In recent years, the use of ASOs has given new impetus to research and the development of effective therapies for many previously untreatable diseases. These include motor neuron diseases, i.e., sporadic and inherited neurodegenerative conditions that entirely or predominantly injure motor neurons and include SBMA, spinal muscular atrophy (SMA), and amyotrophic lateral sclerosis (ALS). In this field, the use of ASOs has led to both great successes and failures. The greatest success was certainly the development of a therapy for SMA based on an ASO known as nusinersen, which is able to compensate for the lack of the SMN protein in SMA by influencing the splice efficiency of exon 7 in the *SMN2* gene. The drug has been shown to significantly improve motor function and increase survival in SMA patients. In just a few years, it has been possible to move from the pre-clinical phase to the approval and marketing of the drug (FDA in 2016 and EMA in 2017) thanks to effective collaboration among different stakeholders to build a robust pathway based on pre-clinical, translational, and clinical evidence to support the regulatory process. Nusinersen has been the first effective therapy for SMA, demonstrating that it is possible to provide patients with effective therapies that can improve symptoms and slow disease progression. This has paved the way for new therapeutic approaches.

Another very positive result was obtained in the treatment of ALS associated with mutations in the *SOD1* gene. Tofersen is an ASO designed for the treatment of ALS patients carrying mutations in the *SOD1* gene. The data collected so far have shown that it reduces biomarker degeneration levels (NfL) and can slow disease progression, especially if treatment is started early after the onset of symptoms. Further long-term clinical studies are still ongoing, but the FDA approved tofersen in 2023 under its Accelerated Approval Program, which allows early approval of drugs that treat serious conditions and fill an unmet medical need based on surrogate markers, and EMA approval arrived in February 2024. This is a milestone in the history of ALS research that has shown for the first time that the disease, at least in some of its forms, can be a treatable condition.

These results have stimulated the search for ASO-based therapies for ALS associated with mutations in other genes. Clinical trials with ASOs targeting *FUS*, *STMN2*, and *ATXN2* are underway and will show whether these therapies are effective in the coming years. The case of hexanucleotide expansion of the *C9orf72* gene deserves a separate discussion. Given the frequency of this mutation in both familial and sporadic forms of ALS, ASOs directed against the sense mRNA, targeting the mRNA containing the repeat expansion,

have been developed and tested with encouraging results in animal models. Based on the promising data, two different companies started phase 1/2 clinical trials with ASOs targeting different regions of the sense repeat mRNA (WVE-004-NCT04931862, Wave Life Sciences; BIIB078-NCT03626012, Biogen/Ionis). Unfortunately, both trials were halted after an interim analysis of results as neither the primary nor secondary endpoints were met.

At this stage, it is not clear what the cause of these failures might be. Various hypotheses have been suggested [123,124]. The ASOs could affect the expression level of wild-type *C9orf72*. These ASOs were designed not to affect the expression of the normal C9orf72 protein, but an effect on global C9orf72 expression in patients could explain the negative effects, as previously observed in mice [125]. In addition, the antisense repeat mRNA may be more important than predicted. This antisense RNA and the DPRs translated from it are not affected by the ASOs tested, and it remains to be clarified whether degradation of the sense RNA affects the antisense RNA. Finally, the question of why ASOs that reduce the amount of sense repeat RNA and the DPRs translated from it appear to have a negative rather than neutral effect on ALS patients remains unanswered.

The positive and negative results obtained so far highlight some important general aspects of the development of ASO-based therapies. First, when considering the treatment of genetic diseases with ASOs, the genetic background/inheritance pattern of the disease must be taken into account when evaluating possible therapeutic approaches.

The first distinction is between two main disease mechanisms caused by pathogenic variants: loss of function (LoF) and gain of function (GoF). Autosomal recessive disorders are usually associated with LoF variants. LoF variants can lead to loss of the gene product, nonsense-mediated decay of RNA transcripts, production of unstable proteins or proteins with no or reduced function [126]. Regardless of the mechanism of action, the general therapeutic approach to LoF is to attempt to restore protein function by resetting the reading frame to either the canonical transcript or a modified transcript that produces a (at least partially) functional protein [127]. In the case of SMA, the presence of the paralogue gene *SMN2* partially facilitated this process, as it was possible to target a specific splicing silencer site in intron 7 of *SMN2* and prevent specific splicing repressors from binding to it, allowing the integration of exon 7 into the final transcript and increasing the synthesis of a full-length functional SMN protein.

In general, LoF variants are relatively easier to deal with than GoF variants. LoF genes are often approached by restoring healthy copies, whereas GoF genes are approached by targeting the diseased allele, gene, or protein for degradation. Examples of such toxic effects include, but are not limited to, missense variants and expanded repeats, which confer additional functions to the protein, increasing its propensity to form aggregates, a common feature of several neurodegenerative diseases. Therefore, one way to develop an effective therapy might be to degrade toxic aggregates or prevent their formation. This approach could stop or slow the progression of the disease, but in principle could also prevent disease manifestation if the treatment is started before the onset of the disease. ASOs could play a key role in such a therapeutic strategy. In this case, there are two different options. A selective strategy involves the use of ASOs that degrade the toxic (mutant) variant while preserving the wild-type form of the protein. The subtle differences between wild-type and pathogenic alleles could be exploited to selectively target the mutant (pre-)mRNA and thus selectively prevent the expression of only the toxic protein variant [128,129]. On the other hand, non-selective targeting of the affected gene could reduce both the toxic and wild-type variants, thus reducing the function of the protein. This is certainly a simpler approach and does not require the use of tailored therapies (different ASOs for different mutations), but it implies that physiologically necessary functions of the wild-type protein are also reduced. A non-specific knockdown of a protein can have serious, unpredictable consequences, so it is extremely important to assess the extent to which the gene can tolerate downregulation without causing additional damage. These negative effects on the wild-type protein could be the reason for the failure of ASO treatment in ALS patients with the *C9orf72* gene mutation, as discussed above. Such negative effects have not been

seen with tofersen treatment in ALS patients with *SOD1* mutations. However, long-term follow-up of these patients is needed, as the observation that recessive null mutations are associated with early and progressive neurological dysfunction [130] suggests that continued suppression of the normal *SOD1* allele may have adverse effects.

Another important aspect to consider is the need for a thorough understanding of the molecular mechanisms underlying the disease (particularly in the presence of alterations in the different genes associated with ALS). This would make it possible to define within what margins it is possible to act, and what can and cannot be done. Research, even basic research, still has a fundamental role to play in this field. This can also be of relevance for the development of more complex therapeutic approaches. One example is the attempt to correct splice defects due to nuclear depletion of TDP-43. The major advantage of this strategy is that a much larger population of ALS patients than just mutation carriers could benefit from this therapeutic strategy, as mislocalisation of TDP-43 is seen in almost all ALS patients. However, in view of its fundamental role, a total downregulation of TDP-43 levels must be ruled out. An alternative approach is to attempt to correct the splicing defects of specific mRNAs that result from nuclear depletion of TDP-43. However, since many mRNAs are aberrantly processed in the absence of nuclear TDP-43, it is unclear whether correcting these single, specific splicing abnormalities will prove effective. It is possible that several of these mis-spliced mRNAs may need to be corrected with a cocktail of ASOs before any therapeutic benefit is achieved. Alternatively, it may be helpful to identify other players that play a key role in the TDP-43-mediated splicing process. SYF2 is a pre-mRNA splicing factor that is recruited to the spliceosome to regulate splicing. When downregulated, it reverses TDP-43 pathology and improves TDP-43 function, including RNA processing, in preclinical models [131]. Thus, ASO-mediated downregulation of SYF2 could restore mis-splicing of multiple mRNAs. To find out whether this strategy also works in patients with ALS, clinical trials will be crucial.

Currently, ASOs are delivered by intrathecal administration, a rather invasive and technically demanding procedure. Although commonly used in the clinical setting, the invasiveness and cost of the procedure is stimulating the development of alternative routes of drug delivery. Advances in chemistry to enhance potency and conjugation of targeting ligands to the ASO are being developed to provide more effective antisense drugs. The use of delivery particles, such as glucose-coated polymeric nanocarriers and peptide-conjugated ASOs, is very promising for the future as they can cross the BBB and may enhance ASO transport into the CNS after systemic administration. However, delivery by nanoparticles may show toxicity linked to the nature of nanoparticles used. For example, protein-based nanoparticles can exert cardiotoxicity, hepatotoxicity, and hypersensitivity; metal-based nanoparticles show anxiogenic effects together with genotoxicity; and lipid-based nanoparticles exhibit cardiopulmonary distress and hypersensitivity [132] (Figure 6).

Another important point to consider is when to start treatment with ASOs. By the time the first symptoms of the disease appear, the motor neurons have already suffered significant damage that cannot be eliminated. Therefore, therapy can only slow down or at best stop the progression of the disease. Two clinical trials in pre-symptomatic individuals with a genetic diagnosis of SMA (NURTURE, NCT023865539) and carriers of mutations in the *SOD1* gene (ATLAS, NCT04856982) are underway to shed light on this issue. If the results are positive, we could see a revolutionary change for some MNDs, from incurable and fatal to not only treatable but also preventable.

In light of these new perspectives, genetic screening for SMA and SOD1-mediated ALS is of paramount importance. In the case of SMA, newborn screening (NBS) allows the immediate initiation of specific treatment for children with SMA to halt irreversible motor neuron loss and disease progression and ensure motor development like that of children without the neuromuscular disease. The Advisory Committee on Heritable Disorders in Newborns and Children (ACHDNC) added NBS for SMA to the Recommended Uniform Screening Panel in July 2018, and thanks to national or regional pilot projects, SMA NBS was implemented in several countries [133]. About ALS, considering that mutations in the

SOD1 gene account for about 20% of fALS patients and up to 2% of sALS cases, prompt screening for *SOD1* mutations should be performed in all new ALS patients with both familial and sporadic presentations.

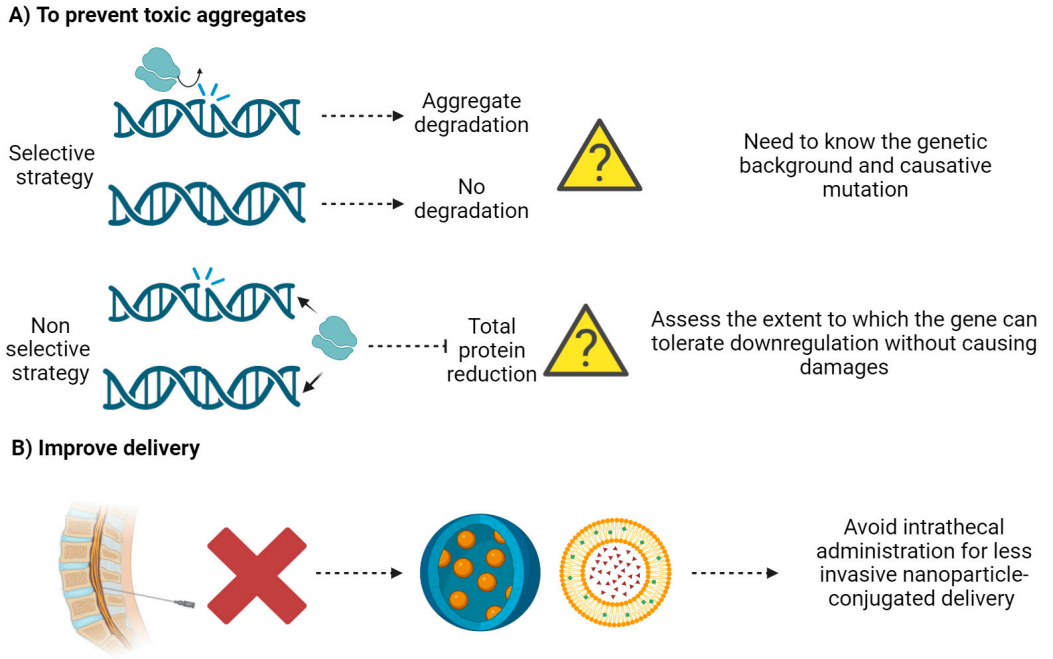

Figure 6. ASO research presents several still open issues. (**A**) To develop an effective therapy, ASOs could be useful in toxic aggregate degradation. By applying a selective strategy, ASOs can degrade the toxic (mutant) variant while preserving the wild-type form of the protein. Alternatively, a non-selective targeting of the affected gene may be chosen, degrading both the toxic and wild-type variants, thus reducing the whole function of the protein. In the first case, the pathogenetic mutation must be known; in the second approach, it is extremely important to assess the extent to which the gene can tolerate downregulation without causing additional damage. (**B**) Commonly, ASOs are intrathecally administered. This represents an invasive procedure that can be replaced by developing nanoparticle-conjugated ASOs.

In summary, ASO therapy has made remarkable progress in recent years, bringing significant benefits to the treatment of motor neuron diseases. The greatest success has been the development of nusinersen, the first effective therapy for SMA approved by the FDA and EMA, able to improve symptoms and slow disease progression. This was followed a few years later by tofersen, which was approved to treat ALS patients with SOD1 mutations. On the other hand, there is still a long way to go regarding other forms of ALS associated with mutations in other genes, particularly *C9orf72*. A deeper understanding of the pathogenetic mechanisms linked to the presence of mutations, together with the development of increasingly effective and high-performance molecules, may make it possible to develop new therapies against these neurodegenerative diseases.

Author Contributions: Conceptualization, C.R. and S.C.; writing—original draft preparation, C.R. and S.C.; writing—review and editing, C.R., S.C. and G.S.; visualization, S.C. All authors have read and agreed to the published version of the manuscript.

Funding: This research received no external funding.

Institutional Review Board Statement: Not applicable.

Data Availability Statement: Not applicable.

Conflicts of Interest: The authors declare no conflicts of interest.

References

1. Shadid, M.; Badawi, M.; Abulrob, A. Antisense Oligonucleotides: Absorption, Distribution, Metabolism, and Excretion. *Expert. Opin. Drug Metab. Toxicol.* **2021**, *17*, 1281–1292. [CrossRef]
2. Bennett, C.F. Therapeutic Antisense Oligonucleotides Are Coming of Age. *Annu. Rev. Med.* **2019**, *70*, 307–321. [CrossRef]
3. Crooke, S.T.; Wang, S.; Vickers, T.A.; Shen, W.; Liang, X.-H. Cellular Uptake and Trafficking of Antisense Oligonucleotides. *Nat. Biotechnol.* **2017**, *35*, 230–237. [CrossRef]
4. Migawa, M.T.; Shen, W.; Wan, W.B.; Vasquez, G.; Oestergaard, M.E.; Low, A.; De Hoyos, C.L.; Gupta, R.; Murray, S.; Tanowitz, M.; et al. Site-Specific Replacement of Phosphorothioate with Alkyl Phosphonate Linkages Enhances the Therapeutic Profile of Gapmer ASOs by Modulating Interactions with Cellular Proteins. *Nucleic Acids Res.* **2019**, *47*, 5465–5479. [CrossRef]
5. Egli, M.; Manoharan, M. Chemistry, Structure and Function of Approved Oligonucleotide Therapeutics. *Nucleic Acids Res.* **2023**, *51*, 2529–2573. [CrossRef]
6. Chan, J.H.P.; Lim, S.; Wong, W.S.F. Antisense Oligonucleotides: From Design to Therapeutic Application. *Clin. Exp. Pharmacol. Physiol.* **2006**, *33*, 533–540. [CrossRef] [PubMed]
7. Prakash, T.P.; Graham, M.J.; Yu, J.; Carty, R.; Low, A.; Chappell, A.; Schmidt, K.; Zhao, C.; Aghajan, M.; Murray, H.F.; et al. Targeted Delivery of Antisense Oligonucleotides to Hepatocytes Using Triantennary N-Acetyl Galactosamine Improves Potency 10-Fold in Mice. *Nucleic Acids Res.* **2014**, *42*, 8796–8807. [CrossRef] [PubMed]
8. Liang, X.-H.; Shen, W.; Sun, H.; Kinberger, G.A.; Prakash, T.P.; Nichols, J.G.; Crooke, S.T. Hsp90 Protein Interacts with Phosphorothioate Oligonucleotides Containing Hydrophobic 2′-Modifications and Enhances Antisense Activity. *Nucleic Acids Res.* **2016**, *44*, 3892–3907. [CrossRef] [PubMed]
9. Dowdy, S.F.; Setten, R.L.; Cui, X.-S.; Jadhav, S.G. Delivery of RNA Therapeutics: The Great Endosomal Escape! *Nucleic Acid Ther.* **2022**, *32*, 361–368. [CrossRef]
10. Ren, X.; Deng, R.; Wang, L.; Zhang, K.; Li, J. RNA Splicing Process Analysis for Identifying Antisense Oligonucleotide Inhibitors with Padlock Probe-Based Isothermal Amplification. *Chem. Sci.* **2017**, *8*, 5692–5698. [CrossRef]
11. Butler, M.; Crooke, R.M.; Graham, M.J.; Lemonidis, K.M.; Lougheed, M.; Murray, S.F.; Witchell, D.; Steinbrecher, U.; Bennett, C.F. Phosphorothioate Oligodeoxynucleotides Distribute Similarly in Class A Scavenger Receptor Knockout and Wild-Type Mice. *J. Pharmacol. Exp. Ther.* **2000**, *292*, 489–496. [PubMed]
12. Finkel, R.S.; Chiriboga, C.A.; Vajsar, J.; Day, J.W.; Montes, J.; De Vivo, D.C.; Yamashita, M.; Rigo, F.; Hung, G.; Schneider, E.; et al. Treatment of Infantile-Onset Spinal Muscular Atrophy with Nusinersen: A Phase 2, Open-Label, Dose-Escalation Study. *Lancet* **2016**, *388*, 3017–3026. [CrossRef] [PubMed]
13. Kordasiewicz, H.B.; Stanek, L.M.; Wancewicz, E.V.; Mazur, C.; McAlonis, M.M.; Pytel, K.A.; Artates, J.W.; Weiss, A.; Cheng, S.H.; Shihabuddin, L.S.; et al. Sustained Therapeutic Reversal of Huntington's Disease by Transient Repression of Huntingtin Synthesis. *Neuron* **2012**, *74*, 1031–1044. [CrossRef] [PubMed]
14. Passini, M.A.; Bu, J.; Richards, A.M.; Kinnecom, C.; Sardi, S.P.; Stanek, L.M.; Hua, Y.; Rigo, F.; Matson, J.; Hung, G.; et al. Antisense Oligonucleotides Delivered to the Mouse CNS Ameliorate Symptoms of Severe Spinal Muscular Atrophy. *Sci. Transl. Med.* **2011**, *3*, 72ra18. [CrossRef] [PubMed]
15. Rigo, F.; Chun, S.J.; Norris, D.A.; Hung, G.; Lee, S.; Matson, J.; Fey, R.A.; Gaus, H.; Hua, Y.; Grundy, J.S.; et al. Pharmacology of a Central Nervous System Delivered 2′- O -Methoxyethyl–Modified Survival of Motor Neuron Splicing Oligonucleotide in Mice and Nonhuman Primates. *J. Pharmacol. Exp. Ther.* **2014**, *350*, 46–55. [CrossRef] [PubMed]
16. Smith, R.A.; Miller, T.M.; Yamanaka, K.; Monia, B.P.; Condon, T.P.; Hung, G.; Lobsiger, C.S.; Ward, C.M.; McAlonis-Downes, M.; Wei, H.; et al. Antisense Oligonucleotide Therapy for Neurodegenerative Disease. *J. Clin. Investig.* **2006**, *116*, 2290–2296. [CrossRef] [PubMed]
17. Hua, Y.; Sahashi, K.; Hung, G.; Rigo, F.; Passini, M.A.; Bennett, C.F.; Krainer, A.R. Antisense Correction of SMN2 Splicing in the CNS Rescues Necrosis in a Type III SMA Mouse Model. *Genes. Dev.* **2010**, *24*, 1634–1644. [CrossRef] [PubMed]
18. DeVos, S.L.; Miller, R.L.; Schoch, K.M.; Holmes, B.B.; Kebodeaux, C.S.; Wegener, A.J.; Chen, G.; Shen, T.; Tran, H.; Nichols, B.; et al. Tau Reduction Prevents Neuronal Loss and Reverses Pathological Tau Deposition and Seeding in Mice with Tauopathy. *Sci. Transl. Med.* **2017**, *9*, eaag0481. [CrossRef] [PubMed]
19. McCampbell, A.; Cole, T.; Wegener, A.J.; Tomassy, G.S.; Setnicka, A.; Farley, B.J.; Schoch, K.M.; Hoye, M.L.; Shabsovich, M.; Sun, L.; et al. Antisense Oligonucleotides Extend Survival and Reverse Decrement in Muscle Response in ALS Models. *J. Clin. Investig.* **2018**, *128*, 3558–3567. [CrossRef]
20. Bennett, C.F.; Krainer, A.R.; Cleveland, D.W. Antisense Oligonucleotide Therapies for Neurodegenerative Diseases. *Annu. Rev. Neurosci.* **2019**, *42*, 385–406. [CrossRef]
21. Benedict, C.; Frey, W.H.; Schiöth, H.B.; Schultes, B.; Born, J.; Hallschmid, M. Intranasal Insulin as a Therapeutic Option in the Treatment of Cognitive Impairments. *Exp. Gerontol.* **2011**, *46*, 112–115. [CrossRef] [PubMed]
22. Wu, H.; Zhou, Y.; Wang, Y.; Tong, L.; Wang, F.; Song, S.; Xu, L.; Liu, B.; Yan, H.; Sun, Z. Current State and Future Directions of Intranasal Delivery Route for Central Nervous System Disorders: A Scientometric and Visualization Analysis. *Front. Pharmacol.* **2021**, *12*, 717192. [CrossRef] [PubMed]
23. Zhang, Y.-T.; He, K.-J.; Zhang, J.-B.; Ma, Q.-H.; Wang, F.; Liu, C.-F. Advances in Intranasal Application of Stem Cells in the Treatment of Central Nervous System Diseases. *Stem Cell Res. Ther.* **2021**, *12*, 210. [CrossRef]

24. Dhuria, S.V.; Hanson, L.R.; Frey, W.H. Intranasal Delivery to the Central Nervous System: Mechanisms and Experimental Considerations. *J. Pharm. Sci.* **2010**, *99*, 1654–1673. [CrossRef] [PubMed]
25. Min, H.S.; Kim, H.J.; Naito, M.; Ogura, S.; Toh, K.; Hayashi, K.; Kim, B.S.; Fukushima, S.; Anraku, Y.; Miyata, K.; et al. Systemic Brain Delivery of Antisense Oligonucleotides across the Blood–Brain Barrier with a Glucose-Coated Polymeric Nanocarrier. *Angew. Chem. Int. Ed.* **2020**, *59*, 8173–8180. [CrossRef]
26. Mercuri, E.; Sumner, C.J.; Muntoni, F.; Darras, B.T.; Finkel, R.S. Spinal Muscular Atrophy. *Nat. Rev. Dis. Primers* **2022**, *8*, 52. [CrossRef] [PubMed]
27. Sugarman, E.A.; Nagan, N.; Zhu, H.; Akmaev, V.R.; Zhou, Z.; Rohlfs, E.M.; Flynn, K.; Hendrickson, B.C.; Scholl, T.; Sirko-Osadsa, D.A.; et al. Pan-Ethnic Carrier Screening and Prenatal Diagnosis for Spinal Muscular Atrophy: Clinical Laboratory Analysis of >72,400 Specimens. *Eur. J. Hum. Genet.* **2012**, *20*, 27–32. [CrossRef]
28. Ogino, S.; Leonard, D.G.B.; Rennert, H.; Ewens, W.J.; Wilson, R.B. Genetic Risk Assessment in Carrier Testing for Spinal Muscular Atrophy. *Am. J. Med. Genet.* **2002**, *110*, 301–307. [CrossRef]
29. Emery, A.E.H. Population Frequencies of Inherited Neuromuscular Diseases—A World Survey. *Neuromuscul. Disord.* **1991**, *1*, 19–29. [CrossRef]
30. Schrank, B.; Götz, R.; Gunnersen, J.M.; Ure, J.M.; Toyka, K.V.; Smith, A.G.; Sendtner, M. Inactivation of the Survival Motor Neuron Gene, a Candidate Gene for Human Spinal Muscular Atrophy, Leads to Massive Cell Death in Early Mouse Embryos. *Proc. Natl. Acad. Sci. USA* **1997**, *94*, 9920–9925. [CrossRef]
31. Crisafulli, S.; Boccanegra, B.; Vitturi, G.; Trifirò, G.; De Luca, A. Pharmacological Therapies of Spinal Muscular Atrophy: A Narrative Review of Preclinical, Clinical–Experimental, and Real-World Evidence. *Brain Sci.* **2023**, *13*, 1446. [CrossRef]
32. Rochette, C.F.; Gilbert, N.; Simard, L.R. SMN Gene Duplication and the Emergence of the SMN2 Gene Occurred in Distinct Hominids: SMN2 Is Unique to Homo Sapiens. *Hum. Genet.* **2001**, *108*, 255–266. [CrossRef]
33. Cartegni, L.; Krainer, A.R. Disruption of an SF2/ASF-Dependent Exonic Splicing Enhancer in SMN2 Causes Spinal Muscular Atrophy in the Absence of SMN1. *Nat. Genet.* **2002**, *30*, 377–384. [CrossRef] [PubMed]
34. Cartegni, L.; Hastings, M.L.; Calarco, J.A.; de Stanchina, E.; Krainer, A.R. Determinants of Exon 7 Splicing in the Spinal Muscular Atrophy Genes, SMN1 and SMN2. *Am. J. Hum. Genet.* **2006**, *78*, 63–77. [CrossRef]
35. Kashima, T.; Manley, J.L. A Negative Element in SMN2 Exon 7 Inhibits Splicing in Spinal Muscular Atrophy. *Nat. Genet.* **2003**, *34*, 460–463. [CrossRef] [PubMed]
36. Kashima, T.; Rao, N.; David, C.J.; Manley, J.L. hnRNP A1 Functions with Specificity in Repression of SMN2 Exon 7 Splicing. *Hum. Mol. Genet.* **2007**, *16*, 3149–3159. [CrossRef] [PubMed]
37. Lorson, C.L.; Hahnen, E.; Androphy, E.J.; Wirth, B. A Single Nucleotide in the SMN Gene Regulates Splicing and Is Responsible for Spinal Muscular Atrophy. *Proc. Natl. Acad. Sci. USA* **1999**, *96*, 6307–6311. [CrossRef]
38. Prior, T.W.; Krainer, A.R.; Hua, Y.; Swoboda, K.J.; Snyder, P.C.; Bridgeman, S.J.; Burghes, A.H.M.; Kissel, J.T. A Positive Modifier of Spinal Muscular Atrophy in the SMN2 Gene. *Am. J. Hum. Genet.* **2009**, *85*, 408–413. [CrossRef]
39. Rudnik-Schöneborn, S.; Berg, C.; Zerres, K.; Betzler, C.; Grimm, T.; Eggermann, T.; Eggermann, K.; Wirth, R.; Wirth, B.; Heller, R. Genotype-Phenotype Studies in Infantile Spinal Muscular Atrophy (SMA) Type I in Germany: Implications for Clinical Trials and Genetic Counselling. *Clin. Genet.* **2009**, *76*, 168–178. [CrossRef]
40. Wirth, B.; Herz, M.; Wetter, A.; Moskau, S.; Hahnen, E.; Rudnik-Schöneborn, S.; Wienker, T.; Zerres, K. Quantitative Analysis of Survival Motor Neuron Copies: Identification of Subtle SMN1 Mutations in Patients with Spinal Muscular Atrophy, Genotype-Phenotype Correlation, and Implications for Genetic Counseling. *Am. J. Hum. Genet.* **1999**, *64*, 1340–1356. [CrossRef]
41. Wirth, B.; Brichta, L.; Schrank, B.; Lochmüller, H.; Blick, S.; Baasner, A.; Heller, R. Mildly Affected Patients with Spinal Muscular Atrophy Are Partially Protected by an Increased SMN2 Copy Number. *Hum. Genet.* **2006**, *119*, 422–428. [CrossRef]
42. Skordis, L.A.; Dunckley, M.G.; Yue, B.; Eperon, I.C.; Muntoni, F. Bifunctional Antisense Oligonucleotides Provide a Trans-Acting Splicing Enhancer That Stimulates SMN2 Gene Expression in Patient Fibroblasts. *Proc. Natl. Acad. Sci. USA* **2003**, *100*, 4114–4119. [CrossRef]
43. Keil, J.M.; Seo, J.; Howell, M.D.; Hsu, W.H.; Singh, R.N.; DiDonato, C.J. A Short Antisense Oligonucleotide Ameliorates Symptoms of Severe Mouse Models of Spinal Muscular Atrophy. *Mol. Ther. Nucleic Acids* **2014**, *3*, e174. [CrossRef]
44. Nizzardo, M.; Simone, C.; Dametti, S.; Salani, S.; Ulzi, G.; Pagliarani, S.; Rizzo, F.; Frattini, E.; Pagani, F.; Bresolin, N.; et al. Spinal Muscular Atrophy Phenotype Is Ameliorated in Human Motor Neurons by SMN Increase via Different Novel RNA Therapeutic Approaches. *Sci. Rep.* **2015**, *5*, 11746. [CrossRef]
45. Hua, Y.; Vickers, T.A.; Okunola, H.L.; Bennett, C.F.; Krainer, A.R. Antisense Masking of an hnRNP A1/A2 Intronic Splicing Silencer Corrects SMN2 Splicing in Transgenic Mice. *Am. J. Hum. Genet.* **2008**, *82*, 834–848. [CrossRef]
46. Singh, N.K.; Singh, N.N.; Androphy, E.J.; Singh, R.N. Splicing of a Critical Exon of Human Survival Motor Neuron Is Regulated by a Unique Silencer Element Located in the Last Intron. *Mol. Cell Biol.* **2006**, *26*, 1333–1346. [CrossRef]
47. Chiriboga, C.A.; Swoboda, K.J.; Darras, B.T.; Iannaccone, S.T.; Montes, J.; De Vivo, D.C.; Norris, D.A.; Bennett, C.F.; Bishop, K.M. Results from a Phase 1 Study of Nusinersen (ISIS-SMN(Rx)) in Children with Spinal Muscular Atrophy. *Neurology* **2016**, *86*, 890–897. [CrossRef]
48. Finkel, R.S.; Mercuri, E.; Darras, B.T.; Connolly, A.M.; Kuntz, N.L.; Kirschner, J.; Chiriboga, C.A.; Saito, K.; Servais, L.; Tizzano, E.; et al. Nusinersen versus Sham Control in Infantile-Onset Spinal Muscular Atrophy. *N. Engl. J. Med.* **2017**, *377*, 1723–1732. [CrossRef]

49. Mercuri, E.; Darras, B.T.; Chiriboga, C.A.; Day, J.W.; Campbell, C.; Connolly, A.M.; Iannaccone, S.T.; Kirschner, J.; Kuntz, N.L.; Saito, K.; et al. Nusinersen versus Sham Control in Later-Onset Spinal Muscular Atrophy. *N. Engl. J. Med.* **2018**, *378*, 625–635. [CrossRef] [PubMed]
50. Xu, L.; Irony, I.; Bryan, W.W.; Dunn, B. Development of Gene Therapies—Lessons from Nusinersen. *Gene Ther.* **2017**, *24*, 527–528. [CrossRef] [PubMed]
51. Hua, Y.; Sahashi, K.; Rigo, F.; Hung, G.; Horev, G.; Bennett, C.F.; Krainer, A.R. Peripheral SMN Restoration Is Essential for Long-Term Rescue of a Severe Spinal Muscular Atrophy Mouse Model. *Nature* **2011**, *478*, 123–126. [CrossRef] [PubMed]
52. De Vivo, D.C.; Bertini, E.; Swoboda, K.J.; Hwu, W.-L.; Crawford, T.O.; Finkel, R.S.; Kirschner, J.; Kuntz, N.L.; Parsons, J.A.; Ryan, M.M.; et al. Nusinersen Initiated in Infants during the Presymptomatic Stage of Spinal Muscular Atrophy: Interim Efficacy and Safety Results from the Phase 2 NURTURE Study. *Neuromuscul. Disord.* **2019**, *29*, 842–856. [CrossRef]
53. Crawford, T.O.; Swoboda, K.J.; De Vivo, D.C.; Bertini, E.; Hwu, W.; Finkel, R.S.; Kirschner, J.; Kuntz, N.L.; Nazario, A.N.; Parsons, J.A.; et al. Continued Benefit of Nusinersen Initiated in the Presymptomatic Stage of Spinal Muscular Atrophy: 5-year Update of the NURTURE Study. *Muscle Nerve* **2023**, *68*, 157–170. [CrossRef]
54. Mead, R.J.; Shan, N.; Reiser, H.J.; Marshall, F.; Shaw, P.J. Amyotrophic Lateral Sclerosis: A Neurodegenerative Disorder Poised for Successful Therapeutic Translation. *Nat. Rev. Drug Discov.* **2023**, *22*, 185–212. [CrossRef] [PubMed]
55. Talbott, E.O.; Malek, A.M.; Lacomis, D. The Epidemiology of Amyotrophic Lateral Sclerosis. In *Handbook of Clinical Neurology*; Elsevier: Amsterdam, The Netherlands, 2016; Volume 138, pp. 225–238. [CrossRef]
56. Hinchcliffe, M.; Smith, A. Riluzole: Real-World Evidence Supports Significant Extension of Median Survival Times in Patients with Amyotrophic Lateral Sclerosis. *Degener. Neurol. Neuromuscul. Dis.* **2017**, *7*, 61–70. [CrossRef] [PubMed]
57. Masrori, P.; Van Damme, P. Amyotrophic Lateral Sclerosis: A Clinical Review. *Eur. J. Neurol.* **2020**, *27*, 1918–1929. [CrossRef]
58. Mejzini, R.; Flynn, L.L.; Pitout, I.L.; Fletcher, S.; Wilton, S.D.; Akkari, P.A. ALS Genetics, Mechanisms, and Therapeutics: Where Are We Now? *Front. Neurosci.* **2019**, *13*, 1310. [CrossRef]
59. Renton, A.E.; Chiò, A.; Traynor, B.J. State of Play in Amyotrophic Lateral Sclerosis Genetics. *Nat. Neurosci.* **2014**, *17*, 17–23. [CrossRef]
60. van Rheenen, W.; van der Spek, R.A.A.; Bakker, M.K.; van Vugt, J.J.F.A.; Hop, P.J.; Zwamborn, R.A.J.; de Klein, N.; Westra, H.-J.; Bakker, O.B.; Deelen, P.; et al. Common and Rare Variant Association Analyses in Amyotrophic Lateral Sclerosis Identify 15 Risk Loci with Distinct Genetic Architectures and Neuron-Specific Biology. *Nat. Genet.* **2021**, *53*, 1636–1648. [CrossRef]
61. Taylor, J.P.; Brown, R.H.; Cleveland, D.W. Decoding ALS: From Genes to Mechanism. *Nature* **2016**, *539*, 197–206. [CrossRef]
62. Rosen, D.R.; Siddique, T.; Patterson, D.; Figlewicz, D.A.; Sapp, P.; Hentati, A.; Donaldson, D.; Goto, J.; O'Regan, J.P.; Deng, H.X. Mutations in Cu/Zn Superoxide Dismutase Gene Are Associated with Familial Amyotrophic Lateral Sclerosis. *Nature* **1993**, *362*, 59–62. [CrossRef] [PubMed]
63. Li, H.-F.; Wu, Z.-Y. Genotype-Phenotype Correlations of Amyotrophic Lateral Sclerosis. *Transl. Neurodegener.* **2016**, *5*, 3. [CrossRef] [PubMed]
64. Bruijn, L.I.; Miller, T.M.; Cleveland, D.W. Unraveling the Mechanisms Involved in Motor Neuron Degeneration in ALS. *Annu. Rev. Neurosci.* **2004**, *27*, 723–749. [CrossRef] [PubMed]
65. Bruijn, L.I.; Cleveland, D.W. Mechanisms of Selective Motor Neuron Death in ALS: Insights from Transgenic Mouse Models of Motor Neuron Disease. *Neuropathol. Appl. Neurobiol.* **1996**, *22*, 373–387. [CrossRef] [PubMed]
66. Foust, K.D.; Salazar, D.L.; Likhite, S.; Ferraiuolo, L.; Ditsworth, D.; Ilieva, H.; Meyer, K.; Schmelzer, L.; Braun, L.; Cleveland, D.W.; et al. Therapeutic AAV9-Mediated Suppression of Mutant SOD1 Slows Disease Progression and Extends Survival in Models of Inherited ALS. *Mol. Ther.* **2013**, *21*, 2148–2159. [CrossRef] [PubMed]
67. Raoul, C.; Abbas-Terki, T.; Bensadoun, J.-C.; Guillot, S.; Haase, G.; Szulc, J.; Henderson, C.E.; Aebischer, P. Lentiviral-Mediated Silencing of SOD1 through RNA Interference Retards Disease Onset and Progression in a Mouse Model of ALS. *Nat. Med.* **2005**, *11*, 423–428. [CrossRef] [PubMed]
68. Miller, T.M.; Pestronk, A.; David, W.; Rothstein, J.; Simpson, E.; Appel, S.H.; Andres, P.L.; Mahoney, K.; Allred, P.; Alexander, K.; et al. An Antisense Oligonucleotide against SOD1 Delivered Intrathecally for Patients with SOD1 Familial Amyotrophic Lateral Sclerosis: A Phase 1, Randomised, First-in-Man Study. *Lancet Neurol.* **2013**, *12*, 435–442. [CrossRef] [PubMed]
69. Heckler, I.; Venkataraman, I. Phosphorylated Neurofilament Heavy Chain: A Potential Diagnostic Biomarker in Amyotrophic Lateral Sclerosis. *J. Neurophysiol.* **2022**, *127*, 737–745. [CrossRef] [PubMed]
70. Miller, T.; Cudkowicz, M.; Shaw, P.J.; Andersen, P.M.; Atassi, N.; Bucelli, R.C.; Genge, A.; Glass, J.; Ladha, S.; Ludolph, A.L.; et al. Phase 1-2 Trial of Antisense Oligonucleotide Tofersen for SOD1 ALS. *N. Engl. J. Med.* **2020**, *383*, 109–119. [CrossRef]
71. Miller, T.M.; Cudkowicz, M.E.; Genge, A.; Shaw, P.J.; Sobue, G.; Bucelli, R.C.; Chiò, A.; Van Damme, P.; Ludolph, A.C.; Glass, J.D.; et al. Trial of Antisense Oligonucleotide Tofersen for SOD1 ALS. *N. Engl. J. Med.* **2022**, *387*, 1099–1110. [CrossRef]
72. Wiesenfarth, M.; Dorst, J.; Brenner, D.; Elmas, Z.; Parlak, Ö.; Uzelac, Z.; Kandler, K.; Mayer, K.; Weiland, U.; Herrmann, C.; et al. Effects of Tofersen Treatment in Patients with SOD1-ALS in a "Real-World" Setting—A 12-Month Multicenter Cohort Study from the German Early Access Program. *EClinicalMedicine* **2024**, *69*, 102495. [CrossRef] [PubMed]
73. Benatar, M.; Wuu, J.; Andersen, P.M.; Bucelli, R.C.; Andrews, J.A.; Otto, M.; Farahany, N.A.; Harrington, E.A.; Chen, W.; Mitchell, A.A.; et al. Design of a Randomized, Placebo-Controlled, Phase 3 Trial of Tofersen Initiated in Clinically Presymptomatic SOD1 Variant Carriers: The ATLAS Study. *Neurotherapeutics* **2022**, *19*, 1248–1258. [CrossRef] [PubMed]

74. Majounie, E.; Renton, A.E.; Mok, K.; Dopper, E.G.P.; Waite, A.; Rollinson, S.; Chiò, A.; Restagno, G.; Nicolaou, N.; Simon-Sanchez, J.; et al. Frequency of the C9orf72 Hexanucleotide Repeat Expansion in Patients with Amyotrophic Lateral Sclerosis and Frontotemporal Dementia: A Cross-Sectional Study. *Lancet Neurol.* **2012**, *11*, 323–330. [CrossRef] [PubMed]
75. Renton, A.E.; Majounie, E.; Waite, A.; Simón-Sánchez, J.; Rollinson, S.; Gibbs, J.R.; Schymick, J.C.; Laaksovirta, H.; van Swieten, J.C.; Myllykangas, L.; et al. A Hexanucleotide Repeat Expansion in C9ORF72 Is the Cause of Chromosome 9p21-Linked ALS-FTD. *Neuron* **2011**, *72*, 257–268. [CrossRef] [PubMed]
76. DeJesus-Hernandez, M.; Mackenzie, I.R.; Boeve, B.F.; Boxer, A.L.; Baker, M.; Rutherford, N.J.; Nicholson, A.M.; Finch, N.A.; Flynn, H.; Adamson, J.; et al. Expanded GGGGCC Hexanucleotide Repeat in Noncoding Region of C9ORF72 Causes Chromosome 9p-Linked FTD and ALS. *Neuron* **2011**, *72*, 245–256. [CrossRef] [PubMed]
77. Haeusler, A.R.; Donnelly, C.J.; Rothstein, J.D. The Expanding Biology of the C9orf72 Nucleotide Repeat Expansion in Neurodegenerative Disease. *Nat. Rev. Neurosci.* **2016**, *17*, 383–395. [CrossRef]
78. Lee, Y.-B.; Chen, H.-J.; Peres, J.N.; Gomez-Deza, J.; Attig, J.; Stalekar, M.; Troakes, C.; Nishimura, A.L.; Scotter, E.L.; Vance, C.; et al. Hexanucleotide Repeats in ALS/FTD Form Length-Dependent RNA Foci, Sequester RNA Binding Proteins, and Are Neurotoxic. *Cell Rep.* **2013**, *5*, 1178–1186. [CrossRef] [PubMed]
79. Rossi, S.; Serrano, A.; Gerbino, V.; Giorgi, A.; Di Francesco, L.; Nencini, M.; Bozzo, F.; Schininà, M.E.; Bagni, C.; Cestra, G.; et al. Nuclear Accumulation of mRNAs Underlies G4C2-Repeat-Induced Translational Repression in a Cellular Model of C9orf72 ALS. *J. Cell Sci.* **2015**, *128*, 1787–1799. [CrossRef] [PubMed]
80. May, S.; Hornburg, D.; Schludi, M.H.; Arzberger, T.; Rentzsch, K.; Schwenk, B.M.; Grässer, F.A.; Mori, K.; Kremmer, E.; Banzhaf-Strathmann, J.; et al. C9orf72 FTLD/ALS-Associated Gly-Ala Dipeptide Repeat Proteins Cause Neuronal Toxicity and Unc119 Sequestration. *Acta Neuropathol.* **2014**, *128*, 485–503. [CrossRef]
81. Zhang, Y.-J.; Jansen-West, K.; Xu, Y.-F.; Gendron, T.F.; Bieniek, K.F.; Lin, W.-L.; Sasaguri, H.; Caulfield, T.; Hubbard, J.; Daughrity, L.; et al. Aggregation-Prone c9FTD/ALS Poly(GA) RAN-Translated Proteins Cause Neurotoxicity by Inducing ER Stress. *Acta Neuropathol.* **2014**, *128*, 505–524. [CrossRef]
82. Zhang, Y.-J.; Gendron, T.F.; Ebbert, M.T.W.; O'Raw, A.D.; Yue, M.; Jansen-West, K.; Zhang, X.; Prudencio, M.; Chew, J.; Cook, C.N.; et al. Poly(GR) Impairs Protein Translation and Stress Granule Dynamics in C9orf72-Associated Frontotemporal Dementia and Amyotrophic Lateral Sclerosis. *Nat. Med.* **2018**, *24*, 1136–1142. [CrossRef]
83. O'Rourke, J.G.; Bogdanik, L.; Yáñez, A.; Lall, D.; Wolf, A.J.; Muhammad, A.K.M.G.; Ho, R.; Carmona, S.; Vit, J.P.; Zarrow, J.; et al. C9orf72 Is Required for Proper Macrophage and Microglial Function in Mice. *Science* **2016**, *351*, 1324–1329. [CrossRef]
84. Burberry, A.; Suzuki, N.; Wang, J.-Y.; Moccia, R.; Mordes, D.A.; Stewart, M.H.; Suzuki-Uematsu, S.; Ghosh, S.; Singh, A.; Merkle, F.T.; et al. Loss-of-Function Mutations in the C9ORF72 Mouse Ortholog Cause Fatal Autoimmune Disease. *Sci. Transl. Med.* **2016**, *8*, 347ra93. [CrossRef]
85. Donnelly, C.J.; Zhang, P.-W.; Pham, J.T.; Haeusler, A.R.; Mistry, N.A.; Vidensky, S.; Daley, E.L.; Poth, E.M.; Hoover, B.; Fines, D.M.; et al. RNA Toxicity from the ALS/FTD C9ORF72 Expansion Is Mitigated by Antisense Intervention. *Neuron* **2013**, *80*, 415–428. [CrossRef]
86. Jiang, J.; Zhu, Q.; Gendron, T.F.; Saberi, S.; McAlonis-Downes, M.; Seelman, A.; Stauffer, J.E.; Jafar-Nejad, P.; Drenner, K.; Schulte, D.; et al. Gain of Toxicity from ALS/FTD-Linked Repeat Expansions in C9ORF72 Is Alleviated by Antisense Oligonucleotides Targeting GGGGCC-Containing RNAs. *Neuron* **2016**, *90*, 535–550. [CrossRef]
87. Cammack, A.J.; Atassi, N.; Hyman, T.; van den Berg, L.H.; Harms, M.; Baloh, R.H.; Brown, R.H.; van Es, M.A.; Veldink, J.H.; de Vries, B.S.; et al. Prospective Natural History Study of C9orf72 ALS Clinical Characteristics and Biomarkers. *Neurology* **2019**, *93*, e1605–e1617. [CrossRef]
88. Tran, H.; Moazami, M.P.; Yang, H.; McKenna-Yasek, D.; Douthwright, C.L.; Pinto, C.; Metterville, J.; Shin, M.; Sanil, N.; Dooley, C.; et al. Suppression of Mutant C9orf72 Expression by a Potent Mixed Backbone Antisense Oligonucleotide. *Nat. Med.* **2022**, *28*, 117–124. [CrossRef]
89. Boros, B.D.; Schoch, K.M.; Kreple, C.J.; Miller, T.M. Antisense Oligonucleotides for the Study and Treatment of ALS. *Neurotherapeutics* **2022**, *19*, 1145–1158. [CrossRef]
90. Liu, Y.; Dodart, J.-C.; Tran, H.; Berkovitch, S.; Braun, M.; Byrne, M.; Durbin, A.F.; Hu, X.S.; Iwamoto, N.; Jang, H.G.; et al. Variant-Selective Stereopure Oligonucleotides Protect against Pathologies Associated with C9orf72-Repeat Expansion in Preclinical Models. *Nat. Commun.* **2021**, *12*, 847. [CrossRef] [PubMed]
91. Liu, Y.; Andreucci, A.; Iwamoto, N.; Yin, Y.; Yang, H.; Liu, F.; Bulychev, A.; Hu, X.S.; Lin, X.; Lamore, S.; et al. Preclinical Evaluation of WVE-004, Aninvestigational Stereopure Oligonucleotide Forthe Treatment of C9orf72-Associated ALS or FTD. *Mol. Ther. Nucleic Acids* **2022**, *28*, 558–570. [CrossRef] [PubMed]
92. Lagier-Tourenne, C.; Baughn, M.; Rigo, F.; Sun, S.; Liu, P.; Li, H.-R.; Jiang, J.; Watt, A.T.; Chun, S.; Katz, M.; et al. Targeted Degradation of Sense and Antisense C9orf72 RNA Foci as Therapy for ALS and Frontotemporal Degeneration. *Proc. Natl. Acad. Sci. USA* **2013**, *110*, E4530–E4539. [CrossRef] [PubMed]
93. Sareen, D.; O'Rourke, J.G.; Meera, P.; Muhammad, A.K.M.G.; Grant, S.; Simpkinson, M.; Bell, S.; Carmona, S.; Ornelas, L.; Sahabian, A.; et al. Targeting RNA Foci in iPSC-Derived Motor Neurons from ALS Patients with a C9ORF72 Repeat Expansion. *Sci. Transl. Med.* **2013**, *5*, 208ra149. [CrossRef] [PubMed]
94. Ratti, A.; Buratti, E. Physiological Functions and Pathobiology of TDP-43 and FUS/TLS Proteins. *J. Neurochem.* **2016**, *138* (Suppl. S1), 95–111. [CrossRef] [PubMed]

95. Vance, C.; Scotter, E.L.; Nishimura, A.L.; Troakes, C.; Mitchell, J.C.; Kathe, C.; Urwin, H.; Manser, C.; Miller, C.C.; Hortobágyi, T.; et al. ALS Mutant FUS Disrupts Nuclear Localization and Sequesters Wild-Type FUS within Cytoplasmic Stress Granules. *Hum. Mol. Genet.* **2013**, *22*, 2676–2688. [CrossRef] [PubMed]
96. Mitchell, J.C.; McGoldrick, P.; Vance, C.; Hortobagyi, T.; Sreedharan, J.; Rogelj, B.; Tudor, E.L.; Smith, B.N.; Klasen, C.; Miller, C.C.J.; et al. Overexpression of Human Wild-Type FUS Causes Progressive Motor Neuron Degeneration in an Age- and Dose-Dependent Fashion. *Acta Neuropathol.* **2013**, *125*, 273–288. [CrossRef]
97. Korobeynikov, V.A.; Lyashchenko, A.K.; Blanco-Redondo, B.; Jafar-Nejad, P.; Shneider, N.A. Antisense Oligonucleotide Silencing of FUS Expression as a Therapeutic Approach in Amyotrophic Lateral Sclerosis. *Nat. Med.* **2022**, *28*, 104–116. [CrossRef] [PubMed]
98. Highley, J.R.; Kirby, J.; Jansweijer, J.A.; Webb, P.S.; Hewamadduma, C.A.; Heath, P.R.; Higginbottom, A.; Raman, R.; Ferraiuolo, L.; Cooper-Knock, J.; et al. Loss of Nuclear TDP -43 in Amyotrophic Lateral Sclerosis (ALS) Causes Altered Expression of Splicing Machinery and Widespread Dysregulation of RNA Splicing in Motor Neurones. *Neuropathol. Appl. Neurobiol.* **2014**, *40*, 670–685. [CrossRef]
99. Wang, X.; Hu, Y.; Xu, R. The Pathogenic Mechanism of TAR DNA-Binding Protein 43 (TDP-43) in Amyotrophic Lateral Sclerosis. *Neural Regen. Res.* **2024**, *19*, 800–806. [CrossRef] [PubMed]
100. Lagier-Tourenne, C.; Polymenidou, M.; Hutt, K.R.; Vu, A.Q.; Baughn, M.; Huelga, S.C.; Clutario, K.M.; Ling, S.-C.; Liang, T.Y.; Mazur, C.; et al. Divergent Roles of ALS-Linked Proteins FUS/TLS and TDP-43 Intersect in Processing Long Pre-mRNAs. *Nat. Neurosci.* **2012**, *15*, 1488–1497. [CrossRef]
101. Polymenidou, M.; Lagier-Tourenne, C.; Hutt, K.R.; Huelga, S.C.; Moran, J.; Liang, T.Y.; Ling, S.-C.; Sun, E.; Wancewicz, E.; Mazur, C.; et al. Long Pre-mRNA Depletion and RNA Missplicing Contribute to Neuronal Vulnerability from Loss of TDP-43. *Nat. Neurosci.* **2011**, *14*, 459–468. [CrossRef]
102. Tsao, W.; Jeong, Y.H.; Lin, S.; Ling, J.; Price, D.L.; Chiang, P.-M.; Wong, P.C. Rodent Models of TDP-43: Recent Advances. *Brain Res.* **2012**, *1462*, 26–39. [CrossRef]
103. Igaz, L.M.; Kwong, L.K.; Lee, E.B.; Chen-Plotkin, A.; Swanson, E.; Unger, T.; Malunda, J.; Xu, Y.; Winton, M.J.; Trojanowski, J.Q.; et al. Dysregulation of the ALS-Associated Gene TDP-43 Leads to Neuronal Death and Degeneration in Mice. *J. Clin. Investig.* **2011**, *121*, 726–738. [CrossRef]
104. Klim, J.R.; Williams, L.A.; Limone, F.; Guerra San Juan, I.; Davis-Dusenbery, B.N.; Mordes, D.A.; Burberry, A.; Steinbaugh, M.J.; Gamage, K.K.; Kirchner, R.; et al. ALS-Implicated Protein TDP-43 Sustains Levels of STMN2, a Mediator of Motor Neuron Growth and Repair. *Nat. Neurosci.* **2019**, *22*, 167–179. [CrossRef] [PubMed]
105. Krus, K.L.; Strickland, A.; Yamada, Y.; Devault, L.; Schmidt, R.E.; Bloom, A.J.; Milbrandt, J.; DiAntonio, A. Loss of Stathmin-2, a Hallmark of TDP-43-Associated ALS, Causes Motor Neuropathy. *Cell Rep.* **2022**, *39*, 111001. [CrossRef]
106. Baughn, M.W.; Melamed, Z.; López-Erauskin, J.; Beccari, M.S.; Ling, K.; Zuberi, A.; Presa, M.; Gonzalo-Gil, E.; Maimon, R.; Vazquez-Sanchez, S.; et al. Mechanism of STMN2 Cryptic Splice-Polyadenylation and Its Correction for TDP-43 Proteinopathies. *Science* **2023**, *379*, 1140–1149. [CrossRef] [PubMed]
107. Scoles, D.R.; Meera, P.; Schneider, M.D.; Paul, S.; Dansithong, W.; Figueroa, K.P.; Hung, G.; Rigo, F.; Bennett, C.F.; Otis, T.S.; et al. Antisense Oligonucleotide Therapy for Spinocerebellar Ataxia Type 2. *Nature* **2017**, *544*, 362–366. [CrossRef]
108. Becker, L.A.; Huang, B.; Bieri, G.; Ma, R.; Knowles, D.A.; Jafar-Nejad, P.; Messing, J.; Kim, H.J.; Soriano, A.; Auburger, G.; et al. Therapeutic Reduction of Ataxin-2 Extends Lifespan and Reduces Pathology in TDP-43 Mice. *Nature* **2017**, *544*, 367–371. [CrossRef] [PubMed]
109. Van Damme, P.; Veldink, J.H.; van Blitterswijk, M.; Corveleyn, A.; van Vught, P.W.J.; Thijs, V.; Dubois, B.; Matthijs, G.; van den Berg, L.H.; Robberecht, W. Expanded ATXN2 CAG Repeat Size in ALS Identifies Genetic Overlap between ALS and SCA2. *Neurology* **2011**, *76*, 2066–2072. [CrossRef]
110. Kennedy, W.R.; Alter, M.; Sung, J.H. Progressive Proximal Spinal and Bulbar Muscular Atrophy of Late Onset: A Sex-linked Recessive Trait. *Neurology* **1968**, *18*, 671. [CrossRef]
111. Banno, H.; Katsuno, M.; Suzuki, K.; Tanaka, F.; Sobue, G. Pathogenesis and Molecular Targeted Therapy of Spinal and Bulbar Muscular Atrophy (SBMA). *Cell Tissue Res.* **2012**, *349*, 313–320. [CrossRef]
112. Guidetti, D.; Sabadini, R.; Ferlini, A.; Torrente, I. Epidemiological Survey of X-Linked Bulbar and Spinal Muscular Atrophy, or Kennedy Disease, in the Province of Reggio Emilia, Italy. *Eur. J. Epidemiol.* **2001**, *17*, 587–591. [CrossRef] [PubMed]
113. Rhodes, L.E.; Freeman, B.K.; Auh, S.; Kokkinis, A.D.; La Pean, A.; Chen, C.; Lehky, T.J.; Shrader, J.A.; Levy, E.W.; Harris-Love, M.; et al. Clinical Features of Spinal and Bulbar Muscular Atrophy. *Brain* **2009**, *132 Pt 12*, 3242–3251. [CrossRef] [PubMed]
114. Fernández-Rhodes, L.E.; Kokkinis, A.D.; White, M.J.; Watts, C.A.; Auh, S.; Jeffries, N.O.; Shrader, J.A.; Lehky, T.J.; Li, L.; Ryder, J.E.; et al. Efficacy and Safety of Dutasteride in Patients with Spinal and Bulbar Muscular Atrophy: A Randomised Placebo-Controlled Trial. *Lancet Neurol.* **2011**, *10*, 140–147. [CrossRef] [PubMed]
115. La Spada, A.R.; Wilson, E.M.; Lubahn, D.B.; Harding, A.E.; Fischbeck, K.H. Androgen Receptor Gene Mutations in X-Linked Spinal and Bulbar Muscular Atrophy. *Nature* **1991**, *352*, 77–79. [CrossRef] [PubMed]
116. Watanabe, M.; Abe, K.; Aoki, M.; Yasuo, K.; Itoyama, Y.; Shoji, M.; Ikeda, Y.; Iizuka, T.; Ikeda, M.; Shizuka, M.; et al. Mitotic and Meiotic Stability of the CAG Repeat in the X-Linked Spinal and Bulbar Muscular Atrophy Gene. *Clin. Genet.* **1996**, *50*, 133–137. [CrossRef] [PubMed]
117. Craig, T.J.; Henley, J.M. Fighting Polyglutamine Disease by Wrestling with SUMO. *J. Clin. Investig.* **2015**, *125*, 498–500. [CrossRef]

118. Grunseich, C.; Fischbeck, K.H. Molecular Pathogenesis of Spinal Bulbar Muscular Atrophy (Kennedy's Disease) and Avenues for Treatment. *Curr. Opin. Neurol.* **2020**, *33*, 629–634. [CrossRef]
119. Lieberman, A.P.; Yu, Z.; Murray, S.; Peralta, R.; Low, A.; Guo, S.; Yu, X.X.; Cortes, C.J.; Bennett, C.F.; Monia, B.P.; et al. Peripheral Androgen Receptor Gene Suppression Rescues Disease in Mouse Models of Spinal and Bulbar Muscular Atrophy. *Cell Rep.* **2014**, *7*, 774–784. [CrossRef] [PubMed]
120. Sahashi, K.; Katsuno, M.; Hung, G.; Adachi, H.; Kondo, N.; Nakatsuji, H.; Tohnai, G.; Iida, M.; Bennett, C.F.; Sobue, G. Silencing Neuronal Mutant Androgen Receptor in a Mouse Model of Spinal and Bulbar Muscular Atrophy. *Hum. Mol. Genet.* **2015**, *24*, 5985–5994. [CrossRef] [PubMed]
121. Wang, Y.; Pang, J.; Wang, Q.; Yan, L.; Wang, L.; Xing, Z.; Wang, C.; Zhang, J.; Dong, L. Delivering Antisense Oligonucleotides across the Blood-Brain Barrier by Tumor Cell-Derived Small Apoptotic Bodies. *Adv. Sci.* **2021**, *8*, 2004929. [CrossRef]
122. Sun, Y.; Kong, J.; Ge, X.; Mao, M.; Yu, H.; Wang, Y. An Antisense Oligonucleotide-Loaded Blood–Brain Barrier Penetrable Nanoparticle Mediating Recruitment of Endogenous Neural Stem Cells for the Treatment of Parkinson's Disease. *ACS Nano* **2023**, *17*, 4414–4432. [CrossRef] [PubMed]
123. Sattler, R.; Traynor, B.J.; Robertson, J.; Van Den Bosch, L.; Barmada, S.J.; Svendsen, C.N.; Disney, M.D.; Gendron, T.F.; Wong, P.C.; Turner, M.R.; et al. Roadmap for C9ORF72 in Frontotemporal Dementia and Amyotrophic Lateral Sclerosis: Report on the C9ORF72 FTD/ALS Summit. *Neurol. Ther.* **2023**, *12*, 1821–1843. [CrossRef]
124. Van Daele, S.H.; Masrori, P.; Van Damme, P.; Van Den Bosch, L. The Sense of Antisense Therapies in ALS. *Trends Mol. Med.* **2024**, *30*, 252–262. [CrossRef] [PubMed]
125. Zhu, Q.; Jiang, J.; Gendron, T.F.; McAlonis-Downes, M.; Jiang, L.; Taylor, A.; Diaz Garcia, S.; Ghosh Dastidar, S.; Rodriguez, M.J.; King, P.; et al. Reduced C9ORF72 Function Exacerbates Gain of Toxicity from ALS/FTD-Causing Repeat Expansion in C9orf72. *Nat. Neurosci.* **2020**, *23*, 615–624. [CrossRef] [PubMed]
126. Backwell, L.; Marsh, J.A. Diverse Molecular Mechanisms Underlying Pathogenic Protein Mutations: Beyond the Loss-of-Function Paradigm. *Annu. Rev. Genom. Hum. Genet.* **2022**, *23*, 475–498. [CrossRef] [PubMed]
127. Lauffer, M.C.; Van Roon-Mom, W.; Aartsma-Rus, A.; N = 1 Collaborative. Possibilities and Limitations of Antisense Oligonucleotide Therapies for the Treatment of Monogenic Disorders. *Commun. Med.* **2024**, *4*, 6. [CrossRef] [PubMed]
128. Hauser, S.; Helm, J.; Kraft, M.; Korneck, M.; Hübener-Schmid, J.; Schöls, L. Allele-Specific Targeting of Mutant Ataxin-3 by Antisense Oligonucleotides in SCA3-iPSC-Derived Neurons. *Mol. Ther. Nucleic Acids* **2022**, *27*, 99–108. [CrossRef] [PubMed]
129. Skotte, N.H.; Southwell, A.L.; Østergaard, M.E.; Carroll, J.B.; Warby, S.C.; Doty, C.N.; Petoukhov, E.; Vaid, K.; Kordasiewicz, H.; Watt, A.T.; et al. Allele-Specific Suppression of Mutant Huntingtin Using Antisense Oligonucleotides: Providing a Therapeutic Option for All Huntington Disease Patients. *PLoS ONE* **2014**, *9*, e107434. [CrossRef] [PubMed]
130. Farrimond, L.; Talbot, K. A Case of SOD1 Deficiency: Implications for Clinical Trials. *Brain* **2022**, *145*, 805–806. [CrossRef]
131. Linares, G.R.; Li, Y.; Chang, W.-H.; Rubin-Sigler, J.; Mendonca, S.; Hong, S.; Eoh, Y.; Guo, W.; Huang, Y.-H.; Chang, J.; et al. SYF2 Suppression Mitigates Neurodegeneration in Models of Diverse Forms of ALS. *Cell Stem Cell* **2023**, *30*, 171–187.e14. [CrossRef]
132. Sharma, S.; Parveen, R.; Chatterji, B.P. Toxicology of Nanoparticles in Drug Delivery. *Curr. Pathobiol. Rep.* **2021**, *9*, 133–144. [CrossRef] [PubMed]
133. Dangouloff, T.; Vrščaj, E.; Servais, L.; Osredkar, D.; Adoukonou, T.; Aryani, O.; Barisic, N.; Bashiri, F.; Bastaki, L.; Benitto, A.; et al. Newborn Screening Programs for Spinal Muscular Atrophy Worldwide: Where We Stand and Where to Go. *Neuromuscul. Disord.* **2021**, *31*, 574–582. [CrossRef] [PubMed]

MDPI AG
Grosspeteranlage 5
4052 Basel
Switzerland
Tel.: +41 61 683 77 34

International Journal of Molecular Sciences Editorial Office
E-mail: ijms@mdpi.com
www.mdpi.com/journal/ijms

Academic Open
Access Publishing

mdpi.com

ISBN 978-3-7258-3507-2